PROCEEDINGS INTERNATIONAL SOLVENT EXTRACTION CONFERENCE 1971

VOL. I

ISEC 71

S.C.I.

Proceedings
of the
International Solvent Extraction Conference
ISEC 71

International Solvent Extraction Conference 1971

Sponsored by : THE SOCIETY OF CHEMICAL INDUSTRY

In association with : KONINKLIJK INSTITUUT VAN INGENIEURS
THE INSTITUTION OF CHEMICAL ENGINEERS
KONINKLIJKE NEDERLANDSE CHEMISCHE VERENIGING

The Working Party on Distillation, Absorption and Extraction of the European Federation of Chemical Engineering participated in the Conference, which was the 101st event of the Federation.

President:

PROFESSOR R. SPENCE, C.B.E., F.R.S.

Vice-President:

DR. IR. A. KLINKENBERG

Conference Committee

Mr. B. F. Warner (Chairman), United Kingdom Atomic Energy Authority
Mr. H. D. Axe, Shell International Chemical Company Ltd.
Dr. Ir. W. J. Beck, Unilever Research Laboratorium
Dr. F. Bradley, 136 Sharps Lane, Ruislip, Middx.
Mr. M. J. Cahalan, Rio Tinto-Zinc Research Secretariat
Professor S. R. M. Ellis, University of Birmingham
Dr. D. S. Flett, Ministry of Technology
Dr. J. A. Gardner, Monsanto Chemicals Ltd.
Professor H. Irving, University of Leeds
Dr. M. J. Jaycock, Loughborough University of Technology
Professor G. V. Jeffreys, University of Aston in Birmingham
Dr. E. Lloyd Jones, B.P. Chemicals Ltd.
Mr. N. G. W. Luitsz, Chairman, Benelux Section, Society of Chemical Industry
Dr. H. A. C. McKay, United Kingdom Atomic Energy Authority
Mr. A. Newton, Imperial Chemical Industries Ltd.
Dr. Ir. G. H. Reman, Koninklijke/Shell Laboratorium
Dr. F. J. C. Rossotti, University of Oxford
Dr. B. F. Saris, Centrale Engineering K.Z.O.
Professor Ir. S. Stemerding, Rijksuniversiteit Groningen
Professor Dr. Ir. D. Thoenes, Technische Hogeschool Twente
Professor J. D. Thornton, University of Newcastle upon Tyne
Professor W. L. Wilkinson, University of Bradford
Professor C. Hanson (Secretary), University of Bradford

U.K. Working Group

Mr. B. F. Warner (Chairman)
Dr. L. J. Austin, Shell International Petroleum Company Ltd.
Dr. M. J. Jaycock
Dr. H. A. C. McKay
Dr. M. W. T. Pratt, University of Bradford
Professor C. Hanson (Secretary)

Netherlands Working Group

Mr. N. G. W. Luitsz (Chairman)
Dr. Ir. J. W. van. Heuven, C.T.I.–T.N.O.
Mr. J. van Kruiselbergen, K.I.V.I.
Ir. N. M. Spaay, Dutch State Mines
Dr. Ir. A. M. Trommelen (Secretary), Unilever Research Laboratorium

SOLVENT EXTRACTION

Proceedings

of the

International Solvent Extraction Conference

ISEC 71

The Hague, 19–23 April, 1971

Vol. I

SOCIETY OF CHEMICAL INDUSTRY
LONDON
1971

MAS 575/001-1

SOCIETY OF CHEMICAL INDUSTRY
14 BELGRAVE SQUARE
LONDON S.W.1

EDITED BY: J. G. GREGORY
B. EVANS
P. C. WESTON
IN CLOSE COLLABORATION WITH
THE SESSION SECRETARIES
(see p. vi)

Figures by:
EAGLE ARTS, SUTTON, SURREY

© 1971 SOCIETY OF CHEMICAL INDUSTRY

In Two Volumes

SBN 901001 16 3
901001 17 1

Universitätsbibliothek Kaiserslautern
Sy.:
SW.:

ALL RIGHTS RESERVED

(86/46-11608/1

Printed in England by Staples Printers Limited at their Kettering, Northants, establishment

PREFACE

The development of solvent extraction as a separation technique has tended to progress in a somewhat fragmented manner. It was first employed on a large scale in the petroleum industry. More or less independently, solvent extraction provided the solution for the nuclear industry to its search for means of processing and reprocessing fuel to exacting limits of purity. The associated research provided much information on the extraction of metals which is now starting to be exploited. In addition to the isolation between solvent extraction workers in different areas of industrial application, communication has not always been good between those responsible for developing process chemistry and those concerned with designing the equipment for exploitation of the processes.

The 1971 International Solvent Extraction Conference was successor to five previous conferences held, respectively, in the U.S.A., Belgium, the U.K., Sweden and Israel. In each of these the emphasis was on the chemistry of solvent extraction, particularly as applied to the extraction of metals. However, from its initiation, ISEC 71 departed from this precedent and aimed to cover the entire science and technology of solvent extraction as applied in all branches of industry. The success with which this objective was realised can be measured by the response to the Conference. 141 papers out of over 200 submitted were presented before an audience of some 550 academic and industrial workers from all parts of the world. These covered both chemical and chemical engineering aspects of the subject as applied over a broad range of industries. Such a major event must provide cohesion between the different groups working in the field and ISEC 71 seems likely to prove a landmark for the future development of solvent extraction.

The initiative for ISEC 71 came through the Solvent Extraction Group of the Society of Chemical Industry. The Society generously agreed to act as Sponsor and a Conference Committee was established. Holland was chosen as the venue and representatives of the Benelux Section of the Society were appointed to the Committee. The Koninklijk Instituut van Ingenieurs, the Institution of Chemical Engineers and the Koninklijke Nederlandse Chemische Vereniging were associated with the Conference. It was the 101st event of the European Federation of Chemical Engineering and enjoyed the active participation of the Federation's Working Party on Distillation, Absorption and Extraction.

The Conference was fortunate in having two distinguished workers from the solvent extraction field as President and Vice-President. Professor R. Spence, C.B., F.R.S., was a central figure in the early application of the technique in nuclear fuel processing while Dr. Ir. A. Klinkenberg played a key role in the development of solvent extraction within the oil industry.

In introducing the Proceedings of the Conference, which include the full texts of all papers presented plus summaries of the discussions, we would like to record on behalf of the Conference Committee our thanks to numerous colleagues without whose help the Conference could never have been mounted. The number of papers involved necessitated a division into parallel sessions. The Session Chairmen carried not only the normal duties associated with such a position but were also charged with presenting reviews of the current situation in the subject areas of the sessions. These made a valuable addition to the proceedings. The secretaries appointed for each session had the heavy responsibility of reviewing the papers submitted and their technical editing. This was followed by the onerous task of recording the discussions. Their efforts have been truly invaluable.

Rapid publication of the Proceedings was felt to be essential for maintenance of their value and this has only been possible with ready collaboration from those responsible. It is impossible to record all names but we would like to express our particular appreciation to the Session Secretaries for prompt production of manuscripts of the discussion periods and to Dr. M. J. Slater who has undertaken a final review of the whole volume. Our thanks are also due to Mr. J. G. Gregory, Mr. B. Evans and other staff of the Society of Chemical Industry for their editorial efforts.

In conclusion, we would like to record our appreciation for the advice and support which was given to the Committee by Dr. D. H. Sharp, General Secretary of the Society of Chemical Industry, and his predecessor Col. F. J. Griffin.

B. F. Warner
Chairman, Conference Committee

C. Hanson
Secretary, Conference Committee

SESSION SECRETARIES

IA	Mr. M. A. Hughes & Dr. G. ten Brink
IB	Dr. J. Hoogschagen & Dr. L. J. Austin
IC	Dr. M. Streat
IIA	Dr. G. J. Lawson & Dr. N. M. Rice
IIB	Dr. J. Ingham & Ir. H. J. v. d. Berg
IIC	Ir. D. v. d. Meer & Ir. W. A. Beverloo
IIIA	Dr. Ir. C. A. P. Bakker & Dr. S. Hartland
IIIB	Dr. D. S. Flett & Dr. Ir. P. Groenveld
IIIC	Dr. A. Naylor
IVA	Dr. N. M. Rice & Dr. G. J. Lawson
IVB	Dr. G. ten Brink & Ir. D. v. d. Meer
IVC	Dr. I. L. Jenkins
VA	Dr. L. J. Austin & Dr. J. Hoogschagen
VB	Ir. W. A. Beverloo & Ir. A. Hamburger
VC	Mr. A. A. North & Dr. M. J. Jaycock
VIIA	Dr. S. Hartland & Dr. Ir. C. A. P. Bakker
VIIB	Dr. Ir. P. Groenveld & Dr. D. S. Flett
VIIC	Dr. A. Naylor & Dr. I. L. Jenkins
VIIIA	Dr. M. J. Jaycock & Mr. M. A. Hughes
VIIIB	Ir. H. J. v. d. Berg & Dr. G. A. Davies
VIIIC	Dr. Ir. P. Groenveld & Dr. D. S. Flett
IX	Mr. M. J. Slater & Ir. E. Ravoo

CONTENTS

Volume I

SESSION 1A: Physical Chemistry of Extraction I

PAGE

(15) SORIANO, J., SHAMIR, J., & MARCUS, Y. (*Hebrew Univ., Israel*)
Distribution of amines between liquid hydrogen fluoride and hexane. 3

(38) SOARES, L., PACKER, L. G., & ELLIS, S. R. M. (*Univ. of Birmingham, U.K.*)
Prediction of ternary liquid equilibria data. 9

(66) TANAKA, M. (*Nagoya Univ., Japan*)
Partition coefficient and extraction constant of non-charged species, as considered from the regular solution theory. 18

(95) TIEPEL, E. W., & GUBBINS, K. E. (*Univ. of Florida, U.S.A.*)
Molecular theory of thermodynamic factors in solvent extraction. 25

(129) WIDMER, H. M. (*Brookhaven National Laboratory, U.S.A.*)
Effects of ionic hydration and ion association on the solvent extraction behaviour of inorganic acids. 37

(204) FROLOV, YU. G., & NASONOVA, G. I. (*Mendeleev Institute of Chemical Technology, U.S.S.R.*)
Salting-out in extraction systems. 50

SESSION 1B: Drops and Dispersions

(24) WILSON, M. P., & JEFFREYS, G. V. (*Univ. of Aston, U.K.*)
Continuous phase backmixing associated with the wake of the dispersed phase droplet. 59

(51) VAN HEUVEN, J. W., (*T. N. O.*) & BEEK, W. J. (*Unilever Research Lab., The Netherlands*)
Power input, drop size and minimal stirrer speed for liquid–liquid dispersions in stirred vessels. 70

(71) EDGE, R. M., & GRANT, C. D. (*Univ. of Strathclyde, U.K.*)
Wakes behind drops falling at their terminal velocity in purified systems. 82

(89) GILES, J. W., HANSON, C., & MARSLAND, J. G. (*Univ. of Bradford, U.K.*)
Drop size distribution in agitated liquid–liquid systems with simultaneous interface mass transfer and chemical reaction. 94

(163) PIKE, F. P., & WADHAWAN, S. C. (*Univ. of S. Carolina, U.S.A.*)
Properties of an emulsion band in a mixer-settler contactor. 112

SESSION 1C: Nuclear Applications I: Chemical Process Technology

(57) MCNEESE, L. E., WATSON, J. S., HANNAFORD, B. A., KEE, C. W., & WHATLEY M. E. (*Oak Ridge National Laboratory, U.S.A.*)
Reductive extraction processing of molten-salt fuels for breeder reactors. 129

(93) AOCHI, T., TSUJINO, T., KOHSAKA, A., & HOSHINO, T. (*Japan Atomic Energy Institute*)
Computer evaluation of chemical flowsheets for plutonium purification with tributyl phosphate. 138

(108) GOURISSE, D., BATHELLIER, A., & BLANCHARD, J.-C. (*Commissariat à l'Energie Atomique, France*)
Use of sulphate in solvent extraction separation processes. 147

(131) STIEGLITZ, L. (*Institut für Heisse Chemie, Karlsruhe, W. Germany*)
Investigation on the nature of degradation products in the system 20 vol.-% tributyl phosphate—dodecane–nitric acid. I. 155

(139) SEGAWA, T., HOSHINO, T., KAYA, A., GONDA, K., TSUBOYA, T., & TANAKA, C. (*Nuclear Fuel Development Co., Japan*)
Flow-sheet studies on reprocessing Japanesse experimental fat reactor fuel in a Purex plant. 160

(179) SCHULZ, W. W. (*Atlantic Richfield Hanford Co. U.S.A.*)
Macroreticular ion-exchange resin clean-up of Purex process tributyl phosphate solvent. 174

(203) BRUNS, L. E. (*Atlantic Richmond Hanford Co. U.S.A.*)
Plutonium-uranium partitioning by a reflux extraction flowsheet. 186

SESSION IIA: Chemistry of Metals Extraction I

(21) HALA, J., & TUCK, D. G. (*Simon Fraser Univ., Canada*)
Extraction equilibria and solvation effects in the system liquid ammonia—tri-n-butyl phosphate, 197

(34) COX, M., (*Hatfield Polytechnic*), and FLETT, D. S., (*Warren Spring Laboratory, U.K.*)
Study of the synergistic extraction of metal ions by a-hydroxyoxime/carboxylic acid mixtures with the AKUFVE apparatus. 204

(40) FLETT, D. S., & WEST, D. W. (*Warren Spring Laboratory, U.K.*)
Extraction of metal ions by LIX 63/carboxylic acid mixtures. 214

(42) JUŽNIĆ, K., & FEDINA, S. (*'Josef Stefan' Institute, Yugoslavia*)
Transfer of iron in a liquid–liquid extraction system. 224

(87) KAMETANI, H. (*National Inst. for Metals, Japan*)
Reduction of cupric ion by ferrous ion with solvent extraction. 227

(98) SATO, T., & NAKAMURA, T. (*Shizuoka Univ., Japan*)
Extraction of iron (III) from sulphuric and hydrochloric acid solutions by di-(2-ethylhexyl) phosphoric acid. 238

SESSION IIB: Extraction Equipment I

(4) BAIRD, M. H. I., MCGINNIS, R. G., & TAN, G. C. (*McMaster Univ., Canada*)
Flooding conditions in a reciprocating plate extraction column. 251

(17) MUMFORD, C. J. (*Univ. of Aston, U.K.*)
Liquid extraction in a continuous agitated horizontal contactor. 260

(90) HANSON, C., INGHAM, J., & STEWARDSON, T. N. (*Univ. of Bradford, U.K.*)
Direct contact heat transfer between immiscible liquids in a mixer-settler apparatus. 270

(144) SPAAY, N. M., SIMONS, A. J. F., & TEN BRINK, G.P. (*D. S.M., The Netherlands*)
Design and operation of a pulsed packed column for liquid–liquid extraction. 281

(218) KARR, A. E., & LO, T. C. (*Hoffman—La Roche Inc., U.S.A.*)
Performance and scale-up of a reciprocating-plate extraction column. 299

SESSION IIC: Application to Petroleum Industry.

(65) SOMEKH, G. S. (*Union Carbide Co., U.S.A.*)
New Union Carbide aromatics extraction process. 323

(68) BERNARD, J. D. T., & VAN MEURS, H. C. A. (*Koninklijke/Shell-Laboratorium The Netherlands*)
Propane deasphalting of difficult feedstocks. 329

(113) WOODLE, R. A., BOZEMAN, P. P., & CUMMINS, B. H. (*Texaco Inc., U.S.A.*)
A new furfural refining process for petrochemical feedstocks. 343

(124) VAN DER MEER, D., ZUIDERWEG, F. J., & SCHEFFER, H. J. (*Koninklijkel Shell-Laboratorium, The Netherlands*) 350
Foam suppression in extract purification and recovery trains.

(125) KOSTERS, W. C. G. (*Bataafse Imternationale Petroleum Mij. N.V., The Netherlands*)
Manufacture of special boiling point solvents by Sulfolane extraction. 359

(176) RAHAJU, S. I., TUPAMAHU, M. S. (*Institut Teknologi*), & SOELISTIJO, (*Directorate of Mines, Indonesia*)
Preliminary study on the possibility of the application of solvent extraction process for sulphur refining. 366

(215) WINWARD, A. (*Univ. of Newcastle-upon-Tyne, U.K.*)
Status of developments in liquid–liquid extraction in the petroleum industry. 373

SESSION IIIA: Coalescence

(35) DAVIES, G. A., JEFFREYS, G. V., & SMITH, D. V., (*Univs. of Manchester and Aston, U.K.*)
Coalescence of liquid droplets—correlation of coalescence times. 385

(50) THOMAS, R. J., & MUMFORD, C. J. (*Univ. of Aston, U.K.*)
Coalescence in packed beds—packing selection and hydrodynamic behaviour. 400

(56) HARTLAND, S., & ROBINSON, J. D. (*Nottingham Univ., U.K.*)
Effect of adjacent drops on the shape of a drop approaching a deformable liquid-liquid interface. 418

(128) HEERTJES, P. M., & DE NIE, L. H. (*Univ. of Technology, Delft, The Netherlands*)
Coalescence and mass transfer. 428

(150) NEKOVAR, P. (*Institute of Chemical Technology, Prague, Czechoslovakia*)
Some results of studying mass transfer in a single drop during coalescence. 434

SESSION IIIB: Process Development I: Metals Extraction

(18) AUE, A., & SKUJTARE, L., (*Gullspang Electrochemical Co.,*), BJORLING, G. (*Royal Inst. of Techn., Stockhom.,*) & REINHARDT, H., & RYDBERG, J. (*Chalmers Univ. of Technology, Goteborg, Sweden*)
Separation of iron, cobalt and nickel from scrap alloy by a solvent extraction process. 447

(20) COOK, L. F., & SZMOKALUK, W. W. (*The Pyrites Co. Inc., U.S.A.*)
Refining of cobalt and nickel sulphate solutions by solvent extraction using di-(2-ethylhexyl) phosphoric acid. 451

(60) RITCEY, G. M., & LUCAS, B. H. (*Dept. of Energy, Mines and Resources, (Canada)*
Process for the recovery of cobalt from ammoniacal solutions using a carboxylic acid. 463

(126) CASSIDY, P. W., & BURKIN, A. R. (*Imperial College, U.K.*)
Extraction of europium from sulphate — perchlorate solutions by di-2-ethylhexylphosphoric acid. 476

(146) RICE, N. M. (*Univ. of Leeds, U.K.*)
The liquid–liquid extraction of iron (III) thiocyanate complexes by Versatic 911 and some other carboxylic acids. 483

(212) FOUCHÉ, K. F., & LE ROUX, H. J. (*Univ. of the Orange Free State, South Africa*)
Solvent extraction of yttrium and lanthanides with N-benzoyl–N–phenylhydroxylamine. 499

SESSION IIIC: Nuclear Applications II: Plant Practice and Technology

(134) BIGELOW, J. E., CHATTIN, F. R., & VAUGHEN, V. C. A. (*Oak Ridge National Laboratory, U.S.A.*)
Plant practice in solvent extraction processing of alpha-emitting nuclides of high specific activity. 507

(147) ORTH, D. A., MCKIBBEN, J. M., & SCOTTEN, W. C. (*E. I. du Pont de Nemours and Co., U.S.A.*)
Progress in tributyl phosphate technology at the Savannah River plant. 514

(148) ORTH, D. A., MCKIBBEN, J. M., PROUT, W. E., & SCOTTEN, W. C. (*E. I. du Pont de Nemours and Co., U.S.A.*)
Isolation of transplutonium elements. 534

(158) MODROW, R. D., OFFUTT, G. F., & WHEELER, B. R. (*Idaho Nuclear Co., U.S.A.*)
Optimized use of multi-purpose fuel processing facilities at the Idaho Chemical Plant. 556

(195) BRESCHET, C., & MIQUEL, P. (*Commissariat a l'Energie Atomique, France*)
Improvement of the procedure used to treat highly irradiated fuels (example of the utilisation of complexing and redox agents in a solvent extraction process). 565

(200) VAN GEEL, J., JOSEPH, C., DETILLEUX, E., HEINZ, W., CENTENO, J., & GUSTAFSSON, B. (*Eurochemic, Belgium*)
Chemical aspects of solvent extraction on plant scale at Eurochemic. 577

(202) JOSEPH, C., VAN GEEL, J., DETILLEUX, E., & CENTENO, J. (*Eurochemic, Belgium*)
Technological experience with extraction equipment at Eurochemic. 593

SESSION IVA: Chemistry of Metals Extraction II

(55) GOLINSKI, M. (*Institute of Nuclear Research, Warsaw, Poland*)
Extraction of tin and indium with tributyl phosphate from hydrochloric acid solutions. 603

(79) SELUCKY, P., RAIS, J., & KRTIL, J. (*Institute of Nuclear Research, Rez, Czechoslovakia*)
Comparison of selectivity of organic nitrosolvents for extraction of alkali metals. 616

(82) SISTKOVA, N. V. (*Institute of Nuclear Research, Rez, Czechslovakia*)
Extraction of sodium by some di-n-alkyl phosphoric acids. 620

(86) ZOLOTOV, Yu. A., & GOLOVANOV, V. I. (*Institute of Geochemistry and Analytical Chemistry, U.S.S.R.*)
Mutual influence of elements during extraction (co-extraction and extraction suppression). 625

(96) LAKSHMANAN, V. I., & LAWSON, G. J. (*Univ. of Birmingham, U.K.*)
Extraction of rhenium (VII) by dilute solutions of Aliquat 336 in organic solvents. 631

(152) DEPTULA, C. (*Institute of Nuclear Research, Swierk, Poland*)
Synergic and antagonistic effects in the extraction of chromium (VI) with a mixture of tri-n-octylamine and alkylphosphotic acids from mineral acid solutions. 638

(155) HERAK, M. J., & JAGODIC, V. (*Rudjer Boskovic Institute, Yugoslavia*)
Solvent extraction of gallium and zinc and their separation by aminophosphoric acids. 656

SESSION IVB: Extraction Equipment II

(13) JEFFREYS, G. V., & MUMFORD, C. J. (*Univ. of Aston, U.K.*)
Droplet break-up mechanisms in a rotating disc contactor. 667

(75) JEFFREYS, G. V., (*Univ. of Aston*), DAVIES, G. A., & PIPER, H. B., (*Univ. of Manchester, U.K.*)
Droplet behaviour in a Scheibel extraction column. 680

(145) ANGELINO, H., & MOLINIER, J. (*Institut du Genie Chimique, Toulouse, France*)
Study of back-mixing effect in a pulsed rotating disc contactor. 688

(160) POPE, R. J., & SHAH, M. R. (*Brigham Young Univ., U.S.A.*)
An improved contactor for liquid–liquid extraction. 699

(165) WIJFFELS, T.-B.,& RIETEMA, K., (*Eindhoven Univ. of Technology, The Netherlands*)
Axial mixing and classification phenomena in liquid-liquid fluid beds. 711

(170) ROD, V. (*Institute of Chemical Process Fundamentals, Prague*), & MISEK, T. (*Research Institute of Chemical Equipment, Prague, Czechoslovakia*)
Residence time distribution of the dispersed phase in agitated extraction columns. 738

SESSION IVC: Nuclear Applications III: Neptunium-Plutonium Separation and Transuranics

(44) KOLARIK, Z. (*Institute fur Heisse Chemie, Karlsruhe, W. Germany*)
Acidic organophosphorus extractants—XV. Extraction of americium and some fission products by di-(2-ethylhexyl) phosphate perchlorate and citrate media. 753

(53) SECEROV, M. M., KOPECHNI, M. M., MAKSIMOVIC, Z. B., & BERAN, M. (*Boris Kidric Institute of Nuclear Sciences, Yugoslavia*)
Solvent extraction of some diprotic nitroaromatic acids and their complexes with some actinides by tributyl phosphate. 762

(105) KOEHLY, G., MADIC, C., & BERGER, R. (*Commissariat a l'Energie Atomique, France*)
Capric acid effect on actinides extraction by trilauryl-ammonium nitrate. 768

(106) GOURISSE, D. (*Commissariat a l'Energie Atomique, France*)
Laboratory studies of nitrous acid and neptunium behaviour in TBP extraction processes. 781

(107) BERGER, R., KOEHLY, G., & ESPIE, J.-Y. (*Commissariat a l'Energie Atomique, France*)
Use of trilaurylamine in the processing of irradiated 237 NP. 792

(174) HYNES, C. J., JENKINS, I. L., & WAIN, A. G. (*Atomic Energy Research Establishment, U.K.*)
A process for the extraction of plutonium—238 from a neptunium solution circulating through a reactor. 801

(197) MYASOEDOV, B. F., CHUMTOVA, M. K., & LEBEDEV, I. A. (*V. I. Vernadski Institute of Geochemistry and Analytical Chemistry, U.S.S.R.*)
Synergistic extraction and its use in analytical chemistry of transplutonium elements. 815

Volume II

SESSION VA: Transport and Interfacial Phenomena

(27) PROCHAZKA, J., & BULICKA, J. (*Institute of Chemical Process Fundamentals, Prague, Czechoslovakia*)
Mass transfer between two turbulent liquids. 823

(97) NAKASHIO, F., TSUNEYUKI, T., INOUE, K., & SAKAI, W. (*Kyushu Univ., Japan*)
The effect of chemical reaction on the rate of solvent extraction 831

(99) YING, W. E., & SAWISTOWSKI, H. (*Imperial College, U.K.*)
Interfacial and mass transfer characteristics of binary liquid–liquid systems. 840

(130) VON BERG, R. L., & HENKEL, W. M., (*Cornell Univ., U.S.A.*)
Simultaneous heat and mass transfer in single drop liquid–liquid extraction. 852

(136) LUHNING, R. W., & SAWISTOWSKI, H. (*Imperial College, U.K.*)
Phase inversion in stirred liquid–liquid systems. 873

(207) YAGODIN, G. A., & TARASOV, V. V. (*Mendeleev Institute of Chemical Technology, U.S.S.R.*)
Some aspects of extraction kinetics. 888

SESSION VB: Process Development II: Extraction of Non-Metals

(46) KRISHNAMOORTHI, V. (*Regional Research Laboratory, Hyderabad, India*)
Edible proteins by solvent extraction. 905

(88) ANWAR, M. M., HANSON, C., & PRATT, M. W. T. (*Univ. of Bradford, U.K.*)
An improved dissociation extraction process for the separation of acidic or basic organic isomers. 911

(112) SHANBHAG, V. P. (*Univ. of Umea, Sweden*)
Rate of transport of proteins across the interface between the two aqueous phases in poly ethyleneglycol-dextran-water systems. 920

(192) JOHANSSON, G. (*Univ. of Umea, Sweden*)
Effects of different ions on the partition of proteins in an aqueous dextram-poly (ethylene glycol) two-phase system. 928

SESSION VC: Extraction of Lanthanides

(28) MICHELSEN, O. B. (*Institutt for Atomenergi, Norway*), & SMUTZ, M. (*Univ. of Florida, U.S.A.*)
Extraction of some rare earth elements with di-(2-ethylhexyl) phosphate acid at high acidities. 939

(29) HARADA, T. SMUTZ, M., & BAUTISTA, R. G. (*U.S.A.E.C., Ames Laboratory, U.S.A.*)
Polymers of iron and rare earths and di-(2-ethylhexyl)-phosphate acid. 950

(30) IOANNOU, T. K., BAUTISTA, R. G., & SMUTZ, M. (*U.S.A.E.C., Ames Laboratory, U.S.A.*)
Correlating multicomponent equilibrium data for the extraction of lanthanides with di-(2-ethylhexyl)-phosphate acid as the solvent. 957

(41) FOOS, J., & GUILLAUMONT, R. (*Institut de Physique Nucleaire, France*)
Solvent extraction from molten salts of some 4f and 5f elements. 966

(69) DAVIS, M. W., HOLT, W., & TOURNIER, R. A. (*Univ. of S. Carolina, U.S.A.*)
Actinide–lanthanide separation in the synergistic systems kerosene-tri-n-butyl phosphate-thenoyltrifluoroacetone. 974

(114) ZUR NEDDEN, P. J., JAMIL, M., & DUYCKAERTS, G. (*Laboratory of Analytical and Nuclear Chemistry, Liege, Belgium*)
Effect of a second organic solvent on the extraction of tri-valent europium by organophosphorus acids into benzene. 993

(189) FIDELIS, I. (*Institute of Nuclear Research, Warsaw, Poland*)
Influence of temperature on the extraction of lanthanides in the HDEHP-HNO3 system. 1004

SESSION VIIA: Mathematical Models and Control

(73) GOTO, T. (*Government Chemical Industrial Research Institute, Japan*)
Calculation of counter-current extraction of lanthanides with a digital computer. 1011

(80) CHENG, S.-I. (*The Cooper Union, U.S.A.*)
Column design and dynamics evaluation for fractional extraction of metals. 1025

(91) JONES, D. A., & WILKINSON, W. L. (*Univ. of Bradford, U.K.*)
A dynamic model of a multiple-mixer solvent extraction column. 1037

(138) TIERNEY, J. W., YANOSIK, J. L., BRUNO, J. A., & BRAINARD, A. J. (*Univ. of Pittsburgh, U.S.A.*)
Solution of equilibrium stage models for solvent extraction processes. 1051

(153) MILLS, A. L., & BELL, P. G. (*U.K.A.E.A.*)
Automatic control and response characteristics of small scale solvent extraction equipment. 1062

(166) VORSTMAN, M. A. G., & THIJSSEN, H. A. C. (*Eindhoven Univ. of Technology, The Netherlands*)
Asymptotic values of disperse phase mass transfer coefficients and their application to extraction calculations. 1071

(182) SLAVICEK, E., & BURES, F. (*Institute of Chemical Technology, Prague, Czechoslovakia*)
Interrupted extraction. 1082

SESSION VIIB: Chemistry of Metals Extraction III

(64) SEVDIC, D., & MEIDER-GORICAN, H. (*Institute Rudjer Boskovic, Yugoslavia*)
Bidentate phosphoryl and thiophosphoryl compounds as extractants for zinc (III), cadmium (II) and mercury (II). 1091

(84) VAN DALEN, A. (*Reactor Centrum*), & GERRITSMA, K. W. (*Free Univ., Amsterdam, The Netherlands*)
Solvent extraction and inclusion compound formation with dinonylnaphthalene-sulphonic acid. 1096

(167) ELEK, A., & SZABO, E. (*Central Research Institute for Physics, Hungary*)
Substoichiometric group separation in activation analysis by metal dithizonate extraction. 1101

(183) PETRUCHIN, O. M., SHEVCHENCO, V. N., IZOSENKOVA, L. A. & ZOLOTOV, Yu. A. (*Vernadsky Institute of Geochemistry and Analytical Chemistry, U.S.S.R.*)
Synergistic extraction of mercury (II), cadmium (II), zinc (II) and silver (I) chelates in the presence of triphenyl-phosphine. 1106

(196) MIKHAILOV, V. A., TORGOV, V. G., GILBERT, E. N., MAZALOV, L. N., & NIKOLAEV, A. V. (*Institute of Inorganic Chemistry, Novosibirsk, U.S.S.R.*)
Dialky sulphoxides and dialkyl sulphides as new extractants for metals. 1112

(198) STARY, J. (*Technical Univ. of Prague, Czechoslovakia*)
Determination of extraction contents of metal chelates. 1120

(208) YAGODIN, G. A., SINEGRIBOVA, O. A., & CHEKMAREV, A. M. (*Mendeleev Institute of Chemical Technology, U.S.S.R.*)
Effect of states of zirconium and hafnium in aqueous solutions on their separation by liquid–liquid extraction. 1124

SESSION VIIC: Nuclear Applications IV: Thorium, Uranium and Amine Systems

(59) PETKOVIC, D. M., & KEZELE, B. A. (*Boris Kidric Institute of Nuclear Sciences, Yugoslavia*)
Determination of tributyl phosphate association contsants and an approach to the problem of solvent effect. 1137

(63) RYON, A. D., FINNEY, B. C., MCBRIDE, J. P., & PARROTT, J. R. (*Oak Ridge National Laboratory, U.S.A.*)
Development and application of solvent extraction processes for the preparation of ThO2 – UO3 and UO2 sols. 1142

(77) LAURENCE, G. T., CHAIEB, M. T., & TALBOT, J. (*Laboratoire de Genie Chimique, ENSCP, France*)
Liquid–liquid extraction of uranyl nitrate and thorium nitrate by aliphatic sulfoxides; separation by di-n-heptyl-sulphoxide. 1150

(109) GERMAIN, M., & BATHELLIER, A. (*Commissariat a l'Energie Atomique, France*)
Studies of trilaurylamine in nuclear fuel processing. 1161

(118) BAROCAS, A., BARONCELLI, F., & DWORSCHAK, H. (*CSN, Casaccia, Italy*)
Influence of some complexing agents on the extraction rate of plutonium from organic to aqueous phase. 1174

(132) PUZIC, R. G., & MAKSIMOVIC, Z. B. (*Boris Kidric Institute of Nuclear Sciences, Yugoslavia*)
Solvent extraction of some actinides in mixed solvents trilaurylamine oxide 2-thenoyltrifluoroacetone system. 1180

(161) THOMAS, R. (*Institute für Chemische Technologie, Jülich, W. Germany*)
Development of an amine-extraction flow-sheet for the recovery of uranium from spent HTR-U-Th fuel elements after a hard-end chlorination (Chlorinex process). 1188

SESSION VIIIA: Physical Chemistry of Extraction II

(9) FREISER, H. (*Univ. of Arizona, U.S.A.*)
Application of solvent extraction principles to the development of ion-selective electrodes. 1199

(45) KRASNOV, K. S. (*Institute of Chemistry and Technology, Ivanova, U.S.S.R.*)
Extraction of ionic associates. Thermodynamics and structure. 1204

(67) APELBLAT, A. (*Israel Atomic Energy Commission, Israel*)
Methyl diphenyl phosphate extraction equilibria. 1208

(115) MODIN, R., PERSSON, B.-A., & SCHILL, G. (*Univ. of Uppsala, Sweden*)
Ion-pair extraction in the isolation of ionisable organic substances. 1211

(191) GROVES, W. D., & FORSYTH, J. S. (*Univ. of British Columbia, Canada*)
Liquid–liquid equilibria in sulphur-aromatic hydrocarbon systems. 1221

(205) FROLOV, Yu. G., OCHKIN, A. V., SERGIEVSKY, V. V., & ZUEV, A. P. (*Mendeleev Institute of Chemical Technology, U.S.S.R.*)
Hydration of substituted ammonium salts. 1229

(206) FROLOV, Yu. G., PUSHKOV, A. A., & SERGIEVSKY, V. V. (*Mendeleev Institute of Chemical Technology, U.S.S.R.*)
Diluent effect on the solvent extraction equilibrium. 1236

(213) KESSLER, Yu. M., GORBANEV, Z. I., & EMELIN, V. P. (*Metallurgical Institute of the Academy of Science, U.S.S.R.*)
Tru interionic potential and salting-out (in) on extraction. 1243

SESSION VIIIB: Extraction Equipment III

(6) PEEL, D., & COGGAN, G. C. (*British Plaster Board Industries, East Leake, U.K.*)
The transurface contactor: A new liquid-liquid extractor. 1251

(37) MEHNER, W., MUELLER, E., & HOEHFELD, G. (*Lurgi Gesellschaft fur Mineraloeltechnik, W. Germany*)
The Lurgi multi-stage liquid–liquid extractor. 1265

(54) CHAKALOZ, T., BUCUKOGLU, Z., (*Middle-East Technical Univ.*), & ARAS, O. (*Petro Chemicals Industries Inc., Turkey*)
Mass transfer studies in a helical solvent extractor. 1277

(102) BERNARD, C., MICHEL, P., & TARNERO, M. (*Commissariat a l'Energie Atomique, France*)
Experience with centrifugal extractors: comparison with other types of extractors. 1282

(159) HENTON, J. E., HAWRELAK, R. A., FORSYTH, J. S., & CAVERS, S. D. (*Univ. of British Columbia, Canada*)
Internal sampling of liquid–liquid spray columns at steady state. Methods, material balances and application to tracer studies without mass transfer. 1302

SESSION VIIIC: Chemistry of Metals Extraction IV

(36) DZIOMKO, V. M., AVILINA, V. N., & IVANOV, O. V. (*All-Union Scientific Research Institute of Chemical Reagents and Ultra High Purity Chemical Substances, U.S.S.R.*)
3, 4, 5-Trialkyl-and 1, 3, 4, 5-Tetra-alkylpyrazoles as new type of amine extractants in liquid–liquid extracting systems. 1319

(135) DESREUX, J. F. (*Univ. of Liege, Belgium*)
Diluent influence on the liquid-liquid extraction of zinc (II) by quaternary and tertiary ammonium chlorides. 1328

(190) NARBUTT, J. (*Institute of Nuclear Research, Warsaw, Poland*)
Effect of the structure of aromatic diluent molecules on extraction of the dithiocyanatotetrakis-(r-picoline) cobalt (II) complex. 1333

(216) DANESI, P. R., DELUCA, B., SCIBONA, G., & SUSINI, P. (*Comitato Nazionale per l'Energia Nucleare, Italy*)
Analysis of the equilibria in the system tetraheptyl-ammonium chloride o-xylene ZnC12 LiCl HCl H2O. 1337

(217) SCIBONA, G., CONTE, A., SCUPPA, B., & DANESI, P. R. (*Comitato Nazionale per l'Energia Nucleare, Italy*)
Interfacial equilibria with quaternary alkylammonium salts. 1344

PLENARY SESSION IX: Case Histories of Industrial Applications

(11) MERIGOLD, C. R., AGERS, D. W., & HOUSE, J. E. (*General Mills Chemicals Inc., U.S.A.*)
LIX 64N—The recovery of copper from ammoniacal leach solutions. 1351

(78) NAYLOR, A., & LARKIN, M. J. (*U.K.A.E.A.*)
Some experiences in the development, design and scale-up of solvent extraction processes for the recovery of irradiated nuclear fuels. 1356

(85) WARWICK, G. C. I., SCUFFHAM, J. B., & LOTT, J. B. (*Power Gas Corp., Ltd., U.K.*)
Considerations in the design of large scale solvent extraction plants for the recovery of metals. 1373

(94) ISRAEL MINING INDUSTRIES STAFF (*Haifa Israel*)
Development and implementation of solvent extraction processes in the chemical process industries. 1386

(175) POWER. (*Ranchers Exploration & Development Co., U.S.A.*)
Operation of the first commercial liquid ion-exchange and electrowinning plant. 1409

(214) ROBINSON, C. G., & PAYNTER, J. C. (*National Institute for Metallurgy, South Africa*)
Optimisation of the design of a countercurrent liquid–liquid extraction plant using LIX-64N. 1416

SUPPLEMENTARY PAPERS by Prof. Thornton and Dr. Rozen 1431

PLENARY PAPERS by Prof. Spence and Dr. Ir. Klinkenberg (Conference President and Vice-President) 1450

DISCUSSIONS AND CHAIRMEN'S REMARKS

IA	Physical Chemistry of Extraction I	Prof. A. S. Kertes	D1
IB	Drops and Dispersions	Dr. H. Sawistowski	D9
IC	Nuclear Applications I	Dr. E. Detilleux	D15
IIA	Chemistry of Metals Extraction I	Mr. A. W. Fletcher	D22
IIB	Extraction Equipment I	Prof. W. L. Wilkinson	D26
IIC	Application to Petroleum Industry	Dr. G. H. Reman	D31
IIIA	Coalescence	Prof. R. C. Kintner	D36
IIIB	Process Development I	Mr. M. J. Cahalan	D38
IIIC	Nuclear Applications II	Dr. W. Schuller	D42
IVA	Chemistry of Metals Extraction II	Prof. H. Irving	D49
IVB	Extraction Equipment II	Prof. J. D. Thornton	D56
IVC	Nuclear Applications III	Mr. A. Chesne	D59
VA	Transport and Interfacial Phenomena	Prof. P. M. Heertjes	D63
VB	Process Development II	Prof. S. R. M. Ellis	D67
VC	Extraction of Lanthanides	Mr. L. G. Sherrington	D70
VI	Commercial Contacting Equipment	Mr. F. J. Zuiderweg	—
VIIA	Mathematical Models and Control	Prof. G. V. Jeffreys	D74
VIIB	Chemistry of Metals Extraction III	Dr. A. R. Burkin	D75
VIIC	Nuclear Applications IV	Dr. M. Zifferero	D79
VIIIA	Physical Chemistry of Extraction II	Dr. H. A. C. McKay	D85
VIIIB	Extraction Equipment III	Prof. S. Stemerding	D87
VIIIC	Chemistry of Metals Extraction IV	Dr. A. R. Burkin	D90
IX	General Discussion / Future Trends in Solvent Extraction	Mr. B. F. Warner	D93

GLOSSARY xxv

LIST OF DELEGATES xxviii

INDEX OF PAPERS, AND SUBJECT GUIDE xli

AUTHOR INDEX xlv

SESSION 1A

PHYSICAL CHEMISTRY OF EXTRACTION, I

CHAIRMAN

Prof. A. S. Kertes

SECRETARIES

Mr. M. A. Hughes
Dr. G. ten Brink

Distribution of amines between liquid hydrogen fluoride and hexane

by J. Soriano, J. Shamir and Y. Marcus

Soreq Nuclear Research Center, Yavneh, and Department of Inorganic and Analytical Chemistry, The Hebrew University, Jerusalem, Israel

The distribution of alkylamines between liquid hydrogen fluoride and aliphatic hydrocarbons has been studied. Chain length, rather than the number of chains, determines the distribution ratio. The effect of Lewis acids on the distribution ratios was determined. The interaction of the amines with hydrogen fluoride was also studied by a dynamic pumping technique. Several polyhydrofluorides of the alkylammonium fluorides were identified.

Introduction

THE EXTRACTION OF solutes from hydrocarbons into liquid anhydrous hydrogen fluoride (AHF), as an industrial process, has been well studied. The desulphuration of crude petroleum is one promising use for this extraction method,[1-3] and details on the extractability of mercaptans, disulphides and thioethers by AHF from heptane have been given by Lien *et al.*[4] The extraction of organic fluorine compounds[5] and of metal contaminants[6,7] from petroleum with AHF has also been suggested.

Only one recent publication suggests the use of AHF extraction to remove nitrogen compounds, in addition to sulphur compounds, from crude oil.[8] The reverse reaction, i.e., the extraction of hydrogen fluoride by amines from gas streams,[9,10] and from aqueous solutions has been studied.[10-13] The reaction of amines and AHF, whether for extraction purposes or otherwise, has not been previously investigated.

Tertiary amines, because of their basic properties, interact very strongly with AHF. They are immediately protonated, the equilibrium:

$$R'R''R'''N + HF \rightleftharpoons R'R''R'''NH^+ + F^- \quad (1)$$

being situated far to the right. Quantitative studies have been made with much less basic compounds, e.g., the aromatic hydrocarbons. The equilibrium:

$$Ar + HF \rightleftharpoons ArH^+ + F^- \quad (2)$$

then lies much more to the left; indeed, the addition of boron trifluoride is required to shift it to the right:[14-17]

$$Ar + HF + BF_3 \rightleftharpoons ArH^+ + BF_4^- \quad (3)$$

Conversely, alkali metal fluorides, dissolved in the AHF, shift the equilibrium to the left. The distribution method has been found to be convenient for studying these equilibria.[14-17]

The extraction of aromatic hydrocarbons with AHF alone, or in the presence of Lewis acids such as boron trifluoride or silver fluoride (which acts also by π-bonding to the aromatic hydrocarbons), has been found to be a useful separation method, e.g. for xylene isomers,[14] for ethylbenzene from xylene[18] or for certain condensed aromatic hydrocarbons.[19]

The present paper deals with the interaction of aliphatic amines with AHF. The preparation of the simple alkylamine fluorides is described, as well as that of several polyhydrofluorides of these compounds. The isothermal decomposition of these is discussed in detail. The distribution of several alkylammonium fluorides, bifluorides and fluoroborates between hexane and AHF is then described, and the effect of some fluoro-Lewis acids on these systems is noted. The results are interpreted in terms of structural effects that the alkylammonium salts have on AHF, and of their aggregation in hexane.

Experimental

Procedure

An all-plastic vacuum line, made of the chlorotrifluoroethylene polymer,

Kel F, was used to handle the AHF. Amines and hydrocarbons were weighed directly into Kel F tubes, and AHF was distilled into it, its amount being determined by weighing. For distribution measurements a Teflon-clad bar magnet actuated from the outside reciprocated in the tube to mix the phases. Samples of each phase were transferred by pressure into preweighed tubes, weighed, and the solvent was allowed to evaporate. The residual amine salt was determined by weighing, and its composition was obtained from the known decomposition curves for the alkylammonium fluoride–AHF adducts.

The decomposition curves were obtained as follows. Excess AHF (more than 40 moles HF per mole amine) was distilled on to the amine and was then allowed to react. Excess HF was then removed at room temperature (22–25 °C) by one of the following three methods: (i) continuous pumping under vacuum; (ii) passage of dry nitrogen over the sample; or (iii) vacuum distillation from the reaction tube into another cooled tube. Since the pressure and temperature were kept constant, weighing at frequent intervals gave a dynamic decomposition curve from which the composition of the intermediate adducts and the final adduct could be determined from the plateaux on the curve. Indeed, this dynamic pumping method gave curves similar to those obtained in thermogravimetric analysis, and a typical one is shown in Fig. 1. The results of all three methods agreed closely with each other.

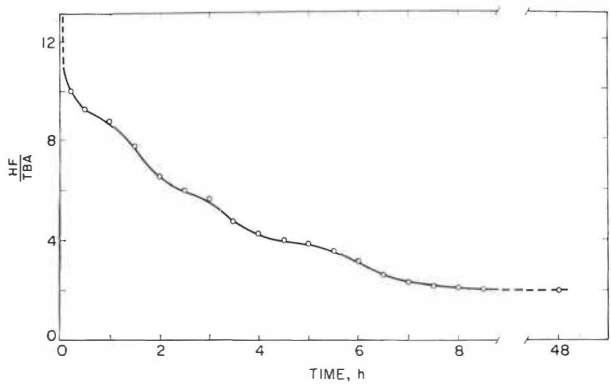

FIG. 1. *Dynamic pumping decomposition curve of tributylamine (TBA) polyhydrofluoride*

Another method was used to determine the composition of the adduct first formed with excess AHF. A solution of 2–10 mole-% amine in hexane was titrated from a weight burette with AHF, until cloudiness appeared, indicating the separation of a second phase. This method was quite sensitive, and yielded results reproducible to $\pm 1\%$ of the amount of AHF used.

Materials

AHF was obtained from Matheson Co., Inc., and was purified by first freezing it in a liquid air bath and degassing to remove non-condensable gases, and then vacuum-distilling it from a dry ice/trichloroethylene bath to a liquid air bath, to free it from water. The specific conductivity of the purified AHF ($\sim 4 \times 10^{-5}$ cm ohm^{-1}) was sufficiently low for the present purposes.

The n-hexane (Fluka, A. R. grade) was dried over metallic sodium and fractionally distilled. The amines (Eastman Kodak and Fluka, purest grade available) were dried over calcium oxide and distilled under vacuum, except for trilaurylamine (Rhône-Poulenc) which was used as received. Inorganic fluorides were obtained from Alpha Inorganics Inc., and were used without further purification.

Results

The neutralisation of alkylamines with hydrofluoric acid does not lead to alkylammonium fluorides since, in every case, bifluorides or even higher polyfluorides were obtained. This was the case whether the amine itself, or its solution in a hydrocarbon, or whether AHF, gaseous hydrogen fluoride, or aqueous hydrofluoric acid were used. However, the simple fluorides were prepared in a metathetical reaction, when a solution of the alkylammonium chloride in a hydrocarbon diluent was contacted with a stoicheiometric amount of silver fluoride in aqueous solution. The alkylammonium fluoride formed in the organic phase was separated from the precipitate, washed once with water, crystallised from the solvent after its partial evaporation, and dried in a desiccator over phosphorous pentoxide. These fluorides were characterised by their melting points, infra-red spectra[20] and proton and fluorine nuclear magnetic resonance spectra.[21]

The compositions of the polyhydrofluorides of the alkylammonium fluorides, obtained by the titration method and by the dynamic pumping methods, are shown in Table I. All the alkyl chains were primary and normal, except that the tri-iso-octyl isomer was also tested.

TABLE I

Hydrofluoride adducts of alkylammonium fluorides

Amine	Moles HF per mole amine				
	From titration	First plateau	Further plateaus		
Monobutyl	12·0	12·2	6·9	4·1	2·0
Dibutyl	9·9	10·3	6·5	4·0	2·0
Tributyl	9·5	9·0	5·9	4·0	2·0
Tetrabutyl	10·0	10·4	6·3	3·9	2·0
Monohexyl	9·4	8·9	~6	~4	2·0
Dihexyl	9·0	8·1	~6	~4	2·0
Trihexyl	5·4	5·9		~4	2·0
Tetrahexyl		8·2	~6	~4	2·0
Mono-octyl	5·5	6·0		~4	2·0
Di-octyl	5·0	5·0		4(?)	2·0
Tri-octyl		4·0			2·0
Tri-iso-octyl	4·8	4·0			
Tetra-octyl	5·1	5·2		4(?)	2·0
Monononyl	4·1	4·7			2·0
Dinonyl	4·6	4·4			2·0
Trinonyl	4·5	3·9			2·0
Monolauryl	4·0	3·8			2·0
Trilauryl	2·5	2·5			—

An inflexion point which is not clearly a plateau is marked by (?)

The compositions of the first adduct, i.e. that found by the titration method or that corresponding to the first plateau in the decomposition curve, are shown in Fig. 2. These two quite dissimilar methods yield concordant results (see Table I). When undiluted amines are titrated with AHF, the product is a liquid which dissolves in excess amine or AHF, without an end-point. Of the amines appearing in Table I, only trilaurylamine yields a product insoluble in excess AHF, and the stoichiometry corresponds to R_3N:2·5 HF. When this ratio is reached, a second phase appears. (See Blundy *et al.*[10] for the behaviour of wet trinonylamine under similar conditions.) It should also be noted that this is the only amine which does not form a stable bifluoride as the end-product, but stabilises at the stoichiometry R_3N:2·5 HF, or $R_3NH^+F^-$:1·5 HF.

The distribution of alkylamine fluorides was studied for AHF and n-hexane as the liquid phases. These solvents are virtually mutually insoluble,[22] so that if $\overline{N}$ is the number of moles of amine per the sum of the moles of amine and

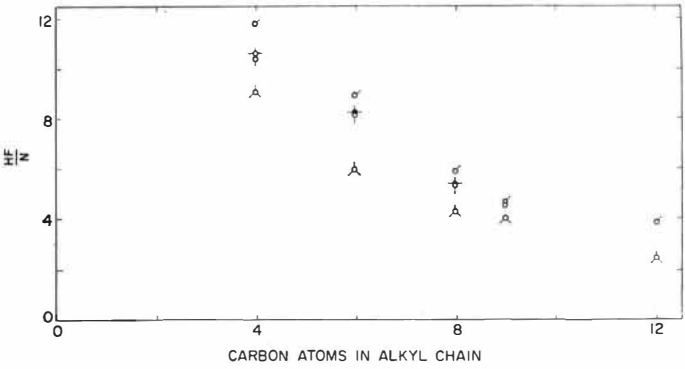

FIG. 2. *Stoicheiometric compositions of the most HF-rich adducts formed from butyl-, hexyl-, octyl-, nonyl- and lauryl-amines, as a function of the number of carbon atoms per alkyl chain (abcissa), and the number of alkyl chains per nitrogen (number of — connected to each ○)*

of hexane in the organic phase, and N is the similar ratio for amine per amine and HF in the AHF phase, then $D = \overline{N}/N$ practically refers to the mole fraction scale. The effect of contamination by the minor component in each phase is neglected. The results for concentration ranges of the amines 2–10 mole-% are shown in Fig. 3.

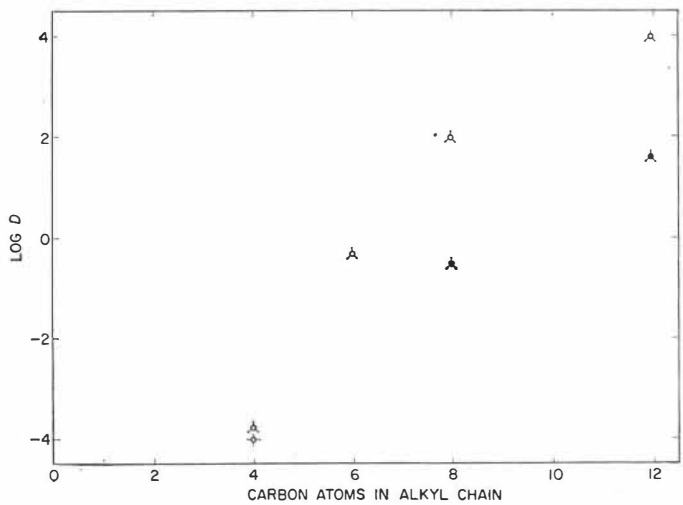

FIG. 3. *Distribution coefficients of alkylammonium fluorides (○) and fluoroborates (●) between hexane and AHF, as a function for the nature of the alkylamine*

Symbols same as in Fig. 2
The organic solvent for tri-iso-octylammonium tetrafluoroborate was benzene, rather than hexane

The effect of Lewis acids on the distribution was tested. Antimony, arsenic and phosphorus pentafluoride, added to the AHF phase, caused charring of the amine, and the vigour of the reaction decreased in the above order. Boron trifluoride, however, yielded stable tetrafluoroborates. Trilaurylammonium tetrafluoroborate was separated as a crystalline solid (m.p. 57–58°c) and so was tri-iso-octylammonium tetrafluoroborate. The distribution coefficients of tetrafluoroborates are also recorded in Fig. 3.

Further experiments were made to test whether metal fluorides at tracer concentrations could be distributed between the two phases. Both lanthanum, as ^{140}La, and tantalum, as ^{182}Ta, preferred strongly the AHF phase, and no activity was found in the hexane solution of trilaurylammonium fluoride.

Discussion

In the three component systems, AHF–hexane–alkylamines, one can neglect the mutual interaction of AHF and hexane[22] and start from the neutralised alkylammonium fluorides (rather than from the amine and HF). Other interaction can then be considered. The interactions are: (i) the self-association in AHF;[22] (ii) the self-association of the alkylammonium fluoride in the hexane solution;[23] (iii) the interaction of this solute with AHF to form hydrofluoride adducts; and (iv) weaker interactions of these adducts with the hexane; of the hexane molecules among themselves, and of associated hydrogen fluoride species among themselves, etc.

As a first approximation, only 'chemical' interactions will be considered, i.e. (i)–(iii) above, and the weaker non-specific interactions of solute with solvent, and of the chemical species of each solvent, will be ignored.

The presence of solutes in AHF was found to cause its partial deaggregation and this effect was seen to increase as the molar volume of the solute increases.[22] The positive enthalpy effect of this reaction is much larger than the positive entropy effect,[22] and only solutes strongly interacting with AHF can overcome this enthalpy barrier. The present results (Table I) show that the lower alkylamines interact with AHF sufficiently strongly to dissolve in it and only trilaurylammonium fluoride, which is so bulky and its hydrogen fluoride adduct so small, separates as an immiscible phase.

Polar solutes, such as the alkylamine hydrohalides, are known to aggregate in solution in non-polar solvents, thereby decreasing their dipole moment.[23–25] The tendency to aggregation decreases from the iodide to the chloride (fluorides were not studied in dry solvents) and increases from aromatic to aliphatic hydrocarbons. The dipole interactions lead eventually to aggregates higher than the dimer or trimer, up to an octamer or even higher (if deviations from ideality are ascribed solely to aggregation[26]). The aggregation of the simple fluoride should be least among the halides, because since it has the smallest anion, the salt has the least dipole moment, but the higher hydrofluoride adducts, having higher dipole moments, should be more aggregated. However, although the aggregation lowers the free energy of the solute, it does not do so sufficiently in the present case to prevent the splitting of the hexane solution of the fluoride into another phase when the highest adduct is formed (Table I). The lower adducts, however, are compatible with hexane. It should be noted that it is mainly the chain length of the alkylamine, and not the number of chains, which determines the number of HF molecules in the adduct required to produce immiscibility (Table I and Figs 2 and 3). The tertiary salts are somewhat exceptional, but Fig. 2 shows clearly the similarity of the primary, secondary and quaternary salts in this respect. Indeed, if N_R is the number of chains and N_C the number of carbon atoms per chain, then the number N_{HF} of HF molecules added to the alkylamine fluoride to give the largest adduct, i.e. that no longer compatible with hexane, is given by the empirical equation:

$$N_{HF} = (13{\cdot}8 \pm 1{\cdot}1) - N_C - (0{\cdot}4 \pm 0{\cdot}1)\,N_R \quad . \quad . \quad . \quad . \quad (4)$$

It may be pointed out that if the added HF molecules form a hydrogen-bonded chain,[10] and since the size of a –HF– group approximates the size of a $-CH_2-$ group, the sum $N_{HF} + N_C$ comes out as approximately twice the length of a hexane molecule. The entropy effect of mixing chain molecules of different length may lead to positive excess entropies, but the concepts of athermal solutions can hardly be applied to the present case. The fact that dodecane and hexane are miscible shows that other factors contribute to the large positive excess free energy. The small effect that branching of the chain has (compare n-octyl with iso-octyl) and the relatively small effect of N_R complicates the matter still further. However, it was noted that a linear combination of N_C and N_R, Equation (4), and not their product, is important in relation to the molar volume of the alkylamine.

The distribution coefficients (Fig. 3) naturally follow the above considerations. The distribution coefficient can be set as the inverse ratio of the activity co-

efficients. Factors which increase the excess partial free energy of a component also increase the activity coefficient. Thus *D* will be large, i.e. highly in favour of the organic phase, for those species, (i) which are more highly aggregated in hexane, (ii) which form the lowest adduct, and (iii) which have the largest bulk of hydrocarbon residue incompatible with AHF. The effect of the tetrafluoroborate anion, in comparison with the fluoride (Fig. 3), is opposite to that which is expected from the size of the anions; thus the aggregation of the fluoroborate salt in hexane should be larger, leading to a higher *D* value. The observed effect leads to the conclusion that the $(C_{12}H_{25})_3NHF:1\cdot5$ HF adduct is capable of higher aggregation in hexane, owing to hydrogen-bonding, in addition to the dipole moment effect.

Acknowledgments

This work constitutes a part of the Ph.D. thesis of J. Soriano at the Hebrew University. The experimental work was done at Soreq Nuclear Research Center.

References

[1] U.S. P. 2,375,675
[2] U.S. P. 2,532,492
[3] Lien, A. P., & Evering, B. L., *Ind. Engng Chem.*, 1952, **44,** 874
[4] Lien, A. P., McCauley, D. A., & Evering, B. L., *Ind. Engng Chem.*, 1949, **41,** 2698
[5] U.S. P. 2,320,629
[6] Universal Oil Products, Fr. P. 1,322,715
[7] Esso, B.P. 915,601
[8] U.S. P. 3,281,350
[9] Fr. P. 1,477,742
[10] Blundy, P. D., Hardwick, W. H., Simpson, M. P., Stevens, I. R., & Wace, P. F., *J. inorg. nucl. Chem.*, 1967, **29,** 1119
[11] Bertocci, U., & Rolandi, G., *J. inorg. nucl. Chem.*, 1961, **23,** 323
[12] Wilson, A. S., & Wogman, N. A., *J. phys. Chem., Ithaca*, 1962, **66,** 1552
[13] Bullock, J. I., Choi, S. S., Goodrick, D. A., Tuck, D. G., & Woodhouse, E. J., *J. phys. Chem., Ithaca*, 1964, **68,** 2687
[14] McCauley, D. A., Shoemaker, B. H., & Lien, A. P., *Ind. Engng Chem.*, 1950, **42,** 2103
[15] McCauley, D. A., & Lien, A. P., *J. Am. chem. Soc.*, 1951, **73,** 2013
[16] Mackor, E. L., Hofstra, A., & van der Waals, J. H., *Trans. Faraday Soc.*, 1958, **54,** 66
[17] Mackor, E. L., Hofstra, A., & van der Waals, J. H., *Trans. Faraday Soc.*, 1958, **54,** 186
[18] U.S. P. 2,426,624
[19] U.S. P. 2,739,992
[20] Soriano, J., Shamir, J., & Marcus, Y., to be published
[21] Soriano, J., Shamir, J., Netzer, A., & Marcus, Y., *Inorg. nucl. Chem. Lett.*, 1969, **5,** 209
[22] Marcus, Y., Shamir, J., & Soriano, J., *J. phys. Chem., Ithaca*, 1970, **74,** 133
[23] Marcus, Y., & Kertes, A. S., 'Ion Exchange and Solvent Extraction of Metal Complexes', 1969, p. 757 (London: Wiley-Interscience)
[24] Kertes, A. S., & Markovits, G., *J. phys. Chem., Ithaca*, 1968, **72,** 4202
[25] Danesi, P. R., Magini, M., & Scibona, G., in 'Solvent Extraction Research', (Kertes, A. S., & Marcus, Y., Eds) 1969, p. 185 (New York: Wiley-Interscience)
[26] Marcus, Y., *Pure appl. Chem.*, 1969, **20,** 85

Prediction of ternary liquid equilibria data

by L. deJ. S. Soares, L. G. Packer and S. R. M. Ellis
Department of Chemical Engineering, The University of Birmingham, U.K.

The selection of parameters for the non-random two-liquid (NRTL) *ternary predicting equation is studied for the systems heptane–aniline–cyclohexane and benzene–water–n-butanol. The* NRTL *equation is then used for the prediction and correlation of liquid–liquid equilibria results for perfluorocarbon–hydrocarbon mixtures.*

Introduction

THE DESIGN OF liquid–liquid extraction equipment for the separation of chemical compounds has very often to be carried out with only very limited or inaccurate data. In many cases the restrictions imposed by analytical techniques limit the determination of adequate design data. It is often necessary, therefore, to extend the equilibrium data by prediction from either semi-empirical or thermodynamically consistent mathematical expressions relating activity coefficients to liquid composition. Subsequently, solute distribution ratios can be calculated.

The non-ideality of liquid mixtures has been expressed by Wohl[1] in terms of the excess Gibbs free energy. From this the more convenient auxiliary thermodynamic function, the activity coefficient, can be derived. Numerous equations have been proposed which relate the activity coefficient on liquid mole fractions, and these have been comprehensively reviewed by Hala *et al.*[2]

Several workers have experienced difficulty in using the Wohl-type equations to describe the behaviour of binary liquid–liquid systems.[3–6] The equations have also been applied in the prediction of ternary liquid–liquid equilibria[7–12] with reasonable agreement being obtained, between the experimental and the predicted equilibria distribution data.

The prediction of solubility curves is more satisfactory for type II systems than type I systems.

More recently, use has been made of the local mole fraction concept[13,14] for defining the excess Gibbs free energy. On this basis, Wilson[14] derived an equation which, in its simplest form, contains two adjustable parameters. The suitability of this equation in vapour–liquid equilibrium studies of completely miscible systems has been carefully investigated by Orye & Prausnitz[15] and Ma *et al.*[16]

When the Wilson equation is applied to mixtures which exhibit phase-splitting, it becomes necessary to include a third constant into the free energy expression. As the values of this third constant must be equal for each binary, this unfortunately restricts its use in the prediction of multi-component liquid–liquid equilibrium data from binary parameters alone.

The limitations of the Wilson equation have led Renon & Prausnitz[17] to combine the local mole fraction concept with the two-liquid theory of Scott[18] in an equation termed the non-random two-liquid (*NRTL*) equation. The last-named equation, in terms of the activity coefficient, can be written:

$$\ln \gamma_i = \frac{\sum_j^N \tau_{ji} G_{ji} x_j}{\sum_k^N G_{ki} x_k} + \sum_j^N \frac{G_{ij} x_j}{\sum_k^N G_{kj} x_k} \left[\tau_{ij} - \frac{\sum_l^N \tau_{lj} G_{lj} x_l}{\sum_k^N G_{kj} x_k} \right] \quad . \quad . \quad . \quad (1)$$

where $\tau_{ji} = (g_{ji} - g_{ii})/RT$
$G_{ji} = \exp(-\alpha_{ji}\tau_{ji})$
$g_{ji} = g_{ij}$

The *NRTL* equation can be applied to completely miscible and partly miscible systems alike and contains three adjustable parameters, one of which (α) can be related[17] to the chemical nature of the binary liquid pairs. Unlike the third

constant in the Wilson equation, different values of α do not restrict the use of the equation in the prediction of multi-component liquid–liquid equilibrium data from binary parameters. The use of the *NRTL* equation has been reported by Renon & Prausnitz[17] and Joy & Kyle[19].

Groves & Forsyth[20] have presented a variable co-ordination number quasi-chemical theory and applied it to the prediction of liquid–liquid and vapour–liquid equilibrium data, from pure component properties.

The present paper is concerned with the application of the *NRTL* equation to the prediction of ternary liquid–liquid equilibria for some type II (open type) systems. Some new equilibrium data are also presented for perfluorocarbon–hydrocarbon systems.

Use of the *NRTL* equation

Joy & Kyle[19] have related the displacement of the solubility curve to the errors in activity estimation. They found that while type II systems were only slightly sensitive, good activity estimation was extremely important for type I systems. Work along these lines has been carried out in this Department.[21]

The sensitivity of the solubility curve position and tie-line slope of type II systems, to selected values of α for the two partially miscible binary pairs, has been investigated.

In order to illustrate the behaviour, two ternary systems were chosen: (a) n-heptane (1)–aniline (2)–cyclohexane (3); and (b) benzene (1)–water (2)–n-butanol (3).

The experimental data of Hunter & Brown[22] and Washburn & Strandskov[23] were used as reference data for systems (a) and (b) respectively.

In system (a) the degree of asymmetry of the two partial binaries is not large, while in system (b) the degree of asymmetry is much greater.

Calculation procedures

For partly miscible systems, the thermodynamic condition for equilibrium can be written:

$$a_{i1} = a_{i2} \qquad (2)$$

where $i = 1, \ldots\ldots N$

if the same standard state is chosen for component i in both the liquid phases. The equation has been rearranged to give:

$$\ln \frac{\gamma_{i1}}{\gamma_{i2}} - \ln \frac{x_{i2}}{x_{i1}} = 0 \qquad (3)$$

where $i = 1, \ldots\ldots N$

In addition, the necessary stoicheiometric relation in terms of the liquid composition is:

$$\sum_{i}^{N} x_{ij} = 1 \qquad (4)$$

where $j = 1, 2$

The substitution of Equation (4) into Equation (3) yields a system of N non-linear equations:

$$F_i(\tau_{12}, \tau_{21}, \ldots; x_{11}, x_{12}, \ldots) = 0 \qquad (5)$$

where $i = 1, \ldots\ldots N$

These equations can be used for: (a) the calculation of binary parameters from mutual solubility data; and (b) the prediction of the ternary solubility curves and tie-line data, provided that a suitable expression, such as the *NRTL* equation, relating the activity coefficients to liquid composition using a restricted number of adjustable parameters, can be found.

The calculation procedure utilises a Newton–Raphson technique, modified to ensure rapid convergence, as described elsewhere.[21] Since it is necessary, in the determination of each tie-line, to fix the composition of one component, that of the solute has been chosen.

TABLE I

Variation of AMD ($\times 10^2$) *with* α *values for the system n-heptane (1)–aniline (2)–cyclohexane (3)*

α_{23}	α_{12} = 0·2			0·25			0·3			0·35			0·4		
	x_{11}	x_{12}	x_{32}	x_{11}	x_{12}	x_{32}	x_{11}	x_{12}	x_{32}	x_{11}	x_{12}	x_{32}	x_{11}	x_{12}	x_{32}
0·2	0·19	−0·19	2·81	0·18	0·01	3·07	0·06	0·13	3·32	−0·22	0·43	4·00	−0·84	1·17	4·68
0·25	0·24	−0·11	2·68	0·20	−0·01	2·83	0·05	0·15	3·12	−0·29	0·44	3·59	−1·11	1·21	4·61
0·3	0·33	−0·15	2·32	0·26	−0·04	2·45	0·12	0·12	2·79	−0·24	0·42	3·25	−1·14	1·27	4·39
0·35	0·47	−0·23	1·68	0·42	−0·10	1·84	0·30	0·06	1·92	−0·05	0·33	2·38	−0·97	1·19	3·93
0·4	0·72	−0·35	0·41	0·74	−0·23	0·59	0·64	−0·11	0·91	0·34	0·15	1·44	−0·56	0·89	2·70
0·425	1·02	−0·60	−1·14	1·07	−0·50	−1·32	1·02	−0·45	−1·00	0·87	−0·28	−0·44	0·01	0·19	0·59

Where the parameters have been determined for the miscible binary mixtures, isothermal vapour–liquid equilibrium data were used with the total pressure method.[24] The minimisation of the objective function

$$\sum_{i}^{M}(P_{i,\,\mathrm{exp.}} - P_{i,\,\mathrm{calc.}})^2$$

was employed, where $P_{i,\,\mathrm{exp.}}$ and $P_{i,\,\mathrm{calc.}}$ are the experimental and calculated total pressures for run i.

n-Heptane (1)–*aniline* (2)–*cyclohexane* (3)

Calculations have been performed with several values of α covering all the permitted range. In these calculations it has been assumed that the miscible system n-heptane–cyclohexane is ideal. This approximation of assuming the miscible system ideal in type II systems has been frequently made by other workers, and particularly so when vapour–liquid equilibrium data for the binary miscible system were not available.

To show tie-line displacement, the arithmetic mean of the deviations (*AMD*) between the calculated and experimental values are given in Table I for a selected number of α values. The arithmetic mean deviation ($\overline{\Delta X}$) can be written:

$$\overline{\Delta X}_l = \frac{\sum_{k}^{M}(X_{lk,\,\mathrm{calc.}} - X_{lk,\,\mathrm{exp.}})}{M} \quad . \quad . \quad . \quad . \quad . \quad . \quad . \quad (7)$$

where n-heptane phase is referred to as phase 1.

From Table I it can be seen that the *AMD* values are all relatively low and are not very sensitive to the selection of α values. Such small differences as exist between the maximum and minimum *AMD* values are, however, significant. For this experimental data maximum deviations are obtained when α_{23} is low. The results also show that α_{23} values associated with aniline–cyclohexane system have slightly more effect on the slope of the tie-lines than the α_{12} values for the n-heptane–cyclohexane system.

If overall *AMD* values of approximately $\pm 1\cdot 5 \times 10^{-2}$ or less are assumed as representing good agreement between the experimental and predicted tie-line slopes, then for the ternary system heptane–aniline–cyclohexane the *NRTL* equation accurately predicts the equilibria data using α_{23} values of 0·4–0·425.

Benzene (1)–*water* (2)–*n-butanol* (3)

For this system, the miscible benzene–n-butanol binary has, in the first instance, been assumed ideal and in further calculations the non-ideality has been taken into account. The binary parameters for the non-ideal case were calculated from the vapour–liquid equilibrium data of Allen *et al.*[25] at 25°C.

Because the compositions in the aqueous phase are so small, only the *AMD* values of the water composition in the hydrocarbon phase (x_{21}) are presented in

TABLE II

Variation of AMD ($\times 10^2$) *with* α *values for system benzene (1)–water (2)–n-butanol (3)*

α_{23}	α_{12}					
	0·2	0·25	0·3	0·2	0·25	0·3
	(1)–(3) Ideal			(1)–(3) Non-ideal		
0·2	−0·84 (6) +5·80 (4)	+12·3	+22·0	−4·84	+6·58	+19·6
0·3	−5·8	+7·2	+18·0	−7·8	−0·8 (7) 2·0 (3)	+14·6
0·425	−11·7	−8·4	+12·16	−12·9	−9·2	−1·2 (6) 7·79 (4)

Table II. Where the calculated solubility curve crosses the experimental solubility curve two different *AMD* values are given, together with the number (*n*) of tie lines from which they are calculated. The closest agreement between the predicted and experimental tie-line data, as indicated by the lowest *AMD* values, is obtained when the non-ideality of the benzene–n-butanol has been allowed for.

Selected calculated and experimental solubility curves are plotted in Figs 1 and 2 in order to illustrate more clearly the influence of the selected α values and the non-ideality of the miscible binary on the predicted solubility curve.

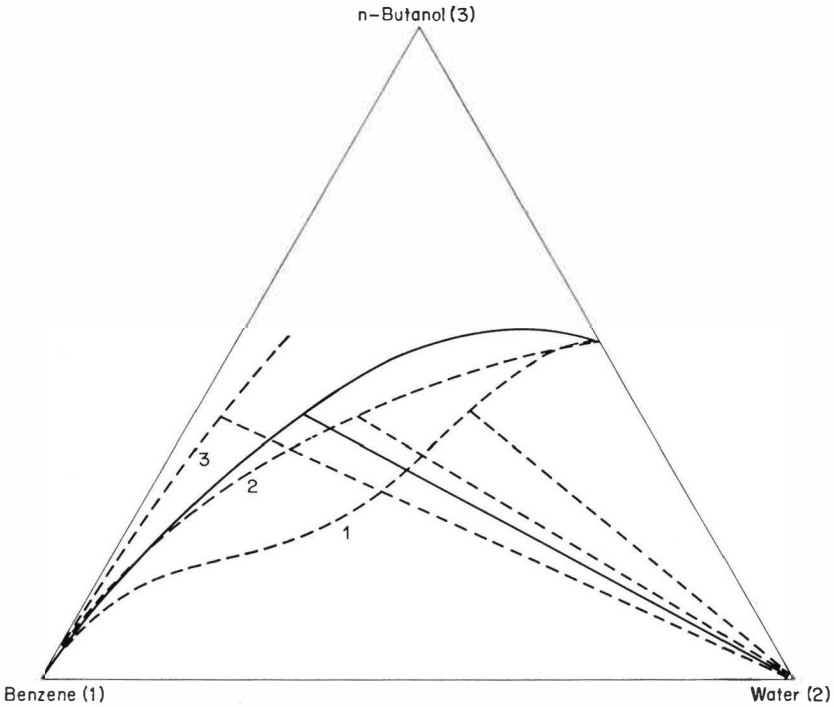

FIG. 1. *Variations in solubility curve with α for system benzene* (1)–*water* (2)–*butanol* (3) (*binary* (1)–(3) *ideal*)

——— Experimental data;[23] – – – – calculated data
1, $\alpha_{12} = 0{\cdot}3$, $\alpha_{23} = 0{\cdot}3$; 2, $\alpha_{12} = 0{\cdot}25$, $\alpha_{23} = 0{\cdot}3$; 3, $\alpha_{12} = 0{\cdot}2$, $\alpha_{23} = 0{\cdot}425$

From Fig. 1, where the miscible system benzene–n-butanol has been assumed ideal, it will be observed that the predicted solubility curve is greatly influenced by the selection of α values.

The predicted curve approaches the experimental one and crosses it in such a way that good agreement cannot be obtained simultaneously for the lower and upper n-butanol concentration regions.

In Fig. 2, where the non-ideality of the benzene–butanol system has been allowed for, there is closer agreement between the predicted and experimental solubility curve. A comparison of Figs 1 and 2 for the same α values, shows that when allowance is made for the non-ideality of the binary system there is a substantial upward displacement of the solubility curve.

Correlation of perfluorocarbon–hydrocarbon equilibria

It has been stated earlier that thermodynamic expressions can be used to extend inaccurate or limited experimental liquid–liquid equilibrium data. Packer[26] has recently determined the ternary equilibrium data for some perfluorocarbon–hydrocarbon systems which exhibit scatter. The *NRTL* equation

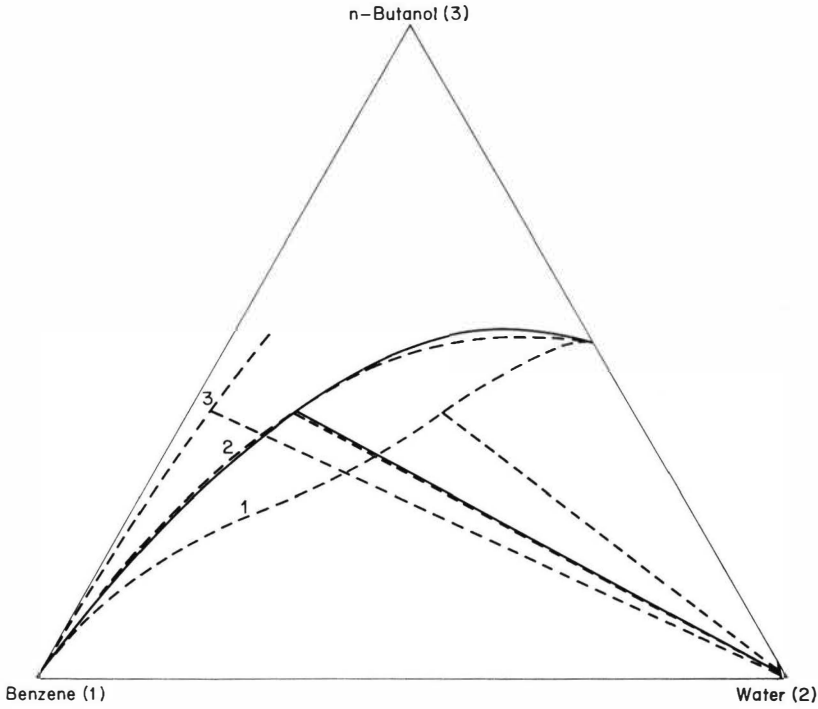

FIG. 2. *Variations in solubility curve with α for system benzene* (1)–*water* (2)–*butanol* (3) (*binary* (1)–(3) *non-ideal*)

——— Experimental data;[23] - - - - calculated data
1. $\alpha_{12} = 0{\cdot}3$, $\alpha_{23} = 0{\cdot}3$; 2. $\alpha_{12} = 0{\cdot}25$, $\alpha_{23} = 0{\cdot}3$; 3. $\alpha_{12} = 0{\cdot}2$, $\alpha_{23} = 0{\cdot}425$

has been used, in conjunction with the previously described prediction methods, to smooth the experimental data.

The ternary equilibria, determined in a small-scale distribution cell, were: (c) n-heptane (1)–perfluorodecalin (2)–heptene (3) at 10°C; and (d) n-heptane (1)–perfluoromethylcyclohexane (2)–heptene (3) at 10°C.

The heptene for both systems was a fraction obtained from the batch distillation of an isomeric heptene mixture, produced by Esso Petroleum Ltd. It consisted mainly of the more highly branched heptene isomers, of which 2,4-dimethyl-2-heptene was the most predominant.

Because no experimental mutual solubility data were determined for the partly miscible binaries, values were initially extrapolated from the ternary data, and subsequently used in the calculation of the binary parameters. Ideality was assumed for the miscible heptane–heptene binary, since it had been found, from the study of the n-heptane–aniline–cyclohexane system, that any slight non-ideality in the binary miscible system had little overall effect on the predicted ternary equilibrium data.

From the calculated binary parameters, the ternary equilibria were predicted for each perfluorocarbon–hydrocarbon system. Where necessary the extrapolated mutual solubilities were adjusted until a good fit was obtained between the experimental and predicted results. Agreement has been expressed in terms of the root mean square deviation (*RMSD*), which can be written:

$$RMSD(X_l) = \frac{\sum_{k}^{M} (X_{lk,\,\mathrm{calc.}} - X_{lk,\,\mathrm{exp.}})^2}{M-1} \qquad (8)$$

The experimental and predicted ternary equilibrium data are presented in Tables III and IV for systems (c) and (d) respectively, together with the binary parameters (corresponding to α values of 0·4) and the *RMSD* values. As the *RMSD* values are relatively small there would appear to be reasonable agreement between the experimental and predicted results.

Fig. 3, corresponding to system (c), shows that the *NRTL* equation describes, reasonably well, the solubility curves and the slopes of the tie-lines. Thus, in these systems, the *NRTL* equation has been of value in interpreting the experimental data.

TABLE III

Ternary liquid equilibria for the system n-heptane (1)–perfluorodecalin (2)–heptene (3) at 10°C

Experimental data				Predicted data			
Hydrocarbon phase		Solvent phase		Hydrocarbon phase		Solvent phase	
x_{11}	x_{31}	x_{12}	x_{32}	x_{11}	x_{31}	x_{12}	x_{32}
0·2809	0·6429	0·0534	0·1519	0·2803	0·6429	0·0573	0·1551
0·3414	0·5809	0·0675	0·1402	0·3441	0·5809	0·0685	0·1371
0·4923	0·4345	0·0869	0·1062	0·4945	0·4345	0·0925	0·0973
0·5670	0·3620	0·1074	0·0798	0·5569	0·3620	0·1031	0·0790
0·7693	0·1658	0·1313	0·0232	0·7701	0·1658	0·1280	0·0337

NRTL parameters:
$\tau_{21} = 2{\cdot}6294$ $\tau_{12} = 2{\cdot}0690$ $\alpha_{12} = 0{\cdot}4$
$\tau_{32} = 2{\cdot}4150$ $\tau_{23} = 1{\cdot}6907$ $\alpha_{23} = 0{\cdot}4$

RMSD values:
0·0024 — 0·0044 0·0072

TABLE IV

Ternary liquid equilibria for the system n-heptane (1)–perfluoromethylcyclohexane (2)–heptene (3) at 10°C

Experimental data				Predicted data			
Hydrocarbon phase		Solvent phase		Hydrocarbon phase		Solvent phase	
x_{11}	x_{31}	x_{12}	x_{32}	x_{11}	x_{31}	x_{12}	x_{32}
0·1735	0·6828	0·0559	0·2657	0·1772	0·6828	0·0589	0·2645
0·2094	0·6533	0·0674	0·2382	0·2085	0·6533	0·0680	0·2490
0·3687	0·5075	0·1053	0·1652	0·3626	0·5075	0·1071	0·1786
0·4244	0·4485	0·1243	0·1476	0·4247	0·4485	0·1205	0·1528
0·4927	0·3825	0·1367	0·1329	0·4941	0·3825	0·1339	0·1256
0·7427	0·1410	0·1819	0·0364	0·7470	0·1410	0·1708	0·0405

NRTL parameters:
$\tau_{21} = 1{\cdot}8940$ $\tau_{12} = 2{\cdot}2634$ $\alpha_{12} = 0{\cdot}4$
$\tau_{32} = 2{\cdot}1230$ $\tau_{23} = 1{\cdot}4249$ $\alpha_{23} = 0{\cdot}4$

RSMD values:
0·0038 — 0·0056 0·0089

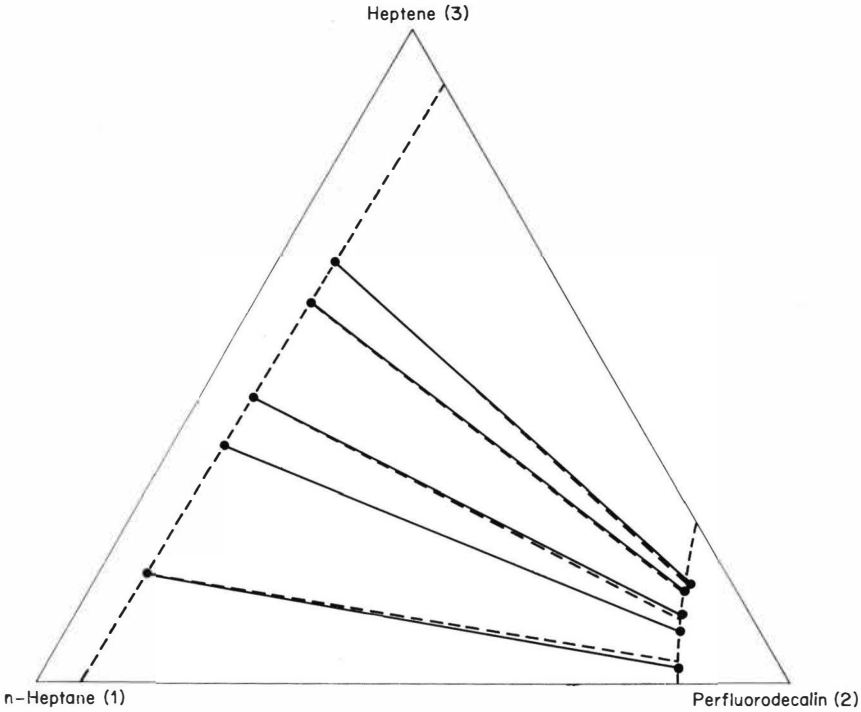

FIG. 3. *Experimental and predicted data for the system n-heptane* (1)–*perfluorodecalin* (2)–*heptene* (3)

●——● Experimental data;[26] – – – predicted data

Discussion

For the type II ternary systems investigated in this work, it has been found that the accurate prediction of the tie-line data and the solubility curve position is dependent on the values of α chosen for the miscible and immiscible binary systems.

For some systems, such as hydrocarbon mixtures extracted with organic solvents, the predicted liquid–liquid equilibria results are not very sensitive to the selected values of α thus giving some latitude in the selection of the α parameters. The assumption often made for such mixtures is that the binary miscible system can be assumed ideal. The assumption is an approximation but is reasonably valid if the partly miscible binaries exhibit similar asymmetry and the solubility of solvent in the hydrocarbon mixture is reasonably high. Generally, if the non-ideality of the binary miscible system is known this should be allowed for in the prediction of ternary liquid–liquid equilibria results.

For highly non-ideal ternary systems the non-ideality of the miscible binary system must be defined and the α-parameters carefully selected for the accurate prediction of ternary liquid–liquid equilibria data. There is little latitude in the selection of values. Systems of this type, such as water–benzene–n-butanol, are characterised by partial miscible binaries with greatly differing degrees of asymmetry and by low mutual solubilities.

The results presented in this paper support the conclusion that a set of parameters can be found which yield a good fit for both the solubility curves and the tie-lines, and that the *NRTL* equation should be regarded as a three-parameter equation when describing the behaviour of partly miscible ternary systems.

The *NRTL* equation, used in conjunction with the method of ternary data prediction described, is particularly valuable for the correlation of scattered experimental results as obtained in the perfluorocarbon–hydrocarbon system.

Nomenclature

a_i	activity of component i
g_{ij}	energy term representing the forces between molecules of species i and j
M	number of experimental runs
N	number of components
P_i	total pressure of run i
R	universal gas constant
T	temperature, K
$\overline{\Delta X_l}$	arithmetic mean deviations: $X_1 = x_{11}$, $X_2 = x_{12}$, $X_3 = x_{32}$
x_i	liquid mole fraction of component i
α_{ij}	non-randomness parameter used in the *NRTL* equation
τ_{ij}	adjustable parameter used in the *NRTL* equation
γ_i	activity coefficient of component i

Acknowledgments

L. deJ. S. Soares thanks the Gulbenkian Foundation for the provision of a scholarship and L. G. Packer thanks the Esso Petroleum Co. Ltd. for the provision of his scholarship.

References

1 Wohl, K., *Trans. Am. Inst. chem. Engrs*, 1946, **42,** 215
2 Hala, E., Pick, J., Fried, V., & Vilim, O., 'Vapour–Liquid Equilibrium', 1967 (Oxford: Pergamon Press)
3 Carlson, H. C., & Colburn, A. P., *Ind. Engng Chem.*, 1942, **34,** 581
4 Treybal, R. E., *Ind. Engng Chem.*, 1944, **36,** 875
5 Ellis, S. R. M., & Garbett, R. D., *Ind. Engng Chem.*, 1960, **52,** 385
6 Brian, P. L. T., *Ind. Engng Chem.*, 1965, **4,** 100
7 Othmer, D. F., & Tobias, P., *Ind. Engng Chem.*, 1942, **34,** 696
8 Hildebrand, J. H., 'Solubility of Non-Electrolytes', 1936 (2nd edn) (New York: Reinhold)
9 Treybal, R. E., 'Liquid Extraction', 1963 (New York: McGraw-Hill)
10 Boberg, T. C., Thesis, Univ. Michigan, 1960
11 Kenny, J. W., *Chem. Engng Sci.*, 1957, **6,** 116
12 Techo, R., Thesis, Georgia Institute of Technology, 1961
13 Guggenheim, E. A., 'Mixtures', 1952 (Oxford: Clarendon Press)
14 Wilson, G. M., *J. Am. chem. Soc.*, 1964, **86,** 127
15 Orye, R. V., & Prausnitz, J. M., *Ind. Engng Chem.*, 1965, **57,** 18
16 Ma, K. T., McDermott, C., & Ellis, S. R. M., *Proc. int. Symp. Distillation*, 1969 (London: Instn chem. Engrs)
17 Renon, H., & Prausnitz, J. M., *J. Am. Inst. chem. Engrs*, 1968, **14,** 135
18 Scott, R. L., *J. chem. Phys.*, 1956, **25,** 193
19 Joy, D. S., & Kyle, B. G., *J. Am. Inst. chem. Engrs*, 1969, **15,** 298
20 Groves, W. D., & Forsyth, J. S., *Proc. int. Symp. Distillation*, 1969 (London: Instn chem. Engrs)
21 Soares, L. deJ. S., Thesis, Univ. of Birmingham, 1970
22 Hunter, T. G., & Brown, T., *Ind. Engng Chem.*, 1947, **39,** 1343
23 Washburn, E. F., & Stradskov, C. V., *J. phys. Chem., Ithaca*, 1944, **48,** 241
24 Ellis, S. R. M., McDermott, C., & Chiang, C.-S., *Br. chem. Engng*, 1967, **12,** 727
25 Allen, B. B., Lingo, S. P., & Felsing, N. A., *J. phys. Chem., Ithaca*, 1939, **43,** 425
26 Packer, L. G., Thesis, Univ. of Birmingham, 1970

Partition coefficient and extraction constant of non-charged species as considered from the regular solution theory

by M. Tanaka
Laboratory of Analytical Chemistry, Faculty of Science, Nagoya University, Chikusa-ku, Nagoya 464, Japan

A method of evaluating the solubility parameter of non-charged metal complexes is proposed, the additive nature being assumed for the molar cohesive energy and molar volume of ligands in complexes. The effect of the substituent on the extraction of ion pairs as well as organic homologues is also quantitatively accounted for. The partition coefficient and the extraction constant of metal complexes are discussed with the aid of the estimated solubility parameters.

Introduction

THE REGULAR SOLUTION theory[1] has been used to interpret the solvent effect on the extraction of metal chelates,[2,3] halide complexes[4,5] and ion pairs.[6] The same theory has been found useful also in discussing the extraction of aliphatic carboxylic acids[7] and their copper(II) complexes.[8]

The present paper describes further considerations on the partition of various species involved in the extraction, i.e. organic substances, metal complexes and their adducts, ion pairs, etc.

Partition coefficient as a function of molar volumes and solubility parameters of species involved

The chemical potential μ_B of a solute B in a regular solution is given by:

$$\mu_B - \mu_B^0 = \boldsymbol{R}T\ln x_B + V_B\varphi_s^2(\delta_s - \delta_B)^2 \quad (1)$$

or

$$\mu_B - \mu_B^0 = \boldsymbol{R}T[\ln\varphi_B - \ln\varphi_s(1 - V_B V_s^{-1})] + V_B\varphi_s^2(\delta_s - \delta_B)^2 \quad (2)$$

where x_B and V_B denote the mole fraction and molar volume, respectively, of the solute B, and φ_s and φ_B, δ_B and δ_s the volume fraction and the solubility parameters of B and solvent, respectively. Pure liquid is chosen as a standard state.

When the solute B is partitioned between the aqueous and organic phases, the following expressions are obtained:

$$\boldsymbol{R}T\ln K_{D,B}^0 = V_B(\delta_w + \delta_o - 2\delta_B)(\delta_w - \delta_o) \quad (3)$$

for the partition coefficient of B in mole fraction, $K_{D,B}^0$ from Equation (1), and

$$\boldsymbol{R}T\ln K_{D,B} = V_B[(\delta_w + \delta_o - 2\delta_B)(\delta_w - \delta_o) + \boldsymbol{R}T(V_o^{-1} - V_w^{-1})] \quad (4)$$

for the partition coefficient of B in molar concentration, $K_{D,B}$ from Equation (2).

Solubility parameters of species involved in the extraction

Small[9] has proposed a method of evaluating solubility parameters of various organic substances utilising the additive nature of molar volumes and molar attraction forces of groups involved. Later Rheineck & Lin[10] found the additive nature of molar cohesive energy and developed a method of calculating solubility parameters of straight-chain compounds. The formula proposed by the latter is:

$$\delta_A = (\Delta E_A/V_A)^{\frac{1}{2}} = (\Sigma\Delta E_i/\Sigma V_i)^{\frac{1}{2}} \quad (5)$$

where ΔE_i and V_i refer to the contributions of group i to the cohesive energy and molar volume, respectively.

Solubility parameters of a homologous series

A plot of solubility parameters δ against the number of carbon atoms in various homologous series has been given.[10] If a compound HB having one more carbon atom than its homologue HR is considered, then, according to Equation (5), the solubility parameter of HB is given by the equation:

$$\delta_{HB}^2 = (\delta_{HR}^2 V_{HR} + \Delta E_{CH_2})/(V_{HR} + V_{CH_2}) \quad . \quad . \quad . \quad . \quad . \quad (6)$$

where ΔE_{CH_2} refers to the molar cohesive energy of CH_2. When V_{HR} is sufficiently large, δ_{HB} can be approximated as:

$$\delta_{HB} = \delta_{HR}[1 - \tfrac{1}{2}V_{CH_2}(1 - \delta_{CH_2}^2\delta_{HR}^{-2})(V_{HR} + V_{CH_2})^{-1}] \quad . \quad . \quad . \quad (7)$$

In other words, when V_{HR} is sufficiently large compared with V_{CH_2}, an additional methylene group does not produce any appreciable change in the solubility parameter. Further examination shows that the solubility parameter is a monotonous and nearly linear function of the number of carbon atoms added in large molecules.

A plot of solubility parameters of aliphatic carboxylic acids against the number of carbon atoms in them is given in Fig. 1. The plot illustrates the validity of the above conclusion. Keeping this in mind, it can be seen from Equations (3) and (4) that the log (partition coefficient) is a linear function of the number of carbon atoms involved in a molecule. The linear relationship has been found for aliphatic carboxylic acids[7] as well as phosphoric acid esters.[11,12] Then, the increment of log K_D for an added methylene group comes mainly from the volume contribution of the methylene group and thus is nearly constant irrespective of solvent and of solute, i.e. $\Delta \log K_D/CH_2 = 0{\cdot}56 - 0{\cdot}60$. The effect of the other group can be considered in a similar manner.

Solubility parameters of ion pairs

Suppose an ion pair A^+X^- is distributed between two phases. Like the preceding case, the change in the solubility parameter of A^+X^- for an added methylene group either in A or in X is given by:

$$\Delta\delta/CH_2 = -\delta_{AX}V_{CH_2}[1 - (\delta_{CH_2}/\delta_{AX})^2]/2(V_{AX} + V_{CH2}) \quad . \quad . \quad (8)$$

for cases when A^+X^- is sufficiently large. As before, the log (partition coefficient) of ion pairs is a linear function of the number of carbon atoms involved. A linear relationship is observed for the extraction of various organic dyes with quaternary ammonium;[13,14] the partition coefficient of the ion pairs then increases about four times for each additional methylene group in the quaternary ammonium compound used as the extractant.

Solubility parameter of a complex

The additive nature of the molar cohesive energy and molar volume of ligands in a complex may be assumed. Then, according to Equation (5), the solubility parameter of a non-charged and unsolvated complex MR_n is given by:

$$\delta_{MR_n} = (n\delta_{HR}^2 V_{HR}/n'V_{HR})^{\frac{1}{2}} = (n/n')^{\frac{1}{2}}\delta_{HR} \quad . \quad . \quad . \quad . \quad . \quad (9)$$

where n is the number of ligand molecules involved in the complex and n' is slightly less than n because of the electro-striction of ligands in the complex. It has been shown[2] that $n \geqslant n' \geqslant 0{\cdot}9\,n$ for some complexes of divalent metal ions.

It can be seen from Equation (9) that the solubility parameter of a complex MR_n, δ_{MR_n}, is equal to or slightly greater than the solubility parameter of the

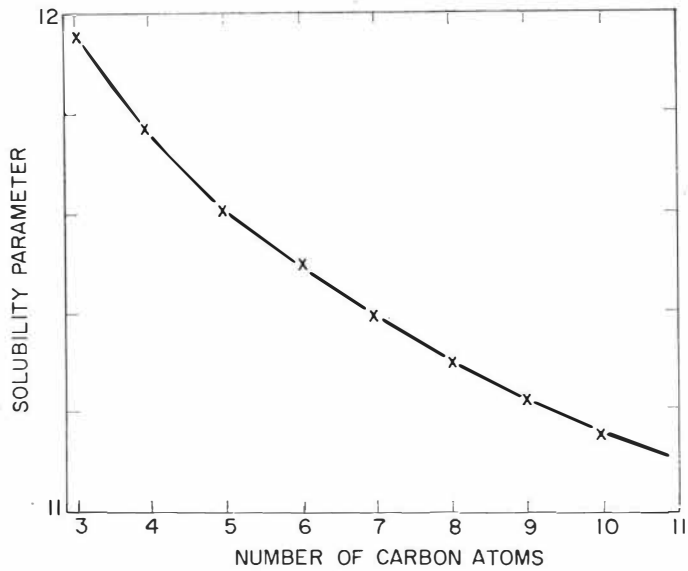

FIG. 1. *Solubility parameter of aliphatic carboxylic acids as a function of the number of carbon atoms*

Molar cohesive energy of CH_2 from Ref. 10.

ligand HR, δ_{HR}. Consideration of Equation (9) together with Equation (3) or (4) leads to the conclusion that the log (partition coefficient) of a complex MR_n is approximately n times that of the ligand HR, i.e.:

$$\log K_{D,MR_n} = n \log K_{D,HR} \qquad (10)$$

This is exactly the case as found for some β-diketonates[2,15,16] and copper carboxylates.[8]

Similarly, an expression is obtained for the solubility parameter of a solvated complex $MR_n mB$, $\delta_{MR_n mB}$:

$$\delta_{MR_n mB}{}^2 = (n\,\delta_{HR}{}^2 V_{HR} + m\delta_B{}^2 V_B)(n' V_{HR} + m V_B)^{-1} \qquad (11)$$

Thus, when δ_B is less than δ_{HR}, an enhanced extraction of the adduct $MR_n mB$ is expected and both volume and solubility parameter favour the partition coefficient of the adduct. On the other hand, when MR_n is hydrated, e.g. $MR_n mH_2O$, the high solubility parameter of water makes the solubility parameter of the adduct considerably high and this results in a low value of the partition coefficient of $MR_n mH_2O$, despite a small but favourable volume contribution of water molecule. Equation (11) is very important in the consideration of synergistic extraction of metal complexes.

Extraction constants of complexes of divalent transition metals

The extraction of a non-charged complex MR_n with a reagent HR is written as follows:

$$M^{n+} + n(HR)_o \overset{K_{ex}(MR_n)}{\rightleftharpoons} (MR_n)_o + nH^+ \qquad (12)$$

and the distribution ratio of the metal M, D_M, is given by:

$$D_M = K_{ex}(MR_n)[HR]_o{}^n[H^+]^{-n} \qquad (13)$$

$K_{ex}(MR_n)$ is composed of various constants and is written as:

$$K_{ex}(MR_n) = \beta_{MR_n} K_{D,MR_n} K_{D,HR}^{-n} K_{HR}^{-n} \quad . \quad . \quad . \quad . \quad . \quad . \quad (14)$$

where β_{MR_n} denotes the overall formation constant of MR_n and K_{HR} the formation constant of the reagent HR.

Substitution of Equation (10) into Equation (14) leads to:

$$K_{ex}(MR_n) = \beta_{MR_n} K_{HR}^{-n} \quad . \quad . \quad . \quad . \quad . \quad . \quad . \quad . \quad (15)$$

Thus the extraction constant is not affected much by the change of solvent and is proportional to β_{MR_n} for a given reagent.

It is often shown that, for complexes of divalent transition metals, the order of $pH_{\frac{1}{2}}$ (or log K_{ex}) is in the order expected from placing the formation constant in the Irving–Williams series. However, an unexpectedly low log K_{ex} is sometimes observed for presumably hydrated complexes,[16] for which the extraction constant is then written as:

$$K_{ex}(MR_n mH_2O) = \beta_{MR_n} K_{D,MR_n mH_2O} K_{D,HR}^{-n} K_{HR}^{-n} \quad . \quad . \quad . \quad . \quad (16)$$

The partition coefficient of $MR_n mH_2O$ is not the same as that of MR_n and should be estimated from the calculated values of molar volume and solubility parameter (see Equations (3), (4) and (11)). After correction of the low log $K_{ex}(MR_n mH_2O)$ value by (log K_{D,MR_n} − log $K_{D,MR_n mH_2O}$), the plot of log K_{ex} against the atomic number appears normal and then conforms to the plot of log (formation constant) against atomic number (Fig. 2).

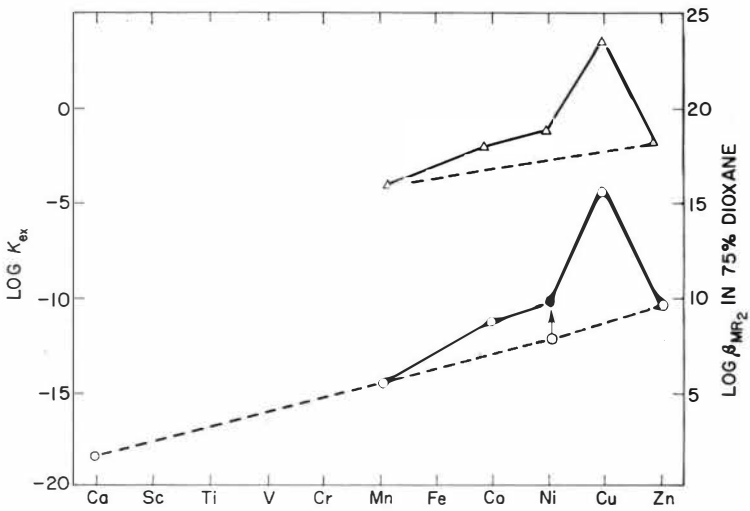

FIG. 2. *Log (extraction constants) and log (formation constants) of benzoylacetonates of some divalent transition metals as a function of atomic number*

Extraction constants from Ref. 16 and formation constants from Ref. 17. Solubility parameter of benzoylacetone 11·2, is calculated with $\delta = 10{\cdot}6$ for acetylacetone and molar cohesive energy of methyl and phenyl given in Ref. 10
△ formation constant; ○ extraction constant; ● corrected extraction constant

Solvent effect on the synergistic extraction

The extraction of a complex MR_n in the presence of a base B is written as:

$$M^{n+} + n(HR)_o + m(B)_o \overset{K_{ex}(MR_n mB)}{\rightleftharpoons} (MR_n mB)_o + nH^+ \quad . \quad . \quad (17)$$

where the extraction constant $K_{ex}(MR_n mB)$ is composed of various constants:

$$K_{ex}(MR_n mB) = \beta_{MR_n} K_{D,MR_n} K_{MR_n mB}^{mB} K_{D,HR}^{-n} K_{HR}^{-n} \quad . \quad . \quad . \quad . \quad (18)$$

In Equation (18), $K^{mB}_{MR_nmB}$ refers to the constant for the following equilibrium in the organic phase:

$$(MR_n)_o + m(B)_o \rightleftharpoons (MR_n mB)_o \quad . \quad . \quad . \quad . \quad . \quad . \quad . \quad (19)$$

The enhanced extraction of a complex in the presence of a base has usually been interpreted[19] in terms of the constant of equilibrium, $K^{mB}_{MR_nmB}$. Now an alternative expression for $K_{ex}(MR_nmB)$ is given by:

$$K_{ex}(MR_nmB) = \beta_{MR_nmB} K_{D,MR_nmB} K^{-n}_{D,HR} K^{-n}_{HR} K^{-m}_{D,B} \quad . \quad . \quad . \quad . \quad (20)$$

where β_{MR_nmB} refers to the overall formation constant of MR_nmB in the aqueous phase. Equation (20) is more convenient than Equation (18) for the consideration of the solvent effect on the synergistic extraction of MR_n in the presence of a base B.

The relative extent of the synergistic enhancement of extraction of MR_n in different solvents can be predicted from the ratio of the partition coefficients:

$$\frac{K_{D,MR_nmB}}{K^n_{D,HR}\, K^m_{D,B}} \quad . \quad . \quad . \quad . \quad . \quad . \quad . \quad . \quad . \quad . \quad . \quad (21)$$

The ratio (21) is readily calculated with knowledge of partition coefficients and/or solubility parameters and molar volumes of solvents and species involved. The solubility parameter of the adduct MR_nmB can be estimated by Equation (11). The difference of the extraction constants in solvents (1) and (2) is conveniently written in the logarithmic form:

$$\begin{aligned}\Delta \log K_{ex} &= \log K_{ex}(MR_nmB)_1 - \log K_{ex}(MR_nmB)_2 \\ &= (\delta_2 - \delta_1)[(\delta_1 + \delta_2)(V_{MR_nmB} - nV_{HR} - mV_B) \\ &\quad - 2(V_{MR_nmB}\delta_{MR_nmB} - nV_{HR}\delta_{HR} - mV_B\delta_B)]/2{\cdot}303RT \quad . \quad (22)\end{aligned}$$

In Equation (22), V_{MR_nmB} is close to $(nV_{HR} + mV_B)$ and because $V\delta$ terms are molar attraction forces, it is anticipated that $V_{MR_nmB}\delta_{MR_nmB}$ is close to $(nV_{HR}\delta_{HR} + mV_B\delta_B)$. Consequently, the extraction constant $K_{ex}(MR_nmB)$ is constant for different solvents, provided that no interaction occurs between solutes and solvents. In other words, the difference in synergistic enhancement for different solvents is caused by the different solvation and/or hydration of the species involved. This conclusion forms a basis for the approach to the synergistic extraction by the determination of activity coefficients of the species.

Recently Akiba *et al.*[18] have studied the role of the solvent in the synergistic extraction of zinc thenoyltrifluoroacetonate ($Zn(TTA)_2$) in the presence of tributyl phosphate (TBP). They have determined the adduct formation constants such as the constant for the equilibrium (19) in various solvents and were successful in explaining the variation of the constants in terms of activity coefficients of all the species taking part in the adduct formation.

The applicability of Equations (11) and (22) is now tested on their experimental results. Equation (11) gives $\delta_{Zn(TTA)_2TBP} = 8{\cdot}95$ when no electrostriction is assumed, and $\delta_{Zn(TTA)_2TBP} = 9{\cdot}4$ when 10% electrostriction of ligands is assumed in the adduct. The value 9·4 is in exact agreement with the observed one.[18] For the calculation of these values, the solubility parameter of pure TBP as calculated from the boiling point is used, viz. $\delta_{TBP} = 7{\cdot}7$*[19].

---

* In calculating the solubility parameter of the adduct, care should be exercised not to use the solubility parameter for *solvated* ligand, since the data from partition experiments sometimes are for *solvated* species.[19,20] On the other hand, in calculating the partition coefficient of ligands, the data from partition experiments should be used. If the partition coefficient itself is available for a particular solvent, it is preferable to use it instead of that calculated from the solubility parameter and molar volume.

TABLE I

Difference of log $K_{ex}(Zn(TTA)_2TBP)$ *in various solvents*

Reference solvent = n-hexane

	δ	$\Delta \log K_{ex}$ (observed)	$\Delta \log K_{ex}$ (calculated)*	$\Delta \log K_{ex}$ (calculated)**
n-Heptane	7·4	−0·09	0·07	−0·27
n-Hexane	7·3	0·00	—	—
Cyclohexane	8·2	0·16	0·63	−0·52
Carbon tetrachloride	8·6	0·74	0·88	0·96
Isopropylbenzene	8·5	1·08	0·83	1·08
Toluene	8·9	1·14	1·07	1·56
Benzene	9·2	1·16	1·24	1·61
o-Dichlorobenzene	10·0	1·27	1·68	1·92
Chlorobenzene	9·5	1·44	1·42	1·81
Methylene chloride	9·7	2·14	1·52	2·26
Bromoform	10·5	2·33	1·92	—
Chloroform	9·3	2·39	1·30	1·90

* Calculated with the following values: $\delta_{Zn(TTA)_2TBP} = 9{\cdot}4$; $\delta_{TTA} = 9{\cdot}9$;[2,18] $\delta_{TBP} = 10{\cdot}2$;[19] $V_{Zn(TTA)_2TBP} = 593 \times 0{\cdot}9$ ml; $V_{TTA} = 160$ ml; $V_{TBP} = 273$ ml.

** Calculated with the known value of the partition coefficients of TTA[18] and the solubility parameters and molar volumes of TBP and the adduct given above.

Also, in calculating the partition coefficient of TBP, δ_{TBP} of 10·2 as determined by the partition experiments is used, though the average value of 10·6 is given in Ref. 19. The value 10·2 is the average of data for nine solvents, higher values for nitrobenzene, ethyl iodide and 1,2-dibromoethane being excluded.

Finally, the difference of the extraction constants of $Zn(TTA)_2TBP$ in various solvents is calculated by means of Equation (22) and the results are given in Table I. The agreement of the calculated values with the observed[18] is good for most solvents, despite the simplicity of the approach and the variety of the sources from which data are taken for calculation.

Conclusions

Although the above treatment involves various assumptions and approximations, the derived expressions are simple and may be used to give a reasonable interpretation of the experimental results. The theory of regular solution is thus effective in many ways in its application to problems of solvent extraction even for some polar solvents, provided that all the solvent–solute interactions (solvation, hydration and higher aggregation) are taken into account. The limitations as well as the applicability of the proposed expressions should, of course, be examined further.

References

1 Hildebrand, J. H., & Scott, R. L., 'Solubility of non-electrolytes', 1957, 3rd Edn (New York: Dover Publishers Inc.)

2 Suzuki, N., Akiba, K., & Kanno, T., *Analytica Chim. Acta*, 1968, **43,** 311, and references cited therein

3 Mottola, H. A., & Freiser, H., *Talanta*, 1966, **13,** 55

4 Irving, H., & Lewis, D. C., *Proc. chem. Soc.*, 1960, p. 222

5 Siekierski, S., & Olszer, R., *J. inorg. nucl. Chem.*, 1963, **25,** 1351

6 Freiser, H., *Analyt. Chem.*, 1969, **41,** 1354

7 Kojima, I., Yoshida, M., & Tanaka, M., *J. inorg. nucl. Chem.*, 1970, **32,** 987

8 Kojima, I., Uchida, M., & Tanaka, M., *J. inorg. nucl. Chem.*, 1970, **32,** 1333

9 Small, P. S., *J. appl. Chem., Lond.*, 1953, **3,** 75

10 Rheineck, A. E., & Lin, D. H., *J. Paint Technol.*, 1968, **40,** 611

11 Dyrssen, D., & Petkovic, Dj., *J. inorg. nucl. Chem.*, 1965, **27,** 1381

12 Dyrssen, D., Ekberg, S., & Liem, D. H.. *Acta chem. scand.*, 1965, **18,** 135

[13] Modin, R., & Schill, G., *Acta pharm. suec.*, 1967, **4,** 301
[14] Gustavii, K., *Acta pharm. suec.*, 1967, **4,** 233
[15] Zolotov, Yu. A., 'Extraction of inner-complex compounds', 1968, pp. 45–48 (Moscow: Izdatelstvo Nauka)
[16] Starý, J., 'The solvent extraction of metal chelates', 1964, p. 32 (Oxford: Pergamon Press)
[17] Sillén, L. G., & Martell, A. E., 'Stability constants of metal-ion complexes', 1964 (London: Chemical Society)
[18] Akiba, K., Suzuki, N., & Kanno, T., *Bull. chem. Soc. Japan*, 1969, **42,** 2537
[19] Siekierski, S., *J. inorg. nucl. Chem.*, 1962, **24,** 205
[20] Kojima, I., Kako, M., & Tanaka, M., *J. inorg. nucl. Chem.*, 1970, **32,** 1651

Molecular theory of thermodynamic factors in solvent extraction

by E. W. Tiepel and K. E. Gubbins
Chemical Engineering Dept., University of Florida, Gainesville, Fla., U.S.A.

A recently developed molecular solution theory provides an improved method of predicting thermodynamic data needed for the selection of an extraction solvent. It is shown how the theory may be used to calculate selectivity and solvency for various systems and temperatures; in addition, it is possible to predict partial molal volumes of the extracted component, so that shifts in fluid phase equilibria with increase in pressure may be estimated. In its present form, the approach to be used considers only those systems in which physical interactions predominate; it is not applicable to systems in which chemical combination occurs.

Examples of the use of this theory are presented for liquid–liquid and gas–liquid equilibria, in which the components may be hydrocarbons, polar liquids, etc. A discussion of the use of mixed solvents, and solutions of ions in polar media, is included.

The theory (a modification of a general perturbation theory) is derived from rigorous statistical mechanical formulae by a series of well-defined approximations. The final equations permit calculations to be made knowing molecular force constants for the pure components together with experimental solvent density data. No experimental activity data are necessary.

Introduction

A FEED CONSISTING of a solution of Components (1) and (1′), which is to be contacted with a solvent (2), is considered; the object is to extract Component (1) (the extension to raffinate phases containing more than two components, and to mixed extracting solvents, will be a straightforward extension of what follows). The role played by a statistical mechanical theory is to predict the equilibrium thermodynamic quantities that are of interest in selecting the solvent and in determining operating conditions; a satisfactory theory may also suggest new classes of solvents for experimental study. Such a theory can not, of course, predict all of the factors to be considered in solvent selection.

Specifically, it is necessary to be able to calculate the activity coefficients of the Components (1) and (1′) in both the raffinate and extract phases as a function of composition, temperature and pressure. At equilibrium, the fugacities (f_i) of any component i will be the same in both phases,

$$f_i^R = f_i^E$$

or

$$x_i^R \gamma_i^R f_i^{oR} = x_i^E \gamma_i^E f_i^{oE}$$

where x is mole fraction, γ is activity coefficient, and f^o is standard state fugacity. When the raffinate phase is a liquid, the pure liquid at the temperature and pressure of the solution will be chosen as the standard state, so that f_i^o is the same in both phases,

$$x_i^R \gamma_i^R = x_i^E \gamma_i^E \quad . \quad . \quad . \quad . \quad . \quad . \quad . \quad . \quad . \quad . \quad (1)$$

For liquid–liquid equilibria, the solvent selectivity, S_2, is defined as[1]

$$S_2 = \frac{x_1^E/x_{1'}^E}{x_1^R/x_{1'}^R} = \frac{\gamma_1^R \gamma_{1'}^E}{\gamma_1^E \gamma_{1'}^R} \quad . \quad . \quad . \quad . \quad . \quad . \quad . \quad . \quad (2)$$

Univ.-Bibl.

where the second form of Equation (2) follows from Equation (1), and assumes the same standard state in both phases. A less general definition of selectivity is often used, and involves the infinite dilution activity coefficients of (1) and (1′) in the solvent:[2]

$$S_2^{\infty} = \frac{\gamma_{1'}^{E,\infty}}{\gamma_1^{E,\infty}} \quad . \quad . \quad . \quad . \quad . \quad . \quad . \quad . \quad . \quad . \quad (3)$$

Equation (3) is obtained from Equation (2) at infinite dilution if it can be assumed that $\gamma_1^R \sim \gamma_{1'}^R$; for many hydrocarbon mixtures of interest this is a good approximation. The effects of temperature and pressure on S_2 and S_2^{∞} are obtained by using the equations:

$$\left(\frac{\partial \ln \gamma_i}{\partial T}\right)_{P,x_j} = \frac{H_i^{\circ} - \overline{H}_i}{RT^2} \quad . \quad . \quad . \quad . \quad . \quad . \quad . \quad . \quad (4)$$

and

$$\left(\frac{\partial \ln \gamma_i}{\partial P}\right)_{T,x_j} = \frac{\overline{V}_i - V_i^{\circ}}{RT} \quad . \quad . \quad . \quad . \quad . \quad . \quad . \quad . \quad (5)$$

where $\overline{H}_i$ and $\overline{V}_i$ are partial molal enthalpy and volume of i, respectively, and H_i° and V_i° are the corresponding values per mole of pure i in the standard state.

For gas–liquid equilibrium, when the pressure is low enough for the gas phase to be assumed to be ideal, the activity coefficient of the dissolved gas can be calculated from:

$$p_i = x_i^E \gamma_i^E f_i^{oE} \quad . \quad . \quad . \quad . \quad . \quad . \quad . \quad . \quad . \quad . \quad (6)$$

where p_i is the partial pressure in the gas phase.

Procedures used previously to estimate activity coefficients in solvent extraction systems have consisted of empirical correlations and regular solution theory. The empirical correlations[3–6] work well for the limited classes of solvent extraction systems for which they were designed; however, extrapolation to other types of system is often unreliable. The regular solution theory has also been applied to solvent extraction with some success.[7–9] While this theory can be derived from statistical mechanics in a fundamental way, its principal drawback is that it is based on the assumption that the excess entropy, s^E, is zero; in most applications the excess volume of mixing is also assumed to be zero. These approximations may be reasonable for solutions containing simple nonpolar molecules, but are likely to lead to significant errors for complex and polar molecules. Because the above approximations cannot be readily improved, it is worth while to look for a new approach.

In this paper, a fundamental statistical mechanical theory is proposed; it is based on a perturbation about a reference system which consists of a solution composed of rigid spheres. Perturbation theories of this type have been very successful when applied to simple liquids.[10] The theory takes advantage of the observation that actual liquid mixtures have properties similar to those of a mixture of rigid sphere particles at the same temperature, density and composition.[10] In contrast to regular solution theory, it is not necessary to make any assumptions concerning s^E or V^E. Similar theories have recently been used to calculate activity coefficients of gases in pure and mixed solvents,[11–13] and to predict the melting line of liquid argon.[14]

The theory presented is not in a finally developed form; it is more appropriate to look upon it as a first step towards a complete theory for systems in which

physical interactions predominate. The possibility of making further improvements by methods which are well defined is one of the most attractive features of the statistical mechanical theory.

Theory

The theory is based on a perturbation method.[15]

Consider a solution containing components 1,2 · · · ν. For any particular configuration (i.e., set of positions) of the molecules, let the system potential energy (due to intermolecular forces) be U. The potential is now written as the sum of two parts:

$$U = U^{o} + U^{p}. \qquad (7)$$

where U^{o} is the potential energy for the unperturbed system, whose properties are assumed to be known, and U^{p} is the perturbation potential energy defined by Equation (7). The configuration Helmholtz free energy (i.e. that part associated with intermolecular forces) is[15]

$$\begin{aligned} A^{c} &= -kT \ln \left[\int \ldots \int \exp(-U^{o}/kT) \exp(-U^{p}/kT) \mathrm{d}r_1 \ldots \mathrm{d}r_N \right] \\ &= A^{c}_{o} + <U^{p}>_{o} - \frac{1}{2kT}\left[<(U^{p})^2>_{o} - <U^{p}>^2_{o}\right] + O(T^{-2}) \qquad (8) \end{aligned}$$

The second form of Equation (8) is obtained by first expanding the term $\exp(-U^{p}/kT)$ and then expanding the logarithm term. In Equation (8), A^{c}_{o} is the configurational Helmholtz free energy for the unperturbed system. It will now be assumed that the series in Equation (8) converges rapidly so that it can be terminated at the $<U^{p}>_{o}$ term; this is the first-order perturbation term. If the intermolecular potentials are pairwise additive, $<U^{p}>_{o}$ is given by:[15, 16]

$$<U^{p}>_{o} = 2\pi \sum_{i=1}^{\nu} \sum_{j=1}^{\nu} \rho_i \rho_j V \int_{0}^{\infty} \varphi^{p}_{ij}(r)\, g^{o}_{ij}(r)\, r^2 \mathrm{d}r \qquad (9)$$

where ρ_i is the number of molecules per unit volume of component i, φ^{p}_{ij} is the perturbation pair potential energy for the ij pair, g^{o}_{ij} is the radial distribution function for the unperturbed system, r is the distance separating molecules i and j, and V is the system volume.

So far a specific choice for the unperturbed state has not been made. This is now taken to be a mixture of rigid sphere molecules at the same temperature, density and composition as the actual solution. This choice has two advantages: (*a*) the actual and rigid sphere solutions have similar thermodynamic properties at the same state conditions,[10] and (*b*) the thermodynamic properties and radial distribution functions are accurately known for rigid sphere mixtures. For this choice, the pair potential energy for the unperturbed system is:

$$\begin{aligned} \varphi^{o}_{ij}(r) &= \infty \quad r \leqslant \sigma_{ij} \\ \varphi^{o}_{ij}(r) &= 0 \quad r > \sigma_{ij} \qquad (10) \end{aligned}$$

where σ is the hard sphere diameter, and the perturbation pair potential is:

$$\begin{aligned} \varphi^{p}_{ij}(r) &= 0 \quad r \leqslant \sigma_{ij} \\ &= 4\varepsilon_{ij}\left[\left(\frac{\sigma_{ij}}{r}\right)^{12} - \left(\frac{\sigma_{ij}}{r}\right)^{6}\right] - \frac{\mu_j^2\alpha_i}{r^6} - \frac{\mu_i^2\alpha_j}{r^6} - \frac{\mu_i^2\mu_j^2}{3kTr^6} \qquad (11) \end{aligned}$$

for $r > \sigma_{ij}$

In Equation (11), the first term is the non-polar part of the perturbation potential energy, where σ_{ij} and ε_{ij} are the potential parameters. The next three terms are the electrostatic interactions, averaged over molecular orientations. The first two electrostatic terms are the dipole-induced dipole interactions, and the last is the dipole–dipole term.[17] In these latter terms, α is polarisability and μ is dipole moment. If one or both of the molecules i and j are non-polar ($\mu_i = 0$ or $\mu_j = 0$), some or all of these electrostatic terms disappear.

The chemical potential (per molecule) of component i, $\bar{g}_i$, can be calculated from Equation (8) using the relation

$$\bar{g}_i = \left(\frac{\partial A}{\partial N_i}\right)_{T,V,N_{j\neq i}} \quad . \quad . \quad . \quad . \quad . \quad . \quad . \quad . \quad . \quad (12)$$

The additional assumption is now made that $g^{o}_{ij} = 1$ in Equation (9) for r values of interest; this amounts to assuming that φ^{p}_{ij} is long-range. From Equations (9)–(12), it is found that:

$$\bar{g}_i = \bar{g}_i^{hs} - \frac{32\pi}{9}\sum_{j=1}^{v} \rho_j\varepsilon_{ij}\sigma_{ij}^3 - \frac{4\pi}{3}\sum_{j=1}^{v}\frac{\rho_j}{\sigma_{ij}^3}\left[\mu_j^2\alpha_i + \mu_i^2\alpha_j + \frac{\mu_i^2\mu_j^2}{3kT}\right] \quad . \quad (13)$$

where $\bar{g}_i^{hs}$ is the chemical potential for rigid spheres. Using the thermodynamic relationship between chemical potential and activity coefficient, Equation (13) gives:

$$\ln(\gamma_i f_i^{o}) = \frac{\bar{g}_i^{hs,r}}{kT} + \ln(kT\rho) - \frac{32\pi}{9kT}\sum_j \rho_j\varepsilon_{ij}\sigma_{ij}^3$$

$$- \frac{4\pi}{3kT}\sum_j \frac{\rho_j}{\sigma_{ij}^3}\left[\mu_j^2\alpha_i + \mu_i^2\alpha_j + \frac{\mu_i^2\mu_j^2}{3kT}\right] . \quad . \quad (14)$$

where ρ is the total number density, and $\bar{g}_i^{hs,r}$ is the residual part of the rigid sphere chemical potential. An equation for f_i^{o} can be obtained by writing Equation (14) for the standard state condition, i.e. taking the limit as $x_i \rightarrow 1$ if the pure liquid standard state is used.

Equation (14) is the final equation that will be used for calculation purposes. Several equations are available for $\bar{g}_i^{hs,r}$. The most accurate of these is that given by Carnahan & Starling:[18,19]

$$\frac{\bar{g}_i^{hs,r}}{kT} = -\ln(1-\zeta_3) + \frac{\pi P^{hs}\sigma_i^3}{6kT} + \frac{3\zeta_2\sigma_i}{(1-\zeta_3)} + \frac{3\zeta_1\sigma_i^2}{(1-\zeta_3)} + \frac{9\zeta_2^2\sigma_i^2}{2(1-\zeta_3)^2}$$

$$+ 3\left(\frac{\zeta_2\sigma_i}{\zeta_3}\right)^2\left[\ln(1-\zeta_3) + \frac{\zeta_3}{(1-\zeta_3)} - \frac{\zeta_3^2}{2(1-\zeta_3)^2}\right]$$

$$- \left(\frac{\zeta_2\sigma_i}{\zeta_3}\right)^3\left[2\ln(1-\zeta_3) + \frac{\zeta_3(2-\zeta_3)}{(1-\zeta_3)}\right] \quad . \quad . \quad . \quad . \quad (15)$$

where the rigid sphere pressure is:

$$P^{hs} = \frac{6kT}{\pi}\left[\frac{\zeta_0}{(1-\zeta_3)} + \frac{3\zeta_1\zeta_2}{(1-\zeta_3)^2} + \frac{3\zeta_2^3}{(1-\zeta_3)^3} - \frac{\zeta_3\zeta_2^3}{(1-\zeta_3)^3}\right] \quad . \quad . \quad (16)$$

and

$$\zeta_l = \frac{\pi}{6}\sum_{i=1}^{v} \rho_i\sigma_i^l$$

Calculations

In order to make calculations for real fluid systems, it is necessary to know only certain molecular parameters and the experimental density of the extractant phase. For systems where component i is a liquid, experimental vapour pressures have been used for the standard state fugacity, f_i^o.

Infinite dilution activity coefficients are calculated below by taking the limit as $x_i \rightarrow 0$ of Equation (14). Heats of solution and partial molal volumes are calculated by taking the temperature and pressure derivatives of $\ln \gamma_i$ in Equation (14).

Parameters

The theory predicts all thermodynamic properties when only the molecular parameters σ_i, ε_i, α_i and μ_i are known for each species in the system. The parameters α_i and μ_i are obtained from standard handbooks,[20,21] and the molecular parameters σ_i and ε_i are obtained from well-defined corresponding states correlations. The theory used here is more sensitive to the size parameter, σ, than to the energy parameter, ε. It is, therefore, important that the σ values be determined accurately.

For non-polar molecules, the Lennard–Jones (6, 12) parameters were first determined from the correlations of Tee *et al.*[22] These correlations were developed from a combination of second virial coefficient and viscosity data, and are given in terms of the critical constants and the Pitzer acentric factor ω. To find the corresponding cut-off Lennard–Jones potential parameters needed, the method of Zwanzig is used.[15] He obtained relations between these two sets of potential parameters by an analysis of reduced second virial coefficients. The final equations are:

$$\sigma = 0{\cdot}9099\sigma^o = \left(\frac{T_c}{P_c}\right)^{\frac{1}{3}} (2{\cdot}1429 - 0{\cdot}0795\omega) \quad . \quad . \quad . \quad . \quad . \quad (17)$$

$$\varepsilon = 1{\cdot}183\varepsilon^o = kT_c(0{\cdot}9363 + 0{\cdot}2003\omega) \quad . \quad . \quad . \quad . \quad . \quad (18)$$

where σ and ε are the cut-off Lennard–Jones parameters and ε^o and σ^o are the parameters for the usual (complete) Lennard–Jones (6, 12) function.

For polar molecules, it is considerably more difficult to obtain the appropriate potential parameters. To determine ε, the recent corresponding states analysis of Bae & Reed[23,24] has been used for polar molecules. Bae & Reed have shown that the pair potential function given by Equation (11) can be rearranged to the usual Lennard–Jones form:

$$<\varphi_{ij}> = 4\varepsilon_{ij}^*\left[\left(\frac{\sigma_{ij}^*}{r}\right)^{12} - \left(\frac{\sigma_{ij}^*}{r}\right)^6\right] \quad . \quad . \quad . \quad . \quad . \quad . \quad (19)$$

where

$$\varepsilon_{ij}^* = \varepsilon_{ij}^o\left[1 + \frac{\mu_i^2\mu_j^2}{6kT(\varepsilon_{ij}^o\sigma_{ij}^{o6})} + \frac{\mu_i^2\alpha_j + \mu_j^2\alpha_i}{4\varepsilon_{ij}^o\sigma_{ij}^{o6}}\right]^2 \quad . \quad . \quad . \quad . \quad (20)$$

and

$$\sigma_{ij}^{*6} = \left(\frac{\varepsilon_{ij}^o}{\varepsilon_{ij}^*}\right)^{\frac{1}{2}} \sigma_{ij}^{o6} \quad . \quad . \quad . \quad . \quad . \quad . \quad . \quad . \quad . \quad (21)$$

From Equation (19) it follows that polar fluids should obey the same law of corresponding states as non-polar fluids, provided that ε^* and σ^* are used as

reducing parameters. To determine the non-polar parameter ε^{o}_{ij} for a polar molecule the empirical relation at the critical point is first used:

$$\frac{\varepsilon_c^*}{k} = 0{\cdot}727\, T_c \quad . \quad . \quad . \quad . \quad . \quad . \quad . \quad . \quad . \quad (22)$$

where ε_c^* is the value of ε^* when $T = T_c$. From Equations (20) and (22):

$$\varepsilon_{ij} = 1{\cdot}183\varepsilon^{o}_{ij} = 0{\cdot}860kT_c\left[1 + \frac{\mu_i^2\mu_j^2}{6kT_c\varepsilon^{o}_{ij}\sigma^{o6}_{ij}} + \frac{\mu_i^2\alpha_j + \mu_j^2\alpha_i}{4\varepsilon^{o}_{ij}\sigma^{o6}_{ij}}\right]^{-2} \quad . \quad . \quad (23)$$

To determine ε from this equation for the like-pair interaction, it is first necessary to have available an expression for $\varepsilon^{o}\sigma^{o6}$, which appears on the right-hand side. Such an expression is provided by the Mavroyannis–Stephen theory for dispersion interactions.[25] An empirical modification[24] of this theory which gives quite good results for polar molecules gives the relation

$$\varepsilon^{o}\sigma^{o6} = 2{\cdot}484 \times 10^{-12}(\alpha^3 Z)^{0{\cdot}5985}\ \text{erg}\,\text{Å}^6 \quad . \quad . \quad . \quad . \quad . \quad (24)$$

where Z is the total number of electrons in the molecule, and α is in Å^3. Equation (24) can be used in Equation (23) to calculate ε_{ij} for like-pair interactions.

When ε^{o} is known, it is possible to estimate σ^{o} for polar molecules from Equation (24). However, the calculations are sensitive to the σ value, and a more accurate method of obtaining this parameter was considered desirable. Consequently, the σ values for polar liquids were calculated by fitting the theoretical equation for γ_i, Equation (14), to experimental activity coefficient data for hexane at infinite dilution in the polar solvent. Hexane was chosen because of the abundance of data for this solute.

The size parameter for ions was obtained from the equation[26, 31]

$$\sigma^{o}_{ion} = 1{\cdot}04\, d_c \quad . \quad . \quad . \quad . \quad . \quad . \quad . \quad . \quad . \quad (25)$$

where d_c is the crystal diameter of the ion. The corresponding ε^{o}_{ion} value was determined from the Mavroyannis–Stephen theory.[25]

For non-polar and polar molecules, and ions, unlike-pair parameters were calculated from like-pair parameters using the mixing rules:

$$\varepsilon_{ij} = (\varepsilon_{ii}\,\varepsilon_{jj})^{\frac{1}{2}} \text{ and } \sigma_{ij} = \tfrac{1}{2}(\sigma_{ii} + \sigma_{jj}) \quad . \quad . \quad . \quad . \quad . \quad . \quad (26)$$

Table I shows the potential parameters used in this study.

Infinite dilution activity coefficient and selectivity

Limiting activity coefficients and selectivities varied widely over the range of solvents studied. From a study of experimental data, Deal & Derr[27] have shown that no definite pattern of selectivity–solvency can be found over a wide range of solvent structures. They have shown, however, that a general trend of selectivity–solvency for hexane–benzene as the raffinate phase can be established. Fig. 1 shows experimental and theoretical selectivity–solvency behaviour for the system hexane–benzene at 25°C. The shaded area is the average experimentally determined behaviour for a large number of solvents as found by Deal & Derr.

The theory predicts the general trend observed experimentally, i.e. a decrease in solvency is usually accompanied by an increase in selectivity. In contrast to the regular solution theory, the present theory is able to account for variations in selectivity at a given solvency.

TABLE I

*Lennard–Jones potential parameters**

	ε^0/k, °K	σ^0, Å
Non-polar molecules		
Methane	141·6	3·958
Pentane	391·6	5·636
Hexane	426·4	5·987
Benzene	638·3	4·776
Cyclohexane	455·3	5·614
Heptane	459·8	6·310
Polar molecules		
Water	96·3	3·390
Methanol	254·2	4·462
Ethylene glycol	361·7	5·242
Aniline	497·6	6·187
Nitrobenzene	368·5	6·198
Dimethyl sulphoxide	421·8	4·695
Methyl Cellosolve	396·7	5·748
Acetone	203·5	5·011
Acetophenone	427·5	6·550
Ions		
K^+	165·2	2·76
OH^-	167·2	3·20
$(CH_3)_4N^+$	258·0	4·98
Br^-	313·0	4·07

* Cut-off Lennard–Jones parameters may be calculated from these ε^0 and σ^0 values using Equations (17) and (18).

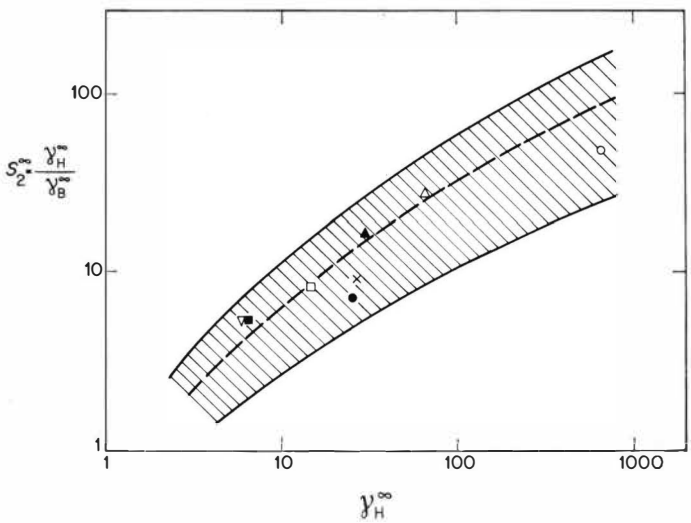

FIG. 1. *Selectivity–solvency behaviour for hexane–benzene as the raffinate phase, 25°C*

The shaded area is the region in which the experimental data are found to lie;[27] the dotted line is a correlation based on regular solution theory.[27]

Points are theoretical calculations from Equation (14) for various solvents: ● MeOH; ▲ aniline; ■ nitrobenzene; ○ ethylene glycol; △ dimethyl sulphoxide; □ methyl Cellosolve; ▽ acetophenone; × 95 vol.-% methyl Cellosolve, 5 vol.-% water.

One cannot tell much about the accuracy of a theory from a plot such as Fig. 1, however. To this end, experimental and theoretical infinite dilution activity coefficients as determined by Equation (14) were directly compared. These results are shown in Table II. The theory predicts the activity coefficient behaviour of non-polar solutes in polar solvents reasonably well. The

behaviour of the slightly polar substances isoprene and 1-pentene shows poorer results; the approximations made in the theoretical calculations are expected to lead to larger errors for such systems.

TABLE II

Activity coefficients at infinite dilution, 25°C

Solute (1)	Solvent (2)	$(\gamma_1^{E,\infty})_{\text{theory}}$	$(\gamma_1^{E,\infty})_{\text{exptl}}$	$(\gamma_1^{E,\infty})^{\dagger}_{RS}$
Pentane	Methanol	28·8	27·0	151
Hexane	Methanol	24·6	27·0	242
Heptane	Aniline	26·8	23·1	29·3
Benzene	Aniline	1·4	2·2	3·8
Hexane	Nitrobenzene	6·7	7·0	10·2
Benzene	Nitrobenzene	1·2	1·2	2·2
Cyclohexane	Ethylene glycol	432	316	451
Hexane	Ethylene glycol	618	625	2346
Pentane	Dimethyl sulphoxide	55·2	61·3	49·1
Cyclohexane	Dimethyl sulphoxide	54·5	40·6	28·2
Benzene	Acetophenone	1·2	1·2	1·5
Pentane	Acetophenone	5·4	5·4	4·8
Isoprene	Acetophenone	3·8	2·1	2·7
Pentane	Methyl Cellosolve	12·7	14·5	—
Hexane	Methyl Cellosolve	14·1	16·0	—
1-Pentene	Methyl Cellosolve	13·6	8·6	—
Pentane	Acetone	5·7	5·3	4·3
Hexane	Acetone	6·9	6·5	4·7
1-Pentene	Acetone	5·8	3·2	4·0

† Calculated from regular solution theory correlation of Weimar & Prausnitz.[7]

Temperature dependence

Perturbation theories based on a hard sphere reference system cannot satisfactorily predict the temperature dependence of thermodynamic properties. To overcome this difficulty, a reference system is used that has a repulsive potential of finite steepness, and the reference system Helmholtz free energy is expanded in terms of a steepness parameter,[28] n; i.e. the A_0^c of Equation (8) is expanded about the hard sphere $A_0^{c,hs}$ in a series in n^{-1}. Truncated at the second term in this series, Barker & Henderson[29] have shown that the value of A_0^c for this 'soft' reference system has the same functional form as that of the hard sphere reference system, but with a temperature-dependent hard core size parameter $d(T)$. The temperature dependence is given by:

$$d(T) = \int_0^{\sigma} [1 - \exp(-\varphi(r)/kT)]\, dr \quad . \quad . \quad . \quad . \quad . \quad . \quad (27)$$

where $\varphi(r)$ is the soft reference repulsion potential, and σ is the potential energy parameter for the perturbation potential $\varphi^p(r)$. This temperature dependence is shown in Fig. 2.

To make a calculation with this modification, the following procedure is used. Equation (14) is again used; however, in calculating $\bar{g}_i^{hs,r}$ from Equation (15), σ_i is everywhere replaced by $d(T)$ as given by Equation (27). This replacement of σ by $d(T)$ is only made in the $\bar{g}_1^{hs,r}$ term, and not in the other terms on the right-hand side of Equation (14).

This modification has little effect on the calculations of concentration- or pressure-dependence of γ_i, but has a marked effect on the temperature-dependence. Fig. 3 shows the great improvement obtained for the partial molal heat of solution for hexane in acetone. With constant σ, the temperature

dependence of γ_i is completely wrong; however, good results are obtained by using Equation (27). Other systems show a similar improvement. Thus the expected increase in solvency (decrease in $\gamma_1^{E,\infty}$) with increasing temperature is correctly predicted by the theory.

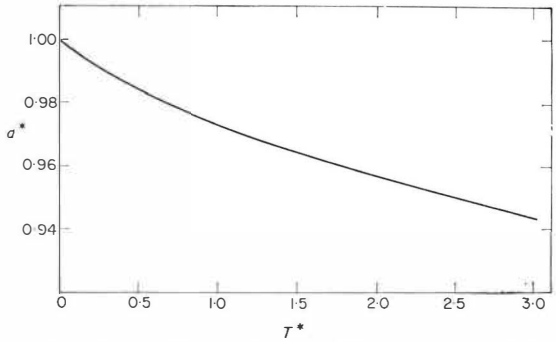

FIG. 2. *Temperature dependence of* d *from Equation (27) with a Lennard–Jones (6, 12) potential* $T^* = kT/\varepsilon°$, $d^* = d(T)/\sigma o$.

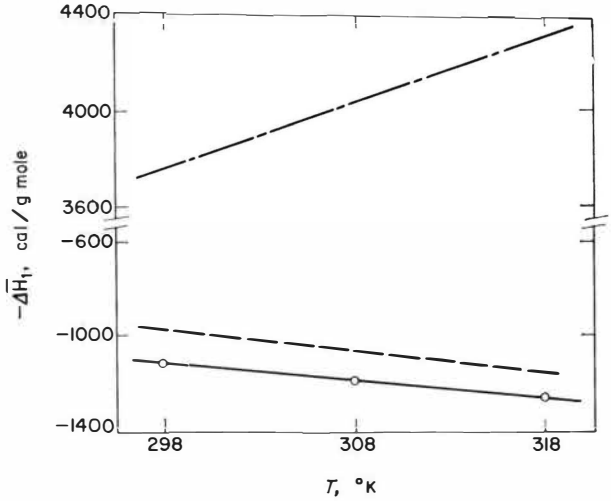

FIG. 3. *Partial molal heats of solution,* $\Delta\bar{H}_1 = \bar{H}_1 - H_1^o$, *for hexane at infinite dilution in acetone*

○ experiment; — — — — — theory with constant σ; - - - - theory with temperature-dependent *d* given by Equation (27).

Pressure dependence

The partial molal volume gives a measure of the pressure dependence of the activity coefficient. The property $\bar{V}_1$ is therefore needed for calculations on extraction processes to be operated at high pressure. It is calculated from the theory by taking the pressure derivitive of Equation (14), and using Equation (5). Calculations for $\bar{V}_1$ at infinite dilution of (1) are given below for two systems which have been studied experimentally.

Solute (1)	Solvent (2)	$\bar{V}_1^{\infty}$ (theory), cm³/mole	$\bar{V}_1^{\infty}$ (exptl), cm³/mole
Benzene	Methanol	92·7	89·4
Benzene	Aniline	68·0	73·9

It is seen that high pressure fugacities would be predicted incorrectly had it been assumed that the partial molal volume for a given solute in different solvents is

the same. Calculations of $\bar{V}_1$ for dissolved gases are given in the next section.

Mixed solvent systems

One of the attractive features of the perturbation theory lies in its simple extension to mixtures. Gas solubilities in mixed solvents[30] and in electrolyte solutions have been examined,[13,31] as well as liquid-phase equilibria in multi-component solvent mixtures.

The practice of adding small amounts of water to extractive distillation solvents to improve selectivity and solvency characteristics is well known. Water, owing to its low solvency behaviour for most hydrocarbons, increases the activity coefficient of these hydrocarbons in the extracting solvent even if it is added in relatively small amounts (5 vol.-%). Fig. 4 shows the activity coefficient behaviour of pentane in mixtures of water and methyl Cellosolve. A marked increase occurs in the activity coefficient of the pentane as more water is added to the mixture. Although solvency characteristics can be drastically altered for mixed solvent systems, the selectivity is often altered very little, so that unless an adjustment to lower solvency is necessary, use of a mixed solvent seldom helps the overall extraction performance. This fact can be seen in Fig. 1 by noting that while γ_H^∞ has increased markedly upon addition of 5 vol.-% of water to methyl Cellosolve, the selectivity remains about the same. This is due to the fact that the value of γ^∞ for the other species in the hydrocarbon mixture also increases, so that the ratio S_2^∞ does not change greatly.

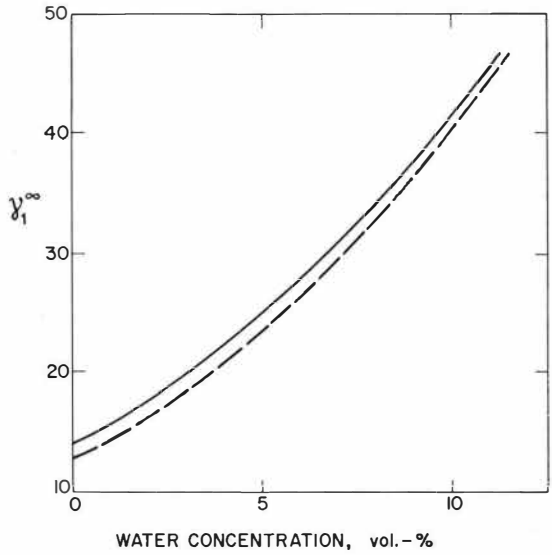

FIG. 4. *Infinite dilution activity coefficient for pentane in a mixed solvent of methyl Cellosolve and water at 25°C*

—— experiment; - - - - theory.

Gas–liquid phase equilibrium in mixed solvent systems is a very interesting subject, because of the diversified pattern of behaviour. For example, on addition of an electrolyte to a solution of solute gas in water, the solute may experience an increase in solvency (salting-in) or a decrease in solvency (salting-out), depending on the salt considered. Fig. 5 shows a comparison of theory and experiment for these two forms of behaviour. The addition of salts will also significantly affect the selectivity in the case of gas mixtures.

Fig. 6 shows the theoretically predicted effect of adding a salt on the partial molal volume of the dissolved gas. The value predicted for $\bar{V}_1$ in pure water is in good agreement with experiment. However, no experimental data are available for $\bar{V}_1$ in salt solutions.

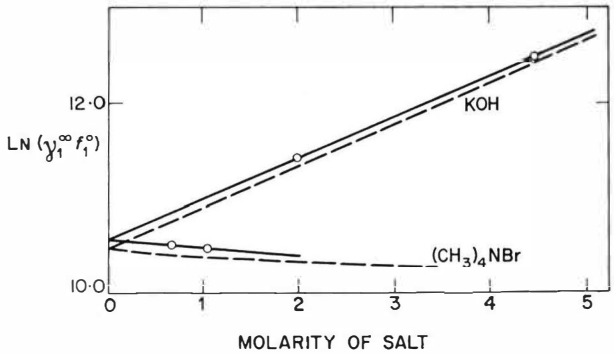

FIG. 5. *Salting-in and salting-out of methane* (1) *at 25°C*

○——○ experiment; - - - - theory.

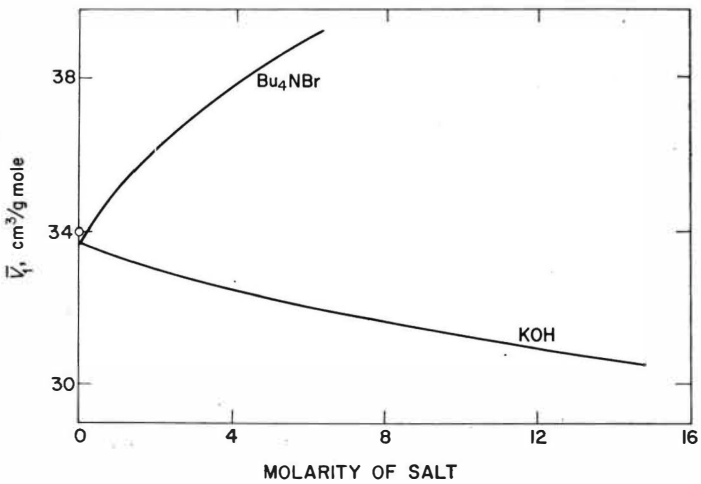

FIG. 6. *Partial molal volumes of methane* (1) *in KOH and Bu_4NBr solutions at 25°C*

- - - - theory; ○ experimental value in water.

Conclusions

The theory presented predicts the concentration-, pressure- and temperature-dependence of activity coefficients quite well. In the case of temperature-dependence, it is necessary to use the temperature-dependent diameter given by Equation (27) to obtain satisfactory results. The theory seems to offer distinct advantages over the regular solution theory.

Further work on the theory is needed to determine the error in neglecting higher order terms in the perturbation treatment, and to evaluate the other approximations in the theory. Such a study should yield improved methods of calculating activity coefficients which are clearly defined, and suitable for engineering use.

Acknowledgments

Financial support of this work by a grant from the National Science Foundation is gratefully acknowledged. One of us (E. T.) acknowledges support from a National Science Foundation Predoctoral Fellowship. Thanks are also due o T. M. Reed for providing a copy of a manuscript prior to publication.

References

[1] Treybal, R. E., 'Mass transfer operations', 1968, 2nd Edn, p. 441 (New York, McGraw-Hill)
[2] Vernier, P., Raimbault, C., & Renon, H., *J. Chim. phys.*, 1969, **66**, 960
[3] Pierotti, G. J., Deal, C. H., & Derr, E. L., *Ind. Engng Chem.*, 1959, **51**, 95
[4] Gerster, J. A., Gorton, J. A., & Eklund, R., *J. chem. Engng Data*, 1960, **5**, 423
[5] Deal, C. H., Derr, E. L., & Papadopoulos, M. N., *Ind. Engng Chem. Fundamentals*, 1962, **1**, 17
[6] Munson, M. S. B., *A.I.Ch.E. Jl*, 1965, **11**, 920
[7] Weimar, R. F., & Prausnitz, J. M., *Hydrocarb. Process.*, 1965, **44**, 237
[8] Humphrey, J. L., & Van Winkle, M., *Ind. Engng Chem. Process Des. Dev.*, 1968, **7**, 581
[9] Skytte-Jensen, B., in 'Solvent extraction chemistry', Dyrssen, D., Liljenzin, J. O., & Rydberg, J., (Eds), 1967, p. 517 (Amsterdam: North-Holland)
[10] Rowlinson, J. S., 'Liquids and liquid mixtures', 1969, 2nd Edn, p. 296 (London: Butterworths)
[11] Pierotti, R. A., *J. phys. Chem., Ithaca*, 1963, **67**, 1840
[12] Pierotti, R. A., *J. phys. Chem., Ithaca*, 1965, **69**, 281
[13] Shoor, S. K., & Gubbins, K. E., *J. phys. Chem., Ithaca*, 1969, **73**, 498
[14] Longuet-Higgins, H. C., & Widom, B., *Molec. Phys.*, 1964, **8**, 549
[15] Zwanzig, R. W., *J. chem. Phys.*, 1954, **22**, 1420
[16] Reed, T. M., & Gubbins, K. E., 'Applied statistical mechanics', 1971, Chap. 9 (New York: McGraw-Hill)
[17] Hirschfelder, J. O., Curtiss, C. F., & Bird, R. B., 'Molecular theory of gases and liquids', 1954, Chap. 1 (New York: Wiley)
[18] Carnahan, N. F., & Starling, K. E., *J. chem. Phys.*, 1969, **51**, 635
[19] Boublik, T., *J. chem. Phys.*, 1970, **53**, 471
[20] Weast, R. C., & Selby, S. M. (Eds), 'Handbook of chemistry and physics', 1969, 49th Edn, (Cleveland: Chemical Rubber Publishing Co.)
[21] Lange, N. A. (Ed.), 'Handbook of chemistry', 1967, 10th Edn (New York: McGraw-Hill)
[22] Tee, L. S., Gotoh, S., & Stewart, W. E., *Ind. Engng Chem. Fundamentals*, 1966, **5**, 356
[23] Bae, J. H., & Reed, T. M., III, *Ind. Engng Chem. Fundamentals*, 1967, **6**, 67
[24] Bae, J. H., & Reed, T. M., III, to be published
[25] Mavroyannis, C., & Stephen, M. J., *Molec. Phys.*, 1962, **5**, 629
[26] Tiepel, E. W., & Gubbins, K. E., to be published
[27] Deal, C. H., & Derr, E. L., *Ind. Engng Chem. Process Des. Dev.*, 1964, **3**, 394
[28] Rowlinson, J. S., *Molec. Phys.*, 1964, **8**, 107
[29] Barker, J. A., & Henderson, D., *J. chem. Phys.*, 1967, **47**, 4714
[30] Tiepel, E. W., & Gubbins, K. E., to be published
[31] Tiepel, E. W., & Gubbins, K. E., paper presented at A.I.Ch.E. meeting, Denver, 1970

Effects of ionic hydration and ion association on the solvent extraction behaviour of inorganic acids

by H. M. Widmer*

Chemistry Department, Brookhaven National Laboratory, Upton, N.Y. 11973, U.S.A.

The use of slope analysis in the interpretation of solvent extraction data and errors that can arise if the effects of ionic hydration and solvation are not considered are discussed. Use of solvent extraction techniques for determining association numbers and association orders of the species involved in the extraction is considered.

Introduction

IN SOLVENT EXTRACTION systems, electrolytes undergo reactions that influence their distribution between organic and aqueous phases. There are many ways to describe these reactions and two different classifications are presented in Fig. 1. It is evident that the simultaneous operation of different interactions causes the stepwise formation of complexes, hydrates or solvates and ion associates, but it must be borne in mind that there is no distinct line between the complex formation, solvation and ion association. Generally, ion associates are considered to be aggregates in which the different ions are separated by solvent molecules while ion pairs in which the ions are not separated by solvent molecules are often referred to as complexes even if the charges are still located at their original sites.

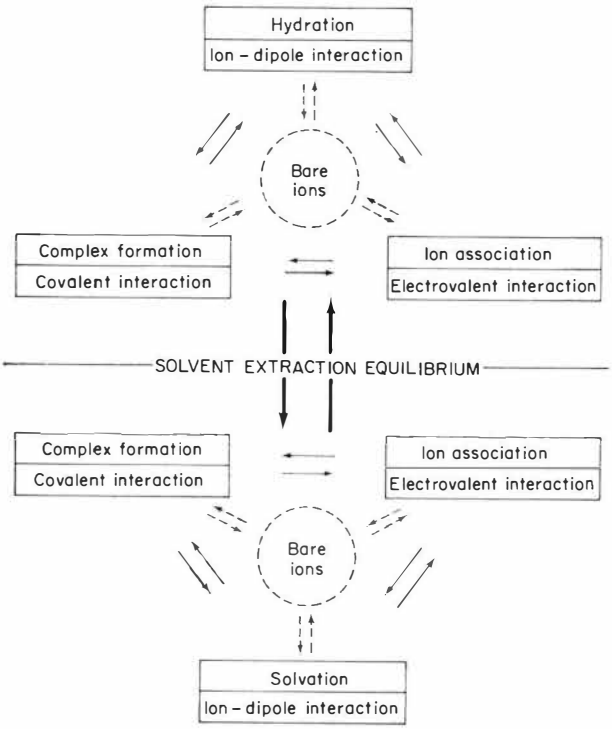

FIG. 1. *Equilibria between principal processes taking place in solvent extraction systems*

*Present address: Department of Chemistry, University of Massachusetts-Boston, Boston, Mass. 02116, U.S.A.

This paper emphasises some effects of ionic hydration on the extraction behaviour of inorganic acids and outlines the influence that the ionic hydration has on the formation of ion associates. This is achieved mainly on the basis of theoretical considerations, but the importance of the results is demonstrated with examples from recently published investigations.[1–4]

Theoretical

The solvation or hydration and complex formation are often characterised by the so-called solvation or hydration number and the co-ordination or ligand number, respectively. By analogy, an association number can be introduced that describes the number of primary particles that are aggregated in an ion associate. However, this number does not (on a thermodynamic basis) completely describe an ion association process. Another concept that might be called the association order must be introduced. It can be defined as the sum of the association numbers of the conjugate species, divided by the number of these species. The two terms are explained in Table I and examples are given for a number of ion associates that play an important role in the solvent extraction behaviour of proton acids.

TABLE I

Characterisation of different ion associates

Ion association equilibrium	Ion associate	Number of conjugated species	Association number	Association order
$H^+ + X^- \leftrightharpoons H^+X^-$	Ion pair	1	2	2
$2H^+ + 2X^- \leftrightharpoons H^+ + HX_2^-$	Ion triplet, triple ion	2	1, 3	2
$2H^+ + 2X^- \leftrightharpoons (H^+X^-)_2$	Ion quadruplet	1	4	4
$3H^+ + 3X^- \leftrightharpoons HX_2^- + H_2X^+$	Ion triplets, triple ions	2	3, 3	3
$3H^+ + 3X^- \leftrightharpoons 2H^+ + HX_3^{2-}$	—	3	1, 1, 4	2

It can be seen from Table I that an association order of 2 can be assigned to a number of ion associates including ion pairs and triple ions and it must be concluded that solvent extraction data do not always give a definitive answer to the question whether or not an acid is dissociated in the organic phase. This fact has not always been considered in its full consequence.

In a logarithmic plot of organic-phase vs. aqueous-phase electrolyte concentration parameters, the slope is determined by the association order of the system in both phases, the slope being identical with the association order of the predominant electrolyte species in the organic phase, if the solute is completely dissociated in the aqueous phase. Table II represents the relation between the expected slopes for different ion associates and the predominant organic-phase species. Figs 2 and 3 represent the same results in graphical form. An acid system in which the triple ion HX_2^- exists as the conjugate

TABLE II

Expected slope for different ion associates in dependence of the predominant organic-phase species

Predominant acid species in the organic phase	Slope of $\log [H_hX_i]_{org}$ vs. $\log a_{HX}$ ($\log [HX]_{org,\ total}$)					
	$h=0, i=1$ (X^-)	$h=1, i=0$ (H^+)	$h=1, i=1$ (HX)	$h=1, i=2$ (HX_2^-)	$h=2, i=1$ (H_2X^+)	$h=2, i=2$ ($(HX)_2$)
$H^+ + X^-$	1 (1)	1 (1)	2 (2)	3 (3)	3 (3)	4 (4)
HX	1 (1/2)	1 (1/2)	2 (1)	3 (3/2)	3 (3/2)	4 (2)
$H^+ + HX_2^-$	0 (0)	2 (1)	2 (1)	2 (1)	4 (2)	4 (2)
$H_2X^+ + HX_2^-$	1 (1/3)	1 (1/3)	2 (2/3)	3 (1)	3 (1)	4 (4/3)
$(HX)_2$	1 (1/4)	1 (1/4)	2 (1/2)	3 (3/4)	3 (3/4)	4 (1)

anion of the hydrogen ion yields the same slope of 2 as an acid ion pair. Only at higher concentrations is the triple ion formation characterised by a slope of 3. This latter situation is expected if the theory of Fuoss & Kraus[5–11] is applied to solvent extraction problems. These authors advanced a thorough theory of ion association, particularly triple ion formation, based on purely electrostatic ion–ion interactions. When applied to acids, the theory predicts equal values for the formation constants of both the triple anion HX_2^- and the cation H_2X^+, and consequently equal concentrations for these two ion associates. This must be so, because in both ions the opposite charges are separated by the same interionic distance, namely the sum of the radii of the two unassociated ions. In Figs 2 and 3 this situation is represented by the thin dashed lines. However, this is only a limiting case, implying that in the associated forms the original ions are still hydrated and solvated to the same extent as they are in the free ion state. Quite often it is observed that in an ion association process, water and solvent molecules are released from the original ion solvation shells. Therefore the formation of the two different triple ions must depend on the water and solvent activities, and as a result the concentration ratio $R = [HX_2^-]/[H_2X^+]$ assumes values that differ from unity.

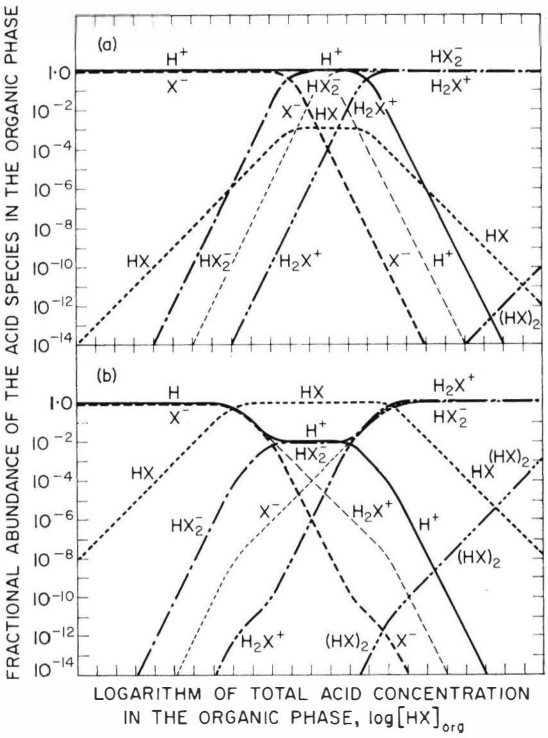

FIG. 2. *Fractional abundance of different acid species in the organic phase as a function of the total organic-phase acid concentration*

(a) Triple anion formation exceeds ion pair formation; (b) Ion pair formation exceeds triple anion formation.

This problem is more thoroughly treated in Appendix I, where the conclusion is drawn that the organic-phase concentration ratio R must be larger than unity for most of the acid extraction systems, in which the hydrogen ion is extensively hydrated and solvated in the organic phase.

The predominant formation of triple anions, as opposed to triple cations, is expected for complex metal acids, resulting in a slope of 2 in a logarithmic distribution plot. Fig. 4 represents solvent extraction and conductance data for the hydrochloric and tetrachloro-iron(III) acid–water–methyl isobutyl

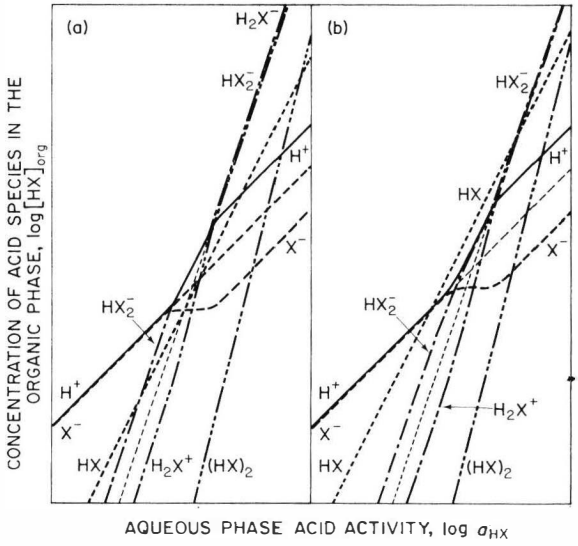

FIG. 3. *Logarithmic plot of the concentration of individual species in the organic phase vs. the aqueous-phase electrolyte activity*

(a) Triple anion formation exceeds ion pair formation; (b) Ion pair formation exceeds triple anion formation.

ketone (MIBK) systems. The two acids represent two different association systems. In the associated form, hydrochloric acid forms predominantly ion pairs, but the complex iron acid remains almost completely dissociated in its associated form, $H(FeCl_4)_2^-$. These examples demonstrate that ion association processes beyond the ion pair formation can be important, and the triple ion formation must be recognised as a major ion association process, that is not limited to a certain class of organic solvents. In recent years it has been shown repeatedly that the formation of triple ions is observed in aqueous solutions[12–17] and organic phases,[16–19] characterised by dielectric constants covering a wide range of values.

Fig. 4 also represents an instructive example of the fact that physico-chemical methods beyond the solvent extraction techniques must be used to characterise the extracted species in the organic phase. Quite often the slope analysis is used to prove that an acid exists in the organic phase in the form of an ion pair. Such a treatment would yield a wrong conclusion in the case of the complex iron acid and, although a constant equivalent conductance is observed at low and high organic-phase electrolyte concentrations for both hydrochloric acid and the complex iron acid, different conclusions must be drawn.

Further important conclusions may be drawn from the mathematical description given in Appendix II. Expressions (19) and (20), and (22) and (23), describe the intercept of the lines with slope 1 and 2 obtained in a logarithmic distribution plot under the conditions discussed in Appendix II. It becomes evident that a dilution study can be used to distinguish between the formation of ion pairs and triple ions, that cause a change of slope from 1 to 2 in a distribution plot. In the ion-pair formation the lines of different slopes intersect at a point that depends on the organic-phase concentration only, provided that the dielectric constant of the medium is not appreciably altered by the variations of the concentrations of the active, solvating extractant S and the diluent, and provided that the dissociated and the ion-paired acid have a common solvation number. However, the location of the intersection depends on the aqueous-phase acid concentration parameters only, when the associated species found in the organic phase is the triple ion (provided that the simple and triple anion are solvated to the same extent).

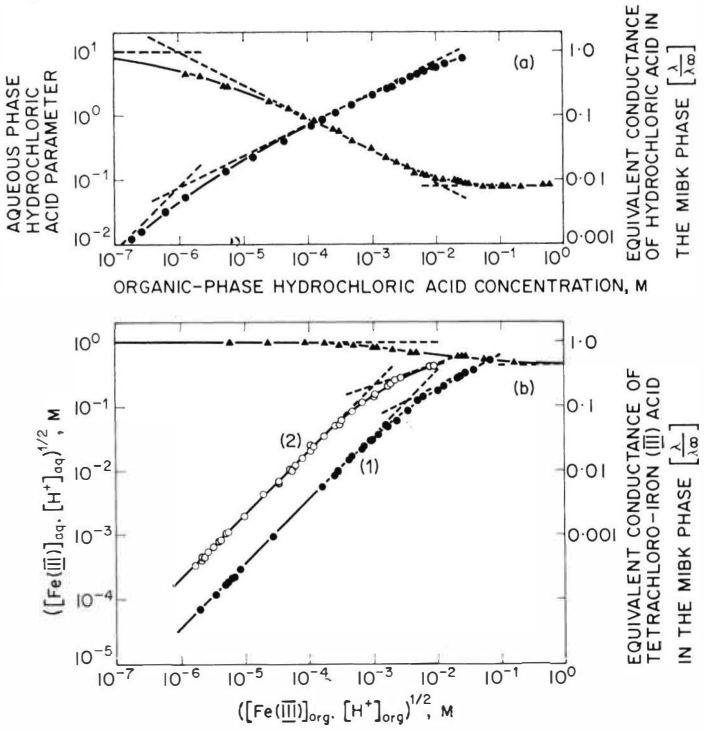

FIG. 4. *Solvent extraction and conductance data for* (a) *the H_2O–HCl–MIBK and* (b) *the H_2O–$HFeCl_4$–MIBK systems*

(1) iron(III) extracted from 2·0M-HCl; (2) iron(III) extracted from 1·0M-HCl

●, ○ = solvent extraction data; ▲ = conductance data

Figs 5(a) and 5(b) represent the solvent extraction of acids forming ion pairs (HX) and triple ions (HX_2^-), respectively, in a dilution study. The solvent activities represented in these plots are from top to bottom $a_s = 0{\cdot}1$, $0{\cdot}01$ and $0{\cdot}001$M, respectively. For simplicity, it is assumed that the dissociated and ion-paired acid exhibit a common solvation number of 2 that can be ascribed to the hydrogen ion (Fig. 5(a)) and that the simple and triple anion (X^- and HX_2^-, respectively) are unsolvated (Fig. 5(b)). The distribution constant $K_{D1} = [H^+]_{org}\,[X^-]_{org}/a_{HX}^2 \cdot a_S^2$ is taken as 10^4 mole^{-2} in both plots. The distribution of the acid between water and the organic phase (solvent S and diluent) is characterised by the presence of an ion pair and triple anion in the organic phase, resulting in distribution constants $K_{D2} = [H^+X^-]_{org}/a_{HX}^2 \cdot a_S^2$ (Fig. 5(a)) and $K_{D3} = [H^+]_{org}\,[HX_2^-]_{org}/a_{HX}^4 \cdot a_S^2$ (Fig. 5(b)) equal to 10^6 mole^{-3} and $2{\cdot}5 \times 10^7$ mole^{-4}, respectively.

Such a dilution study is a convenient method for investigating independently the ion-pair and triple-ion formation of the same acid, provided that the organic solvent S is powerful enough that it can be effectively diluted by an inert solvent. The extraction behaviour of an ion pair as shown in Fig. 5(a) is often observed and discussed in the literature. The system shown in Fig. 5(b) is not often described, but there is evidence that the water–nitric acid–TOPO system, diluted with a solvent of rather high dielectric constant, represents such a system. It can be expected that other mineral and also many complex metal acids behave similarly. Such a system may have important practical application, since the cost of separating processes may be lowered by the proper choice of the solvent extraction conditions. Customary high distribution quotients are achieved by the increase of the active solvent concentration, thus shifting the system into the concentration range where the ion pair is

extracted predominantly. Favourable distribution quotients may also be obtained by an increase of the aqueous-phase concentration of the extracted compounds or a decrease of the water activity in the aqueous phase without changing the solvent concentration.

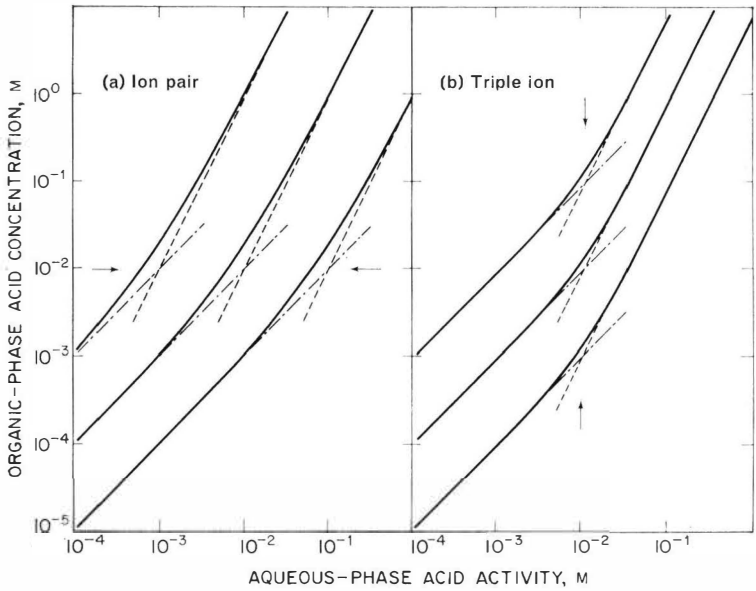

FIG. 5. *Expected distribution behaviour of an acid forming* (a) *ion pairs and* (b) *triple ions in the organic phase of a dilution system with solvent activities* (a_s) *from top to bottom equal to 0·1, 0·01 and 0·001M, respectively*

(a) ion pair. The dependence of the intersection of upper and lower curve on the organic-phase acid concentration is stressed. The following distribution constants describe the system: $K_{D1} = 10^4$ mole^{-2} and $K_{D2} = 10^6$ mole^{-3}, resulting in an ion-pair formation constant $K_A = 10^2$ mole^{-1}.
(b) triple ion. The dependence of the intersection of upper and lower curve on the aqueous-phase acid activity is stressed. The following distribution constants describe the system: $K_{D1} = 10^4$ mole^{-2} and $K_{D3} = 2 \cdot 5 \times 10^7$ mole^{-4}. Similar distribution curves are also obtained from an acid forming ion pairs that are solvated by only one solvent molecule rather than two as assumed in (a). The corresponding distribution constant would be $K_{D2} = [H^+X^-]_{org}/(a_{HX^2} \cdot a_s) = 10^4$ mole^{-2}.

So far hydration effects have been considered that directly influence the ion association process and which are reflected in the distribution constants K_{D2} and K_{D3} (Equations (18) and (21)). But there are also some effects that find their expression in the distribution constant K_{D1} (Equation (17)). These effects may arise from the hydration phenomena of the hydrogen ion as well as the corresponding anion. If comments are restricted to the behaviour of proton acids, then any differences in K_{D1} which are due to hydration differences of different acids in the same solvent system must be caused by differences of the anion hydration. It is convenient to distinguish between structure-forming and structure-breaking acids and this classification can at least in part be related to two different anion hydration models that have been discussed earlier.[3] Fig. 6, taken from a paper by Everett & Coulson,[20] describes the two hydration models in terms of the potential energy associated with the different structural arrangements of the hydration shell. Structure A is assumed only by large anions and complex anions in particular that can stabilise the structure by the formation of hydrogen bonds between electronegative groups of the complex and the hydrogen atoms of the water molecule. Structure A lacks a rotational freedom around the O–H bond that is preserved in the arrangement of structure B. Consequently, only weak bonds can be formed between the primary hydration shell and the bulk water of anion A, but the same bonds are much stronger for the anion B, that fits into the structure of the bulk water. For the same reasons, anion A is pushed from the aqueous solution into the organic

phase and is extracted much better than anion B. It is also possible that anion A carries more water molecules into the organic phase than anion B, although the water is bound more strongly in the hydration shell of the structure-forming electrolyte B. The large differences between the distribution constants K_{D1} of hydrochloric and perchloric acid which is generally observed is in agreement with this model. In the MIBK system, the distribution constants for HCl and $HClO_4$ at 25°C are $K_{D1} = 1 \cdot 42 \times 10^{-10}$ and $1 \cdot 21 \times 10^{-4}$, respectively, and it is found that the perchlorate anion is more extensively hydrated in the organic phase than the chloride ion.[1-3]

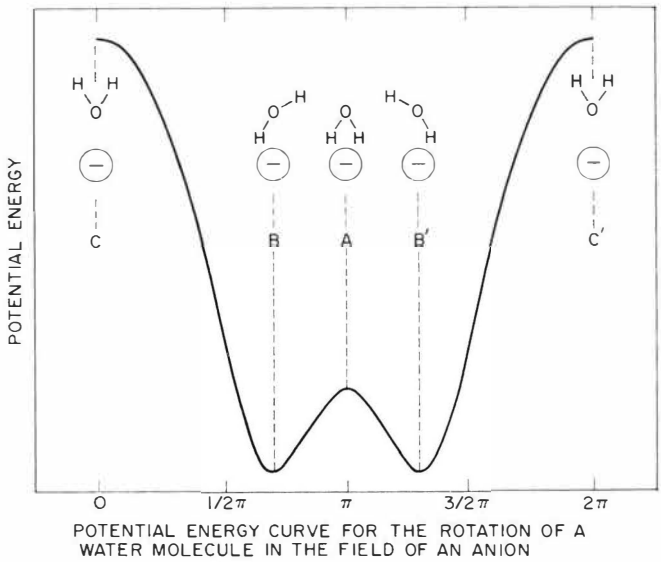

FIG. 6. *Orientation of water molecules in the primary hydration shell of anions and its influence on the stability of the structural arrangement*[20]
A: suggested by Azzam[21,22] and Buckingham;[23] B: suggested by Bernal & Fowler;[24] C: unfavourable

A rather different hydration effect arises from the fact that the extracted species in the organic phase are characterised by different hydration numbers than the corresponding ionic species in the aqueous phase. Such an effect can be expressed in terms of the water activity that must be raised to the power of the difference between the hydration numbers of the thermodynamically active equilibrium species in the two phases. Such an effect is explained and illustrated in Fig. 7, where distribution data of the hydrochloric acid–MIBK system are plotted. If the distribution ratio is plotted against the aqueous-phase acid concentration, then a slope representing a high association order is obtained. A slope close to $2 \cdot 0$ describes the behaviour at acid concentrations $> 1 \cdot 0$M, and an association order of 3 could be assigned to the organic-phase species. If the distribution ratio is plotted against the aqueous-phase acid activity, a slope close to $\frac{1}{2}$ is found at higher acid activities. This result indicates an ion association in the aqueous phase rather than in the organic medium. Obviously both conclusions are wrong. Conductance measurements (Fig. 4) indicate that the predominant hydrochloric acid species in the organic phase is the ion pair as soon as the organic-phase acid concentration rises above 10^{-6}M. By rearrangement of Equation (18), the difference of the organic and aqueous-phase hydration number ΔH_2 is obtained as the slope in a logarithmic plot of the extraction parameters vs. the water activity:

$$\Delta H_2 = \frac{\mathrm{d} \log ([\mathrm{H}^+\mathrm{X}^-]_{\mathrm{org}}/a_{\mathrm{HX}}^2\, a_{\mathrm{s}}^{\Delta S_2})}{\mathrm{d} \log a_{\mathrm{w}}}$$

Such a plot is represented in Fig. 8 which presents extraction data for the hydrochloric acid– and perchloric acid–MIBK systems. The slopes of 5·0 and 9·0 agree with the hydration numbers derived by the analyses of the organic-phase solutes. These results indicate that the activities used in this plot represent the bare, unhydrated ions (similar results are obtained from the rearrangement of Equations (17) and (21) that must be used when the free unassociated ions and the triple anion are the predominant species in the organic phase, respectively). If the value of ΔH_2 derived in this manner is used to correct the aqueous-phase hydrochloric acid parameters in Fig. 7, the correct slope and intercept that agree with the results or the conductance experiments are obtained.

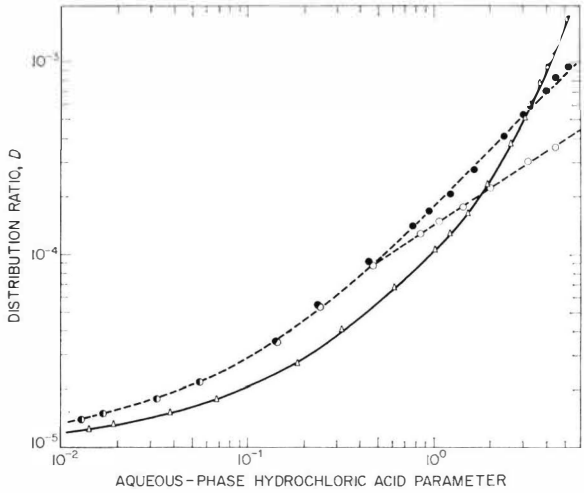

FIG. 7. *Distribution ratio* D *as a function of the aqueous-phase hydrochloric acid parameters*

△ [HCl] (concentration), $D = [HCl]_{org}/[HCl]$; ○ a_{HCl} (activity), $D = [HCl]_{org}/a_{HCl}$; ● $a_{HCl} \cdot a_w^{2\cdot5}$, $D = [HCl]_{org}/(a_{HCl} \cdot a_w^{2\cdot5})$.

Such an effect is not limited to solvent extraction systems in which the electrolyte concentration of the aqueous phase is altered. It is also observed in systems where the aqueous-phase ionic strength is maintained at a constant value. However, medium changes that do not alter the ionic strength may cause variations in the water activity that affect the distribution of an acid in an enhanced way, since the water activity must be raised to a power that quite often assumes rather high values. This is best explained with an example. In 1·0M hydrochloric acid, iron(III) exists predominantly as the monochloride[25] that is hydrated with five water molecules. However it is the tetrachloride, $FeCl_4^-$, that is extracted as acid by most of the common extractants. It is generally believed that the anion $FeCl_4^-$ is not hydrated. The distribution must therefore be formulated as:

$$H(H_2O)_y^+{}_{org} + FeCl_4^-{}_{org} + (3j+5+i-y)\,H_2O \rightleftharpoons H(H_2O)_i^+ + FeCl(H_2O)_5^{2+} + 3\,Cl(H_2O)_j^-$$

The water activity enters the distribution equilibrium with a power that easily exceeds 10 and eventually assumes a value closer to 20 if it is assumed that the hydrogen ion is capable of carrying its full aqueous-phase hydration shell into

the organic phase. It is not well established how many water molecules are needed to hydrate the free chloride ion in aqueous solutions, but there is evidence in the literature that j assumes values around 3–4.[21,26–28] It is such an effect, in combination with others, that causes the slope to be too high in the distribution plot representing the extraction of iron(III) from 1·0M hydrochloric acid by MIBK (Fig. 4).

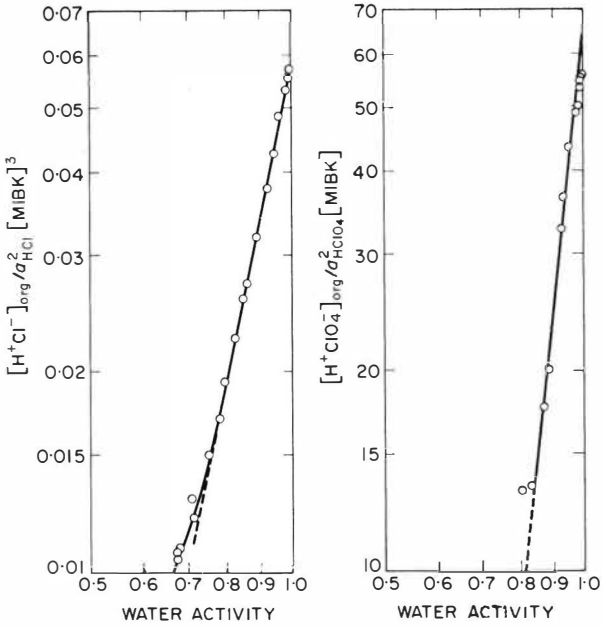

FIG. 8. *Determination of the difference between the hydration number of the equilibrium species in an aqueous and MIBK phase*

Activities of HCl taken from Harned & Owen;[29] activities of $HClO_4$ taken from Pearce & Nelson[30]

Conclusions

In this paper, an attempt has been made to stress and illustrate the difficulties that are involved in the application of the most widely used method, the slope analysis. Examples have been chosen that would result in wrong conclusions if the effects of the ionic hydration and solvation were not properly considered in the interpretation of solvent extraction data. It has also been demonstrated that solvent extraction techniques are a powerful method for the determination of association numbers and association orders of the species involved in the extraction. The study of the solutes present in the organic phase not only provides information on extraction mechanisms, but also provides a tool to gain information on association processes that are not limited to non-aqueous solutions. However, owing to the high dielectric constant of water, the electrovalent interactions are overshadowed by covalent and ion–dipole interactions, and become important only at high electrolyte concentrations, where the dielectric constant of the aqueous solutions breaks down to values that usually characterise organic solvents. In this concentration range, other effects are observed simultaneously with the ion association and it is a tedious task to separate hydration effects from those caused by ion associates. As a result, only little is known on the ion association of univalent ions in general and strong acids in particular in aqueous solutions.

Appendix I

In the following description, only the ionic hydration is considered and the solvation by the organic solvent is neglected. Such a treatment is incomplete

as it is often found that the aqueous-phase hydrogen ion is extensively solvated. However, this description is attractive because of its great simplicity and the results are not altered qualitatively and in addition it can easily be extended to include the solvation effects.

Square brackets are used to denote concentrations. Therefore the derived equilibrium constants represent concentration constants rather than thermodynamic quantities, but the true constants can be derived on introduction of the corresponding activity coefficients.

The hydrated hydrogen ion and anion exist in equilibrium with less hydrated species and formally this equilibrium includes the bare unhydrated ions as well as all the species with hydration numbers up to the maximum value m for the hydrogen ion and n for the anion. The predominant ions are, however, characterised by the hydration numbers p and q, respectively.

According to the theory of Fuoss & Kraus,[5–11] each particularly hydrated hydrogen ion, $H(H_2O)_i^+$, must be combined with each of the particularly hydrated anions, $X(H_2O)_j^-$, to form the corresponding ion pair and triple ion formation constant:

$$H(H_2O)_i^+ + X(H_2O)_j^- \rightleftharpoons HX(H_2O)_{i+j} \quad (1)$$

$$HX(H_2O)_{i+j} + X(H_2O)_j^- \rightleftharpoons HX_2(H_2O)_{i+2j}^- \quad (2)$$

$$HX(H_2O)_{i+j} + H(H_2O)_i^+ \rightleftharpoons H_2X(H_2O)_{2i+j}^+ \quad (3)$$

Each combination is characterised by a definite interionic distance $r_{i,j}$ which, together with the dielectric constant of the medium, determines the magnitude of the ion pair and triple ion formation constants. Because of the same interionic distance, the triple anion and triple cation formation constant must be the same as indicated in Equation (5):

$$K'_{A,i,j} = \frac{[HX(H_2O)_{i+j}]}{[H(H_2O)_i^+][X(H_2O)_j^-]} \quad (4)$$

$$K'_{T,j} = \frac{[HX_2(H_2O)_{i+2j}^-]}{[HX(H_2O)_{i+j}][X(H_2O)_j^-]} = K'_{T,i}$$

$$= \frac{[H_2X(H_2O)_{2i+j}^+]}{[HX(H_2O)_{i+j}][H(H_2O)_i^+]} \quad (5)$$

The ion pair and triple ion formation constants, $K'_{A,i,j}$, $K'_{T,i}$ and $K'_{T,j}$, assume increasing values when i and j are decreased because the interionic distance $r_{i,j}$ is smaller for less hydrated ions. However, the more i and j deviate from the hydration numbers of the predominant unassociated ions, p and q, respectively, the smaller will be the concentrations of the simple ions $H(H_2O)_i^+$ and $X(H_2O)_j^-$ relative to the total electrolyte concentration. The ion associates can be significantly formed only if the effect of the increasing formation constant compensates the effect of the relatively small concentrations that characterise the less hydrated species. In general, the association constants are expressed in terms of the macroscopic ion concentrations, $[H^+]$ and $[X^-]$ rather than in terms of the concentrations of the hydrates, $[H(H_2O)_i^+]$ and $[X(H_2O)_j^-]$ that are formally involved in the observed ion association. Equations (6)–(9) describe the relation between these different concentrations and the more convenient association constants are defined by Equations (10)–(12):

$$[H^+] = \sum_{i=0}^{m} [H(H_2O)_i^+] \quad (6)$$

$$[X^-] = \sum_{j=0}^{n} [X(H_2O)_j^-] \quad (7)$$

$$\alpha_i = \frac{[H(H_2O)_i^+]}{[H^+]} \quad (8)$$

$$\alpha_j = \frac{[X(H_2O)_j^-]}{[X^-]} \quad (9)$$

$$K_{A,i,j} = \frac{[HX]}{[H^+][X^-]} = K'_{A,i,j} \cdot \alpha_i \cdot \alpha_j \quad (10)$$

$$K_{T,j} = \frac{[HX_2^-]}{[HX][X^-]} = K'_{T,j} \cdot \alpha_j \quad (11)$$

$$K_{T,i} = \frac{[H_2X^+]}{[HX][H^+]} = K'_{T,i} \cdot \alpha_i \quad (12)$$

The corresponding association constants of the predominant ions are $K_{A,p,q}$ $(=K'_{A,p,q} \cdot \alpha_p \cdot \alpha_q)$, $K_{T,p}$ $(= K'_{T,p} \cdot \alpha_p)$ and $K_{T,q}$ $(= K'_{T,q} \cdot \alpha_q)$. It is the value of these quantities that must be outweighed by the effects of the less hydrated species before ion association processes can be observed in which water is released from the hydration shell of the original ions. Only if these conditions are fulfilled can the concentration ratio $R = [HX_2^-]/[H_2X^+]$ assume values that deviate strongly from unity. R can be calculated from Equation (13) if it is assumed that HX is the only electrolyte present in the solution.

$$\frac{[HX_2^-]}{[H_2X^+]} = \frac{K'_{T,j} \cdot \alpha_j [HX][X^-]}{K'_{T,i} \cdot \alpha_i [HX][H^+]} = \frac{\alpha_j [X^-]}{\alpha_i [H^+]} = \frac{[X(H_2O)_j^-]}{[H(H_2O)_i^+]}. \quad (13)$$

The concentration of the predominant ion species can be expressed by Equations (14) and (15), which yield the relation given by Equation (16) on combination with Equations (6)–(9) and (13).

$$[H(H_2O)_p^+] = [H(H_2O)_i^+] \cdot \beta_{p,i} \cdot a_w^{p-i} \quad (14)$$

$$[X(H_2O)_q^-] = [X(H_2O)_j^-] \cdot \beta_{q,j} \cdot a_w^{q-j} \quad (15)$$

$$\frac{[HX_2^-]}{[H_2X^+]} = \frac{\alpha_j [X^-]}{\alpha_i [H^+]} = \frac{\alpha_q [X^-]}{\alpha_p [H^+]} \cdot \frac{\beta_{p,i}}{\beta_{q,j}} a_w^{p+j-q-i} \quad (16)$$

$\beta_{p,i}$ and $\beta_{q,j}$ denote the cumulative constants of the aquo complexes, describing the formation of the predominant hydrates, $H(H_2O)_p^+$ and $X(H_2O)_q^-$, in terms of the species, $H(H_2O)_i^+$ and $X(H_2O)_j^-$, that are involved in the formation of the triple ions, $HX_2(H_2O)_{i+2j}^-$ and $H_2X(H_2O)_{2i+j}^+$, respectively.

From Equation (16) it can be seen that the concentration ratio R is influenced by three different quantities, the relative fractional abundance of the predominant ion species, the relative strength of the hydrated ions, and the water activity. Of these, the ratio of the cumulative hydration constants $\beta_{p,i}/\beta_{q,j}$ is able to produce extreme values of R. In general, the hydrogen ion is capable of binding water and solvent molecules with greater strength than the anion. This is particularly so for large, complex anions, as opposed to small, atomic anions. For these acids, the concentration ratio R becomes much larger than 1·0. In this case, the triple anion is formed long before the triple cation can be observed.

Appendix II

The distribution of the unassociated and associated species can be expressed in terms of the appropriate distribution constant, K_D, the aqueous-phase acid activity, a_{HX}, the water activity, a_w, and the solvent activity, a_s, according to Equations (17), (18) and (20).

Dissociated species:

$$[H^+]_{org}\,[X^-]_{org} = K_{D1}\,a_{HX}^2\,a_w^{\Delta H_1}\,a_s^{\Delta S_1} \qquad (17)$$

Ion pair:

$$[H^+X^-]_{org} = K_{D2}\,a_{HX}^2\,a_w^{\Delta H_2}\,a_s^{\Delta S_2} \qquad (18)$$

If $[H^+]_{org} = [X^-]_{org}$,

$$\frac{[H^+X^-]_{org}}{[X^-]_{org}} = \frac{K_{D2}}{K_{D1}} \cdot a_w^{\Delta H_2 - 1}\,a_s^{\Delta S_2 - 1}\,[H^+]_{org} \qquad (19)$$

If the dissociated and ion-paired acid forms are solvated and hydrated to the same extent, the intersection of the slopes 1 and 2 of a logarithmic plot is given by Equation (20):

$$\frac{[H^+X^-]_{org}}{[X^-]_{org}} = 1{\cdot}0 = \frac{K_{D2}}{K_{D1}}\,[H^+]_{org} = 1/2\,K_A\,[HX]_{org,\,total} \qquad (20)$$

Triple ion:

$$[H^+]_{org}\,[HX_2^-]_{org} = K_{D3}\,a_{HX}^4\,a_w^{\Delta H_3}\,a_s^{\Delta S_3} \qquad (21)$$

and:

$$\frac{[HX_2^-]_{org}}{[X^-]_{org}} = \frac{K_{D3}}{K_{D1}} \cdot a_{HX}^2\,a_w^{\Delta H_3 - 1}\,a_s^{\Delta S_3 - 1} \qquad (22)$$

If the two different anions are solvated and hydrated to the same extent the intersection of the slope 1 and 2 of a logarithmic distribution plot is given by Equation (23):

$$\frac{[HX_2^-]_{org}}{[X^-]_{org}} = 1{\cdot}0 = \frac{K_{D3}}{K_{D1}} \cdot a_{HX}^2 \qquad (23)$$

In these equations ΔH and ΔS denote the difference of the hydration and solvation numbers of the corresponding equilibrium species.

Acknowledgment

This research was performed under the auspices of the U.S. Atomic Energy Commission.

References

[1] Widmer, H. M., *158th natn Meet. Am. chem. Soc.*, New York, 1969; *Abstr. phys. Chem.*, 1969, No. 84
[2] Widmer, H. M., *J. phys. Chem., Ithaca*, 1970, **74**, 3251
[3] *Idem, ibid.*, 1970, **74**, 3618
[4] *Idem, ibid.*, in preparation
[5] Fuoss, R. M., & Kraus, C. A., *J. Am. chem. Soc.*, 1933, **55**, 21
[6] *Idem, ibid.*, 476
[7] *Idem, ibid.*, 1019
[8] *Idem, ibid.*, 2387
[9] *Idem, ibid.*, 3614
[10] *Idem, ibid.*, 1957, **79**, 3301

[11] *Idem, ibid.*, 1958, **80,** 5059
[12] Broene, H. H., & de Vries, T., *J. Am. chem. Soc.*, 1947, **69,** 1644
[13] Martin, D. L., & Rossotti, F. J. C., *Proc. chem. Soc.*, 1959, p. 60
[14] Selvaratnam, M., & Spiro, M., *Trans. Faraday Soc.*, 1965, **61,** 360
[15] Pethybridge, A. D., & Prue, J. E., *Trans. Faraday Soc.*, 1967, **63,** 2019
[16] Tuck, D. G., *Prog. inorg. Chem.*, 1968, **9,** 161, and references therein
[17] Marcus, Y., and Kertes, A. S., 'Ion exchange and solvent extraction of metal complexes', 1969, p. 673 and references therein (New York: Wiley-Interscience)
[18] Kolthoff, I. M., Bruckenstein, S., & Chantooni, M. K., *J. Am. chem. Soc.*, 1961, **83,** 3927, 5051
[19] Maddock, A. G., Smulek, W., & Tench, A. J., *Trans. Faraday Soc.*, 1962, **58,** 923
[20] Everett, D. H., & Coulson, C. A., *Trans. Faraday Soc.*, 1940, **36,** 633
[21] Azzam, A. M., *Z. Elektrochem.*, 1954, **58,** 889
[22] Azzam, A. M., *Can. J. Chem.*, 1960, **38,** 2203
[23] Buckingham, A. D., *Discuss. Faraday Soc.*, 1957, **24,** 151
[24] Bernal, J. D., & Fowler, R. H., *J. chem. Phys.*, 1933, **1,** 515
[25] Rowley, J. K., & Sutin, N., *J. phys. Chem., Ithaca*, 1970, **74,** 2043
[26] Brady, G. W., *J. chem. Phys.*, 1958, **28,** 464
[27] Rutgers, A. J., & Hendrikx, Y., *Trans. Faraday Soc.*, 1962, **58,** 2184
[28] Rutgers, A. J., Rigole, W., & Hendrikx, Y., *Chem. Weekbl.*, 1963, **59,** 33
[29] Harned, H. S., & Owen, B. B., 'The physical chemistry of electrolyte solutions', 3rd edn, 1958, p. 716 (New York: Reinhold Publ. Corp.)
[30] Pearce, J. N., & Nelson, A. F., *J. Am. chem. Soc.*, 1933, **55,** 3075

Salting-out in extraction systems

by Yu. G. Frolov and G. I. Nasonova
D. I. Mendeleev Institute of Chemical Technology, Moscow, U.S.S.R.

The effect of salting-out agents on the extraction of sulphuric acid with N-octylaniline and the separation of uranium and thorium using tri-n-octylamine is discussed.

For the bisulphate salting-out agents used for sulphuric acid the effect decreased in the order lithium bisulphate > sodium bisulphate > ammonium bisulphate. The system $UO_2(NO_3)_2$–$Th(NO_3)_4$–TOA–$LiNO_3$ is used to show that the separation of uranium and thorium is influenced by all the salting-out effects.

Introduction

RECENT WORK[1] ESTABLISHED the equality of osmotic coefficients of components in isopiestic solutions without significant interaction between components. This allowed Zdanovsky's rule which was found empirically in 1936[2] to be derived and it could be shown that this rule is more general and can be applied to systems of electrolytes without common ions. Moreover, in the systems where Zdanovsky's rule is applicable it is possible to calculate not only the properties of multicomponent solutions from properties of binary solutions and the thermodynamic properties of components (activity coefficients of components can be calculated from Mikulin's equation[3]) but also osmotic coefficients and activity coefficients of ions.[4]

Some authors[5,6] considered that ideal mixing of isopiestic solutions is necessary for these systems, but in fact it is sufficient if the excess free energy of mixing is zero,[7,8] that is if

$$\Delta G^{E} = 0 \text{ or } \Delta H^{E} - T\Delta S^{E} = 0 \,. \qquad (1)$$

where ΔG^{E} = excess free energy of mixing,
ΔH^{E} = excess enthalpy of mixing,
ΔS^{E} = excess entropy of mixing.

When these rules and also the salting-out equation are applied to heterogeneous systems[9,10] it is possible to calculate the contributions of salting-out effects and their influence on the separation of electrolytes for extraction. This paper will show the influence of salting-out agents on the extraction of sulphuric acid with *N*-octylaniline (OA) and the separation of uranium and thorium using tri-n-octylamine (TOA).

Theoretical

The extraction isotherm for sulphuric acid extracted with a 0·355M solution of OA in benzene is given in Fig. 1. Because sulphuric acid dissociates mainly into bisulphate ions, the salting-out agent was lithium bisulphate which probably interacts only slightly with sulphuric acid.

In the following calculations it is assumed that the mixed aqueous solution behaves according to Zdanovsky's rule and that the activity coefficients of components can be calculated in accordance with Mikulin's equation.[3] Also a knowledge of the dependence of water activity in binary solutions upon electrolyte concentration is necessary for these calculations. These data, for $LiHSO_4$ solutions, could not be found in the literature. Therefore, osmotic coefficients of $LiHSO_4$ were calculated from those of the ions[4] used in the following scheme:

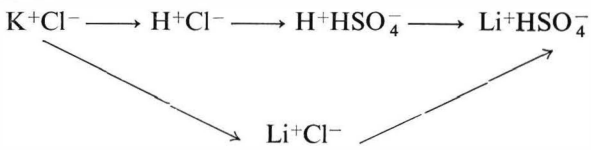

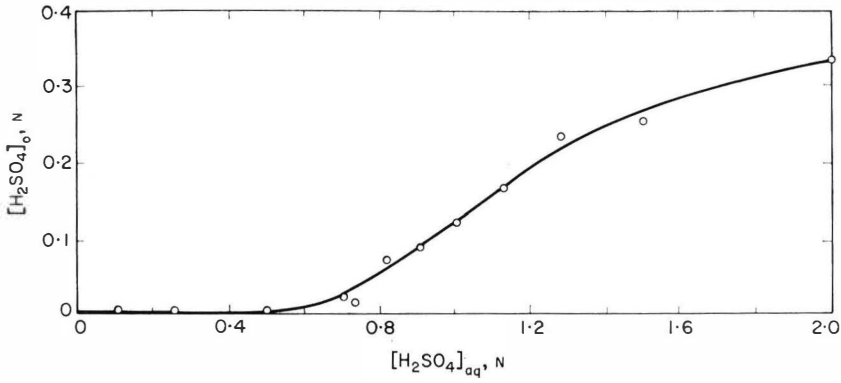

FIG. 1. *Extraction isotherm for sulphuric acid with a 0·355 mole/l solution of n-octylamine in benzene*

A stoicheiometric coefficient, $\nu = 2$, was used in the calculation of the osmotic coefficient and the activity coefficient of sulphuric acid and lithium bisulphate.

Salting-out effects were calculated for the reaction

$$n\bar{A} + B \rightleftarrows \overline{A_nB} \qquad (2)$$

It has been shown: [8,9]

$$W_{gen} = \left(\frac{m_{s1}}{m_{s2}}\right)^{\nu-1} \left(1 + \frac{\nu_{-salt}\, m_{salt}}{\nu_-\, m_{s1}}\right)^{\nu_-} \left(\frac{\gamma_{\pm S_1}}{\gamma_{\pm S_2}}\right)^{\nu} \cdot \frac{\bar{\gamma}_{A_nB_2}}{\bar{\gamma}_{A_nB_1}} \cdot \left(\frac{\bar{a}_{A_1}}{\bar{a}_{A_2}}\right)^{n}$$

$$= W_c \cdot W_{ci} \cdot W_{\gamma\pm} \cdot \overline{W}_\gamma \cdot \overline{W}_A \qquad (3)$$

where, (i) $W_{gen} = D_1/D_2$ is the general salting-out effect defined as the ratio of the distribution coefficient of compound B with salting-out agent D_1 to that of B without salting-out agent D_2 (subscript 1 denotes systems with salting-out agents, whereas subscript 2 denotes systems without them); (ii) $\left(\frac{m_{s1}}{m_{s2}}\right)^{\nu-1} = W_c$ is the concentration effect due to the alteration of the equilibrium concentration m_B in the aqueous phase; (iii) $\nu = \nu_+ + \nu_-$ are stoicheiometric coefficients of compound B, its cation and anion respectively; (iv) $\left(1 + \frac{\nu_{-salt}\, m_{salt}}{\nu_-\, m_{s1}}\right)^{\nu_-} = W_{ci}$ is an effect of the common ion in the aqueous phase, ν_{-salt} being the stoicheiometric coefficient of the anion of the salting-out agent and m_{salt} being the concentration of the salting-out agent; (v) $(\gamma_{\pm 1}/\gamma_{\pm 2})^{\nu} = W_{\gamma\pm}$ is an effect due to the alteration of the activity coefficients of compound B in the aqueous phase and is calculated according to Mikulin's equation; (vi) $\frac{\bar{a}^n_{A_1}}{\bar{a}^n_{A_2}} = \overline{W}_A$ is an effect due to the alteration of the activity of the extractant; in this work activities were considered equal to concentrations of either 'free' TOA in the extraction of H_2SO_4 or nitrate of TOA in the extraction of the elements; (vii) $\frac{\bar{\gamma}\, A_nB_1}{\bar{\gamma}\, A_nB_2} = \overline{W}_\gamma$ is an effect due to the alteration of activity coefficients of complexes formed in the organic phase and this effect was determined from experimental W_{gen} and other calculated effects.

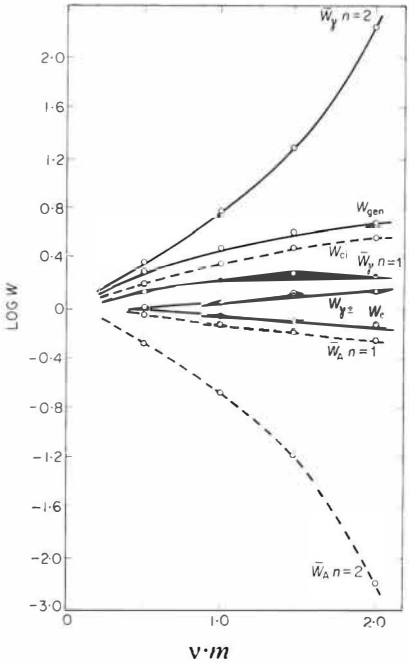

FIG. 2. *Effects of the salting-out of sulphuric acid by lithium bisulphate on extraction with 0·355 mole/l solution of n-octylamine in benzene*

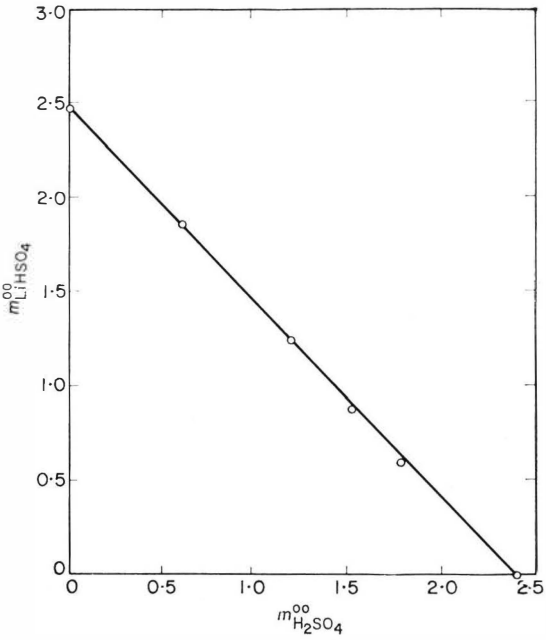

FIG. 3. *Isotherm-isobar of the sulphuric acid–lithium bisulphate–water system at water activity 0·87*

The salting-out effects on the extraction of sulphuric acid with solutions of OA in benzene at various concentrations of lithium bisulphate are presented in Fig. 2. The initial concentration of sulphuric acid was 0·5M. The effects W_{ci} and $W_{\gamma\pm}$ are positive. The salting-out effects in the organic phase were determined when formation of the bisulphate ($n=1$) and the sulphate ($n=2$) of OA was presumed. $\overline{W}_{\gamma}$ and $\overline{W}_{A}$ are very large for $n=2$ whereas the description of this system is more realistic when $n=1$. Hence it is possible to presume that OA forms mainly bisulphate because it is a weaker base than TOA.

The bisulphate of OA is able to associate and its association increases when its concentration increases. This explains positive effects of salting-out owing to alteration of activity coefficients of bisulphate of OA in the organic phase (salting-in for the organic phase). The negative sign for the effects $\overline{W}_{c}$ and $\overline{W}_{A}$ is reasonable. The other effects are positive and the line of the general effect, which is the sum of all the constituents, is higher than the other lines.

In order to calculate the activity coefficients in mixtures of sulphuric acid and alkali metal bisulphates, the water activity has been measured by an isopiestic technique. The equipment and the conditions have been reported elsewhere.[11] The results have shown that the isotherm–isobar of the system sulphuric acid–lithium bisulphate, is practically a straight line (Fig. 3). The isotherms–isobars of the sulphuric acid–sodium or ammonium bisulphate systems are similar.

Activity of water is a function of ion concentration of electrolytes:

$$a_{H_2O} = f(\nu \cdot m)_{\text{electrolyte}}$$

Deviations of these systems from Zdanovsky's rule are not more than 3%. A discrepancy of about 0·5% between calculated and experimental lines for the lithium bisulphate results gives a difference of about 1·5% between the activity coefficients of sulphuric acid in mixtures with lithium bisulphate. The salting-out effect of sulphuric acid decreases in the order: lithium bisulphate > sodium bisulphate > ammonium bisulphate, i.e. with decrease of their osmotic coefficients.

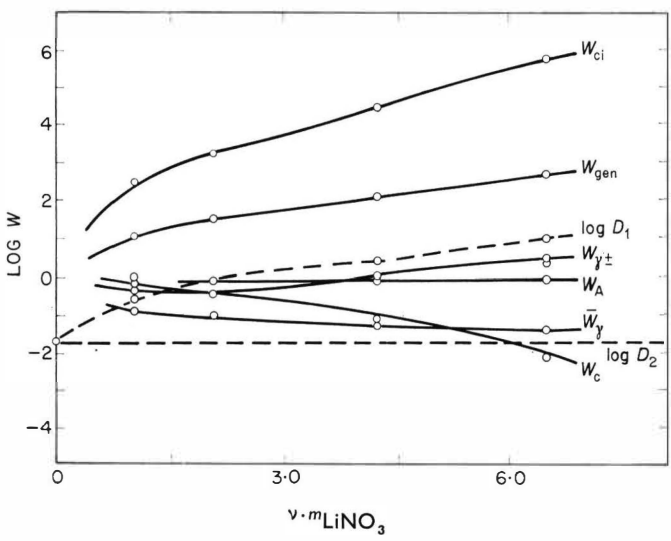

FIG. 4. *Salting-out effects of uranyl nitrate on extraction with a 0·4 mole/l solution of TOA in benzene from solutions containing nitrates of thorium and lithium*

The system $UO_2(NO_3)_2$–$Th(NO_3)_4$–TOA–$LiNO_3$ is given here as an example of the influence of salting-out on the separation of elements. The initial concentrations of the elements were 5 g/l, that of TOA in benzene was 0·4M and pH = 2·0. The concentration of lithium nitrate varied from 0 to 3·5M. The calculated effects of salting-out of uranyl nitrate and thorium nitrate in mixtures are shown in Figs 4 and 5; the absence of mutual interaction is assumed. Effects on the separation for each salting-out system are given in Fig. 6. They were calculated according to equation:

$$Q_{gen} = \frac{W^{Th}_{gen}}{W^{U}_{gen}} = \frac{W^{Th}_{c}}{W^{U}_{c}} \cdot \frac{W^{Th}_{ci}}{W^{U}_{ci}} \cdot \frac{W^{Th}_{\gamma\pm}}{W^{U}_{\gamma\pm}} \cdot \frac{\overline{W}^{Th}_{\gamma}}{\overline{W}^{U}_{\gamma}} \cdot \frac{\overline{W}^{Th}_{A}}{\overline{W}^{U}_{A}} = Q_c \cdot Q_{ci} \cdot Q_{\gamma\pm} \cdot \overline{Q}_{\gamma} \cdot \overline{Q}_{A} \quad . \quad (4)$$

Separation of the elements is influenced by all the salting-out effects but the effects of common ion and activity coefficients in the organic and aqueous phases are the most important. The effect of the common ion is more important for thorium than for uranium because of the difference in the valences between these two elements and because of the better extraction of thorium which occurs when a salting-out agent is absent. The separation becomes worse owing to the alteration of the activity coefficients of components in the aqueous phase where the activity coefficients of thorium decrease more strongly in the presence of salting-out agent than do those of uranium. The difference between the stoicheiometric coefficients and the effect of the organic phase is essential. The result is that an improvement in the separation of the elements is obtained when the salting-out agent is added.

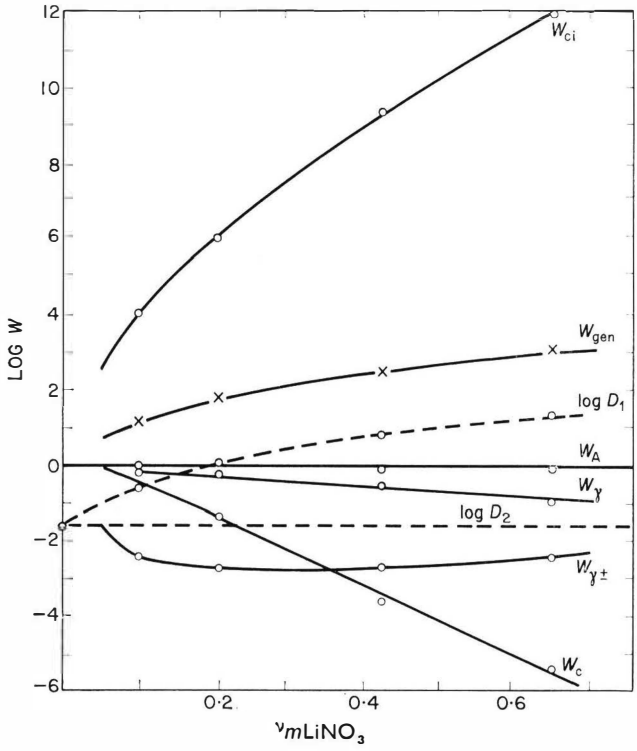

FIG. 5. *Salting-out effects of thorium nitrate on extraction with a 0·4 mole/l solution of TOA in benzene from solutions containing uranyl and lithium nitrates*

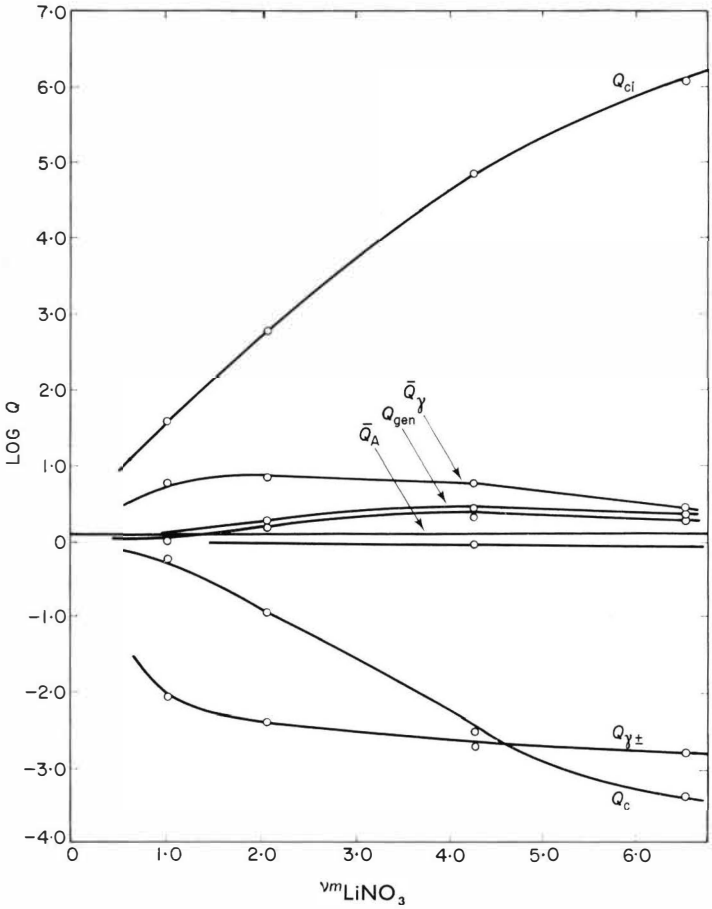

FIG. 6. *Effects on separation of uranyl and thorium nitrates, due to their salting-out by lithium nitrate, on extraction with a 0·4 mole/l solution of TOA in benzene*

In conclusion, this approach allows an appreciation of the influence of various factors on the separation when salting-out agents have been added to the extraction systems.

References

[1] Frolov, Yu. G., & Gavrilov, N. V., *Trudȳ mosk. khim.-tekhnol. Inst.*, 1967, **56**, 282; 1968, **58**, 55; *Atomn. Energ.*, 1968, **25**, (1), 39

[2] Zdanovsky, A. V., *Trudȳ sol. Lab. Akad. Nauk SSSR*, 1936, **6**, 1

[3] Mikulin, G. I., Abstr. of paper presented at the Ukrainian Republican Conf. on Phys. Chem., Kiev, USSR, 1962, p. 177

[4] Frolov, Yu. G., & Nikolaev, V. P., *Trudȳ mosk. khim.-tekhnol. Inst.*, 1968, **58**, 64

[5] Vdovenko, V. M., & Rjazanov, M. A., *Radiokhimiya*, 1965, **7**, 442

[6] Kirgintsev, A. N., & Lukyanov, A. V., *Zh. fiz. Khim.*, 1970, **44**, 1766

[7] Frolov, Yu. G., & Nikolaev, V. P., *Trudȳ mosk. khim.-tekhnol. Inst.*, in press

[8] Frolov, Yu. G., Nikolaev, V. P., Vlasenko, K. K., & Karapetjyants, M. Ch., *Izv. Vysch. Schkoly. Khim. khim. tekhnol.*, in press

[9] Frolov, Yu. G., *Trudȳ mosk. khim.-tekhnol. Inst.*, 1968, **58**, 60

[10] Frolov, Yu. G., Nasonova, G. I., Belousova, L. A., & Apter, I. D., *Atomn. Energ.*, 1969, **26**, 423

[11] Nikolaev, V. P., & Frolov, Yu. G., *Trudȳ mosk. khim.-tekhnol. Inst.*, in press

SESSION 1B

DROPS AND DISPERSIONS

CHAIRMAN

Dr. H. Sawitowski

SECRETARIES

Dr. L. Hoogschagen
Dr. L. J. Austin

Continuous phase backmixing associated with the wake of the dispersed phase droplet

by M. P. Wilson and G. V. Jeffreys

Dept. of Chemical Engineering, University of Aston in Birmingham, Gosta Green, Birmingham, U.K.

An investigation into the geometry of the closed loop vortex at the rear of a moving droplet, has resulted in the observation of a relationship between the droplet Reynold's number (Re) *and the vortex volume of the form:*

$$(Re) = 17 + 186 \cdot 2 \left(\frac{6V}{\pi d^3}\right) - 42 \cdot 3 \left(\frac{6V}{\pi d^3}\right)^2$$

This relationship is shown to be valid for droplets moving in the regime below a critical value of the droplet Reynold's number which has been related to the development of internal circulation of the drop.

The pattern of vortex development above this critical (Re) *value is discussed in relation to a proposed mechanism of surfactant loss owing to the proximity of the separation ring and the leading edge of the immobile cap.*

Introduction

SEVERAL AUTHORS[1–3] HAVE discussed the backmixing characteristics of spray columns, and the relative importance of the entrainment of the continuous phase by the established flow pattern outside the individual dispersed phase droplets.

Investigations[4,5] of the continuous phase concentration discontinuity, at the entrance of that phase, in counterflow spray columns, have indicated that a number of factors combine to effect this observed backmixing.

The important mechanisms of continuous phase backmixing are: recirculation of the continuous phase by induction and/or displacement; release of the associated vortex at droplet arrest; mass transfer in the flocculation zone.

Jensen *et al.*[6] discussed the role of vortex entrainment in spray columns used in the continuous hydrolysis of animal fats and oils. Predicted mass transfer coefficients were exceeded in practice, and the authors suggested that this may be due to the raffinate recycle effected by the wake patterns assisting in the initiation of the reaction.

Letan & Kehat,[7,8] in a study of the mechanics of a spray column heat exchanger, concluded that the observed backmixing could wholly/partly be considered to be due to vortex entrainment. A significant observation from this work, however, was that during a period immediately after droplet release from the nozzle, the measured transfer of heat from the dispersed phase droplet was not recorded as a transfer to the bulk of the continuous phase. The conclusion that transfer during this period was totally into the closed loop vortex, together with the realisation that the mass and heat transfer coefficients immediately after droplet release have been observed to be very much higher than those observed during steady state progression, indicates the wider importance of the study of wake characteristics.

The single drop

A full review of the literature concerning the mechanics and transfer characteristics of drops in liquid/liquid systems, and the effect of surfactant material upon droplet performance, is considered beyond the scope of this paper.

An extensive review by Gal-Or *et al.*[9] covers fundamental work in many aspects of bubble and droplet phenomena. Baker[10] has discussed the mechanics and mass transfer characteristics of single drops and spheres, and coverage of experimental and theoretical studies of the wake of a spherical body is found in the work by Torobin & Gauvin.[11]

Magarvey & Bishop[12] have photographed and classified (Table I) the wakes of immiscible spheres corresponding to $0 < (Re) < 2500$. It was found that

identical wake patterns correspond to approximately the same (*Re*) independent of the system physical properties. They noted that the exact transition values of (*Re*) could not be precisely stated, as these depend upon the degree of drop deformation.

TABLE I

Class	(*Re*) range	Character
I	0–210	Single thread
II	210–270	Double thread
III	270–290	Double thread with waves
IV	290–410	Procession of vortex loops
V	410–700	Double row of vortex rings
VI	700–2500	Asymmetrical wake

Garner *et al.*,[13] in a study of the characteristics of solid spheres, reported that oscillation and the shedding of material from the vortex did not initiate until a value (*Re*) = 450.

The linear dimensions of the vortex at the rear of a solid sphere were measured by Taneda.[14] He observed a linear relationship between the sphere (*Re*) and the ratio of sphere diameter to vortex length. Jensen[15] developed a relaxation technique for the solution of the Navier-Stokes equation for viscous flow around a sphere at low (*Re*) (< 40). The theoretical value for the initiation of boundary layer separation was found to be (*Re*) = 17, compared with Taneda's experimental value of (*Re*) = 24.

Tayeban,[16,17] in an investigation of mass transfer from single drops, calculated the concentration of transfering material in the associated closed loop vortex. Use of a variable length transfer column allowed the determination of the mass transfer that would occur for zero column length. Elimination of the transfer that occurred during drop formation and during coalescence, allowed this zero length value to be equated to the total vortex content. In the calculation of the concentration in the vortex, the vortex volume was approximated by the volume of a cylinder surmounted by a cone.

Hendrix *et al.*[18] attempted a calculation of the volume of the vortex pattern for drops of various systems. Immiscible drops, formed in a dyed continuous phase field, were allowed to travel for various lengths through an un-dyed field before being collected and withdrawn, together with the dyed volumes of vortex regions. The vortex volume was calculated from the value of the concentration of dye in the total volume of withdrawn continuous phase, it being assumed that the vortex concentration at capture was equal to the concentration in the initial dyed field. This assumption appeared to be valid for drops having a value of (*Re*) below that at which drop oscillation was observed to initiate. A linear relationship was shown to hold between droplet diameter and vortex volume for non-oscillating drops. At the initiation of oscillation, however, vortex shedding resulted in a high degree of scatter in the data obtained.

Experimental

Equipment and materials

Observations of the flow pattern and velocity of translation for single drops were carried out in a glass-sided column of 10 cm square cross-section, and a maximum path length of 1·5 m (Fig. 1). The edges of the glass faces of the cell were precisely ground and were clamped on to PTFE strip, thus avoiding the necessity for a plasticised sealant. The base of the cell was sealed in a similar manner.

The desire for confidence in purity in this work required that all materials of construction should be compatible with the chemical reagents used during experimentation, and with those used in the involved cleaning procedure. The

PTFE was of an electrical grade containing no plasticiser. The compatibility of this material with a number of the reagents used was indicated by chromatographic analysis of a reagent sample, both before and after refluxing with the PTFE.

Introduction of the dispersed phase into the base of the cell was through a stainless steel capillary, to an interchangeable hypodermic needle. Release of the dispersed phase droplet was effected by the magnetic impulse system, as indicated in Fig. 1.

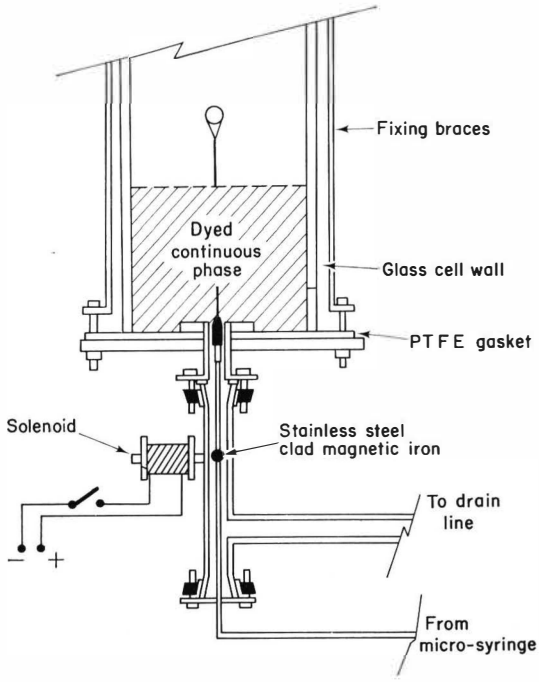

FIG. 1. *Base section of observation column indicating drop release system*

All reagents used throughout this work were of 'Analar' grade, or were redistilled from general purpose reagents (G.P.R. grade) when the 'Analar' grade was not available. Distilled water was the aqueous phase throughout.

For systems in which a tracer dye was required for flow pattern visualisation, the dyes used were chosen for their non-surfactant characteristics, these characteristics being confirmed during the experimentation (Table II).

TABLE II

Tracer dyes used during experimentation

Continuous phase	Dye
Aqueous	5% potassium permanganate solution in water
Organic	Calco Oil Red [19]

Photographic observations were made using both still and ciné equipment.

For the still photographs: Asahi Pentax camera with 135 mm Prinz Galaxy telephoto lens. Kodak Panatomic–X, 35 mm, black and white film, FX 135–36 (ASA/BS 32).

For the ciné photographs: Beaulieu, R–16 ciné camera with 75 mm Angenieux telephoto lens. Kodak Plus–X, 16 mm negative film.

Experimental procedure

All parts of the equipment that would be in contact with the continuous or dispersed phases were thoroughly cleaned following the procedure outlined by Lawson.[20]

The assembled cell, with a suitable charge of continuous phase and dye, remained undisturbed in the constant temperature environment for a suitable period to allow for dynamic and thermal equilibrium. Most tests were carried out at 25°C, a temperature which could be maintained to an accuracy of $\pm 0 \cdot 2$°C in the system.

A volume of dyed continuous phase was allowed to flow from the reservoir at a regulated rate such that the minimum disturbance was caused in the cell. It was found possible to obtain a fairly sharp interface between the dyed and undyed sections of the continuous phase, without the necessity of a diffuser similar to the type used by Hendrix *et al.*[18] in a similar approach. This interface was maintained at a level 8 cm above the hypodermic tip for all observations.

The desired volume of dispersed phase liquid was delivered from a microsyringe, through the capillary, to form a droplet at the hypodermic nozzle, from where it was detached by an impulse from the magnetic system.

The time taken for the drop to travel a distance between two set positions, 80 cm apart, was measured using an accurate stop-watch. The lower set position was 40 cm above the nozzle tip, a distance considered suitable for the damping of disturbances caused by the method of droplet formation and release, and for the terminal velocity to have been attained.

Each drop was photographed at the mid-point of its timed travel (80 cm above the nozzle tip). The drop size was indicated by comparison with an etched glass graticule attached to the rear face of the cell. The parallax effect was alleviated by use of a telephoto lens with the camera, thus allowing the plane of the film to be $1 \cdot 25$ m from the mid-plane of the cell.

Observations involving the ciné camera were carried out in a similar manner. The camera, however, was supported on the platform of a precisely balanced pulley system, thus allowing an easy vertical movement. Distance of travel in this case was indicated by a scale fixed to the rear face of the cell.

The ciné technique was also adopted for runs in which the dyed continuous phase was contaminated with $4 \cdot 0$ ppm of sodium lauryl sulphate. The development of the vortex and the droplet mechanics were then observed after emergence from the dyed phase, and during the drop's progress through the uncontaminated continuous field.

Analyses of droplet and vortex characteristics were made by projection of the negative using standard 16 mm or 35 mm equipment. Where necessary the profile of the drop and its associated flow pattern were traced on to the projection screen, from where measurements were taken. The areas of the closed loop vortices were determined using a standard type of planimeter.

Results

The six classifications of wake proposed by Magarvey *et al.*[12] have been observed in this work. The main interest, however, has been centred upon the closed loop vortices classified as groups I, II and III.

Although the property of the vortex most relevant to this study is its volume, a convenient variable was found to be the ratio of the areas of the drop and vortex profiles. This ratio is plotted as A/d^2 for all the results presented. Whereas the majority of drops observed showed negligible deformation, it was found for situations in which deformation was significant that the major axis was the pertinent dimension, and this was used throughout. This was also noted by Magarvey *et al.*[12]

The terminal velocity values as measured were corrected for wall effect by the Faxen-Ladenburg[21] equation (Equation 1), assuming the equivalent diameter of the cell to be 9 cm.

$$v_1 = v_0 \left(1 - 2 \cdot 1 \frac{d}{D}\right) \quad . \quad . \quad . \quad . \quad . \quad . \quad . \quad . \quad (1)$$

Measurements of vortex area from photographs taken by Taneda[14] for solid spheres having $20 < (Re) < 140$, indicated the base line for the vortex dimension data.

Both the drag coefficient and the wake dimension data for systems subjected to massive surfactant contamination showed good agreement with this solid sphere line.

It was during the tests on these highly contaminated systems that the agreement with Magarvey's classification was observed. Particularly noted was the transition between the single thread (class I) and the double thread (class II) wakes in the region of $(Re) = 200$–220, this value being in agreement with Magarvey. The transition between classes II and III was less precise as few observations were carried out in this range.

The results indicate that the classification proposed by Magarvey is only significant for solid spheres, or for drops having the characteristics of solid spheres. Results obtained during tests in which 'Analar' grade reagents were used, and for which contamination by surfactant material was avoided, indicated a type of behaviour in which drop characteristics deviated from the solid sphere model (Fig. 2).

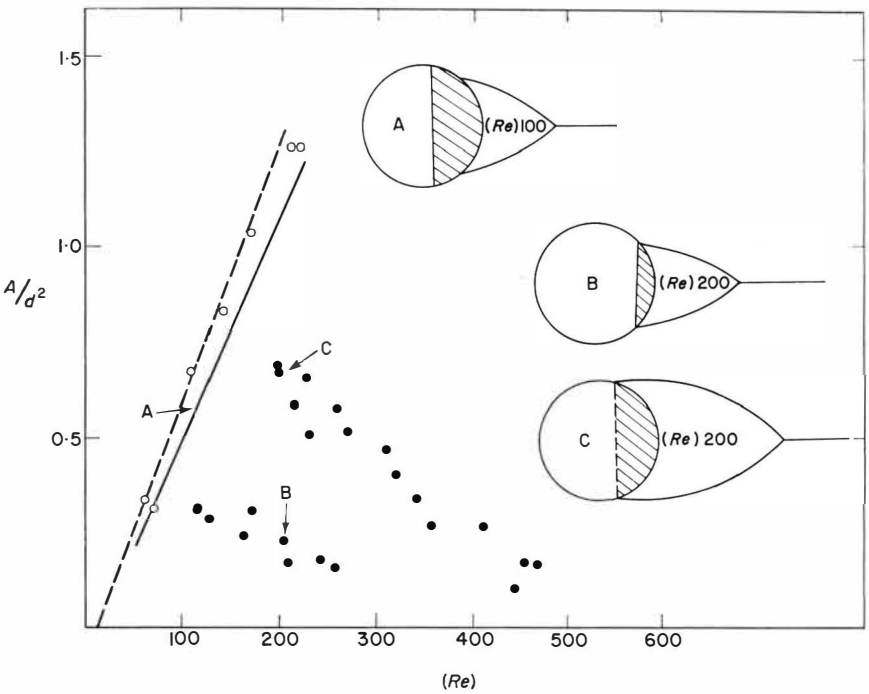

FIG. 2. *Variation in vortex area ratio with* (Re) *for various degrees of purity*
— — — Solid sphere data; ——— non-circulating data; ● benzene, Analar-C, purified-B; ○ benzene, massive surfactant contamination

Data for drops having a value of (Re) below a critical value, followed the solid sphere curve, independent of the physical property combination. The data did not correspond precisely with the solid sphere curve, the vortex volume being smaller and the separation ring being nearer the rear stagnation point than observed in solid sphere studies.

These data were used in the determination of the drop/vortex volume ratios plotted against droplet Reynold's number (Re) in Fig. 3. The points indicated

may be adequately represented by the relationship of Equation (2) within 5% accuracy limits.

$$(Re) = 17 + 186{\cdot}2\left(\frac{6V}{\pi d^3}\right) - 42{\cdot}3\left(\frac{6V}{\pi d^3}\right)^2 \quad . \quad . \quad . \quad . \quad (2)$$

Above a critical value of droplet (Re) the drop characteristics deviated from the solid sphere pattern of behaviour in that the terminal velocity was increased and the separation retreated towards the rear stagnation point, resulting in a decrease in relative vortex volume. The highest value of this critical value of (Re), for any of the supposedly uncontaminated systems, was noted to be in the range $200 < (Re) < 220$. It will be noted that this is the same range over which the transition from class I to class II wakes was observed in the solid sphere behaviour.

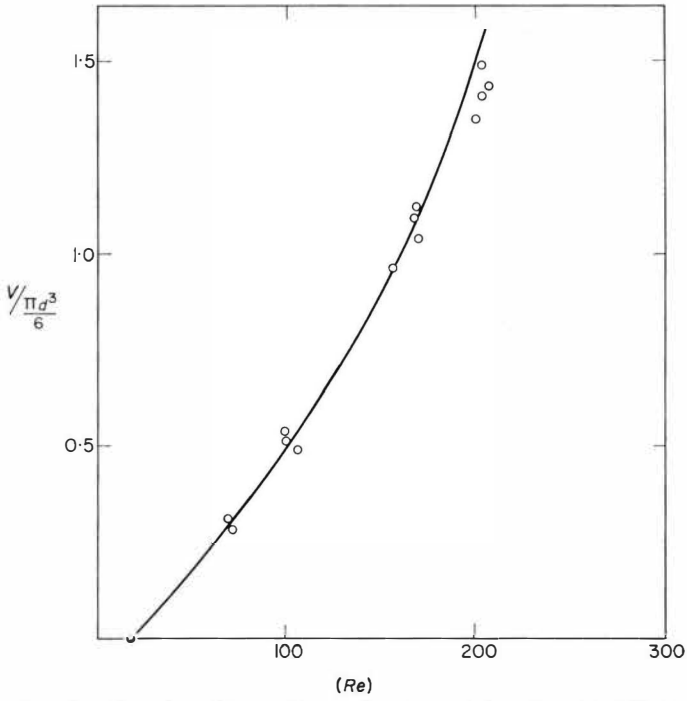

FIG. 3. *Variation of vortex/drop volume ratio below the critical* (Re)
○ Non-circulating data; ● Jensen's[15] theoretical value $(Re) = 17$
—— curve of $(Re) = 17 + 186{\cdot}2\left(\frac{6V}{\pi d^3}\right) - 42{\cdot}3\left(\frac{6V}{\pi d^3}\right)^2$

Theoretically[21] all drops of pure substances which are free from surfactant contamination, should circulate no matter how low their (Re). It was noted in this work, however, that drops having a value of (Re) below the critical value acted in all respects in a pattern similar to that noted for solid spheres. The supposition is, therefore, that the systems contain material capable of immobilisation of the interface.

It was noted that for all runs, apart from those in which surfactant was purposely added, that the interfacial tensions, bulk viscosities, and specific gravities did not differ appreciably from those published or derived from published data for the systems used. The concentrations of dyes used in these tests were also shown to cause no change in the interfacial tensions for all systems, within the experimental accuracy of the test method.

Comparison of the terminal velocity dependence on droplet diameter for a typical system (Fig. 4) in the absence of, and after addition of, the dyed continuous phase, indicated that there was no significant alteration of the droplet

performance. This would indicate that the dyes used were not the agents of surface immobilisation.

Intensive purification of dispersed phase reagents, however, resulted in a reduction in the critical value of (*Re*) (Fig. 2). It was not found possible to reduce the critical (*Re*) below a value approximately equal to (*Re*) = 100 for the method of solvent purification used. This method of purification involved filtration through a bed of purified active carbon, followed by double distillation in an all-glass still.

Attainment of terminal velocity prior to the test section was confirmed for all normal systems by use of the ciné technique. The results of this technique were also shown to noticeably reduce the scatter in the data obtained. Scatter is also reduced for drops above the critical (*Re*) by plotting the vortex/drop dimension ratios against the drag coefficient of the drop, as in Fig. 5, the relationships being linear for these axes.

Addition of surfactant to the dyed continuous phase indicated the existence of two types of behaviour for drops progressing through the uncontaminated

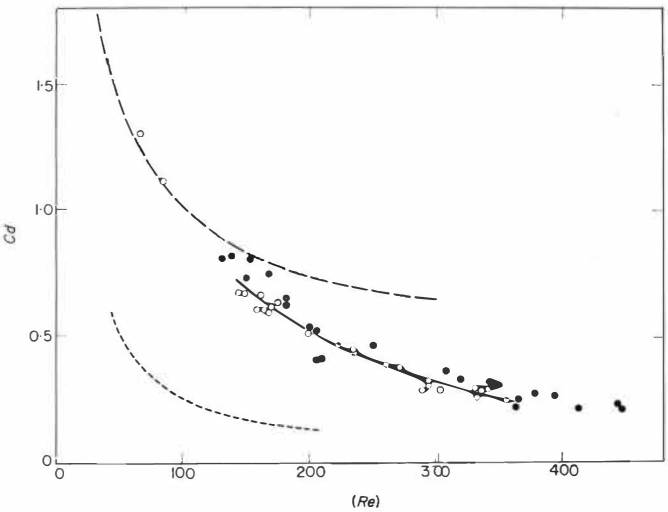

FIG. 4. *Drag coefficient versus* (Re) *for benzene drops in water with and without permanganate dye*

● Benzene with tracer dye; ○ Benzene dye-free; — — — solid sphere line; - - - - - - data of Winnikow & Chao[28] for fully circulating spheres

continuous field, as illustrated in Fig. 6. Drops having an initial 'terminal' velocity giving rise to a value of (*Re*) below a critical value maintained this value throughout their life. Drops having an initial 'terminal' velocity giving rise to a (*Re*) above this critical value, however, progressively increased their velocity, with an accompanying reduction in vortex volume and angle of separation.

Discussion

The well-documented observation of the reduction in the terminal velocities of liquid drops in the presence of surfactant material has been confirmed by this work. Agreement has also been noted with Garner's statement[23] that agents may affect the velocity, even when present in concentrations insufficient to cause a measurable change in the interfacial tension for the liquid/liquid system. Systems in this series of experiments which had interfacial tensions equal to those of the pure components, were shown to exhibit terminal velocity and vortex geometry characteristics, for drops having the (*Re*) below a critical value, corresponding to those for solid spheres. The correspondence with the solid sphere pattern of behaviour was not complete, however, in that the drops

showed a decreased vortex size, and a separation ring nearer the rear stagnation point than that observed for the solid sphere.

This deviation from solid sphere performance may be related to partial internal circulation of the drop. Kintner[24,25] observed drops of $(Re) < 10$ exhibiting this partial circulation pattern during studies of droplet internal motion, and he related this to an immobile cap model of surfactant contamination. It will be noted that in the results for the system involving massive contamination with sodium lauryl sulphate, the droplet and vortex behaviour agreed more closely with that expected for solid spheres, indicating, in this case, that the whole of the drop was stagnant.

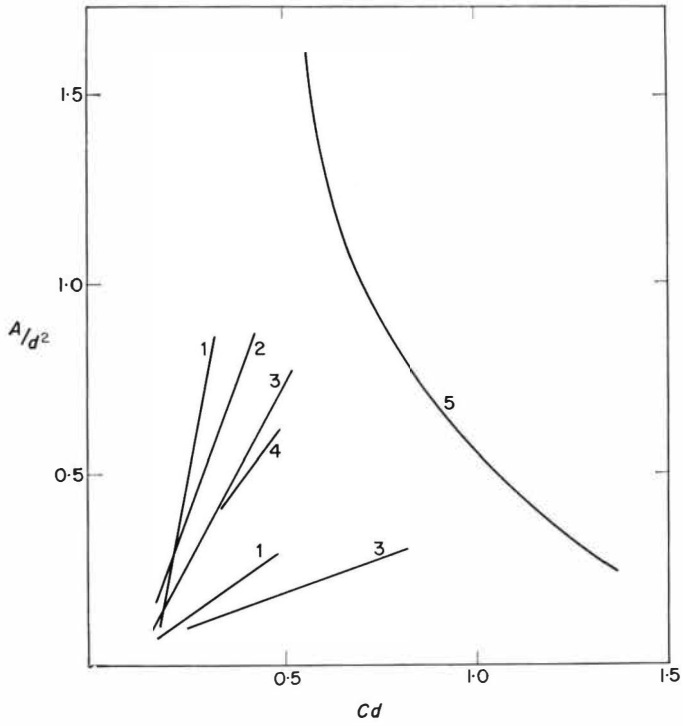

FIG. 5. *Variation of vortex area ratio with drag coefficient*
1, Toluene; 2, iso-octane; 3, benzene; 4, MIBK; 5, non-circulating data

Fig. 2 indicates the migration of the separation ring towards the rear stagnation point during development of internal circulation of the drop. The increase in terminal velocity, reduction in drag and change in vortex geometry above the critical (Re) may be related to the development of internal circulation of the droplets.

The interfacial tension gradient model of surfactant contamination of drops would support the suggestion that the critical (Re) corresponds to the initiation of total internal circulation,[26] when the shear forces owing to flow overcome the interfacial forces at the equator of the drop. Many authors,[25,27] however, have criticised this model for being unable to explain the coexistence of stagnant and circulating regions of the drop, and the existence of the immobile cap.

It was noted that the maximum value obtained for the critical (Re), for all systems free from surfactant contamination, was in the range $200 < (Re) < 220$. It is in this region of (Re) that vortex instability is first observed in solid sphere studies,[12] and consideration may be given to the possibility that internal circulation may be initiated by an interfacial turbulence resulting in the breakdown of a weakly bonded barrier at the interface.

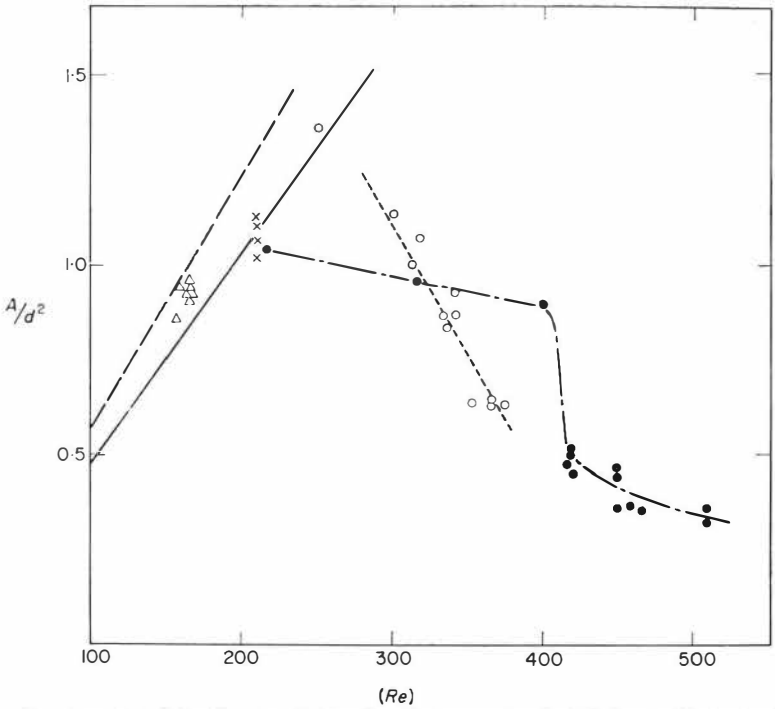

FIG. 6. *Development of the characteristics of surfactant-contaminated drops of benzene during their progress through an uncontaminated aqueous continuous phase*
d (cm): ○ 0·31; ● 0·346; × 0·283; △ 0·253
——— non-circulating data; — — — — solid sphere line

The suggestion by Savic[27] that intermolecular or hydrogen bonding at the interface may be the agent of interface immobilisation seems to be refuted by the present work. For a particular two-phase system, the critical (*Re*) should always remain constant for constant system conditions if the bonding were of a molecular/hydrogen type, as it would not be expected that the strength of the bonding could be changed. It was in fact found that extensive purification of two of the systems used (Fig. 2), resulted in a marked reduction of the value of the critical (*Re*). It is concluded that, unless the impurities removed were themselves agents of intermolecular bonding at the interface, this method of interface immobilisation is not significant for the systems and (*Re*) ranges studied. It is, however, possible that such forces gain significance below the lowest critical (*Re*) here attained ((*Re*) = 100).

The existence of the immobile cap[25] and the observation of an abrupt halt in surface streaming at the leading edge of this cap,[27] suggest a useful model. For the situation in which the circumference of the immobile cap is greater than the circumference of the separation ring, the immobilised surface would present the hydrodynamic characteristics of the solid sphere. The angle of separation of the boundary layer would be close to that of the solid sphere, but its value would be modified by the effect of the mobile area of interface at the front of the drop.

The observation[27] that interfacial streaming stopped abruptly at the leading edge of the immobile cap, resulting in a boundary layer separation at that position, and Kintner's note[25] that this leading edge was never observed to progress further forward than the equator, even in highly contaminated systems. is significant to the possible explanation for a critical (*Re*) value. It would be relevant to note that as (*Re*) approaches a value of 200, the separation ring approaches the equator. The proximity of this vortex boundary layer separation to the edge of the immobile cap, it is suggested, would give rise to instability in the boundary layer, resulting in dissociation of the interfacial forces and

transport of surfactant material, at the edge of the cap, into the boundary layer. The progressive removal of surfactant material in this manner, would result in the observed development of internal circulation.

This model satisfies the condition of a reduced critical (*Re*) for the purified systems. The reduced cap area, in this instance, relates to a reduction in the active component of the dispersed phase.

The evidence of the tests, illustrated in Fig. 6, lends support to the model proposed. The loss of surfactant material from a highly contaminated drop, during its progression through an uncontaminated field, should depend upon the proximity of the separation ring to the drop equator. It was noted that drops travelling in the 'non-circulating' mode, having a value of $(Re) < 220$, progressed through the uncontaminated field without showing a change in behaviour which would characterise the development of internal circulation. This may be considered as significant of the retention of the surfactant material at the interface. Drops which would have $(Re) > 220$, however, when travelling in the 'non-circulating' mode, were observed to exhibit the characteristics of a developing internal circulation. This behaviour may be considered as signifying the transport of surfactant material into the boundary layer, in the region of the leading edge of the immobile cap.

Conclusions

Systems involving the performance of droplets moving in the 'solid sphere' regime would be adequately satisfied by the vortex volume data indicated in Fig. 3 and expressed by the relationship of Equation (2).

It may be proposed that, for most situations, the highest degree of backmixing associated with the vortex of the dispersed phase droplet would be for the regime of stagnant droplet phenomena in which the closed vortex of Magarvey's classifications I and II predominate.

Above the droplet (*Re*) range of 220 to 240 the periodic shedding of the vortex into the wake for the solid sphere regime would reduce the importance of the vortex concentration differential, relative to the overall mass transfer.

It is also proposed that entrainment backmixing would be less for systems in which the dispersed phase hold-up is high. It will be noted that the average residence time for a particular volume element of continuous phase would be reduced by the vortex shedding induced by inter-droplet collision and interaction.

For a situation in which residence time in the vortex is low, it may be anticipated that the continuous phase backmixing associated with the vortex would be smaller for high degrees of separation. This results from the observation that the maximum equilibrium concentration in the vortex would be equal to the product of the distribution coefficient and the concentration in the dispersed phase drop. A high residence time, however, would maintain vortex concentration at the level relating to the initial droplet concentration until drop arrest, and would thus increase the significance of the entrainment to the performance of the column.

Observation during this work, of the development of internal circulation, above a critical Reynold's number (*Re*), has resulted in conclusions which may be summarised as follows: despite intensive purification, the dispersed phases studied included an agent capable of interface immobilisation; this agent did not affect the values of the specific gravities, bulk viscosities, or interfacial tension of the system, within the limits of accuracy of the standard experimental test methods; intermolecular bonding or hydrogen bonding does not appear to be significant to interface immobilisation for the systems and (*Re*) ranges studied; the maximum (*Re*) for which development of internal circulation may be suppressed is in the range $200 < (Re) < 230$, for systems not involving high surfactant contamination; the behaviour of the drops is adequately described by a model in which the immobile cap, at the rear of the drop, is progressively broken down from its leading edge when the separation ring approaches this leading edge.

The model described would benefit from further research to determine its independence from system physical properties and surfactant type. Research in this direction is currently in progress.

Acknowledgment

One of the authors (M.P.W.) wishes to thank the Science Research Council for the financial support in the form of a research studentship, during the period of this work.

Nomenclature

A	Area of the closed loop vortex profile, cm^2
Cd	Drag coefficient
d	Diameter of the drop, cm
D	Equivalent diameter of the column, 9 cm
(Re)	Droplet Reynold's number, $vd\rho_c/\mu_c$
r	Radius of the drop, cm
v	Velocity of the drop, cm/sec
V	Volume of the closed loop vortex, cm^3
μ_c	Continuous phase bulk viscosity
π	3·1429
ρ_c	Continuous phase specific gravity, g/cm^3
σ	Interfacial tension

References

1 Geankopliss, C. J., *Ind. Engng Chem.*, 1952, **44,** 2458
2 Letan, R., & Kehat, E., *A.I.Ch.E. Jl*, 1965, **11,** 804
3 Rod, V., *Br. chem. Engng*, 1964, **9,** 300
4 Geankopliss, C. J., Wells, P. L., & Hawk, E. L., *Ind. Engng Chem.*, 1951, **43,** 1848
5 Newman, M. L., *Ind. Engng Chem.*, 1952, **44,** 2457
6 Jensen, V. G., Jeffreys, G. V., & Edwards, R. E., *C.r. hebd. Séanc. Acad. Sci., Paris*, 1967, **T32(3),** 694
7 Letan, R., & Kehat, E., *A.I.Ch.E. Jl*, 1968, **14,** 831
8 Letan, R., & Kehat, E., *A.I.Ch.E.Jl*, 1968, **14,** 398
9 Gal-Or, B., Klinzing, G. E., & Tavlarides, L. L., *Ind. Engng Chem.*, 1969, **61,** 21
10 Baker, K. G., Ph.D. thesis, University of Birmingham, 1963
11 Torobin, L. B., & Gauvin, W. H., *Can. J. chem. Engng*, 1959, **37,** 167
12 Magarvey, R. H., & Bishop, R. L., *Can. J. Physics*, 1961, **39,** 1418
13 Garner, F. H., Jensen, V. G., & Keey, R. B., *Trans. Instn chem. Engrs*, 1959, **37,** 191
14 Taneda, S., *J. phys. Soc. Japan*, 1956, **11,** 1104
15 Jensen, V. G., *Proc. R. Soc. A*, 1959, **249,** 346
16 Tayeban, M., Ph.D. thesis, University of Birmingham, 1958
17 Garner, F. H., & Tayeban, M., *An. R. Soc. esp. Fis Quím.*, 1960, **56-B,** 479
18 Hendrix, C. D., Dave, S. B., & Johnson, H. F., *A.I.Ch.E. Jl*, 1967, **13,** 1072
19 Kintner, R. C., Horton, J. J., Graumann, R. E., & Amberkar, S., *Can. J. chem. Engng*, 1961, **39,** 235
20 Jeffreys, G. V., & Lawson, G. B., *Trans. Instn chem. Engrs*, 1965, **43,** 294
21 Griffith, R. M., *Chem. Engng Sci.*, 1962, **17,** 1057
22 Hamielec, A. E., & Johnson, A. I., *Can. J. chem. Engng*, 1962, **40,** 41
23 Garner, F. H., & Skelland, A. H., *Ind. Engng Chem.*, 1956, **48,** 51
24 Kintner, R. C., Horton, J. J., & Fritsch, T. R., *Can. J. chem. Engng*, 1965, **43,** 140
25 Huang, W. S., & Kintner, R. C., *A.I.Ch.E. Jl*, 1969, **15,** 735
26 Schecter, R. S., & Farley, R. W., *Can. J. chem. Engng*, 1963, **41,** 103
27 Savic, P., *Rep. natn. Res. Coun. Can.*, 1953, No. M.T.-22
28 Winnikow, S., & Chao, B. T., *Physics Fluids*, 1966, **9,** 50

Power input, drop size and minimum stirrer speed for liquid–liquid dispersions in stirred vessels

by J. W. van Heuven* and W. J. Beek**

Laboratorium voor Fysische Technologie, Technische Hogeschool, Delft, The Netherlands.

The aim of this investigation was to find design or scale-up rules for power input, drop size and minimum stirrer speed to achieve complete dispersion in turbulent liquid–liquid systems in stirred vessels. Experiments were performed in cylindrical vessels with a turbine impeller and four baffles. The results were compared with theories based on a distinction between large- and small-scale flow. In all cases, design or scale-up rules were obtained. The results are discussed in the light of a complete dimensional analysis, and the well-known rule of scale-up on a basis of equal energy input per unit mass is compared with the outcome.

Introduction

THERE IS A NEED for design rules for the construction of liquid extraction apparatus. If these rules are known, it should be possible to scale-up from results obtained on a laboratory or semi-technical scale. Research work is described in this paper to set up such design and scaling-up rules for one type of apparatus, a cylindrical vessel with a six-blade turbine stirrer and four baffles.

The following quantities will be important for design purposes:

1. power consumption of the stirrer;
2. drop size distribution of the dispersed phase;
3. the minimum stirrer speed to achieve complete dispersion;
4. the coalescence frequency of the drops;
5. the mass transfer coefficient in the continuous and dispersed phase.

The present study is limited to the first three points.

Apparatus

All experiments were performed in vessels of a standard geometry, shown in Fig. 1. The diameter (T) and the height (H) of the vessel are equal. The width of the four baffles is one tenth of the vessel diameter. The dimensions of the stirrer, which is placed centrally in the vessel, are given in Fig. 1. Stirrer speed can be read off from a tachometer. All vessels but one are provided with a cover to prevent air entrainment at high stirrer speeds. The vessel and the cover are provided with inlets for the continuous and the dispersed phase and an outlet to take samples from the dispersion. Vessel volumes range from $1 \cdot 6 \times 10^{-3}$ to $1 \cdot 36$ m^3. The largest vessel is not provided with a cover and has a relatively slightly larger stirrer diameter: $D = 0 \cdot 33\ T$. A survey of the different vessels is given in Table I.

TABLE I

Dimensions of vessels and stirrers

Vessel number	V1	V2	V3	V4	V5	V6	V7
Vessel volume, m^3	$1 \cdot 56 \times 10^{-3}$	$3 \cdot 28 \times 10^{-3}$	$5 \cdot 5 \times 10^{-3}$	$1 \cdot 44 \times 10^{-2}$	$7 \cdot 1 \times 10^{-2}$	$7 \cdot 1 \times 10^{-2}$	$1 \cdot 36$
Vessel diameter, m	0·125	0·161	0·191	0·264	0·45	0·45	1·20
Stirrer diameter, m	0·0375	0·048	0·057	0·076	0·135	0·135	0·40

* Centraal Technisch Instituut, T.N.O., Delft, The Netherlands

** Unilever Research Laboratorium, Vlaardingen, The Netherlands

For the interpretation of the experimental results it is necessary to know the hydrodynamic flow conditions in the vessels. As low viscosity liquids are used for the experiments, the flow must be turbulent to obtain complete dispersion. The transition from laminar to fully turbulent flow takes place over a fairly large range of the Reynolds number, (Re_D), related to the stirrer. Fully turbulent flow is obtained when

$$(Re_D) = \frac{\rho N D^2}{\eta} > 10^4 \quad . \quad . \quad . \quad . \quad . \quad . \quad . \quad . \quad (1)$$

Roughly speaking, two different kinds of flow can be distinguished. Firstly, large scale flow: this is the circulation flow which starts from the stirrer radially. An extensive description of this kind of flow can be found in the literature.[1–4] Secondly, small scale flow: this is caused by the velocity fluctuations of the

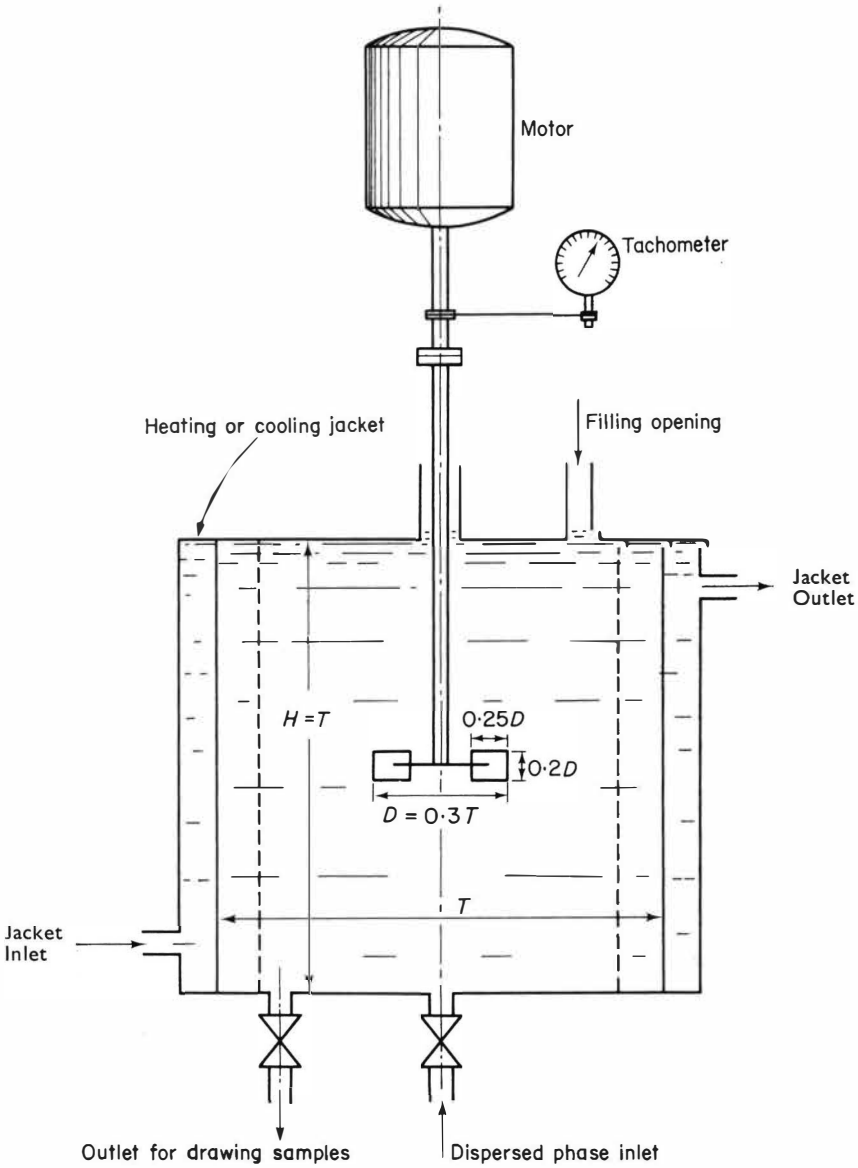

FIG. 1. *Apparatus*

turbulent flow. Shinnar & Church[5,6] described this type of flow using Kolmogoroff's theory on locally isotropic turbulence. According to their conclusions, small-scale flow is determined by the local energy dissipation. It should be kept in mind that close to the impeller, energy dissipation density is much higher than the average energy dissipation density in the vessel.

Power consumption

It is clear that the power consumption of the stirrer has to be calculated for the design of the drive of the stirrer. However, power consumption also determines the nature of the large and small scale flow and thus the phenomena that are taking place.

The literature on power consumption in systems with one liquid phase is very extensive. A survey has been given by Voncken.[7] Fick *et al.*[8] made measurements with four-blade stirrers in liquid–liquid dispersions. Measurements with six-blade turbines in liquid–liquid dispersions were not noticed in the literature. In order to calculate the power consumption, the torque exerted on the vessel was measured. The method has been described in detail by Reith[9] who used it to measure power consumption in gas–liquid dispersion; water was used as the continuous phase in all experiments. Hexane and octanol were used as two different dispersed phases. They differ in density and interfacial tension and therefore show different drop sizes at a given power input. All the measurements were performed in vessels V3 and V6. The dispersed phase volume fraction was varied from 0 to 40%. For a single phase system with fully turbulent flow, the power number (P_o), defined as follows, is practically constant:

$$P_o = \frac{P}{\rho N^3 D^5} = \text{constant} \quad . \quad . \quad . \quad . \quad . \quad . \quad . \quad . \quad (2)$$

From the results obtained with two-phase systems, power numbers were calculated, taking the average density of the system, and are given in Fig. 2 as a function of the impeller Reynolds number. It can be seen from Fig. 2 that the power number is practically constant and that the values for water alone and the dispersions coincide. In so far as power consumption is concerned, the dispersion behaves as a homogeneous liquid with a density equal to the average density of the dispersion. This is in agreement with the results obtained by Fick *et al.*[8] Fig. 2 shows a small but systematic difference between the measurements in both vessels. In the literature,[10–12] power numbers ranging from 4·9 to 6·3 are found without there being an explanation for these differences. A value of 5·4 ± 0·5 is in good agreement with recent studies and the results presented here.

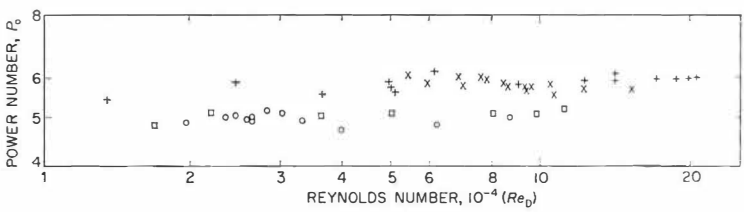

FIG. 2. *Power number as a function of impeller Reynolds number for water and dispersions of hexane and octanol in water*

Vessel V3: □ water; ○ water with hexane or octanol (1–40%)
Vessel V6: + water; × water with hexane or octanol (1–30%)

Drop size distribution

Experimental

Various methods have been used to measure drop size distribution or the average drop size, including: light absorption,[13,14] a fast chemical reaction,[15] photographical techniques[16,17] and the Coulter counter.[18,19] With the first two

methods, only the average drop size (Sauter mean diameter) can be determined. In choosing a measuring technique, a simple method of drawing stable and representative samples from the dispersion in the vessel was sought which did not require special fittings on the vessels.

Two methods of obtaining stable samples were developed. The first is based upon encapsulation of the droplets by a thin polymer film by means of a so-called interfacial polycondensation reaction. Madden & McCoy[20] were the first to point out this possibility. However, there was a tendency for the encapsulated droplets to stick together. A procedure which solves this problem has been described by van Heuven & Hoevenaar.[21,22] Local as well as average dropsize distribution in the vessel can be determined since the encapsulation can be carried out inside as well as outside the vessel.

The second method is based upon stabilising a sample drawn from the vessel by means of a surface-active agent: samples were caught in and subsequently thoroughly mixed with a solution of sodium lauryl sulphate. This procedure was also described by van Heuven & Hoevenaar.[21,22] The stable samples obtained in this way were photographed under a microscope. The drop size distribution was measured from the photographs.

The encapsulation technique was applied solely to the water–benzene system. The second method was applied to four systems. A survey of the most important properties of these systems is given in Table II.

TABLE II

Densities and interfacial tensions of systems at 20°C

Continuous phase	Dispersed phase	Density of continuous phase, kg/m^3	Interfacial tension, kg/sec^2
Water	Benzene	998	$35{\cdot}0 \times 10^{-3}$
Water	Hexane	998	$49{\cdot}5 \times 10^{-3}$
Water	Octanol	998	$8{\cdot}5 \times 10^{-3}$
Water	Styrene	998	$35{\cdot}5 \times 10^{-3}$

Experiments were performed with volume fractions of dispersed phase ranging from 0·4 to 35%. Impeller Reynolds number as defined by Equation (1) was varied from $1{\cdot}6 \times 10^4$ to $4{\cdot}5 \times 10^5$. In this way, Sauter mean drop diameters were obtained ranging from 21 to 240 μm.

Interpretation of results

The theory developed by Shinnar & Church[5,6] was used. This predicts that a Weber number, (We), is a constant:

$$(We) = \frac{\rho N^2 D^{4/3} d_{max}^{5/3}}{\sigma} = \text{constant} \qquad (3)$$

Equation (3) is restricted to cases where the influence of coalescence on drop size can be neglected. If the ratio between d_{max} and the Sauter mean diameter, d_{32}, is a constant, Equation (3) gives:

$$d_{32}\left(\frac{\rho^{3/5} N^{6/5} D^{4/5}}{\sigma^{3/5}}\right) = \text{constant} \qquad (4)$$

The Sauter mean diameter is defined as:

$$d_{32} = \frac{\Sigma d_d^{\,3}}{\Sigma d_d^{\,2}} \qquad (5)$$

where d_d is the diameter of an individual drop.

The constant in Equation (3), which cannot be derived from the theory of Shinnar & Church,[5,6] was calculated by van Heuven:[21]

$$d_{max}\left(\frac{\rho^{3/5}N^{6/5}D^{4/5}}{\sigma^{3/5}}\right) = 12 \times 10^{-2} \quad . \quad . \quad . \quad . \quad . \quad . \quad (6)$$

The main step was the calculation of the highest local energy dissipation, which determines the size of the largest drops in the dispersion. At present it is not possible to calculate the ratio of d_{32} and d_{max} so that a theoretical prediction of the constant in Equation (4) cannot be given. Finally, it should be pointed out that Equations (3), (4) and (6) are valid if the drops are larger than the microscale of turbulence. This condition is satisfied if the droplet Reynolds number is greater than unity:[5,6]

$$(Re_d) = \frac{ND^{2/3}d_{32}{}^{4/3}}{\nu} > 1 \quad . \quad . \quad . \quad . \quad . \quad . \quad . \quad (7)$$

Agreement between theory and experiments can now be checked by comparison of the results of the experiments on small volume fractions of dispersed phase with Equations (4) and (5). However, the problem arises as to which value of the interfacial tension is to be used. The measured values obtained from samples of the dispersion are lower than the values given in Table II. The latter originating from the literature were determined with very pure liquids. In the present study, liquids of 'technical purity' were used, however. Besides, when working on a relatively large scale, some contamination can hardly be avoided. Yet the best agreement between different systems was found when the values given in Table II were used. This may be explained by two facts. Firstly, a very large surface area is obtained in the dispersion and thus a relatively low degree of contamination. Secondly, during the process of break-up, a new and clean surface is created in the first instance.

In Fig. 3, the left-hand term in Equation (4), calculated with the values of the interfacial tension given in Table II, is given as a function of droplet Reynolds number.

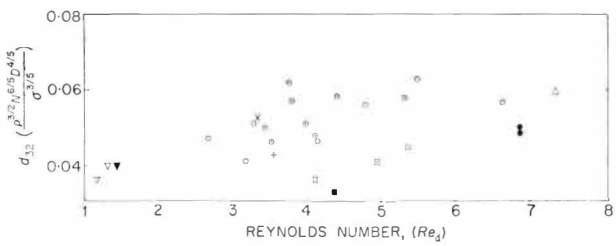

FIG. 3. *Dimensionless drop diameter* (Equation 4) *as a function of droplet Reynolds number for liquids of 'technical purity'*

	V1	V2	V3	V4	V5	V6	V7
benzene	○	×		+	○		●
hexane			□			⊡	■
octanol			▽			▽	▼
styrene				△			

Only the results obtained with the second technique (stablisation with sodium lauryl sulphate) are shown in Fig. 3. It can be seen that the left-hand term of Equation (4) is not far from being constant although a slight increase with droplet Reynolds number can be discerned. Also the results are scattered. The results obtained with the first technique (encapsulation of the droplets) are given separately in Fig. 4. Here the actually measured value of the interfacial tension had to be inserted because some of the chemicals necessary for the encapsulation reaction had to be dissolved in both phases beforehand (e.g. sodium hydroxide in the water and sebacoyl dichloride in the benzene). No values of the interfacial tension of these solutions could be taken from the literature. A higher value of the left-hand term of Equation (4) is obtained.

It can be concluded that for an accurate prediction of the Sauter mean drop diameter, a few experiments should preferably be performed on a small scale at

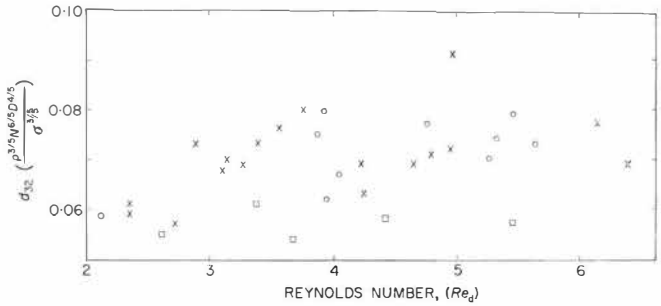

FIG. 4. *Dimensionless drop diameter* (Equation (4)) *as a function of droplet Reynolds number for water + sodium hydroxide and benzene + sebacoyl dichloride*
○ V1; × V2; □ V3

the same value of the droplet Reynolds number as on full scale. Without performing experiments, an approximate value can be obtained, however.

The experimental results are now compared with Equation (6). From the results in Fig. 3, it follows that:

$$d_{32}\left\{\frac{\rho^{3/5}N^{6/5}D^{4/5}}{\sigma^{3/5}}\right\} = 4{\cdot}7 \times 10^{-2} \quad . \quad . \quad . \quad . \quad . \quad . \quad (8)$$

From an average of all experiments, it was found that:

$$d_{\max} = 2{\cdot}0\, d_{32} \quad . \quad . \quad . \quad . \quad . \quad . \quad . \quad . \quad . \quad (9)$$

Combining Equations (8) and (9):

$$d_{\max}\left\{\frac{\rho^{3/5}N^{6/5}D^{4/5}}{\sigma^{3/5}}\right\} = 9{\cdot}4 \times 10^{-2} \quad . \quad . \quad . \quad . \quad . \quad . \quad (10)$$

Taking into account that the theory leading to Equation (6) is rather approximate, the agreement between the constants in Equations (6) and (10) seems to be good. The correctness of the suppositions underlying the theory of Shinnar & Church[5,6] is consequently supported.

The results obtained in this investigation are in good agreement with those found by others. Chen & Middleman[17] and Sprow[18] obtained the value $5{\cdot}1 \times 10^{-2}$ for the constant in Equation (8), a difference of only 8% from the result of this investigation. For the ratio of $d_{\max}$ and d_{32}, they found 1·6 and 2·6, respectively, compared with 2·0 in the present investigation.

The results of the experiments with large fractions of dispersed phase (up to 35%) are now discussed. Only the second measuring technique was used in this part of the investigation. The results are shown in Fig. 5. The ratio of the Sauter mean diameter $d_{32}(\varphi)$ belonging to a fraction of dispersed phase φ and the Sauter mean diameter belonging to a very small fraction of dispersed phase $d_{32}(\varphi=0)$ under otherwise similar conditions is given as a function of φ. For all systems, the result can be expressed with reasonable accuracy as:

$$\frac{d_{32}(\varphi)}{d_{32}(\varphi=0)} = 1 + 2{\cdot}5\,\varphi \quad . \quad . \quad . \quad . \quad . \quad . \quad . \quad . \quad (11)$$

This is in agreement with measurements by Vanderveen.[23] Vermeulen *et al.*[14] obtained 3·3 instead of 2·5 for the value of the constant in Equation (11). From Equations (8) and (11), it follows that:

$$d_{32}\left\{\frac{\rho^{3/5}N^{6/5}D^{4/5}}{\sigma^{3/5}}\right\} = 0{\cdot}047\,(1 + 2{\cdot}5\varphi) \quad . \quad . \quad . \quad . \quad . \quad (12)$$

It should be pointed out that this result is obtained from measurements with liquids of 'technical purity' and with no dissolved components in either phase.

It is remarkable that the influence of the fraction of dispersed phase is the same for all systems. This indicates that it is not primarily coalescence but rather the influence of the droplets on the small-scale flow that is mainly

responsible for the increase in drop size with the fraction of dispersed phase. This conclusion follows from the fact that the influence of coalescence on drop size would not be the same with different systems.

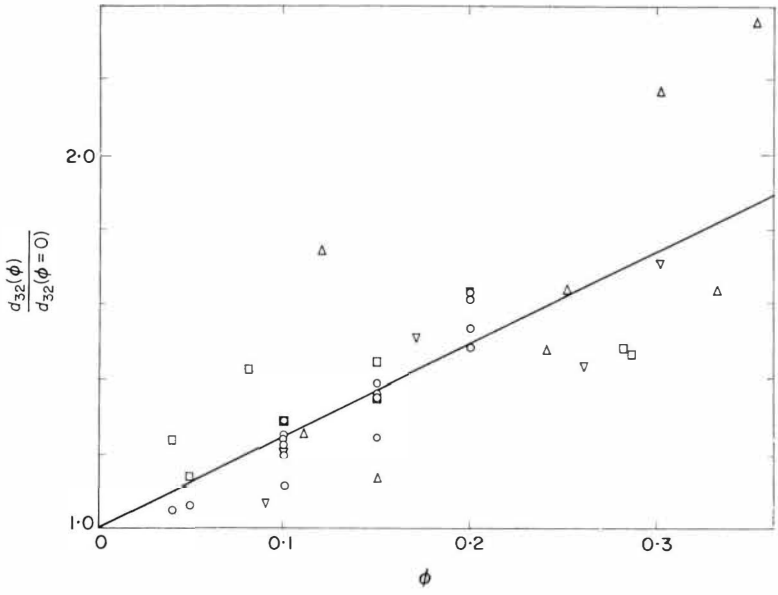

FIG. 5. *Influence of the fraction of dispersed phase on drop size*
○ water–benzene; □ water–hexane; △ water–octanol; ▽ water–styrene

Minimum stirrer speed

When a liquid–liquid dispersion is being made, it has to be borne in mind that below a certain stirrer speed no complete dispersion will be obtained. The term 'complete dispersion' is used for a situation in which no large drops or agglomerates of droplets are found on the bottom of the vessel or at the liquid surface. This situation should not be confused with 'homogeneous dispersion', a situation in which the concentration of droplets is constant throughout the whole vessel. Criteria to achieve the latter situation were obtained by Pavlushenko *et al.*[24,25] It can be concluded from their study that the velocity of the large-scale flow (circulation flow) has to be sufficiently large compared with the rise or fall velocity of the droplets.

In order to obtain 'complete dispersion', small-scale flow will play an important role. The velocity on this scale has to be sufficiently high compared with the rise or fall velocity of the droplets. From this consideration, it follows that for small fractions of dispersed phase, a dimensionless number, G_o, should be a constant:[21]

$$G_o \equiv \frac{\rho^{1/2} N_m D^{2/3}}{g^{1/2} \Delta\rho^{1/2} d_{32}{}^{1/6}} = \text{constant (for } \varphi \ll 1) \quad . \quad . \quad . \quad . \quad (13)$$

For large volume fractions of dispersed phase, the constant in Equation (13) will be a function of this fraction. If it is assumed that the influence of the fraction of dispersed phase is due to the influence of the droplets on small-scale flow only, it can be proved, starting from Equation (12), that this constant, G_ϕ, should have the following form:

$$G_\phi \equiv \frac{\rho^{1/2} N_m D^{2/3}}{g^{1/2} \Delta\rho^{1/2} d_{32}{}^{1/6}} = G_o(1 + 2{\cdot}5\varphi)^{5/6} \quad . \quad . \quad . \quad . \quad . \quad (14)$$

Equations (13) and (14) can now be compared with the results obtained with the systems mentioned earlier using vessels V3, V4, V5, V6 and V7. The experiments were performed visually. The results obtained with small volume

fractions of dispersed phase are presented in Fig. 6, which shows that G_o is not constant but is slightly dependent on the impeller Reynolds number, (Re_D). Physically this means that the minimal stirrer speed is slightly dependent on large-scale flow. A line drawn in a conservative way through the highest points satisfies the equation:

$$G_o = 10(Re_D)^{-0\cdot1} \quad . \quad . \quad . \quad . \quad . \quad . \quad . \quad . \quad (15)$$

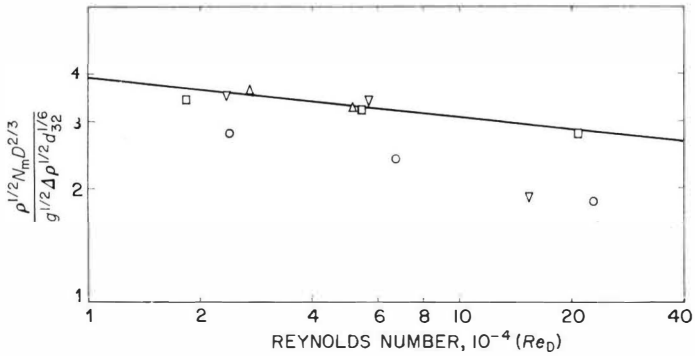

FIG. 6. *Dimensionless minimum stirrer speed* (Equation (13)) *as a function of impeller Reynolds number*

○ water–hexane; □ water–octanol; △ water–styrene; ▽ water–benzene

Fig. 7 shows the experimental results for all fractions of dispersed phase. The ratio of G_ϕ and G_o is given as a function of φ. The lower line drawn in this figure represents Equation (14). The agreement with experiment is quite good, although the majority of the points lie above the line. The results are represented in the best way by the following equation:

$$\frac{G_\phi}{G_o} = 1 + 2\cdot5\varphi \quad . \quad . \quad . \quad . \quad . \quad . \quad . \quad . \quad . \quad (16)$$

From Equations (14), (15) and (16):

$$\frac{\rho^{1/2}N_m D^{2/3}}{g^{1/2}\Delta\rho^{1/2}d_{32}{}^{1/6}} = 10(Re_D)^{-0\cdot1}\,(1 + 2\cdot5\varphi) \quad . \quad . \quad . \quad . \quad . \quad (17)$$

Again, it should be stressed that all experiments were performed with liquids of 'technical purity'.

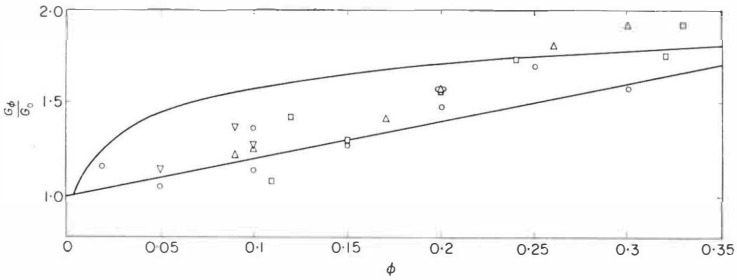

FIG. 7. *Influence of the fraction of dispersed phase on minimum stirrer speed*

○ water–hexane; □ water–octanol; △ water–styrene; ▽ water–benzene

Upper line: results from Equation (18)[26]

The results of this study are now compared with those for 'complete suspension' of solid particles. Zwietering[26] gives an empirical correlation for the same geometry of vessel and stirrer as was used in the present work. His correlation, after some rearrangement, can be written as:

$$\frac{\rho^{1/2}N_m D^{2/3}}{g^{1/2}\Delta\rho^{1/2}d_p{}^{1/6}} = 11\cdot2(Re_D)^{-0\cdot1}\left(\frac{d_p}{D}\right)^{0\cdot05}\beta^{0\cdot14} \quad . \quad . \quad . \quad . \quad (18)$$

In order to compare Equation (18) with Equation (15), an average value for d_p/D and 0·5% by weight for β (the lowest value in the experiments by Zwietering) are taken. This results in:

$$\frac{\rho^{1/2} N_m D^{2/3}}{g^{1/2} \Delta\rho^{1/2} d_p^{1/6}} = 8 (Re_D)^{0 \cdot 1} \quad . \quad . \quad . \quad . \quad . \quad . \quad . \quad (19)$$

This is in fair agreement with Equation (15), taking into account that the constant in Equation (15) would be 9 instead of 10 when d_{max} is used instead of d_{32}. The deviations in $(d_p/D)^{0 \cdot 05}$ from the average value are relatively small ($\pm 7\%$). In order to compare the influence of the fraction of dispersed phase as given by Equation (18) with the results of the present study, this equation is represented by the upper line in Fig. 7. A density difference $\Delta\rho = 200$ kg/m^3 was taken for the calculations, this being about the average of the systems used. The agreement is not very satisfactory. However, there are no good reasons to suppose that a great difference exists between the mechanism of 'complete dispersion' and 'complete suspension'.

In conclusion, it can be said that it follows from the foregoing that both 'complete dispersion' and 'complete suspension' are determined mainly by small scale flow and that a relatively simple relationship for the minimum stirrer speed is obtained.

Discussion

The dependent variable (q) in each of the previous studies is, principally speaking, a function of the following independent variables:

$$q = f(N, D, \varphi, \rho, \Delta\rho, \eta_c, \eta_d, \sigma, g) \quad . \quad . \quad . \quad . \quad . \quad . \quad (20)$$

where η_c and η_d are the dynamic viscosities of the continuous and dispersed phase, respectively. If Q is a dimensionless number containing q, it follows from dimensional analyses that:

$$Q = f\left(\frac{ND^2}{\nu}, \frac{N^2 D}{g}, \varphi, \frac{\rho\nu^2}{\sigma D}, \frac{\Delta\rho}{\rho}, \frac{\eta_c}{\eta_d}\right) \quad . \quad . \quad . \quad . \quad . \quad . \quad (21)$$

When working with the same liquid–liquid system on both small and large scale, it is impossible to keep all these dimensionless numbers constant. This means that complete similarity (i.e. simultaneous geometric, kinematic and dynamic similarity) cannot be achieved (see, e.g. Langhaar[27]). However, when a certain quantity is determined by either small- or large-scale flow only, and when small- and large-scale flows do not influence each other, similarity may be obtained either on one or other scale. Similarity on a small scale is obtained if the power input per unit mass is kept constant provided that large-scale flow has no influence, or, in other words, small-scale turbulence has to be isotropic. In geometrically similar stirred vessels, power input per unit mass is kept constant as long as N^3D^2 is kept constant. This has to be borne in mind for the following discussion on power input, drop size and minimum stirrer speed.

Power input

$$q = P \text{ and } Q = \frac{P}{\rho N^3 D^5} \quad . \quad . \quad . \quad . \quad . \quad . \quad . \quad . \quad (22)$$

Experimentally it was found that:

$$\frac{P}{\rho N^3 D^5} = 5 \cdot 4 \quad \left(\frac{ND^2}{\nu} > 10^4\right) \quad . \quad . \quad . \quad . \quad . \quad . \quad . \quad (23)$$

if the average density of the dispersion is taken for ρ. When Equations (23) and (21) are compared, it can be seen that in this case Q is not a function of any of the other dimensionless numbers. There is no similarity problem. It follows from Equation (23), as has been stated earlier, that the power input per unit mass is kept constant as long as N^3D^2 is kept constant.

Drop size

$$q = d_{32} \text{ and } Q = \frac{d_{32}}{D} \quad . \quad . \quad . \quad . \quad . \quad . \quad . \quad . \quad (24)$$

Rearrangement of Equation (12) gives:

$$\frac{d_{32}}{D} = 0{\cdot}047\left(\frac{ND^2}{\nu}\right)^{-6/5}\left(\frac{\rho v^2}{\sigma D}\right)^{-3/5}(1 + 2{\cdot}5\varphi) \quad . \quad . \quad . \quad . \quad (25)$$

When Equations (25) and (21) are compared, it can be concluded that gravity (g), the density difference between the phases ($\Delta\rho$) and the viscosity of the dispersed phase (η_d) do not influence drop size. It follows from Equations (12) and (25) that d_{32} can be kept constant in geometrically similar vessels by keeping N^3D^2 constant. Flow on a small scale, at least close to the stirrer, is fully determined by power input per unit mass and the influence of large scale flow is negligible.

Minimum stirrer speed

$$q = N_m \text{ and } Q = \frac{N_m{}^2 D}{g} \quad . \quad . \quad . \quad . \quad . \quad . \quad . \quad . \quad (26)$$

Rearrangement of Equation (17) and elimination of d_{32} by using Equation (12) gives:

$$\frac{N_m{}^2 D}{g} = 22\left(\frac{N_m D^2}{\nu}\right)^{-3/5}\left(\frac{\rho v^2}{\sigma D}\right)^{-1/5}\left(\frac{\Delta\rho}{\rho}\right)(1 + 2{\cdot}5\varphi)^{7/3} \quad . \quad . \quad (27)$$

It must be pointed out that stirrer speed in this case is the dependent variable. Comparison with Equation (21) shows that all the variables with the exception of the viscosity of the dispersed phase are relevant. For the scale-up, it follows from Equation (27) that $N_m{}^{2{\cdot}6}D^2$ has to be kept constant. Thus scaling up on a basis of power input per unit mass is not exact in this case. Minimum stirrer speed is not determined by small-scale flow only, but there is some influence of large scale flow on this process.

A study on other small-scale processes (coalescence and mass transfer) in turbulent liquid–liquid dispersions by van Heuven[21] has indicated that scaling-up on a basis of power input per unit mass cannot be done for these processes either.

Conclusions

Power input

A simple design rule is available which is analogous to the well-known rule for single phase systems.

Drop size

A design rule was found for dispersions of liquids of 'technical purity'. In practice, it is desirable to perform a few experiments on a small scale. Scale-up on the basis of equal power input per unit mass is adequate.

Minimum stirrer speed

A design rule is available, although higher accuracy may be obtained by performing a few experiments on a small scale and scaling-up with the aid of a simple rule. Power input per unit mass is an unsatisfactory basis for scale-up.

Finally, it can be said that rules have been found for design or scaling-up of power input, drop size and minimum stirrer speed. Also the commonly used basis of equal power input per unit mass for scale-up is not applicable for all processes in turbulent liquid–liquid dispersions in a stirred vessel.

Acknowledgment

The authors are grateful to ir. H. J. Beverdam, ir. H. H. Boswinkel, ir. W. M. M. Dekkers, ir. P. Geerlings, ir. J. C. Hoevenaar and ir. A. C. W. Leenards who performed some of the measurements.

Nomenclature

d_{32}	Sauter mean drop diameter	m
d_{max}	diameter of the largest drops in the dispersion	m
d_p	particle size	m
D	diameter of the impeller	m
g	acceleration due to gravity	m/sec^2
G_o	dimensionless number (see Equation (13))	—
G_ϕ	dimensionless number (see Equation (14))	—
H	height of liquid in the vessel	m
N	stirrer speed	sec^{-1}
N_m	minimum stirrer speed for complete dispersion	sec^{-1}
P	power	W
P_o	power number (see Equation (2))	—
q	dependent variable	different dimensions
Q	dimensionless number containing q	—
(Re_d)	droplet Reynolds number (see Equation (7))	—
(Re_D)	impeller Reynolds number (see Equation (1))	—
T	vessel diameter	m
(We)	Weber number (see Equation (3))	—
β	wt.-% of solid particles in the suspension	—
η	dynamic viscosity	kg/m sec
η_c	dynamic viscosity of continuous phase	kg/m sec
η_d	dynamic viscosity of dispersed phase	kg/m sec
ν	kinematic viscosity of the continuous phase ($= \eta_c/\rho$)	m^2/sec
ρ	density	kg/m^3
$\Delta\rho$	density difference between continuous and dispersed phases	kg/m^3
σ	interfacial tension	kg/sec^2
φ	fraction of dispersed phase	—

References

[1] Voncken, R. M., Thesis, Delft Technol. Univ., 1966
[2] Voncken, R. M., *Symp. Ser. Instn chem. Engrs*, 1965, No. 10
[3] Holmes, D. B., Voncken, R. M., & Dekker, J. A., *Chem. Engng Sci.*, 1964, **19**, 201
[4] Voncken, R. M., Holmes, D. B., & den Hartog, H. W., *Chem. Engng Sci.*, 1964, **19**, 209
[5] Shinnar, R., & Church, J. M., *Ind. Engng Chem.*, 1960, **52** (3), 253
[6] Shinnar, R., *J. Fluid Mech.*, 1961, **10** (2), 259
[7] Voncken, R. M., *Br. chem. Engng*, 1965, **10** (12), 179
[8] Fick, J. L., Rea, H. E., & Vermeulen, T., *Rep. Congr. atom. Energy Commn U.S.*, 1954, UCRL-2545
[9] Reith, T., Thesis, Delft Technol. Univ., 1968
[10] Miller, R. S., Ralph, J. L., Curl, R. L., & Towell, G. D., *A.I.Ch.E. Jl*, 1963, **9**, 196
[11] Rushton, J. H., Costich, E. W., & Everett, H. J., *Chem. Engng Prog.*, 1950, **46** (395), 467
[12] Bates, R. L., Fondy, P. L., & Corpstein, R. R., *Ind. Engng Chem. Process Des. Dev.*, 1963, **2**, 310
[13] Rodger, W. A., Trice, V. G., & Rushton, J. H., *Chem. Engng Prog.*, 1956, **52**, 515
[14] Vermeulen, T., Williams, G. M., & Langlois, G. E., *Chem. Engng Prog.*, 1955, **51**, 85
[15] Fernandes, J. B., & Sharma, M. M., *Chem. Engng Sci.*, 1967, **22**, 1267
[16] Endoh, K., & Oyama, Y., *Sci. Pap. Inst. phys. chem. Res., Tokyo*, 1958, **52**, 131
[17] Chen, H. T., & Middleman, S., *A.I.Ch.E. Jl*, 1967, **13**, 989
[18] Sprow, F. B., *Chem. Engng Sci.*, 1967, **22**, 435
[19] Sprow, F. B., *A.I.Ch.E. Jl*, 1967, **13**, 995
[20] Madden, A. J., & McCoy, B. J., *Chem. Engng Sci.*, 1964, **19**, 506

[21] van Heuven, J. W., Thesis, Delft Technol. Univ., 1969
[22] van Heuven, J. W., & Hoevenaar, J. C., *Proc. 4th chem. Reaction Engng Symp.*, Brussels, 1968
[23] Vanderveen, J. H., *Rep. Congr. atom. Energy Commn U.S.*, 1960, UCRL-8733
[24] Pavlushenko, I. S., & Ianishevskii, A. V., *J. appl. Chem. USSR*, 1958, **31,** 1334
[25] Pavlushenko, I. S., & Braginskii, L. N., *J. appl. Chem. USSR*, 1963, **36,** 303
[26] Zwietering, T. N., *Chem. Engng Sci.*, 1958, **8,** 244
[27] Langhaar, H. L., 'Dimensional analysis and theory of models', 1951 (New York: John Wiley & Sons)

Wakes behind drops falling at their terminal velocity in purified systems

by R. M. Edge and C. D. Grant

Department of Chemical Engineering, University of Strathclyde, Glasgow, U.K.

A study was made of the wake behind drops of specially purified organic liquids falling through water. It was observed that as the volume of the drop was increased there was a transition region where the wake changed from a thread-like wake behind a non-oscillating drop to a vortex street behind an oscillating drop. The wake structures observed in this transition region are classified and are discussed with reference to the Ohnesorge number.

In the oscillating range, the frequency of oscillation of the drops both determined and was equal to the frequency of wake shedding. Semi-empirical equations are proposed for correlation of the frequency of shedding of the wake.

Introduction

THE HYDRODYNAMIC PHENOMENA relating to the fall of single liquid drops through another liquid have been the subject of much research work. Measurements have been reported of the terminal velocity of the drops, the shape of non-oscillating drops and the frequency of oscillation of oscillating drops. Edge & Grant[1] have reviewed this work. However, comparatively little is known about the flow of the continuous phase past these drops and without such knowledge drop phenomena cannot be fully understood. Also, many of the experimental investigations have used systems not of the highest purity and it is known that the presence of a minute quantity of a surface-active impurity can considerably alter the drop behaviour and can cause conflicting results to be obtained for seemingly identical systems. The work reported in this paper is concerned mainly with the flow of the continuous phase past oscillating drops falling in purified systems. Oscillating drops were chosen for this investigation because it is known that oscillating drops give high mass transfer rates in spray columns[2] and comparatively little is known about their hydrodynamics.

The flow past a liquid drop can be predicted theoretically when the droplet is falling in the Stokesian region, at Reynolds numbers (*Re*) less than 0·1, but at Reynolds numbers significantly above this a theoretical analysis is extremely difficult. The best attempt to date appears to be that of Harper & Moore[3] who analysed the simple model of a fully circulating sphere with no interfacial contamination. The Reynolds number was assumed to be sufficiently high for boundary layer theory to hold, and the analysis predicted that the flow would separate very near the rear of the drop to form a thin wake.

Experimentally observed flow patterns have been reported in the literature, but there is considerable disagreement as the purity of the systems used has varied widely. Garner[4] and Garner & Skelland[5] observed that flow separation from the drop surface first occurred at a Reynolds number of about 20, and that an attached wake was then formed at the rear of the drop. Garner & Tayeban[6] estimated the size of the attached wakes behind both stagnant drops of 2-ethylhexane-1,3-diol and circulating drops of benzyl alcohol. Their work suggests that the flow past a circulating drop separates much nearer the rear of the drop than when the drop is stagnant, and that the wake size is smaller. Elzinga & Banchero[7] observed from shadowgraphs of contaminated and uncontaminated drops that the flow separated on the front half of contaminated drops and on the rear half of uncontaminated drops, and attributed this shift in the position of the flow separation to the greater internal circulation in the uncontaminated drops.

Magarvey *et al.*[8–12] reported wake configurations for drops falling through water. The wakes were rendered visible by adding a water-soluble aniline dye to the dispersed phase. The wake types were classified[10] according to the nature of the motion in the continuous phase some distance downstream from the drop. Six distinct types of wake were observed, and to each type a range of Reynolds number was assigned. A symmetrical periodic shedding of vorticity was observed in the range $290 < (Re) < 700$ and above a Reynolds number of 700 the wake was asymmetrical. The authors[10] made no mention of the position of flow separation.

Winnikow & Chao[13] obtained still shadowgraphs of the wake behind drops in carefully purified systems. The variation in density in the continuous phase owing to mass diffusion of the drop solvent was sufficient to reveal the wake structure. For non-oscillating drops the wake was thread-like and the angle of flow separation was in all cases considerably greater than for a solid sphere at the same Reynolds number. The observed wake configuration differed considerably from those reported by Magarvey & Bishop,[10] and Winnikow & Chao attributed this difference to contamination of the liquid–liquid interface by the aniline dye used by Magarvey & Bishop. They also observed shedding of the attached wake only when the drops were oscillating. From measurements on oscillating drops of nitrobenzene they concluded that the frequency of drop oscillation was significantly greater than the frequency of wake shedding. They offered no explanation of this. A number of other authors[7,13–15] have speculated on the relationship between the oscillation of the drop and the shedding of the attached wake but as yet no quantitative relationship appears to have been established between the two phenomena.

Experimental

Method

The drop phase liquids were slightly soluble in the continuous phase and the resulting density gradients in the boundary layer separating from the drop and in the wake were made visible by means of a conventional Schlieren optical system which is shown in Figs 1 and 2. The light source was a mercury vapour lamp fed from a d.c. supply, and the optical components between the slit and the plane P, where the light beam was brought to a focus, were of Schlieren quality. The continuous phase was contained in a glass column consisting of a 6 × 4 in nominal bore Quickfit Visible Flow cross-piece, supplemented by additional sections of 4 in nominal bore tubing positioned above the cross-piece. The light beam passed horizontally through the 6 in arms of the cross-piece which were blanked off by Schlieren quality glass windows with surfaces flat to within 1 fringe/in.

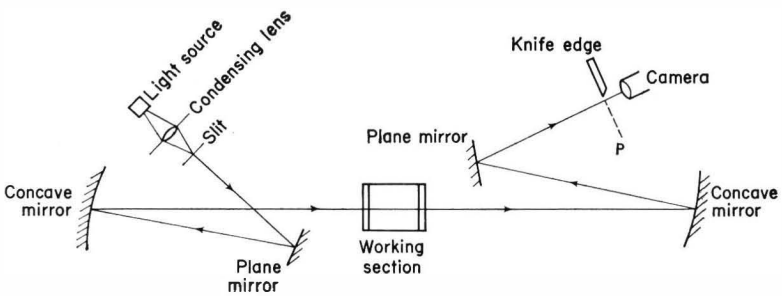

FIG. 1. *Schlieren optical system*

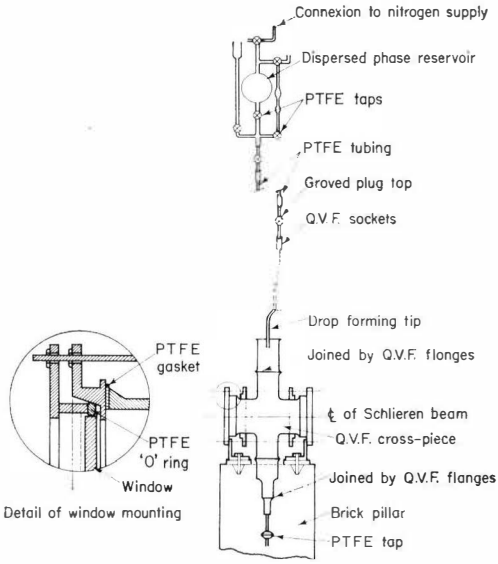

FIG. 2. *Column and supports*

The larger drops were formed from stainless-steel tips with sharp circular ends and the smaller drops from the inside diameter of glass capillary tubing. The tips were connected to the dispersed phase reservoir by PTFE tubing. All parts of the apparatus which were in contact with either phase were made of glass, PTFE, or stainless steel. These were enclosed in an air bath which maintained the liquid temperature at $25 \cdot 0 \pm 0 \cdot 1$ °C.

The falling drops were filmed with a Bolex 16 mm cine camera operating at a nominal 64 frames/sec and were visible on the film over a vertical distance of fall of 14 cm. A stainless-steel length scale was positioned inside the column, and a marked wheel driven by a synchronous electric motor was positioned in the light beam close to the column. These were visible on each frame of the film and provided the length scale and the time scale respectively. The drops were formed in the field of view, or up to 24 cm above the field of view. The rate of drop formation was varied between 1 drop every 10 sec for the largest drops and 1 drop every 3 sec for the smallest drops. The rate of formation was coarsely set by means of a grooved plug-tap and the fine adjustment was made by altering the pressure in the dispersed phase-reservoir. For each system the range of drop sizes was chosen so that all drop diameters were greater than the diameter corresponding with the peak in the curve of terminal velocity against drop diameter.[1] The drop size was found by weighing a number of drops which were formed at the required rate into a small amount of the continuous phase contained in a weighing bottle. For each experiment the passage of approximately 9 drops down the column was filmed.

Great care was taken to avoid contamination of the system, and all surfaces which came into contact with either phase were cleaned with chromic acid at least once each week, and whenever the system was changed. The chromic acid was left in contact with the various pieces of apparatus for 24 h and all traces of it were then removed by repeated washings with distilled water.

Properties of materials

Double distilled water was used as the continuous-phase liquid and 5 drop phase liquids were used. The physical properties of the liquids at 25 °C are shown in Table I. The organic liquids were of A.R. grade and were fractioned

TABLE I

Physical properties at 25°C of the liquids used

Liquid	Density, g/cm³	Viscosity,[19] cP	Interfacial tension, dynes/cm
Water	0·997	0·894	
Chlorobenzene	1·099	0·756	36·5
1,2-Dichloroethane	1·240	0·778	27·8
Ethyl bromide	1·451	0·371	32·4
sym-Tetrachlorethane	1·587	1·58	30·9
1,2-Dibromoethane	2·167	1·61	36·0

before use at a high reflux ratio in a 30-plate all-glass Oldershaw column. The interfacial tension between the drop phase and the continuous phase was measured by the drop-weight method, using the correction factor of Harkins & Brown.[16]

Results

Classification of wake patterns

The observed wake patterns were classified into five types. These are described in Table II and are illustrated in Fig. 3. The wake class and the corresponding Reynolds number for each size of drop and for the various systems are given in Table III. The transition from one wake type to another was not sharply defined and at certain drop sizes the wake resembled a mixture of two classes. In such cases both wake classes are quoted in Table III, the first number corresponding to what appears to be the predominant type.

TABLE II

Classification of wake types

Class	Description
I	Non-oscillating drop. Single thread wake
II	Drop oscillating with small amplitude. Single thread wake with 'pulses'
III	Drop oscillating. Chain of vortices formed along the axis of fall
IV	Drop oscillating and zig-zagging. Vortices shed from alternate sides of the drop
V	Random wobble of the drop. Irregular detachment of vortices

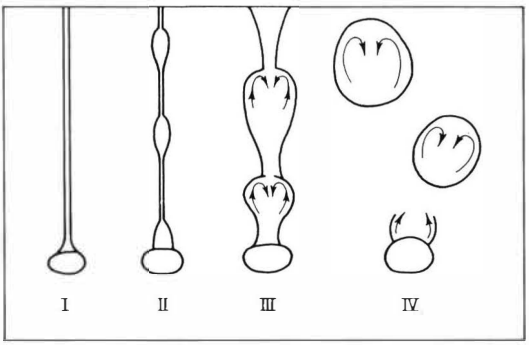

FIG. 3. *Classification of wake types*

TABLE III

Wake types and frequencies of oscillation

Chlorobenzene				Dichloroethane			
D_E, cm	Wake class	(*Re*)	ω, sec^{-1}	D_E, cm	Wake class	(*Re*)	ω, sec^{-1}
0·882	V	1318	5·35	0·600	IV	975	7·8
0·770	IV	1202	6·54	0·578	IV	948	8·1
0·674	III	1082	8·04	0·512	IV	880	9·5
0·620	III	1065	8·80	0·410	III–IV	770	13·0
0·560	III	974	9·76	0·360	III	676	15·1
0·438	I	850		0·320	II	652	
0·376	I	755		0·300	I	622	
				0·242	I	526	

Ethyl bromide				Tetrachloroethane			
D_E, cm	Wake class	(*Re*)	ω, sec^{-1}	D_E, cm	Wake class	(*Re*)	ω, sec^{-1}
0·426	IV	831	13·2	0·444	IV	900	11·9
0·370	IV	755	15·9	0·390	IV	821	13·7
0·339	IV	710	18·1	0·340	IV	755	16·3
0·292	III	643	22·2	0·313	IV	711	18·2
0·274	III	623		0·280	III	662	20·6
0·264	II	624		0·238	I	608	

Dibromoethane			
D_E, cm	Wake class	(*Re*)	ω, sec^{-1}
0·309	IV	790	17·9
0·276	IV	725	21·3
0·249	IV	666	24·3
0·212	III–IV	601	28·1
0·204	III	606	
0·192	II	590	
0·162	I	531	

Wake behind non-oscillating drops

The non-oscillating drops had the shape of a distorted ellipsoid with the front being more flattened than the rear (Fig. 4). The angle of flow separation, θ_s, and the diameter of the flow separation ring, D_S, were estimated for the dichloroethane and chlorobenzene drops. With the other systems, the non-oscillating drops were too small for the position of the flow separation to be clearly visible. Table IV gives values of S, E and θ_s where S is the ratio $D_S : D_H$, E is the ratio $D_H : D_V$ and D_S, D_H, D_V, and θ_S are defined as in Fig. 4.

TABLE IV

Non-oscillating drops

System	D_E, cm	S	E	θ_s, °
Chlorobenzene	0·438	0·347	1·77	150
	0·376	0·392	1·52	150
Dichloroethane	0·300	0·221	1·61	163
	0·261	0·244	1·54	162
	0·242	0·267	1·43	163

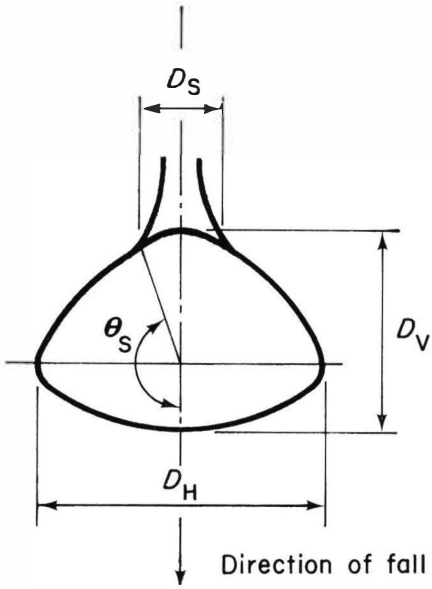

FIG. 4. *Shape of a non-oscillating drop*

Wake behind oscillating drops

The wake behind oscillating drops was unsteady and periodic in nature. At drop sizes slightly greater than the size at which oscillations began, the oscillations of the drop were of small amplitude, and the periodicity in the wake appeared as small 'pulses' disturbing the thread-like trail (class II). The frequency at which these pulses appeared was the same as the frequency of oscillation of the drop. When the size of the drop was increased the amplitude of the oscillations became greater and the position at which the flow separated varied appreciably throughout the cycle of the drop oscillation (classes III and IV). The angle between the separating boundary layer and the surface of the drop also varied considerably. The result of these complicated changes in the position and angle of the flow separation was a periodic injection of vorticity into the detached wake, at a frequency which was the same as the frequency of oscillation of the drop.

When the wake was of the class III type, discrete vortices could not be distinguished and the vortices appeared to be linked together in a vortex chain along the axis of fall. However, when the wake was of the class IV type, one discrete vortex was shed at each oscillation of the drop, and the drops fell in a zig-zag path with a rocking motion so that the vortices were shed on alternate

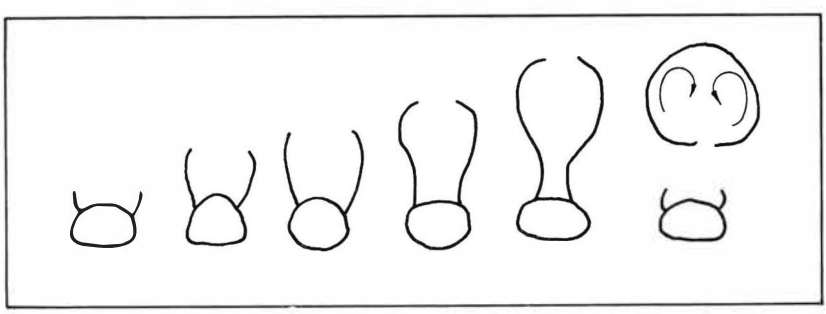

FIG. 5. *Oscillation cycle for a drop with a class IV wake*

sides of the axis of fall. The frequency of the rocking motion was the same as the frequency of oscillation of the drops. An oscillation cycle for a drop with a class IV wake is shown in Fig. 5. The frequencies at which vortices were shed into the wake are given in Table III. These were obtained by measuring the average time between sheddings over the full 14 cm of fall visible on the film.

Volume of the attached wake shed during an oscillation cycle

As a drop falls, some of the continuous phase is contained within the sheet formed by the separating boundary layer and travels with the drop. In the case of classes I and II wakes this volume was very small compared with the drop volume and could not be easily measured. For classes III and IV wakes

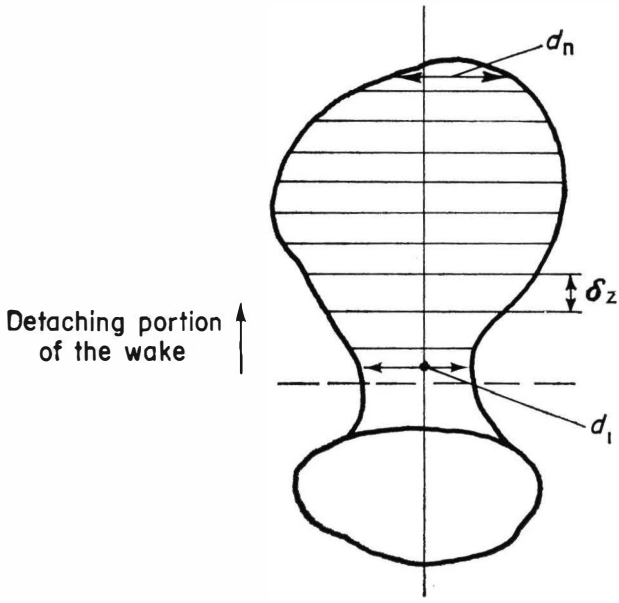

FIG. 6. *Class IV wake immediately prior to detachment*

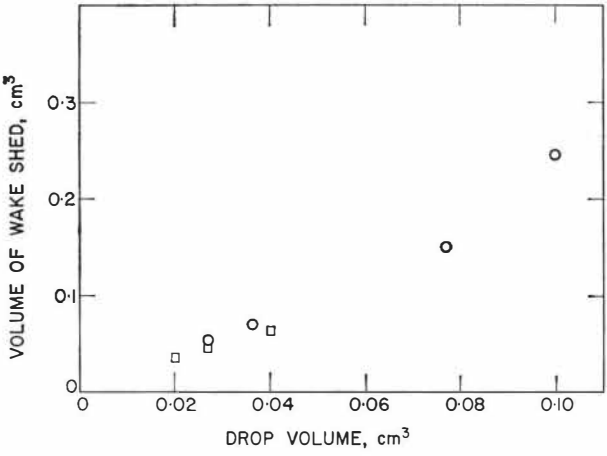

FIG. 7. *Volume of the wake shed at each oscillation of the drop*
○ Dichloroethane; □ ethyl bromide

the volume of the attached wake varied during the oscillation cycle. Because of the interlinking of the vortices, when the wake was of the class III, the volume of the attached wake was not easily estimated. However, for class IV wakes an estimate was made of the volume of the shed vortex, by assuming that this volume was given by $\sum_{i=1}^{n} \frac{\pi}{4} d_i^2 \, \delta z$ (Fig. 6). This volume is shown plotted against the volume of the drop in Fig. 7 and the relationship between the two is approximately linear. The volume of the wake attached to the drop immediately after the shedding of a vortex was small compared with the volume shed and was not easily measured.

Strouhal number

Periodic wake phenomena are frequently correlated by the Strouhal number, (*Sr*). A Strouhal number was calculated from the frequency of shedding of the attached wake for classes III and IV wakes, and from the frequency of the pulses in the thread-like wake for class II wakes. The Strouhal number is shown plotted against Reynolds number in Fig. 8, and for each system the Strouhal number is approximately constant. Because the frequency of shedding of the wake is equal to the frequency of oscillation of the drop the characteristic Strouhal number for wake shedding can be correlated empirically by the equations given by Edge & Grant[1] for the Strouhal numbers for oscillating drops.

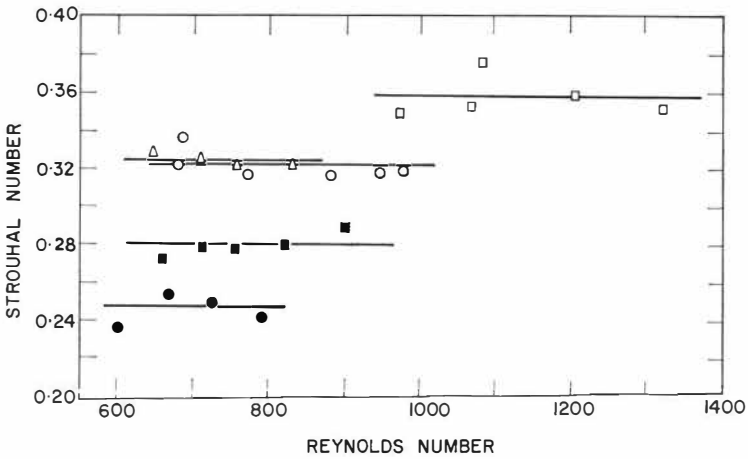

FIG. 8. *Strouhal number of oscillating drops*

□ Chlorobenzene; ○ dichloroethane; △ ethyl bromide; ■ tetrachloroethane; ● dibromoethane

Discussion

Classification of the wake

The wake configurations observed in this work confirm that the wakes classified by Magarvey & Bishop do not correspond with wakes behind drops in pure systems. For example they found that the shedding of vortices in the wake occurred at Reynolds numbers above 290, whilst in this work the wakes were still thread-like up to Reynolds numbers of 530–850 depending on the system. It is likely that the drops were so contaminated in the work of Magarvey & Bishop that there was no circulation inside the drops, and the observed wakes were essentially the same as those behind solid spheres. This is supported by Goldburg & Florsheim[17] who performed experiments similar to those of Magarvey & Bishop but using solid spheres dipped in dye. They obtained all six of Magarvey & Bishop's wake configurations, and also verified the ranges of Reynolds number corresponding to each classification. In the work reported

here the Reynolds number range of each classification was not the same for all systems and the Reynolds number corresponding with the transition between two wake types tended to decrease as the density of the dispersed phase increased.

It was shown previously[1] that the transition between a thread-like wake (class I) and a vortex street (class IV) was characterised by a break in the curve of the modified Weber number, $(We_M) = \dfrac{\rho_d U_\infty^2 D_E}{\sigma}$ against the modified Ohnesorge number, $Z_M = \dfrac{\mu_d}{(\rho_d \sigma D_E)^{\frac{1}{2}}}$. This break occurred at a transition Ohnesorge number given by:

$$Z_T = \frac{\mu_d^{\frac{1}{2}}}{(\rho_d \sigma D_{E,T})} \quad . \quad . \quad . \quad . \quad . \quad . \quad . \quad (1)$$

Where D_{ET}, the transition diameter, is given by the empirical equation[1]

$$D_{E,T} = \frac{0{\cdot}162}{(\Delta\rho/\rho_d)}$$

In Fig. 9 is shown the modified Weber number plotted against the ratio Z_M/Z_T.

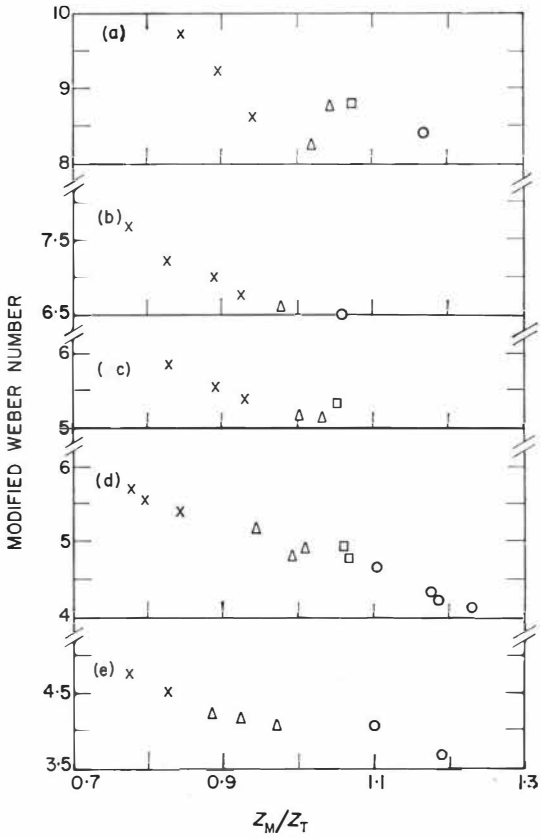

FIG. 9. *Variation of the modified Weber number* $\dfrac{\rho_d U_\infty^2 D_E}{\sigma}$ *and the type of wake with the ratio* Z_M/Z_T *where* $Z_M = \dfrac{\mu_d}{(\sigma \rho_d D_E)^{1/2}}$ *and* $Z_T = \dfrac{\mu_d}{(\sigma \rho_d D_{E,T})^{\frac{1}{2}}}$

○ Class I; □ class II; △ class III; × class IV
(a) Dibromoethane; (b) tetrachloroethane; (c) ethyl bromide; (d) dichloroethane; (e) chlorobenzene

Below the value $Z_M/Z_T = 0 \cdot 9$ a vortex street is present and above the value $Z_M/Z_T = 1 \cdot 1$ a thread-like wake is present. In the region $0 \cdot 9 < Z_M/Z_T < 1 \cdot 1$ the wake changes from class I to class IV by way of class II and class III wakes.

Wakes behind non-oscillating drops

The wakes observed behind non-oscillating drops (class I) are in agreement with the wakes observed by Winnikow & Chao[13] for non-oscillating drops in pure systems. The delay in the flow separation compared with the separation from the surface of a solid body indicates that there is well developed circulation of the drop liquid. Although the drops are far from spherical a comparison can be made with the analysis of Harper & Moore[3] which predicts that the diameter of the wake at the rear of a circulating liquid sphere is the order of $(Re)^{-1/6} \times D_E$ (i.e. that D_S/D_E is of the order of $(Re)^{-1/6}$). The non-oscillating drops in this work have Reynolds numbers in the range $500 < (Re) < 850$ and thus $(Re)^{-1/6}$ is about $0 \cdot 34$, which is in reasonable agreement with the experimental results that $0 \cdot 22 < D_S/D_H < 0 \cdot 39$.

Wakes behind oscillating drops

The wakes behind oscillating drops were complex and difficult to describe and quantify, but the results did show that the frequency of shedding of the attached wake was the same as the frequency of oscillation of the drop, irrespective of the wake configuration. Edge & Grant found that ω, the frequency of oscillation of a drop falling through a purified system, was given by the equation:

$$\omega = \omega^* - \left[\frac{0 \cdot 695}{\left(\frac{\Delta\rho}{\rho_d}\right)^{0 \cdot 2}} \cdot \frac{1}{D_E^2} \right] \quad . \quad . \quad . \quad . \quad . \quad . \quad . \quad . \quad (2)$$

where ω^* is the frequency of oscillation of an inviscid fluid sphere suspended in an inviscid fluid and is given by the following equation which was derived by Lamb:[18]

$$\omega^* = \frac{1}{2\pi} \left[\frac{192\,\sigma}{(2\,\rho_c + 3\,\rho_d)\,D_E^3} \right]^{\frac{1}{2}} \quad . \quad . \quad . \quad . \quad . \quad . \quad . \quad . \quad (3)$$

Therefore, Equation (3) can also be used to predict the frequency of shedding of vorticity from the attached wake behind an oscillating drop. This finding is in disagreement with the findings of Winnikow & Chao. Their limited data on nitrobenzene drops indicated that the frequency of shedding of the attached wake and the frequency of oscillation of the drop were different. However, it is likely that their measurements of the frequency of shedding of the attached wake were in error, since these frequencies were estimated from single still shadowgraphs. Their measurements of the frequency of oscillation of the drop, which were made from cine film, agree with Equation (2) to within $\pm 3\%$.

The frequency of shedding of the attached wake provides a further quantitative difference between the wake in pure and impure systems. In this work it was found that the Strouhal number for each system was approximately constant whereas Magarvey & Bishop and Goldburg & Florsheim found that it increased with increasing Reynolds number.

There has been some speculation as to whether the shedding of the wake is responsible for the oscillation of the drop or *vice versa*. Immediately after a large drop is detached from the tip on which it is formed it falls with a thread-like wake and it is not until after it has fallen a distance equal to several drop diameters than an attached wake is formed. Although it is not easy to obtain an accurate measure of the frequency of oscillation of the drop before the attached wake is formed, measurements do show that this frequency is close to

the frequency of oscillation of the drop when it is falling at its terminal velocity and has an attached wake. Therefore, as the frequency of shedding of the attached wake and the frequency of oscillation of the drop are the same it can be concluded that for an oscillating drop the frequency of shedding of the wake is determined by the frequency of oscillation of the drop.

Conclusions

1. The structure of the wake behind falling drops in a liquid–liquid system is dependent on the purity of the system.

2. In pure systems the wake behind non-oscillating drops is consistent with the existence of vigorous circulation in the drop.

3. In pure systems as the diameter of the drop is increased and as the drop begins to oscillate there is a transition of the wake structure from a thread-like wake to a vortex street. This transition can be related to the Ohnesorge number.

4. In pure systems periodic shedding in the wake occurs only when the drop is oscillating. The frequency of oscillation of the drop both determines, and is the same as, the frequency of shedding of the wake.

Acknowledgment

One of the authors (C.D.G.) wishes to express his gratitude to the Science Research Council for the provision of a Research Studentship.

Nomenclature

D_E equivalent spherical diameter of the drop, cm
D_H major axis of the drop, cm
D_V minor axis of the drop, cm
D_S diameter of the flow separation ring, cm
E eccentricity of the drop, D_H/D_V
(Re) Reynolds number, $\frac{D_E U_\infty \rho_c}{\mu_c}$
S D_S/D_H
θ_s angle of flow separation
U_∞ terminal velocity of the drop, cm/sec
(Sr) Strouhal number, $\frac{\omega D_E}{U_\infty}$
(We_M) modified Weber number, $\frac{\rho_d U_\infty^2 D_E}{\sigma}$
Z_M modified Ohnesorge number, $\frac{\mu_d}{(\rho_d \sigma D_E)^{\frac{1}{2}}}$
μ viscosity, P
ρ density, g/cm^3
σ interfacial tension, dynes/cm
ω frequency of oscillation, sec^{-1}
ω^* frequency of oscillation predicted by Lamb, Equation (3), sec^{-1}

Subscripts

c continuous phase
d dispersed phase
T at the transition point

References

[1] Edge, R. M., & Grant, C. D., *Chem. Engng. Sci.* (in press)
[2] Jeffreys, G. V., *Chem. Process Engng*, 1968, **49,** 111
[3] Harper, J. F., & Moore, D. W., *J. Fluid Mech.*, 1968, **32,** 367
[4] Garner, F. H., *Trans. Instn chem. Engrs*, 1950, **28,** 88
[5] Garner, F. H., & Skelland, A. H. P., *Chem. Engng Sci.*, 1955, **4,** 149
[6] Garner, F. H., & Tayeban, M., *An. R. Soc. esp. Fís. Quím.*, 1960, **56B,** 497
[7] Elzinga, E. R., & Banchero, J. T., *A.I.Ch.E. Jl*, 1961, **7,** 394
[8] Magarvey, R. H., & Bishop, R. L., *Nature, Lond.*, 1960, **188,** 735
[9] Magarvey, R. H., & Bishop, R. L., *Physics Fluids*, 1961, **4,** 800
[10] Magarvey, R. H., & Bishop, R. L., *Can. J. Phys.*, 1961, **39,** 1418
[11] Magarvey, R. H., & Blackford, B. L., *Can. J. Phys.*, 1962, **40,** 1036
[12] Magarvey, R. H., & Maclatchy, C. S., *A.I.Ch.E. Jl*, 1968, **14,** 260
[13] Winnikow, S., & Chao, B. T., *Physics Fluids*, 1966, **9,** 50
[14] Hughes, R. R., & Gilliland, E. R., *Chem. Engng Prog.*, 1952, **48,** 497
[15] Schroeder, R. R., & Kintner, R. C., *A.I.Ch.E. Jl*, 1965, **11,** 5
[16] Harkins, W. D., & Brown, F. E., *J. Am. chem. Soc.*, 1919, **41,** 499
[17] Goldburg, A., & Florsheim, B. H., *Physics Fluids*, 1966, **9,** 45
[18] Lamb, H., 'Hydrodynamics,' 1945, 6th edn (Dover)
[19] Timmermans, J., 'Physico-chemical constants of pure organic compounds', 1950 (Amsterdam: Elsevier)

Drop size distributions in agitated liquid–liquid systems with simultaneous interface mass transfer and chemical reaction

by J. W. Giles,* C. Hanson and J. G. Marsland
Postgraduate School of Chemical Engineering, University of Bradford, Bradford, 7, Yorkshire, U.K.

Mean drop sizes and drop size distributions have been studied in a stirred tank reactor during the nitration of toluene.

The drop size has been found to be dependent on the dispersed phase hold-up and on the agitator speed. The mixing and drop breakdown processes can be treated theoretically by the concept of local isotropy. It is shown that Kolmogorov's statistical theory can be applied to the turbulent flow regime in stirred tanks and can be used as a basis for correlations to predict drop sizes in such dispersions. The results of previous workers are reviewed. It is shown that the existence of mass transfer and chemical reaction in the nitration system decreases the mean drop size and hence increases the interfacial area.

The drop size distribution is well represented by a log-normal distribution. Reasons for a slight skewness are presented and various anomalies in the published literature are reviewed.

Preliminary experiments designed to measure interfacial tension in reacting heterogeneous systems are also discussed.

Introduction

IN RECENT YEARS, increasing attention has been paid to the study of mass transfer accompanied by chemical reaction in liquid–liquid systems.[1] It has been recognised that kinetic effects are important in some metal extraction processes. This is indicated when stage efficiencies in a stagewise contactor become a function of residence time. Such effects obviously become important when scaling up a process, e.g. if data obtained under or near equilibrium conditions in a laboratory mixer are applied to equipment having shorter contact times such as centrifugal contactors.

Heterogeneous liquid–liquid reactions common in the organic chemical industries are now being studied. In particular, the nitration of aromatic compounds is receiving attention. Albright[2] and Hanson *et al.*[3] have reviewed the findings reported by previous workers and have shown that considerable doubt exists as to whether the effect of mass transfer on such processes has in fact been eliminated, as claimed, by working under conditions of severe agitation. More recent work by Hanson *et al.*[4] has demonstrated that the nitration of toluene in a miniature continuous stirred tank reactor is, in fact, mass transfer or diffusion controlled even with very intense agitation. This work has been continued and attempts are being made to construct a satisfactory model of the nitration process, as this would aid in the design of reactors for such processes. A knowledge of the interfacial area is essential to such calculations and hence experiments have been carried out to provide this information. During this work, it soon became evident that existing published correlations for mean drop size in stirred tanks did not predict accurately the mean drop sizes encountered in the experiments. The causes of the discrepancy could lie in the correlations themselves or in the fact that mass transfer and chemical reaction were also taking place, whereas experimental confirmation of the correlations had invariably been obtained with systems at equilibrium. Accordingly, the

*Present address: I.C.I. Ltd., Dyestuffs Division, Huddersfield, U.K.

assumptions underlying the theory of droplet breakup were examined critically in order to establish the validity and applicability of the correlations. At the same time, further experiments were carried out to try to estimate the effects of mass transfer and chemical reaction on the physical properties of the system.

Mechanics of the dispersion of fluids

The interdispersion of immiscible fluids is brought about by the interaction of fluid dynamic forces in the continuous phase and surface forces of interfacial tension and viscous stress in the dispersed phase. Three major stresses act on the dispersed phase:

(i) external shear stress $= f$ . . . . . (1)

(ii) surface resistance $\propto \frac{\gamma}{d}$ . . . . . (2)

(iii) viscous stress in dispersed phase $\propto \frac{\mu_D}{d}\sqrt{\frac{f}{\rho_D}}$ . . . . (3)

Formal dimensional analysis leads to two useful dimensionless groups.[5] These are (i) the Weber Number ($N_{We} = \frac{fd}{\gamma}$); and the Ohnesorge Number ($N_{Ohn} = \frac{\mu d}{\sqrt{\rho_D \gamma d_{vs}}}$). As the external force becomes increasingly greater than the opposing interfacial tension force, so the Weber Number (their ratio) increases, as does the deformation of the drop. At a critical value of N_{We}, the drop breaks up. As the imbalance increases still more, the break-up process becomes increasingly chaotic. The Critical Weber Number ($N_{We_{crit}}$) will be a function of the Ohnesorge Number (frequently ignored) and Hinze[5] proposed the relationship:

$$N_{We_{crit}} = C_1 (1 + b(N_{Ohn})) \quad . \quad . \quad . \quad . \quad . \quad . \quad . \quad (4)$$

in which C_1 is a constant, and the function $b \rightarrow 0$ as $N_{Ohn} \rightarrow 0$.

Kolmogorov[6] considered the dimensions of the eddies occurring in turbulent flow. The primary eddies are similar in scale to the main flow stream dimensions, but are unstable and decay into smaller eddies. The process continues until the energy is dissipated by viscous flow. He concluded that all eddies which are much smaller than the primary eddies are statistically independent of them and that their properties are governed by the local energy dissipation per unit mass of fluid. He deduced an eddy length, l, given by:

$$l = \frac{\mu_c^{0.75}}{\rho_c^{0.5}} \left(\frac{P}{V}\right)^{-0.25} \quad . \quad . \quad . \quad . \quad . \quad . \quad . \quad . \quad . \quad (5)$$

If the drop diameter, d, is greater than the eddy length, then fluctuations in the fluid velocity around the drop will take place over the drop surface, contributing to break-up (Kolmogorov's First Case). Conversely, if the drop size is less than the eddy length, there will be no such fluctuations, and break-up occurs because of viscous drag rather than inertial forces (Kolmogorov's Second Case).

Kolmogorov's First Case

For the former case, Batchelor[7] has derived an expression for the mean square fluctuating velocity over the maximum drop diameter:

$$\bar{v}^2 = C_2 (E d_{max})^{0.667} \quad . \quad . \quad . \quad . \quad . \quad . \quad . \quad . \quad (6)$$

when $q \gg d \gg l$, (q is impeller blade width, E is power dissipated per unit mass of the continuous phase, C_2 is a constant.)

The Critical Weber Number may be written as:

$$N_{We_{crit}} = \rho_c \frac{\bar{v}^2 d_{max}}{\gamma} \quad . \quad . \quad . \quad . \quad . \quad . \quad . \quad . \quad (7)$$

If viscous forces are neglected, Hinze[5] showed that:

$$d_{max} \left(\frac{\rho_c}{\gamma}\right)^{0\cdot 6} E^{0\cdot 4} = C_3 \quad . \quad . \quad . \quad . \quad . \quad . \quad . \quad . \quad (8)$$

which transforms simply into

$$d_{max} = \frac{C_4 \gamma^{0\cdot 6}}{\rho_c^{0\cdot 2} \left(\frac{P}{V}\right)^{0\cdot 4}} \quad . \quad . \quad . \quad . \quad . \quad . \quad . \quad . \quad (9)$$

since $E\rho_c = P/V$

If d_{max} and d_{vs} are linearly related (for which see section on drop size distributions) then $d_{vs} = \dfrac{C_5 \gamma^{0\cdot 6}}{\rho_c^{0\cdot 2} \left(\frac{P}{V}\right)^{0\cdot 4}}$ . . . . . (10)

Introducing another dimensionless group,

the Power Number $\left(N_p = \dfrac{P g}{\rho N^3 D^5}\right)$ gives:

$$\frac{d_{vs}}{D} \propto N_{We}^{-0\cdot 6} N_p^{-0\cdot 4} \left(\frac{D^3}{V}\right)^{-0\cdot 4} \quad . \quad . \quad . \quad . \quad . \quad . \quad . \quad (11)$$

where D is agitator diameter, N is agitator speed (T^{-1})

Since the Power Number is constant for a fully-baffled, agitated vessel operating in the turbulent region,[8] then for scale-up maintaining geometric similarity,

$$\frac{d_{vs}}{D} = C_6 N_{We}^{-0\cdot 6} \quad . \quad . \quad . \quad . \quad . \quad . \quad . \quad . \quad . \quad (12)$$

Chen & Middleman[9] and Sprow[10] working at very low hold-ups ($H_v < 0\cdot 015$) have obtained correlations of this form. Other workers, e.g. Vermeulen *et al.*,[11] Calderbank[12] and Pitt,[13] have discovered that dispersed hold-up is an important parameter. All their results can be correlated by expressions of the form:

$$\frac{d_{vs}}{D} = C_7 (1 + C_8 H_v) N_{We}^{-0\cdot 6} \quad . \quad . \quad . \quad . \quad . \quad . \quad (13)$$

C_6 and C_7 are typically of the order 0·5–0·65 for stirred tanks of standard configuration. C_8 is very sensitive to the distance of the probe from the impeller. However, Rodgers *et al.*[14] correlated their results by:

$$\frac{d_{vs}}{D} = C_9 N_{We}^{-0\cdot 36} \left(\frac{D}{D_T}\right)^{-p} \quad . \quad . \quad . \quad . \quad . \quad . \quad . \quad (14)$$

where D_T is tank diameter; $0\cdot 75 < p < 1\cdot 4$ and $C_9 = f(D_T)$. Their work was carried out at only one value of hold-up ($H_v = 0\cdot 5$). This high value of hold-up might explain the different form of the correlation. Most workers have found drop size to increase with hold-up, even in the isotropic turbulence

region near the impeller: they have assumed that this is due to coalescence. However, Pitt,[13] using both non-coalescing and coalescing systems, found that the same correlation held good for each. This suggests that, in fact, this effect may be due to the damping effect of the dispersed phase on the scale of the turbulent eddies in the impeller stream. This is in line with the observations of Taylor[15] and Hinze[5] that the Critical Weber Number for single droplets is a function of the viscosity ratio of the two phases.

Kolmogorov's Second Case

In this case, the mean square fluctuating velocity was shown by Batchelor[7] to be:

$$\bar{v}^2 = \frac{C_{10}\, E \rho_c\, d_{max}^2}{\mu_c} \qquad (15)$$

where $\eta \gg d$; $l \gg d$.

If these fluctuations lead to drop breakup, the Critical Weber Number is given by:

$$N_{We_{crit}} = \frac{\rho_c\, \bar{v}^2\, d_{max}}{\gamma} \text{ as before} \qquad (16)$$

$$\text{or } N_{We_{crit}} = \frac{C_{10}\, \rho_c^{\,2}\, d_{max}^3\, E}{\mu_c\, \gamma}$$

If Ohnesorge Number can again be ignored and if the maximum and mean diameters are simply related, this gives:

$$d_{vs}^{\,3} = \frac{C_{11}\, \mu_c\, \gamma}{\rho_c^{\,2} E} = \frac{C_{11}\, \mu_c\, \gamma}{\rho_c \left(\frac{P}{V}\right)} \qquad (17)$$

Thornton & Bouyatiotis[16] measured drop sizes near the bottom corner of a tank of standard geometry and correlated their results thus:

$$d_{vs} = d^{o}_{vs} + m\, H_v \qquad (18)$$

where d^{o}_{vs} is drop size extrapolated to zero hold-up and m is the rate of change of drop size with hold-up. d^{o}_{vs}, in turn, was well correlated by:

$$\left[\frac{d^{o}_{vs}{}^2\, \rho_c^{\,2}\, g}{\mu_c^{\,2}}\right] = 29{\cdot}0 \left[\frac{\left(\frac{P}{V}\right)^3 g_c^3}{\rho_c^{\,2}\, \mu_c\, g^4}\right]^{-0{\cdot}32} \left[\frac{\rho_c^{\,3}\, \gamma}{\mu_c^{\,4}\, g}\right]^{0{\cdot}14} \qquad (19)$$

m was dependent upon the physical properties of the system:

$$m = 1{\cdot}18 \left[\frac{\gamma^2}{\mu_c^{\,2}\, g}\right] \left[\frac{\Delta\rho\, \gamma^3}{\mu_c^{\,4}\, g}\right]^{-0{\cdot}62} \left[\frac{\Delta\rho}{\rho_c}\right]^{0{\cdot}05} \qquad (20)$$

The correlation of d^{o}_{vs} may be readily transformed to:

$$d^{o3}_{vs} = C_{12}\, \frac{\mu_c^{\,1{\cdot}76}\, \gamma^{0{\cdot}42}}{\rho_c^{\,2{\cdot}18}\, E^{0{\cdot}96}} \qquad (21)$$

This has strong similarities to Equation (17) derived above and suggests that Kolmogorov's Second Case is applicable to those regions of the stirred-tank which are well away from the impeller. The hypothesis presented here receives added support from the work reported by Sprow[17] and Rushton.[18] They measured drop sizes at various points within a tank and found that their results

did not fit the flow circulation pattern as proposed by Rietema.[19] In the plane of the impeller, there was a marked increase in drop size along a radial path to the tank wall. At the wall, the flow splits into upper and lower circulation loops, with an initial decrease in drop size. Little further variation was found in the upper loop, but drop size in the lower loop again increased as the distance from the impeller increased. The largest drop sizes were observed at the bottom corners of the tank.

Variation of drop size with agitator speed

If the drop sizes were to follow a correlation which is in agreement with Kolmogorov's First Case, they would have to agree with Equation (10), where for a given system:

$$d_{vs} \propto \left(\frac{P}{V}\right)^{-0\cdot4} \qquad (22)$$

However, most practical cases must occur in the fully turbulent region where the Power Number is constant:[8]

$$\text{i.e. } \frac{P}{V} \propto N^3 \qquad (23)$$

$$\text{leading to } d_{vs} \propto N^{-1\cdot2} \qquad (24)$$

If, on the other hand, the correlation is based upon Kolmogorov's Second Case, then Equation (17) gives:

$$d_{vs} \propto \left(\frac{P}{V}\right)^{-0\cdot333} \qquad (25)$$

$$\text{or } d_{vs} \propto N^{-1\cdot0} \qquad (26)$$

Drop size distributions

The most common distributions are the normal and the log-normal distributions.

Normal distribution

This law applies when differences of equal amounts in excess of or deficiency from a mean value are equally likely. This is represented by:

$$y = \frac{1}{s\sqrt{2\pi}} \exp\left(\frac{-(d-\bar{d})^2}{2s^2}\right) \qquad (27)$$

where y = probability density
d = drop diameter
$\bar{d}$ = arithmetic mean drop diameter
s = standard deviation

$$s^2 = \sum_{o}^{\infty} \frac{(d-\bar{d})^2}{M-1}$$

M = total number of drops measured

A dispersion whose drop size distribution fits the 'normal' equation can be characterised by two parameters, i.e. mean value and standard deviation; a straight line will result from plotting drop diameter against cumulative percentage frequency.

Log-normal distribution

Many distributions obey a law where ratios of equal amounts in excess of or deficiency from a mean value are equally likely:

$$y = \frac{1}{\log s \sqrt{2\pi}} \exp\left(\frac{-(\log d - \log\bar{d})^2}{2(\log S)^2}\right) \quad . \quad . \quad . \quad . \quad . \quad (28)$$

Such a distribution yields a straight line when log d is plotted against cumulative percentage frequency.

Svarovsky[20] has suggested a modified form of the log-normal distribution. The distribution of drop size is usually required, and is more useful than the distribution of log d:

$$y = A' \exp\left(-b' \ln^2\left(\frac{d}{d_g}\right)\right) \quad . \quad . \quad . \quad . \quad . \quad . \quad . \quad (29)$$

d_g is the mode, or most common dropsize, A' and b' are constants characteristic of the distribution, and are obtained from the slope of the graph of log d plotted against the probability.

It can be shown[21] that for a log-normal distribution a simple relationship exists between d_{vs} and d_g, e.g.

$$d_g = 0{\cdot}926\, d_{vs} \quad . \quad . \quad . \quad . \quad . \quad . \quad . \quad . \quad . \quad (30)$$

This suggests that a similar relationship may exist between d_{vs} and d_{max}. This has, in fact, been reported by Sprow,[10] Chen & Middleman,[9] and Brown & Pitt[22] who all obtained:

$$d_{vs} = C_{13}\, d_{max} \quad . \quad . \quad . \quad . \quad . \quad . \quad . \quad . \quad . \quad (31)$$

However, few workers have reported any work on droplet size distributions in stirred tanks. Ward & Knudsen[23] have studied the phenomenon in turbulent pipe flow and observed two peaks in the size distribution. The one at lower diameter was attributed to drop breakdown and the other to coalescence. The latter tended to disappear at low hold-ups. One possible conclusion is that a skewed distribution is an indication that coalescence is occurring. Sprow[10] and Chen & Middleman[9] both tried to express their distribution mathematically. Sprow obtained a skewed distribution, whereas Chen & Middleman obtained normal curves. However, the latter workers used very small values of H_v, and hence little coalescence could be expected. Sprow, on the other hand, worked with a variety of hold-ups, although none was high ($H_v < 0{\cdot}015$) and also used a Coulter counter in place of the more normal photographic technique for measurement of drop sizes.

Experimental

Drop size measurement

The specific surface diameter, or Sauter mean diameter, is one of the commonest and most useful quantities for characterising the drop size of the dispersed phase in a liquid–liquid system. It is the diameter of the drop having the same surface area–volume ratio as exists in the whole of the dispersed phase. It is defined as $d_{vs} = \frac{\Sigma n_i d_i^3}{\Sigma n_i d_i^2}$ where n_i is the number of drops of diameter d_i. If the fractional hold-up of dispersed phase is H_v, and the volume of the system is V, then the total interfacial area is given by $a = \frac{6 H_v V}{d_{vs}}$, and the interfacial area per unit volume by $A = \frac{6 H_v}{d_{vs}}$.

Two methods were considered for measuring the drop sizes; light transmittance, as used by several previous workers;[11,12,14,18] and a photographic method, in which the dispersion is photographed and the drop sizes are measured on a scaled enlargement.[9,16] The latter method was adopted for the following reasons. (i) The stoichiometry of the reaction entailed the use of large hold-ups of the dispersed organic phase. The light transmittance technique is best suited for systems with low hold-up. At higher hold-ups, a correction must be made for the multiple reflections of the light as it traverses a dense swarm of drops. (ii) The physical properties of the system change as reaction proceeds and hence the light transmittance method would have to be calibrated over a wide range of reaction conditions, and this would involve photography. (iii) The effects of coloured by-product formation might be difficult to correct for if the transmittance technique were used. (iv) The photographic method enables drop size distributions to be examined, whereas the other method gives information only on interfacial area and mean drop size.

Equipment

The dimensions of the continuous flow stirred tank reactor, C.F.S.T.R., used are shown in Fig. 1. The reactor was 15·25 cm high × 15·25 cm diameter (volume = 2·5 l) and constructed throughout in EN58J stainless steel. It was designed as closely as possible to the Standard Tank Configuration.[24]

The reactants were pumped from glass aspirators, in which they were stored, to the reactor using metering pumps. Two metering pumps of different

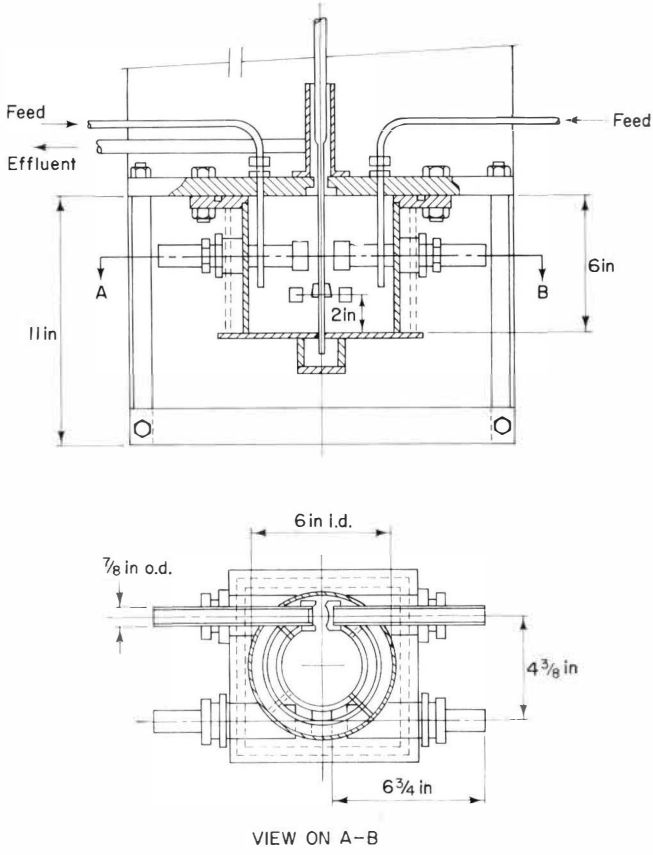

FIG. 1. *Reactor dimensions*

capacity were used to give a range of residence times in the reactor from 6 to 60 minutes.

The reactor probes were designed for use of the light transmittance and photographic techniques for measurement of drop sizes. Both techniques require two probes positioned directly opposite each other. With the photographic technique, one probe directs light into the reactor, whilst the other houses the photographic probe. One set of probes was positioned opposite the impeller at the reactor wall and the other midway between the impeller and the top of the reactor at the wall. Each set of probes consisted of two $\frac{7}{8}$ in o.d. stainless steel tubes sealed inside the reactor by screwed caps with glass windows. Since the stainless steel tubes were sealed at the reactor wall by 'Ermeto' fittings, the gap between the two could be varied depending on the hold-up, H_v, in the reactor. The greater the hold-up, the more light was absorbed by the dispersion and the closer the probes had to be positioned.

The photographic probe was built from a microscope which was modified so as to fit into the stainless steel reactor probes. The objective lens was screwed onto the end of a length of copper tubing, whilst the eyepiece fitted into a holder at the opposite end. A graticule was arranged in the holder for the eyepiece so that, after calibration, the graticule could be used for measuring the drop sizes. Photographs of the drops were obtained by a standard microscope camera which fitted onto the eyepiece holder. There was no shutter in the camera arrangement, but the speed of the drops was stopped by use of a high speed

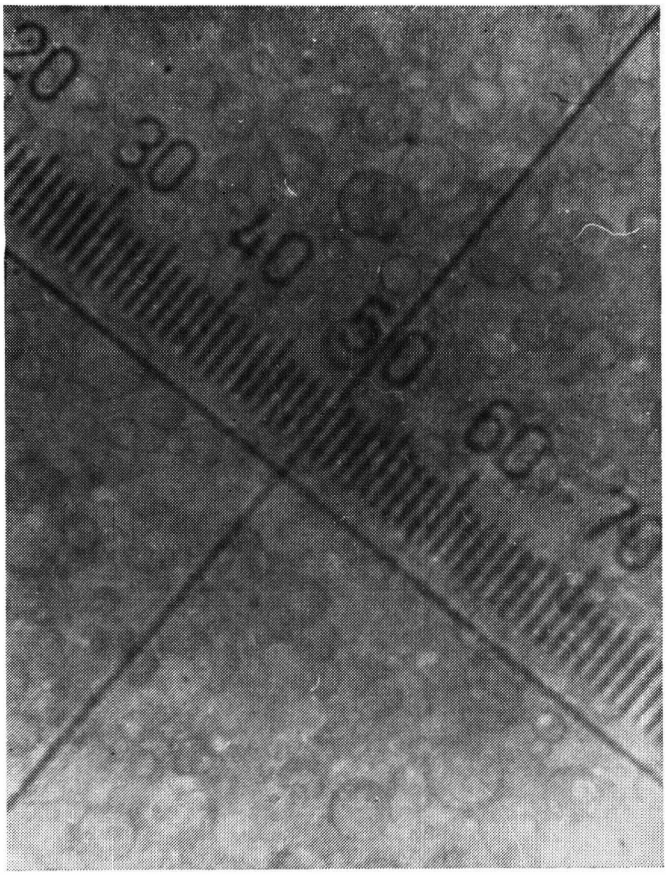

FIG. 2. *Photograph of typical dispersion*
scale marked in cm

flash. After much trial and error, Ilford F.P.4 film developed for 7 min at 68 °F in Acutol developer was found to give a satisfactory negative. A typical photograph from which the drops were measured is shown in Fig. 2. By measuring at least 300 drops, a maximum error of 3% was involved in the determination of d_{vs}.[25]

Systems

Drop sizes were studied during the nitration of toluene with the nitrating acids shown in Table I.

TABLE I

Acid mixtures used in the nitration of toluene

Component, mole-%	A	B	C
H_2SO_4	30	25	20
HNO_3	15	15	10
H_2O	55	60	70
	100	100	100

The physical properties of the system varied with the extent of reaction. Operating conditions for some of the experiments are included in Table II.

Procedure

The reactor was initially filled with water, the agitator switched on and the toluene and acid streams pumped in at the commencement of an experiment. When steady state conditions had been obtained, the dispersion was photographed. The power input to the reactor was measured by both electrical and mechanical means.

On completion of an experiment the agitator was stopped, the reactants drained from the reactor and H_v, the hold-up of dispersed phase in the reactor, measured. There was a critical agitator speed below which the hold-up in the reactor was less than in the feed. This critical value of approximately 1000 rev/min for the system used, appears to correspond to the start of the turbulent region of Rushton's Power Curve[8] for such a configuration. Only above the critical agitator speed was the power input proportional to the cube of the agitator speed. The latter is a property of the turbulent region of the Power Curve.

TABLE II

Details of experimental runs

Run No.	Acid composition	τ, min	T, °C	N, rev/min	P, h.p.	H_v	d_{vs}, μm	$a \times 10^4$, m^2/m^3	ρ_c at 30°C, g/cm^3	μ_c at 30°C, cP
1	A	10	30	1,000	0·023	0·425	175	1·48	1·620	8·90
2	A	10	30	1,200	0·040	0·440	161	1·64	1·595	7·40
3	A	10	30	1,500	0·056	0·438	148	1·78	1·617	8·46
4	A	10	30	1,700	0·084	0·437	125	2·10	1·613	8·21
5	A	10	30	2,000	0·139	0·448	106	2·53	1·604	8·10
6	A	10	30	2,400	0·250	0·445	84	3·18	1·595	8·04
7	A	40	30	1,500	0·059	0·430	139	1·86	1·591	7·35
8	A	10	30	1,500	0·063	0·377	115	1·97	1·627	9·60
9	A	40	30	1,500	0·059	0·430	139	1·86	1·591	7·35
10	A	50	30	1,500	0·061	0·44	140	1·890	1·588	7·09
11	B	20	30	1,500	0·059	0·50	169	1·775	1·570	6·60
12	B	20	30	1,500	0·062	0·361	127	1·705	1·571	6·64
13	B	20	30	1,500	0·060	0·275	95	1·74	1·577	6·85
14	B	20	30	1,500	0·060	0·398	140	1·71	1·572	6·61
15	C	6·55	30	1,500	0·061	0·190	80	1·43	1·547	6·23
16	C	30	30	1,500	0·063	0·283	118	1·44	1·510	5·37

Results and discussion

Effect of agitator speed

The logarithms of the drop sizes obtained during the study of the effect of agitation on the reaction rate are plotted against the logarithm of the agitator speed in Fig. 3. A line of slope —1·2 can be drawn through the points obtained at higher agitation speeds ($N > 1500$ rev/min), thus showing good agreement with Equation (24), based on Kolmogorov's First Case. At speeds of less than 1500 rev/min turbulent conditions may not have been fully established, as evidenced by the volume fractions within the reactor differing from the volumetric ratio of the feed streams. However, a line of slope —1 is also shown on the graph and it is possible that these points can, in part, be explained by Kolmogorov's Second Case, where break-up is due to viscous forces in a less turbulent stream.

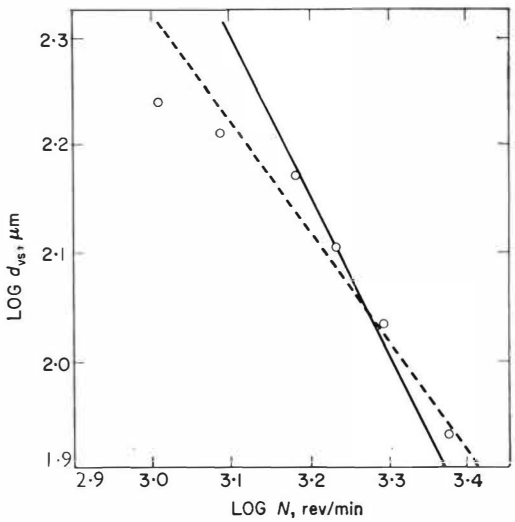

FIG. 3. *Effect of agitator speed on drop diameter*
$H_v = 0{\cdot}40$; $T = 30°C$; —— Slope = −1·2; - - - Slope = −1·0

N, rev/min	d_{vs}, μm
1000	172
1200	161
1500	148
1700	125
2000	106
2400	84

Variation of drop size with vessel hold-up and position in vessel

In the experimental programme aimed at establishing a model able to describe satisfactorily the nitration of toluene, the majority of the experiments were carried out at an agitator speed of 1500 rev/min. The mean drop sizes obtained in these runs are shown in Fig. 4 as a function of the organic phase hold-up, H_v. A considerable spread of drop sizes was expected since the physical properties of the system vary with the extent of reaction. Extrapolating to zero hold-up yields a drop size at zero hold-up d^o_{vs}, of approximately 9 μm. Substituting this value into Calderbank's correlation[12] for zero hold-up:

$$\frac{d^o_{vs}}{D} = 0{\cdot}06\ N_{We}^{-0{\cdot}6} \qquad (32)$$

and using an average value of 1·6 g/cm³ for the density of the continuous phase, a value of 8 dynes/cm is obtained for the apparent interfacial tension. This is much less than any value determined for mixtures of toluene and *o*-nitrotoluene

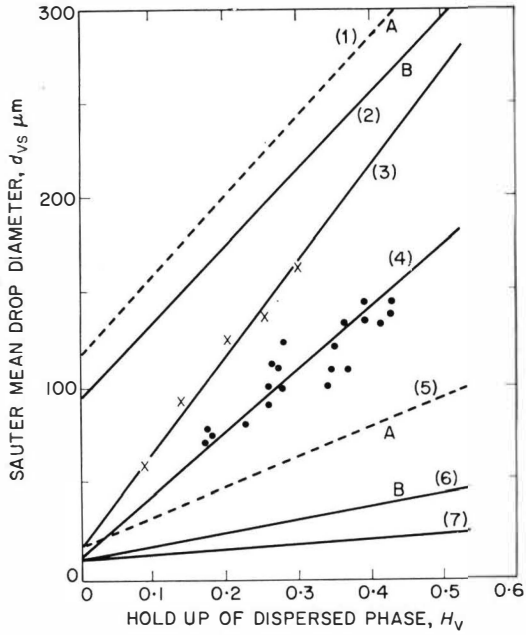

FIG. 4. *Variation of drop diameter with hold-up*

(1), (2) Thornton & Bouyatiotis[16]; (3) no mass transfer or chemical reaction; (4) nitration experiments; (5), (6) Calderbank[12]; (7) Pitt[13]; $N = 500$ rev/min, $T = 30°C$

with 30 mole-% sulphuric acid (Fig. 5). This acid is comparable to a nitrating acid which has been exhausted of nitric acid by reaction. These values of interfacial tension were obtained using the drop weight method described by Findlay.[26]

Such a large discrepancy between estimated and measured interfacial tensions for the system could well be due to the effects of mass transfer and/or chemical reaction. This was further investigated by agitating *o*-nitrotoluene and nitrating acid at different values of hold-up until the phases were mutually saturated and no further mass transfer took place. The drop sizes were then measured by the photographic method. The results are also plotted in Fig. 4. The mean drop size at zero hold-up, d^{o}_{vs}, was 13·5 μm. When this is substituted into Calderbank's equation, the apparent interfacial tension is 13·5 dynes/cm. The value obtained from Fig. 5 is 18·5 dynes/cm but in the actual experiments mutually saturated phases were used and hence the interfacial tension would be less than 18·5 dynes/cm. This relative agreement is encouraging. It can be seen from Fig. 4 that the runs with neither mass transfer nor reaction gave larger drop sizes than the nitration runs. The major reason for this difference appears to be the lower effective interfacial tension in the system where mass transfer and chemical reaction occur.

The results from these two systems were correlated by Calderbank's equation:[12]

$$d_{vs} = d^{o}_{vs}\,(1 + w\,H_v) \qquad (33)$$

where w is a coefficient dependent on position in vessel.

The value of w obtained from the nitration runs is 36·7; for the simple runs d is 40·0, which represents very good agreement when the large extrapolation of the nitration data is taken into account. Calderbank[12] obtained a value of 9 for measurements made in the impeller region. Pitt[13] obtained a value of 3·14 very close to the impeller.

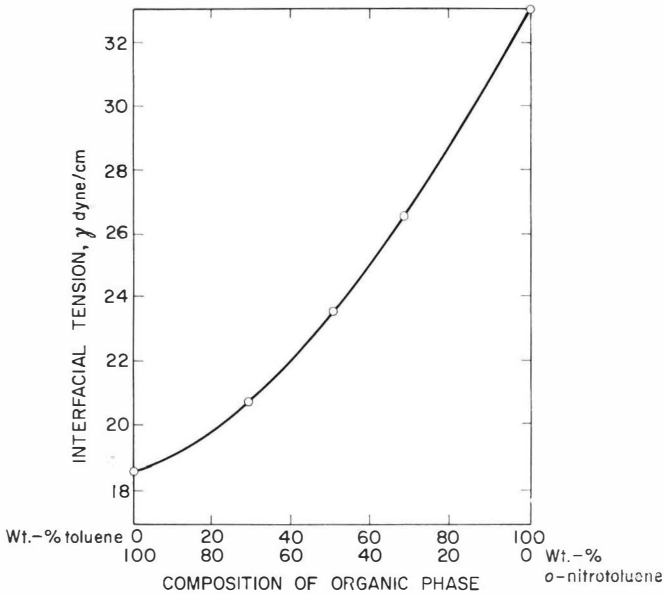

FIG. 5. *Interfacial tensions of 30 mole -%H_2SO_4 and mixtures of toluene and o-nitrotoluene*

The drop sizes predicted from the correlations proposed by Pitt,[13] Calderbank[12] and Thornton & Bouyatiotis[16] are also plotted in Fig. 4. The lines labelled 'A' were obtained using values of interfacial tension of the corresponding organic phase and 30 mole-% sulphuric acid (Fig. 5). Lines labelled 'B' use the apparent value of 8 dynes/cm derived from the nitration data. Organic phase compositions observed in a typical nitration run were used.

It can be seen from the graphs that the correlations predict an increase in drop size as the drop flows from the impeller to the vessel wall and thence into the lower circulation loop (Thornton's correlation). The data for the nitration experiments fit very well into this scheme. This stresses yet again that the correlations so far proposed predict a mean drop size only at the position in the vessel for which they were derived.

The results obtained from the nitration runs and from the straightforward mixing runs span the range of predicted drop sizes, agreeing with Pitt[13] and Calderbank[12] at low hold-ups, and with Thornton & Bouyatiotis[16] at higher values of hold-up. This is in agreement with the argument previously put forward that the effect of increasing the hold-up of the dispersed phase is to damp out the turbulent eddies more rapidly and hence hasten the transition from Kolmogorov's First Case to the Second Case, i.e. as hold-up increases so the mechanism of drop break-up changes, permitting the larger drops caused by coalescence of smaller drops to continue as a stable entity.

The variation of drop size in the upper circulation zone was also investigated during some of the runs. In such experiments the photographic probe in the upper half of the tank was used. Little variation was found. The results obtained in run 8 are typical. The mean drop size using the lower probe in the agitator plane was 115 μm whereas it was 124 μm using the probe in the upper circulation loop. This confirms the observation reported by Sprow[17] and Rushton.[18]

Interfacial tension in the toluene–nitrating acid system

An attempt was made to substantiate the previous arguments regarding interfacial tensions in the reacting system. A modified Du Nouy torsion balance

was used. The standard ring normally employed (see Findley[26]) was replaced by a very thin glass plate. The interfacial tension of the system should then be proportional to the force required to detach the plate from the interface. One volume of toluene was carefully superimposed on two volumes of nitrating acid (30 mole-% H_2SO_4; 15 mole-% HNO_3; 55 mole-% H_2O) in a glass dish. The interfacial tension was determined immediately, and then at intervals over the next few hours. The results obtained are shown in Fig. 6, in which the balance readings, which are proportional to the interfacial tension, are plotted against time. A small thermometer was also positioned at the interface, and the

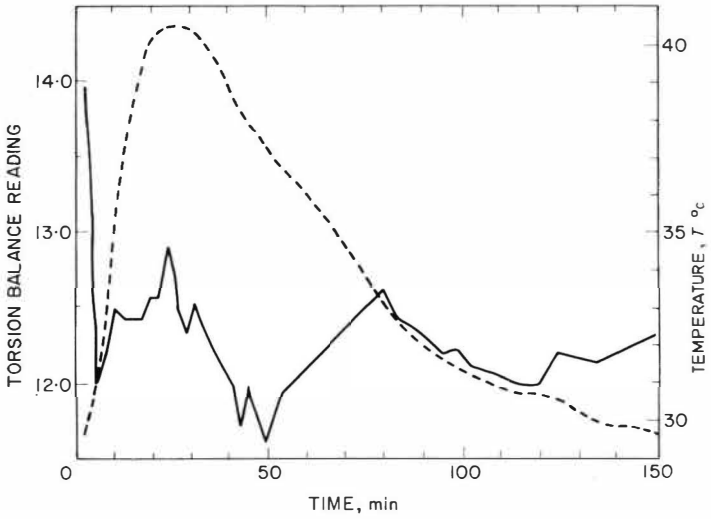

FIG. 6. *Variation of the interfacial tension of toleune and nitrating acid*

— Interfacial tension; - - - temperature

temperature of the interface followed. It can be seen that the interfacial tension rapidly decreased by 14% of its initial value, and the temperature increased by 15°C. The interfacial tension in the non-reacting toluene–30 mole-% H_2SO_4 system decreases by only 4·6% for such a temperature rise. The interfacial tension is further reduced by the formation of mononitrotoluene (MNT), for as shown in Fig. 5, the interfacial tension in the MNT–30% H_2SO_4 system is some 40% less than that of the toluene–50% H_2SO_4 system. However, this alone would not explain the smaller drop sizes obtained during the nitration runs. The indication is that interfacial phenomena reduce the effective interfacial tension, thus explaining the smaller drop sizes observed in the presence of mass transfer and chemical reaction.

Drop size distribution

Results from runs 8 and 15 are plotted in Fig. 7. It can be seen that the smaller drops seem to follow the normal distribution but that the larger drops show large deviations. This is probably attributable to coalescence.

Results from run 11 are plotted in Fig. 8. It can be seen that the number distribution approximates closely to a log-normal distribution. The surface and volume distributions are also plotted. These do not agree quite so well but, taking into consideration the variation in physical properties due to the reaction, the agreement is reasonable. The volume distributions for several runs are plotted in Fig. 9. Taking an average slope and applying Svarovsky's

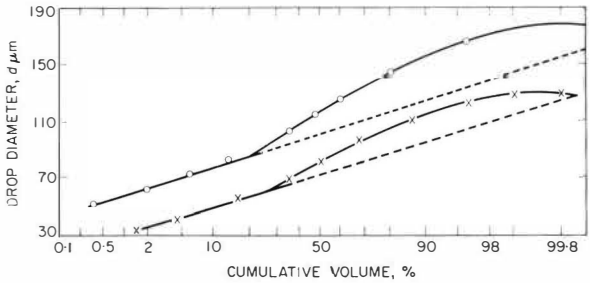

FIG. 7. *Application of the data of the present study to a normal distribution*
○ Run 8; × Run 15

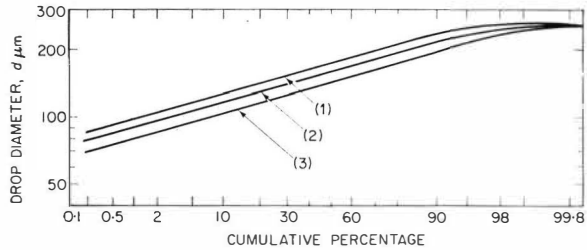

FIG. 8. *Number, surface area and volume distributions for nitration Run 11*
(1) Volume; (2) area; (3) number

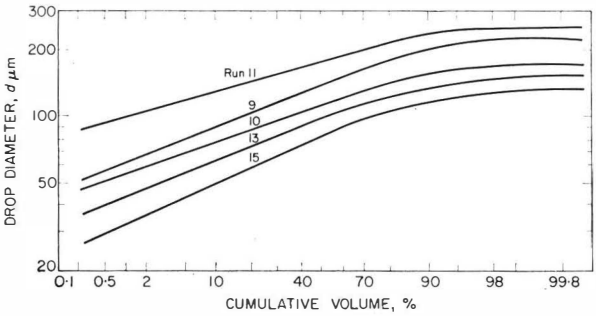

FIG. 9. *Various distributions obtained during the nitration of toluene*

method,[20] the following equation was obtained to describe the various distributions:

$$y = 0{\cdot}01 \exp\left(-4{\cdot}0 \ln^2\left(\frac{d}{d_g}\right)\right) \quad . \quad . \quad . \quad . \quad . \quad . \quad . \quad (34)$$

Fig. 10 is a plot of Equation (34) and the distribution obtained in run 11. The theoretical maximum probability is less than the actual one, because with an actual log-normal distribution it is theoretically possible to obtain a drop of infinite size. However, in a turbulent emulsion there is a maximum possible drop size above which break-up will occur. Therefore, there would be a tendency for more drops with the maximum size, as was actually obtained.

The relationship between mean drop size and the mode was found to be:

$$d_g = 0{\cdot}87\, d_{vs} \quad . \quad . \quad . \quad . \quad . \quad . \quad . \quad . \quad . \quad (35)$$

(*cf.* $d_g = 0{\cdot}926\, d_{vs}$, Equation (30))

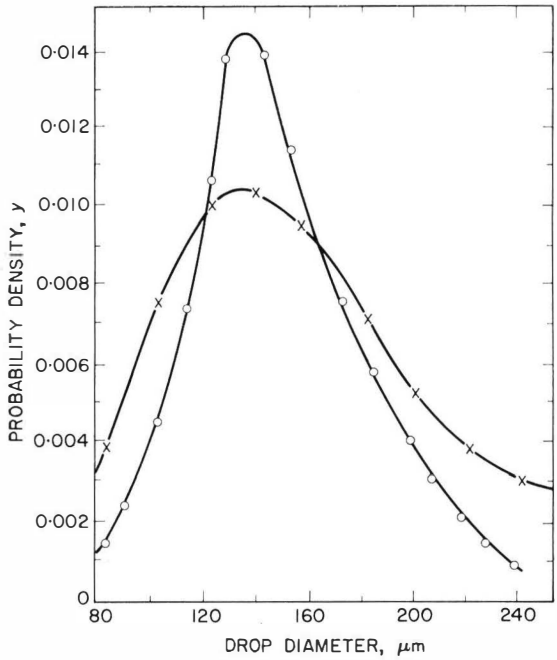

FIG. 10. *Application of drop size distribution equation to run 11*

○ Actual; × theoretical

This is further evidence that the distribution is not truly log-normal.

The relationship between mean and maximum drop sizes was obtained by the procedure used by Sprow,[10] who fitted his data to the equation:

$$\ln V\% = n\ 100 + \frac{a'}{d_{max}} - \frac{a'}{d} \quad . \quad . \quad . \quad . \quad . \quad . \quad . \quad (36)$$

where $V\%$ is cumulative volume percentage of the drops below diameter d and a' is a characteristic diameter.

A plot of $\ln V\%$ against $\frac{1}{d}$ gave a straight line. Data from runs 7, 8, 13 and 15, are plotted in this way in Fig. 11. Run 15 used the less dense 20 mole-% sulphuric acid. Good agreement was obtained, although deviations still occurred at large drop sizes. From the average slopes of these graphs:

$$d_{vs} = 0{\cdot}65\ d_{max} \quad . \quad . \quad . \quad . \quad . \quad . \quad . \quad . \quad . \quad (37)$$

This may be compared with the values obtained for the constant of 0·38 (Sprow), 0·625 (Chen & Middleman) and 0·675 (Brown & Pitt).

It would appear that coalescence caused the drop size distribution to be skewed. Such a result has been obtained in this present study. This is in agreement with most previous workers, the principal exception being Chen & Middleman. They obtained a normal distribution, but their maximum hold-up of dispersed phase was only 0·005%. The work of Nagata & Yamaguchi,[27] who worked at similarly low hold-ups, indicates that mass transfer and chemical reaction can promote a skewed distribution. Their work may be suspect, however, as they withdrew their samples from the tank prior to photographing them.

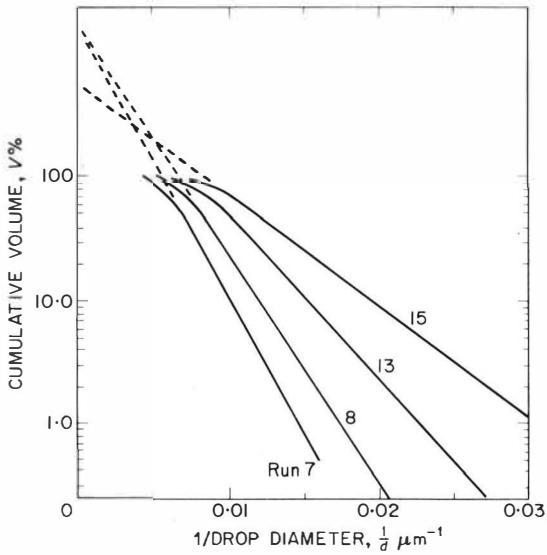

FIG. 11. *Application of Sprow's[10] correlation to the data of the present study*

Conclusions

The Sauter mean diameter of drops of the dispersed organic phase in experiments on the nitration of toluene by mixed nitrating acids have been measured. It appears that drop formation and break-up can be caused by two mechanisms. The first, observed at low dispersed phase hold-up or in regions of intense turbulence, is due to the imbalance between the external shear stress imposed by the turbulence and the interfacial tension striving to maintain drop sphericity and prevent gross distortion. This is characteristic of Kolmogorov's First Case. At higher hold-ups or in regions away from the agitator where the turbulent eddies have been damped out, break-up is due to viscous forces stripping smaller drops off the parent drop. The low external shear stress allows larger drops to retain their stability. This is Kolmogorov's Second Case. It has been shown that the results obtained by previous workers are in agreement with those presented here.

The mean drop size varies with position in the tank and hence existing correlations for mean drop size are only applicable for the position at which they were derived. This result may be explained by applying Kolmogorov's theory. The same is true for the effect of agitator speed on drop sizes.

The distribution of drop sizes has been investigated and has been shown to approximate to a log-normal distribution. Deviations from this distribution occur at large drop sizes. One possible explanation for this is that a log-normal distribution allows the existence of a very small number of very large drops, and even an infinitesimal chance of an infinite drop, whereas, in practice, in a turbulent emulsion there is a maximum possible drop size above which break-up inevitably occurs. This will tend to 'skew' the distribution for the larger drop sizes. Mass transfer and chemical reaction may enhance this effect.

The preliminary experiments attempting to measure the interfacial tension in the reacting toluene–nitrating acid system show that interfacial phenomena (including concentration and temperature gradients) can considerably reduce the interfacial tension. This lowers the surface forces opposing drop break-up and hence leads to a smaller drop size and increased surface area. This is likely to enhance mass transfer rates.

Nomenclature

A	interfacial area per unit volume
A'	coefficient in Equation (29)
a	interfacial area
a'	characteristic diameter in Equation (36)
b	function of N_{vi} in Equation (4)
b'	coefficient in Equation (29)
$C_1, C_2, \ldots C_{13}$	coefficients in various equations
D	impeller diameter
D_T	tank diameter
d	drop diameter
$\bar{d}$	arithmetic mean drop diameter
d_g	modal drop diameter
d_i	drop diameter
d_{max}	maximum drop diameter
d_{vs}	Sauter mean drop diameter $= \dfrac{\Sigma n_i d_i^3}{\Sigma n_i d_i^2}$
d^o_{vs}	Sauter mean drop diameter at zero hold-up
E	power dissipated per unit mass of the continuous phase
f	external shear stress acting on a drop
g	acceleration due to gravity
g_c	gravitational constant
H_v	hold-up of dispersed phase
l	eddy length
M	number of drops measured (Equation (27))
m	rate of change of drop size with hold-up (Equation (18))
N	agitator speed
n_i	number of drops of diameter d_i
P	power input
p	exponent in Equation (14)
q	impeller blade width
s	standard deviation
V	volume of system
$V\%$	cumulative volume percentage
$\bar{v}^2$	mean square fluctuating velocity over maximum drop diameter
w	coefficient in Equation (33)
y	probability density
γ	interfacial tension
μ_c	viscosity of continuous phase
μ_D	viscosity of dispersed phase
ρ_c	density of continuous phase
ρ_D	density of dispersed phase
τ	mean residence time
N_p	Power Number $= \dfrac{P_g}{\rho N^3 D^5}$

N_{Ohn} Ohnesorge Number $= \frac{\mu d}{\sqrt{e_D \sigma d_{vs}}}$

N_{We} Weber Number $= \frac{fd}{\gamma}$

References

[1] Hanson, C., (Ed.) 'Recent Advances in Solvent Extraction', 1971, Chap. 12 (Oxford: Pergamon Press)
[2] Albright, L. F., *Chem. Engng, Albany*, 1966, 73, (9) 169
[3] Hanson, C., Marsland, J. G., & Wilson, G., *Chemy Ind.*, 1966, p. 675
[4] Hanson, C., Marsland, J. G., & Wilson, G., to be published
[5] Hinze, J. O., *A.I.Ch.E. Jl*, 1955, **1**, 289
[6] Kolmogorov, A. N., *C.r. Acad. Sci. USSR*, 1941, **30**, 301; 1942, **31**, 538; 1943, **32**, 16
[7] Batchelor, G. K., *Proc. Camb. phil. Soc. math. phys. Sci.*, 1951, **47**, 359
[8] Rushton, J. H., Costich, E. W., & Everett, H. J., *Chem. Engng Prog.*, 1950, **46**, 467
[9] Chen, H. T., & Middleman, S., *A.I.Ch.E. Jl*, 1967, **13**, 989
[10] Sprow, F. S., *Chem. Engng Sci.*, 1967, **22**, 435
[11] Vermeulen, T., Williams, G. M., & Langlois, G. E., *Chem. Engng Prog.*, 1955, **51**, 85
[12] Calderbank, P. H., *Trans. Instn chem. Engrs*, 1958, **36**, 443
[13] Pitt, K., Ph.D. Thesis, University of Manchester, 1968
[14] Rodger, W. A., Trice, V. G., & Rushton, J. H., *Chem. Engng Prog.*, 1956, **52**, 515
[15] Taylor, G. I., *Proc. R. Soc. A*, 1934, **146**, 501
[16] Thornton, J. O., & Bouyatiotis, B. A., *Instn chem. Engrs Symposium*, Newcastle, 1967
[17] Sprow, F. S., *A.I.Ch.E. Jl*, 1967, **13**, 995
[18] Rushton, J. H., & Love, J. R., Purdue University, U.S.A., personal communication
[19] Rietema, K., *Adv. chem. Engng*, 1964, **5**, 237
[20] Svarovsky, L., personal communication, to be published in *Powder Technol.*
[21] Giles, J. W., Ph.D. Thesis, University of Bradford, 1970
[22] Brown, D., & Pitt, K., *Proc. Chemica 70, Melbourne–Sydney*, 1970, p. 83
[23] Ward, J. P., & Knudsen, J. G., *A.I.Ch.E. Jl*, 1967, **13**, 356
[24] Holland, F. A., & Chapman, F. S., 'Liquid mixing and processing in stirred tanks', 1966 (New York: Reinhold)
[25] B.S. 3406, Part 4, 1963, p. 35
[26] Findlay, A., 'Practical physical chemistry', 8th ed., 1954 (London: Longmans)
[27] Nagata, S., & Yamaguchi, I., *Mem. Fac. Engng Kyoto Univ.*, 1960, **22** (2), 249

Properties of an emulsion band in a mixer–settler contactor

by F. P. Pike and S. C. Wadhawan*

College of Engineering, University of South Carolina, Columbia, S.C. 29208, U.S.A.

The few published studies on the flow capacity and scale-up of mixer–settler contactors imply that the emulsion band is essentially homogeneous in its properties and that its thickness is simply related to the flow variables. On this basis, the rate of coalescence is the same for each unit area of coalescing interface; consequently it is proportional to total area, and scale-up becomes simple. The present study tests this hypothesis by measurements on a bench-scale rectangular mixer–settler operating on an oil–water system. A coarse oil-in-water emulsion was produced that settled so rapidly that it could only be studied in situ. *Measurements on the emulsion-band thickness confirmed that the rate of coalescence is controlled primarily but not exclusively by the extent of the surface separating the emulsion band from that coalesced phase which was once dispersed. Three different regimes were indicated, and impeller speed was a major factor. The physical properties of the emulsion, particularly that of density and viscosity, showed sharp discontinuities with respect to flow rate, at constant organic : aqueous ratio. This surprising pattern in the settler is consistent with the finding of Hillestad that two distinct operating regimes exist in the mixer section.*

Introduction

ALTHOUGH THE MIXER–SETTLER contactor is one of the oldest liquid–liquid contacting devices known and has been much studied in industry, there is a serious lack of published information, particularly with regard to the factors that limit flow capacity. The major definitive study is by Ryon *et al.*[1] They found that the logarithm of the emulsion band thickness gave a straight line relationship when plotted against the logarithm of the flow rate of the discontinuous phase expressed as a superficial velocity, that is, gal/min/ft^2 of horizontal disengaging area. Parallel lines were obtained for differing phase ratios of the two feed streams. The relationships found were very simple, but the key finding was that the variations in equipment size made no difference over an area scale-up of 1000 to 1. One can deduce that this could be true only if all units of horizontal area were equally effective in permitting coalescence independent of the range of horizontal dimensions. In turn, this implies complete uniformity in the emulsion phase. This finding has been debated and may hold only for the Dapex system studied by Ryon *et al.* Gondo *et al.*[2] also expressed equipment capacity as a superficial velocity and tested the behaviour of a kerosene–water system. They expressed the system flow capacity as the sum of the superficial velocities of the two inlet phases and found that this permitted a correlation of all of their emulsion band thickness data into one equation involving the flow ratio, the impeller speed and the sum of the two superficial velocities. Again, their correlation implies that the emulsion phase coalesces uniformly over the separating interface. However, they tested only one equipment size.

In addition, some information on flow capacity is contained in the paper by El-Roy & Gonen.[3] Hillestad[4] showed that the coalescing action in the mixer separated sharply into two differing patterns, depending upon the impeller speed. It would be difficult for the settling zone not to reflect the dichotomy of

* Present address: Pennsylvania Engineering Corp., 32nd Street, Pittsburgh, Pa. 15201, U.S.A.

the mixing zone, but neither Ryon *et al.* nor Gondo *et al.* detected more than one regime. Because of the questions raised, the present study was concerned with the properties of the emulsion band itself.

Experimental

Mixer–settler contactor

Fig. 1 shows a schematic arrangement of the entire apparatus, particularly the flow patterns of the two phases. It was originally intended to recirculate both phases so that mass transfer would be eliminated. However, a haze of secondary droplets developed so rapidly in the aqueous phase that this flow pattern was abandoned. Accordingly, tap water was employed on a once-through basis. However, the oil phase was recirculated and, hence, reached equilibrium with respect to the water content.

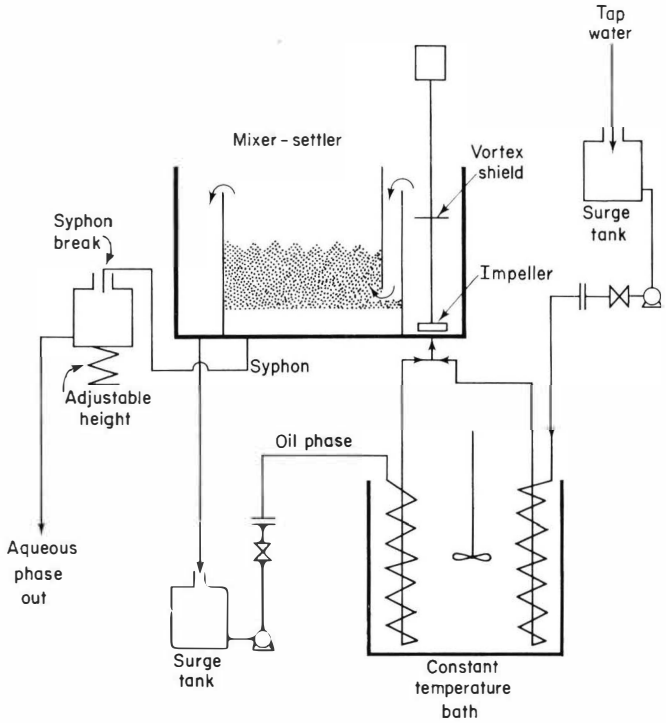

FIG. 1. *Experimental apparatus*

In this arrangement, the surge tanks were found to be virtually essential in disassociating changes in total volume and phase composition of the emulsion band. Otherwise, the system was very difficult to bring to equilibrium. Also it was necessary to break the syphon on the outlet aqueous line. The use of the constant-temperature bath restricted the temperature changes to $\pm$ 0·5°C.

The lines, pumps, and valves were made of polyethylene with an occasional seal using Viton rubber O-rings. The mixer–settler unit was constructed of glass (Pyrex) and a chemical-resistant thermosetting plastic (Laminac, American Cyanamid), sealed with epoxy cement. The flow was metered with precision glass rotameters using floats of stainless steel, titanium or Hastalloy.

The turbine impeller was a shrouded, flat-blade impeller of conventional design, and had six blades with an outer diameter of 58·8 mm. For this impeller the tip speed in m/sec = 0·03076 rev/min. The impeller diameter was fixed at one-half of the mixing-tank side dimension, in accordance with the recommendation of Rushton.[5] The impeller was carefully centred above the flow inlet and spaced with a clearance of 6·4 mm above it. A disc collar was installed on the impeller shaft to reduce the vortex action. This collar had the same diameter as the impeller and was 3·2 mm thick. It was placed 254 mm above the impeller and 127 mm below the liquid surface. The vortex shield greatly reduced the vortexing action and virtually eliminated air entrainment. It was felt to have influenced the circulation patterns in the mixer to a major degree. The speed of the impeller was controlled by a stepless transmission. The power input was measured by use of mechanical arrangements adapted from the equipment design of Bates.[6]

The mixer–settler unit was rectangular in cross-section. The mixer section was 119 × 119 × 368 mm deep to the overflow. The passageway to the settler was 119 × 38 × 197 mm down from the overflow level, thus introducing the emulsion starting at a point 171 mm above the settler floor. The upper part of the settler, where the coalescing occurred, was 119 × 340 mm in cross-section, and 355 mm deep to the overflow.

The mixer–settler was constructed by sealing the Pyrex plate glass walls into grooves cut in the plastic sheets. In this manner, the use of glass gave visual access to the settling zone and made photography possible, while the plastic permitted attachment of fittings with tapered pipe threads. These purposes were well served, but it was unfortunately found that the bonded combination could not stand much thermal stress. Earlier models cracked when the temperature was raised 10–15°C above ambient.

The entire apparatus was grease-free and chemically resistant, virtually inert. It possessed the following approximate ranges in capability:

Flow rate of the aqueous phase	0–250 cm^3/sec
Flow rate of the organic phase	0–250 cm^3/sec
Flow ratio of the two phases	10 : 1 to 1 : 10
Temperature	25–35°C
Impeller speed	0–1100 rev/min
Emulsion band thickness	5–305 mm
Power input	0–9·7 W
Coalescing area	432 cm^2

Material system

The aqueous phase was water from the City of Columbia system, considered to be a good grade of filtered and treated municipal water. The hydrocarbon phase employed was a commercial aliphatic petroleum fraction marketed as AMSCO 460 Solvent by the American Mineral Spirits Company, Palatine, Ill. The listed specifications for this fraction include the following information:

Density	0·811 g/cm^3 at 15·6°C
Initial boiling point	190°C
50% recovery point	218°C
Dry point	238°C
Aniline number	64·4
Flash point (closed cup)	63·9°C
Standard component analysis	42% paraffins, 40% naphthenes, 18% aromatics

The selection of AMSCO 460 Solvent was made because it was a reproducible, narrow-boiling fraction, relatively safe because of its high flash point and with a viscosity only about twice that of water.

At 30°C, the measured physical properties of the two phases were as follows:

	Tap water	AMSCO 460
Density, g/cm³	0·995	0·793
Viscosity, cP	0·80	1·2
Surface tension, mN/m	73·1	44·2

An attempt to measure the interfacial tension of the oil–water system at 30°C showed a slow trend with time. The value in mN/m was 30·75 at 0 h, 27·90 at 6 h and 27·45 at 21·5 h. The Wilhelmy plate technique was employed with a platinum plate; it thus appears that a slow selective adsorption occurred on the platinum.

Run procedure

Generally, it was possible to obtain either an oil–water or a water–oil emulsion, and occasionally the type would invert during a run. It was intended to operate with the oil–water type, and the start-up procedure was adapted to produce that type.

The thin emulsion produced in the mixer overflowed into the settling chamber and started to accumulate there. As the emulsion band aged, it changed in size and in phase ratio. These changes in turn induced a change in the inventory of the oil phase, usually accompanied by a vertical drift of the position of the emulsion band. It was necessary to monitor all flows and levels continually and to make continued adjustments.

A run was continued until the various measurements indicated that equilibrium had been attained. In order to ease this judgement, the apparatus was completely shut down and allowed to settle before each new run was started. This procedure gave a meaning to the time required to reach equilibrium. It was pertinent that an interfacial precipitate was continually formed at a slow rate during operation, in spite of the cleanliness of the system. This film was light coloured, initially nearly white but later grey. In appearance it was somewhat silky or fibrous and solid rather than liquid. Upon evaporation of a 10-cm³ sample of 'dirty' emulsion, no weighable residue could be detected to 1 mg. This film tended to accumulate at the far end of the settling zone. When allowed to accumulate to an appreciable extent, it retarded the rate of coalescence by physically blocking the interfaces. Fortunately, the rate of formation was quite slow. It sufficed to remove the accumulation approximately every 15–20 min during a run. The criterion for removal was a blockage of more than one linear inch of active coalescing interface. Removal was accomplished by suction, sweeping the pertinent area with the glass tip of a pipette.

Measurement of properties

Time to reach equilibrium

Each run was started from a complete shutdown, thus defining zero time. As a run proceeded, measurements were made of band thickness and the emulsion density and viscosity at a standard position. These values were plotted against time and fitted by eye with a smooth curve asymptotic to a limiting value. These curves were used to define the time to reach equilibrium.

Emulsion band thickness

It was observed that the emulsion band was rarely of uniform thickness. Generally, it had a wedge shape, thicker at the entrance. Furthermore, the thickness at the entrance had a slow cyclical variation about an average. At the far end, the emulsion band often curved up or down compared with the surfaces extending up to there. Sometimes the emulsion band did not reach the far end. In that case, the end thickness was measured about a short distance,

say 1 cm, from the end. Owing to the uncertainties, and to obtain a single thickness value, the following formula was adopted to measure the average band thickness:

$$\text{Average band thickness} = \frac{2\,(\text{middle thickness}) + (\text{sum terminal thicknesses})}{4}.$$

When the band thicknesses were appreciable, say 100–250 mm, the manner of defining the average made little difference. However, for thicknesses less than 20 mm, the manner of definition was important.

Emulsion density

The density was measured at specific points within the emulsion by determination of the buoyant force on a small glass sphere of 1·58 cm diameter. The density readings themselves were made on a modified Model No. 4028 Mohr-Westphal balance. By calibration on a series of liquids of known density, the density of the emulsion phase was measured to 0·001 g/cm.^{3} The movements within the emulsion prevented extension of the precision to the customary 0·0001 g/cm.^{3}

Emulsion viscosity

The viscosities of the emulsion band were determined with a Brookfield SynchroLectric Viscometer, Model LVT 8. In order to read the viscosity of the emulsion over a narrow vertical spacing, a special spindle was obtained that was essentially a smooth, thin, flat disc mounted on a centre rod.

In use, the special spindle was immersed at various depths, hence requiring an adjustable length of support. This was provided by three extension supports.

A series of tests were made to determine the appropriateness of the procedure. First, tests were made to determine the magnitude of the interference between the walls of a test vessel and the viscous drag of the rotating test spindle. The results are presented in Table I, for tests at constant room temperature using a viscosity standard.

TABLE I

Effect of vessel size on viscosity (cP)

Spindle speed, rev/min	Vessel inside diameter, mm			
	63·5	76·2	88·9	101·6
30	10·0	9·8	9·8	9·8
12	10·35	9·8	9·8	9·8
6	10·95	9·8	9·8	9·8
3	17·4	9·8	9·8	9·8

It is apparent that the wall effect dissipates rapidly and has essentially vanished when the vessel diameter has reached 76·2 mm. This gave an average clearance between the spindle and the walls of 8·8 mm. In practice, the spindle was kept at least 10 mm from the walls of the mixer–settler.

The test spindle when placed in the emulsion necessitated the use of varying lengths of suspending shaft, up to ~300 mm. Results of tests are presented in Table II.

TABLE II

Effect of shaft immersion on indicated viscosity (cP)

Test liquid: 10 cP standard, at 29·5°C; Inside diameter of test vessel 76 mm; Standard immersion 39 mm

Spindle speed, rev/min	Depth of immersion beyond the 39-mm standard, mm				
	0	25	44	76	152
30	9·80	9·83	9·85	9·85	9·85
12	9·80	9·83	9·85	9·86	9·87
6	9·80	9·82	9·84	9·86	9·86
3	9·80	9·85	9·86	9·86	9·86

The correction for the additional length of shaft was not only small, but was found to decrease as the indicated viscosity increased. Since most of the measured viscosities were above 100 cP, the immersion effect was ignored.

Two questions are associated with the measurements of the viscosity of the coarse oil–water emulsions. One is whether or not the coarse emulsion is Newtonian in character. Readings of the viscosity at different shear rates are presented in Table III.

TABLE III

Indicated emulsion viscosity (cP) at various shear rates

Test emulsion	Setting on Brookfield instrument, rev/min					
	60	30	12	6	3	1·5
A	*	*	*	*	3300	3200
B	*	*	*	1360	1350	1340
C	*	*	380	375	400	400
D	5·6	5·8	5·7	5·7	*	*
E	3·6	3·5	3·5	3·5	*	*

*Instrument off-scale

The conclusion drawn from Table III is that the readings were independent of shear-rate, and the coarse emulsions substantially Newtonian in character.

The other question concerned the behaviour of the rotating spindle of the viscometer. Using relationships derived by Schlicting,[7] the Reynolds Number was calculated at the tip for various emulsions. This was found to vary from about 0·02 at the minimum to a maximum of 4770 for the highest spindle speed, average density and lowest possible viscosity. From data presented by Schlicting,[7] laminar flow exists for all values of tip Reynolds Number less than 35,000. It was concluded therefore that the flow conditions were laminar over the entire rotating spindle under all conditions, that the emulsions encountered were Newtonian, and that the indicated viscosities were essentially correct measurements.

The special spindle was calibrated using standard viscosity solutions.

Hydraulic gradient

For the measurement of hydraulic gradient, three paper scales from transparent graph paper were pasted on the outside of the glass wall. These scales were carefully levelled by means of a spirit level. The level of the top surface of the emulsion, or other features, was read on these scales by a horizontal sighting on the scales.

Power input

The measurement of the power input was made possible by the special arrangements built into the equipment.[6] The drive motor of the stirrer shaft was supplied with a special, circular, ball-bearing support that was essentially frictionless. A mechanical arrangement transmitted the torque of the impeller to register as a force on a balance.

Droplet size

An attempt was made to photograph the emulsion through the glass walls and from the photographs to measure the average drop size. In a few cases, the photographs were quite revealing and useful. However, in most cases the presence of innumerable, very small drops rendered the photographs indistinct.

Results

General

The major finding of this study was that the behaviour patterns of the emulsion band are multiple and extraordinarily complex. Many different phenomena are distinguishable, but they are obviously interrelated.

After most of the data were obtained, the questions raised necessitated a closer visual study. Normally, it is impossible to see into the emulsion more than a few mm. However, by using very intense photoflood lamps for back-lighting, it became possible to see through the 120 mm width of emulsion contained between two plateglass walls. It was then found that the so-called emulsion band was, in fact, usually two bands of considerably different composition, one above the other. At low impeller speeds, only one band was observable and with it much less haze was associated. At higher impeller speeds, two layers appeared. The upper layer, larger in size, contained a high percentage of emulsified oil, 50–80 vol.-%. However, the lower band was much more dilute, containing typically only a few vol.-% of oil. Furthermore, the drop size averaged much less in the dilute band.

At relatively high impeller speeds, an additional third emulsion band sometimes appeared as a thin wedge between the two main layers. It was felt that these bands are simply a consequence of creaming behaviour, a well-known phenomenon in emulsion technology. For these coarse emulsions, the larger drops settle out much faster than the smaller drops, leading inevitably to some fractionation owing to differential settling.

By suitable use of the controls built into this system, it was possible to vary vertically the positions of the emulsion band. When this was done, it was possible to separate the emulsion into two sub-bands, the lower one dilute. Alternately, one could bring two sub-bands together by interpenetrating one into the other. It is easy to speculate that the coalescing of two intermeshed layers should be different from the net rate when they are separated. This operating control of the nature of the emulsion band means that studies should be made of the effect of vertical positioning of the main band.

Another critical observation was that there existed a complex flow pattern within the emulsion band. Generally, there was a flow band from the entrance which was approximately horizontal and moving away from the entrance. As this stream reached the far end of the settler, usually a stream turned up and flowed backward along the top of the emulsion band. Sometimes there was also a backflow underneath the primary horizontal flow. In other words, the emulsion band was not thoroughly mixed but rather was stratified. A volume element that flowed across the length of the settling zone, then back again, aged considerably compared with an entering volume element. Since ageing leads to compaction, and compaction leads in turn to higher viscosity and higher oil:water ratios, one could expect considerable differences in density

and viscosity at various spot locations. The finding of Wadhawan[8] was that this was clearly the case. Differences in viscosity by factors up to 5 were readily observed at different locations. However, the situation was further complicated by vertical mixing owing to some coalescing internal to the emulsion and no overall pattern was discernable for the variations in properties.

The appearance of haze was another highly variable phenomenon. At the lowest impeller speeds, sometimes no appreciable haze appeared in either phase. However, generally a haze was observed to exist in the continuous phase (water) only. But at the highest impeller speeds, a small quantity of haze was also observed in the coalesced discontinuous phase (oil). The common haze in the aqueous phase represented only a small amount of oil, considerably less than 1%. But it obviously did not settle out or coalesce rapidly for when the aqueous phase was recycled, a run of only 30 min would convert the entire aqueous phase to something like skimmed milk in appearance.

Another phenomenon of note was the occurrence of 'dimpling', as described by Frankel & Mysels[9] and by Allan *et al.*[10] 'Dimpling' is the appearance of a circular depression on a fluid drop on its front and centre as it approaches closely a solid interface, in this case the glass wall. Some of the successful photographs clearly revealed the occurrence of 'dimpling'. Another interesting revelation of the photography was the appearance of double and triple emulsions, drops inside drops inside drops.

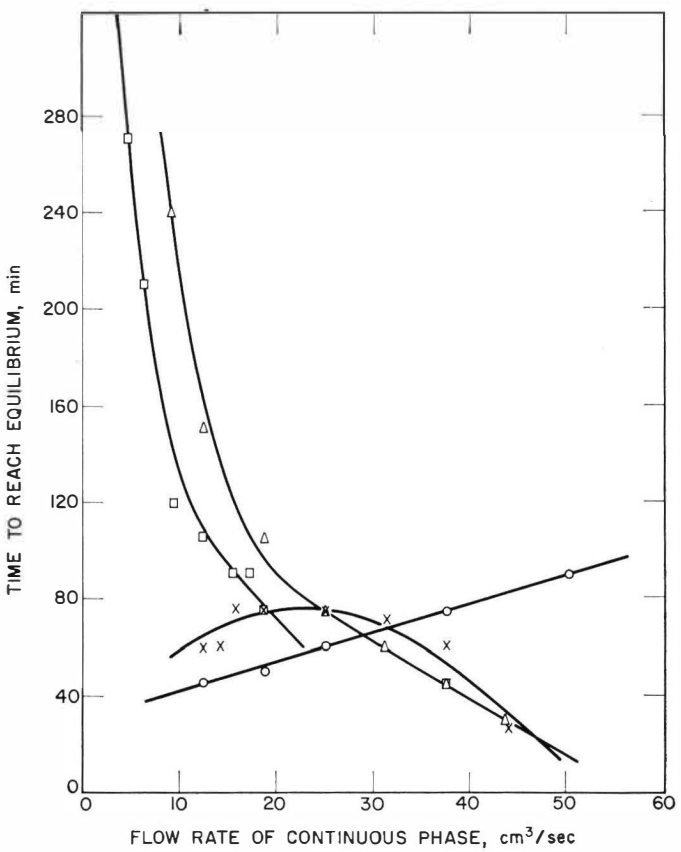

FIG. 2. *Time for the emulsion band to reach equilibrium in its properties*

Oil–water emulsion. Organic/aqueous ratio = 2·00; temp. = 30°C; viscosity of oil = 1·2 cP; viscosity of water = 0·8 cP.

Tip speeds (m/sec): ○ 1·12; × 1·52; △ 1·96; □ 2·97.

Finally, for some of the runs that give the thinnest bands, the emulsion did not spread out over the entire area available to it. As the emulsion moved forward, processes took place that finally came to an end with complete coalescence. This was a striking illustration that the emulsion band is not homogeneous although admittedly these bands were too thin to be industrially important.

The coalescing behaviour of the emulsion band was carefully observed with respect to the contention of Ryon *et al.*[1] that coalescence occurs solely at the interface between the emulsion and that coalesced phase which was previously dispersed. It was agreed by five observers that without doubt most of the coalescence did take place at the interface in question. However, both the photographs and the visual observations indicated that some coalescence did occur also within the body of the emulsion.

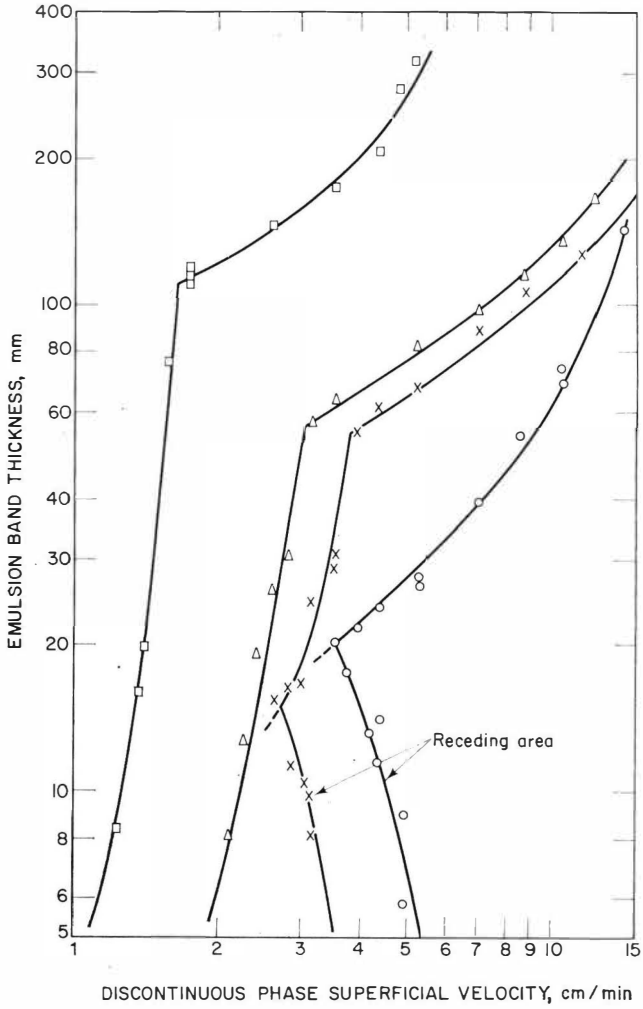

FIG. 3. *Emulsion band thickness as a function of operating variables*

Conditions as in Fig. 2

Measurements on the emulsion bands

A large number of measurements exploring the emulsion band were reported by Wadhawan.[8] For these runs, the emulsion type was restricted to oil/water, the temperature was held at 30° ± 0·5°C, and the O/A (organic/aqueous) ratio was fixed at 2·00. Four tip speeds were used for the impeller (1·12, 1·52, 1·96 and 2·79 m/sec), selected to cover an industrial range of practice. The major experimental variation was in flow rate of the aqueous phase, from ~60 cm³/sec downward by a factor of 10. The organic flow rate was tied to the aqueous rate by the fixed ratio of O/A = 2·00.

Fig. 2 presents the time to reach equilibrium, after start-up from no operation. Fig. 3 shows the emulsion band thicknesses for four different impeller speeds, as a function of the organic (discontinuous) flow rate expressed as a linear velocity with respect to the surface area active in coalescence. Note that for these runs O/A is constant. Figs 4, 5 and 6 represent the pattern of three behavioural responses as a function of operating variables (but O/A is constant), at one selected position in the settling zone. Data on other positions have been reported by Wadhawan.[8]

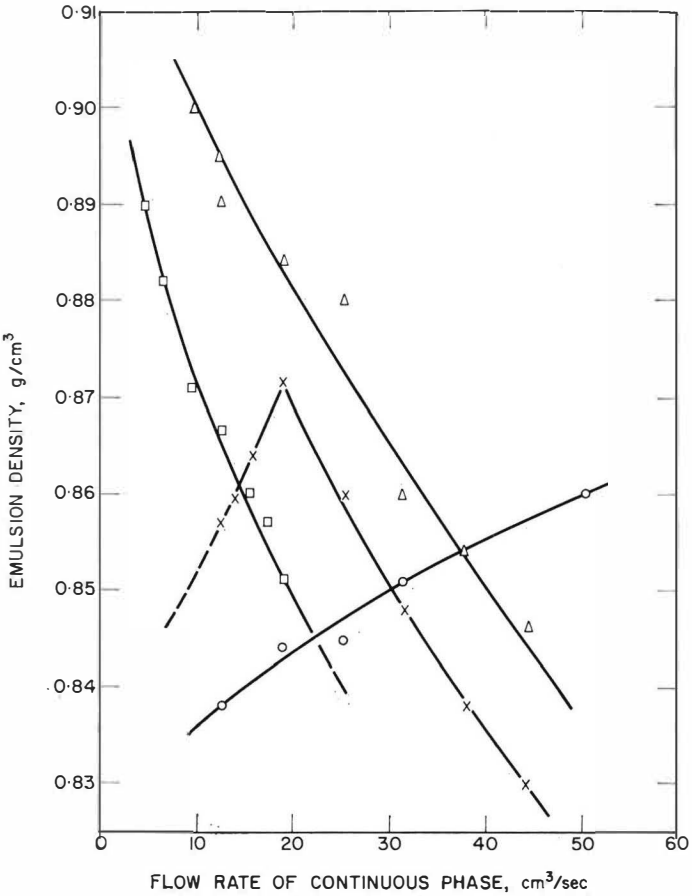

FIG. 4. *Density of the emulsion band in the centre of the settler and near the top of the band*

Conditions as in Fig. 2

An attempt was made to measure the O/A ratio within the emulsion band by sampling. A number of measurements were made and reported by Wadhawan;[8] these showed good internal consistency. However, it becomes clear that, with the large drop-size range that exists for these coarse emulsions, the sampling technique is critical. It is felt that the probe employed was too small in diameter, but the potential exists to measure another important characteristic of such emulsions bands.

The power input was measured for each run with an unexpected result. It was found that the power requirement was fixed by the tip speed of the impeller and that the flow rate through the mixing chamber had no influence at all on the power input. The simple relationship derived was that power was proportional to the tip speed raised to the power 3·63.

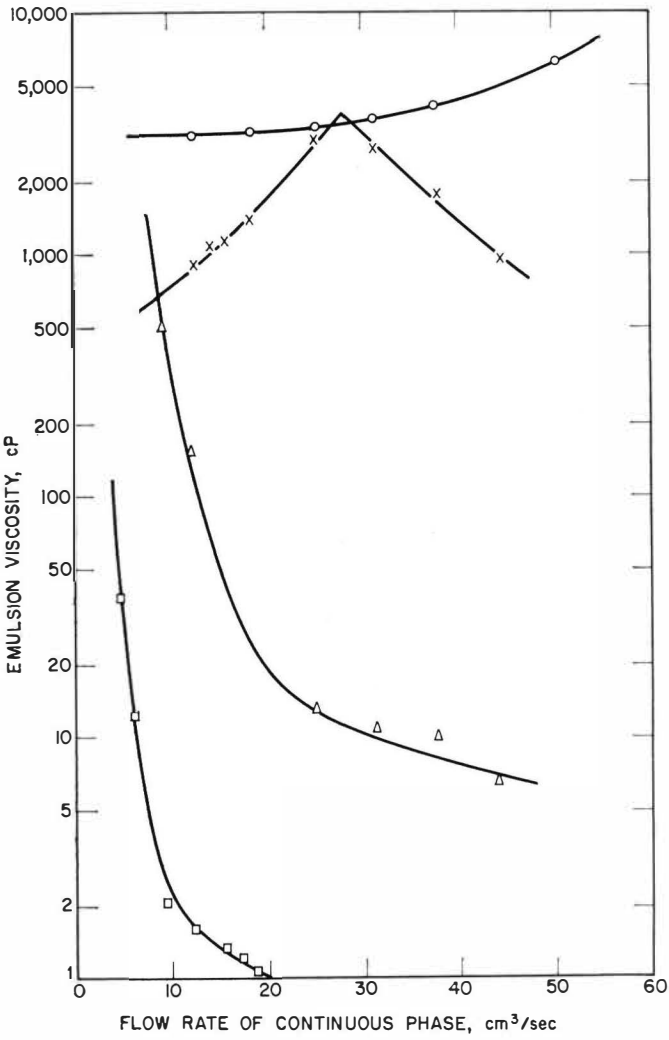

FIG. 5. *Viscosity of the emulsion band in the centre of the settler and near the top of the band*

Conditions as in Fig. 2

A series of runs was made to examine specifically the influence of the O/A ratio at constant flow rate of the organic phase. This would presumably check on the contention of Ryon[1] that only the flow rate of the discontinuous phase per unit of coalescing area was important and that the O/A ratio *per se* was of much less importance. The results are presented in Table IV. These measurements were made on the system after a period of shut-down. The data are not consistent with the previous data but are felt to be internally consistent.

TABLE IV

Effect of O/A ratios on emulsion band thickness

Tip speed, m/sec	Coalescence rate*, cm/min	Av. emulsion band thickness, mm		
		O/A 2·0	O/A 3·0	O/A 4·0
2·79	1·32	146	130	131
2·79	2·63	316	305	310
1·96	2·63	82	75	89
1·96	5·27	132	137	127
1·12	4·39	53	51	46
1·12	7·03	143	132	133

*Flow rate of the discontinuous phase (organic) with respect to the coalescing interface

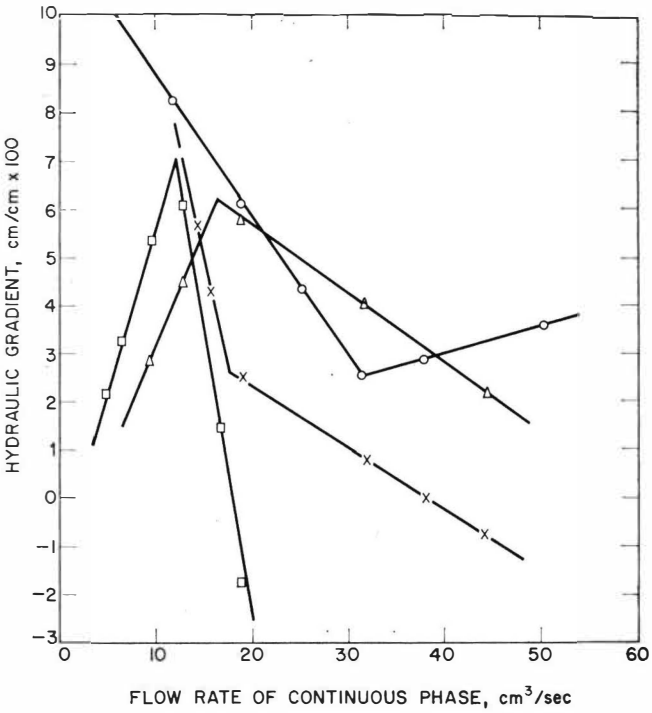

FIG. 6. *Top hydraulic gradient in the emulsion band*

Conditions as in Fig. 2

Discussion

There has been debate (Ryon, A. D., personal communication, 1968) over the relationships that control the thickness of the dispersion band and the generality of the straight line relationship presented by Ryon.[1] The results of this study do not agree with those of Ryon, nor do the results of Gondo *et al.*[3] agree with either. Yet each set is self-consistent. Perhaps the best conclusion is that the manner of dispersion and the spectrum of drop sizes differed enough between the three systems to account for the different behaviour patterns. The manner of breaking up the inlet discontinuous phase stream differs considerably between the three studies. The revelations of this study that the emulsion band is not a homogeneous structure, but rather is exceedingly complex, points to a route to an explanation.

A point of issue is the contention of Ryon[1] that the coalescence rate is controlled mainly by the flow rate of the discontinuous phase per unit area of coalescing interface. The O/A ratio has little or no effect, according to Ryon. Using this concept, it is appropriate to measure the coalescing rate as a superficial linear velocity. This study agrees in general with Ryon on this point. The experiments reported in Table IV specifically confirm that the O/A ratio is not significant. However, Gondo *et al.*[2] found it necessary in effect, to include the O/A ratio in their correlation. Their data are extensive, and their final correlation is effective in handling their data. It is noted that in the experiments of Gondo *et al.*,[2] the settling zone was small in diameter. There was literally no opportunity for their emulsion to travel laterally for an appreciable distance, as in the present experiments. Since lateral travel leads to an ageing effect, it is now clear that different geometries for settlers may well lead to different types of correlations.

The results presented in Figs 2–6 show remarkable agreement on one point, relating to five responses each quite different in character. They all are consistent in agreeing that the emulsions studied reflect some abrupt change or changes in regime. The trend in behavioural responses for one set of conditions can be the opposite to that of another set of conditions. The viscosity data and the density data clearly show abrupt transitions during a given experiment. It is difficult not to accept the conclusion of Hillestad[4] that abrupt changes in regime can occur in the mixer. If such a transition occurs in the mixer, it inevitably would find some reflection in the settler.

Incidentally, a number of authors have pointed to the need for careful attention to the hydraulic balance in a mixer-settler, to prevent emulsion from spilling from one unit to another. In this context, it is disconcerting to see in Fig. 6 that sometimes the hydraulic gradient, as judged by the top surface of the emulsion, can become negative. This behaviour was observed at other times also. There seems to be no explanation for this other than the inherent fact that the emulsions as studied were decidedly not homogeneous. It is pertinent that the viscosities of the emulsion are characteristically high, and reached the high value of >6000 cP. With such viscosities, non-homogeneity is promoted.

Conclusions

It has been shown that the physical structure of an emulsion band in a mixer–settler is extraordinarily complex, particularly when the emulsion flows an appreciable distance horizontally as in many rectangular commercial designs. Perhaps the differences in equipment geometry together with the specific manner in which the discontinuous phase is dispersed can explain the differences reported by the three available studies on the effect of operating variables on flooding capacity (as measured by emulsion band thickness). The differences must be resolved before scale-up can be reasonably assured.

Coalescence occurs primarily, but not exclusively, at the interface between the emulsion band and that coalesced layer which was once dispersed. This model places primary importance on the flow rate of the discontinuous phase per unit

of coalescing surface and dictates logically that the rate of coalescence should be expressed as a superficial velocity (such as cm/sec). The scale-up relationships will probably be simplified by the use of this variable.

The coarse emulsion in an operating mixer–settler tends to change rapidly with time at any one location and to age if it is allowed to flow along any extended path. Hence, an emulsion band can only be studied *in situ*. Suitable techniques have been developed to measure point values for emulsion density and emulsion viscosity. However, one should also study the phase ratio and drop spectrum at point locations, and the various internal circulation patterns. A means for seeing inside the emulsion is virtually essential. In turn, this means an intense lighting source plus clear walls that are preferably flat.

Acknowledgments

The authors acknowledge with gratitude the support of the Lithium Corporation of America for the construction and initial operation of the equipment.

References

[1] Ryon, A. D., Daley, F. L., & Lowrie, R. S., *Chem. Engng Prog.*, 1959, **55** (10), 70
[2] Gondo, S. I., Hisatomi, K., Kusunoki, K., & Nakamori, I., *Kagaku Kogaku* (*Chem. Engng, Tokyo*), 1968, **32**, 923
[3] El-Roy, M., & Gonen, D., *Israel J. Technol.*, 1964, **2**, 253
[4] Hillestad, J. G., Ph.D. Thesis, Purdue Univ., 1965
[5] Rushton, J. H., *Chem. Engng Prog.*, 1951, **47**, 485
[6] Bates, R. L., *Ind. Engng Chem.*, 1959, **51**, 1245
[7] Schlicting, H., 'Boundary-layer theory', 4th edn, 1966, 83–90 (New York: McGraw-Hill)
[8] Wadhawan, S. C., M.S. Thesis, Univ. South Carolina, 1968
[9] Frankel, P. S., & Mysels, J. K., *J. phys. Chem., Ithaca*, 1962, **66**, 190
[10] Allan, R. S., Charles, G. E., & Mason, S. G., *J. Colloid. Sci.*, 1961, **16**, 150

SESSION 1C

NUCLEAR APPLICATIONS, I

CHAIRMAN

Dr. E. Detilleux

SECRETARY

Dr. M. Streat

Reductive extraction processing of molten-salt fuels for breeder reactors

by L. E. McNeese, J. S. Watson, B. A. Hannaford, C. W. Kee and M. E. Whatley
Chemical Technology Division, Oak Ridge National Laboratory,
Oak Ridge, Tennessee 37830, U.S.A.

Reductive extraction affords a method of removing rare earth fission products and isolating ^{233}Pa from molten salt breeder reactors. The chemistry of reductive extraction of lanthanides and actinides is reviewed. Engineering experiments and development of countercurrent contactors for molten salt and metal are discussed. Data are presented on flooding, hold-up, axial mixing and mass transfer in packed columns.

Introduction

A UNIQUE FORM of liquid–liquid extraction is under development at the Oak Ridge National Laboratory for processing the fuel salt of a molten salt breeder reactor. The reference reactor[1] is a 1000 Mw(e), single fluid, two-region machine containing approximately 1700 ft^3 of salt having the composition 71·7 mole-% ^7LiF, 16 mole-% BeF_2, 12 mole-% ThF_4 and 0·3 mole-% UF_4. Efficient operation of the reactor requires the continuous removal of ^{233}Pa (an intermediate between ^{232}Th and ^{233}U) and rare earth fission products from the fuel salt.

The required separations can be effected by reductive extraction, a form of liquid–liquid extraction, in which materials present in the molten salt are extracted into a liquid bismuth stream containing a reductant.

This paper presents typical data for the distribution of important materials between molten salts and bismuth in the presence of a reductant, briefly describes a typical reductive extraction flowsheet based on these data and discusses engineering data concerning the development of packed column contactors for use with high density fluids.

Distribution of various metals between molten salts and bismuth

Bismuth is essentially immiscible with the molten salts but dissolves to a useful extent lithium, thorium, uranium and most of the fission products. Beryllium, an exception, is virtually insoluble in bismuth. Data for the distribution of a number of metals between molten salts and bismuth containing a reductant are reported elsewhere;[2,3] therefore, only sufficient information to characterise separation factors, on which a typical process flowsheet is based, will be given.

Under the conditions of interest the extraction of a metal halide, MX_n, can be expressed as the equilibrium reaction

$$MX_{n(salt)} + nLi_{(Bi)} = M_{(Bi)} + nLiX_{(salt)}$$

in which n is the valence of the metal in the salt phase. It has been found that, at constant temperature, the distribution coefficient, D, for metal M depends on the lithium concentration in the metal phase (mole fraction), X_{Li}, as follows:

$$\log D = n \log X_{Li} + \log K' \qquad (1)$$

where K' is a constant and the distribution coefficient is defined by:

$$D = \frac{\text{mole fraction of M in metal phase}}{\text{mole fraction of } MX_n \text{ in salt phase}}$$

The ease with which one component can be separated from another is indicated by the ratio of their respective distribution coefficients, that is, the separation factor. As the separation factor approaches unity, separation of the components becomes increasingly difficult.

Distribution coefficients obtained at 600°C with $LiF-BeF_2-ThF_4$ (72–16–12 mole-%) are summarised in Fig. 1. For the materials shown, zirconium,

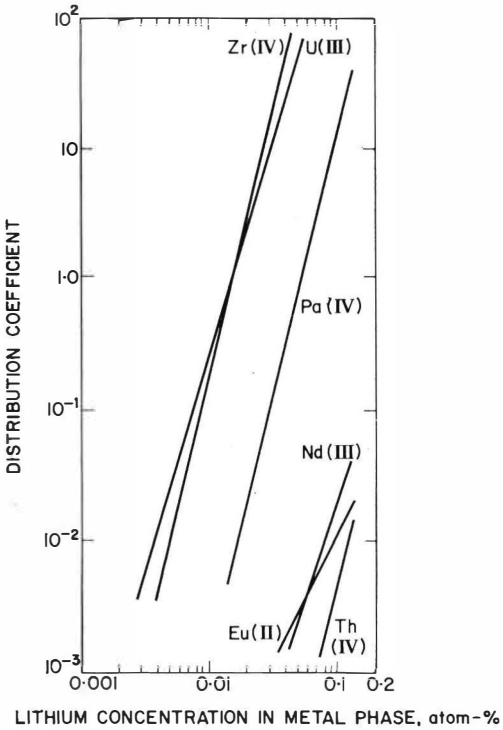

FIG. 1. *Distribution coefficients for various materials between molten salt and bismuth containing reductant at 600°C*

72–16–12 mole-% $LiF-BeF_2-ThF_4$

protactinium and thorium are tetravalent, uranium and neodymium are trivalent salts, and europium is a divalent salt. Uranium and zirconium are most easily extracted, but the separation factor between them is near unity. The separation of protactinium from uranium and thorium is straightforward since the U–Pa separation factor is approximately 100 and the Pa–Th separation factor is approximately 3000. These separation factors form the basis for the protactinium isolation method.

Separation of the rare earths from thorium in the presence of a fluoride salt is difficult since the thorium–rare-earth separation factors are only 1·2 to 3·5 under the most favourable operating conditions. However, with LiCl, much more favourable thorium–rare-earth separation factors are obtained (Fig. 2). For example, the thorium–trivalent rare-earth (Nd and La) separation factors are approximately 10^4 and the thorium–divalent rare-earths (Sm and Eu) and the thorium–alkaline-earth metal separation factors are both about 10^8. Similar separation factors also have been observed with LiBr. Thus, the separation of rare-earths from thorium is relatively easy.

Conceptual process flowsheet

A typical flowsheet for processing a single-fluid MSBR is shown in Fig. 3.

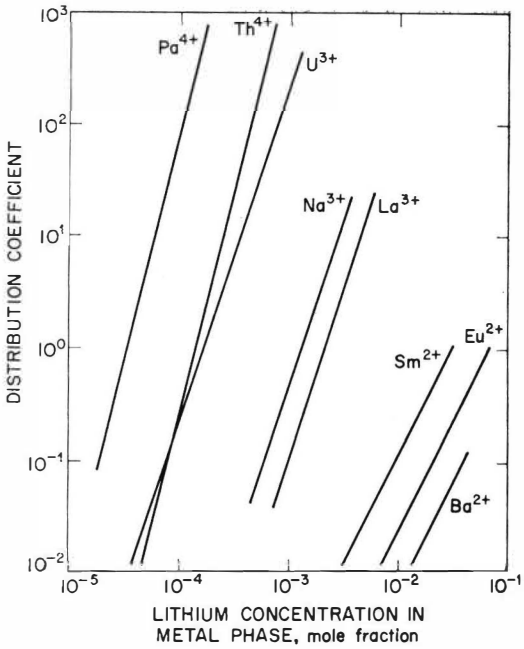

FIG. 2. *Distribution coefficients for various materials between LiCl and bismuth containing reductant at 640°C*

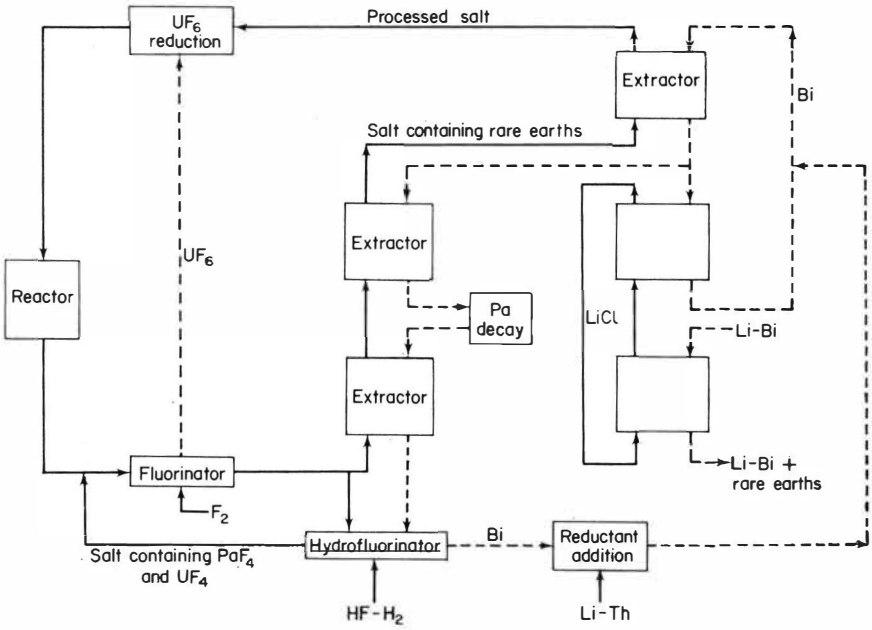

FIG. 3. *Typical flowsheet for processing a single-fluid molten-salt breeder reactor*

Salt is withdrawn from the reactor on a 10-day cycle; for a 1000-Mw(e) reactor, this represents a flow rate of 0·88 gal min^{-1}. The salt, containing UF_4 and PaF_4, is fed to a fluorinator where about 95% of the uranium is removed as UF_6. Ninety per cent of the salt, still containing protactinium and some uranium, is fed to a six-stage extractor where it is mixed with a countercurrent of bismuth containing lithium and thorium.

In the lower part of the extractor, uranium is preferentially reduced into the bismuth stream. The protactinium proceeds further up the extractor but is also reduced into the bismuth. Since relatively high protactinium concentrations can accumulate in the bismuth phase, this stream is diverted through a decay tank having a volume (about 160 ft^3) sufficient to contain most of the protactinium in the reactor system. The bismuth stream leaving the tank contains some protactinium, as well as the uranium that has not been removed by the fluorinator and the uranium that has been produced by decay of protactinium in the decay tank. This metal stream is hydrofluorinated in the presence of about 10% of the salt leaving the fluorinator in order to transfer the extracted materials to the salt stream that is recycled to the fluorinator for uranium removal.

The salt stream leaving the extractor is essentially free of protactinium and uranium but contains the rare-earths at approximately the same concentrations as present in the reactor. About 30% of the rare-earths are removed from the salt by countercurrent contact, in a three-stage contactor, with a 12·5 gal min^{-1} bismuth stream containing thorium. Following this step, the metal stream is countercurrently contacted with a 33 gal min^{-1} LiCl stream in a three-stage contactor, where significant amounts of the rare-earths and a negligible fraction of the thorium are transferred to the LiCl. The final process step is removal of the rare-earths from the LiCl by mixing with a bismuth stream containing lithium.

The processed salt is combined with the uranium that was removed initially to yield fuel salt, which is returned to the reactor.

Studies of packed column contactors for reductive extraction

Packed columns have been widely used in aqueous–organic solvent extraction systems. However, the present application results in significant deviations from that technique. For example, the fluids may not wet the packing material and have much higher densities, density differences and interfacial tensions than those in conventional systems. The authors have found that design correlations developed for organic–aqueous systems are unreliable under these conditions and have found it necessary to study the packed column operation with fluids which have properties similar to those of the molten salt–bismuth systems. A convenient choice is the mercury–water system, which is similar to the molten salt–bismuth systems in most respects. The mercury–water system has a high density difference and a comparable interfacial tension; the principal discrepancy is between the viscosity of water and the molten salts of interest (1 centipoise *vs* ~15 centipoises).

Studies with the mercury–water system have produced data on dispersed phase hold-up, column capacities (flooding rates), axial diffusion and column pressure drop. The packed columns studied had a length of 24 in and inside diameters of 1 and 2 in. The packing, made of polyethylene or Teflon, was not wet by water or mercury. The column diameter to packing diameter ratio ranged from 4 to 8, which is smaller than that needed for negligible wall effect; however, the column diameter was limited by the mercury supply and pump capacity.

Hold-up measurements are made by suddenly closing a ball valve at each end of the column in order to isolate the column. The volume of trapped mercury was then measured. The results obtained with 1/4-in Raschig rings having a void fraction of 0·71 are shown in Fig. 4. Hold-up increased as the flow rate

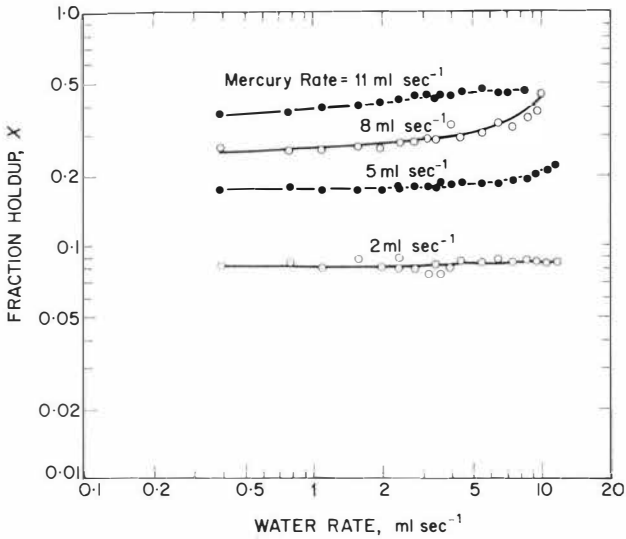

FIG. 4. *Dispersed phase hold-up in a mercury–water column packed with 1/4-in Raschig rings* 0·71 void fraction; 24 × 1 in i.d. column

of either phase increased. The data can be correlated by assumption of a constant superficial slip velocity which is commonly defined as follows

$$\frac{V_c}{1-X}+\frac{V_d}{X}=V_s \qquad (2)$$

where V_c = superficial velocity of the continuous (water) phase
V_d = superficial velocity of the dispersed (metal) phase
V_s = superficial slip velocity
X = fraction of column void volume occupied by dispersed phase.

A superficial slip velocity of 0·0618 ± 0·0063 m sec^{-1} was observed for 1/4-in Raschig rings. No apparent dependence of slip velocity on the flow rate of either phase was noted. Conversely in organic–aqueous systems with wetted packing a constant slip velocity is not normally observed.[5]

Equation (2) should also apply at flooding and can be used to predict flooding rates. Flooding is assumed to occur when

$$\frac{\partial V_c}{\partial X}=\frac{\partial V_d}{\partial X}=0 \qquad (3)$$

According to Equation (2), these conditions are met when

$$(V_c)^{1/2}_{\text{flooding}}+(V_d)^{1/2}_{\text{flooding}}=V_s^{1/2} \qquad (4)$$

Thus, a plot of $V_d^{1/2}$ *vs.* $V_c^{1/2}$ at flooding should produce a straight line with a slope of −1 and an intercept of $V_s^{1/2}$. Experimentally, the column was considered to be flooded when the pressure drop and/or hold-up increased and did not stabilise within 15 min or when either phase was forced out of the wrong end of the column. Flooding data with 0·25 in Raschig rings are shown in Fig. 5. The data fall along a straight line corresponding to the superficial slip velocity calculated from hold-up measurements.

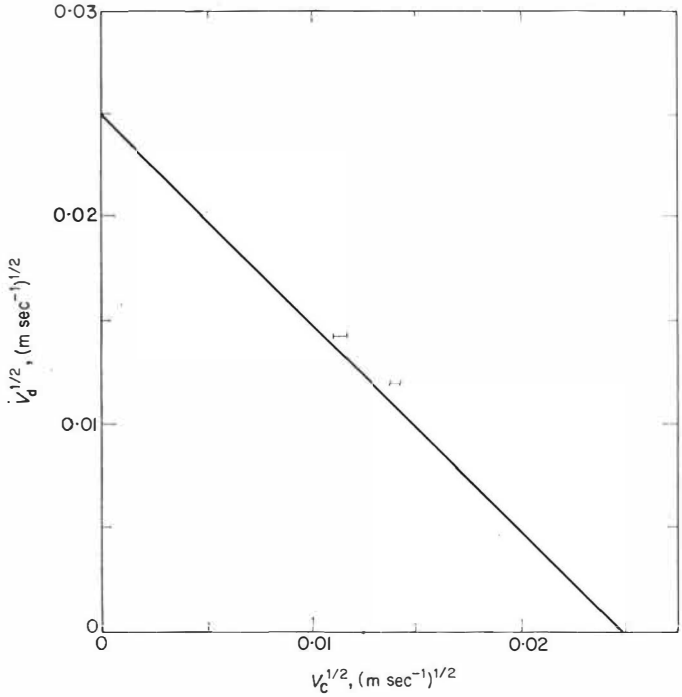

FIG. 5. *Comparison of measured and predicted flooding rates in a column packed with 1/4-in Raschig rings during countercurrent flow of mercury and water at 25°C*
0·071 void fraction

Extrapolation of these results to a salt–bismuth system involves a considerable number of uncertainties since the physical properties were not varied in the mercury–water studies. The most important of these are probably continuous phase viscosity and difference in densities of the phases. In flowing down the column, the dispersed phase interacts with both the packing and the continuous phase. Interaction with the continuous phase occurs in the interstitial region, where viscosity is expected to have only a slight effect. Thus, the slip velocity depends upon the density difference raised to a power between 1/2 (interaction with continuous phase) and 1 (interaction with packing); the dependence will probably be closer to 1. No attempt has been made to account for changes in interfacial tension since this quantity, which is not of great importance in conventional systems, is believed to be approximately the same for both systems. The relation for predicting flooding rates for countercurrent flow of bismuth and molten salt was obtained by assuming the superficial slip velocity to be proportional to both the difference in densities of the phases and the packing void fraction. The resulting predicted flooding relation for 1/4-in Raschig rings is

$$(V_c)_{\text{flood}}^{1/2} + (V_d)_{\text{flood}}^{1/2} = 0{\cdot}0207\sqrt{\varepsilon\Delta\rho} \qquad (5)$$

where V_c = superficial velocity of continuous phase, m sec^{-1}
V_d = superficial velocity of dispersed phase, m sec^{-1}
ε = packing void fraction
$\Delta\rho$ = difference in density of phases, g ml^{-1}

The flooding curve predicted from Equation (5) for countercurrent flow of bismuth and molten salt (72–16–12 mole-% LiF–BeF_2–ThF_4) through a column (0·61 m long, 2·1 cm i.d.) packed with 1/4-in molybdenum Raschig rings having a void fraction of 0·84 is shown in Fig. 6. Also experimental data

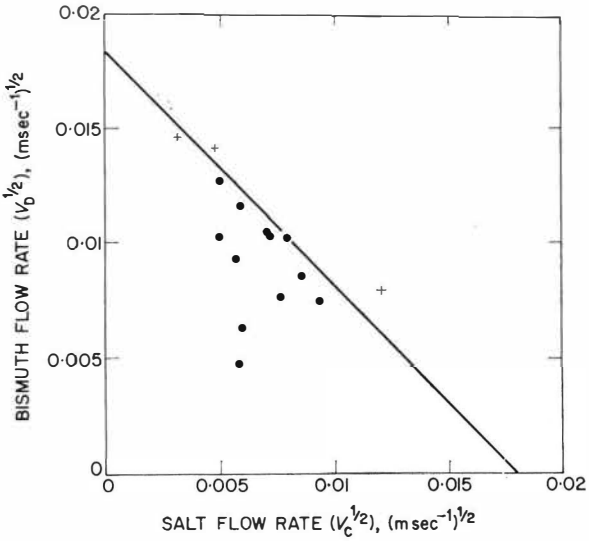

FIG. 6. *Comparison of measured and predicted flooding rates in a column packed with 1/4-in molybdenum Raschig rings during countercurrent flow of molten salt and bismuth at 600°C*

0·84 void fraction, 0·69 m × 2·1 cm column
72–16–12 mole-% $LiF-BeF_2-ThF_4$
+ flooded; ● not flooded

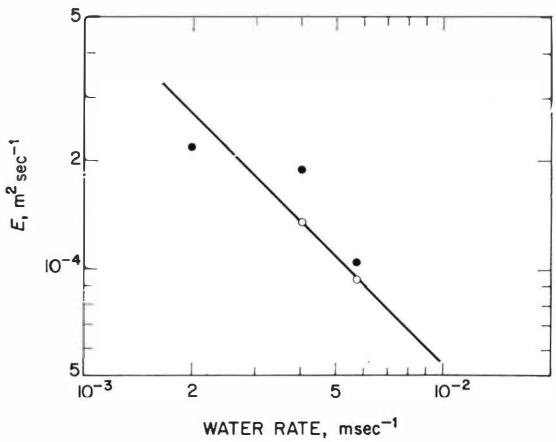

FIG. 7. *Axial dispersion coefficients (in the water phase) measured during countercurrent flow of mercury and water in a column packed with 1/4-in Raschig rings*

0·7–1·5 m × 2 in column
○ 0·00296 m sec^{-1}; ● 0·00694 m sec^{-1}

indicating whether the column was flooded or not are shown for comparison. Good agreement is observed between the predicted curve and the experimental data.

Axial mixing can adversely affect column performance, particularly when high dispersed phase to continuous phase flow rate ratios are required. In such cases, the flow rate of the continuous phase will be low in order to avoid flooding of the column. The authors have recently found a simple equation which closely approximates more complicated relations for predicting the effect of axial dispersion on column performance.[6] The equation relates the column height required with axial mixing to the height required with no axial mixing and is a function of flow rates, required separation (number of transfer units),

the slope of the equilibrium curve and the axial dispersion coefficient.

Axial dispersion coefficients were measured using a steady-state technique in which a tracer solution of cupric nitrate is injected into the water phase near the top of the column and the concentration of tracer is measured up or down the column. The concentration measurements are made by continuously circulating small side streams of water through photocells and returning them to the column at the same axial position. Results obtained with 1/4-in Raschig rings in a 2-in i.d. column 0·7 to 1·5 m in length are shown in Fig. 7. The dispersion coefficients lie between 0·9 and 2·2 $cm^2\ sec^{-1}$ and appear to be inversely proportional to the water or continuous phase flow rate. There is no apparent dependence of the dispersion coefficient on the metal flow rate; this does not agree with data from conventional low-density systems with wetted packing.[5]

For some flowsheets axial dispersion would result in uneconomical column lengths, and thus devices for reducing axial dispersion have been developed. A typical device, called a preventer, is illustrated schematically in Fig. 8. The

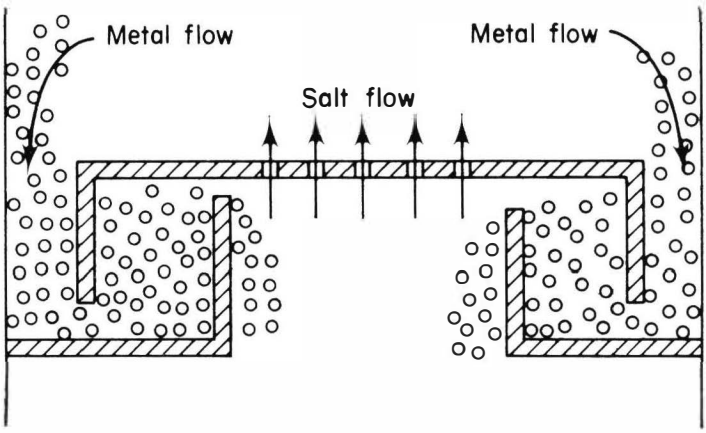

FIG. 8. *Schematic diagram of an axial mixing preventer*

metal phase flows down through an annular device that functions in a similar manner to a bubble cap to prevent the flow of the continuous phase (salt or water) by directing it through constricted openings in sieve plates or through small tubes. This results in a higher continuous phase velocity through these openings and backmixing across the openings is reduced. The results obtained when using sieve openings are given in Fig. 9. The amount of backmixing, defined as the fraction of continuous phase flow recycled or backmixed through the preventer, is a function of both the diameter and the flow rate through the openings. Although these results were obtained with mercury and water, salt and bismuth are expected to behave similarly. Less than 15% backmixing, which is adequate to allow practical column lengths for all proposed operating conditions, have been achieved with sieve openings of up to 3/8-in in diameter. Although the use of tubes for salt or water flow reduces backmixing slightly, it allows much higher metal flow rates. The use of tubes has permitted metal flow rates which are greater than 50% of flooding for columns packed with 1/4-in Raschig rings.

Mass transfer between bismuth and salt streams in packed columns have also been studied; however, the data available at present are preliminary. The column used in these studies (2·1 cm i.d., 0·7 m long) is packed with 1/4-in molybdenum Raschig rings. In the initial experiment, more than 95% of the uranium was extracted from the salt by a bismuth phase containing lithium and thorium.

The studies to date have shown that high density systems behave differently

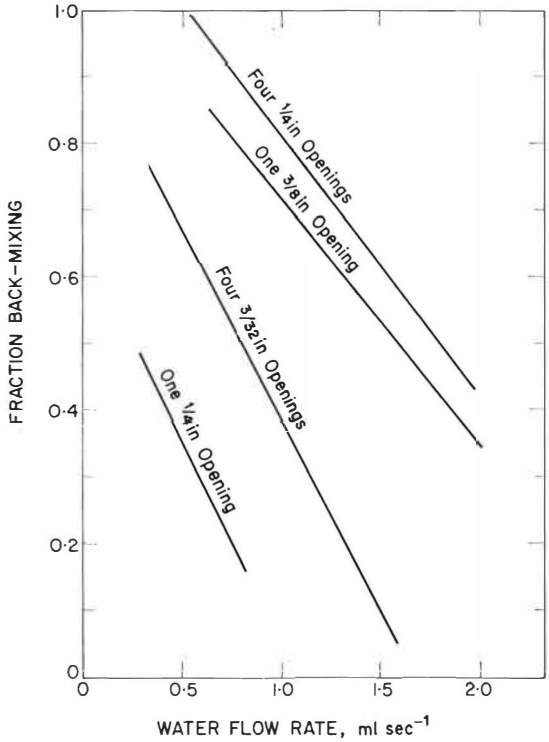

FIG. 9. *Summary of experimentally determined fractional backmixing data during countercurrent flow of mercury and water in a column packed with 3/8-in Raschig rings*
1·5 m × 2 in column

from the conventional systems, and that the effects of changes in physical properties of the phases used can be predicted. A major objective of future studies is to determine why these systems differ from conventional systems. Additional measurements will be made with packing materials that are not wet by the dispersed (metal) phase as well as with materials that are wet. These measurements should indicate whether the difference in behaviour results from wetting or from the density difference and interfacial tension. Data will also be obtained to verify the assumed effect of continuous phase viscosity.

Currently, the major effort is aimed at studying mass transfer in reductive extraction systems. In addition to measurements of uranium, thorium and lithium transfer rates between molten salt and bismuth phases, studies of tracer exchange (e.g., the exchange of labelled isotopes with unlabelled isotopes of the same element) are planned. The results should aid in understanding and describing more complex reductive extraction processes.

Acknowledgments

This work was sponsored by the U.S. Atomic Energy Commission under contract with the Union Carbide Corporation.

References

[1] *Rep. Congr. U.S. atom. Energy Commn*, 1970, ORNL 4548, p. 41
[2] Ferris, L. M., Mailen, J. C., Lawrence, J. J., Smith, F. J., & Nogueira, E. D., *J. inorg. nucl. Chem.*, 1970, **32**, 2079
[3] Ref. 1, p. 289
[4] Miyauchi, T., & Vermeulen, T., *Ind. Engng Chem. Fundamentals*, 1963, **2**, 113
[5] Pratt, H. R. C., *et al.*, *Trans. Instn chem. Engrs*, 1951, **29**, 110
[6] Watson, J. S., & Cochran, H. D., Jr., to be published

Computer evaluation of chemical flowsheets for plutonium purification with TBP

by T. Aochi, T. Tsujino, A. Kohsaka and T. Hoshino*

Reprocessing Development Laboratory, Japan Atomic Energy Research Institute, Tokai-mura, Ibaraki-ken, Japan

In order to evaluate the plutonium purification process with tributyl phosphate (TBP), a calculation code for the system TBP–HNO_3–Pu was prepared on the basis of a batchwise counter-current extraction cascade. By using this code, concentration profiles for transient or steady state conditions, and numbers of theoretical stages required, can be computed for a given process.

The outline of the code is described and the calculated results are compared with those of experimental process studies. Results are also given for the application of this method to flowsheet calculations in connection with the JAERI Reprocessing Test Plant.

Introduction

A SOLVENT EXTRACTION PROCESS of the Purex type is the only practical method at present for the reprocessing of irradiated fuels.

It is a typical multi-component system involving tri-n-butyl phosphate (TBP), nitric acid, uranium, plutonium and fission products.

These multi-component problems are intractable except with the use of a digital computer and/or an experimental proving test. The latter technique is, however, very laborious and time-consuming.

As the first stage in the use of a computer for solving multi-component extraction problems, a calculation code was prepared for the system TBP–HNO_3–Pu employing the model of a batchwise counter-current extraction cascade. The concentration profiles and the numbers of theoretical stages required under transient or steady state conditions can be computed for a given process.

To prove the validity of the calculation programme, the calculated results are compared with those obtained in experimental process studies with miniature mixer–settlers; flowsheet calculations were also made for the specific conditions of the JAERI Reprocessing Test Plant.[1]

Some calculation codes for reprocessing flowsheets have been prepared by Olander[2] and Burton & Mills;[3] the detailed programmes, however, are not available here in Japan. It seems that these workers use a conventional trial and error technique similar to that employed in the graphical approach on an operating diagram. By this method, it is difficult to evaluate transient phenomena.

The present calculation code, based on the model of a batchwise counter-current extraction cascade, is very simple to programme and covers the extraction, scrubbing and stripping processes under transient or steady state conditions.

Whilst writing the present paper, an ORNL technical report[4] was received. It states that a calculation programme, based on the same principle as the present paper, is being prepared with a view to evaluating chemical flowsheets for FBR spent fuel.

Theory

Summarised distribution data for nitric acid and plutonium in 30 vol.-% TBP–H_2O

For the system under consideration, the extraction of nitric acid and plutonium with TBP can be expressed as

*Present address: Power Reactor and Nuclear Fuel Development Corporation (PNC), Japan.

$$H^+ + NO_3^- + TBP \rightleftarrows HNO_3 \cdot TBP \quad (1)$$

$$H^+ < 5_N,$$

$$Pu^{4+} + 4NO_3^- + 2TBP \rightleftarrows Pu(NO_3)_4 \cdot 2TBP \quad (2)$$

The actual partition data in 30 vol.-% TBP have already been summarised[5] and the following empirical equations are derived from these data.

In the system TBP–HNO_3:

For $0 \leq y_H \leq 0{\cdot}5$,

$$K'_H = -0{\cdot}37_5\, y_H + 0{\cdot}35_0 \quad (3)$$

For $0{\cdot}5 < y_H \leq 1$,

$$K'_H = 0{\cdot}16_5 \quad (4)$$

In general,

$$K'_H = y_H/(x_H \cdot x_{NO_3^-} \cdot y_{TBP}) \quad (5)$$

where x and y are molar concentrations in the aqueous and organic phases, respectively and K'_H indicates an apparent equilibrium constant for equation (1). In the system TBP–HNO_3–Pu(IV) (concentration of Pu below several g/l):

For $x_H \leq 1{\cdot}5$

$$\log K_d = 1{\cdot}6_3 \log x_H + 0{\cdot}41_3 \quad (6)$$

For $1{\cdot}5 < x_H \leq 6$

$$\log K_d = 1{\cdot}3_1 \log x_H + 0{\cdot}46_8 \quad (7)$$

where K_d is the distribution ratio of plutonium in 30 vol-% TBP

($K_d = y_{Pu}/x_{Pu}$).

Batchwise counter-current extraction

As already reported,[6] according to theoretical and general principles, the repeated batchwise extraction cascade essentially simulates a continuous counter-current extraction process. The model of a batchwise counter-current extraction cascade is convenient for programming a calculation code as well as for experimental proving tests.

Mass balance and stage efficiency

The mass balance is taken at each batch stage, assuming no volume change of the two phases during extraction.

In the present paper, a single stage efficiency η_s is defined to represent the actual partition in each stage.

$$\eta_s = \left| y/y^* \right|_x \quad \text{(extraction)}$$
$$\eta_s = \left| y^*/y \right|_x \quad \text{(scrubbing and stripping)} \quad (8)$$

where y^* and y are the organic molar concentrations respectively, at equilibrium and under the actual conditions of partition with a given aqueous concentration x.

Calculation programme

Based on the above principle and empirical equations, a code was programmed according to the flow scheme shown in Fig. 1.

The programme, named REPROSY-P (REprocessing PRocess StudY-Pu),

is written in FORTRAN IV for IBM 7044. The complete programme list and flow chart are summarised in a JAERI internal report.[7]

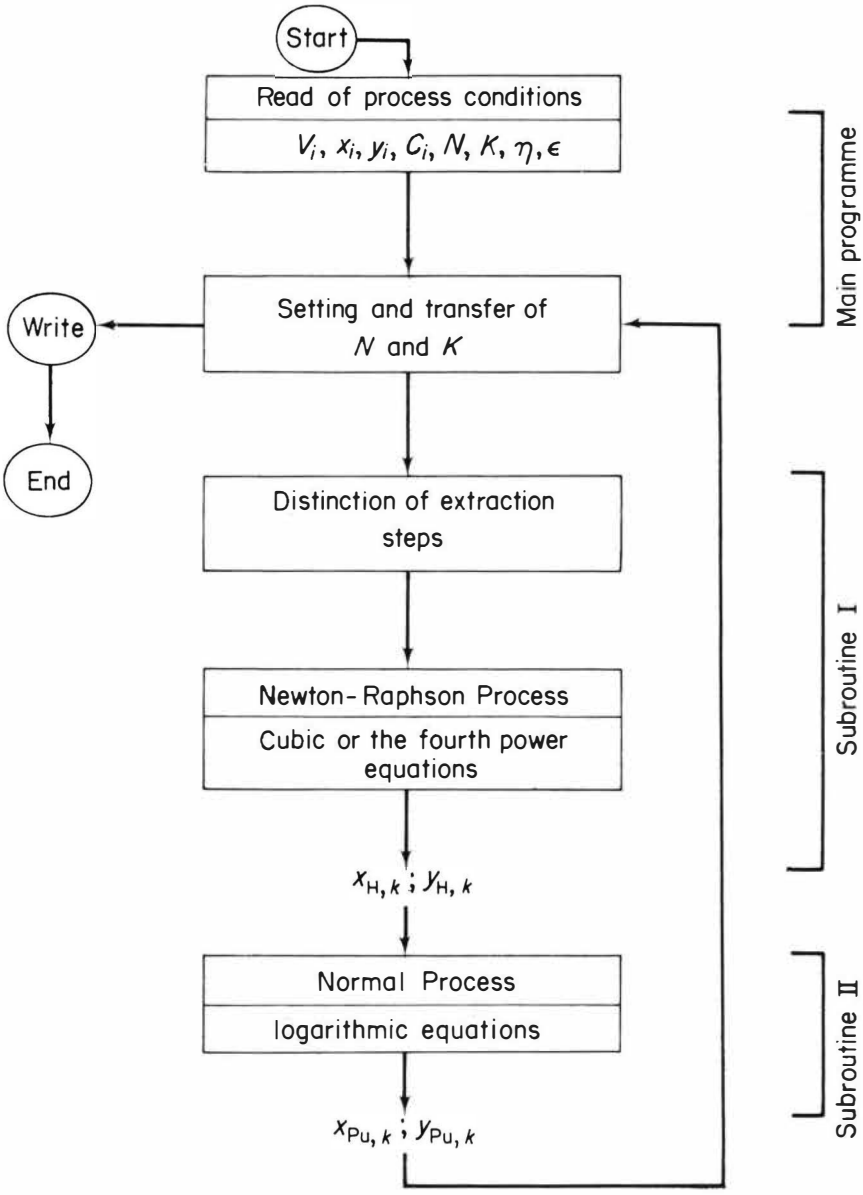

FIG. 1. *Calculation scheme of REPROSY-P*

V_i flow rate of i species solution; x_i, y_i molar concentrations; c_i empirical coefficients; N cycle number; K stage number; η_i stage efficiency; ε significant figure

Calculation

Flowsheet for laboratory process study

The evaluated chemical flowsheet is shown in Fig. 2. It was selected from data obtained in the experimental proving tests for plutonium purification in the JAERI Reprocessing Test Plant.

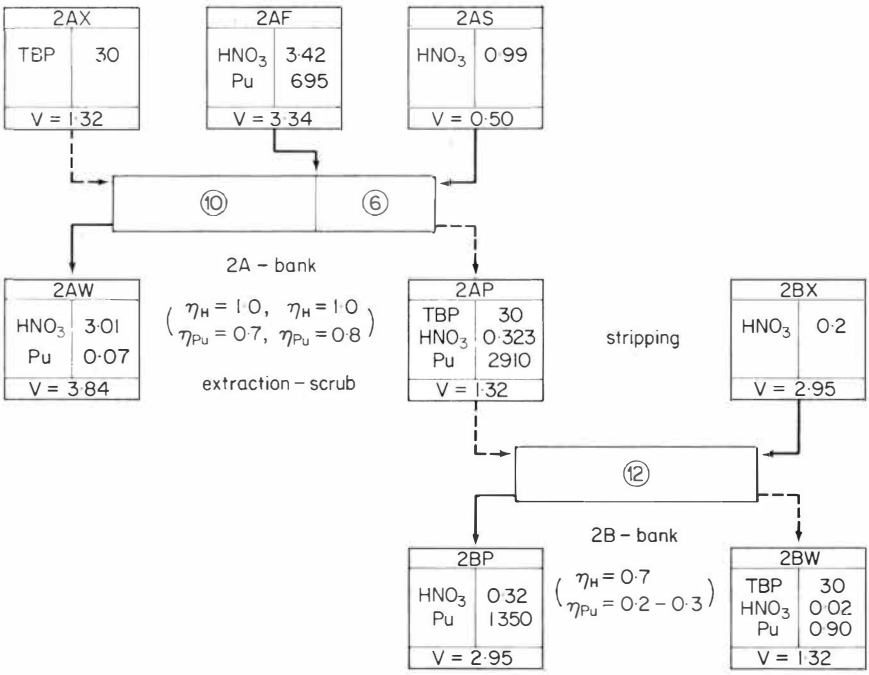

FIG. 2. *Standard chemical flowsheet of process studies*
[HNO_3] expressed as normality; [Pu] as mg/l; [TBP] as vol.-% with dodecane; flow rate V as ml/min; ○ stage number

Flowsheet for the JAERI Reprocessing Test Plant

Fig. 3 shows a calculated chemical flowsheet for the plutonium purification process with TBP.

Variable factors for the calculation are given in Table I. Since the actual stage efficiencies have not been found for the CC-1 bank (extraction and scrubbing) and the CC-2 bank (stripping), the estimated values from the results of laboratory process studies are used.

TABLE I

Variable factors in the flowsheet calculation for JAERI Reprocessing Test Plant

	H^+, normality:	0·05, 0·1, 0·2
2BX	flow rate, l/h:	1, 2, 2·6, 3, 4
	flow ratio R: (2BX/2AP)	0·5, 1, 1·3, 1·5, 2
2AF	H^+ normality:	3·6, 4·0

Calculation

Calculations were performed on the IBM 7044 which was available in the Computing Centre of JAERI. For each run the computing and printing were completed in 3 seconds and 16 seconds, respectively.

Experimental

Process studies with miniature mixer–settlers

According to the chemical flowsheet shown in Fig. 2, process studies were carried out, as previously reported,[8,9] with two miniature mixer–settlers (made

by Wastelake Manufacturing Co., U.S.A.) in a glove-box. The mixer-settlers are of the pump-mixing type and have capacities, in the mixing and settling sections, of 4·5 and 8·0 ml, respectively. Flow rates were controlled to within ±3% of the design values.

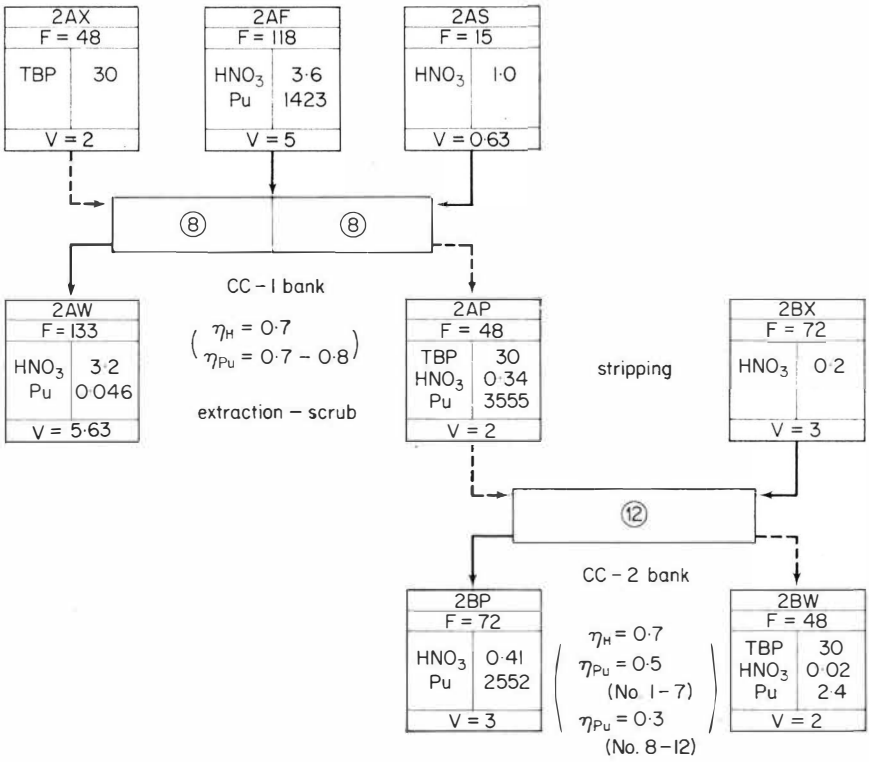

FIG. 3. *Calculated chemical flowsheet for the JAERI Reprocessing Test Plant (Pu purification Process)*

[HNO_3] expressed as normality; [Pu] as mg/l; V flow rate as l/h; F total volume as l; ○ stage number

Analysis

Nitric acid was analysed by titration with NaOH. The concentration of plutonium was determined by α-counting and checked by titration with ceric ions when necessary.

Results and discussion

Proving of the calculation code by process studies

Some examples of calculated concentration profiles together with the experimental values are shown in Figs 4 and 5.

Nitric acid

As shown in Fig. 4, the calculated values for all stages are in good agreement with experiment. It is noted that the stage efficiency for nitric acid is fairly high in the present system.

Plutonium

As shown in Fig. 5, the calculated results agree well with the experimental values, except at plutonium concentrations below 10 mg/l.

Discrepancies in the extraction stages may be explained by the presence of americium and/or inextractable species like plutonium hydroxide polymers.

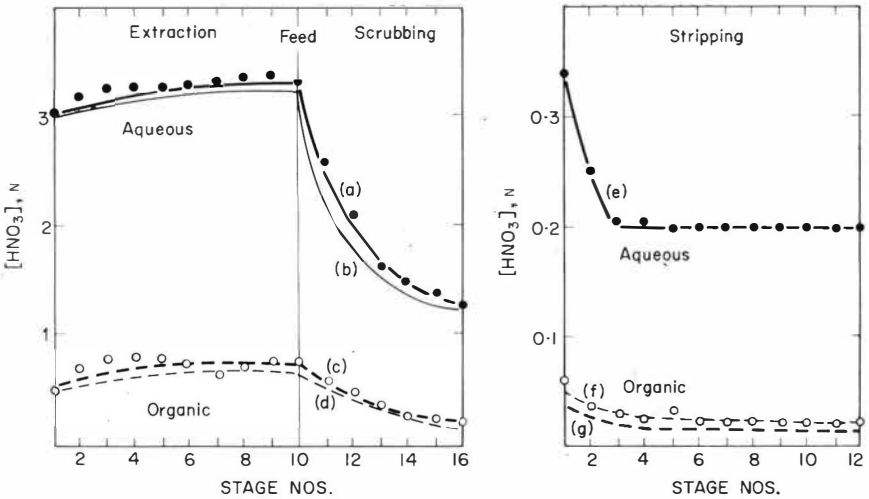

FIG. 4. *Concentration profiles for HNO_3 in the process studies*
● ○ experimental value, ---- calculated value
η_H values: (a) = 1·0; (b) = 0·8; (c) = 1·0; (d) = 0·8; (e) = 1·0, 0·7; (f) = 0·7; (g) = 1·0

It is quite normal for such a tailing to appear in an actual process, and it would be difficult to simulate the tailing phenomenon exactly because the tailing depends upon the history of the plutonium feed solution.

Deviations in the stripping stage may be due to species, such as plutonium–dibutyl phosphate complexes, which are difficult to remove from the organic phase, and, as shown in Fig. 5, such phenomena can be simulated in the computer code by the assumption of low stage efficiences.

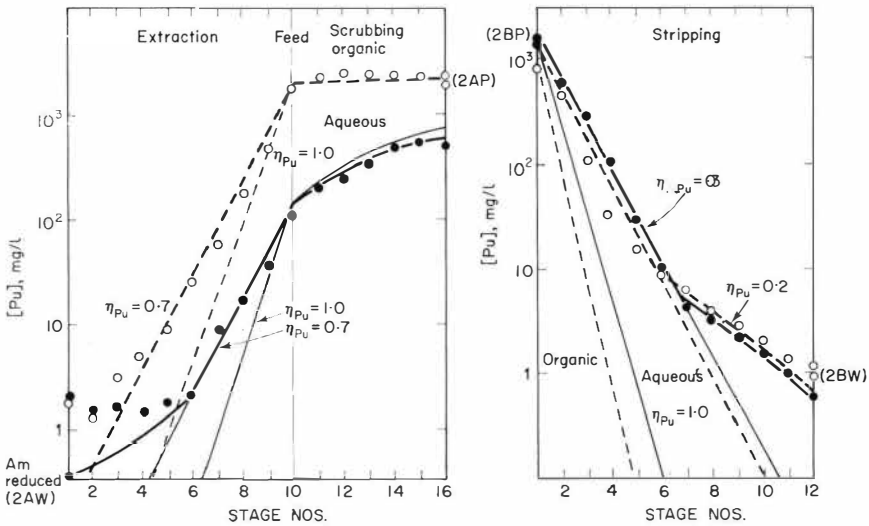

FIG. 5. *Concentration profiles for Pu in the process studies*
● ○ experimental values; ---- calculated value

Comparison of stage efficiencies

From the experimental operating diagrams and the calculated results, the number of theoretical stages required for extraction and stripping are easily determined. Comparison of the single stage and overall contactor efficiencies, as defined by Equations (8) and (9), are shown in Table II.

TABLE II

Comparison of apparent stage efficiencies

Section		Extraction	Scrubbing	Stripping
HNO_3	η_H	~1·0	~1·0	0·7–1·0
	η_o	~1·0	~1·0	~0·9
Pu	η_{Pu}	~0·7*	~0·8	0·2–0·3
	η_o	~0·7*	~1·0	0·2–0·3

*excluding stages 1–5

The overall contactor efficiency is given by

$$\eta_0 = N^*/N \quad . \quad . \quad . \quad . \quad . \quad . \quad . \quad . \quad . \quad . \quad (9)$$

where N is the actual number of stages required and N^* is the calculated number of theoretical stages.

It is empirically shown from Table II that the single stage efficiency defined here, is of the same order as the overall contactor efficiency.

From the above results it can be shown that the calculation code (REPROSY-P), with the assumption of particular values for the single stage efficiencies, is applicable to the actual evaluation of the plutonium purification process with TBP for Pu concentrations below several g/l.

Calculated flowsheets for the JAERI Reprocessing Test Plant

The calculation for the test plant was used to estimate the minimum permissible flow ratio R and to determine the effect of nitric acid on the stripping process.

Minimum permissible flow ratio

The importance of the flow ratio is seen in Fig. 6, which shows that plutonium losses in the 2BW stream decrease with increasing flow ratio.

It can be concluded from Fig. 6 that a flow ratio R of 1·3–1·5 is the minimum permissible under the present conditions. In an actual active run on the test plant,[1] stripping with $R=1\cdot5$ was used and the measured concentration of plutonium in the 2BW stream was nearly the same as that calculated.

Effect of nitric acid concentration

It was shown quantitatively by calculation that decrease of nitric acid concentration is very effective for efficient stripping of plutonium if the hydrolysis of plutonium can be avoided. This hydrolysis may be inhibited by introducing nitric acid of high concentration into the 2BP solution.

Some differences were observed in the aqueous concentration of nitric acid in the extraction stages when 3·6 and 4·0N-HNO_3 feeds were used, whereas the organic profiles were apparently the same. No large difference was observed in the plutonium concentration profiles.

Potential applications and extensions of the programme

For TBP–HNO_3–Pu systems, various applications have been shown above.

With an extension of this code, estimates of extraction behaviour can also be made for any three[10] or four extractable components; for example, for nitric acid, plutonium, uranium and fission products under a wide variety of conditions.

The potential applications include calculations of concentration profiles during transient states and estimates of the effects of operating parameters such as variations in the concentrations of components, flow rate, number of stages and stage efficiency. Mal-operation phenomena can also be estimated, especially for criticality and inventory control.

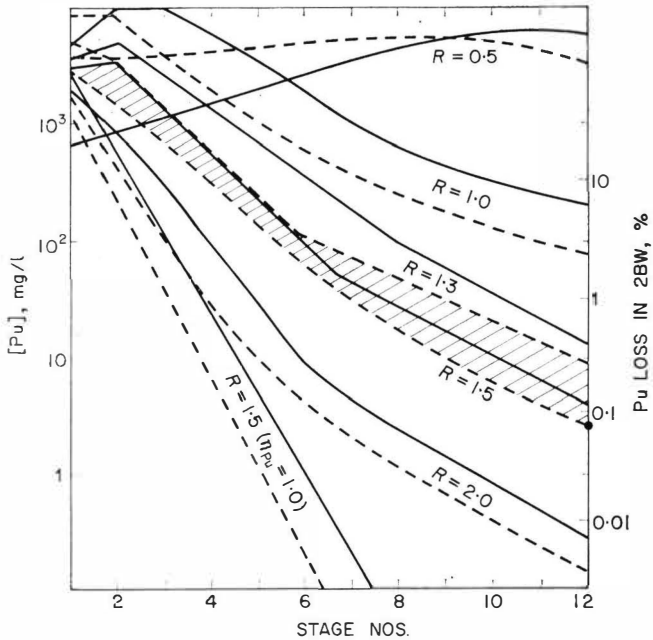

FIG. 6. *Calculated concentration profiles of plutonium in the stripping process*

$\eta_H = 0 \cdot 7$; $\eta_{Pu} = 0 \cdot 5$ (stage no. 1–7); $\eta_{Pu} = 0 \cdot 3$ (stage no. 8–12)
● experimental value obtained in the JAERI Reprocessing Test Plant, R=2BX/2AP;
—— aqueous; - - - organic

Conclusions

The calculation code for the TBP–HNO_3–Pu system was programmed successfully for evaluating the plutonium purification process with TBP. The number of theoretical stages required and the concentration profiles for nitric acid and plutonium can be computed in 20 seconds for given conditions.

The calculated concentration profiles were found to agree well with those obtained in the experimental process studies assuming a single stage efficiency.

The code was applied in practice to the JAERI Reprocessing Test Plant.

These types of calculation would be of value in process design and flowsheet optimisation studies, especially before undertaking experimental proving tests.

In order to cover all reprocessing systems, the code must be extended further to cover systems of higher Pu concentration and of more than four components including uranium[10] and fission products.

Further studies are necessary to elucidate the tailing phenomenon with dilute concentrations of plutonium.

Acknowledgments

The authors are grateful to Mr. Y. Kawashima and Mr. S. Yasu of the Power Reactor and Nuclear Fuel Development Corporation, Japan, for their technical, assistance in the experimental process studies. They also wish to express their thanks to members of the authors' laboratory, especially to Mr. E. Yagi for helpful discussions on the application of the code to the test plant.

References

[1] Aochi, T., *Atoms Japan*, 1969, **13,** 23
[2] Olander, D. R., *Ind. Engng Chem.*, 1961, **53,** 1
[3] Burton, W. R., & Mills, A. L., *Nucl. Engng, Lond.*, 1963, p. 248
[4] Horner, D. E., *Rep. Congr. atom. Energy Commn U.S.*, 1970, ORNL-TM-2711
[5] Aochi, T., Tsujino, T., Segawa, T., & Hoshino, T., *JAERI Memo.*, 1969, 3745 (unpublished)
[6] Scheibel, E. G., *Ind. Engng Chem.*, 1954, **46,** 16
[7] Aochi, T., Tsujino, T., Konsaka, A , & Hoshino, T., *JAERI Memo.*, 1969, 3746 (unpublished)
[8] Aochi, T., Tsujino, T., & Yagi, E., *JAERI*, 1967, 12790
[9] Tsujino, T., Hoshino, T., *et al.*, *PNC* Ann. Rep.*, 1968 *PNCT-AR* **67,** 22
[10] Segawa, T., Hoshino, T., Kaya, A., Gonda, K., Tsuboya, T., & Tanaka, C., *Proc. Int. Solvent Extraction Conf.*, 1971 (London: Society of Chemical Industry)

*PNC=Power Reactor & Nuclear Fuel Development Corp., Japan

Use of sulphate in solvent extraction separation processes

by D. Gourisse, A. Bathellier and J.-C. Blanchard
Département de Chimie, Commissariat à l'Énergie Atomique, Centre d'Études Nucléaires de Fontenay-aux-Roses, France

The complexing power of sulphate anions for tetravalent actinide elements is a very useful tool for improving solvent separation processes in a nitric acid medium and most interesting results were obtained in this field.

The stripping of tetravalent actinide elements from tertiary amine solutions is easily done with sulphuric–nitric acid solutions. Typical experiments with Pu(IV) and Np(IV) show that stripping with a concentration factor ⩾ 5 may be made with recovery ⩾ 99·9%.

Np–U and Pu–U separations by quantitative tributyl phosphate (TBP) extraction of uranium are largely improved by introducing sulphuric acid in the aqueous nitric acid solution. Distribution of elements results of competition between TBP organic complexes and aqueous sulphate complexes. Since sulphate complexes are stronger for tetravalent elements, the separation factor is largely increased. In typical Pu–U separations uranium decontamination factors for plutonium > 10^7 were obtained in 16-stage countercurrent extractions.

Introduction

SULPHATE ANIONS HAVE a high complexing power for tetravalent actinide cations. As the sulphuric acid concentration increases, the complexing induces a decrease in distribution coefficients of the actinide elements into basic solvents from nitric acid media. This property can be used to strip tetravalent plutonium[1–4] and neptunium[5,6] from tertiary amine solutions.

The use of sulphate greatly improves the separation processes which utilise tributyl phosphate (TBP) or trilaurylamine (TLA) extraction. Since the complexing power of sulphate anions is higher for tetravalent than for hexavalent actinide elements,[7] the decrease in the hexavalent actinide distribution coefficients is smaller than the corresponding decrease for tetravalent elements.

The decrease in tetravalent actinide distribution coefficients increases the percentage of these elements in the aqueous phase and consequently the reduction by aqueous reductants [for example, Fe(II)] becomes faster. This property can be used to improve uranium–plutonium separation processes by TBP extraction and neptunium–plutonium separation processes by TLA extraction in a reducing medium.

This paper contains typical results obtained in this field.

Equilibrium experiments

TBP extraction

In the literature there is information on the influence of sulphate on TBP extraction of uranium(VI)[8,9] and plutonium(IV)[10–12] from studies made on separation processes. The studies made on stability constants of plutonium (IV)–sulphate complexes by solvent extraction[13–15] also give some values of plutonium(IV) distribution coefficients.

Figs 1 to 4 show results obtained in these laboratories. These results concern plutonium(IV) (Fig. 1) and neptunium(IV) (Fig. 2) extraction by 30 vol.-% TBP in dodecane, uranium(VI) and plutonium(IV) extraction by 20% TBP–dodecane (Fig. 3) and uranium(VI) and neptunium(IV) extraction by 15% TBP–dodecane (Fig. 4). The variations of the separation factor $S(M^{VI}/M^{IV})$, defined as the ratio of distribution coefficients, are given in Tables I and II.

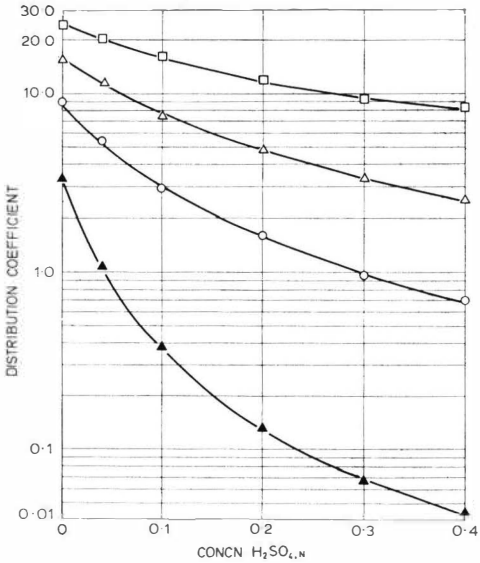

FIG. 1. *Distribution coefficients of plutonium(IV) in the system 30% dodecane–HNO_3–H_2SO_4–H_2O*
□ 4N-HNO_3; △ 3N-HNO_3; ○ 2N-HNO_3; ▲ 1N-HNO_3

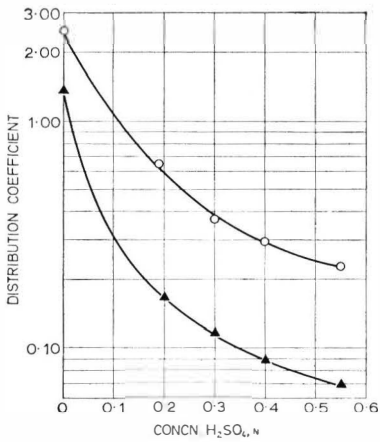

FIG. 2. *Distribution coefficients of neptunium(IV) in the system 30% dodecane–HNO_3–H_2SO_4–H_2O*
○ 2N-HNO_3; ▲ 1N-HNO_3

TABLE I

Uranium(VI)–plutonium(IV) separation factors $S(U^{VI}/Pu^{IV})$ in 20% TBP–dodecane

$(H_2SO_4)_{aq}$, N	0·0	0·25	0·50	1·0	1·5
$(HNO_3)_{aq}$ = 1N	2·9	32	54	70	70
$(HNO_3)_{aq}$ = 2N	1·5	7·2	12	17	21

A small increase in sulphuric acid concentration increases the separation factor sharply in nitric acid medium. As expected, the separation factor increases with the ratio $\frac{(H_2SO_4)}{(HNO_3)}$ at constant nitric acid or sulphuric acid concentration.

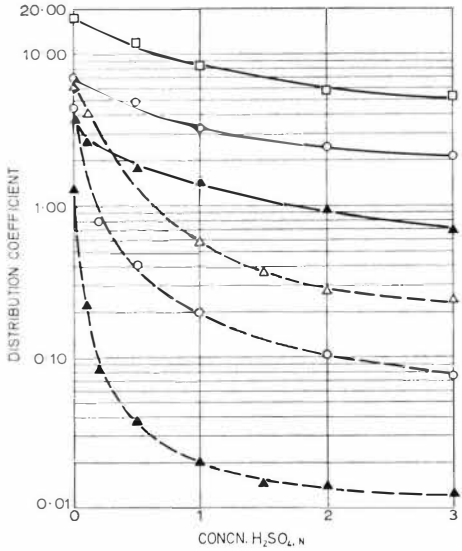

FIG. 3. *Distribution coefficients of uranium(VI)* (———) *and plutonium(IV)* (– – –) *in the system 20% TBP–dodecane–HNO_3–H_2SO_4–H_2O*
□ 4N-HNO_3; △ 3N-HNO_3; ○ 2N-HNO_3; ▲ 1N-HNO_3

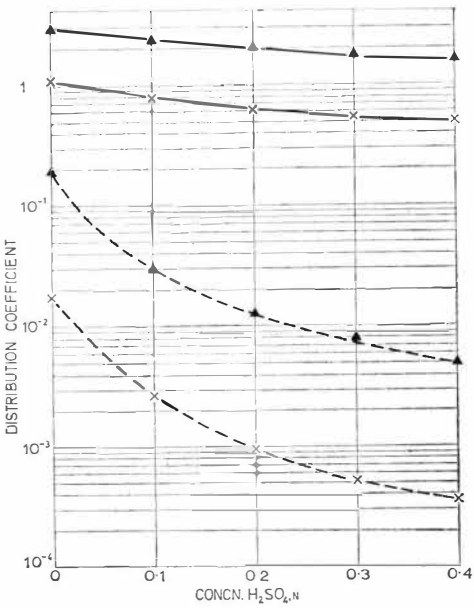

FIG. 4. *Distribution coefficients of uranium(VI)* (———) *and neptunium(IV)* (– – –) *in the system 15% TBP–dodecane–HNO_3–H_2SO_4–H_2O*
▲ 1N-HNO_3; × 0·5N-HNO_3

TABLE II

Uranium(VI)–neptunium(IV) separation factors $S(U^{VI}/Np^{IV})$ in 15% TBP–dodecane

$(H_2SO_4)_{aq}$, N	0·0	0·10	0·20	0·30	0·40
$(HNO_3)_{aq}$ = 0·5N	30	290	680	1060	1400
$(HNO_3)_{aq}$ = 1N	15	80	170	220	350

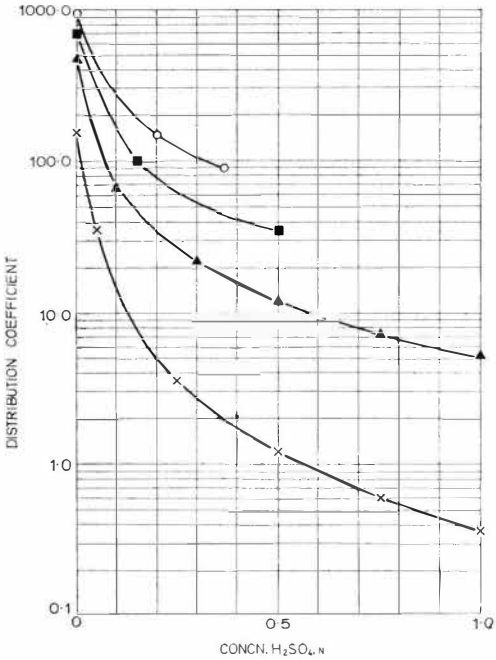

FIG. 5. *Distribution coefficients of plutonium(IV) in the system 20% TLA–dodecane–HNO_3–H_2SO_4–H_2O*
○ 2N-HNO_3; ■ 1·5N-HNO_3; ▲ 1N-HNO_3; × 0·5N-HNO_3

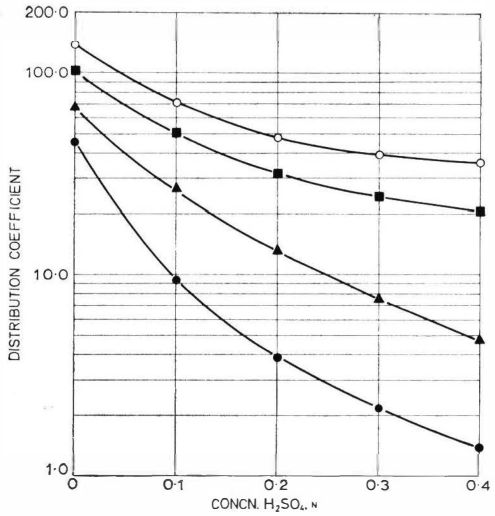

FIG. 6. *Distribution coefficients of neptunium(IV) in the system 20% TLA–dodecane–HNO_3–H_2SO_4–H_2O*
○ 2N-HNO_3; ■ 1·5N-HNO_3; ▲ 1N-HNO_3; ● 0·7N-HNO_3

TLA extraction

There is information in the literature on the influence of sulphate on plutonium(IV)[1,4] and neptunium(IV)[5] extraction by tertiary amine solutions for high values of the ratio $\frac{(H_2SO_4)}{(HNO_3)}$ (stripping). Figs 5 and 6 respectively show the results obtained on the influence of sulphate on plutonium(IV) and

neptunium(IV) extraction by 20 vol.-% TLA in dodecane. The distribution coefficients decrease slightly when the sulphuric acid concentration increases but their values remain sufficiently high to allow quantitative extraction in counter-current processes.

MO_2^{2+} – M^{4+} separation processes

In pure nitric acid medium, the separation between hexavalent and tetravalent actinide elements obtained by TBP extraction is not very effective, as the difference between their distribution coefficients is too small. The use of sulphate increases the separation factor and consequently enhances the separation efficiency.

Uranium(VI)–plutonium(IV) separation

In 'Purex' processes the separation between plutonium and uranium is generally obtained by the use of a reductant [Fe(II), U(IV), N_2H_4, etc.]. As shown in Fig. 7, a separation scheme without reductant can be used. Testing this flow-sheet in mixer-settler experiments a uranium decontamination factor with respect to plutonium of $2 \cdot 25 \times 10^4$ was obtained whereas the plutonium decontamination factor with respect to uranium is 4×10^5.

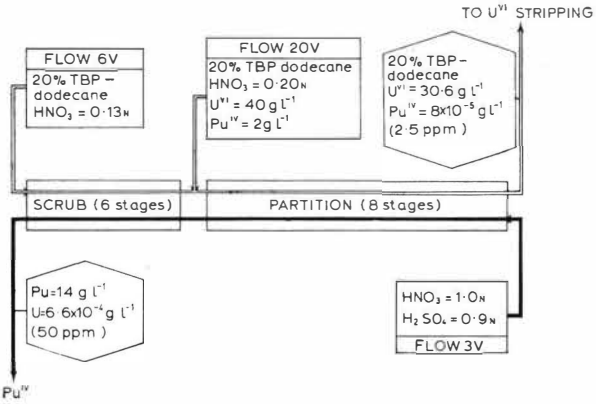

FIG. 7. *Flow-sheet for uranium(VI)–plutonium(IV) separation by 20% TBP extraction*

Uranium(VI)–neptunium(IV) separation

In the study of the processing of irradiated U–Al fuel, the recovery of neptunium and plutonium was investigated according to the following scheme for the first cycle:

Extraction I: uranium(VI) + neptunium(IV) + plutonium(IV) co-extraction by 15% TBP–dodecane.
Extraction II: neptunium(IV) + plutonium(III) stripping.
Extraction III: uranium(VI) stripping.

The flow-sheet for Extraction II is shown in Fig. 8. On testing this scheme a uranium decontamination factor with respect to neptunium of 2×10^4 was obtained and a neptunium decontamination factor with respect to uranium of $1 \cdot 6 \times 10^4$ whereas neptunium is concentrated by a factor of $18 \cdot 5$.

Separation processes in reducing medium

These processes use the reduction of plutonium to the inextractable trivalent state. Overall distribution coefficients correspond to a mixture of trivalent and tetravalent plutonium. Sulphate ions have a mixed effect on these coefficients, viz.: (1) they decrease the value of the plutonium(IV) distribution coefficient, and (2) they increase the percentage of plutonium in the aqueous phase and consequently increase the reduction rate by aqueous reductant.

These two effects result in a decrease of the plutonium overall distribution coefficients.

Uranium–plutonium separation by TBP extraction

In the flow-sheet shown in Fig. 8, relating to U–Al fuel processing, uranium is decontaminated by a factor of 5×10^5 with respect to plutonium in spite of the high concentration factor for plutonium.

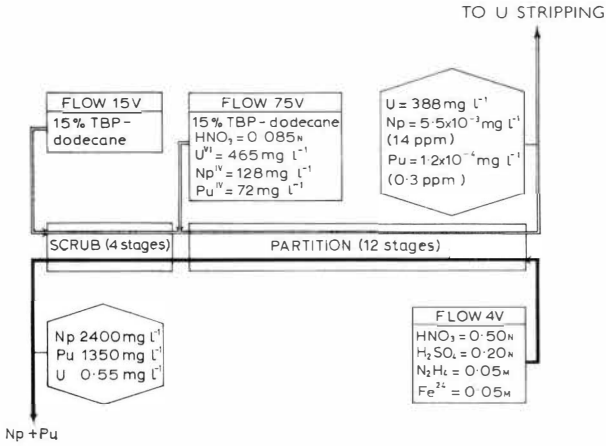

FIG. 8. *Flow-sheet for uranium(VI)–neptunium(IV) + plutonium(III) separation by 15% TBP extraction*

When operating conditions are simpler, the choice of an appropriate flow-sheet leads to a more efficient separation. In Fig. 9 the separation scheme for the third cycle of mixed UO_2–PuO_2 fuels processing by 30% TBP–dodecane is given. A uranium decontamination factor of $1 \cdot 3 \times 10^7$ with respect to plutonium (24 ppb Pu) and a plutonium decontamination factor of $9 \cdot 6 \times 10^3$ with respect to uranium (345 ppm U) were obtained. Uranium from this separation may be sent directly to gaseous diffusion plants for further isotopic enrichment without any other plutonium decontamination.

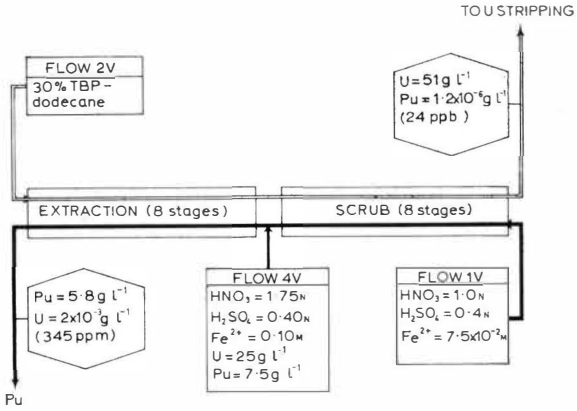

FIG. 9. *Flow-sheet for the uranium(VI)–plutonium(III) separation by 30% TBP extraction*

These results show clearly that the use of sulphate might sharply increase the efficiency of the uranium–plutonium partition in 'Purex' processes.

Neptunium–plutonium separation by TLA extraction

^{237}Neptunium recovery from 'Purex' plant wastes and ^{238}plutonium purification from irradiated ^{237}Np targets are often made by TLA extraction.[5,6,16,17] The main difficulty lies in separating neptunium(IV) from plutonium(III). Scrubbing the solvent with a reducing solution in dilute nitric acid medium is ineffective, since plutonium(IV) distribution coefficients are too high to allow any effective reduction of plutonium by aqueous reductant [Fe(II)]. The use of sulphate increases the separation sharply.[18] For instance, in a typical experiment, a neptunium decontamination factor of 2 with respect to plutonium was obtained by scrubbing a loaded solvent in a 5-stage unit by a solution of $0{\cdot}7$N-HNO_3 + $0{\cdot}05$M-Fe(II) + $0{\cdot}05$M-N_2H_4 whereas scrubbing under the same conditions with a solution of $1{\cdot}0$N-HNO_3 + $0{\cdot}3$N-H_2SO_4 + $0{\cdot}05$M-Fe(II) + $0{\cdot}05$M-N_2H_4 gave a decontamination factor of 50.

As a result of this the feasibility of neptunium–plutonium partition from a loaded TLA solvent was tested according to the flow-sheet shown in Fig. 10. A neptunium decontamination factor with respect to plutonium of 335 and a plutonium decontamination factor with respect to neptunium of 220 were obtained while the reflux of neptunium in the scrub section is only 20% of the overall neptunium quantity.

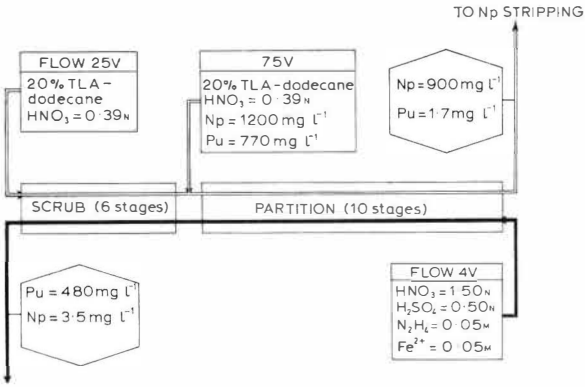

FIG. 10. *Flow-sheet for the neptunium(IV)–plutonium(III) separation by 20% TLA extraction*
Correction: for FLOW 4V read FLOW 40V

This separation might be extremely helpful in the first cycle of the processing of irradiated ^{237}Np targets before the purification cycles which follow for ^{237}Np and ^{238}Pu.

Conclusions

The differences between the complexing powers of sulphate ions for hexavalent and tetravalent actinide elements can be very useful in improving solvent separation processes in nitric acid media.

Uranium(VI)–plutonium(IV) and uranium(VI)–neptunium(IV) separations by TBP extraction may be performed without contamination of the stripped tetravalent actinide by aqueous metallic reductant.

When aqueous reduction is feasible, uranium(VI)–plutonium(IV) separations by TBP extraction are sharply improved. The use of sulphate even allows the direct separation of trivalent plutonium from tetravalent neptunium by stripping plutonium from TLA solutions with a reducing solution in a mixed nitric–sulphuric acid medium.

Acknowledgments

The authors would like to thank M. André Chesné for his encouragement and helpful discussions.

References

[1] Brown, K. B., *Rep. Congr. atom. Energy Commn U.S.*, 1961, CF-61-3-141
[2] Coleman, C. F., *Rep. Congr. atom. Energy Commn U.S.*, 1961, ORNL-CF-61-5-74
[3] Chesné, A., Bathellier, A., & Koehly, G., *Nucl. Sci. Engng*, 1963, **17**, 557; Bathellier, A., Koehly, G., Perez, J. J., & Chesné, A., *Rapp. CEA*, 1964, CEA-R-2594
[4] Hultgren, Å., in 'Solvent extraction chemistry of metals', (McKay, H. A. C., Healy, T. V., Jenkins, I. L., & Naylor, A., Eds), 1965, p. 275 (London: MacMillan)
[5] Champion, J., & Chesné, A., *Rapp. CEA*, 1964, CEA-R-2607
[6] Schulz, W. W., *Ind. Engng Chem. Process Des. Dev.*, 1967, **6**, 115
[7] Sillen, G. L., 'Stability constants', *Spec. Publs chem. Soc.*, 1964, No. 17
[8] Bartlett, T. W., *Rep. Congr. atom. Energy Commn U.S.*, 1951, K-706
[9] Lang, G. P., & Nethaway, M. O., *ibid.*, 1961, MCW-1456
[10] Codding, J. W., Haas, W. O., & Heumann, F. K., *ibid.*, 1951, KAPL-602
[11] Smith, L. L., *ibid.*, 1962, DP-700
[12] Detilleux, E., Rolandi, G., G., Geoffroy, A., & van Geel, J., *Eurochemic Rep.*, 1962, EIR-90
[13] Laxminarayanan, T. S., Patil, S. K., & Sharma, H. D., *J. inorg. nucl. Chem.*, 1964, **26**, 1001
[14] Lucas, M., *Radiochim. Acta*, 1964, **3**, 126
[15] Rao, C. L., *Radiochim. Acta*, 1969, **12**, 135
[16] Berger, R., Koehly, G., & Sontag, R., *Notes CEA*, 1968, CEA-N-1044, p. 283
[17] Gourisse, D., & Bathellier, A., *Radiochim. Acta*, 1970, **13**, 187; 1970, **13**, 191
[18] Fr.P. 6,933,809

Investigation on the nature of degradation products in the system 20 vol.-% tributyl phosphate–dodecane–nitric acid

I. Enrichment of complexing products and infra-red study

by L. Stieglitz

Institut für Heisse Chemie, Gesellschaft für Kernforschung mbH, 75 Karlsruhe, Postfach 3640, W. Germany

The nature of the diluent degradation products responsible for the retention of zirconium in the Purex process is still a matter of dispute. As hitherto described in the literature, zirconium retention is attributed either to nitroparaffins or to hydroxamic acids. The present work shows that the complexing agents are mostly formed on irradiation with low nitric acid concentrations, with a maximum yield at a nitric acid concentration of 0·4M in the organic phase. No relation was found between the amount of hafnium complexed in the solvent and the concentration of nitroparaffins. High-vacuum molecular distillation produced a concentrated residue with strong extracting power. From the appearance of absorptions at 1720, 1660 and 1615 cm^{-1}, it is concluded that the carbonyl function is most probably responsible for the complexing action of degraded solvents.

Introduction

THE USEFUL LIFE of hydrocarbon–tributyl phosphate extraction systems in the Purex process is limited by the formation of previously unidentified products, which are supposedly formed from the hydrocarbon diluent by chemical or radiolytic reactions. Since these degradation products are not removed by the alkali scrub, they accumulate in the solvent. The main consequences of the resulting low process performance are the retention of fission products (mainly zirconium) in the organic phase, increase of the activity levels in recycled systems and the contamination of the uranium and plutonium products owing to leakage of retained fission products into the product streams.

Blake *et al.*[1] at the Oak Ridge National Laboratory report that the extraction behaviour of degraded solvents can be assigned to the presence of nitroparaffins which complex zirconium as a nitroparaffin enol adduct or enol salt. According to Lane,[2] and Huggard & Warner,[3] however, the detectable primary products of irradiation are not responsible for the fission product retention. They found evidence to suggest that one of the main complexing agents formed during the chaos of chemical and radiolytic reactions are hydroxamic acids, which are known to be very potent complexing agents.[4] Hydroxamic acids are assumed to be formed from primary nitroparaffins by rearrangement (Victor Meyer reaction), or as by-products via acid salt formation and reacidification (Nef reaction). While both sides have experimental evidence for their hypotheses, the nature of the diluent degradation products is still a matter of dispute. Feeling that the problem can be solved best by isolation and identification of at least the main complexing products, a research programme was started at the Nuclear Research Centre, Karlsruhe. The main drawback to the investigation of the problem is the fact that the complexing agents, though very effective in retaining fission products, are present below the ppm level. The present work therefore started with establishing reaction conditions for optimum yield and procedures for the enrichment of the interesting degradation products.

Experimental

Materials

Tributyl phosphate (TBP) (Merck A.-G.) was purified by successive washing with 1M sodium carbonate solution, water, and distillation at reduced pressure (0·2 mm Hg, 80°C). n-Dodecane (free of olefins; gas-chromatographic purity >99%) was used as received from Fluka, Switzerland. All experiments were carried out with mixtures of 20 vol.-% TBP–80 vol.-% dodecane. As a substitute for ^{95}Zr, a mixture of $^{175}Hf + ^{181}Hf$ (Radiochemical Centre, Amersham) was used; this avoids the necessity of separating ^{95}Zr from its radioactive daughter ^{95}Nb before each experiment. The equivalence of zirconium and hafnium tracer in solvent degradation studies was tested by Field & Jenkins.[5] The hafnium stock solution, received in the chloride form, was converted to the nitrate by evaporating with nitric acid to near dryness and taken up in 3M nitric acid to give a concentration of 5×10^{-7} M hafnium.

Methods

The 20 vol.-% TBP–dedocane samples were equilibrated (volume ratio organic : aqueous phase = 1) with water or nitric acid (concentrations: 0·2, 0·5, 0·75, 1·0, 2·0, 3·0, 4·0 and 5·0M), and the organic phase was irradiated in a Gammacell 220 (AECL). The radiation power was ~0·6 Watts/l and the temperature was 30–35°C. After irradiation, the low molecular weight acid products, such as mono- and di-butyl phosphate, were removed by scrubbing with 1M sodium carbonate solution. Then the degraded solvent was contacted for 10 min with the hafnium tracer solution in 3M nitric acid at a phase ratio of unity. In the distribution experiments, care was taken to maintain an excess of metal ions in order to achieve full saturation of the complexing agents. Heavily degraded solvents with high extraction capacities were diluted if necessary to maintain an excess concentration of metal ions in the aqueous phase. An 'H-number', i.e. an index giving the number of moles of Hf retained in 10^9 l of degraded solvent, was evaluated from the hafnium concentration of the organic phase after taking into consideration and subtracting the amount of Hf extracted by the 20 vol.-% TBP system alone.

Infra-red absorption measurements were made using a Beckman IR-7 double-beam instrument with 0·1- and 1·0-mm cells. For the enrichment of the degradation products, a special high-vacuum molecular distillation apparatus was found to be very efficient. The procedure is described elsewhere.[6]

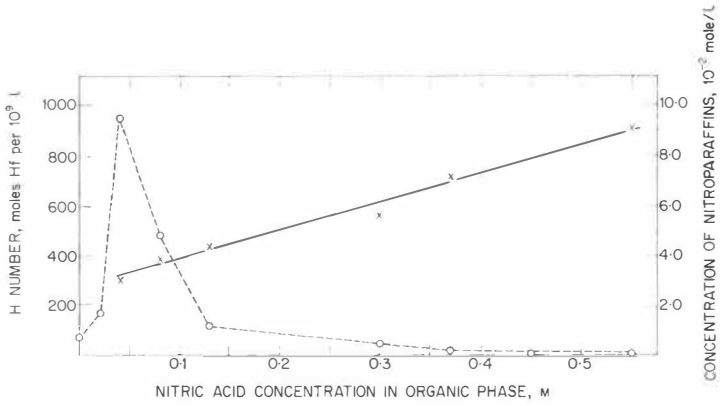

FIG. 1. *Effect of nitric acid concentration during irradiation on the extracting power and the nitroparaffin concentration*

○ H-number; × nitroparaffin concentration

Results and discussion

Effect of nitric acid concentration during irradiation

The concentration of nitric acid during the irradiation proved to be very important for the formation of extracting agents. Results are shown in Fig. 1 for samples irradiated to a total dose of 40 Wh/l. The H-number (moles of Hf extracted per 10^9 l of solvent) was 75 if the system had been equilibrated with water, and increased to 170 and 950 for solvents with organic nitric acid concentrations of 0·02 and 0·04M, respectively, during irradiation. For final $HNO_{3(org)}$ concentrations of 0·45 and 0·55M the corresponding H-numbers were as low as 9 and 6, respectively, i.e. lower by a factor of 100 or 150 compared with an irradiation with an $HNO_{3(org)}$ concentration of 0·04M. Apparently two counteracting processes take place: at low nitric acid concentration, considerable amounts of complexing products are formed, which are suppressed or destroyed at high nitric acid concentration.

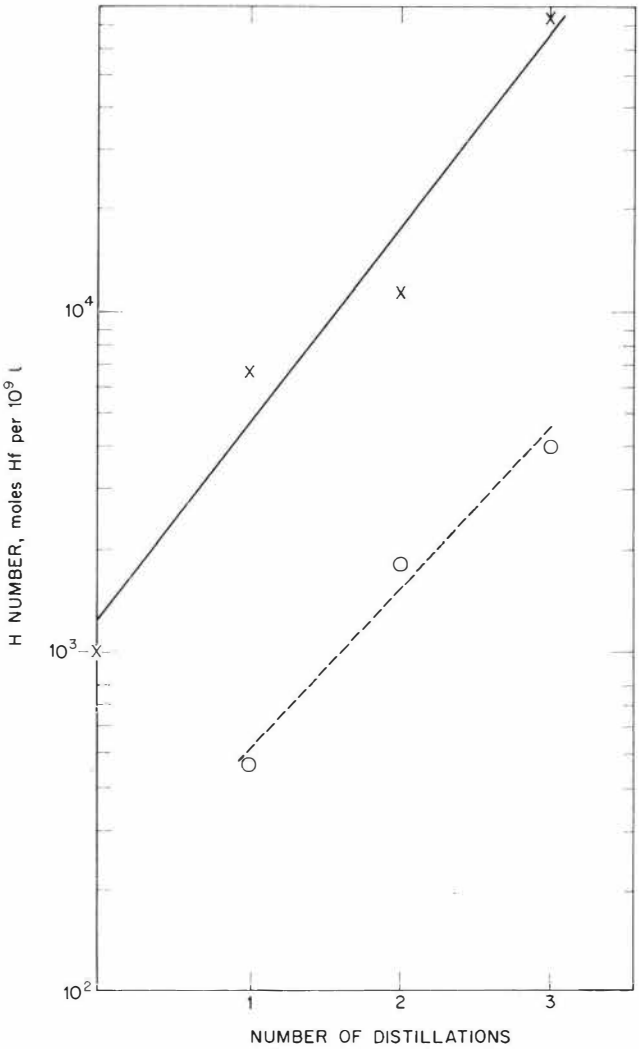

FIG. 2. *Enrichment of complexing degradation products by high-vacuum molecular distillation*

× H-number of residue; ○ H-number of distillate

Included in Fig. 1 are the concentrations of nitroparaffins as obtained from infra-red measurements at 1550 cm^{-1}. There is a roughly linear relationship between nitroparaffin and nitric acid concentrations during irradiation. If these results are compared with the H-numbers, it may be concluded that no direct relation exists between the presence of nitroparaffins and the extraction of hafnium.

Enrichment of complexing agents by molecular distillation

After establishing the optimum conditions for the formation of the complexing degradation products, the next step was a distillation procedure to achieve their separation from undegraded diluent and TBP. 500 ml of solvent (equilibrated with 0·5M nitric acid) was irradiated to a total dose of 40 Wh/l. After scrubbing with 1M sodium carbonate solution, water, and 0·5M nitric acid the sample showed an H-number of 1000. High-vacuum molecular distillation at

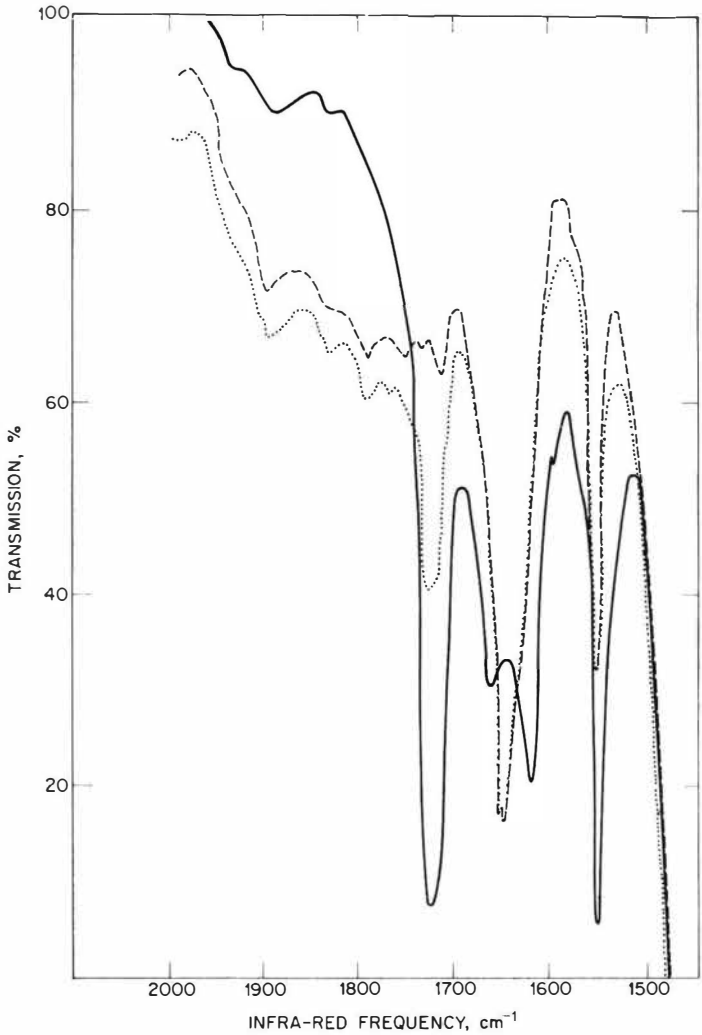

FIG. 3. *Infra-red spectra of distillation residues*

Residue 1 (– – – – –): H-number 6,700; Residue 2 (. . . . . .): H-number 11,000; Residue 3 (————): H-number 72,000

10^{-2} mm Hg and 40°C gave a distillate and a residue with H-numbers of 450 and 6700, respectively. The results are shown in Fig. 2. Further enrichment was achieved by a second and third run, resulting in a concentrated residue (H-number 72,000). The infra-red spectra of the residues after distillation are shown in Fig. 3 for the range 1450–2000 cm^{-1} together with the corresponding H-numbers. Marked absorptions at 1550 and 1640 cm^{-1} indicate the presence of equal amounts of nitroparaffins and nitrate esters in residues 1 and 2, whilst the extraction powers differed significantly. This again suggests that nitroparaffins have no influence on the retention of hafnium. Noteworthy, however, is the appearance of a substantial peak at 1720 cm^{-1} after the second distillation; this peak is even more intense with the third residue. Absorptions at 1720 cm^{-1} are generally assigned to the carbonyl function. In the spectrum of residue 3, further peaks at 1615 and 1660 cm^{-1} are emerging and are also tentatively assigned to the carbonyl group, e.g. in diketones.[7] It is obvious from the present results that the high extracting power can be related to carbonyl compounds rather than nitroparaffins.

Conclusions

The degradation products responsible for the retention of fission products can be characterised as follows:

As scrubbing with sodium carbonate solution is ineffective in removing the compounds, the substance may be either a weak acid, or a sodium salt with a high solubility in the organic phase.

The volatility is lower than that of TBP, pointing to a high molecular weight, possibly combined with polar functional groups.

No relation was found between the presence of primary nitroparaffins and the specific action with respect to hafnium or zirconium. On the other hand, an increase of the extraction power was noted in cases where infra-red absorptions due to the carbonyl function had increased.

The concentration of complexing agents even after high radiation doses (40 Wh/l) is of the order of 10^{-6} mole/l, while monofunctional degradation products such as nitroparaffins and unsubstituted ketones are formed at a rate that is higher by a factor of 1000. The low concentration of the extracting compounds may be explained if the primary products must undergo further substitution or conversion to form a compound where several functional groups are in a favourable position for complexing zirconium.

Acknowledgments

The author wishes to thank Prof. Dr. F. Baumgärtner for his valuable discussion and encouragement during this work. The help of Mrs. H. Feiler and Mr. F. Leonhard is greatly appreciated.

References

[1] Blake, C. A., Davis, W., Jr., & Schmitt, J. M., *Nucl. Sci. Engng*, 1963, **17**, 626
[2] Lane, E. S., *Nucl. Sci. Engng*, 1963, **17**, 620
[3] Huggard, A. J., & Warner, B. F., *Nucl. Sci. Engng.* 1963, **17**, 638
[4] Baroncelli, F., & Grossi, G., *J. inorg. nucl. Chem.*, 1965, **27**, 1085
[5] Field, B. O., & Jenkins, E. N., *Rep. U.K. atom. Energy Auth.*, 1960, AERE-R-3507
[6] Frank, W., *Chemikerzeitung–chem. Appar.*, 1963, **87**, 365
[7] Bellamy, L. J., 'Ultrarot-Spektrum und chemische Konstitution', 1966, 2 Auflage, p. 102 (Darmstadt: Dr. Dietrich Steinkopff)

Flow-sheet studies on reprocessing of Japan Experimental Fast Reactor fuel in a Purex plant

by T. Segawa, T. Hoshino, A. Kaya, K. Gonda, T. Tsuboya and C. Tanaka
Development & Research Section, Technology Division, Power Reactor & Nuclear Fuel Development Corporation, Tokai, Ibaraki, Japan

At the I.A.E.A. panel on reprocessing of highly irradiated fuels held in Vienna in 1969, a development plan of the reprocessing technique for the Japan Experimental Fast Reactor (JEFR) fuel in a Purex plant was reported.

The flow-sheets proposed are characterised by the following points: (1) a dilution system (about 1/15 dilution) except for the third Pu cycle; (2) use of 10% tributyl phosphate (TBP)/dodecane as a solvent. Detailed examination of these preliminary design flow-sheets was started at the beginning of 1969. Firstly, measurements of the distribution ratio for uranium, plutonium and ruthenium in 10% TBP/dodecane–HNO_3 system were performed since these were necessary for flow-sheet design. A computer code for calculating concentration profiles in a contactor bank was developed and used for flow-sheet simulation. Proving tests of designed flow-sheets were subsequently carried out using unirradiated uranium and plutonium in a glove box.

In the present paper, the results of distribution ratio measurements, of the proving tests, and of the flow-sheet simulation are described in detail.

Introduction

THE CONSTRUCTION of an experimental fast reactor has been scheduled by the Power Reactor and Nuclear Fuel Development Corporation (PNC). This reactor (Japan Experimental Fast Reactor, JEFR, recently named as Joyo) will be critical in 1973. It will have a thermal output of 10 MW and mixed uranium/plutonium oxides will be used as core fuel and liquid sodium as a coolant.

On the other hand, the construction of a reprocessing plant which was designed on the basis of the Purex process by Saint-Gobain Techniques Nouvelles, has been also planned by PNC.[1,2] It will be completed in 1973 and hot operation will be started at the end of 1974. The capacity of this plant is ~0·7 ton/day, and Magnox-clad natural uranium fuel burnt up to 3,900 MW days/ton (MWD/T) and Zircalloy- or stainless steel-clad enriched uranium oxide fuel (up to 4%) burnt up to 28,000 MWD/T can be treated in this plant. Cooling times for these two fuels are 155 and 180 days, respectively.

According to the JEFR construction programme, the reprocessing of irradiated fuels will be necessary from 1975. The amount of the core fuel discharged from this reactor will be ~1 ton/year and the blanket will be ~2 ton/year. The prospect of treating these fuels in the PNC reprocessing plant has been considered.[3]

In contrast to the case of light water reactor fuels, there are many factors to be considered such as the removal of sodium coolant, the removal of decay heat released from the fuel containing a great deal of fission products (FPs), the dissolution including the feasibility of a chopping machine, the off-gas treatment, the expected low decontamination factors caused by the change of FPs composition and solvent damage. The problems of criticality and the extraction behaviour of plutonium caused by higher plutonium content must also be solved.

For the treatment of JEFR core fuel in the PNC plant, the following three methods are considered:

(1) Treatment of the core and the blanket separately in order to recover enriched uranium which remains in the core fuel.

(2) Treatment of the core and blanket simultaneously.

(3) Treatment of the core and blanket with the light water reactor fuels which will be treated routinely.

In the first case, enriched uranium can be recovered without isotopic dilution but reprocessing costs will be rather high. In the last case, except for the head-end process including dissolution, the flow-sheet and operating conditions for light water reactor fuel treatment could be used with slight modification. In the first and second cases, however, an independent campaign for the JEFR fuels must be carried out.

As a first step, the first case has been considered, and in order to establish the reprocessing technique, chemical flow-sheets of the extraction and separation processes have been designed and a series of proving tests have been carried out with the aid of these flow-sheets.

In the present paper, the preliminary design of the chemical flow-sheets and the results of the measurement of basic data necessary for the flow-sheet design are described. Also, the results of the flow-sheet simulation using a computer and of the proving tests using unirradiated uranium and plutonium are discussed.

Design basis of the flow-sheets

Specification of JEFR fuel

Since, according to the conceptual design of JEFR, the length of the fuel is less than that of the light water reactor fuel, there will be no problem concerning the reception of the fuel. The cladding is of SUS-32, and the meat of core fuel is composed of 76·9% of 20% enriched UO_2 and 23·1% of PuO_2. The radial blanket is made of natural UO_2. Burn-up of the core is 48,000 MWD/T and that of the blanket is 860 MWD/T, and the fission ratio, Pu:U, is 1:0·91.[3]

On the other hand, the FPs composition of the irradiated fuel, after 180 days' cooling, is calculated according to the method of Burris & Dillon.[4] The results are shown in Table I.

TABLE I

Fission products composition of irradiated fuel (β Ci/kg)

Cooling time 180 days

Isotope	LWR	JEFR (core)	JEFR (ax. blanket)
Total activity	$4{\cdot}6\times10^{3}$	$1{\cdot}4\times10^{4}$	$2{\cdot}3\times10^{2}$
^{85}Kr	$1{\cdot}1\times10$	$1{\cdot}3\times10$	$3{\cdot}7\times10^{-1}$
^{129}I		$5{\cdot}3\times10^{-6}$	$6{\cdot}6\times10^{-8}$
^{131}I	$1{\cdot}5\times10^{-4}$	$1{\cdot}3\times10^{-3}$	$8{\cdot}9\times10^{-5}$
^{103}Ru	$5{\cdot}5\times10$	$2{\cdot}3\times10^{2}$	3·5
^{103m}Rh	$5{\cdot}5\times10$		
^{106}Ru	$3{\cdot}9\times10^{2}$	$1{\cdot}3\times10^{3}$	3·3
^{141}Ce	$3{\cdot}7\times10$	$1{\cdot}1\times10^{2}$	1·9
^{144}Ce	$1{\cdot}0\times10^{3}$	$1{\cdot}7\times10^{3}$	$3{\cdot}5\times10$
^{95}Zr	$2{\cdot}5\times10^{2}$	$9{\cdot}5\times10^{2}$	$2{\cdot}0\times10$
^{95}Nb	$5{\cdot}3\times10^{2}$	$1{\cdot}8\times10^{3}$	$3{\cdot}7\times10$
^{89}Sr	$1{\cdot}4\times10^{2}$	$3{\cdot}1\times10^{2}$	7·8
^{90}Sr	$9{\cdot}6\times10$	$9{\cdot}0\times10$	2·1
^{137}Cs	$9{\cdot}0\times10$	$1{\cdot}5\times10^{2}$	2·9
^{237}U	$3{\cdot}0\times10^{-11}$ g/kg		
^{237}Np	$8{\cdot}2\times10^{-5}$ (0·12 g/kg)		
^{241}Am	0·15 (0·045 g/kg)		
^{242}Cm	$6{\cdot}5\times10^{-3}$ ($2{\cdot}0\times10^{-6}$ g/kg)		
Heat generation, W/kg	14	61	0·92

Throughput of the plant

In the case of core fuel reprocessing, it has been concluded that the throughput of the core fuel must be reduced to 44·4 kg/day (4 elements/day), owing to the through-put of the third Pu cycle and nuclear safety of the dissolver vessel and adjusting tanks. The quantity of ^{131}I in JEFR fuels compared with that

of the light water reactor fuel shows that the cooling period must exceed at least 180 days and additional shielding of the caves is necessary without capacity reduction. Heat removal of the irradiated fuel and release of ^{85}Kr will pose no problem (cf. Table I).

Tail end

Evaporation and concentration of plutonium nitrate solution

Since the through-put of plutonium will be limited to nearly the same as that of the light water reactor fuel treatment, no problem will arise in this process.

Denitration of uranium

Since initially 20% enriched uranium is loaded in the core of the JEFR fuel, although the enrichment of uranium will be lowered by a few per cent after irradiation, it will still be higher than in the case of the light water reactor fuel. From the viewpoint of criticality, safety of the process must be checked.

Waste treatment and storage

Liquid and solid waste treatment and storage will not pose any difficulty.

FPs quantity and decontamination factor (DF)

The FPs quantity will be $\sim$1/6 of that for the case of light water reactor fuels, and the content of ^{106}Ru will be higher than that in light water reactor fuels, but there will be no problem concerning solvent damage and DF.

Preliminary design chemical flow-sheets

As described above, the core fuel will be treated in a plant designed for light water reactor fuel on the basis of ordinary chemical flow-sheets. In order to use the equipment, i.e. pumps, tanks, and instrumentation equipped for light water reactor fuel, the modification of process conditions must be limited to a minimum. Since the through-put of the plant is reduced to 44·4 kg/day, the degree of solvent saturation will be low and DF will be relatively low except for the third Pu cycle. To keep solvent saturation relatively high, 10% tributyl phosphate (TBP)/dodecane is used as a solvent in place of 30% TBP/dodecane in the preliminary design flow-sheets. Thus the DF will be high enough to obtain final uranium and plutonium products. These flow-sheets are shown in Figs 1–3. The same flow-sheet for light water reactor treatment will be used for the third Pu cycle.

The study of these preliminary design flow-sheets can be carried out by drawing an operating diagram using precise distribution data for the 10% TBP/dodecane–Pu–U–HNO_3 system, and can be verified by proving tests using miniature mixer–settlers. The distribution data of this system have not been studied in detail, except for a few points which are available in the published literature. Accordingly, the systematic distribution ratios thought to be necessary for the analysis of process conditions were measured. The distribution ratios of ruthenium were also measured but only under the first cycle process conditions.

A computer code for calculating concentration profiles in a contactor bank was developed for 10% and 30% TBP systems. This code is useful for flow-sheet simulation in order to determine optimum conditions and to analyse process stability and the results of proving tests.

The results of the studies such as the measured distribution ratios and the outline of the computer code are described in detail and the results of proving tests are also shown.

Measurement of the distribution ratios

Experimental

A constant volume of aqueous phase and the same volume of organic phase were taken in a polyethylene capsule and shaken for 3 min and settled for 15 min (in the case of a ruthenium experiment, 1 min for mixing and 3 min for settling). Each phase was then taken for analysis of U, Pu, HNO_3 and Ru. By calculation, the distribution ratio of each component was obtained. Before

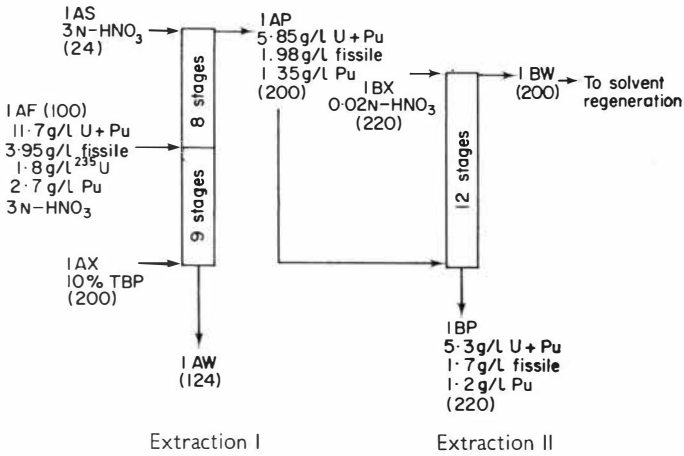

FIG. 1. *First cycle flow-sheet*

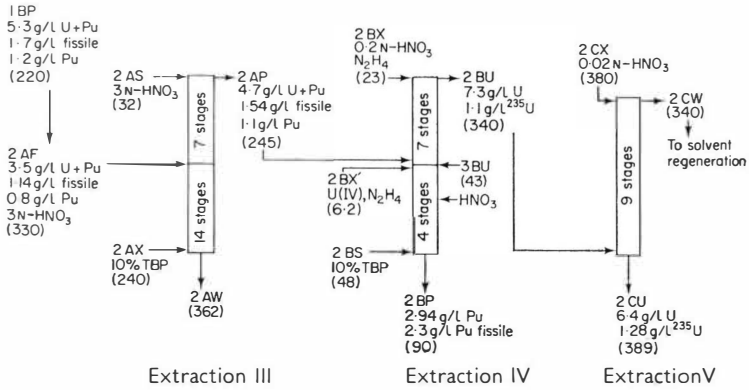

FIG. 2. *Second cycle flow-sheet*

Corrections: for 1·1 g/l^{235}U read 1·46 g/l^{238}U; for (389) read (387); on left-hand arrow add HNO_3.

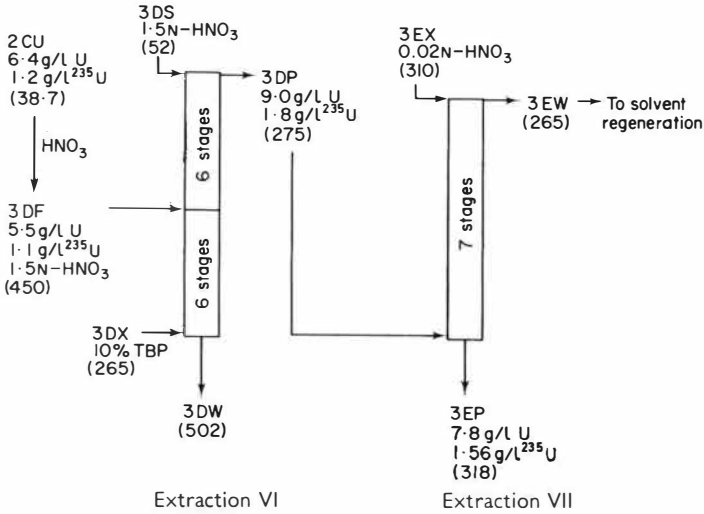

FIG. 3. *Third U cycle flow-sheet*

contact of two phases the aqueous phase was prepared to a fixed composition and the organic phase was prepared by washing with Na_2CO_3, HNO_3 and H_2O in turn. All extraction experiments were carried out at room temperature.

Reagents

TBP and nitric acid used were of reagent grade, and n-dodecane was obtained from Maruzen Oil Co.

Plutonium was used after the purification by the ordinary anion-exchange technique using Diaion SA–200 resin (Mitsubishi Chemical Co.).

The valency of plutonium was adjusted with ferrous sulphamate (extra-pure grade) and sodium nitrite (reagent grade). As a stabiliser of plutonium valency, hydrazine (extra-pure grade) was used and also ferrous sulphamate was used as a holding agent of plutonium(III).

The solution of ruthenium was prepared by the method described by Jenkins & Wain.[5]

Analysis

All analyses of samples were carried out in the Analysis Section of the Technology Division (PNC Tokai works). The methods adopted for each component were as follows:

Pu and Am: α-counting or α-spectrometry (if the separation of Pu from Am and/or U was necessary, an anion-exchange technique is used for this purpose).

U: colorimetry with dibenzoyl methane, DBM (after the separation of uranium from plutonium with ethyl acetate).

Free HNO_3: titration with NaOH.

Ru: β-counting for total concentration and reversed-phase paper chromatography[6, 7] followed by the β-counting technique for complex composition.

Results

The distribution data of the system containing Pu(IV) are shown in Figs 4 and 5. Fig. 4 shows that aqueous plutonium concentration (x_{Pu}) has no significant effect on uranium distribution (Kd_U) and Kd_U is almost constant up

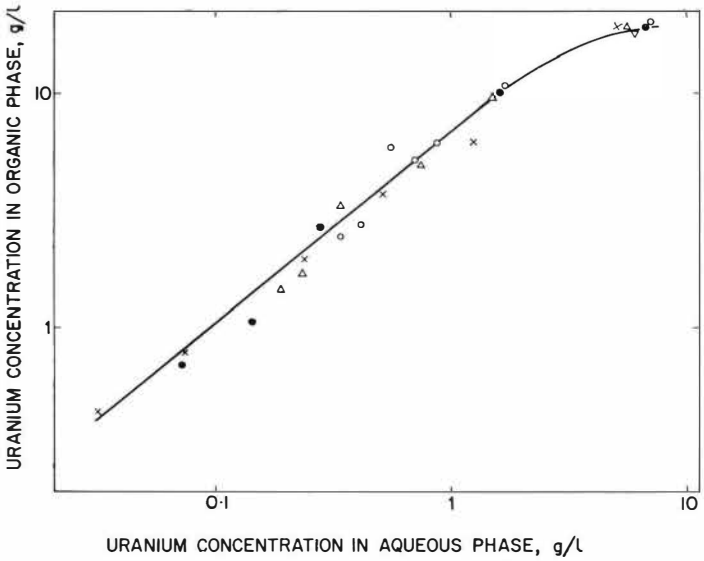

FIG. 4. *Distribution curve of 10% TBP–U–Pu(IV)–HNO₃ system*

Extraction I, x_H = 3N
Initial Pu concn. in aqueous phase (g/l): ○ 5; △ 2·5; ▽ 1·0; ● 0·25; × 0

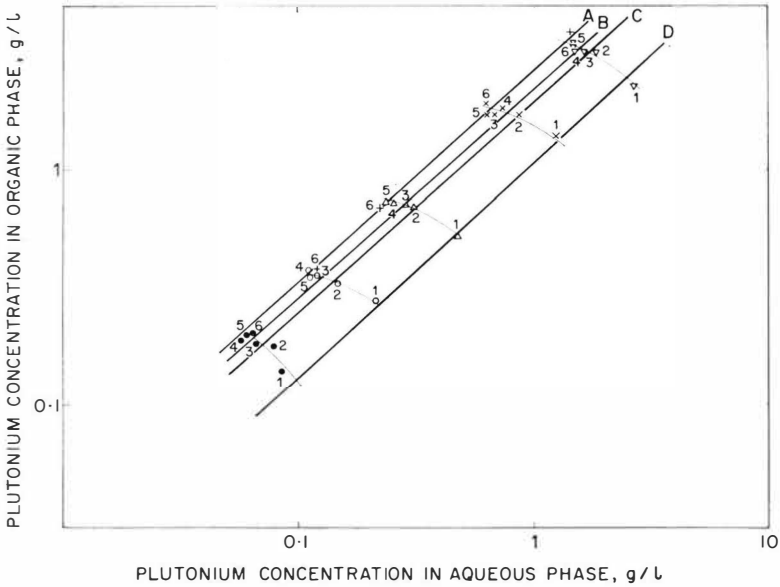

FIG. 5. *Distribution curves of 10% TBP–U–Pu(IV)–HNO_3 system*

Extraction I, x_H = 3N
Initial Pu concn. in aqueous phase (g/l): ▽ 5; × 2·5; △ 1·0; ○ 0·5; ● 0·25
U concn. in aqueous phase (g/l): A 0·2; B 0·7; C 1·5; D 6·0

to an aqueous uranium concentration (x_U) of 2 g/l. With increasing x_U above 2 g/l, Kd_U tends to decrease. Plutonium distribution curves are shown in Fig. 5 where x_U is taken as a parameter. The distribution ratio of plutonium (Kd_{Pu}) decreases gradually with increasing x_{Pu} and x_U significantly affects Kd_{Pu} (for example, at x_U = 6 g/l, Kd_{Pu} is one third less than the initial value at x_U = 0). Uranium equilibrium curves (aqueous nitric concentration (x_H) and x_{Pu} are taken as parameters) show that Kd_U is almost constant in all tested regions. The nitric acid distribution ratio (Kd_H) increases with increasing x_H up to 1N and Kd_H is then nearly constant at any higher x_H.

The results of a comparison between 30% TBP and 10% TBP systems are shown in Table II. It can be seen that Kd_U and Kd_{Pu} at low x_U (x_U = 0·15 g/l) are proportional to $(TBP)^{1\cdot6-1\cdot8}$ and at higher x_U (x_U = 6 g/l), Kd_U and Kd_{Pu} are proportional to $(TBP)^{1-1\cdot25}$ and also that the ratio Kd_U:Kd_{Pu} is 3–4 over the whole range used in this work.

The distribution data of the system containing Pu(III) are presented in Fig. 6 which shows that the distribution ratio (Kd_{Pu}) decreases slightly with increasing x_{Pu} in the higher concentration region. The effect of x_U on Kd_{Pu} is not found at a low nitric acid concentration (x_H = 0·2N) but at higher nitric acid concentration, Kd_{Pu} decreases with increasing x_U. The distribution ratio

TABLE II

Effect of TBP concentration (at 3N aq. HNO_3)

	U concn. in aq. phase, g/l					
	0·15			6·0		
	TBP concn., %					
	3	10	30	3	10	30
Kd_{Pu}	0·34	3·3	19	0·12	1·2	4·0
Kd_U	1·5	10	73	0·4	3	13

of nitric acid, Kd_H, increases with increasing aqueous nitric acid concentration (x_H), and the increasing rate of Kd_H decreases gradually at $x_H \geqslant 1$N. It can also be seen that Kd_H is independent of uranium and plutonium concentrations in the aqueous phase, and that Kd_U is independent of x_{Pu} and in the higher concentration region Kd_U decreases slightly with increasing x_U.

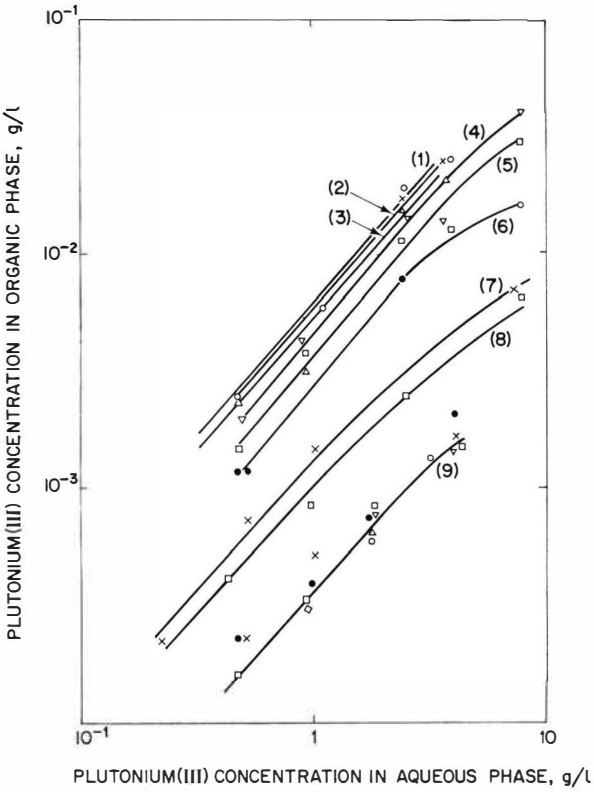

FIG. 6. *Distribution curves of 10% TBP–U–Pu(III)–HNO₃ system*
Extraction IV
U concn. in aqueous phase (g/l): (1) 0·1; (2) 0·2; (3) 0·3; (4) 1·2; (5) 3·3; (6) 7; (7) 0·3; (8) 6; (9) 0·5–16
HNO_3 concn. in aqueous phase (N): (1)–(6) 2·0; (7)–(8) 0·5; (9) 0·2

Distribution of Ru in 10% TBP–U–HNO_3 system

The relatively extractable nitrato complexes are tri- and tetra-nitrato complexes and there is only a slight difference between the extractabilities of the two complexes. The high extractability of the tetra-nitrato complex as shown in the system of higher TBP concentration, was not found in the 10% TBP system. The ratio of these two complexes to the total ruthenium complexes increases with increasing uranium concentration in the aqueous phase. The extractability of the complexes decreases remarkably with increasing aqueous uranium concentration.

It is assumed that the extraction of these complexes is performed by free TBP in the solvent and a linear relationship has been found between log Kd_{Ru} and log $(TBP)_{free}$ (cf. Fig. 7).

Examination of preliminary design flow-sheets

The number of stages of the flow-sheets was checked by drawing an operating diagram based on the distribution data which were measured previously. Some process conditions were modified so as to obtain the initially expected recovery of uranium and plutonium. On the other hand, mathematical equations were

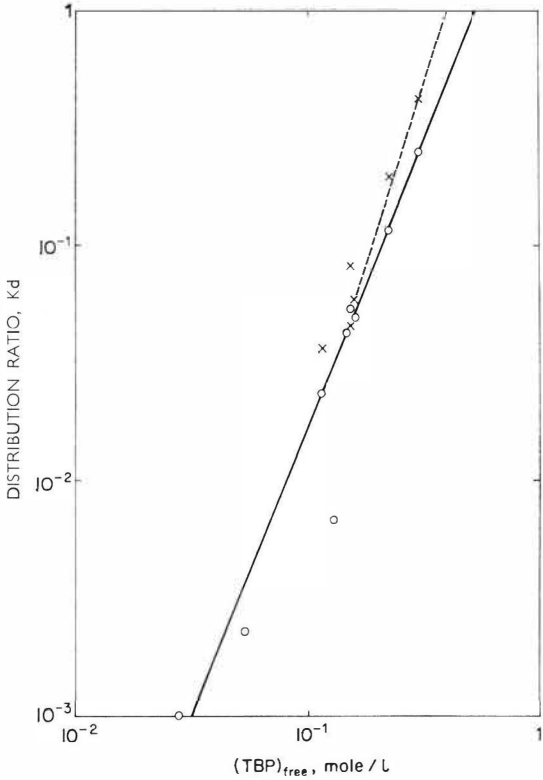

FIG. 7. *Relations between distribution ratio of Ru complexes and free TBP concentration*
○ ———— ○ distribution ratio of tri- and tetra-nitrato complexes;
× - - - - - - × distribution ratio of tetra-nitrato complex

derived to express the distribution data of 10% TBP system. A calculation code for obtaining concentration profiles in a bank was developed and the code was used for the analysis of the flow-sheet characteristics.

Outline of the code

The calculation codes so far reported for calculating concentration profiles have been reviewed by Mills,[8] but these programs are not available in Japan. Therefore, a code for 30% and 10% TBP systems has been developed starting from the code REPROSY–P[9] and the flow chart of REPROSY–UP developed at JAERI (Japan Atomic Energy Research Institute).

The principle of calculation is based on a batchwise countercurrent extraction principle where the concentration of each phase is calculated using the distribution equations and material balance equations of each component. The flow-chart of the code is shown in Fig. 8. The concentrations of nitric acid and uranium are calculated by first considering that the distribution is affected by these concentrations. Secondly, the distribution of plutonium is calculated from these nitric acid and uranium concentrations, where it is assumed that the distribution of nitric acid and uranium is not affected by the distribution of plutonium.

Number of theoretical stages in each bank

The calculations using a graphical method and the computer code have been carried out to check the number of theoretical stages. The results obtained are summarised in Table III, which shows that the extraction section requires eight stages to treat the feed containing 100 mg/l of Pu(VI) and 2·6 g/l of

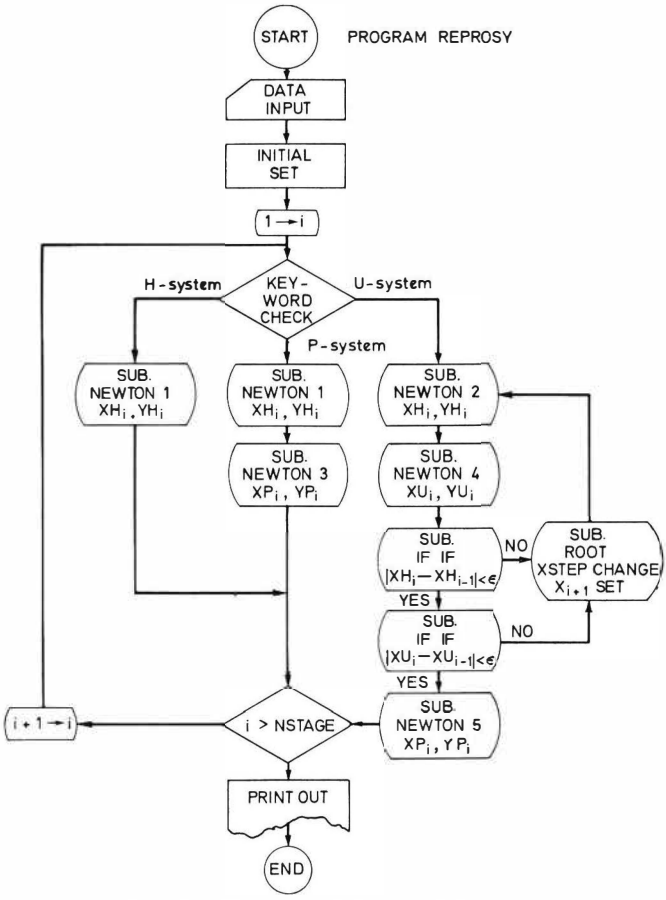

FIG. 8. *Flow chart of the calculation code*
X = aqueous; Y = organic; H = nitric acid;
P = plutonium; U = uranium; i = parameter for calculation.

Pu(IV) in the first cycle. In the second cycle, nine stages are required for the extraction section in order to obtain a permissible leakage of plutonium in the aqueous raffinate. It is supposed that since the distribution ratio of U(IV) in 10% TBP system is rather low, the leakage of U(IV) in the plutonium stream will be high, and that the quantity of U(IV) to be added to the partition bank as a reductant must be minimised as far as possible. The optimum quantity of U(IV) can be determined by a proving test or by an actual test run of the plant.

As an example of the operating diagram for Pu, that of the Extraction I bank (the first cycle) is shown in Fig. 9. The concentration profiles of Extraction III (the second cycle) calculated by the computer code are given in Fig. 10 as an example. In this case, 30% TBP/dodecane is used as a solvent and the calculated profiles will be compared with experimental results later.

For the process conditions of the third Pu cycle, it is seen that the feed concentration of plutonium will be 2·7 g/l (plus 35% to the original flow-sheet) containing 2·15 g/l of fissile plutonium. In this cycle, 20% enriched U(IV) will be added as a reductant, this corresponds to a concentration of 1·88 g/l fissile material, but in Extraction IX (partition bank) plutonium is stripped into the aqueous stream whilst uranium remains in the organic stream. The critical concentration of this cycle is designed for ~36 g/l, consequently the fissile concentration in both phases will be low in comparison with this critical concentration.

TABLE III
Calculated number of stages required

Cycle	Number of stages		
	Section	Calculated	LWR plant design
First	Extraction	3 for U 6 for Pu 8 for Pu (10% Pu(VI))	9
	Strip	3 for U	12
Second	Extraction	3 for U 9 for Pu	14
	Pu-strip	Not calculated	7
	Pu-scrub	Not calculated	4
	Strip	4 for U	9
Third U	Extraction	5 for U	6
	Strip	4 for U	7
Third Pu	Extraction	Not calculated	9
	Pu-strip	Not calculated	8
	Pu-scrub	Not calculated	5

Since, in this cycle, 30% TBP system is used, loaded solvent from the Extraction IX bank cannot be recycled to the Extraction IV bank of the second cycle. To solve this problem, two modifications are considered: (a) is to add a uranium strip bank and solvent regeneration bank, thus making the third Pu cycle an independent cycle, and (b) eliminate the addition of U(IV) and to modify the flow-sheet so as to remove only FPs from the plutonium stream with or without a solvent regeneration cycle.

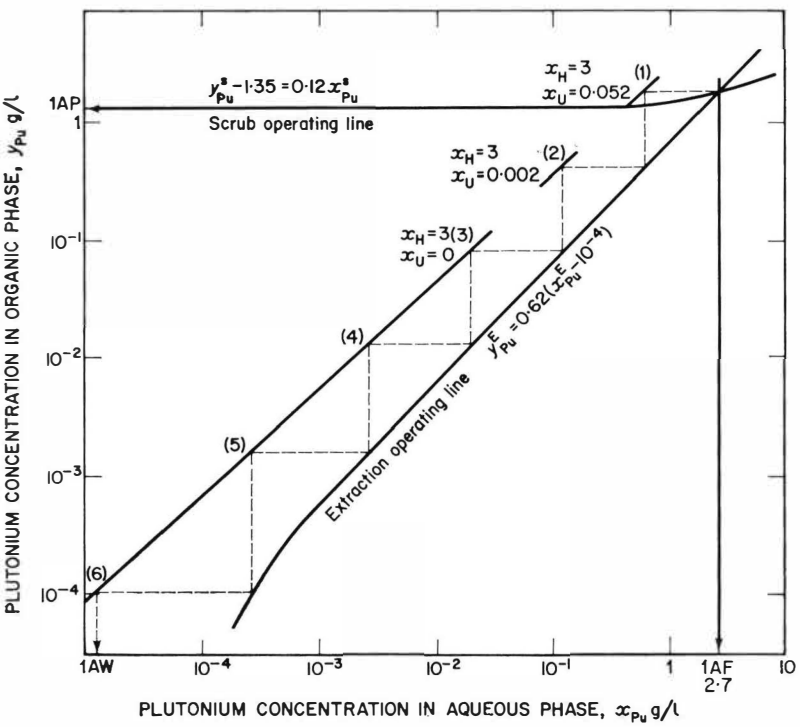

FIG. 9. *Operating diagram of Extraction I bank (first cycle) for plutonium*

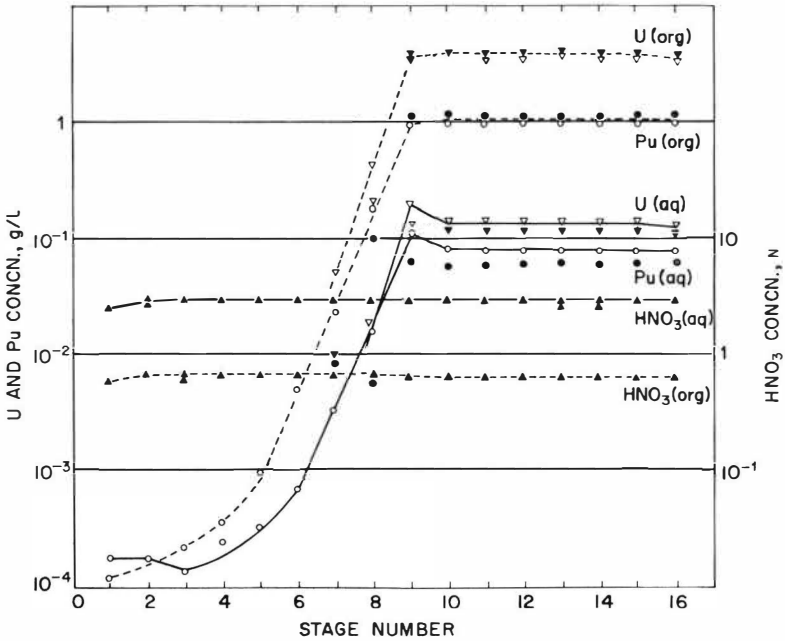

FIG. 10. *Concentration profiles in Extraction III bank (second cycle, 30% TBP system)*
○ Pu exp.; ● Pu calc.; ▽ U exp.; ▼ U calc.; △ HNO_3 exp.; ▲ HNO_3 calc.
———— aqueous phase; - - - - - - organic phase

For the third U cycle, if the same flow ratio is adopted and the uranium recycle to the second cycle from the third Pu cycle is about three times that of plutonium, eight stages will be required for the extraction section. But the actual number of stages is six, and by changing the flow ratio (aq./org.) in the extraction section from 1·92 to 1·20, the extraction of uranium can be performed even with five stages. This modification can be done by decreasing the strip flow rate in Extraction V bank of the second cycle without using an evaporator for concentration.

Proving tests

A series of proving tests using un-irradiated uranium and plutonium was carried out.

Equipment

In a glove box for plutonium (900 × 900 × 1200 mm), two miniature mixer–settlers (Sonal, CEA standard type) were set up and used for the proving tests. This mixer–settler has 16 stages in a bank and each stage has a hold-up of 25 ml (mixer 5·6 ml; settler 16·7 ml; dead volume 2·7 ml). It can be used with an arbitrary number of stages within the total of 16. The bank is made of Plexiglass and is completely transparent; each stage has a screw to regulate the height of the two phase interfaces and an impeller which is composed of a shaft and a perforated plate of stainless steel. Three types of Japanese pumps were used in the tests.

Experimental

The flow rate of the pumps was measured every 30 min and when the deviation exceeded ±3% of the fixed flow rate, it was readjusted. The composition of discharged streams was analysed every hour in order to check

for steady state. After steady state was obtained, the operation was continued for a few hours and at the end of the test stage samples of each bank were taken and analysed to obtain the concentration profiles of uranium, plutonium and nitric acid.

The contact time in the mixers of the extraction section was kept as specified for the actual plant.

Results

The results are summarised in Table IV, which shows that the losses of uranium and plutonium in the first cycle are all acceptable. From the concentration profiles in Extraction I bank, it can be concluded that the extraction section requires eight stages for effective uranium and plutonium extraction. The number of stages necessary for the scrub section cannot be obtained by the α-proving test and a series of γ-tests must be carried out in an α–γ-cave using irradiated fuels. According to the concentration profiles in Extraction II bank, the number of stages necessary for the stripping will be six.

For the second cycle, the losses of uranium and plutonium in the aqueous raffinate are reasonable. From the concentration profiles in Extraction III bank, it is found that the number of stages required to obtain satisfactory results will be 11. On the other hand, in Extraction IV (partition bank), uranium leakage in the plutonium stream is ~1·32 g/l, as shown in Table IV (uranium:plutonium = 0·452). This value is nearly the same as that of the feed solution to the third Pu cycle in the original flow-sheet. The leakage of plutonium in the uranium product stream is ~0·04 mg/l (12·4 ppm, cf. Table IV). This stream can be purified in the third U cycle and the value obtained in the second cycle tests is of the same order as designed. It is concluded that the tested flow-sheet is reasonable to obtain the initially expected uranium/plutonium partition. The quantity of U(IV) giving the best result is ~1·8 times that of plutonium by weight.

The final test of this cycle was carried out with 30% TBP/dodecane as solvent. The results of the losses of uranium and plutonium and of the

TABLE IV

Summarised results of the proving tests

	Aqueous raffinate		Organic raffinate	
First cycle, 10% TBP system	U	Pu	U	Pu
	10 mg/l> 0·12% >	1 mg/l 0·13%	10 mg/l>> 0·19% >	1·75 mg/l 0·16%
	Aqueous raffinate		U product	Pu product
Second cycle, 10% TBP system	U	Pu	Pu	U
	10 mg/l> 0·25% >	0·51 mg/l 0·046%	0·04 mg/l 12·4 ppm	1·32 g/l U: Pu 0·452
	Aqueous raffinate		U product	Pu product
Second cycle, 30% TBP system	U	Pu	U	Pu
	10 mg/l> 0·067%>	0·158 mg/l 0·022%	0·02 mg/l 1·7 ppm	41·37 mg/l U: Pu 0·0177
	Aqueous raffinate		Organic raffinate	
Third U cycle, 10% TBP system	U		U	
	160 mg/l 2·18%		13·5 mg/l 0·18%	

partition of uranium/plutonium are all satisfactory, as shown in Table IV. These results are better than those of the previous tests using 10% TBP/dodecane as a solvent.

As a typical example, the experimental concentration profiles in Extraction III bank obtained by the proving test are shown in Fig. 10, which also shows the concentration profiles calculated by the computer code. From Fig. 10, it is found that the calculated profiles agree well with the results of the proving test.

For the third Pu cycle, the flow-sheet designed for light water reactor fuel treatment can be used without any modification because the through-put of plutonium will be about the same as in the case of JEFR fuel treatment. The proving test of this cycle, therefore, was not undertaken.

For the third U cycle, the losses of uranium in the organic raffinate and the aqueous raffinate are 0·18% and 2·18%, respectively. Though the loss of uranium in the organic raffinate is acceptable, the loss of uranium in the aqueous raffinate is rather high. This might be attributed to U(IV) leakage (cf. Table IV). From the concentration profiles in the extraction section, it is concluded that in order to obtain a uranium concentration below 10 mg/l in the aqueous raffinate, four stages must be added to the extraction section, but that since the actual number of stages is six in the PNC plant, 30% TBP/dodecane must be used as solvent as required in the original flow-sheet.

It is expected that satisfactory results might be obtained by the original third U cycle flow-sheet which is already proven in the case of JEFR core fuel treatment and thus a further proving test was eliminated.

From the results mentioned above, it is concluded that the preliminary design flow-sheets for the first and second cycles are reasonable and that uranium and plutonium can be separated and recovered satisfactorily with the aid of these flow-sheets.

For the third cycle, it is supposed that plutonium and uranium will be purified by the original flow-sheets with acceptable results.

According to the theoretical considerations, it is supposed that, for the final product of uranium and plutonium, satisfactory decontamination factors can be obtained under the process conditions. However, this can be verified only by proving tests using the irradiated fuels.

In order to perform the γ-test of the preliminary design flow-sheets, one compartment of the α–γ facility which is now under construction at Oharai Engineering Centre of PNC is being prepared and will be completed by the middle of 1971. The γ-test for finishing the preliminary flow-sheet design will be carried out on completion of this facility.

Conclusions

To establish a technique for reprocessing irradiated core fuel of JEFR in the PNC plant for light water reactor fuel, the following studies have been carried out:

(1) design of the preliminary flow-sheets;

(2) measurement of the distribution ratio related to flow-sheet design;

(3) a series of proving tests on the preliminary flow-sheets.

As a result of these studies, it is concluded that the core fuel discharged from JEFR can be treated satisfactorily by the use of the preliminary design flow-sheets for the first and the second cycles using 10% TBP as a solvent. For the third uranium cycle, the original flow-sheet using 30% TBP as a solvent is recommended for satisfactory recovery of uranium.

To obtain exact information on decontamination factors the effect of solvent damage and performance of solvent regeneration and a series of γ-tests in an α–γ-cave using irradiated core fuels will have to be carried out.

Acknowledgments

The authors are indebted to Mr. T. Aochi and his colleagues of JAERI for their assistance and facilities at JAERI Reprocessing Test Facility, and the helpful advice of Mr. T. Tsujino of JAERI in programming the computer code is appreciated. The authors would also like to thank Messrs S. Sato, T. Sakakura and Y. Kitahara of PNC, Tokyo, for their considerable assistance in the flow-sheet design and safety analysis of the process, and Mr. K. Miyahara and the reprocessing analysis group of Technology Division, PNC Tokai, for sample analysis. Thanks are also due to Messrs S. Yasu, N. Kawashima and S. Nemoto of Technology Division, PNC Tokai, for their help in carrying out the proving tests.

References

[1] Curillon, R., & Viennot, J., *Énergie nucl.*, 1968, **10,** 160
[2] Lefort, G., Miquel, P., & De Rubercy, M., *Énergie nucl.*, 1968, **10,** 169
[3] Naito, K., Sato, S., & Hoshino, T., Paper presented at I.A.E.A. Panel on Reprocessing of Highly Irradiated Fuels, Vienna, 1969
[4] Burris, L., Jr., & Dillon, I. D., *Rep. Congr. atom. Energy Commn U.S.*, 1957, ANL–5742
[5] Jenkins, I. L., & Wain, A. G., *J. inorg. nucl. Chem.*, 1956, **27,** 28
[6] Scargill, D., *Rep. U.K. atom. Energy Auth.*, 1964, AERE–R 4583
[7] Fletcher, J. M., Lyon, C. E., & Wain, A. G., *J. inorg. nucl. Chem.*, 1965, **27,** 1841
[8] Mills, A. L., *Rep. U.K. atom. Energy Auth.*, 1965, TRG 902(D)
[9] Aochi, T., Tsujino, T., Konsaka, A., & Hoshino, T., *JAERI Memo.*, 1969, 3746 (unpublished)

Macroreticular ion-exchange resin clean-up of Purex process tributyl phosphate solvent

by W. W. Schulz
Atlantic Richfield Hanford Company, Richland, Washington, U.S.A.

Strong-base macroreticular anion-exchange resins effectively remove fission products and degradation products produced from TBP and the diluent from used Purex process solvent. Application of such resins in routine clean-up of Purex process extractant is potentially attractive to eliminate the large volumes of radioactive waste generated by the solvent wash procedures used at present.

The capacity of macroreticular resins for sorbing extractant impurities is very high judging from batch and column data. Over 240 bed volumes of unwashed Hanford Purex plant first cycle solvent were passed downflow (at 40°C and 4 bed volumes/h) through a 59-ml bed of 14- to 50-mesh resin without any detectable breakthrough of impurities. All the effluent solvent was water-white as opposed to the faint yellow colour of the feed; its fission product content and plutonium retention number were both substantially lower than those of typical washed (alkaline permanganate) plant solvent. Elution of loaded resin with a few bed volumes of 3M-HNO_3–0·05M-HF and 4M-NaOH removes all the sorbed yellow colour and ^{95}Zr–^{95}Nb activity but only 55–65% of the ^{106}Ru–^{106}Rh load.

Introduction

THE CLASSIC PUREX process[1] or some modification thereof is now universally used to re-process all kinds of irradiated nuclear reactor fuel. All Purex plants routinely perform 'solvent treatment' operations to maintain the quality of the tri-n-butyl phosphate (TBP) extractant. Solvent treatments conventionally involve a combination of alkaline and acid washes, sometimes in conjunction with alkaline permanganate solutions, to remove dibutylphosphoric acid (HDBP), residual fission products, and, at least partially, diluent degradation products. (A typical wash sequence is that used to treat Hanford Purex plant first-cycle solvent and is discussed in the Appendix.) Chemical and radiolytic degradation of TBP extractants and solvent treatment procedures have been reviewed by several authors.[2–5]

Sustained, satisfactory operation of various Purex plants in the United States and elsewhere attests to the efficiency of present-day solvent washing techniques. A major disadvantage of these methods, however, is that they generate large volumes of radioactive aqueous waste which must be stored or otherwise treated as high-level waste. Development of an alternative solvent treatment procedure which does not generate such wastes is both economically and environmentally desirable.

Very promising results have been obtained in this direction utilising the properties of macroreticular ion-exchange resins. Such resins are identical to their conventional microreticular counterparts except that they have much larger pore diameters. These large pores do not disappear when the swelling solvent (water) is removed; macroreticular resins are thus especially suited for use with non-aqueous, even non-polar, solutions.[6,7]

Japanese workers[8,9] previously applied microreticular ion-exchange resins for removal of various acidic components from degraded TBP–diluent solutions. The present work extends the concept to the more suitable macroreticular resins and to experiments with actual Purex plant solvent.

The Hanford Purex plant changed in 1966 from Soltrol-170 (Phillips Petroleum Co.), a mixture of 100% branched paraffins, to NPH, a mixture of C_{10} to C_{14} normal paraffins, as a diluent for TBP (other Purex plants have made similar

diluent changes). Subsequently, overall plant decontamination performance improved markedly, and, especially important to this work, the concentration of fission products in the unwashed first-cycle solvent decreased 20- to 40-fold. The concentration of nitroalkanes in the recycled solvent also decreased noticeably. These favourable changes in solvent quality and stability significantly enhance applicability of ion-exchange solvent clean-up procedures.

Experimental

Materials

Rohm & Haas Co. macroreticular resins (Amberlyst®) were used throughout. Amberlyst-15 (cation exchange) and Amberlyst A-21 (weak-base anion-exchange) resins were used in the as-received condition (H^+- and OH^--forms, respectively). Amberlyst A-26 and A-29 (strong-base anion-exchange) resins were converted from the as-received chloride to the hydroxide form by exhaustive washing with 4M-NaOH. Air-dried resins were screened (U.S. Standard Sieve series) to obtain fractions encompassing desired particle sizes for use in batch equilibration tests.

As-received TBP (Commercial Solvents Corp.) was diluted with NPH (South Hampton Co.) to prepare 30% TBP solvent; HDBP (Victor Chemical Co.), purified from monobutylphosphoric acid, was added in some cases to a concentration of 0·058M.

Unwashed Hanford Purex plant first-cycle solvent (1CW solution) was used in fission product retention studies. This pale yellow material contained, nominally, 30% TBP; and, depending on plant performance, 18–350 μCi/l of ^{95}Zr–^{95}Nb (~50% ^{95}Zr) and 75–350 μCi/l of ^{106}Ru–^{106}Rh. Small amounts of ^{103}Ru and HNO_3 (<0·005M) were also present; the concentration of HDBP in plant solvent was not measured. Plant 1CW solution was obtained fresh as needed and was not allowed to age more than ~7 days before use. For comparative purposes, representative washed (cf. Appendix) Hanford Purex plant first-cycle solvent was also procured—composition and properties of this solvent are listed later.

All other chemicals were of reagent grade quality.

Distribution ratio tests

Portions of screened, air-dried resin (2 g) were contacted (30 min at 25°C; mechanical stirring) twice with fresh 10-ml portions of 30% TBP–NPH and then (at various times and temperatures) with 10 ml of either plant 1CW solution or laboratory-prepared 30% TBP–0·058M HDBP–NPH. (All liquid–solid separations were by centrifugation.) Initial and final liquid phases from the last contact were analysed either for fission product content (γ-energy pulse height analyses with NaI or Ge(Li) detectors) or for HDBP (Beckman Automatic Titrator; derivative mode titration with alcoholic KOH). Distribution ratios (K_d) for the loading step were calculated as

$$K_d = \frac{\text{amount of material on resin per g of air-dried resin.}}{\text{amount of material in solution per ml of solution}}$$

Batch fission product elution tests were performed with 2-g samples of 14- to 20-mesh A-29 resin previously equilibrated twice with 30% TBP–NPH and once (30 min at 40°C) with plant 1CW solution. The resultant resin was washed twice at 40°C with 10-ml portions of NPH and then contacted for 15 min at either 20° or 50°C with 10 ml of eluent solution.

Column runs

Jacketed glass columns (1·88 cm i.d.) were filled with 25 ml (~17 g) of air-dried 14- to 50-mesh A-26 resin. After classification by upflow of water, the bed height was ~21 cm, corresponding to a bed volume of 59 ml. Successive

4 bed volume portions of 4M-NaOH and laboratory-prepared 30% TBP–NPH were passed downflow at 25°C and at a rate of 4 bed volumes/h. No change in bed volume occurred during these latter treatments.

All column runs with 1CW solution were made with downflow loading at 40°C. Three runs were made at flow rates of 1·1, 4·3 and 8·6 bed volumes/h, respectively, to determine the effects of flow rate upon fission product retention. In each test, 50–55 bed volumes of 1CW solution were loaded.

Additional tests were made to establish A-26 resin capacity and behaviour during consecutive load and elution cycles. Initially, 245 bed volumes of 1CW solution (taken at various times during plant operation) were loaded on to a fresh resin bed at a rate of 4 bed volumes/h. Consecutive portions of water, 3M-HNO_3–0·05M-HF and 4M-NaOH (4, 15 and 12 bed volumes, respectively) were used to wash, elute, and regenerate the resin. Elution was carried out upflow at 25°C and at a rate of 4 bed volumes/h. Following reclassification of the eluted bed with water, an additional 107 bed volumes of 1CW solution were loaded. Except that it was carried out at 40°C and at 2 bed volumes/h, the second elution cycle was identical to the first.

Solvent quality tests

Various physical and chemical properties of plant solvent were measured after ion-exchange clean-up. Similar measurements were made with washed and unwashed plant solvents. TBP concentrations were determined by gas–liquid chromatography.[10] The apparatus of Moore & Mendel[11] served to measure disengaging times when a TBP solvent was mixed at 25°C with an equal volume of 1·84M-$UO_2(NO_3)_2$–0·5M-HNO_3 solution. The uranium extraction distribution ratio (E_a^o) for each solvent was determined by contacting it with an equal volume of 3M-HNO_3–0·25M-$UO_2(NO_3)_2$.

Plutonium retention tests involved contacting the TBP phase (5 min at 25°C) with one-fifth volume of 3M-HNO_3–0·001M-$Pu(NO_3)_4$ solution; the resultant organic phase was scrubbed three times with fresh double-volume portions of 0·01M-HNO_3. The Pu retention number was calculated by multiplying the molarity of plutonium in the final organic phase by 10^9.

Results and discussion

Batch tests

Loading tests

Results of various batch loading tests with macroreticular resins are presented in Figs 1–5. Data from these tests provided valuable guidance for selection of optimum column operating conditions.

The two strong base exchangers, A-26 and A-29 resins, exhibit about the same affinity for sorbing fission products from unwashed Purex process solvent. For this purpose, both A-26 and A-29 resins are superior to either A-21 (weak-base exchanger) or Amberlyst-15 (cation-exchanger) resins. In turn, affinity of the A-21 resin for both ^{106}Ru–^{106}Rh and ^{95}Zr–^{95}Nb was greater than that of Amberlyst-15 resin. This same resin ranking order was also observed with smaller resin particles than the 14- to 20-mesh fractions used to obtain the data shown in Figs 1 and 2.

Kinetics of sorption of fission products from used Purex extractant by macroreticular ion-exchange resins are significantly faster at 40°C than at 25°C (Figs 3 and 4); to take advantage of this fact, subsequent column runs were carried out at 40°C. A-26 resin was used in these column runs since manufacturers' literature indicates that the thermal stability of A-26 resin is slightly greater than that of the A-29 resin.[7]

The kinetics of fission product uptake by the macroreticular resins also vary with resin particle size. As expected, the smaller particles sorb activity faster than large beads at both 25° and 40°C. At long contact times, the particle size

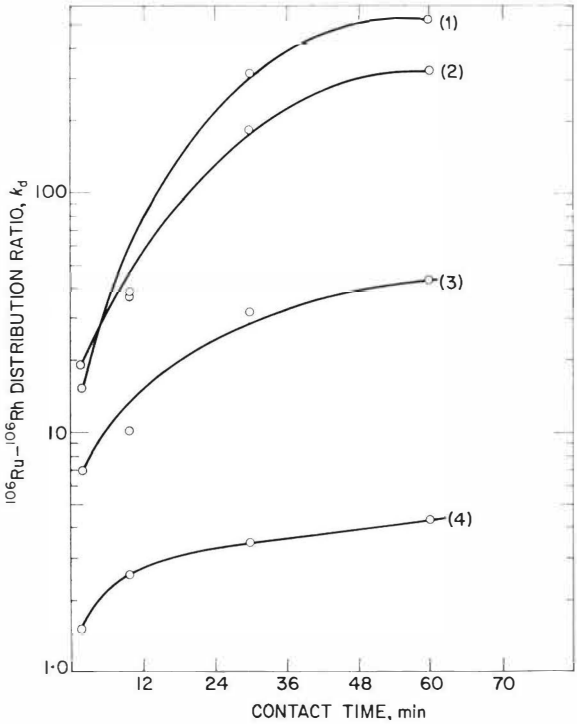

FIG. 1. *^{106}Ru-^{106}Rh loading distribution ratios—variation with resin type*
2 g resin (14–20 mesh) contacted at 25°C with 10 ml 1CW solution
(1) A-29; (2) A-26; (3) A-21; (4) Amberlyst 15

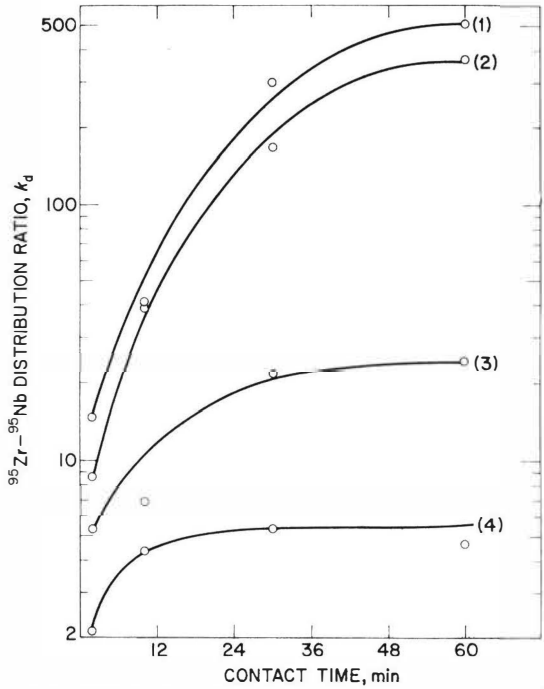

FIG. 2. *^{95}Zr–^{95}Nb loading distribution ratios—variation with resin type*
2 g resin (14–20 mesh) contacted at 25°C with 10 ml 1CW solution
(1) A-29; (2) A-26; (3) A-21; (4) Amberlyst 15

effect disappears and the equilibrium distribution for a particular resin is attained. Column runs were made with as-supplied 14- to 50-mesh A-26 resin; classification into smaller particle size fractions is considered impractical for projected plant-scale application.

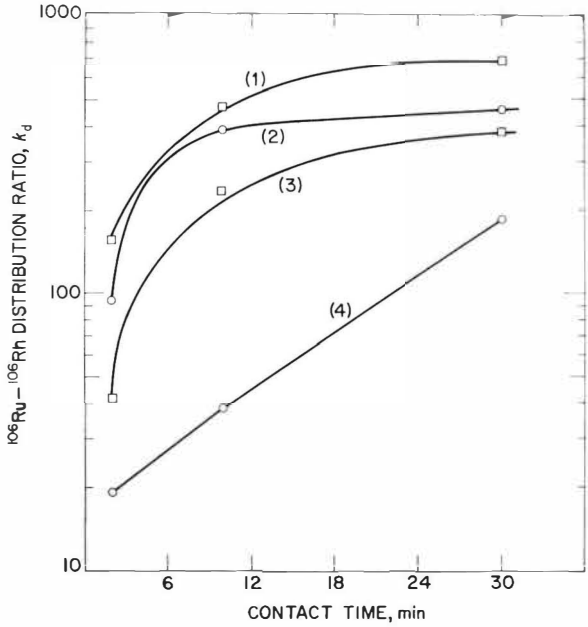

FIG. 3. *Loading of ^{106}Ru–^{106}Rh on to Amberlyst A-26 resin*
2 g portions of air-dried resin (OH^- form) contacted with 10 ml 1CW solution
(1) 28–35 mesh, 40°C; (2) 28–35 mesh, 25°C; (3) 14–20 mesh, 40°C; (4) 14–20 mesh, 25°C

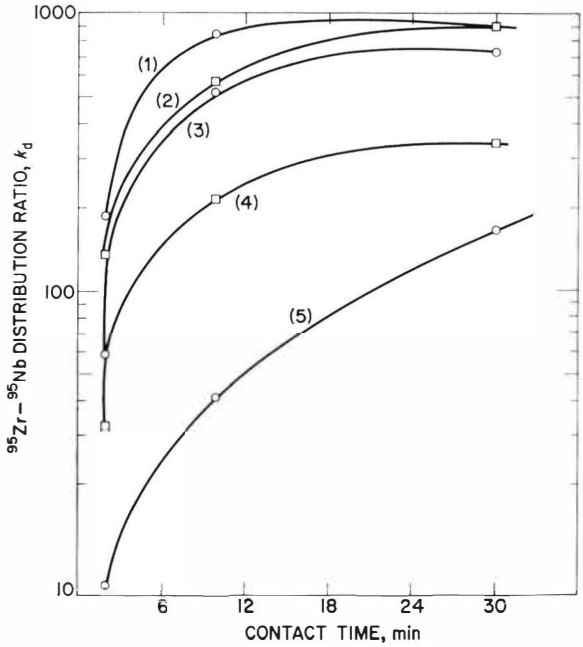

FIG. 4. *Loading of ^{95}Zr–^{95}Nb on to Amberlyst A-26 resin*
2 g portions of air-dried resin (OH^- form) contacted with 10 ml 1CW solution
(1) 35–48 mesh, 40°C; (2) 28–35 mesh, 40°C; (3) 28–35 mesh, 25°C; (4) 14–20 mesh; 40°C; (5) 14–20 mesh, 25c°

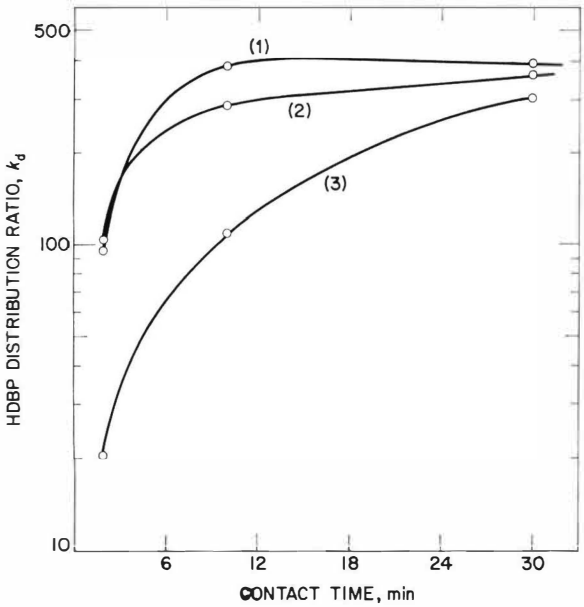

FIG. 5. *Loading of HDBP on to Amberlyst A-26 resin*

2 g portions of air-dried resin (OH^- form) contacted with 10 ml 30% TBP–0·058M HDBP–NPH at 40°C
(1) 35–48 mesh; (2) 28–35 mesh; (3) 14–20 mesh

All the 1CW solutions used in this work contained about equal concentrations of ^{95}Zr and ^{95}Nb. Individual ^{95}Zr and ^{95}Nb concentrations in the organic phases from the batch contacts listed in Figs 2 and 4 were not measured. However, anticipating results presented later, effluent obtained in column-loading cycles also contained equal concentrations of ^{95}Zr and ^{95}Nb, thus demonstrating that A-26 resin has an equal affinity for both nuclides.

That niobium and, especially, zirconium are sorbed so strongly from unwashed Purex process solvent by *anion*-exchange resins is somewhat surprising. Efficient uptake of positively charged species by cation-exchange resins would normally be expected and, indeed, was so observed in earlier work.[8] In the plant solvent used in the present work, however, zirconium and niobium, and presumably ruthenium also, are apparently associated with negatively charged TBP and diluent degradation products; sorption of these latter entities on the anion-exchange resin affects removal of the fission products also.

Characteristics of the strong sorption of HDBP by strong-base macroreticular anion-exchange resins are shown in Fig. 5. Kinetic effects operative in this case and their variation with particle size are similar to those noted for uptake of fission products. In earlier work,[8] it was shown that in addition to HDBP, various other acidic components (e.g., monobutylphosphoric acid and carboxylic acids) present in degraded TBP solutions also reported strongly to the resin phase. Indirect evidence for sorption of acidic components other than HDBP and fission products from Purex 1CW solution was obtained in column runs; this evidence is considered later.

Elution tests

Various reagents were screened on a batch basis to determine their ability to elute fission product activity from loaded macroreticular resin. Results of some of these tests are listed in Table I. Nitric acid solutions containing low concentrations of fluoride are highly effective for eluting ^{95}Zr–^{95}Nb; as shown

by the data in Table I, three successive contacts with 3M-HNO_3–0·05M-HF solution eluted all the ^{95}Zr–^{95}Nb from a batch of resin. (Beneficial effects of fluoride ion in removing ^{95}Zr–^{95}Nb from anion-exchange resins have been noted earlier.[12]) Conversely, no completely satisfactory elutriant for removing ^{106}Ru–^{106}Rh activity from the loaded macroreticular resin has yet been found. Of the reagents tested for this purpose, NaOH and HNO_3–HF solutions appeared best and were used in column tests.

TABLE I

Fission product elution batch tests

2 g of 14- to 20-mesh A-29 resin containing ~12 μCi of ^{95}Zr–^{95}Nb and ~1·6 μCi of ^{106}Ru–^{106}Rh contacted 15 min at either 25° or 50°C with 10 ml of eluent solution

Eluent composition	Percent eluted			
	^{95}Zr–^{95}Nb		^{106}Ru–^{106}Rh	
	25°C	50°C	25°C	50°C
1M-HNO_3	52·9	24·6	55·9	59·0
3M-HNO_3	67·9	19·1	53·6	58·7
5M-HNO_3	60·3	16·1	55·4	61·9
1M-NaOH	27·6	34·4	64·7	50·0
1M-$NaHCO_3$	10·9		37·2	
1M-$Na_2S_2O_3$	2·8			
1M sodium citrate	14·8			
3M-HNO_3–0·05M-HF*				
Contact 1	79·9		66·2	
Contact 2	18·3†		20·1†	
Contact 3	4·7†		6·0†	
3M NaOH*				
Contact 1	64·3		63·4	
Contact 2	11·1†		14·8†	
Contact 3	2·8†		7·9†	

* Three successive contacts with fresh 10-ml portions of eluent.
† Percent of total activity initially present on resin.

Column tests

Column tests with A-26 resin extended the new solvent treatment scheme to a dynamic system; data obtained in these runs generally substantiated effects noted in the batch work.

Flow rate effects

Illustrative of the kinetic aspects of the new solvent treatment process is the way fission product sorption increases with decreasing feed flow rate (Figs 6 and 7). For the conditions used, over 97% of both ^{106}Ru–^{106}Rh and ^{95}Zr–^{95}Nb in the 1CW feed was retained by the resin bed at a flow rate as high as 4 bed volumes/h. At all flow rates, column effluent fission product concentrations remained essentially constant over the entire 50 to 55 column volumes, thus evidencing the great capacity of the A-26 resin.

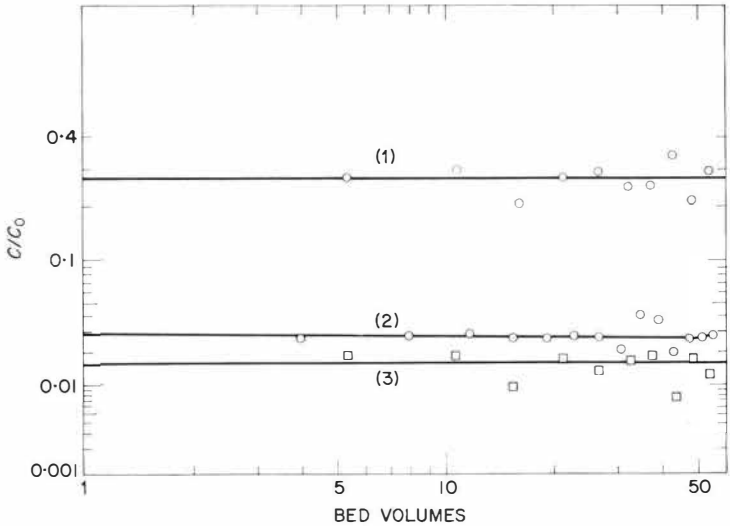

FIG. 6. *Variation of* ^{106}*Ru loading with flow-rate*

A-26 resin, 14–50 mesh at 40°C; 1CW solution: 80–90 μCi/l ^{106}Ru–^{106}Rh
Bed volumes/h: (1) 8·6; (2) 4·0; (3) 1·1

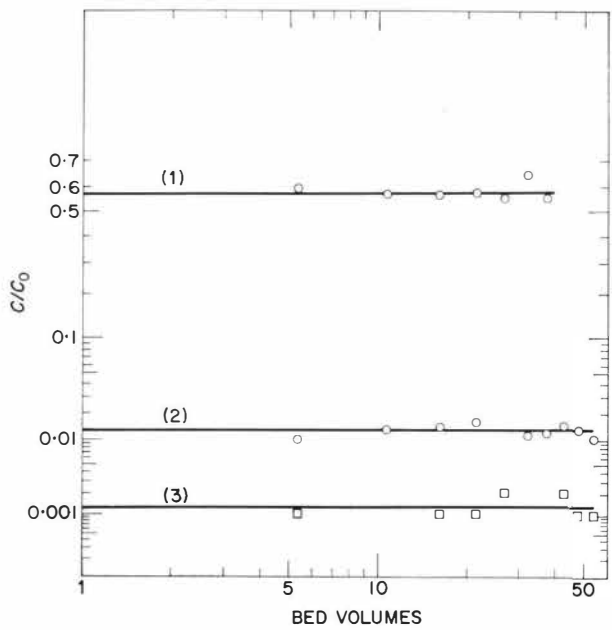

FIG. 7. *Variation of* ^{95}*Zr–*^{95}*Nb loading with flow-rate*

A-26 resin, 14–50 mesh at 40°C; 1CW solution: 65μCi/l ^{95}Zr–^{95}Nb
Bed volumes/h: (1) 8·6; (2) 4·0; (3) 1·1

Cyclic load-elution tests

Spectacular confirmation of the ability of the A-26 resin to clean up large quantities of used Purex solvent was provided by cyclic load and elution tests. Results of the loading portion of these runs are plotted in Figs 8 and 9. Throughout the first loading cycle (245 column volumes), the effluent fission

product content remained at a very low level with no indication that breakthrough was approaching. The first loading cycle was terminated and the bed eluted at this point only because 1CW feedstock was temporarily unavailable. Effluent product obtained in a second loading cycle (107 bed volumes) was comparable in all respects with that produced in the first cycle and again there was no evidence for any breakthrough.

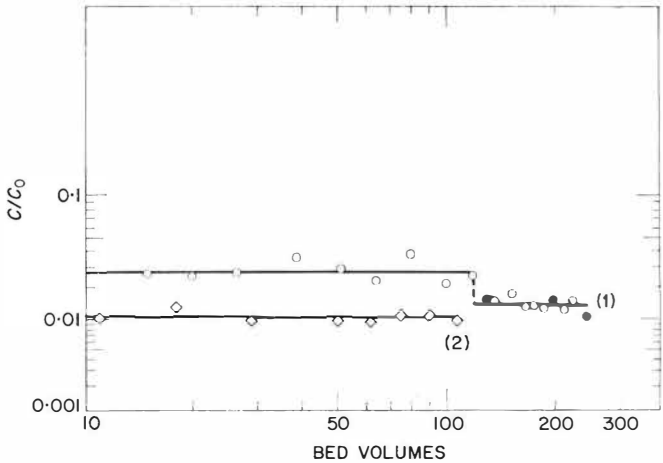

FIG. 8. ^{106}*Ru behaviour in cyclic loading tests*

A-26 resin (OH⁻form), 14–50 mesh at 40°C

		Bed volumes	^{106}Ru–^{106}Rh, μCi/l in 1CW solution
(1)	Load cycle 1:	0–119	81
		119–187	258
		187–245	344
(2)	Load cycle 2:	0–107	310

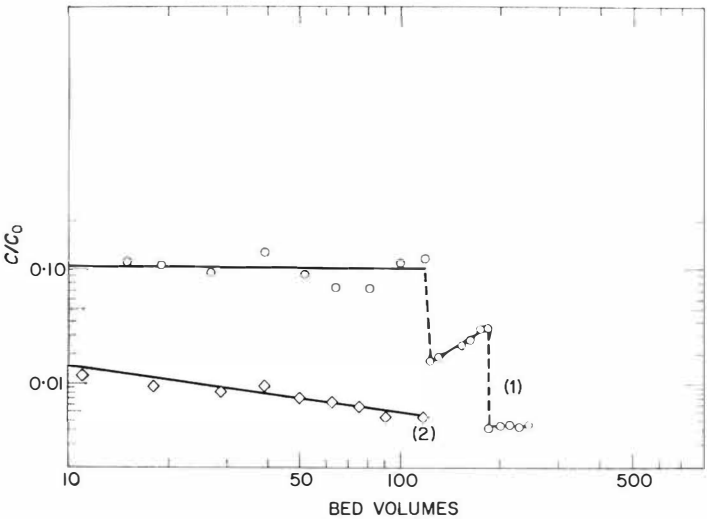

FIG. 9. ^{95}*Zr–*^{95}*Nb behaviour in cyclic loading tests*

A-26 resin (OH⁻form), 14–50 mesh at 40°C

		Bed volumes	^{95}Zr–^{95}Nb, μCi/l in 1CW solution
(1)	Load cycle 1:	0–119	18
		119–187	105
		187–245	180
(2)	Load cycle 2:	0–107	305

Throughout both loading cycles, the fission product content of the organic effluent remained approximately constant. As a consequence, the fraction (C/C_0) of each fission product reporting to the effluent stream varied with its concentration in the influent 1CW feed. This effect is very evident in the ^{95}Zr–^{95}Nb results shown in Fig. 9 and, to a lesser extent, also in the ^{106}Ru–^{106}Rh data plotted in Fig. 8. Such behaviour emphasises the kinetic aspects of the absorption process; operation at a flow rate lower than 4 bed volumes/h would have reduced C/C_0 values correspondingly.

A significant feature of the column tests was the removal of the yellow colour from the degraded feed solvent. All the effluent, including that obtained after the first elution cycle, was water-white just like virgin solvent. During both loading cycles, a yellow colour-front slowly moved down the resin bed. The identity of the yellow material has not yet been established, but it presumably represents part of the nitrated diluent present in the 1CW solution. The first portions of 4M-NaOH eluent appeared to remove all the yellow colour from the bed in both elution cycles.

Essentially all the ^{95}Zr–^{95}Nb but only ~64% of the ^{106}Ru–^{106}Rh present on the loaded resin bed were removed in the first elution cycle. The second elution cycle made at 40°C was not as effective as the first (made at 25°C) in that only 71% of the ^{95}Zr–^{95}Nb and 55% of the ^{106}Ru–^{106}Rh activity on the bed were eluted (the latter percentage takes into account the ^{106}Ru–^{106}Rh left on the bed after the first elution cycle). Of the ^{95}Zr–^{95}Nb and ^{106}Ru–^{106}Rh eluted in each cycle, 97% and 80%, respectively, were removed by the HNO_3–HF eluent. The poorer ^{95}Zr–^{95}Nb elution observed in the second elution cycle agrees with the temperature effects noted in batch work (Table I).

The elution cycle results illustrate the relative ineffectiveness of HNO_3–HF and NaOH solutions for removing radioruthenium from loaded macroreticular anion-exchange resin. In plant applications, however, exhausted beds might be simply discarded as solid waste without any need for regeneration. This favourable position could exist if both resin capacity and resin stability were sufficiently great to offset economic penalties involved in resin replacement.

TABLE II

Properties of ion-exchange-treated Purex solvent

Test/Property	Plant 1CW*	Plant 100*	Ion-exchange-treated solvent, Bed volumes† 119	Ion-exchange-treated solvent, Bed volumes† 195	Lab.-prepared solvent
TBP, vol.-%	29·6	29·2	28·8	29·9	30·0
Colour	Yellow	Yellow	Colourless	Colourless	Colourless
Density, g/cm³	0·8111	0·8122	0·8108	0·8114	0·8126
Fission product content, μCi/l					
^{95}Zr	90	3·4	0·62	0·35	—
^{95}Nb	98	2·1	0·69	0·54	—
^{106}Ru	170	9	1·2	3·0	—
Disengaging time, sec	37	61	28	50	67
U extraction, E_a^o	14·6	14·2	14·1	17·6	17·4
Pu retention number	2070	50	6	9	23

* Typical plant material

† From run described in Figs 1 and 2

Solvent quality

New procedures proposed for cleaning up Purex process solvent must do at least as good a job as the aqueous wash schemes presently in use—and preferably better. Against this standard, the merits of the macroreticular ion-exchange treatment stand out clearly (Table II). Particularly noticeable are the low fission product content and Pu retention number of the resin-treated extractant; both values are substantially lower than those for alkaline permanganate-washed plant solvent. The Pu retention number, like the analogous 'Z' and 'H' numbers,[13] has traditionally been considered as a sensitive measure of the presence of deleterious diluent and/or TBP degradation products in used Purex solvent. The colourless appearance of the resin-treated TBP extractant and its very low Pu retention number are convincing evidence that the ion-exchange procedure effectively removes these degradation products. It is truly a 'solvent clean-up' method (in the sense defined by Blake *et al.*[4]) and not just a mechanism for removing radioactivity.

The other properties listed in Table II (TBP concentration, density, etc.) all confirm that ion-exchange treatment neither removes nor adds components to the Purex solvent which affect its hydraulic and chemical performance as an extractant for uranium and plutonium (variation of a factor of two in disengaging time with the apparatus used is not regarded as significant).

Conclusions

Application of macroreticular ion-exchange resins to clean-up of used Purex process solvent has been successfully demonstrated on a laboratory scale. A primary advantage of the ion-exchange method is that it eliminates the large volumes of radioactive waste generated by present-day aqueous wash schemes. Also, the quality of the product obtained by the ion-exchange procedure is equal or superior to that of solvent washed with conventional alkaline permanganate solutions.

Further laboratory and/or pilot plant-scale work are needed to accurately establish resin capacity for removing fission products and various degradation products from used TBP solvent. Improved techniques for eluting radio-ruthenium from the loaded resin are also needed and assessment of the economic potential of the ion-exchange solvent treatment procedure is required.

Acknowledgments

The author thanks Messrs C. W. Hobbick and A. P. Hammitt for their assistance in performing the experimental work and Mr. R. L. Walser for helpful discussions.

References

[1] Stoller, S. M., & Richards, R. B., Eds, 'Reactor handbook', 1961, Vol. II, p. 146 (New York: Interscience Publishers Inc.)
[2] Orth, D. A., & Olcott, T. W., *Nucl. Sci. Engng*, 1963, **17**, 593
[3] Lane, E. S., *Nucl. Sci. Engng*, 1963, **17**, 620
[4] Blake, C. A., Jr., Davis, W., Jr., & Schmitt, J. M., *Nucl. Sci. Engng*, 1963, **17**, 626
[5] Huggard, A. J., & Warner, B. F., *Nucl. Sci. Engng*, 1963, **17**, 638
[6] Dean, J. A., 'Chemical separation methods', 1969, p. 90 (New York: Van Nostrand Reinhold Co.)
[7] 'Amberlyst A-26 and Amberlyst A-29, Technical Bulletin', 1967 (Philadelphia: Rohm & Haas Co.)
[8] Ohwada, K., *J. nucl. Sci. Technol.*, 1967, **4**, 361
[9] Shiba, T., B.P. 1,051,978
[10] Campbell, M. H., *Analyt. Chem.*, 1966, **38**, 237
[11] Moore, R. H., & Mendel, J. E., *Rep. Congr. atom. Energy Commn U.S.*, 1953, HW-27807
[12] Isaacson, R. E., & Judson, B. F., *Ind. Engng Chem. Process Des. Dev.*, 1964, **3**, 296
[13] Field, B. O., & Jenkins, E. N., *Rep. U.K. atom. Energy Auth.*, 1960, AERE-R 3507

Appendix

A simplified version of the flowsheet used at Hanford to wash the organic waste stream (1CW) from the First Decontamination and Partition Cycle is shown in Fig. 10. The 1CW stream is initially given a semi-batch contact with an Na_2CO_3–$KMnO_4$ solution to remove fission products, traces, if any, of plutonium and uranium, and, to some extent, solvent degradation products.

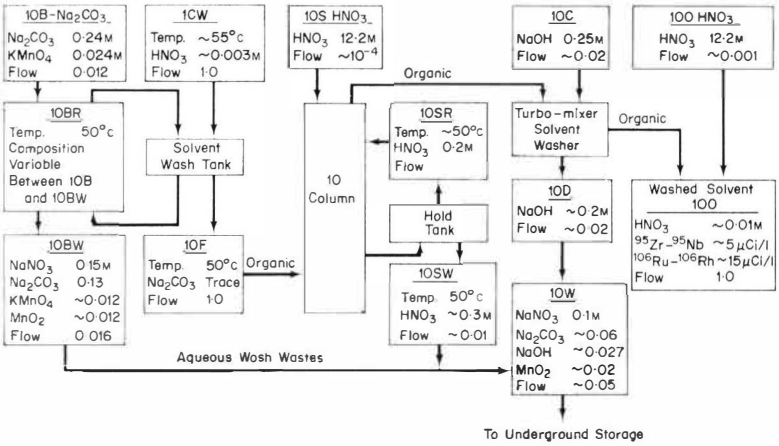

FIG. 10. *Hanford Purex first-cycle solvent wash scheme*

Subsequently, the solvent stream is pumped to the 10 column where contact with dilute HNO_3 removes entrained carbonate and MnO_2. From the 10 column, the organic phase overflows to a Turbomixer tank where it is given a final wash with dilute NaOH before routing to the 100 Pump Tank. Entrained NaOH is continuously neutralised in the 100 Pump Tank by addition of a small flow of HNO_3. The aqueous wash solutions are charged out on a scheduled basis—the frequency depending on the quality of the clean solvent.

Plutonium–uranium partitioning by a reflux extraction flowsheet

by L. E. Bruns
Atlantic Richfield Hanford Company, Richland, Washington, U.S.A.

A new solvent extraction flowsheet has been developed for the processing of unirradiated plutonium–uranium scrap. By refluxing plutonium product as Pu(III) in a multi-stage plutonium stripping–partitioning system, uranium is salted into the organic phase and pure plutonium is quantitatively separated from uranium. A hydrofluoric acid strip removes the final traces of plutonium from the organic phase containing the uranium. The flowsheet was plant-tested, and problems evident in the plant test were solved by comprehensive laboratory tests. The fully developed flowsheet is ready for plant application.

Introduction

A NEW SOLVENT extraction flowsheet has been devised for the separation and purification of plutonium from systems containing uranium. The flowsheet permits the purification and concentration of plutonium in a single solvent extraction cycle. This new concept was developed by Atlantic Richfield Hanford Company personnel in the Plutonium Reclamation Facility, a plutonium scrap processing plant operated under prime contract for the Atomic Energy Commission.

It appears that this flowsheet could be applied directly to the processing of scrap from fuel fabrication for both the light water and fast breeder reactors. With further development, it might be useful in the processing of irradiated fuels.

The development of the flowsheet and the parameters pertinent to process performance are described in this paper.

Experimental

After the plutonium–uranium scrap is dissolved or leached, the resulting solution is adjusted for salting strength and the plutonium is adjusted to the extractable (IV) and (VI) states. Uranium and plutonium are coextracted in a multi-stage extractor (Unit I, Fig. 1), using 20% TBP (tributyl phosphate) in CCl_4 (carbon tetrachloride) as the solvent. In the same extractor, the loaded solvent is scrubbed for impurity removal.

In a second multi-stage unit (Unit II, Fig. 1), plutonium is reduced to the aqueous-favouring plutonium(III) state with hydroxylamine nitrate. The purified Pu(III) leaving the concentrated end of this second multi-stage unit is split into a product stream and a reflux stream which flows to a hold-up tank where it is oxidised to the extractable Pu(IV) state by merely adding nitric acid. This Pu(IV) stream is re-introduced as a scrub stream in the first extractor. Plutonium (III)product is withdrawn from the system when a 30 to 60 g Pu/litre concentration is attained. Uranium is removed from the Pu(III) by a 20% TBP–CCl_4 scrub in the initial stages of this second extractor (see Fig. 1).

The uranium quantitatively leaves the second extractor via the organic stream. The plutonium impurity (about 1%) in this uranium stream is removed by a novel hydrofluoric strip in a third extractor (Unit III, Fig. 2). Further conventional extractors (not discussed in this paper) remove the uranium and organic impurities from the organic stream.

The flowsheet has been tested in the laboratory and the plant to identify and correct process difficulties. Full-scale plant application is planned.

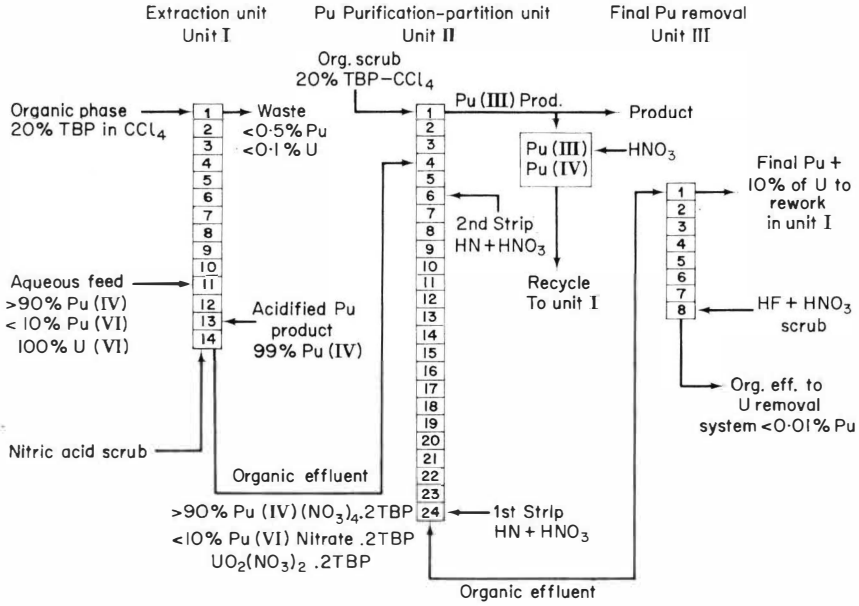

FIG. 1. *Representation of theoretical flowsheet*

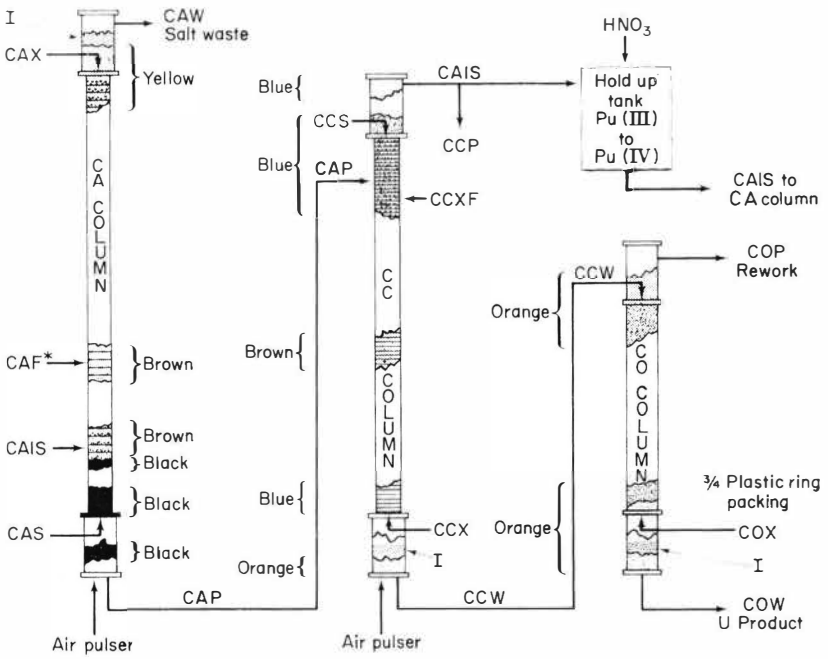

FIG. 2. *Plant flowsheet*

Colour code: brown, Pu(IV) (1–15g/l); black, Pu(IV) (15–30 g/l); blue, Pu(III) (5–60 g/l); yellow, 20% TBP in CCl_4, negligible Pu; orange, U(VI) (1–20 g/l)

Discussion

Basic flowsheet

Scrap bearing plutonium and uranium is dissolved or leached, and appropriate salting and plutonium valence adjusting agents are added as required. Both plutonium and uranium are quantitatively coextracted from the feed by a mixture of 20% TBP in a CCl_4 diluent. This extraction operation can be performed in some type of multi-stage equipment, e.g. a mixer–settler unit or a packed or pulsed column unit. The solvent extraction system is depicted in Fig. 1.

Addition of nitric acid and, sometimes, nitrite ion to the aqueous extraction unit feed ensures a predominance of Pu(IV), with some Pu(VI). This valence combination is extractable within 10 mixer–settler stages. The uranium in the stable hexavalent state is easily extractable. Sufficient stages are used to ensure negligible plutonium and uranium losses in the salt waste.

Additional scrub stages are required for removing entrained and extracted impurities from the plutonium and uranium in the organic phase. Two scrub streams are used. The initial two-stage scrub section uses refluxed plutonium product as the scrub stream and removes the bulk of the impurities from the uranium and plutonium. One additional scrub stage uses a pure nitric acid scrub stream and removes the final impurities from the refluxed plutonium product with repeated washings. The number of stages required will depend upon the degree of impurity removal required.

The coextracted plutonium and uranium flow to a combination plutonium stripping and plutonium–uranium partitioning unit (Unit II in Fig. 1). The organic stream enters Unit II at the fourth stage, leaving three stages of scrub section for removal of the uranium from the plutonium stream. The number of scrub stages used depends upon the desired capacity. For the maximum-sized equipment allowable to provide criticality control (e.g. geometrically favourable 6-in diameter sieve plate pulse column) and using a 20% TBP extractant, three stages of uranium scrub provide a potential of 100 kg per day uranium capacity. Organic of the same composition as used in Unit I is used as scrub in Unit II and is introduced in Stage I (see Fig. 1).

Two stripping solutions are introduced into the stripping partitioning unit, Unit II, one at the 24th stage and one 2 stages below the organic feed stream entry point, the sixth stage. The stripping streams contain various amounts of reducing agents, hydroxylamine nitrate (HN) and nitric acid. An estimated 20 stages are required for quantitative stripping of the plutonium from the organic phase.

The two effluent streams from Unit II are the pure plutonium product and the organic effluent which contains the uranium and a minor amount of the plutonium (usually less than 0·1 g/l). Almost all the plutonium product is refluxed to the thirteenth stage of Unit I as the intermediate scrub. When the refluxed plutonium stream reaches the desired concentration, plutonium is drawn off as product.

The partition principle is based on maintaining a high concentration (30 to 60 g/l) of plutonium, predominantly Pu(III), in the scrub section and the initial stripping stages (stages 5 and 6). Plutonium(IV) and plutonium(VI) favour the organic phase in a salted medium whereas plutonium(III) favours the aqueous phase even in a salted medium. The high concentration of plutonium (III) nitrate salts the uranium into the organic phase. The Unit II scrub stream (20% TBP in CCl_4) removes the uranium quantitatively, and the plutonium is only slightly refluxed in this scrub section.

The high plutonium(III) nitrate salting strength is maintained with a reducing agent. Selection of the reducing agent is the key to the one-cycle system. The reducing agent must be strong enough to cause a predominance of plutonium (III) in the scrub section and the concentrated product portion of the stripping section. The reducing agent must not introduce impurities, since much of it remains with the concentrated plutonium product.

The reducing agent found to be optimum was hydroxylamine nitrate (HN). This chemical can reduce plutonium(IV) to plutonium(III) in low nitric acid media (0·5 to 1·5M). Other reaction products are gases – N_2O (major constituent), N_2, and a small amount of NO_2. However, the equilibrium shifts quantitatively to plutonium(IV) in nitric acid concentrations greater than 3·5M.

One problem with HN is the formation of the NO_2 gas from the reaction of plutonium(IV) with HN. Some of the NO_2 is solubilised and forms a nitrite ion which oxidises plutonium(III) to plutonium(IV). The NO_2 reacts with HN, forming N_2O, N_2, and small amounts of addition NO_2. The conversion back to plutonium(IV) can be minimised.

The stripping agent introduced at the dilute plutonium end of the stripping-partition unit, Unit II (see Fig. 1, Stage 24), forms plutonium(III). As the aqueous or light phase goes from Stage 24 to 23, etc., an autocatalytic breakdown of HN takes place owing to the formation of the nitrite ion in the plutonium(IV) to plutonium(III) reaction. The excess NO_2 oxidises plutonium(III) to plutonium(IV), and plutonium(IV) may predominate in the middle stages (13, 14, 15, etc.). If plutonium(IV) predominates, the flowsheet is not workable (this will be discussed later under Plant Testing). If a second HN stream is added at about the sixth stage, a plutonium(III) medium can be maintained at the top of the column; and the formation of excessive plutonium(IV) below the addition point is minimised. This second stream, 1·2M-HN and 1·0M-HNO_3 is added approximately two stages below the organic stream entry point. It cannot be added too many stages from the plutonium end because, again, the kinetics involved in the formation of nitrite ion may cause a predominance of plutonium(IV) at the product end of the unit.

One additional unit is important to the one-cycle system – Unit III. This unit is necessary owing to the formation of DBP (dibutyl phosphate), the breakdown product of tributyl phosphate (TBP). Dibutyl phosphate complexes plutonium as an almost unstrippable plutonium(IV) compound, $Pu(NO_3)_4.2DBP$. Hydroxylamine nitrate(HN) will not strip plutonium efficiently from DBP but hydrofluoric acid will strip plutonium quantitatively from DBP. The stripping agent used is 2·5M-HNO_3–0·25M-HF. Nitric acid serves two purposes: to ensure the bulk of the uranium stays in the organic phase (owing to salting action of nitric acid), and to prevent PuF_4 precipitation. The solubility of PuF_4 increases from 1 to 8 g/l as the nitric acid concentration is increased from 0·0 to 2·5M.

With an estimated 8 stages in Unit III, the plutonium may be reduced to the parts-per-billion level. The organic stream is transferred to a simple water strip system; and the uranium is removed for further processing as a relatively pure uranium stream. Dibutyl phosphate is removed from the organic in another unit by use of a carbonate wash. The organic is re-acidified and returned to Unit I and Unit II as extractant and scrub, respectively (see Fig. 1).

Plant application

The Atlantic Richfield Hanford Company's Plutonium Reclamation Facility was designed and built as a plutonium scrap (no uranium) recovery facility.[1] Plutonium-bearing scrap is dissolved or leached with a mixture of nitric and hydrofluoric acids. The resulting solutions are purified in a single cycle solvent extraction system. The extraction column, called the CA Column (see Nomenclature for description of plant columns and streams, and Fig. 2 for flow sketch of Plutonium Reclamation Facility columns); and the plutonium stripping column, the CC Column, are 4-in diameter sieve plate pulsed columns. The CA Column represents Unit I and the CC Column represents Unit II (see Fig. 1). A short packed column (CO Column, Unit III) is used for removing the final plutonium from the organic by an HF wash.

This column system appeared adaptable to the basic flowsheet approach previously described, and Pu–U scrap was available; hence, the decision was made to test the Pu(III) reflux principle in the Plutonium Reclamation Facility (PRF). Plant stages available were not sufficient for high capacities (2 to 3 organic scrub stages, Unit II; and 2 to 3 stages in HF strip column, Unit III), but a significant capacity (10 kg uranium + plutonium per day) could be realised with only minor changes and additions. Later, additional stages could be added to increase plant capacity (up to 30 kg U + Pu/day is thought possible).

Initial separation flask laboratory studies showed that a single stripping solution (last stage, Unit II) in the plutonium purification–partition column should be adequate. To study the overall valence balance and kinetics, a plant test was needed.

Plant testing

Several hundred pounds of plutonium–uranium scrap were processed through the Plutonium Reclamation Facility. However, the first attempt was not successful since plant kinetics using a single stripping agent were such that a Pu(IV) medium predominated in the top of the CC Column. A brown Pu(IV) colour was apparent where a blue colour (characteristic of Pu(III)) should have been present. Although Pu(IV) has a smaller extraction coefficient than U, the law of mass action prevailed and the Pu(IV) took over the bulk of the immediate available organic sites in the organic scrub stream. The end result was Pu refluxing down the column and U building up in the recycled Pu product stream to as high as 10%.

Plutonium(IV) and uranium accumulated in the centre of the column, resulting in over-saturation of the organic and precipitation of the Pu(IV) nitrate–DBP complex [only Pu(IV) can form this complex]. Also, the high Pu(IV) accumulation resulted in high Pu losses in the CC Column organic effluent called the CCW. The high amount of Pu overloaded the final Pu clean-up unit, the CO Column. The HF strip precipitated PuF_4, and high Pu in the U product resulted. Although the first plant test was unsuccessful, flowsheet problem areas were identified for subsequent comprehensive laboratory investigation.

Laboratory testing

Laboratory testing was conducted in two different sets of equipment. One was a minimixer-settler unit to study the kinetics in certain areas; and the other a mock-up of the plutonium stripping–partitioning column to study *HTUs* (height of a transfer unit) and column gassing.

Mixer-settler

In this unit, plant solutions could be used and the number of plant stages and residence times could be duplicated. The scale-down ratio was 500 : 1. All stages were visible, permitting colour determination. The tests were set up to first duplicate plant problems, and then varied to solve those problems.

Plant problems were successfully duplicated. By using only a single CC Column stripping agent at the last stage [bottom stage in the plant], a plutonium (III) medium could not be attained and the plutonium product soon contained excessive amounts of uranium.

Two flowsheet changes were made and each produced excellent results. One was the addition of a second HN stripping stream added two stages below the organic inlet, as previously discussed. The other was use of hydrazine as a holding agent in the CC Column bottom stripping stream. The hydrazine

reacted with excess nitrite and the mixer-settler system showed a blue Pu(III) colour throughout. Although inexpensive, hydrazine has a serious flowsheet disadvantage, viz. nitric acid alone will not convert the Pu(III) returning to the CA Column back to Pu(IV) if hydrazine is present. Nitrite must be added to destroy the hydrazine, and a snowballing effect can easily occur if excess nitrite is added. Serious gassing and reversals to predominant plutonium(IV) media can result. Therefore, the more easily controlled hydroxylamine nitrate (HN) approach was selected.

The mixer-settler study concluded with a long demonstration run.[2] It demonstrated that the plant CA, CC, and CO Columns could probably handle 5 kg U/day (plus associated plutonium) with only the addition of a side HN stream.

Mock-up of CC Column

The mock-up column duplicated the top 15 stages of the CC Column.[3] Uranium was used; but plutonium could not be used in the pilot plant area available. To simulate the plutonium nitrate salting strength, sodium nitrate was added to the HN side stream. The same type of perforated stainless steel plates as in the PRF plant CC Column (Unit II) were used. This was followed by a test with Raschig rings between the plates in the scrub section of the laboratory column (rings were also added to the PRF column.

The results showed:

Gassing in the CC Column actually improved column efficiency. To test severe gassing, excess nitrite was added to the system; however, no column flooding occurred. Gassing should be minimised in the plant to avoid organic entrainment into the plutonium recycle stream and eventual cavitation of pump in the product recycle hold-up tank.

Height of a transfer unit (*HTU*) is lowered only slightly by the addition of 3/4-inch plastic Raschig rings between the plates in the scrub section of the column. The rings were added to increase mixing in the lower volume velocity scrub section.

Height of a transfer unit studies showed that with optimisation of column amplitude and frequency, at least four transfer units could be realised in the plant scrub section.

Plant flowsheet

The final plant flowsheet for processing unirradiated plutonium–uranium scrap in the PRF is depicted in the flow sketch shown in Fig. 2. The abbreviations used in Fig. 2, plus other abbreviations and symbols used throughout the paper are explained in the nomenclature. Existing equipment was used so there are some capacity limitations. For example, the CC Column originally designed as a plutonium stripping column was divided into a stripping–scrub column. Hence, some stripping area was lost and not as many scrub stages as desired could be added. The CO Column is a simple packed column with only two to three stages (eight shown in Fig. 1) available.

A colour code is also used showing the valence balance throughout a column system. The brown colour shows a high concentration of plutonium(IV) [some green plutonium(VI) is present, but it is dwarfed by the predominant plutonium(IV)]. Plutonium(III) in the aqueous phase (the light phase) is blue. The organic, when free of actinides, is a yellowish colour.

The CA Column is an organic-continuous unit with the aqueous being the dispersed phase. Here, the interface is at the top. In the CC and CO Columns, the aqueous phase is continuous and the interface is at the bottom (I stands for interface, Fig. 2).

Conclusions

A new plutonium–uranium scrap processing flowsheet (see Fig. 2) has been developed from theoretical considerations, laboratory testing, and plant testing. Important conclusions based on this work include the following:

A Pu stripping column or combination Pu–U partition–Pu stripping column (as discussed above) operating on the reflux flowsheet principle can operate on a Pu(III) system. Use of the reducing agent, hydroxylamine nitrate and minimal use of nitrite in the extraction feed can give an easily controlled Pu(III) column. The Pu(III) system not only has the advantage of an excellent column profile (variation of Pu concentration with column height), but it avoids Pu polymer precipitation (possible in low-acid media like the CC Column) and $Pu(NO_3)_4.2DBP$ precipitation in the middle of the stripping column.

A flowsheet for Pu–U scrap processing has been developed that can avoid additional Pu and U cycles. The extra Pu cycles can be avoided by the reflux flowsheet principle, which gives a concentrated, pure Pu product. Many solvent extraction systems are once-through systems (i.e. no refluxing) with several Pu and U cycles. Such systems demand high nitric acid concentrations for partitioning; hence an impurity laden (iron), powerful reducing agent like ferrous sulphamate is required. In once-through systems, the Pu product from the partitioning column will frequently be low in Pu (especially in a Pu–U scrap processing facility with its variable Pu content in the scrap), and metallic impurities will be excessive. At least one more complete cycle is required – and probably two – to attain required purity level if the once-through principle is maintained in the additional cycles.

Further U cycles may be avoided by use of the HF strip column. The PRF uses an existing column, and the facility layout was such that column dimensions could not be economically altered to meet U specifications (10 parts Pu/billion parts U). A new facility can avoid this problem.

Geometrically favourable equipment is required with the reflux flowsheet system. However, geometrically-favourable systems are usually selected for final plutonium purification with any flowsheet. Geometrically-favourable means nuclear safe by geometry (usually minimum diameter, annulus, or slab thickness) for the worst foreseeable abnormal occurrence in the facility.

An adaptation of the proposed flowsheet might be useful in power reactor fuel reprocessing, especially where breeder reactors are concerned (high Pu concentrations, e.g., 20% Pu). A new facility could conceivably process 500 kg/day of U plus Pu if limited to a cylindrical geometrically favourable facility.

Plutonium can be removed from the organic degradation product DBP with dilute hydrofluoric acid–nitric acid mixtures. Other reducing agents (like ferrous sulphamate) are unsatisfactory for this purpose.

Nomenclature

PRF	Plutonium Reclamation Facility.
Geometrically favourable facility	A facility processing fissionable material that is safe from criticality by equipment design.
CA Column	The PRF sieve plate, air-pulsed, continuous extraction column. This column co-extracts the plutonium and uranium and the impurities from the plutonium and uranium in the organic stream.

CAF	The aqueous feed to the CA Column.
CAX	The organic stream used in the CA Column. It contains 20% of the TBP extractant in the CCl_4 diluent. The organic phase is the continuous and the heavy phase.
CAIS	The refluxed plutonium product stream. This stream gives extra volume velocity to the scrub section, improving the plutonium–uranium clean-up efficiency.
CAS	A nitric acid scrub at the bottom of the CA Column. For most feeds, 2M-HNO_3 is used. With refluxing product [CAIS], the CAS is able to recontact the plutonium product for purification many times before the plutonium product is removed from the system.
CAP	The organic effluent from the CA Column containing all the co-extracted plutonium and uranium. The plutonium concentration will normallly be higher than the uranium, since plutonium is refluxed.
I	Interface between the two phases. The interface will either be in the bottom or top disengaging section, depending upon which is the continuous phase; e.g. organic phase – I at top; aqueous phase – I at bottom.
CC Column	The combination plutonium stripping–partitioning column. It is a sieve plate, air-pulsed column.
CCS	The organic scrub which removes the uranium from the plutonium product in the CC Column.
CCX	The initial CC Column strip, 0·2 to 0·5M-HN and 0·15M-HNO_3, added at the bottom of the column.
CCXF	The second CC Column strip, 1·2M-HM–1·0M-HNO_3, added about two stages below the CAP entry point.
CCW	The CC Column organic effluent containing all the uranium and usually less than 0·1 g/l plutonium.
CCP	The final purified plutonium product.
CO Column	The column for removing the final plutonium from the uranium-laden organic.
COX	The hydrofluoric acid strip for the CO Column, 0·25M-HF–2·5M-HNO_3.
COW	The CO Column organic effluent. This stream goes to conventional uranium and organic handling equipment; i.e. a packed water strip column for removing nitric acid and uranium from the organic and a column for removing such degradation products as DBP from the organic by a carbonate strip.
COP	The aqueous effluent from the CO Column which contains the remaining plutonium and 10% of the uranium entering the CO Column via the CCW. The COP flows to the extraction feed system for rework.
HN	Hydroxylamine nitrate.

References

[1] Bruns, L. E., *Chem. Engng Prog. Symp. Ser.*, 1967, **63**, (80), 156

[2] Bruns, L. E., 'Plutonium-Uranium Processing in the Plutonium Reclamation Facility by Coextraction-Partitioning', ARH-1343, Atlantic Richfield Hanford Company, Richland, Washington, Sept. 25, 1969

[3] Bonner, W. F., & Richardson, G. L., *Pilot Plant Demonstration of the Plutonium Reclamation Facility CC, CR, and CS Columns*, BNWL-CC-2461, February, 1970

SESSION 2A

CHEMISTRY OF METALS EXTRACTION, I

CHAIRMAN

Mr. A. W. Fletcher

SECRETARIES

Dr. G. J. Lawson
Dr. N. M. Rice

Extraction equilibria and solvation effects in the system liquid ammonia – tri-n-butyl phosphate

by J. Hala* and D. G. Tuck
Department of Chemistry, Simon Fraser University, Burnaby 2, B.C., Canada

The characteristics of the liquid ammonia–tri-n-butyl phosphate (TBP) two-phase equilibrium system are reviewed. Studies of the partition of Group IA thiocyanates, and of ammonium halides, reveal marked differences from the aqueous solution–TBP system. These differences are discussed in terms of the effects of the basicity of the ammonia molecule, which results in strong solvation of cations in the liquid ammonia phase.

Introduction

THE LITERATURE OF solvent extraction is largely concerned with the equilibrium distribution of solute species between aqueous solution and an immiscible solvent, and the application of a variety of physicochemical techniques has produced a good understanding of the overall principles that govern such extraction equilibria. In general, the nature of the two phases can be varied in two ways. The chemical and physical characteristics of the organic phase are readily altered by changing from one solvent to another, and changes in the properties of the aqueous phase can be brought about by the addition of appropriate solutes. There has been relatively little work on systems of two immiscible non-aqueous solvents, other than studies of liquid metal or molten electrolyte systems at high temperatures. For reasons set out below, there is current interest in solvent extraction equilibria in systems of two non-aqueous immiscible liquids, one of which is an inorganic solvent. The present paper reviews briefly some recent work on the interaction of liquid ammonia with the well known organic solvent tri-n-butyl phosphate (TBP), and presents results on the extraction of some simple salts from liquid ammonia into that solvent.

Before considering the detailed results, it is worth reviewing the sort of information which can be obtained from a study of solute partition between two immiscible non-aqueous solvents. Firstly, by studying the physical chemistry of such systems, it should be possible to obtain useful data about solvent–solvent interactions in such non-aqueous systems. This approach should lead to useful comparisons with aqueous systems, and models for the latter should be tested against information for completely non-aqueous systems. Secondly, solvent extraction studies should yield information about the state of solute species in a solvent such as liquid ammonia. This approach is analogous in many respects to that often used previously for aqueous solutions. In this same context, it may be possible in some cases to study species which are insoluble in water, or which cannot exist in aqueous solution because of hydration or other solvolysis reactions. Thirdly, it may be possible to find new separation methods for analytical, industrial or academic use, taking advantage of the variety of non-aqueous solvents which are known, and of the increased temperature range which becomes available by the use of such solvents. In work with liquid ammonia and TBP, for example, it was possible to work down to −65°C, and no doubt there are other solvent systems where lower temperatures are possible. One of the present interests of Canadian industry is in the possibility of metallurgical operations in those areas where ambient temperatures are commonly well below the freezing point of water,

*Permanent address: Department of Physical Chemistry, University of Brno, Czechoslovakia.

and it may be that separations by non-aqueous solvent extraction techniques have something to offer in this respect.

Experimental

General

The solvent purification and handling techniques used have been fully described in published[1] and unpublished work (Hala, J., & Tuck, D. G., unpublished results); the most important point is the exclusion of moisture. In work on the equilibrium solubility of ammonia in TBP, liquid–liquid equilibria studies were carried out over the range -65 to $-35°C$. Above $-35\cdot5°C$ (the boiling point of ammonia at 1 atm.), it was possible to saturate TBP with dry ammonia gas.

Experiments on the distribution of solutes between TBP and liquid ammonia were carried out at a fixed temperature of $-40°C$. The two phases were shaken vigorously for 20 min, although preliminary experiments showed that equilibrium was reached after about 5 min. Distribution coefficients were determined by analysing the organic phase for halide or thiocyanate by titration against aqueous silver nitrate solution, after suitable dilution and neutralisation; the equilibrium concentration in the ammonia phase was then obtained by difference from the known initial concentration. The method yielded partition data expressed as:

$$D_{MX} = \frac{\text{moles MX per kg TBP}}{\text{moles MX per kg } NH_3}$$

Materials

Solutions were prepared with analytical grade materials. Thiocyanates of Group I metals were as in previous work.[2] The thiocyanates of calcium, cobalt and zinc were prepared by dissolving the corresponding carbonates in aqueous thiocyanic acid, obtained by cation exchange of an aqueous solution of sodium thiocyanate. After evaporation, the solid materials were dried over phosphorus pentoxide *in vacuo*, and analysed titrimetrically for thiocyanate (*Found:* for the calcium salt: CNS^- 59·9, $Ca(CNS)_2.2H_2O$ requires CNS^- 60·5%; for the cobalt salt: CNS^- 66·8, $Co(CNS)_2$ requires CNS^- 66·3%; for the zinc salt: CNS^- 64·2, $Zn(CNS)_2$ requires CNS^- 64·0%). The silver complex $[Ag(NH_3)_2]NO_3$ was prepared by passing gaseous ammonia through a solution of silver nitrate in acetonitrile (*Found:* Ag 53·7, $[Ag(NH_3)_2]NO_3$ requires Ag 53·5%).

Results and discussion

Ammonia–tri-n-butyl phosphate system

Liquid ammonia is known to have much higher solubility than water in a number of organic solvents,[3] and in agreement with this, the mutual solubilities of ammonia and TBP are appreciably higher than those for water and TBP. The temperature dependence of the solubility of ammonia in TBP is shown in Fig. 1. Two main differences from the much studied[4] water–TBP system are clear; the NH_3:TBP mole ratio is always greater than unity in the liquid ammonia temperature range, and the temperature dependence of the solubility in the liquid range is opposite in sign to that observed for H_2O:TBP. These results, which have been discussed in detail in an earlier paper,[1] together with spectroscopic and other evidence, show that the high solubility of ammonia in TBP is the result of weak NH_3–TBP intermolecular interactions, which in turn result from the lower polarity and higher basicity of ammonia compared with water.

In keeping with these results, TBP is more soluble in ammonia than in water[1] (32 $\pm$ 1 g TBP per l of ammonia at $-40°C$, as against 0·422 g per l of water at 25°C), but the solubility is still sufficiently small to be neglected

in the present discussion. These results on the NH_3–TBP interaction are of considerable significance in understanding the distribution of some simple electrolytes between liquid ammonia and TBP.

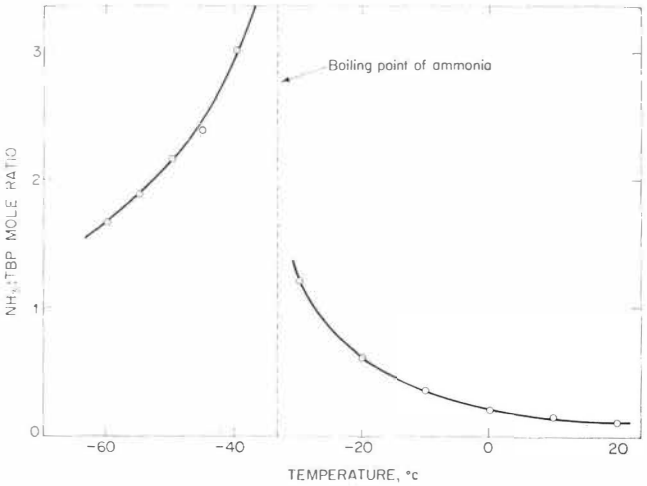

FIG. 1. *Temperature dependence of the solubility of ammonia in tri-n-butyl phosphate*

Distribution of ammonium halides and thiocyanate

The distribution of mono- and di-basic acids between aqueous solution and TBP has been investigated earlier.[5] The distribution coefficient depends *inter alia* on the size and basicity of the anion, and the extraction equilibria can be treated[5] as a competition between three bases (water, TBP and the anion) for the single acidic species, the proton. The first experiments, therefore, examined the distribution of the readily soluble ammonium halides and thiocyanate, which are acids in liquid ammonia, between ammonia and TBP. Ammonium chloride is insufficiently soluble in liquid ammonia at $-40°C$ for extraction measurements to be made. No extraction was detected with ammonium bromide ($D < \sim 5 \times 10^{-4}$), and only slight extraction with ammonium iodide ($D \sim 1 \cdot 5 \times 10^{-3}$), but with ammonium thiocyanate significant concentrations of salt were detected in the TBP phase. The distribution coefficient is concentration-dependent over the range studied (Table I).

The first interesting point is that the order of extractability ($NH_4Br < NH_4I < NH_4CNS$) is not the order of the solubility of these salts in TBP ($NH_4Cl < NH_4Br < NH_4I \sim NH_4CNS$),[2] so that a simple solubility-controlled partition system is not being dealt with here. It is instructive to examine the above

TABLE I

Distribution of ammonium thiocyanate between ammonia and TBP at $-40°C$

Equil. concn. of NH_4CNS (ammonia phase), moles per kg NH_3	Equil. concn. of NH_4CNS (TBP phase), moles per kg TBP	$D(NH_4CNS)$
5·25	38	$7 \cdot 2_4 \times 10^{-3}$
6·13	50	$8 \cdot 1_5 \times 10^{-3}$
7·35	90	$12 \cdot 2 \times 10^{-3}$

results in terms of the views advanced earlier on the important factors in the extraction of mineral acids from aqueous solution into a basic organic solvent.[5,6] The distribution of NH_4X between liquid ammonia and TBP should be regarded as a series of acid–base competitions, possibly influenced by factors such as anion size. The fact that the thiocyanate is much better extracted than the iodide anion is then related to the higher basicity of the thiocyanate anion. This is a more attractive explanation than one based on size, since the thiocyanate and iodide ions are not markedly different in volume. It has been argued[6] that the size effect is a function of the highly structured nature of liquid water, and a comparison of the properties of water and ammonia suggests that the latter should be much less structured, so that size may be relatively unimportant in influencing the relative extractability of solutes from ammonia solution; this point obviously requires further investigation.

The low values of the distribution coefficients, even for ammonium thiocyanate, are also significant. Since the ammonium cation is known to become hydrogen-bonded to the phosphoryl oxygen of TBP in solution,[2] the low extraction implies strong solvation in the ammonia phase. The most obvious form of solvation is of the cation by ammonia to give $[NH_4(NH_3)_n]^+$, analogous to $[H_3O(H_2O)_3]^+$, which is known to exist in aqueous solution.[7,8] There is at present no direct evidence of such a solvated cation in liquid ammonia, but Kebarle[9] has shown that in the gas phase clusters of $[NH_4(NH_3]_n)^+$ are thermodynamically stable up to $n \sim 5$. The analogous gas-phase hydronium ion species were also identified. The overall balance of stabilising factors in the gaseous and the liquid phases may be very different of course, but the parallel between ammonium and hydronium ions strongly suggests the existence of solvated ammonium ions in liquid ammonia. It has not been possible so far to determine directly the amount of ammonia co-extracted with the TBP phase along with the ammonium cation; in contrast to the aqueous system, the relatively large amount of ammonia present in the organic phase (see Fig. 1), together with the slight extraction of ammonium thiocyanate, makes any such experiment intrinsically inaccurate.

Distribution of alkali metal thiocyanates

The distribution coefficients for the partition of alkali metal thiocyanates between liquid ammonia and TBP are given in Table II, along with relevant data on solubilities.

TABLE II

Distribution of alkali metal thiocyanates between liquid ammonia and TBP at −40°C

MCNS	Radius of anion,[10] Å	D_{MCNS} for 5-molal MCNS in ammonia	Solubility of MCNS in TBP,[2] g per 100 g TBP	Solubility of MCNS in ammonia,[11] g per 100 g NH_3
LiCNS	0·60	0·0076	12·0	—
NaCNS	0·95	0·0124	12·5	205·5 (25°C)
KCNS	1·33	0·0438	6·96	v. soluble
RbCNS	1·48	~0·05*	3·4	—
NH_4CNS	1·48	0·0072	11·6	312·0 (25°C)

*Extrapolated value

The only study of the extraction of an alkali metal thiocyanate refers to the partition of the sodium salt[12] between aqueous solution and TBP. The (molar) distribution coefficient for equilibria aqueous phase salt concentrations of 2–4 M is ~0·35, and water molecules are extracted along with salt. Baldwin

et al.[13] investigated the distribution of Group IA halides, and found the effect of the cation followed the order HX > LiX > NaX > KX > CsX; for the iodides, for example, the (molal) distribution coefficients are ~0·5, 0·3, 0·1, and 0·04 for HI, LiI, NaI and KI, respectively. It seems reasonable to assume that this same order would hold for the corresponding thiocyanates in the aqueous solution–TBP system.

The results in Table II show that the distribution favours the organic phase much less in the ammonia–TBP case, and that the order is essentially the reverse of that in the aqueous system, namely, $NH_4CNS \leqslant LiCNS < NaCNS < KCNS \leqslant RbCNS$. This order holds over the range of concentrations in which sensible measurements can be made.

The explanation is as follows. The ammonia–TBP system is a competition between two basic and probably unstructured solvents for the various cations (ignoring the anion, which is common to all the salts in question). Although the salts are all appreciably soluble in TBP, solvation of the cation by TBP, as detected by changes in the P=O stretching frequency,[2] is only significant for NH_4CNS, and LiCNS, with $\Delta\nu \sim 20$ cm^{-1} in both cases. As noted above, there is little information on solvation numbers, etc., in ammonia solution, but the basicity of the ammonia molecule, and its well-known complexing interaction with many metal ions, lead one to expect stronger solvation of a given cation in ammonia than in water. If the solvation of the alkali metal cations is a dipole–charge interaction, the order of solvation energies should be of the order of the ionic radii, namely Li > Na > K > Rb. This will then be the inverse order of the extractability from ammonia solution, provided there are no overriding effects in the TBP phase, and the infra-red evidence shows that only in the case of the lithium salt is solvation by TBP detectable. Apparently, this organic phase interaction is not sufficiently strong to overcome the solvation in the ammonia phase, since the extraction of lithium thiocyanate is small, and since the order of extraction is the same as that of the presumed solvation energies. As in the ammonium work discussed above, reliable evidence on the transfer (if any) of ammonia molecules with the extracted salt is not available, so that at present no estimates of the solvation number for these cations in liquid ammonia can be made.

Comparison of the results in Table II with those for the aqueous solution–TBP systems shows that the competition between water and TBP is in favour of the organic phase to a greater extent in the latter, as predicted by the relative basicities of the solvents.

It should be noted that the ionic size argument breaks down when the extraction of ammonium thiocyanate is considered relative to that of the alkali metal salts. The explanation is similar to that used to explain the strong hydration of the hydronium ion.[8] Despite the large ionic radius, the solvation of ammonium ion by ammonia can occur by specific hydrogen-bonding interactions, owing to the effective concentration of the positive charge at the hydrogen atoms of the NH_4^+ group, so that NH_4^+ will interact much more strongly with ammonium than does Rb^+, with an identical ionic radius. Thus, in spite of the known solvation of NH_4^+ by TBP,[2] the extraction of ammonium thiocyanate is weaker than that of the salts studied because of strong solvation in the ammonia phase.

As a further example of the effect of strong solvation in the ammonia phase, it is found that $[Ag(NH_3)_2]NO_3$ is not extracted into TBP from ammonia solution. The ionic radius of Ag^+ (1·26Å) lies between those of Na^+ and K^+, but the solvation by ammonia, which persists even in the solid state, evidently prevents extraction.

Some $M(CNS)_2$ salts

Since some thiocyanates of divalent metals have been found to have high solubility in both liquid ammonia and TBP (see Table III), it was attempted to extend the partition studies to this class of electrolytes, using calcium, zinc and

cobalt(II) thiocyanates. Of these, only the zinc salt was extracted sufficiently to permit measurement of the distribution coefficient by the titrimetric method, with $D = 4 \cdot 5 \times 10^{-5}$ at an equilibrium ammonia phase concentration of 2M. This partition is lower than with univalent metal thiocyanates, presumably owing to strong $Zn(II)$–NH_3 interactions in the ammonia phase. Brown anhydrous $Co(CNS)_2$ yielded a dark brown solution and a brown solid on contacting with liquid ammonia; no thiocyanate transfer into the organic phase was observed on shaking with TBP. Similarly, when a blue solution of $Co(CNS)_2$ in dry TBP was brought into contact with liquid ammonia, the blue colour disappeared and the same brown product was obtained in the ammonia phase. The blue solution in TBP is evidently the four-coordinate $Co(CNS)_2(TBP)_2$ species, but this coordinate solvation of cobalt by TBP is not sufficient to overcome solvation by ammonia.

TABLE III

Solubility of some divalent metal thiocyanates in tri-n-butyl phosphate at 22°C

$M(CNS)_2$	Solubility of $M(CNS)_2$ in TBP, g per 100 g TBP	Mole ratio TBP : $M(CNS)_2$ in satd. soln.*	$\Delta\nu$(P–O),** cm^{-1}	$\Delta\nu$(P–O) for $M(NO_3)_2$ in TBP,[14] cm^{-1}
$Ca(CNS)_2.2H_2O$	$19 \cdot 7 \pm 0 \cdot 4$	2·98	33	33
$Zn(CNS)_2$	33 ± 1	2·05	53	48
$Co(CNS)_2$	$25 \cdot 8 \pm 0 \cdot 2$	2·55	38	36

*Estimated error $\pm 0 \cdot 05$
**From the ν (P–O) frequency of 1275 cm^{-1} in anhydrous TBP

Some direct evidence of the solvation of calcium, zinc and cobalt thiocyanate by TBP was obtained in studies of the solubility of these salts in TBP, and of the infra-red spectrum of TBP in the resultant solutions. The results shown in Table III demonstrate that a strong interaction occurs, with infra-red spectral changes very similar to those reported for the nitrates of the same elements.[14] Following the arguments used previously[2] it is concluded that for Zn(II) thiocyanate, the saturated solution represents the $Zn(CNS)_2.2TBP$ complex. Similar complexes are probably formed also with thiocyanates of Co(II) and Ca with some free TBP present at saturation. The strength of the M(II)–TBP interaction is however not sufficient to overcome the M(II)–NH_3 solvation in the ammonia phase in the two-phase system, so that extraction from ammonia does not occur.

Conclusions

The experimental evidence to date suggests that the differences between the TBP–aqueous solution and TBP–ammonia solution systems can be explained in terms of the higher basicity of ammonia relative to water. Extensions of the present work are planned so that other factors can be examined.

Acknowledgment

This work was supported in part by an Operating Grant from the National Research Council of Canada.

References

[1] Hala, J., & Tuck, D. G., *J. chem. Soc. A*, 1970, p. 3242
[2] Hala, J., & Tuck, D. G., *Can. J. Chem.*, 1970, **48**, 2843
[3] Smith, H., 'Organic reactions in liquid ammonia', 1963 (New York: Interscience)
[4] Kertes, A. S., & Marcus, Y., 'Ion exchange and solvent extraction of metal complexes', 1969, p. 660 (New York: Wiley)

[5] Tuck, D. G., *J. chem. Soc.*, 1958, p. 2783
[6] Diamond, R. M., & Tuck, D. G., *Prog. inorg. Chem.*, 1961, **2,** 109
[7] Bell, R. P., 'The proton in chemistry', 1958 (Ithaca: Cornell University Press)
[8] Tuck, D. G., & Diamond, R. M., *J. phys. Chem., Ithaca*, 1961, **65,** 193
[9] Kebarle, P., *Adv. Chem. Ser.*, 1968, (72), p. 24 and refs therein
[10] Wells, A. F., 'Structural inorganic chemistry', 3rd Edn, 1962, p. 71 (Oxford: Oxford University Press)
[11] Jander, J., 'Chemie in wasserfreiem flüssigem Ammoniak', 1966, pp. 53 *et seq.* (New York: Interscience)
[12] Arcand, G. M., & Carroll, W. R., *J. phys. Chem., Ithaca*, 1962, **66,** 1014
[13] Baldwin, W. H., Higgins, C. E., & Soldano, B. A., *J. phys. Chem., Ithaca*, 1959, **63,** 118
[14] Katzin, L. I., *J. inorg. nucl. Chem.*, 1961, **20,** 300

Study of the synergistic extraction of metal ions by α-hydroxyoxime/carboxylic acid mixtures with the AKUFVE apparatus

by M. Cox and D. S. Flett
Hatfield Polytechnic and Warren Spring Laboratory, Stevenage, Herts, U.K.

The synergistic extraction system copper(II)/α-hydroxyoxime/carboxylic acid has been studied using the AKUFVE apparatus for the two acids, naphthenic acid and α-bromolauric acid. It has been shown that the copper is extracted as a monomeric mixed ligand complex copper(II)/α-hydroxyoxime/carboxylic acid with the stoicheiometry 1:2:4 for α-bromolauric acid. A detailed spectroscopic investigation of the system indicates the presence of only one mixed complex in solution. The role of each of the organic reagents in the mixed complex is discussed.

Preliminary investigation of the iron(III)/α-hydroxyoxime/naphthenic acid system, where little synergism has been observed, has provided evidence of hysteresis in the log D *vs. pH plots.*

Introduction

THE TERM SYNERGISM has a well-established usage in the field of solvent extraction of metals being defined as the enhancement of extraction of a metal/ligand complex by the addition of a second donor molecule to the system. Taube[1] has defined a synergistic coefficient as:

$$\text{synergistic coefficient} = \log \frac{D\ (\text{expt. value in presence of both reagents})}{D\ (\text{calc. additive value in absence of synergism})}$$

Since the first recognition of this phenomenon in 1954 many examples have been reported and reviews have been presented at two previous solvent extraction conferences.[2,3] Marcus & Kertes[4] classify four different types of synergistic combinations: (i) chelating agent—neutral ligand; (ii) alkylphosphoric acid–neutral ligand; (iii) two neutral ligands; and (iv) two acid ligands. The majority of published examples are concerned with types (i), especially the systems involving β-diketones and organophosphorus esters, and (ii), where the neutral ligand is again often an organophosphorus ester. In both these combinations high synergistic coefficients ($\sim 10^5$) are observed and the mechanism is explained in terms of the formation of mixed ligand complexes, $[M(A\text{–}A)_nS_x]^o$ for type (i), and $[M(X.HX)_mS_x]^o$ for type (ii), which have a higher extractability than either of the two parent complexes (A–A denotes β-diketone and HX denotes alkyl phosphoric acid).

Data concerned with the last two combinations are less detailed and the mechanism is less well characterised. Thus it has been reported[4] that several metals, including uranium(VI), iron(III), zirconium(IV), and the rare earths, can be synergistically extracted by mixtures of various ethers, ketones, alcohols, and esters, although the synergistic coefficients are much lower[2–5] than types (i) and (ii) and sometimes no synergism occurs at all. Finally, in a study of metal extraction by mixtures of two β-diketones, Newman[5] noted that in most cases no synergism occurred although formation of mixed complexes $[M(A\text{–}A)_{n-m}(B\text{–}B)_m]^\circ$ could be established.

For historical reasons only the solvation of metal complexes by molecules of the complexing reagent itself is not considered as synergism although the phenomenon is very similar in that mixed complexes are formed. Similarly the well-known[6,7] extraction of metals by carboxylic acids with the formation of mixed complexes of the type $[MX_n(HX)_m]^o$ is not considered to be a synergistic process. The replacement of the solvating carboxylic acid molecules by other donors might be expected to produce a synergistic system but no useful degree of synergism has been observed with, for example, the combinations of alkylamine/naphthenic acid[8] and amine/salicyclic acid[9] for copper(II) extraction.

Similar results were obtained for tributyl phosphate/salicylic acid mixtures with several metal ions.[10,11] However, enhanced extraction of caesium was found[12] with mixtures of 4-phenylvaleric acid and 4-s-butyl-2-(α-methylbenzyl)phenol (BAMBP). In this system the phenol behaves as the neutral solvating agent. Synergism by carboxylic acids has also been recently reported[13] for tris(benzoyltrifluoroacetato)europium(III) and the enhanced extraction was explained by adduct formation with the undissociated carboxylic acid, $[Eu(bztfac)_3\ (HX)_2]^o$.

Following the announcement of synergism by mixtures of an α-hydroxyoxime (LIX63, General Mills Inc.) with di-2-ethylhexylphosphoric acid mixtures,[14] preliminary results[15] showed useful synergism with mixtures of the α-hydroxyoxime and naphthenic acid for copper(II) and cobalt(II), and this has been extended to include mixtures of other acids with LIX63 and the use of the synergism for the selective extraction of one element from another.[16] The results reported here are concerned with a detailed investigation of the systems copper(II)/LIX63/naphthenic acid and copper(II)/LIX63/α-bromolauric acid to ascertain the nature of the extracted species and to try to elucidate the role of each of the two reagents in the synergistic extraction. A preliminary study of the extraction of iron(III) with these mixed reagents is also included as it had been noted that little synergism occurred in this case.[16]

Experimental

Apparatus

The results were obtained using an AKUFVE 100 system with ancillary detecting apparatus. The AKUFVE system has been fully described elsewhere[17] and results of experiments have been published.[18–20] The principal advantage of this system over conventional shake-flask tests is the rapid accumulation of data points (10–100 times faster depending on detection apparatus and the kinetics of the extraction). Also, because it operates on a recycling closed loop for each phase, random errors are reduced and less scatter is observed. In this work the metal concentration in each phase was measured, after suitable dilution and treatment, by atomic absorption spectroscopy, although visible spectrophotometry of the organic phase using flow-through cells was also used in a few runs. The analysis of samples proved to be the biggest time factor in the determinations but unfortunately flow-through scintillation counting equipment was not available for this study. The aqueous phase was also continuously monitored for pH using a glass calomel combination electrode calibrated against known buffer solutions. Good agreement was obtained between this electrode under flowing conditions and samples measured by another pH meter (Beckman Research pH meter) under static conditions and calibrated with the same buffer solutions. Operating in this way any errors arising from drift of the pH meters or malfunction of the electrodes was eliminated. In the case of the copper extraction the aqueous phase was also continuously monitored for copper ion activity using a specific ion electrode (Orion Research Inc., Cupric model 94-29A) in conjunction with a reference electrode (Orion Research Inc., 90-01) and a digital pH meter (Orion Research Inc., Model 801). Here it was not possible to use a combined electrode and differences in the potentials were noted under flowing conditions. However, the system was used only for measurement of changes of activity, using values obtained by atomic absorption measurements on selected samples to fix the absolute values. Once again good agreement was found between the two methods of monitoring the copper ion concentration. Even without the facility of on-line analysis of the two phases, 50 data points could easily be collected in a day and in all runs the system was checked for hysteresis by addition of both acid and alkali.

In an investigation of this type it is necessary to study the effect on metal extraction of the variation in reagent concentration. This is usually achieved by performing a large number of extraction coefficient vs. pH determinations, each at a fixed reagent concentration. Thus a family of log D vs. pH curves is obtained as in Fig. 1. Selection of a suitable pH allows the construction of

a log D vs. reagent concentration graph with points obtained from this family of curves. To accelerate this process of obtaining log D vs. reagent concentration dependence, the operation of the AKUFVE system at a constant pH and varying reagent concentration was investigated. The apparatus consisted of a pH stat, (Metrohm Impulsomat E473 coupled to a Metrohm pH meter E300B and a Metrohm Dosimat E415 automatic piston burette), operating on the aqueous phase. This allowed variation of reagent concentration in the system while maintaining it at a constant pH by addition of acid or alkali. Thus the variation of distribution coefficient with reagent concentration could be obtained from one experimental run rather than from a larger number of distribution coefficient vs. pH experiments. Tests showed coincidence of the log D vs. log [reagent] plot by this method with data derived from the family of log D vs. pH plots, (see Fig. 5), thus giving confidence in this method.

LIX 63 was used as received, and its active principle, 5,8-diethyl-7-hydroxydodecane-6-oxime, was also prepared according to the method of Swanson.[21] Although it was suspected that the commercial material was not pure the level and nature of impurities did not alter the extraction performance from that of the pure reagent. Naphthenic acid (Shell Chemical Co. Ltd.) and α-bromolauric acid (Ralph N. Emanuel Ltd.) were used without purification and all other chemicals were of analytical quality.

Procedure

The aqueous phase contained copper sulphate (5mM) in potassium nitrate (1M) solution to provide a constant ionic strength medium. The organic phase contained the two reagents LIX63 and carboxylic acid in various molar concentrations. Equal volumes of each phase (400 ml) were added to the mixing chamber of the AKUFVE and the mixer and centrifuge started. When equilibrium had been established (2–3 min) samples (1 ml) were withdrawn from each phase for analysis, and the pH and copper ion activity readings of the meters were recorded. Adjustment of the pH was then made by addition of sodium hydroxide (1M) or sulphuric acid (5M). In a typical run the total volume of added acid/alkali was not greater than 10% of initial aqueous volume.

For experiments at constant pH the same procedure was applied with the reagent, whose concentration was being varied, added to the mixing chamber as a concentrated solution in kerosene containing the other reagent at the desired fixed level. The pH was adjusted automatically with sodium hydroxide (1M) added to the aqueous detection loop to ensure that the desired pH was maintained. This method necessitates slow addition of alkali and hence the time to reach equilibrium is longer and readings were taken at about 20 min intervals. Once again volume changes were less than 10% of initial volumes. Because of the importance in this type of measurement of accurate pH measurement the pH-stat was supported by another pH-meter in the aqueous loop and by measurement of each sample under static conditions by a third meter.

All experiments were carried out at 25 ± 1°C.

Results and discussion

Interaction between the extraction reagents LIX63 and carboxylic acids

For meaningful conclusions to be drawn from the application of the law of mass action to the distribution data it is essential to know the form in which the two extractants exist in the organic phase and the degree of interaction between them which may lead to formation of species which must be included in the overall equilibrium expression. For this study α-bromolauric acid was used exclusively as being the purer acid together with, for the same reason, the LIX63 synthesised in the laboratory.

The mutual interaction between LIX63 and α-bromolauric acid was studied by the cryoscopic measurement of the molecular weight of α-bromolauric acid in benzene solution in the presence of LIX63. It was found that the carboxylic

acid was still dimeric in this solvent even after the addition of an equimolar amount of the hydroxyoxime, and the LIX63 behaved as a monomer. The values obtained were 246 for LIX63 and 543 for α-bromolauric acid, with the calculated monomer values 274 and 279 respectively.

Further confirmation of the lack of interaction between these two reagents was afforded by their infra-red (i.r.) and ultra-violet (u.v.) spectra. The u.v. spectra were recorded in hexane solution and it was found that the addition of the acid had no affect on the spectrum of LIX63. Unfortunately the presence of a strong absorption in the LIX63 spectrum completely masks any absorption arising from the acid. However, the i.r. spectra of benzene solutions of the acid alone and in the presence of an equimolar amount of LIX63 showed no variation either in the position or intensity of the two carbonyl bands at approximately 1800 and 1600 cm^{-1} arising from the free and hydrogen-bonded carboxylic acid group.

From this evidence therefore it can be assumed that the two reagents LIX63 and α-bromolauric acid do not interact with one another in hydrocarbon solutions.

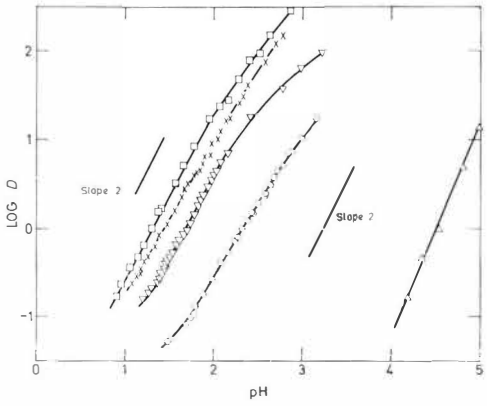

FIG. 1. *Extraction of copper with LIX63/naphthenic acid in kerosene*
△ 0·1M naphthenic acid; ○ 0·3M LIX63; ▽ 0·3M LIX63/0·1M naphthenic acid; × 0·3M LIX63/0·03M naphthenic acid; □0·3M LIX63/0·9M naphthenic acid

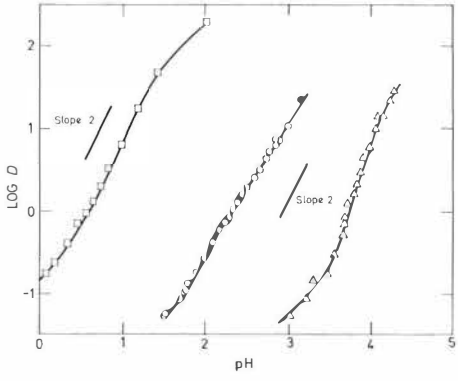

FIG. 2. *Extraction of copper with LIX63/α-bromolauric acid in kerosene*
△ 0·1M α-bromolauric acid; ○ 0·3M LIX63; □ 0·3M LIX63/0·1M α-bromolauric acid

Equilibrium studies on extraction of metals by the mixed reagents LIX63/carboxylic acid

Effect of pH on copper extraction

The earlier observations of Flett & Titmuss[15] of the synergism in the copper extraction system were confirmed and the effect of replacing the naphthenic acid by the stronger α-bromolauric acid was studied (Figs 1 and 2). Each plot results from a large number of data points and, with the pH range covered at least twice, no evidence of hysteresis was observed. However, in the case of the extraction with LIX63/α-bromolauric acid, when sulphuric acid was used to adjust the acidity, changes in slope were observed as the system was cycled from acid to alkali, although no change was noticed when nitric acid was used. This change of slope presumably arises from the formation in the aqueous phase of sulphato copper complexes, which are known to occur at high sulphate ion concentrations,[22] whereas no such nitrato complexes are known. This hypothesis is supported by the observation that a similar variation in extraction behaviour could be caused by adding a concentrated aqueous sodium sulphate solution at fixed pH (Fig. 3).

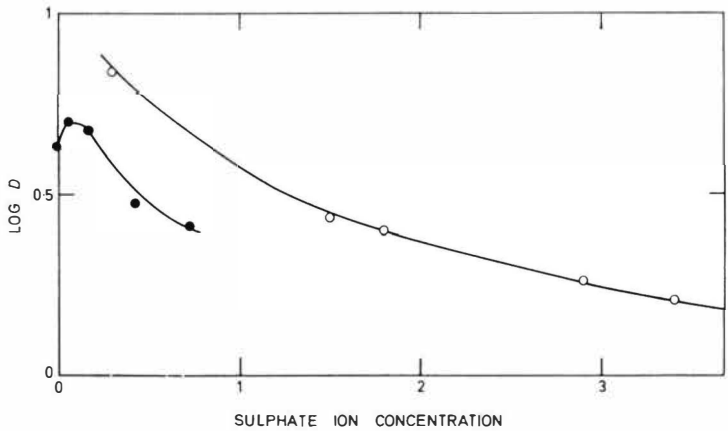

FIG. 3. *Effect of sulphate ion concentration on extraction of copper with LIX63/α-bromolauric acid in kerosene*

○ Data extrapolated from log D vs. pH plots with 0·3M LIX63/0·1M α-bromolauric acid (pH 1); ● obtained by addition of Na_2SO_4 solution to LIX63/α-bromolauric acid (0·01M, pH 2·14)

The extraction of divalent metal ions by LIX63/carboxylic acid mixtures can be represented by:

$$M^{2+} + n\overline{HL} + m\overline{R_2H_2} \rightleftharpoons \overline{M(L_nR_{2m}H_{2m+n-2})} + 2H^+ \quad . \quad . \quad . \quad (1)$$

where HL represents LIX63, R_2H_2 the carboxylic acid dimer and the bars denote organic-phase species.

The mass action constant for the equilibrium is:

$$K = \frac{\overline{[M(L_nR_{2m}H_{2m+n-2})]}\,[H^+]^2}{[M^{2+}]\,[\overline{HL}]^n\,[\overline{R_2H_2}]^m} \quad . \quad . \quad . \quad . \quad . \quad . \quad . \quad (2)$$

Defining a distribution coefficient, D, as:

$$D = \frac{\overline{[M(L_nR_{2m}H_{2m+n-2})]}}{[M^{2+}]} \quad . \quad . \quad . \quad . \quad . \quad . \quad . \quad . \quad (3)$$

Substituting in Equation (2) and taking logarithms:

$$\log D = \log K + 2pH + n \log [\overline{HL}] + m \log [\overline{R_2H_2}] \quad . \quad . \quad . \quad (4)$$

Examination of Figs 1 and 2 shows that, as predicted by Equation (4) when $\overline{[HL]} \gg [M]_{total}$, the log D vs. pH plots for the extraction of copper by the mixed reagent systems have slopes of approximately 2. It should be noted that the measured value of D is in fact the expression:

$$D_{obs.} = \frac{\text{total copper concentration in organic phase}}{\text{total copper concentration in aqueous phase}}$$

Effect of pH on iron(III) extraction

A preliminary investigation of the extraction of iron(III) with naphthenic acid and with the mixed reagent LIX63/naphthenic acid has also been carried out. The aqueous phase was a 5mM solution of ferric ammonium sulphate in 1M potassium nitrate. The results are shown in Fig. 4, and it can be seen that considerable hysteresis was observed. The nature and cause of this phenomenon will be studied in detail later.

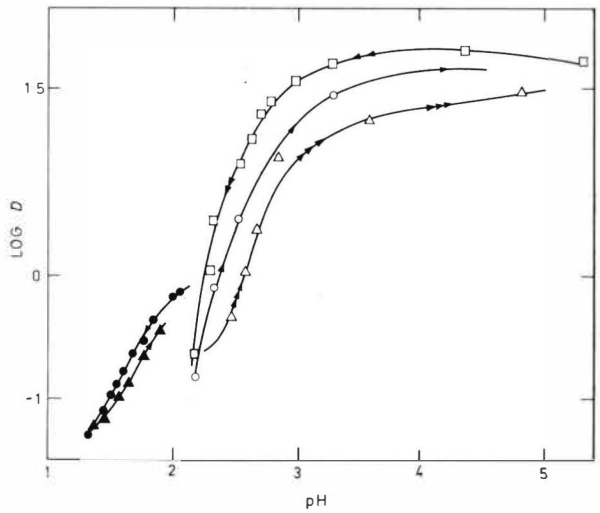

FIG. 4. *Effect of pH on extraction of Fe(III) with LIX63/naphthenic acid in kerosene*
●, ▲ 0·3M LIX63/0·1M naphthenic acid; ○, □, △ 0·1M naphthenic acid

Variation in LIX63 concentration at constant pH and carboxylic acid concentration

Using the pH-stat facility in conjunction with the AKUFVE system, the pH of the extraction mixture was kept constant while the LIX63 concentration was varied by the addition of a concentrated solution of LIX63 in kerosene with the carboxylic acid maintained at a constant level. The results for the two acids are shown in Fig. 5.

From Equation (4), assuming that the total copper concentration in the organic phase related to a complex of the form given in Equation (1), then the value of n will be given by the slope of the plot of log D vs. log $\overline{[HL]}$ at constant pH and R_2H_2 concentration. Examination of Fig. 5 shows that in both cases straight lines are obtained over a substantial range of HL concentration giving slopes of 1·7 and 2·0 for naphthenic acid and α-bromolauric acid, respectively. The coincidence of the data from the pH-stat runs with data from individual log D vs. pH plots is emphasised.

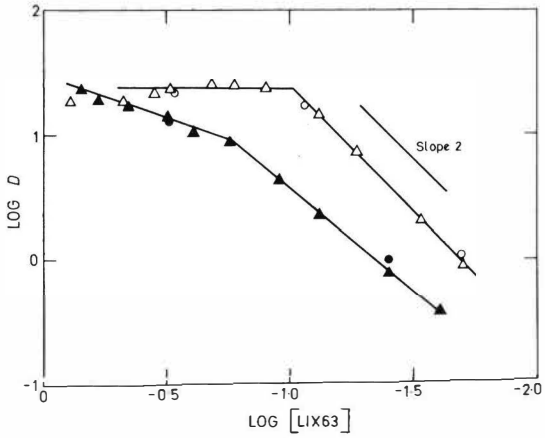

FIG. 5. *Variation of LIX63 concentration at constant pH for extraction of copper with LIX63/carboxylic acid in kerosene*

●, ▲: 0·1M naphthenic acid, 0·005M Cu, pH 2·57;
○, △: 0·1M α-bromolauric acid, 0·005M Cu, pH 1·23
Circles represent data extrapolated from individual log *D* vs. pH plots; triangles represent data from single run at constant pH

Variation of carboxylic acid concentration at constant pH and LIX63 concentration

Similar experiments to those outlined above were carried out with changing carboxylic acid concentrations at constant pH and LIX63 concentration (Fig. 6).

As above, from Equation (4) the value of m may be obtained from the plot of log D vs. log $\overline{[R_2H_2]}$, (= log $\overline{[RH]}$—log 2), at constant pH and HL concentration. Examination of Fig. 6 shows that for α-bromolauric acid, $m = 2$, but in the case of naphthenic acid a rather flat curve is obtained. The reason for this discrepancy lies in the pH at which the results were obtained, i.e. pH 2·12. At this pH value significant amounts of copper are extracted by LIX63 itself. Reference to Fig. 1 shows that for $\overline{[LIX63]} = 0{\cdot}3$M at pH 2·12, log D has a

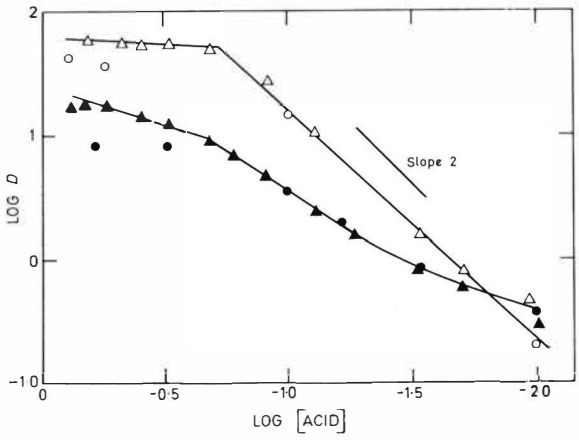

FIG. 6. *Variation of carboxylic acid concentration at constant pH for extraction of copper with LIX63/carboxylic acid in kerosene*

●, ▲: 0·3M LIX63, 0·005M Cu, pH 2·12; ○, △: 0·3M LIX63, 0·005M Cu, pH 1·13
Circles represent data extrapolated from individual log *D* vs. pH plots; triangles represent data from single run at constant pH

value of $\sim -0 \cdot 5$, a value which the plot in Fig. 6 is approaching. Thus unfortunately no meaningful conclusion may be drawn from the naphthenic acid data.

Spectral studies

In order to assist in the interpretation of the distribution data visible spectral studies were carried out on the organic phase extracts for the whole range of LIX63/carboxylic acid ratios and at various acidities. The recorded spectra showed the same species was extracted under all conditions (Fig. 7). This evidence was supported by mixing solutions of the parent complexes copper(II)/LIX63 and copper(II)/α-bromolaurate in varying molar ratios. The results show the formation of only one mixed complex by the presence of two isosbestic points (Fig. 8). Thus the assumption that the total copper concentration in the organic phase relates to a single complex species is justified except as shown above for the variation of naphthenic acid at constant LIX63 concentrations.

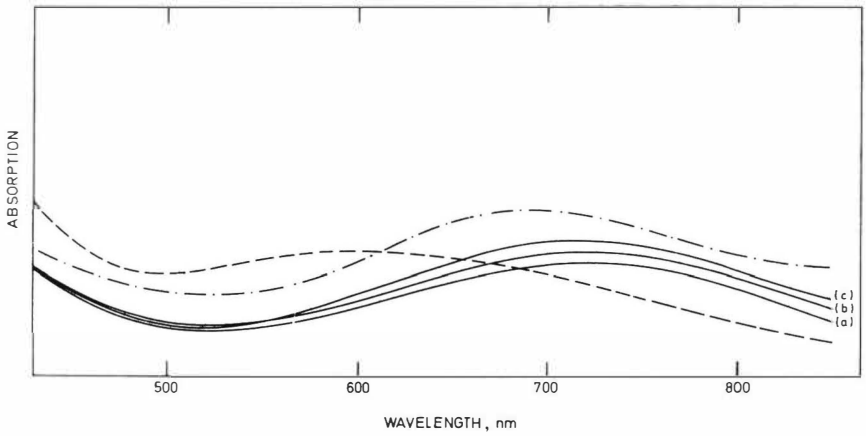

FIG. 7. *Absorption spectra for extraction of copper with LIX63/naphthenic acid in kerosene*
(a) 0·3M LIX63/0·1M naphthenic acid; (b) 0·3M LIX63/0·6M naphthenic acid;
(c) 0·3M LIX63/0·9M naphthenic acid
– – – – LIX63; —·—· naphthenic acid

Stoicheiometry

The distribution data for the extraction of copper by LIX63/α-bromolauric acid mixtures can be interpreted by slope analysis based on Equation (1) to yield the following ratio: Cu : LIX63 : α-bromolauric acid = 1 : 2 : 4. Unfortunately, because of the overlap in extraction by one of the components of the mixture, the data for the LIX63/naphthenic acid system cannot be unambiguously interpreted but it seems likely that a similar ratio would apply to the copper complex in this case.

In order to formulate the complex with confidence it is necessary to know its molecular complexity in the organic phase, i.e. monomer, dimer, etc. This question may be resolved by the method of Tanaka[8] as follows.

Consider a polymeric species where only the j-mer is important. Then condensing the two reagents into a single species HA which represents the LIX63 and α-bromolauric acid in the proportions given above:

$$D = K_j \cdot \frac{\overline{[\mathrm{HA}]}^j [\mathrm{M}^{2+}]^{j-1}}{[\mathrm{H}^+]^{2j}} \quad . \quad . \quad . \quad . \quad . \quad . \quad . \quad . \quad (5)$$

Thus at constant $\overline{[\mathrm{HA}]}$:

$$\log D - (j-1) \log [\mathrm{M}^{2+}] = \log K_j + 2j \,\mathrm{pH} \quad . \quad . \quad . \quad . \quad (6)$$

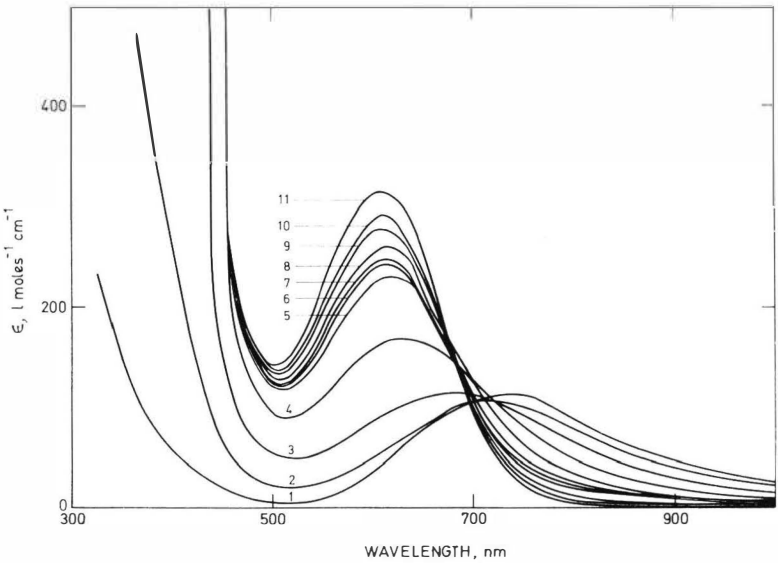

FIG. 8. *Spectra of mixed solutions of copper/α-bromolaurate and copper/LIX63 in kerosene showing two isosbestic points*

Curve	Ratio	
	Cu/α-bromolaurate	Cu/LIX63
1	1·0	0
2	0·9	0·1
3	0·8	0·2
4	0·7	0·3
5	0·6	0·4
6	0·5	0·5
7	0·4	0·6
8	0·3	0·7
9	0·2	0·8
10	0·1	0·9
11	0	1·0

and a plot of log $D - (j-1)$ log $[M^{2+}]$ vs. pH should give a straight line of slope $2j$. Plots of this function for several values of j are shown in Fig. 9 and the best straight line is obtained for $j = 1$ when the slope is 2 as predicted by Equation (6).

Thus the copper/LIX63/α-bromolauric acid complex may be formulated as $[CuH_4L_2R_4]$.

Synergism in the system LIX63/carboxylic acid arises therefore by the formation of a mixed ligand complex which presumably has an increased organic solubility over the parent compounds. This complex is of interest because it contains two reagents which are potentially acids with replaceable protons and it would be interesting to discover which is acting as the solvating agent. Unambiguous conclusions cannot be drawn from the distribution (Equation (4)). However, it is known that carboxylic acids can act as solvating agents in the extraction of metals[7,8,13] and this possibility could be considered here.

The effect of replacing the carboxylic acid by other oxygen donors is being studied to test this hypothesis and the results will be published later.

Acknowledgments

One of the authors (M.C.) would like to thank the Governors of the Hatfield Polytechnic for leave of absence to undertake this work.

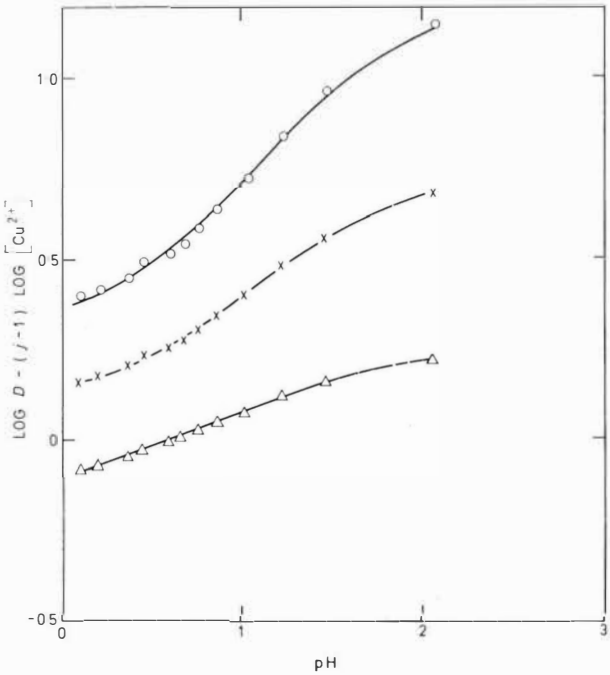

FIG. 9. *Log* D−(j−l) *log* [Cu^{2+}] versus *pH for extraction of copper with LIX63/α-bromolauric acid in kerosene*

△ $j = 1$; × $j = 2$; ○ $j = 3$

References

[1] Taube, M., & Siekierski, S., *Nukleonika*, 1961, **6,** 489

[2] Irving, H. M. H. N., in 'Solvent Extraction Chemistry', Dyrssen, D., Liljenzin, J. O., & Rydberg, J. (Eds.), 1967, p. 91 (Amsterdam: North Holland)

[3] Healy, T. V., in 'Solvent Extraction Research', 1969, p. 257 (New York: Wiley-Interscience)

[4] Marcus, Y., & Kertes, A. S., 'Ion Exchange and Solvent Extraction of Metal Complexes', 1969, Ch. 11, p. 815 (London: Wiley-Interscience)

[5] Newman, L., & Klotz, P., in 'Solvent Extraction Chemistry', Dyrssen, D., Liljenzin, J. O., & Rydberg, J. (Eds.), 1967, p. 128 (Amsterdam: North-Holland)

[6] Fletcher, A. W., & Flett, D. S., *J. appl. Chem., Lond.*, 1964, **14,** 250

[7] Tanaka, M., & Niinomi, T., *J. inorg. nucl. Chem.*, 1965, **27,** 431

[8] Flett, D. S., *Trans. N.R.I.M. Tokyo*, 1967, **9,** 215

[9] Aggett, J., & Billinghurst, M. W., *J. inorg. nucl. Chem.*, 1969, **31,** 513

[10] Aggett, J., & Crossley, P., *J. inorg. nucl. Chem.*, 1967, **29,** 1113

[11] Aggett, J., Crossley, P., & Hancock, R., *J. inorg. nucl. Chem.*, 1968, **30,** 2529

[12] Zingaro, R. A., & Coleman, C. F., *J. inorg. nucl. Chem.*, 1967, **29,** 1289

[13] Shigematsu, T., Tabushi, M., Matsui, M., & Honjyo, T., *Bull. chem. soc. Japan*, 1969, **42,** 976

[14] Joe, E. G., Ritcey, G. M., & Ashbrook, A. W., *J. Metals, N.Y.*, 1966, **18,** 18

[15] Flett, D. S., & Titmuss, S., *J. inorg. nucl. Chem.*, 1969, **31,** 2612

[16] Flett, D. S., & West, D. W., *Proc. int. Solvent Extraction Conf.*, 1971, (London: Society of Chemical Industry)

[17] Rydberg, J., *Acta chem. scand.*, 1969, **23,** 647

[18] Reinhardt, H., & Rydberg, J., *Acta chem. scand.*, 1969, **23,** 2773

[19] Johansson, H., & Rydberg, J., *Acta chem. scand.*, 1969, **23,** 2797

[20] Lilenzin, J. O., Starý, J., & Rydberg, J., in 'Solvent Extraction Research', 1969, p. 13 (New York: Wiley-Interscience)

[21] U.S.P. 3,224,873

[22] Lumme, P., *Spec. Publs chem. Soc.*, 1964, No. 17

Extraction of metal ions by LIX 63/carboxylic acid mixtures

by D. S. Flett and D. W. West
Warren Spring Laboratory, Stevenage, Herts, U.K.

Studies on the extraction of several metal ions (Cu, Fe, Ni, Co, Cd, Zn) with various carboxylic acid/α-hydroxyoxime mixtures showed that appreciable synergism occurred in many cases. The degree of synergism varied with the type of carboxylic acid and with the metal ion. Changes in separation factor between certain pairs of cations were noted and modification of the extraction kinetics for one metal ion observed. The separation of copper from ferric iron is studied in more detail. Development of a viable separation process is hindered by the protonation of the oxime nitrogen thus preventing satisfactory backwash operation.

Introduction

THE EXTRACTION OF metal ions by carboxylic acids is well known and has been studied by many workers.[1,2] Several stoicheiometric investigations have been made and general agreement with regard to species present in the organic phase has been achieved.[2–5] However, little information is available regarding mixed complex formation and synergism in solvent extraction of metal ions with carboxylic acids. Mixed complex formation has been reported in copper ammine/naphthenic acid systems[6,7] and the copper ammine/salicylic acid system,[8] but no useful degree of synergism was obtained. Aggett *et al.* have studied the extraction of several metal ions[9,10] by salicylic acid using tributyl phosphate (TBP) as diluent and have observed the formation of di-solvated metal salicylates but again no synergism resulted. Synergism, however, has been reported in the extraction of caesium by mixtures of 4-sec-butyl-2-(α-methylbenzyl)phenol (BAMBP) and 4-phenylvaleric acid.[11] Here the carboxylic acid satisfies the valency requirements of the caesium while the BAMBP assumes the role of a solvating agent. A solvating role for carboxylic acids is assigned by Japanese workers[12] who observed synergism in the extraction of europium by benzoyltrifluoroacetone (HBFA) in the presence of carboxylic acids. The workers conclude that the carboxylic acid acts as a Lewis base and estimate the stoicheiometry of the adduct as $Eu(BFA)_3.2RH$ where RH denotes the carboxylic acid.

Joe[13] has shown that mixtures of an α-hydroxyoxime (LIX 63, General Mills Inc.)[14] and di-(2-ethylhexyl)phosphoric acid enhanced the extraction of copper from aqueous solution above the levels achieved by the individual extractants, although no attempt was made to discover the nature of this enhancement. Because this system has subsequently been the subject of patent action, the effect of replacement of the expensive dialkyl phosphoric acid with the cheaper carboxylic acids was investigated. Preliminary studies[15] showed that significant synergism occurred in the extraction of copper and cobalt with LIX 63/naphthenic acid mixtures. Further work was therefore undertaken in order to determine the extent of this enhancement, the effect of different carboxylic acids and the changes, if any, occurring in the well-known selectivity series for extraction of metals with carboxylic acids.[1]

Experimental and results

In all, three carboxylic acids were examined: naphthenic acid (Shell Chemical Co. Ltd.); Versatic 9–11 (Shell Chemical Co. Ltd.); and α-bromolauric acid (Ralph N. Emanuel Ltd.). The acids were employed as 0·1 M solutions in kerosene with a 10% vol.-% LIX 63 content.

Equilibrium studies

Aliquots of organic phase and aqueous phase (5 mM metal ion in 1 M-KNO_3) were equilibrated for 1 h (except Ni where 3 h were required to achieve equilibrium) in a thermostat at 25°C. The phases were then separated, the pH of the aqueous phase measured and the metal ion distribution between the two phases determined. The pH was varied by the addition of acid or alkali to the aqueous phase prior to equilibration. The metal ions studied were Cu^{2+}, Fe^{3+}, Ni^{2+}, Co^{2+}, Cd^{2+} and Zn^{2+}.

The extraction results for copper, iron, nickel and cobalt for α-bromolauric acid, Versatic 9–11, naphthenic acid/LIX 63 mixtures and LIX 63 are shown in Figs 1–4 as percentage extraction vs. pH plots. The relative selectivity of the organic phases for the metal ions can be seen by the table of $pH_{0.5}$ values in Table I.

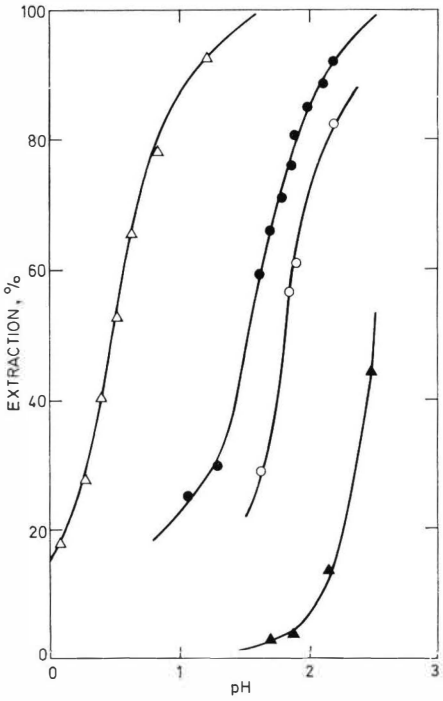

FIG. 1. *Extraction of copper by LIX 63 and LIX 63/carboxylic acid*

▲ 10 vol.-% LIX 63 in kerosene; ○ 10 vol.-% LIX 63/0·1 M naphthenic acid in kerosene; ● 10 vol.-% LIX 63/0·1 M Versatic 9–11 acid in kerosene; △ 10 vol.-% LIX 63/0·1 M α-bromolauric acid in kerosene

TABLE I

$pH_{0.5}$ values in the extraction of metal ions with LIX 63/carboxylic acid mixtures

Extractant	$pH_{0.5}$					
	Cu^{2+}	Fe^{3+}	Ni^{2+}	Co^{2+}	Cd^{2+}	Zn^{2+}
LIX 63/α-bromolauric acid	0·46	1·30	1·02	1·48	ND*	ND*
LIX 63/Versatic 9–11	1·51	1·77	ND*	ND*	ND*	ND*
LIX 63/naphthenic acid	1·78	1·78	2·20	3·05	3·38	3·72
LIX 63 (10%)	2·50	2·22	5·32	5·65	ND*	Not extracted
†α-bromolauric acid (0·1 M)	3·10	1·70	3·70	4·70	ND*	ND*
naphthenic acid (0·1 M)	4·54	2·75	6·80	6·99	ND*	ND*

* ND = not determined; † from Blumberg & Meltzer[16]

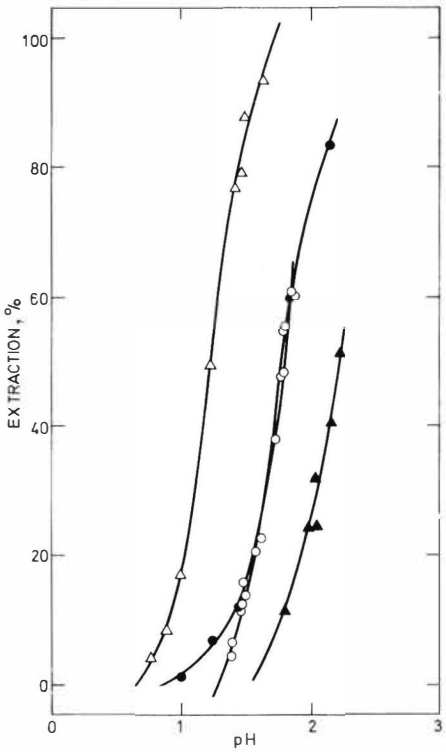

FIG. 2. *Extraction of ferric iron by LIX 63 and LIX 63/carboxylic acid*
▲ 10 vol.-% LIX 63 in kerosene; ○ 10 vol.-% LIX 63/0·1 M naphthenic acid in kerosene; ● 10 vol.-% LIX 63/0·1 M Versatic 9–11 acid in kerosene; △ 10 vol.-% LIX 63/0·1 M α-bromolauric acid in kerosene

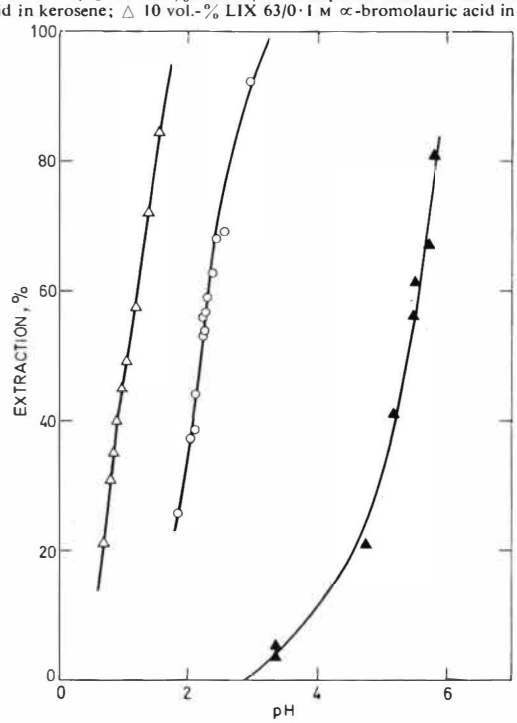

FIG. 3. *Extraction of nickel by LIX 63 and LIX 63/carboxylic acid*
▲ 10 vol.-% LIX 63 in kerosene; ○ 10 vol.-% LIX 63/0·1 M naphthenic acid in kerosene; △ 10 vol.-% LIX 63/0·1 M α-bromolauric acid in kerosene

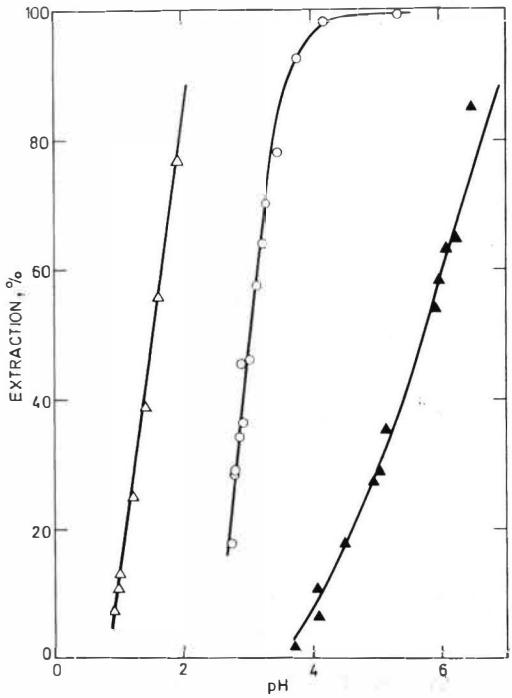

FIG. 4. *Extraction of cobalt by LIX 63 and LIX 63/carboxylic acid*

▲ 10 vol.-% LIX 63 in kerosene; ○ 10 vol.-% LIX 63/0·1 M naphthenic acid in kerosene; △ 10 vol.-% LIX 63 0·1 M α-bromolauric acid in kerosene

The results show that significant synergism occurs with divalent metal ions but only slight enhancement occurs with ferric iron. A shift in the selectivity series is also found which in the case of the α-bromolauric acid/LIX 63 system yields a selectivity reversal for copper and ferric iron and nickel and ferric iron. This is exemplified in Fig. 5 where the results for this system are shown as log D vs. pH plots. It will also be noted from Table I that a significant increase in separation factor between nickel and cobalt has occurred compared with the parent systems, particularly for the LIX 63/naphthenic acid system.

Based on the results shown in Fig. 5, it can be seen that α-bromolauric acid/LIX 63 should be a useful extractant for copper. Further development was therefore undertaken.

Separation of copper and ferric iron

Extraction tests

Extraction isotherms were obtained in the following manner. Various volumes of the organic phase (10% LIX 63 /0·1 M α-bromolauric acid in kerosene) were contacted with various volumes of aqueous phases containing copper so as to yield results covering a range of final concentrations of metal ions in both the organic and aqueous phases. Tests showed that two minutes contact time was sufficient to reach equilibrium and this equilibration time was employed in all tests. After equilibration the phases were separated, the pH was measured and the metal distribution determined. The results for a 2 g/l solution of copper as sulphate at initial pH values of 2·0, 1·5 and 1·0 are shown in Fig. 6, and for a 10 g/l solution of copper at pH 2·0 in Fig. 7. The results show that a satisfactory countercurrent extraction of copper up to concentrations of 10 g/l can be achieved with this system.

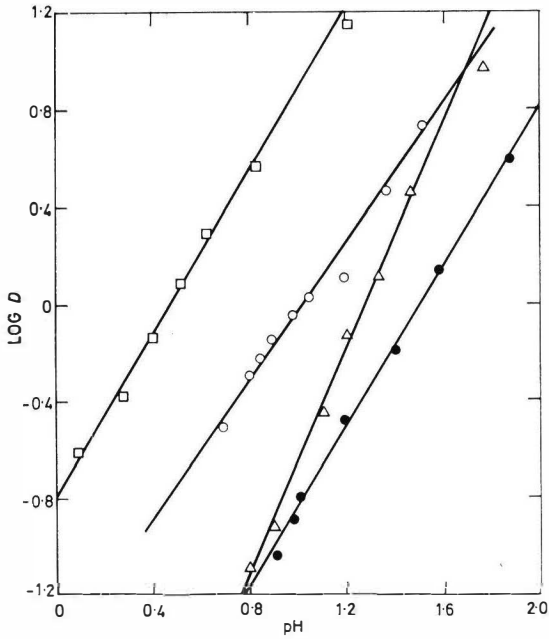

FIG. 5. *Extraction of Cu, Fe(III), Ni and Co by LIX 63/α-bromolauric acid/kerosene: variation of log* D *wth pH*

□ Cu; △ Fe(III); ○ Ni; ● Co

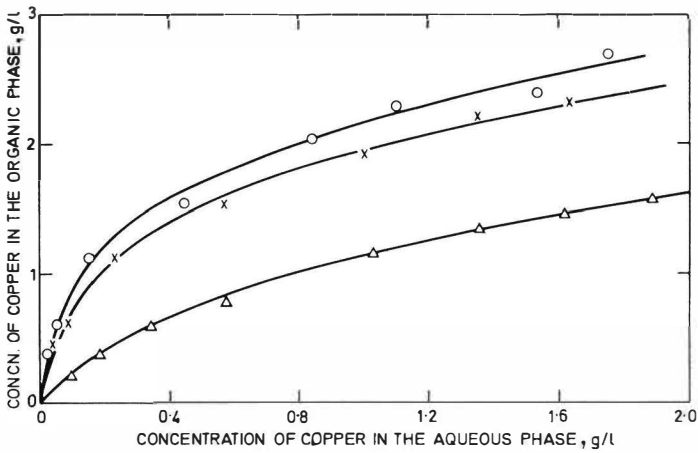

FIG. 6. *Extraction of copper by LIX 63/α-bromolauric acid: effect of pH of the feed solution*

○ pH 2·0; × pH 1·5; △ pH 1·0

Backwashing tests

The effect of sulphuric acid concentration on the backwashing of copper from the organic phase was examined by contacting organic phases containing ~ 2·0 g/l copper with equal volumes of aqueous phases of various sulphuric acid concentrations. The results are shown in Fig. 8. Surprisingly, there is a maximum in the amount of copper backwashed at 150 g/l H_2SO_4.

Further tests showed that the backwash isotherm at room temperature did not provide satisfactory results and a further isotherm was obtained at 50°C using 150 g/l H_2SO_4. The two isotherms are shown in Fig. 9.

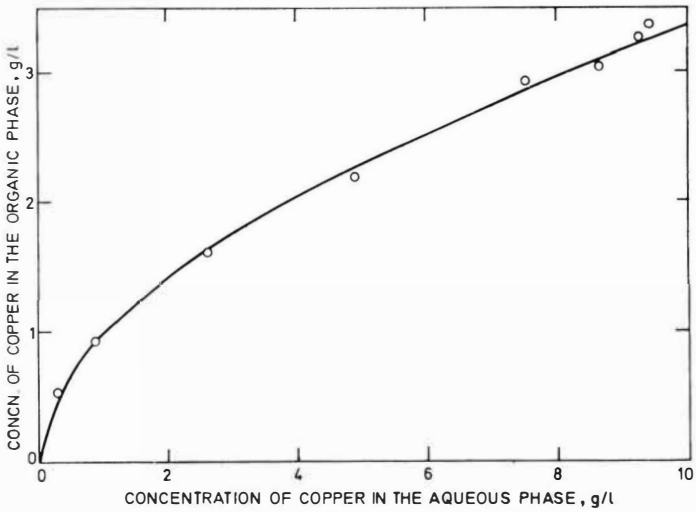

FIG. 7. *Extraction of copper from a 10 g/l solution by LIX 63/α-bromolauric acid*

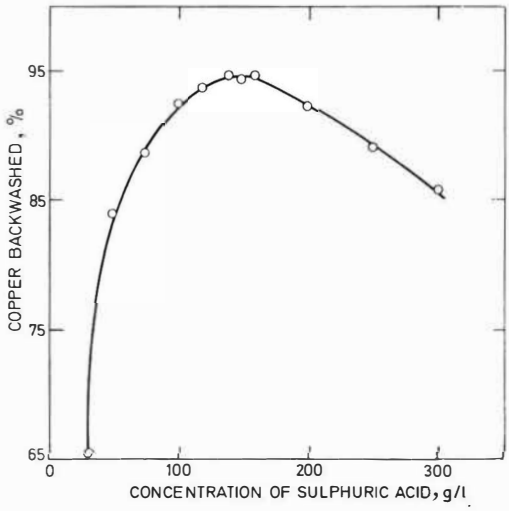

FIG. 8. *Backwashing of copper from LIX 63/α-bromolauric acid, effect of sulphuric acid concentration at room temperature*

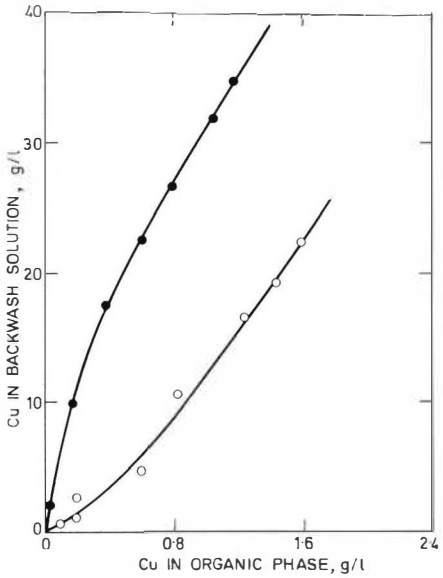

FIG. 9. *Backwashing isotherms: Cu-loaded LIX 63/α-bromolauric acid with dilute H_2SO_4*
○ Loaded organic phase containing 2·7 g/l Cu backwashed with 10 vol.-% H_2SO_4 at room temperature; ● loaded organic phase containing 2·1 g/l Cu backwashed with 150 g/l H_2SO_4 at 50°C

Discussion

Synergism has been defined as the enhancement in extraction achieved by a combination of solvents (or extractants) S_1 and S_2 in excess of that which could be expected from the distribution ratios of the components separately, viz,

$$D_{exp} = D_{S_1} + D_{S_2} + \Delta D$$

where ΔD is the magnitude of the synergistic enhancement of extraction.

The existence of synergistic enhancement of extraction with LIX 63/carboxylic acid mixtures has been demonstrated for the extraction of copper and cobalt[15] where the carboxylic acid is naphthenic acid. Examination of Table I shows the presence of appreciable synergism for copper, nickel and cobalt in all systems and shows the very small enhancement for ferric iron. There is insufficient data to comment on the cadmium and zinc results except to note that LIX 63 alone does not extract zinc appreciably. The order of extractability in the case of LIX 63/naphthenic acid tends to be closer to that of LIX 63 than naphthenic acid because nickel and cobalt are preferred to cadmium and zinc. The increasing enhancement of copper extraction as the carboxylic acid is changed from naphthenic acid through Versatic 9–11 to α-bromolauric acid coupled with the relatively small changes in the extraction of ferric iron, thus giving rise to the selectivity reversal of copper and ferric iron, suggests that it is the carboxylic acid that is solvating the LIX 63 chelate rather than *vice versa* as suggested previously.[15]

This conclusion is based on the co-ordinately unsaturated condition of LIX 63 chelates with metals such as nickel and cobalt, where two co-ordination positions are available to form carboxylic acid adducts thus giving rise to large enhancements in extraction. The results show the expected synergism even to the extent of a nickel/ferric iron selectivity reversal with α-bromolauric acid. It is likely that stoicheiometric studies might show a 1:1 ratio of LIX 63: carboxylic acid in the Ni and Co complexes. Copper is different because a four co-ordination state exists, but other co-ordination states are well known and it will be of interest to study this ion further. In the case of ferric ion, therefore, the LIX 63 could be expected to co-ordinately saturate the iron. To

incorporate carboxylic acid molecules, then, either a higher co-ordination state must be achieved or chelate bonds must be broken. Hence large enhancements in the extraction of ferric iron are unlikely.

From the above deduction it is clear that the donor properties of the carbonyl oxygen are of importance and it will be of interest to see the effect of compounds with more basic oxygen atoms.

The extraction of nickel in these systems is worthy of comment. Preliminary tests showed that nickel extracts very slowly taking ~ 3 h to come to equilibrium at room temperature. This slow rate of extraction is found only with the LIX 63/carboxylic acid system for equilibrium is reached in a matter of minutes with the individual components. Comparison of the rate of extraction of nickel with LIX 63 and nickel with LIX 63/naphthenic acid is shown in Fig. 10. The reason for this slow extraction is not known.

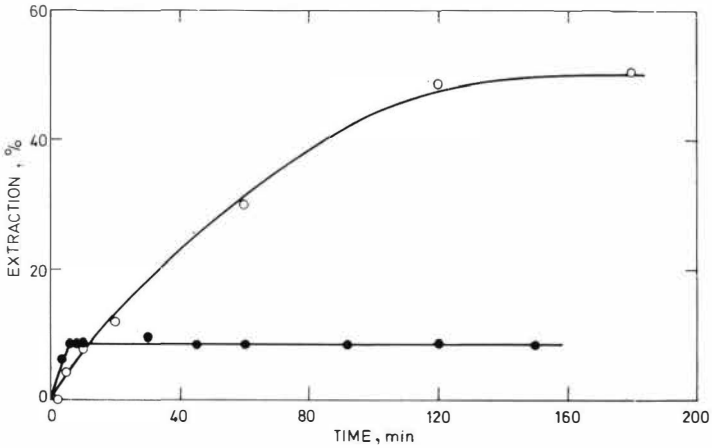

FIG. 10. *Rate of nickel extraction by LIX 63/kerosene and LIX 63/naphthenic acid in kerosene*
● 10 vol.-% LIX 63 in kerosene; ○ 10 vol.-% LIX 63/0·1 M naphthenic acid in kerosene

The low pH range for copper extraction with LIX 63/α-bromolauric acid coupled with the selectivity reversal between copper and ferric iron bears favourable comparison with LIX 64, the 2-hydroxybenzophenoneoxime introduced by General Mills for copper recovery from iron bearing dilute acidic leach liquors.[17–19] At the $pH_{0.5}$ value for copper the separation factor $\log \beta \frac{Cu^{2+}}{Fe^{3+}} =$ 2·15 for LIX 63/α-bromolauric acid compared with 2·05 for LIX 64,[20] while the respective $pH_{0.5}$ values are 0·46 and 1·05 (Flett, D. S., & West, D. W., unpublished data). Data for the newer reagent LIX 64N are not available. Thus, while the copper–iron separation is similar, the range of operation of the LIX 63/α-bromolauric acid system extends to lower pH values. This is demonstrated in Fig. 6 where a 2 g/l copper solution at an input pH of 1·0 still yields a satisfactory extraction isotherm. The ability of the system to operate at lower pH values also allows the system to handle solutions containing much higher copper concentrations, as shown in Fig. 7 for a 10 g/l copper solution at pH 2·0.

While satisfactory operation of an extraction system is therefore anticipated, the behaviour of the copper-loaded organic phase in backwash conditions is less satisfactory. The maximum in the amount of copper backwashed on increasing the sulphuric acid concentration, Fig. 8, is quite unusual and requires explanation. The answer would seem to lie in the nitrogen of the oxime group which will be weakly basic. Thus, at a certain acidity this nitrogen will protonate and will thus be capable of forming ion pairs with anions. This was tested by contacting LIX 63/α-bromolauric acid solution with sulphuric acid of

different concentrations at room temperature and measuring the change of acid concentration in the aqueous phase. The results, including one for HCl, are shown in Table II.

TABLE II

Uptake of mineral acid by LIX 63/α-bromolauric acid

	Sulphuric acid					Hydrochloric acid
Concentration in aqueous phase, g/l	150	243·87	298·24	343·57	388·53	116·8
Concentration in organic phase, g/l	0	1·13	1·76	3·43	6·97	3·2

Table II shows clearly that above 150 g/l H_2SO_4 uptake of acid becomes measurable and this agrees well with the maximum in Fig. 8. It appears that the copper is being retained in the organic phase as a sulphato complex. A noticeable change in colour of the organic phase occurs and spectrophotometric studies should confirm this. Some difficulty was found by Swanson & Agers[20] in achieving a satisfactory backwash of copper from LIX 63 alone and this is undoubtedly due to the protonation of the oxime nitrogen. It is also significant that the nitrogen is much less basic in LIX 64 and consequently no backwashing problems occur.

Examination of the copper backwash isotherm (Fig. 9), therefore, shows that the backwashing of copper with a solution containing ~ 30 g/l copper, which might occur in a spent tankhouse electrolyte, would not be possible because operating lines on a McCabe–Thiele Construction would lie on the wrong side of the isotherm. Operation would be possible at an input copper concentration of ~ 15 g/l and 150 g/l H_2SO_4 with a final aqueous backwash concentration of ~ 20 g/l. It may be possible to operate a tankhouse under these conditions but there is too little flexibility in the system for it to be commercially attractive.

Similarly, while the increase in nickel/cobalt separation factors are attractive and the selectivity reversal of nickel and ferric iron is a spectacular success for the system, the adverse kinetics of nickel extraction are likely to preclude commercial application of LIX 63/carboxylic acid systems to the solvent extraction of these metals.

Conclusions

Studies on the extraction of several metal ions (Cu, Fe, Ni, Co, Cd, Zn) with various carboxylic acids/α-hydroxyoxime mixtures have showed that appreciable synergism occurred in many cases. The degree of synergism varied with the type of metal ion and with the carboxylic acid type. A selectivity reversal between copper and ferric iron in the system LIX 63/α-bromolauric acid was of sufficient magnitude to warrant further investigation. Development of a viable separation process was hindered by the protonation of the oxime nitrogen, thus preventing satisfactory backwash operation. The unexpectedly slow rate of extraction of nickel by the mixed reagents is likely to discourage development of separation processes of nickel from cobalt with LIX 63/naphthenic acid and of nickel from ferric iron with LIX 63/α-bromolauric acid.

References

[1] Fletcher, A. W., & Flett, D. S., in 'Solvent extraction chemistry', 1965, p. 359 (London: Macmillan)

[2] Marcus, Y., & Kertes, A. S., 'Ion exchange and solvent extraction of metal complexes', 1969, p. 551 (London: Wiley-Interscience), and references contained therein

[3] Tanaka, M., Nakasuka, N., & Sasane, S., *J. inorg. nucl. Chem.*, 1969, **31,** 2591

[4] Schweitzer, G. K., & Clifford, F. C., *Analytica chim. Acta*, 1969, **45,** 57

[5] Schweitzer, G. K., & Stevens, R. H., *Analytica chim. Acta*, 1969, **45,** 192

[6] Flett, D. S., & West, D. W., *J. inorg. nucl. Chem.*, 1967, **29,** 1365

[7] Flett, D. S., *Trans. N.R.I.M. Tokyo*, 1967, **9,** 215

[8] Aggett, J., & Billinghurst, M. W., *J. inorg. nucl. Chem.*, 1969, **31,** 513

[9] Aggett, J., & Crossley, P., *J. inorg. nucl. Chem.*, 1967, **29,** 1113

[10] Aggett, J., Evans, D. J., & Hancock, R., *J. inorg. nucl. Chem.*, 1968, **30,** 2529

[11] Zingaro, R. A., & Coleman, C. F., *J. inorg. nucl. Chem.*, 1967, **29,** 1287

[12] Shigematsu, T., Tabushi, M., Matsui, M., & Honjyo, T., *Bull. chem. Soc. Japan*, 1969, **42,** 976

[13] Joe, E. G., Ritcey, G. M., & Ashbrook, A. W., *J. Metals, N.Y.*, 1966, **18,** 18

[14] Swanson, R. R., U.S. P. 3,224,873

[15] Flett, D. S., & Titmus, S., *J. inorg. nucl. Chem.*, 1969, **31,** 2612

[16] Blumberg, R., & Meltzer, P., *7th int. Miner. Process. Conf.*, 1964, Part III, 139 (New York: Gordon & Breach)

[17] Agers, D. W., House, J. E., Swanson, R. R., & Drobnick, J. C., *Trans. Soc. mech. Engrs*, 1966, **235,** 191

[18] Agers, D. W., & DeMent, E. R., Paper to joint meeting Rocky Mountain Minerals Conf. and Fall Meeting of Soc. Mech. Engrs, Las Vegas, Sept. 1967

[19] Swanson, R. R., U.S. P. 3,428,449

[20] Swanson, R. R., & Agers, D. W., Paper presented to 23rd Annual Meeting, A.I.M.E., New York, Feb. 1964

Transfer of iron in a liquid–liquid extraction system

by K. Južnič and Š. Fedina
Institute 'Jozef Stefan', Ljubljana, Yugoslavia

The self-diffusion and liquid–liquid interfacial transfer coefficients of iron(III) species have been measured in an equilibrated extraction system at different temperatures by the capillary technique. Absolute viscosities of both phases of the extraction system under study were determined at the respective temperatures with Ubbelohde's viscometer. From the data obtained, the radii of the iron(III) species in solution and the free energies of activation for the diffusion and the transfer across the liquid–liquid interface were calculated.

Introduction

THE TRANSFER PROCESSES taking place in a static extraction system in equilibrium are self-diffusion and transfer across the liquid–liquid interface. It is interesting to have data for these processes, because if the viscosities are known the size of the diffusing particles and the magnitude of the energy barrier at the liquid–liquid interface can be calculated. The transfer in two such systems has been studied[1,2] in this laboratory, viz. the transfer of zinc(II) and the transfer of antimony(III). In both cases hydrochloric acid was used in the aqueous medium, while tri-n-octylamine (TOA) and trioctylphosphine oxide (TOPO) in *m*-xylene, respectively, formed the organic phase. This paper reports the transfer of iron(III) in an extraction system in which the metal is distributed between aqueous hydrochloric acid and an organic solution of TOA in *m*-xylene.

Experimental

Reagents

Iron(III) chloride, hydrochloric acid (analytical grade) and *m*-xylene (Puriss) were supplied by Riedel de Haen Co. Tri-n-octylamine (TOA) was obtained from Koch-Light Co. ^{59}Fe as chloride with a specific activity greater than 3 mCi/mg was obtained from the Radiochemical Centre, Amersham.

Procedure

The extraction systems were prepared by shaking together equal volumes of 0·0686M iron(III) chloride in 4M hydrochloric acid and 0·0686M TOA in *m*-xylene in a thermostated shaker for two hours at the selected temperature. For each equilibration a separate smaller quantity of a chemical identical system labelled with radioisotope was prepared in the same way. This was used to fill the capillaries for measuring the diffusion and interfacial transfer coefficients. A detailed description of the procedure is given in a previous paper.[2] The viscosities were determined with Ubbelohde's suspended meniscus viscometer. Densities were measured with a 100 ml pycnometer. All measurements were performed in a water bath with temperature fluctuations within $\pm 0 \cdot 03$ °C.

Results

The values of the distribution coefficients (K_a^o) for iron in the prepared extraction systems at different temperatures together with the results for the self-diffusion (D) and interfacial transfer coefficients (α) are shown in Table I.

TABLE I

Self-diffusion and interfacial transfer coefficients

t, °C	K_a^o	D, 10^{-6} cm²/sec aqueous	D, 10^{-6} cm²/sec organic	α, 10^{-4} cm/sec
25	1·27	6·11	2·90	0·4
35	1·31	7·37	3·75	0·6
45	1·45	9·11	4·78	—
55	1·55	10·87	6·15	1·2

Each result of D and α given in Table I is the arithmetic mean of three results obtained in a single run. The precision and deviations from the mean of the observed values were the same as reported previously.[2] The energies of activation for diffusion in the aqueous and organic phases were found to be 3689 and 4223 cal/mole, respectively.

The results of measured flow times (τ) in the viscometer together with densities (ρ) and absolute viscosities (η) are given in Table II. Doubly distilled water was used as a reference liquid[3] to determine the characteristics of the viscometer.

TABLE II

Flow times, densities and viscosities

t, °C	τ, sec water	τ, sec aqueous	τ, sec organic	ρ, g/cm³ aqueous	ρ, g/cm³ organic	η, cP aqueous	η, cP organic
25	245·1	291·7	223·8	1·06643	0·86419	1·1427	0·7005
35	200·0	245·0	200·0	1·06203	0·85605	0·9527	0·6194
45	167·4	209·3	180·8	1·05782	0·84750	0·8083	0·5543
55	143·9	182·7	165·0	1·05373	0·84024	0·6983	0·4990

By means of the Stokes–Einstein relation, $r = kT/6\pi\eta D$, where k is Boltzmann's constant, η is the absolute viscosity, and T is the absolute temperature, the radii (r) of iron(III) species were calculated. Free energies of activation for the diffusion (F_d) and transfer across the interface (F_i) were obtained according to the following equations:[4]

$$D = l^2kT/h \exp(-F_d/RT) \text{ and}$$
$$\alpha = lkT/h \exp(-F_i/RT)$$

where l is the distance between two equilibrium positions in a liquid. Approximate values of 6×10^{-8} cm for *m*-xylene and 4×10^{-8} cm for water were obtained from $l = (V/N)^{1/3}$ where V is the molar volume of the liquid and N is Avogadro's number. The results of the radii and free energies of activation are summarised in Table III.

TABLE III

Radii of iron(III) species and free energies of activation for diffusion and interfacial transfer

t, °C	r, 10^{-8} cm aqueous	r, 10^{-8} cm organic	F_d, 10^3cal/mole aqueous	F_d, 10^3cal/mole organic	F_i, 10^4cal/mole
25	3·12	10·74	4·38	5·30	1·3
35	3·21	9·71	4·43	5·43	1·4
45	3·16	8·79	4·46	5·38	—
55	3·16	7·82	4·51	5·40	1·4

Discussion

Since its introduction[5] the capillary technique has been widely used for the measurement of self-diffusion coefficients. Its accuracy and reliability and comparisons of the results with those obtained by other methods have been reported by several authors.[6,7]

To obtain good results by this method it is recommended that the i.d. of capillaries should be less than 1 mm and the length sufficient to ensure that disturbances at the capillary mouth become negligible. To meet these requirements capillaries with i.d. 0·4 mm and 3 cm long were used. As stated previously[2] the accuracies of the interfacial transfer coefficients determined by the modified capillary technique depend on their relative magnitude with regard to the rate of diffusion in a liquid. In the present case the transfer across the interface was relatively fast in comparison with the rate of diffusion in the liquid, and therefore the transfer coefficients are relatively inaccurate. Deviations from the mean of parallel measurements were up to 30%.

Only a few comparable data on self-diffusion of iron(III) species in aqueous solutions can be found in the literature. The values of $6{\cdot}7 \times 10^{-6}$ and $5{\cdot}4 \times 10^{-6}$ cm^2/sec for 1·0M and 0·033M iron(III) chloride respectively, given by Ziolkowski[8] are similar to the present authors' results at corresponding temperatures.

A comparison of the diffusion data for iron(III) species with those for antimony(III)[2] in a similar extraction system shows that the values for the latter are about 20 and 60% higher in the aqueous and organic phases, respectively. Consequently, the calculated radii of iron species were found to be appreciably greater than for those of antimony. This suggests higher hydration of iron(III) chloride in hydrochloric acid and furthermore that the iron complex is more aggregated in the organic phase than is that of antimony. The energies of activation for the diffusion of both metals in the aqueous phase are relatively similar, while those for organic phase differ; the higher value for iron is probably due to dissociation of its complex with elevation of temperature.

As seen in Table III, the free energies of activation for the diffusion are much lower than those for the transfer across the interface. According to the theory the former represent the energies necessary for formation of holes for the particles to diffuse into and are usually fractions of the vaporisation energies of molecules. The transfer energies may be attributed to a chemical reaction taking place on transfer across the interface, viz. breakage of hydrogen bonds between metal species and water molecules. Since the breakage of hydrogen bonds requires 2·5 kcal/mole of O–H . . . O in water[9] and a similar value may be expected in the present case, it may be said that the separation of several water molecules from the metal species is associated with the transfer across an interface.

References

[1] Južnič, K., *J. inorg. nucl. Chem.*, 1968, **30,** 2270
[2] Južnič, K., & Fedina, Š., *J. inorg. nucl. Chem.*, 1970, **32**, 3673
[3] Korson, L., Hansen, W. D., & Milero, F. J., *J. phys. Chem., Ithaca*, 1969, **73,** 34
[4] Glasstone, S., Laidler, K. J., & Eyring, H., 'Theory of rate processes', 1941 (New York: McGraw-Hill Book Co. Inc.)
[5] Anderson, J. S., & Saddington, K., *J. chem. Soc.*, 1949, p. 381
[6] Wang, J. H., *J. Am. chem. Soc.*, 1952, **74,** 1182
[7] Mills, R., & Kennedy, J. W., *J. Am. chem. Soc.*, 1953, **75,** 5696
[8] Ziolkowski, J., *Nukleonika*, 1967, **12,** 619
[9] Walrafen, G. E., 'Hydrogen-bonded solvent systems', (Eds Covington, A. K., & Jones, P.), 1968, p. 9 (London: Taylor and Francis Ltd.)

Reduction of cupric ion by ferrous ion with solvent extraction

by H. Kametani
National Research Institute for Metals, 2 Chome, Nakameguro, Meguro-ku, Tokyo, Japan

The reduction of cupric ion in chloride solutions to a cuprous complex and that of the cuprous complex to metallic copper by ferrous ion were studied using an organic solvent, a kerosene solution of Versatic acid 911. If the pH is increased by the addition of sodium hydroxide solution the reactions

$$Cu^{2+} + Fe^{2+} + 3\,H_2O + 2\,Cl^- = CuCl_2^- + Fe(OH)_3 + 3\,H^+$$
$$CuCl_2^- + Fe^{2+} + 3\,H_2O = Cu^0 + Fe(OH)_3 + 3\,H^+ + 2\,Cl^-$$

proceed to the right, and the precipitation of ferric hydroxide is eliminated by the extraction of the iron by the solvent. The first reduction takes place in the pH range 1·5–4, and the second reduction from pH 5–6 for chloride solutions of initial concentrations, 0·1M-Cu^{2+}, 0·1–0·2M-Fe^{2+}, and 3M-NaCl.

The reduction processes proceeded nearly quantitatively and fast at 40°C, but difficulties were encountered owing to the poor phase separability between the aqueous solution and the solvent in the presence of ferric ion in the pH region lower than 4, the co-extraction of ferrous ion with ferric ion in the pH region higher than 2, and the extraction of calcium ion by the solvent in the pH region higher than 5, when calcium hydroxide was used in place of sodium hydroxide.

Introduction

IT HAS BEEN reported that in a chloride solution cupric ion is reduced by ferrous ion first to cuprous ion and then to metallic copper at pH values of ~ 3 and 5, respectively.[1] It is also known that ferrous ion, ferric ion, and cupric ion in dilute chloride solutions are extracted by kerosene solutions of carboxylic acids at pH values higher than 4·5, 2, and 4, respectively.[2–4] Cuprous ion, which appears in the reduction process as an intermediate species, is not extracted by the solvent from chloride solution at a pH lower than 6. The purpose of this study was to separate the metallic copper formed from the simultaneously precipitated ferric hydroxide.

Experimental

Experiments on the reduction with simultaneous solvent extraction were made using a 2-l flask with a stirring screw made of glass, a glass electrode, a Pt electrode, and a saturated calomel electrode (S.C.E.), with which the pH and the potential of the chloride solutions and the solvent, of total volume 1·5 l, were measured directly and continuously. A 50-ml burette was connected to the flask so as to permit dropwise addition of a solution of 4N or 5N sodium hydroxide to the chloride solution to change the pH. Air in the flask was expelled by argon gas, and the reaction was carried out at a temperature of 40 ± 1°C.

The concentrations of chlorides in the aqueous phase were 3·0M-NaCl 0·1 M-$CuCl_2.2H_2O$, and 0·1–0·2 M-$FeCl_2.4H_2O$, and a 20 vol.-% kerosene solution of Versatic acid 911 was used as the solvent. The volume ratio of the solvent to aqueous solution was 1 : 1.

The aqueous solution and an equal volume of the solvent were placed in the flask and mixed by stirring. After the addition of a few ml of NaOH solution, stirring was continued until the pH was constant. The mixture was allowed to settle for 10 min and then sampled. The sample solutions of the aqueous phase taken at proper intervals of pH were immediately titrated by $KMnO_4$ to determine the total amount of cuprous ion and ferrous ion, followed by individual

determination of total Fe and total Cu after separation by NH_4OH. Samples of the organic phase were back-extracted by 6N-HCl solution under nitrogen gas. In cases of poor phase separability, the samples were centrifuged. It was found that the pH value of the stirred emulsion was generally somewhat lower than that of the separated aqueous solution.

Results and discussion

Reduction of cupric ion by ferrous ion

The thermodynamic and kinetic details of the reduction reactions have been reported[1] for the sulphate solution-system and the chloride solution-system. The reduction of Cu^{2+} to Cu^0 in chloride solution takes place in two steps as illustrated by a theoretical potential–pH diagram at 25°C, Fig. 1.

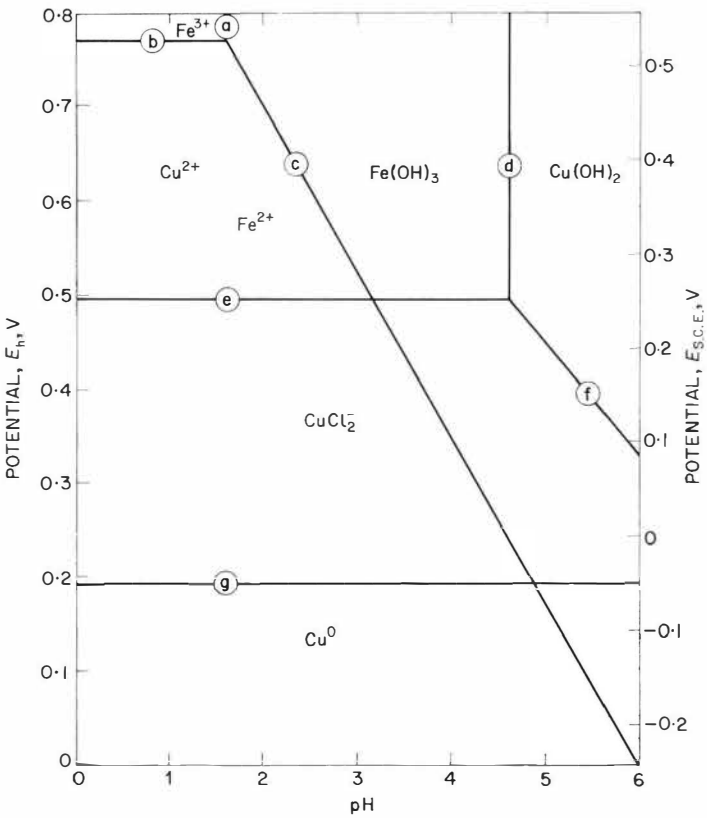

FIG. 1. *Potential–pH diagram for the chloride system at 25°C*

(a) $Fe^{3+} + 3H_2O = Fe(OH)_3 + 3H^+$
(b) $Fe^{2+} = Fe^{3+} + e$
(c) $Fe^{2+} + 3H_2O = Fe(OH)_3 + 3H^+ + e$
(d) $Cu^{2+} + 2H_2O = Cu(OH)_2 + 2H^+$
(e) $CuCl_2^- = Cu^{3+} + 2Cl^- + e$
(f) $CuCl_2^- + 2H_2O = Cu(OH)_2 + 2H^+ + 2Cl^- + e$
(g) $Cu^0 + 2Cl^- = CuCl_2^- + e$

The first step is the reduction of Cu^{2+} to Cu^+, which forms a chloride complex, $CuCl_2^-$. In Fig. 1 (for 1·0M concentration) the horizontal straight line (e) which represents the redox reaction (1) intersects the inclined straight line (c) which represents the reaction (3) at pH 3·2, the value being dependent to some extent on the concentrations of Cu^{2+}, $CuCl_2^-$, Cl^-, and Fe^{2+} according to Equations (2) and (4).

$$Cu^{2+} + 2\,Cl^- + e = CuCl_2^- \quad . \quad . \quad . \quad . \quad . \quad . \quad . \quad (1)$$

$$E_h = 0{\cdot}496 + 0{\cdot}059 \log [Cu^{2+}] - 0{\cdot}059 \log [CuCl_2^-] + 0{\cdot}118 \log [Cl^-] \quad . \quad . \quad . \quad . \quad . \quad . \quad . \quad (2)$$

$$Fe^{2+} + 3\,H_2O = Fe(OH)_3 + 3H^+ + e \quad (3)$$

$$E_h = 1{\cdot}057 - 0{\cdot}177\,pH - 0{\cdot}059 \log [Fe^{2+}] \quad (4)$$

The overall reaction is as follows:

$$Cu^{2+} + Fe^{2+} + 2\,Cl^- + 3\,H_2O = CuCl_2^- + Fe(OH)_3 + 3\,H^+ \quad (5)$$

It is reasonable to consider that $CuCl_2^-$ is oxidised by Fe^{3+} or $Fe(OH)_3$ if the pH falls below the value at the point of intersection which corresponds to the equilibrium of the reaction (5) and the reaction then proceeds to the left whereas Cu^{2+} is reduced by Fe^{2+} if the pH is greater than the value at this point and the reaction (5) then proceeds to the right.

In practical cases when a solution is prepared by dissolving the chlorides $CuCl_2$ and $FeCl_2$ it is inevitable that the solution contains a little amount of ferric ion and the concentration ratio, ferric/ferrous, determines the potential, which falls generally in the range 0·3–0·4 V (Pt electrode vs. S.C.E.). The horizontal line for the constant ferric/ferrous ratio, therefore, lies between the horizontal line (b) for ferric/ferrous = 1 and the horizontal line (e), and the pH of the intersecting point becomes lower than 3·2. The higher the value of the pH, the lower the potential becomes along the inclined line. It follows an increasing concentration of $CuCl_2^-$ and a decreasing concentration of Cu^{2+} according to Eqn (2), that is, the progress of the reduction shown in Eqn (1).

The cuprous chloride complex thus formed is further reduced to metallic copper in the second step. In Fig. 1 the horizontal straight line (g) which represents the reaction (6) intersects the inclined straight line (c), representing the reaction (3), at pH 4·9, which is also dependent on the concentration of $CuCl_2^-$ and Fe^{2+}.

$$CuCl_2^- + e = Cu^0 + 2\,Cl^- \quad (6)$$

$$E_h = 0{\cdot}194 + 0{\cdot}059 \log [CuCl_2^-] - 0{\cdot}118 \log [Cl^-] \quad (7)$$

The overall reaction is as follows.

$$CuCl_2^- + Fe^{2+} + 3\,H_2O = Cu^0 + Fe(OH)_3 + 2\,Cl^- + 3\,H^+ \quad (8)$$

An ideal cycle of a hydrometallurgical process for leaching of cupric sulphide and reduction to metallic copper is illustrated in Fig. 2. The cycle starts by addition of cupric sulphide (1 mole) into a ferric solution (2M, 1 l) at a pH somewhat lower than the pH value of hydrolysis of the ferric solution. The sulphide is dissolved oxidatively according to the reaction (9), reducing ferric ion to ferrous ion, and the potential is depressed to a value around 0·590 V (point A) where the leaching approaches completion.

$$CuS = Cu^{2+} + S^0 + 2\,e \quad (9)$$

$$E_h = 0{\cdot}590 + 0{\cdot}059 \log [Cu^{2+}] \quad (10)$$

The overall reaction is as follows:

$$CuS + 2\,Fe^{3+} = Cu^{2+} + 2\,Fe^{2+} + S^0 \quad (11)$$

The leach liquor is then filtered to recover elemental sulphur. By increasing the pH of the filtrate the point moves first horizontally until the intersecting point B, then falls along the inclined straight line which corresponds to Eqn (4) for $[Fe^{2+}] = 2$M. To be exact, the point does not move precisely along the line, but it deviates gradually from the line to the right owing to progress of the first step reduction. In the final stage of this reduction the point moves along the inclined line for $[Fe^{2+}] = 1$M.

The second step reduction begins to take place at a point C, where two straight lines, representing Eqn (4) for $[Fe^{2+}] = 1$M and Eqn (7) for $[CuCl_2^-] = 1$M, intersect. Keeping the ratio $[CuCl_2^-]$ to $[Fe^{2+}]$ equal to 1, the point moves linearly from point C to point D, where 99% completion of the reduction is assumed.

The final solution is a slurry-like mixed suspension of precipitated metallic copper and ferric hydroxide, so that either of the two precipitates must be separated from the solution to win metallic copper product. Because the formed particles of metallic copper are extremely fine at 40°C, solvent extraction of

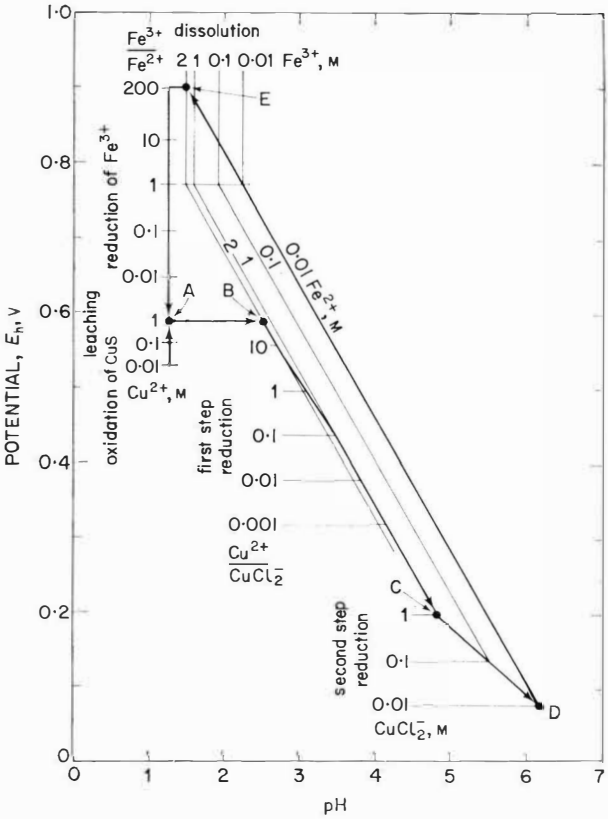

FIG. 2 *Ideal cycle for leaching of copper sulphide and reduction to metallic copper*

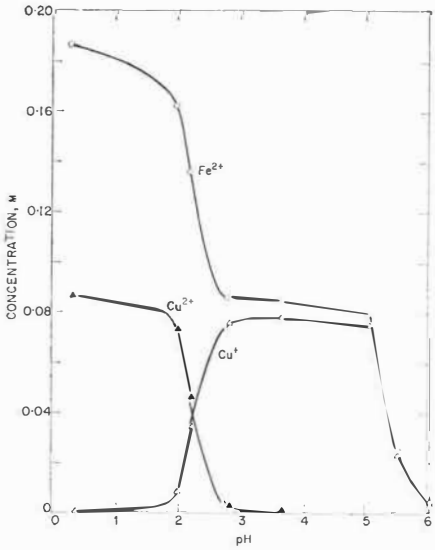

FIG. 3. *Reduction of cupric ion by ferrous ion in aqueous solution*
$Cu^{2+} : Fe^{2+} = 1 : 2$, at 40°C

the precipitated ferric hydroxide by Versatic acid is studied in this paper as a means of separation.

The solution containing ferric hydroxide (2M) and a very low concentration of ferrous ion, if precipitated copper is eliminated, is then acidified. By decreasing the pH the point moves along the inclined straight line representing Eqn (4) for $Fe^{2+} = 0 \cdot 01$M. It follows the simultaneous increase of ferric ion concentration owing to re-dissolution of the hydroxide and the solution is ready for re-use at the end point (E), which has a potential corresponding to $Fe^{3+}/Fe^{2+} = 200$ and a pH value just under the hydrolysis of 2M ferric solution.

The result for a chloride solution of the concentration ratio, $0 \cdot 1$M-Cu^{2+} : $0 \cdot 2$M-Fe^{2+}, in the absence of the solvent is shown in Fig. 3, as the variation of the concentrations of species as a function of pH. The first step reduction takes place in the pH range 2–3, and the second step reduction in the range 5–6. These variations illustrated in Fig. 3 can be explained by the reaction mechanism described above. The reductions take place nearly quantitatively and are fast at 40°C.

Extraction of individual metal ions

In Fig. 4 the results for chloride solutions containing only one species are summarised. The pH values at half-extraction are $5 \cdot 3$, $0 \cdot 9$, and $3 \cdot 2$ for Fe^{2+}, Fe^{3+}, and Cu^{2+}, respectively. These values are comparable with those previously reported for dilute chloride solutions.[2–4] Cuprous ion (a chloride complex) was not extracted in the pH range studied.

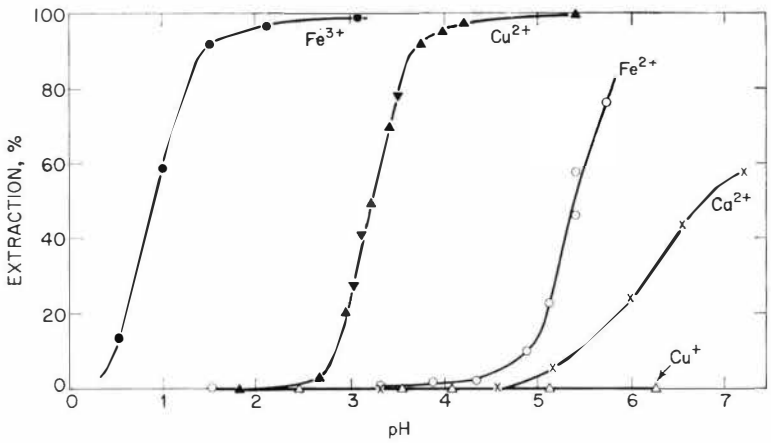

FIG. 4. *Extraction of individual metal ions by Versatic acid 911*

Reduction of cupric ion with simultaneous solvent extraction

It is expected that the reaction takes place essentially by the same process as that without solvent extraction, an example of which was shown above. The results are shown in Figs 5 and 6 for the first step reduction and in Fig. 7 for the second step.

Fig. 5 illustrates the variations of the concentration of species in the aqueous phase (Fig. 5 b) and the organic phase (Fig. 5 a) with increasing pH for the first step reduction for the initial concentrations $0 \cdot 1$M-Cu^{2+} and $0 \cdot 1$M-Fe^{2+}. The reduction begins to take place at pH $\sim 1 \cdot 5$, which is somewhat lower than that for the reduction without extraction, and approaches completion at pH ~ 4.

The results for the initial concentrations $0 \cdot 1$M-Cu^{2+} and $0 \cdot 2$M-Fe^{2+} are shown in Fig. 6. The reduction takes place as a whole in the same manner as that shown in Fig. 5. However, a great difference was found between Fig. 6

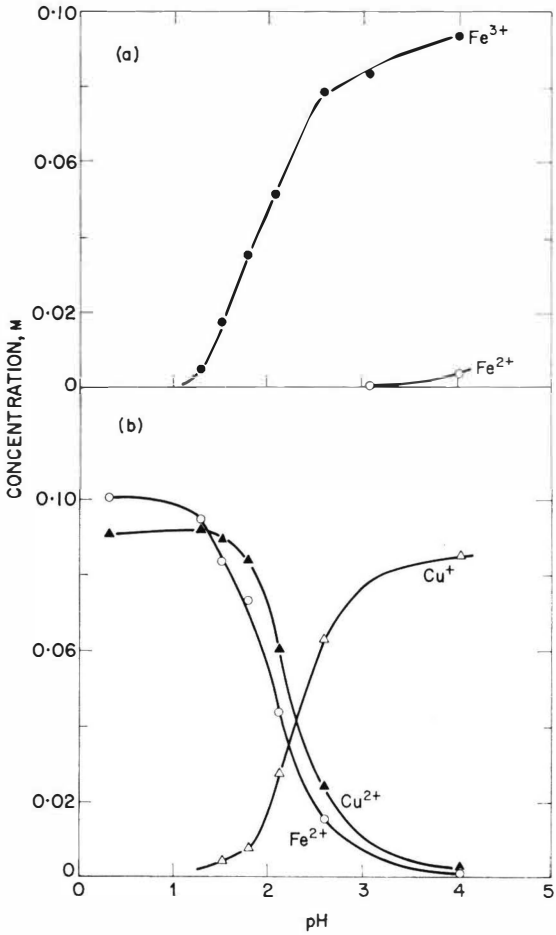

FIG. 5. *First step reduction* (Cu^{2+} : Fe^{2+} = *1* : *1*) *with extraction*
(a) Organic phase; (b) aqueous phase

and Fig. 5 in that ferrous ion was extracted by the solvent above pH 2, when the solution contains excess ferrous ion for use in the subsequent stage of reduction.

The reduction with simultaneous solvent extraction throughout the two steps is experimentally very difficult, because the viscosity of the heavily loaded solvent is so high that the emulsion turns into a liquid gel like a clay slurry in the second step, and agitation is unsatisfactory and the phase separation becomes very poor.

The second step reduction was, therefore, carried out separately from the first step. The pH of a chloride solution of initial concentrations 0·1M-Cu^{2+} and 0·1M-Fe^{2+} was raised in the presence of the solvent to reduce cupric ion to the cuprous complex, then the loaded solvent was removed from the vessel. After fresh solvent of equal volume and the proper amount of the ferrous chloride to yield a concentration of 0·1M-Fe^{2+} were added to the flask, the second step reduction was started.

Fig. 7 illustrates the second step reduction thus carried out for the initial concentrations 0·1M-$CuCl_2^-$ (which decreased to 0·08M during the first step) and 0·1M-Fe^{2+}. As a result of the extraction of ferrous ion, which was as

much as 40% of the initial concentration in accordance with the extraction results for ferrous ion shown in Fig. 4 for pH values greater than 5, about half of the total copper remained in the aqueous solution after the completion of the reduction reaction.

Metallic copper precipitated in this step as very fine particles and most of these were caught in the organic phase forming red brown flocculates.

Potential change during the reductions

The changes of potential, which were measured with a Pt electrode and a

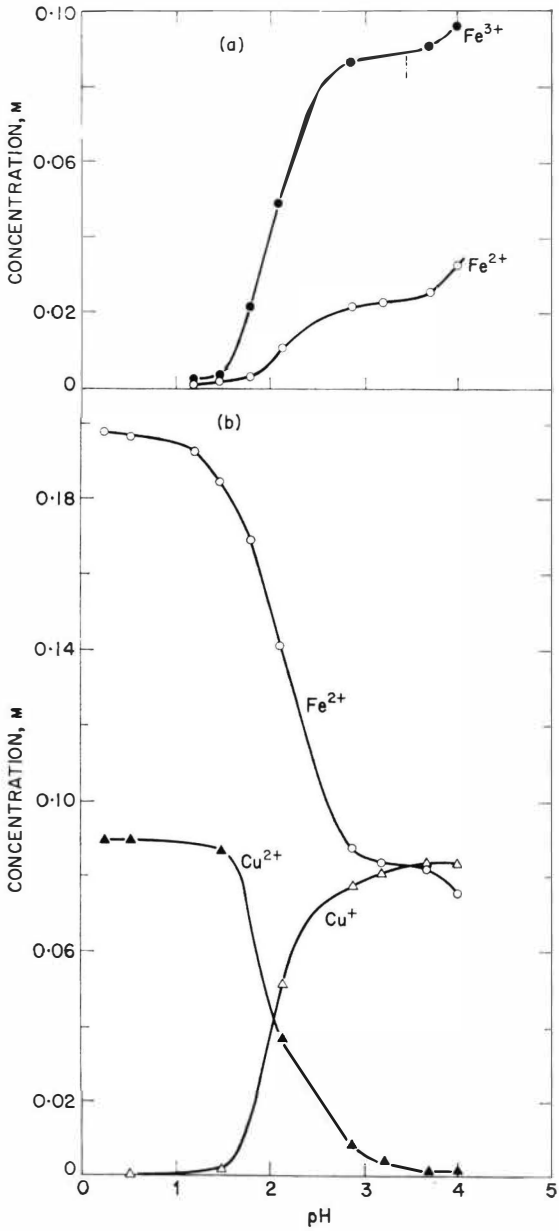

FIG. 6. *First step reduction (Cu^{2+} : Fe^{2+} = 1 : 2) with extraction*
(a) Organic phase; (b) aqueous phase

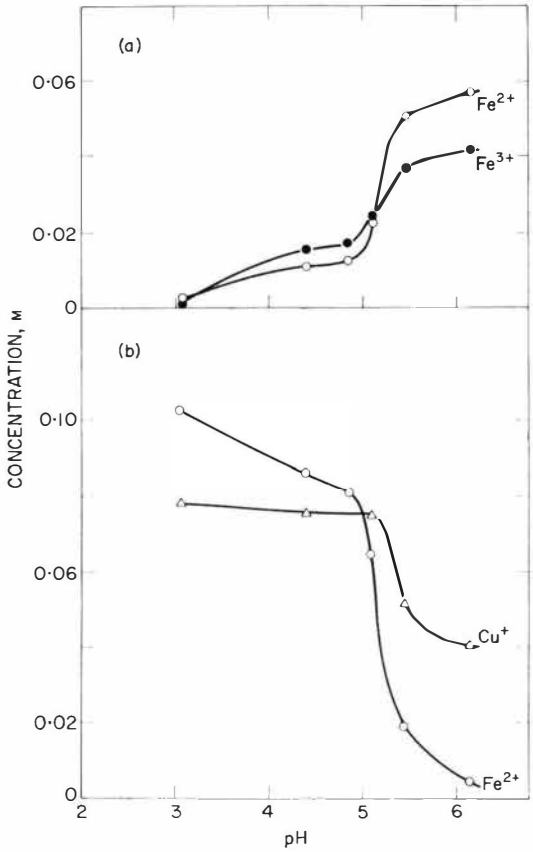

FIG. 7. *Second step reduction (Cu^{2+} : Fe^{2+} = 1 : 1) with extraction*
(a) Organic phase; (b) aqueous phase

saturated calomel electrode at 40°C, are summarised in Fig. 8. The inclined broken line in Fig. 8 represents Eqn (4) for $[Fe^{2+}] = 0 \cdot 1$ M and the horizontal broken line Eqn (7) for $[CuCl_2^-] = 0 \cdot 1$M and $[Cl^-] = 1$M at 25°C.

The first step reduction starts at the bend of the curves at about 0·4 V, pH 1·5, proceeds along the inclined nearly linear portion of the curves, and approaches completion at ~ 0 V, pH 4, where the ratio, $Cu^{2+}/CuCl_2^-$, is around 10^{-4} according to Eqn (2). This inclined portion of the curves is nearly parallel to the theoretical inclined line represented by the broken straight line. The second step reduction takes place at the second bend at about −0·2 V, pH 5, which corresponds to the intersection point of the two theoretical lines in Fig. 1. The difference between the measured curves and the theoretical lines may be attributed to differences in activities and temperatures. Together with the curves for the reductions, a curve for the simple extraction of ferrous ion is also shown in Fig. 8.

Difficulties encountered

Two important abnormalities which make experiments difficult have been found: one is the poor phase separability between the aqueous phase and the organic phase, and the other is the coextraction of ferrous ion.

It was found that during the first step reduction the phase separability between the two phases was markedly influenced by the pH of the chloride solution. Normally, aqueous phases hardly dissolve the solvent, but here the solvent, which seemed to be a brown turbid single phase after long settling, was

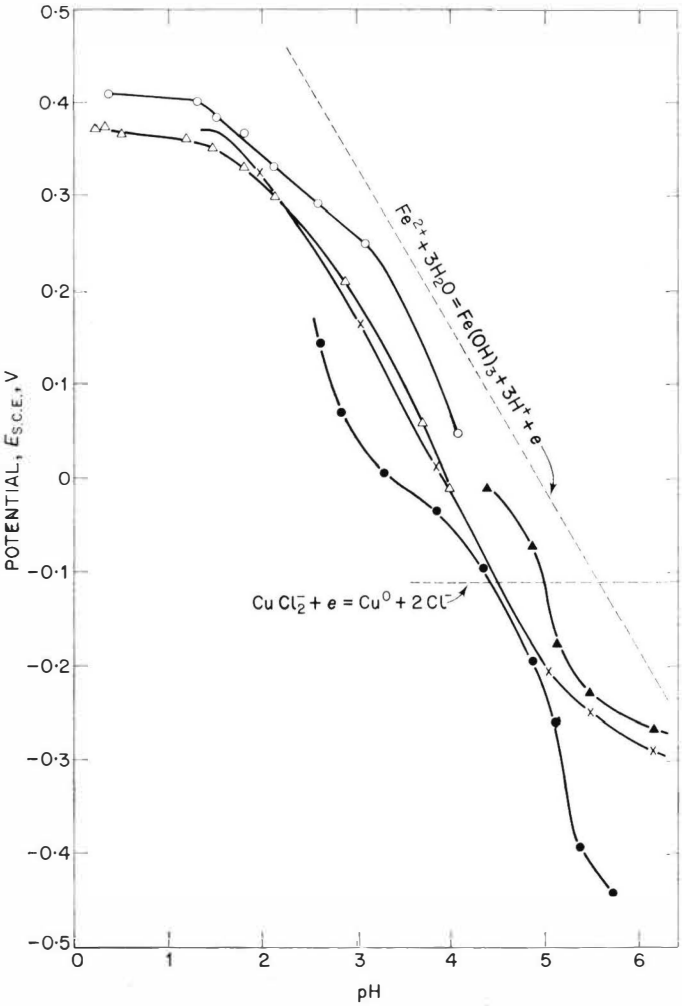

FIG. 8. *Variations of the potential (Pt—S.C.E.) with increasing pH*

	$[Cu^{2+}]$	$[Fe^{2+}]$ (M)		
●	—	0·1		With extraction
○	0·1	0·1		With extraction
△	0·1	0·2	1st step	With extraction
▲	0·1	0·2	2nd step	With extraction
×	0·1	0·2	Without extraction	

seen to contain large amount of aqueous solution, which existed in a colloidal state forming a soft gel in the organic phase, and could be separated from the organic phase with the aid of a centrifugal separator.

The maximum amount of aqueous solution contained in the solvent is ~ 15% at pH 2 and decreases with increasing pH, as shown by the closed circles in Fig. 9. The phase separability becomes normal above pH 4, when the first step reduction is already over.

The pH dependence of the water content in the solvent was further examined for a ferric chloride solution of 0·1M-Fe^{3+} and 3·0M-NaCl, and the result is shown by the open circles in Fig. 9. In the pH range 1–3 the organic phase contains as much as 30% by volume of the aqueous solution.

The second abnormality is the co-extraction of ferrous ion with ferric ion from a chloride solution by the solvent above pH 2, as already shown by Figs 6 and 7.

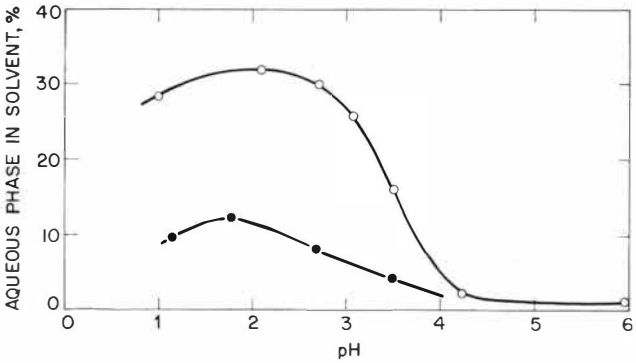

FIG. 9. *Variation of aqueous solution content in the solvent with pH*

● Reduction with extraction (Fig. 5); ○ 0·1M-$FeCl_3$, 3M-NaCl

To ascertain the reason for this co-extraction, which might be attributed to formation of certain double salts, or complexes between ferrous ion and ferric ion, the concentration of sodium chloride was decreased while maintaining a constant concentration ratio, $Fe^{3+} : Fe^{2+} = 0{\cdot}1\text{M} : 0{\cdot}1\text{M}$.

As shown in Fig. 10 the co-extraction of ferrous ion takes place in the pH region higher than 2 independently of the chloride concentration, and the step in the extraction curves at about 20% and 40% suggests the formation of certain hydroxide complexes between $Fe(OH)_2$ and $Fe(OH)_3$, as emphasised by Robins.[5]

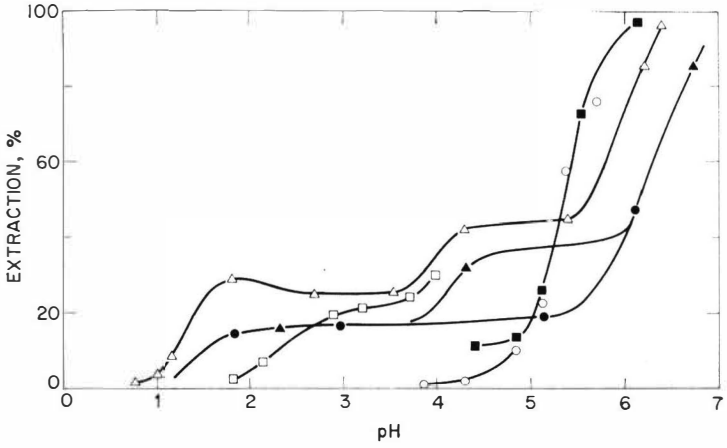

FIG. 10. *Co-extraction of ferrous ion with ferric ion*

○ 0·1M-$FeCl_2$, 3M-NaCl; △ 0·1M-$FeCl_2$, 0·1M-$FeCl_3$, 3M-NaCl; ● 0·1M-$FeCl_2$, 0·1M-$FeCl_3$; ▲ 0·1M-$FeSO_4$, 0·1M-$Fe(SO_4)_{1\cdot5}$, 1M-Na_2SO_4; □ first step reduction (Fig. 6); ■ second step reduction (Fig. 7)

Precipitation-extraction process

Other than the reduction with simultaneous extraction, that is the reaction–extraction process, described above, there is a method called the precipitation–extraction process, in which a hydroxide is first precipitated by addition of an alkaline reagent and then the precipitate is extracted to separate it from soluble values in the aqueous solution.

The process was applied to the reduction and the results are shown in Table I.

TABLE I

Results of the precipitation–extraction process

Reduction	Initial concentration, M		pH		$E_{S.C.E.}$, V		Equilibrium distribution, %					
							Aq. phase			Org. phase		
	Cu^{2+}	Fe^{2+}	Initial	Final	Initial	Final	Cu^{+}	Cu^{2+}	Fe^{2+}	Fe^{2+}	Fe^{3+}	Cu^{0}*
First step	0·078	0·090	5·4	4·5	−0·105	0·080	94·5	4·8	1·1	3·2	95·7	(0·7?)
Second step	0·087	0·189	6·9	6·2	−0·303	−0·200	12·1	—	tr†	15·6	84·4	87

* Metallic copper suspended in the organic phase; † tr = trace

The values obtained for the first step reduction are comparable to the result in Fig. 5, that is, the reaction–extraction process. The second step reduction was 88% complete, a better value than that shown in Fig. 7, but far from satisfactory. The extraction of ~ 15% of the ferrous ion might be attributed to a shift of the equilibrium represented by Eqn (8) caused by the addition of the solvent.

Extraction of calcium ion

Generally sodium chloride and sodium hydroxide are so expensive that it is not practical to use these materials in the reduction. Cheaper materials for chloride solution make-up and neutralisation exist, for example calcium chloride and calcium hydroxide or carbonate, respectively. Therefore, the extraction of Ca^{2+} from a chloride solution by the solvent was examined. As shown in Fig. 4, together with other metal ions, Ca^{2+} becomes extractable above pH 5. This fact, together with the extraction of ferrous ion in the high pH region, suggests that application of both the reaction–extraction process and the precipitation–extraction process is restricted to the first step reduction, that is, the reduction of cupric ion to the cuprous chloride complex.

Conclusion

Cupric ion in a chloride solution (Cl^{-} 3M) is reduced by ferrous ion in a high pH region first to a soluble cuprous chloride complex and then to metallic copper, and ferric hydroxide precipitates simultaneously.

Application of a reaction–extraction process and a precipitation–extraction process using Versatic acid 911 was examined to separate the precipitated ferric hydroxide from the desired products, i.e. the cuprous chloride complex in the solution or the precipitated metallic copper.

The reduction with simultaneous extraction takes place nearly quantitatively and fast at 40°C in the pH range 1·5–4 for the first step reduction and pH 5–6 for the second step reduction. The reaction–extraction process is applicable only to the first step reduction of cupric ion with a stoicheiometric concentration of ferrous ion, but problems arise owing to the poor phase separability between the aqueous phase and the organic phase in that pH region has to be solved. In the second step reduction the co-extraction of ferrous ion makes the application impossible. The precipitation–extraction process is applicable to the second step reduction, but the pH of the solution should be precisely controlled throughout.

References

[1] Gerlach, J., Kametani, H., & Pawlek, F., *Z. anorg. allg. Chem.*, 1970, **378**, 22

[2] Fletcher, A. W., Flett, D. S., & Wilson, J. C., *Trans. Instn Min. Metall.*, 1964, **73**, 766

[3] Fletcher, A. W., & Flett, D. S., Int. Conf. on the Chemistry of the Solvent Extraction of Metals, A.E.R.E., Harwell, 27–29 Sept., 1965

[4] Murayama, K., *J. Min. metall. Inst. Japan*, 1969, **85**, 187

[5] Robins, R. G., Report No. LR 80 MST, Warren Spring Lab., June, 1968

Extraction of iron(III) from sulphuric and hydrochloric acid solutions by di-(2-ethylhexyl)phosphoric acid

by T. Sato and T. Nakamura

Department of Applied Chemistry, Faculty of Engineering, Shizuoka University, Hamamatsu, Japan.

The partition of iron(III) between sulphuric or hydrochloric acid and solutions of di-(2-ethylhexyl)phosphoric acid in kerosene was investigated by varying the concentrations of acid, solvent and aqueous iron at different temperatures. The sulphate or chloride concentration and the water content of the organic phase were examined. Both the aqueous and organic phases were studied by spectrophotometry, and an infra-red spectral study was carried out for the organic phase. For the compounds prepared by evaporating the organic phase, saturated with iron by extraction from sulphuric or hydrochloric acid, the apparent molecular weight was determined in benzene, and the magnetic moment was measured. The mechanism of the extraction is discussed on the basis of the results obtained.

Introduction

THE EXTRACTION of iron(III) from acid solutions by dialkyl phosphoric acid has been studied by several workers,[1-3] but observations on the extraction mechanism are few. One of the present authors has previously investigated the extraction of uranium(VI) and thorium from sulphuric and hydrochloric acid by di-(2-ethylhexyl)phosphoric acid (DEHPA).[4-7] This study extends the work to the extraction of iron(III).

Experimental

Reagents

The DEHPA (Union Carbide Corp.) was purified by washing several times successively with 10% sodium carbonate solution, 6N hydrochloric acid and water.[4] The kerosene used as diluent was also washed successively with concentrated sulphuric acid, dilute sodium hydroxide and water. The cyclohexane used as a solvent for ultra-violet spectroscopy was also prepared by washing successively with a mixture of nitric and sulphuric acids, dilute sodium hydroxide and water. The aqueous iron(III) solutions were prepared by dissolving ferric sulphate or chloride in sulphuric or hydrochloric acid of the required concentration, respectively. The other chemicals were of analytical reagent grade.

Extraction and analytical procedures

Equal volumes (20 ml) of DEHPA solution and aqueous iron(III) solution, placed in 50-ml stoppered conical flasks, were shaken for a given time in a water bath maintained by a thermostat at the required temperature. Preliminary experiments showed that equilibrium between the phases was complete in 10 and 90 min, respectively, for the extractions from hydrochloric and sulphuric acid. After equilibration, the phases were separated by a centrifuge, and then the distribution coefficient (the ratio of the equilibrium concentration of iron in the organic phase to that in the aqueous phase) was obtained. Iron in the organic phase was back-extracted with 1M hydrochloric acid. The iron concentration was determined by back-titration of the aqueous solution, after adding an excess of EDTA, with thorium nitrate solution using xylenol orange as indicator at pH 2.[8]

The sulphate concentration in the organic phase was determined as follows: lead nitrate solutions was added to the sample solution diluted with ethanol at pH 2, the resulting precipitate was dissolved in EDTA solution, and then the

free EDTA was back-titrated with magnesium chloride solution using Eriochrome Black T as indicator at pH 10.[9] The chloride concentration and water content in the organic phase were determined by Volhard's method in the presence of nitrobenzene and Karl Fischer titration, respectively.

Spectrophotometry and infra-red spectral measurement

The absorption spectra were obtained on a Shimazu Model QV-50 spectrophotomet r by using matched 1·00-cm fused silica cells for the ultra-violet and visible range. The infra-red spectra of the organic extracts were determined with kerosene as reference liquid on a Japan Spectroscopic Co. Model IR-S recording infra-red spectrophotometer equipped with potassium chloride prisms, in a matched pair of cells of fixed path length 0·1 mm with thallium halide windows. The spectra of the complexes prepared by evaporating organic phases saturated with iron, obtained by extraction of iron from sulphuric or hydrochloric acid with a solution of DEHPA in n-hexane, were measured as a capillary film between thallium halide plates.

Measurements of apparent molecular weight and magnetic moment

For the iron(III)–DEHPA complexes, the apparent molecular weight was determined in benzene on a Hitachi Model 115 isothermal molecular weight apparatus, and the magnetic moment was measured by the Gouy method.[10]

Results and discussion

Dependence of iron(III) extraction on acid and solvent concentrations

The extraction of iron(III) from aqueous solutions containing 1 g/l of ferric chloride in hydrochloric acid at various concentrations by DEHPA in kerosene at 20°C gave the results shown in Fig. 1. This shows that the distribution coefficient decreases with increasing aqueous acidity below 4·5M, and above this acidity the curve rises. The variation of the distribution coefficient is interpreted as follows: at low aqueous acidity, iron is extracted by a cation-exchange reaction in which hydrogen is liberated, and at high aqueous acidity by a solvating reaction similar to that with non-ionic reagents.

If it is assumed that the initial decrease in the partition coefficient is governed by an ion-exchange reaction similar to that in the extraction of uranium(VI),[6] viz.:

$$Fe^{3+}_{(aq)} + 3(HX)_{2(org)} \rightleftharpoons FeX_6H_{3(org)} + 3H^{+}_{(aq)} \quad (1)$$

where X is the anion $(C_8H_{17}O)_2PO_2^-$ and $(HX)_2$ the dimeric solvent, then the following relationship must hold:

$$\log 8\, E^{o}_{a} = \log K + 3 \log (C_S - 6\, C_{Fe})/C_H \quad (2)$$

in which E^{o}_{a} is the distribution coefficient, K the equilibrium constant, C_S the total DEHPA concentration, C_{Fe} the iron concentration of the organic phase and C_H the aqueous acidity. However, since the log–log plots of E^{o}_{a} vs. $(C_S–6C_{Fe})/C_H$ at constant hydrochloric acid concentration indicate that Equation (2) is not satisfied, it is inferred that iron(III) is extracted as a polymeric species:

$$FeX_6H_{3(org)} + Fe^{3+}_{(aq)} + 2(HX)_{2(org)} \rightleftharpoons Fe_2X_{10}H_{4(org)} + 3H^{+}_{(aq)} \quad (3)$$

The overall reaction:

$$2Fe^{3+}_{(aq)} + 5(HX)_{2(org)} \rightleftharpoons Fe_2X_{10}H_{4(org)} + 6H^{+}_{(aq)} \quad (4)$$

leads to the relationship:

$$\log 8\, E^{o}_{a} = \log K_1 + 3 \log(C_S - 3\, C_{Fe})/C_H \quad (5)$$

where K_1 is a constant. The log–log plots of E^{o}_{a} vs. $(C_S-3C_{Fe})/C_H$ show that Equation (5) is satisfied at hydrochloric acid concentrations of 0·05–1M. It is therefore postulated that although the monomeric species is formed when the

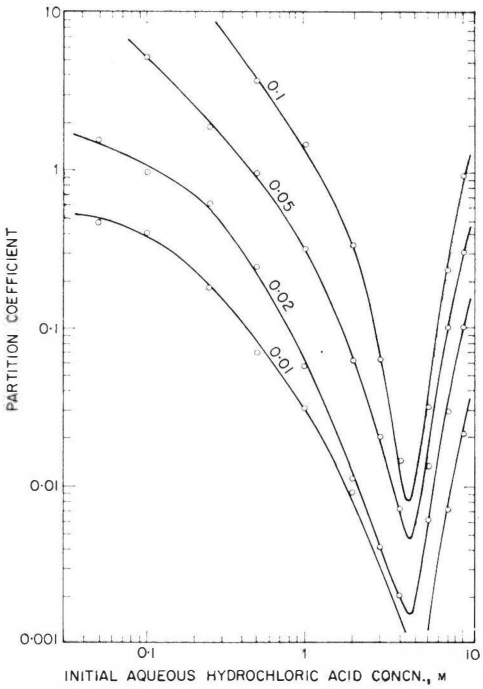

FIG. 1. *Extraction of iron(III) from hydrochloric acid by DEHPA in kerosene*
Numerals on curves are DEHPA concentrations, M

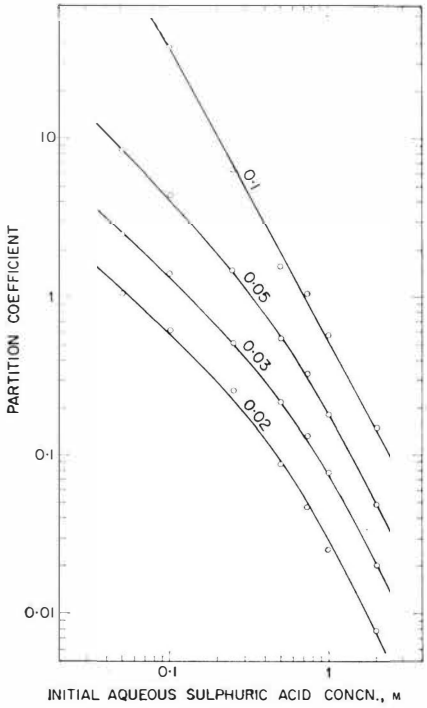

FIG. 2. *Extraction of iron(III) from sulphuric acid by DEHPA in kerosene*
Numerals on curves are DEHPA concentrations, M

DEHPA is present in excess, the increase in the iron concentration of the organic phase involves the formation of a polymeric iron(III)–DEHPA complex.

At high aqueous acidity, if the extraction involves the combination of m molecules of the DEHPA dimer $(HX)_2$, which is bonded as the monomer 2HX, with each iron ion by a reaction similar to that for TBP, viz.:

$$Fe^{3+}_{(aq)} + 3Cl^-_{(aq)} + m(HX)_{2(org)} \rightleftharpoons FeCl_3.(HX)_{2m(org)} \quad . \quad . \quad . \quad (6)$$

then:

$$\log 2^m E^o_a = \log K_2 + 2m \log(C_S - 2m\, C_{Fe}) \quad . \quad . \quad . \quad . \quad (7)$$

where K_2 is a constant. Log–log plots of E^o_a vs. $(C_S–2mC_{Fe})$ in 8- and 10-M-HCl gave slopes of 1·30 and 1·40, respectively, for m = 1–3. Thus it is expected that m = 1·5 in Equation (6), i.e.

$$Fe^{3+}_{(aq)} + 3\ Cl^-_{(aq)} + 3/2\ (HX)_{2(org)} \rightleftharpoons FeCl_3.3HX_{(org)} \quad . \quad . \quad . \quad (8)$$

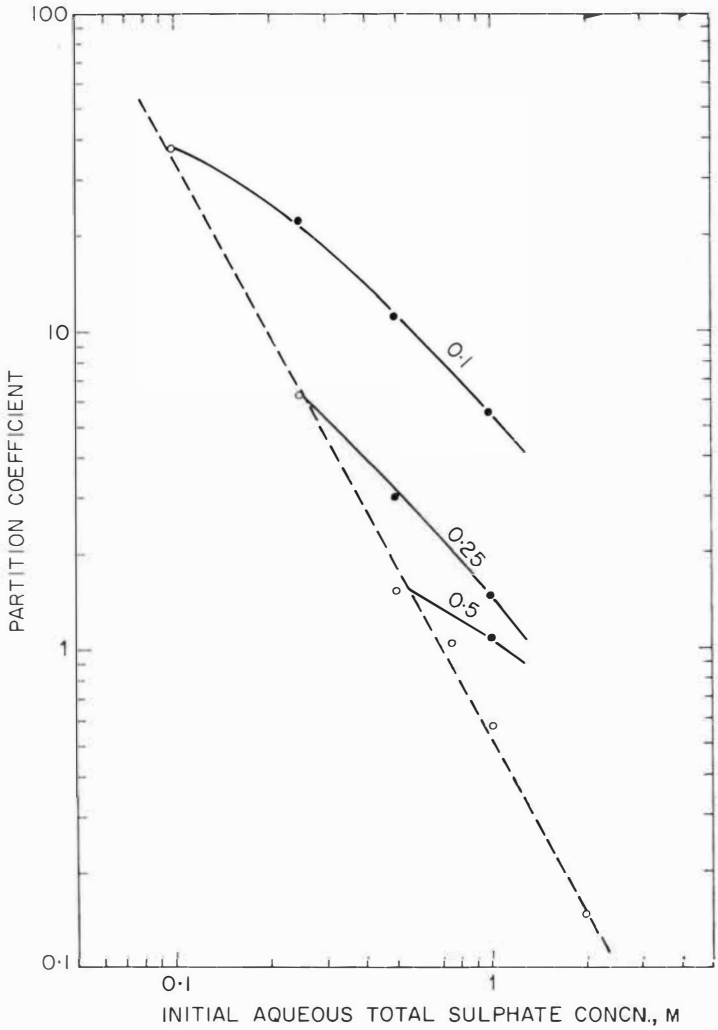

FIG. 3. *Extraction of iron(III) from sulphuric acid containing sodium sulphate by 0·1M-DEHPA in kerosene*

Numerals on curves are initial aqueous sulphuric acid concentrations, M
– – – – – curve for H_2SO_4 alone

In contrast, the extraction of iron(III) from aqueous solutions containing 1 g/l of ferric sulphate in sulphuric acid at various concentrations by DEHPA in kerosene at 20°C gave the results shown in Fig. 2. From the dependence of the distribution coefficient on the concentration of DEHPA, it was found that the extraction from sulphuric acid solutions is dominated by the ion-exchange reaction of Equation (4) rather than Equation (1). Accordingly, the following equation, expressed as the ion-exchange reaction involving the formation of polymeric species, is given in general for the extraction of iron(III) from acid solutions by DEHPA:

$$n\,Fe^{3+}_{(aq)} + (2n+1)(HX)_{2(org)} \rightleftharpoons Fe_nX_{2(2n+1)}H_{n+2(org)} + 3n\,H^{+}_{(aq)} \quad (9)$$

where $n \geqslant 1$.

For the extraction from sulphuric acid solutions, Blake *et al.*[1] have postulated an equilibrium such as:

$$Fe^{3+}_{(aq)} + 2(HX)_{2(org)} + H_2O_{(aq)} \rightleftharpoons Fe(OH)X_4H_{2(org)} + 3\,H^{+}_{(aq)} \quad (10)$$

which leads to the relationship:

$$\log 4\,E^{0}_{a} = \log K' + 2\log(C_S - 4\,C_{Fe}) - 3\log C_H \quad (11)$$

where K' is the equilibrium constant, but Equation (11) is not satisfied under the conditions in this investigation.

Extraction in the presence of sodium sulphate or lithium chloride

The extraction of iron(III) from aqueous solutions containing 1 g/l of ferric sulphate in sulphuric acid and sodium sulphate with 0·1M-DEHPA in kerosene at 20°C shows that the distribution coefficient is only slightly influenced by the sulphate ion concentration, but decreases with increasing hydrogen ion concentration, as shown in Fig. 3. The gradual decrease in the distribution coefficient with increasing sulphate or chloride ion concentration may be explained by the presence of aqueous species containing sulphate, e.g. $FeSO_4^+$,[11] on the assumption that the extracted species contains no sulphate. This assumption is supported by the fact that the infra-red spectra of extracted organic species do not exhibit the absorption band due to the sulphate group, in accordance with the chemical analysis for the sulphate concentration of the organic phase. A similar phenomenon was also observed in the extraction of iron(III) from aqueous solutions containing ferric chloride in hydrochloric acid and lithium chloride. In this case, the slight decrease in the distribution coefficient with the chloride ion concentration may be ascribed to the presence of $FeCl^{2+}$.[12]

Dependence on iron concentration

The extraction of iron(III) from aqueous solutions containing ferric sulphate at various concentrations in 0·1M sulphuric acid with 0·1M-DEHPA in kerosene at 20°C gave the results shown in Fig. 4. With the variations in the mole ratios of DEHPA concentration and water content to iron concentration in the organic phase plotted as a function of initial aqueous iron concentration, it is seen that the former approaches a limiting value of three, and the latter nearly unity. This result implies that a complex containing iron : DEHPA : water in the mole ratio 1 : 3 : 1 is formed at higher iron concentrations. A similar result was obtained in the extraction of iron(III) from aqueous solutions containing ferric chloride in hydrochloric acid.

Temperature effect

In the extraction of iron(III) from aqueous solutions containing ferric sulphate or chloride in sulphuric or hydrochloric acid with 0·05 or 0·1M-DEHPA in kerosene at temperatures between 20° and 50°C, the distribution coefficient decreases with rising temperature as indicated in Table I. This

dependence on temperature is analogous to that for uranium(VI) or thorium.[4,7] The heats of reaction (change in enthalpy, $-\Delta H$) in Equations (4) and/or (8) were estimated to be 2·3 and 1·6 kcal/mole in 0·1 and 0·5 M-H_2SO_4 with 0·05M-DEHPA, respectively; 2·9 and 2·8 kcal/mole in 0·1 and 0·5M-HCl with 0·05M-DEHPA, respectively; and 3·1 kcal/mole in 10M-HCl with 0·1M-DEHPA.

TABLE I

Temperature dependence of partition coefficient on the extraction of iron(III) from hydrochloric and sulphuric acid by DEHPA in kerosene

Temp., °C	Partition coefficient*				
	HCl, M			H_2SO_4, M	
	0·1	0·5	10	0·1	0·5
20	5·18	0·931	0·900	4·28	0·549
30	4·80	0·890	0·849	3·86	0·522
40	4·32	0·808	0·723	3·61	0·480
50	3·70	0·675	0·582	3·25	0·447

*All extractions were carried out with 0·05M-DEHPA, except 10M-HCl solution with 0·01M-DEHPA

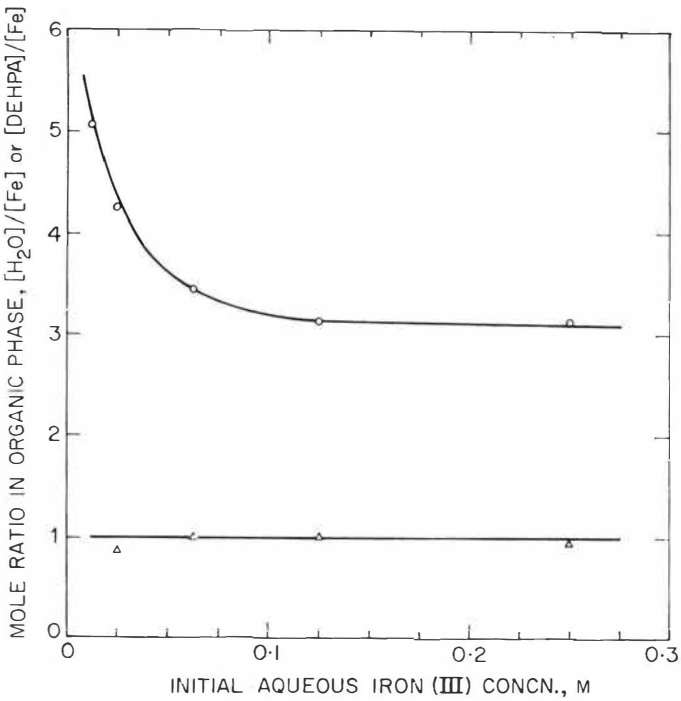

FIG. 4. *Variation in mole ratios of water content and DEHPA concentration to iron concentration in organic phase with initial aqueous iron concentration, for the extraction of iron(III) from 0·1M sulphuric acid solution by 0·1M-DEHPA in kerosene*

○ $[DEHPA]/[Fe]_{org}$; △ $[H_2O]/[Fe]_{org}$

Absorption spectra

The ultra-violet absorption spectra of both the aqueous and organic phases in the extraction of iron(III) from aqueous solutions containing ferric sulphate of 1, 10 and 50 g/l in 0·1 and 2M sulphuric acid with 0·04M-DEHPA in cyclohexane at 20°C are given in Figs 5 and 6.

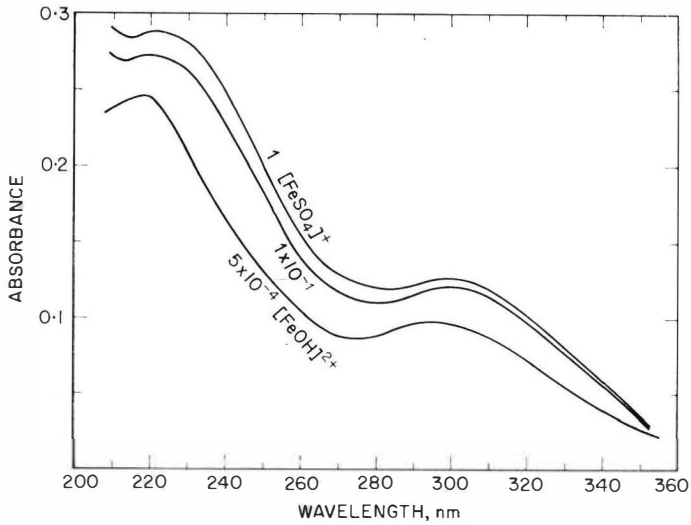

FIG. 5. *Absorption spectra of aqueous ferric sulphate solutions (0·01 g/l) in the presence of sulphuric acid at different concentrations*

Numerals on curves are initial aqueous sulphuric acid concentrations, M

In the spectra of the aqueous solutions (Fig. 5), the absorption band which arises from a charge-transfer transition in $FeOH^{2+}$ at 295 nm is observed at sulphuric acid concentration 5×10^{-4}M, and that in $FeSO_4^+$ at 300 nm at acid concentration $> 1 \times 10^{-1}$M.[11] Therefore it is thought that the species Fe^{3+} and $FeSO_4^+$ exist in the initial aqueous ferric sulphate solutions containing sulphuric acid in the concentration range under this experimental condition, corresponding to the result shown in Fig. 3. However, the spectra of the organic phases from the extraction of aqueous solutions containing ferric sulphate do not show the charge-transfer bands in $FeOH^{2+}$ and $FeSO_4^+$. In Fig. 6, the absorption due to the charge-transfer transition appears at 270 nm when the iron loading is low, as illustrated in the extraction from 2M sulphuric acid, and shifts to a wavelength of 240 nm with increasing iron concentration, as indicated in the extraction from 0·1M sulphuric acid. These results suggest that although the extraction does not follow Equation (10), the species formed in the organic phase depends on the loading iron concentration.

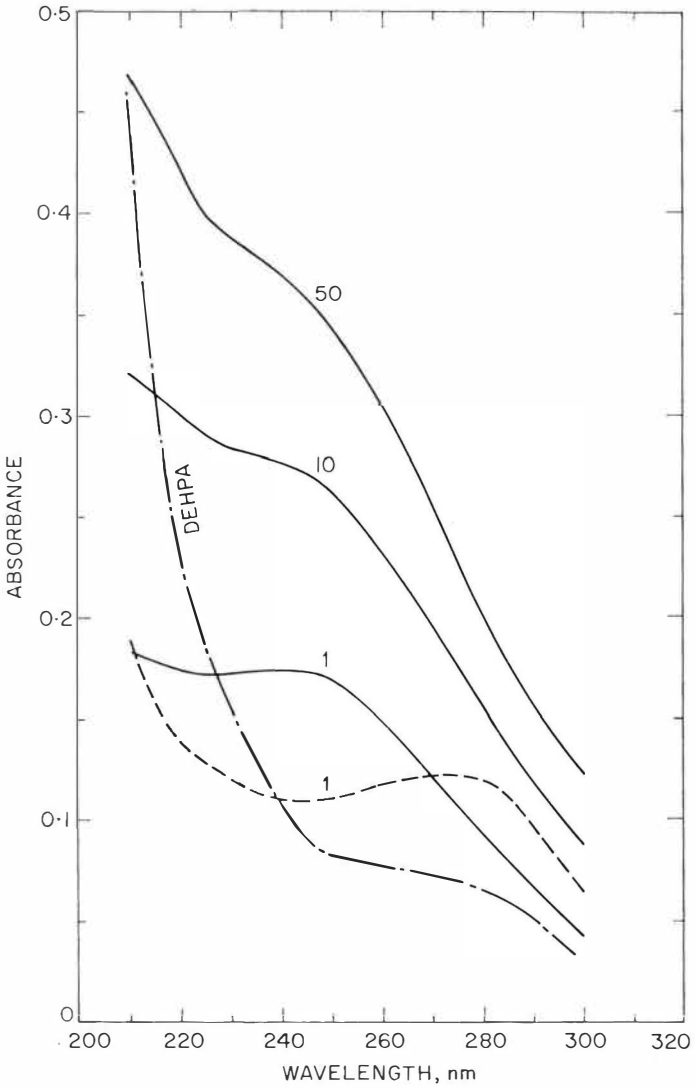

FIG. 6. *Absorption spectra of organic solutions from the extraction of iron(III) from sulphuric acid with 0·04M-DEHPA in cyclohexane*

Numerals on curves are initial aqueous ferric sulphate concentrations, g/l; sulphuric acid concentrations: —— 0·1M (dilution × 200); - - - - 2M (dilution × 20). Thickness of cell 1.00 cm.

Furthermore, as shown in Fig. 7, the absorption spectra of the organic phase from the extraction of aqueous solutions containing ferric chloride of 1, 10, 50 and 100 g/l in 0·1M hydrochloric acid with 0·02M-DEHPA in cyclohexane closely resemble those for the extraction from sulphuric acid solution: the absorption due to the charge-transfer transition shifts from 250 to 240 nm as the initial aqueous iron concentration increases.

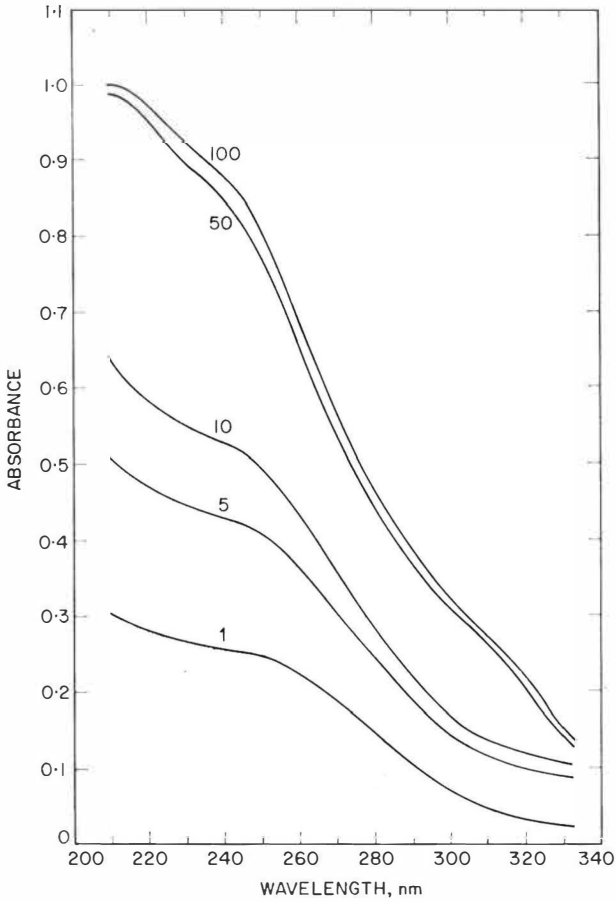

FIG. 7. *Absorption spectra of the organic solutions from the extraction of iron(III) from aqueous solutions containing hydrochloric acid at 0·1M with 0·02M-DEHPA in cyclohexane*

Numerals on curves are initial aqueous ferric chloride concentrations, g/l; dilution × 50; thickness of cell 1·00 cm

Infra-red spectra

The organic phases from the extraction of aqueous solutions containing ferric sulphate or chloride of 5, 10, 25, 50 and 100 g/l in 0·1M sulphuric or hydrochloric acid with 0·1M-DEHPA in kerosene at 20°C were examined by infra-red spectroscopy. The spectra are given in Fig. 8.

The infra-red spectrum of DEHPA in kerosene shows the P→O stretching band at 1230 cm^{-1}, the OH stretching band at 2680 and 2350 cm^{-1}, which are ascribed to the hydrogen bond in the formation of dimer, the OH bending band at 1690 cm^{-1}, and the [P–O]–C stretching band at 1030 cm^{-1}. In the spectra of the extracts from ferric sulphate solutions, as the iron concentration increases the intensities of the OH stretching bands at 2680 and 2350 cm^{-1}, and of the OH bending band at 1690 cm^{-1}, decrease, while the P→O absorption band at 1230 cm^{-1} shifts to lower frequencies. Simultaneously, an absorption at 1055 cm^{-1} appears in addition to the peak at 1030 cm^{-1} in the DEHPA. The peak at 1085 cm^{-1} has a slightly lower intensity than that of the former, and that at 985 cm^{-1} has a shallow shoulder. Also, a very broad band in the region 1700–700 cm^{-1}, which is observed in the organic solution from the extraction of ferric

sulphate solution at an initial aqueous concentration of 5g/l, decreases in intensity at higher iron loadings. These are observed more clearly in the spectrum of the complex prepared by evaporating the organic phase saturated with iron. Although the absorption band at 1150 cm^{-1} appears in addition to the [P–O]–C stretching band at 1930 cm^{-1}, there is no sign of the absorption in the region 1700–700 cm^{-1}. According to Whateley *et al.*,[13,14] the background absorption in the region 1700–700 cm^{-1} indicates the presence of short, strong symmetrical or near-symmetrical hydrogen bonding. As the absorption band at 1085 cm^{-1} is assigned to the POO^- symmetric vibration,[15] it is considered that the absorption at 1150 cm^{-1} is due to the POO^- asymmetric frequency of the X^- group doubly co-ordinated to iron. A similar result is also observed in the extraction from hydrochloric acid. Thus the infra-red results confirm that iron extracted into DEHPA by cation exchange is bonded to the phosphoryl oxygen atom

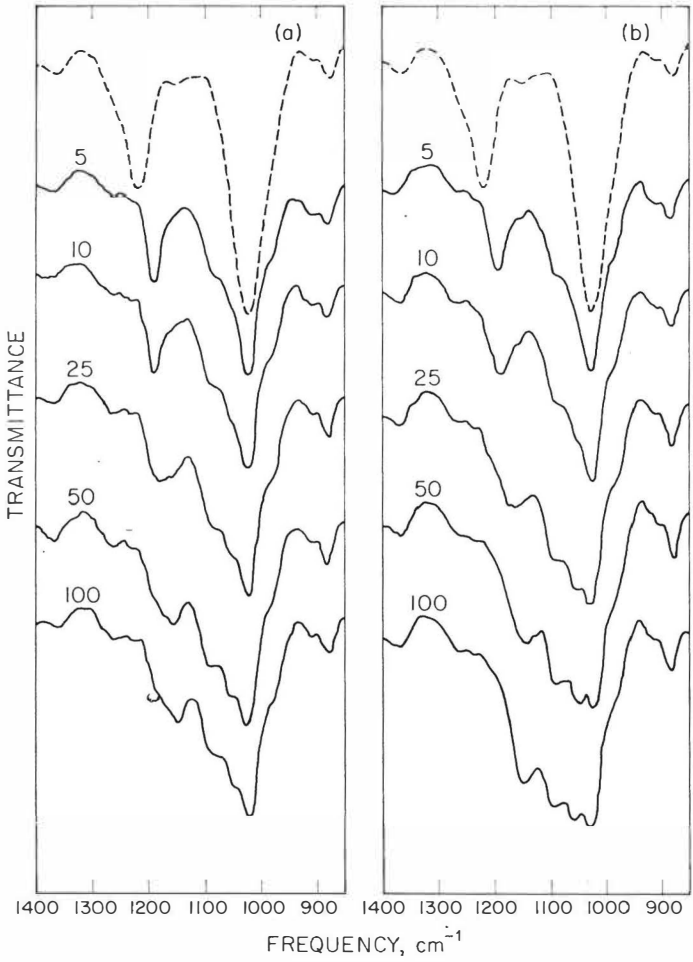

FIG. 8. *Infra-red spectra of the organic solutions from the extraction of iron(III) from aqueous solutions containing sulphuric or hydrochloric acid at 0·1M with 0·1M-DEHPA in kerosene*

Numerals on curves are concentrations of ferric sulphate or chloride, g/l
(a) ferric sulphate solutions; (b) ferric chloride solutions
– – – – curve for 0·1M-DEHPA

Molecular weight and magnetic moment of the complex

The analytical data for the complexes freed from organic solvent are illustrated in Table II.

TABLE II

Analytical data for iron(III) – DEHPA complexes

Extraction system*	Composition, mole ratio Fe : DEHPA : H_2O	Apparent molecular weight	Magnetic moment, B.M. (at 10°C)	Probable formula
Fe(III)–HCl–DEHPA	1 : 3·04 : 1·13	1985	3·65	$(FeX_3.H_2O)_2$**
Fe(III)–H_2SO_4–DEHPA	1 : 3·00 : 1·03	1980	3·66	

*Extractions were carried out from aqueous solutions containing acid at 0·1M with 0·1M-DEHPA in n-hexane at 20°C

**Molecular weight 1966

The complexes formed in the extraction from acid solutions by ion-exchange reaction exhibit an apparent molecular weight of 1980–1985, corresponding to the theoretical value of 1966 as $(FeX_3.H_2O)_2$ in benzene. This result indicates that the formation of a polymeric iron(III)–DEHPA complex is involved when the iron concentration of the organic phases increases. This is also supported by the fact that iron(III)–DEHPA complexes have three unpaired electrons, as evidenced by a magnetic moment of 3·65–3·66 B.M. In general, the compounds of iron(III) have one or five unpaired electrons,[16] but it has been reported that a binuclear hydroxyl-bridged complex is in a quartet ($S = 3/2$) spin state for the iron.[17] According to Mattock,[18] the tendency towards dimerisation by metal ions increases with the probable increase of covalence in metal–hydroxyl bonds. Accordingly it is inferred that the iron(III)–DEHPA complex exists as the dimer or polymer, corresponding to the data for the apparent molecular weight. Consequently, it is proposed that for the species extracted by the ion-exchange reaction, iron displays a co-ordination number of six in both the monomeric species, chelated to three HX_2^- groups, and the polymeric species, doubly co-ordinated by the formation of a polymer chain.

Acknowledgment

The authors thank Mr. S. Kurihara for assistance with the experimental work.

References

[1] Blake, C. A., jun., Baes, C. F., jun., Brown, K. B., Coleman, C. F., & White, J. C., *Proc. 2nd int. Conf. peaceful Uses atom. Energy, Geneva, 1958*, 1958, **28,** 289
[2] Baes, C. F., jun., & Baker, H. T., *J. phys. Chem., Ithaca*, 1960, **64,** 89
[3] Baes, C. F., jun., *J. inorg. nucl. Chem.*, 1962, **24,** 707
[4] Sato, T., *J. inorg. nucl. Chem.*, 1962, **24,** 699
[5] Sato, T., *J. inorg. nucl. Chem.*, 1965, **27,** 1395
[6] Sato, T., *J. inorg. nucl. Chem.*, 1965, **27,** 1853
[7] Sato, T., *Z. anorg. allg. Chem.*, 1968, **358,** 296
[8] Kinnunen, J., & Wennerstrand, B., *Chemist Analyst*, 1957, **46,** 92
[9] Sporek, K. F., *Analyt. Chem.*, 1958, **30,** 1032
[10] Garner, W. E., (Ed.), 'Chemistry of the solid state', 1955, p. 147 (London: Butterworths)
[11] Whiteker, R. A., & Davidson, N., *J. Am. chem. Soc.*, 1953, **75,** 3031
[12] E.g., Myers, R. J., & Metzler, D. E., *J. Am. chem. Soc.*, 1950, **72,** 3772, 3776; Gamlen, G. A., & Jordan, D. O., *J. chem. Soc.*, 1953, p. 1435
[13] Whateley, T. L., *Nature, Lond.*, 1966, **212,** 279
[14] Smythe, L. E., Whateley, T. L., & Werner, R. L., *J. inorg. nucl. Chem.*, 1968, **30,** 1553
[15] Ferraro, J. R., *J. inorg. nucl. Chem.*, 1962, **24,** 475
[16] E.g., Reiff, W. M., Baker, W. A., jun., & Erickson, N. E., *J. Am. chem. Soc.*, 1968, **90,** 4794
[17] Mulay, L. N., & Selwood, P. W., *J. Am. chem. Soc.*, 1955, **77,** 2693
[18] Mattock, G., *Acta chem. scand.*, 1954, **8,** 777

SESSION 2B

EXTRACTION EQUIPMENT, I

CHAIRMAN

Prof. W. L. Wilkinson

SECRETARIES

Dr. J. Ingham

Ir. H.J.v.d. Berg

Flooding conditions in a reciprocating plate extraction column

by M. H. I. Baird, R. G. McGinnis* and G. C. Tan
Chemical Engineering Department, McMaster University, Hamilton, Ontario, Canada

The flooding of a 2-in diameter reciprocating plate column has been investigated for four different liquid systems in the absence of mass transfer. It is found that existing flooding correlations for pulsed plate columns do not apply to the present results, since the diameter of the holes in the reciprocating plates is relatively large (0·5 in). However, the results are correlated quite well by a model based on the dispersion of drops by turbulent energy dissipation, assuming that at flooding the conditions are analogous to those in a fluidised bed.

Introduction

PULSED PLATE EXTRACTION columns and reciprocating plate extraction columns differ in that in one case the plates are fixed, while in the other the plates move relative to the rest of the column. In both cases, there is oscillatory motion of the liquid phases relative to the plates. The usually cited original pulsed column[1] was, strictly speaking, a reciprocating plate column. As indicated in a recent review,[2] pulsation of the fluid by pistons or bellows has been used more widely than reciprocating plate drive.

However, an industrially established example of the reciprocating plate genre is the Karr column (Chem Flow Corporation, Little Falls, New Jersey, U.S.A.) which has been manufactured since 1965 in sizes up to diameter 18 in. The only hitherto published performance study of this column[3] has shown that the minimum *HTU* is obtained fairly close to the flooding point, i.e., at near the maximum throughput. This characteristic distinguishes it from pulsed columns[4] in which the minimum *HTU* occurs at an agitation level (or flow) well below the flooding point. As already noted, the fluid mechanics of pulsed and reciprocating plate columns are basically similar. The Karr column differs from normal pulsed plate columns, however, in the plate design. The free area is relatively large (61 %) and the hole diameter is 0·5 in, much larger than in typical pulsed plate columns.

The present investigation of flooding rates has been carried out with the aim of obtaining a soundly based correlation, and comparing the data with an existing correlation[5] for pulsed plate columns. It may be noted that mass transfer was not occurring in any of the present work.

Experimental

The column and ancillary equipment are shown in Fig. 1.

The column itself was made of 2 in i.d. Pyrex glass sections of a total height of 8 ft. Agitation was provided by a 6 ft column of perforated 1/8 in thick Teflon plates, mounted at 1·14 in intervals on a central shaft. Each plate was perforated with six 1/2 in diameter holes and six hole segments at the periphery; the clearance between the plates and the column wall was about 0·02 in but contact occurred in some cases. The plates were spaced vertically by 1 in Teflon sleeves on the 1/4-in diameter stainless-steel drive shaft. The drive mechanism was a variable speed motor (3–4 h.p., 0–400 rev/min) with an adjustable yoke; the amplitude (stroke) of the plates could be varied up to 4·5 cm.

Table I shows the systems used and their physical properties. Viscosities were measured by a capillary viscometer, and interfacial tensions by a ring tensiometer. In all cases, the organic phase preferentially wetted the Teflon, so

*Present address: Chemical Engineering Department, University of Alberta, Edmonton, Alberta, Canada.

the column was operated with the organic phase continuous. The total number of data points was 231, of which 174 were obtained at values of Af in excess of 3 cm/sec.

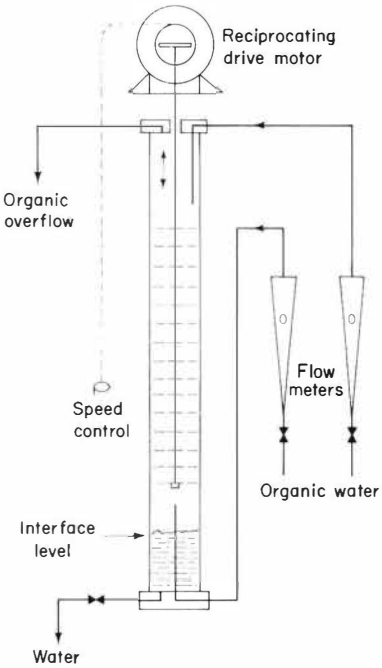

FIG. 1. *Karr reciprocating plate column and ancillaries (not to scale)*

TABLE I

System properties

System	Symbol on Figs 5 & 6	Continuous phase	ρ_C, g/cm^3	μ_C, cP	Interfacial tension, dyne/cm
A	□	Kerosene	0·805	1·07	28·2
B	○	Kerosene, Mineral oil	0·843	1·37	32·7
C	△	Kerosene, Carbon tetrachloride	0·878	1·20	31·0
D	×	Kerosene, Carbon tetrachloride, Mineral oil	0·871	1·92	29·9

Dispersed phase: water in all cases

Results

Qualitative

In pulsed columns,[6] two distinct types of flooding can occur. At low rates of agitation the dispersed phase cannot pass through the plates and forms a discrete layer at each plate, while emulsion flooding occurs at high rates of agitation. In the Karr column, because of the large hole size, only the second type of flooding was observed. The usual procedure was to set the flows of the two phases, and the amplitude of the plates, and very slowly increase the

frequency. Flooding was identified as the formation of an emulsion layer of the dispersed phase, distinct from freely falling drops. This phenomenon is shown in Fig. 2, and it may be noted that the emulsion layer did not always necessarily appear at the same point in the column. Once formed, the emulsion layer tended to grow up the column unless the frequency was decreased in which case it was possible, by careful adjustment, to regulate its extent.

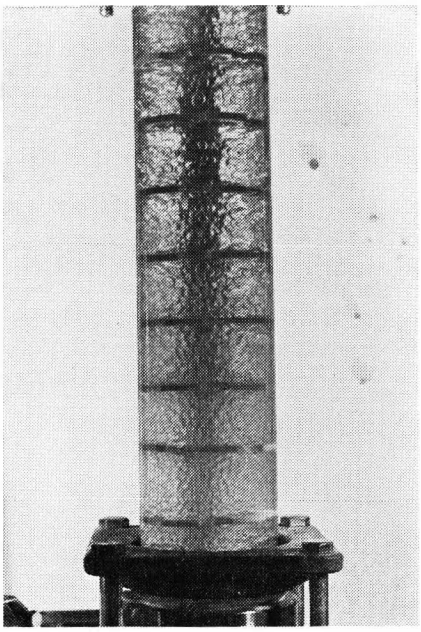

FIG. 2. *Incipient flooding, kerosene–water system*

Quantitative

Fig. 3 shows some typical flooding data for the kerosene–water system. Whereas in conventional pulsed plate columns[6] no counterflow is possible in the absence of agitation, Fig. 3 shows that the flow in the absence of external agitation is only slightly less than the maximum. At frequencies above about 1 Hz, the dispersed phase flow at flooding decreases with frequency as the drop size becomes smaller. Measurements of flooding by the visual method described above became difficult at high frequencies because of the presence of very finely dispersed drops.

The interrelation between U_C and U_D at fixed agitation is important. Previous workers on pulsed columns[5,7,8] have used the sum $(U_D + U_C)$, but the present results suggest that, for frequencies above about 1 Hz, the sum $(U_D + 0{\cdot}67U_C)$ is constant for a given system and agitation level.

The next question to be studied concerned the definition of agitation level. The product Af appears in the expression[9] for power dissipation, and is taken as the usual measure of agitation in pulsed columns. In the present investigation the two flow rates were held constant and the combinations of amplitude and frequency for flooding were noted. The results in Fig. 4 show a slope of -1 on a log–log plot, confirming that Af is the correct agitation parameter in the Karr column as in pulsed columns.

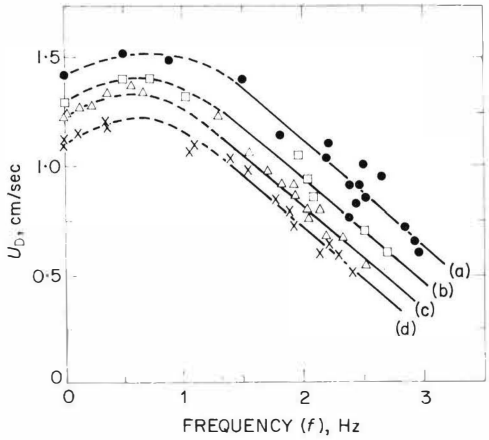

FIG. 3. *Typical flooding data*

Amplitude = 2·7cm for system A (kerosene–water)
(a) $U_C = 0$; (b) $U_C = 0{\cdot}23$; (c) $U_C = 0{\cdot}47$; (d) $U_C = 0{\cdot}71$ cm/sec

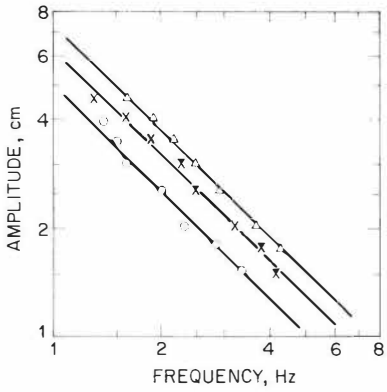

FIG. 4. *Relationship between amplitude and frequency at flooding for kerosene–water system*

△ $U_D = 0{\cdot}49$, $U_C = 0{\cdot}36$ cm/sec; × $U_D = 0{\cdot}49$, $U_C = 0{\cdot}51$ cm/sec; ○ $U_D = 0{\cdot}88$, $U_C = 0{\cdot}51$ cm/sec

Comparison of present data with previous correlations

Several published correlations of flooding in pulsed extraction columns are available. The most extensive is that of McAllister *et al.*,[7] but numerical problems were encountered in comparing the present data with it. The correlation of Smoot *et al.*[5] is also very extensive, and the present data are compared with it on Fig. 5.

It will be seen that the experimental data are about 40% below the predicted values.[5] Moreover, the data points for system D (high μ_C) are significantly separated from other data points. It is thought that these discrepancies are due partly to the fact that the correlation[5] covers plate hole diameters up to only 0·19 in, compared with 0·5 in in the present work. The correlation of Thornton[8] has also been compared and in this case the experimental flooding rates are about 25% of the predicted values, although the correlation[8] does combine the effects of viscosity etc. better than that of Smoot *et al.*[5]

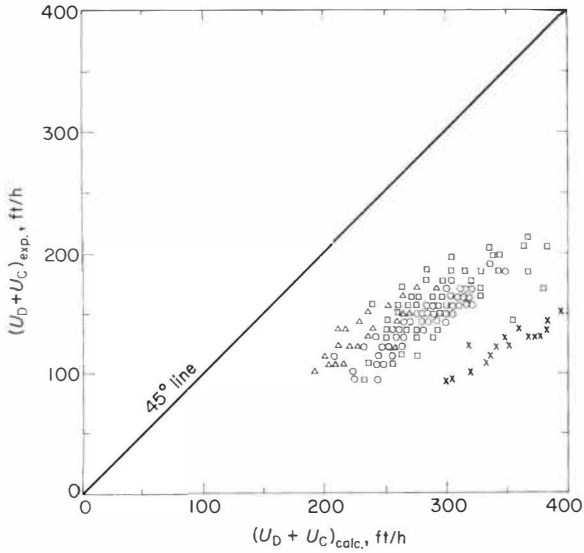

FIG. 5. *Present data compared with correlation of Smoot* et al.[5]

Symbols: see Table I
Not all points are shown, in order to reduce congestion

Discussion

Flooding model

The qualitative observations of the emulsion layer (Fig. 2) suggest an analogy with a fluidised bed. This analogy has been pointed out[10] for flooding in a spray column, but it does not appear to have been applied to agitated columns.

The relative velocity between the two phases is given by:[11]

$$u_S = \frac{U_D}{\varepsilon} + \frac{U_C}{1-\varepsilon} \quad . \quad . \quad . \quad . \quad . \quad . \quad . \quad . \quad . \quad (1)$$

The superficial velocity of the continuous phase, relative to the dispersed phase, is thus:

$$U_S = (1-\varepsilon)\, u_S = U_D\left(\frac{1-\varepsilon}{\varepsilon}\right) + U_C \quad . \quad . \quad . \quad . \quad . \quad . \quad (2)$$

As noted above, observation suggests that in the Karr column, $(U_D + 0{\cdot}67U_C)$ is constant at flooding, which is consistent with a value of ε of about 0·4. Direct measurements of ε in the emulsion were not taken, but the value 0·4 appears reasonable, being somewhat less than the value for closest-packed spheres, and comparable to values found in fluidised beds. Hence:

$$U_S = 1{\cdot}5\,[U_D + 0{\cdot}67\,U_C] \quad . \quad . \quad . \quad . \quad . \quad . \quad . \quad (2a)$$

According to the fluidised bed model,[10] the pressure gradient for flow of the continuous phase through the emulsion is:

$$-\frac{dP}{dz} = \varepsilon g\,\Delta\rho \quad . \quad . \quad . \quad . \quad . \quad . \quad . \quad . \quad . \quad (3)$$

This must be equated with the frictional pressure gradient. In their early paper, Elgin & Foust[10] assumed laminar flow; in this work, however, the more general form of the pressure drop equation for a packed bed will be written, as obtained by Ergun:[12]

$$-\frac{dP}{dz}\left(\frac{d(1-\varepsilon)^3}{\rho_C U_S^2 \varepsilon}\right) = \frac{150\varepsilon}{(Re)} + 1{\cdot}75 \quad . \quad . \quad . \quad . \quad . \quad . \quad . \quad (4)$$

where $(Re) = U_S d \rho_C / \mu_C$. . . . . (5)

In adopting Equation (4) it is assumed that the dispersed phase drops behave as rigid spheres of uniform diameter. Sample calculations based on visual estimates of d confirm the suggestion of Gayler *et al.*[11] that the drop Reynolds number is of the order of 100–300; in other words, the flow conditions around the drop are neither wholly laminar nor wholly turbulent. Equation (3) may be inserted in Equation (4) which can then be solved quadratically for U_S, but the solution can be used only if a measured value of d is available. In the present investigation, the variation of d with agitation could only be inferred approximately (see below), so a simpler version of Equation (4) was sought.

Gayler *et al.*[11] pointed out that for single particles at intermediate Reynolds numbers, the drag coefficient was approximately proportional to $(Re)^{-0{\cdot}5}$ Similarly, Equation (4) for packed beds may be rewritten approximately for intermediate flow conditions:

$$-\frac{dP}{dz}\left(\frac{d(1-\varepsilon)^3}{\rho_C U_S^2 \varepsilon}\right) = K(Re)^{-0{\cdot}5} \quad . \quad . \quad . \quad . \quad . \quad . \quad (5a)$$

Substituting Equation (3) in Equation (5a) and rearranging gives:

$$U_S = d\left[\frac{(1-\varepsilon)^3 g}{K}\right]^{2/3} \frac{\Delta\rho^{\,2/3}}{(\rho_C \mu_C)^{1/3}} \quad . \quad . \quad . \quad . \quad . \quad . \quad (6)$$

If it is assumed that the term in brackets is essentially constant, Equation (6) may be rewritten in the form:

$$\{U_S (\rho_C \mu_C)^{1/3} (\Delta\rho)^{2/3}\} \propto d \quad . \quad . \quad . \quad . \quad . \quad . \quad . \quad (7)$$

Although the diameter d was not measured, the interaction between d and Af may be inferred approximately. The drop size depends on the turbulent energy dissipation due to the reciprocating plates, and an expression which has been deduced theoretically[13] and found useful[14] in predicting drop sizes in stirred tanks may be used:

$$d \propto \frac{\gamma^{0{\cdot}6}}{\psi^{0{\cdot}4}\,\bar{\rho}^{0{\cdot}2}} \quad . \quad . \quad . \quad . \quad . \quad . \quad . \quad . \quad . \quad (8)$$

As shown in Table I surface tension and density were varied only very slightly in this work. The energy dissipation per unit volume ψ was a function of Af as calculated[8,9] for pulsed columns:

$$\psi = \frac{\pi^2 (1-\sigma^2)(Af)^3 \bar{\rho}}{2\sigma^2 C_o^{\,2} l} \quad . \quad . \quad . \quad . \quad . \quad . \quad . \quad . \quad (9)$$

The only terms in Equation (9) which were appreciably varied in this work were A and f. Hence from Equations (7), (8) and (9):

$$\{U_S (\rho_C \mu_C)^{1/3}\ \Delta\rho^{-2/3}\} \propto (Af)^{-1{\cdot}2} \quad . \quad . \quad . \quad . \quad . \quad . \quad (10)$$

This equation is in a suitable form for comparison with the experimental data, bearing in mind that γ, l, σ etc. were not varied significantly in this work.

Comparison of data with model

Fig. 6 shows all the present results as a modified velocity *versus* Af. The modified velocity is defined from Equation (10) as follows:

$$U_M = (U_D + 0{\cdot}67\, U_C)\rho'_C{}^{1/3}(\rho'_D - \rho'_C)^{-2/3}(\mu_C/\mu_{Co})^{1/3} \quad . \quad . \quad (11)$$

According to Equation (10) this velocity should vary as $(Af)^{-1{\cdot}2}$. Fig. 6 confirms this at high values of Af, but when $Af < 3$ cm/sec the data deviate from Equation (10). The reason is that, at low agitation, the drop size depends not only on agitation but also on the characteristics of the drop nozzle, the dispersed phase flow rate, etc. The deviation is very pronounced for system A (kerosene–water) in which the value of U_S was greatest.

The usefulness of this model is not only that it predicts the effect of Af at the high agitation levels normally used in practice, but that it brings together the points for different system properties. As part of this investigation, expressions based on the 'wholly laminar' and 'wholly turbulent' forms of Equation (4) were also tried but they were much less satisfactory than Fig. 6.

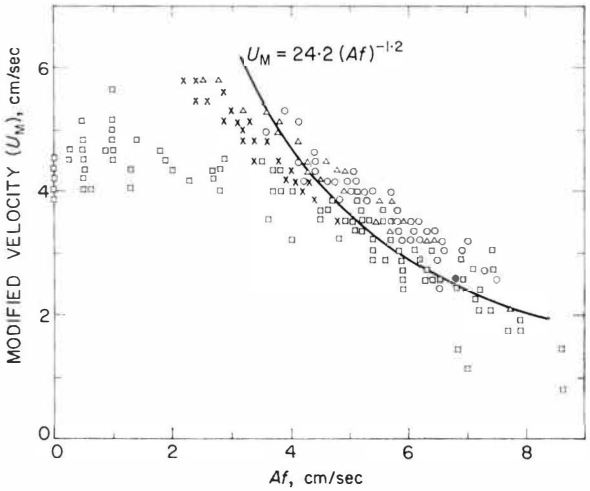

FIG. 6. *Present data, plotted according to theoretical model*

Symbols: see Table I
Not all points are shown, in order to reduce congestion

Comparison of model with previous correlations[5,8]

As shown in Fig. 5, a previous correlation[5] is not very accurate in regard to the present data. It is useful to compare the present model directly with the previous correlation expressions.[5,8] When Equations (6) and (8) are combined, the following dimensionally consistent expression is obtained:

$$U_S = C\left(\frac{\gamma^3}{\psi^2\bar{\rho}}\right)^{0{\cdot}2}\left(\frac{g^2\,\Delta\rho^2}{\rho_C\mu_C}\right)^{1/3} \quad . \quad . \quad . \quad . \quad . \quad . \quad . \quad (12)$$

(velocity) (length) (time)$^{-1}$

The proportionality constant C for experimental data (cases where $Af > 3$ cm/sec) is $2{\cdot}24 \times 10^{-2}$, with a standard deviation of $2{\cdot}36 \times 10^{-4}$. The previous correlations defined flooding velocity as $(U_D + U_C)$ rather than as in Equation (2a), but the main point of interest is the exponent to which each independent variable is raised on the right hand side of the equation. The comparison is shown in Table II. The exponent of $\Delta\rho$ in the model agrees quite well with the correlations. The continuous phase viscosity effect in the model agrees reasonably with Thornton's correlation[8] but not with that of Smoot *et al.*[5] It may also be noted from Fig. 5 that Smoot correlation[5] does not allow properly for the effect of continuous phase viscosity as regards the present data.

TABLE II

Comparison between present model and previous correlations

	Present work	Thornton[8]	Smoot *et al.*[5]
Exponent of $(\rho_D-\rho_C)$	0·67	0·79	0·63
,, ,, μ_C	−0·33	−0·26	0·49
,, ,, μ_D	0	0·30	−0·20
,, ,, ψ	−0·40	−0·24	−0·21
,, ,, γ	0·60	−0·17	−0·14
,, ,, d_o	0	0·90	0·46
,, ,, g	0·67	1·01	0·81

The model assumes no effect of dispersed phase viscosity while the correlations predict a small effect; however, the stated effect of μ_D on flooding velocity is negative in one case[5] and positive in the other.[8] The model predicts a stronger dependence on power input and interfacial tension than the correlations,[5,8] but no effect of hole diameter. This latter prediction is in marked contrast with the correlations, particularly that of Thornton.[8] The probable reason is that in Thornton's investigation[8] the maximum hole size was only 0·125 in. In Smoot *et al.*'s correlation,[5] the maximum hole size was 0·19 in and it is significant that they found a smaller exponent for d_o than Thornton.[8] It seems reasonable to suppose that as the hole diameter increases in relation to the drop diameter, it gradually ceases to be an important variable. In the Karr column, with a hole diameter of 0·5 in, the drop size is normally much less than the hole size and is dictated by the turbulence level alone. This may also account for the larger effect of ψ postulated in the model and illustrated by the data in Fig. 6. The last variable in Table II, gravity, has been included in the correlations[5,8] for the sake of dimensional correctness. There is no experimental data on its effect on flooding conditions, though such data could be obtained by operating an extractor on a centrifuge.

Conclusions

The flooding model proposed in this work is derived from several previous investigations; the fluidised bed analogy of Elgin & Foust,[10] the intermediate flow equation for friction,[11] the turbulent drop dispersion mechanism[13] and the power dissipation expression[8] in pulsed plate columns. It fits the present data better than the previous correlations[5,8] for pulsed plate columns, in which the hole diameter is an important factor. Further work is recommended to see whether the effects of interfacial tension and plate spacing are in agreement with the present model. It would also be useful to find out whether increasing the column diameter has any effect on flooding, although none is predicted in the model. Another possible application of the model might be the oscillating-baffle contactor recently developed by Thomas[15] in which the hole diameter is 0·25 in.

Nomenclature

A	amplitude, cm
C	dimensionless constant, Equation (12)
C_o	orifice coefficient, Equation (9)
d	drop diameter, cm
d_o	hole diameter, cm
f	frequency, Hz
g	gravitational acceleration, cm/sec^2
K	dimensionless constant, Equation (5a)
l	plate spacing, cm
p	pressure, dyne/cm^2
(Re)	drop Reynolds number $(=dU_S\rho_C/\mu_C)$

u velocity, cm/sec
U superficial velocity at the flooding point, cm/sec
U_M modified velocity, Equation (11), cm/sec
z distance up column, cm
γ interfacial tension, dyne/cm
$\Delta\rho$ density difference ($\rho_D - \rho_C$), g/cm^3
ε volume fraction of dispersed phase
μ viscosity, P
μ_{Co} reference viscosity = 0·01 P
ψ energy dissipation per unit volume, erg/cm^{3}sec
ρ density, g/cm^3
ρ' specific gravity, dimensionless
$\bar{\rho}$ average density ($=\varepsilon\rho_D + (1-\varepsilon)\rho_C$), g/cm^3
σ fraction free area

Subscripts

C continuous phase
D dispersed phase
S relative between phases

Acknowledgments

The authors wish to express their gratitude to Chem Flow Corporation who donated the reciprocating plate column, to the National Research Council of Canada for partial financial support, and to Mr. D. Burney for experimental assistance.

References

[1] U.S. P. 2,011,186
[2] Hanson, C., *Chem. Engng*, 1968, **75** (18), 76
[3] Karr, A. E., *A.I.Ch.E. Jl*, 1959, **5**, 446
[4] Chantry, W. A., Von Berg, R. L., & Weigandt, H. F., *Ind. Engng Chem.*, 1955, **47**, 1153
[5] Smoot, L. D., Mar, B. W., & Babb, A. L., *Ind. Engng Chem.*, 1959, **51**, 1005
[6] Sege, G., & Woodfield, F. W., *Chem. Engng Prog.*, 1954, **50**, 396
[7] McAllister, R. A., Groenier, W. S., & Ryon, A. D., *Chem. Engng Sci.*, 1967, **22**, 931
[8] Thornton, J. D., *Trans. Instn chem. Engrs*, 1957, **35**, 316
[9] Jealous, A. C., & Johnson, H. F., *Ind. Engng Chem.*, 1955, **47**, 1159
[10] Elgin, J. C., & Foust, H. C., *Ind. Engng Chem.*, 1950, **42**, 1127
[11] Gayler, R., Roberts, N. W., & Pratt, H. R. C., *Trans. Instn chem. Engrs*, 1953, **31**, 57
[12] Ergun, S., *Chem. Engng Prog.*, 1952, **48**, 89
[13] Shinnar, R., & Church, J. M., *Ind. Engng Chem.*, 1960, **52**, 253
[14] Calderbank, P. H., *Trans. Instn chem. Engrs*, 1958, **36**, 443
[15] Thomas, W. J., *Trans. Instn chem. Engrs*, 1969, **47**, 304

Liquid extraction in a continuous agitated horizontal contactor

by C. J. Mumford
Department of Chemical Engineering, The University of Aston in Birmingham, Gosta Green, Birmingham, U.K.

The Morris contactor is a novel continuous agitated horizontal extractor. The operation of a laboratory-scale liquid–liquid contactor with 5 mixing/transfer sections is described. At continuous to dispersed phase ratios of less than 1 or at low agitator speeds, operation corresponded to that of a mixer–settler chain.

Performance data are presented for the system water–toluene–acetone (or acetic acid). Maximum volumetric throughput was dependent on internal geometry but increased with phase ratio and decreased linearly with impeller speed. Hold-up and extraction efficiency both increased with impeller speed up to 400 rev/min.

Phase flowrates and hold-up were related by the equation:

$$\frac{V_d}{X} + \frac{V_c}{(1-X)} = \bar{V}_N (1-X)$$

It is concluded that the contactor merits consideration for non-pressure applications, where phase separation or particulate solids are a problem, and for leaching processes.

Introduction

CONTINUOUS AGITATED CONTACTORS find wide application in liquid–liquid extraction. These include pulsed columns and the more common rotary agitated columns, viz. the rotating disc contactor, Scheibel and Oldshue–Rushton extractors. Intimacy of contact between the phases is primarily dependent upon the mechanical energy input, i.e. for rotary agitated designs, the impeller speed. Since this also enhances the coefficients of mass transfer, optimum conditions can be achieved for any extraction process.

The influence of the main operating variables, viz. volumetric throughput, solvent to feed ratio and rotor speed is fairly well established for most columns.[1] Conversely little information has been published on the horizontal contactor patented by Morris.[2] This comprises a rectangular vessel subdivided into a series of compartments by alternate vertical weirs and baffles. The weirs have their upper edges submerged below the liquid level whilst the baffles extend from above the liquid surface to within a short distance of the bottom of the vessel. The weirs and baffles are spaced so as to provide narrow zones, or transfer sections, alternating with mixing sections. Each mixing section contains a gate impeller suspended from a vertical shaft and powered by a common overhead drive. In liquid contacting, the phases are fed into the two extreme mixing sections so as to pass through the contactor in countercurrent flow. The agitators cause one liquid to be dispersed. If the less dense liquid is dispersed, droplets are swept under the dividing baffle and into the adjacent transfer section where they ascend. The more dense continuous phase is swept over the weirs in the opposite direction. An interface normally exists only at the dispersed phase outlet so that the separation difficulties often associated with a mixer–settler chain can be avoided.

The contactor is claimed to be adaptable for continuous extraction, reaction or ion-exchange processes in both liquid–liquid and liquid–particulate systems.[3] Its original use was in the continuous manufacture and treatment of trinitrotoluene and it has since been found suitable for washing and lye treatment of soap curds. Nevertheless, application has been limited due, in part, to lack of data.

Hartland & Wise[4] have investigated the degree of backmixing in a liquid–liquid contactor. For kerosene in water, backmixing of the dispersed phase

was found to be negligible under normal operating conditions. Backmixing of the continuous phase passed through a maximum as the impeller speed was increased and varied inversely with continuous phase flowrate. Values of the backmixing coefficient, F, and Peclet number, P obtained from steady-state tracer experiments were found to be related for stagewise and differential models by:

$$M \log \left[1 + \frac{1}{F}\right] = P \qquad (1)$$

where

$$F = 53 \left[\frac{1}{X_t}\right]^{0\cdot46} \left[\frac{\mu_c}{D\, V_{ct} \rho_c}\right]^{1\cdot2} \qquad (2)$$

The present paper summarises work which has been performed to investigate the influence of the main operating variables on the extraction performance of a Morris contactor and to assess its potential for liquid–liquid contacting. A similar investigation has been carried out with a liquid–solid contactor (Smith, E. L., *et al.*, unpublished work).

Experimental and results

The equipment used is shown in Fig. 1. This consisted of a brass vessel 36·5 in long × 9·25 in deep × 3·25 in wide. The vessel had a glass front and was divided to give 5 mixing and transfer sections each 3 in wide. Weir and baffle heights were adjustable; these were set initially to give a weir height of 4 in and a baffle depth of 6 in. The mixing sections contained 1 in × $\frac{3}{4}$ in gate impellers each located with the bottom edge 2 in from the bottom of the vessel. The impellers were chain driven from a 0·15 h.p., 600 rev/min electric motor; the speed was adjusted by varying the input voltage and measured by

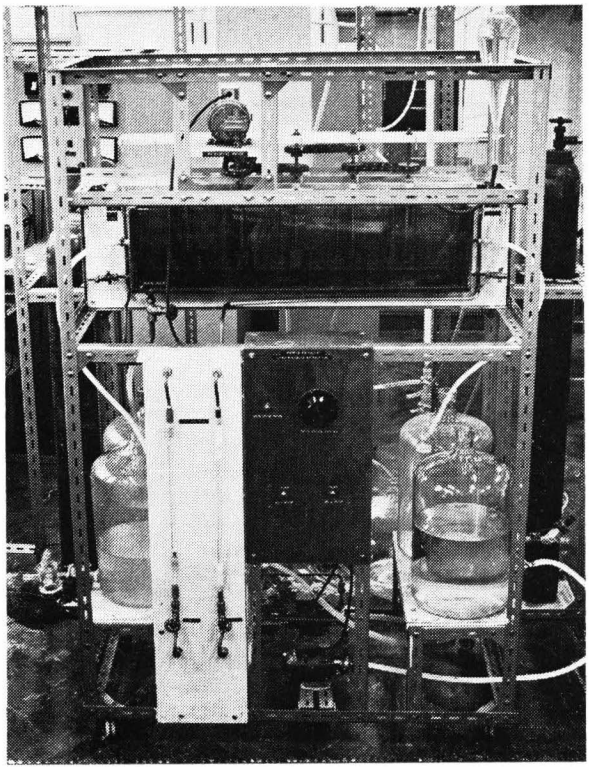

FIG. 1. *Pilot-scale Morris Contactor for liquid–liquid extraction*

means of a portable tachometer placed in direct contact with each impeller shaft. Liquids were stored in glass aspirators and transferred by means of Stuart-Turner No. 10 centrifugal pumps. All interconnecting tubing was of PTFE. Flow-rates into the contactor were controlled by needle valves and measured by independently calibrated rotameters. The system toluene–water was used with either acetone or acetic acid as solute. Typical conditions of operation are illustrated in Fig. 2. Absolute cleanliness was essential in order to obtain reproducible data. After any series of runs the equipment was therefore drained, washed through with Teepol solution and then flushed continuously with water for 30 min.

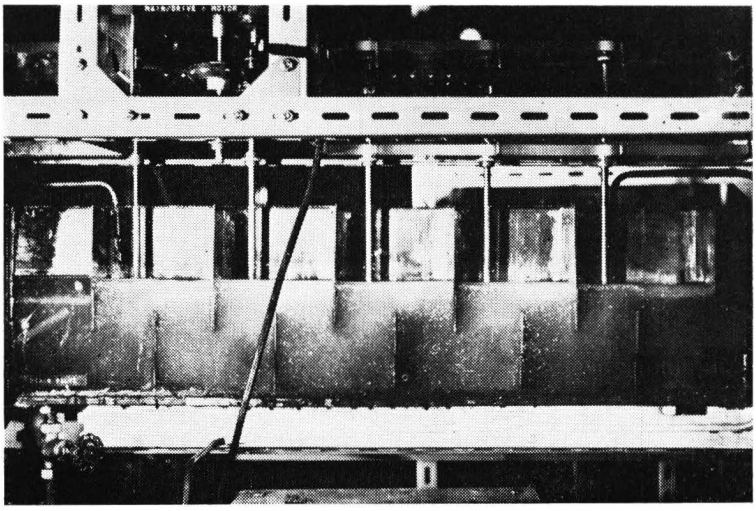

FIG. 2. *Contactor operating under typical conditions*
$V_C = 1 \cdot 5$ l/min, $V_D = 0 \cdot 25$ l/min, $N = 350$ rev/min
Dispersed phase flowing from right to left

Volumetric capacity

In common with other contactors the volumetric capacity is dependent on the phase ratio, the degree of agitation and the internal geometry. Initially runs were performed with mutually saturated phases in the absence of mass transfer.

At very low agitator speeds, e.g. 200 rev/min, a dispersed phase flow-rate existed at which the impellers were incapable of completely dispersing this phase and transferring it along the contactor. A separate interface existed in each compartment and 'flooding' resulted from an accumulation of dispersed phase. Characteristically, at practical operating speeds, flooding commenced with rejection of the dispersed toluene phase at the transfer section nearest the inlet. (It is of interest that, over the range of phase ratios in this work, either liquid could be made to constitute the continuous phase by charging it to the contactor first.) Two techniques were used to determine flood-points: (i) by incremental variation of dispersed phase flow-rate at 5 min intervals with a constant impeller speed and a selected continuous phase flow-rate; (ii) by slowly increasing the impeller speed at a constant phase ratio.

A sharper determination of the onset of flooding was found possible by method (ii). Typical results are shown in Figs 3 and 4. These incorporate results obtained when 10% acetic acid was initially present as solute in the dispersed phase. Phase ratios are on a continuous : dispersed phase basis. In general maximum volumetric throughput increases with an increase in phase ratio but decreases linearly with impeller speed. An increase in the capacity, of the order of 100%, occurred when mass transfer was from the dispersed phase. This was associated with a noticeable increase in droplet size compared with

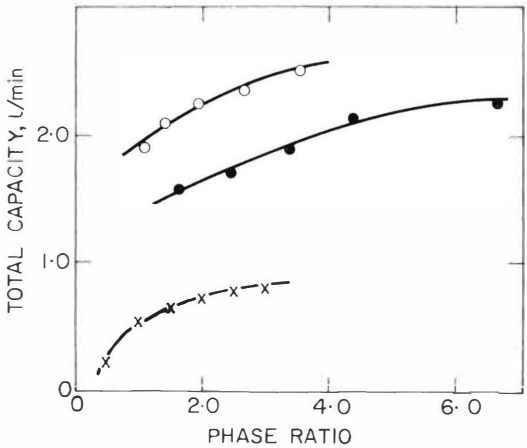

FIG. 3. *Variation of maximum throughput with phase ratio*
○ N = 350 rev/min; ● N = 400 rev/min; × N = 400 rev/min (kerosene–water[4])

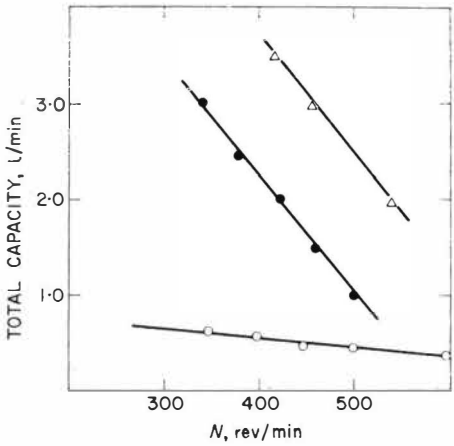

FIG. 4. *Variation of maximum throughput with rotor speed (phase ratio* = 1)
● No mass transfer; △ mass transfer from disperse phase; ○ kerosene–water[4]

solute-free conditions; this phenomenon is well established in other contactors, and is attributable to enhanced coalescence rates.[1]

Capacity is closely related to contactor internals; these results were obtained with the geometry described earlier (corresponding to a liquid head of approximately 3 cm above the weirs). No attempt was made to optimise this but the effect of a 1 cm increase in weir height, i.e. a one-third reduction in overflow area, was determined in a separate series of runs. When plotted the results gave curves similar to those in Fig. 3 but with a reduction in total capacity of the order of 20–25%. Separate runs with the baffles lowered by 1 cm yielded only slightly reduced capacities; this was as expected since the reduction in flow area so produced was only approximately 12%.

Under normal conditions of operation at high phase ratios and up to 80% of flooding, the dispersed phase persisted as droplets throughout the equipment. The contactor therefore operated as a continuous differential extractor. At low phase ratios, e.g. less than 1, bulk coalescence of the dispersed phase occurred in the transfer sections. The mode of operation was then that of a series of mixer–settlers.

Hold-up

Dispersed phase hold-up at different impeller speeds was determined by samples withdrawn from each of the four centre mixing and transfer sections in the presence and absence of mass transfer. Individual sections showed a maximum deviation of 7% from the mean value. Hold-up was found to

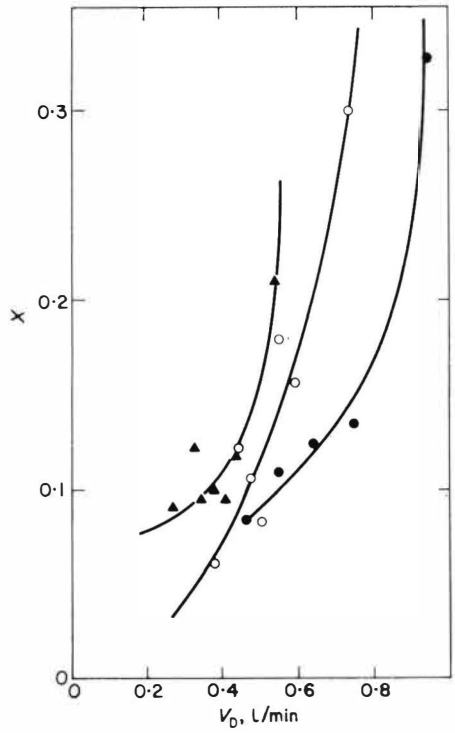

FIG. 5. *Fractional mean hold-up in transfer sections* (N = 350 *rev/min*)
● V_C = 1·0; ○ V_C = 1·5; ▲ V_C = 2·0 l/min

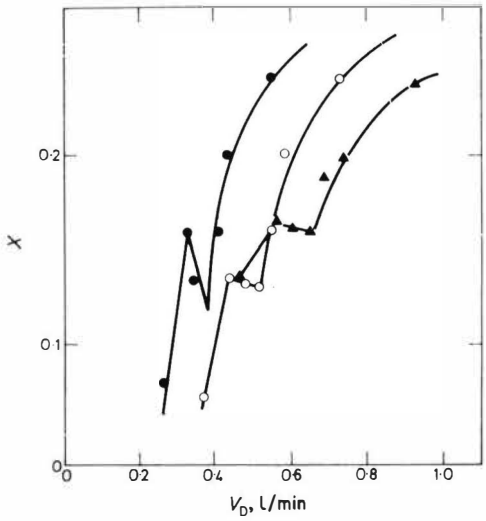

FIG. 6. *Mean fractional hold-up in mixing sections* (N = 350 *rev/min*)
▲ V_C = 1·0; ○ V_C = 1·5; ● V_C = 2·0 l/min

increase with increasing impeller speed owing to the reduction in drop size produced in the mixing sections. Thus, in the solute-free system at 350 rev/min, the mean drop size was of the order of 0·1 cm and at 200 rev/min it was 0·27 cm. Typical hold-up data are shown in Figs 5 and 6. Results obtained for the transfer sections were of similar form to those obtained by Hartland & Wise.[4] Curves of hold-up *versus* dispersed phase flowrate for the mixing sections all showed a well defined break where hold-up decreased, for an increase in flow-rate. This occurred at 70–80% of the flooding point and was greater the higher was the continuous phase flow-rate. Such phenomena are well known in packed columns,[5,6] and are best defined with high interfacial tension systems at high continuous phase flow-rates. In columns they are associated with an increase in drop size;[6] this was not observed in this work and there were only slight indications of a corresponding break occurring in the transfer sections. The fractional hold-up in both mixing and transfer sections was greatly reduced when mass transfer was taking place. No break point was observed in curves plotted for the mixing section data; this may have been attributable to the lowering of the interfacial tension by the presence of acetic acid[7] or to the inherently larger drop sizes observed. The hold-up at flooding was approximately three times greater when solute was present, consistent with an increased mean droplet size and greater throughput.

Whilst hold-up in the mixing sections was in all cases greater than in the transfer sections, which operated as spray columns, correlations of the form previously proposed,[4] viz.:

$$X_m = 11\cdot4\, N^{-0\cdot53}\, V_{dt}^{0\cdot66} \qquad (3)$$

$$X_t = 7\cdot0 \times 10^{-8}\, N^{3\cdot7}\, V_{dt}^{1\cdot5} \qquad (4)$$

did not prove valid for this work. For packed columns and some agitated columns,[1] phase flow-rates and hold-up can be correlated by an equation of the form:

$$\frac{V_d}{X} + \frac{V_c}{(1-X)} = \bar{V}_N\,(1-X) \qquad (5)$$

where V_N is the mean relative velocity of the droplets extrapolated to essentially zero flow-rates. The validity of this equation for this contactor was examined by following the procedure developed by Thornton.[8] Good agreement was obtained as indicated by the straight lines capable of extrapolation through the origin obtained when V_{df} was plotted against $X_f^2\,(1-X_f)$ as in Fig. 7. Values of the characteristic velocity calculated by this procedure from flooding and

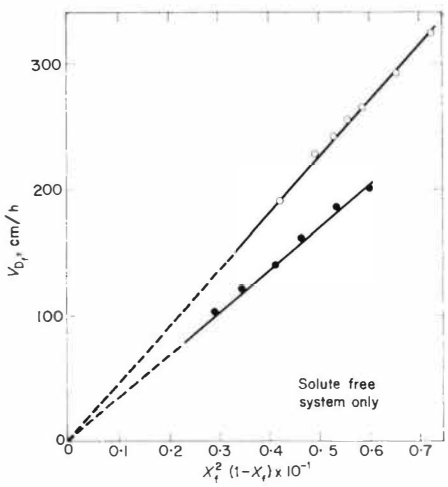

FIG. 7. *Correlation of flooding data after Thornton*[8]
Solute-free system only
○ N = 350 rev/min; ● N = 400 rev/min

experimental hold-up data showed a maximum deviation of only 10%. When mass transfer was occurring, however, the correlation was found to be invalidated by the enhanced characteristic velocities.

For the solute-free system, a series of hold-up profiles along the contactor were also determined by rapidly isolating the equipment and allowing the phases to separate. Typical results are shown in Fig. 8. In general, profiles below flooding showed a slight increase in hold-up in moving away from the dispersed phase inlet; at flooding the profiles were reversed.

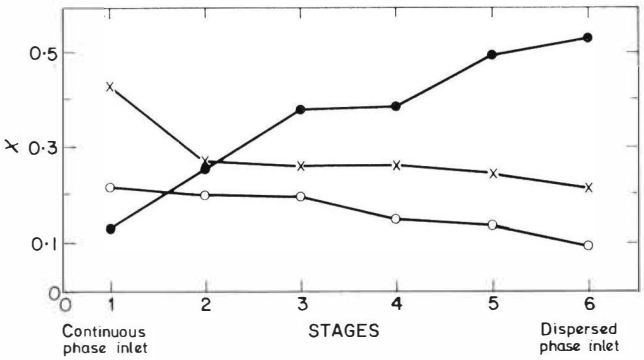

FIG. 8. *Hold-up profiles along contactor*
○ N = 300 rev/min; × N = 350 rev/min; ● N = 400 rev/min (flooding)

Back-mixing

Back-mixing concentration profiles were determined using acetic acid as tracer in the usual way[4] but at 75% of flooding. Back-mixing was found to increase with impeller speed to reach a maximum at 300 rev/min with a phase ratio of unity and then to decrease. This confirms the observations of Hartland & Wise.[4] Further, at constant impeller speed, back-mixing was greatest when the phase ratio was small; F decreased sharply with increasing flow of continuous phase as shown in Fig. 9.

Mass transfer

Mass transfer was investigated using acetone as solute giving a distribution coefficient of almost unity and facilitating analysis by measurement of refractive

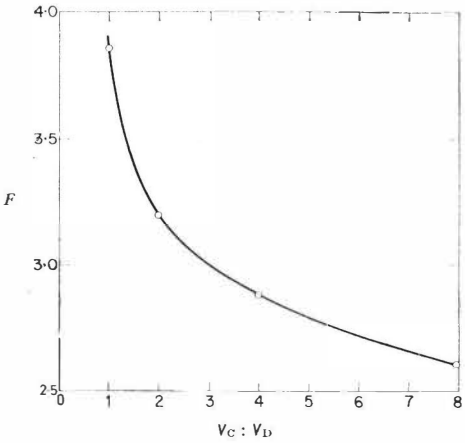

FIG. 9. *Variation of back-mixing factor with phase ratio* (N = 300 *rev/min*)

indices. Approximately 20 wt.-% solutions were used. The number of transfer units $(NTU)_{OR}$ was calculated by graphical integration in the usual way.[9] Typical results showing the variation of $(NTU)_{OR}$ with rotor speed are given in Fig. 10. In general extraction efficiency increased with impeller speed. The enhanced efficiency generally associated with mass transfer from the continuous phase[1] is not well defined. The variation of $(NTU)_{OR}$ with phase ratio is shown in Fig. 11.

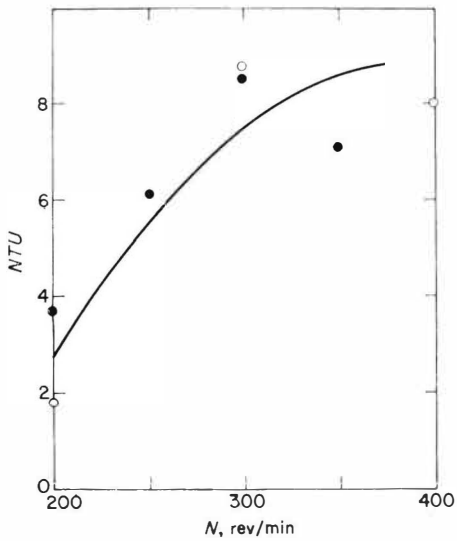

FIG. 10. *Variation of* $(NTU)_{OR}$ *with impeller speed*
Phase ratio 1 : 1
Direction of transfer: ○ water to toluene; ● toluene to water

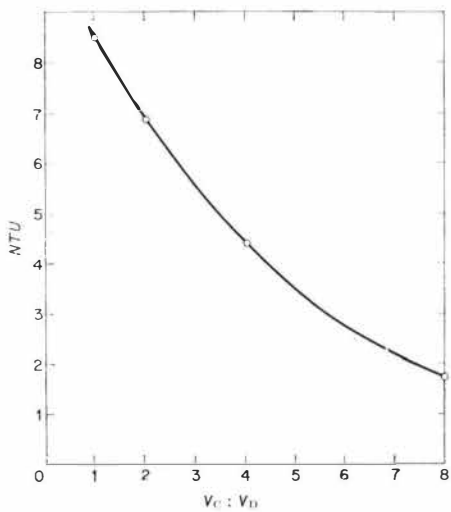

FIG. 11. *Variation of* $(NTU)_{OR}$ *with phase ratio*
$N = 300$ rev/min
Mass transfer from toluene to water

As mentioned earlier, no attempt was made to optimise internal geometry and an increased residence time of the dispersed phase could be achieved by reduction of the lower baffle orifice heights. Some reduction in the extent of con-

tinuous phase back-mixing could also be achieved by the insertion of packing or baffles in the transfer sections as in the Scheibel and similar columns.[1]

The contactor is relatively inexpensive to fabricate and extremely simple and and versatile in operation. Volumetric capacity is undoubtedly greater than for a mixer–settler chain owing to the absence of intermediate interfaces. The potential exists for applying different degrees of agitation in consecutive sections thus allowing for changes in interfacial tension associated with different solute concentrations as extraction proceeds. Also, as pointed out by Morris,[3] the ability to operate with either liquid as the disperse phase by adjusting the height of the end separator outlets enables viscous liquids to be processed.

It is believed to merit consideration for non-pressure liquid–liquid extraction applications particularly where phase separation or the presence of particulate solids may present difficulties in conventional mixer–settlers or packed columns. Thus work is in progress to extend this study to investigate systems of low interfacial tension and to correlate $\overline{V}_N$ in Equation (5) with rotor speed and physical properties, by means of an equation of the form found satisfactory for the rotating disc contactor[8] and Oldshue–Rushton[10] columns, viz, at constant geometry:

$$\frac{\overline{V}_N \mu_c}{\sigma} = k\left[\frac{\Delta\rho}{\rho_c}\right]^a \left[\frac{g}{RN^2}\right]^b \qquad (6)$$

Apart from in the two end compartments, it appears that hold-up and hence mean drop size varies little throughout the equipment. Since discrete droplets persist throughout, a design procedure may be based on single drop mass transfer data using predicted or photographically determined mean drop sizes (Hshemi, M., unpublished work). in any practical application, however, with a variable impeller drive and adjustable weir, baffle and impeller heights, in-plant optimisation would be relatively simple and an empirical design procedure may be adequate.[2]

The contactor has probably greatest potential for liquid–solid processing, e.g. leaching (Smith, E. L., *et al.*, unpublished work). With dense solids it is simply necessary to slope the base of the transfer sections to assist forward flow of the solid[3] (and Smith, E. L., *et al.*, unpublished work).

Acknowledgment

The author is indebted to Messrs D. J. Green, J. F. Gallacher, A. R. Payne and B. M. Samson for performing much of the experimental work described.

Nomenclature

D = contactor width, (characteristic dimension) cm

F = continuous backmixing coefficient (stagewise model)

g = acceleration due to gravity

M = number of stages in contactor

N = impeller speed, rev/min

NTU = number of transfer units

P = Peclet number of continuous phase (differential model)

V = superficial velocity of phase, cm sec^{-1}

$\overline{V}_N$ = characteristic velocity, cm sec^{-1}

x = concentration of solute in continuous phase

X = holdup, fraction of dispersed phase

ρ = density

μ = viscosity

σ = interfacial tension

Subscripts

c = continuous phase

d = dispersed phase

f = at flood point

m = mixer section

n = stage number

t = transfer section

References

[1] Mumford, C. J., *Br. Chem. Engng*, 1968, **13,** 981

[2] B.P. 885,503 and 974,829

[3] Morris, W. H., paper presented to Soc. Chem. Ind. Conference on Industrial Solvent Extraction Equipment, London, 27 March, 1969

[4] Hartland, S., & Wise, G. D., *Trans. Instn chem. Engrs*, 1967, **45,** 353

[5] Dell, F. R., & Pratt, H. R. C., *Trans. Instn chem. Engrs*, 1951, **29,** 89

[6] Ballard, J. H., & Piret, E. L., *Ind. Engng Chem.*, 1950, **42,** 1088

[7] Murphy, N. F., Lastorica, J. E., & Fallis, J. C., *Ind. Engng Chem.*, 1957, **49,** 1035

[8] Logsdail, D. H., Thornton, J. D., & Pratt, H. R. C., *Trans. Instn chem. Engrs*, 1957, **35,** 301

[9] Treybal, R. E., 'Liquid extraction', 1963 (2nd edn) (New York: McGraw-Hill)

[10] Bibaud, R. E., & Treybal, R. E., *A.I.Ch.E.Jl*, 1966, **12,** 472

Direct contact heat transfer between immiscible liquids in a mixer–settler apparatus

by C. Hanson, J. Ingham and T. N. Stewardson

Post-Graduate School of Chemical Engineering, University of Bradford, Bradford 7, U.K.

Heat transfer experiments were carried out using the direct contacting of two immiscible liquids in a high throughput mixer–settler. The effects of propeller speed, flow-rate, and flow ratio on the heat conductances were investigated, and high values of the order of 1200 Btu/h°F were obtained for the 2-gal capacity unit. Comparison of the results with theoretically derived values indicated a change in the basic droplet transfer mechanism from rigid sphere to circulating drop behaviour as a consequence of a relative increase in the dispersed phase flow-rate. The experimental results agreed well with those of other studies, indicating a basic relationship between the rate of heat transfer and the interfacial area generated in the system.

Introduction

THE GROWING REQUIREMENT for more efficient methods of heat transfer has aroused interest in the possibility of achieving this by contacting immiscible liquid pairs directly together. The subject of direct liquid–liquid heat transfer has been reviewed several times in the literature.[1–3] Originating as an aid to mass transfer studies, heat transfer by direct liquid–liquid contacting has become an interesting and independent area of activity within the sphere of liquid–liquid operations, with numerous advantages over more conventional techniques. Advantages include enhanced rates of transfer, the absence of any resistance due to tube surfaces, and the absence of fouling considerations in contactors of simplified mechanical construction. Whilst the present investigation was undertaken primarily in order to provide design information for process studies, it has nevertheless raised several points of more fundamental significance.

Previous studies

The process of direct contact heat transfer is exactly analogous to mass transfer in that the same forms of physical law apply. Several studies have utilised this fact by measuring temperature changes rather than the less convenient measurement of concentration. This has resulted, however, in most of the studies being concerned with small temperature changes so as not to effect large changes in the physical properties of the system.

A very low temperature difference of the order of 0·5°C was utilised by Davis & Colven[4] in order to compare the mixing efficiencies of various impellers in a 20-gal capacity pump-mix mixer–settler. Mottel[5] utilised a temperature difference of only 2°C in studies of the mixing efficiency of a shrouded paddle in a mixer–settler, and the same order of temperature difference was employed by Mottel & Colven[6] in work on shrouded paddles in a turbine contactor. These latter results were analysed by Webster,[7] who found good agreement between these and theoretically calculated values of the heat conductances. Results involving mass transfer studies, however, were nearly two orders of magnitude higher than the theoretical values. This was explained as being due to an impedance to heat transfer to the drops due to impurities at the interface, which was disrupted under conditions of the simultaneous heat and mass transfer to give enhanced rates of transfer. Webster's calculations for the heat transfer conditions demonstrated the underlying similarity of the results obtained for mixer–settler contactors ranging in flow-rate from 1·6 to 100 galmin/. Coughlin & von Berg[8] studied the process of simultaneous heat and mass

transfer in an industrial scale 'pump-mix' mixer–settler. Good agreement was obtained between the experimental results and theoretical values based on models of the transfer processes.

Whilst these and other studies demonstrate the applicability of theoretical analysis to problems of direct contact heat transfer in mixer–settlers, it was felt that the possible effects of significant temperature differences on performance required further study, hence leading to the research programme described in this paper.

Experimental

A flow diagram of the apparatus is given in Fig. 1. This flow system enabled the direct contacting of a hot oil–cold water system to be studied. The particular oil employed, Shell-B.P. Turbo Oil 27, has good stability at elevated temperatures, a flash point of 410°F, and although the viscosity is relatively high at room temperature, this was considerably reduced over the range of working temperature employed (i.e. 75–95°C).

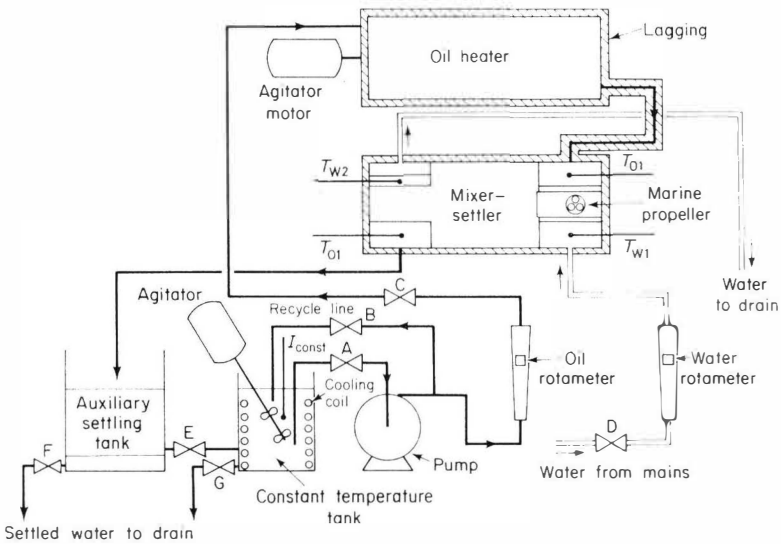

FIG. 1. *Flow diagram of apparatus*

The contactor used was a high throughput mixer–settler as developed by Hanson & Kaye.[9] This was chosen because of the very high flow capacity, which is independent of propeller speed, and the complete hydraulic independence of the mixing and settling stages, such that no backmixing is possible. The unit had a capacity of ~ 2 gal and was fabricated from stainless steel with observation glasses at each end of the mixing and settling compartments. The mixing compartment had overall dimensions of 6 in. × 6 in × 6 in. The oil and water entered over 3-in high weirs situated at opposite sides of the mixer and were contacted by means of a marine propeller rotating inside a draught tube, of 1·5-in diameter, slightly larger than the propeller. This not only dispersed one liquid phase in the other, but also lifted the two phases up the draught tube on to a tray, which then delivered the dispersion into the settler. The height of the draught tube was 3 in. Vortex formation in the draught tube was prevented by the use of a small internal baffling arrangement. The overall dimensions of the settler were 6 in × 6 in × 24 in long, the settled phases being removed via appropriate underflow and overflow weirs. The power supplied to the propeller was measured by a watt meter, and the

propeller speed by means of a stroboscope. The complete assembly was insulated and boxed-in to prevent heat loss. The temperatures of the entering and exit phases were measured in the respective inlet and outlet weir compartments, using mercury-in-glass thermometers calibrated in 0·1 °C divisions.

Heating of the circulating oil system was effected by means of an electrical heater assembly of 12 kW total capacity, fitted with a thermostatic control device. Flow-rates were measured by means of rotameters, the oil rotameter being calibrated over the range of operating temperature in order to compensate for the effect of changing system properties. Operation of the apparatus was always such that the aqueous phase was dispersed. Full tabulated values of the experimental results, calculated results and system physical properties are available.[10]

Results and discussion

Overall heat conductances (UA values) were calculated from the measured heat load on the basis of a logarithmic mean temperature, computed from the inlet and outlet temperature for the apparatus as a whole. Thus:

$$UA = \frac{Q}{\Delta T_m}$$

$$\text{where } \Delta T_m = \frac{(T_{O1} - T_{W1}) - (T_{O2} - T_{W2})}{\ln\left(\dfrac{T_{O1} - T_{W1}}{T_{O2} - T_{W2}}\right)}$$

where A is total interfacial area; Q is total heat load; T is temperature; U is overall heat transfer coefficient; subscripts o, w, 1 and 2 denote oil, water, mixer inlet and settler outlet, respectively.

The use of the temperature mean, it should be noted, is of rather doubtful theoretical validity as it ignores the very complex fluid regime in the mixer and the effects of the heat transfer in the settler. The first effect, however, is an unknown quantity, whilst the total heat transfer occurring in the settler was shown experimentally to be very small. Although the UA values thus obtained are in accordance with common practice, their limitations must be recognised.

In the experiments, the separate effects of propeller speed, phase ratio and total flow-rate on the heat conductances were investigated. Results obtained with a phase flow ratio, oil:water, of 1:1 are shown in Figs 2, 3 and 4; those for an oil:water phase ratio of 2:1 are shown in Figs 5, 6 and 7, with water the dispersed phase. The results all show considerable scatter, owing to the very high rates of heat transfer obtained and the consequent close approach to equilibrium at the settler outlet. This gave temperature differences of the order of only 1–0·5 °C, and thus gave corresponding difficulties in measurement. The heat conductances were found to increase with increasing rates of agitation, and the high values obtained, 1200 Btu/h °F at 1:1 flow ratio, and 600 Btu/h °F at 2:1 flow ratio, are noteworthy. The UA values also showed a slight tendency to increase with increasing total flow-rate, but this may not be significant as the variation, in general, appeared to be in the same region as that due to the experimental error.

The effect of increasing propeller speed in increasing the UA values is as expected, owing to the increasing turbulence produced in the continuous phase and the resulting decrease in the mean droplet size and thus the increased interfacial area. The large difference in the magnitudes of the UA values at equivalent stirring conditions for the two different phase ratios was, however, unexpected. Furthermore, there appear to be different forms of the dependence

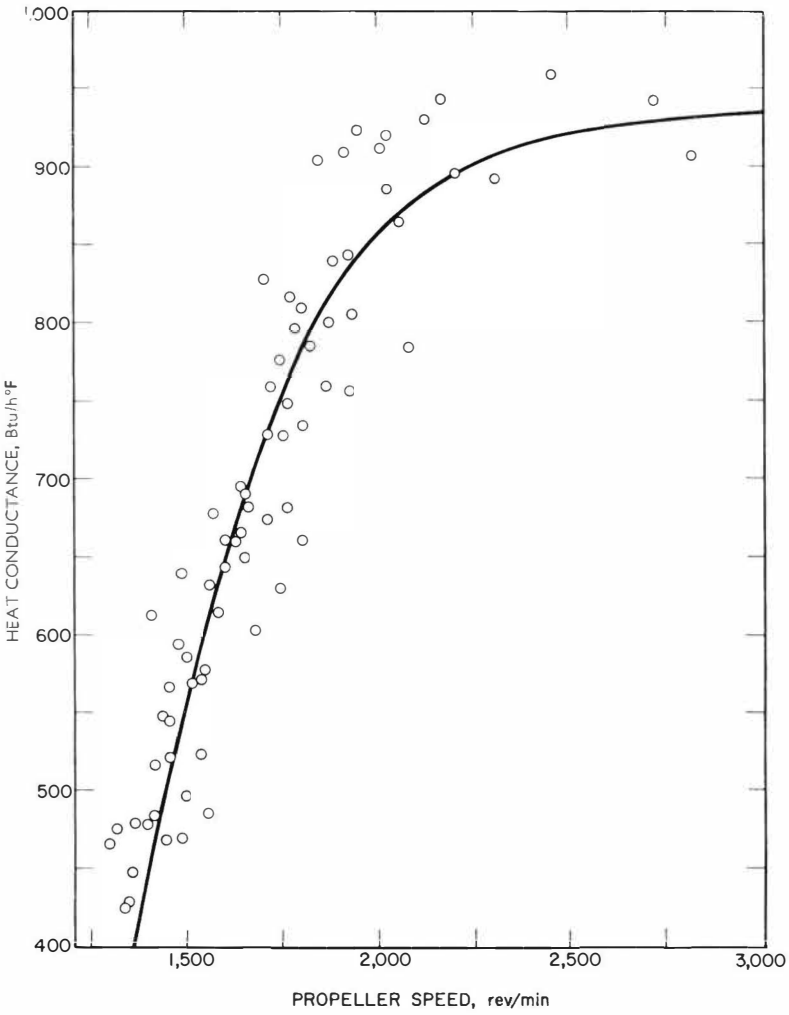

FIG. 2. *Plot of heat conductance results for 1 : 1 flow ratio of oil : water (by wt.) and an oil flow-rate of 420 lb/h*

in the *UA* values *versus* propeller speed. At 1:1 phase ratio, the rate of increase in the heat conductance tended to decrease with increasing propeller speed and approached a limiting value, whereas at the 2:1 phase ratio, for the same range of propeller speeds, the heat conductances were still tending to increase with increasing speed. The large difference in the magnitude of the heat conductances and the differing dependence on propeller speed suggested that the net rate of heat transfer for the two phase-ratio conditions might be generated by different functions of the properties of the system. These different

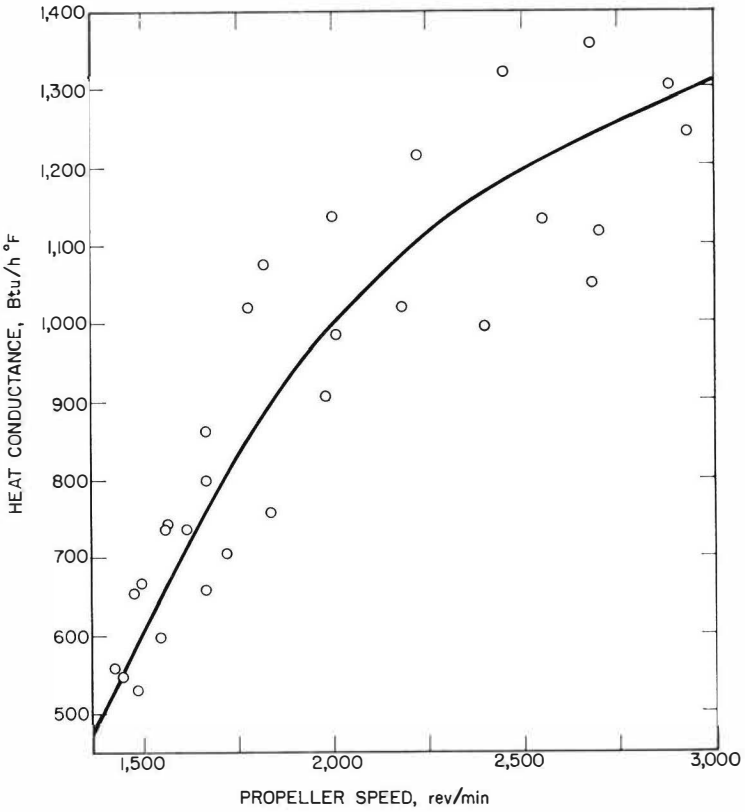

FIG. 3. *Plot of heat conductance results for 1 : 1 flow ratio of oil : water (by wt.) and an oil flow-rate of 550 lb/h*

functions might occur with different conditions in the dispersed phase, such as droplets undergoing transfer by a rigid sphere mechanism involving purely molecular heat conduction into the drop, and other mechanisms such as the presence of internal circulation currents in the droplets and the effects of droplet–droplet interaction, both of which would tend to increase the net rate of transfer.

In order to test this hypothesis, information concerning the mean droplet size in the dispersion was required. No experimental determinations were available in this case and, therefore, established correlations had to be used. Three correlations were finally considered; that of Webster,[7] based on those of Vermeulen *et al.*[11] and Roger *et al.*;[12] that of Coughlin & von Berg;[8] and that of Bouyatiotis & Thornton.[13] Of these, the correlation of Bouyatiotis & Thornton,[13] developed from a similar type of mixing system to the draught tube used in this case, but on a much larger scale, and based on theoretical consideration of the relative slip velocity between the phases and the power dissipated into the system, was thought to be the most applicable. This cor-

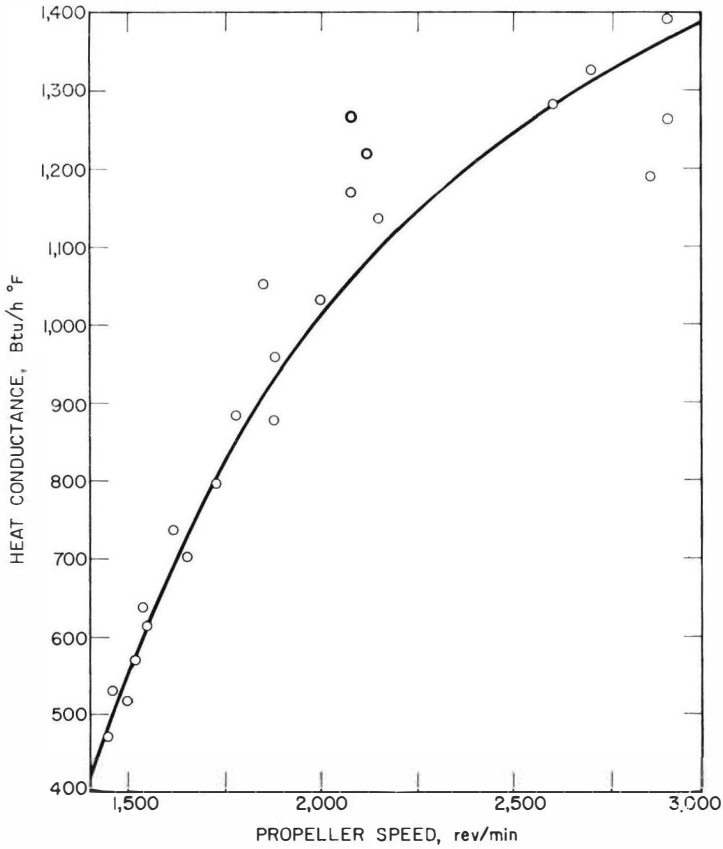

FIG. 4. *Plot of heat conductance results for 1 : 1 flow ratio of oil : water (by wt.) and an oil flow-rate of 670 lb/h*

relation was also found to be in very good agreement with the correlation and experimental results of Coughlin & von Berg.[8] The correlation of Webster predicted mean drop sizes an order of magnitude lower. Over the range of conditions employed, and based on the correlation of Bouyatiotis & Thornton,[13] the predicted mean droplet size for 1:1 flow-ratio conditions was found to vary from 0·85 to 1·2 mm diameter, and for 2:1 flow ratio conditions from 0·5 to 0·75 mm diameter. Under these conditions of small droplet size and low droplet Reynolds Number in the mixer (this was only slightly greater than unity), transfer by a rigid sphere mechanism would normally be expected. Theoretical predictions of the droplet and continuous film coefficients for the heat transfer were calculated, therefore, on the basis of models assuming (a) rigid sphere behaviour and (b) droplets with internal circulation only, as it was considered that the possibility of the droplets exhibiting oscillating behaviour under these conditions was extremely unlikely. The correlations subsequently chosen for

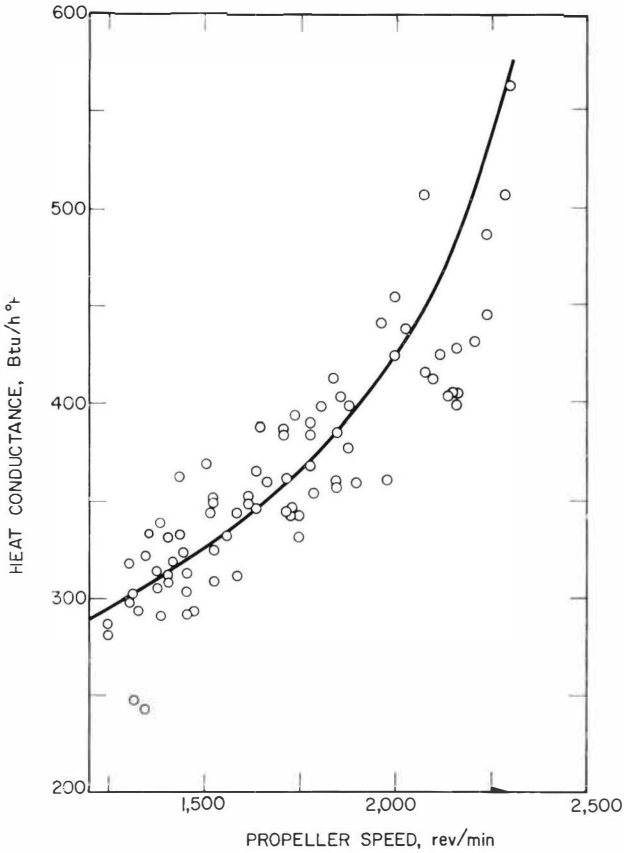

FIG. 5. *Plot of heat conductance results for* 2 : 1 *flow ratio of oil : water (by wt.) and an oil flow-rate of* 470 *lb/h*

the heat transfer were combinations of those of Steinberger & Treybal[14] and Treybal[15] for the rigid drops, and those of Elzinga & Banchero,[16] Boussinesq,[17] Kronig & Brink[18] and Handlos & Baron,[19] for the drops with internal circulation. Values for the continuous and dispersed phase film heat transfer coefficients were calculated from these correlations using the relevant heat transfer analogy. Mean values of the liquid physical properties for use in the correlations were evaluated at the bulk mean temperature for each phase. Although this is accepted procedure, it should be noted that this method for determining the droplet regime by comparison with the theoretical values is largely circumstantial and usually only limited conclusions can be drawn.

The experimental results obtained at 2:1 flow ratio showed best agreement with the values corresponding to rigid sphere behaviour, as expected. This was also the case for the results obtained with the 1:1 flow ratio at low propeller speeds, but as the propeller speed was increased, these results showed the best correspondence with values predicted assuming circulating drop behaviour, intermediate to the Handlos & Baron, and Kronig & Brink models. A feature of the theoretical models was the very large range in values obtained even for the same assumed mode of droplet behaviour. Under these conditions, therefore, any conclusions drawn become even more tenuous. The disparity in

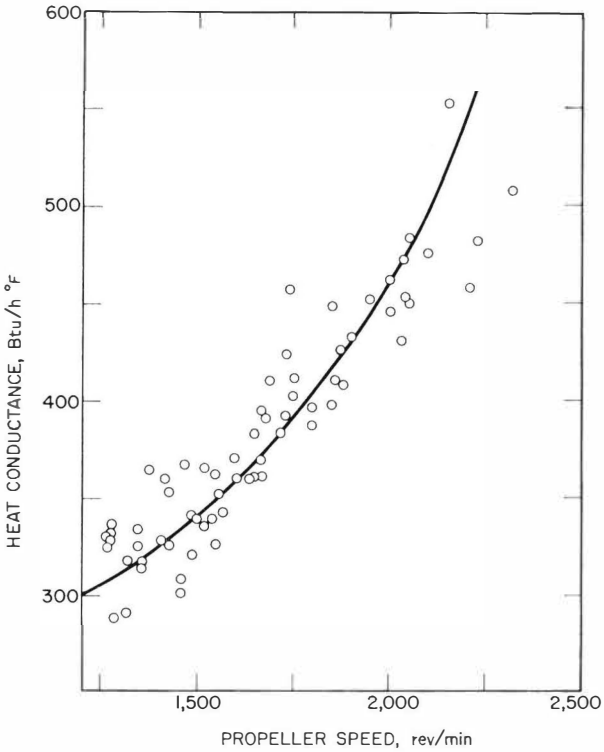

FIG. 6. *Plot of heat conductance results for 2 : 1 flow ratio of oil : water (by wt.) and an oil flow-rate of 600 lb/h*

the results, however, raises the question as to why the 1:1 phase ratio results differ in apparent mechanism from those at 2:1 flow ratio. At 1:1 phase ratio with low propeller speeds, the calculated drop size was < 1 mm and the correspondence with rigid drop behaviour at these ratio conditions may indicate a transitional stage in the droplet behaviour. At 1:1 phase ratio, the drop sizes are generally larger than those at 2:1 phase ratio, thus giving some increase in the tendency for internal droplet circulation. It has also been shown that the disruption of the liquid–liquid interface by a concentration gradient can cause internal circulation to be set up in droplets of smaller diameter than would normally be expected.[7] Another factor contributing to the adoption of an internally circulating flow regime is the fact that, at 1:1 phase ratio, there is twice the quantity of dispersed phase flowing through the same quantity of continuous phase as at 2:1 phase ratio. This means an increase in the relative velocity at 1:1 phase ratio, and, therefore, an increase in the viscous drag between the phases, which is one of the factors inducing internal droplet circulation. However, the most probable cause of the enhancement in the heat transfer rate is that due to increasing droplet–droplet interaction as a result of the increased holdup of dispersed phase in the mixer at the higher dispersed: continuous phase ratio. Thornton[20] has shown that the mass transfer processes in stirred vessels may be dominated by an intensive coalescence–redispersion mechanism, giving mass transfer rates more in accordance with a turbulent eddy-mixing mechanism, than to the expected process of molecular diffusion through a stagnant drop.

In order to see whether a link could be established between this and other work, the results were compared with those of Mottel & Colven.[6] These were

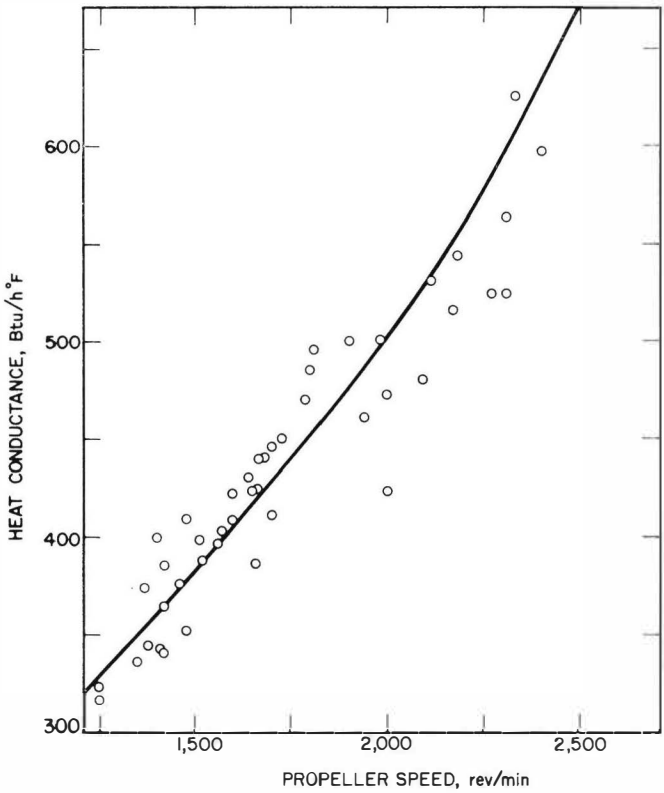

FIG. 7. *Plot of heat conductance results for 2 : 1 flow ratio of oil : water (by wt.) and an oil flow-rate of 710 lb/h*

also obtained in a mixer–settler apparatus, but in one using shrouded paddle turbine contactors of different impeller sizes. When plotted on the same graph, as a function of propeller size (Fig. 8), the agreement between the values of heat conductances obtained in the two investigations for the 1:1 phase ratio is quite good. The results of this investigation for 2:1 phase ratio, oil:water are in agreement with those of Mottel & Colven[6] for phase ratio conditions of 0·5:1, which, although a coincidence, appears at first to have no relevance. A similarity exists, however, in that, with the present work, the water was the dispersed phase, whereas in the studies of Mottel & Colven[6] the oil phase was dispersed. Therefore, the two sets of results are comparable in representing a 2:1, continuous: dispersed phase ratio. This reinforcement in the agreement between the two investigations tends to suggest that direct contact heat transfer in mixer–settlers does not vary greatly according to difference in that type of impeller employed, and that the true relationship is probably between the heat transferred and the interfacial area generated. The heat transfer is defined, therefore, by the droplet size and by the power dissipation, also taking into account possible differences in the mode of droplet behaviour, as affected by varying phase ratio.

Conclusions

The high throughput mixer–settler is an extremely efficient form of direct-contact heat exchanger. In these studies, the capacity of the apparatus was limited only by the difficulties of efficient phase disengagement for the very high degree of dispersion obtained at high rates of agitation, and a larger settler capacity would have enabled substantially higher flow capacities to be handled,

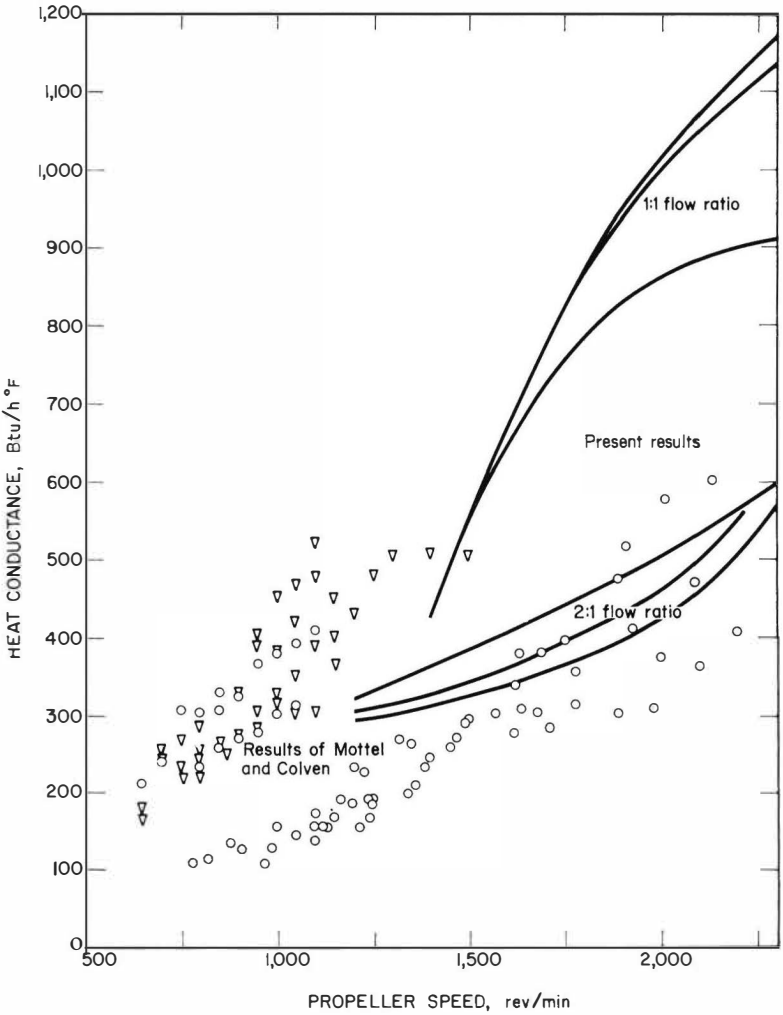

FIG. 8. *Comparison of experimental results with those obtained by Mottel & Colven*[6]
▽ approx. 1 : 1 flow ratio; ○ approx. 0·5 : 1 flow ratio.

still with effective rates of heat exchange.

Theoretical comparisons with the experimental results indicate a rigid sphere heat transfer mechanism to be dominant at a 2:1 oil:water flow ratio. At 1:1 flow ratio, the increased relative flow of dispersed phase, with its effects of increasing droplet–droplet interaction, increasing droplet size and increasing viscous drag on the droplet surfaces, causes sufficient disruption of the liquid–liquid interfaces so that the heat transmitted is greatly enhanced compared to considerations of rigid drop behaviour. The influence of variation of dispersed: continuous flow ratios on the droplet transfer mechansim may, therefore, be of great importance in the design and operation of large-scale mixer–settlers for both heat transfer and mass transfer applications.

The excellent correspondence between the results of this study, and those obtained by Mottel & Colven[6] for shrouded paddle turbine impellers of differing dimensions, when correlated against propeller speed, confirms the essential dependence of heat conductance on interfacial area and droplet transfer mechanism, as opposed to differences in the type and dimensions of the mixer–settler apparatus.

References

[1] Sideman, S., *Adv. chem. Engng*, 1966, **6,** Chapter 4
[2] Kehat, E., & Sideman, S., 'Recent Advances in Liquid–Liquid Extraction', 1971, Chapter 12 (Oxford : Pergamon Press)
[3] Hanson, C., & Ingham, J., *Br. chem. Engng*, 1965, **10,** 391
[4] Davis, A. T., & Colven, T. J., *A.I.Ch.E. Jl*, 1961, **7,** 72
[5] Mottel, W. J., *Rep. Congr. atom. Energy Commn U.S.*, 1955, D.P.-130
[6] Mottel, W. J., & Colven, T. J., *Rep. Congr. atom. Energy Commn U.S.*, 1957, D.P.-254
[7] Webster, D. S., *Rep. Congr. atom. Energy Commn U.S.*, 1964, D.P.-847
[8] Coughlin, R. W., & von Berg, R. L., *Chem. Engng Sci.*, 1966, **21,** 3
[9] Hanson, C., & Kaye, D. A., *Chem. Process Engng*, 1963, **44,** 27; 1963, **44,** 651
[10] Stewardson, T. N., M.Sc. Thesis, 1968, University of Bradford
[11] Vermeulen, T. G., Williams, G. M., & Langlois, G. E., *Chem. Engng Prog.*, 1955, **51,** 85F-94F
[12] Roger, W. A., Trice, V. J., & Rushton, J. H., *Chem. Engng Prog.*, 1956, **52,** 515
[13] Bouyatiotis, B. A., & Thornton, J. D., *Instn chem. Engrs Symp. Ser.*, 1967, No. 26
[14] Steinberger, R. L., & Treybal, R. E., *A.I.Ch.E. Jl*, 1963, **6,** 227
[15] Treybal, R. E., 'Liquid Extraction', 1951, 1st Edn., (N.Y.: McGraw-Hill)
[16] Elzinga, E. R., & Banchero, J. T., *Chem. Engng Prog. Symp. Ser.*, 1959, **55,** No. 29
[17] Boussinesq, M. J., *J. Math. Pures appl.*, 1905, **1,** 285
[18] Kronig, R., & Brink, J. C., *Appl. Sci. Res.*, 1951, **A2,** 142
[19] Handlos, A. E., & Baron, T., *A.I.Ch.E. Jl*, 1957, **3,** 127
[20] Thornton, J. D., *Ind. Chem.*, 1964, **40,** 13

Design and operation of a pulsed packed column for liquid–liquid extraction

by N. M. Spaay, A. J. F. Simons and G. P. ten Brink
DSM Central Laboratory, Geleen, The Netherlands

The paper describes the results of investigations carried out in pulsed packed columns (PPC) *both on a laboratory scale (5-, 10- and 22-cm diameter) and on an industrial scale (75 cm diameter, 500 cm packed height).*

On the basis of the information so obtained, a process-engineering model has been developed in which drop diameter, hold-up of dispersed phase, axial mixing coefficients and mass-transfer coefficients of the dispersed and continuous phase are of essential importance.

Industrial application over a prolonged period (6 months) has been most satisfactory; the extraction figures were in good agreement with those used in designing the column.

Introduction

A PULSED PACKED COLUMN consists of a vertical cylindrical vessel partly filled with packing. Two liquid phases, one of which is present in the form of drops, pass countercurrently through the column. In the top, or base, of the column, the dispersed phase coalesces at an interface layer. The two phases in the column are moved up and down by means of a pulsating device connected to the column base.

The present investigation was carried out on columns packed with Raschig rings. The column diameters varied from 5 to 75 cm and the height of the packed section from 1 to 5 m. The material of the rings was such that the dispersed phase remained drop-shaped whilst travelling through the bed.

The aim of the study was to develop a process-engineering model for the pulsed packed column which contains useful correlations for the various parameters. Such a model enables a pulsed packed column to be designed without additional experiments. It was attempted to adapt the correlations as closely as possible to existing know-how and theories.

In this process-engineering model, the following relation holds for the column height required:

$$H = NTU \times HTU \qquad (1)$$

Normally, the principal resistance to mass-transfer in pulsed packed columns is found in the dispersed phase; hence, NTU and HTU can best be related to the overall driving force for the dispersed phase:

$$H = NTU_{Od} \times HTU_{Od} \qquad (1a)$$

In a given extraction process, NTU_{Od} can be calculated from equilibrium data and mass balances by means of the known procedures.

According to Miyauchi,[1,2] $HTU_{Od} = (HTU_{Od})_p + HDU_O$ (2)
where $(HTU)_{Od})_p$ denotes the height of a transfer unit for the dispersed phase under conditions where the two phases pass through the column in piston-flow while HDU_O stands for the height of a diffusion unit, i.e. the length to be added to $(HTU_{Od})_p$ in order to compensate for the axial mixing effect. This axial mixing is described by an effective superficial longitudinal diffusivity E for each phase.

Miyauchi[2] and Sleicher[3] published the solutions of the differential equations that describe the process in tabular form. Stemerding & Zuiderweg[4] used these data in preparing empirical equations by means of which HDU_O can be calculated. In order to calculate HDU_O for a pulsed packed column, correlations are needed for the axial mixing coefficient in the continuous and dispersed phases E_c and E_d. The search for these correlations and the results achieved are considered later.

$(HTU_{Od})_p$ obeys the equation:

$$(HTU_{Od})_p = \frac{v_d}{K_d A} \quad . \quad . \quad . \quad . \quad . \quad . \quad . \quad . \quad . \quad (3)$$

where A is the specific interfacial area: $A = \dfrac{6\,\varepsilon\varphi}{d_{vs}}$ . . . . . (4)

while K_d is defined as: $\dfrac{1}{K_d} = \dfrac{1}{k_d} + \dfrac{m}{k_c}$ . . . . . (5)

In publications on several extraction devices,[5] the relation between φ and the superficial velocities of the two phases is given by the expression:

$$\frac{v_d}{\varphi\varepsilon} + \frac{v_c}{\varepsilon\,(1-\varphi)} = v_o\,(1-\varphi) \quad . \quad . \quad . \quad . \quad . \quad . \quad . \quad . \quad (6)$$

This expression has been applied also to the pulsed packed column, so that the hold-up studies have been directed at relating v_o to the other variables.

The column diameter must be such that the linear velocities of the two phases equal 65% of the flooding velocities.

Thornton[6–9] showed that the hold-up at flooding can be calculated from:

$$\varphi_{df} = \frac{[(v_{df}/v_{cf})^2 + 8\,v_{df}/v_{cf}]^{0\cdot5} - 3\,v_{df}/v_{cf}}{4\,(1-v_{df}/v_{cf})} \quad . \quad . \quad . \quad . \quad . \quad (7)$$

Substitution of φ_{df} in Equation (6) yields the values of v_{df} and v_{cf}. The design velocities thus found are: $v_d = 0\cdot65\,v_{df}$ and $v_c = 0\cdot65\,v_{cf}$.

To be able to use Equations (1)–(7) for designing a *PPC*, correlations for d_{vs}, v_o, E_c, E_d, k_d, and k_c are consequently needed.

Drop diameter: d_{vs}

Theory

To describe the dispersion of one liquid in another, under conditions of turbulent flow, several workers, e.g. Chen & Middleman,[10] successfully used Hinze's theory.[11]

This theory leads to the following relation for the drop diameter:

$$d_{vs} = C_1\,\frac{\sigma^{0\cdot6}}{\rho_c^{0\cdot6}\cdot W^{0\cdot4}}, \quad . \quad . \quad . \quad . \quad . \quad . \quad . \quad . \quad . \quad (8)$$

it being assumed that the ratio between the maximum drop diameter and d_{vs} is constant. It has been endeavoured to describe the measured results by means of Equation (8).

For calculating W, it is supposed that the drop diameter is determined by the maximum frictional energy dissipated in the column the moment the pulsation rate is highest.

Then: $W = \dfrac{\Delta p\cdot\pi\cdot a\cdot f}{H\cdot\varepsilon\cdot\rho_c}$ . . . . . (9)

In this relation, v_c has been omitted because it is considered negligible compared with $a\cdot f$.

Assuming that the flow conditions establish instantaneously as soon as the flow velocity becomes maximum, one can conclude from Carman's experimental results[12] that in the range of Reynold's values concerned [$100 < (Re) < 450$]:

$$\frac{\Delta p\cdot\varepsilon^3}{H\cdot S\,(1-\varepsilon)\,\rho_c\,(\pi a f)^2} = 8\left(\frac{\pi\cdot a f\cdot\rho_c}{S\cdot\eta_c\cdot(1-\varepsilon)}\right)^{-0\cdot2} \quad . \quad . \quad . \quad . \quad . \quad (10)$$

Combination of Equations (8), (9) and (10) yields

$$\frac{1}{d_{vs}\cdot S} = C_2\left(\frac{1-\varepsilon}{\varepsilon}\right)^{1\cdot6}\left(\frac{\rho_c\cdot a\cdot f}{\eta_c\cdot S\,(1-\varepsilon)}\right)^{1\cdot12}\left(\frac{S\cdot\eta_c^2}{\rho_c\cdot\sigma}\right)^{0\cdot6} \quad . \quad . \quad . \quad (11)$$

It will be shown that the correlation can be improved by extending Equation (11) with a constant term in the way shown below:

$$\frac{1}{d_{vs}\cdot S} - \frac{1}{d_o\cdot S} = C_3\left(\frac{1-\varepsilon}{\varepsilon}\right)^{1\cdot 6}\left(\frac{\rho_c\cdot a\cdot f}{\eta_c\cdot S(1-\varepsilon)}\right)^{1\cdot 12}\left(\frac{S\,\eta_c^2}{\rho_c\,\sigma}\right)^{0\cdot 6} \quad . \quad . \quad (12)$$

Experiments

The measurements were carried out with mutually saturated liquids. Table I shows a survey of the physical properties of the liquid–liquid systems concerned.

The average drop diameter was measured in photographs showing the drops issuing from the packing. The drops were photographed together with a reference object of known diameter. The measurements were carried out on the enlarged prints, and the average diameters were calculated by Sauter's procedure.

TABLE 1

Saturated systems using water as the continuous or dispersed phase at 20°C

	ρ, kg/m³	$\Delta\rho$, kg/m³	σ, 10^{-3} N/m	η, 10^{-3} Nsec/m²
Methyl isobutyl ketone (MIBK)	805	193	10·1	0·614
Ethyl acetate	905	95	6·5	0·490
Iso-octane	691	307	40·0	0·486
Butyl acetate	881	116	14·2	0·748
Toluene	867	131	32·0	0·586
MIBK–acetic acid	805	193	5·0	0·750
Hexane	670	330	50·0	0·500
Benzene	879	121	33·0	0·650
Additional system: benzene–water with 39% of $(NH_4)_2SO_4$ at 40°C				
Benzene	868	368	28	0·49
39% $(NH_4)_2SO_4$ solution in water	1236	368	28	1·20

Results and discussion

It was found that within the range of pulse rates normally applied in a pulsed packed column, all the systems examined showed a linear relationship between the reciprocal drop diameter and the pulse rate:

$$\frac{1}{d_{vs}} = \frac{1}{d_o} + C_4\cdot a\cdot f \quad . \quad . \quad . \quad . \quad . \quad . \quad . \quad . \quad (13)$$

Studies by various investigators[13] on unpulsed packed columns operated at low liquid velocities yielded the following relation:

$$d_{vs} = 0\cdot 92\left(\frac{\sigma}{\Delta\rho\cdot g}\right)^{0\cdot 5}$$

The experimental values of d_o (Equation (13)) were correlated with the same variables and very well fitted the curve:

$$d_o = 1\cdot 39\left(\frac{\sigma}{\Delta\rho\cdot g}\right)^{0\cdot 5} \quad . \quad . \quad . \quad . \quad . \quad . \quad . \quad . \quad (14)$$

In Fig. 1, the $1/d_o$ values obtained by extrapolation have been plotted *versus* $\left(\frac{\Delta\rho\cdot g}{\sigma}\right)^{0\cdot 5}$

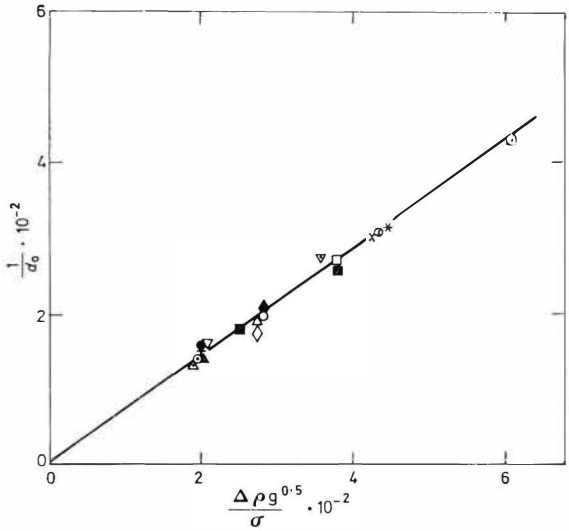

FIG. 1. d_o *correlation according to Equation* (14)

2-in column, 10-mm polyethylene rings: ■ water–hexane
2-in column, 15-mm carbon rings: ▲ water–toluene
2-in column, 15-mm ceramic rings: ⊗ methyl isobutyl ketone–water
▼ ethyl acetate–water
◇ iso-octane–water
♦ butyl acetate–water
2-in column, 16-mm polyethylene rings: ⊙ water–toluene
4-in column, 12-mm ceramic rings: * MIBK–water
⊡ MIBK–water–acetic acid
4-in column, 25-mm ceramic rings: × MIBK–water
□ ethyl acetate–water
△ iso-octane–water
○ butyl acetate–water
● toluene–water
▽ toluene–water; *a* has been varied
▽ benzene–39% $(NH_4)_2SO_4$ solution in water
9-in column, 25-mm ceramic rings: + toluene–water
9-in column, 35-mm ceramic rings: △ benzene–water

Further, the suitability of Equation (12) for giving a description of the experimental drop diameter was examined. For this purpose the power to which the right-hand member of the equation must be raised to warrant the best possible description of the drop diameters measured was determined. This power equals 0·66 (see Fig. 2).

To find a correlation that would give a better description of the experimental results, a group with $\Delta\rho$ was introduced in addition to the existing dimensionless groups, viz. $\left(\frac{\Delta\rho \cdot g}{\sigma S^2}\right)$.

Using the method of the least squares, it was then found:

$$\frac{1}{d_{vs}} - \frac{1}{d_o} = 6700 \left(\frac{1-\varepsilon}{\varepsilon}\right)^{0.95} \left(\frac{\rho_c \cdot a \cdot f}{\eta_c \cdot S}\right) \left(\frac{\eta_c^2 S}{\sigma \rho_c}\right)^{0.53} \left(\frac{\sigma S^2}{\Delta\rho \cdot g}\right)^{0.23} \quad . \quad . \quad (15)$$

(d_{vs} and d_o being expressed in metres).

Fig. 3 shows the spread of the measuring points around this correlation. It is seen that for 85% of the values the deviation is less than 20%.

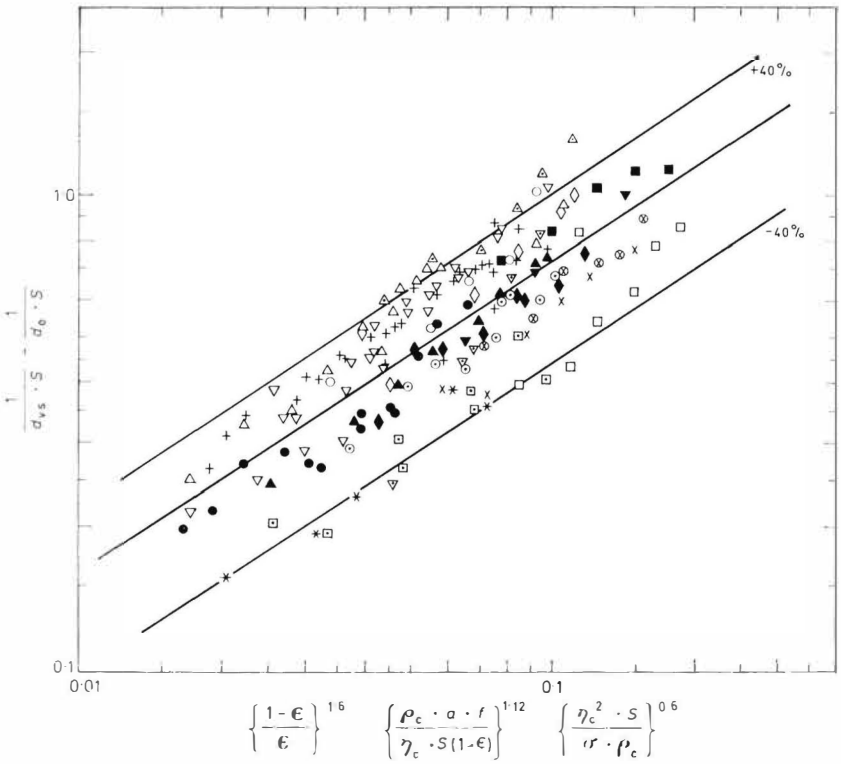

FIG. 2. *Check of theoretical Equation* (12)
Symbols as in Fig. 1

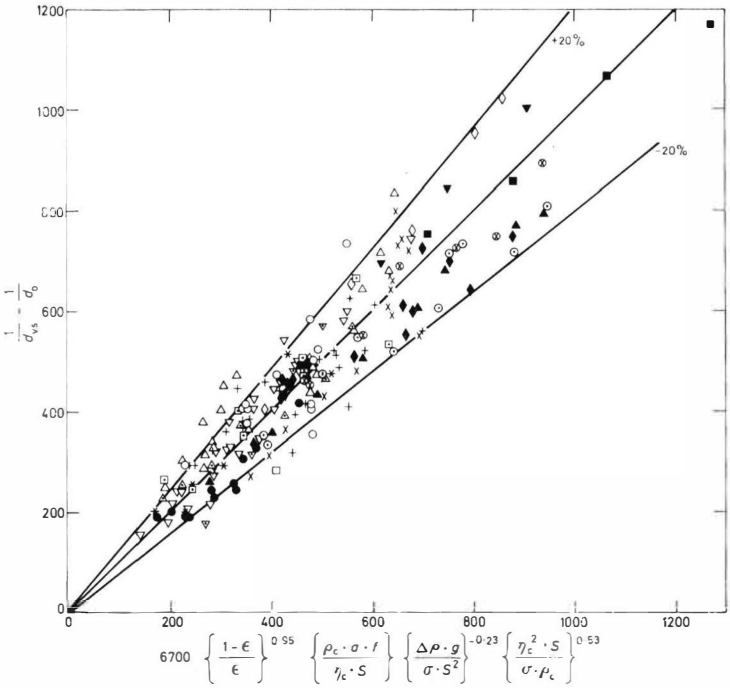

FIG. 3. *Check of experimental Equation* (15)
Symbols as in Fig. 1

Comparison with the correlations known from the literature reveals that Correlation (15) differs considerably from Karpacheva's relation:[14]

$$d_{vs} = 7{\cdot}25.10^{-4}\left(\frac{\sigma}{\Delta\rho\, g}\right)^{0{\cdot}5}\left(\frac{a{\cdot}f\,\eta_c}{\sigma}\right)^{-1{\cdot}4} \quad . \quad . \quad . \quad . \quad . \quad (16)$$

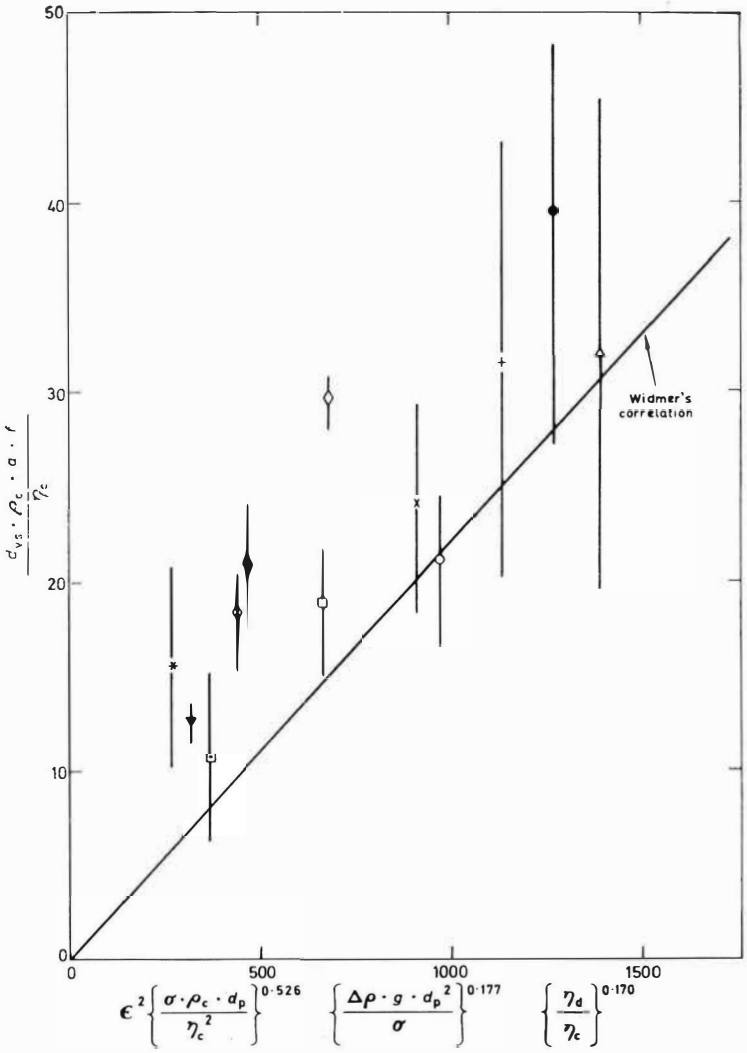

FIG. 4. *Comparison of* d_{vs} *values with Widmer's correlation* (*Equation* 17)

2-in column, 15-mm ceramic rings: ⊗ methyl isobutyl ketone–water
▼ ethyl acetate–water;
◇ iso-octane–water;
♦ butyl acetate–water

4-in column, 12-mm ceramic rings: * MIBK–water;
⊡ MIBK–water–acetic acid

4-in column, 25-mm ceramic rings: × MIBK–water;
□ ethyl acetate–water;
△ iso-octane–water;
○ butyl acetate–water;
● toluene–water

9-in column, 25-mm ceramic rings: + toluene–water

and, as far as the exponents of the various groups are concerned, is in reasonable agreement with Widmer's correlation:[15]

$$\frac{d_{vs}\rho_c f \cdot a}{\eta_c} = 2 \cdot 21 . 10^{-2}\, \varepsilon^2 \left(\frac{\sigma \rho_c d_p}{\eta_c^2}\right)^{0 \cdot 526} \left(\frac{\Delta\rho\, g d_p^2}{\sigma}\right)^{0 \cdot 177} \left(\frac{\eta_d}{\eta_c}\right)^{0 \cdot 17} . \quad (17)$$

Fig. 4 gives a comparison of our measurements with Widmer's correlation. Upon substitution of our experimental data in Widmer's correlation, the spread is considerably larger than that found by Widmer in his own experiments. The differences between our and Widmer's experimental conditions will be discussed in greater detail later.

Characteristic velocity: v_o

Theory

In the range of the usual hold-up values, Relation (6)

$$\frac{v_d}{\varepsilon\varphi} + \frac{v_c}{\varepsilon(1-\varphi)} = v_o(1-\varphi)$$

has proved to be applicable. In this formula, v_o denotes the velocity of a single drop of the dispersed phase under conditions where $v_c = 0$, and in the limiting case that $v_d \sim 0$ and $\varphi \sim 0$.

v_o must depend not only on the physical properties of the liquid–liquid system considered and the properties of the packing, but also on the amplitude, frequency and shape of the pulse. The existing theoretical views on this point[16–21] do not yet provide an adequate basis for an estimation of the degree to which v_o depends on the pulse characteristics.

Experiments

Almost all experiments carried out for determining the drop diameter have been used also for measuring the hold-up of dispersed phase φ, from which v_o is calculated by means of Equation (6). The determination of φ was performed by the drainage method described in Ref. 22. In most measurements v_c equalled zero. In a number of experiments, the influence of the viscosity of the continuous phase has been examined by adding CMC (carboxymethylcellulose) to the continuous aqueous phase, thereby varying η_c between 1 and 5 cP. The pulse in all measurements was sinusoidal.

Results and discussion

The first tentative analysis of the measured results yielded the following information:

(i) The quantities a and f influence v_o almost exclusively in so far as they have an effect on d_{vs}; in other words, the effect of a and f on v_o works almost exclusively through d_{vs}.

(ii) The small direct influence of a and f on v_o can best be represented by a term containing $a \cdot f^2$ (acceleration).

(iii) In the relation between v_o and d_{vs}, two distinct regions can be distinguished: at low d_{vs} values, v_o varies in approximately linear proportion with d_{vs} and is virtually independent of the packing diameter; in the range of high d_{vs} values, v_o is practically independent of d_{vs} but varies with the packing diameter.

(iv) In some cases, v_o increased with v_d; it was found then that d_{vs} also increased with v_d owing to coalescence with increasing hold-up.

(v) The characteristic velocity v_o was found to be proportional to $\eta_c^{-0 \cdot 35}$.

After this analysis, it was examined whether v_o in the two ranges (lower and higher d_{vs} values) can be described by correlations of the following shape:

$$v_o = \text{const.}\ d_{vs}^{\alpha} \cdot (af^2)^{\beta} \cdot \Delta\rho^{\gamma} \cdot [S(1-\varepsilon)]^{\delta} \cdot \eta_c^{-0.35}$$

It was found:

(a) $v_o = 6 \cdot 32.\ 10^{-3} \cdot d_{vs}^{0.727} \cdot \Delta\rho^{0.815} \cdot (af^2)^{-0.254} \cdot [S(1-\varepsilon)]^{-0.184} \cdot \eta_c^{-0.35}$. (18)

if:

$L \equiv d_{vs}^{0.787}\ \Delta\rho^{0.255}\ (af^2)^{-0.144} \cdot [S(1-\varepsilon)]^{0.426} \leqslant 0 \cdot 406$. . . . (19)

(b) $v_o = 2 \cdot 57.\ 10^{-3} \cdot d_{vs}^{-0.06} \cdot \Delta\rho^{0.56} \cdot (af^2)^{-0.11} \cdot [S(1-\varepsilon)]^{-0.61} \cdot \eta_c^{-0.35}$. (20)

if: $L \geqslant 0 \cdot 406$. . . . . (21)

These correlations are not dimensionless; all quantities must be expressed in S.I. units. In addition, the relation

$$\frac{d_{vs}}{d_p} \leqslant 1 \cdot 37 \cdot \Delta\rho^{-0.5} \quad . \quad . \quad . \quad . \quad . \quad . \quad . \quad . \quad . \quad (22)$$

must be satisfied, i.e. the diameter of the Raschig rings must not be too small. Further explanation on this point is given at the end of this paragraph. Correlations (18) and (20) are illustrated in Figs 5 and 6.

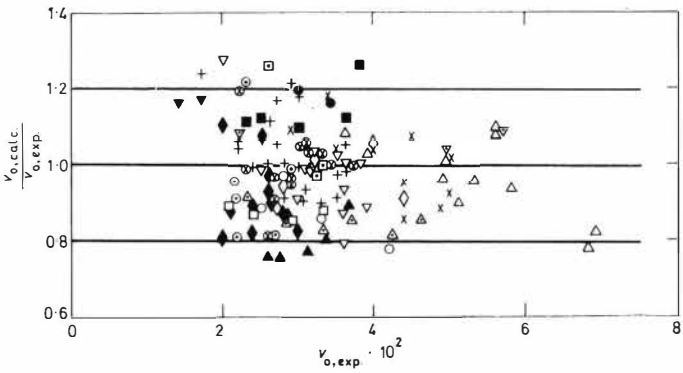

FIG. 5. *Check of Equation* (18)

Symbols as in Fig. 1

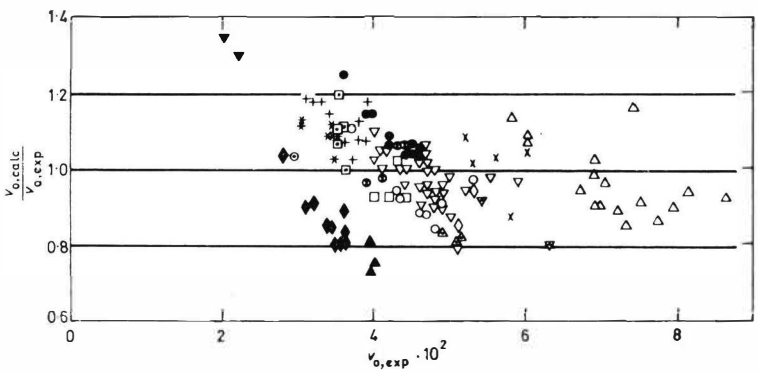

FIG. 6. *Check of Equation* (20)

Symbols as in Fig. 1

In Correlation (18), d_{vs} and $\Delta\rho$ are the main variables: their exponents show a close resemblance to those in a correlation given by Klee & Treybal[23] for the terminal velocity of smaller drops in an unpacked column:

$$v \sim d_{vs}^{0.70}\,\Delta\rho^{0.58} \quad . \quad . \quad . \quad . \quad . \quad . \quad . \quad . \quad (23)$$

In this case, the normal flow resistance of the drops in the channels between the packing is involved, the higher pulse velocities pertaining to this lower d_{vs} value keep the drops from attaching to the packing.

In Correlation (20), $\Delta\rho$ and S (or d_p) are the main variables; here v_o is evidently determined not only by $\Delta\rho$, but also by the packing resistance. The resemblance of Sitaramayya & Laddha's[24] correlation for non-pulsed packed columns (high d_{vs}) to Correlation (20) is striking; Sitaramayya & Laddha found:

$$v_o = 0{\cdot}683\cdot\left[\frac{\varepsilon\cdot g\cdot\Delta\rho}{S(1-\varepsilon)\rho_c}\right]^{0.5} \quad . \quad . \quad . \quad . \quad . \quad . \quad . \quad (24)$$

A comparison of our results with those of Widmer is shown in Fig. 7; it is seen here that the differences are fairly large. Widmer's correlation reads:

$$v_o = \left(\frac{\Delta\rho}{\rho_c}\right)^{0.5}\cdot\left(\frac{0{\cdot}428 d_{vs}}{9{\cdot}12.10^{-3} + d_{vs}}\right) \quad . \quad . \quad . \quad . \quad . \quad . \quad (25)$$

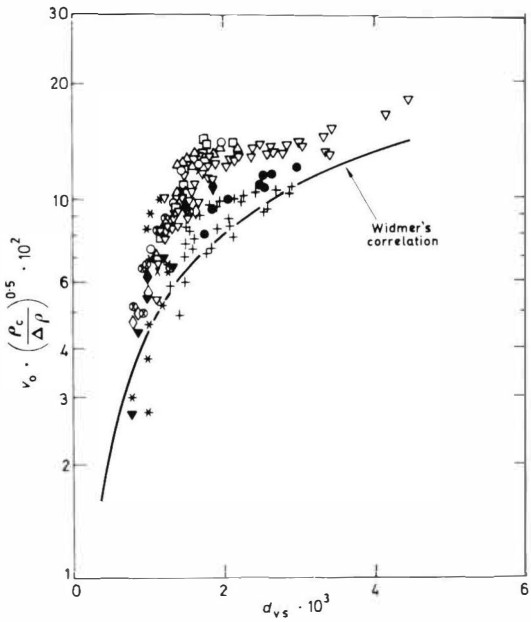

FIG. 7. *Comparison of* v_o *values with Widmer's correlation* (*Equation* 25)

Symbols as in Fig. 1

A possible explanation for these large differences is that Widmer performed his measurements on relatively small Raschig rings (7, 9, 13, 15 and 20 mm) and relatively large drops because the interfacial tension in nearly all his liquid–liquid systems was $> 30.10^{-3}$ N/m.

The results of the present experiments on the system toluene–water ($\sigma = 31.10^{-3}$ N/m) in a 10-cm column packed with 12-mm ceramic Raschig rings are illustrated in Fig. 8. On the right of the maximum the normal behaviour is seen: a decrease of v_o with increasing $a{\cdot}f$, owing to the decrease of d_{vs}; on the left of the maximum, the probability of the drops colliding with the packing increases with decreasing $a{\cdot}f$.

Widmer performed many of his experiments in the region on the left of the maximum. In deriving Correlations (18) and (20), use has been made only of the values on the right of the maximum (the practical range). It should be pointed out, however, that the present authors have found this maximum only in experiments on columns packed with Raschig rings $\leqslant 12$ mm. From the maxima measured, the following criterion can be derived:

$$\frac{d_{vs}}{d_p} \leqslant 1 \cdot 37\,(\Delta\rho)^{-0 \cdot 5} \qquad (22)$$

This should be satisfied before the Correlations (18) and (20) can be applied.

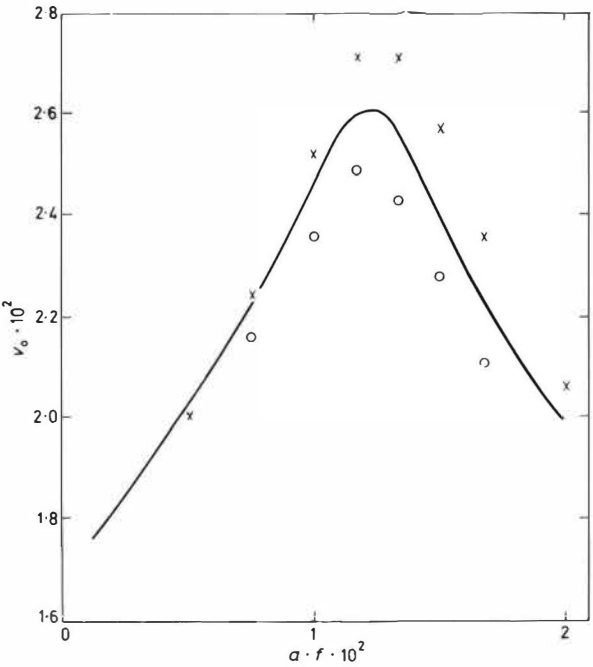

FIG. 8. v_0 *values for the system toluene–water measured in a 10-cm column packed with 12-mm ceramic Raschig rings*

× $v_d = 0 \cdot 145.10^{-2}$ m/sec, $v_c = 0$; ○ $v_d = 0 \cdot 145.10^{-2}$ m/sec, $v_c = 0 \cdot 212.10^{-2}$ m/sec

Axial mixing coefficients: E_c and E_d

Theory

Since Geankoplis & Hixson,[25] Pratt[26] and Gier & Hougen[27] drew attention to the influence of axial mixing on the extraction efficiency, the mathematical models for describing this have been steadily improved; in addition, a great many results of experiments with a wide variety of extraction devices have been reported in the literature. Experiments on packed columns, with and without pulsation, were done by Jacques *et al.*,[28] Moon *et al.*,[29] and by Rozen *et al.*[30] In the model used for describing axial mixing, it is assumed that an adequate description can be obtained by means of axial mixing coefficients for the continuous and dispersed phases.

All measurements on unpulsed flows through a granular bed have shown that $E \sim v \cdot d_p$.[31, 32] Hence the relation for a pulsed column will, in all probability, also be of the shape $E_c \sim a \cdot f \cdot d_p$. It is to be expected that the relation for the dispersed phase will be much more complicated. In unpulsed columns, as well

as in columns operated at low pulse rates, the dispersed phase will show a wide spread in drop size and a corresponding spread in drop velocities. At higher pulse rates the drops become more uniform in size, but the spread in residence time increases owing to the violent agitation.

Experiments

The axial mixing coefficients have been determined from the response curve of a step function for columns of 5-, 10- and 22-cm diameter.

The measurements for the continuous phase were carried out with water and a dilute KCl solution as a tracer. The breakthrough curve was measured by means of a conductivity cell consisting of two stainless steel grids spaced 6 mm apart.

To examine the influence of the dispersed phase on E_c, toluene was introduced on the column axis at a distance of 15 cm above the conductivity cell. In several measurements a dye (Waxoline Blue CBS) in methyl isobutyl ketone was used as the tracer, and the breakthrough curve recorded by means of a photocell. The other measurements were carried out by a method described by Jacques *et al.*[28] In this method, the breakthrough curve for the dispersed phase is determined from the amount per unit time of dispersed phase arriving in the top of the column after admission of this phase to the column base.

Results and discussion

Axial mixing coefficient in the continuous phase: E_c

As regards the axial mixing coefficient in the continuous phase, a distinction can be made between the contributions of the pulse rate, the continuous phase velocity and the dispersed phase velocity:

(i) The contribution of the pulse rate can be described very well by means of the relation:

$$E_c = \varphi_1 \cdot a_i \cdot f \cdot d_p \qquad (26)$$

where φ_1 is a function of the amplitude (see Fig. 9). At high values of a_i, φ_1 is independent of a_i.

The values for $\varphi_{1,\,max}$ here are virtually equal to those mentioned by Rozen *et al.*:[30]

25-mm Raschig rings: $\varphi_{1,\,max} = 0 \cdot 51$ (Rozen *et al.*: $0 \cdot 52$).
8-, 10-, 12-mm Raschig rings: $\varphi_{1,\,max} = 0 \cdot 60$ (Rozen *et al.*: $0 \cdot 57$).

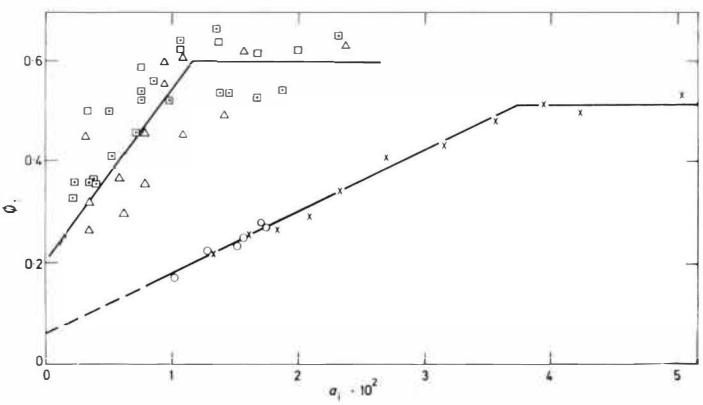

FIG. 9. *Correlation for* φ_1

	Column, cm	Ceramic Raschig rings, mm
×	10	25
○	22	25
△	5	8
□	5	10
⊡	10	12

At lower a_i values, the axial mixing coefficient decreases with the amplitude. An explanation may be that as the amplitude decreases, a steadily growing portion of the liquid is retained in the same channel (e.g. a given Raschig ring) over one pulse cycle and, in consequence, can no longer make a contribution to the spread in residence time. The shift from the one range to the other must then take place at an amplitude in the order of the Raschig ring dimensions.

(ii) For the spread in residence time caused by the flow rate of the continuous phase at zero pulse rate it was found:

$$E_c = B \cdot v_c \cdot d_p \qquad (27)$$

The value of B is still dependent on the packing diameter:

$d_p = 12$ mm: $B = 2 \cdot 51$,
$d_p = 25$ mm: $B = 1 \cdot 31$.

During an increase of the pulse rate, the influence of v_c on E_c decreases, probably owing to improved radial mixing. It was found that also under these conditions, a low a_i value reduces the contribution of v_c to E_c by a larger amount than does a high a_i value at the same pulse rate.

The contribution of v_c to E_c in a large number of measurements could be described by means of the term: $\varphi_2 \cdot B \cdot v_c \cdot d_p$, where φ_2 is a function of $\frac{\varphi_{1,\max}}{\varphi_1} \cdot a_i \cdot f$ (see Fig. 10).

(iii) The influence of the dispersed phase on the axial mixing coefficient in the continuous phase was examined with toluene being used as the dispersed phase. Measurements over the whole range of pulse rates and flow velocities showed that E_c was increased by 20% (see Fig. 11). Hence, the relation for E_c in a pulsed packed column is:

$$E_c = 1 \cdot 2\,(\varphi_1 \cdot a_i \cdot f \cdot d_p + \varphi_2 \cdot B \cdot v_c \cdot d_p) \qquad (28)$$

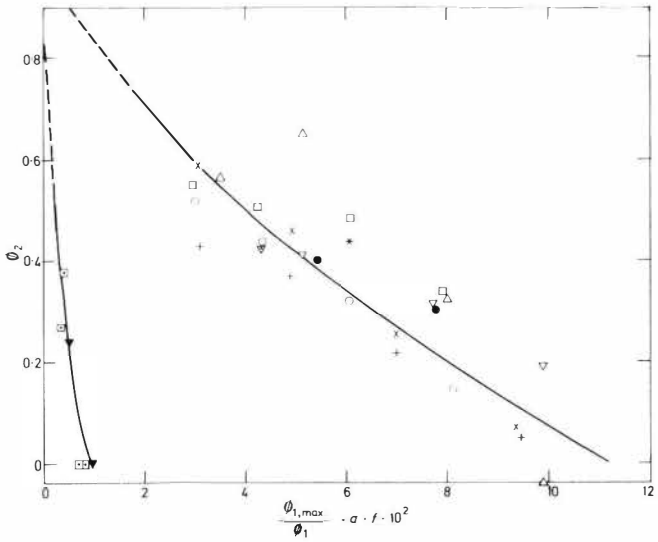

FIG. 10. *Correlation for* φ_2

	v_c, 10^{-2} m/sec	a, 10^{-2} m	
○	0·25	0·5	22-cm column, 25-mm ceramic Raschig rings
×	0·25	0·7	
△	0·25	0·9	
□	0·42	0·5	
+	0·42	0·7	
●	0·42	0·8	
▽	0·42	0·9	
*	0·51	0·5	
▽	0·60	0·5	

▼ 5-cm column, 8-mm ceramic Raschig rings;
⊡ 5-cm column, 10-mm ceramic Raschig rings

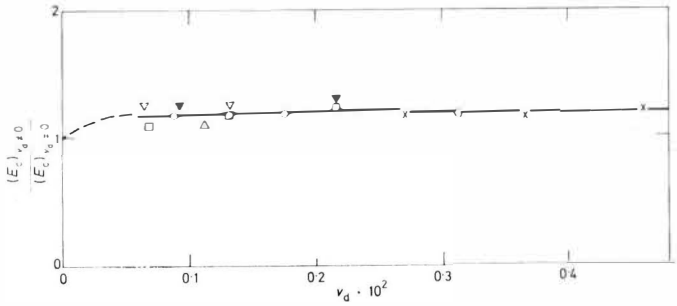

FIG. 11. *Influence of the dispersed toluene phase on the residence time distribution in the continuous water phase*

	Column, cm	Ceramic Raschig rings, mm	a, 10^{-2} m	f, sec^{-1}	v_c, 10^{-2} m/sec
×	10	25	1·79	1·05	0·33
△	10	25	3·06	1·11	0·169
▽	25	25	0·7	2·38	0·25
□	25	25	0·7	2·38	0·40
○	25	25	0·9	2·67	0·25

It should be noted that E_c is a superficial mixing coefficient; in the relations for HDU_O it must therefore be combined with the superficial continuous phase velocity (v_c). Measurements on columns of 10- and 22-cm diameter have revealed that the axial mixing coefficient for the continuous phase is independent of the column diameter.

Axial mixing coefficient in the dispersed phase: E_d

Under the heading 'Theory', it was remarked that E_d might be a very complicated function of a large number of variables. Fortunately, it has appeared that the influence of E_d on the extraction efficiency is slight, so that the development of an accurate correlation for E_d (superficial mixing coefficient for the dispersed phase) is not essential for designing a reasonably good column.

The results obtained on columns operated with 25-mm Raschig rings and the system toluene–water, and with 12-mm Raschig rings and the system methyl isobutyl ketone–water (Fig. 12), demonstrate that the 'actual' mixing coefficient, $E_d/\varepsilon\varphi$, is almost independent of $a \cdot f$.

Recommendation for design purposes:

12-mm Raschig rings: $E_d/\varepsilon \cdot \varphi = 6.10^{-4}$ m^2/sec;

25-mm Raschig rings: $E_d/\varepsilon \cdot \varphi = 10.10^{-4}$ m^2/sec.

Mass-transfer coefficients: k_d and k_c

Theory

Partial mass-transfer coefficient in the dispersed phase: k_d

A theoretical approach of the mass-transfer coefficient in the dispersed phase can be made only by means of models. At higher pulse rates the drops of the dispersed phase are normally so small that there is no or hardly any flow inside, in other words the drops are rigid. For rigid drops, various authors[33,34] derived the relation:

$$k_d = \frac{2\,\pi^2\,D_d}{3\,d_{vs}} \qquad (29)$$

For non-rigid drops, a correlation was used of the shape:

$$(Sh)_d = C(Re')_d^n\,(Sc)_d^{\frac{1}{3}} \qquad (30)$$

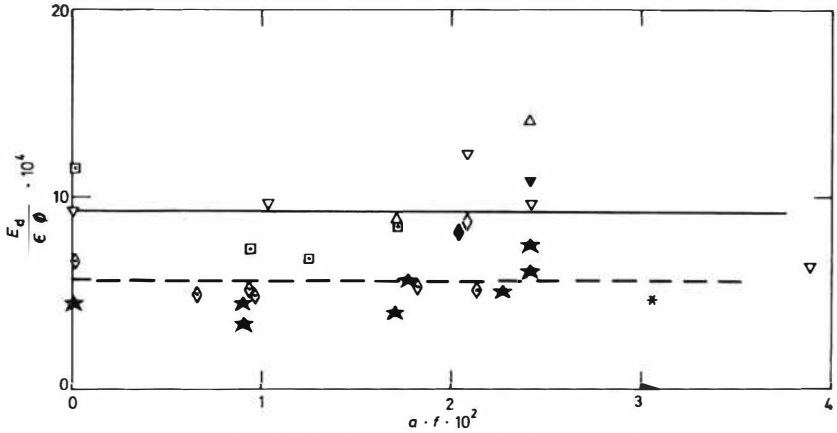

FIG. 12. *Axial mixing coefficient in the dispersed phase*

22-cm column, 25-mm ceramic Raschig rings, toluene–water

	v_c, 10^{-2} m/sec	v_d, 10^{-2} m/sec
△	0	0·21
▽	0	0·25
*	0	0·29
▽	0	0·31
♦	0·25	0·24
◇	0·147	0·24

5-cm column, 12-mm ceramic Raschig rings, MIBK–water

◇	0·09	0·33
⊡	0·09	0·16
★	0·05	0·33

Partial mass-transfer coefficient in the continuous phase: k_c

The partial mass-transfer coefficient in the continuous phase of a pulsed packed column is usually very large compared with k_d, i.e. the term $\frac{m}{k_c}$ in the second member of Equation (5) can almost be neglected unless the distribution coefficient m is very large.

Experiments

The mass-transfer coefficient in the dispersed phase, k_d, was measured on five liquid–liquid systems: methyl isobutyl ketone–acetone–water; ethyl acetate–acetone–water; butyl acetate–acetone–water; toluene–acetone–water; and benzene–caprolactam–water.

In the first four systems, the mass-transfer was from the continuous to the dispersed phase, and in the last system it was from the dispersed to the continuous phase.

In the majority of the experiments, the drop diameters and hold-ups needed for calculation of the mass-transfer coefficient were measured; in the experiments with the system benzene–caprolactam–water in the 75- and 22-cm columns, the hold-ups only were measured and the drop diameters were derived by means of the v_o correlation.

The content of solute (acetone) in the continuous phase of the first four systems was at most 5 wt-%. The average content of caprolactam in the dispersed benzene phase was 17 wt.-%.

The solute concentrations in the feed and exit flows were determined in all experiments. From the data so obtained, the number of transfer units NTU_{Od} were derived by means of the known relations.[35] The column length being known, HTU_{Od} could subsequently be calculated. After correction for the axial mixing effect, $(HTU_{Od})_p$ was then found. Combination of Equations (3) and (4) with the hold-up values and the drop diameters yielded the overall mass-transfer coefficient K_{Od}. The partial mass-transfer coefficient k_d could then be calculated by means of Equation (5), provided the partial mass-transfer coefficient in the continuous phase is known.

For the determination of k_c, two experiments were carried out with the system water (dispersed)–acetic acid–carbon tetrachloride (continuous) in which the acetic acid was extracted from the CCl_4. Under equilibrium conditions, the acetic acid shows a distinct preference for the aqueous phase: $m = \frac{y}{x} \sim 100$.

Application of the above procedure enabled K_{Oc} to be calculated for the two experiments. From the value so found, the partial mass-transfer coefficient in the continuous phase was derived: $k_c = 3.10^{-4}$ m/sec. This result shows that the resistance in the continuous phase can normally be neglected in comparison with that in the dispersed phase (according to Equation (29), $k_d \sim 10^{-6}$–10^{-5} m/sec).

Results and discussion

Fig. 13 shows a plot of $(Sh)_d = \frac{k_d \cdot d_{vs}}{D_d}$ *versus* $(Re')_d = \frac{\rho_d (2\, a \cdot f + v_o)\, d_{vs}}{\eta_d}$; the Sherwood number $(Sh)_d$ contains the experimental values found for k_d. (When $a \cdot f$ increases, $(Re')_d$ decreases.)

The molecular diffusion coefficient of the solute in the dispersed phase (D_d) appearing in the Sherwood number has been calculated by the method of Wilke–Chang.[35]

It appears from Fig. 13 that a distinction must be made between a non-polar organic phase (benzene, toluene) and a polar organic phase (methyl isobutyl ketone, ethyl acetate, butyl acetate). The explanation is that the polar organic phase coalesces more readily than the non-polar organic phase. Coalescence and

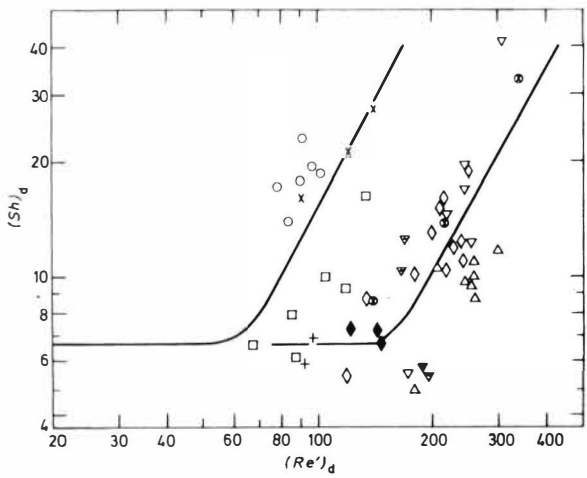

FIG. 13. $(Sh)_d$ versus $(Re')_d$

	System	Column, cm	Ceramic Raschig rings, mm
△	Toluene–acetone–water	10	25
+	,, ,, ,,	10	12
◇	,, ,, ,,	22	25
♦	,, ,, ,,	5	12
▽	Benzene–caprolactam–water	75	25
*	,, ,, ,,	22	25
▽	,, ,, ,,	75	35
⊗	,, ,, ,,	22	35
×	MIBK–acetone–water	5	15
□	Ethyl acetate–acetone–water	5	15
○	Butyl acetate–acetone–water	5	15

redispersion increase the mass-transfer coefficient in the dispersed phase owing to accelerated renewal of the surface.[36] From Fig. 13, it also appears that at high pulse rates, i.e. at low $(Re')_d$ values, the two systems have the same Sherwood number, $(Sh)_d \sim 6 \cdot 6$.

It has been assumed earlier that with circulating flow in the drop: $(Sh)_d \sim (Re')_d^n (Sc)_d^{\frac{1}{2}}$. In Fig. 14, the data from Fig. 13 have therefore been re-plotted as $(Sh)_d/(Sc)_d^{\frac{1}{2}}$ *versus* $(Re')_d$.

The fairly large spread of the values around the two average curves was to be expected because any errors made in measuring the solute concentration, drop diameter, hold-up, linear flow rates, as well as any errors in the process engineering model (including the calculation of HDU_O) and in the system characteristics (calculated D_d) would obviously show up in Fig. 14.

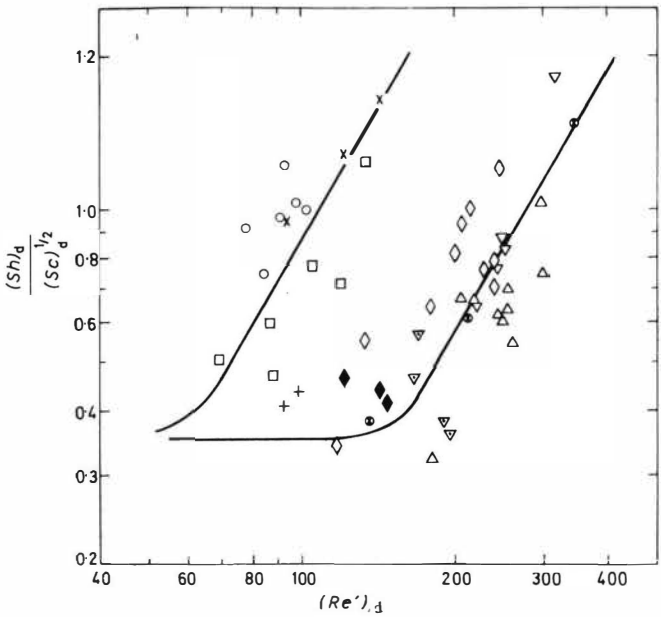

FIG. 14. $(Sh)_d/(Sc)_d^{\frac{1}{2}}$ versus $(Re')_d$

Symbols as in Fig. 13

Conclusions

The principal factor involved in the design of a *PPC* is the drop diameter, which is of decisive importance in establishing the column diameter (via the hold-up φ) and the column height (via the specific interfacial area A). The corresponding pulse rate has only a slight direct influence on v_o but is an important factor in the calculation of the axial mixing coefficients. Small deviations of the system characteristics, e.g. the interfacial tension, can easily be remedied by slight alteration of the pulse rate, which must, of course, be variable. As a result, the drop diameter can always be adjusted to its original design value. Columns for strongly coalescing systems (mass-transfer from the dispersed phase to the continuous phase) can also be dimensioned, provided the pulsator can be controlled within reasonable limits. DSM has been operating an experimental *PPC* of 75-cm diameter and 500-cm packed height for 6 months in an industrial process for the extraction of caprolactam from benzene (dispersed phase) with water (continuous phase); the packing consisted of 25-mm ceramic Raschig rings. The design principles outlined above appeared to be

sound and the expectation that the upscaling factor would be unity was confirmed. A large diameter column may evidently be looked upon as a combination of columns of a smaller diameter and the same height whose collective cross-sectional area is equal to that of the large column. The pulses were produced with a pneumatic pulsator as described in several DSM patents.[37–41]

For some industrial extraction processes, the cost of extraction in a *PPC* has been calculated and compared with that for the same extraction process in more conventional equipment. Extraction in the *PPC* proved to be much cheaper; this has been confirmed in the operation of the 75-cm *PPC* mentioned above.

References

[1] Miyauchi, T., & Vermeulen, Th., *Ind. Engng Chem. Fundamentals*, 1963, **2**, 113
[2] Miyauchi, T., *Rep. Congr. atom. Energy Commn U.S.*, 1957, UCRL-3911
[3] Sleicher, C. A., *A.I.Ch.E. Jl*, 1959, **5**, 145
[4] Stemerding, S., & Zuiderweg, F. J., *Chem. Engr*, 1963, p. CE156
[5] Gayler, R., Roberts, N. W., & Pratt, H. R. C., *Trans. Instn chem. Engrs*, 1953, **31**, 57
[6] Thornton, J. D., *Chemy Ind.*, 1954, p. 1581
[7] Thornton, J. D., *Chem. Engng Sci.*, 1956, **5**, 201
[8] Thornton, J. D., *Chem. Engng Prog. Symp. Ser.*, 1954, no. 13
[9] Thornton, J. D., & Pratt, H. R. C., *Trans. Instn chem. Engrs*, 1953, **31**, 289
[10] Chen, H. T., & Middleman, S., *A.I. Ch. E. Jl*, 1967, **13**, 989
[11] Hinze, J. O., *A.I.Ch.E.Jl*, 1955, **1**, 289
[12] Carman, P.C., *Trans. Instn chem. Engrs*, 1937, **15**, 150
[13] Gayler, R., & Pratt, H. R. C., *Trans. Instn chem. Engrs*, 1953, **31**, 69
[14] Karpacheva, S. M., Zakharov, E. I., & Kiseleva, L. F., *J. appl. Chem. USSR*, 1964, **37**, 2631
[15] Widmer, F., *Chemie-Ingr-Tech.*, 1967, **39**, 900
[16] Baird, M. H. J., Senior, M. G., & Thompson, R., *Chem. Engng Sci.*, 1967, **22**, 551
[17] Houghton, G., *Proc. R. Soc., A*, 1963, **33**, 272
[18] Houghton, G., *Can. J. chem. Engng*, 1966, **44**, 90
[19] Houghton, G., *Can. J. chem. Engng*, 1968, **46**, 79
[20] Molerus, O., & Werther, J., *Chemie-Ingr-Tech.*, 1968, **40**, 522
[21] Molerus, O., *Chemie-Ingr-Tech.*, 1964, **36**, 866
[22] Gayler, R., & Pratt, H. R. C., *Trans. Instn chem. Engrs*, 1951, **29**, 110
[23] Klee, A. J., & Treybal, R. E., *A.I.Ch.E. Jl*, 1956, **2**, 444
[24] Sitaramayya, T., & Laddha, G. S., *Chem. Engng Sci.*, 1961, **13**, 263
[25] Geankoplis, C. J., & Hixson, A. N., *Ind. Engng Chem.*, 1950, **42**, 1141
[26] Pratt, H. R. C., *Trans. Instn chem. Engrs*, 1951, **29**, 195
[27] Gier, T. E., & Hougen, J. O., *Ind. Engng Chem.*, 1953, **45**, 1362
[28] Jacques, G. J., Cotter, J. E., & Vermeulen, Th., *Rep. Congr. atom. Energy Commn U.S.*, 1959, UCRL-8658
[29] Moon, J. S., Hennico, A., & Vermeulen, Th., *Rep. Congr. atom. Energy Commn U.S.*, 1963, UCRL-10928
[30] Rozen, A. M., Rubezhnyy, Y. G., & Martynov, B. V., *Chem. Ind.* [*Khim. Prom.*], 1970, p. 66
[31] Cairns, E. J., & Prausnitz, J. M., *Chem. Engng Sci.*, 1960, **12**, 20
[32] Hiby, J. W., 'Symposium on the interaction between fluids and particles', London, 1962, Paper C 71
[33] Barrer, R. M., 'Diffusion in and through solids', 1941 (Cambridge: Cambridge University Press)
[34] Hobler, T., 'Mass transfer and absorbers', 1966 (Oxford: Pergamon Press)
[35] Treybal, R. E., 'Liquid extraction', 1963, 2nd ed. (New York: McGraw-Hill)
[36] Treybal, R. E., & Schindler, H. D., *A.I.Ch.E. Jl*, 1968, **14**, 790
[37] B.P. 1,070,101
[38] Neth. P. Appln. 295,891 and 6,401,432
[39] B.P. 1,164,710
[40] Neth. P. Appln. 6,611,676
[41] Further patent applications pending

Nomenclature

A	interfacial area/m^3 column volume	m^{-1}
a	amplitude: total stroke length in unpacked column section	m
a_i	a/ε; total stroke length in packed column section	m
B	constant in Eqn (27)	—

C	constant	—
D	molecular diffusion coefficient of the solute	$m^2\ sec^{-1}$
d_o	$= 1 \cdot 39 \left(\frac{\sigma}{\Delta\rho g}\right)^{0 \cdot 5}$	m
d_p	packing diameter	m
d_{vs}	average drop diameter according to Sauter	m
E	superficial axial mixing coefficient	$m^2\ sec^{-1}$
f	frequency	sec^{-1}
g	gravitational acceleration	$m\ sec^{-2}$
H	packed column height	m
HDU	height of a diffusion unit	m
HTU	height of a transfer unit	m
K	overall mass-transfer coefficient	$m\ sec^{-1}$
k	partial mass-transfer coefficient	$m\ sec^{-1}$
L	quantity defined in Eqn (19)	—
m	distribution coefficient: $m = y/x$	—
n	exponent in Formula (30)	—
NTU	number of transfer units	—
Δp	pressure difference	$N\ m^{-2}$
(Re)	Reynolds number: $\frac{\rho \cdot v}{S \cdot \eta \cdot (1-\varepsilon)}$	—
$(Re')_d$	modified Reynolds number related to dispersed phase: $(Re')_d = \frac{\rho_d\,(2a \cdot f + v_o) \cdot d_{vs}}{\eta_d}$	—
S	ring area per unit volume of ring material	m^{-1}
(Sc)	Schmidt number: $(Sc) = \nu/D$	—
(Sh)	Sherwood number: $(Sh) = k \cdot d_{vs}/D$	—
v	superficial velocity	$m\ sec^{-1}$
v_o	characteristic velocity of the drops	$m\ sec^{-1}$
$v_{o,\ exp.}$	experimental value of v_o calculated from φ, v_c, v_d and ε by means of Eqn (6)	$m\ sec^{-1}$
$v_{o,\ calc.}$	v_o calculated by means of Eqn (18) or (20)	$m\ sec^{-1}$
W	energy dissipated per unit mass and unit time	$J\ kg^{-1}\ sec^{-1}$
x	weight fraction of solute in continuous phase	—
y	weight fraction of solute in dispersed phase	—
ε	bed porosity	—
η	dynamic viscosity	$N\ sec\ m^{-2}$
ν	kinematic viscosity	$m^2\ sec^{-1}$
ρ	specific mass	$kg\ m^{-3}$
$\Delta\rho$	difference in specific mass between the two liquid phases	$kg\ m^{-3}$
σ	interfacial tension	$N\ m^{-1}$
φ	hold-up of the dispersed phase, i.e. volume of dispersed phase/volume of dispersed + continuous phase	—
φ_1	see Eqn (26)	—
φ_2	see Eqn (28)	—

Subscripts

c	continuous phase
d	dispersed phase
f	flooding
O	overall
p	piston flow
R	raffinate phase

Performance and scale-up of a reciprocating-plate extraction column

by A. E. Karr and T. C. Lo
Hoffmann-La Roche Inc., Nutley, New Jersey, U.S.A.

Data are presented which form the basis of an empirical scale-up procedure for an open-type perforated reciprocating-plate extraction column. Data obtained in a 12 in dia. column and a 1 in dia. column on the system methyl isobutyl ketone (MIBK)–acetic acid–water were correlated with data previously reported on a 3 in dia. column. The 12 in dia. column consisted of three plate sections, each containing perforated reciprocating plates spaced 1 in apart, and each section was separated by a baffle plate having approximately the same free area, 58%, as the perforated plates. The baffle plates were found to be necessary in most types of operation with respect to the dispersed phase and the direction of mass transfer in order to prevent excessive axial mixing. A minimum height of an equivalent theoretical stage (HETS) of 6·2 in and volumetric efficiencies up to 311 h^{-1} were achieved in the 12 in dia. column.

To scale up performance from a column of small diameter to one of large diameter, the recommended procedure is as follows:

1. *The plate spacing, amplitude and total throughput per unit cross sectional area are kept constant.*
2. *The HETS is taken as being proportional to the 0·25 power of the column diameter, and the optimum reciprocating speed is taken as inversely proportional to the 0·14 power of the column diameter. Final adjustment to the optimum speed of reciprocation should be made during actual operation of the large column.*

Introduction

IN 1959, performance data on a 3 in dia. reciprocating-plate extraction column were reported.[1] The column was shown to have a high volumetric efficiency compared to other columns for two systems: methyl isobutyl ketone (MIBK)–acetic acid–water and *o*-xylene–acetic acid–water. The reciprocating-plate column has been commercially accepted in columns of up to 18 in dia.[2–5] In recent years, data on various columns characterised by reciprocating, perforated plates or packing have appeared in the literature.[6–11] Most of the data have lent support to the conclusion that reciprocating-plate columns, especially in small diameters, generally have high volumetric efficiencies.

The data presented in this paper were obtained with the view toward understanding the performance of reciprocating-plate columns having diameters larger than 3 in with the further object of establishing a scale-up procedure.

Experimental

Description of column

The reciprocating-plate column employed in the present work is shown in Figs 1, 2 and 3. The column consisted of a 48 in length of 12 in o.d. Quickfit pipe specially selected to have a fairly uniform i.d. of $\sim 11\frac{5}{8}$ in.

The plates were of 11·205 in dia., which was the maximum that could be utilised without excessive friction against the glass pipe. The perforated plates, made of $\frac{1}{16}$ in stainless steel sheet, contained $\frac{5}{8}$ in dia. holes on $\frac{25}{32}$ in triangular centres which provided 58% open area. The plates were turned over at their edges to provide the necessary strength. 25 plates spaced 1 in apart were mounted on a central shaft of $\frac{5}{8}$ in dia. and were assembled in a rigid fashion by the use of $\frac{15}{16}$ in high by $1\frac{5}{8}$ in dia. spacers and locking collars.

The central shaft which supported the plates was reciprocated by means of a reciprocating drive mechanism located at the top of the column. The amplitude was variable although the present series of runs was carried out at a

constant amplitude of $\frac{1}{2}$ in. By the use of a variable speed drive, it was possible to operate the column at speeds ranging from 84 to 844 rev/min.

The light and heavy streams were introduced 3 in below and above, respectively, the plate section by 96 tubes of 0·131 in i.d. manifolded at the top and the bottom of the column.

The first series of runs was made with 25 uniformly spaced plates of the type described above. In the second series of runs, four plates were removed and replaced by two special plates or baffle plates. The spacing of the regular plates and the baffle plates and the dimensions of the baffle plates are shown in Fig. 1. The baffle plate was designed to have 58 % open area after correcting for the hub and spokes.

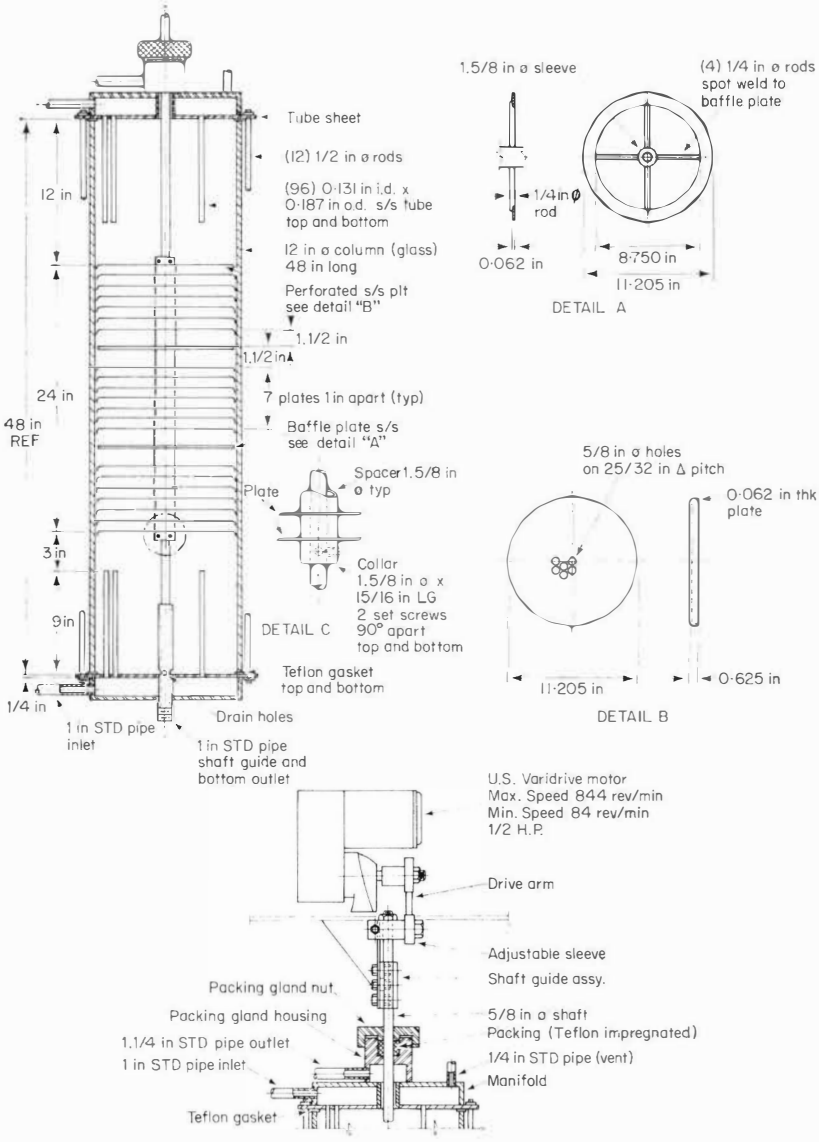

FIG. 1. *Extraction column details*

Operating procedure

The system used in this investigation was MIBK–acetic acid–water. The distribution data employed were the same as those previously reported.[12, 13] The solute was first extracted from the aqueous solution by the MIBK phase. In the following run, the solute was extracted from the organic phase by the aqueous phase. As previously mentioned, in all runs the amplitude was

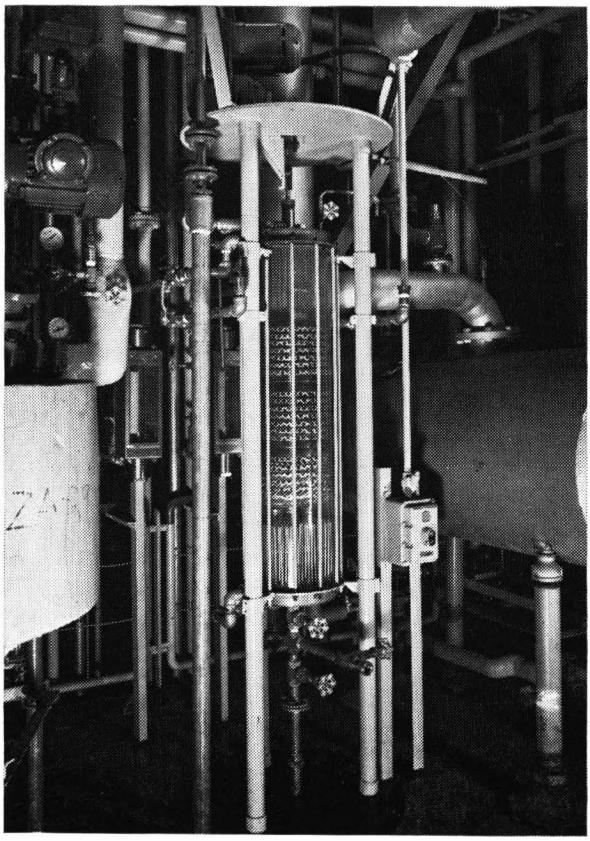

FIG. 2. *12 in reciprocating-plate extraction column*

½ in and the plate spacing was 1 in. The following are the four types of runs made in the 12 in dia. column: water dispersed, MIBK extractant; water dispersed, water extractant; MIBK dispersed, water extractant; and MIBK dispersed, MIBK extractant.

The solvent ratios were mainly such that the operating line was approximately parallel to the equilibrium curve. The solvent ratios employed are given in the tables of data. The concentration of acid in the feed solutions was maintained within narrow limits (13·6–16·5%) in order to minimise the effect of solute concentration on the results.

The liquid extraction system used is shown in Fig. 4. The feed solutions were maintained at ~22°C. The solutions were mutually saturated in the 200 and 300 gal glass-lined kettles. The aqueous and organic feed streams

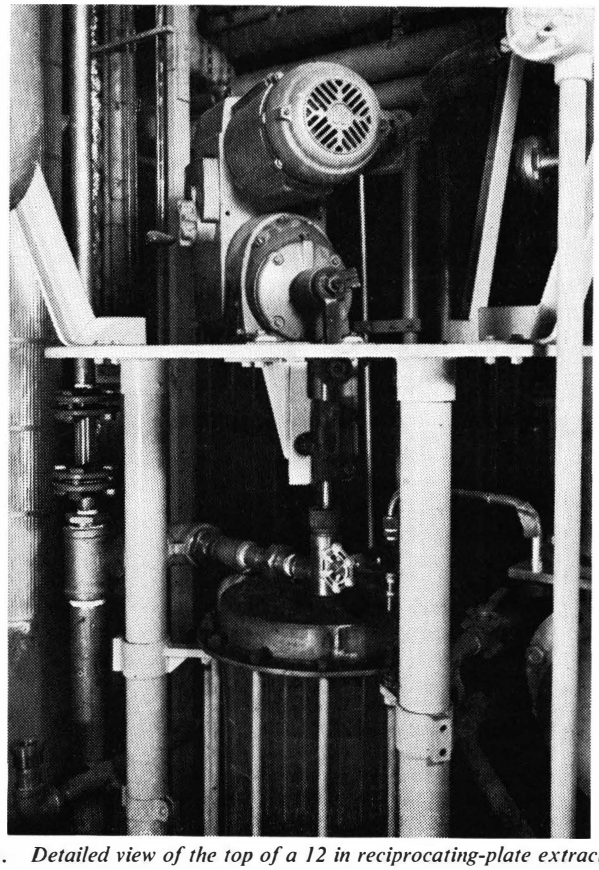

FIG. 3. *Detailed view of the top of a 12 in reciprocating-plate extraction column*

were introduced into the column by centrifugal pumps via calibrated rotameters, and the feed rate was controlled by needle valves. All lines were made of stainless steel, and care was taken to avoid contamination of the solvents by using Teflon gaskets and packings.

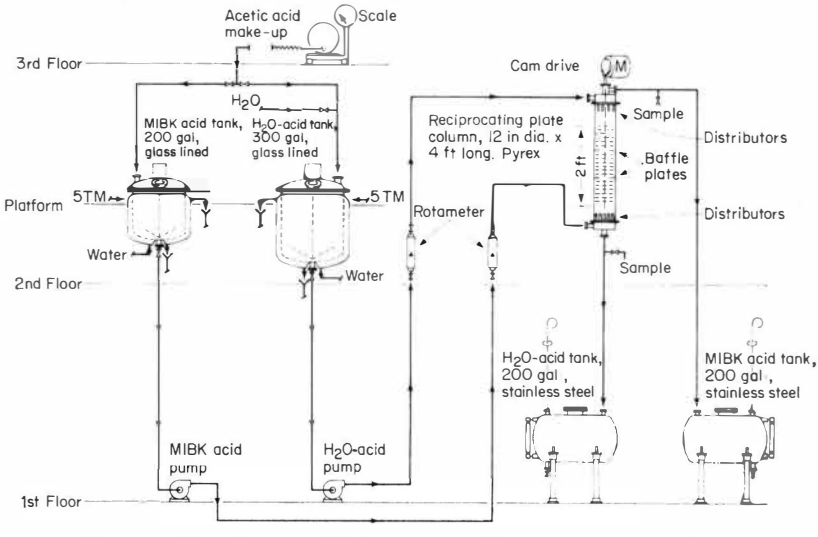

FIG. 4. *Flow diagram of 12 in reciprocating-plate extraction system*

The column was first filled with continuous phase, and then the interface was established at either the top or bottom of the column. The flow rate was adjusted, and the desired reciprocating speed was set by adjustment of the variable speed drive. The interface was kept in as constant a position as possible by controlling the bottom draw-off needle valve. The interface was usually maintained at ~4–6 in from the top or bottom of the column, depending on which phase was dispersed. The column came to a steady state by the time the contents of the column had been replaced three times. Usually more than three times the volume of the column was fed before the samples of the exit streams were taken for analysis. The acid in the extract and raffinate were analysed by titration with 0·1N standard caustic solution.

In addition to the runs in the 12 in dia. column, the following two types of runs were made in a 1 in dia. column: water dispersed, MIBK extractant; and water dispersed, water extractant.

The plates used for the 1 in dia. column were punched out of Teflon sheet and had a free area of ~50% as shown in a previous paper.[1]

Results

The data are shown in Tables I–VIII. Tables I–III present the data obtained in the 12 in column fitted with 25 perforated plates spaced 1 in apart. Tables IV–VI show similar data for the column fitted with two baffle plates as shown in Figs 1 and 2. In addition, data on a 1 in extraction column operated with 1 in plate spacing and ½ in amplitude are presented in Tables VII and VIII, and for easy reference and comparison, the data on the 3 in dia. column[1] for 1 in plate spacing and ½ in amplitude are shown in Tables IX and X.

Effect of reciprocating speed, strokes/min

Figs 5 and 6 show all the data for the various types of operation for the 12 in column with and without the baffle plates, the 3 in column, and the 1 in column. For an understanding of the various types of data presented, reference should be made to the definitions of the symbols employed in Figs 5 and 6. For example, Fig. 5(b) shows the data for the case water dispersed, MIBK extractant for a total throughput in the range of 913–1216 gal/h/ft^2 for the 1 in column, the 3 in column and the 12 in column with and without the baffle plates. As shown, the minimum HETS achieved was 2·8 in in the 1 in column, 6·3 in in the 3 in column, 11·4 in in the 12 in column without the baffle plates, and 7·2 in in the 12 in column with the baffle plates. A summary of the minimum HETS values achieved for all types of operation is given in Table XI.

Effect of throughput

The effect of throughput on the minimum HETS obtained in the 3 in column and the 12 in column with and without baffle plates is shown in Fig. 7. The benefit of using the baffle plates is apparent for two of the four cases studied. In both cases, the direction of mass transfer was from the aqueous to the organic phase.

Volumetric efficiency

In Table XII, volumetric efficiencies achieved with and without the baffle plates in the 12 in dia. column are presented along with similar data reported in the literature on columns of at least 6 in dia. Volumetric efficiencies achieved with the baffle plates are consistently higher than those obtained without baffle plates. Volumetric efficiencies up to 311 h^{-1} were achieved which compare favourably with most of the data on the other columns listed. It is to be expected that modifications in baffle plate arrangement will improve the volumetric efficiency.

TABLE I

12 in reciprocating-plate extraction column: Summary of data (with no baffle-plates)

System: MIBK–acetic acid–water; water dispersed, MIBK extractant

Run no.	Symbol	No. of plates	Plates spacing, in	Amplitude, in	Agitator speed, strokes/min	Flow rates of feed streams, gal/h/ft²			Concentration of acetic acid, wt.-%				No. of theoretical stages	Plate efficiency, %	HETS, in	(*H*/*L*) Rot.* / (*H*/*L*) M.S.C.**
						MIBK	H_2O	Total	MIBK in	MIBK out	H_2O in	H_2O out				
11	$\blacktriangle_1$	25	1	0·5	360	305	299	604	1·28	8·05	14·2	8·53	1·6	6·4	15·6	1·085
15	$\blacktriangle_1$	25	1	0·5	350	305	299	604	4·92	10·63	16·42	12·12	1·3	5·2	19·2	0·958
17	$\blacktriangle_1$	25	1	0·5	300	301	306	607	1·82	8·19	11·98	6·72	3·0	12·0	8·3	0·953
19(1)	$\blacktriangle_1$	25	1	0·5	300	306	300	606	0·82	12·22	17·99	8·08	3·2	12·8	7·8	0·969
19(2)	$\blacktriangle_1$	25	1	0·5	350	306	300	606	0·82	10·58	17·99	10·01	1·7	6·8	14·7	0·957
29(1)	$\blacktriangle_1$	25	1	0·5	250	305	300	605	3·40	10·50	15·55	9·46	2·6	10·4	9·6	1·005
29(2)	$\blacktriangle_1$	25	1	0·5	0	305	300	605	3·40	8·14	15·55	12·01	0·8	3·2	31·3	0·850
31(1)	$\blacktriangle_1$	25	1	0·5	250	299	298	597	3·44	11·07	16·59	10·27	2·3	9·2	10·9	1·015
31(2)	$\blacktriangle_1$	25	1	0·5	200	295	293	588	3·44	10·83	16·59	10·39	2·1	8·4	11·9	1·062
33(1)	$\blacktriangle_2$	25	1	0·5	200	600	600	1200	4·13	11·50	16·97	11·03	2·2	8·8	11·4	0·970
33(2)	$\blacktriangle_2$	25	1	0·5	250	600	600	1200	4·13	9·52	16·97	12·76	1·0	4·0	25·0	1·110
35(1)	$\blacktriangle_2$	25	1	0·5	150	596	620	1216	4·71	10·34	16·34	12·16	1·35	5·4	18·5	1·002
35(2)	$\blacktriangle_2$	25	1	0·5	100	596	612	1208	4·71	9·87	16·34	12·48	1·1	4·4	22·7	1·008
23(1)	$\blacktriangle_3$	25	1	0·5	250	946	887	1833	3·53	8·77	16·57	12·54	0·92	3·7	27·2	0·998
23(2)	$\blacktriangle_3$	25	1	0·5	300	946	887	1833	3·53	8·69	16·57	12·37	0·92	3·7	27·2	1·045
25(1)	$\blacktriangle_3$	25	1	0·5	150	930	880	1810	4·76	9·43	16·79	13·27	0·85	3·4	29·4	0·952
25(2)	$\blacktriangle_3$	25	1	0·5	100	930	880	1810	4·76	9·17	16·79	13·28	0·81	3·2	31·0	0·982

* Heavy to light phase flow rate from rotameter readings
** Heavy to light phase flow from analyses and mutual solubility curve

TABLE II

12 in reciprocating-plate extraction column: Summary of data (with no baffle-plates)

System: MIBK–acetic acid–water; water dispersed, water extractant

Run no.	Symbol	No. of plates	Plates spacing, in	Amplitude, in	Agitator speed, strokes/min	Flow rates of feed streams, gal/h/ft²			Concentration of acetic acid, wt.-%				No. of theoretical stages	Plate efficiency, %	HETS, in	(H/L) Rot.* / (H/L) M.S.C.**
						MIBK	H_2O	Total	MIBK in	MIBK out	H_2O in	H_2O out				
20(1)	■1	25	1	0·5	350	360	187	547	14·59	5·28	0·21	13·86	2·1	8·4	11·9	1·010
20(2)	■1	25	1	0·5	300	360	187	547	14·59	4·04	0·21	13·79	2·5	10·0	10·0	0·940
22(1)	■1	25	1	0·5	250	364	190	554	14·55	2·66	0	15·15	3·9	15·6	6·4	0·953
22(2)	■1	25	1	0·5	200	364	190	554	14·55	2·91	0	14·93	3·6	14·4	6·95	0·965
28(1)	■1	25	1	0·5	150	353	182	535	13·42	4·17	0	13·03	2·4	9·6	10·4	1·175
28(2)	■1	25	1	0·5	0	353	182	535	13·42	6·30	0	10·54	1·2	4·8	20·8	0·935
30(1)	■1	25	1	0·5	250	353	184	537	14·18	3·61	0·15	14·99	3·4	13·6	7·35	1·065
30(2)	■1	25	1	0·5	200	353	184	537	14·18	3·55	0·15	14·83	3·4	13·6	7·35	1·038
32(1)	■2	25	1	0·5	200	708	461	1169	12·74	2·66	0	11·27	2·5	10·0	10·0	1·020
32(2)	■2	25	1	0·5	250	727	456	1183	12·74	4·67	0	9·73	1·4	5·6	17·8	0·930
34(1)	■2	25	1	0·5	150	708	465	1173	15·42	3·53	0	12·97	2·3	9·2	10·9	0·983
34(2)	■2	25	1	0·5	100	712	465	1177	15·42	4·80	0	12·40	1·8	7·2	13·9	0·978
24(1)	■3	25	1	0·5	150	1043	663	1706	13·93	3·92	0	12·50	2·2	8·8	11·4	1·070
24(2)	■3	25	1	0·5	200	1043	663	1706	13·93	5·74	0	11·76	1·5	6·0	16·7	1·150
26(1)	■3	25	1	0·5	100	1030	663	1693	14·04	4·72	0	11·72	1·7	6·8	14·7	1·060
26(2)	■3	25	1	0·5	0	1030	663	1693	14·04	5·71	0	11·03	1·4	5·6	17·9	1·190

*,** See footnote, Table I

TABLE III

12 in reciprocating-plate extraction column: Summary of data (with no baffle-plates)

System: MIBK–acetic acid–water

Run no.	Symbol	No. of plates	Plates spacing, in	Amplitude, in	Agitator speed, strokes/min	Flow rates of feed streams, gal/h/ft²			Concentration of acetic acid, wt.-%				No. of theoretical stages	Plate efficiency, %	HETS, in	(H/L) Rot.* / (H/L) M.S.C.**
						MIBK	H_2O	Total	MIBK in	MIBK out	H_2O in	H_2O out				
						MIBK dispersed, water extractant										
42(1)	●1	25	1	0·5	250	362	184	546	13·86	3·53	0·06	14·19	3·1	12·4	8·1	1·025
42(1)	●1	25	1	0·5	350	362	184	546	13·86	3·22	0·06	14·62	3·5	14·0	7·1	0·935
44(1)	●1	25	1	0·5	400	362	184	546	14·41	5·21	0	13·25	2·0	8·0	12·5	1·003
44(2)	●1	25	1	0·5	450	362	184	546	14·41	5·35	0	12·29	1·8	7·2	13·9	0·942
36(1)	●2	25	1	0·5	200	710	465	1175	14·32	3·43	0·12	12·22	2·2	8·8	11·4	0·983
36(2)	●2	25	1	0·5	250	706	461	1167	14·32	2·96	0·12	12·51	2·5	10·0	10·0	0·983
38(1)	●2	25	1	0·5	300	710	465	1175	13·72	4·53	0·32	10·22	1·5	6·0	16·7	0·923
38(2)	●2	25	1	0·5	350	710	465	1175	13·72	5·53	0·32	10·12	1·3	5·2	19·2	1·030
40(1)	●2	25	1	0·5	225	718	448	1166	15·16	4·13	0·23	13·58	2·4	9·6	10·4	1·056
40(2)	●2	25	1	0·5	275	718	448	1166	15·16	5·39	0·23	11·95	1·6	6·4	15·6	0·982
						MIBK dispersed, MIBK extractant										
41(1)	×1	25	1	0·5	200	306	300	606	5·0	10·57	16·68	12·34	1·4	5·6	17·9	0·940
41(2)	×1	25	1	0·5	150	306	300	606	5·0	11·58	16·68	11·54	2·2	8·8	11·4	1·042
43(1)	×1	25	1	0·5	100	306	300	606	4·38	11·65	16·97	10·88	2·4	9·6	10·4	1·047
43(2)	×1	25	1	0·5	0	306	300	606	4·38	10·93	16·97	11·71	1·6	6·4	15·6	1·020
37(1)	×2	25	1	0·5	200	600	607	1207	3·47	9·47	16·51	11·97	1·1	4·4	22·7	1·012
37(2)	×2	25	1	0·5	150	600	607	1207	3·47	9·78	16·51	11·79	1·2	4·8	20·8	0·995
39(1)	×2	25	1	0·5	100	602	610	1212	4·89	10·20	16·62	12·52	1·2	4·8	20·8	0·967
39(2)	×2	25	1	0·5	85	598	610	1208	4·89	10·15	16·62	12·48	1·2	4·8	20·8	0·973

*,** See footnote, Table I

TABLE IV

12 in reciprocating-plate extraction column: Summary of data (with baffle-plates)

System: MIBK–acetic acid–water; water dispersed, MIBK extractant

Run no.	Symbol	No. of plates	Plates spacing, in	Amplitude, in	Agitator speed, strokes/min	Flow rates of feed streams, gal/h/ft²			Concentration of acetic acid, wt.-%				No. of theoretical stages	Plate efficiency, %	HETS, in (H/L) Rot.* / (H/L) M.S.C.**	
						MIBK	H_2O	Total	MIBK in	MIBK out	H_2O in	H_2O out				
49(1)	$\triangle_1$	21	1	0·5	300	304	301	605	4·52	11·16	16·50	11·06	2·10	10·0	11·7	0·985
49(2)	$\triangle_1$	21	1	0·5	325	304	301	605	4·52	10·59	16·50	11·09	1·82	8·7	13·5	0·932
51(1)	$\triangle_1$	21	1	0·5	250	304	298	602	4·82	11·87	16·40	10·40	3·40	16·2	7·2	1·005
51(2)	$\triangle_1$	21	1	0·5	225	304	298	602	4·82	12·0	16·40	11·16	3·27	15·6	7·5	0·890
53(1)	$\triangle_1$	21	1	0·5	200	304	298	602	5·12	11·44	16·08	11·14	2·70	12·9	9·1	0·957
53(2)	$\triangle_1$	21	1	0·5	150	304	298	602	5·12	11·02	16·08	11·54	1·99	9·5	12·35	0·962
45(1)	$\triangle_2$	21	1	0·5	200	601	600	1201	5·94	12·30	17·17	11·88	2·80	13·3	8·75	0·965
45(2)	$\triangle_2$	21	1	0·5	250	601	600	1201	5·94	11·78	17·17	12·24	1·99	9·5	12·35	0·995
47(1)	$\triangle_2$	21	1	0·5	225	600	600	1200	4·09	11·87	16·58	9·92	3·40	16·2	7·2	1·030
47(2)	$\triangle_2$	21	1	0·5	200	600	600	1200	4·09	11·50	16·58	10·50	2·58	12·3	9·5	0·990
59(2)	$\triangle_2$	21	1	0·5	150	600	600	1200	5·67	11·23	16·27	11·88	1·98	9·4	12·35	1·000
61(1)	$\triangle_2$	21	1	0·5	225	600	600	1200	2·54	11·08	16·04	8·91	2·92	13·9	8·4	1·988
61(1)	$\triangle_2$	21	1	0·5	225	600	600	1200	2·54	10·75	16·04	8·90	2·70	12·9	9·1	0·060
55(1)	$\triangle_3$	21	1	0·5	150	938	883	1821	4·89	10·82	16·60	11·70	1·75	8·3	14·0	0·995
57(1)	$\triangle_3$	21	1	0·5	125	938	887	1825	5·07	10·37	16·62	11·83	1·52	7·2	16·15	1·057
57(2)	$\triangle_3$	21	1	0·5	100	938	887	1825	5·07	10·10	16·62	12·47	1·17	5·6	21·0	1·010

*,** See footnote, Table I

TABLE V

12 in reciprocating-plate extraction column: Summary of data (with baffle-plates)

System: MIBK–acetic acid–water; water dispersed, water extractant

Run no.	Symbol	No. of plates	Plates spacing, in	Amplitude, in	Agitator speed, strokes/min	Flow rates of feed streams, gal/h/ft²			Concentration of acetic acid, wt.-%				No. of theoretical stages	Plate efficiency, %	HETS, in	(H/L) Rot.* / (H/L) M.S.C.**
						MIBK	H_2O	Total	MIBK in	MIBK out	H_2O in	H_2O out				
50(1)	□1	21	1	0·5	250	365	190	555	14·43	4·12	0·38	14·93	3·03	14·4	8·1	1·090
50(2)	□1	21	1	0·5	300	365	190	555	14·43	4·64	0·38	13·79	2·34	11·1	10·5	0·970
52(1)	□1	21	1	0·5	225	365	190	555	14·36	2·88	0·32	14·51	3·50	16·7	7·0	0·930
52(2)	□1	21	1	0·5	175	365	190	555	14·36	3·69	0·32	13·66	2·70	12·9	9·1	0·995
46(1)	□2	21	1	0·5	200	710	460	1170	14·29	3·02	0·21	12·48	2·58	12·3	9·5	0·975
46(2)	□2	21	1	0·5	225	710	460	1170	14·29	2·94	0·21	12·58	2·58	12·3	9·5	1·005
48(1)	□2	21	1	0·5	250	707	460	1167	13·62	3·19	0·08	12·07	2·45	11·7	10·0	1·060
56(1)	□2	21	1	0·5	150	715	460	1175	14·35	3·62	0·22	12·30	2·22	10·6	11·05	1·004
56(2)	□2	21	1	0·5	275	715	460	1175	14·35	3·76	0·22	12·70	2·22	10·6	11·05	1·045
54(1)	□3	21	1	0·5	200	1065	642	1707	14·19	5·03	0·22	12·31	1·75	8·3	14·0	1·100
54(2)	□3	21	1	0·5	150	1052	642	1694	14·19	3·89	0·22	12·49	2·22	10·6	11·05	0·976
58(1)	□3	21	1	0·5	100	1065	642	1707	14·12	5·01	0·33	11·89	1·82	8·7	13·5	1·030

*,** See footnote, Table I

TABLE VI

12 in reciprocating-plate extraction column: Summary of data (with baffle-plates)

System: MIBK–acetic acid–water

Run no.	Symbol	No. of plates	Plates spacing, in	Amplitude, in	Agitator speed, strokes/min	Flow rates of feed streams, gal/h/ft²			Concentration of acetic acid, wt.-%				No. of theoretical stages	Plate efficiency, %	HETS, in (H/L) Rot.*	(H/L) M.S.C.**
						MIBK	H_2O	Total	MIBK in	MIBK out	H_2O in	H_2O out				
						MIBK dispersed, water extractant										
62(1)	○2	21	1	0·5	250	706	460	1166	13·56	2·74	0·20	11·85	2·58	12·3	9·5	0·993
62(2)	○2	21	1	0·5	175	706	460	1166	13·56	3·85	0·20	11·47	1·98	9·4	12·35	1·040
64(1)	○2	21	1	0·5	275	718	461	1179	14·56	2·64	0	12·32	2·58	12·3	9·5	0·935
64(2)	○2	21	1	0·5	300	718	461	1179	14·56	3·62	0	12·42	2·22	10·6	11·05	0·985
						MIBK dispersed, MIBK extractant										
65(1)	×1	21	1	0·5	200	299	296	595	4·72	11·92	16·42	10·67	3·14	14·9	7·8	0·928
65(2)	×1	21	1	0·5	150	299	296	595	4·72	11·81	16·42	10·72	2·92	13·9	8·4	1·015
69(1)	×1	21	1	0·5	300	304	302	606	3·38	10·49	16·02	10·33	2·10	10·0	11·7	0·993
69(2)	×1	21	1	0·5	250	304	302	606	3·38	10·80	16·02	9·65	2·58	12·3	9·5	1·072
63(1)	×2	21	1	0·5	150	600	602	1202	3·41	11·63	16·13	8·84	4·02	19·2	6·2	1·085
63(2)	×2	21	1	0·5	200	600	602	1202	3·41	11·15	16·13	10·81	2·22	10·6	11·05	0·860
67(1)	×2	21	1	0·5	150	600	602	1202	3·59	11·60	16·05	9·30	3·72	17·7	6·6	1·032
67(2)	×2	21	1	0·5	100	600	602	1202	3·59	11·10	16·05	9·70	2·80	13·3	8·75	1·040

*,** See footnote, Table I

TABLE VII

1 in reciprocating-plate extraction column: Summary of data

System: MIBK–acetic acid–water; water dispersed, MIBK extractant

Run no.	Symbol	No. of plates	Plates spacing, in	Amplitude, in	Agitator speed, strokes/min	Flow rates of feed streams, gal/h/ft²			Concentration of acetic acid, wt.-%				No. of theoretical stages	Plate efficiency, %	HETS, in	(H/L) Rot.* / (H/L) M.S.C.**
						MIBK	H_2O	Total	MIBK in	MIBK out	H_2O in	H_2O out				
9	△1	25	1	0·5	360	249·0	323·0	572·0	0	14·545	18·705	5·715	8·0	32·0	3·1	1·000
11	△1	25	1	0·5	345	249·0	323·0	572·0	0	14·295	18·75	5·43	7·5	30·0	3·3	0·985
13	△1	25	1	0·5	320	249·0	323·0	572·0	0	14·32	18·735	5·80	7·1	28·4	3·5	0·985
7	△1	25	1	0·5	373	249·0	323·0	572·0	0	—	18·705	—	—	—	—	Column flood
1	△2	25	1	0·5	401	456·5	456·5	913·0	0	12·15	17·05	2·91	8·8	35·4	2·8	1·021
2	△2	25	1	0·5	417	456·5	456·5	913·0	0	11·75	16·53	3·31	6·6	26·4	3·8	1·000
3	△2	25	1	0·5	393	446·0	479·0	925·0	0	12·53	17·04	4·01	8·1	32·4	3·1	0·983
5	△2	25	1	0·5	312	446·0	482·0	928·0	0	12·46	17·50	5·58	5·65	22·6	4·4	1·025
19	△2	25	1	0·5	0	446·0	482·0	928·0	0	8·29	15·84	8·75	1·4	5·6	17·5	0·951
23	△2	32	1†	0·5	322	446·0	482·0	928·0	0	11·67	15·78	4·64	7·5	30·0	3·3	1·009
2	△2	25	1	0·5	446	456·5	456·5	913·0	0	—	16·53	—	—	—	—	Column flood

† Top 6 in of column plate spacing is 1·5 in, middle 8 in is 1 in, bottom 10 in is 0·5 in

*,** See footnote, Table I

TABLE VIII

1 in reciprocating plate extraction column: Summary of data

System: MIBK–acetic acid–water; MIBK dispersed, water extractant

Run no.	Symbol	No. of plates	Plates spacing, in	Amplitude, in	Agitator speed, strokes/min	Flow rates of feed streams, gal/h/ft²			Concentration of acetic acid, wt.-%				No. of theoretical stages	Plate efficiency, %	HETS, in	(H/L) Rot.* / (H/L) M.S.C.**
						MIBK	H_2O	Total	MIBK in	MIBK out	H_2O in	H_2O out				
6	⊡1	25	1	0·5	278	376·8	181·7	458·5	16·785	0·815	0	16·075	6	24·0	4·2	1·033
8	⊡1	25	1	0·5	280	376·8	181·7	458·5	—	—	3·02	—	—	—	—	Column flood
2	⊡2	25	1	0·5	152	670·5	359·1	1029·6	16·53	2·65	0	14·74	3·1	12·4	8·1	0·996
4	⊡2	25	1	0·5	115	670·5	359·1	1029·6	16·53	3·67	0	13·79	2·3	9·2	10·9	0·961
10	⊡2	25	1	0·5	0	670·5	359·1	1029·6	11·79	6·73	3·11	11·525	1·5	6·0	16·7	0·953

*,** See footnote, Table I

TABLE IX

3 in reciprocating-plate extraction column: Summary of data

System: MIBK–acetic acid–water

Run no.	Symbol	No. of plates	Plates spacing, in	Amplitude, in	Agitator speed, strokes/min	Flow rates of feed streams, gal/h/ft²			Concentration of acetic acid, wt.-%				No. of theoretical stages	Plate efficiency, %	HETS, in	(H/L) Rot.* / (H/L) M.S.C.**
						MIBK	H_2O	Total	MIBK in	MIBK out	H_2O in	H_2O out				
						Water dispersed, MIBK extractant										
17	▼1	22	1	0·5	300	301	298	599	4·1	12·5	17·9	9·47	3·5	15·9	6·3	1·202
19	▼1	22	1	0·5	201	301	297	598	5·14	13·75	19·3	11·3	3·1	14·1	7·1	1·090
22	▼1	22	1	0·5	330	302	298	600	2·805	8·85	12·52	7·17	4·5	20·2	4·9	1·080
23	▼2	22	1	0·5	245	601	592	1193	2·805	8·71	12·52	7·67	3·5	15·9	6·3	1·005
42	▼1	22	1	0·5	0	302	297	599	1·155	5·98	13·55	9·75	0·79	3·6	27·9	1·131
43	▼2	22	1	0·5	126	605	590	1195	1·155	8·73	16·21	10·1	1·3	5·8	16·9	1·048
						Water dispersed, water extractant										
16	▽1	22	1	0·5	285	356	190	547	14·95	1·76	0·078	15·25	4·7	21·4	4·7	0·932
18	▽1	22	1	0·5	207	354	190	544	16·35	2·53	0·107	16·2	3·75	17·0	5·9	0·928
20	▽1	22	1	0·5	320	358	190	548	11·52	1·34	0·082	12·62	5·1	23·2	4·3	0·938
21	▽2	22	1	0·5	185	716	452	1168	11·52	2·14	0·082	10·50	2·75	12·5	8·0	0·944
24	▽2	22	1	0·5	230	716	452	1168	11·67	1·17	0·118	11·30	3·3	15·0	6·7	0·953
25	▽2	22	1	0·5	0	716	452	1168	11·67	4·80	0·118	8·23	1·2	5·5	18·3	0·933

*,** See footnote, Table I

TABLE X

3 in reciprocating-plate extraction column: Summary of data

System: MIBK–acetic acid–water

Run no.	Symbol	No. of plates	Plates spacing, in	Amplitude, in	Agitator speed, strokes/min	Flow rates of feed streams, gal/h/ft²			Concentration of acetic acid, wt.-%				No. of theoretical stages	Plate efficiency, %	HETS, in	(H/L) Rot.* / (H/L) M.S.C.**
						MIBK	H_2O	Total	MIBK in	MIBK out	H_2O in	H_2O out				
						MIBK dispersed, water extractant										
32	⊙₂	22	1	0·5	285	715	452	1167	13·21	1·42	0·24	12·2	3·85	17·5	5·7	0·922
33	⊙₁	22	1	0·5	430	357	190	547	13·21	2·30	0·24	13·5	3·8	17·3	5·8	0·930
36	⊙₂	22	1	0·5	0	715	452	1167	13·45	5·26	0·21	9·7	1·25	5·7	17·6	0·926
37	⊙₁	22	1	0·5	0	357	190	547	13·45	6·2	0·21	10·19	1·2	5·5	18·3	0·932
44	⊙₂	22	1	0·5	122	717	452	1169	11·45	3·57	0·105	9·06	1·6	7·3	13·8	0·927
45	⊙₁	22	1	0·5	122	358	190	548	11·45	3·79	0·105	10·20	1·9	8·6	11·6	0·912
						MIBK dispersed, MIBK extractant										
34	▽₁	22	1	0·5	244	302	297	599	3·26	10·58	14·4	8·2	5·0	22·7	4·4	1·012
35	▽₂	22	1	0·5	170	603	590	1193	3·26	10·28	14·4	8·37	3·9	17·5	5·6	0·980
38	▽₁	22	1	0·5	0	302	297	599	1·34	9·07	14·85	8·5	1·9	8·6	11·6	0·980
39	▽₂	22	1	0·5	0	605	590	1195	1·34	11·49	17·2	8·9	2·5	11·3	8·8	0·982

*,** See footnote, Table I

TABLE XI

Summary of minimum HETS values

Column diameter, in	Symbol	Minimum HETS	Throughput, gal/h/ft²	Agitator speed, strokes/min
1	△1	3·1	572	360
	△2	2·8	913	401
1	⊡1	4·2	458·5	278
	⊡2	8·1	1029·6	152
3	▼1	4·9	600	330
	▼2	6·3	1193	245
	▽1	4·3	548	320
	▽2	6·7	1168	230
	⊙1	5·8	547	430
	⊙2	5·7	1167	285
	×1	4·4	599	244
	×2	5·6	1193	170
12 (with baffle)	△1	7·2	602·4	250
	△2	7·2	1200	225
	△3	14·0	1821	150
	□1	7·0	555	225
	□2	9·5	1170	200
	□3	11·05	1694	150
	○2	9·5	1179	275
	▽1	7·8	595	200
	▽2	6·2	1202	150
12 (without baffle)	▲1	7·8	606·6	300
	▲2	11·4	1200	200
	▲3	27·2	1833·6	250
	■1	6·4	555·8	250
	■2	10·0	1168·8	200
	■3	11·4	1706·4	150
	●1	7·1	546	350
	●2	10·0	1166·4	250
	×1	10·4	606	100
	×2	20·8	1206·6	150

TABLE XII

Comparison of volumetric efficiencies

MIBK–acetic acid–water system

Type of column	Reference	Column dia., in	Dispersed phase	Direction of mass transfer	Maximum total throughput		Minimum HETS		Volumetric efficiency V_t/HETS, h^{-1}
					gal/h/ft²	V_t, ft³/h/ft²	in	ft	
Rotating disc; R.D.C.	14	8·0	Water		980	131·0	4·3**	0·36	364
			Water		1030	137·8	6·3†	0·525	262
Turbine agitator, horizontal baffles	15	11·5	Water	d→c*	458	61·2	3·0	0·25	245
Alternate agitated and packed sections	13	11·5	Water	d→c	595	79·5	9·2	0·77	104
Reciprocating plate	1	3·0	Water	d←c	547	73·1	4·3	0·36	203
			Water	d←c	1172	156·8	5·0	0·42	376
			Water	d←c	1707	228·5	7·75	0·65	353
			Water	d→c	1837	245·6	7·5	0·63	393
Reciprocating plate with baffle	This work	12·0	Water	d→c	602	80·5	7·2	0·60	134
			Water	d→c	1200	160·4	7·2	0·60	268
			Water	d→c	1821	243·5	14·0	1·17	208
			Water	d←c	555	74·2	7·0	0·58	127
			Water	d←c	1170	156·4	9·5	0·79	197
			Water	d←c	1694	226·4	11·05	0·92	246
Reciprocating plate without baffle	This work	12·0	Water	d→c	607	81·1	7·8	0·65	125
			Water	d→c	1200	160·4	11·4	0·95	169
			Water	d→c	1834	245·1	27·2	2·26	109
			Water	d←c	556	74·3	6·4	0·53	139
			Water	d←c	1169	156·2	10·0	0·83	188
			Water	d←c	1706	228·1	11·4	0·95	240
Turbine agitators in baffled compartments	16	6·0	MIBK	d→c	286	38·2	3·7	0·31	124
			MIBK	d→c	500	66·8	5·5	0·46	146
Reciprocating plate with baffle	This work	12·0	MIBK	d→c	1179	157·6	9·5	0·79	199
			MIBK	d←c	595	79·6	7·8	0·65	123
			MIBK	d←c	1202	160·8	6·2	0·52	311
Reciprocating plate without baffle	This work	12·0	MIBK	d→c	546	73·0	7·1	0·59	124
			MIBK	d→c	1167	155·9	10·0	0·83	188
			MIBK	d←c	606	81·0	10·4	0·87	93
			MIBK	d←c	1208	161·5	20·8	1·73	93

* d = dispersed phase, c = continuous phase † Rotor diameter = 4·7 in; stator opening = 6·3 in ** Rotor diameter = 3·1 in; stator opening = 4·9 in

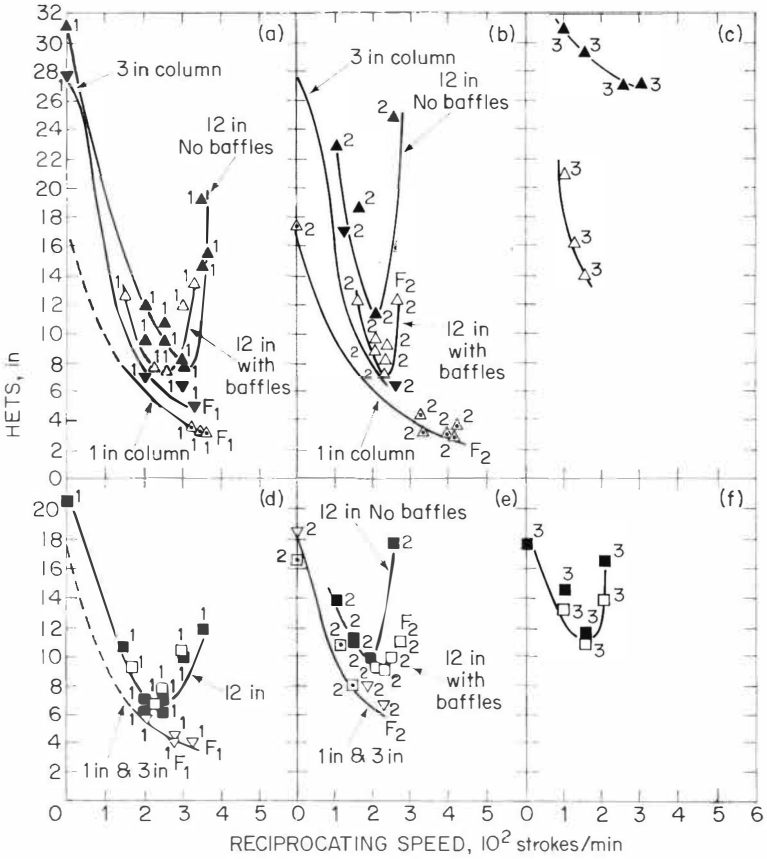

FIG. 5. *Effect of reciprocating speed on HETS, water dispersed, MIBK extractant; water dispersed, water extractant*

Symbol	Column dia., in	Effective column height, in	No. of perforated plates	Plate spacing, in	Amplitude, in	No. of baffle plates
		*Water-dispersed, MIBK extractant d→c**				
▲	12	25	25	1	0·5	0
△	12	25	21	1/1·5	0·5	2
▼	3	22	22	1	0·5	0
△	1	25	25	1	0·5	0
		Water-dispersed, water extractant d←c				
■	12	25	25	1	0·5	0
□	12	21	21	1/1·5	0·5	2
▽	3	22	22	1	0·5	0
⊡	1	25	25	1	0·5	0

* *d* = dispersed phase, c = continuous phase

No. adjacent to symbol	Total throughput, gal/h/ft²		
	1-in column	3-in column	12-in column
1	458–572	544–600	502–606
2	913–1030	1161–1197	1166–1216
3	—	1706–1841	1693–1834

F = floodpoint

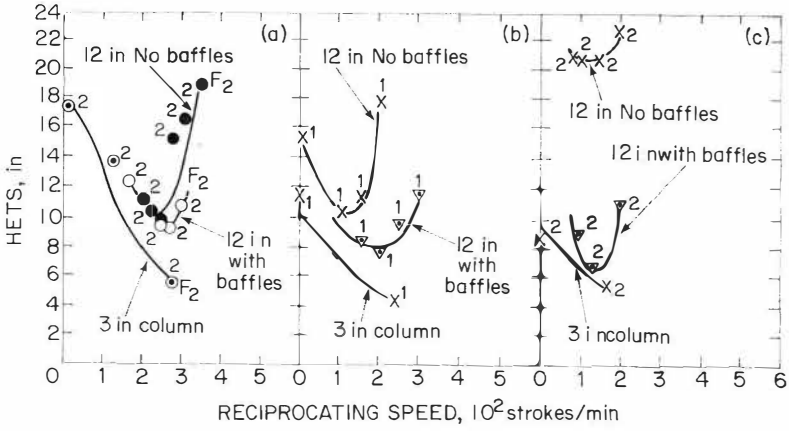

FIG. 6. *Effect of reciprocating speed on HETS, MIBK dispersed, water extractant; MIBK dispersed, MIBK extractant*

Symbol	Column dia., in	Effective column height, in	No. of perforated plates	Plate spacing, in	Amplitude, in	No. of baffle plates
		*MIBK dispersed, water extractant d→c**				
●	12	25	25	1	0·5	0
○	12	25	21	1/1·5	0·5	0/2
⊙	3	22	22	1	0·5	0
		MIBK dispersed, MIBK extractant d← c				
×	12	25	25	1	0·5	0
▽	12	25	21	1/1·5	0·5	0/2
×	3	2	22	1	0·5	0

* *d* = dispersed phase, c = continuous phase
F = floodpoint
Numbers adjacent to symbols as in Fig. 5

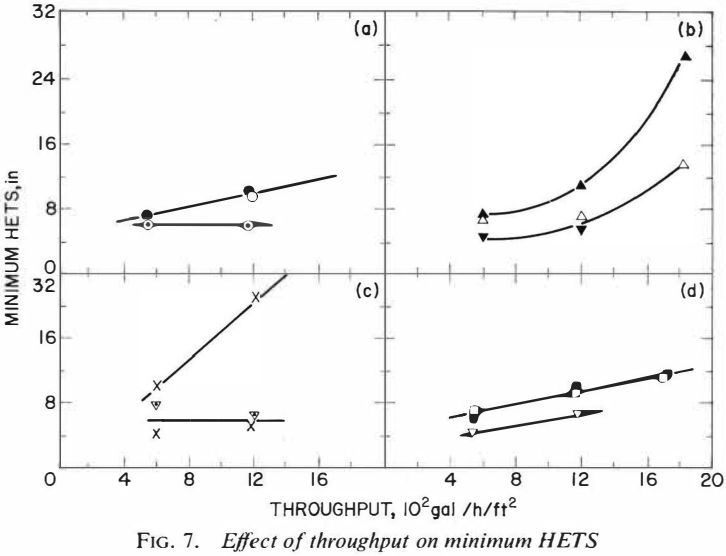

FIG. 7. *Effect of throughput on minimum HETS*

Fig.	3-in column	12-in column, no baffles	12-in column, with baffles
(a)	○	●	○
(b)	▼	▲	△
(c)	×	×	▽
(d)	▽	■	□

Discussion

When the column consisted of a series of identical perforated plates mounted on a central shaft, definite minima in the HETS vs. reciprocating speed curves were observed. Thus, the phenomenon of axial mixing was quite pronounced and, in this respect, was quite different from the performance in a 3 in dia. column. In 3 and 1 in dia. columns, most of the data obtained on the MIBK–acetic acid–water system showed HETS decreasing continuously with the reciprocating speed until the flood point. The performance curves obtained for the 12 in column depended greatly on which was the dispersed phase and the direction of extraction. But, in some cases, it was felt that the performance was not satisfactory because of the obvious evidence of axial mixing. Special notice should be taken of the case MIBK dispersed, MIBK extractant. The minimum HETS achieved in this case was significantly higher than that achieved in the 3 in column. The minimum HETS values achieved for most of the other types of operation were reasonable so far as being acceptable for scale-up from a 3 in to a 12 in column. Nevertheless, it was concluded that steps had to be taken to minimise axial mixing.

Based on the data discussed above, the decision was made to install the baffle plates previously described and shown in Fig. 1. Two baffle plates were used, and the column consisted of seven regular perforated plates spaced 1 in apart, a baffle plate, a second series of perforated plates, a baffle plate, and a third series of perforated plates. The spacing between baffle plates and perforated plates was 1·5 in. The purpose of the baffle plates was to prevent the circulation of liquid up one side of the column and down the other side which was a flow pattern that could actually be observed, especially at high throughputs and high reciprocating speeds.

The performance obtained with the baffle plates was significantly improved in most cases, especially in those cases where performance without the baffle plates was poor, specifically for the case of MIBK dispersed, MIBK extractant and for the case water dispersed, MIBK extractant at the higher throughputs. The performance curve was apparently also somewhat improved in the case of MIBK dispersed, water extractant. For the case water dispersed, water extractant, it may be difficult to conclude that performance was significantly improved by the use of the baffle plates although, at a total throughput of approximately 1200 gal/h/ft^2, there appears to be an improvement with respect to axial mixing at reciprocating speeds above the minimum HETS.

Apparently, because of the existence of minima in the HETS vs. reciprocating speed curves for most cases with the baffle plates, it has to be concluded that, although axial mixing has been significantly reduced, additional baffling should be investigated to determine whether further improvements toward eliminating axial mixing can be achieved. Nevertheless, the present data are sufficiently encouraging to warrant the development of a scale-up correlation based on the data in 3 and 12 in dia. columns with baffle plates. The factors considered in the scale-up are: direction of extraction; the continuous phase; the total throughput; the column diameter; the minimum HETS; and the reciprocating speed at the minimum HETS.

Over the range of column diameters studied, minimum HETS and the corresponding reciprocating speeds can be expressed as power functions of diameter. The constants are summarised in Table XIII, and the respective correlations are shown in Figs 8 and 9. It can be seen that the average exponent for HETS is ~0·25 although the exponent varies from 0·19 to 0·36, depending on which phase is dispersed and which phase is the extractant. The exponent for the reciprocating speed corresponding to the minimum HETS is either 0 or 0·14 depending on which phase is dispersed and which phase is the extractant. Thus, a preliminary simplified correlation for scaling up data on an experimental column of D_1 in dia. would be:

$$\frac{(\text{HETS})D_2}{(\text{HETS})D_1} = \left(\frac{D_2}{D_1}\right)^{0\cdot 25} \qquad (1)$$

The corresponding reciprocating speed (SPM) at which the large-diameter column should be operated is given by:

$$\frac{(\mathrm{SPM})D_2}{(\mathrm{SPM})D_1} = \left(\frac{D_1}{D_2}\right)^{0\cdot 14} \quad . \quad . \quad . \quad . \quad . \quad . \quad . \quad (2)$$

The above correlations are obviously approximate, but they have been used successfully for scaling up columns of 1, 2 and 3 in dia. to up to 18 in dia. It is to be expected that the scale-up correlation can be extended to columns of >18 in dia. It should also be noted that additional improvements in performance are possible by more efficient baffling arrangements.

Scale-up procedure

Based on the present data and assuming the use of a column with baffle plates similar to those employed in present work, the following is a proposed method of scale-up:

1. Data are obtained on a 1, 2 or 3 in dia. column which need not have baffle plates, inasmuch as axial mixing in a column of up to 3 in dia. is relatively small.
2. The optimum performance of the small diameter column is determined, and, for the purpose of the present discussion, the criteria for optimum performance will be assumed to be maximum volumetric efficiency.
3. The large-diameter column is designed with approximately the same number of baffle plates per foot of column as that employed in the present work. It is also recommended that baffle plates be used at the top and bottom of the plate section. The inclusion of such plates in the present work would probably have resulted in better performance.
4. The plate spacing is the same as in the small diameter column.
5. The amplitude is the same as in the small diameter column.
6. The total throughput/ft^2 is the same as in the small diameter column. The expected HETS is calculated by means of Equation (1).
7. The reciprocating speed required is estimated by Equation (2).

Commercial applications

The reciprocating-plate extraction column fitted with the baffle plates described herein has been employed successfully in columns of up to 18 in dia. The column has been found to be quite suited to the extraction of fermentation broths, which tend to emulsify in other types of extraction equipment. Both filtered and whole broths have been extracted successfully in a 12 in dia. reciprocating-plate column.[3] A 2 in dia. reciprocating-plate column was used in the pilot plant work leading to the development of tetraethylene glycol as an efficient solvent in the Udex process.[5] Many other small diameter columns are being used for developing basic data for eventual scale-up to commercial columns.

Pilot plant tests on a toluene–aqueous extraction system in the reciprocating-plate column and in two other commercially accepted columns[17] have shown that the reciprocating-plate column had 5–8 times the volumetric efficiency of the other columns. Assuming the scale-up procedure described herein is valid, the reciprocating-plate column should also enjoy the advantage of higher volumetric efficiencies in large-diameter columns.

Acknowledgment

The authors are grateful to Hoffmann-La Roche Inc. for the use of their facilities and for permission to publish this work. Thanks are due to Mr. A. Frunzi for the fabrication of the various columns, to Mr. A. Quiam for some assistance in the calculations, and to Messrs T. Harty and A. Pisani for assistance in performing the experiments.

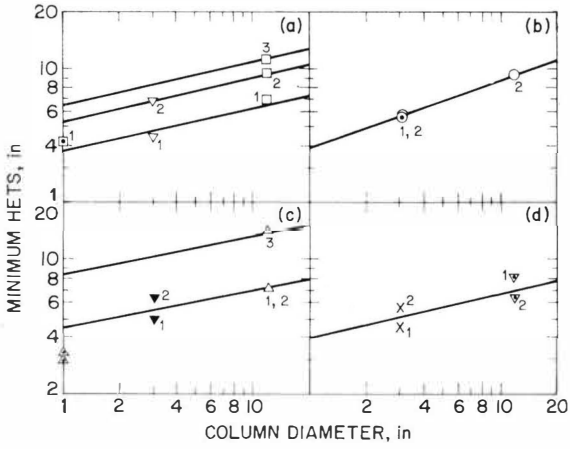

FIG. 8. *Effect of column diameter on minimum HETS*

Fig.	1-in column	3-in column	12-in column, with baffles
(a)	⊡	▽	□
(b)	—	⊙	○
(c)	△	▼	△
(d)	—	×	▽

Numbers adjacent to symbols as in Fig. 5

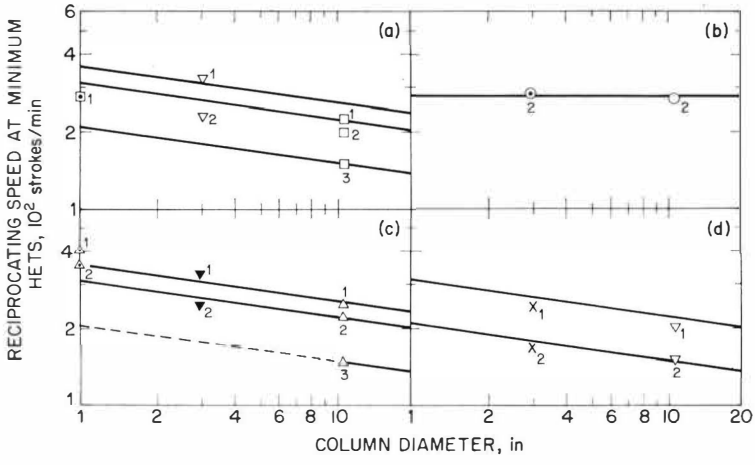

FIG. 9. *Effect of column diameter on reciprocating speed at minimum HETS*

Fig.	1-in column	3-in column	12-in column, with baffles
(a)	⊡	▽	□
(b)	—	○	○
(c)	△	▼	△
(d)		×	▽

Numbers adjacent to symbols as in Fig. 5

TABLE XIII

HETS and reciprocating speed as a function of column diameter

System: MIBK–acetic acid–water

HETS = KD^a (Equation (1))
Reciprocating speed (strokes/min) = k/D^b (Equation (2))

Total throughput	HETS scale-up		Reciprocating speed scale-up	
	K	a	k	b
	Water dispersed, water extractant			
Case 1	3·7	0·226	360	0·140
Case 2	5·3	0·226	310	0·140
Case 3	6·5	0·226	210	0·140
	Water dispersed, MIBK extractant			
Case 1	4·5	0·190	360	0·140
Case 2	4·5	0·190	310	0·140
Case 3	8·5	0·190	210	0·140
	MIBK dispersed, water extractant			
Case 1	3·9	0·360	—	—
Case 2	3·9	0·360	280	0
	MIBK dispersed, MIBK extractant			
Case 1	3·9	0·236	310	0·140
Case 2	3·9	0·236	210	0·140

References

[1] Karr, A. E., *A.I.Ch.E. Jl*, 1959, **5**, 446
[2] *Chem. Process., Lond.*, Nov. 19, 1965, p. 6; Mooney Brothers Corp., Chem-Flow Products, Little Falls, N.J., Bulletins KC–1 and KC–2
[3] *Chem. Process., Lond.*, Mid-Nov. 1966, p. 92
[4] Karr, A. E., private communication
[5] Somekh, G. S., & Friedlander, B. I., *Hydrocarb. Process.*, Dec. 1969, p. 128
[6] Elenkov, D., Boyadzhiev, L., & Krustev, I., *Izv. Khim. Inst., Sof. (Izv. bulg. Akad. Nauk)*, 1966, **4**, 181
[7] Gelperin, N. I., *et al.*, *Khim. Prom.*, 1965, (1), 37; *Br. chem. Engng Abstr.*, 1966, **11**, 528
[8] Issac, N., & DeWitte, R. L., *A.I.Ch.E. Jl*, 1958, **4**, 498
[9] Landau, J., *et al.*, *Colln Czech. chem Commun.*, 1964, **29**, 3003
[10] Prochazka, J., Landau, J., Souhrada, F., & Nekovar, P., Paper presented at 3rd Congress CHISA, 1969, Czechoslovakia
[11] Wellek, R., *et al.*, *Ind. Engng Chem. Process Des. Dev.*, 1969, **8**, 515
[12] Karr, A. E., & Scheibel, E. G., *Chem. Engng Prog. Symp. Ser.*, 1954, **50** (10), 73
[13] Scheibel, E. G., & Karr, A. E., *Ind. Engng Chem.*, 1950, **42**, 1048
[14] Reman, G. H., & Olney, R. B., *Chem. Engng Prog.*, 1955, **51**, 141
[15] Scheibel, E. G., *A.I.Ch.E. Jl*, 1956, **2**, 74
[16] Oldshue, J. Y., & Rushton, J. H., *Chem. Engng Prog.*, 1952, **48**, 297
[17] Lo, T. C., *et al.*, unpublished report

SESSION 2C

APPLICATION TO PETROLEUM INDUSTRY

CHAIRMAN

Dr. G. H. Reman

SECRETARIES

Ir. D. v. d. Meer

Ir. W. A. Beverloo

New Union Carbide aromatics extraction process

by G. S. Somekh
Union Carbide Corporation, Chemicals and Plastics
Research and Development Department, Tarrytown, New York, U.S.A.

A new extraction process is proposed in which a gasoline fraction is first treated in a primary extraction with a polar, selective solvent. Aromatics are then transferred into a high-boiling aliphatic fraction in a secondary extraction. Finally, aromatics are fractionally distilled from the second extract. In this process no water is distilled, no extractor reflux is distilled, and the aromatics are vaporised only once. Thus, the process has significantly better economics compared with conventional processes.

Introduction

THE BENZENE–TOLUENE–C_8 aromatics fraction is at present the principal raw material used for the manufacture of petrochemicals. This fraction (usually referred to as BTX) is employed in even greater quantities than ethylene as a raw material. These aromatics are available in reformed gasolines in concentrations ranging from about 30 to 60%. BTX is also available from coke oven light oils, cracked gasolines and dripolenes, which after hydrogenation can contain about 70–98% aromatics.

Conventional processing

In the present commercial processing methods, the individual aromatics are obtained from these feedstocks by an extraction process which also involves an extractive distillation, followed by a fractionation train. Fig. 1 shows the 'conventional' processing scheme. The Udex Process is depicted for the extraction process.[1,2] In recent years numerous Udex plants have improved their operations by employing UCAR® tetraethylene glycol together with technology proprietary to Union Carbide Corporation.[3,4] In this process the feedstock enters the extractor near the middle and percolates up the column and is depleted of aromatics by a tetraethylene glycol–water solution, which enters near the top and percolates down the column. In the lower section of the extractor the C_8 aromatics in the extract are purified by the countercurrent action of a light hydrocarbon reflux, which enters near the bottom.

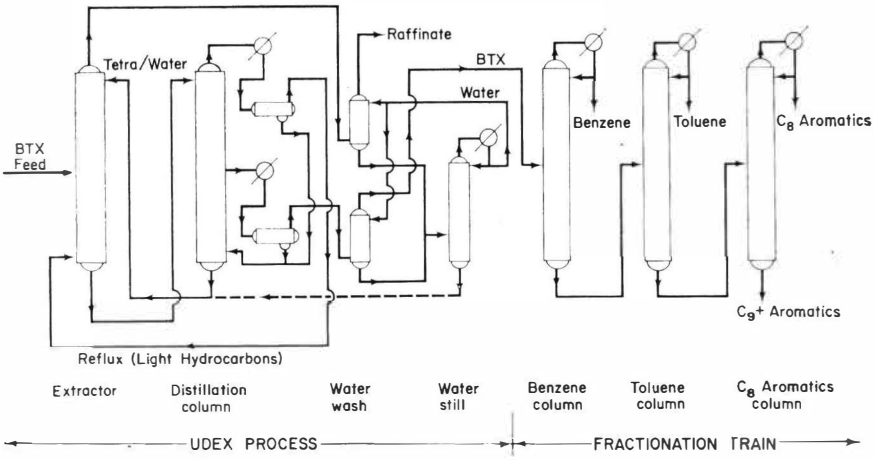

FIG. 1. *Conventional processing scheme*

The extract, consisting of tetraethylene glycol/water, BTX and reflux, is sent to the top of the two-step distillation column. The first step is an extractive distillation in which the extractor reflux, which consists mainly of C_6 aliphatics and benzene, is distilled from the extract. This is accomplished in the upper half of the column. The reflux-to-feed ratio is of the order of 1/1. Some water is also distilled along with this reflux. In the second step, the BTX, again together with some water, is distilled from the glycol solution which returns to the extractor. Both the raffinate and the BTX are water-washed to recover dissolved and entrained glycol and the water is distilled.

There are other similar processes that do the same thing as the tetraethylene glycol Udex and at about the same operating cost. The Sulpholane Process is an example.[5] In the case of sulpholane, the distillations are operated in two separate columns. The reflux together with some water is distilled in the first column, and the BTX together with some water is distilled in the second column.

In another process, the Arosolvan Process, a solution of *N*-methylpyrrolidone and ethylene glycol is used at present.[6] The extractor reflux, together with some wash water, is distilled in the first distillation column. In the second distillation column, the BTX, along with some ethylene glycol, is distilled.

These extraction processes are similar to each other and each produces a liquid solution of the aromatics as feed to the fractionation train. Such a processing scheme involves the distillation of a substantial amount of extractor reflux, water and polar solvents, as well as the revaporisation of the aromatics.

Union Carbide extraction process

The Union Carbide Corporation has been researching the aromatics separations field for over ten years. As a result of these efforts a low-cost processing scheme has been evolved and is shown as Fig. 2.[7] The fractionation train is an integral part of the extraction process. There are two extractions. The primary extractor is analogous to the Udex extractor. Tetraethylene glycol, in this case *free* of water, enters near the top, feed enters near the middle, and a dodecane reflux enters near the bottom. The extract leaving the bottom of the primary extractor is essentially free of feed aliphatics, and no further purification is necessary. In 'conventional' processes, however, the additional step of distilling the reflux together with some water is required.

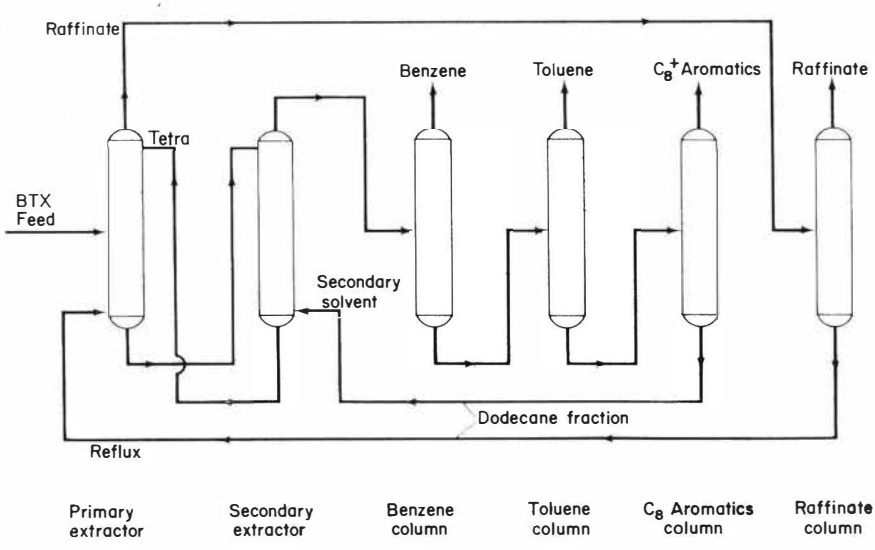

FIG. 2. *Union Carbide aromatics extraction process*

The extract is fed to the top of the secondary extractor, and the aromatics are removed from the glycol by extraction with more dodecane. The tetraethylene glycol, stripped of aromatics, is merely recycled back to the primary extractor. Thus, the bulk of the glycol does not contact high distillation temperatures.

The solution of dodecane, BTX and a slight proportion of dissolved and entrained glycol passes to the distillation train. Benzene, toluene and C_8 aromatics are successively distilled from the dodecane. The slight proportion of glycol is withdrawn together with the dodecane from the bottom of the C_8 aromatics column. No water washing is necessary to recover this glycol. However, the most important benefits of this distillation scheme are that the aromatics are distilled just once, and water and polar solvents are not distilled at all.

The raffinate from the primary extractor contains the feed aliphatics, dodecane and some dissolved and entrained glycol. This stream must be distilled to recover the process solvents. In 'conventional' processes the raffinate need not be distilled, so that this step detracts somewhat from the favourable economics of the Union Carbide process. However, the economic advantages far outweigh this disadvantage. Furthermore, the trend in the industry is to produce feedstocks containing lower aliphatic concentrations, as for example by increasing reformer severity.

Other advantages of this process are that: solvent losses are very low because of low degradation rates and the small proportions of solvent in raffinate and extract streams are recovered in multi-stage fractionations; fired heaters can be used in the stills, as hardly any polar solvent enters the distillation columns; and extraction pressures are low, because of the presence of high-boiling secondary solvent in both extractors.

Experimental

Pilot plant experiments were carried out using the system depicted in Fig. 3 to demonstrate the feasibility of the process. The primary and secondary extractors and one distillation were operated in a continuous manner. In the distillation the benzene was taken overhead and its freezing point was determined. Toluene, C_8 aromatics and the dodecane fraction were taken as the bottoms product and discarded.

UCAR® tetraethylene glycol (extraction grade), manufactured by Union Carbide Corporation, was employed as the primary solvent. Isopar M, an

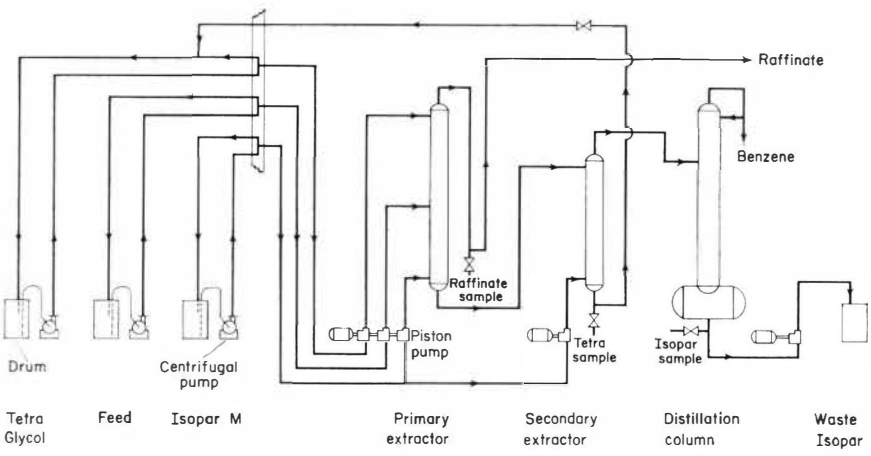

FIG. 3. *Schematic flow diagram of pilot plant*

aliphatic fraction containing dodecanes and higher, and produced by the Humble Oil and Refining Company, was employed both as secondary solvent and as primary extractor reflux. The feed used in the experiments was prepared from individual components, and its composition was similar to that of a hydrogenated dripolene obtained from naphtha cracking:

	Vol.-% at 25°C
Benzene	39·3
Toluene	25·1
C_8 aromatics	22·5
C_6 aliphatics	5·2
C_7 aliphatics	7·9
	100·0

Drums of UCAR® tetraethylene glycol (TETRA), feed, and Isopar M were well mixed by recirculation using centrifugal pumps. The glycol and Isopar M drums were maintained at about 110°C so that they would enter the extraction column close to 100°C. TETRA, feed and 'Isopar M' were fed through piston metering pumps to the primary extractor at the top, middle and bottom, respectively.

The primary extractor is a 2-in i.d. Karr reciprocating plate extractor, consisting of a vertical column with a centre shaft on which plates are attached.[8] The plates are separated with spacers and the plate-spacer stack is attached to the shaft with set screws at the top and bottom. Each plate is in the shape of a wheel and has an o.d. of $1\frac{3}{4}$ in. A reciprocating motion is given to the stack by a motor mounted overhead. The agitated section is eight feet long with one-foot settling zones at each end of the column. The column is made of glass, all metallic parts in contact with process liquids are made of 316 stainless steel, and the plates and spacers are made of Teflon. This column had previously been calibrated to have approximately ten theoretical stages.

The glycol extract was sent to the top of the secondary extractor. This extractor is identical to the primary extractor in all respects, except that the agitated section is only $5\frac{1}{2}$ feet long. This section could be equivalent to about seven theoretical stages. A ratio of Isopar M/TETRA of 0·7/1 (by vol. at 100°C) was maintained in the secondary extractor.

The aromatics-laden Isopar M was withdrawn from the top of the secondary extractor and sent to the distillation column. The distillation column is a 4-in i.d. by 19-ft high Corning glass distillation column. It has a 10-ft section packed with $\frac{1}{4} \times \frac{1}{4}$ in extruded stainless steel packing. This column has approximately 25 theoretical stages. The feed to this column entered three feet below the top of the packing. A reflux ratio of 1·5/1 (by vol.) was used to produce the benzene distillate. This reflux ratio is close to that theoretically required to separate the benzene from the toluene in the absence of Isopar M. A bottoms temperature of about 180°C was maintained. The still bottoms (containing toluene, C_8 aromatics and Isopar M) were sent to a waste drum.

All the flow rates were first set before starting a run, and were measured several times during each run. The system was then allowed to operate until the extractor interface levels, distillation temperatures and the analyses of certain streams all became constant. A typical run usually took between four and six hours to complete. Samples of raffinate, glycol from the secondary extractor, distillate and still bottoms were taken. All the samples were analysed by vapour–liquid chromatography, except the benzene samples which were analysed by freezing point determination using the ASTM method.

Results

The results are shown in Fig. 4. Aromatics recoveries were very high. The TETRA/feed ratio was usually between 6·6/1 and 7/1. These are somewhat higher than those employed in the Udex Process, so that extractor dia-

meters would be larger. At TETRA/Isopar M ratios ranging from about 8·5/1 to about 11/1 recoveries of benzene and toluene were always over 99·5%. Recoveries of C_8 aromatics were always above 94%.

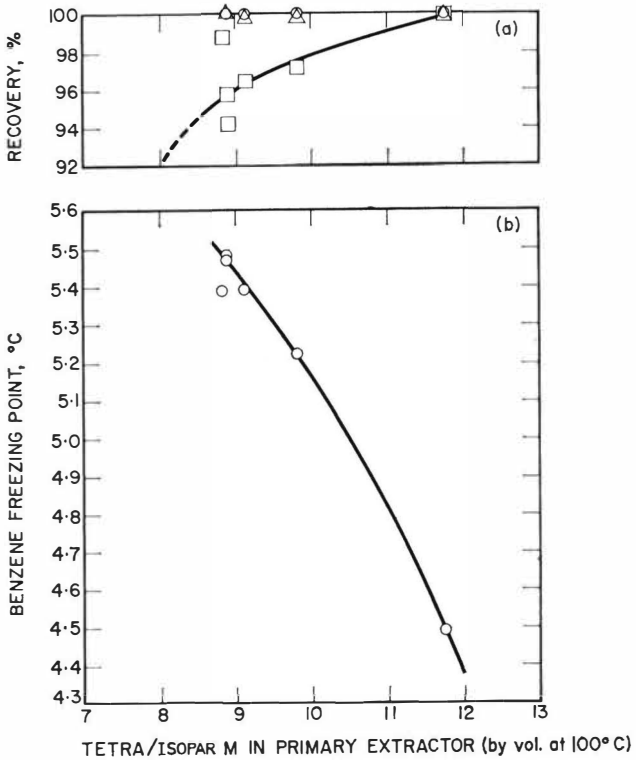

FIG. 4. (*a*) *Aromatics recovery and* (*b*) *benzene freezing point vs. TETRA/Isopar ratio*

6·6 < S/F < 7·2 (by vol.)
○ Benzene; △ toluene; □ C_8 aromatics

Part (b) of Fig. 4 shows that benzene purity is determined by the TETRA/Isopar M ratio. The curve shows that at TETRA/Isopar M ratios below about 9/1 benzene having a freezing point of almost 5·50°C was obtained, and this corresponds to about 99·9% purity. At a TETRA/Isopar M ratio slightly above 9/1 benzene having a freezing point of about 5·40°C was obtained. This freezing point corresponds to a purity of about 99·8%.

There is only one run at a TETRA/feed ratio as high as 7·20/1. This is the run at a TETRA/Isopar M ratio of 8·84. At these conditions, the recovery of C_8 aromatics was increased to 98·8%. Yet, the benzene freezing point still had a high value at 5·39°C.

Discussion

These results, while they are encouraging, are for a feed that is high in benzene content, which tends to result in high benzene purity. The feed is also low in aliphatics content, which tends to result in high recoveries of C_8 aromatics. Furthermore, it is not precisely known how many theoretical stages can be assigned to the extractors and the distillation column for each run. The main conclusion to be drawn from the experimental work reported herein is, therefore, that the Union Carbide Process has been demonstrated to be a good workable process with excellent potential.

Work is proceeding on the choice of the optimum system for various types

of feeds. For primary solvent it is preferred to use glycols, because of their low cost, ready availability, excellent stability and proven use in extraction processes. For the solvents of choice, work is proceeding on the determination of the optimum extraction temperatures, theoretical stage requirements and flow ratios. Various methods for recovering the significant amount of heat remaining in the secondary solvent returning to the extractors from the distillation train are also being studied.

If these studies progress as anticipated, this process could be offered commercially by the end of this year.

Conclusions

The Union Carbide process has been demonstrated as being an easily operable process. This process has low operating costs, because: extractor reflux is not distilled; the aromatics are distilled only once; and water and polar solvents are not distilled at all.

References

[1] Read, D., Production of High-Purity Aromatics for Chemicals, presented at the May 14, 1952, A.P.I. meeting, San Francisco, California, U.S.A.

[2] Grote, H. W., *Chem. Engng Prog.*, 1958, **54**, (8), 43

[3] Somekh, G. S., & Friedlander, B. I., *Hydrocarb. Process.*, 1969, **48**, (12), 127

[4] Hoover, T. S., *Hydrocarb. Process.*, 1969, **48**, (12), 131

[5] Deal, C. H., jun., Evans, H. D., Oliver, E. D., & Papadopoulos, M. N., *Petrol. Refiner*, 1959, **38**, (9), 185

[6] Arosolvan Process, *Hydrocarb. Process.*, 1965, **44**, (11), 181

[7] U.S. P. 3,492,365

[8] Karr, A. E., *A.I.Ch.E.Jl*, 1959, **5**, 446

Propane deasphalting of difficult feedstocks

by J. D. T. Bernard and H. C. A. van Meurs
Koninklijke/Shell-Laboratorium, Amsterdam, The Netherlands
(Shell Research N.V.)

Propane deasphalting of some North African feedstocks on a pilot-plant scale was found to be difficult owing to clogging of the equipment, which resulted in entrainment of asphaltic material with the deasphalted oil. It was proved that this is an intrinsic effect with the feedstock under investigation and is not caused by contamination.

The pertinent phase behaviour was determined and the results were used to devise ways of avoiding the difficulties under practical deasphalting conditions. The phase diagrams obtained were also used for determination of the number of stages in a pilot-plant extractor.

Introduction

DURING PILOT-PLANT SCALE evaluation of Zarzaitine (a crude from the central Sahara)[1] as a potential lubricating oil feedstock, difficulties were experienced with the propane deasphalting of the short residue in a rotating disc contactor (RDC).

Starting with a clean plant it was possible to obtain a good quality deasphalted oil (DAO) for only 60–80 h. Thereafter the DAO gradually became dark coloured and when examined it was found to consist of two completely different phases. The composition of the heavier phase was that of a light bitumen and similar to the reflux which is formed in the top of the RDC by increasing the temperature in the top section (see Table III for reflux analysis). Washing out the RDC with toluene, after it had been completely drained, showed that a large quantity of deposit was partially blocking it in the area around and immediately below the short residue feed inlet.

Very few references to this type of problem could be found in the literature,[2] although a patent exists[3] which claims a way of preventing the formation of solid deposits during propane deasphalting. It would seem from the information that is available that solid deposit formation occurs only with residues which are highly paraffinic, have a low sulphur content and a very low asphaltene content.

Bench-scale experiments have been carried out to investigate the phase behaviour of mixtures of Zarzaitine short residues and propane under various conditions. From the information obtained in this way suitable operating conditions could be chosen for the pilot plant so as to prevent blockages occurring and also to enable the number of stages in the pilot-plant RDC to be evaluated.

Experimental

The bench-scale batch experiments were carried out using jacketed autoclaves (1- and 2-litre capacity) which were heated by circulating hot oil from a thermostatic bath.

Weighed quantities of residue and propane were brought to the desired temperature and then shaken for 30 min. After settling for 1 h the DAO phase was drawn off through a dip tube and the bitumen phase through a drain point in the bottom of the autoclave. Any solid deposits, sticking to the walls and the dip tube, were washed out with toluene after complete removal of the liquid phases. After evaporation of the solvent, the yields of DAO, bitumen and solid deposit were calculated on a no-loss basis.

To calculate the phase compositions small quantities of both the oil and the bitumen phase were drawn into hot receivers, to which a wet gas meter was connected to measure the quantity of propane evaporated during sampling. The remaining propane was removed under vacuum at high temperature and

after weighing the solvent-free oil and bitumen the phase compositions could be calculated.

The continuous deasphalting experiments were carried out in a pilot-plant RDC, the details of which are given in Fig. 1. The contactor was divided into 5

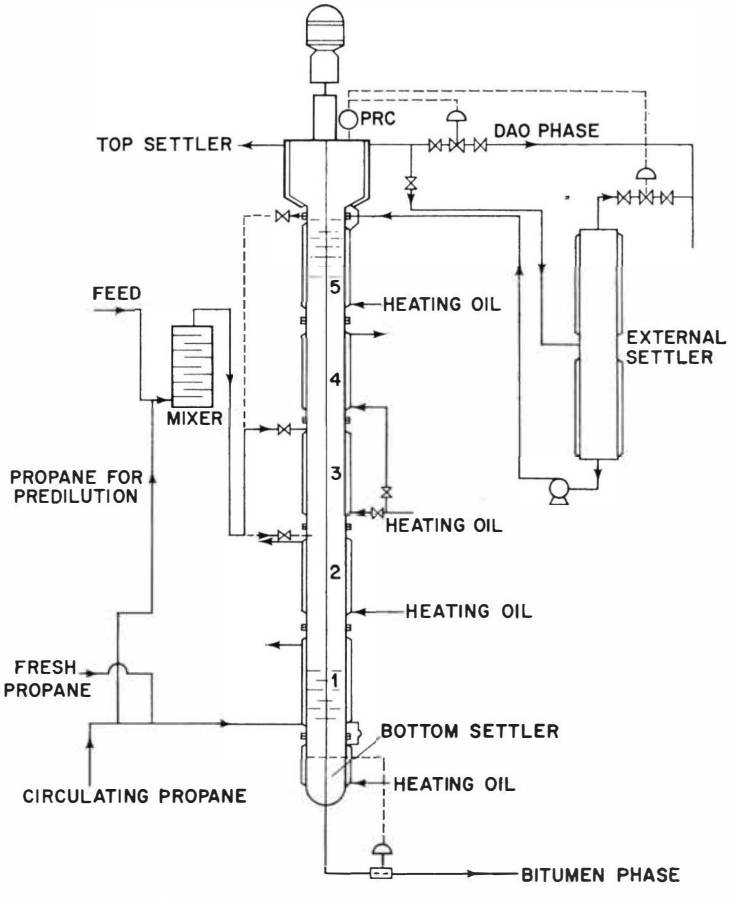

FIG. 1. *Diagram of rotating disc contactor pilot plant*

RDC dia. = 100 mm; stator dia. = 70 mm; rotor dia. = 60 mm; height of each compartment = 19·5 mm; number of compartments = 150; total height = 3440 mm. (1), (2) etc., refer to section number

sections plus a top and bottom settler. Each of the sections could be heated independently to produce a temperature profile along the length of the column, as shown in Fig. 2. Normally the column was operated with the profile B, which is similar to that used in commercial units.[4]

After each experiment the contents of the RDC were drawn off at the operating temperature and any solid deposits which had been formed were removed by washing out with toluene at 100°C. In order to locate where the deposit was concentrated the contactor was filled with increasing amounts of toluene, which were drawn off and analysed separately.

Some experiments were carried out to determine the number of theoretical mass transfer stages in the pilot-plant RDC when used for propane deasphalting. For these experiments the whole contactor, including the top settler (see Fig. 1), was kept at 50°C. The reflux was formed in an external settler kept at 70°C and pumped back into the RDC at the top of section 5.

One experiment to assess the number of stages below the residue feed point

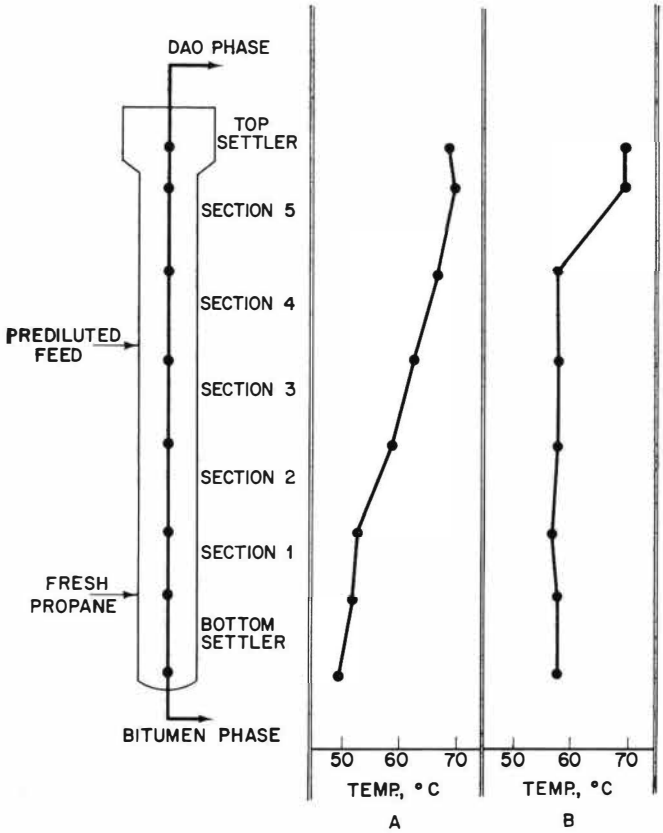

FIG. 2. *Examples of temperature profiles in pilot-plant RDC*

TABLE I

Properties of Zarzaitine short residues

Residue	A very short	B medium	C long
Specific gravity, *d* 70/4°C	0·9127	0·9072	0·9028
Sulphur content, % wt.	0·44	0·50	0·46
Wax content, % wt.	11·3	10·0	—
Congealing point of wax, °C	65	72·5	—
Viscosity, cS/210°F	197·9	125·3	97·4
Ramsbottom carbon content, % wt.	8·5	8·0	—
n-C_7 asphaltenes, % wt.	0·4	0·4	0·4
n-C_5 asphaltenes, % wt.	2·1	1·6	1·7
Flocculation ratio, FR_5, %-vol. xylene	0	4	—
Flash point, PMcc,* °C	—	260	—
Hot filtration test, % wt.	—	0·022	—
Ash content, % wt.	—	0·022	—
Vanadium content, ppm	16	—	—
Nickel content, ppm	9	—	—
Resins, % wt.	28·5	25·1	24·7
Saturates, % wt.	35·5	39·3	39·8
Mono + diaromatics, % wt.	28·1	27·7	27·7
Tri + polyaromatics, % wt.	5·8	6·3	6·4

* Pensky-Martin closed cup

TABLE II

Comparison of average properties of solid deposit and C_3 bitumen from short residue B

	Solid deposit washed from RDC at place of feed input–typical	C_3 bitumen –typical
Average yield, % wt. on feed	0·05–0·1	25–40
Specific gravity, *d* 70/4°C	0·975	0·975
Sulphur content, % wt.	1·6	1·4
C_7 asphaltenes, % wt.	20	2
C_5 asphaltenes, % wt.	28	—
Ramsbottom carbon content, % wt.	22	18
Softening point, R & B, °C	83	60
Wax content, % wt.	5·5	7·5
Congealing point of wax, °C	67	58
Ash content, % wt.	1·1	0·1

more accurately was carried out with the feed entering the RDC at the top of section 5, below the top settler.

In the experiments where a bitumen recycle was applied, propane-free bitumen from the bitumen stripper was pumped back into the contactor combined with the fresh feed.

Discussion of results

Analysis of typical samples of the solid deposit, the bitumen and the short residue feeds indicate (Tables I and II) that the solid deposit is not present as a solid in the residue feed. It has many similar properties to the bitumen (see

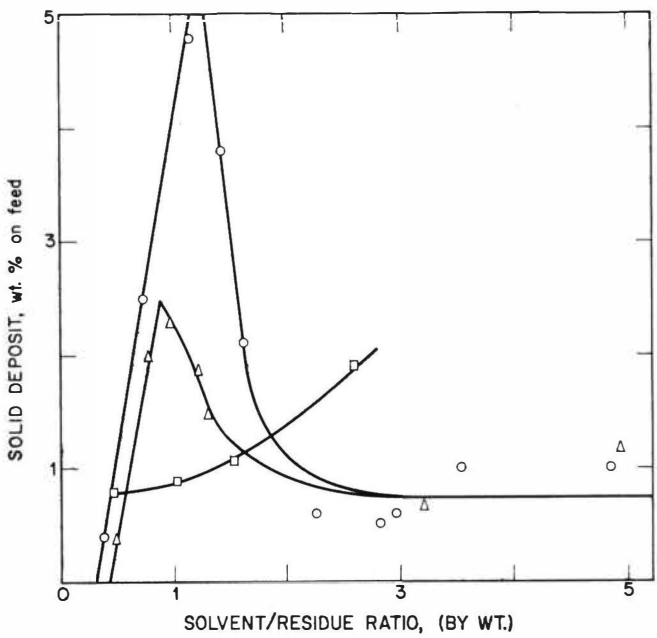

FIG. 3. *Formation of solid deposits during propane deasphalting of various short residues in batch*

△ Residue A; ○ Residue B; □ Middle East short residue

Table II), particularly in content and properties of wax, but is much more asphaltenic in nature than the bitumen, and could justifiably be called 'propane asphaltenes'.

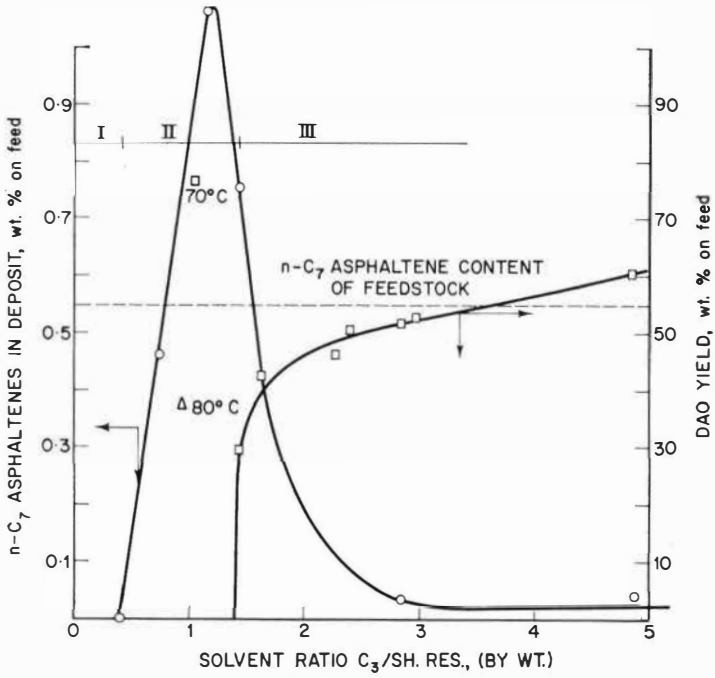

FIG. 4. *Batch propane deasphalting of Zarzaitine short residue B at 50°C*

DAO yield and deposit formation as a function of solvent ratio:
I = propane + short residue homogeneous, no precipitation of solids; II = propane + short residue homogeneous, increasing deposit formation at increasing solvent ratio; III = formation of DAO and bitumen phases, decreasing deposit formation at increasing solvent ratio

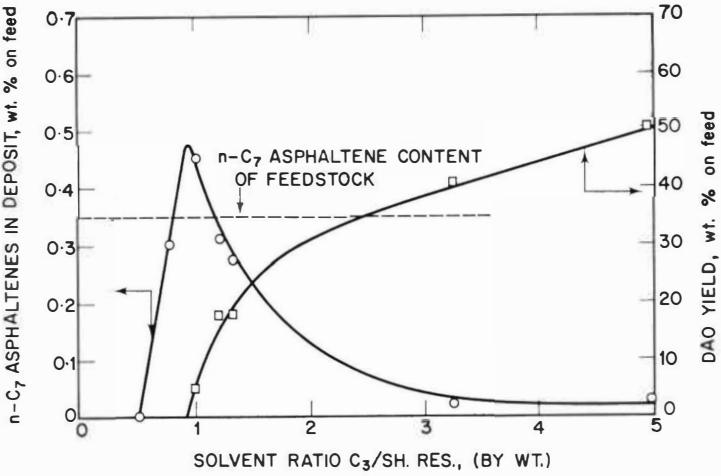

FIG. 5. *Batch propane deasphalting of Zarzaitine short residue A at 50°C*

DAO yield and deposit formation as a function of solvent ratio

Bench-scale batch experiments

Bench-scale batch experiments were carried out with two of the Zarzaitine short residues (A and B) to determine the effect of temperature and solvent/residue ratio on the phase separations occurring during propane deasphalting. A similar study was made, for comparative purposes, with a typical Middle East short residue which is not known to give problems with solid deposits. The results of these studies are presented in Figs 3, 4, 5 and 6. In Fig. 3 the

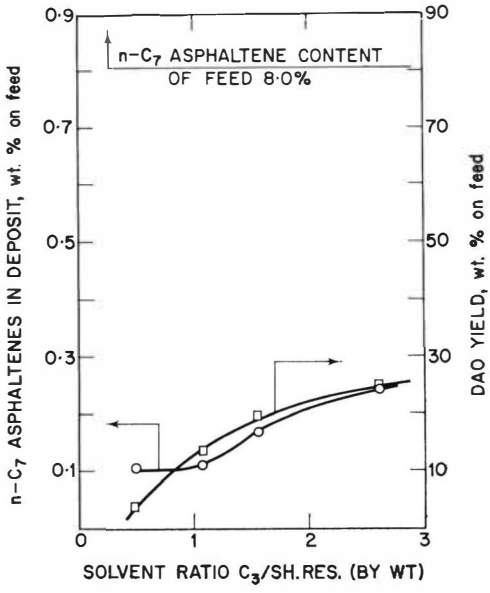

FIG. 6. *Batch propane deasphalting of a Middle East short residue at 50°C*

DAO yield and deposit formation as a function of solvent ratio
n-C_7 asphaltene content of feed 8·0%

amount of solid deposit formed from three short residues is shown, as a function of the solvent ratio, the temperature remaining constant at 50°C. This figure gives some idea of the magnitude of the problem with up to 5% wt. deposit formed under certain conditions. Owing to the method of measurement the solid deposits can have differing quantities of bitumen associated with them and in order to minimise this effect, the amount of n-C_7 asphaltenes in the deposits, as a % of the total residue feed, has been used as a measure for comparison. This is possible because of the great difference in the n-C_7 asphaltene contents of the bitumen and the solid deposit (see Table II). Figs 4, 5 and 6 are drawn on this basis. The behaviour of the two Zarzaitine residues was qualitatively the same. Three regions were found, depending on the solvent ratio applied (see Fig. 4):

(I) At low solvent ratios all the propane dissolves in the short residue and only one phase exists.

(II) At higher solvent ratios a sharply increasing quantity of solid deposit is formed. At these solvent ratios the bulk of the short residue and propane exists in one phase. It is interesting to note here that apparently more n-C_7 asphaltenes are found in the deposit than were originally present in the residue feedstock.

(III) At still higher solvent ratios, three phases are observed, a DAO phase, a bitumen phase, and a rapidly decreasing quantity of solid deposit phase.

The above phenomena are more pronounced for the medium short residue B than for the very short residue A (Fig. 5).

The Middle East short residue does not display the phenomena described above (Fig. 6). The total amount of n-C_7 asphaltenes in the toluene washings is very much lower than that in the feedstock and the concentration of the n-C_7 asphaltenes in the toluene washings does not differ much from that in the corresponding bitumen. This indicates that the bulk of the material washed out of the autoclaves during the latter experiments was normal bitumen.

As shown in Fig. 4 operation at higher extraction temperatures tends to reduce the amount of solid deposit formed in the critical solvent/residue ratio region. The nature of the relationships between the amount of solid deposit and the solvent ratio (Figs 4 and 5) indicates that this phenomenon occurs only over a small range of solvent ratios (approximately 0·5 to 2·0 by wt.). It is thought that at high solvent ratios no solid deposits would be formed if the propane and residue could be mixed instantaneously. The small amounts of solid deposit formed at high solvent ratios are thought to be due to the fact that during the mixing process the residue has to move through the critical dilution region and unless this is accomplished very quickly flocculation of some of the asphaltenes is inevitable. It is estimated[5] that the initial flocculation of asphaltenes can take as little as 10^{-3} sec and once flocculation has occurred repeptisation takes considerably longer. In this situation the speed with which complete mixing is achieved is of crucial importance.

The reason why asphaltenes should be flocculated from some residues and not from others is difficult to see. At temperatures well below the critical temperature, pentanes and paraffins of higher molecular weight, when mixed with residual oils, will precipitate solid, particulate asphaltenes. Asphaltenes are present as a colloidal suspension in residual oils and it is thought that the resin fraction has a stabilising or peptising function which is exerted by adsorption of the resin molecules on to the surface of the large asphaltene molecules.[6,7] When pentane is added in sufficient quantities to a residue it dissolves all the lighter components and most of the resin components and the asphaltenes then flocculate to form pseudo-crystallites.[8] If butane or other lower molecular weight solvents less polar than pentane are added to a residue they do not dissolve so much of the resin fraction and so the asphaltenes remain in a colloidal suspension in the bitumen phase. What seems to have happened in the case of the propane deasphalting of Zarzaitine residues is that the mixture of propane and high molecular weight paraffins from the residue (in the range of solvent/residue ratios 0·5 to 2·0 by wt.) has the same effective non-polarity as n-paraffins in the range C_5 to C_7 which will dissolve some of the resin fraction and thus cause the asphaltenes to flocculate. The temperature is important here because as the temperature is increased towards the critical point of propane (97 °C) the non-polarity of the propane increases sharply and so the effective non-polarity of the propane/high molecular weight paraffins mixture will also increase. Thus less resin fraction will be dissolved, at a given solvent ratio, and less asphaltene flocculation will occur.

The fact that solid deposit formation occurs only with residues from a very few crudes can only be attributed to a very high paraffinicity and a low asphaltene content in these crudes. Support for this hypothesis is given in the difference in behaviour of the two Zarzaitine residues tested. The shorter residue has a ratio of saturates/C_5 asphaltenes of 17 by wt. and produces considerably less solid deposit than the longer residue, which has a ratio of saturates/C_5 asphaltenes of 25 by wt. Further support comes from the fact that as soon as the normal phase split occurs (into DAO and bitumen) the solid deposit formation is reduced to very low values (Figs 4 and 5). When this happens most of the saturates go into the DAO phase while the asphaltenes and resins remain in the bitumen phase.

During the course of the bench-scale batch experiments information was obtained on the composition of the two liquid phases formed. From this it is possible to construct phase diagrams (Figs 7 and 8). In these constructions the method described by Sawistowski & Smith[9] has been used, where the scale

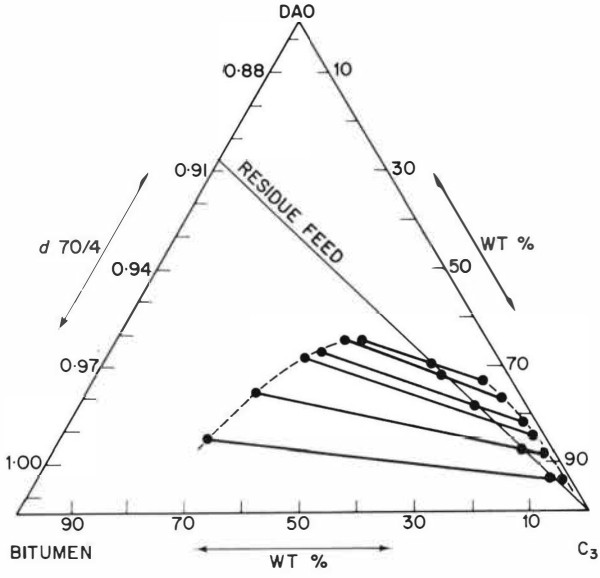

FIG. 7. *Phase diagram for propane deasphalting of Zarzaitine short residue B at 50°C*

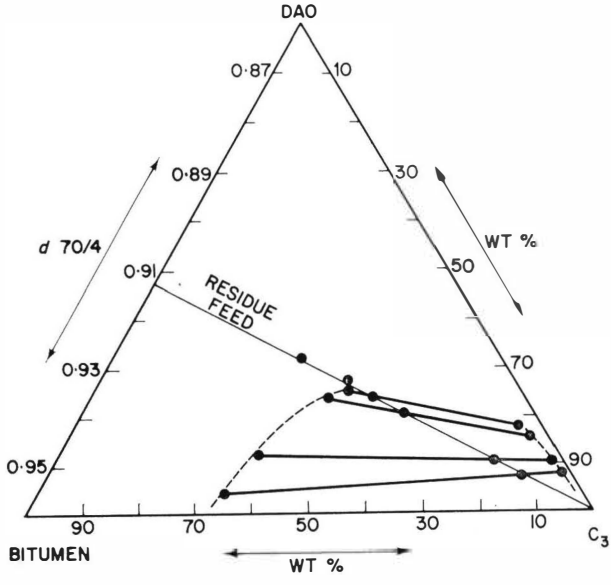

FIG. 8. *Phase diagram for propane deasphalting of Zarzaitine short residue A at 50°C*

describing the split into DAO and bitumen is represented by the sp. gr. of the solvent-free products. The DAO and bitumen poles do not represent pure components and the triangular diagram drawn should be regarded as part of a larger triangular diagram which does have poles representing 'pure' components. The third pole represents the pure solvent, propane, and the grid lines from the DAO/bitumen side converge to this pole. In order to make graphical constructions the distance between the propane pole and the DAO/bitumen scale must be divided into equal parts to give a scale representing wt.% propane in DAO/bitumen mixture. It is also necessary that the sp. gr. scale be linear with

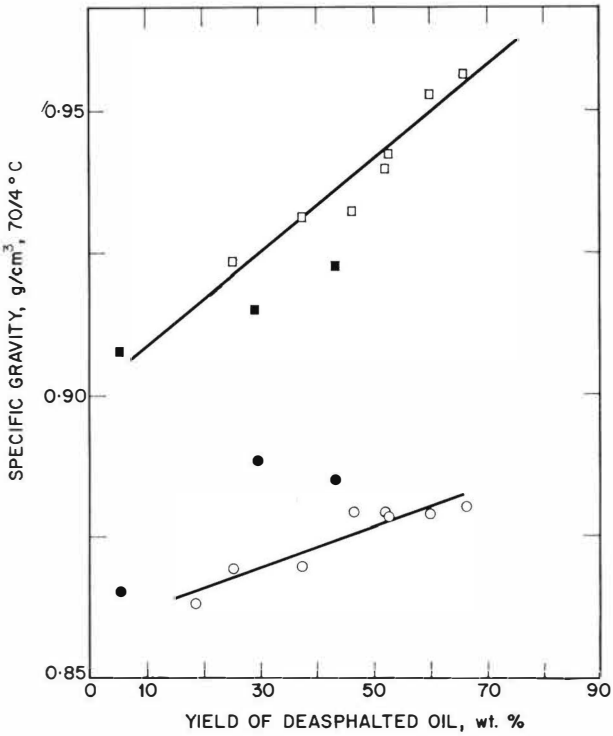

FIG. 9. *Correlation between the yield of DAO and the specific gravity of the oil and bitumen products from short residue B*

○ DAO; □ bitumen; ■ ● values in critical solvent ratio region

DAO yield on a weight basis. This is shown to be generally true (Fig. 9) for both the bitumen and the DAO. Deviations do, however, occur in the products obtained by deasphalting in the critical range of solvent ratios (0·5 to 2·0 by wt.) where solid deposits are formed. This means that in Fig. 7 the top two tie lines are probably distorted and that use of this part of the phase diagram in graphical constructions could lead to errors.

In line with the hypothesis that the principal reason for the solid deposit formation is a very high ratio of paraffinic to asphaltenic materials in the Zarzaitine residues a few batch deasphalting experiments were carried out in which Zarzaitine residue B was mixed with various materials which were comparatively more aromatic in nature. These materials were:

(a) its own bitumen from propane deasphalting

(b) furfural bright stock

(c) Middle East short residue

(d) the resin fraction from a Venezuelan residue.

The effects of the furfural bright stock extract and the bitumen were more or less the same; both reduced the solid deposit formation considerably. Mixtures of equal proportions of residue and additive, when mixed with 0·7 by wt. propane (i.e., 1·4 by wt. solvent/residue ratio) produced only $\frac{1}{4}$ (by wt.) as much solid deposit as the residue on its own.

On the other hand, mixtures of equal proportions of Middle East and Zarzaitine short residues when deasphalted with propane in the critical solvent ratio region (1·2 to 1·7 by wt. solvent/Zarzaitine residue ratios in this case) produce enormous amounts of solid deposits (10 to 20% wt.). The n-C_7 asphaltene content of this deposit is 4·0 % wt. on total feed at the maximum

and is equal to the total present in the two short residues. It appears that the solvent power of the mixture of propane and high molecular weight paraffins from the Zarzaitine residue is sufficient to dissolve enough of the resin fractions in the Middle East residue to cause the flocculation of its asphaltenes in addition to the asphaltenes from the Zarzaitine residue.

In order to try and increase the protective layer of resinous material round the asphaltenes, a small quantity (3 % wt.) of some resins prepared from Venezuelan residue was added to the Zarzaitine residue B. When mixed with propane in the critical solvent ratio region (1·6 by wt.), however, a large amount of solid deposit was again formed (6% wt. on residue). This amount of deposit is equal to the amount that is formed by the residue itself plus the total amount of resin added. It appears, therefore, that the added resin fraction, although succeeding in the primary objective of remaining adsorbed on the asphaltenes, was not present in sufficient quantities to prevent flocculation occurring.

Continuous pilot-plant experiments

Although the batch experiments were unable to indicate conditions under which no solid deposit formation would occur, the following conditions produced distinct improvements:

(*a*) use of high solvent/residue ratios

(*b*) use of as short a residue as possible

(*c*) applications of high extraction temperatures

(*d*) mixing short residue with its own bitumen.

A series of experiments were therefore carried out in the pilot plant to see if conditions could be found under which no blocking of the RDC occurred. The results are summarised in Fig. 10, where the n-C_7 asphaltene content of the solid deposit, measured by toluene washing, as a function of the total feed throughput, is plotted against the solvent/residue ratio.

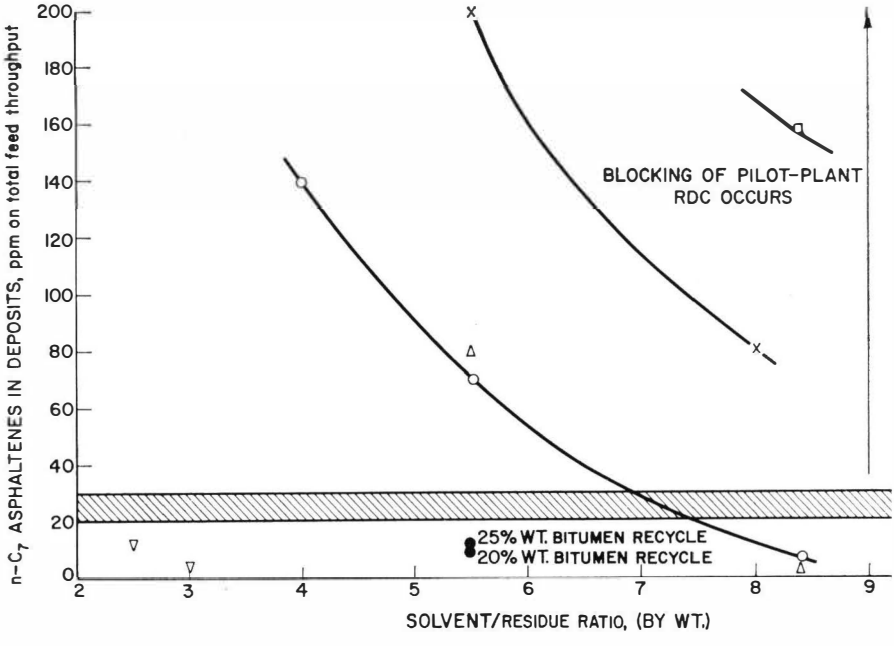

FIG. 10. *Influence of various parameters on the formation of solid deposits in pilot-plant RDC*

● ○ Zarzaitine residue B; × Zarzaitine residue B with temperature profile 'A' in Fig. 2; △ Zarzaitine residue A; □ Zarzaitine residue C; ▽ Middle East residues

In order to control the quality of the DAO produced (particularly the viscosity) either the solvent ratio or the temperature has to be a dependent variable. In this work the temperature was used to control the DAO viscosity so that when operating at high solvent ratios, in order to prevent solid deposit formation, a high extraction temperature must be applied to keep a constant viscosity level. This, of course, in turn further reduces the amount of solid deposit formed.

It can be seen from Fig. 10 that the same conditions that produced improvements in the batch experiments also produce improvements in the continuous pilot-plant operation. It was found that the two shorter residues could be processed indefinitely in the pilot plant without causing blockages if the solvent ratio was above 7 by wt. Under the same conditions the longer short residue blocked the RDC very quickly.

Recycling bitumen into the short residue feed B such that the feed contained 20 and 25% wt. of its own bitumen also enabled trouble-free operation even at the lower solvent/residue ratio of 5·5 by wt. The quality of the DAO obtained during these experiments was, however, considerably poorer.

It was found that if a different temperature profile was used in the RDC (profile A in Fig. 2), blockage caused by solid deposits occurred within a few hours, even when using high solvent residue ratios.

In Fig. 10 a tentative limit to the amount of solid deposit (on n-C_7 asphaltene basis) that can be produced without causing blockages in the pilot-plant RDC is indicated. For comparative purposes figures obtained from pilot-plant deasphalting of two Middle East feedstocks which do not normally give any problems are included.

It will be noticed that the quantities of solid deposit apparently formed in the batch extractions is in the range 200–400 ppm (on n-C_7 asphaltene basis) even at high solvent/residue ratios (Figs 4 and 5) and values of 20–30 ppm in the continuous pilot-plant experiments. There are two possible reasons for this. First, the small amounts of deposit obtained in the batch experiments are virtually impossible to measure accurately because of contamination with bitumen and these figures are therefore probably too high. Secondly, it is probable that most of the solids formed in the continuous experiments, even at low solvent ratios, will leave the extractor together with the bitumen and only a small fraction will remain in the RDC.

Calculation of the number of theoretical mass transfer stages in an RDC when propane deasphalting

A few experiments have been carried out to investigate the mass transfer staging in the pilot-plant RDC during propane deasphalting. As described earlier, phase diagrams were available from the bench scale batch experiments, but only at 50°C. So preliminary experiments were carried out to see if the yield and quality of the DAO and bitumen produced when using an external settler, as a reflux forming device, was the same as that produced when using the top section of the RDC to form a reflux in the normal way. The results, shown in Table III, indicated reasonable correspondence and therefore allowed the whole RDC to be operated at 50°C, making it simpler to collect the necessary samples and calculate the number of theoretical stages. The quantity of reflux formed by a 20°C temperature rise in the external settler was extremely small and gave a reflux ratio of only 0·02 by wt.

The calculation of the number of stages in the top sections, above the normal residue feed point, was not attempted because it involved the use of that part of the phase diagram which is unreliable owing to the solid deposit formation. However, because of the very small quantity of reflux formed in the top sections and the similar DAO quality obtained from the RDC and single-stage batch extractions, under the same conditions, there can be very little staging in these sections. With the short residue feed entering between section 3 and 4 (see Fig. 1) between 2 and 3 theoretical stages were estimated in the three asphalt

TABLE III

Determination of number of theoretical stages of the pilot-plant RDC with Zarzaitine short residue B

Experimental conditions	1	2	3	4	5*
Temperature, °C: Top	70	50	50	50	50
Bottom,	50	50	50	50	50
External settler	—	70	70	70	—
Sections 3 + 4	50	50	50	50	50
Section 5	70	50	50	50	50
Feed rate, kg/h	8	8	8	8	12
Solvent ratio: C_3/sh. res., by wt.	8·5	8·5	8·5	8·5	5·5
Predilution: C_3/sh. res., by wt.	0·5	0·5	0·5	0·5	0·5
Stirrer speed, rev/min	100	100	0	400	100
Yields					
DAO, % wt.	81·5	82·6	81·7	83·4	85·8
Bitumen, % wt.	18·5	17·4	18·3	16·6	14·2
Properties					
DAO					
Phase composition C_3/DAO, by wt.	10·3	—	—	—	—
Refractive index n_D^{70}	1·4943	1·4949	1·4940	1·4950	1·4960
Specific gravity, *d* 70/4°C	0·8850	0·8864	0·8850	0·8863	0·8878
Ramsbottom carbon content, % wt.	2·1	2·4	2·4	2·5	2·7
Viscosity, cS/210°F	61·46	63·76	62·09	64·79	68·51
Bitumen					
Phase composition C_3/bit., by wt.	0·14	—	—	—	—
Specific gravity, *d* 70/4°C	1·024	1·025	1·025	1·033	1·028
Softening point R & B, °C	92·5	93	93	101·5	95
Penetration at 25°C, 0·1 mm	<1	<1	<1	<1	2
Reflux ex *external settler*					
Refractive index, n_D^{70}	—	1·520	1·516	1·518	—
Specific gravity, *d* 70/4°C	—	0·9224	0·9180	0·9187	—
Ramsbottom carbon number, % wt.	—	7·1	6·0	6·3	—
Viscosity, cS/210°F	—	300·0	253·3	258·4	—

* Feed input at top of RDC

stripping sections. The method used for the graphical construction of the number of theoretical mass transfer stages was that of Hunter & Nash.[10]

In a final experiment the short residue feed was introduced at the top of the RDC. The results of this test indicate a significant increase in yield (comparing Experiments 2 and 5 in Table III) and only a slight deterioration in quality, which is probably due to the lower solvent/residue ratio used. The constructions for the estimation of the number of theoretical stages is shown in Fig. 11, from which it can be seen that between 3 and 4 ideal stages exist in the five sections below the residue feed point. This compares reasonably well with experience on a commercial-sized RDC,[4] where 4 theoretical stages were found during propane deasphalting in an 8 ft diameter tower 32 ft long.

In making the graphical constructions shown in Fig. 11 it was necessary to extrapolate the tie lines. To do this a method described by Alders[11] has been used, as indicated in the figure.

From this study it can be seen that a recycle of bitumen, which has the same effect as backmixing, will tend to reduce the number of stages in the bottom section where, it has been found, the majority of the staging occurs. Consequently, a reduction in the yield and quality of the DAO produced is inevitable.

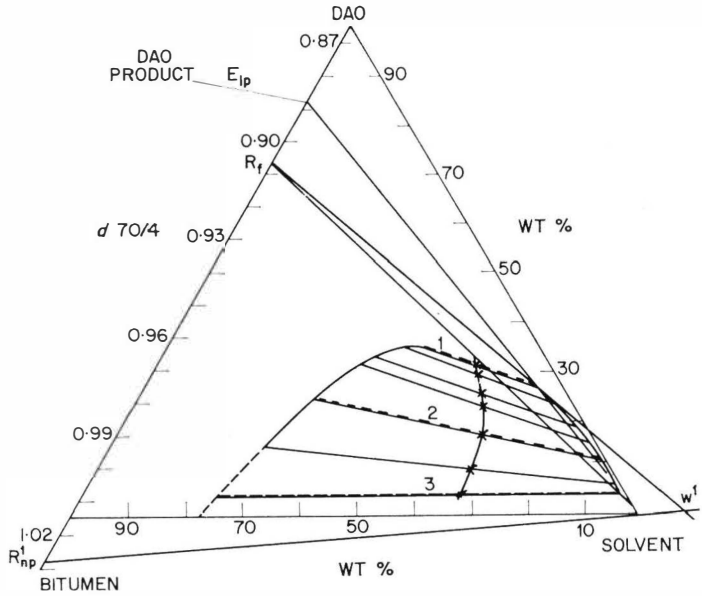

FIG. 11. *Calculation of the number of theoretical mass transfer stages.*

Short residue feed inlet at top of RDC (Run 5, Table III)

- - - - Extrapolated phase equilibrium data

1 Stage constructions

×——× Construction or tie line extrapolation[11]

Conclusions

The formation of solid deposits during the propane deasphalting of Zarzaitine short residues has been attributed to the extreme paraffinicity and low asphaltene content of this feedstock. At low solvent/residue ratios it is thought that propane and high molecular weight paraffins from the residue form a mixture which, in solvent power towards the resin fraction, is equivalent to pentane or hexane This causes the colloidal suspension of asphaltenes to collapse and the asphaltenes to flocculate. The solvent power of this mixture is such that it will also cause flocculation of asphaltenes feed stocks of, e.g., Middle East origin which normally, on their own, produce no deposit even at low solvent/residue ratios.

No conditions could be found, either in batch or continuous experiments, which completely prevented the formation of solid deposits. However, operation at very high solvent/residue ratios and high extraction temperatures reduced the amounts of deposit formed to levels which did not cause blockages in the pilot-plant RDC. It was also found essential to use a residue which is as short as possible. One residue tested, which was about 25% longer, could not be deasphalted, without forming solid deposits, under any of the conditions tried.

Recycling part of the bitumen product was also found to prevent blockages occurring in the pilot plant even at lower solvent ratios. However, the yield and quality of the DAO produced in this way was reduced owing to a reduction in the staging in the bottom part of the RDC caused by this backmixing.

The number of theoretical mass transfer stages could not be measured for the sections above the residue feed inlet, but no more than one stage is thought to exist because of the very small reflux in these sections. In the sections below the residue feed inlet approximately 0·75 theoretical stages per section of the pilot RDC was measured. This value agrees fairly well with the value obtained from a commercial scale unit. In these circumstances it is clearly best to introduce

the residue feed as close to the top of the RDC as is practical, that is, just below the reflux-forming heater.

References

[1] le Fournier, J., *Revue Inst. fr. Pétrole*, 1969, **8**, 579

[2] Kalichevsky, V. A., & Kobe, K. A., 'Petroleum refining with chemicals', 1956, p. 392 (New York: Elsevier)

[3] Benedict, B. C., *et al.*, U.S. P. 2,570,044

[4] Thegze, V. B., Wall, R. J., Train, K. E., & Olney, R. B., *Oil Gas J.*, May 8, 1961, pp. 90–94

[5] Overbeek, J. Th. E., & Kruyt, H. R., 'Colloid science', Vol. 1, Chapter 7 (Amsterdam: Elsevier)

[6] Beuther, H., & Schmid, B. K., 6th Wld Petrol Congr., Frankfurt a.M. (Germany), 1963, Section III, Paper 20–PD 7

[7] Yen, T. F., Erdman, J. G., & Pollack, S. S., *Analyt. Chem.*, 1961, **33**, 1587

[8] Ferris, S. W., Black, E. P., & Clelland, J. B., *Ind. Engng Chem. Prod. Res. Dev.*, 1967, **6**, 127

[9] Sawistowski, H., & Smith, W., 'Mass transfer process calculations', 1963, pp. 394–401 (New York: Interscience)

[10] Hunter, T. G., & Nash, A. W., *J. Soc. chem. Ind., Lond.*, 1934, **53**, 95 T

[11] Alders, L., 'Liquid–liquid extraction', 1955, p. 20 (Amsterdam: Elsevier)

A new furfural refining process for petrochemical feedstocks

by R. A. Woodle, P. P. Bozeman, jun., and B. H. Cummins
Texaco Inc., Port Arthur, Texas, U.S.A.

The furfural refining process has been modified for the manufacture of gas oil extracts which are highly concentrated in dinuclear aromatics. The result is a double-solvent process in which a second solvent washes the extract phase essentially free of non-aromatics, and azeotropes with the furfural to aid in solvent recovery. The effects of the main process variables on extract yield and quality are reported. Investment and utilities required are presented.

Introduction

TEXACO'S RESEARCH LABORATORIES have developed a new furfural refining process for producing dinuclear aromatic concentrates for petrochemicals applications from fluid cracked (FC) cycle gas oil.

At the time this work was carried out, it appeared that high-tonnage production of naphthalene from petroleum might require large volumes of feedstocks highly concentrated in dinuclear aromatics. Existing refinery streams, such as reformer bottoms, which were naturally concentrated in aromatics of the desired boiling range, were available in very limited amounts. Light FC cycle gas oil represented a large-volume, readily available source of aromatics but the concentration was only of the order of 50%.

The target aromatic concentrate specifications that were established early in the development were: total aromatics, 90 vol.-% minimum; dinuclear aromatics, 70 vol.-% minimum; recovery of dinuclear aromatics, 80% minimum.

Attainment of the desired concentrations involved a hydrocarbon-type separation, and thus solvent extraction was the first process considered. Furfural was the solvent closest to Texaco's background from its use for lubricating oil and middle distillate refining. Furfural refining units for lubricating oil manufacture have been installed throughout the world.[1] A smaller number of units designed for refining gas oils for manufacture of diesel fuel, burning oils, or cracking stocks are in operation.[2] The gas oil process was designed for meeting refined oil specifications; it was not capable of achieving the above extract oil specifications except at extraction temperatures of the order of 10°C.

Therefore, work was undertaken on a new modification of the furfural solvent-extraction process. A second solvent would be introduced to wash the extract phase essentially free of non-aromatics; also, the second solvent would be chosen to azeotrope with furfural. Thus the use of a second solvent as a backwash would enable highly aromatic extracts to be produced by furfural refining at above-atmospheric temperatures and also would aid in recovery of the solvents.

Several factors guided the selection of the second solvent:

(1) It should displace feedstock non-aromatic compounds from the extract mix and be sparingly soluble in furfural. This suggested the use of a paraffinic solvent.

(2) It should form an azeotrope relatively rich in furfural. A literature review[3] (results in Fig. 1) suggested the use of a paraffinic fraction boiling in the 150–220°C range.

(3) It should not boil in the range of the feedstock. Since the probable initial boiling point of the feedstock was about 200°C, a nominal 150–175°C boiling range was indicated for the second solvent.

(4) It should be available in quantity and be inexpensive.

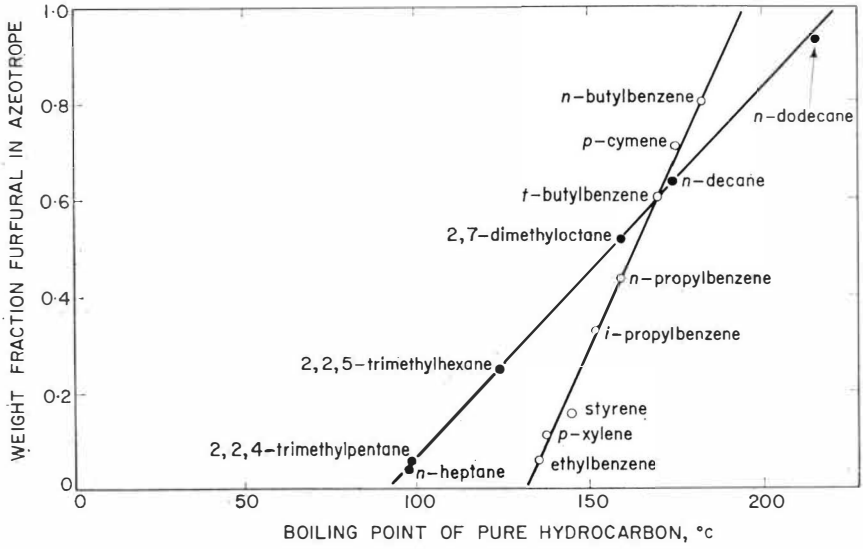

FIG. 1. *Binary furfural–hydrocarbon azeotropes*

These factors led to the choice of a 150–175°C fraction of Udex raffinate as the second solvent for the present work; other fractions similar in composition and boiling range could be used.

The development work was carried out in continuous pilot-scale equipment with no difficulty from the process-design standpoint. The new process has been further proven in a demonstration plant-scale run, and is covered by a patent.[4]

Experimental

The equipment required for the process is at a minimum. Essentially, it consists of an extractor, an extract fractionator, a raffinate fractionator and a decanter to separate the furfural from the second solvent for recycling of the two solvents.

Fig. 2 is a schematic flow diagram of the pilot unit. The extractor consists of a rotating disc contactor (RDC) having an internal diameter of 10 cm, a height of 1·6 m and containing forty 3·8-cm compartments. The rotor is driven by a 1 h.p. motor through a variable-speed drive having a range from 50 to 520 rev/min. The liquid–liquid interface is maintained above the extractor in an external settler.

The extract fractionator is a 6-m section of 15-cm diameter carbon-steel pipe. It is packed to a height of approximately 5 m with 1-cm carbon Raschig rings.

The raffinate fractionator is a 7·5-cm diameter tower containing approximately 3·7 m of 1-cm carbon Raschig rings.

Both fractionators are provided with multiple feed-entry points. Both are also electrically wound for adiabatic operation.

The unit was designed for the following maximum charge rates to the RDC (l/h):

Charge oil	20
Furfural	50
Second solvent	20

The operating procedure consists of charging furfural at the top of the extractor, charge oil at the middle and the second solvent near the bottom. Raffinate leaves the top of the extractor through the settler, from which it

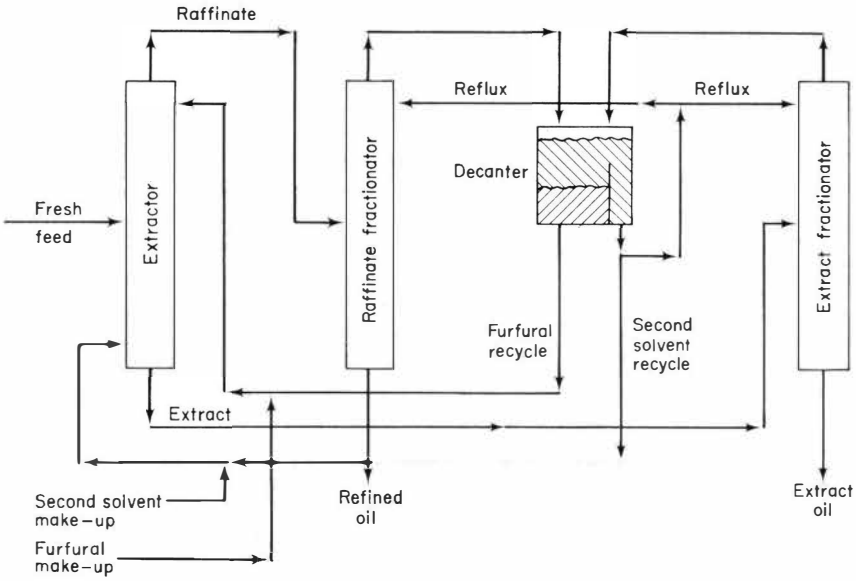

FIG. 2. *Schematic flow diagram of pilot unit*

passes to the raffinate fractionator. Extract discharges from the bottom of the RDC and flows to the extract fractionator.

The refined oil, free of solvent, is recovered as bottoms from the raffinate fractionator. The overhead consists of a mixture of furfural and second solvent, which is condensed and settled in a separator. The recovered light phase consists mainly of second solvent, while the heavy phase is mainly furfural. Both solvents are recycled. In addition, the tower is refluxed with the recovered light phase.

The extract is handled in a similar manner in the extract fractionator.

The furfural was redistilled solvent from a commercial lubricating oil refining unit. As received from the plant it was free of oil, essentially dry and light in colour. Before charging to the process, the furfural was saturated with water at atmospheric temperature.

The second solvent was a nominal 150–175°C fraction of Udex raffinate from extraction of reformed gasoline. Inspection tests are shown in Table I. In all the work reported here, the term 'second solvent' refers to this Udex raffinate fraction.

Table I also shows tests on the two charge stocks used. Stocks A and B are fractions of light FC cycle gas oils from two different FCC Units operating on different charge stocks at different operating conditions.

Results

The ability of the furfural refining process described here to produce extracts highly concentrated in dinuclear aromatics has been demonstrated over a wide range of operating conditions. Operations have included extended runs of several weeks' duration during which the solvent additions required have been mainly the amounts needed to replace samples taken from the unit. Long-term solvent losses should not exceed 0·03 vol.-% of circulation.

Results obtained while charging Stock A over a broad range of operating conditions are shown in Table II. The process readily produced extracts analysing 95 to 100% aromatics, with dinuclear aromatic recoveries in the extract of 85 to 92%.

TABLE I
Tests on hydrocarbon stocks

Test	Second solvent	Charge stock 'A'	Charge stock 'B'
Gravity, ASTM D–287, °API	58·3	29·2	28·6
Density at 15°C, ASTM D–1298, kg/l	0·7453	0·8801	0·8833
Closed cup flash point, ASTM D–93, °C	—	102	—
Kinematic viscosity at 100°F, ASTM D–445, cS	—	2·06	2·14
Colour, ASTM D–1500	—	<1·5	—
Pour point, ASTM D–97, °C	—	−37	—
Sulphur, ASTM D–2622, wt.-%	—	0·83	0·19
Conradson carbon residue on 10% distillation residue, ASTM D–189, wt.-%	—	0·22	—
Ash, ASTM D–482, wt.-%	—	None	—
Refractive index at 70°C, ASTM D–1218	1·3960	1·4792	1·4830
Distillation, ASTM D–86, °C at:			
Initial boiling point	151	229	234
10% Overhead	160	237	239
50% Overhead	163	244	244
90% Overhead	171	257	257
End point	198	274	274
Total aromatics, ASTM D–1319, vol.-%	4·7	46·8	48·2
Mononuclear aromatics, vol.-%*	—	14·3	13·7
Dinuclear aromatics, vol.-%*	—	32·5	34·5
Olefins, ASTM D–1319, vol.-%	2·6	6·2	4·8

* The aromatic portion from ASTM D–1319 was separated and analysed for mononuclear and dinuclear aromatics by gas chromatography

TABLE II
Operating conditions and results

	Run no. and charge stock							
	46–A A	37–B A	42–A A	48–A A	33–B A	47–A A	40–B A	60 B
Solvent dosage, vol.-%								
Furfural	66	98	100	150	202	235	203	201
Second solvent	32	25	40	22	41	32	25	50
Extractor temperature, °C								
Top	38	30	60	52	78	52	77	77
Bottom	38	26	49	38	49	38	50	50
Yield, vol.-%								
Extract	19·8	27·9	29·2	37·2	38·0	38·0	43·2	37·2
Raffinate	80·2	72·1	70·8	62·8	62·0	62·0	56·8	62·8
Extract product								
Total aromatics, ASTM D–1319, vol.-%	96·7	99·8	97·2	97·4	96·2	95·4	91·3	100·0
Dinuclear aromatics, vol.-%*	87·2	82·1	79·6	75·4	74·5	74·0	69·5	84·8
% Recovery total aromatics	40·8	59·5	60·7	77·3	78·1	77·5	84·2	77·2
% Recovery dinuclear aromatics	53·1	70·5	71·5	86·3	87·0	86·5	92·3	91·4
Refined oil product								
Total aromatics, ASTM D–1319, vol.-%	34·6	26·3	26·0	16·9	16·5	17·0	13·0	17·5
Dinuclear aromatics, vol.-%*	19·0	13·3	13·1	7·1	7·2	7·1	4·4	4·7

* The aromatic portion from ASTM D–1319 was separated and analysed for dinuclear aromatics by gas chromatography

An extended production run was made on Charge Stock B with the results also shown in Table II. The refined oil from that run was subjected to extensive testing as shown in Table III; it was found to meet high-quality diesel fuel requirements.

TABLE III

Product tests – Run no. 60

Test	Product	
	Extract	Refined oil
Gravity, ASTM D–287, °API	12·3	40·7
Density at 15°c, ASTM D–1298, kg/l	0·9834	0·8213
Closed cup flash point, ASTM D–93, °c	—	102
Colour, ASTM D–1500	—	<0·5
Pour point, ASTM D–97, °c	—	−30
Sulphur, ASTM D–2622, wt.-%	0·48	0·012
Conradson carbon residue on 10% distillation residue, ASTM D–189, wt.-%	—	0·006
Refractive index at 70°c, ASTM D–1218	1·5612	1·4375
Cetane number, ASTM D–976	—	52·0
Aniline point, ASTM D–611, °c	—	67·7
Total aromatics, ASTM D–1319, vol.-%	100·0	17·5
Dinuclear aromatics, vol.-%*	84·8	4·7
Olefins, ASTM D–1319, vol.-%	0	6·6

* The aromatic portion from ASTM D–1319 was separated and analysed for dinuclear aromatics by gas chromatography

Effects of variables

The specific results obtained at a given set of operating conditions depend upon the charge stock characteristics. However, for a given charge stock the effects of the main process variables are shown in a qualitative way in Table IV.

Charge-stock boiling range

It is economically important to recover and re-use the solvents. In this process, the ability to do this is related to the charge-stock boiling range, or more specifically, the front-end volatility.

TABLE IV

Relationship of variables

Dependent variable	Independent variable		
	Furfural dosage	Extraction temperature	Second-solvent dosage
Extract yield	Direct	Direct	Inverse
Extract aromatics concentration	Inverse	Inverse	Direct
Extract aromatics recovery	Direct	Direct	Inverse
Extract dinuclear aromatics recovery	Direct	Direct	Inverse
Refined oil aromatics concentration	Inverse	Inverse	Direct

The charge-stock should contain not more than 2 vol.-% boiling lower than 200°C as measured by a precision distillation. With a lower-boiling stock, there is a possibility of a build-up of paraffinic light ends in the recovered second solvent or of aromatic light ends in the recovered furfural.

Where the purpose of the operation is to recover methylnaphthalenes, it may be desirable to pre-fractionate the charge-stock to about 225°C initial boiling point in order to exclude from the feed most of the mononuclear aromatics, even though the extraction conditions can be adjusted to reject these preferentially to the refined oil stream.

Recycle stream analyses

With a properly fractionated charge-stock, as described above, the process readily recovers the two solvents in satisfactory purity for recycle without requiring any special provisions for solvent clean-up.

Table V shows the range of recycle-solvent analyses observed during the runs shown in Table II.

TABLE V

Recycle stream analyses

Furfural-rich phase	
Vol.-% oil	2·4–4·8
Oil refractive index at 70°C, ASTM D–1218	1·4156–1·4309
Hydrocarbon-rich phase	
Vol.-% oil	95·7–97·7
Oil refractive index at 70°C, ASTM D–1218	1·3939–1·3965
Oil gravity, ASTM D–287, °API	58·4–59·3
Oil density at 15°C, ASTM D–1298, kg/l	0·7449–0·7414

Economics

Table VI shows the estimated investment and utilities requirements for a unit designed to operate at the conditions of Run no. 60 (Table II), and sized to produce 300 metric tons per day of aromatic concentrate. This quantity is sufficient to supply a unit producing 45,000 metric tons of naphthalene per year. Operating costs are not shown since these will depend upon the particular plant situation; however, the operating costs are estimated to be in line with those for lubricating-oil furfural refining units.

TABLE VI

Economics

Basis: Charge stock B	
Operating conditions – as for Run 60	
Extract production – 300 metric tons per day	
Investment, $ millions	2·5–3·0
Utilities	
10·5 kg/cm² steam	2·1 metric tons per hour
Fuel	25×10^6 kcal/h
Power	375 kW

Conclusion

A new furfural refining process has been developed for preparing highly concentrated dinuclear aromatic extracts for petrochemicals application. Advantages of this process include: minimum equipment requirements; low-cost, easily recovered solvents; moderate operating conditions; and a high degree of flexibility.

This process is covered by a U.S. patent[4] and is available for licensing through Texaco Development Corporation.

References

[1] *Hydrocarb. Process.*, 1968, **47** (9), 180

[2] *Hydrocarb. Process.*, 1968, **47** (9), 179

[3] Dunlop, A. P., & Peters, F. N., *Am. chem. Soc. Monogr.*, *No.* 119, 1953, p. 328 (New York: Reinhold Publishing Corp.)

[4] Texaco Inc., U.S.P. 3,239,456

Foam suppression in extract purification and recovery trains

by D. van der Meer, F. J. Zuiderweg and H. J. Scheffer
Koninklijke/Shell-Laboratorium, Amsterdam, The Netherlands
(Shell Research N.V.)

In the sulpholane extraction process small amounts of saturates in the extract are removed in an extractive distillation stripping step. Since the solutions are highly non-ideal, the removal of the saturates causes an appreciable increase in surface tension. Under certain conditions this may lead to foaming on the trays of the stripper column, due to the 'Marangoni effect', which might limit plant throughput; foaming can be suppressed by conventional silicone-type defoamers. Analysis of the foaming mechanism, however, suggested that in this particular case higher molecular-weight saturates might also be active as anti-foaming agents. This was confirmed in both laboratory experiments and commercial plant-scale application.

Introduction

PURE LIGHT AROMATICS form an important group of petrochemical products. For their extraction from suitable feeds, such as a cut from the product stream of a platformer, various processes are available.[1] One of these, the Shell sulpholane extraction process,[2] has found worldwide applications; so far some 40 plants have been commissioned.

In the Shell sulpholane extraction process the feed stream, consisting of aromatics (benzene, toluene, xylenes), naphthenes and paraffins, is contacted with sulpholane ($C_4H_8SO_2$) in a rotating-disc contactor (RDC). In Fig. 1, a flow scheme of the process is given. The raffinate is water-washed to remove traces of solvent. Before the solvent is recovered, the extract passes through an extractive stripper, in which the small amounts of dissolved non-aromatic hydrocarbons are removed by vapour generated in the reboiler of the stripper. To increase the relative volatilities of the non-aromatics even more, more fresh

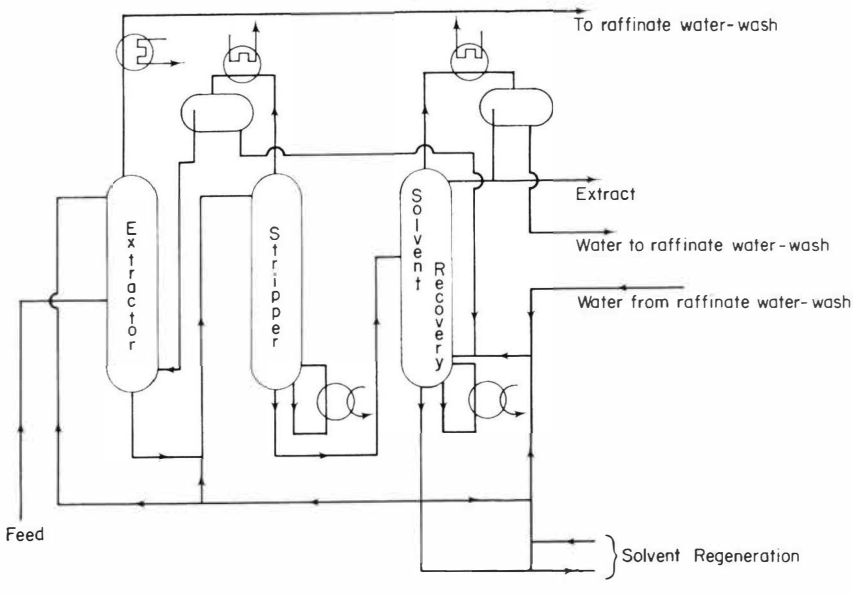

FIG. 1. *Flow scheme for the Shell sulpholane extraction process*

sulpholane is mixed with the extract stream before this enters the column. The top product of the stripper is fed back to the bottom of the RDC as reflux or backwash after coooling and separating some of the water originally present in the feed and sulpholane streams.

When, some time ago, it was tried to increase the throughput of one of the units, the operation of the extractive stripper became unstable. The phenomena observed were similar to those reported by Bolles,[3] who was faced with a foam problem. *X*-Ray investigation revealed that the top section of the column was flooding. Yet, in tests on similar trays with the system benzene–toluene, the trays could cope with the increased throughput. This paper is a report of the investigations which then followed to overcome the capacity limitations in the recovery train.

Hydrodynamic and physico-chemical conditions on the extractive stripper trays

Since the trays in the extractive stripper apparently had sufficient capacity to handle the required amounts of liquid and vapour when distilling a normal mixture, foaming was strongly suspected in the sulpholane stripping operation. For foaming to occur, however, both a hydrodynamic and a physico-chemical condition must be fulfilled. The hydrodynamic condition requires that the trays should operate in the so-called bubbling regime. The physico-chemical aspects concern the surface properties of the liquid mixture by which in a vapour-bubbling system the bubbles are stabilised to such an extent that a real foam is formed.

The situation with respect to the fulfilment of the hydrodynamic condition can be analysed on the basis of some recent studies published in the literature[4–6] on the transition between the vapour-bubbling and liquid-spraying regimes on distillation trays. From the rather extensive study on a probably sufficiently large scale by Porter & Wong[6] it can be shown that for sieve trays the transition between the two regimes is dependent on liquid holdup, hole size and

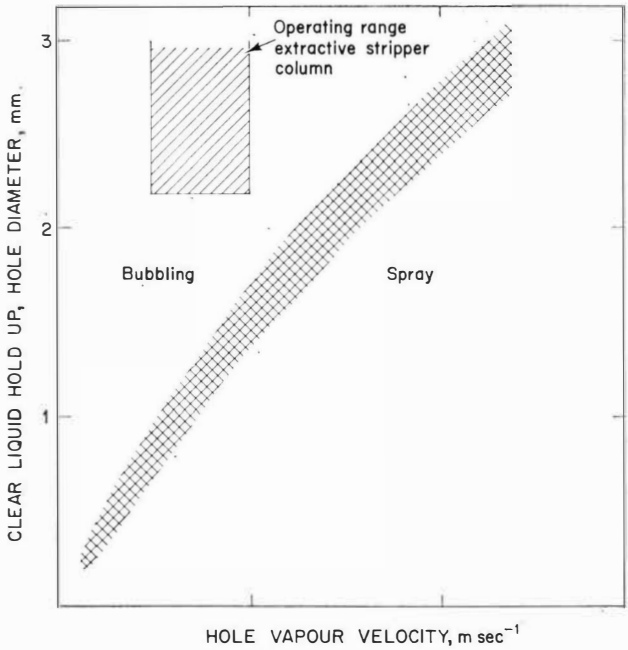

FIG. 2. *Transition between bubbling and spray regimes on distillation trays*

hole vapour-loading factor. This relation is shown in Fig. 2. To judge whether the extractive stripper was operating in the bubbling regime the liquid holdup was calculated on the basis of weir height, froth density[7] and crest over weir.[8] Thus, a liquid holdup of 44 mm clear liquid was found. Since the trays were of the valve type with 40 mm valves having a lift opening of 10 mm, the equivalent hole diameter relative to sieve trays is estimated at 10 to 20 mm. With the hole vapour-loading factors ranging between 0·30 and 0·50 m/sec, the operating regime of the trays in the stripper appears to be well in the bubbling regime, as indicated in Fig. 2.

To check whether the second physico-chemical condition was fulfilled, i.e., whether the liquid properties were such that a bubbling regime could be stabilised into a foam, first a simple foam test was made by bubbling air through a sulpholane–hydrocarbon mixture. It was found that in such a test the liquid had no foaming properties. Since the conditions in the actual stripping operation are quite different from those in the simple foam test, however, it was decided to simulate the stripping process in the laboratory. Thus, stripping experiments were carried out with actual plant feed in a 20-tray Oldershaw

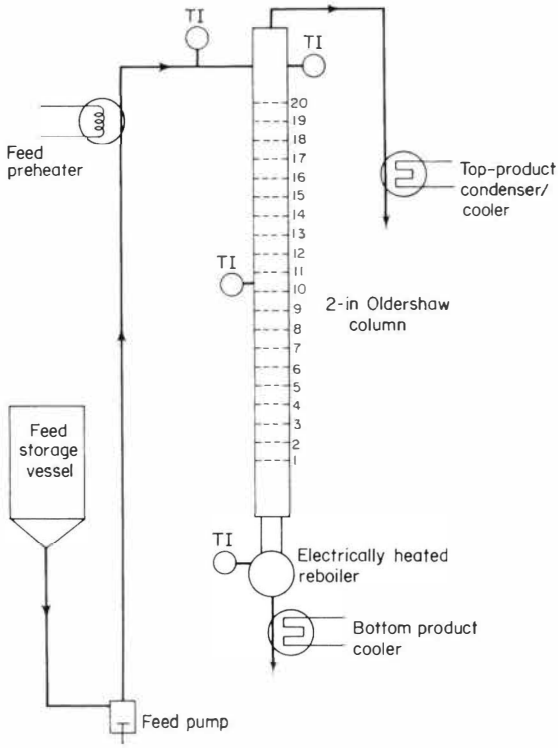

FIG. 3. *Schematic drawing of 20-tray laboratory Oldershaw column*

glass sieve plate column (Fig. 3). The column capacity was determined for both the sulpholane system and the non-foaming test system, benzene–toluene. It was found that the column flooded at a five times lower vapour load for the sulpholane system under the same liquid load, while the bed heights were two to three times higher for the sulpholane system under the same hydrodynamic conditions. For a feed temperature of about 60 °C, the maximum bed heights occurred in the middle of the column (Fig. 4) and a foamy structure was observed. Lower in the column the trays operated at normal bed levels without foaming. Thus these experiments suggested that the stripping-off of paraffins causes foaming, which limits the stripper throughput. This was confirmed by

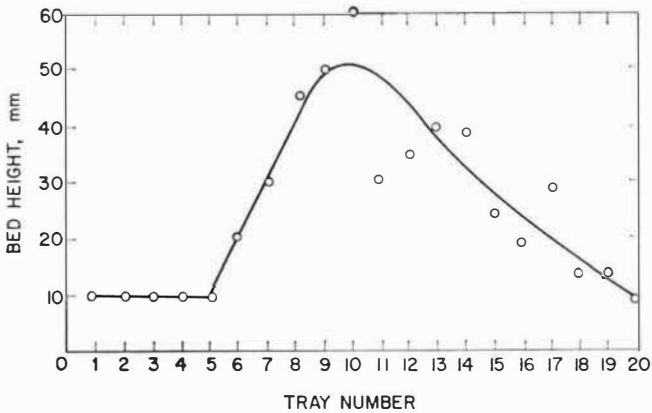

FIG. 4. *Liquid bed heights in simulated stripping tests*
2-in diameter Oldershaw sieve plate column

experiments in a 0·45-m dia. distillation column containing 4 valve trays, which was operated under both stripping and absorbing conditions. Under stripping conditions a fixed amount of cooled reboiler liquid was premixed with the condensed vapours and fed to the top tray (Fig. 5). During the travel of this liquid back to the reboiler paraffins are stripped off. Under absorbing

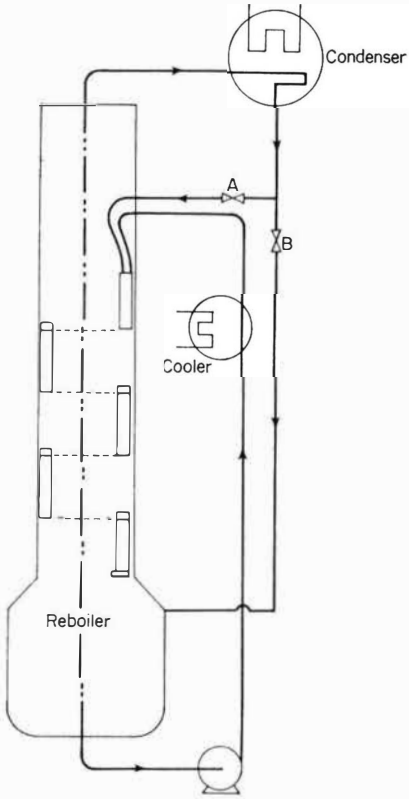

FIG. 5. *Schematic set-up of distillation column*
0·45-m diameter column

conditions only a fixed amount of cooled reboiler liquid is fed to the top tray and the condensed top vapours are returned to the reboiler.

During the stripping operation severe foaming was observed on the trays, whereas under absorbing conditions no foaming took place. This is illustrated in Fig. 6.

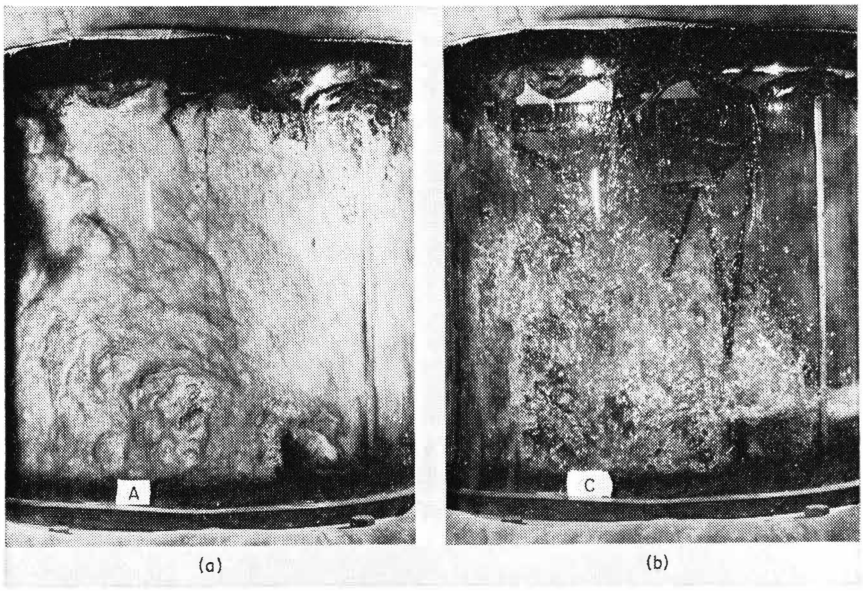

FIG. 6. *Foaming on trays*
(*a*) Tray under stripping conditions
(*b*) Tray under absorbing conditions

Thus, from the analysis presented in this section it appears that, on the basis of both hydrodynamic and physico-chemical conditions, the limited throughput of the commercial plant stripper is due to foaming. This foaming is related to the stripping-off of the paraffins from the sulpholane–hydrocarbon mixture.

Foaming by the Marangoni effect

The phenomena discussed above suggest that the foaming is caused by the Marangoni effect.[9] On this basis foaming develops when the liquid surface tension increases due to mass transfer. The liquid film just between two adjacent vapour bubbles is closer to equilibrium than the liquid at some distance from these vapour bubbles. When the equilibrium conditions on the tray correspond with a higher surface tension, liquid will be sucked into the film between the two bubbles. When this suction dominates the drainage from the froth, foaming stabilised by the Marangoni effect occurs.

In aromatics extraction, non-ideal liquid mixtures are encountered; the affinity of the aromatics to the solvent is much higher than that of the paraffins and the naphthenes. This means especially that the concentration of paraffins at the surface is much higher than that in the bulk of the liquid, so the surface tension of sulpholane–aromatic–paraffin mixtures will be strongly dependent on the paraffin concentration. This is illustrated in Fig. 7, where surface tension measurements of sulpholane–toluene–iso-octane–water mixtures are given as a function of the iso-octane concentration. Fig. 7 shows that the surface tension decreases by 5 dynes cm^{-1} when the iso-octane concentration is brought from 0 to 1 wt.-%.

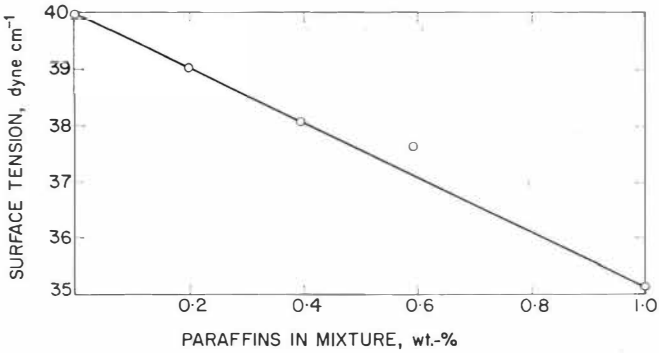

FIG. 7. *Surface tension of sulpholane–hydrocarbon–water mixtures*
20°C; weight ratio 80·4 : 18·9 : 0·75

The feed to the stripper normally contains 3·5 to 4·5% paraffins and naphthenes. Usually nine equilibrium stages suffice to reduce the non-aromatics content of the extract to 0·02%. The concentration profile over the column is given in Fig. 8 and the corresponding temperature profile in Fig. 9.

The concentration profile shows a rather sharp decrease of the paraffin concentration in the top of the column. Consequently, a steep rise in surface tension occurs there. On the basis of the data presented in Figs 7, 8 and 9,

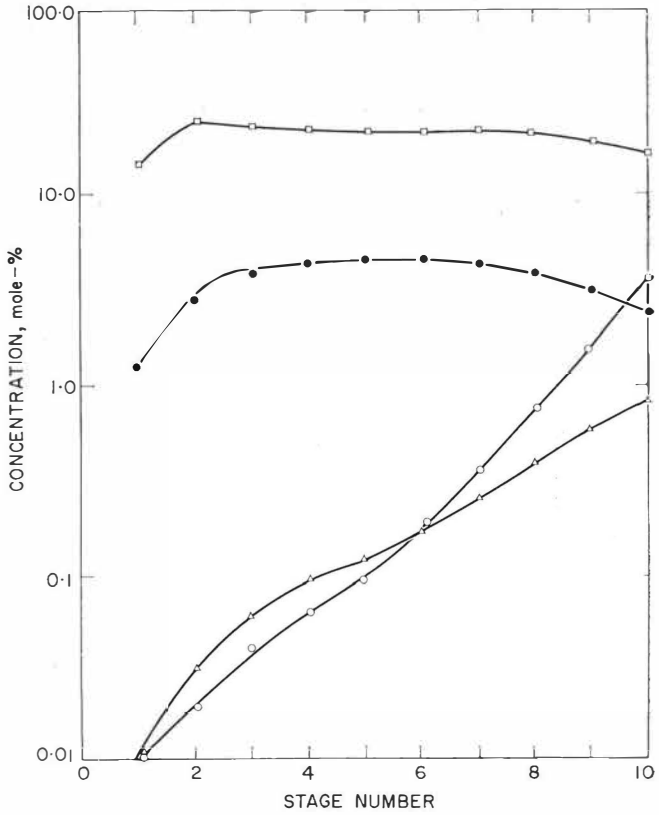

FIG. 8. *Concentration profits in extractive stripper*
□ Aromatics; ● water; △ naphthenes; ○ paraffins

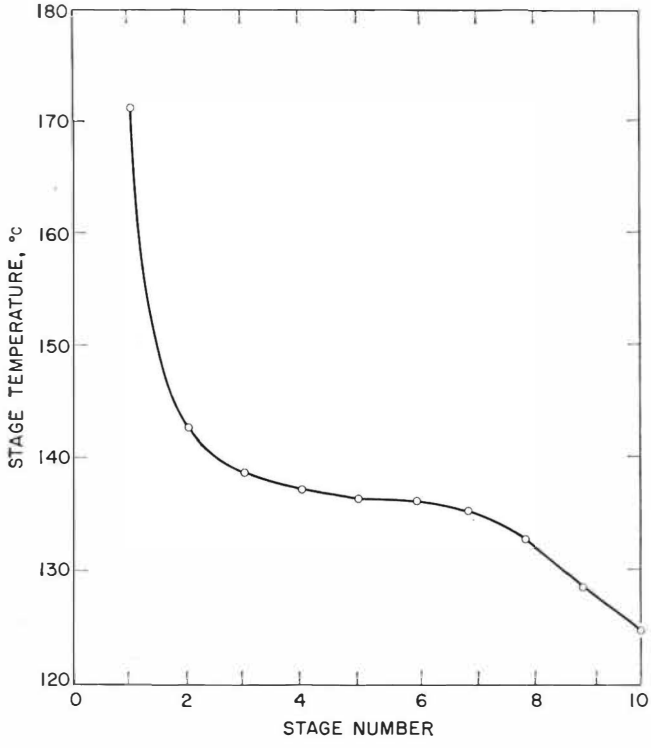

FIG. 9. *Temperature profile in extractive stripper*

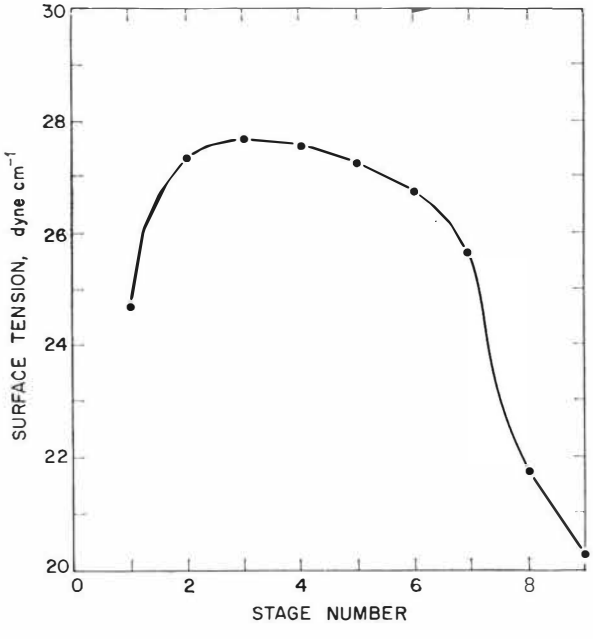

FIG. 10. *Surface tension profile in extractive stripper*

the surface tension profile over the column was calculated, taking into account an average temperature influence on the surface tension of 0·1 dyne cm^{-1} $°C^{-1}$. The further assumptions were:

(*a*) the influence of the various paraffins is the same

(*b*) naphthenes behave as paraffins

(*c*) the decrease of the surface tension with the paraffin concentration over the relevant range is linear

(*d*) the relatively small change in aromatics concentration does not affect the surface tension significantly.

The resulting surface tension profile is given in Fig. 10. From this figure it can be seen that there is a marked rise in surface tension in the top section of the stripper, especially at stage 7 where the surface tension increases by 4 dynes cm^{-1}. This surface tension profile shows very clearly that as far as the physico-chemical condition is concerned, flooding of the stripper by foaming stabilised by the Marangoni effect was to be expected.

Foam suppression

Once it had become apparent that flooding of the commercial stripping column was caused by foaming, 0·5 ppm of a silicone-type antifoam agent was continuously injected into the feed, which led to the desired increase of the throughput. This was also demonstrated in the laboratory Oldershaw column, where, with 0·5 ppm antifoam, bed heights between 5 and 15 mm were measured under the same conditions as in Fig. 3. The effectiveness of the antifoam agent may be explained by considering that it causes such a reduction in the overall surface tension that the surface-tension gradient due to the mass transfer is practically eliminated. In addition, it might act in the conventional way.[10]

This consideration and the observation of the strong surface activity of the saturated hydrocarbons in sulpholane–hydrocarbon mixtures suggests an alternative and probably even more elegant way of foam suppression. Small amounts of heavy paraffins injected into the extract and not removed in the stripper might also effectively reduce the overall interfacial tension and thus neutralise the Marangoni effect. The reductions in bed height in the laboratory column for actual plant feeds obtained with odourless kerosene and with silicone antifoam are compared in Fig. 11. With antifoam, the reduction rises very sharply when the concentration is increased from 0·1 to 10 ppm, which probably indicates that the surface becomes saturated with antifoam molecules, so that

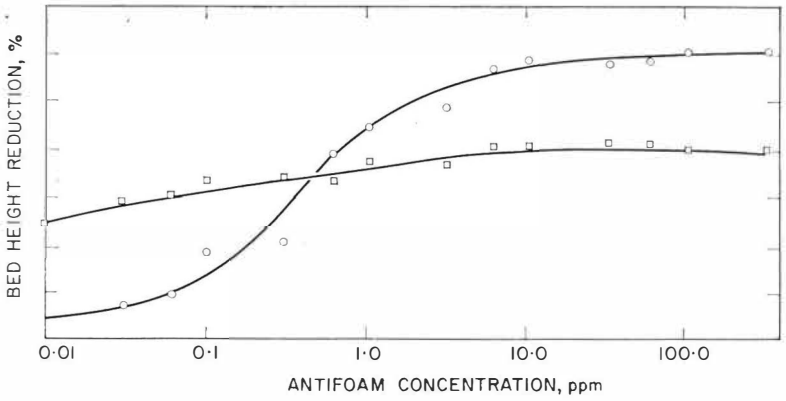

FIG. 11. *Bed height reduction of actual stripper feed as a function of antifoam concentration in a 20-tray Oldershaw column*

○ silicone-type antifoam agent; □ odourless kerosene

beyond a certain concentration no further reduction is obtained. With the 'unconventional' kerosene antifoam a more continuous reduction of the bed heights with increasing concentration is observed, indicating that the heavy paraffins are not only present at the liquid surface, but are also dissolved in the liquid. Here the maximum bed-height reduction is determined by the solubility of the paraffins in the sulpholane–hydrocarbon mixture.

More generally it can be said that foaming caused by the stripping-off of light components that lower the surface tension can be reduced by adding a heavy homologue. This rules out the possibility of contamination of end products with antifoam agents.

Conclusion

The performance of complex extraction units may be seriously affected if potential problems in the recovery section are overlooked. By nature, the systems encountered are highly non-ideal and can suffer from foam stabilised by the Marangoni effect. This is not generally recognised. Bolles' foam problem[3] can easily be explained along the lines given in this paper. The use of heavy homologues to suppress foaming may find wider application.

References

[1] Vashist, F. N., & Beckmann, R. B., *Ind. Engng Chem.*, 1968, **60**, 43
[2] Voetter, M., & Kosters, W. C. G., VI World Petrol. Congr., Sect. III, Paper 11, 1963
[3] Bolles, W. L., *Chem. Engng Prog.*, 1967, **63**, 48
[4] De Goederen, C. W. J., *Chem. Engng Sci.*, 1965, **20**, 1115
[5] Ho, G. E., Muller, R. L., & Prince, R. G. H., in 'Distillation 69' (Int. Symp. Distillation, Brighton, 1969), 1970, Sect. 2, p. 5 (London: Institution of Chemical Engineers)
[6] Porter, K. E., & Wong, P. F. Y., *ibid.*, Sect. 2, p. 7
[7] Zuiderweg, F. J. & Van der Meer, D., *3rd CHISA Congr.*, *Mariánské Lázně* (*Czechoslovakia*), September 1969
[8] Leibson, I., Kelley, R. E., & Bullington, L. A., *Petrol. Refiner*, 1957, **36**, 127 and 288
[9] Zuiderweg, F. J., & Harmens, A., *Chem. Engng Sci.*, 1958, **9**, 89
[10] Ross, S., *Chem. Engng Prog.*, 1967, **63**, 41

Manufacture of special boiling point solvents by sulfolane extraction

by W. C. G. Kosters
Bataafse Internationale Petroleum Mij. N.V., The Hague, Netherlands

The specifications on aromatic content for hydrocarbon solvents have become more stringent in the course of the last few years, especially for maximum allowable benzene content. The scheme for the manufacture of a large variety of solvents from a number of base components includes a process for the reduction of the aromatics content of the base material. For this processing step sulfolane extraction or hydrogenation can be used. The merits of both processes are discussed.

Introduction

HYDROCARBON SOLVENTS ARE fractions which boil in the gasoline range. If the final boiling point is below 160°C these solvents are commonly termed SBP solvents, while for solvents boiling between 145 and 205°C the name 'white spirits' is more often used.

These solvents are used for a variety of industrial purposes and are often manufactured to suit the special needs of a number of small customers in competitive markets.

For this reason SBP solvents are usually manufactured in comparatively small batches or short runs. Normally, this type of manufacture is economic only if a number of grades with widely different specifications can be produced simultaneously or in series by means of flexible and versatile equipment and/or by choosing between different possible production routes.

The selection of the most attractive processing route is dependent on the number of solvents required as well as on product specifications. The latter point especially is often the determining factor.

Possible manufacturing processes

Originally hydrocarbon solvents were manufactured by redistillation of suitable fractions from selected crude oils. In this way products meeting the specifications valid at that time could be made, although the segregation of the feedstock was a heavy burden on overall refinery operation.

Over the past 10 years the aromatic content of hydrocarbon solvents has been receiving increasing attention. On the one hand the specification for benzene content was tightened in view of its toxic nature, while on the other hand individual users were setting specifications for total aromatic content in order to obtain sufficient solvent power for their particular application.

In order to comply with the new specifications, additional process steps capable of removing or converting the aromatics had to be added. Such a process should preferably also concentrate the aromatics. Processes applied for this purpose are: oleum treatment, adsorption, extraction and hydrogenation. Their merits will be briefly discussed:

Oleum treatment

Although this is one of the oldest processes it is still in use. Capital costs are usually low, while operating costs depend largely on the aromatic content of the feedstock. Very low aromatic contents can be obtained by using relatively large amounts of oleum.

A serious disadvantage of the process is the problem of disposal of the spent oleum; under the most favourable conditions the value of the spent oleum is

zero, but often high additional costs are involved. Moreover, the aromatics present in the feed are destroyed (with resultant low yield) and add to the extra costs for spent oleum disposal. Aromatics from an outside source are required for back-blending in order to meet product specifications.

Adsorption

Adsorption of the aromatics on silica gel or other suitable adsorbents is possible. The process, however, is normally operated in semi-batch, while high costs are involved in stripping the aromatics from the loaded adsorbent.

Operating costs are mainly dependent on the aromatic content of the starting material.

Extraction

Extraction processes are very suitable for aromatics removal from light distillate fractions. The use of high boiling solvents (e.g. sulfolane) has particular advantages, since in this case the operating costs are only marginally influenced by the quality of the starting material.

The aromatics can be obtained in a pure form and as such have a high value either as a gasoline component, as high aromatic solvent or as starting material for the manufacture of pure aromatics. As extraction is a continuous process it becomes more attractive when large capacities are required.

Hydrogenation

This process converts the aromatics into naphthenes, which sometimes are valuable components for hydrocarbon solvents, depending on their application. Suitable catalysts, usually containing a noble metal, are usually sulphur-sensitive, so a preceding hydrodesulphurisation step is required. However, in modern refineries this is carried out in any case (e.g. for catalytic reforming). Hydrogen requirements, directly coupled with the aromatic content of the feedstock, substantially contribute to the operating costs.

Very low aromatic contents can be obtained with this process, but an aromatic concentrate is not produced. Hydrogenation has the same advantage as the extraction process in that it becomes attractive when large capacities are required.

It is clear, therefore, that for large capacities only extraction and hydrogenation can be regarded as suitable processes for control of the aromatic content in the manufacture of hydrocarbon solvents. In the Royal Dutch/Shell Group sulfolane extraction is used in the manufacturing of hydrocarbon solvents.

The sulfolane extraction process

This process (Fig. 1)[1,2] was originally developed by the Royal Dutch/Shell Group for the manufacture of high-purity light aromatics, and this is still its major application.[3] It has been found, however, that it can be equally well applied to other uses. A short description of the process follows.

The starting material is contacted countercurrently with the solvent in an extractor (usually a rotating disc contactor). Nearly all the aromatics plus a part of the non-aromatics (the lighter ones) are dissolved in the solvent. The extract phase is withdrawn at the bottom of the extractor and fed to the extractive-stripping column. In this column the non-aromatics are removed by extractive distillation, together with part of the light aromatics. This stream is returned to the bottom of the extractor.

The bottom product of the extractive stripper, consisting of sulfolane and pure aromatics, is separated in the recovery column. This column operates at sub-atmospheric pressure and stripping steam is introduced at the bottom in order to facilitate the removal of hydrocarbons from the sulfolane, which is recycled to the extractor. The top product (aromatics), which contains only

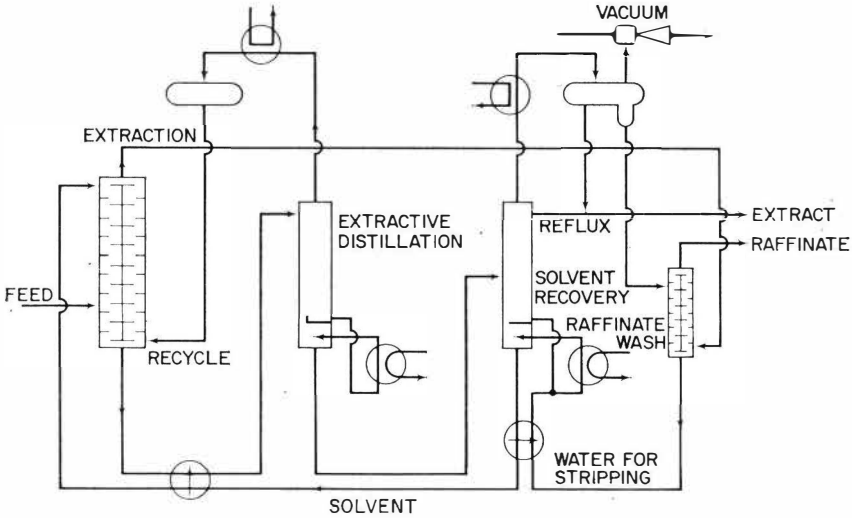

FIG. 1. *The sulfolane extraction process*

traces of sulfolane, can be fed to distillation equipment if so required, or used as such. If even the last traces of sulfolane have to be removed a once-through water wash can be applied. The raffinate obtained as top product of the extractor contains all the non-aromatics together with small amounts of aromatics. As this stream is saturated with sulfolane, water washing is necessary; for this step the water phase from the top of the recovery column is normally used.

The spent wash water is returned to the recovery column to serve again as stripping steam; at the same time the sulfolane dissolved in the water is recovered.

The washed raffinate, which normally contains 1–10 ppm sulfolane, can be fed to further processing equipment. Complete removal of sulfolane, if required, can be obtained by adding a once-through water wash step. The aromatic content of the raffinate can be easily controlled by changing the amount of solvent used in the extractor.

Extract purity is mainly governed by the operation of the extractive stripper; high purity can be obtained by operating with a high top product flow. Decreasing the amount of top product will decrease the purity of the extract. If only small amounts of aromatics have to be removed or extract purity required is low (e.g. 80–85% aromatics), a simplified scheme, consisting only of an extractor and a recovery column, can be used. If only light products (e.g. with boiling ranges of 50–90°C) with low aromatic contents have to be processed, it is sometimes advantageous to omit the extractor. The unit in this case is operated as an extractive distillation unit. Combinations of these three modes of operation are of course also possible, i.e. the unit is used as a full extraction unit for one type of feedstock while for other feedstocks either the extractor or the extractive stripper is by-passed.

Overall processing scheme

Originally hydrocarbon solvents were manufactured by redistillation of suitable light distillates. In this scheme all solvents were made directly as final products. Benzene and total aromatics contents of the product are in this case completely dependent on feedstock quality. However, when customers demanded special boiling ranges for their own specific use, the number of solvents to be prepared in this way increased rapidly, requiring not only a large

number of tanks but also a rather frequent change of operating conditions in the distillation units, with resultant production of off-specification products.

A better and more advantageous scheme is used nowadays. In this scheme a number of fractions of low aromatic content and of different narrow boiling ranges are prepared by distillation and these fractions, together with individual aromatics or high-purity aromatic fractions, can be blended to produce the final solvents. In this way the requirements of individual users can easily be met by changes in blending ratio only, while the number of tanks required is also greatly reduced and little or no change is required in the operation of the processing units.

Use of the extraction process

The sulfolane extraction step can be incorporated in the processing scheme at different points. Basically two possibilities exist, viz.:

Extraction of the feedstock

In this case suitable light distillates are fed to the extraction unit. The raffinate is separated into the required fractions, which can be used for blending of final products. If so required the extract can also be fractionated and part of the aromatics back-blended in order to meet specifications for minimum aromatic content.

The advantage of this scheme is that normally only one feed of constant quality has to be processed. Switch-overs and changes in operating conditions with resultant loss of production are not required.

However, a fuller extraction, especially of benzene, is often required so as to meet the specifications of the final product, since concentration of aromatics may occur in the following fractionation step. Moreover, if not all of the raffinate fractions can be included in the finished product, the extraction capacity required will be relatively large.

Extraction of intermediate products

In this case the base materials are first fractionated and part or all of these fractions fed to the extraction unit. The products of the extraction unit can be used as such for blending or fractionated again into narrow boiling range products.

In this case, better direct control of the aromatic content of the products is possible by selecting appropriate extraction conditions. Moreover, those fractions which do not require extraction can be used directly, thereby decreasing the required capacity of the extraction unit.

A drawback to this system is that a number of feedstocks have to be pro-

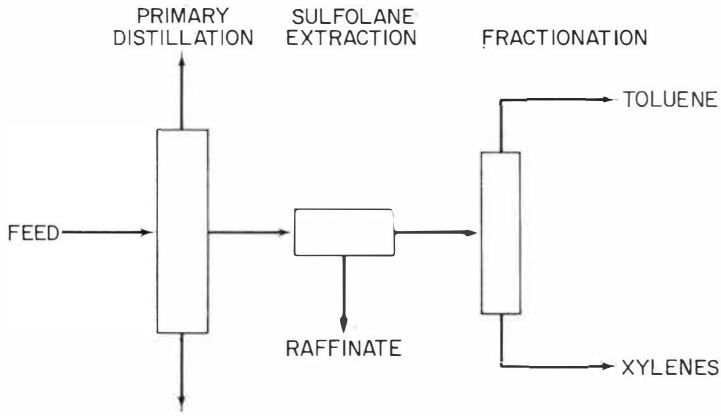

FIG. 2. *Extraction of feedstock to obtain toluene*

cessed in the extraction unit, necessitating repeated switching. A certain loss of production due to flushing of the extraction unit after each switch is in this case inevitable.

Which of the two schemes is the more attractive depends to a large extent on the finished product and specifications and on the feedstock. It is also possible to use both methods in one complex by changes in line-up of the different units. For example, in one complex for manufacturing hydrocarbon solvents nitration-grade toluene was also required. For the toluene operation the first method was used (Fig. 2) viz. the toluene heart cut was first extracted and the extract was fed to the fractionator to obtain the toluene as a top product. For the other operation on hydrocarbon solvents a suitable narrow boiling range fraction was prepared in the fractionator, and was sub-

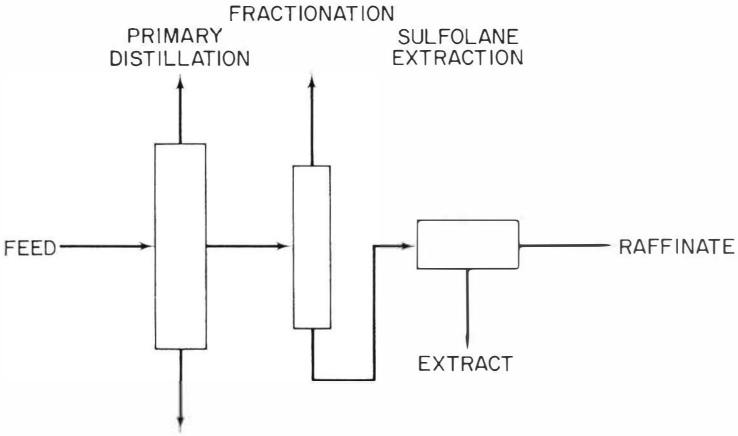

FIG. 3. *Extraction of intermediates to obtain raffinate for blending*

sequently extracted (Fig. 3). The raffinates in this case were used directly as blending components.

Both systems are in use in the Royal Dutch/Shell Group and have given satisfactory performance.

TABLE I

Extraction for manufacture of hydrocarbon solvents feedstock

	Feedstock A		Feedstock B	
	Design	Actual	Design	Actual
Feed				
benzene, %	1·0	0·2	0·5–1·0	0·07
total aromatics, %	3·0	1·1	12·5	9·2
ASTM boiling range, °C	70–95	70–100	85–160	81–163
Raffinate				
benzene, ppm	150	<10	150	<5
total aromatics, %	0·1	<0·01	0·3	0·2
sulfolane, ppm		<5		5·7
Extract				
total aromatics, %		55–60*	95	95
sulfolane, ppm		<5		<5

* As total amount of extract was small, no requirements as to purity were foreseen in the design

TABLE II

Extraction of light distillate fractions

	Feed A		Feed B		Feed C		Feed D	
	Design	Actual	Design	Actual	Design	Actual	Design	Actual
Feed								
ASTM dist., °C	110–145	110–145	100–140	100–140	40–90	30–100	60–90	60–90
total aromatics, % . .	77	76	12	10	0·8	1	0·8	0·7
Raffinate								
total aromatics, % . .	5–10	7	<1	<1	<0·1	0·08	<0·1	<0·01
Extract								
total aromatics, % . .	99·9	99·9*		>99		†		†

* For toluene manufacture (toluene recovery: 99·7%)

† No requirements for extract purity in view of small amounts of aromatics

Some typical results are given in Tables I and II. From these results it is evident that very low benzene contents can easily be obtained. Percentage removal of toluene and xylenes (which is always lower than for benzene) depends on the extraction conditions. If the final products have a specification for a minimum total aromatic content it is often not desirable to remove all the toluene and xylenes, as these have then to be added in the final blending. Fortunately the extraction process is so versatile that a certain flexibility can be obtained.

Application of the sulfolane extraction process

As described above the sulfolane extraction process[4,5] can be applied easily to the manufacture of SBP solvents, which normally have boiling ranges between 30 and 160°C. The process is, however, also suitable for the extraction of higher boiling fractions, viz.: (*a*) white spirits, boiling range 145–205°C. In this case an extract with an aromatic content of 95–99% can be obtained, and this can be used for the manufacture of solvents with a high aromatic content; (*b*) kerosols, kerosene-type solvents boiling in the range 160–300°C. Either a slight extraction for smoke point improvement or a full extraction in which virtually all the aromatics are removed can be applied with only a marginal difference in operating costs. Extract purity is normally 90% or higher, which is substantially higher than can be realised with, e.g., SO_2 extraction.

Economic comparison

The costs of sulfolane extraction and the costs of the hydrogenation route for the preparation of 125,000 ton/year of feedstock of low aromatics content for the manufacture of hydrocarbon solvents have been compared. It was found that for the starting material used (a Middle East distillate with 0·3% benzene and 2–3% toluene) the capital and operating costs were about the same, viz., capital costs approximately Nederland *fl.*2,500,000 and operating costs including capital charge about Nederland *fl.*10 per ton of low aromatic content product. The following assumptions have been made in preparing this cost estimate: (i) sufficient hydrogen available from other sources. (If this were not the case, costly hydrogen manufacturing facilities would be required, which would considerably increase the costs of the hydrogenation route); (ii) no extra desulphurisation of the starting material required to protect the catalyst; (iii) no extra value included for the extract from the sulfolane extraction process.

Normally the value of this extract is the same or is even higher than that of

the starting material when used as a blending component for motor gasoline or as starting material for aromatics production. This would reduce operating costs by Nederland *fl.*1·00 to 3·50/ton of low aromatic content product, depending on aromatic content of the starting material. The following points should, however, be taken into account:

Sulfolane extraction is more flexible. By back-blending of the raffinate (fractions) and the extract (fractions) a whole range of aromatic contents can be obtained. When hydrogenation is used, separate sources of aromatics are required.

When using starting material of higher aromatic content the operating costs of the hydrogenation process (hydrogen consumption) will rise quickly. Sulfolane extraction is less sensitive in this respect, since a larger solvent circulation, required to extract more aromatics, can be realised with only a minor increase in heat requirements.

Costs of the sulfolane extraction step can be reduced considerably when the manufacture of feedstock for hydrocarbon solvents is combined with aromatics manufacture. In this case two possibilities exist, viz.: (*a*) In the aromatics manufacture a fuller extraction than normally required is applied in order to make a raffinate which is suitable for solvent manufacture. Operating costs for this route are only slightly higher than for normal aromatics manufacture. (*b*) The raffinate of low aromatic content normally obtained in the aromatics production step is re-extracted with fresh solvent. In this case combinations of the different solvent streams are possible, which result in only marginal extra operating costs.

Conclusion

In the manufacture of hydrocarbon solvents an additional process step is required in order to meet present-day requirements on aromatic content. Commercial experience with sulfolane extraction has proved this process to be an excellent and versatile tool, with advantages over other processing routes.

References

[1] Deal, C. H., Evans, H. D., Oliver, E. D., & Papadopoulos, M. N., *Proc. 5th Wld Petrol. Congr., New York*, 1959, Section III, p. 283

[2] Voetter, H., & Kosters, W. C. G., *Proc. 6th Wld Petrol. Congr., Frankfurt*, 1963, Section III, p. 131

[3] Broughton, D. B., & Asselin, G. F., *Proc. 7th Wld Petrol. Congr., Mexico*, 1967, **IV**, 65

[4] Voetter, H., & Kosters, W. C. G., *Erdöl Kohle*, 1966, **19**, 267

[5] Kosters, W. C. G., *Erdöl Kohle*, 1970, **23**, 205

Preliminary study on the possibility of application of solvent extraction process for sulphur refining

by Susanto Imam Rahaju, M. S. Tupamahu, and Soelistijo*
Department of Chemistry, Institut Teknologi Bandung, Bandung, Indonesia

Investigations were carried out into the nature of sulphur deposits in the form of mud at Kawah Putih, West Java, Indonesia. Data are presented on the mineralogical and chemical composition, and conditions for its extraction, in particular with CS_2, are discussed.

Introduction

THE PRESENT WORK is a preliminary investigation into the possibility of using a solvent extraction method to purify sulphur from a low- and medium-grade sulphur mud. Although other methods of sulphur refining are known, the presence of sulphur deposits in the form of mud at the crater, Kawah Putih, West Java, Indonesia, presents an opportunity to examine the solvent extraction method. The object of this work was to study the state of the raw material, and to determine the optimum conditions for applying solvent extraction methods.

The sulphur deposits are of volcanic origin, and were apparently formed by the various oxidative and reductive processes involving water, air, hydrogen sulphide and sulphur dioxide;[1] the latter two substances are commonly found in volcanically-active regions. Sulphur was formed by direct aerial oxidation of H_2S:

$$2\ H_2S + O_2 \longrightarrow 2\ S + 2\ H_2O \qquad (1)$$

or by the reaction:

$$2\ H_2S + SO_2 \longrightarrow 3\ S + 2\ H_2O \qquad (2)$$

Reaction (2) also occurs in aqueous media but this involves some side reactions and the end products, in addition to free sulphur, also contain polythionic acids.

Free sulphur thus formed was deposited on the slopes of craters or fumaroles, or floated on the surface of crater lakes. Rain washed the deposits from the slopes into lakes or bottoms of craters, and, in the process, mixed them with clay and other minerals or decaying organic matter to form a mud. It is in this form that the present deposit is found.

Experimental

Mineralogical analysis

The mineral composition of the mud was determined by polarisation microscopy, as described by Milner[2] and Taggart.[3] Sieve analysis was carried out by wet-screening, using woven–wire screen and square hole perforated plate screen for precision testing (ASTM E11–39); standard size testing is ASA M5–1932.[4]

Chemical analysis[5]

Total sulphur was determined by total oxidation to sulphate and gravimetric determination as $BaSO_4$. Free sulphur was converted into thiosulphate by refluxing with sodium sulphate, and determined iodometrically.

The metal ion concentrations were determined spectrophotometrically, using a Beckmann model UV spectrophotometer: iron was determined with

* Mining and Metallurgy Research Center, Directorate of Mines, Bandung, Indonesia

o-phenanthrolene at 525 nm; aluminium with aluminon at 525 nm; titanium with hydrogen peroxide at 410 nm; manganese was converted to MnO_4^- and determined at 525 nm; and sulphate was determined by a turbidimetric method.

Physico-chemical properties

Sulphur was extracted from the mud mainly by Soxhlet extraction but with some pulping and filtering. Solubility of pure and raw sulphur were determined in a controlled thermostat, using a mechanical stirrer,[6] and allowing 30 minutes for complete solution.

Heat of solution of sulphur in carbon disulphide was determined calorimetrically by the standard method[7] using a Dewar flask, fitted with a small nickelin wire heater, stirrer and a Beckmann differential thermometer, as calorimeter.

Results

Results of sieve analysis are shown in Tables I and II.

TABLE I

Grain size distribution of sulphur mud

Mesh	%-Weight
+10	10·7
−10+100	19·8
−100+400	18·4
−400	51·1

TABLE II

Grain size distribution of the sulphur mud as the result of wet-screening

	Size testing I			Size testing II		
Mesh	Weight of fractions, g	%-Weight of fractions	% Cumulative weight of fractions	Weight of fractions, g	%-Weight of fractions	% Cumulative weight of fractions
+ 10	98·2	9·82	9·82	116·40	11·64	11·64
− 10+ 18	27·2	2·72	12·54	65·00	6·50	18·14
− 18+ 35	44·0	4·40	16·94	36·00	3·60	21·74
− 35+ 60	92·0	9·20	26·14	43·10	4·31	26·05
− 60+100	49·8	4·98	31·12	38·50	3·85	29·90
−100+140	83·1	8·31	39·43	85·00	8·50	38·40
−140+200	52·5	5·25	44·68	53·60	5·36	43·76
−200+270	26·6	2·66	47·34	21·20	2·12	45·88
−270+325	18·3	1·83	49·17	8·50	0·85	46·73
−325+400	13·2	1·32	50·49	5·70	0·57	47·30
−400	495·1	49·51	100·00	527·00	52·70	100·00
Total	1000·0	100·00		1000·00	100·00	

The results in Table III and Fig. 1 show that the free sulphur content of the mud depends on grain size.

TABLE III

Dependence of free sulphur content on grain size

Mesh	Sulphur content, %-Weight
−10	44·86
−10+100	55·36
−100+400	24·79
−400	48·83
−100	35·17

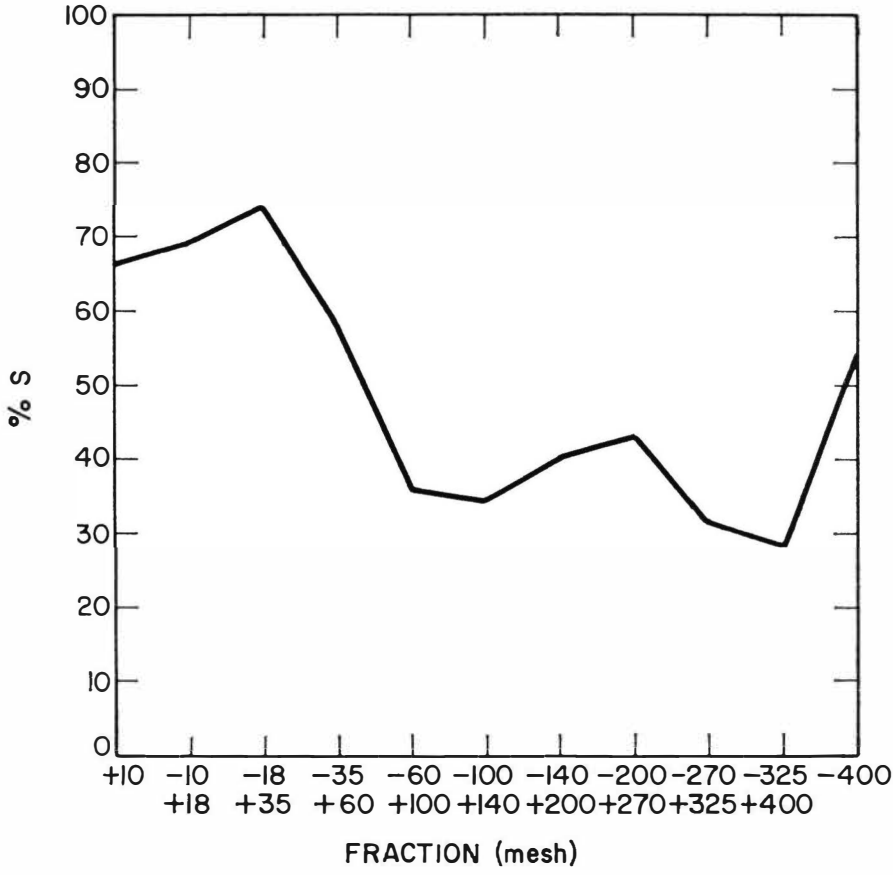

FIG. 1. *Sulphur distribution vs. fraction (mesh) of wet-screened sulphur mud*

The fractions of mud used for sieve analysis were shown, by microscopic analysis, to contain: light minerals, comprising sulphur particles, quartz and the feldspar group, as the major component of the mud; and heavy minerals, comprising: ilmenite, magnetite, leucoxene, zircon, anatase, pyrite, tourmaline, hornblende, rutile, monazite, biotite and the pyroxene group.

Samples not subjected to sieve analysis were found to contain water-soluble minerals belonging to the sulphate and silicate groups as well as degradation products of organic materials (Table IV).

TABLE IV

*Mineralogical composition of the sulphur mud of − 60 + 100 and − 100 + 325 mesh fractions**

Minerals	% Composition −100+325 mesh	−60+100 mesh
Light minerals:		
Uncoated sulphur (S)	40·3	62·7
Coated sulphur (S)	47·1	37·1
Quartz (SiO_2)	11·3	0·0
Feldspar group (K, Na, Al, Ca silicate)	1·2	0·0
Heavy minerals:	0·1	0·2
Ilmenite ($FeO.TiO_2$)	(+)	(+)
Magnetite (Fe_3O_4)	(+)	(+)
Leucoxene (TiO_2)	(+)	(+)
Zircon ($ZrSiO_4$)	(+)	(+)
Anatase (TiO_2)	(+)	(+)
Tourmaline (Na $Fe_3B_3Al_3$ $(Al_3Si_6O_{27})$ $(OH)_4$)	(+)	(+)
Hornblende $\{Ca_2(Mg.Fe.Al)_5(OH)_2\ [(Si\ Al)_4O_{11}]_2\}$	(+)	(+)
Monazite $(Ce,La,Dy,Th)_2O_3.P_2O_5$	(+)	(+)
Pyroxene group ($MgSiO_3$)	(+)	(+)
Pyrite (FeS_2)	0·0	(+)
Biotite ($K_2O_4(Fe,Mg)0{\cdot}2(Al,Fe)_2O_3.6SiO_2.H_2O$)	0·0	(+)
Rutile (TiO_2)	(+)	0·0

* Observed at the Laboratory of Mineralogy, Directorate of Geology, Bandung, 1970

Sulphur particles were present in various states: without coating materials (anisotropic); completely coated (isotropic); and partially coated. The coating materials are either transparent, or subtransparent (Fig. 2). The transparent material consists of silica groups (opal), whereas the subtransparent materials are insoluble silicates (e.g., feldspar group) and soluble silicates or sulphates. The thickness of coating materials of the − 60 + 325 mesh fraction was estimated, by the ASTM Designation A 219–58 microscopic method, and found to be 7–12 nm.

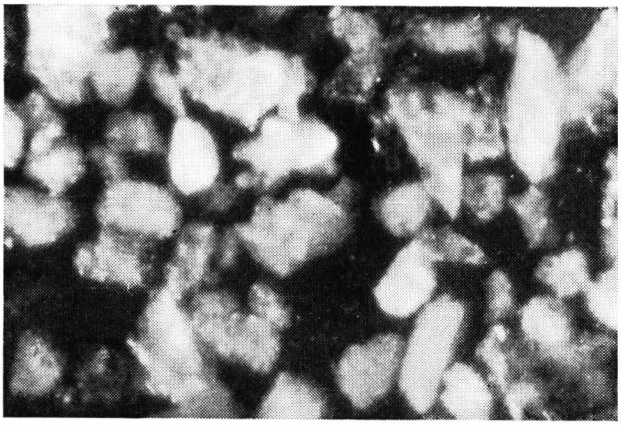

FIG. 2. *Coating materials on the sulphur particles in sulphur mud* (−60+325 *mesh*)
Magnification: 100×

The results of chemical analysis of the mud as a whole are shown in Table V.

TABLE V

Chemical analysis of major components of sulphur mud

Component	%-Wt.
Total sulphur	51·90
Free sulphur	49·50
SiO_2	32·96
Al_2O_3	1·59
TiO_2	0·45
Fe_2O_3	0·75

The solubility of pure sulphur in several solvents systems at 30°C, namely: CS_2–benzene, CS_2–toluene and CS_2–CCl_4 are given in Fig. 3.

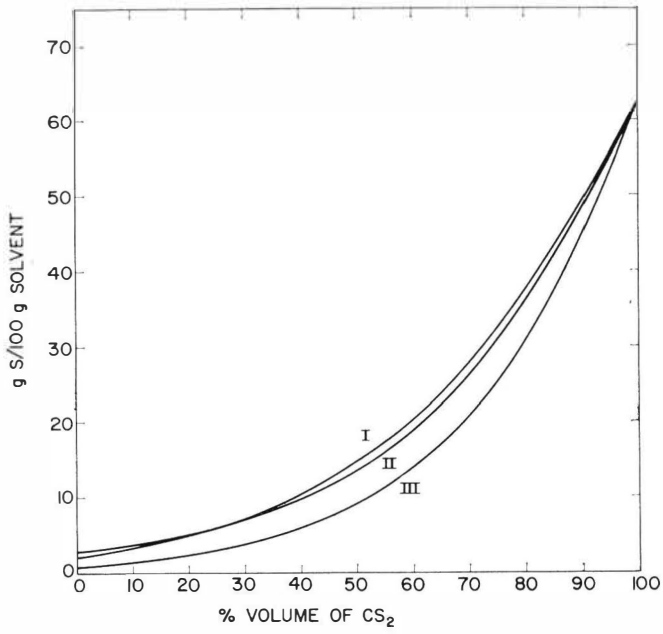

FIG. 3. *Solibility curves of sulphur in solvent systems* (I) *CS_2–benzene,* (II) *CS_2–toluene and* (III) *CS_2–CCl_4 at* 30°C

The integral heat of solution of pure sulphur in carbon disulphide at 27°C is shown in Fig. 4.

The result can be expressed by:

$$\Delta H = 26{\cdot}6\, C$$

where ΔH is the integral heat of solution (cal) and C is concentration (g S/100g CS_2).

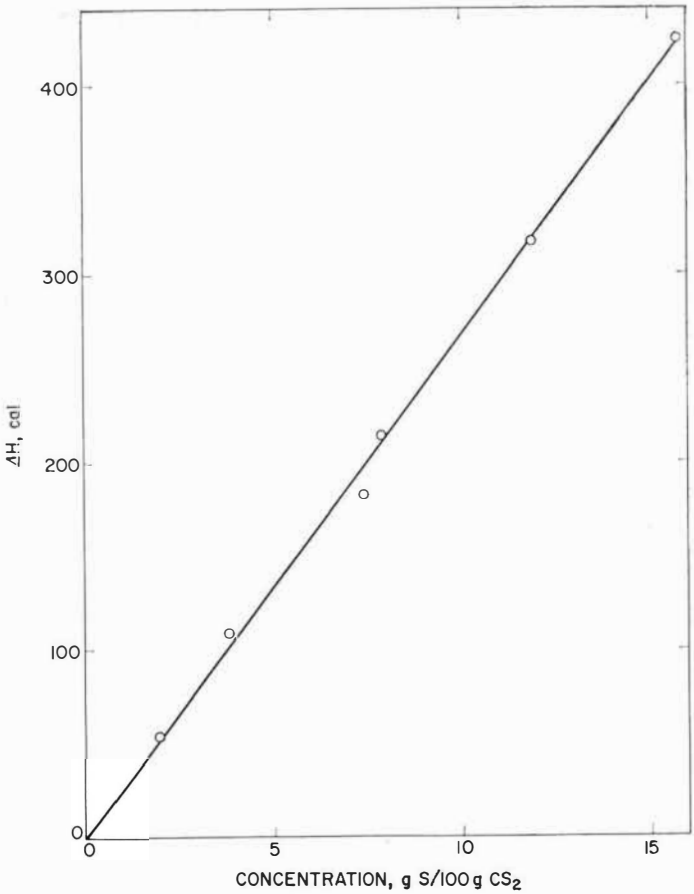

FIG. 4. *Integral heat of solution* (ΔH) *vs. concentration of sulphur in* CS_2 *at* 27°C

Discussion

The choice of carbon disulphide in the investigation of solvent extraction of sulphur from mud is based on the excellent solubility of sulphur in this solvent (Fig. 5).

Sulphur can be recovered from the extract by evaporation of the solvent or by partial crystallisation. As some organic matter might also have dissolved in the organic solvent, complete evaporation will result in contamination of the sulphur, and so partial crystallisation might be the better method.

In this case, the choice of solvent should be such that it has a large temperature gradient, and a low solubility at low temperatures. This may be achieved by using a mixed solvent, e.g., CS_2–benzene, where the temperature dependence will lie between that of CS_2 and benzene in Fig. 5. Further work on solvent combination is in progress.

The presence of coating materials on a part of the sulphur particles poses further problems in that depending on the nature of the coating material, it could prevent direct contact between solvent and sulphur and, therefore, decrease the rate of solution during extraction. This decrease in rate depends primarily on whether the particles are completely or partially coated, and on the porosity of the coating. Further investigation is necessary into the removal of this thin coating material.

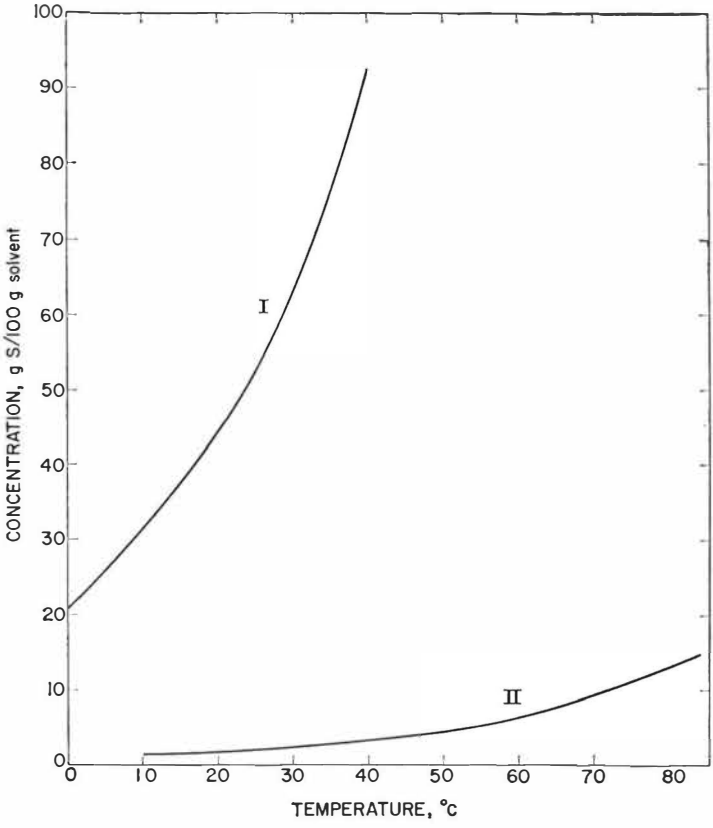

FIG. 5. *Solubility of sulphur in CS_2 and in benzene*
I CS_2; II benzene

Acknowledgment

This research was made possible through an affiliation between the Mining & Metallurgy Research Centre, Directorate of Mines, Ministry of Mines of the Republic of Indonesia, and the Department of Chemistry, Institut Teknologi Bandung, Indonesia.

References

[1] Sergeyev, V. P., & Afanasiev, N. A., 'Technological Tests of the Sulphurous Ores from the Republic of Indonesia', 1965 (Moscow–Liubertsy: GIGHS)

[2] Milner, H. B., 'Sedimentation Petrography', 1940, 3rd Edn, pp. 82–94; 31–40 (London: Thomas Murby & Co.)

[3] Taggart, A. F., 'Handbook of Mineral Dressing', 1956, Sect. 19, pp. 72–85 (New York: John Wiley & Son)

[4] *Idem, ibid.*, Sect. 19, pp. 99–109

[5] Meetes, L., Ed. 'Handbook of Analytical Chemistry', 1963 (New York: McGraw-Hill)

[6] Partington, J. R., 'Textbook of Inorganic Chemistry', 1957, 6th Edn, pp. 68–69 (London: Macmillan)

[7] Findlay, A., & Kitchener, J. R., 'Practical Physical Chemistry', 1954, 8th Edn, p. 190 (London: Longmans Green & Co.)

Status of developments in liquid–liquid extraction in the petroleum industry

by A. Winward
University of Newcastle-upon-Tyne, Newcastle-upon-Tyne, U.K.

Recently published information on new solvent systems is reviewed. Data on solvent systems are difficult to compare in view of wide differences in feedstock quality. Depending on the process duty, about 4–15 theoretical stages of separation appear to cover optimum conditions. Increasing use is being made of developments in extraction equipment. Solvent recovery methods and integration of the extraction process with other refinery operations are key features of recent developments. Displacement solvents are being more extensively used to improve separation efficiency and solvent recovery and attention is being paid to the reduction of foaming and emulsification tendencies.

While liquid – liquid extraction will continue to be used on a very large scale, its relative lack of selectivity for sulphur compounds and somewhat lower product yields may favour the installation of hydrotreating units when new plant is required for fuels and lubricants. Also, for high purity petrochemical feedstocks the further development of highly selective solvent systems, with improvements in extraction equipment, will be needed to compete successfully with other separation processes.

Introduction

THE OBJECT OF this paper is to review published information on recent developments in the application of liquid–liquid extraction for petroleum products and petrochemical feedstocks. This special attention appears well justified since the petroleum industry uses extraction processes on a scale which is greatly in excess of other process industries. Also, despite the longevity of some established processes for more conventional petroleum products, these processes have been continually improved because of economic pressures and internal competition within the industry. A wide variety of new solvent systems is also being studied to match new product requirements.

Most of the developments referred to in this paper deal with extraction operations which depend on physically selective solvents. Many of the refining finishing operations which depend on chemical action, i.e. dissociative extraction, have been well established for some years and are well documented. Examples of these are hydrogen sulphide removal, mercaptan extraction, recovery of diolefins with cuprous salts, and sulphonation.

General background

It is well known that the first (~ 1909) important commercial application for liquid–liquid extraction in Europe was the Edeleanu process, using sulphur dioxide – a highly selective solvent for aromatic hydrocarbons.[1] By 1936, 180,000 barrels/day of distillate feedstocks were being treated for kerosene production. Also, in the 1930s, other solvents were in extensive use for lubricant production and these included furfural, phenol and cresol. Compared with sulphur dioxide these solvents had more suitable solvency and selectivity properties for the high molecular weight cyclic hydrocarbons present in heavier and waxier feedstocks. However, the use of benzene to modify the selectivity of sulphur dioxide, i.e. a mixed solvent system, was used to a smaller extent for distillates. The mixed solvent system (propane–cresylic acid, phenol) was also being used in the 'Duosol' process for heavy distillates and residua.

Despite the changes in yield/pattern required from crude petroleum over the years (including a reduced vol.% of burning kerosene) the petroleum industry still uses extraction solvents on a tremendous scale – probably over 600,000 barrels/day of hydrocarbon feedstock capacity. It is of interest that

although some solvents used commercially for lubricant production have fallen into disuse (e.g. aniline, nitrobenzene) the solvents furfural, phenol and Duosol are still in use with improved processes. Latest figures on U.S. solvent refining capacity indicate about 100,000 barrels/day lubricant feedstocks each for furfural and phenol and about 30,000 barrels/day for Duosol solvent.

Liquid–liquid extraction became well suited for the petroleum industry, not only because of its intrinsic merit of separating heat-sensitive materials more according to hydrocarbon type rather than molecular weight, but also because of the commercial value of wide-boiling range products, moderately enriched in either aliphatic hydrocarbons or aromatics. Also, extraction conditions could often be readily adjusted to changes in the crude source of the distillate feedstock.

With the development of catalytic reforming, steam cracking and hydrodealkylation processes for octane improvement and unsaturated gases, the petroleum industry created for itself a big capacity for producing aromatic concentrates in the C_6–C_{10} range. This paralleled the recent upsurge in demand (greater than 25% per year in most industrial countries) for benzene, toluene, xylene isomers and naphthalene as chemical feedstocks. It can also be stated that this growth in 'aromatic' capacity coincided with drastic changes in the pattern of the gas industry; these changes resulted in a reduced capacity for light aromatic hydrocarbon production because of factors relating to natural gas and steel production.

With the help of liquid–liquid extraction the petroleum industry is meeting the challenge so that petroleum is becoming the major source of naphthalene as well as of benzene, toluene and xylenes. These aromatics are feedstocks for petrochemicals including styrene, maleic anhydride, linear alkylbenzenes, phthalic anhydride, terephthalic and isophthalic acids and caprolactam.

Recent developments

Solvent systems

Table I covers the recently published developments on extraction solvents for petroleum and petrochemical feedstocks.[2–60] Feedstocks vary considerably in molecular weight range and volatility, and include unsaturated C_4 hydrocarbons and petroleum tars, derived from cracking operations, as well as straight-run distillates. Main products include olefins, high purity C_6, C_7 and C_8 aromatics as solvent extracts and, also, paraffinic raffinates for diesel fuel, improved cracking feedstocks and lube oils.

TABLE I

Developments in extraction solvents[a] for petroleum products and petrochemicals

Single solvent systems[b]

Solvent	Feedstock	Main products	References
Dimethyl formamide (DMF)	Catalytic cycle oil (204–316°c, b.p.)	Alkyl naphthalenes aliphatic-rich stream	2, 3
Dimethyl formamide	C_4 hydrocarbons	Butadiene	4
β-Methoxyproprionitrile (β-MOPN)	C_4 hydrocarbons	Butadiene	29
Dimethyl formamide (diethyl formamide)	Urea adducts (2·6% aromatics impurities)	Paraffins (240–360°c, b.p.)	5, 51
Nitromethane	Catalytic naphtha	Diesel fuel and aromatics (94% pure)	6
Sulphur dioxide	Straight run distillates	Burning kerosenes	7
Furfural	Process gas oils	Carbon black feed, and cat. cracking feed	8
	Coker distillates	Carbon black feed	9
	Vacuum distillates	Lube oil blend stocks	10
		Polycyclic aromatics	11

Solvent	Feedstock	Main products	References
Phenol	Distillates	Lube oil blend stocks	10, 12
	Vacuum distillate	Polycyclic aromatics	11
Sulpholane	Naphthas	C_5–C_8 aromatics	13, 14, 15, 16, 17, 18, 19, 30
Dimethyl sulphoxide	Naphthas	C_6–C_8 aromatics	20, 21
Ammonia	De-aromatised naphthas, process naphthas heavy distillates	Olefinic rich extracts Aromatics, Paraffinic raffinates	22
Methyl carbamate (Carmex)	Hydrogenated process naphthas	C_6–C_8 aromatics	23
Substituted phospholanes	Hydrocarbon mixtures	Aromatics	24
N-Hydroxyethylpropylene-diamine	Hydrocarbon mixtures	Aromatics	25
Glycols: dipropylene diethylene triethylene tetraethylene	Heavy naphtha catalytic reformate urea adducts cracked gasoline	C_6–C_8 aromatics and n-paraffins	5, 15, 26, 27, 28
		C_6–C_8 aromatics	29, 31, 32
Mixed xylenes[c]	Carboxylic acid salt mixtures	e.g. 5-t-butyl-isopthalic acid	33
N-*Methyl-2-pyrrolidone (NMP)*	Heavy distillate	Lube oil stocks	34, 35, 36
	Naphtha	High purity aromatics (C_6, C_7, C_8)	37
	C_4 streams	Butadiene	38, 39
ω-Methoxyalkylpyrrolidine	—	Aromatics	40
Fluorinated hydrocarbons and alkanols	Test hydrocarbon mixtures	—	41
Hydrogen fluoride	Petroleum tars	Naphthalene	42, 43
1,3-Dicyanobutane (methyl glutaronitrile)	Naphtha	Aromatics, unsaturates	29, 44
Mixed solvent systems[d]			
Phenol and ethyl alcohol	Petroleum residues	Lube stocks	45
Diglycolamine and NMP, monoethanolamine and NMP, glycerol and NMP	Mixed hydrocarbons	C_6–C_8 aromatics	46, 47
Furfural, furfural alcohol, water	Cycle oil	Heavy aromatics	48
Furfural and C_6–C_{10} monoketones	Lube oil feed	Lube oil	49, 50
Furfural and alcohols	Lube oil feed	Lube oil	52
N-Alkylpyrrolidine, urea (or thiourea), water	Hydrocarbon mixture	Aromatics	53
Hydrotropic salt solutions (e.g. sodium aryl sulphonates)	Hydrocarbon mixtures	Paraffins and aromatics	54
ε-caprolactam and water	Hydrocarbon mixtures	Paraffins and aromatics	55
Alkyl carbamates and water	Hydrocarbon mixtures	C_6–C_7 aromatics	56
Carbamate, thiocarbamate esters and water	Steam-cracked naphtha	C_6–C_7 aromatics	57
Hydrogen fluoride and boron trifluoride	Mixed xylenes C_6–C_9	*p*-and *o*-xylene, *m*-xylene (extract)	58, 59
Dual solvent system			
Dimethyl formamide (or amide) + glycerol (hydroxy compound) for re-extraction of extract	Hydrocarbon oil	Paraffinic and aromatic oil	60

[a] Solvents known to be used commercially are italicised

[b] This definition does not exclude use of minor proportions of water as 'anti-solvent'

[c] Dissociative extraction

[d] Term excludes displacement solvents (see text)

Improved process schemes, using sulphur dioxide, furfural and phenol solvents, are now available for the commercial separation of high purity aromatics from petroleum reformates as well as for the production of kerosene and lubes; plants for these latter products tend to have a smaller number of theoretical stages. Table I also shows that other selective solvents now in use commercially for aromatics production are sulpholane (tetramethylene sulphone), aqueous glycols, *N*-methylpyrrolidone (NMP), dimethyl sulphoxide, dimethylformamide (DMF) and methyl carbamate. NMP and DMF liquid solvents are also being used for the selective separation of gases such as C_4 hydrocarbons[38, 39] or ethylene recovery from ethylene–acetylene mixtures.[61] (Strictly speaking, this is liquid–gas extraction.)

Interesting, and relatively new, solvent systems developed for treating petroleum fractions include ammonia and hydrogen fluoride. The former solvent can be used for recovery of aromatics and also unsaturates, depending on the nature of the feedstock. Fenske[22] has pointed out the commercial potential of ammonia for making chemicals and solvents as well as fuels and lubricants. Hydrogen fluoride is proposed[42, 43] for extraction of naphthalene from tar, and, in combination with boron trifluoride, is the mixed, 'complexing' solvent used in a commercial process for the production of pure xylenes.[58, 59]

Comparative data

Despite these developments there are still considerable gaps in published information on the effect of operating variables, even for a single solvent system. Also, the comparison of data on the effectiveness of various solvent systems is often difficult because of different conditions in the contactor arising from water injection, temperature gradients, back-mixing and the feedstock itself. Any overall comparison of solvent systems for a particular product would need to include an assessment of power requirements and other factors affecting operating cost, such as selectivity, size of equipment needed and the preferred method for solvent recovery.

However, some interesting data on glycol solvent systems are reported; in particular, the benefits to be gained by the careful selection of solvent properties have been well illustrated by recent experiences of the Sun Oil Company. These show that big savings have been achieved by changing the solvent in a UDEX aromatic extraction plant.[62, 32] Unit throughput and aromatics recovery were raised by about 10%, following a change from the mixed dipropylene glycol–diethylene glycol solvent to the higher molecular weight solvent, tetraethylene glycol. More detailed pilot-plant data on aromatics extraction with aqueous glycols are given by Somekh & Friedlander.[31] These show a two-fold increase in extraction capacity by replacing diethylene glycol–8% water solvent with triethylene glycol–5% water. Also, a further doubling of capacity has been obtained by replacing the latter solvent with tetraethylene glycol–3·9% water. Hoover[32] has also reported that no antifoamant is needed with the latter solvent and this probably reflects previous separation difficulties. Useful data, of more general application, have also been obtained by Russian workers on the solubility of aromatic hydrocarbons and the relative extractability of bicyclic and monocyclic aromatics with triethylene glycol. These data may be useful for naphthalene extraction processes.

Process data, in terms of product purity and yield, solvent and utility consumptions, have also been reported for the methyl carbamate process. This process was developed originally for the separation of aromatics from hydrogenated steam-cracked naphtha.[23] For a specific hydrocarbon feedstock, containing only a small proportion of aromatics, work by Ledyashova[5] shows that DMF is more effective than triethylene glycol for de-aromatisation. For the extraction of aromatic hydrocarbons from a gas condensate Muradov and co-workers rate DMF somewhat higher than ethylene chlorohydrin.[63] The selectivity of DMF improves more rapidly with an increase in water content. Quittzch and co-workers at Leipzig have continued to accumulate thermo-

dynamic data on binary liquid mixtures, including DMF; these data could be useful for the prediction of partly miscible systems used in the liquid extraction of aromatics from catalytic reformates. Vapour–liquid equilibria, activity coefficients and excess enthalpies are included in data available on n-heptane–formamide binaries.[51]

Using ammonia as solvent, the effects of operating variables on product yields and purities are reported by Fenske.[22] The variables, covered in extensive pilot-plant work include thermal gradients, water as antisolvent and various alkylamines as pro-solvents for the system methylcyclohexane–n-heptane and ammonia. Two other selective solvents have recently been highly rated;[29] these are 1,3-dicyanobutane for light aromatic extraction and β-methoxypropionitrile (β-MOPN) for butadiene extraction plants. The former solvent has a higher capacity than sulpholane, a lower melting point (thus avoiding the need for steam tracing) and a higher thermal stability. This allows stripping operations at higher pressures. Also, a minor advantage is that the absence of water (contrasted with many commercial solvents) means less heat requirement. From pilot-plant data β-MOPN compares favourably with furfural and replacement of the latter solvent would require very little adaptation of existing plant.

Among solvents with single hydroxyl groups, nitropropanols appear to be the most selective of various alcohols for aromatic extraction. Laboratory data obtained by Diyarov[64] confirm that selectivity decreases with increasing length of hydrocarbon chain (in the solvent). Binary and ternary solubility data are also available on benzene–n-hexane–sulpholane model systems. Nechaeva *et al.*[65] conclude that, in particular, 3-methoxy sulpholane should be evaluated further for commercial use.

A general study on fluoro-hydrocarbons, which are moderately selective extraction solvents, has been carried out at Pennsylvania State University.[41] Critical solution temperature for four fluorinated solvents, with various hydrocarbons, are tabulated. The solubility relationships of partly fluorinated and perfluorinated hydrocarbons with paraffins, olefins, naphthenes, aromatics and polynuclear aromatics have been examined. A useful study on nitromethane as an extraction solvent for aromatics from light catalytic gas oil has also been carried out.[6] This shows that nitromethane appears to be preferable to furfural as an extraction agent because of its relatively low tendency to emulsification. The value of a lower molecular weight displacement solvent, e.g. isoctane, which can be combined with nitromethane, is emphasised. This combination enables the production of almost 100% aromatics extract against about 94% purity for nitromethane alone (conditions are six stages of countercurrent extraction at 45°C with solvent ratios in the range 0·6 to 2·4:1).

Ram[54] has reported that a solvent extraction process for hydrocarbon mixtures based on hydrotropic solutions of sodium xylene sulphonate and sodium cymene sulphonate look economically and technically feasible. Solubility data on aromatics have been obtained and a useful equation derived for predicting solubilities; this is applicable to four component systems.

The extraction of napthalenes from middle distillates (200–350°C, b.pt.) is of increased interest and an interesting comparative study made by Riad *et al.*[66] gives data on the selectivity of a range of solvents (furfural, phenol, anilines, morpholine and *p*-cresol). The solvents were tested at 50 and 90°C, well below the critical solution temperatures of the various mixtures, and the benefits gained by water saturation of solvents, i.e. better selectivity, are confirmed. Useful supplementary information has also been reported by Klimenok[67] on temperature effects on solvent capacity and selectivity for the system docosane–diphenylhexane and furfural. For high purity aromatic extracts the importance of small concentrations of water and high solvent: charge stock ratios has also been demonstrated by Shcherbina *et al.*[20] Their laboratory data show that dimethyl sulphoxide is outstanding for extraction of benzene from mixtures with cyclohexane or n-hexane.

Rather inconclusive data comparing aqueous phenol with anhydrous furfural extraction of light lube oil feedstock have been obtained by Rudenko *et al.*[10, 55] Both solvents yield oils of comparable quality although furfural may give a higher yield. A study of the extraction of polycyclic aromatics from catalytic gas oil for carbon black manufacture also enables some comparison between furfural and phenol solvents.[68] Furfural was more selective than phenol in the extraction of aromatic polycyclics but the dissolving power of phenol was slightly higher. In view of the similarity of these solvents (widely used commercially) other factors would affect the choice.

Other interesting data which apply to the treatment of petroleum residua have been obtained by Mitrofanov;[68] these enable a comparison between dual solvent extraction (the original Duosol process) and separate phenol extraction, after propane de-asphalting. The Duosol process appears more selective than the two-stage treatments with a smaller loss of useful oil components.

Some work has also been carried out on ethyl alcohol as a component of a mixed solvent system. Ivankma[45] and co-workers have shown its value, compared with various other components, for improving the selectivity of aqueous phenol for refining petroleum residues. Operating conditions of the plant for phenol refining, with the addition of ethyl alcohol, are tabulated. A Russian study on the value of various alcohols as a component in the furfural treatment of lubricating oil has also been made.[52]

Shell patent data, relating to lubricating oil fractions, show advantages for a mixed solvent, i.e. furfural and di-isobutylketone. At the same temperature, much less of the mixed solvent is required than for furfural alone.[50]

Integrated processes

In petroleum refining, liquid–liquid extraction has always been a relatively expensive process – solvent recovery being a costly item. However, more recently, by integration with the other processes, new technology has been developed which has enabled substantial savings in equipment, operating costs and site area requirements. Heat integration, in particular, can result in the recovery of heat that would otherwise be wasted.[69] Often, good flow-sheet design practice will mean a smaller number of furnaces and compressors.

A good example of combination plant is the ESI integrated lube plant at Augusta, in Sicily, which has operated for the last 5 years. A key feature of the plant is a phenol 'hot belt'. Heat, from the condensation of phenol used for lube oil extraction, is conveyed to the de-asphalting and dewaxing units for vaporising the propane solvent. As a result, operating costs are reduced and the furnaces needed for the liquid extraction plant can provide all the heat needed for the entire lube oil production unit.

Another example of a combination plant uses aqueous dimethyl formamide solvent[2] in a new dual column extraction process called Redex. This produces a heavy aromatic concentrate (95–100%) containing alkyl naphthalenes, and a diesel fuel raffinate. Significant cost savings are claimed over the conventional one column extraction process; a unique feature of the Redex process is the use of a light displacer oil containing both aromatics and paraffinics (e.g. xylene and naphtha). Good data on the effect of operating conditions on the two-product yield and quality are reported.

The use of a light boiling hydrocarbon fraction as a counter-solvent for the recovery of high purity aromatics using aqueous *N*-methylpyrrolidone is described in a patent by Eisenlohr & Wirth.[37] Combination of solvent extraction and extractive distillation is also mentioned.[69] Other examples of combination processing aimed at reducing product losses and improving purity are described in recent patents.[17, 18, 35] A scheme[8] for solvent extraction of two hydrocarbon fractions using furfural should enable the low cost production of two products, i.e. catalytic cracking feed and carbon black feed. Raffinates are combined in a dual-step process and the extract from the first step is used as the solvent in the second step. Also, a combination process of liquid

extraction and reforming is described in a U.O.P. patent[71] in which aromatics are produced by recovery from extracts which are obtained from solvent extraction of the feedstock followed by reforming the raffinate, and solvent extraction of the reformate.

Product and solvent losses

Plant experience from the petroleum industry teaches that counter-current treatment towers can lose design efficiency and give unexpected product and solvent losses. These problems are often associated with haze formation, emulsification and foaming. These effects are not necessarily due to the provision of inadequate settling zones, but are often caused by contamination from solvent[72] or feedstock deterioration. Much attention has therefore been paid to the removal of impurities. The general use of adsorbent treatment for solvent is described[70] and, more specifically, filtration is indicated for sulpholane after distillation of aromatics therefrom and after dilution with water or toluene.[15] A U.O.P. patent[71] describes the recovery of sulpholane-type solvents from raffinate streams by activated carbon below 125°F. The carbon is periodically back-flushed with an aromatic hydrocarbon stream to desorb the solvent. Similarly, a Shell patent outlines the use of silica gel for purification of the raffinate phase or extract.[73] While basic substances may be effective in preventing deterioration of sulpholane, it is claimed that this solvent itself is a good additive for minimising deposit problems during sulphur dioxide extraction.[74]

An interesting patent of Philips Petroleum[75] describes a method of removal of emulsion accumulating at the interface of each contacting zone. This emulsion is removed by entrainment with a light liquid flowing at a high velocity through a conduit of a small uniform diameter.

Azeotroping may be a method for reducing solvent loss[23] from the raffinate stream. Another possible method is re-extraction with a paraffinic fraction having a different boiling range[55] than the raffinate, extract or solvent.

Solvent selectivity for sulphur compounds

In solvent extraction processes for the petroleum industry the distribution of organic sulphur compounds effected by different solvents is of continual interest. In general, the sulphur compounds tend to concentrate in solvent extracts and this has proved quite beneficial when using sulphur dioxide for the preparation of high quality burning oils (raffinates). In addition, some basic work by Hanson *et al.*[76] suggests that a thiophene removal step could be incorporated into the sulfolane process after separating aromatics from aliphatics.

However, for many hydrocarbon products the high content of sulphur compounds in the feedstock, coupled with the relatively poor selectivity of solvents for these sulphur compounds, indicates that a preliminary hydrogenation process would be necessary to reduce sulphur content before extraction.[33] Detailed studies have, in fact, been carried out by Pecka *et al.*[14] on the use of sulfolane for the removal of sulphurous compounds from lighter petroleum fractions. Distribution coefficients of sulphurous compounds with sulphur dioxide and other solvents are low and, in general, solvents have a low extraction capability for these compounds. For example, sulfolane is a solvent with rather low efficiency and selectivity for the extraction of mercaptans – the most polar type of sulphur-containing hydrocarbon. Being acidic they can, of course, be removed by chemical means; this includes several stages of dissociative solvent extraction, with alkali and secondary solvent (e.g. the Solutizer Process).

Extraction equipment

The petroleum industry has, traditionally, relied on vertical counter-current column contactors for liquid–liquid extraction. These include packed and different forms of perforated plate columns and also the mechanically agitated

rotating disc contactor. Over the years many improvements in designs of plate and packed columns have been patented. An interesting recent example[77] refers to the refining of lube oil stocks with phenol and an X-shaped contacting device. Column section efficiency rates at 30–35% compared with 10–12% for ceramic rings or sieve plate trays.

There have also been improvements to mechanically agitated columns for refinery operation claimed to reduce back-mixing effects, thus increasing the advantage which these contactors have over plate and packed columns in terms of compactness. More recently, following the first application for antibiotics, several makes of vertical and horizontal multistage centrifugal extractors have found fairly wide use in petroleum liquid–liquid extraction operations. While many of these applications (as for agitated columns) are for chemical finishing treatments, several papers[78–81] have appeared which cover the successful commercial application of large-scale centrifugal units for phenol and furfural extraction of lube oils and cycle stocks.

Discussion

In making an assessment of recent progress in liquid–liquid extraction in the petroleum industry, there are several general points which emerge from the published information. The operation is needed for many more products than in the past, ranging from low molecular weight olefins for polymerisation to heavy polycyclic aromatics for carbon black manufacture. A main development emphasis has been on the production of high purity aromatic hydrocarbons.

With regard to solvent systems, a wide range of mixed and single solvents are being studied, for example, dimethylformamide and *N*-methyl-2-pyrrolidone which are both being used commercially and, also, 1,3-dicyanobutane. Important factors in the selection of a solvent include feedstock quality and the level of product quality which it is desired to achieve. For example, DMF and sulphur dioxide may be especially suitable for high purity n-paraffins from a feedstock with a low% of aromatics; however, for an aromatic-rich feedstock a solvent system with modified phase-temperature relationships is needed for the production of high purity aromatic hydrocarbons. For these reasons and because of the many molecular species involved, it is understandable that there are considerable gaps in information on the relative performance of different solvent systems. More data on solubility relationships have become available which are of direct value, e.g. Fenske's work on ammonia-based solvents and Russian work on the extraction of bicyclic aromatics. Also, Humphrey & Winkle have derived some empirical equations for the prediction of solvent capacity and selectivity.[82] These equations relate to the extraction of mixtures of alkanes, alkenes, cycloalkenes and aromatics by some substituted aliphatic solvents. However, existing extraction parameters are not satisfactory with hydrogen bond-forming solvents.

While not covered in this review, it will be apparent from other papers that results from basic studies on factors relating mass transfer with hydrodynamics cannot yet be applied directly to mixed solvents and feedstocks of commercial interest. The design of a liquid–liquid extraction process still depends on laboratory and pilot-plant data. Experimental measurements for the calculation of the number of equilibrium stages in a process design has been reviewed by Gester.[83] In particular, well-designed laboratory mixer-settler units such as the AKUFVE, or the Fenske stacked stage extractor, are invaluable in extending knowledge of solvency and selectivity characteristics, including the effect of temperature and possible solvent modifiers for internal reflux control.

A wider range of contacting equipment is now in use in the petroleum industry; improvements have been made in plate and packed columns and the more compact mechanically agitated columns and multistage centrifugal extractors are being used to a greater degree. Published information suggests that over the years the number of theoretical stages used in practice for extrac-

tion of distillate fuel and lubricant feedstocks has increased from about 4 to 7, primarily to reduce solvent requirements, while for the commercial production of petrochemical feedstocks, 6–15 contacting stages are used – more because of the higher degree of product quality which is needed.

Process design for liquid–liquid extraction within the industry shows considerable ingenuity by way of integration with other processes. There is also greater use of displacement solvents to aid separation efficiency and solvent recovery. The Redex dual column extraction process, using a light displaced oil containing both an aromatic hydrocarbon and a paraffin, is a particular example.

Future developments

Liquid–liquid extraction will undoubtedly continue to be an important separation tool for the petroleum industry. Further useful refinements will be made to process design; these will follow from work on improved solvent systems, the development of improved contactors, integration with other processes and control procedures arising from a more basic understanding of the factors affecting mass transfer. There are some restrictions, however, which are beginning to operate against further applications, e.g. the lack of selectivity towards sulphur compounds. Indeed, hydrogenation processes for lube oils as well as distillates are becoming more acceptable alternatives for de-aromatisation as well as desulphurisation. For these broad cut feedstocks the hydrogenation route can show a greater product yield.

For pure petrochemical feedstocks production, competing processes are becoming more successful – for example, azeotropic distillation for aromatics and molecular sieves for n-paraffins. However, the further development of highly selective solvent systems, with improvements in control and extractor equipment, may have a significant effect on this trend.

References

[1] Edeleanu, A., *Instn Petrol. Technol.* 1932, **18**, 898
[2] Benham, A. L., Plummer, M. A., & Robinson, K. W., *Hydrocarb. Process. Petrol. Refin.*, 1967, **46**, (9), 134
[3] Marathon Oil, U.S. P. 3,415,743; Fr. P. 1,424,225
[4] *Chem. Wkly*, 1968, **103**, (5), 34
[5] Ledyashover, G. E., & Bairbuskaya, E. L., *Khimiya Tekhnol. Topl. Masel*, 1968, **13**, (4), 21
[6] Bondarenko, M. F., Kolychev, V. M., & Rudnova, O. N., *Khimiya Tekhnol. Topl. Masel*, 1967, **12**, (8), 27
[7] Black, C., & Harting, G. M., *Chem. Engng Prog.*, 1968, **64**, 66, 77
[8] Cities Service Oil Co., U.S. P. 3,349,028
[9] Andreevu, A. S., *et al.*, *Khimiya Tekhnol. Topl. Masel*, 1968, **13**, (4), 24
[10] Rudenko, N. D., *et al.*, *Nefteperab. Neftekhim.*, 1969, **4**, 12
[11] Andreeva, A. S., *et al.*, *Khimiya Tekhnol. Topl. Masel*, 1969, **14**, (9), 22
[12] Nesterov, P. M., *et al.*, *Khimiya Tekhnol. Topl. Masel*, 1967, **12**, (10), 44
[13] Kosters, W. C., *Erdöl Kohle*, 1970, **23**, 205; *Chemy Ind.*, 1968, p. 1177
[14] Pecka, K., *et al.*, *Chem. Abstr.*, 1967, **67**, 13469
[15] U.O.P. Co., U.S. P. 3,385,783; 3,385,784; 3,398,083
[16] U.O.P. Co., U.S. P. 3,433,735
[17] U.O.P. Co., U.S. P. 3,466,344–6
[18] U.O.P. Co., U.S. P., 3,468,792–3
[19] *Eur. Chem. News*, 1969, **16**, 406
[20] Scherbina, E. I., *et al.*, *Izv. Vyssh. ucheb. Zaved. Neft Gaz*, 1969, **12**, 69
[21] Raimbault, C., *et al.*, *Erdöl Kohle*, 1968, **21**, (5), 275
[22] Barton, P., McCormick, R. H., & Fenske, M. R., *Ind. Engng Chem. Process Des. Dev.*, 1968, No. 713, 366
[23] *Chim. Ind. Génie Chim.*, 1968, **99**, 926
[24] Shell Oil Co., U.S. P. 3,345,287
[25] Koppers G.m.b.H., Ger. P. 1,275,039
[26] Dow Chemical, Ger. P. 1,252,647
[27] Ismailov, P., *et al.*, *Izv. vyssh. ucheb. Zaved. Neft Gaz*, 1968, **11**, 43
[28] U.O.P. Co., U.S. P. 3,436,435
[29] *Oil Gas J.*, 1969, **67** (42), 86
[30] Broughton, D. B., & Asselm, G. F., *Proc. 7th Wld Petrol. Congr.*, 1967, **4**, 65
[31] Somekhand, G. S., & Friedlader, B. I., *Am. Chem. Soc. Div. Petrol. Chem.Prepr.*, 1969, **14**, D179
[32] Hoover, T. S., *Hydrocarb. Process Petrol. Refin.*, 1969, **48**, (12), 131

[33] Chevron Research Co., *Petro/Chem. Engr*, 1968 (July), **40**, 61
[34] Texaco Development, U.S. P. 3,472,757
[35] Texaco Inc., U.S. P. 3,476,681
[36] Texaco Inc., U.S. P. 3,476,680
[37] Metallgesellschaft A.G., U.S. P. 3,433,849
[38] Klein, H., & Weitz, H. M., *Hydrocarb. Process. Petrol. Refin.*, 1968, **47** (11), 135
[39] Morrison, J., *Oil Gas, J.*, 1968, **66**, (39), 102
[40] B.A.S.F., Belg. P. 694,131
[41] Hughes, J. R., Thesis, Penn. State Univ., 1966
[42] Plyusnin, V. G., *et al.*, *Chem. Abstr.*, 1967, **67**, 13546r
[43] Esso Research and Engineering Co., B. P. 1,135,293
[44] Feldman, J., *Am. chem. Soc. Div. Petrol. Chem. Prepr.*, 1969, **14**, D179
[45] Ivankina, E. B., *et al.*, *Chem. Abstr.*, 1967, **67**, 13454p
[46] Metalgesellschaft A.-G., U.S. P. 3,415,739–42
[47] Mueller, E., & Hoefield, G., *Proc. 7th Wld Petrol. Congr.*, 1967, **4**, 13
[48] Marathon Oil Co., Fr. P. 1,424,226
[49] Shell Int. Research, S. Afr. P. 66/6571
[50] Shell Oil Co, U.S. P. 3,449,462
[51] Quittzch, K., *et al.*, *Z. phys. Chem.*, 1969, **240**, 107
[52] Murshudli, C. D., & Volokh, S. M., *Izv. vyssh. ucheb. Zaved. Neft Gaz*, 1968, **11**, (12), 52
[53] B.A.S.F., Ger. P. 1,275,038
[54] Ram, M. J., *Diss. Abstr.*, 1967, **28**, 163B
[55] Ministerial Petrolului, Neth. P. Appln., 67/16597
[56] Vishynyakova, T. P., *et al.*, *Khimiya Tekhnol. Topl. Masel*, 1968, **13**, (11), 13
[57] Entreprise Minière et Chimique, Fr. P. 1,556,765
[58] Japan Gas-Chemical Co. Ltd. (Process), *Chem. Wkly*, 1968, **103**, (11), 79
[59] Japan Gas-Chemical Co. Inc., Belg. P. 724,148
[60] B. P. 1,125,177
[61] Sugai, K., *Sekiya Gakkai Sh.*, 1970, **13**, 37
[62] *Chem. Engng*, 1969, **76**, (16), 66
[63] Maradov, T., *Nefteperab. Neftekhim.*, 1969, **5**,
[64] Dijarov, I. N., *et al.*, *Khimiya Tekhnol. Topl. Masel*, 1969, **14**, (7), 21
[65] Nechaeva, M. A., *et al.*, *Neftekhimiya*, 1969, **9**, 784
[66] Riad, M. A., *et. al.*, *J. Inst. Petrol.*, 1969, **55**, 168
[67] Klimenok, B. V., *Khimiya Tekhnol. Topl. Masel*, 1969, **14**, (3), 3
[68] Mitrofanov, M. G., *et al.*, *Khimiya Tekhnol. Topl. Masel*, 1969, **14**, (8), 13
[69] Hydrocarbon Research Inc., U.S. P. 3,291,728
[70] Universal Oil Products Co., Neth. P. Appln., 67/04862
[71] Universal Oil Products Co., U.S. P. 3,470,087
[72] Shell International, Ger. P. 1,270,569
[73] Shell International, Belg. P. 713,854
[74] Phillips Petroleum Co., U.S. P. 3,474,030
[75] Phillips Petroleum Co., U.S. P. 3,356,459
[76] Hanson, C., *et al.*, *J. appl. Chem.*, *Lond.*, 1969, **19**, 320
[77] Maksimenko, V., *et al.*, *Khimiya Tekhnol. Topl. Masel*, 1968, **13**, (12), 34
[78] Fox, J. M., *Hydrocarb. Process. Petrol. Refin.*, 1963, (Sept.), 2
[79] Cox, R. P., & Atteridge, P. T., *ibid.*, 1960, (March), 17
[80] Tears, C. F., *Oil Gas J.*, 1963, (June 15), 34
[81] Ishigaki, S., & Kaiser, H. R., *Petro/Chem Engr*, May 1963
[82] Humphrey, J. L., & van Winble, M., *Ind. Engng Chem.*, 1968, (Oct.), 581
[83] Gester, J. A., *Chem. Engng. Prog.*, 1966, **62**, (Sept.) 62

SESSION 3A

COALESCENCE

CHAIRMAN

Prof. R. C. Kintner

SECRETARIES

Dr. Ir. C. A. P. Bakker

Dr. S. Hartland

Coalescence of liquid droplets–correlation of coalescence times

by G. A. Davies, G. V. Jeffreys* and D. V. Smith

Department of Chemical Engineering, University of Manchester Institute of Science and Technology, U.K.

Investigations of the coalescence of liquid droplets have been carried out and factors affecting film drainage are discussed. Although this provides a better understanding of the mechanisms involved, insufficient data on overall coalescence times are available to allow correlation in terms of the system parameters. This is necessary if data on coalescence are to be used for the important problems associated with the separation of liquid dispersions. Data for a wide range of binary liquid systems are presented together with a developed correlation which can be used to predict overall coalescence times.

Introduction

MUCH WORK HAS been carried out to elucidate the mechanism of coalescence of a drop at a phase boundary. In all cases experimenters have observed that in a given system, in the absence of mass transfer to or from the dispersed phase and keeping all conditions apparently constant, there is no unique value for the drainage time, i.e. the time the drop resides at the phase boundary prior to rupture of the film of continuous phase separating the drop from the bulk coalesced phase. A distribution is always obtained about some mean value and workers have found that in order to obtain a reproducible average value for the drainage time measurements must be made for a number of drops. A qualitative explanation for this was first put forward by Gillespie & Rideal.[1] The minimum number of measurements specified by various workers has varied and is undoubtedly influenced by the design of equipment, experimental method and method of preparation of the liquid phases used. For example, Gillespie & Rideal found it necessary to measure the coalescence times of between 100 and 200 drops whereas Hawksley & Jeffreys[2] in an improved all-glass apparatus measured only 70–100 drops; more recently Hodgson & Lee[3] in a smaller apparatus were able to obtain reproducible results from 30 measurements. As techniques have improved in using all-glass equipment and, in particular, in providing efficient methods for removing contamination at the interface between the phase reproducibility in results has improved.

However, it is likely that some variation in coalescence time (for single step coalescence time and drainage time can be considered interchangeable since in practical systems transfer of liquid from the drop to bulk phase after film rupture is very much less than the drainage time) between drops is inevitable since it has been demonstrated that drainage of the intervening film of continuous phase between drops and interface is not uniform across the drop.[4] In many instances the drop appears to tilt about the vertical mid-axis resulting in asymmetrical rupture of the film. No regular pattern is observed.

Notwithstanding these difficulties it would be helpful in assessing the coalescence times of particular systems if some method of correlating the mean coalescence time was available. This would be especially useful if coalescence times of single drops could be related to the separation of dispersions when such information could be used to estimate residence times required in equipment to obtain phase separation. The purpose of the present paper is to report results on coalescence and separation times and to propose correlations for mean coalescence time in terms of the system properties. Such an approach was first reported by Jeffreys & Hawksley[2] who considered that the coalescence time was a function of drop diameter, φ, densities and interfacial tension of the phases,

* Department of Chemical Engineering, University of Aston in Birmingham, U.K.

viscosity of the continuous phase, distance of fall or rise of the drop to the interface and temperature. They carried out a dimensional analysis and estimated the significance of the parameters and exponents by factorial experimentation. The resulting correlation for the 'half-life' rest time $t_{\frac{1}{2}}$ was:

$$t_{\frac{1}{2}} = K\left[\left\{\frac{\mu_c^{0\cdot5}\,\Delta\rho^{1\cdot2}}{\gamma^2}\right\}\left\{\frac{T}{25}\right\}^{-0\cdot7}\mu_c^{0\cdot5}\left\{\frac{\varphi}{2}\right\}^{0\cdot02}\left\{\frac{\gamma^2}{\mu_c}\right\}^{0\cdot55}L^{0\cdot001}\left\{\frac{\gamma^2}{\mu_c}\right\}^{0\cdot5}\right]^{0\cdot91} \quad (1)$$

Jeffreys & Lawson[5] later simplified the analysis, by restricting their investigation, by stating that temperature affected the physical properties only so that temperature as such need not be considered as a variable. The resulting correlation became:

$$\left[\frac{\bar{\tau}^1\gamma}{\mu\varphi}\right] = 1\cdot32 \times 10^5\left\{\frac{L}{\varphi}\right\}^{0\cdot18}\left\{\frac{\varphi^2\Delta\rho g}{\gamma}\right\}^{0\cdot32} \quad . \quad . \quad . \quad . \quad . \quad (2)$$

This work was restricted to a relatively narrow range of physical properties. Furthermore, if such data are to be used in assessing separation rates of dispersions then information is required on drop/drop coalescence. It has been established that separation of primary droplet dispersions is accomplished by coalescence of droplets with the phase boundary by drop/interface mechanism and drop/drop coalescence within the dispersion.[6,7] To investigate this and provide improved correlations measurements of coalescence times were carried out.

Experimental

Two types of apparatus were used. Following previous workers, an all-glass cell was first used to measure coalescence times but as this work was part of a larger programme to investigate coalescence in and separation of droplet dispersions, measurements of coalescence time were repeated in a column apparatus. This was particularly useful since it allowed coalescence rates in groups of drops at an interface to be measured and also, since the distance of fall (or rise) of drops to the interface was an order of magnitude greater than that in the simple glass cell, it allowed this effect to be more accurately determined than in previous experiments.

Glass coalescence cell

This was based on the design originally used by Hawksley[7] and later improved by Smith.[8] It was somewhat smaller than the former models and supply lines to the cell were shortened and kept to a minimum. There can be little doubt that the size and complexity of many of the cells that have been used, in particular the many glass joints and long transfer lines, has been a hindrance to the attainment of high levels of purity. The cell (Fig. 1) measured 5 cm dia. and the internal volume was approximately 500 ml. Four connexions were made through the walls of the cell to supply dispersed phase to the drop forming assembly and interface, to introduce the continuous phase and a drain to remove any contaminated phase after flushing of the interface.

The drop-forming assembly consisted of a long tube passing through the top of the cell to which a nozzle was connected at the lower end. A set of interchangeable nozzles was made by sealing to standard sockets short lengths of capillary tube which were ground flat at the ends to obtain reproducible drop sizes. To ensure that drops formed from the inner surface of the capillary tubing rather than the outer edge the nozzles were made non-wetting by the dispersed phase.* When using aqueous phase dispersed this was achieved by treating the glass with a silicone de-wetting agent.

In order to adjust the distance of fall of the drop to the interface it was necessary to vary the position of the complete nozzle assembly relative to the

* A solution of dimethyldichlorosilane in carbon tetrachloride was used. After forming a film of this solution on the nozzles they were heated to 200°C for 3 h.

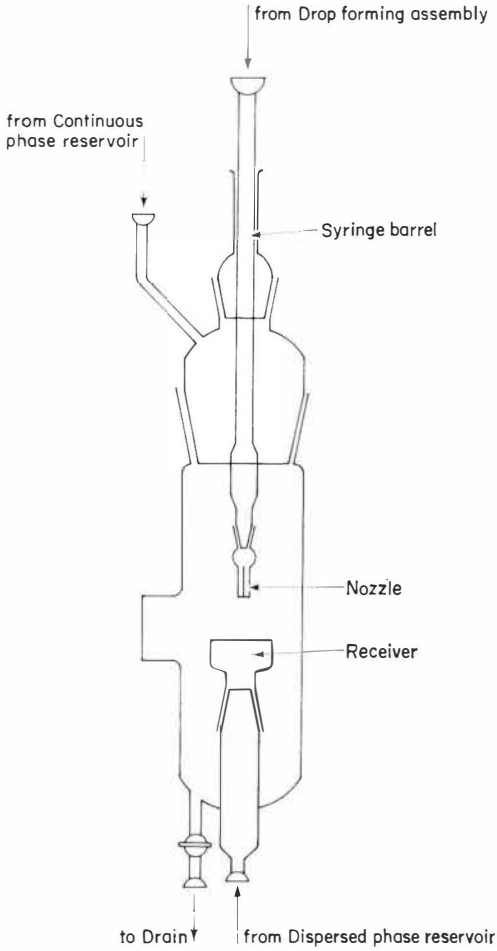

FIG. 1. *Diagram of coalescence cell*

cell. This was achieved by using part of a 10 ml syringe to form a liquid-tight sliding seal. The plunger was incorporated into the tube supplying the dispersed phase to the nozzle. The outer barrel was joined to the top of the cell by a standard joint. The interface was formed at the ground rim of a receiver or cup in the lower part of the cell. The apparatus was assembled on a rigid framework that was bolted to an external wall of the building via vibration pads in order to prevent vibrations reaching the interface. The cell itself was then immersed in a large thermostated water bath and the complete apparatus was surrounded by a thermostated air bath. At steady operating conditions the variation in the water bath was $< \pm 0{\cdot}05$°C while the variation in the air cabinet was of the order $\pm 0{\cdot}1$°C.

Column apparatus

A diagram of the column apparatus is shown in Fig. 2. A glass column (2 in dia. × 24 in long) was used.

The column was filled with the liquid phases. The phase boundary could be positioned at any point in the column and controlled by continuously removing the coalesced phase via a lute to a reservoir. Drops were formed either by using a perforated distributor, as shown in Fig. 2, or by using an all-glass apparatus fed by gravity from a reservoir similar in design to that used in the glass cell.

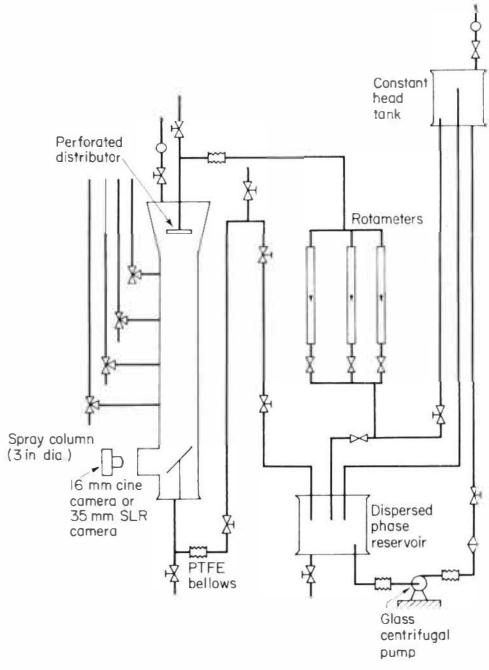

FIG. 2. *Diagram of column apparatus*

Again it was necessary to have both the distributor plates and glass nozzles non-wetted by the dispersed phase. Distributors were made of either Teflon or stainless steel depending on whether the dispersed phase was the water or organic phase. The hole size, pitch and thickness of these plates were carefully chosen to minimise the variation in size of the droplets and prevent 'bridging'.[9] When using the distributors to form drops in the column a continuous recycle system was used. Dispersed phase was continuously circulated, using a glass centrifugal pump, from a reservoir to a constant head tank. Liquid was fed from the constant head tank under gravity to the distributor. The flow rate was controlled using a glass–Teflon needle valve and measured by rotameters or for very low flow rates by metering the flow from the column using a burette included in the outlet line. The column was fitted with 4 off-take lines spaced at equal intervals between the distributor and end section. These were used to flush the interface between the two liquid phases in the column. At the outlet end of the cell a tee junction was fitted. Into this was fitted a stainless-steel mirror inclined at 45°. The tee was sealed with an optical flat. This arrangement was used to view the phase boundary between the liquids. Photographs were taken (35 mm still and 16 mm movie), using background illumination provided by a projector, of droplets coalescing at the phase boundary. The apparatus was mounted on a rigid framework, the pump being isolated from the rest of the apparatus to reduce vibrations. All flow lines tanks etc., were made of glass, the only other materials used being Teflon and stainless steel. The whole apparatus was enclosed in an air bath.

This apparatus was primarily designed to study the separation of droplet dispersion bands.[10] In this work it was observed that the nature of the wall of the column, i.e. whether it was wetted or non-wetted by the dispersed phase, influenced the separation rate. Thus as part of the programme of work on single drops and groups of drops different wall conditions (making the phase boundary either concave or convex) was investigated. This was done by coating the column with a silicone surface as discussed earlier. After treatment part of this surface was removed by immersing the column to the required

position in a concentrated hot alcoholic solution of potassium hydroxide. This gave a very sharp transition in surface of the column. All the equipment was carefully cleaned by degreasing with acetone followed by acid cleaning, washing in distilled water and drying before use. The column was cleaned in this way before surface treatment.

Selection of phases

The systems used in this work were chosen to cover a wide range of physical properties (viscosities, interfacial tension, density difference). It was important also that they should have a reasonably high flashpoint, low toxicity and could be easily purified, and did not undergo chemical reaction. In all the systems used water was used as one phase. A further restriction was that the refractive indices of the organic phase should be suitable to allow photographs to be taken. In some systems the formation of secondary hazes was especially troublesome from this point of view. A list of phases used is shown in Table I. The phases were carefully purified by distillation before use; A.R. grade was used wherever possible. After purification the physical properties of each phase were checked before equilibrating at the operating temperature. The viscosities, interfacial tension and densities of the mutually saturated phases were then measured using an Oswald viscometer, drop-weight volume method[11] and pyknometer, respectively.

TABLE I

Physical properties of mutually saturated phases at 25°C

No.	System	Aqueous phase		Organic phase		Interfacial tension, dynes/cm
		Density, gm/cm³	Viscosity, cP	Density, gm/cm³	Viscosity, cP	
1.	Diethyl carbonate–water	0·9995	1·06	0·9756	0·821	13·1
2.	Methyl isobutyl ketone–water	0·9949	1·25	0·8114	0·623	9·93
3.	Cyclohexane–water	0·9984	1·35	0·9512	2·28	3·75
4.	Amyl alcohol–water	0·9922	1·15	0·8254	4·21	4·88
5.	Anisole–water	0·9982	1·00	0·9941	1·09	16·1
6.	Iso-octane–water	0·9981	1·02	0·6916	0·509	50·17
7.	70% Dibutyl phthalate 30% kerosene–water	0·9996	1·30	0·970	14·0	30·0
8.	Kerosene–water	0·9982	1·01	0·7880	1·93	52·5

Results and discussion

Coalescence of single drops

Coalescence times were measured in the cell and in the column apparatus. These were compared and in this way the effect of distance of fall and relative purity could be assessed. In the cell, despite the use of a careful technique that placed emphasis on maintaining the phases in a high state of purity, on the exclusion of disturbances and on the measurement of the rest times of a large number of drops (~ 100) the reproducibility of the mean single drop coalescence times was disappointing. Sample results for the systems studied showing the mean coalescence time and standard deviation are shown in Table II. In each case the form of the distribution was examined and following previous workers the application of an equation of the form:

$$\ln\left(\frac{N}{N_0}\right) = kt^n \qquad (3)$$

was investigated. Results are included in Table II where the values of k and n calculated from the experimental results are tabulated. The correlation coefficients would indicate that an equation of this form can be used. The constant k does not have any physical significance apart from being the value of

TABLE II

Single drop coalescence times

System	Apparatus	Volume of drop, ml	Mean coalescence time, sec	Standard deviation, sec	K Equation (3)	n Equation (3)	Regression coefficient	$t_{\frac{1}{2}}$
Water–diethyl carbonate	cell	0·0899	4·55	2·17	$6{\cdot}0 \times 10^{-2}$	1·83	0·991	3·68
	cell	0·0490	8·71	3·33	$4{\cdot}0 \times 10^{-2}$	2·55	0·996	8·05
	col.	0·204	11·01	4·41	$1{\cdot}8 \times 10^{-2}$	1·60	0·914	9·59
	col.	0·112	2·21	1·28	$9{\cdot}14 \times 10^{-2}$	2·66	0·844	2·14
	col.	0·107	2·58	0·26	$1{\cdot}46 \times 10^{-2}$	1·49	0·976	2·55
	cell	0·090	5·45	1·27	$5{\cdot}92 \times 10^{-3}$	2·88	2·859	5·23
	cell	0·094	3·24	2·16	$2{\cdot}72 \times 10^{-1}$	1·14	0·950	2·28
	col.	0·203	6·04	5·22	$8{\cdot}12 \times 10^{-2}$	1·38	0·949	4·74
	col.	0·275	5·54	4·33	$1{\cdot}85 \times 10^{-1}$	1·05	0·988	3·54
Water–methyl isobutyl ketone	col.	0·038	1·88	0·85	$3{\cdot}5 \times 10^{-1}$	1·70	0·973	1·49
	col.	0·026	2·67	1·38	$6{\cdot}0 \times 10^{-1}$	0·78	0·966	1·20
	col.	0·011	4·23	1·78	$5{\cdot}0 \times 10^{-2}$	2·12	0·998	3·57
	col.	0·020	4·19	2·24	$1{\cdot}5 \times 10^{-1}$	1·29	0·944	3·26
	col.	0·0043	2·97	1·42	$1{\cdot}3 \times 10^{-1}$	1·78	0·989	2·57
	col.	0·0052	0·62	0·07	$5{\cdot}5 \times 10^{-2}$	1·84	0·993	0·58
	cell	0·021	1·05	0·31	$5{\cdot}9 \times 10^{-1}$	2·38	0·949	1·04
	cell	0·090	1·27	0·75	$9{\cdot}2 \times 10^{-1}$	0·95	0·956	0·74
Water–cyclohexanone	col.	0·0306	8·01	3·71	$3{\cdot}03 \times 10^{-3}$	2·68	0·969	7·59
	cell	0·0952	3·42	1·90	$9{\cdot}68 \times 10^{-2}$	1·87	0·988	2·89
	col.	0·0152	12·26	5·39	$7{\cdot}69 \times 10^{-3}$	1·87	0·971	11·09
	cell	0·0111	2·58	1·09	$1{\cdot}24 \times 10^{-1}$	2·02	0·955	2·34
Water–amyl alcohol	col.	0·023	2·13	0·36	$2{\cdot}0 \times 10^{-1}$	3·89	0·992	2·09
	col.	0·0136	1·18	0·12	$1{\cdot}2 \times 10^{-1}$	5·81	0·982	1·16
	col.	0·0105	1·03	0·12	$5{\cdot}2 \times 10^{-1}$	4·72	0·885	1·03
	col.	0·0059	0·91	0·06	$2{\cdot}3 \times 10$	5·65	0·940	0·90
Water–anisole	cell	0·441	29·20					
	cell	0·398	20·47					
	col.	0·50	12·50	1·83	$1{\cdot}37 \times 10^{-5}$	4·24	0·829	12·88
	col.	0·243	12·37	2·75	$1{\cdot}16 \times 10^{-4}$	3·43	0·958	12·60
	col.	0·40	28·77	4·82	$6{\cdot}0 \times 10^{-6}$	5·24	0·986	28·40
Water–iso-octane	All coalescence times measured < 1 sec							
Water–kerosene	cell	0·336	10·17	4·16	$2{\cdot}0 \times 10^{-1}$	2·49	1·984	9·53
	cell	0·12	5·89	3·00	$1{\cdot}1 \times 10^{-1}$	1·28	0·989	4·34
	cell	0·038	2·95	1·32	$1{\cdot}0 \times 10^{-1}$	2·08	0·998	2·55

In (N/N_0) at $t = 1$. The exponent n, however, is a measure of the slope of the cumulative coalescence time curve and may be thus expected to be inversely proportional to the standard deviation. This trend is evident in Fig. 3, although much of the data is concentrated in the region bounded by $n = 1$ and $n = 3$. However, it is evident that the value of $n = 4$ proposed by Hawksley does not fit the data.

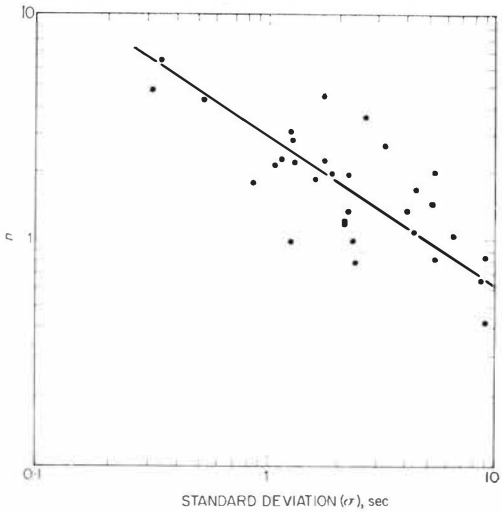

FIG. 3. *Standard deviation vs. exponent* n

Results for single drop coalescence times

An attempt was made to relate the mean coalescence times obtained to the system properties (despite the rather poor reproducibility obtained). Considering the factors interfacial tension, density difference, viscosities and drop size as influencing coalescence an equation of the form:

$$\frac{\bar{\tau}^1\gamma}{\varphi\mu_c} = K\left[\frac{\varphi^2\Delta\rho g}{\gamma}\right]^a\left[\frac{\mu_c}{\mu_d}\right]^b \qquad (4)$$

can be obtained. Computed in this way a regression analysis of the data yielded:

$$\frac{\bar{\tau}^1\gamma}{\varphi\mu_c} = 6{\cdot}2 \times 10^3\left[\frac{\varphi^2\Delta\rho g}{\gamma}\right]^{-1{\cdot}14}\left[\frac{\mu_c}{\mu_d}\right] \qquad (5)$$

The scatter about Equation (5) is high as illustrated in Fig. 4. The results are presented, however, to illustrate that there was no significant difference between the results obtained in the cell and column where the conditions could not be so rigidly controlled and where the level of contamination was probably higher. A further difference between the results was that the distance of fall in the column was approximately 10 times greater than in the cell. Thus the combined effects of contamination and distance of fall in these experiments are less than the variation caused by other (unaccountable) sources.

During these experiments observations of partial coalescence were recorded and the number of stages in the partial coalescence series was noted. These are shown in Table III. Three types of behaviour were observed: (i) a tendency for drops that coalesced immediately ($\bar{\tau} < 1$ sec) to coalesce in a single stage,[1] (ii) in partial coalescence after the coalescence of the original drop the second drop formed had a longer rest time than either the original drop or any of the succeeding stages; and (iii) sometimes the partial coalescence series branched, i.e. the coalescence of the original drop produced two secondary drops (one large

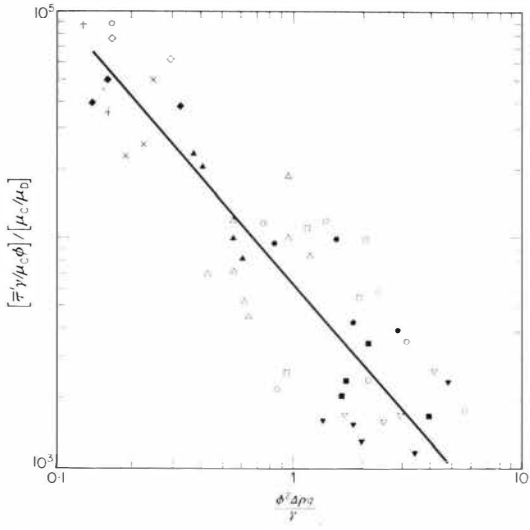

FIG. 4. *Correlation of results for single drop coalescence times*

System	Column	Cell
1	△	▲
2	○	●
3	□	■
4	▽	▼
5	+	×
8	◇	♦

and one small) that then coalesced separately. These are noted in Table III. Although the number of stages in the longer series could not be determined exactly without high-speed photography, owing to the speed at which the final drops coalesced, there was a clear difference between the systems that always

TABLE III

Number of partial coalescence stages for various systems

System	Number of partial coalescence stages	Viscosity ratio (μ_d/μ_c)
Diethyl carbonate	4–7[c]	1·29
Methyl isobutyl ketone	several	2·01
Cyclohexanone	1–2[a,b]	0·592
Amyl alcohol	1	0·273
Anisole	6–7	0·917
Iso-octane	several[b]	2·00
Kerosene–dibutyl phthalate	1	0·073
Kerosene	1–6[a,b]	0·524

[a] A tendency for the drops that coalesced immediately (< 1 sec) to coalesce in a single stage
[b] The drop left after the coalescence of the original drop had a longer rest time than either the original drop or any of the succeeding stages
[c] Sometimes the partial coalescence series branched, i.e. the coalescence of the original drop produced two secondary drops (one large and one small) that then coalesced separately

produced a partial coalescence series and those that did not. Reference to the properties of the systems shows that when the viscosity of the dispersed phase was close to, or greater than, the continuous phase, a long partial coalescence series always occurred and for decreasing values of $[\mu_d/\mu_c]$ the length of the partial coalescence series decreased. These results broadly agree with the work of Charles & Mason,[12] although with the difference that partial coalescence was

not observed in the systems amyl alcohol, $[\mu_d/\mu_c] = 0{\cdot}273$ and kerosene–dibutyl phthalate, $[\mu_d/\mu_c] = 0{\cdot}073$ whereas Charles & Mason reported a lower limit of 0·02 below which single step coalescence took place.

As the major part of this work was to study coalescence and separation of dispersion bands emphasis was next placed on measuring coalescence frequencies, both drop interface and drop–drop, in groups of drops at a phase boundary. These experiments were carried out in the column apparatus. The flow rate of dispersed phase and position of the phase boundary in the column were held constant and photographs of the drop distribution at the phase boundary were taken. From these films the relative coalescence frequency could be measured. The apparent drop diameters were measured from projections of the film. These had to be corrected for distortion since, by photographing from beneath the phase boundary, only that part of each drop in contact with the phase boundary was visible. This was done by using previously published tables.[13,14] Such photographs are shown in Figs 5–7. The drop distributors used were designed and operated to obtain as uniform a drop size as possible; this was relatively easy to achieve at the low rates discussed here. From the photographs it is evident that the distribution of drop sizes at the interface varies from system to system indicating varying rates of interdrop coalescence. Interdroplet coalescence is shown in Fig. 5(a) in the system diethyl carbonate–water. Evidence of stepwise coalescence is shown in Fig. 6, anisole–water, where the

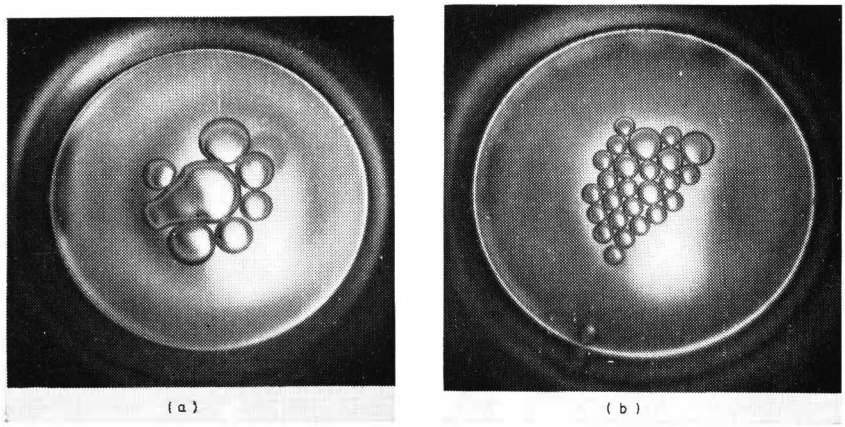

FIG. 5. *Droplet coalescence*

(a) diethyl carbonate–water; (b) cyclohexanone–water

smaller drops the result of partial coalescence. Fig. 7 is particularly interesting in that, apart from illustrating the increase in size of drops at the phase boundary by drop/drop coalescence (system diethyl carbonate–water) it also shows the effect of a coalescence event on surrounding drops at the phase boundary. The large drop in the centre is coalescing with the interface. The disturbance set up by this has caused the surrounding drops to distort becoming 'pear shaped'. This disturbance subsequently causes oscillation and rearrangement of the remaining drops at the phase boundary and rather than destabilising these drops it interupts the film drainage process which on average causes an increase in coalescence time. On some films drops were occasionally observed to coalesce immediately a neighbouring drop had coalesced being evidence of the disturbance reducing coalescence. These were relatively rare and in such cases presumably the drainage process had progressed to a point where slight mechanical vibrations would induce film breakdown.

Measurements of coalescence times were made from the films, the apparent drop size being corrected as discussed above. Since the apparatus was being operated continuously the possible effect of the arrival of a drop at the phase

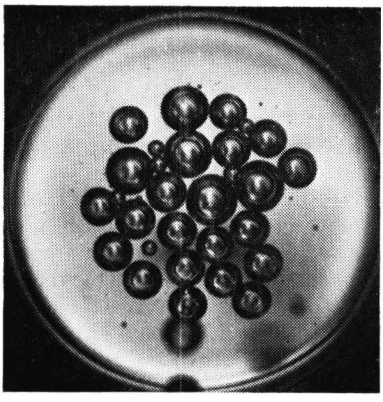

FIG. 6. *Droplet coalescence for anisole–water system*
Small drops result of partial coalescence

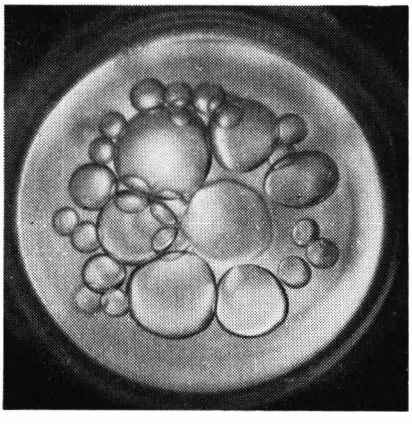

FIG. 7. *Droplet coalescence for diethyl carbonate–water system*

boundary on coalescence of drops resting there was first examined. Measurements of coalescence times (drop/interface) were made at varying flow rates. Mean values were computed at each condition, the results being shown in Fig. 8. From this it can be seen that, as for the single drop coalescence times, the mean coalescence time is inversely proportional to the drop size over the range considered. Furthermore, as the arrival of drops at the interface increases, the mean coalescence time slowly decreases. When considering this, the controlling factor is likely to be the average number of disturbances inflicted on each drop between its arrival or formation by interdroplet coalescence and coalescence. Denoting the mean coalescence time of a drop size i by $\bar{\tau}_i^1$ and average number of such drops present n_i then the average number of disturbances is:

$$\frac{\sum_{i=0}^{i=j} \bar{\tau}_i^1 \, n_i}{\sum_{i=0}^{i=j} n_i} \times N$$

where N is the drop arrival rate. In the range covered in these experiments this varied from 10–200. Lower values were not suitable for analysis by this technique but could be best studied by modifying the cell apparatus.[15] Results in the range $\bar{\tau}^1 N = 0 \cdot 5$ to 2 would be particularly interesting as they would show

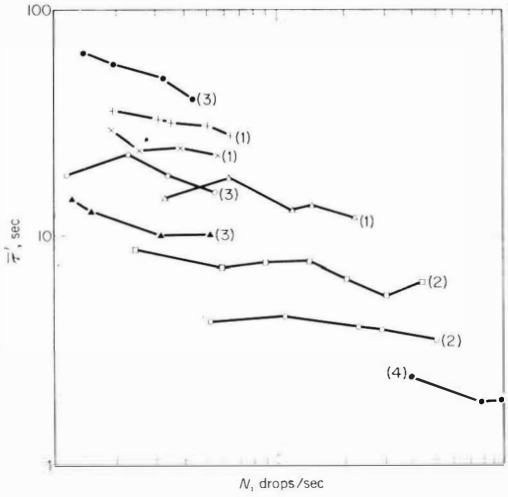

FIG. 8. *Mean drop interface coalescence times vs. drop arrival rate*

(1)–(4) refer to system numbers
φ: ● 0·30; + 0·50; × 0·59; △ 0·68; ○ 0·38; ▲ 0·44; □ 0·25 cm

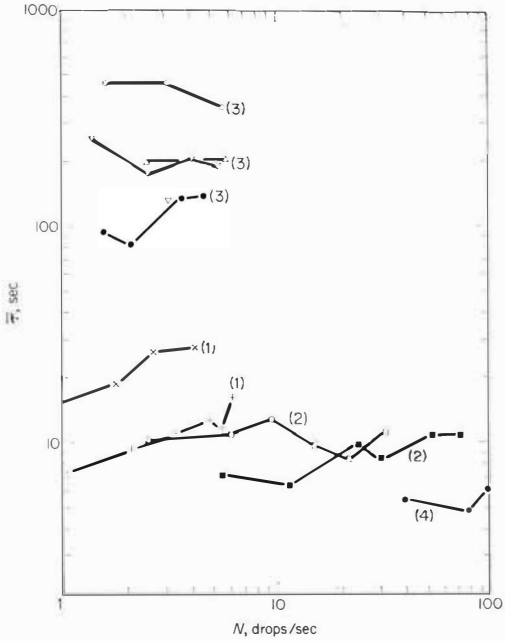

FIG. 9. *Mean drop/drop coalescence times vs. drop arrival rate*

(1)–(4) refer to system numbers
φ: ● 0·30; ○ 0·45; △ ▽ 0·39; × 0·58; + 0·50; □ 0·26; ■ 0·32 cm

the effect of a single disturbance occurring at the critical stage in the drainage process.

Interdroplet coalescence times were also obtained. In this case fewer measurements were possible and the resultant variation was higher. It was found that the amount of interdrop coalescence increased rapidly as the diameter of the inlet drops decreased and, to a lesser extent, as the drop arrival rate decreased (Fig. 9), the disturbance in the interface tending to cause the drops to separate. As discussed above, the rate of interdrop, coalescence was found to

vary throughout the systems studied; this is qualified in Table IV where the range of ratios of drop/interface and drop/drop coalescence times observed is given. Comparing these results with the physical properties the ratio decreases with increasing continuous phase viscosity and decreasing interfacial tension.

TABLE IV

Range of ratios of drop/interface and drop/drop coalescence times

System	Ratio $\bar{\tau}^1/\tau$ observed
Diethyl carbonate	1–5
Anisole	0·25–1·25
Methyl isobutyl ketone	0·25–0·75
Amyl alcohol	0·25–0·4
Cyclohexanone	0·03–0·5

To obtain the overall effects of the experimental variables, the data for both drop/drop and drop/interface coalescence was expressed in the dimensionless groups:

$$\frac{\bar{\tau}^1\gamma}{\varphi\mu_c}, \frac{\varphi^2\Delta\rho g}{\gamma}, \bar{\tau}^1 N, \frac{\mu_d}{\mu_c}$$

and the constants calculated by regression analysis as before. For drop/interface coalescence the following equation was obtained:

$$\frac{\bar{\tau}^1\gamma}{\varphi\mu_c} = 31 \times 10^3 \left(\frac{\varphi^2\Delta\rho g}{\gamma}\right)^{-1\cdot 24} \left(\frac{\mu_d}{\mu_c}\right)^{1\cdot 03} \quad . \quad . \quad . \quad . \quad . \quad (6)$$

the confidence limits of the two exponents were $\pm 0\cdot 16$ and $\pm 0\cdot 22$ respectively. The results are shown graphically in Fig. 10. The rate of disturbance characterised by $\bar{\tau}^1 N$ had no significant effect as the exponent obtained was $0\cdot 002 \pm 0\cdot 1$. A comparison of the results obtained from the monolayers and single drop method shows that although there is some agreement in the effect of the groups $\left(\frac{\varphi^2\Delta\rho g}{\gamma}\right)$ and $\left(\frac{\mu_d}{\mu_c}\right)$ the constants in Equations (5) and (6) are quite different and result in predicted mean coalescence times for drops in a monolayer somewhat greater than those computed from single drop experiments. This must be due to interaction between drops restricting the film drainage process and to disturbances generated on coalescence. In the experimental range studied the disturbance generated by arrival of a drop into the layer had apparently little effect.

In the case of interdrop coalescence the results analysed in a similar way gave:

$$\frac{\bar{\tau}\gamma}{\varphi\mu_c} = 412 \times 10^3 \left(\frac{\varphi^2\Delta\rho g}{\gamma}\right)^{-0\cdot 3} (\bar{\tau}^1 N)^{-0\cdot 5} \left(\frac{\mu_d}{\mu_c}\right)^{0\cdot 3}. \quad . \quad . \quad . \quad (7)$$

but in this case owing to the width of the confidence limits ($\pm 0\cdot 3$, $\pm 0\cdot 3$ $\pm 0\cdot 4$ respectively) the result was inconclusive.

If one considers the observations made on the stability of the secondary drops formed by partial coalescence, where it was noted that in some instances the secondary drop formed was more stable, this apparently conflicts with predictions from Equation (6). For these cases the drop size was of the order of 0·1 to 1 mm and was outside the range of measurements. There is some evidence that at low values of $(\varphi^2\Delta\rho g/\gamma)$ $(<0\cdot 1)$ the measured values are less than those predicted in this work.[3] In this range there is scope for further work, particularly since in agitated extractors the droplet sizes are likely to be smaller than those studied here.

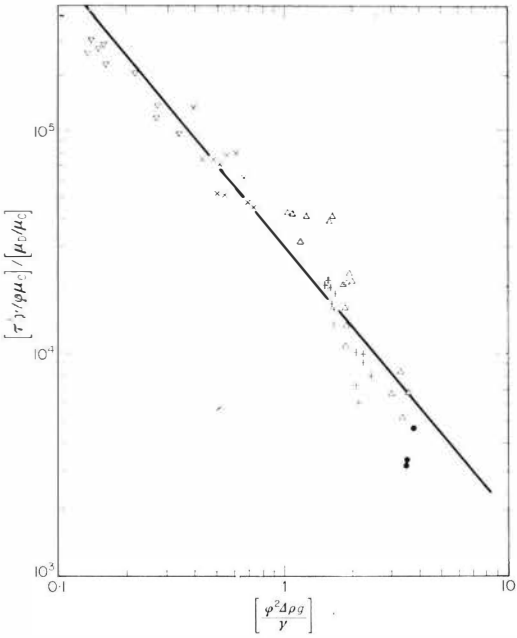

FIG. 10. *Correlation of results for drop/interface coalescence times*

● amyl alcohol–water; + methyl isobutyl ketone–water; △ anisole–water; △ cyclohexanone–water; × DEC

Coalescence at a convex interface

During the work, observations were made of coalescence of groups of drops at a convex interface such that the walls of the column were not wetted by the dispersed phase. This condition was found to be particularly interesting when dispersion bands were formed at the phase boundary at higher throughputs.[10] Under non-wetting conditions droplets collected around the walls of the column. Drop/drop coalescence appeared to take place preferentially with these drops and when one of them eventually coalesced with the interface the drops from the centre of the interface rolled to the wall through the resulting gap and invariably immediately coalesced with the interface. This process continued for 2 or 3 sec until a drop lodged against the wall and proceeded to grow fairly rapidly by drop/drop coalescence. Thus it appeared that when the drops were in contact with the wall (i.e. not cushioned by a thin film of dispersed phase adhering to the wall) both drop/drop and drop/interface coalescence was promoted. A typical photograph of this is shown in Fig. 11. The smaller drops at the centre are drops of continuous phase formed during coalescence.[16] These collect underneath the phase boundary in the bulk coalesced phase and subsequently recoalesce into the continuous phase. This illustrates the complexity of phase separation in dispersion bands where within the band not only is there counterflow of the phases and drop/drop coalescence but also coalescence in both directions with the interface.

Conclusions

It has been found that coalescence times of drops measured by studying the separation of clusters of drops and single layers at a phase boundary are higher than the corresponding measurements for single drops. The effect of disturbance from adjacent drops appears to increase the rest time by disrupting the drainage process. In this work better reproducibility was obtained in the multidrop experiments. A correlation is proposed to relate the mean coalescence time to system properties. Drop/drop coalescence times have been

measured and these were found to increase with increasing continuous phase viscosity and droplet size.

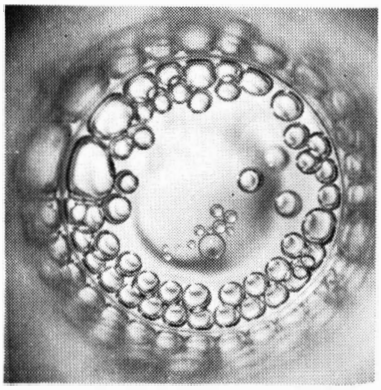

FIG. 11. *Droplet coalescence for kerosene–water system (walls not wetted by dispersed phase)*

Nomenclature

a	constant dimensional analysis
b	constant dimensional analysis
k	constant Equation (3)
K	constant dimensional analysis
L	distance of fall or rise of drop
n_i	number of drops diameter i
N	drop arrival rate
N_t	number of drops that have not coalesced after t sec
N_0	total number of drops in sample
R	regression coefficient
t	time
$t_{\frac{1}{2}}$	half-life coalescence time
T	temperature, °C
γ	interfacial tension
μ	viscosity
ρ	density
φ	mean drop volume diameter
τ	coalescence time
$\bar{\tau}^1$	mean drop/interface coalescence time
$\bar{\tau}$	mean drop/drop coalescence time
σ	standard deviation

Subscripts

c	properties of continuous phase
d	properties of dispersed phase

References

[1] Gillespie, T., & Rideal, E. K., *Trans. Faraday Soc.*, 1956, **52,** 173
[2] Jeffreys, G. V., & Hawksley, J. L., *A.I.Ch.E. Jl*, 1965, **11,** 413
[3] Hodgson, T. D., Ph.D. Thesis, University College of Wales, 1966

[4] Hartland, S., *Trans. Instn chem. Engrs*, 1967, **45,** 102
[5] Lawson, G. B., *Chem. Process Engng*, 1967, **47,** 45
[6] Davies, G. A., & Jeffreys, G. V., *3rd CHISA Congr., Mariánské Lázně (Czechoslovakia)*, 1969
[7] Hawksley, J. L., Ph.D. Thesis, Univ. of Birmingham, 1963
[8] Smith, D. V., M.Sc. Thesis, Univ. of Manchester, 1965
[9] Hayworth, C. B., & Treybal, R. E., *Ind. Engng chem.*, 1950, **42,** 1174
[10] Smith, D. V., & Davies, G. A., *Can. J. chem. Engng*, 1970, **48,** 628
[11] Harkins, W. B., & Brown, F. H., *J. Am. chem. Soc.*, 1919, **41,** 499
[12] Charles, G. E., & Mason, S. G., *J. Colloid Sci.*, 1960, **15,** 236
[13] Bashforth, F., & Adams, J. C., 'An attempt to test the theories of capillary action', 1883 (Cambridge: Cambridge University Press)
[14] Princen, H. M., *J. Colloid Sci.*, 1963, **18,** 178
[15] Smith, D. V., Ph.D. Thesis, Univ. of Manchester, 1969
[16] Davies, G. A., Jeffreys, G. V., Smith, D. V., & Ali, F. A., *Can. J. chem. Engng*, 1970, **48,** 328

Coalescence in packed beds—packing selection and hydrodynamic behaviour

by R. J. Thomas and C. J. Mumford
Department of Chemical Engineering, University of Aston in Birmingham, Gosta Green, Birmingham, U.K.

The hydrodynamic behaviour of dispersed phase droplets in knitted mesh packed beds has been examined with regard to the breakdown/coalescence mechanisms which govern the exit droplet size and to assist selection of this type of packed bed as a coalescing device for primary dispersions.

The behaviour has been shown to be dependent upon the 'wetting' properties of the packing material; the most efficient coalescers being those 'wetted' by the dispersed phase.

For packings 'wet' by the dispersed phase, coalescence predominates and enlarged exit droplets are produced. The exit mechanisms are dependent upon system and packing physical properties. This exit drop-size, in a stationary continuous phase and at low dispersed phase flow rate, has been correlated by means of an equation.

The behaviour of packings 'wet' by the continuous phase was analogous to droplet behaviour in conventional packed columns, viz. Raschig rings and Berl saddles. The breakdown/coalescence equilibrium was shown to be dependent upon packing and system physical properties. The existence of a 'characteristic' exit dropsize has been demonstrated and correlated for high voidage packings (> 95%).

A 'flooding' correlation, covering a wide range of system and packing properties has been developed.

Introduction

IN LIQUID–LIQUID extraction a large interfacial area for solute transfer is produced by the dispersion of one phase as droplets and ultimately, when mass transfer is complete, it is necessary to separate the phases. Similarly oil-in-water type emulsions treatment in effluent streams and water-in-fuel dispersions frequently require separation.

These dispersions are of two types. The first, a primary or coarse emulsion, contains droplets greater than 100 μm dia. which given time, will settle under the influence of gravity to form a heterogeneous layer. Whether sufficient time is available for such gradual settling is dependent on the throughput of the process flowstream. Finally, separation occurs via inter-droplet and droplet/interface coalescence.

A secondary emulsion containing large numbers of very small droplets may also be present. These droplets have a diameter of less than 1 μm, and settle extremely slowly. For example, a 1 μm size droplet of kerosene in water has a settling rate of the order of 2 cm/day. Therefore, the coalescence and clarification of secondary emulsions presents considerable difficulty.

Numerous mechanical and chemical methods may be used to induce liquid dispersions to coalesce. Four main types of mechanical separation techniques are available:[1] (a) simple gravity settling; (b) accelerated settling in a centrifuge, hydrocyclone or electrical coalescer; (c) preferential flow through a selective membrane; and (d) induced coalescence caused by passage through packed beds.

For highly stable emulsions chemical techniques such as the addition of an electrolyte or a surface-active agent[2] are available to promote inter-droplet coalescence. After enlargement of the dispersed phase droplets, recourse is made to one of the mechanical separation techniques.[3]

The selection of a mechanical coalescence device is largely a matter of trial and error since no standard design methods or selection criteria are available. This is particularly true of packed-bed coalescers.

In packed-bed coalescers, coagulation occurs within the body of the packed section. The mechanisms and operational characteristics remain the subject of considerable research. Several prerequisites for successful operation have been proposed, viz.: the coalescer material should be preferentially wet by the dispersed phase; they should possess a large surface to volume ratio; the interstices should be small enough to cover the range of droplet sizes encountered; and they should cause as low a pressure drop as possible.

Among the materials currently in use are cotton, glasswool, metal and polymer fibrous beds; knitted mesh packings formed from interlocking loops of metallic, polymeric and natural fibres; pebble or ballotini beds and beds composed of conventional column packings, for example Raschig rings and Berl saddles. The type of packed section employed is dependent upon the nature of the dispersion encountered. Factors affecting the efficient coalescence of secondary dispersions by packings have been investigated.[4–6] Work on the equally important problem of primary dispersions is described in this paper.

In the coalescence of primary dispersions, Raschig rings or similar column packings, pebble or ballotini beds and knitted mesh beds are most commonly used. There are considerable published data on droplet behaviour in conventional packings in extraction columns, but the characteristics of pebble beds and knitted mesh packings have received scant attention. Therefore, the hydrodynamic behaviour of droplets in knitted mesh packings was investigated in order to establish their operational characteristics and to provide criteria for packing selection.

Since some analogy is probable between the factors affecting the behaviour of droplets in knitted mesh packed beds and those in packed extraction columns, work on the latter was reviewed. The results of the present research have been interpreted in a similar manner.

Droplet behaviour in Raschig ring packed extraction columns

The most extensive study of droplet behaviour in packed liquid–liquid extraction columns is that of Lewis and others.[7–12] With a 2 in dia. × 3 ft packed height column, provided the packing was greater than a limiting size, defined by:

$$d_p = 2{\cdot}42\left(\frac{\gamma}{\Delta\rho g}\right)^{\frac{1}{2}} \quad . \quad . \quad . \quad . \quad . \quad . \quad . \quad . \quad . \quad (1)$$

the exit droplet size was independent of the size of packing used. Equation (1) gives the size of packing at which the characteristics of droplet flow change drastically. The size of packing so defined, is that in which the mean void size is equal to the mean droplet size.

The exit drop size was independent of the size of droplets entering the packing. Thus large inlet droplets were gradually broken down to some equilibrium size whilst small inlet droplets grew, by coalescence, to attain the same equilibrium drop size. Although Pratt[7] made a general observation that the rate of coalescence of droplets was considerably slower than the breakdown process, no study was made of the breakdown–growth equilibrium. The exit droplet Sauter mean diameter, produced by a range of aqueous–organic solvent systems, after passing through 6 ft of packing, whose diameter was greater than the critical packing size, could be correlated by:

$$\frac{d_{vs}\Delta\rho\gamma}{\mu_c^2} = 1{\cdot}42\left(\frac{\Delta\rho\gamma^3}{\mu_c^4 g}\right)^{0{\cdot}475}\left(\frac{V\varepsilon_o x}{V_d}\right) \quad . \quad . \quad . \quad . \quad . \quad . \quad (2)$$

This could be simplified with slight loss of accuracy to give,

$$d_{vs} = 0{\cdot}92\left(\frac{\gamma}{\Delta\rho g}\right)^{0{\cdot}5}\left(\frac{V_o\varepsilon x}{V_d}\right) \quad . \quad . \quad . \quad . \quad . \quad . \quad . \quad (3)$$

Pratt also found that the droplet diameter at substantially zero flow rate, d^{o}_{vs}, could be correlated by the expression;

$$d^{o}_{vs} = 0{\cdot}92 \left(\frac{\gamma}{\Delta\rho g}\right)^{0{\cdot}5} \quad . \quad . \quad . \quad . \quad . \quad . \quad . \quad . \quad (4)$$

The first term on the right of Equation (3) takes account of the effect of physical properties and the second term the effects of changes in phase flow rates. V_o is the droplet 'characteristic velocity', i.e. the mean velocity of the droplets relative to the continuous phase at substantially zero flow rates. This is defined by:

$$\frac{V_d}{x} + \frac{V_c}{1-x} = \varepsilon V_o (1-x) \quad . \quad . \quad . \quad . \quad . \quad . \quad . \quad (5)$$

V_o may be found from experimental data by plotting $V_d + \frac{x}{1-x} V_c$ against $x(1-x)$ to give a straight line passing through the origin with a gradient of firmed by Wicks & Beckmann.[13] Pratt has presented a graphical correlation for prediction of V_0 from packing and system physical properties, together with a nomogram which relates V_0 and the phase flow rates to the hold-up of dispersed phase. Thus it is possible using Equations (2) and (3) to predict the Sauter mean droplet diameter in a packed extraction column. Furthermore from the relationship:

$$a = \frac{6\varepsilon X}{d_p} \quad . \quad . \quad . \quad . \quad . \quad . \quad . \quad . \quad . \quad . \quad (6)$$

the interfacial area for mass transfer is calculable. From Equations (3) and (6):

$$a = \frac{6V_d}{0{\cdot}92\left(\frac{\gamma}{\Delta\rho g}\right)^{0{\cdot}5} V_o} \quad . \quad . \quad . \quad . \quad . \quad . \quad . \quad . \quad (7)$$

$$a = \text{constant} \times V_d \quad . \quad . \quad . \quad . \quad . \quad . \quad . \quad . \quad . \quad . \quad (7(a))$$

Thus rapid estimation of the interfacial area for mass transfer is possible. Equation (7(a)) has been verified experimentally by Puranik & Sharma.[14]

These correlations are only applicable to packings wetted by the continuous phase. No corresponding work has been carried out for packings wetted by the dispersed phase although some qualitative observations have been made regarding general flow phenomena in packed columns.[15–17]

Pratt demonstrated the existence of an equilibrium droplet size distribution, attained after passage through a packed section. Therefore, during their passage through the packings the droplets undergo some process, viz. breakdown of larger droplets and growth of smaller droplets, which results in an equilibrium size distribution being approached. The equilibrium between growth and breakdown determines the exit droplet size distribution.

To clarify these phenomena Thornton[18] examined the size distribution of toluene droplets in an aqueous continuous phase as they passed through 18 in packed sections of $\frac{3}{4}$-in Raschig rings in a column 6 ft high × 3 in dia. The distribution became progressively skewed with column height and could be represented approximately by means of a log-normal distribution function. A stable distribution was only reached after the droplets had passed through several feet of packing. Consequently, the Sauter mean droplet diameter, d_{vs}, became progressively smaller with column height and only approached an

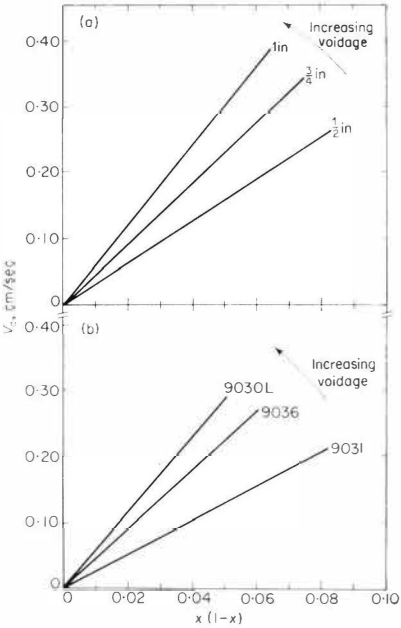

FIG. 1. *Typical dispersed phase hold-up data for determining 'characteristic' velocity*
(a) Conventional packings; (b) knitted mesh packings

equilibrium value towards the top of the column (Fig. 2). The change in d_{vs} with column height could be represented by an exponential equation:

$$d_{vs} = d_{vs_{(eq.)}} + 0{\cdot}27 \exp(-0{\cdot}0157\, h) \qquad (8)$$

The equilibrium value of the mean droplet size $d_{vs_{(eq.)}}$ was found to have a value of 0·45 cm for toluene droplets dispersed in water.

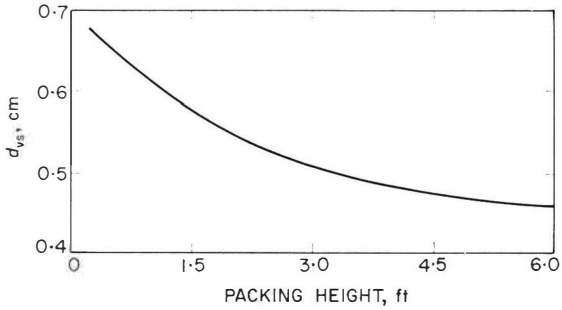

FIG. 2. *Approach to equilibrium dropsize in Raschig ring packing*[18]

It was assumed however, that the effect of each of the discrete packed sections was additive, i.e.: the exit drop size from two consecutive 18 in packed sections was the same as from a single 36 in depth of section. It has since been demonstrated that this is not valid because droplets leaving the exit surface of a packed section are able to accelerate to a velocity higher than that they would achieve within the voids of the packing (Thomas, R. J., unpublished results). Thornton suggested that droplets travel at 80% of their terminal velocity within the packed sections. However, calculations show that 50% is a more realistic value. No work has been reported regarding the effect of packing size upon the approach to equilibrium drop size.

An impact–breakdown mechanism has been proposed to explain the attainment of an equilibrium size distribution.[19] This may be summarised as follows. Provided the packing is greater than the limiting size, defined by Equation (1), the droplets rise freely within the interstices of the packing and are brought to rest by random collisions with packing elements. Energy is therefore dissipated which may result in droplet breakdown. Thus there is a gradual reduction in d_{vs} with increasing number of collisions, and therefore column height. This breakdown process is opposed by a coalescence process due to droplets being arrested in the smaller interstices of the packing and coalescing until a sufficiently large head is built up to redisperse them as fresh droplets. As the void size decreases, i.e. with decreasing packing size, the coalescence mechanism may predominate, particularly with packings less than the critical size.

Thornton[20] examined the impact of single droplets travelling at their terminal velocity on fixed baffles representing packing elements. It was demonstrated that a critical drop size existed, below which breakdown on impact did not occur. In an energy balance, before and after symmetrical collision with a packing element, an equation was derived which could be solved for the critical droplet size:

$$1{\cdot}79\,(d_c^2 \Delta\rho g) + (d_c V_t^2 \rho_d) = 3{\cdot}12\gamma \qquad (9)$$

However, this equation is based upon a symmetrical collision producing two equal sized 'daughter' droplets; unsymmetrical collisions are equally probable, resulting in only a small portion of the original droplet being sheared. This would produce a greater spread in the droplet size distribution.

V_t is the terminal velocity of the droplet on impact with the baffle, i.e. the terminal velocity in an infinite medium. Good agreement was observed between predicted and actual values of d_c. In practical packed columns, the velocity, V, with which the droplet collides with an element of packing, will be a function of hold-up and the continuous phase superficial velocity so that:

$$V = \Phi\, V_t - \frac{V_c}{\varepsilon(1-x)} \qquad (10)$$

where Φ is a correction factor for droplets rising in a restricted medium. Using the calculated values of d^o_{vs} from Equation (4), and the calculated values of the critical droplet size, d_c, from Equation (9), it was shown that over a limited range of flowrates and physical properties:

$$d^o_{vs} = 0{\cdot}5\, d_c \qquad (11)$$

For the toluene–water system, the experimental results referred to earlier could be represented by:

$$d_{vs(eq.)} = 0{\cdot}85\, d_c \qquad (12)$$

Equations (11) and (12) indicate that it should be possible to predict the value of $d_{vs(eq.)}$ from the impact theory, but a great deal of work is required to establish a general form of Equation (12). There is evidence that the numerical constant in Equation (12) is dependent upon the physical properties of the systems.[19]

Considerable work has been carried out concerning other important flow phenomena in packed extraction columns, for example, the condition referred to as 'flooding'. For a given flow rate of one phase in a column, there is a maximum flow of the other phase, which if exceeded, results in accumulation of one of the phases in the column. This limiting flow or 'flooding' condition is a function of the particular liquid system and packing under consideration. Clearly a knowledge of the limiting flow is essential for extraction column design. Numerous graphical correlations of flooding data have been published.[21–23]

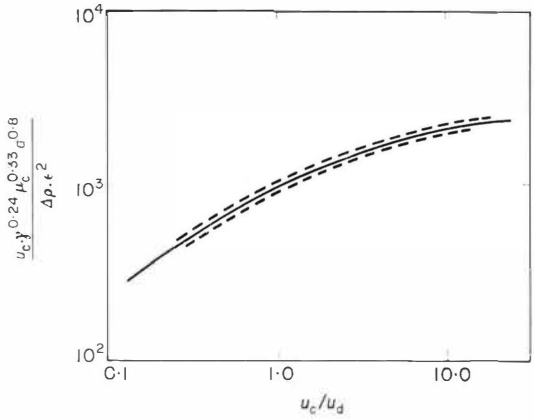

FIG. 3. *Flooding correlation for conventional packings*[21]

The correlation of Breckenfield & Wilke[21] shown in Fig. 3 is typical.

No reference has been made in any published work to the wetting effects of the systems with regard to the droplet behaviour within the packing. It is apparent that all the reported work has been concerned with 'non-wetted' packings, i.e. packings 'wetted' by the continuous phase.

A direct measure of the surface 'wettability' is given by the contact angle of a drop of liquid on the solid surface. This is defined as the angle between the tangent to the drop and the solid surface measured into the drop, as illustrated in Fig. 4. The experimental methods for measuring the contact angle of a droplet on a solid surface have been reviewed by Osipow.[24] If the contact angle is zero the surface is completely wetted by the dispersed phase; if the contact angle is 180° the surface is completely 'non-wetted'. Usually contact angles less than 90° are considered as partial wetting.

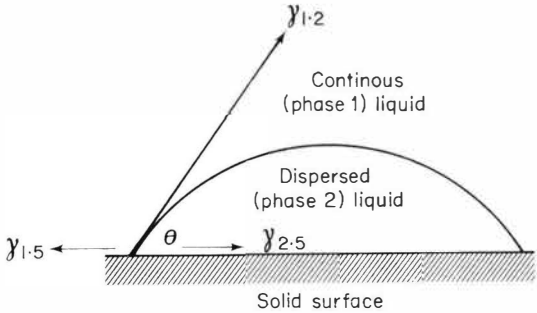

FIG. 4. *Contact angle of a sessile drop at a solid/liquid/liquid boundary*

θ contact angle; $\gamma_{1\cdot2}$ interfacial tension; $\gamma_{1\cdot5}$ liquid/solid tension of phase 1; $\gamma_{2\cdot5}$ liquid/solid tension of phase 2

Recent work (Thomas, R. J., unpublished) has indicated that surface preparation is of paramount importance in the 'wetting' behaviour of surfaces. It has been demonstrated that most surfaces, when scrupulously clean and dry, display preferential wetting effects, i.e. that phase which first wets the dry surface will be the 'wetting' phase. Thus, for example, with stainless steel it is possible to prepare the surface in such a manner that either the aqueous or the organic phase is 'wetting'. This behaviour is more pronounced with high energy surfaces (stainless steel, glass) than with low energy surfaces (polypropylene, polytetrafluoroethylene (PTFE)).

Hill[25] has demonstrated an experimental method which enables surfaces to be ranked in order of hydrophobic or hydrophilic behaviour. This facilitates the prediction of the likely 'wetting' properties of suitable materials of construction.

Hydrodynamic studies in knitted mesh packed beds

Research regarding the hydrodynamic behaviour of droplets in knitted mesh packed beds has been very limited and has been mainly concerned with their application in Scheibel extraction columns. Here the role of the packing is to isolate the mixing sections and prevent backmixing within the column.[26]

Perry[27] describes the Scheibel extractor as a series of mixer-settlers in which the packed sections coalesce the emulsion formed by the turbines. Although some coalescence takes place in the packed section, this is dependent upon the properties of the system, the preferential wetting ability of the packing, and the hydrodynamics of operation.[28]

Several workers[29–31] have studied droplet flow through the packings in a Scheibel column. Honeykamp & Burkhart[29] concluded that the effects on exit drop size of continuous phase flow rate, dispersed phase flow rate and inlet drop size were insignificant. However, packed height had a significant effect on the exit droplet size, with evidence of the existence of a 'characteristic' drop size similar to that found in conventional packings. Indeed, further analysis of the results of Honeykamp & Burkhart presented in the form of Fig. 5 demonstrate that high voidage knitmesh packings have droplet flow characteristics similar to conventional packings greater than the critical packing size.

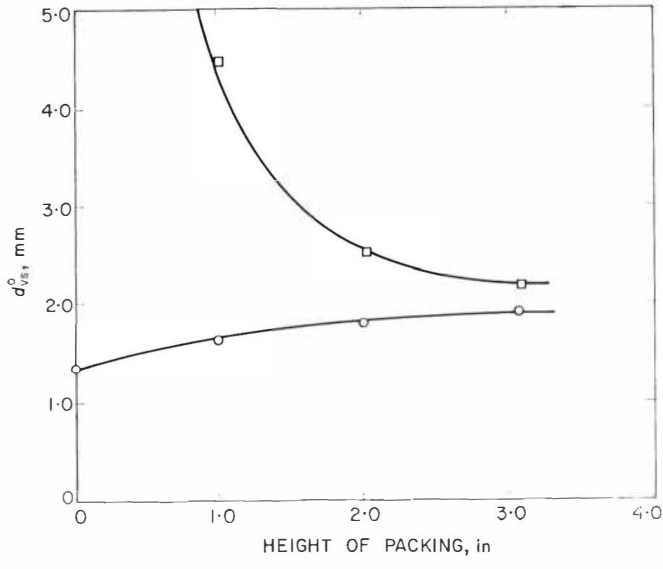

FIG. 5. *Approach to equilibrium dropsize*[29] (*'non-wetted' packing*)
Yorkmesh packing: stainless steel Type 9033, surface area 120 ft²/ft³, voidage 0·975, methyl isobutyl ketone–water

Piper[31] studied limiting flow phenomena in knitted mesh packings, wetted by the continuous phase, covering voidages in the range 97·5–98·75%. He found that the working range of the packings increased with increasing voidage, a conclusion also reached by Slatter[30] and that the limiting flow was dependent upon the inlet droplet size. Large inlet drops (7·5 mm) rapidly accumulated as a coalesced layer at the inlet surface of the packing and caused a reduction in the limiting flow rates. With the smaller inlet drops (3·5 mm) the core did not form., the number of drops accumulating below the packing increasing gradually

with flow rate. Piper experienced difficulty in defining the onset of flooding and this limited the analysis to general observations of factors affecting 'flood-point' phenomena. Further analysis of his results indicates that a general 'flooding rate' correlation, similar to that of Crawford & Wilke, is possible.

The studies referred to were all largely qualitative and concerned with droplet behaviour in packings wetted by the continuous phase. No similar work has been reported for packings wetted by the dispersed phase. However Juma[32] has investigated the coalescence of droplets on solid surfaces and packings with particular reference to the influence of surface properties. With respect to the coalescence of primary dispersions in packings he concluded that the efficiency of coalescence was higher if the dispersed phase wets the packing surface. Over the range of surface/volume ratios which were studied, viz. 60–250 ft^2/ft^3, no significant difference was observed in performance. Again, with respect to knitted mesh packings, the observations were essentially confined to providing a guide to the general coalescence behaviour of packed beds. Jeffreys & Davies[6] have examined the coalescence of primary dispersions and conclude that two distinct mechanisms of coalescence exist, dependent upon the 'wetting' situation prevailing. For packings wetted by the dispersed phase, droplet/interface coalescence predominates, whilst for packings wetted by the continuous phase the interdroplet mode predominates. Thus the factors controlling these two types of behaviour will govern the efficiency of coalescence of the particular packing situation.

Experimental

Preliminary investigations were carried out in a 3 in dia. column, constructed entirely from Q.V.F. glassware. This enabled a high standard of cleanliness to be maintained and allowed easy access for photographic equipment. All other connexions were made with chemically inert PTFE tubing.

Since temperature[33] and mass transfer[34] significantly affect liquid properties, viz. interfacial tension, density and viscosity, mutually saturated systems were used under constant temperature conditions. To achieve temperature control the entire apparatus was enclosed in a constant temperature air bath. Subsequent experimental work was carried out in a 4 in dia. column. The latter had more sophisticated temperature control facilities including automatic temperature control of both phase reservoirs.

Organic solvents were used as the dispersed phase with an aqueous continuous phase. The solvents were selected to provide a range of interfacial tensions from 8·50 to 45·0 dynes/cm. In the 3 in dia. column, phase dispersal was achieved via a brass plate distributor, with the distributor holes drilled and punched as recommended by Treybal.[35] No facility was provided for circulation of the continuous phase since it is well established that this has negligible effect on droplet hydrodynamics.[7,29] Using a range of distributor plates, inlet droplet sizes in the range 2–7 mm could be accurately reproduced.

In the 4 in dia. columns, phase dispersal was achieved via interchangeable glass nozzles, which were fitted to a constant head distributor, enclosed within the column. Owing to the 'wetting' of glass by water, the tips of the nozzles were coated with an insoluble, non-surfactive organic repellent solution[36] when the aqueous phase was dispersed.

The organic solvents used were of Analar grade and the physical properties of each system were determined prior to and during each set of experiments using conventional techniques;[37] these were found to remain constant.

Prior to each series of runs the equipment was cleaned by leaving it overnight, filled with a solution of biological decontaminant, 'Decon 70'. After soaking, the whole apparatus was rinsed thoroughly with de-ionised water, and finally with distilled water. The packed sections were cleaned by soaking in chromic acid, thorough water washing and then drying in an oven at 120°C. The subsequent treatment of the packings depended upon the wetting conditions required.

The performance of the packed sections was analysed based upon the measurement of the inlet and exit droplet sizes. The Sauter mean droplet diameter was used since this diameter gives directly the specific surface (area per unit volume) of the dispersed phase. Since droplet coalescence and breakdown are essentially surface phenomena this was considered the most appropriate mean diameter.

Droplet diameters were determined from photographs of the inlet and exit drop size distributions. Photographs were taken using a Miranda Sensorex 35 mm camera with a 135 mm telephoto lens attached to a 20 mm extension tube. This combination gave sufficient depth of field such that, after accurate focusing on the centre of the column, the whole depth of the column was adequately in focus. Illumination was provided by diffused rear lighting through a Perspex window in the air bath cabinet. Two 500 W photographic lamps generally provided an adequate light intensity. Kodak Panatomic X film, a fine grain film, was used, which provided sharp black and white contrasts. Errors due to the magnification and distortion at the column wall have been shown to be negligible except at the extreme edges of the column.[30]

A Beaulieu cine camera was used to record the various phenomena observed. A film speed of 64 frames/sec was used throughout. Hold-ups were determined by the standard displacement method.[7]

Results and discussion

An initial study was made of the manner in which the droplet size distribution varied with: the height of the packed section; the properties of the bed, viz. voidage; the physical properties of the dispersed phase; and the surface properties of the bed. Stainless steel packings (Knitmesh Ltd., Greenfield, Haywell, Flintshire) were used; these are specified in Table I.

TABLE I

Properties of Knitmesh packings

Packing type	Surface area, ft^2/ft^3	Voidage
Compressed	1200	0·7500
9031 U	1300	0·8500
9031	500	0·9500
9033	120	0·9750
9030	90	0·9800
9036	60	0·9875
9031 L	50	0·9925

A variation in the 'wetting' properties of the packing was obtained by modification of the method of preparation. Plastic packings and pebble beds are being investigated separately.[38] The packings were first cleaned and dried as described earlier. The dry packings were then either soaked in the dispersed phase for 1 h (this produced a packing preferentially wet by the dispersed phase) or soaked in distilled water for 1 h (this produced a packing preferentially wet by the aqueous continuous phase). After such treatments the 'wetting' properties were found to remain constant despite prolonged use.

The study was initially restricted to the use of two systems: methyl isobutyl ketone–water and iso-octane–water. These represented the extremes of the range of systems selected, which are specified in Table II.

The change in mean drop size due to passage through packed sections of Knitmesh packings were investigated. Packed sections up to 9 in depth were used. The investigation covered both dispersed phase 'wet' and continuous phase 'wet' packings.

TABLE II

Physical properties of organic solvents at 20°C

Organic solvent	Density, mg/ml	Viscosity, cP	Interfacial tension with water, dynes/cm
Iso-octane	0·692	0·505	45·0
Toluene	0·863	0·552	34·5
Amyl acetate	0·870	0·811	27·6
Nitrobenzene	1·201	2·013	24·1
Ethyl acetate	0·899	0·450	8·50
Methyl isobutyl ketone	0·800	0·580	8·50

Drop capture by a fibre element is governed by several factors, viz. drop-fibre element geometry; thinning of the continuous phase film between drop and fibre element, adhesive interaction between the drop and the fibre and drop disengagement.

The approach of a drop to a fibre element has generally been treated according to the classical theories of aerosol science. Thus droplet-fibre interception is dependent on such factors as fibre size, shape and flow streamlines. These theories cannot at present be applied to describe the more complex phenomena occurring in packed sections.

Ultimate contact between the drop and the fibre element follows retardation due to the film thinning process. During this stage the necessary forces for film thinning derive from flow streamlines and van der Waals forces. Unless micron and sub-micron droplets are considered Brownian motion is negligible.

On rupture of the continuous phase film, the drop makes contact with the fibre element, With a 'wetted' packing, the fibre element is covered with a film of dispersed phase liquid and coalescence occurs into this film. The movement of the coalesced dispersed phase is governed by flow of this 'wetting' film under the influence of gravity forces and flowstream drag forces.

For a 'non-wetted' packing the extent of dispersed phase 'filming' over the packing is reduced. The dispersed phase droplets remain discrete and growth occurs by random collisions which occur between moving drops in the continuous and either stationary drops attached to the packing element or collisions in the restricted paths of the packing. In this case the packing acts to promote interdroplet coalescence. Breakage due to collision with packing elements was also a feature of this mode of operation however, and the resultant exit drop-size was thus a function of the breakdown/coalescence equilibrium. Droplet behaviour was analogous to the dispersed phase behaviour reported by Thornton and in agreement with the observation of Honeykamp & Burkhart. Typical results are shown in Fig. 6. These demonstrate that large inlet droplets are rapidly broken to the equilibrium drop size. However, this equilibrium drop size was achieved much more rapidly for knitted mesh packings (~8 in) than for Raschig ring packings (~6 ft). Observations, made with single packing elements, indicated that the collisions in knitted mesh beds more closely resembled the ideal behaviour proposed by Thornton than do collisions within Raschig ring packed sections.

The behaviour of the dispersed phase droplets was shown to be dependent upon the voidage of the packed section. For voidages below 95·0% the coalescence mode predominates and enlarged exit droplets are produced. A feature of this operation was the build up of a flocculated zone of dispersed phase droplets at the inlet surface of the packings. This was due to the dispersed phase droplets queueing at the available inlet voids. With these low voidage packings, the voids are so small that the droplets are locked in the interstices and cannot move until impacted from behind by those following. Frequent interdroplet coalescence occurs resulting in enlarged droplets at the

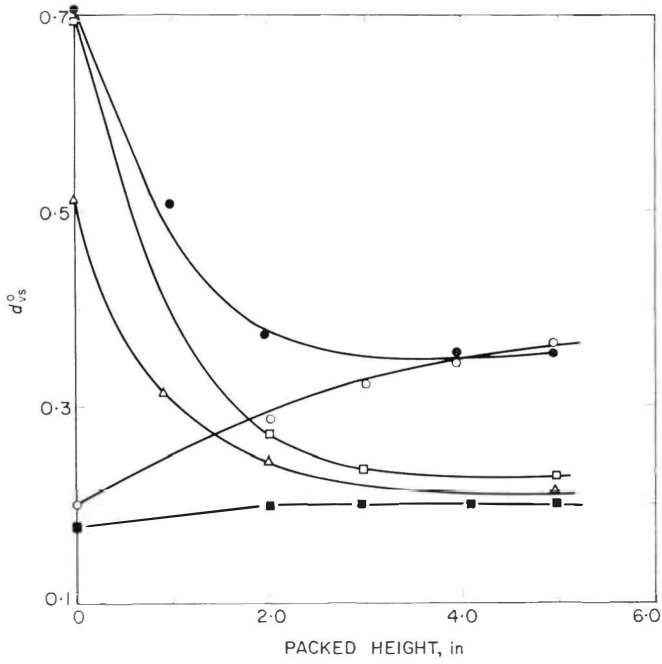

FIG. 6. *Approach to equilibrium dropsize in packings 'wet' by the continuous phase*
continuous phase wetting; stainless steel packing, Type 9036
○, ● iso-octane; □, △, ■ methyl isobutyl ketone

exit of the packed section. Clearly, as the voidage of the packings increases, the mechanical holding effect is reduced and behaviour approaches the acceleration–impact mechanism of Thornton.

For packings 'wet' by the dispersed phase, droplets coalesced upon the surface of the packing to form a continuous film and drainage of this film through the packing took place. Subsequently, enlarged droplets detached from the exit surface of the packed bed. Since basically drop/interface coalescence occurred, the factors which control this mode of coalescence,[36,39] will determine the effectiveness of coalescence of the dispersed phase by the packing. Thus the time required for separation would increase with increasing drop diameter, density difference between the phases and continuous phase viscosity and also with decreasing interfacial tension. Hence the greatest separation efficiency would be expected with systems of high interfacial tension and low continuous phase viscosity. Since it has been shown that the curvature of the interface into which a drop is coalescing also affects the time of separation[40] then the ratio of fibre diameter to droplet diameter is likely to be a factor influencing packing efficiency. As the ratio droplet diameter : fibre diameter increases so separation will occur more easily. Typical results are shown in Fig. 7.

At low flow rates and with high voidage packings (95·0–99·0%), the exit proplet detachment mechanism was by 'drip-point' formation as shown in Fig. 8(a) and (b) with the associated possibility of the formation of fine secondary droplets, which are detrimental to efficient operation. At higher flow rates and with lower voidages 'jetting' occurred, as in Fig. 8(c) and (d) and the dispersed phase left the packing in the form of a continuous stream. Discrete droplets were formed due to Rayleigh-type instabilities[41] in this stream, leading to exit droplets smaller than those produced by the 'drip-point' mechanism.

For the mechanism of drip point detachment some success has been achieved in correlating the exit drop size at low dispersed phase flow rate, with physica-properties of the systems separated. To facilitate correlation the methods of

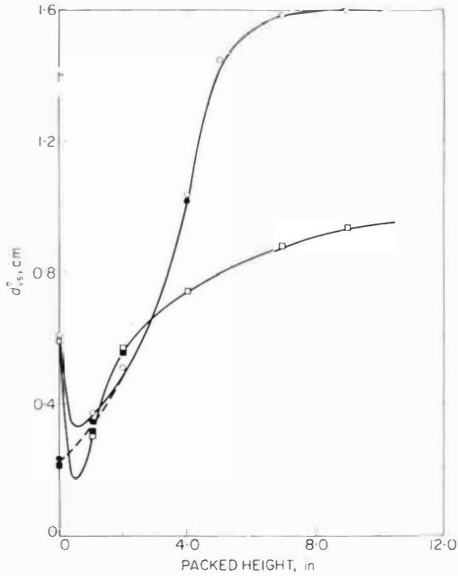

FIG. 7. *Approach to equilibrium dropsize in packings 'wet' by the dispersed phase*
Dispersed phase wetting; stainless steel packing, Type 9036
○, ● iso-octane; □, ■ methyl isobutyl ketone

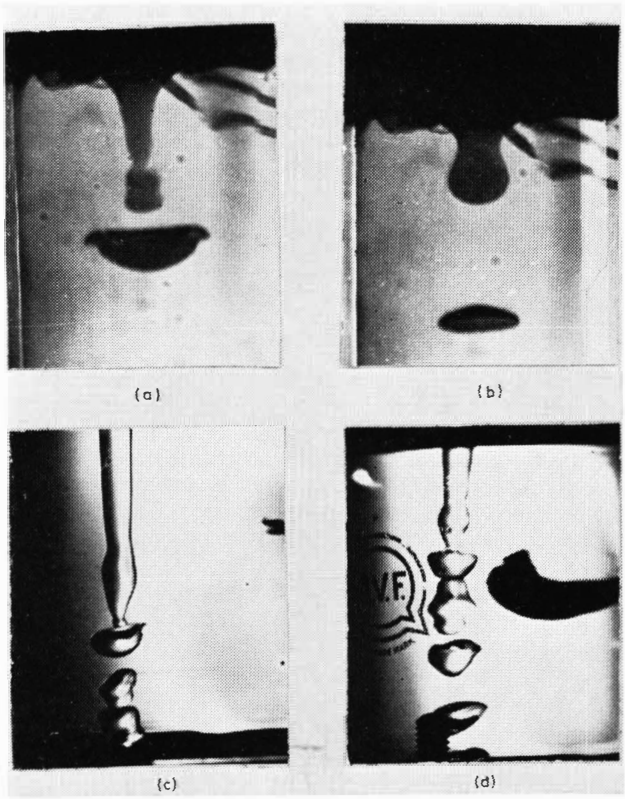

FIG. 8. *Exit mechanisms of dispersed phase 'wetting'*
(a), (b) 'drip-point' detachment; (c), (d) 'jetting' and jet disruption

dimensional analysis were used. It was assumed that the exit drop diameter could be represented as a power function of: the density difference, the interfacial tension, the viscosities of the phases and the gravitational acceleration. This analysis led to:

$$\frac{d^{o}_{vs}\,\Delta\rho\gamma}{\mu_c^{2}} = k\left(\frac{\Delta\rho\gamma^{3}}{\mu_c^{4}g}\right)^{a}\left(\frac{\mu_d}{\mu_c}\right)^{b} \quad . \quad . \quad . \quad . \quad . \quad . \quad . \quad (13)$$

This is of the same general form as Equation (3) presented by Pratt.

Pratt assumed that the exponent of the viscosity ratio term was zero. On this basis the experimental data for coalescence in knitted mesh packings could be correlated by:

$$\frac{d^{o}_{vs}\,\Delta\rho\gamma}{\mu_c^{2}} = 2{\cdot}44\left(\frac{\Delta\rho\gamma^{3}}{\mu_c^{4}g}\right)^{0{\cdot}523} \quad . \quad . \quad . \quad . \quad . \quad . \quad . \quad (14)$$

This is illustrated in Fig. 9.

Equation (14) can be simplified to:

$$d^{o}_{vs} = 2{\cdot}44\left(\frac{\gamma}{\Delta\rho\cdot g}\right)^{0{\cdot}5} \quad . \quad . \quad . \quad . \quad . \quad . \quad . \quad . \quad (15)$$

From Equations (4) and (15):

$$\frac{d^{o}_{vs}(\text{Knitmesh})}{d^{o}_{vs}(\text{Raschig rings})} = \frac{2{\cdot}44\left(\dfrac{\gamma}{\Delta\rho\cdot g}\right)^{0{\cdot}5}}{0{\cdot}92\left(\dfrac{\gamma}{\Delta\rho\cdot g}\right)^{0{\cdot}5}} \quad . \quad . \quad . \quad . \quad . \quad (16)$$

$$= 2{\cdot}65 \quad . \quad . \quad . \quad . \quad . \quad . \quad (17)$$

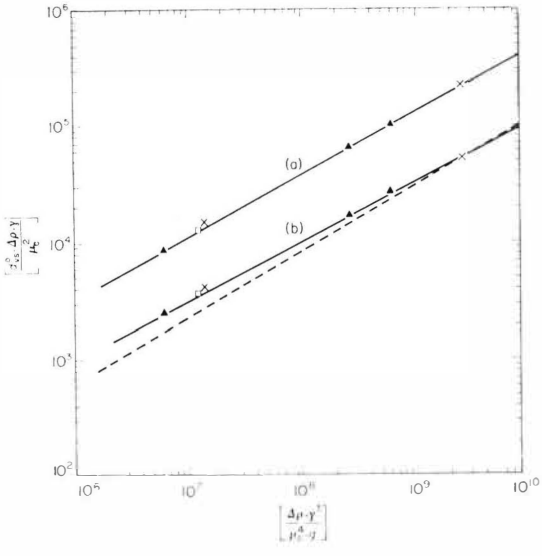

FIG. 9. *Correlation of equilibrium exit dropsize for high voidage packings*

(a) knitted mesh dispersed phase 'wetting'; (b) knitted mesh packing continuous phase 'wetting'; - - - conventional packing

○ iso-octane–water; ▲ toluene–water; × methyl isobutyl ketone–water; □ benzaldehyde–water; △ ethyl acetate–water; △ amyl alcohol–water

In a similar investigation covering packings 'wet' by the continuous phase the following general correlation was obtained (Fig. 9):

$$\frac{d^{o}_{vs}\,\Delta\rho\gamma}{\mu_c^{\,2}} = 0{\cdot}917\left(\frac{\Delta\rho\,\gamma^3}{\mu_c^{\,4}\cdot g}\right)^{0\cdot506} \quad . \quad . \quad . \quad . \quad . \quad . \quad . \quad (18)$$

which upon simplification yields:

$$d^{o}_{vs}\,(\text{non-wetted Knitmesh}) = 0{\cdot}92\left(\frac{\gamma}{\Delta\rho\cdot g}\right)^{0\cdot5} \quad . \quad . \quad . \quad . \quad (19)$$

Thus, comparing Equations (19) and (14):

$$\frac{d^{o}_{vs}\,(\text{wetted Knitmesh})}{d^{o}_{vs}\,(\text{non-wetted Knitmesh})} = 2{\cdot}65 \quad . \quad . \quad . \quad . \quad . \quad . \quad (20)$$

Equations (17) and (20) demonstrate the improved coalescing performance of knitted mesh packings 'wet' by the dispersed phase as opposed to 'non-wetted' knitted mesh and Raschig rings. Investigations are in progress to refine the accuracy of Equations (14) and (18) and to investigate further the effect of phase flow rates.

For efficient coalescer performance, with 'wetted' packings, the maximum flow rate of dispersed phase, corresponds to the transition between 'drip point' detachment and 'jet' formation. This is a function of the system physical properties and the hydraulic dimensions of the packed section. As stated previously, this transition is approached most rapidly with low voidage packed sections. It was observed that the exit dropsize decreased with increasing dispersed phase flow, until the transition to 'jetting' occurred; the exit dropsize after the transition regime was governed by the break-up mechanisms of jet disruption. In general, over the range of flows examined, the droplet size produced by jet disruption (0·50–0·80 cm) were still greater than the inlet sizes considered in the present work (0·20–0·60 cm) (Fig. 10).

As an extension to this work an attempt has been made to predict the transition from the 'drip' point to 'jetting' regimes. Using conventional packed-bed theory to predict interstitial path dimensions and the 'jetting' velocity correlations of Meister & Schede[41] to predict the transition flow rate, reasonable agreement between predicted and experimental results has been demonstrated (Thomas, R. J., unpublished results). Prediction of the droplet size due to 'jet' disruption based upon stability analysis of the 'jet' stream[42] was also possible.

Thus the Sauter mean drop size after passage through a knitted mesh packed section can be predicted for the operating conditions outlined in this paper. Work is continuing to investigate the effect of continuous phase flow rate, although qualitative observations have been made. For example, in counter-current flow, a decrease in the effective density difference and hence of droplet velocity would be expected, resulting in enlarged exit droplet sizes and higher jetting velocities. This has been observed in practice (Thomas, R. J., unpublished results).

Droplet behaviour in 'non-wetted' knitted mesh packings, with voidages greater than 95% can be related to the behaviour of dispersed phase droplets in conventional packings. This was found to be practical in the evaluation of the 'characteristic velocity' V_o, and dispersed phase interfacial area, from experimentally determined values of dispersed phase hold-up (Fig. 1(a) and (b)). Table III compares typical results for Raschig ring and knitted mesh packings.

Similarly a general correlation of the 'flooding' velocities in 'non-wetted' packings has been attempted. The object in the development of the general correlation was to determine relationships between the variables, so that the curves for all experimental runs could be superimposed on a single curve. In the absence of any quantitative mathematical theory for flow in such systems

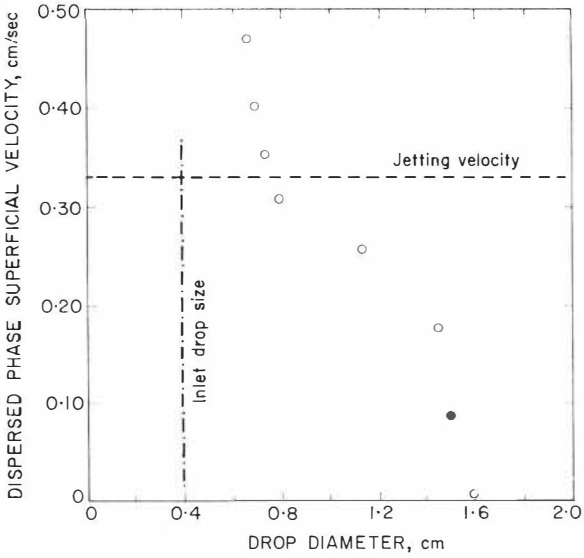

FIG. 10. *Effect of dispersed phase flow rate on exit dropsize ('drip-point' to 'jetting' transition)*

Dispersed phase wetting; packing 9031; iso-octane–water

TABLE III

Comparison of 'characteristic velocity' for iso-octane–water system

Packing	Voidage, %	V_0*. cm/sec	Packing	Voidage, %	V_0, cm/sec
1 in Raschig rings	80·30	7·90	9030	99·25	5·76
¾ in ,, ,,	75·60	6·35	9036	98·75	5·00
½ in ,, ,,	72·80	4·62	9031	95·00	3·09

*Reference 10

an empirical approach was necessary. Certain variables would be expected to effect limiting flows, for example, phase density difference, interfacial tension and packing characteristics. The effect of each variable has been isolated graphically.

The 'flooding' point was taken as being the condition at which the dispersed phase accumulated as a flocculated layer below the packing, the depth of this layer gradually increasing with time. The initial correlation, which represents all the experimental data to within 15%, is presented in Fig. 11 and this is to be refined.

Some general observations of droplet behaviour were made. Below the 'flooding' point, the dispersed phase consisted of nearly spherical droplets of approximately constant size owing to the dispersed phase distributor producing drops less than the critical size, defined by Equation (9). The streams of discrete droplets passed upwards through the packed section, deforming where necessary, to pass through the interstices of the packing. As the 'flood' point was approached the hold-up of the dispersed phase increased with an increase in the degree of interdroplet coalescence, the breakdown/coalescence mechanism described earlier becoming a feature of this regime. At the 'flood' point, the dispersed phase droplets collected below the packed section, whilst the dispersed phase within the packing remained as discrete close packed droplets.

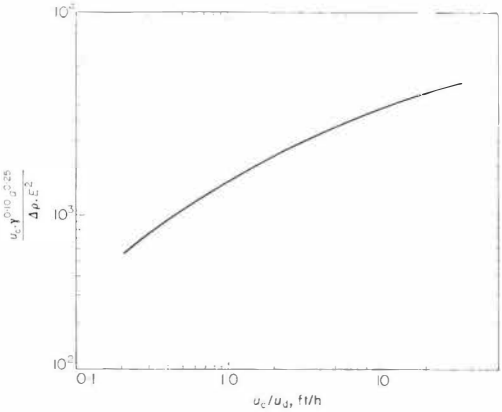

E = voidage

FIG. 11. *General flooding correlation for knitted mesh packing*

There was some evidence that the 'flooding' characteristics of knitted mesh packings are a function of the inlet droplet sizes, an observation also reported by Piper and this requires clarification.

Some observations have been made of the droplet size distributions, but a complete analysis is not feasible at present. The size distribution is determined by two opposing mechanisms; breakdown by impact with packing elements and growth due to interdroplet or drop/interface coalescence. The relative magnitudes of each effect are governed by the packing properties, phase flow rates and wetting phenomena; the differing rates producing a heterogeneous (multimodal) log-normal size distributions. Log-normal distributions have been reported by Thornton for droplet distribution changes in γ conventional packings.

Conclusions

1. The surface properties of the knitted mesh packings, with regard to 'wetting' or 'non-wetting' by the dispersed phase are of paramount importance in packing selection and operational characteristics. This is well illustrated in the single fibre collision study (Thomas, R. J., unpublished results) shown in Fig. 12(a) and (b). Coalescence efficiency is greatest in the case of 'wetted' packings.

2. For 'non-wetted' packings, there is some analogy with the breakdown-coalescence mechanism proposed by Thornton[18] and droplet behaviour can be interpreted as for conventional packings.

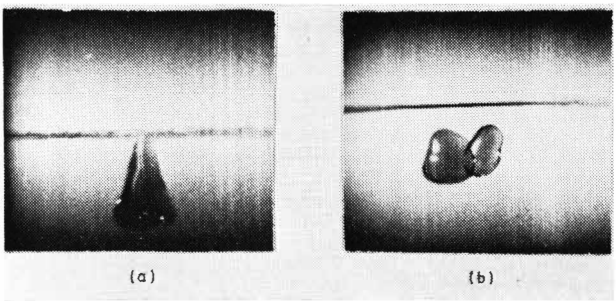

FIG. 12. *Droplet impact on single fibre*
(a) 'Wetted' fibre; (b) 'non-wetted' fibre

3. For 'wetted' packings, the coalescence mechanism predominates and prediction of the equilibrium exit dropsize is possible using Equation (14).

It is clear from the experimental work to date, that the inherent non-homogeneity of the packings precludes absolute description of droplet behaviour and all correlations must be viewed as representing the most probable, or most often observed behaviour.

There is every indication that the preliminary conclusions stated above, coupled with work in progress, will lead to the establishment of a satisfactory design procedure for knitted mesh coalescers. The results presented are also applicable to the operation of the Scheibel column (or any column) containing open-knitted wire or plastic mesh packings.

Acknowledgments

The authors wish to express appreciation of the advice and assistance of Prof. G. V. Jeffreys under whose direction this work was undertaken. One of them (R.J.T.) would like to thank the Science Research Council for support during this work.

Nomenclature

d_{vs}	Sauter mean droplet diameter at finite flowrates
d^{o}_{vs}	Sauter mean droplet diameter at substantially zero flowrates
d_p	critical packing size as defined by Equation (1)
d_c	critical droplet size
$d_{vs(eq.)}$	equilibrium value of d_{vs}
γ	interfacial tension
$\Delta\rho$	density difference between phases
μ_d, μ_c	viscosity of the dispersed and continuous phases, respectively
V_d, V_c	superficial velocities of the dispersed and continuous phases, respectively
V_t	terminal velocity in finite medium
V_o, v_o	velocity of the dispersed phase relative to the continuous phase at substantial zero flow rates, i.e. 'characteristic velocity'
a	specific interfacial area of dispersed phase
h	height of packed section
ε	voidage of packed section
x, X	fractional hold-up of the dispersed phase
g	acceleration due to gravity
Φ	function
ρ_d	dispersed phase density.

References

[1] Thomas, R. J., & Mumford, C. J., to be published
[2] Becher, P., 'Emulsions, Theory and Practice', 1965 (New York: Reinhold)
[3] Purchas, D. B., 'Industrial Filtration of Liquids', 1967 (London: Leonard Hill)
[4] Kintner, R. C., Sareen, S. S., Rose, P. M., & Gudesen, R. C., *A.I.Ch.E. Jl*, 1966, **12**, 1045
[5] Hazlett, R. N., *N.R.L. Rep.*, 1968, 68–383
[6] Jeffreys, G. V., & Davies, G. A., *Filtration Separation*, 1969 (July), p. 349
[7] Lewis, J. B., Jones, I., & Pratt, H. R. C., *Trans. Instn chem. Engrs*, 1951, **29**, 136
[8] Gayler, R., & Pratt, H. R. C., *Trans. Instn chem. Engrs*, 1953, **31**, 69
[9] Gayler, R., & Pratt, H. R. C., *Trans. Instn chem. Engrs*, 1951, **29**, 110
[10] Gayler, R., Roberts, N. W., & Pratt, H. R. C., *Trans. Instn chem. Engrs*, 1953, **31**, 57
[11] Dell, F. R., & Pratt, H. R. C., *Trans. Instn chem. Engrs*, 1951, **29**, 270
[12] Dell, F. R., & Pratt, H. R. C., *Trans. Instn chem. Engrs*, 1951, **29**, 89
[13] Wicks, C., & Beckman, R. B., *Ind. Engng Chem.*, 1950, **42**, 1078
[14] Puranik, S. A., & Sharma, M. M., *Chem. Engng Sci.*, 1970, **25**, 257
[15] Porter, K. E., *Trans. Instn chem. Engrs*, 1968, **46**, 69
[16] Schulmann, H. L., & Mellish, W. G., *A.I.Ch.E. Jl*, 1967, **13**, 1137
[17] Ellis, S. R. M., & Garner, F. H., & Hill, J. W., *A.I.Ch.E. Jl*, 1955, **2**, 185
[18] Thornton, J. D., & Ramshaw, C., *Instn chem. Engrs Symp. Series*, 1967, No. 26, 86
[19] Thornton, J. D., *Ind. Chemist*, 1964, (Jan.), p. 13

[20] Thornton, J. D., & Ramshaw, C., *Instn chem. Engrs Symp. Series*, 1967, No. 26, 73
[21] Breckenfield, R. R., & Wilke, C. R., *Chem. Engng Prog.*, 1950, **46,** 187
[22] Blanding, F. H., & Elgin, J. C., *A.I.Ch.E. Jl*, 1942, **33,** 305
[23] Crawford, R., & Wilke, C. R., *Chem. Engng Prog.*, 1951, **47,** 423
[24] Osipow, L. I., 'Surface Chemistry', 1962 (New York: Reinhold)
[25] Hill, J. W., *Chem. Engr, Lond.*, 1954, **5,** 43
[26] Scheibel, E. G., *Chem. Engng Prog.*, 1948, **44,** 681
[27] Perry, J. H., 'Chemical Engineering Handbook', 4th edn (New York: McGraw-Hill)
[28] Jeffreys, G. V., & Mumford, C. J., *3rd CHISA Congr., Mariánské Lázně (Czechoslovakia)*, 1969
[29] Honeykamp, J. R., & Burkhart, L. E., *Ind. Engng Chem. Process Des. Dev.*, 1962, **1,** 177
[30] Slatter, M. A., Thesis, Univ. of Aston, 1968
[31] Piper, H., Thesis, Univ. Manchester Inst. Science & Technol., 1965
[32] Juma, S. M., Thesis, Univ. Manchester Inst. Science & Technol., 1969
[33] Lawson, G. B., *Chem. Process Engng*, 1967 (May), p. 45
[34] Groothuis, H., & Zuiderweg, F. J., *Chem. Engng Sci.*, 1960, **12,** 288
[35] Treybal, R. E., 'Liquid–Liquid Extraction', 1963, Vol. II (New York: McGraw-Hill)
[36] Lawson, G. B., 1968, Thesis, Univ. Manchester Inst. Science & Technol.
[37] Jacobs, M. B., & Scheflan, L., 'Chemical Analysis of Industrial Solvents', 1953 (New York: Interscience)
[38] Lashkari, M., Project, Univ. of Aston, 1970
[39] Jeffreys, G. V., & Hawksley, J., *A.I.Ch.E. Jl*, 1968, **14,** 15
[40] Neilsen, L. E., Wall, R., & Adams, G., *J. Colloid Sci.*, 1958, **13,** 441
[41] Meister, B. J., & Scheele, G. F., *A.I.Ch.E. Jl*, 1969, **14,** 15
[42] Sherony, D., Thesis, Illinois Inst. Technol., 1969

Effect of adjacent drops on the shape of a drop approaching a deformable liquid–liquid interface

by J. D. Robinson and S. Hartland
Chemical Engineering Department, The University, Nottingham, U.K.

The effect of adjacent drops, in a two dimensional array, on the arc length of the draining film beneath a drop approaching a bulk interface was investigated photographically. For a single horizontal row of drops the arc length is less than that beneath a single drop. The arc length is least for the middle drop in the row and, for this drop, reaches a constant minimum value when about five drops are present. In a vertical column of two drops having equal volume, the arc length beneath the drop at the interface is greater than that for a single drop due to the increased vertical force acting on the drop. When horizontal rows of drops are arranged in a vertical column, the arc length at the interface increases with the height of the vertical column. However, the arc length is less than that for a single vertical column of two drops, even when up to four rows are present, due to the horizontal force exerted by the adjacent drops in the row.

The residence time of a drop at the bulk interface decreases as the dispersion height increases since the rate of drainage increases with the applied vertical force. When drops are continuously introduced the rate of coalescence at the bulk interface must equal the feed rate when the steady state dispersion thickness is attained. Three regions are observed in the close-packed dispersion; initially the voidage is relatively high, but the centre of the dispersion assumes a regular polygonal shape like that of a gas–liquid foam; finally the voidage again increases as continuous phase is liberated by groups of drops coalescing at the bulk interface. Circulation does not occur in viscous two-dimensional dispersions and coalescence is consequently slower than in three-dimensional dispersions.

Introduction

MASS TRANSFER BETWEEN two liquids may be enhanced by increasing the interfacial area and interfacial turbulence. This is usually brought about by sidpersing one phase in another in the form of drops. When the mass tranfers is complete the drops must be recombined to form the bulk phase. The drops are allowed to collect in a close-packed dispersion in which they may coalesce with each other but finally coalescence at the bulk interface must occur.[1,2] Circulation patterns play an important part in the behaviour of such dispersions but essentially the disperse phase is moving through a continuous phase in which there is no overall flow. As the disperse phase flowrate increases so does the thickness of the close packed dispersion.[3,4] At the steady state, the rate of coalescence at the bulk interface must equal the flowrate. This rate of coalescence of a drop at the bulk interface depends on the rate of drainage of the film of continuous phase trapped between the drop and the interface.[5] The rate of drainage increases with the force pressing on the drop and decreases as the area of the film increases; however, the problem is complicated by the fact that this area itself depends on the applied force.[6,7] In a close packed dispersion, the drops above press on the drops at the interface and increase the rate of drainage. As the drops are moving towards the interface the viscous drag force as well as the buoyancy force must be subtracted from the weight of the drops.

This paper sets out to investigate the effect of adjacent drops on the size of the draining film between a drop and the bulk interface. The effects of horizontal rows of drops and vertical columns are studied. The drops are contained in a two-dimensional cell since it is difficult to observe the drops in a three-dimensional dispersion. In order to minimise the optical distortion and slow down the rate of coalescence, pairs of liquids with close refractive indices and high viscosities are used for the disperse and continuous phases.

Experimental

The liquid–liquid systems were studied as follows: (i) liquid paraffin drops rising through golden syrup containing water (5% by vol.) and approaching an interface with liquid paraffin; (ii) liquid paraffin drops rising through glycerol and approaching an interface with liquid paraffin; (iii) 50% by vol. aqueous glycerol drops falling through silicone fluid and approaching an interface with 50% by vol. aqueous glycerol; and (iv) golden syrup drops containing potassium iodide (25% by wt.) falling through sextol phthalate (a mixture of isomeric dimethyl cyclohexyl phthalates) and approaching an interface with golden syrup containing 25% potassium iodide (25% by wt.).

The physical properties of these liquids are given in Table I. Refractive indices were measured on an Abbé refractometer, viscosities using a Ferranti–Shirley cone and a plate viscometer and interfacial tensions by the pendant drop method.[8] Water or potassium iodide was added to golden syrup, and water to glycerol to adjust their refractive indices.

TABLE 1

Physical properties of liquids measured at 22·5°C

	Golden syrup +5vol.-%	Liquid paraffin	Glycerol	50vol.-% aqueous glycerol	Silicone fluid	Golden syrup +25vol.-%KI	Sextol phthalate
Refractive index	1·488	1·483	1·472	1·405	1·405	1·511	1·516
Density, kg/m³	1410	879	1240	1142	973	1560	1069
Viscosity, Nsec/m²	2·750	0·185	0·810	0·008	1·211	18·5	13·70
Interfacial tension, mJ/m²	37·0	27·5		30·0		23·9	

The two immiscible liquids were placed in a Perspex cell (height 7 cm, length 7 cm) with a width similar to the diameter of a sphere equal in volume to the drops used. The drops were introduced from a syringe needle and allowed to approach their static equilibrium position before being photographed as previously described.[5] In the static equilibrium position the drops did not move relative to each other. In some experiments, lycopodium powder was placed at the interface to indicate the direction of drainage in the film. In another series of experiments liquid paraffin drops were continuously dispersed in glycerol or golden syrup containing 5% by vol. water. The drops were introduced into a Perspex cell (height 33 cm, length 25 cm and width 0·6 cm) through twelve stainless-steel nozzles (0·25 cm diameter), and allowed to approach an interface with liquid paraffin. The dispersion was photographed when the steady state was reached as described above.

Liquid paraffin drops were also dispersed in glycerol or golden syrup containing 5% by vol. water in a cubical glass cell with sides 7 cm long. Photographs of the drops approaching the interface were taken from above, the cell being illuminated from below by light from a mirror inclined at 45° to the horizontal.

Results and discussion

Typical photographs of the two-dimensional drops are shown in Figs 1, 2 and 3, for the static system, and in Figs 4, 5 and 6 for the continuous system. The negatives were projected on to a screen and the values of x and φ indicated in Fig. 7 were obtained for the drops at the bulk interface, the magnification being obtained from the known diameter of the syringe needle. Because of the equal densities of the liquids bounding the draining film the overall shape of the draining film is spherical[9,10] and so the maximum cross-sectional arc length of the draining film was calculated from $L = x\varphi/\sin\varphi$. Since the walls of the cell deform the drops, the area of the draining film could not easily be calculated and so only the arc lengths were compared.

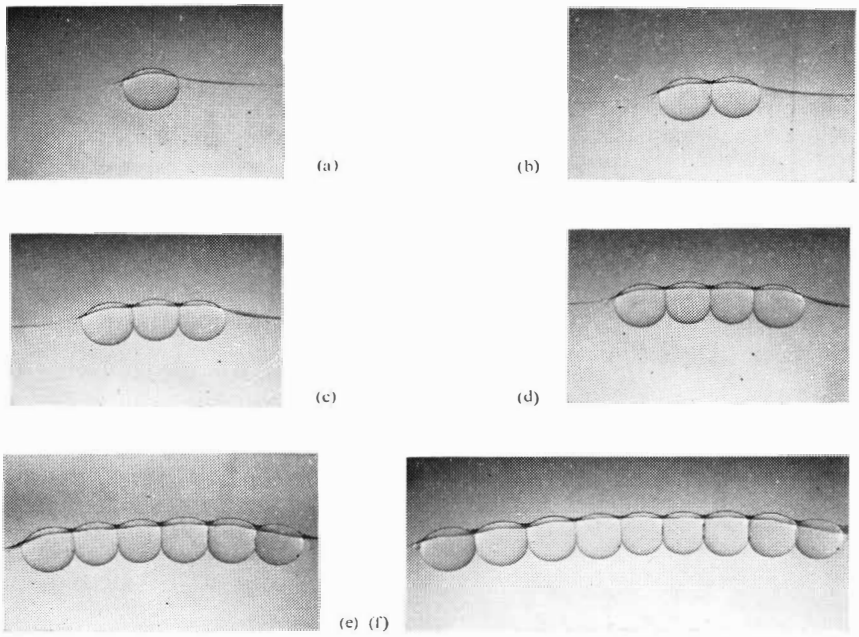

FIG. 1. *A single horizontal row of liquid paraffin drops each of volume 0·13 ml, in glycerol, and approaching an interface with liquid paraffin*

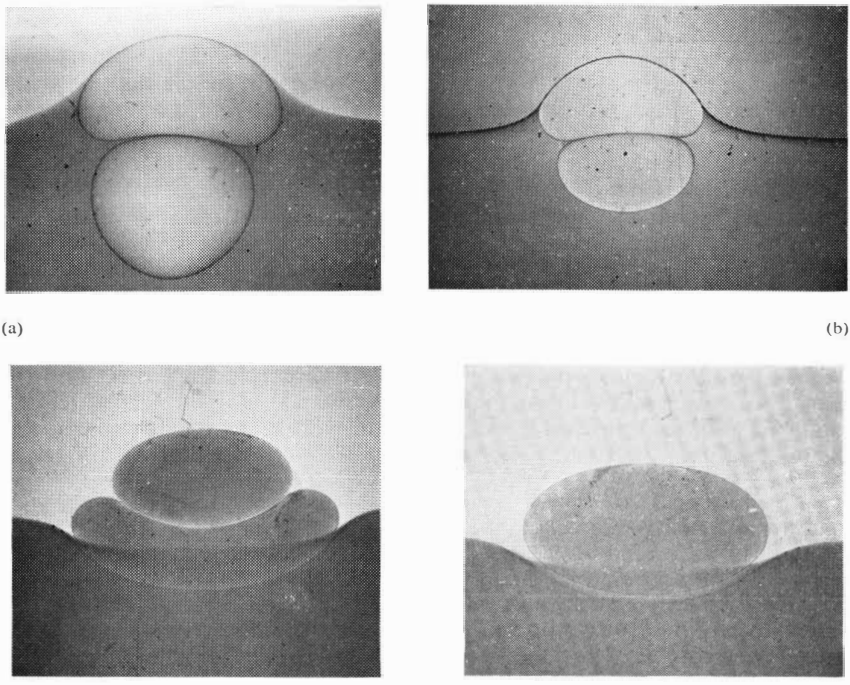

FIG. 2. *A vertical column of two drops approaching an interface*

(a) liquid paraffin drops each of volume 0·3 ml, in golden syrup and approaching an interface with liquid paraffin
(b) liquid paraffin drops each of volume 0·2 ml, in glycerol and approaching an interface with liquid paraffin
(c) golden syrup drops each of volume 0·3 ml, in sextol phthalate and approaching an interface with golden syrup
(d) single golden syrup drop of volume 0·3 ml, in sextol phthalate and approaching an interface with golden syrup, for comparison

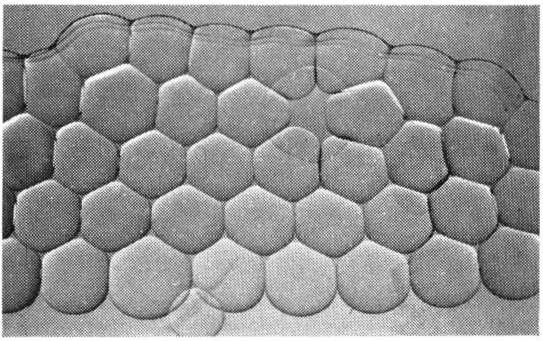

FIG. 3. *Five rows of liquid paraffin drops of volume 0·13 ml in a vertical column, in glycerol and approaching an interface with liquid paraffin*

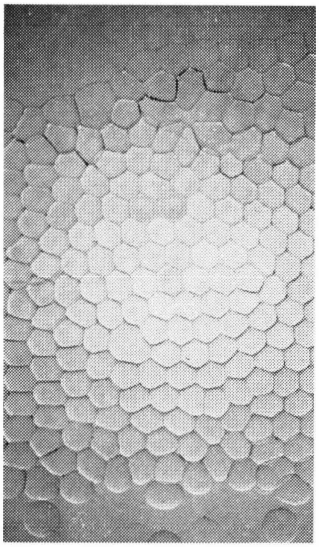

FIG. 4. *A continuous dispersion of liquid paraffin drops in glycerol and approaching an interface with liquid paraffin*

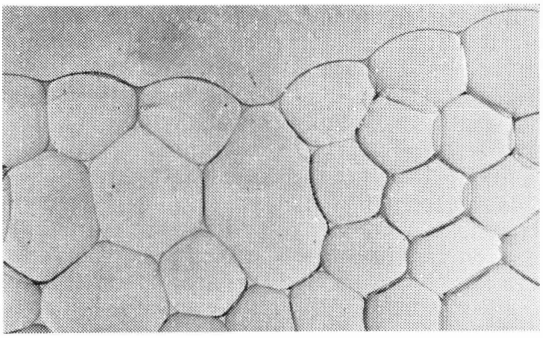

FIG. 5. *A continuous dispersion of liquid paraffin drops in glycerol and approaching an interface with liquid paraffin, showing coalescing interface*

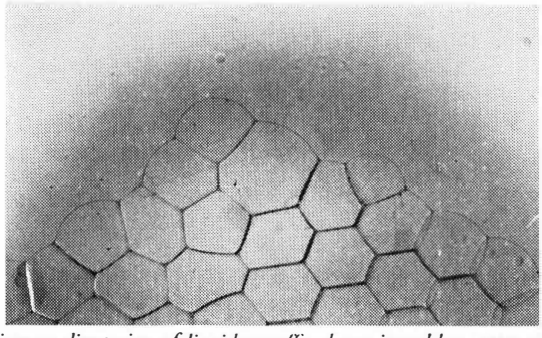

FIG. 6. *Continuous dispersion of liquid paraffin drops in golden syrup and approaching an interface with liquid paraffin, showing coalescing interface*

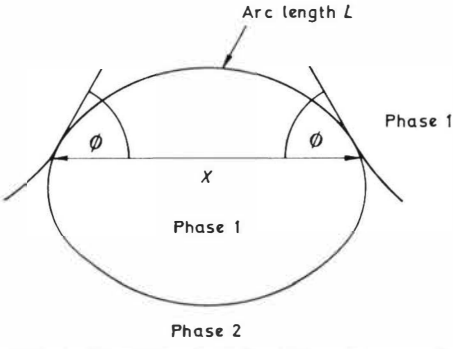

FIG. 7. *Characteristic dimensions for a liquid drop in a two-dimensional array approaching a deformable interface*

Figs 1(a)–(f) show the drop shape when 1, 2, 3, 4, 6 and 9 drops respectively are approaching the bulk interface. The variation in the arc length beneath a drop, with the number and volume of drops present in the row, is shown in Tables II and III. The arc length is least for the drops in the middle of the row and reaches a minimum when there are about five drops present. The decrease in arc length is due to the horizontal forces exerted by the adjacent drops. The arc length for a drop in the middle of a long row is about 30% less than that for a single drop for both the liquid paraffin–golden syrup and liquid paraffin–glycerol systems. However, the difference is only about 12% for the aqueous glycerol–silicone system. In a row of drops of volume 0·2 ml or less the middle drop usually coalesces with the bulk interface first since its arc length is smallest. However, when the drop volume is large, binary coalescence tends to occur before coalescence at the bulk interface. The inclusion of lycopodium powder at the bulk interface shows that symmetrical drainage usually occurs in the films beneath the drops in a regular row.

When a drop of equal volume is balanced on top of the drop at the bulk interface, the arc length at the bulk interface is greater than that for a single drop as shown in Fig. 2 because of the additional vertical force exerted by the second drop. Table IV shows that the arc lengths are about 50% greater than those for a single drop for both the liquid paraffin–glycerol and golden syrup–sextol phthalate systems. However, the difference is only about 15% for the liquid paraffin–golden syrup system. In such a vertical column of two drops, binary coalescence usually occurs when the drop volume is greater than 0·1 ml, showing that the effect of the smaller area between the drops is greater than that of the increased vertical force acting on the draining film adjacent to the bulk interface. The presence of lycopodium powder shows that symmetrical drainage occurs in both the films at the bulk interface and between the two drops.

TABLE II

Effect of number of drops on the maximum cross-sectional arc lengths of the draining films beneath drops in a horizontal row at a deformable liquid–liquid interface

Drop volume, ml	Number of drops	Arc length, cm															
		Phase 1 = liquid paraffin; phase 2 = golden syrup															
0·10	1								0·50								
	2							0·45		0·45							
	3						0·44		0·42		0·45						
	4					0·46		0·38		0·38		0·45					
	5				0·45		0·39		0·35		0·38		0·46				
	6			0·40		0·39		0·37		0·36		0·38		0·43			
	7		0·40		0·38		0·36		0·36		0·37		0·39		0·42		
	8	0·40		0·39		0·36		0·37		0·36		0·39		0·38		0·40	
		Phase 1 = liquid paraffin; phase 2 = glycerol															
0·13	1								0·47								
	2							0·44		0·44							
	3						0·38		0·33		0·38						
	4					0·39		0·33		0·33		0·39					
	5				0·40		0·35		0·32		0·35		0·40				
	6			0·37		0·35		0·32		0·32		0·34		0·37			
	9	0·37	0·36		0·34		0·31		0·31		0·31		0·34		0·37		0·40
		Phase 1 = aqueous glycerol; phase 2 = silicone fluid															
0·15	1								0·41								
	2							0·37		0·39							
	3						0·41		0·40		0·41						
	4					0·38		0·35		0·36		0·39					
	5				0·37		0·36		0·37		0·38		0·38				
	6			0·38		0·37		0·37		0·35		0·39		0·40			

TABLE III

Effect of drop volume on the maximum cross-sectional arc lengths of the draining films beneath drops in a horizontal row at a deformable liquid–liquid interface

Drop volume, ml	Number of drops	Arc length, cm						
Phase 1 = liquid paraffin; phase 2 = golden syrup								
0·2	1			0·72				
	2		0·63		0·64			
	3	0·69		0·55		0·66		
	4	0·65	0·45		0·53		0·63	
	5	0·66 0·47		0·47		0·52		0·64
0·3	1			0·92				
	2		0·80		0·80			
	3	0·77		0·55		0·84		
	4	0·80	0·53		0·56		0·79	
0·4	1			1·00				
	2		0·94		0·94			
	3	0·97		0·77		0·94		
Phase 1 = liquid paraffin; phase 2 = glycerol								
0·2	1			0·87				
	2		0·71		0·68			
0·3	1			1·00				
	2		0·88		0·90			
0·4	1			1·16				
	2		1·04		1·04			
Phase 1 = golden syrup + KI; phase 2 = sextol phthalate								
0·1	1			0·70				
	2		0·65		0·59			
	3	0·60		0·53		0·59		
0·2	1			0·84				
	2		0·75		0·78			
	3	0·72		0·60		0·73		
0·4	1			1·36				
	2		1·03		1·03			
	3	1·00		0·74		1·02		

TABLE IV

Maximum cross-sectional arc lengths of draining films beneath drops in a single vertical column

Drop volume, ml	Arc length at bulk interface, cm	Arc length between drops, cm
Phase 1 = liquid paraffin; phase 2 = golden syrup		
0·1	0·61	0·27
0·2	0·84	0·28
0·3	1·04	0·36
Phase 1 = liquid paraffin; phase 2 = glycerol		
0·1	0·69	0·30
0·2	1·24	0·63
0·3	1·53	0·85
Phase 1 = golden syrup + KI; phase 2 = sextol phthalate		
0·2	1·33	0·91
0·3	1·72	1·02

Fig. 3 shows the shape of drops when five horizontal rows are present in a vertical column. The effect of the number of rows on the arc length of the middle drop in the row at the bulk interface is shown in Table V. Any vertical column. The effect of the number of rows on the arc lengths of the middle drops in the row at the bulk interface is shown in Table V. Any variation is due to the increased number of rows pressing on the interface, as Table III shows that the effect of the drops on either side is constant for a long row. For both the liquid paraffin–golden syrup and aqueous glycerol–silicone systems, the arc length increases by about 22% as the number of rows increases from one to four. However, the arc length for the liquid paraffin–glycerol system initially decreases as the number of rows increases.

TABLE V

Effect of number of rows on the arc length of the draining film beneath middle drop in row at the deformable liquid–liquid interface

Drop volume, ml	Number of rows of drops pressing on bulk interface	Arc length of draining film at bulk interface, cm
Phase 1 = liquid paraffin; phase 2 = golden syrup		
0·10	1	0·36
	2	0·33
	3	0·39
	4	0·44
Phase 1 = liquid paraffin; phase 2 = glycerol		
0·13	1	0·31
	2	0·46
	3	0·43
	4	0·38
	5	0·34
Phase 1 = aqueous glycerol; phase 2 = silicone fluid		
0·15	1	0·37
	2	0·39
	3	0·42
	4	0·45

Comparison of the arc length at the bulk interface for a single column of two drops, given in Table IV, with the values given in Table V, emphasises the effect of the horizontal force exerted by the adjacent drops in a row. For the liquid paraffin–golden syrup system, the arc length for a single column of two 0·1 ml drops is 38% greater than that when four rows are present.

The static study of liquid drops was extended to one in which drops were continuously introduced for both the liquid paraffin–golden syrup and liquid paraffin–glycerol systems. The height of the dispersion increases with time until at the steady state the flow rate of disperse phase equals its rate of coalescence at the bulk interface. For a given liquid paraffin flow rate the steady state dispersion thickness is less when glycerol is the continuous phase because the viscosity of the draining films is less than when golden syrup is the continuous phase. In both systems three regions may be discerned within the dispersion band. Initially, the drops collect together and form a region where the voidage is relatively high. In the centre of the dispersion the draining films become very thin and a regular polygonal structure is formed in which the drops usually have five or six sides as shown in Fig. 4. Finally there is a region close to the bulk interface where the voidage again increases, because continuous phase is liberated when drops coalesce as shown in Fig. 5 for the liquid paraffin–glycerol system. Due to the large differences in density and viscosity between the two phases in the liquid paraffin–golden syrup system, the regular polygonal structure is similar to that in gas–liquid foams[11] and may extend up to the bulk interface as shown in Fig. 6, because less continuous phase is liberated from the thinner draining films.

Interdrop coalescence, forming larger drops as shown in Fig. 5, may occur with both systems but more usually direct coalescence at the bulk interface occurs. However, a drop may coalesce at the walls of the cell (as seen earlier in Fig. 3) which promotes coalescence of the surrounding drops. Coalescence at the bulk interface usually occurs in groups of four or five drops for the liquid paraffin–golden syrup dispersion and in groups of ten to fifteen drops for the paraffin–glycerol dispersion. This leaves the bulk interface uneven and may lead to unsymmetrical drainage as shown in Fig. 5.

A single horizontal layer of drops at the bulk interface assumes a close packed arrangement with each drop surrounded by six others. Fig. 8 shows a single horizontal layer of liquid paraffin drops in golden syrup approaching an interface with liquid paraffin.

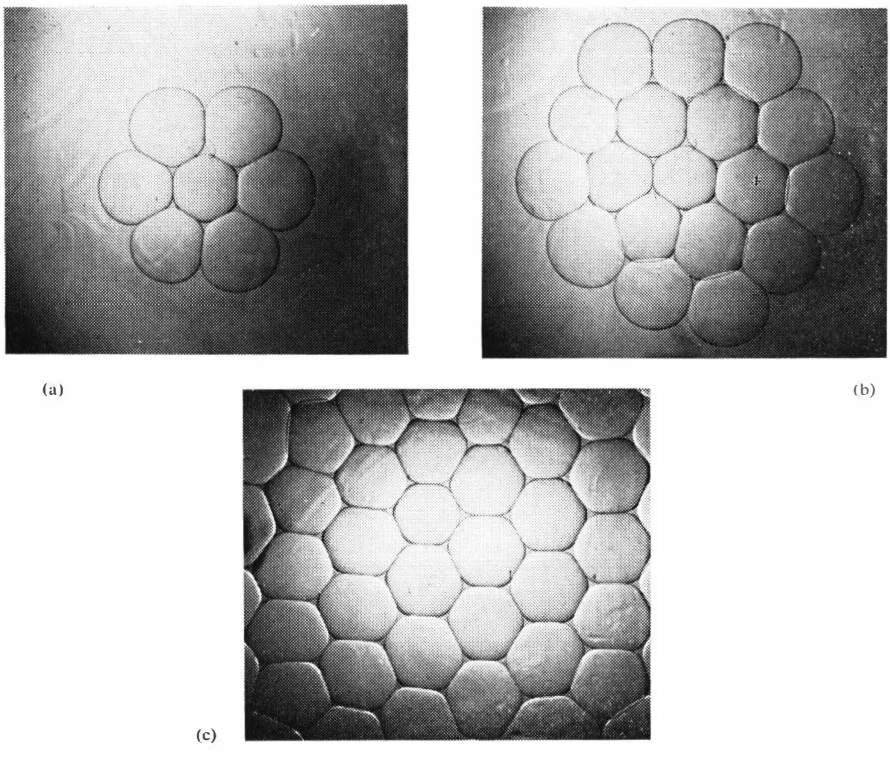

FIG. 8. *A single horizontal layer of liquid paraffin drops in golden syrup approaching an interface with liquid paraffin (viewed from above)*

(a) Symmetrical arrangement for 7 drops (b) Symmetrical arrangement for 18 drops
(c) Section of arrangement for large number of drops

However, as more horizontal layers of drops are added, the regular polygonal structure does not persist throughout the three dimensional dispersion which is formed. Circulation usually occurs as the larger drops, formed by binary coalescence, have a smaller viscous drag force per unit volume and so rise quicker through the dispersion carrying continuous phase with them.[12] This quickly transports drops to the coalescing interface and prevents formation of the regular polygonal structure. For the same disperse phase flowrate per unit area three dimensional dispersion heights are consequently smaller than those for two dimensional dispersions in which the proximity of the cell walls restricts circulation and allows the regular polygonal structure to develop.

Conclusions

The shape of a liquid drop approaching a deformable liquid–liquid interface is affected by the presence of adjacent drops. In a two-dimensional system, the arc length of the draining film between a drop in a horizontal row and the bulk interface is less than the corresponding value for a single drop. The middle drop in the row, which has the smallest arc length, usually coalesces with the bulk interface first but as the drop volume increases binary coalescence may occur. For a vertical column of two drops, the arc length of the draining film at the bulk interface is greater than the corresponding value for a single drop, due to the additional vertical force exerted by the second drop. For this case binary coalescence occurs before coalescence at the bulk interface.

When horizontal rows of drops are arranged in a vertical column the arc lengths of the draining films at the bulk interface increase with the number of rows. However, the arc length is less than that for a single vertical column of two drops even when four rows are present due to the horizontal force exerted by the adjacent drops in the row.

The residence time of a drop at the bulk interface decreases as the number of rows increases because the rate of drainage increases with the applied vertical force. When drops are continuously introduced the height of dispersion increases until at the steady state the rate of coalescence at the bulk interface is equal to the feed rate. Three regions are observed in the close packed dispersion; initially, the voidage is relatively high, later the centre of the dispersion assumes a regular polygonal shape like that of a gas–liquid foam and finally the voidage again increases as groups of drops coalesce at the bulk interface and liberate continuous phase. Circulation does not occur in viscous two dimensional close packed dispersions and coalescence is slower than in three dimensional dispersions.

Acknowledgment

The authors would like to thank Professor W. Smith for his encouragement, and the Ministry of Technology, Warren Spring Laboratory, Stevenage, England, for financial assistance.

Nomenclature

L maximum cross-sectional arc length of the draining film
x chord length between edges of draining film
φ inclination of edge of draining film to chord

References

[1] Atkinson, E., & Freshwater, D. C., *Br. chem. Engng*, 1958, p. 554
[2] Jackson, R., *Chem. Engr, Lond.*, 1964, **178,** CE107
[3] Ryon, A. D., Daley, F. L., & Lowrie, R. S., *Chem. Engng Prog.*, 1955, **55,** 70
[4] Davies, G. A., Jeffreys, G. V., & Smith, D. V., *A.I.Ch.E.Jl*, 1970, **16,** 823
[5] Hartland, S., *Trans. Instn chem. Engrs*, 1967, **45,** T102
[6] Hartland, S., *Chem. Engng Sci.*, 1969, **24,** 987
[7] Hartland, S., *Can. J. chem. Engng*, 1969, **47,** 221
[8] Andreas, J. M., Hauser, E. A., & Tucker, W. B., *J. phys. Chem., Ithaca*, 1938, **42,** 1001
[9] Princen, H. M., *J. Colloid Sci.*, 1963, **18,** 178
[10] Hartland, S., *Trans. Instn chem. Engrs*, 1967, **45,** T97
[11] Hartland, S., 'The Coalescence of Liquid Drops' (Ciné Film), 1970, Dept. of Chemical Engineering, University of Nottingham
[12] Hartland, S., *Chem. Engng J.*, 1970, **1,** 258

Coalescence and mass transfer

by P. M. Heertjes and L. H. de Nie
University of Technology, Delft, The Netherlands

Coalescence of drops at a liquid–liquid interface has been studied for a binary and for a ternary system.

It has been concluded that mass transfer during drainage can be described by diffusion in a rigid sphere apart from other possible contributions from interfacial phenomena.

Observations on a binary system indicate that instabilities at the interface are not the only cause of the remarkable spread in coalescence time observed. Circulation in the drops, caused by density differences, might also be an important factor.

Introduction

THE PROCESS OF coalescence of drops and the accompanying phenomena get increasing attention. As is well known from investigations over the past ten years on the effect of mass transfer on coalescence with ternary systems, mass transfer into drops increases the stability of the drops whereas mass transfer from drops into the continuous phase promotes coalescence.

For binary systems, instabilities of the interface have also been reported[1,2] which will influence coalescence.

In the present contribution, some experiments are reported on coalescence and mass transfer for a binary system and for a ternary system.

Coalescence and mass transfer

The main point of study has been the influence of mass transfer on coalescence. Drop size and the rate of coalescence at the boundary of phase separation at the end of a contacting step are thereby directly influenced.

The possible contribution to mass transfer during coalescence at a flat interface was determined in a general study on mass transfer at formation and release of drops.

Three stages have to be recognised in the process of coalescence:

settling of the drop and drainage of the film between drop and interface;

rupture; and

coalescence proper.

The process might be repeated in the case where secondary droplets are formed after coalescence.

In the present study, only the first stage has been considered because rupture and coalescence proper take an extremely short time compared with the first step.

Binary systems

Experimental

In the binary system of isobutanol drops in a continuous water phase, experiments were carried out in which all the successive drops arrived at the same place at the interface of coalescence.

The glass apparatus used is shown in Fig. 1. A removable metal cylinder A with a glass cylinder B was installed in such a way that the interface of coalescence could be maintained at the position C. Samples of the homophase could be taken with the hypodermic needle D fixed on the top E, which was constructed in such a manner that any position beyond the interface could be reached for sampling.

Samples of 2·5 mm^3 were taken at a frequency of one per min so that no disturbance would be caused at a drop frequency of one per sec and a drop volume of 4 mm.^{3}

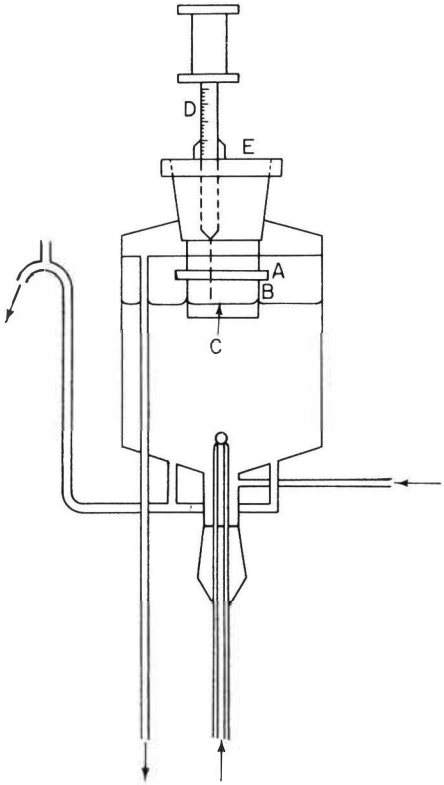

FIG. 1. *Apparatus for measurement of concentration profiles*

In the coalescence time experiments, the time between drop arrival and disappearence was measured electronically for short times and with a stopwatch for long times. The drops were formed at such low frequencies that the drop had disappeared before the arrival of the following drop.

The rate of coalescence was measured at various initial concentrations of water in the isobutanol drops and for different capillaries.

The temperature was kept constant at $20 \cdot 0 \pm 0 \cdot 1$°C.

Results

A typical example of the concentration profiles in the receiving cylinder B at different heights above the interface under stationary conditions, reached after a few hours, is given in Fig. 2. The zero point at the horizontal axis is the point where drops touched the interface. In the central part of B (around zero) no measurements could be made because of the repeated passage of drops.

From the measured profiles combined with visual observation of drops, coloured with cobalt chloride, a schematic presentation of the situation in the homophase as presented in Fig. 3 can be given.

In zone I, a steep concentration gradient exists, in zone II a low and uniform concentration (near to the water content of the drop) is maintained even after 30 h or more, while in zone III the ascending drops keep their identity for some time while rising in the homophase. After a few cm of rise, the drops lose their identity.

The coalescence times for drops formed at different capillaries and with various initial concentrations of water in the isobutanol drop showed a marked dependence on this water concentration and therefore of the influence of the mass transfer, as demonstrated in Fig. 4.

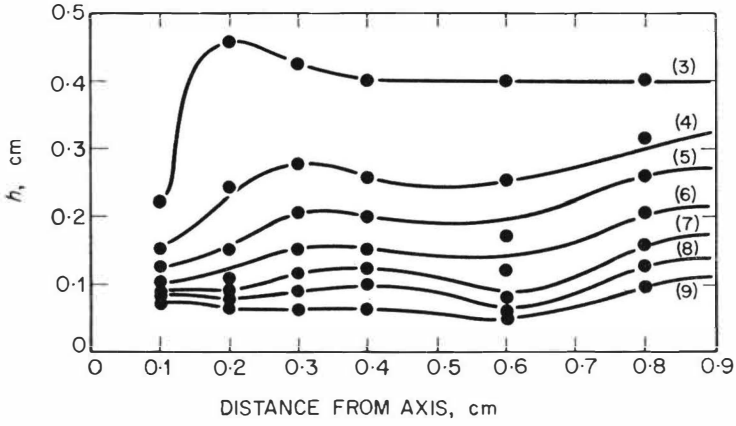

FIG. 2. *Concentration profiles for a cross-section in the receiving tube B*
Numbers in brackets are water concentrations (%)

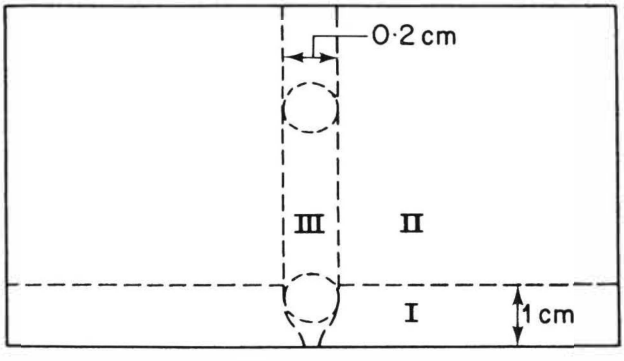

FIG. 3. *Schematic presentation of different concentration regions in the homophase*

Discussion

As indicated in the introduction, an appreciable contribution to the mass transfer exists only during the drainage period. It is understood that at the interface between the continuous phase and homophase, mass transfer takes place also. For profiles as given in Fig. 2, values such as 2×10^{-8} mole/sec cm^2 have been found leading to an amount of mass transfer of the same order of magnitude as during drainage.[3]

A stable concentration gradient causes zero mass transfer in the experiments. For practical conditions where drops arrive at different places at the interface, it can be concluded from Fig. 3 that the comparatively small disruption at the interface will not increase mass transfer considerably.

It should be noted that mass transfer during coalescence is small compared with the other contributions such as drop formation and rise of the drops. Even in experiments with a relatively short rise of the drops (~ 1 cm) and with an interface of coalescence of 2 cm diameter and a coalescence time of a few seconds, the contribution to mass transfer at coalescence and at the interface was less than 5% of the total.[3]

The influence of the initial concentration of water on the rate of coalescence is remarkable. According to Sawistowski & Austin[4], the system isobutanol–water has a stable interface with respect to mass transfer. Merson & Quinn[2] reported interfacial activity for the unsaturated systems. These combined findings do not seem to lead to a conclusion on the influence of mass transfer on coalescence similar to that known for ternary systems.

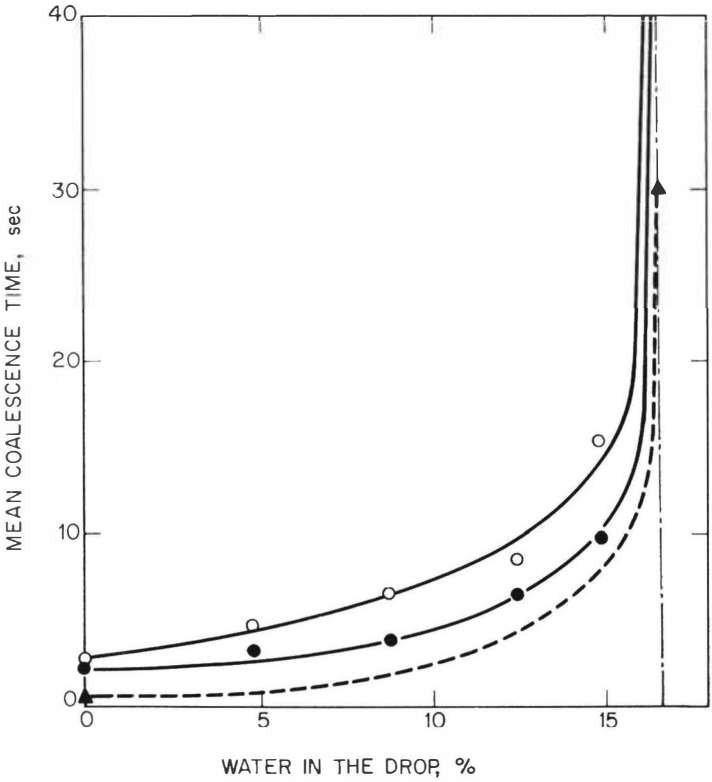

FIG. 4. *Mean coalescence time for isobutanol drops as a function of the initial water concentration in the drop*
V_{dr} (mm³): ▲ 1·3; ● 3·1; × 6·7

An explanation could follow from the circulation patterns in a settling drop as given by Hartland.[5] Density differences due to mass transfer can be the driving forces for a downward circulation inside the drop during drainage which will promote the drainage process. The influence will be larger if the water concentration in the drop is smaller.

Ternary systems

A study of the coalescence behaviour during mass transfer of acetone from water into benzene drops during drainage was made, in which no mass transfer occurred during drop formation, the transfer during drop rise was negligible and the time of drainage could be adjusted.

Experimental

The apparatus used is shown in Fig. 5. Drops were formed at capillary (1) inside a tube (2). The system was benzene drops in a continuous phase of water containing acetone as a solute.

The continuous phase inside tube (2) contained no acetone so that no mass transfer occurred during drop formation. Because of the wake formed in this period, the mass transfer during drop rise was negligible until arrival at the interface of coalescence (3).

The third requirement of an adjustable time of coalescence as mentioned above was realised by the installation of a thin needle (4). This needle was connected to a coil and a spring directed by the phototransistor (5) in such a way that the needle moved downward ($\sim$2 mm) at any installed delay time after arrival of the drop and drop rupture occurred.

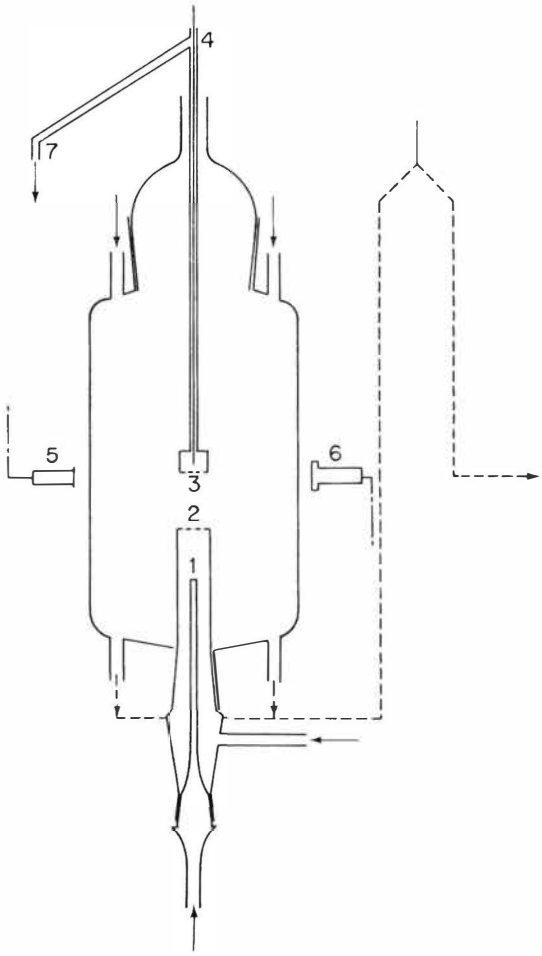

FIG. 5. *Apparatus for measurement of mass transfer during drainage*

The samples for analysis of the mass transfer were collected at overflow (7).

Three series of runs were made for three different concentrations of acetone in the continuous phase.

In all experiments, the temperature was kept constant at $20 \cdot 0 \pm 0 \cdot 1\,^{\circ}\mathrm{C}$.

Results and discussion

It can be seen from Fig. 6 that for the low driving forces applied, the mass transfer during drainage (E_c) is independent of the concentration driving force. A comparison with mass transfer by diffusion into a rigid drop shows that the mass transfer as measured is $2 \cdot 6$ times greater than the value predicted from pure diffusion. This ratio is about the same as can be found from the experiments of Sawistowski & Goltz[6] for drop formation with the same system.

The findings do not permit a final quantitative conclusion but do show that mass transfer during drainage can be described by diffusion fortified by interfacial instability. Because of the relatively low contribution of mass transfer, these findings are of more importance for the study of drop interfaces than for extraction apparatus.

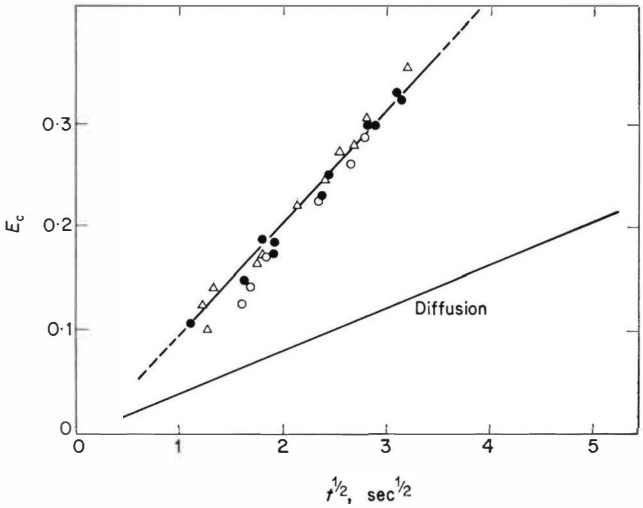

FIG. 6. *Comparison between experimental mass transfer and that as predicted from diffusion*

Acetone in continuous phase (%): ○ 3; ● 4; △ 5
$d = 0{\cdot}360$ cm

Conclusions

The dependence of the rate of coalescence of drops on mass transfer in binary systems cannot be explained entirely by interfacial phenomena.

The mass transfer can essentially be described by diffusion into a rigid body, and thus drops during drainage can be used for the determination of the influence of the behaviour of the interface.

Acknowledgments

Thanks are due to Ir. L. Tjioe and Ir. C. Coulaloglou who carried out the experiments.

References

[1] Austin, L. J., Ying, W. E., & Sawistowski, H., *Chem. Engng Sci.*, 1966, **21,** 1109
[2] Merson, R. L., & Quinn, J. A., *A.I.Ch.E. Jl*, 1965, **11,** 391
[3] de Nie, L. H., Thesis, Technische Hogeschool, Delft, 1970
[4] Sawistowski, H., & Austin, L. J., *Chemie-Ingr-Tech.*, 1967, **39,** 224
[5] Hartland, S., *Chem. Engng Sci.*, 1969, **24,** 611
[6] Sawistowski, H., & Goltz, G. E., *Trans. Instn chem. Engrs*, 1962, **41,** 174

Some results of studying mass transfer in a single drop during coalescence

by P. Nekovář

Department of Chemical Engineering, Institute of Chemical Technology, Prague 6, Czechoslovakia

Some results concerning the occurrence of the vortex ring which is formed as a result of coalescence of a single drop on the phase boundary, as well as mass transfer from the surroundings into the vortex ring are discussed.

Introduction

THIS WORK IS a continuation of previous papers[1-4] dealing with problems of mass transfer from a stagnant liquid phase into the growing and falling drops, accompanied by a fast chemical reaction within the drop between components from the stagnant phase and a component originally present inside the drop in question. By means of an indicator the unreacted part of the drop was distinguished from the part where the reaction had taken place. This procedure was used for coalesced drops in order to investigate the mass transfer from the stagnant phase after decay of the drop.

The flow from drops after breaking an external film and formation of the vortex ring were described qualitatively by Charles and Mason.[5] Chapman and Critchlow[6] discussed the formation and the translation of the vortex ring which is formed after decay of a drop on the surface of the same fluid.

In this paper the method of Pedley,[7] recently also applied to the study of toroidal bubbles, will be used. Furthermore, some experimental results of mass transfer will be presented.

The nature of the experiment is shown in Fig. 1. The drop which is formed as a result of the outflow from a nozzle falls on the boundary of light (l) and heavy (h) phases where coalescence occurs. The dispersed phase (d) consists of the solvent D containing component B with the initial concentration c_{Bo} and indicator E. The light phase is formed by a solvent C containing a component A with the concentration c_{Al}, the heavy phase contains a solvent D and a component A (concentration c_{Ah}). Both phases l and h are in phase equilibrium. Moreover, both solvents C and D are mutually immiscible. For $c_{Al}=c_{Ah}=0$ mass transfer does not occur. If mass transfer takes place, i.e. in the presence of the component A, a fast chemical reaction

$$A+B \rightarrow AB+D \qquad (1)$$

occurs as a result of the contact of the drop with the light phase l. Also after coalescence of the drop, i.e. in the residuum formed from the broken drops, the reaction continues as long as the component B is present.

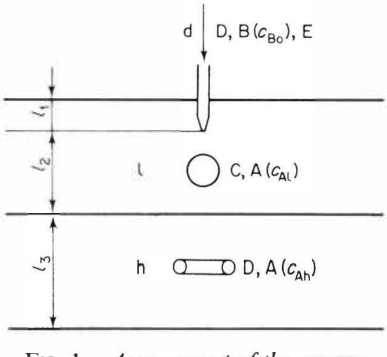

FIG. 1. *Arrangement of the process*

Experimental

In these experiments A=acetic acid, B=sodium hydroxide, C=benzene, D=water, E=phenolphthalein. Both the concentration and the physical properties of systems of fluids investigated are presented in Table I. In all experiments 1 ml of a 2% solution of phenolphthalein in ethanol was added to 100 ml of the phase d. The physical variables have been measured by the usual techniques.

TABLE I

Properties of systems studied (25°C)

System	Phase	C_A, mole/l	C_B, mole/l	ρ, g/cm^3	η, cP	σ_{l-h}, dyn/cm
I	d	0	0·2	1·008	1·018	
	l	0	0	0·872	0·610	
	h	0	0	0·997	0·895	26·6
II	d	0	0·2	1·008	1·018	
	l	0·01	0	0·874	0·635	
	h	0·2	0	1·001	0·955	19·7
III	d	0	0·01	0·999	0·989	
	l	0·28	0	0·917	0·692	
	h	3·46	0	1·002	1·086	10·7

The drops were formed on the sharp edge of a nozzle at a constant volumetric flow-rate.[1–4] Both the inner diameter of the nozzle and the volumetric flow rate are given in Table II.

TABLE II

Formation of drops

Run	d, mm	$\dot{V}$, mm^3/sec	System I V_K	System I V	System II V_K	System II V
			mm^3			
1	1·37	8·68	92·6	91·2	94·0	93·8
2	1·07	8·60	74·6	72·9	70·5	69·7
3	0·70	8·15	51·9	50·8	52·2	50·3
4	0·29	4·77	24·5	23·7		

The experiments were carried out in a glass vessel 18×15 (bottom)×21 cm. Referring to Fig. 1, l_1=1 cm, l_2=7 cm, l_3=12 cm. The liquid in the vessel was maintained at 25°±0·1°C by means of glass tubing heated by water from a thermostat. The nozzle was placed above the centre of the bottom of the vessel.

In Table II the volumes of the drops are given. These were determined from the volumetric flow rate in the nozzle and formation-time of a drop, as well as from the volumes of liquid transferred after coalescence in the heavy phase. These have been estimated after subtracting the volume of the secondary drop and the original volume of the particular drop. The volume of the secondary drop has been determined photographically.

The splash of the liquid stream from the drop after coalescence at the boundary of the light and heavy phases, as well as the formation of the vortex ring in the heavy phase, have been photographed in the region 0–6 cm beneath the interface between the light and heavy phases, using an Exacta-Varex IIb camera with objective Trioplan 2·8/100 equipped with a green filter, and ORWO NP 15 film. A flash-gun placed opposite the camera and screened by a single sheet of paper was used for illumination.

On the photographs the splash of the liquid stream as well as the formation of an ellipsoid have been observed. This ellipsoid changes sequentially in shape

and finally forms a toroid, which sinks, while growing in diameter. Decay of this geometrical body takes place around certain centres (2–5). From these centres a stream emerges and, in addition, a new toroid is created so that the whole phenomenon is repeated. The particular phases of this phenomenon are shown in Fig. 2.

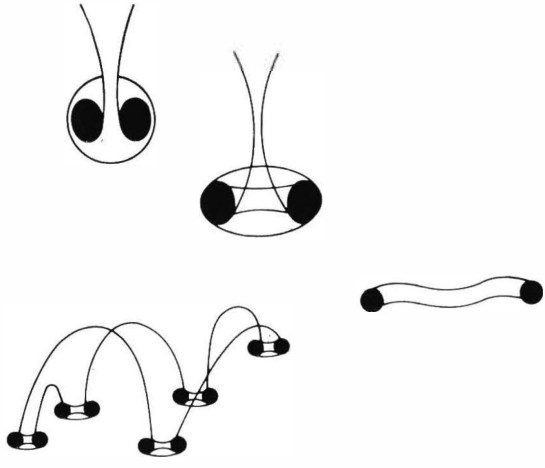

FIG. 2. *Diagramatic formation and decay of the toroid*

Based on the photographs, the typical dimensions of the coloured vortex ring as well as the distance from the boundary, i.e. the variables a, b, h in Fig. 3 have been evaluated. The linear scale of the pictorial projection is subject to error because of a perspective distortion, unless the object in question is placed in the plane where the calibration of the linear scale has been carried out. It has been observed that for given experiments the frequency of drops exhibited the normal distribution in all directions, with a maximum in the axis of the nozzle. In turn, maximum coalescence occurs on a circle of radius $1 \cdot 1$ cm with the origin in the axis. The errors in measuring ratios for this length do not exceed the errors of measurement of linear sizes in photographs where the distance may be estimated with an accuracy of $\pm 0 \cdot 2$ mm.

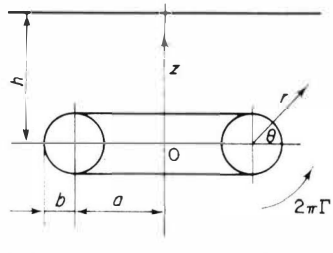

FIG. 3. *Notation of variables and co-ordinates*

Development of the vortex ring

The dependence of the radius of the vortex ring on the distance from the boundary may be developed in an analogous manner to Pedley's[7] considerations for a toroidal bubble. The notation is apparent from Fig. 3. Let us assume that the circulation $2\pi\Gamma$ around the injected fluid is the same as around the core of the homogeneous vortex ring having the same size, circulation and distribution of the azimuthal vorticity. Furthermore, let us suppose both the constant vorticity $2\Gamma/b^2$ in the core of the circular cross-section and the constant volume of the toroid:

$$V = 2\pi^2 ab^2. \qquad (2)$$

where $b \ll a$. For an axially symmetric flow induced by an isolated circular vortex ring in an nonviscid ambient fluid the velocity of translation of the vortex ring, according to Lamb,[8] is given by

$$u = \frac{\Gamma}{2a}\left[\ln\frac{8a}{b} - \frac{1}{4}\right] \qquad (3)$$

According to Pedley, with respect to both Lamb's results for the impulse of the system and the translation velocity given by Eq. (3),

$$P \doteq 2\pi^2 \rho a^2 \Gamma, \qquad (4)$$

where

$$\rho = \rho_h \doteq \rho_d. \qquad (5)$$

The vertical impulse can be described by Eq. (6)

$$\frac{dP}{dt} = \Delta\rho g V. \qquad (6)$$

where the right-hand side is the resultant force due to the buoyancy and, moreover,

$$\Delta\rho = \rho_d - \rho_h. \qquad (7)$$

After integration of Eq. (6) for the change of the radius a with time can be obtained

$$a^2 = a_0^2 + mt \qquad (8)$$

where

$$m = \frac{\Delta\rho g V}{2\pi^2 \rho \Gamma}. \qquad (9)$$

The variable a_o is the radius for $t = O$.

For motion in a viscous fluid, according to Tung and Ting's[9] results, the following may be written:

$$u = \frac{\Gamma}{2a}\left[\ln\frac{8a}{b_e} - 0{\cdot}688\right] \qquad (10)$$

where b_e is an equivalent radius defined as

$$b_e^2 = 4\nu\tau \qquad (11)$$

and

$$\tau = \int_0^t \frac{a(t')\,dt'}{a(t)}. \qquad (12)$$

After combination with Eq. (8) and assuming

$$a_0^2 \ll mt \qquad (13)$$

we obtain an equation similar to Pedley's relation

$$u = \frac{\Gamma}{2a}\left[\ln\frac{8a}{(\frac{8}{3}\nu t)^{1/2}} - 0{\cdot}688\right]. \qquad (14)$$

In addition, Equations (8) and (10) give

$$\frac{dz}{da} = \frac{\Gamma}{m}\left[\ln\left(\frac{24m}{\nu}\right)^{1/2} - 0{\cdot}688\right]. \qquad (15)$$

The integration of Equation (15) from h_0 to h and a_0 to a, respectively, results in

$$h - h_0 = \left[\frac{\Gamma}{2m}\ln\frac{24m}{3{\cdot}96\nu}\right](a - a_0) \qquad (16)$$

Let us assume that for flow in a viscous fluid Equation (9a)

$$m = k_1\frac{\Delta\rho g V}{2\pi^2\rho\Gamma} \qquad (9a)$$

is valid and that as for circulation of a toroidal bubble developed by Walters and Davidson,[10] Equation (17) can be formulated:

$$2\pi\Gamma = k_2(gV)^{1/2}, \qquad (17)$$

where k_1 and k_2 are constants for a particular system, then Equation (16) may be written

$$a - a_0 = \frac{4k_1\Delta\rho}{k_2\rho\ln\left[24k_1\Delta\rho(gV)^{1/2}/3{\cdot}96\pi k_2\rho\nu\right]}\,h - h_0 \qquad (18)$$

Comparison with experiments

The validity of our assumption of a constant volume in Equation (2) has been checked by comparison of the volume of stream injected (horizontal line) and the volume of toroid in the photographs. With respect to the size of the experimental error no important difference has been found as may be noted in Fig. 4 for the configuration of the experiment I-3.

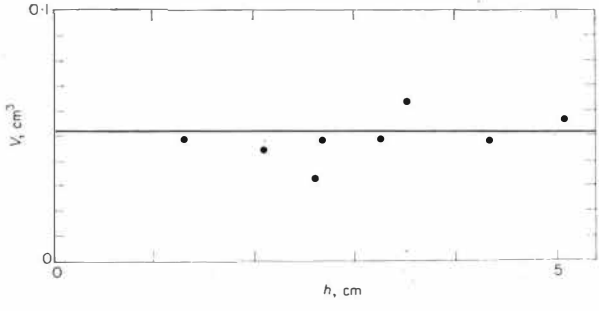

FIG. 4. *Volume of the toroid*

Fig. 5 shows the results of the run I-3. It is obvious that in accordance with our assumptions the upper part of the relationship a vs. h is linear and that the points match quite well the line computed from Equation (18) for $k_1 = 0{\cdot}232$ and $k_2 = 0{\cdot}139$. The value of k_1 has been obtained from two values of the time and the distance of the vortex ring from the boundary. Fig. 6 displays the analogous results for the run II-3, where mass transfer and chemical reaction take place. For the other experimental runs with systems I and II an analogous agreement in the same region has been found. A discussion quantitatively of the results obtained with system III is not presented. An undefined change of the direction of the stream injected and a flow towards the interface has been observed due to the opposite sign for $\Delta\rho$. It is apparent from the results that Equation (18) describes quite well the effects of volume, density and viscosity.

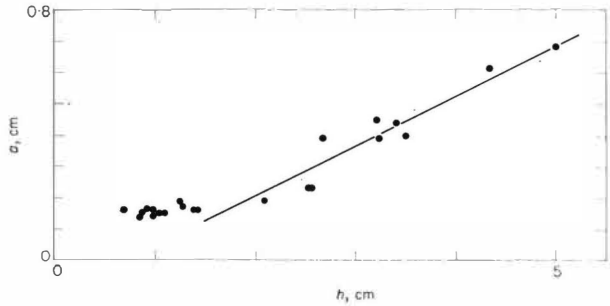

FIG. 5. *Growth of the external radius of the vortex ring (without mass transfer)*

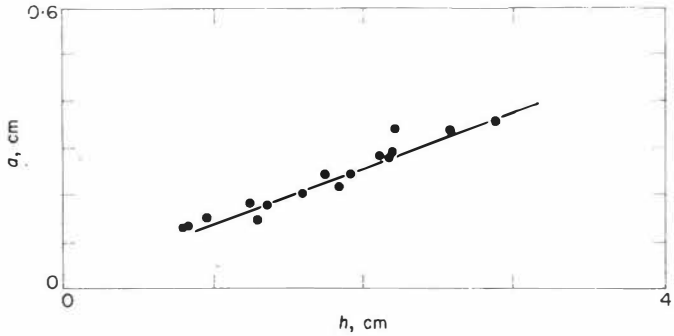

FIG. 6. *Growth of the external radius of the vortex ring (mass transfer and chemical reaction)*

Mass transfer in a vortex ring

Let us assume that within the toroid two regions exist which are bounded by the 'reaction surface' where

$$c_A = c_B = 0. \qquad (19)$$

Thus, we may consider the mass transfer problem for a system of components A–D and B–D in two distinct parts. For mass transfer of A into the medium in question and, furthermore, for a rapid chemical reaction given by Equation (1) the concentration of B may be supposed to be equivalent to a negative concentration of A. Let us write

$$c = c_A \, . \qquad (20a)$$

for the component A in the part of the system where chemical reaction takes place and, further,

$$c = -c_B \qquad (20b)$$

for the component B in the nonreacting region.

Supposing

$$D_{AD} = D_{BD} = D \qquad (21)$$

the continuity equation in cylindrical co-ordinates may be written

$$\frac{\partial c}{\partial t} + v_r \frac{\partial c}{\partial r} = D\left(\frac{\partial^2 c}{\partial r^2} + \frac{1}{r}\frac{\partial c}{\partial r}\right) \qquad (22)$$

assuming $\partial c/\partial\theta = 0$ and $\partial c/\partial\chi = 0$. The co-ordinates r and θ are shown in Fig. 3; χ is the third co-ordinate. The initial and boundary conditions may be

considered in the form

$$c = c_{\mathrm{Ah}} \qquad r = b(t) \tag{23}$$

$$c = -c_{\mathrm{Bo}} \qquad t = 0 \tag{24}$$

respectively, supposing that mass transfer occurs after the formation of the vortex ring. According to Pedley[7]

$$v_r = \frac{r}{b}\frac{\mathrm{d}b}{\mathrm{d}t}. \tag{25}$$

After introducing dimensionless variables

$$R = \frac{r}{b}. \tag{26}$$

$$T = \int_0^t \frac{D}{b^2}\,\mathrm{d}t \tag{27}$$

$$C = \frac{c + c_{\mathrm{Bo}}}{c_{\mathrm{Ah}} + c_{\mathrm{Bo}}} \tag{28}$$

and by combination with Equation (25) a set of equations results

$$\frac{\partial C}{\partial T} = \frac{\partial^2 C}{\partial R^2} + \frac{1}{R}\frac{\partial C}{\partial R} \tag{29}$$

$$C = 1 \qquad R = 1 \tag{30}$$

$$C = 0 \qquad T = 0 \tag{31}$$

The solution of Equations (29)–(31) is given by Crank[11]

$$C = 1 - 2\sum_{n=1}^{\infty} \frac{J_0(R\alpha_n)}{\alpha_n J_1(\alpha_n)} \exp(-\alpha_n^2 T) \tag{32}$$

where α_n are the positive roots of Equation (33)

$$J_0(\alpha_n) = 0 \tag{33}$$

After using Equation (19), i.e.

$$C = C_s = \frac{c_{\mathrm{Bo}}}{c_{\mathrm{Ah}} + c_{\mathrm{Bo}}} \tag{34}$$

we may write for $R=0$

$$C_s = 1 - 2\sum_{n=1}^{\infty} \frac{1}{\alpha_n J_1(\alpha_n)} \exp(-\alpha_n^2 T_k) \tag{35}$$

Equation (35) yields a relation which can be used for an evaluation of the time T_k of complete conversion of B. From Equations (27) and (8) and taking into consideration both assumptions (2) and (14) a relation between T and t holds

$$T = \frac{4}{3}\frac{D}{V}\pi^2 m^{1/2} t^{3/2}. \tag{36}$$

After combination with Equations (9a) and (17) relation (37) may be written

$$t = \frac{1}{\pi}\left(\frac{3}{4}\frac{T}{D}\right)^{2/3} \frac{V^{1/2}}{g^{1/6}} \left(\frac{k2\rho}{k_1 \Delta\rho}\right)^{1/3} \tag{37}$$

Comparison with experiments

The time from coalescence to the complete loss of the colour of the vortex ring has been measured. The concentrations in system II were chosen in such a way that the discoloration occurred before decay. In order to compare these results with Equation (37) for T_k, it is necessary to check the validity of the relation (31), i.e. the effects of mass transfer during formation, downwards motion and coalescence, on the results obtained.

The latter effect has been examined by taking colour photographs of drops in system III remaining at the interface. It is obvious from the pictures that before maximum coalescence 40% of the volume has lost its colour. In addition, the secondary drop has been formed only from the discoloured volume. The drops in system II did not lose colour unless coalescence took place. Assuming c_{Bo} is the original concentration of B in a growing drop then at the boundary between both colour and colourless region the concentrations in system II and system III are $C_s=0\cdot5$ and $C_s=2\cdot89\ .\ 10^{-3}$, respectively, i.e. in 60% of the volume $C<0\cdot003$ and in 40% $0\cdot003<C<0\cdot5$.

After coalescence of drops in system III it has been observed that a discoloration of the toroid takes place just after formation. This seems to be an effect of mixing. During experimental runs with system II no discoloration was observed and, furthermore, no differences in the volume of toroid in systems I and II were estimated. It can be expected that the dimensionless concentration is again in the region $0\cdot003<C<0\cdot5$. Moreover, let us take into consideration that for system III, according to Equation (35), the discoloration time T_k is $T_k=3\cdot82\ .\ 10^{-2}$ which corresponds to the mean concentration $\bar{C}=0\cdot4$. The concentration $\bar{C}$is defined as

$$\bar{C} = \frac{\bar{c}+c_{Bo}}{c_{Ah}+c_{Bo}} \qquad (38)$$

and for $\bar{C}$ Crank[11] presents

$$\bar{C} = 1-4\sum_{n=1}^{\infty} \alpha_n^{-2} \exp(-\alpha_n^2 T_k). \qquad (39)$$

For the first assessment of mass transfer, unless the toroid is formed, let us take $\bar{C}=0\cdot2$. The corresponding value C_{Bo} is $c_{Bo}=0\cdot12$ mole/l and furthermore the new value $C_s=0\cdot375$. Equation (35) yields $T_k=0\cdot164$ (instead of $T_k=0\cdot200$ for $C_s=0\cdot5$).

In Fig. 7 the time of completion of the reaction is plotted against volume. The line corresponding to Equation (37) is drawn for $T_k=0\cdot164$. Agreement can be obtained for the average diffusivity $1\cdot1\ .\ 10^{-4}$ cm²/sec. For the highest value V decay of the toroid occurred during the final period of discoloration.

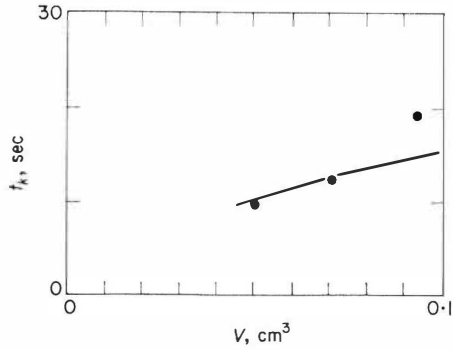

FIG. 7. *Time of completion of the reaction*

Referring to Fig. 8, the movement of the reaction surface for run 3 can be studied. The line drawn corresponds to Equation (32) for $C=C_s$. The variable b has been evaluated from assumption (2) and the value r has been obtained from photographs (subject to error, the magnitude of which has been discussed). For runs 1 and 2 the course was analogous.

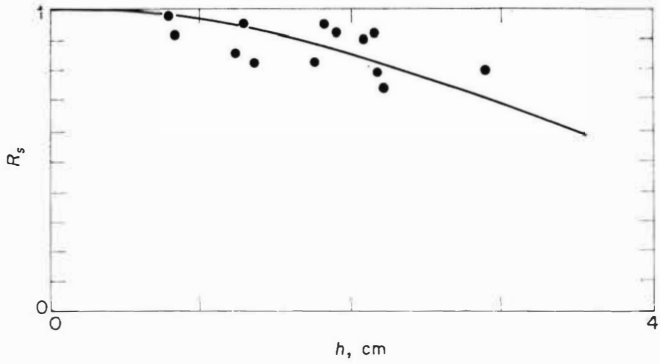

FIG. 8. *Movement of the reaction surface*

Nomenclature

a	external radius of vortex ring
b	internal radius of vortex ring
c	concentration, see Equation (20)
c_i	concentration of component i
C	dimensionless concentration, see Equation (28)
$\bar{C}$	mean concentration
d	inner diameter of nozzle
D	diffusivity
g	gravitational acceleration
h	distance from interface
J_k	Bessel function of $_k$th order
k_1, k_2	constant, see Equation (9a) and (17), respectively
l	length
m	constant, see Equation (8)
P	impulse
r	length co-ordinate (Fig. 3)
R	dimensionless length co-ordinate, see Equation (26)
t	time
T	dimensionless time, see Equation (27)
u	velocity
V	volume
$\dot{V}$	volumetric flow rate
z	co-ordinate (Fig. 3)
α	roots of Equation (33)
$2\pi\Gamma$	circulation
χ	co-ordinate, cylindrical system
η	dynamic viscosity
ν	kinematic viscosity
ρ	density

$\Delta\rho$ differences in densities, see Equation (7)
σ interfacial tension
τ time, see Equation (12)

Subscripts

A,B,D components
d dispersed phase
h heavy phase
l light phase
k drop
e equivalent value
o initial value
s value at the reaction surface
r, θ, χ components in co-ordinate system (r, θ, χ)

References

[1] Šalamon, Š., & Nekovář, P., *3rd Conf. Liquid–Liquid Extraction Leningrad*, 1967
[2] Šalamon, Š., Nekovář, P., & Grymová, L., *15th CHISA Conf., Mariánské Lázně*, 1968
[3] Nekovář, P., Vacek, V., & Šalamon, Š., *3rd CHISA Congr., Mariánské Lázně*, 1969
[4] Nekovář, P., *17th CHISA Conf., Mariánské Lázně*, 1970
[5] Charles, G. E., & Mason, S. G., *J. Colloid Sci.*, 1960, **15,** 105
[6] Chapman, D. S., & Critchlow, P. R., *J. Fluid Mech.*, 1967, **29,** 177
[7] Pedley, T. J., *J. Fluid Mech.*, 1968, **32,** 97
[8] Lamb, H., 'Hydrodynamics', 6th ed., 1945 (New York: Dover Publ.)
[9] Tung, C., & Ting, L., *Physics Fluids*, 1967, **10,** 101
[10] Walters, J. K., & Davidson, J. F., *J. Fluid Mech.*, 1963, **17,** 321
[11] Crank, J., 'The Mathematics of Diffusion', 1956 (Oxford: Clarendon Press)

SESSION 3B

PROCESS DEVELOPMENT, I

CHAIRMAN

Mr. M. J. Cahalan

SECRETARIES

Dr. D. S. Flett
Dr. Ir. P. Groenveld

Separation of iron, cobalt and nickel from scrap alloy by a solvent extraction process

by A. Aue,* L. Skjutare,* G. Björling,† H. Reinhardt‡ and J. Rydberg‡
‡ Dept. of Nuclear Chemistry, Chalmers University of Technology, Gothenberg, Sweden

The increasing use of super-alloys leads to the accumulation of large amounts of waste with high metal value content. In an investigation of various techniques for reclaiming the metal value, a solvent extraction–electrolytic process has been designed and tested in a pilot plant. The raw material is scrap alloy containing mainly Mo, W, Fe, Co and Ni. Through a special process only Fe, Co and Ni are brought into a chloride solution. The separation of these metals is achieved by solvent extraction in mixer-settler batteries using Alamine 336 (25% tertiary amine) in kerosene as organic solvent. This produces three streams, each containing one of the metals in high purity. The metals are recovered from these streams electrochemically in such a way that no waste solutions leave the plant.

Introduction

A PROCESS FOR recovery of Mo, W, Fe, Co and Ni from scrap alloy is being investigated by a joint group from industry and universities in Sweden. The process contains four main steps:[1–4] (i) pyrometallurgical pretreatment; (ii) electrolytic dissolution; (iii) separation through solvent extraction; (iv) electrolytic recovery of valuable metals.

Pretreatment of raw material[5]

The raw material is scrap used in the form of grindings, turnings, solids, etc. The scrap contains mainly Mo, W, Fe, Co, Ni, Cr and smaller amounts of Al, Si, Ti, Ta, and Nb. In order to remove non-metallic elements (up to 20% of total weight) as well as oil, water etc. (also about up to 20% of total weight) the raw material is melted in an arc furnace together with slag-forming substances (e.g. lime). This produces a fairly homogeneous metal. It is remelted in an HF furnace together with 3–4% graphite, after which the melt is granulated The purpose of this procedure is twofold. It transfers the high melting metals (Mo, W, etc.) into carbides, which do not dissolve in the subsequent electrolytic treatment. It also prepares the other metals (Fe, Co, Ni, etc.) for an easy electrolytic dissolution.

Electrolytic dissolution

Diaphragm-type electrolytic cells are used for anodic dissolution of the granulate, and for simultaneous cathodic deposition of the metals which have been separated through a solvent extraction cycle (see below). A $CaCl_2$ solution is used as supporting electrolyte.

The granulate is fed into titanium baskets, which act as anodes. Fe, Co, Ni and small amounts of Cr are brought into solution by the current. The anodic residue consists mainly of carbides of Mo, W and Cr, which is treated in a special process to form a calcium molybdate–tungstate. The anolyte carrying the metal ions having a total chloride ion concentration of 50–100 g/l and pH 2, leaves the electrolytic cells for the separation of iron and cobalt from nickel by solvent extraction.

Solvent extraction

Solvent extraction using tertiary alkylamines in kerosene[6] is probably the most efficient technique for selective separation of Fe(III), Co(II) and Ni(II) in

* Gullspång Electrochemical Co., Gullspång, Sweden
† Dept. of Process Metallurgy, Royal Institute of Technology, Stockholm, Sweden

chloride solutions.[2,7] Fig. 1 shows the dependence of chloride ion concentration on the extraction of these and some other metals. The amine chloride system is suitable because by changing the chloride ion concentration it is possible to separate the metals one by one. At low chloride ion concentration, iron(III) can be extracted into the organic phase while cobalt(II) and nickel(II) are not affected. At higher chloride ion concentration cobalt is extracted, but not nickel. The organic phase contains Alamine 336 (25% tertiary amine) as extractant dissolved in kerosene. Dodecanol is used as third phase inhibitor.

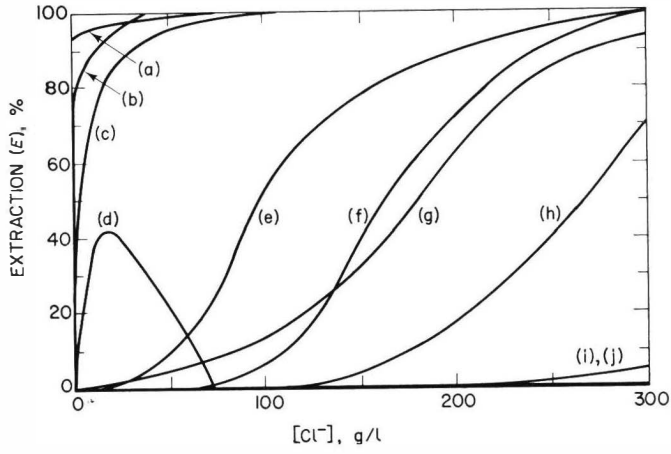

FIG. 1. *Percentage extraction of various metals as a function of chloride ion concentration at 40°C*

(a) Mo; (b) Zn; (c) Fe^{3+}; (d) Sn; (e) Cu; (f) Co; (g) Fe^{2+}; (h) Mn; (i), (j) Ni, Cr
Organic phase: 25% tertiary amine (Alamine 336), 15% dodecanol (Loval C12), 60% kerosene (Nysolvin 75A)
Aqueous phase: $CaCl_2$ solutions, [Me] = 1 g/l, pH ~ 2

The chemical reaction which takes place between a tertiary alkyl amine hydrochloride in an organic phase and cobalt in a strong chloride solution is:

$$2\ R_3NHCl_{org} + CoCl_4^{2-}{}_{aq} \rightleftharpoons (R_3NH)_2CoCl_{4\ org} + 2\ Cl^-{}_{aq}$$

The resulting uncharged molecule is soluble in the organic phase.

Because the dissolution of the granulate will introduce minor concentrations of other metals other than Fe, Co and Ni, the behaviour of these other metals in the solvent extraction process had to be investigated. The experimental technique used was an arrangement for continuous measurements of the distribution ratios in solvent extraction (AKUFVE[8]). Extraction variables such as metal, reagent and chloride ion concentrations, temperature, kinetics of extraction, and influence of some organic and inorganic impurities were studied.

Extraction of iron and cobalt

As can be seen from Fig. 1, the chloride ion concentration must be varied in order to achieve a complete separation of iron, cobalt and nickel. Fe(III) is first extracted from solution at low chloride ion concentration. The solution is then evaporated to raise the chloride ion concentration and cobalt is extracted. The resulting condensate is well suited for stripping purpose. Such a procedure permits stripping of the metals without addition of extra water. This leads to the very attractive possibility of a completely closed system. Using these principles the separation process shown in Fig. 2 was developed.

In order to separate iron from Co(II) and Ni(II), iron must be in the Fe(III) state. The anodic dissolution produces Fe(II). The oxidation is carried out electrochemically in a cell where the anodic part is separated from the cathodic

by a diaphragm. Chlorine, generated at the graphite anodes, causes the oxidation. Before extraction, small amounts of slime, consisting of insoluble metal hydroxides and chlorides obtained from the electrolytic cells, are removed in a filter press of 10 m^2 total surface.

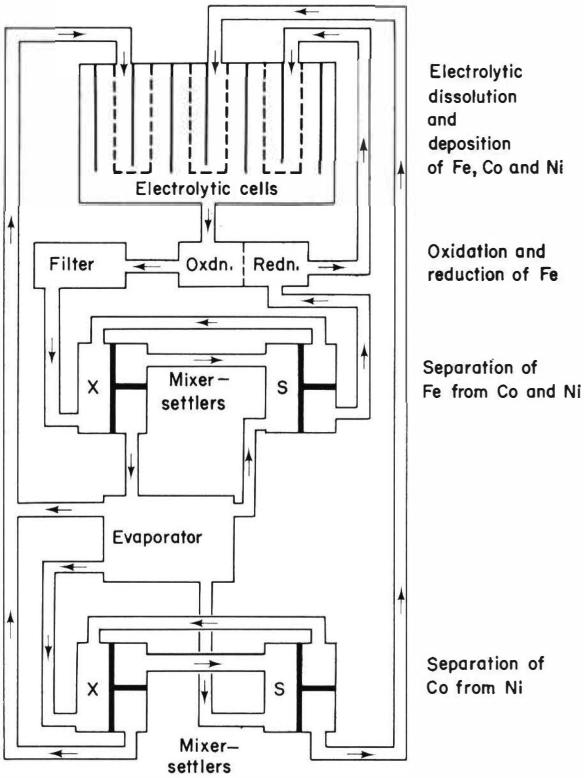

FIG. 2. *Flowsheet for separation of iron, cobalt and nickel from scrap alloy*

Iron as Fe(III) is nearly quantitatively extracted from the solution in three mixer-settler steps by an organic phase containing 25% Alamine 336 (General Mills Inc.), 15% dodecanol (Lorol 12, Henkel) and 60% kerosene (Nysolvin 75A, Nynäs Petroleum). The organic phase is recirculated internally in the mixer-settlers to achieve organic continuous conditions.

As can be seen in Fig. 1, cobalt will also be extracted to some extent at a chloride ion concentration of 50–100 g/l. Nevertheless, experience shows that iron prevents cobalt from being taken up into the organic phase. This is because the iron chloride complex is much stronger than the cobalt chloride complex. The resulting effect is that practically no cobalt is lost to the organic phase.

Using the same composition of the organic phase, cobalt can be extracted at a chloride ion concentration $\geqslant$ 200 g/l. The high chloride concentration is obtained by evaporation of the solution from the iron extraction to achieve a volume reduction of 50 to 75%. The necessary heat energy is transmitted by steam in a heat exchanger made of titanium. Cobalt is extracted from nickel countercurrently in six mixer-settler steps.

Isolation of iron, cobalt and nickel

The organic phase from the Fe extraction is stripped in eight steps, and that from the Co extraction in three steps, with the sligtly acid (pH 2–3) condensate from the evaporation.

Iron exists in the strip solution mainly as Fe(III). It is reduced to Fe(II) in the cathodic part of the same cell as is used for its oxidation to the Fe(III) state, as mentioned above.

The iron solution is pumped into the cathodic compartments of the diaphragm electrolytic cells intended for recovery of the iron. The cobalt solution is pumped to similar cells. The chloride ion concentration is 30–40 g/l in both solutions. The metals are deposited on iron-wire nettings.

The raffinate from the cobalt extraction is diluted with condensate so that the resulting chloride ion concentration is 120–150 g/l. Nickel is then recovered similarly as iron and cobalt.

Discussion

Although the process described has been running for only a few months, some experience has already been gathered. Small impurities of metals, silica and other materials build slowly up as precipitates, leading to the necessity of filtration. Further, it is necessary to keep the organic phase homogeneous during the extraction cycle, in order to avoid unbreakable emulsions. The presence of organic phase in the evaporator, was found to cause disturbing effects. All these problems are minor, however, and do not overshadow the advantages of the process which are: (i) by using diaphragm-type electrolytic cells, electrical energy is used in an optimum manner for dissolution and deposition; (ii) the amine chloride system is well suited for separation of Fe, Co and Ni, and is easy to control; (iii) using an evaporator for raffinate concentration and production of aqueous strip, a closed wet cycle is obtained; (iv) the low consumption of chemicals and energy indicates an economic advantage over similar open cycle processes; and (v) no gases or aqueous waste pollute the environment.

Acknowledgment

Financial support from the Swedish Board for Technical Development is gratefully acknowledged.

References

[1] Brooks, P. T., & Rosenbaum, J. B., *Rep. Invest. U.S. Bur. Mines*, 1963, No. 6159
[2] Brooks, P. T., Potter, G. M., & Martin, D. A., *ibid.*, 1969, No. 7316
[3] Baggott, E. R., Fletcher, A. W., & Kirkwood, T. A. W., *Proc. 9th Commonw. Min. metall. Congr.*, 1969, Paper 23
[4] Wesley, W. A., & Carry, J. W., *Trans. electrochem. Soc.*, 1939, **75**, 209
[5] Swed. P. Appln 16823/68
[6] Coleman, C. F., *Rep. Congr. atom. Energy Commn U.S.*, 1962, ORNL 3516
[7] Ioffe, E. Sh., & Dushkina, L. V., *Tsvet. Metallŷ, Mosk.*, 1965, **38**, 38
[8] Reinhardt, H., & Rydberg, J., *Chemy Ind.*, 1970, p. 488

Lorol 12: C-12 carbon chain: 95–99%; boiling interval: 250–265°C; melting point: 19–23°C; specific gravity (25°C): 0·83.

Nysolvin 75A: aromatic content: 0·1 vol.-%; boiling interval: 165–260°C; flash point: 50°C; specific gravity (15°C): 0·77

Refining of cobalt and nickel sulphate solutions by solvent extraction using di-(2-ethylhexyl)phosphoric acid

by L. F. Cook and W. W. Szmokaluk
The Pyrites Company, Inc., Wilmington, Delaware, U.S.A.

A process has been developed to remove heavy metal impurities from cobalt and nickel sulphate solutions prior to precipitation of the cobalt and nickel as the hydroxides or carbonates. A commercial application of this process is currently operated by The Pyrites Company, Inc., to refine sulphate solutions derived from leaching the solids discharged from a fluo-solids reactor used in the production of sulphuric acid from cobalt- and copper-bearing pyrites.

Sulphate solutions containing various levels of cobalt, zinc, iron, manganese, nickel and copper are refined by extracting the metals, other than cobalt and nickel, with the sodium salt of di-(2-ethylhexyl)phosphoric acid. The current plant solvent extraction system is designed primarily to remove high levels of zinc and provide a scavenging process for removal of copper, manganese and iron after a primary separation of these metals by precipitation and electrochemical methods. The feed to this system averages 10 g/l Zn, 0·05 g/l Mn, 10 g/l Co and 0·8 g/l Ni. Raffinates have metal levels of 0·10 g/l Zn, 0·005 g/l Fe, 0·008 g/l Mn, 10 g/l Co and 0·8 g/l Ni. 13 stages are used in the system: 5 extraction, 3 scrubbing, 2 stripping and 3 solvent treatment. Various strengths of sulphuric acid are used for scrubbing and stripping metals other than iron. Iron is stripped with a caustic chelate solution.

Introduction

THE PYRITES COMPANY uses a number of different feedstocks in their production of cobalt hydrate, oxide and metal. Their major source of cobalt is from by-product sulphate solutions derived from a sulphuric acid plant using a cobalt-bearing pyrite feed. Secondary supplies of cobalt are obtained from residues, spent catalyst and sludges. It is the general practice to leach or dissolve these secondary sources of cobalt with sulphuric acid and enter the sulphate solutions into various areas of the refinery, depending on the impurities that are present in these secondary solutions.

Past refining practices of these sulphate solutions have used classical precipitation methods of separating impurities from the cobalt. The precipitation of these impurities led to high losses of cobalt in the discarded precipitates. In the preliminary study of ways to combat these losses, solvent extraction offered the best solution. Solvent extraction techniques also appeared to be an attractive route to purify nickel sulphate solutions. The nickel sulphate circuit was not an immediate problem but was considered a good prospect in the future diversification plans of the Company.

The initial investigation of various solvent extraction systems indicated that the best economics could be achieved by extracting the impurities from the cobalt, rather than cobalt from the impurities. Test work on various extractants indicated that the sodium salt of di-(2-ethylhexyl)phosphoric acid (D2EHPA) gave the best results for the mass extraction of the wide ranges of copper, iron, manganese and zinc found in the various sulphate feedstocks. Sulphate solutions with high levels of copper, iron, manganese and zinc required two separate D2EHPA circuits, one for iron–zinc removal and the other for copper–manganese extraction. The strip solution from the copper–manganese unit is used as a feed to an electrolytic copper circuit. Sulphate solutions containing high nickel levels, together with copper, manganese, zinc and iron, required a third extraction unit using a tertiary amine extractant for the cobalt–nickel separation.

The process that is in commercial use at Pyrites is a combined precipitation–solvent extraction system and was installed with considerable urgency to combat a serious elevation of zinc levels in the primary feedstocks. The precipitation process formerly used to make the separation of cobalt and zinc was incapable of coping with the increased levels of zinc without damaging economic losses of cobalt.

Experimental

Metal extractant studies

Considering the various metal extractants that appeared to have potential use with sulphate solutions, extractants that were selective for specific metals were initially considered. Consequently, LIX-63 and LIX-64 (General Mills), were investigated for their ability to separate copper from other metals in sulphate solutions. Reports dealing with these extractants formed the basis for this work.[1,2]

These extractants are highly specific for copper and extract it preferentially from other cations over a narrow pH range.

The extraction equation is:

$$\underline{2RH} + Cu^{2+} \rightarrow 2H^{+} + \underline{R_2Cu} \quad . \quad . \quad . \quad (1)$$

where the underlined species reside in the organic phase.

Since hydrogen ions are exchanged for copper as the extraction proceeds, the pH of the feed is lowered, inhibiting further extraction. For dilute feeds, i.e. copper values of ~2–4 g/l, the effect is not too serious and the hydrogen ion concentration does not increase enough in the feed to preclude complete extraction.

Since copper levels in the feeds are 15–30 g/l, extraction of the copper by the LIX reagents would not proceed past a 2–4 g/l reduction in copper levels.

An attempt was made to treat the LIX reagents with caustic to convert them to the sodium salt, i.e.,

$$\underline{RH} + NaOH \rightarrow \underline{RNa} + H_2O \quad . \quad . \quad . \quad (2)$$

then to exchange sodium for the copper without affecting pH:

$$\underline{2RNa} + Cu^{2+} \rightarrow \underline{R_2Cu} + 2Na^{+} \quad . \quad . \quad (3)$$

and to strip the copper with acid:

$$\underline{R_2Cu} + 2H^{+} \rightarrow \underline{2RH} + Cu \quad . \quad . \quad . \quad (4)$$

then recycle the organic phase.

Reaction (2), however, did not proceed to any observable degree.

An interstage pH adjustment was considered to neutralise hydrogen ions generated in the feed by Reaction (1). This was not attractive from an operational viewpoint. Also, although LIX-63 would load to 20 g/l at about 20% concentration in kerosene, a thick, viscous hard-to-handle organic phase resulted. LIX-64 would load only to ~3–4 g/l and would necessitate an impractically large organic phase to aqueous phase volume ratio (O/A), considering the copper levels in the present feedstock. The higher costs of LIX-63 and -64 were also determining factors.

Carboxylic acids were considered, and exploratory work was carried out on the use of naphthenic acids as extractants. Results from the investigation were not attractive because interstage pH adjustment was required, and solvent losses appeared excessive when the sodium salts of the acids were used.

Of the extractants tested, D2EHPA seemed the most attractive for our use. The D2EHPA obtained from commercial sources was found to average 96% D2EHPA and the remainder mostly the mono-2EHPA, which is water-soluble. Only compounds with high flash points were considered as possible diluents. Both aromatic and aliphatic diluents were tested. Shell Cyclo-Sol 53 (a tri-aliphatic benzene) worked well for all cation extractions except Fe^{3+}. Even with the addition of 15% of isodecanol, a third phase formed upon

extraction. Hence, Shell Sol 140, a high flash point (140°F) mineral spirit (kerosene) was adopted as the standard diluent.

Batch tests

Extractions

Shakeout tests performed on a qualitative basis with various concentrations of D2EHPA diluted with kerosene-type diluents and isodecanol as a third-phase inhibitor showed the following results:[3] iron was extracted from sulphate liquors in various degrees; zinc was extracted at a relatively low pH; copper and manganese were co-extracted and only a slight preference for copper over manganese was shown; cobalt and nickel were extracted at about the same pH,[4] after the iron, zinc, copper and manganese; and loadings to almost 20 g/l copper were possible with a 20% D2EHPA organic solution.

The extraction equation

$$\underline{2RH} + M^{2+} \rightarrow \underline{R_2M} + 2H^+ \quad . \quad . \quad . \quad (5)$$

is, of course, identical with Reaction (1). Reaction (2), converting the extractant to the sodium salt, does go to completion with D2EHPA, however, and Reactions (3) and (4) are then possible, allowing extraction of copper and other metals without adverse pH lowering.

D2EHPA when converted to the sodium salt formed a third phase when diluted with kerosene. 5% of isodecanol or tri-n-butyl phosphate eliminated this third phase.

From extraction tests on various feedstocks containing the cations of interest, the graph in Fig. 1 was constructed. The sodium salt of D2EHPA (20%) was used in the shakeout tests along with 5% of isodecanol. A few observations were made which guided future work: ferrous iron, manganese, and copper are all extracted at about the same pH; iron extraction will occur at all pH ranges between 1 and 5, Fe^{3+} at the lower end and Fe^{2+} at the higher end; the natural equilibrium $Fe^{2+} \leftrightharpoons Fe^{3+}$ would drive itself to completion as Fe^{3+} was removed from the aqueous stream by D2EHPA, at low pHs; and the common rule of thumb that a metal is best extracted at a pH just below that at which its hydroxide precipitates, does not hold completely.

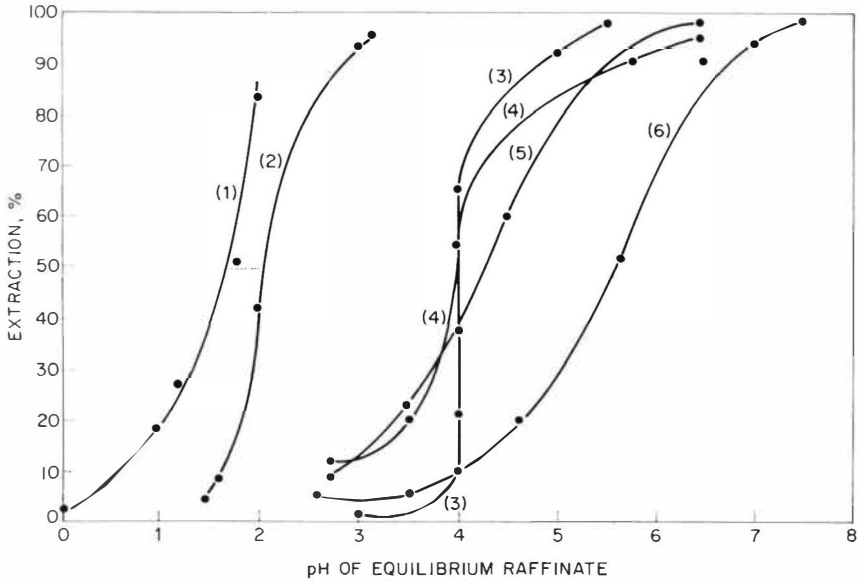

FIG. 1. *Degree of extraction vs. equilibrium pH*
(1) Fe^{3+}; (2) Zn (data from Ref. 3); (3) Fe^{2+}; (4) Cu; (5) Mn; (6) Co

In a carboxylic acid extraction, manganese would be extracted after cobalt and nickel at about pH 7. With D2EHPA, it is extracted before cobalt and nickel and shows extraction characteristics similar to copper. Zinc also shows some anomalous behaviour.

To establish the iron extraction characteristics, extracted iron values from the ferrous sulphate feeds were checked for the presence of both Fe^{2+} and Fe^{3+}. The results are plotted in Fig. 2.

The copper–manganese separation was another item of concern. To explore more fully the behaviour of these metal ions with D2EHPA, Fig. 3 was constructed. A feed solution (17·02 g/l copper, 22·5 g/l cobalt, 36·7 g/l manganese and pH 4·15) was prepared. An organic phase containing 20% D2EHPA and 5% isodecanol was contacted successively with equal volumes of the feed for 1 min. The results show the preference of D2EHPA for copper over manganese and cobalt. It also shows the ability of one metal (copper) to replace another metal (manganese) in the organic phase, even though there are only slight differences in their extraction characteristics.

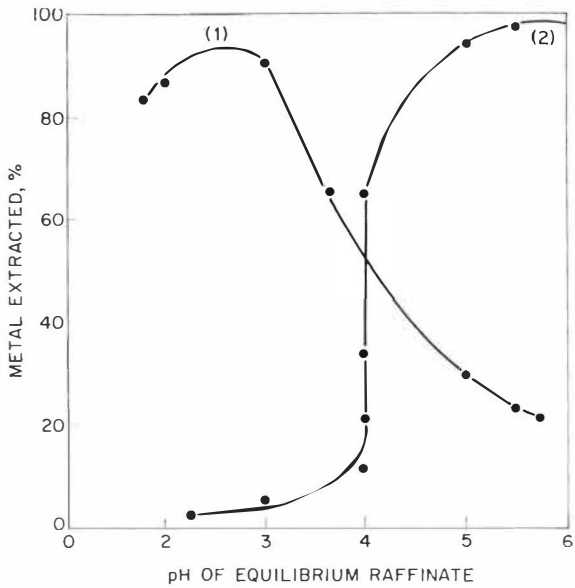

FIG. 2. *Degree of extraction vs. equilibrium pH with Fe^{2+} feed*

Feed: $FeSO_4$; pH 1·8; O/A 0·1–10
Organic phase: 20% D2EHPA (Na), 5% isodecanol, 75% Shell Sol 140; contact time 1 min.
(1) Fe extracted as Fe^{3+}; (2) total Fe extracted

Some observations were made at this point which formed implicit and tacit parts of the procedure in later continuous work: hydrogen could be considered an extractable species by the sodium (or ammonium or calcium) salt of D2EHPA along with the metals iron, zinc, copper, etc.; for a feed of low pH, the D2EHPA (Na) will extract hydrogen ions until the pH is such that Fe^{3+} is extracted, and so forth; the following order of preference was obtained with increasing pH by the sodium salt of D2EHPA: H^+, Fe^{3+}, Zn^{2+}, Cu^{2+}, Fe^{2+}, Mn^{2+}, Co^{2+}, Ni^{2+}. Thus, the D2EHPA (Na) will exchange essentially all its sodium ion present for the metals (or hydrogen) in the above order.

The concept of treating the hydrogen ion as an extractable species by D2EHPA salts of Na, Ca or NH_4 provides a convenient method of controlling the pH of the raffinate without interstage adjustments to maintain the maximum extraction of the desired metals.

Control of the pH is accomplished by limiting the amount of D2EHPA (Na) in contact with the feed and the raffinate in the extraction stages. The

amount of D2EHPA in contact with the aqueous phase is proportional to the O/A ratio. Using this technique, it is possible to design systems that will separate a metal or groups of metals from one another.

A 20% solution of D2EHPA should load to about 20 g/l of copper or any other divalent metal in the same molecular weight range. In fact, 17–18 g/l was found to be the maximum loading, or a solvent efficiency of ~85%.

In the Pyrites plant treatment of the cobalt solution, the iron (8 g/l) is removed by chlorine oxidation and neutralisation. Large amounts of cobalt are lost, probably through occlusion, with the precipitated iron. Although iron presents many problems in a solution to be treated by solvent extraction, it was considered as an impurity to be removed by solvent extraction, along with zinc and the others.

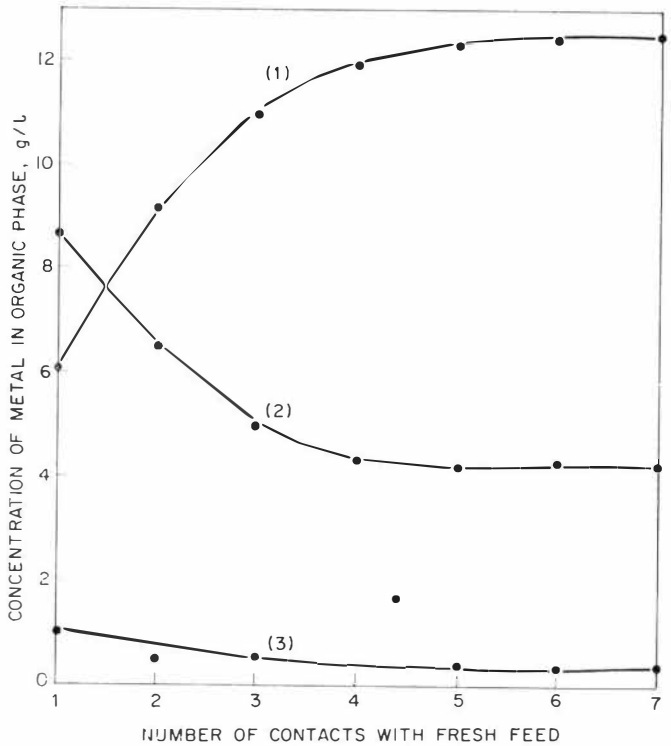

FIG. 3. *Scrubbing of manganese and cobalt by copper*

Feed: 17·02 g/l Cu, 22·5 g/l Co, 36·7 g/l Mn; pH 4·15; O/A 1·0
Organic phase: 20% D2EHPA, 5% isodecanol, 75% Shell Sol 140
(1) Cu; (2) Mn; (3) Co

Stripping

Iron was first removed from the organic phase by using a 6N–HCl strip and then a 10N–H_2SO_4 wash.

Two phenomena occurred. The 6N–HCl would remove most of the iron from the organic phase, but the isodecanol (or TBP), present as a modifier in the organic phase, would re-extract it as the $FeCl_6^{3-}$ complex. The 10N–H_2SO_4 did not strip the remaining iron out, and the water wash following the acid treatment, prior to the caustic treatment, succeeded only in raising the pH sufficiently to allow re-extraction of the iron by the D2EHPA.

This iron was subsequently removed from the organic phase as $Fe(OH)_3$ by the dilute caustic treatment. The mess it created in the settlers, however, was intolerable. It was known that saccharides and other organic compounds

with multiple OH groupings such as polyanhydric alcohols, e.g. mannitol and sorbitol, and the glycerides would sequester or chelate iron and keep it in solution at a pH at which it would normally precipitate as the hydroxide.

Tests were made to check the performance of these compounds. Cane sugar, molasses and corn syrup were all effective in chelating the iron at high pH. The resulting solutions were stable and showed no signs of precipitate after days of standing. The pH varied from 6 to 12 in all cases.

Since these substances, called sugars for convenience, are also reducing agents, it was postulated that caustic would remove the iron from the organic phase as before, and the sugar would both reduce it to the ferrous state and chelate it.

A search was started for a sugar that was cheap and readily available. EO-81, an enzose hydrol (Corn Products), is 80% solids and very high in dextrose content. It is a residue from sugar refining.

Using D2EHPA loaded with ferric iron, an EO-81–caustic–salt mixture was used to strip out the iron. The iron stripped from the organic phase was reduced, and remained in solution (the reaction is exothermic). The organic phase required a water wash before it could be reused in extraction. From current estimates, it appears that 2 lb of EO-81 are required to chelate 1 lb of iron.

Continuous runs were set up to study these solutions in a small pilot plant.

Solvent treatment and conversion of the D2EHPA to a salt form

Ammonia had been the first choice for a solvent 'neutralisation' medium because of its lower cost/lb-equivalent. In sulphate solutions containing low amounts (20 g/l) of cobalt, this ammonium salt of D2EHPA worked well as the exchange ion. In solutions containing greater amounts of cobalt, saturation was quickly reached with regard to the cobalt ammonium sulphate salt, and this crystallised out in both mixers and settlers. Another deterrent to the use of ammonia was evidence that in the extraction of copper some ammonia extracted with the copper, probably as a cationic complex.

Limestone was attractive from a cost standpoint, but the equipment needed to handle the calcium sulphate that would be formed by the exchange reaction in the mixer–settlers precluded its use. Caustic was therefore chosen as the neutralisation medium.

Continuous tests

Equipment

For some of the earliest continuous work, Plexiglas mixer–settlers (General Mills Inc.) were used.

These units had mixer capacities of ~160 ml which allowed a flow rate of aqueous feed of ~30–40 ml/min. These flows were not considered great enough on which to base scale-up.

Mixer–settlers having a 1-l mixer capacity and a 5-l settling capacity were built for the bulk of the work. These units allowed a more reasonable scale-up factor of 25 for the full plant-size equipment.

The mixer–settlers were constructed of epoxy-coated plywood in banks of six cells each. Constant head tanks for feed to the units through rotameters proved to be the most accurate and precise method of metering flows. Feed solutions were fed to the system at ground level, and were continuously pumped to the constant head tanks; the excess overflowed back to the feed tanks at ground level.

Tankage was of polyethylene material, tubing was Tygon, and interface controllers were glass Y-tubes which were raised or lowered by a turnbuckle arrangement. Stainless steel mixer–impellers were used at first but suffered severe corrosion under continuous use with copper-bearing liquors and 6N-HCl. Shafts and mixer–impellers were fabricated from polyethylene and worked well. Rheostats controlled mixer speed.

Extraction and stripping

The solution, a synthetic feed, representing a derivative of a sulphuric acid-leached cobalt residue, had the following analysis for cations (g/l): cobalt 50·4; copper 5·1; nickel 0·3; manganese 8·5; iron 0·6; and zinc 2·6.

This was fed into a five-stage counter-current extraction unit with a 20% D2EHPA (Na), 5% isodecanol solvent.

The raffinate had the following impurity analysis (g/l): manganese 0·02; copper 0·02; iron 0·01; and zinc was not detectable.

The cobalt products produced from this raffinate by present plant practices had the analysis in Table I; for comparison, product produced by the classical separation procedures are shown.

TABLE I

Cobalt oxide analyses

Cation	Run I, wt.-%	Run II, wt.-%	Present plant product, wt.-%
Copper	0·05	0·07	0·02
Calcium oxide	0·12	0·11	0·35
Iron	0·015	0·015	0·10
Manganese	0·05	0·07	0·05
Nickel	0·04	0·06	0·20
Zinc	<0·01	<0·01	1·50
Sulphur	0·80	1·30	0·05

The high sulphur contents of the products are due to poor washing and are not connected with the solvent extraction process.

A diagram of the circuit is shown in Fig. 4, along with the analyses made. Some non-equilibrium conditions through unavoidable surges in flow rates caused slight discrepancies in the material balance in the circuit.

In the extraction stages, the results show some cobalt tracing a circular path, being extracted in the last stages by the organic phase and being scrubbed in the first stages by the manganese, copper and zinc.

The cobalt scrub is recycled back to the feed (in the pilot plant this was not done, which explains the lower cobalt levels in the raffinate vs. the feed).

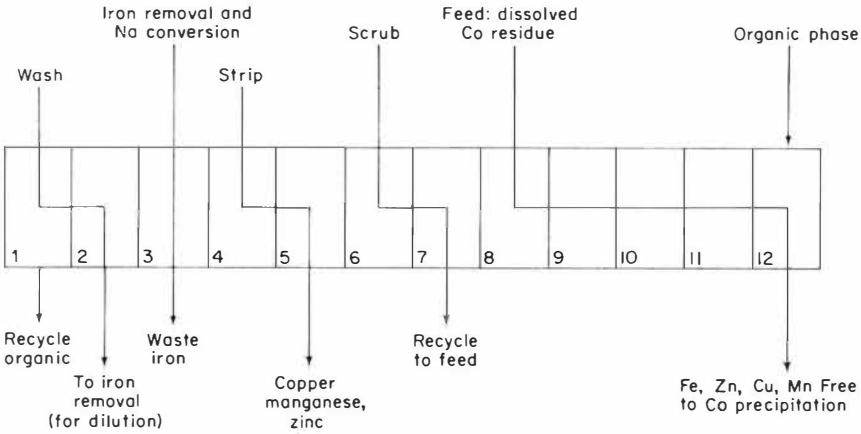

FIG. 4. *Diagram of circuit*

Feed: 16% Co, 2% Cu, 4% MgO, 0·5% Fe, 20% CaO, 12% S, 2% Al_2O_3, 3% Mn, 15% H_2O
Organic phase: 20% D2EHPA, 5% isodecanol, 75% Shell Sol 140
Scrub and strip liquors: 88 g/l H_2SO_4
Iron removal and Na coversion liquor: 8% NaOH, 30 g/l NaCl, 3% EO-81
wash liquor: 30 g/l NaCl used to dilute NaOH and EO-81
Flow rates (ml/min): feed 130; organic phase 155; scrub liquor 13; strip liquor 22; iron removal liquor 35; wash liquor 30

The amount recycled amounts to 6% of the cobalt, 20% of the manganese and 15% of the copper.

The overall cobalt recovery is >99% between the values left in the raffinate and the recycled amounts from the scrub stages.

The flow rate in the strip stages was not adequate to fully remove the zinc, and it was not removed from the organic phase until the iron removal stage.

Parameters in the treatment of the dissolved cobalt residue are shown in Table II.

TABLE II

Treatment of dissolved cobalt residue

All results in g/l

Phase	Stage no.	Copper	Cobalt	Manganese	Iron	Zinc	pH
Feed	—	5·1	50·4	9·0	0·6	2·6	2·1
			Extraction—125–130 ml/min				
Raffinate	18	0·05	43·6	0·04	0·02	<0·01	5·95
Organic	18	<0·01	15·6	0·16	0·04	0·78	—
Aqueous	17	0·2	43·6	1·84	0·2	—	5·45
Organic	17	0·06	15·0	0·7	0·04	0·75	—
Aqueous	16	0·4	64·4	3·13	0·2	—	5·20
Organic	16	0·14	11·5	2·5	0·04	0·78	—
Aqueous	15	0·4	60·8	3·78	0·2	—	5·10
Organic	15	1·0	6·5	5·4	0·06	0·78	—
Aqueous	14	2·4	60·8	5·62	0·2	—	4·10
Organic	14	2·9	2·66	4·9	0·46	2·5	—
			Cobalt scrub—13 ml/min				
Recycle	13	6·9	31·7	18·0	0·2	—	3·75
Organic	13	3·2	1·64	5·9	0·46	2·1	—
Aqueous	12	12·7	11·3	25·0	0·2	—	2·8
Organic	12	3·1	0·10	4·5	0·40	2·1	—
			Strip—22 ml/min				
Strip liquor	11	20·0	<1·0	31·0	0·2	0·75	2·65
Organic	11	1·4	0·01	1·9	0·4	4·9	—
Aqueous	10	12·0	—	19·5	0·2	15·5	1·5
Organic	10	0·06	0·01	0·06	0·4	3·2	—
			Iron strip—35 ml/min				
Strip liquor	9	0·50	—	0·7	2·0	22·8	11·0
Organic	9	<0·01	<0·01	<0·01	0·04	0·06	—

Economics

An estimation of the economics involved for refining this dissolved cobalt residue on a plant scale by solvent extraction is given below, based on a 1-min operation–8 g/min, 3·33 lb cobalt/min.

Reagent costs used

Sulphuric acid at 94%, \$0·014/lb; caustic solution at 50%, \$0·032/lb; rock salt, \$0·0077/lb; and EO-81 (sugar), \$0·035/lb.

Recycle cost

Acid: 0·585 lb/min=\$0·00875/min (caustic cost included in solvent treatment).

Strip cost

Acid: 1·05 lb/min=\$0·0157/min.

Solvent treatment cost

Caustic, 1·83 lb/min=$0·0587/min; sugar (EO-81), 1·135 lb/min=$0·0396/min; and rock salt, 0·542 lb/min=$0·00416/min.

Costs are summarised in Table III, and show a most attractive chemical cost for the dissolved cobalt residue.

TABLE III

Summary of costs

	lb/min	$/min	$/lb cobalt
Recycle acid	0·585	0·00875	0·00262
Strip acid	1·05	0·0157	0·00472
Solvent treatment			
Caustic	1·83	0·0587	0·0176
Sugar	1·135	0·0396	0·0119
Rock salt	0·542	0·0042	0·0013
Total	—	0·127	0·03814
Solvent loss (estimated)			0·01
			0·048/lb cobalt

Plant operation

A 13-stage solvent extraction system capable of handling 15 gal/min of feed at an O/A ratio of 1:1 and a contact time of 2 min in the extraction area has been on-stream since April 30, 1970, at The Pyrites Company plant at Wilmington. The current feed to this system is a sulphate solution from a fluo-solids reactor which has had the copper removed by electro-winning and iron precipitated with limestone at pH 4–5.

Circuit parameters

Extraction

Feed rate 11 g/min; O/A 1:1; contact time 3 min; number of stages 5.

Feed analysis (g/l): Cu 0·13; Fe 0·13; Mn 0·10; Zn 11·0; Co 11·0; pH 4·5.

Raffinate analysis (g/l): Cu 0·006; Fe 0·006; Mn 0·008; Zn not detected; Co 10·9.

Scrubbing

Scrub liquor, H_2SO_4 180 g/l; feed rate 0·1–0·4 g/min; number of stages 3.

Action—removes Co from the loaded solvent and recycles scrub liquor back to extraction.

Stripping

Strip liquor, H_2SO_4 180 g/l; feed rate 1 g/min; number of stages 2; pH of strip liquor 1·5.

Action—strips the copper, zinc and Mn in strip liquor.

Solvent treatment

Treatment liquor: 8% NaOH, 3% sugar; feed rate 1·2 g/min; number of stages 1; pH of raffinate 9–10.

Action—strips iron and hydrogen ions and converts the D2EHPA to sodium form.

Solvent wash

Wash liquor 3% NaCl; feed rate 1 g/min; number of stages 2.

Action—removes excess sugar and NaOH from extractant before recycling the solvent.

Solvent

12 vol.-% D2EHPA, 3% isodecanol; diluent Shell Sol 140.

These parameters represent typical figures. Flows are changed from time to time depending on physical conditions.

Equipment

Mixer–settlers

Pyrites design (Fig. 5): mixer 2 ft × 2 ft 3 in × 2 ft; settler 2 ft × 2 ft 3 in × 5 ft 8 in; material of construction Hetron 197 FRP (Hooker Chemical Co.).

Tankage

Material of construction Derakane (Dow Chemical Co.).

The outside tankage consists of a Lixator for rock salt dissolution with a storage tank for the saturated brine. A brine dilution tank stores the 30 g/l salt solution. Also outside is the 50% liquid caustic storage tank which feeds the iron scrub make-up tank as necessary. The iron scrub make-up tank, in addition to the caustic feed, is fed also from the saturated brine tank and also from drums of sugar. An acid make-up tank completes the outside tankage and is fed from a distant acid storage tank. A 3-in water line services all tanks.

The inside tanks are the feed and constant head tanks to the solvent extraction circuit. The wash, caustic and acid feed tanks are filled from the outside tanks as required. The solutions are continually pumped to 96-gal constant head tanks which overflow back to the feed tanks. Solutions are tapped from the constant head tanks through Rotameters to the correct stage in solvent extraction.

The cobalt solution to be refined is stored and fed from a 25,000-gal wooden tank, again tapped from a constant-head tank with excess flowing back to storage.

Mixers, pump and piping

The mixer motors are Lightnin (Mixing Co., Inc.) which have given good service. Shafts are 316 stainless steel with polyethylene tubing slid over the metal. Locally fabricated mixer–impellers were pinned on the tip and sealed with polyethylene welding rod.

Initially, magnetic-driven pumps were used that were of essentially polypropylene heads. These proved to be unserviceable for this application and are being replaced with metal (316 stainless steel or Ca20, depending on service) packed gland models.

Outside piping is primarily thermowelded polypropylene and PVC piping is used indoors and for intra- and inter-cell lines (1·5-in standard). Polypropylene ball valves are used throughout.

Operation

One man monitors the circuit on each shift and changes flows as required to maintain manganese levels in the raffinate at or below 0·01 g/l. An additional man on day work makes up solutions as required for the circuit.

Control of recycles to maintain organic continuous mixing, in the stages where aqueous streams leaves the system, results in crystal-clear streams. Aftersettlers collect very little organic phase.

Conclusions

Solvent extraction has proved to be an effective technique for refining cobalt solutions and it is felt that the same method can be used to refine other metal-

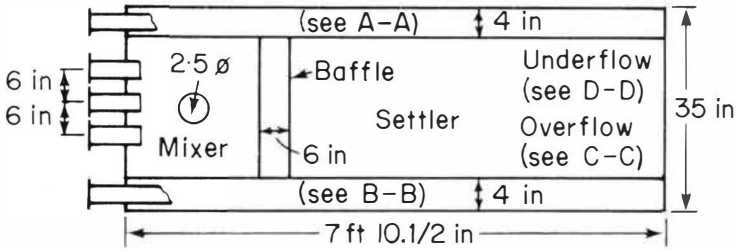

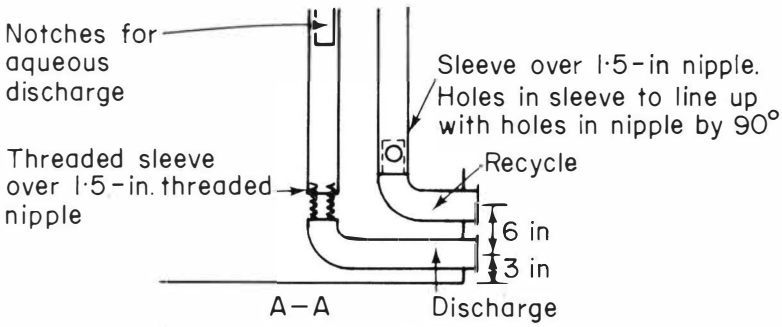

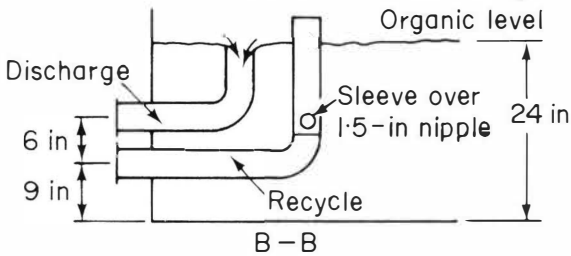

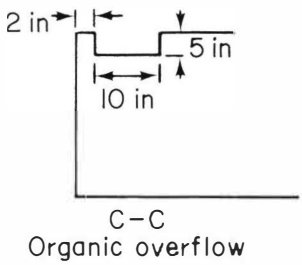

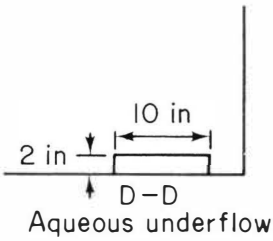

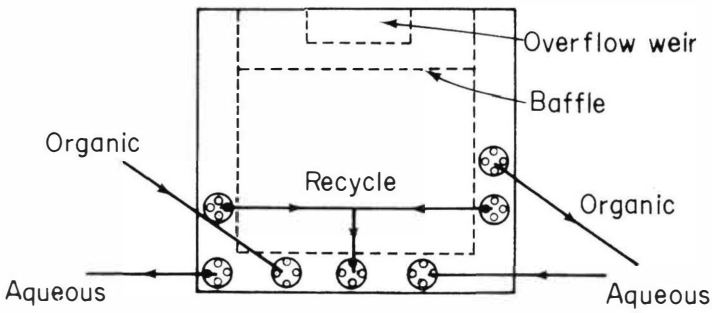

FIG. 5. *Sketch of mixer–settler used by Pyrites Company*

All piping 1·5-in PVC

bearing sulphate solutions. At 10 g/l Co, the cost of production/lb of metal is approximately the same as with precipitation procedures but considerable savings are realised owing to reduction of cobalt losses in precipitates. As the cobalt levels in the feeds increase, the cost/lb of metal decreases below precipitation costs and the savings due to better recoveries are retained.

References

1 Agers, D. W., & Swanson, R. R., 'A new reagent for the extraction of copper', 1963 (Minneapolis: General Mills)

2 Agers, D. W., & Dement, E. R., 'LIX-64 as an extractant for copper', 1967 (Minnesota: General Mills)

3 Cook, L. F., & Szmokaluk, W. W., 'Refining of sulphate solutions using DEHPA', 1969 (Wilmington: Pyrites Co.)

4 Ashbrook, A. S., & Ritcey, G. M., 'The Eldorado Process for the separation of cobalt and nickel by liquid–liquid extraction from acid solutions', 1966 (Toronto: Eldorado Mining & Refining Ltd.)

Process for the recovery of cobalt from ammoniacal solutions using a carboxylic acid

by G. M. Ritcey and B. H. Lucas
Hydrometallurgy Section, Department of Energy, Mines and Resources, Mines Branch, Ottawa, Canada

In most nickel ores, cobalt is found associated with the nickel, and the separation of the two metals has often proved to be difficult. One of the methods in use for the dissolution of nickel sulphide ores is the ammonia pressure-leach process, which provides a leach solution of metal-ammine sulphates. The work described shows the development of a new process for the preferential separation of cobaltous cobalt by liquid–liquid extraction from a concentrated ammoniacal ammonium sulphate solution containing dissolved cobalt and nickel. This is accomplished by the use of a tertiary monocarboxylic acid (Shell Versatic 911) dissolved in an organic diluent. The cobalt is extracted as the cobaltous form from an aqueous solution at pH ~8·0. The bench-scale results have indicated that the separation of cobalt from nickel is affected by the oxidation state of cobalt, feed pH, ammonium sulphate concentration, number of stagewise contacts during extraction, and the scrubbing procedure used. The cobalt is stripped from the organic phase by sulphuric, nitric, or hydrochloric acid. Results are also shown for the separation of cobalt from nickel in ammoniacal chloride, nitrate and carbonate solutions.

Introduction

IN CANADA, one of the present methods for treating nickel sulphide ores is by pressure-leaching at elevated temperatures using ammonia and air.[1] The dissolved copper, nickel and cobalt are recovered from the leach solution by precipitation techniques which involve several steps as well as many pieces of equipment. The copper is removed by distillation and hydrogen sulphide precipitation.[1,2] The copper-free solution is then oxidised, and the nickel precipitated by hydrogen reduction at 350°F.[3,4] The resultant 'barren' solution with a pH of 6·5, containing ~1 g/l each of cobalt and nickel and 500 g/l of ammonium sulphate, is contacted with hydrogen sulphide at atmospheric pressure in order to precipitate the residual nickel and cobalt.

The cobalt is recovered from this mixed sulphide in several stages.[4] The sulphides are first dissolved in dilute sulphuric acid under oxidising conditions. The nickel is removed by precipitation as nickel ammonium sulphate, and the cobalt is recovered from the solution by hydrogen reduction to the metal powder at elevated temperature and pressure.

The system described above has obvious disadvantages. Many process steps are necessary for nickel and cobalt recovery, and several pieces of process equipment, which take up a relatively large processing area, are required.

The aim was to devise a simpler flowsheet than the one now being used whereby the cobalt can be removed from the saturated ammonium sulphate solution containing nickel and cobalt. It was decided that solvent extraction could be a possible alternate route to the production of a highly purified cobalt stream amenable to reduction to cobalt metal powder.

A considerable amount of work on the separation of cobalt or nickel from various solutions has been reported. Ritcey & Ashbrook[5,6] reported a successful separation of cobalt from nickel at pH 5–6 in acid sulphate solution, and at pH 11–12 in ammoniacal sulphate using di-(2-ethylhexyl)phosphoric acid (D2EHPA). In the alkaline pH range, not greater than 40 g/l of ammonium sulphate could be tolerated whereas in the acid pH range, sulphate ion concentration of 200 g/l (as sodium sulphate) caused a slight decrease in cobalt extraction.

Drobnick & Millsap[7] described the use of α-hydroxy oximes to extract and separate nickel from cobalt in alkaline solutions (10 g of ammonia/l, 30 g of ammonium carbonate/l), after prior oxidation of the cobalt. Carboxylic acids have also been shown to be suitable for the separation of nickel and cobalt in acid solutions[8–12] where nickel is again selectively extracted. Little has been published on the extraction and separation of cobalt from nickel in an alkaline solution containing a high salt content, e.g. 500 g of ammonium sulphate/l, apart from a recent patent by Williams & Bayless[13] who claim the separation can be achieved above pH 8·6 using C_8-C_{38} naphthenic acids. This patent described the used of oleic acid for separating cobalt from nickel in 4 M ammonium chloride solutions.

Haffenden & Lawson[14] recently described the use of Versatic 9, a carboxylic acid product of the Shell Chemical Co. Ltd., for the extraction of copper, nickel and cobalt. They noted in the extraction of cobalt at pH 8 from a 1·0 M ammonium nitrate solution, that the mauve colour of the cobalt–Versatic 9 complex indicated the possible formation of an extractable ammine complex, and that the presence of ammonium ions may enhance the separation of cobalt and nickel.

On the basis of the above literature review, it was decided to investigate those extractants which might be suitable for the separation of cobalt and nickel present in an ammonium sulphate system in the pH range 5–8. The object of the investigation was to identify a satisfactory extractant for the treatment of a solution of this type, and to identify those variables that would be significant to an industrial solvent extraction operation.

This paper describes first a series of screening tests using extractants, selected on the basis of previously published work. A subsequent detailed investigation of the most promising extractant, Versatic 911, a tertiary carboxylic acid from Shell Chemical Co. Ltd., is then discussed. The object of the work was to produce separate streams of cobalt and nickel of high purity.

Experimental

A series of preliminary bench shake-out tests using separating funnels were carried out to screen selected solvents. Subsequently, bench tests were performed on Versatic 911 extractant only, and these determined the effects of variables such as feed pH, oxidation state, loading characteristics, retention time and stripping conditions on the extraction and separation of cobalt from nickel.

Results

Preliminary tests

The first work carried out was a series of exploratory tests on a synthetic solution containing 1 g of nickel/l, 1 g of cobalt/l and 531 g of ammonium sulphate/l, in which LIX-63, LIX-64, D2EHPA, mixtures of the three, as well as Versatic 911 were used as extractants. These bench shake-out tests were conducted with 5% solutions of the organic extractant dissolved in Shell 140 Flash Naphtha kerosene. No pre-equilibration of the organic phase, and no additive was necessary in the organic mixtures. All these tests involved a 2-min retention time at room temperature with an aqueous phase to organic phase volume ratio (A:O) of 1:1. Because preliminary tests had indicated that nickel and cobalt were precipitated if the pH of the aqueous feed solution dropped below 6·5, the pH range investigated in this work was 6·5–8·0. The results are shown in Table I.

The results in Table I show that of the extractants investigated, LIX-64 gave the best separation of cobalt from nickel with an extraction coefficient (E_A^0) relative to cobalt of 4·1, the highest obtained in this series of tests. Within the range investigated, a pH value of 8 was desirable. Although LIX-64 gave a satisfactory separation of cobalt from nickel, stripping the extracted metal from

TABLE I

Comparison of extractants for separation of cobalt and nickel

Feed concentrations, g/l: Co 1·1; Ni 1·1; $(NH_4)_2SO_4$ 531

Extractant	Feed pH	Extraction % Co	Extraction % Ni	Extraction E_A^0 Co	Extraction E_A^0 Ni	Separation factor, Co/Ni
D2EHPA, 0·1M	6·5	27	30	0·37	0·43	1
	7·0	12	10	0·14	0·11	1
	8·0	9	7	0·10	0·08	1
D2EHPA–LIX-64, 0·1M, 5%	6·5	34	50	0·51	1	0·5
	7·0	17	36	0·2	0·57	0·3
	8·0	35	16	0·45	0·18	2
D2EHPA–LIX-63, 0·1M, 5%	6·5	41	52	0·71	1·1	0·6
	7·0	38	36	0·62	0·57	1
	8·0	53	14	1·14	0·16	8
LIX-63, 5%	6·5	24	20	0·32	0·25	1
	7·0	22	10	0·27	0·11	2
	8·0	34	6	0·51	0·07	7
LIX-64, 5%	6·5	41	32	0·71	0·46	1·5
	7·0	43	12	0·75	0·13	6
	8·0	80	15	4·1	0·17	24
Versatic 911, 10%	8·0	75·1	40·3	3·02	0·68	4·5
Naphthenic acid,* 5%	7·0	36	23	0·57	0·31	1·8
	8·0†	31	0	0·45	0	∞

* Anachemia Chemicals
†Stable emulsions formed after contact of phases; broken by addition of isodecanol

the solvent was difficult. For this reason, no further work was done with LIX-64.

As shown in Table I, the next best extractant, both for separating cobalt from nickel and also for maximum extraction in one stage was Versatic 911. This extractant was shown to have an E_A^0 relative to cobalt of 3·02. On the basis of the E_A^0 (cobalt) values, Versatic 911 appeared to be almost as good as LIX-64 while it had the additional advantage of being readily stripped of the extracted metal. In view of all these factors, it was decided to conduct a detailed study of Versatic 911 as an extractant for the cobalt–nickel–ammonium sulphate system.

Extraction

Tests were conducted using 10 vol-% Versatic 911 to determine whether pre-equilibration of the organic phase after stripping prior to extraction was necessary, as well as to determine the effect of any pre-treatment on the extraction. Stripping of a loaded extract with an acidic or basic solution could be considered as a typical example where the solvent will have undergone a pre-treatment stage. The Versatic 911 was pre-equilibrated with a 10 vol-% sulphuric acid solution in one test, and in the other with a 10 vol-% ammonium hydroxide solution. The pre-equilibration was followed by contact of the solvents with the regular cobalt–nickel feed solution of pH 8·0 for 2 min.

The results in Table II show that the ammonium hydroxide treatment was completely detrimental to the extraction of cobalt and nickel, while the sulphuric acid treatment slightly improved the extraction. In other words, if an acid

such as sulphuric acid is used for stripping, no additional treatment of the solvent is necessary prior to extraction.

Previous work with the nickel–cobalt ammonium sulphate system using LIX-64 showed that increased ageing of the feed solution resulted in a decrease in the Co/Ni separation factor, possibly owing to the oxidation of the cobalt. Similar extraction tests were therefore conducted using 10 vol-% Versatic 911 to determine the change in the oxidation state of the cobalt, as indicated by the e.m.f. of the solution, with time, and the effect of this change on the subsequent extraction and separation of cobalt and nickel. The solvent was contacted at an A:O ratio of 3 : 1 with the feed solution which contained 1·13 g of nickel/l and 1·11 g of cobalt/l at pH 8·0. The results in Table III show that increased ageing of the feed up to 100 h resulted in an increase in the oxidation state of the cobalt, as well as a decrease in the separation factor for cobalt–nickel from 10·8 to 6·9. Subsequent tests were on solutions of cobalt in the reduced state.

TABLE II

Effect of pre-equilibration of Versatic 911 on extraction

A : O 2 : 1; Co 1·14 g/l; Ni 1·14 g/l

Pre-equilibration solution	Raffinate, g/l			Extract, g/l		Extraction, %		Extraction coeff., E_A^0	
	Co	Ni	pH	Co	Ni	Co	Ni	Co	Ni
None	0·38	1·06	7·60	1·52	0·16	67	7	4·0	0·14
10% H_2SO_4	0·31	1·00	7·35	1·66	0·28	73	12	5·3	0·28
10% NH_4OH	1·14	1·14	8·0	0	0	0	0	0	0

TABLE III

Effect of ageing on cobalt–nickel separation

Ageing time, h	E.m.f., mV	Extraction, %		E_A^0		$\frac{E_A^0(Co)}{E_A^0(Ni)}$
		Co	Ni	Co	Ni	
1·5	58	65	15	5·5	0·53	10·8
4·0	72	61	10	4·7	0·32	14·7
73	120	59	13	4·4	0·46	9·5
100	220	58	17	4·2	0·61	6·9

The effect of pH on the extraction and separation of cobalt and nickel was then determined. Feed solutions containing 1·08 g of Co^{2+}/l, 1·09 g of nickel/l and 531 g of ammonium sulphate/l were contacted at an A : O ratio of 3 : 1 for 2 min with 10% Versatic 911. Feed pH values from 6·5 to 8·5 were investigated. The results given in Fig. 1 show an increase in the extraction coefficients, E_A^0, to a maximum for cobalt at pH 8·0 and for nickel at pH 7·5. Also, the maximum separation of Co^{2+} and nickel was at pH 8·0.

Equilibrium isotherms for two solutions, one containing 1·16 g of Co^{2+}/l and the other 1·08 g of nickel/l in contact with 10% Versatic 911 are shown in Fig. 2. The feed pH was 8·0 and the contact time was 2 min. The A : O ratio was varied from 1 : 5 to 20 : 1. A 10 vol-% solution of Versatic 911 is shown to load to ~3·2 g of cobalt/l or 0·5 g of nickel/l at equilibrium.

In another series of tests, the feed solution, which contained 1·15 g of cobalt/l, 1·09 g of nickel/l and 531 g of ammonium sulphate/l, was contacted with 10,

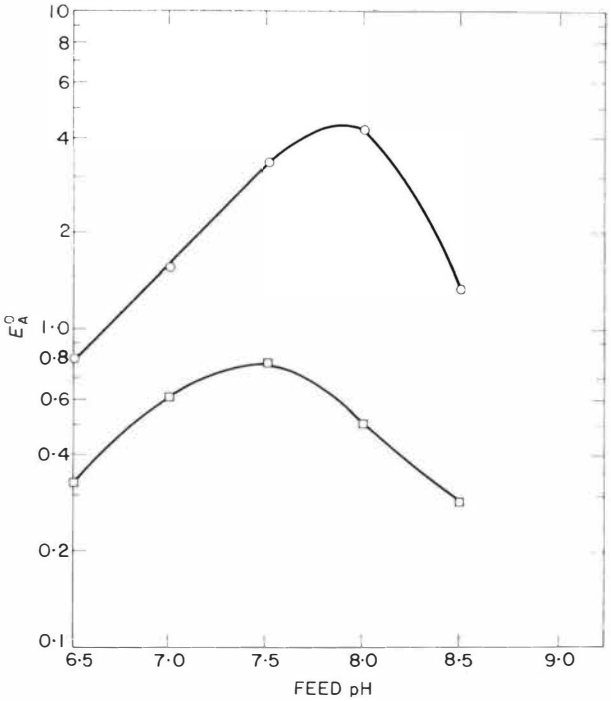

FIG. 1. *Effect of feed pH on extraction coefficients*

o Co: □ Ni Feed (g/l): Co^{2+} 1·08, Ni 1·09, $(NH_4)_2SO_4$ 531 A : O 3 : 1. 10% Versatic 911

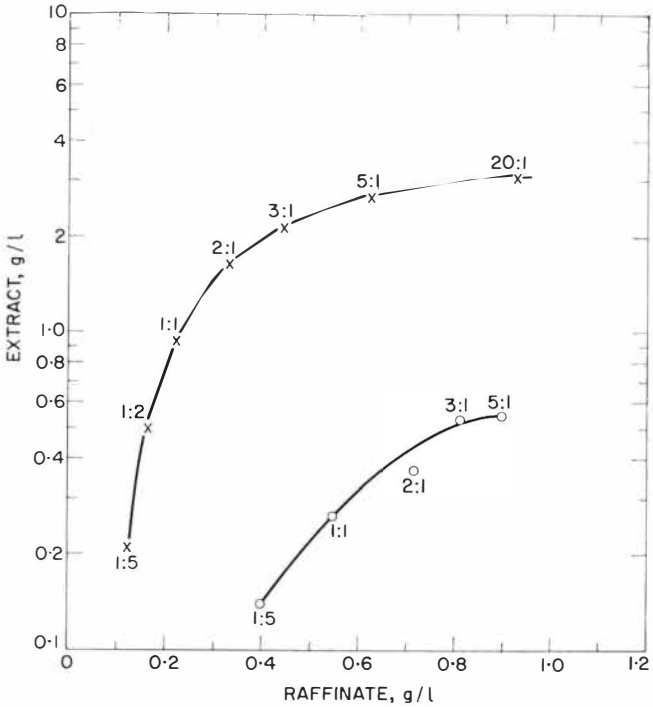

FIG. 2. *Equilibrium isotherms for separate solutions*

× Co^{2+}; o Ni Feed (g/l) : Co^{2+} solution 1·16; Ni solution 1·08; $(NH_4)_2SO_4$ 531; pH 8·0. 10% Versatic 911
Numbers along curves are A : O ratios

20 or 30 vol-% Versatic 911 for 2 min at a feed pH of 8·0. The A : O ratio was varied from 1 : 5 to 5 : 1. The equilibrium isotherms, at an equilibrium pH of 7·5, are shown in Fig. 3 and indicate a preferential extraction of cobalt over nickel, as well as a higher loading of Co^{2+} over Co^{3+}. The separation factor at an A : O ratio of 5 : 1 was 5 for Co^{2+}/Ni, compared with 3·5 for Co^{3+}/Ni. Using 10% Versatic 911, a loading of 2·5 g of Co^{2+}/l was achieved with 2·0 g of Co^{3+}/l. The nickel loading was ~0·7 g/l. A decrease in the Co : Ni ratio in the extract from 4·5 to 3·0 resulted from the increase in the Versatic 911 concentration from 10 to 30%.

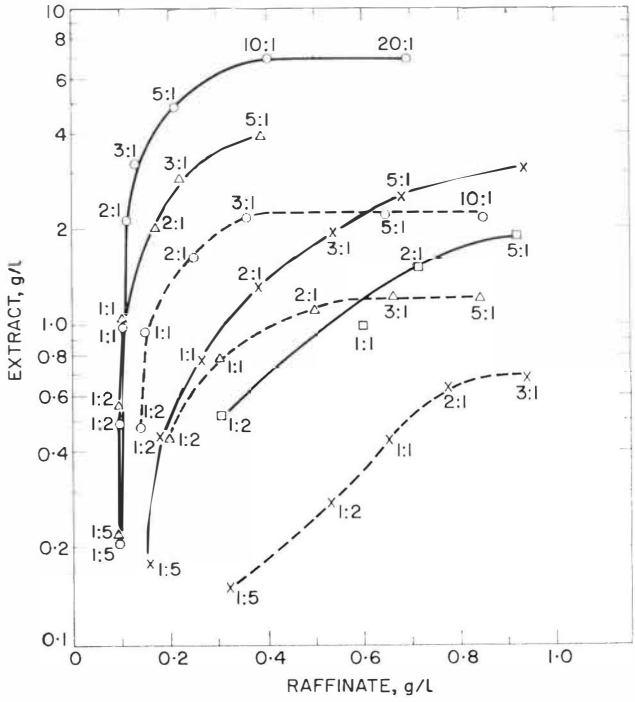

FIG. 3. *Equilibrium isotherms for Co and Ni at various Versatic 911 concentrations*

Feed pH 8·0
○—○ 30% Co^{2+}; △—△ 20% Co^{2+}; ×—× 10% Co^{2+}; □—□ 10% Co^{3+};
○ - - - ○ 30% Ni; △ - - - △ 20% Ni; × - - - × 10% Ni
Numbers along curves are A : O ratios

Tests at an A : O ratio of 4 : 1 and pH 8·0 were conducted on a solution containing 1·06 g of cobalt/l and 1·09 g of nickel/l where the contact time was varied from 10 sec to 2 h. The results showed that maximum extraction occurred in 30 sec. In this one stage of extraction ~60% of the cobalt and 20% of the nickel were extracted. In another series of tests, at an A : O ratio of 15 : 1, the retention time was varied up to 96 h. The cobalt was maintained in the Co^{2+} form with an atmosphere of nitrogen. The results in Fig. 4 show an increase in the Co : Ni ratio in the extract with increased retention time. No change in the saturation loading occurred.

Tests were performed at 25, 40 and 60°C to determine the effect of temperature on the extraction and separation of cobalt and nickel, using 10 vol-% Versatic 911 in contact with a feed solution containing 1·07 g of cobalt/l, 1·07 g of nickel/ and 531 g of ammonium sulphate/l at pH 8, and an A : O ratio of 3 : 1. No change either in the extraction of nickel or cobalt, or in the separation of Co and Ni resulted with increase in temperature up to 60°C and retention times up to 5 h under a nitrogen atmosphere.

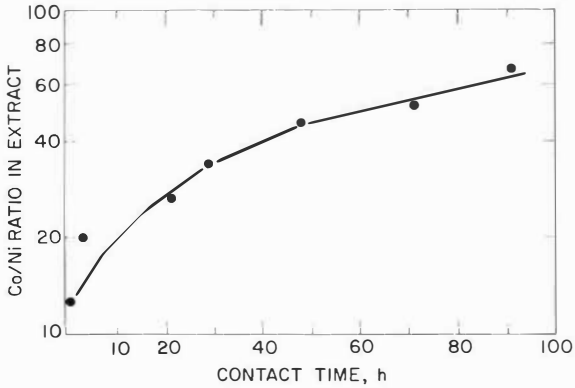

FIG. 4. *Effect of contact time on Co : Ni ratio in extract*

1·06 g Co/l; 1·09 g Ni/l; 531 g $(NH_4)_2SO_4$/l
pH 8·0; A : O ratio 15 : 1; N_2 atmosphere

To determine whether the ammonium sulphate concentration had an effect on the separation of cobalt and nickel, a series of shake-out tests at pH 8·0 was performed in which the ammonium sulphate concentration ranged from 50 to 531 g/l. The contact time was 2 min with 10 vol-% Versatic 911 at an A : O ratio of 5 : 1. The results indicated that increasing the ammonium sulphate concentration had no appreciable effect on the loading, but the separation of cobalt from nickel did increase with increasing ammonium sulphate concentration. These results are shown in Fig. 5.

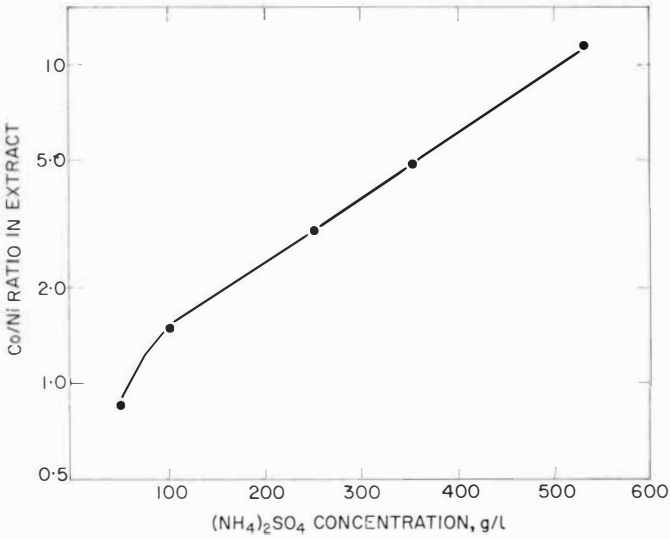

FIG. 5. *Effect of ammonium sulphate concentration on the separation of cobalt from nickel*

10 vol.-% Versatic 911, pH 8·0; A : O ratio 5 : 1

The Co : Ni ratio in the feed solution was varied from 1 : 10 to 20 : 1 to determine if increased nickel concentration would adversely affect the Co/Ni separation. The tests were carried out on solutions containing 531 g of ammonium sulphate/l at pH 8·0 for 2 min in contact with 10 vol-% Versatic 911 and at an A : O ratio of 3 : 1. The results in Fig. 6 show that when the Co : Ni ratio

in the feed was increased, the Co : Ni ratio in the extract increased after a single-stage extraction.

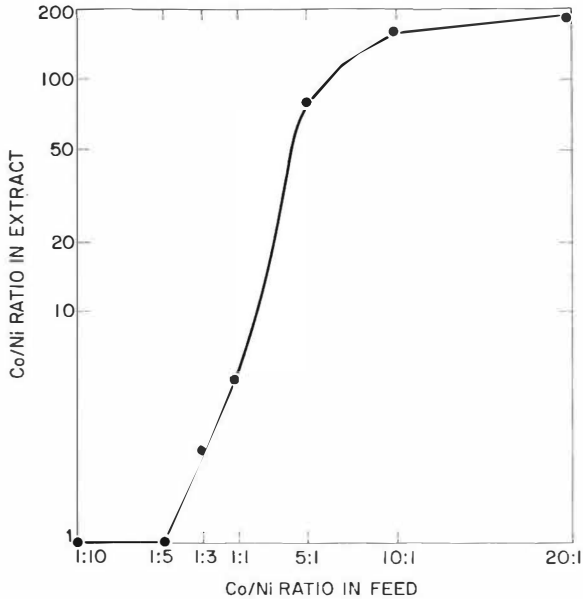

FIG. 6. *Effect of Co : Ni ratio in feed on the Co : Ni ratio in the extract*

In another series of tests, the cobalt concentration of the feed solution was examined in the range 1 to 40 g/l while the nickel concentration was kept at 1 g/l in a solution containing 531 g of ammonium sulphate/l. Equilibrium isotherms for cobalt at pH 8·0 for these feed solutions, when they were contacted with 10 vol-% Versatic 911 at varying A : 0 ratios, showed than an increase in the saturation loading of cobalt occurred with an increase in the Co : Ni ratio in the feed solution. The results of these tests are shown in Fig. 7. Saturation of the Versatic 911 was achieved with the feed solutions containing concentrations of cobalt $\geqslant$20 g/l. These results indicate that 2 moles of Versatic 911 are required per mole of Co^{2+} at saturation.

Scrubbing

It was observed that during the contact of the cobalt–nickel solution with the Versatic 911, a certain amount of nickel is co-extracted. To determine whether a multi-contact extraction system would improve the Co : Ni ratio, successive stagewise contacts of the extract with fresh feed solution at pH 8·0 were performed. Fig. 8 shows the effect of such a multi-stage extraction. After ten stages of contact at an A : O ratio of 3 : 1, the Co : Ni ratio in the extract was increased to 17 from 3·5, the value after one stage of extraction. Thus the loaded extract is amenable to scrubbing, in order to replace co-extracted nickel with additional cobalt. This scrubbing can take place during extraction, or an additional stage of scrubbing could be introduced, depending on the desired cobalt purity.

Tests were then carried out to determine whether successive stages of contact of the loaded extract with an aqueous cobalt scrub solution would increase the Co : Ni ratio on the extract by replacement of the nickel by cobalt. Scrubbing tests on a Versatic 911 extract, containing 1·86 g of cobalt/l and 0·3 g of nickel/l, were carried out using an ammonium sulphate solution at pH 8.0, containing 30–50 g Co^{2+}/l (previously preliminary tests indicated a cobaltous–ammonium sulphate medium at pH 8·0 to be better than a cobaltous sulphate solution.) The

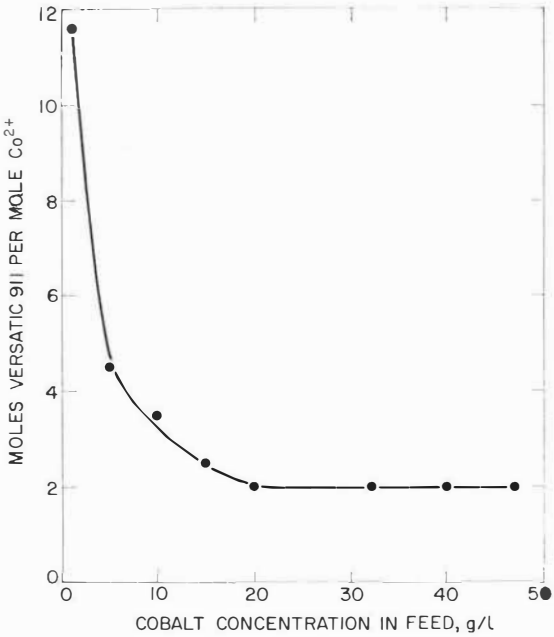

FIG. 7. *Effect of cobalt concentration in feed on cobalt loading of Versatic 911*

10 vol.-% Versatic 911; pH 8·0
Each point represents saturation at the particular level of cobalt concentration of feed.

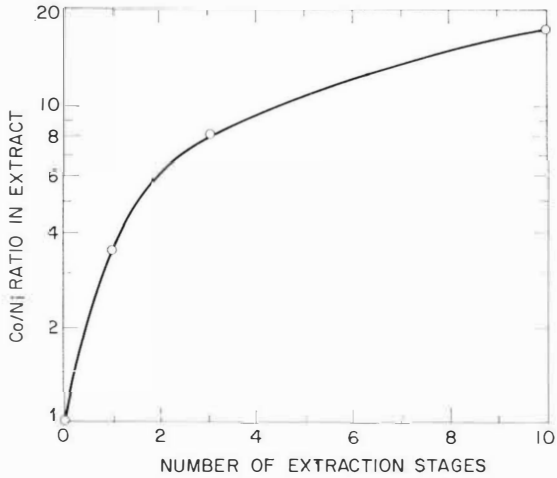

FIG. 8. *Effect of stagewise extraction on Co : Ni ratio in extract*

10 vol.-% Versatic 911
Co 1·1 g/l; Ni 1·1 g/l; $(NH_4)_2SO_4$ 531 g/l; pH 8·0; A : O ratio 3 : 1

extract was contacted three successive times at an A : O ratio of 1 with the cobalt–ammonium sulphate solution. The concentration of ammonium sulphate in the cobalt scrub solution was varied from 100 to 500 g/l. After scrubbing, the extract was stripped with 15 vol-% sulphuric acid. The strip results shown in Table IV indicate that although the Co : Ni ratio in the loaded extract was increased from 6 to 30 through the use of a scrub solution

TABLE IV

Scrubbing of 10 vol-% Versatic 911 extract

pH = 8·0

Scrub solution feed, g/l			Co : Ni ratio in strip solution
Co	Ni	$(NH_4)_2SO_4$	
42·6	6·0	100	30
47·1	—	300	3900
32·0	—	500	5400

containing 100 g of ammonium sulphate/l, a much higher purification level of greater than 4000 can be obtained with a scrub solution containing 300–500 g of ammonium sulphate/l. This optimum range of ammonium sulphate concentration for scrubbing agrees with the range required for maximum Co/Ni separation during extraction (Fig. 5).

Stripping

Preliminary stripping tests, using various concentrations of nitric, hydrochloric or sulphuric acid, showed that in one stage of stripping, nitric and sulphuric acid were equally effective, recovering 95% of the cobalt, while hydrochloric acid was almost as effective, giving 90% recovery. These results, shown in Table V, also indicated that a 5 vol-% sulphuric acid solution was almost as effective as a 15 vol-% solution. A loaded extract containing 2·67 g of cobalt/l and 0·154 g of nickel/l was subjected to four successive contacts with fresh 5% sulphuric acid at an A : O ratio of 1 : 1 for 2 min contact time at room temperature. These results showed that cobalt was readily removed from the extract. After three stages of stripping with the 5 vol-% sulphuric acid, the solvent contained 0·012 g of cobalt/l which represented a cobalt recovery of 99·5%.

TABLE V

One-stage stripping of 10% Versatic 911

	Stripping solution, vol.-%								
	HCl				HNO_3			H_2SO_4	
	2	5	10	20	2	5	10	5	15
Cobalt recovered, %	70	90	90	90	87	96	96	95	96

Subsequent stripping tests, conducted at elevated temperatures, showed no improvement or selectivity in stripping the cobalt up to 50°C. Also, stripping tests carried out over a period of 0·5–10 min showed that complete stripping took place after 0·5 min contact, with no selectivity of cobalt over nickel occurring with increased time.

Effect of anions other than sulphate

A series of tests was performed to determine whether ammoniacal solutions of anions other than sulphate could be tolerated in the extraction and separation of cobalt from nickel using 10 vol.-% Versatic 911. The tests were performed on solutions containing about 1 g/l each of Co^{2+} and nickel, and 300 g/l of either ammonium chloride, nitrate, carbonate or sulphate. The A : O ratios

investigated were 1 : 1, 3 : 1 and 5 : 1, and the pH of the feed was 8·0. The extracts were stripped with 10% nitric acid at an A : O ratio of 1 : 1, for comparison of extraction values. The results in Table VI show extraction and separation of cobalt from nickel occurring from each type of solution, with the following orders achieved for Co/Ni separation and total metal loading:

Order of Co/Ni separation: $NO_3^- > Cl^- > SO_4^{2-} > CO_3^{2-}$

Order of total metal loading: $NO_3^- > SO_4^{2-} > CO_3^{2-} > Cl^-$.

Because it is known from the scrubbing results on the sulphate system that co-extracted nickel can be effectively removed, a system with a high metal loading would be preferable in the plant. So, although the chloride system has a high Co/Ni separation compared with the sulphate system, the loading capacity is relatively low compared with the sulphate or nitrate systems.

Ageing of the feed solutions described above for one week followed by contact with 10 vol.-% Versatic 911 showed a decrease in loading capacity as well as a decrease in the Co : Ni ratio in the extract. These results are also shown in Table VI.

Recycling of Versatic 911

To determine whether significant amounts of the Versatic 911 were lost during extraction and stripping, a sample of the extractant was successively loaded and stripped several times. No change in the saturation loading of 10% Versatic 911 solvent or in the recovery occurred after five complete cycles of three-stage extraction followed by a one stage stripping with 15 vol.-% sulphuric acid.

Proposed flowsheet

An example of a possible flowsheet for the process is shown in Fig. 9. After contact of the leach feed solution at pH 8·0 with Versatic 911, the extract is purified by scrubbing with a cobalt ammine sulphate solution at pH 8 to remove small amounts of co-extracted nickel. A bleed of the scrub recycle stream is returned to the extraction circuit as the nickel content increases due to scrubbing. The scrubbed extract containing the cobalt can be stripped by various mineral acids, and sulphuric acid stripping is shown in the flowsheet. The resultant cobalt sulphate solution is reduced by hydrogen in the conventional manner,[2] and the residual ammonium sulphate is recovered by crystallisation. A portion of the cobalt sulphate solution is returned to the scrub circuit to maintain the necessary cobalt balance in that circuit.

The nickel contained in the extraction raffinate is recovered by subsequent extraction into Versatic 911, followed by stripping with sulphuric acid. This adjusted strip solution would be amenable to hydrogen reduction to produce nickel powder.[3] Another alternative would be recovery by precipitation of the sulphide.

Recently, work has been described in the literature on the direct reduction of the loaded extract to produce metal powders.[15,16] This route might be applicable to the recovery of both the cobalt and the nickel from the metal carboxylate without the requirement of a stripping circuit.

Conclusions

A process has been described for the separation of cobalt from nickel in an ammoniacal sulphate solution using Versatic 911. The extraction and separation of cobalt from nickel is highly dependent on pH and is best carrried out at pH 8·0. The oxidation state of the cobalt is critical, and maximum extraction occurs when the cobalt is in the cobaltous form. The extract can be readily scrubbed to remove any co-extracted nickel, and is easily stripped with dilute mineral acids to recover the cobalt. The process appears to be amenable to the treatment of ammoniacal leach solutions, and more specifically for the recovery of cobalt from the barren solution that results from production of nickel

TABLE VI

Effect of anions on Co/Ni separation from ammoniacal solutions using 10 vol.-% Versatic 911

HNO_3 strip solution

Anion	A : O ratio	Equilibrium pH	Same day					After 7 days				
			Co, g/l	Ni, g/l	Total metals, g/l	Co:Ni ratio	E.m.f., mV	Co, g/l	Ni, g/l	Total metals, g/l	Co:Ni ratio	E.m.f., mV
NO_3^-	1 : 1	7·7	0·86	0·72	1·56	1·2		0·72	0·72	1·44	1·0	
	3 : 1	7·8	2·38	0·62	3·00	3·8		1·56	0·94	2·50	1·7	
	5 : 1	7·9	2·80	0·42	3·22	6·7	+120	1·72	0·76	2·48	2·3	+120
Cl^-	1 : 1	7·7	0·78	0·24	1·02	3·2		0·30	0·20	0·50	1·5	
	3 : 1	7·8	1·12	0·28	1·40	4·0		0·50	0·26	0·76	1·9	
	5 : 1	7·9	1·08	0·26	1·34	4·15	−130	0·56	0·24	0·80	2·3	− 40
SO_4^{2-}	1 : 1	8·0	0·80	0·45	1·75	2·0		0·62	0·45	1·07	1·45	
	3 : 1	8·0	1·9	0·65	2·55	2·9	+ 58	1·48	0·65	2·13	2·28	
	5 : 1	8·0	2·5	0·70	3·20	3·6		1·95	0·65	2·60	3·00	+140
CO_3^{2-}	1 : 1	8·0	0·70	0·40	1·10	1·75		0·42	0·40	0·82	1·05	
	3 : 1	8·0	1·10	0·44	1·54	2·5		0·68	0·32	1·00	2·10	
	5 : 1	8·0	1·40	0·48	1·88	2·9	−210	0·94	0·46	1·40	2·04	−120

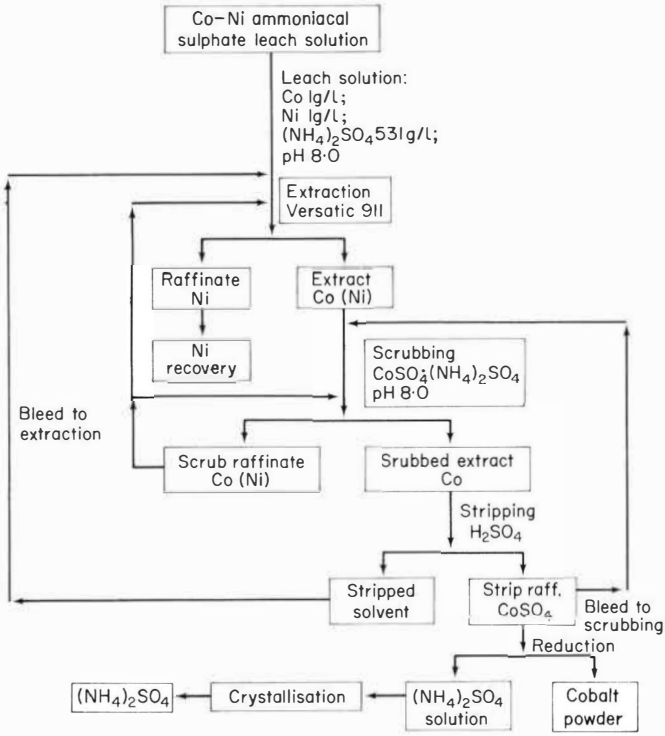

FIG. 9. *Proposed flowsheet*

powder by hydrogen reduction. Solutions of this type are produced, for example in the Sherritt–Gordon process.[1–4]

Acknowledgments

The authors gratefully acknowledge the work of Messrs K. Price, L. Carter, R. Umpherson and R. Chagnon of the Hydrometallurgy Section who carried out the numerous tests that were required for collecting the data, and also the work of Messrs R. Guest, R. Pugliese, D. Sheldrick and D. MacPherson of the Chemical Analysis Section for the chemical analysis.

References

[1] Technical Editor, *Chem. Engng, Albany*, 1969, **76** (7), 108
[2] Stauffer, R., & Lindsay, S., *Trans. Can. Inst. Min. Metall.*, 1967, **70,** 161
[3] Mackiw, V. N., Lin, W. C., & Kunda, W., *J. Metals, N.Y., Metals Trans.*, 1957, **209,** 786
[4] Kunda, W., Warner, J. P., & Mackiw, V. N., *Trans. Can. Inst. Min. Metall.*, 1962, **65,** 21
[5] Ritcey, G. M., & Ashbrook, A. W., U.S. P. 3,399,055
[6] Ritcey, G. M., & Ashbrook, A. W., *Trans. Instn Min. Metall., C*, 1969, **78,** 57–63; U.S. P. 3,438,768
[7] Drobnick, J. L., & Millsap, W. A., U.S. P. 3,276,863
[8] Blumberg, R., & Melzer, P., *Proc. 7th int. Miner. Congr. 1964*, 1966, pp. 139–145 (New York: Gordon & Breach)
[9] Flett, D. S., & Fletcher, A. W., 'The separation of nickel from cobalt by solvent extraction with a carboxylic acid', Paper presented at AIME Annual Meeting, Washington, Feb. 1969
[10] Spitzer, E. L. T. M., *et al.*, 'Selective extraction of metals from aqueous solutions by synthetic carboxylic acids', Paper 113, Gr. V, S. 14, presented at 36th Congress on Industrial Chemistry, Brussels, Sept. 12–16, 1966
[11] Spitzer, E. L. T. M., Radder, J., & Muys, H. M., *Trans. Instn Min. Metall., C*, 1966, **75,** 265
[12] Hawes, W. B., B.P. 959,813
[13] Williams, R. E., & Bayless, J. H., U.S. P. 3,380,801
[14] Haffenden, W. J., & Lawson, G. J., *Proc. Instn Min. Metall.*, 1967, pp. 678–685
[15] Burkin, A. R., *Powder Metall.*, 1969, **12,** 243
[16] Richardson, F. D., *Jernkont. Annlr*, 1969, **153,** 359

Extraction of europium from sulphate–perchlorate solutions by di-2-ethylhexylphosphoric acid

by P. W. Cassidy and A. R. Burkin

Department of Metallurgy, Imperial College, London, S.W.7.

The extraction of europium from sulphate–perchlorate solutions by di-2-ethylhexylphosphoric acid, $(HX)_2$, has been analysed quantitatively in terms of the equation:

$$\log D_{Eu} = \log K'_{Eu} + 3 \log [(HX)_2] + \log \alpha_o + 3\,pH$$

where $D_{Eu} = [Eu(HX_2)_3]_{org}/[\Sigma Eu]_{aq}$;

$$K'_{Eu} = \frac{[Eu(HX_2)]_{org}\,\{H^+\}^3_{aq}}{[Eu^{3+}]_{aq}\,[(HX)_2]^3_{org}}$$

$-\log \{H^+\} = pH$ and $\alpha_o = [Eu^{3+}]_{aq}/[\Sigma Eu]_{aq}$.

Values of K'_{Eu} are given for initial sulphate concentrations between 0·00 and 0·30 molar.

Introduction

WHEN A METAL M^{n+} in an aqueous solution does not form strong complexes with any anion or ligand present, and when loading of the organic phase is low, the extraction of the metal by dimeric di-2-ethylhexylphosphoric acid (D2EHPA) can usually be represented at equilibrium by the equation:

$$M^{n+}_{aq} + n(HX)_{2\,org} = M(HX_2)_{n\,org} + nH^+_{aq}$$

where HX denotes the monobasic dialkylphosphoric acid. This has been demonstrated in the cases of lanthanides,[1,2] actinides[1] and uranium(VI).[3–5]

When complexing of the metal occurs in the aqueous phase, correction of the value of the concentration of M^{n+}_{aq}, or of its activity, in the appropriate equations for the equilibrium constants is necessary. The work reported in this paper deals with the effects on the extraction of europium by D2EHPA due to the formation of complexes of the metal with sulphate and bisulphate ions. It is part of a programme of work designed to analyse distribution data quantitatively in terms of extraction constants, activity coefficients, component concentrations and stability constants of complexes in the aqueous phases.

Experimental

D2EHPA was Koch Light 'Pure' grade, the equivalent weight determined by titration was 318·5, theoretical 322·4. Solutions of concentration 0·100F (formula weight per litre of solution) in 'crystallisable' benzene were used for extraction, diluted if necessary. Europium sulphate solutions were prepared from europium oxide (99·9%, Johnson Matthey Co. Ltd.), Analar sodium sulphate and sulphuric acid, and G.P.R. sodium perchlorate, were used to control the pH and ionic strength.

Extraction of europium was carried out batchwise in 100 ml separating funnels, using 25 ml of each phase. A contact time of 20 minutes, using a shaking machine, was sufficient to achieve equilibrium. Experiments were carried out at room temperature, 18–25°, and within this range a temperature change had no detectable effect on the results. Experiments were carried out in triplicate.

Aqueous solutions of europium were labelled with $^{152+154}Eu$ tracer (Radiochemical Centre, Amersham, U.K.) and gamma scintillation counting with a Tl/NaI phosphor was used to measure the equilibrium concentration of europium in each phase. The radioactive europium was supplied dissolved in hydrochloric acid, and a chloride-free solution of europium in bisulphate form was produced by ion exchange on Amberlite IRA 400 resin. The pH of the aqueous phase at equilibrium was measured using a Pye 'Dynacap' pH meter and Pye 401 electrode.

Results and discussion

Writing the equilibrium equation for the extraction of europium from sulphate solution by D2EHPA in benzene as:[2]

$$Eu^{3+}_{aq} + 3\,(HX)_{2\,org} = Eu\,(HX_2)_{3\,org} + 3H^{+}_{aq}$$

permits an extraction constant K_{Eu} to be written:

$$K_{Eu} = \frac{\{Eu(HX_2)_3\}_{org}\,\{H^+\}^3_{aq}}{\{Eu^{3+}\}_{aq}\,\{(HX)_2\}^3_{org}} \qquad (1)$$

where { } denotes activity.

If the ionic strength of the aqueous phase is constant and the concentration of $Eu(HX_2)_{3\,org}$ is low then activity in Equation (1) may be replaced by concentrations, [ ], giving a constant K'_{Eu}.

At concentrations of 0·10 molal (monomer basis) and below the acid behaves as an ideal dimer in 'wet' and 'dry' benzene.[6] The maximum concentration of D2EHPA used in this investigation was 0·10F.

If the distribution coefficient for europium, D_{Eu}, is $[Eu(HX_2)_3]_{org}/[\Sigma Eu]_{aq}$ and he fraction α_o of europium present in the aqueous phase as Eu^{3+} is given by $\alpha_o = [Eu^{3+}]_{aq}/[\Sigma Eu]_{aq}$, then

$$K'_{Eu} = \frac{D_{Eu}\,\{H^+\}^3_{aq}}{\alpha^{\circ}[(HX)_2]^3}$$

and

$$\log D_{Eu} = \log K'_{Eu} + 3\log[(HX)_2] + \log\alpha_o + 3\,pH \qquad (2)$$

The relationship between log D_{Eu} and pH, with initial sulphate concentrations ranging from zero to 0·30M (molar) was investigated at an ionic strength of

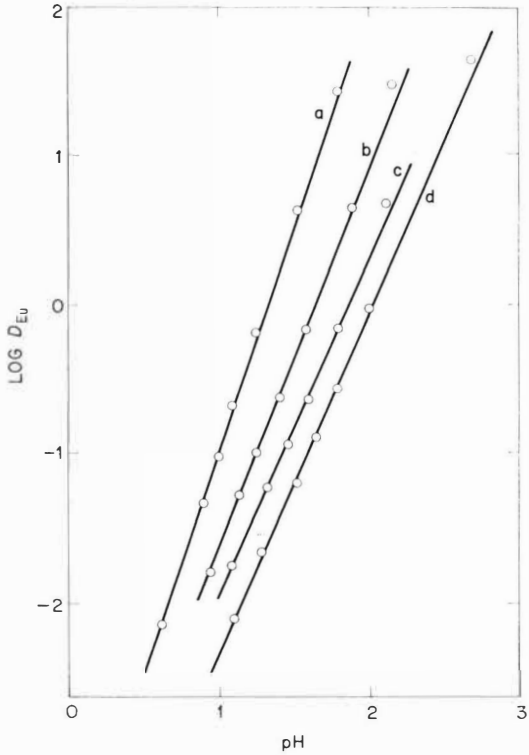

FIG. 1. *Log* D *against pH at different total sulphate concentrations*
Ionic strength 1·0; [D2EHPA] = 0·100 F;
a, 0·00M; b, 0·10M, c, 0·20M; d, 0·30M

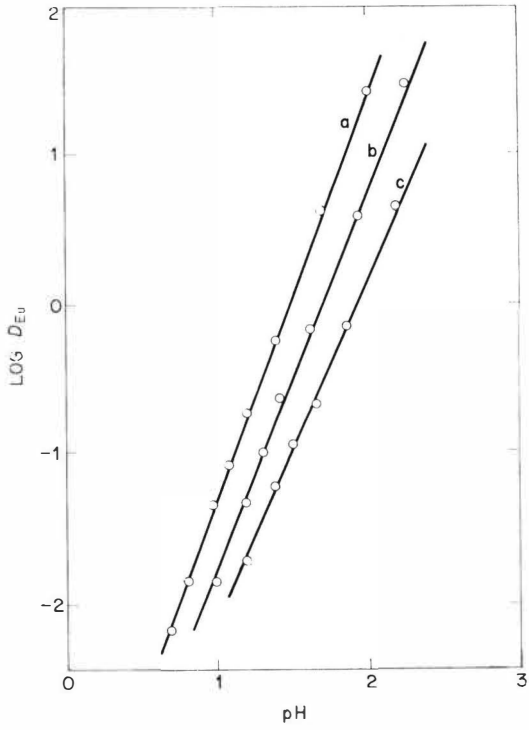

FIG. 2. *Log* D *against pH at different total sulphate concentrations*
Conditions as Fig. 1
a, 0·05M; b, 0·15M; c, 0·25M

unity with total europium concentration 10^{-4}M. The results are shown in Figs 1 and 2 as least squares plots; the slopes, correlation coefficients, intercepts at pH = 0 and intercepts at log D_{Eu} = 0 are given in Table I.

TABLE I

Results from Figs 1 and 2: plots of log D_{Eu} *against pH at varying sulphate concentrations*

Initial $[SO_4^{2-}]$, M	Correlation coefficient	Slope	pH = 0 intercept	Log D_{Eu} = 0 intercept
0·00	0·9997	3·07	−4·06	1·32
0·05	0·9998	2·72	−4·05	1·49
0·10	1·0000	2·56	−4·18	1·63
0·15	0·9998	2·62	−4·45	1·70
0·20	0·9989	2·37	−4·39	1·85
0·25	0·9994	2·36	−4·52	1·92
0·30	0·9988	2·36	−4·73	2·00

TABLE II

Results from Fig. 3: plots of log D_{Eu} *against log* $[HX]$ *at varying sulphate concentrations*

Initial $[SO_4^{2-}]$, M	Correlation coefficient	Slope	Log [HX] intercept	Log D_{Eu} = 0 intercept
0·00	0·9995	2·99	5·04	−1·69
0·05	0·9992	2·84	4·25	−1·50
0·10	0·9998	2·91	3·87	−1·33
0·20	0·9997	2·76	3·20	−1·16
0·30	0·9998	2·96	2·95	−1·00

Fig. 3 shows the relationship between log D_{Eu} and log [HX], with initial sulphate concentrations from 0·00M to 0·30M at pH 2·00. Relevant data obtained from this are given in Table II.

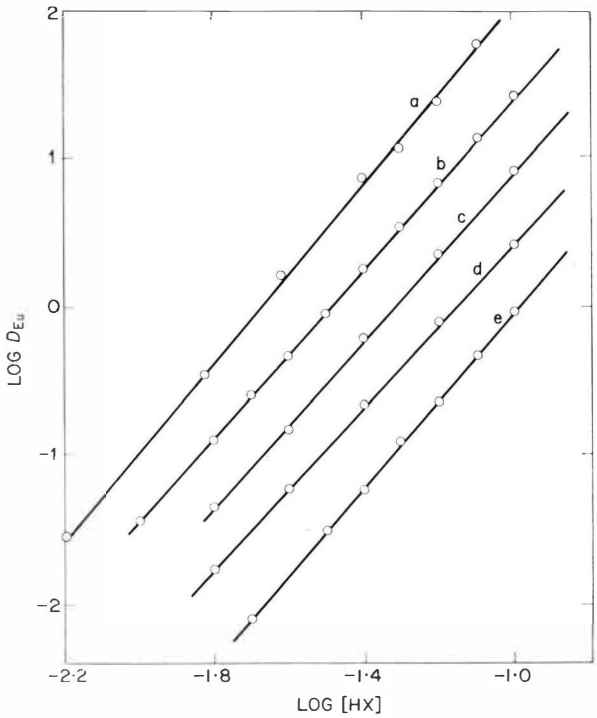

FIG. 3. *Log* D *against log [HX] at different total sulphate concentrations*
Ionic strength 1·0; pH 2·0
a, 0·00M; b, 0·05M; c, 0·10M; d, 0·20M; e, 0·30M

In the absence of sulphate ions $\alpha_o = 1$; also since the europium concentration in the aqueous phase initially was 10^{-4}M, the equilibrium concentration of free D2EHPA may be assumed to be equal to its initial concentration. Hence

$$\frac{d \log D_{Eu}}{d\,pH} = \frac{d \log D_{Eu}}{d \log [(HX)_2]} = 3$$

This is in good agreement with the results obtained with zero sulphate concentration.

In the presence of sulphate the value of α_o must be computed from relevant stability constant data, using the relationship:

$$\alpha_o = (1 + \sum_1^n \beta_n [L]^n)^{-1}$$

where β represents the overall stability constant and L the aqueous anion(s) to be considered. In the present system, at pH values less than 2, the anions requiring consideration are sulphate and bisulphate. The stability constant data for ionic strength of unity are as follows: Eu^{3+}–SO_4^{2-}, $\beta_1 = 37$, $\beta_2 = 250 \pm 30$;[8] $\beta_1 = 35 \pm 1 \cdot 15$, $\beta_2 = 490 \pm 1 \cdot 12$;[9] Eu^{3+}–HSO_4^-, $\beta_1 = 6 \cdot 7$.[7] The SO_4^{2-}–HSO_4^- equilibrium constant was taken as 11·0.[10] The values of β_1 and β_2 used in this work were 36 and 370 respectively. Calculations showed that no hydroxy species of europium occur to a significant extent below pH 5·2 and these were ignored. Extraction of a 10^{-2}M solution of europium from sulphate solution by D2EHPA in benzene gave no extraction of sulphate as

shown by stripping with hydrochloric acid. Hence extraction of sulphate or bisulphate complexes of europium need not be considered.

From Equation (2) when sulphate is present:

$$\frac{d \log D_{Eu}}{d\,pH} = 3 + \frac{d \log \alpha_o}{d\,pH}$$

so that the slopes of lines obtained by plotting log D_{Eu} against pH are not 3. Since SO_4^{2-} ions form complexes with Eu^{3+} ions rather more readily than do HSO_4^- ions, the value of α_o decreases as the pH increases. Thus d log α_o/d pH is negative and the slopes should be less than 3. The higher the initial concentration of sulphate in the aqueous solution, the more pronounced is the

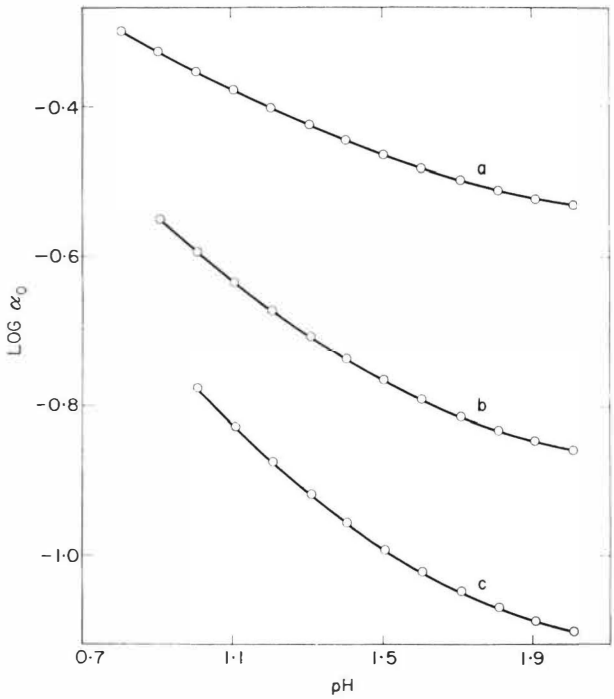

FIG. 4. *Log α_o against pH at different total sulphate concentrations*
Ionic strength 1·0
a, 0·05M; b, 0·10M; c, 0·15M

TABLE III

Predicted slopes of log D_{Eu}–pH graphs at different initial sulphate concentrations

pH range	Initial $[SO_4^{2-}]$, M					
	0·05	0·10	0·15	0·20	0·25	0·30
0·80–0·90	2·75	—	—	—	—	—
0·90–1·00	2·74	2·59	—	—	—	—
1·00–1·10	2·74	2·59	2·49	2·42	2·37	2·36
1·10–1·20	2·75	2·61	2·53	2·47	2·43	2·38
1·20–1·30	2·76	2·64	2·56	2·51	2·47	2·45
1·30–1·40	2·78	2·66	2·59	2·55	2·52	2·48
1·40–1·50	2·80	2·71	2·65	2·62	2·59	2·57
1·50–1·60	2·83	2·74	2·71	2·67	2·64	2·64
1·60–1·70	2·85	2·78	2·74	2·72	2·68	2·69
1·70–1·80	2·87	2·81	2·78	2·75	2·77	2·72
1·80–1·90	2·89	2·85	2·82	2·80	2·80	2·81
1·90–2·00	2·91	2·87	2·85	2·84	2·83	2·81
Measured slope	2·72	2·56	2·62	2·37	2·36	2·36

change in α_o with pH; thus the value of d log α_o/d pH becomes increasingly more negative. The calculated relationships between log α_o and pH at different initial sulphate concentrations are shown in Figs 4 and 5. Mean gradients obtained from these have been used to predict the slopes of D_{Eu} – pH graphs and the results are shown in Table III. The straight lines shown in Figs 1 and 2 neglect any changes in slope owing to variation of d log α_o/d pH.

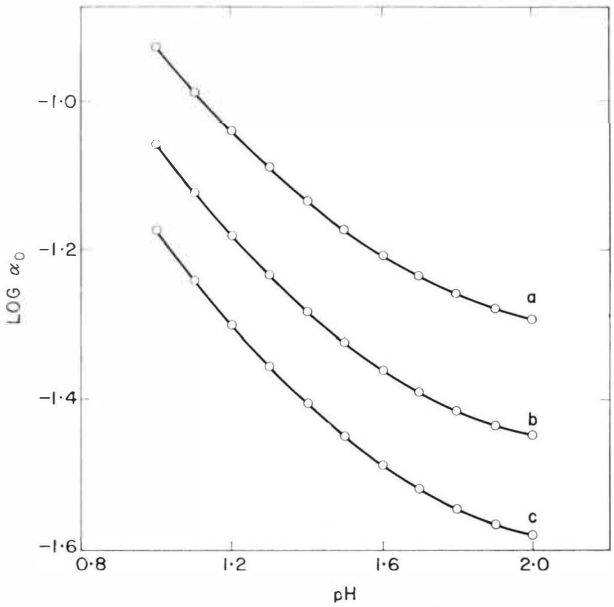

FIG. 5. *Log α_o against pH at different total sulphate concentrations*
Ionic strength 1·0
a, 0·20M; b, 0·25M; c, 0·30M

Values of K'_{Eu} may be calculated from Figs 1 and 2 using the log $D_{Eu} = 0$ intercepts. Under this condition and since $[HX] = 2[(HX)_2]$, Equation (2) becomes:

$$\log K'_{Eu} = -3\log[HX] + 3\log 2 - \log\alpha_o - 3\,pH \quad . \quad . \quad . \quad (3)$$

The calculated results are given in Table IV.

TABLE IV
Values of K'_{Eu} from Figs 1 and 2

Initial $[SO_4^{2-}]$, M	Log $D_{Eu} = 0$ intercept	$[SO_4^{2-}]$ free, M	$[HSO_4^-]$ free, M	α_o	K'_{Eu}
0·00	1·32	0·00	0·00	1·00	1·140
0·05	1·49	0·0369	0·0131	0·343	0·791
0·10	1·63	0·0795	0·0205	0·158	0·653
0·15	1·70	0·123	0·027	0·089	0·713
0·20	1·85	0·173	0·027	0·054	0·417
0·25	1·92	0·221	0·029	0·0367	0·378
0·30	2·00	0·270	0·030	0·0264	0·303

At constant values of pH, ionic strength, and europium and sulphate concentration, since the total europium concentration is small, d log D_{Eu}/d log $[HX] = 3$. The slopes of the lines in Fig. 3 are in satisfactory agreement with this predicted value. Values of K'_{Eu} may be calculated from Fig. 3 using the intercepts at log $D_{Eu} = 0$ and at log $[HX] = 0$. At pH = 2 from Equation (2) and by analogy with (3)

$$\log K'_{Eu} = -5{\cdot}097 - \log \alpha_o - (3 \log [HX])_{\log D_{Eu}=0}$$

and

$$\log K'_{Eu} = -5{\cdot}097 - \log \alpha_o - (\log D_{Eu})_{\log [HX]=0}$$

The calculated values of K'_{Eu} are given in Table V.

TABLE V

Values of K'_{Eu} from Fig. 3

Initial $[SO_4^{2-}]$, M	$[SO_4^{2-}]$ free, M	$[HSO_4^-]$ free, M	α_o	K'_{Eu} from $\log D_{Eu} = 0$ intercept	K'_{Eu} from $\log HX = 0$ intercept
0·00	0·00	0·00	1·000	0·940	0·877
0·05	0·045	0·005	0·294	0·861	0·484
0·10	0·090	0·010	0·137	0·572	0·433
0·20	0·180	0·020	0·051	0·473	0·249
0·30	0·270	0·030	0·0264	0·303	0·270

TABLE VI

Values of K'_{Eu} from Figs 1–3

Initial $[SO_4^{2-}]$, M	K'_{Eu} from Figs 1 and 2	K'_{Eu} from Fig. 3		Mean K'_{Eu}
0·00	1·140	0·940	0·877	0·986
0·05	0·791	0·861	0·484	0·712
0·10	0·653	0·572	0·433	0·553
0·15	0·713	—	—	(0·713)
0·20	0·417	0·473	0·249	0·380
0·25	0·378	—	—	(0·378)
0·30	0·303	0·303	0·270	0·292

All of the values of K'_{Eu} are summarised in Table VI. The results suggest that K'_{Eu} decreases as the initial sulphate concentration increases. This effect may be attributable to a decrease in the mean activity coefficient of the Eu^{3+} ion as the perchlorate present in the solution is progressively replaced by a sulphate–bisulphate mixture. This is equivalent to suggesting that the equilibrium constant used for the europium–sulphate complex formation is slightly inaccurate.

Acknowledgment

One of the authors (P.W.C.) is grateful to the Science Research Council for financial assistance while this work was carried out.

References

[1] Peppard, D. F., Mason, G. W., Maier, J. L., & Driscoll, W. J., *J. inorg. nucl. Chem.*, 1957, **4**, 334
[2] Peppard, D. F., Mason, G. W., Driscoll, W. J., & Sironen, R. J., *J. inorg. nucl. Chem.*, 1958, **7**, 276
[3] Baes, C. F., jun., Zingaro, R. A., & Coleman, C. F., *J. phys. Chem., Ithaca*, 1958, **62**, 129
[4] Sato, T., *J. inorg. nucl. Chem.*, 1962, **24**, 699
[5] Peppard, D. F., Mason, G. W., Hutcher, I., & Brandao, F. A. J. A., *J inorg. nucl Chem.*, 1962, **24**, 1387
[6] Burkin, A. R., & Cassidy, P. W., to be published
[7] Burkin, A. R., & Cassidy, P. W., to be published
[8] Bansal, B. M. L., Patil, S. K., & Sharma, H. D., *J. inorg. nucl. Chem.*, 1964, **26**, 993
[9] Sekine, T., *J. inorg. nucl. Chem.*, 1964, **26**, 1463
[10] *Spec. Publs chem. Soc.*, 1964, No. 17

Liquid–liquid extraction of iron(III) thiocyanate complexes by Versatic 911 and some other carboxylic acids

by N. M. Rice

Department of Mining and Mineral Sciences, University of Leeds, Leeds LS2 9JT, U.K.

Difficulties in the interpretation of the extraction of iron(III) thiocyanate complexes with carboxylic acids (HR) in benzene, caused by adsorption of iron on to experimental glassware have been resolved by treating the adsorbed material as a non-extractable aqueous species. The composition of this species corresponds to $(Fe_q(OH)_p)^{(3q-p)+}$ *with* $q = 1 \cdot 99 \pm 0 \cdot 17$, $p = 4 \cdot 08 \pm 0 \cdot 58$ *and formation constant,* $^*\beta_{pq} = (5 \cdot 73 \pm 4 \cdot 98) \times 10^{-8}$. *This device enabled the average composition of the extracted species* $(Fe(SCN)_s(OH)_h R_r(HR)_m(H_2O)_w(NO_3)_t)_f$ *to be derived from the experimental data for extraction using Versatic 911. The scatter in the data was too great for reliable values of* f, (h + r), (m + r), s *and* t *to be obtained but the results indicated that* f *was probably about 2 and that the values of the other parameters vary with the composition of the phases. Suggestions for improving the experimental technique to obtain more adequate data are put forward.*

Introduction

FROM THE LITERATURE on the extraction of metals by carboxylic acids there is general agreement that the extraction mechanism is more than a simple exchange of cations and that some form of solvated complex of the metal is actually extracted.[1–3] The solvating molecules may be either the carboxylic acid itself or water which has been shown to co-extract with certain metals.[2,3] The most efficient extraction takes place at pH values close to those where the metal hydroxides precipitate,[1–4] hence it is probable that the extracted species is partially hydrolysed, and there appears to be no reason other than the rules governing chemical bond formation why any cationic metal complex should not be extracted by a carboxylic acid.

Evidence that such complexes are extracted was found by Flett & West[5] who observed that $Cu(NH_3)_4^{2+}$ is extracted by naphthenic acid in the presence of *p*-nonylphenol in the organic phase. Haffenden & Lawson[6] have suggested that amminocobalt(II) complexes are extracted by Versatic 9 (Shell Chemical Co. Ltd.) from ammoniacal cobalt solutions. Similar behaviour with di-2-ethylhexylphosphoric acid was observed by Baes & Baker[7] who state that the iron(III) species extracted by this reagent contains water as well as hydroxide and perchlorate ligands.

When iron(III) is extracted from solutions containing SCN^- ligands by Versatic 911 (Shell Chemical Co. Ltd.) the organic phase is pink and has an absorption maximum at 506 nm[8] compared with the reddish brown colour (peak 460 nm) observed in the absence of SCN^-.[4] This indicates that the extracted species in the former case contains SCN^-. Detailed results of a study of the iron(III) thiocyanate–Versatic 911 extraction system have been reported elsewhere[8] but interpretation of these results, which were very scattered, was hampered by the low and variable iron mass balances obtained. These were caused by adsorption of some of the iron on to experimental glassware. A later report[9] describes attempts to overcome these effects by silicone treatment of the glassware, the use of stirred, sealed separating funnels to prevent evaporation of volatile diluents and to ensure uniform contacting of the phases during the relatively long (2–3 h) contact times required to approach equilibrium as well as close control of temperature with a thermostat bath. In addition some other carboxylic acids were studied in the hope that extraction in a lower pH range might reduce losses by adsorption. Lauric, pivalic and α-bromolauric acids were tried all without success. The last reagent was capable of extracting

iron at lower pH values than the rest but from the spectra of the organic phases it was apparent that no SCN^- was being co-extracted.

In this paper mathematical methods are developed for interpreting the previous results.[8] The device of treating the iron lost by adsorption as a non-extractable aqueous hydroxy-species is adopted. It was necessary to determine the apparent stoichiometry of this species although it should be realised that its actual nature will depend on the surface area available for adsorption and may well be vastly different from the mathematical formulation. It is considered that as this device enables the extraction results to be interpreted – the main purpose of this work – its use is justified.

In the interpretation it has been necessary to calculate the fractional distribution of iron between various species in the aqueous phase from published stability constant data, which were obtained from the references cited in Table I. Values of the various constants were corrected to an ionic strength of 0·25 using the Debye–Hückel equation with the values of the parameters listed in Table I where the constants have the following meanings (omitting charges) and [ ] denotes concentration:

$$\text{(i)}\quad Fe_j(OH)_{i-1} + H_2O \rightleftharpoons Fe_j(OH)_i + H^+ \qquad (1)$$

$$^*K_{ij} = [Fe_j(OH)_i][H^+]/[Fe_j(OH)_{i-1}] \qquad (2)$$

$$\text{(ii)}\quad Fe^{3+} + NO_3^- \rightleftharpoons Fe(NO_3)^{2+} \qquad (3)$$

$$K_{NO_3} = [Fe(NO_3)^{2+}]/[Fe^{3+}][NO_3^-] \qquad (4)$$

$$\text{(iii)}\quad Fe(SCN)_{n-1} + (SCN^-) \rightleftharpoons Fe(SCN)_n \qquad (5)$$

$$K_n = [Fe(SCN)_n]/[Fe(SCN)_{n-1}][SCN^-] \qquad (6)$$

$$\text{(iv)}\quad 2Fe^{3+} + 6SCN^- \rightleftharpoons Fe_2(SCN)_6 \qquad (7)$$

$$\beta_{62} = [Fe_2(SCN)_6]/[Fe^{3+}]^2[SCN^-]^6 \qquad (8)$$

TABLE I

Stability constant data for iron(III)

Complex	Constant	Debye–Hückel parameters			K_n values for ionic strengths of 0 and 0·25		References
		$\mathring{a}B$	C	ΔZ^2	0	0·25	
$Fe(OH)^{2+}$	$10^3{}^*K_{11}$	2·4	0	−4	6·4	2·24	10, 11
$Fe(OH)_2^+$	$10^5{}^*K_{21}$	2·4	0	−2	7·7	4·48	10, 11
$Fe_2(OH)_2^{4+}$	$^*K_{22}$	2·1	0	+8	36	344	10, 11
$Fe_3(OH)_4^{5+}$	$10^6\ \beta_{43}$	2·1	0	+2	1·7	3·024	12
$Fe(NO_3)^{2+}$	K_{NO_3}	1·7	0·015	−6	10	1·508	13
$Fe(SCN)^{2+}$	K_1	1·5	0·30	−6	1070	173·0	14
$Fe(SCN)_2^+$	K_2	1·5	0·044	−4	98·0	28·6	14
$Fe(SCN)_3$	K_3	1·5	0	−2	77·0	39·6	14
$Fe(SCN)_4^-$	K_4	1·5	0	0	20·0	20·0	14
$Fe(SCN)_5^{2-}$	K_5	1·5	0	+2	0·277	0·538	14
$Fe(SCN)_6^{3-}$	K_6	1·5	0	+4	0·087	0·306	14
$Fe_2(SCN)_6$	$10^{16}\beta_{62}$	—	—	—	—	0·500	15, 16

Theory

Adsorbed species

For any particular surface area in contact with the aqueous phase an equilibrium should exist between the concentration of iron in the aqueous phase and the quantity of iron adsorbed on the glassware. The aqueous phase and hence also the adsorbed iron are in equilibrium with the organic phase. The adsorbed iron will be treated as a non-extractable complex in equilibrium with the other aqueous iron species i.e. it will be considered as part of the aqueous

iron concentration, C_{Fe}, which will then be given by the difference between the measured organic iron concentration, $\bar{C}_{Fe}$, and the initial iron concentration, $(C_{Fe})_0$, for equal phase volumes

$$\text{i.e.} \quad C_{Fe} = (C_{Fe})_0 - \bar{C}_{Fe} \qquad (9)$$

whence the iron distribution ratio, D_{Fe}, is

$$D_{Fe} = \bar{C}_{Fe}/[(C_{Fe})_0 - \bar{C}_{Fe}] \qquad (10)$$

The 'concentration' of adsorbed iron, C_A, is given by the difference between C_{Fe} as calculated by Equation (1) and the analytically determined aqueous iron concentration, $(C_{Fe})_M$

$$\text{i.e.} \quad C_A = C_{Fe} - (C_{Fe})_M \qquad (11)$$

From the experimental data[8] it is clear that the fraction of iron adsorbed, $C_A/C_{Fe})_0$, depends on pH and free iron concentration $[Fe^{3+}]$. It increases with rising pH and also with rising $(C_{Fe})_0$ up to about 8×10^{-4}M when it starts to decrease, presumably because the surface is then saturated with iron and the percentage adsorbed becomes relatively less at higher concentrations. $C_{Fe}/(C_{Fe})_0$ is also lower at higher SCN^- concentrations which indicates that it depends on the free iron concentration. Thus it seems that the adsorbed species is probably a polynuclear hydroxy-complex of iron(III) which may be formulated: $Fe_q(OH)_p^{(3q-p)+}$.

Ignoring changes the formation equilibrium may be written as

$$q\,Fe^{3+}_{(aq)} + pH_2O_{(aq)} \rightleftharpoons Fe_q(OH)_{p(glass)} + pH^+_{(aq)} \qquad (12)$$

with overall formation quotient

$$*\beta_{pq} = \frac{[Fe_q(OH)_p][H^+]^p}{[Fe^{3+}]^q} \qquad (13)$$

The value of $*\beta_{pq}$ will naturally vary with the surface area available for adsorption, but with a relatively constant surface area it should remain relatively constant in a constant ionic medium.

The fraction of 'aqueous' iron in the adsorbed species:

$$\alpha_{pq} = \frac{q\,[Fe_q(OH)_p]}{C_{Fe}} = \frac{C_A}{C_{Fe}} \qquad (14)$$

From Equations (13) and (14) taking logarithms:

$$\log C_A = \log q\,*\beta_{pq} + q \log (Fe^{3+}) + p.\text{pH} \qquad (15)$$

Provided that $*\beta_{pq}$, q and p are constant, a plot of $\log C_A$ against $\log [Fe^{3+}]$ at constant pH should be linear with a slope of q and intercept, $I_1 = \log q\,*\beta_{pq} + p.\text{pH}$ at $\log [Fe^{3+}] = 0$.

From a series of such plots for different pH values the variation of $\log C_A$ with pH may be obtained for a given value of $[Fe^{3+}]$ and a plot of $\log C_A$ against pH should have a slope of p and intercept, $I_2 = \log q\,*\beta_{pq}\,[Fe^{3+}]^q$ at pH = 0.

Thus provided the assumptions are reasonable it should be possible to evaluate p and q.

Liquid–liquid extraction

There are several possible cationic species that may be extracted but individual treatment of each equilibrium is mathematically difficult.[8] Thus it is simplest to assign an overall average composition to the extracted species,[17] deduce this and then attempt to interpret the various individual extraction equilibria. Also it is conceivable that these individual extracted species may combine to form mixed-ligand polymers in the organic phase.

Using the notation below for convenience, assume that the extracted species is:

$$(Fe(SCN)_s R_r (HR)_m (OH)_h (NO_3)_t (H_2O)_w)_f$$

where R^- is the carboxylate ion of carboxylic acid HR. It is also assumed that a negligible fraction of HR enters the aqueous phase. NO_3^- is included because KNO_3 was used to maintain a constant ionic strength in the aqueous phase and at least one cationic ion pair is formed between Fe^{3+} and NO_3^-.[13]

If the extractant is assumed to exist as a dimeric species in the organic phase[1] then the extraction equilibrium may be written:

$$Fe^{3+}_{aq} + s\,SCN^-_{aq} + (h+w)H_2O_{aq} + \frac{m+r}{2}(HR)_2 + tNO^-_{3aq} \rightleftharpoons$$

$$\frac{1}{f}\left(\overline{(Fe(SCN)_s R_r (HR)_m (OH)_h (NO_3)_t (H_2O)_w)_f}\right) + (h+r)H^+_{aq} \quad . \quad (16)$$

where aq denotes the aqueous and —— the organic phase using the notation of Marcus & Kertes.[1]

The extraction constant is therefore

$$K_{ex} = \frac{(C_{Fe}/f)^{1/f}\,[H^+]^{h+r}}{[Fe^{3+}]_{aq}\,[SCN^-]^s_{aq}\,[NO_3^-]^t_{aq}\,[(HR)_2]^{(m+r)/2}} \quad . \quad . \quad . \quad (17)$$

where [ ] is taken to mean concentration because in general the experiments were carried out in a medium of constant ionic strength and hence the aqueous activity coefficient quotients are constant.

$$[Fe^3]^+ = C_{Fe}/X \quad . \quad . \quad . \quad . \quad . \quad . \quad . \quad . \quad . \quad (18)$$

where X is the complex formation sum in the aqueous phase and in this system

$$X = 1 + K_{NO_3}[NO_3^-] + \sum_1^2 {}^*\beta_{i1}[H^+]^{-n} + \sum_1^6 \beta_n [SCN^-]^n$$
$$+ 2\,{}^*\beta_{22}[Fe^{3+}][H^+]^{-2} + 3\,{}^*\beta_{43}[Fe^{3+}]^2[H^+]^{-4}$$
$$+ 2\,\beta_{62}[Fe^{3+}][SCN^-]^6 + C_A/[Fe^{3+}] \quad . \quad . \quad . \quad . \quad (19)$$

where $\beta_N = \prod_0^N K_N$ for K_n as given in Table I.

The initial concentrations of NO_3^- and SCN^-, C_{NO_3}, and C_{SCN} are both very much greater than C_{Fe}. $\bar{C}_R$, the total organic extractant concentration, is very much greater than $\bar{C}_{Fe}$. Hence the approximations may be made that $[NO_3^-] = C_{NO_3}$, $[SCN^-] = C_{SCN}$ and $\bar{C}_R = 2\,[(HR)_2]$.

Also, $[Fe^{3+}]$ may be calculated from Equations (18) and (19) by an iterative method[18] using the above approximations and assuming that no polynuclear species exist when an initial value for X is calculated.

The term $C_A/[Fe^{3+}]$ may also be ignored if $(C_{Fe})_M$ is used for C_{Fe} since it is readily shown that

$$[Fe^{3+}] = \frac{C_{Fe}}{X} = \frac{(C_{Fe})_M}{X - C_A/[Fe^{3+}]} \quad . \quad . \quad . \quad . \quad . \quad . \quad (20)$$

The extraction equation then becomes:

$$K_{ex} = \frac{(\bar{C}_{Fe}/f)^{1/f}\,[H^+]^{h+r}\,X}{C_{Fe}\,C^s_{SCN}\,C^t_{NO_3}\,(C_R/2)^{(m+r)/2}} \quad . \quad . \quad . \quad . \quad . \quad . \quad (21)$$

Now the iron distribution ratio,[3]

$$D_{Fe} = \frac{\bar{C}_{Fe}}{C_{Fe}} = \frac{(\bar{C}_{Fe}/f)^{1/f}\,(\bar{C}_{Fe})^{(f-1)/f}}{C_{Fe}\,(1/f)^{1/f}} \quad . \quad . \quad . \quad . \quad . \quad . \quad (22)$$

Substituting (22) in (21), rearranging and taking logarithms gives:

$$\log D_{Fe} = \log K_{ex} + \frac{1}{f}\log f - \frac{m+r}{2}\log 2 + \frac{f-1}{f}\log \bar{C}_{Fe}$$
$$+ s\log C_{SCN} + t\log C_{NO_3} + \frac{m+r}{2}\log \bar{C}_R + (h+r)\,\mathrm{pH} - \log X \,. \quad (23)$$

which is the equation previously used.[8]

Direct application of (23) proved difficult because of the simultaneous variation of D_{Fe} and $\bar{C}_{Fe}$. Hence the variation of $\mathrm{pH}_{0\cdot5}$ at which $D_{Fe} = 1$ and hence $\bar{C}_{Fe} = \frac{1}{2}(C_{Fe})_0$ was studied. . . . . (24)

Substitution of $\mathrm{pH}_{0\cdot5}$ and (24) into (23) gives the equation:

$$(h+r)\,\mathrm{pH}_{0\cdot5} = -\log K_{ex} - \frac{1}{\log f} + \frac{m+r}{2}\log 2 - \frac{f-1}{f}\log (C_{Fe})_0$$
$$+ \frac{f-1}{f}\log 2 - s\log C_{SCN} - t\log C_{NO_3} - \frac{m+r}{2}\log \bar{C}_R + \log X \,. \quad (25)$$

Again, application of this equation proved difficult because of the varying mass balances but this difficulty may be overcome by means of the procedure outlined in the previous section.

In the subsequent equations the following notation is used for convenience: X_{SCN} is the thiocyanate complex formation sum:

$$X_{SCN} = \sum_{1}^{6} n\,\alpha_n + 6\,\alpha_{62} \quad . \quad . \quad . \quad . \quad . \quad . \quad . \quad . \quad (26)$$

where α_n is the fraction of aqueous iron present as $Fe(SCN)_n^{3-n}$ and α_{62} is the fraction of aqueous iron in the polynuclear species $Fe_2(SCN)_6$.

X_{PN} is the polynuclear complex formation sum:

$$X_{PN} = \alpha_{62} + \alpha_{22} + 2\,\alpha_{43} \quad . \quad . \quad . \quad . \quad . \quad . \quad . \quad (27)$$

where α_{ij} is the fraction of aqueous iron in the polynuclear hydrolysis products $Fe_j(OH)_i$.

X_{OH} is the hydroxy-complex formation sum:

$$X_{OH} = \alpha_{11} + 2\,\alpha_{21} + 2\,\alpha_{22} + 4\,\alpha_{43} \quad . \quad . \quad . \quad . \quad . \quad . \quad (28)$$

where α_{ij} is defined as above.

Partial logarithmic differentiation of Equation (25) yields the following expressions:

(i) *At constant* $\bar{C}_R$, C_{NO_3} *and* $(C_{Fe})_0$

$$(h+r)\,\frac{\partial\,\mathrm{pH}_{0\cdot5}}{\partial \log C_{SCN}} = -s + X_{SCN} \quad . \quad . \quad . \quad . \quad . \quad . \quad . \quad (29)$$

(ii) *At constant* $\bar{C}_R$, $\bar{C}_{NO_3}$ *and* C_{SCN}

$$(h+r)\,\frac{\partial\,\mathrm{pH}_{0\cdot5}}{\partial \log (C_{Fe})_0} = \frac{1-f}{f} - \left(\frac{X_{PN} + (q-1)\,\alpha_{pq}}{1 + X_{PN} + (q-1)\,\alpha_{pq}}\right)\left(\frac{s + X_{SCN}}{X_{SCN}}\right) \quad (30)$$

(iii) *At constant* $\bar{C}_R$, $\bar{C}_{SCN}$ *and* $(C_{Fe})_0$

$$(h+r)\,\frac{\partial\,\mathrm{pH}_{0\cdot5}}{\partial \log C_{NO_3}} = t + \frac{\mathrm{d}\log X}{\mathrm{d}\log C_{NO_3}} \quad . \quad . \quad . \quad . \quad . \quad . \quad . \quad (31)$$

The latter term is most easily evaluated empirically because of the variation in stability constants with ionic strength which varies as C_{NO_3} varies.

(iv) *At constant* C_{NO_3}, C_{SCN} *and* $(C_{Fe})_0$

$$\frac{\partial\,\mathrm{pH}_{0\cdot5}}{\partial \log \bar{C}_R} = -\frac{m+r}{2(h+r)} \quad . \quad . \quad . \quad . \quad . \quad . \quad . \quad . \quad (32)$$

In practice the difficulty in applying Equations (29) to (32) is that no independent estimate is available for $(h+r)$ from Equation (25).

The problem of the simultaneous variation of log D_{Fe} and log $\bar{C}_{Fe}$ in Equation (23) may be overcome as follows:

D_{Fe} and $\bar{C}_{Fe}$ are not independent variables but are related by the equation

$$\bar{C}_{Fe} = \frac{D_{Fe}}{1 + D_{Fe}} (C_{Fe})_0 \quad . \quad . \quad . \quad . \quad . \quad . \quad . \quad . \quad (33)$$

for a phase volume ratio of 1 : 1.

Substitution of (33) in (23) and rearrangement with all the terms involving D on the left hand side gives:

$$\left(\frac{f-1}{f}\right) \log (1 + D_{Fe}) + \frac{1}{f} \log D_{Fe} = \log K_{ex} + \frac{1}{f} \log f$$
$$- \frac{m+r}{2} \log 2 + \frac{f-1}{f} \log (C_{Fe})_0 + s \log C_{SCN} + t \log C_{NO_3}$$
$$+ \frac{m+r}{2} \log \bar{C}_R + (h+r)\,\mathrm{pH} - \log X \quad . \quad . \quad . \quad . \quad . \quad (34)$$

Differentiation of the left hand side of Equation (34) w.r.t. any variable log C gives the following:

$$\frac{1}{f} \frac{\mathrm{d} \log D_{Fe}}{\mathrm{d} \log C} + \left(\frac{f-1}{f}\right) \frac{\mathrm{d} \log (1+D_{Fe})}{\mathrm{d} \log C}$$
$$= \frac{1}{f} \frac{\mathrm{d} \log D_{Fe}}{\mathrm{d} \log C} + \left(\frac{f-1}{f}\right) \frac{\mathrm{d} \log (1 + D_{Fe})}{\mathrm{d} \log D_{Fe}} \frac{\mathrm{d} \log D_{Fe}}{\mathrm{d} \log C}$$
$$= \frac{1}{f} \frac{\mathrm{d} \log D_{Fe}}{\mathrm{d} \log C} + \left(\frac{f-1}{f}\right) \left(\frac{D_{Fe}}{1 + D_{Fe}}\right) \frac{\mathrm{d} \log D_{Fe}}{\mathrm{d} \log C}$$
$$= \frac{1 + f D_{Fe}}{f(1 + D_{Fe})} \frac{\mathrm{d} \log D_{Fe}}{\mathrm{d} \log C} \quad . \quad . \quad . \quad . \quad . \quad . \quad . \quad . \quad (35)$$

Hence it is readily shown that logarithmic partial differentiation of Equation (34) gives the following expressions (all for a phase ratio of 1 : 1).

At constant $(C_{Fe})_0$, C_{SCN}, C_{NO_3} *and* $\bar{C}_R$

$$\frac{\partial \log D_{Fe}}{\partial\, \mathrm{pH}} = \left(\frac{f(1 + D_{Fe})}{1 + f D_{Fe}}\right) [(h+r) - X_{OH} - p\,\alpha_{pq}] \quad . \quad . \quad . \quad (36)$$

Plots of log D_{Fe} versus pH for a series of values of C_{SCN}, C_{NO_3}, $(C_{Fe})_0$ and $\bar{C}_R$ should enable the variation of log D_{Fe} with each of these parameters at constant pH to be measured.

At constant pH, C_{SCN}, C_{NO_3} *and* $\bar{C}_R$

$$\frac{\partial \log D_{Fe}}{\partial \log (C_{Fe})_0} = \frac{(1 + D_{Fe})}{1 + X_{PN} + (q-1)\,\alpha_{pq} + f D_{Fe}}$$
$$\times [f - (1 + X_{PN} + (q-1)\,\alpha_{pq}] \quad . \quad . \quad . \quad . \quad . \quad . \quad (37)$$

At constant pH, $(C_{Fe})_0$, C_{NO_3} *and* $\bar{C}_R$

$$\frac{\partial \log D_{Fe}}{\partial \log C_{SCN}} = \frac{f(1 + D_{Fe})}{(1 + f D_{Fe})} [s - X_{SCN}] \quad . \quad . \quad . \quad . \quad . \quad . \quad (38)$$

At constant pH, $(C_{Fe})_0$, C_{SCN} *and* $\bar{C}_R$

$$\frac{\partial \log D_{Fe}}{\partial \log C_{NO_3}} = \frac{f(1 + D_{Fe})}{(1 + f D_{Fe})} (t - \alpha_{NO_3}) \quad . \quad . \quad . \quad . \quad . \quad . \quad . \quad (39)$$

At constant pH, $(C_{Fe})_0$, C_{SCN} *and* $\bar{C}_R$

$$\frac{\partial \log D_{Fe}}{\partial \log \bar{C}_R} = \frac{f(1 + D_{Fe})}{1 + fD_{Fe}} \left(\frac{m+r}{2}\right) \quad . \quad . \quad . \quad . \quad . \quad . \quad (40)$$

From Equation (37) it is thus possible to establish a value for f independent of all other stoichiometric parameters. Then using this value Equation (36) may be used to obtain $(h+r)$ and then Equations (38) to (40) or (29) to (32) may be used to evaluate s, t and $(m+r)$. It is difficult to obtain separate values of m, h and r, and w cannot be obtained without a study of the water uptake by the organic phase.

Equations (36) to (40) are equivalent to the general equations derived by Irving *et al.*[17] but are in a form convenient for the study of the present system with the available stability constant data and the difficulties caused by adsorption losses.

Experimental

Details of the experimental technique are to be found in references 8 and 9. Briefly, iron distribution data were obtained by γ scintillation counting of ^{59}Fe tracer added to non-active iron. Both phases were counted. KNO_3 was used to maintain an ionic strength of 0·25 except in one series of experiments when its concentration was varied. The pH was adjusted before extraction by adding a few drops of KOH and making up to volume. The pH values after extraction were measured.

For Versatic 911, phase contact was by shaking for 2 to 3 h in separating funnels at an ambient temperature of 25°C ± 3°C using freshly prepared aqueous phase.

Experiments on pivalic, lauric and α-bromolauric acids were carried out by stirring in sealed separating funnels at a constant rate of 1275 rev/min at a temperature of 25°C ± 0·1°C in a thermostat bath. Again, contact times were 2–3 h.

The experimental data recorded in the previous reports[8] were recalculated on the basis of Equations (9) to (11) using the University of Leeds KDF-9 computer. The values of X, X_{SCN}, X_{PN} and X_{OH} were also calculated by computer from the stability constant data of Table I.

Results

Adsorption

Values of log C_A obtained from a series of experiments where $(C_{Fe})_0$ varied between $1{\cdot}024 \times 10^{-5}$M and $5{\cdot}12 \times 10^{-3}$M with $\bar{C}_R$, C_{SCN} and C_{NO_3} constant at 0·10, 0·01 and 0·25M respectively, are shown plotted in Fig. 1 against corresponding values of log $[Fe^{3+}]$ for a series of different pH values. (For clarity, plots at intermediate pH values have been omitted.) The slopes of the linear portions of the curves (equal to q in Equation 15) had a mean value of 1·99 ± 0·17. From the data of Fig. 1, log C_A was plotted against pH for a series of values of log $[Fe^{3+}]$. The curves were linear with a mean slope $p = 4{\cdot}08 \pm 0{\cdot}58$ (in these results ± indicates one standard deviation).

From the values of C_A, $[Fe^{3+}]$ and pH for each of the 30 points plotted in Fig. 1, the value $^*\beta_{pq}$ was calculated by Equation (13) taking $p = 4$ and $q = 2$. A mean value of $^*\beta_{pq} = (5{\cdot}73 \pm 4{\cdot}98) \times 10^{-8}$ was obtained.

The flat portion of the curves in Fig. 1 indicates that saturation of the glass surface occurs for C_A values in the region of about 5×10^{-4}M which corresponds to about 1·4 Å^2 per Fe^{3+} adsorbed taking an approximate surface area from the dimensions of the glassware. No significant adsorption occurs at $[Fe^{3+}]$ values below about 10^{-5} to 10^{-7}M, the value decreasing as the pH rises.

Extraction with Versatic 911

Varying $(\bar{C}_{Fe})_0$

Table II shows the experimental data for the variation of D_{Fe} with pH for a series of values of $(C_{Fe})_0$ with C_{SCN}, C_{NO_3} and $\bar{C}_R$ constant at 0·01M, 0·25M and

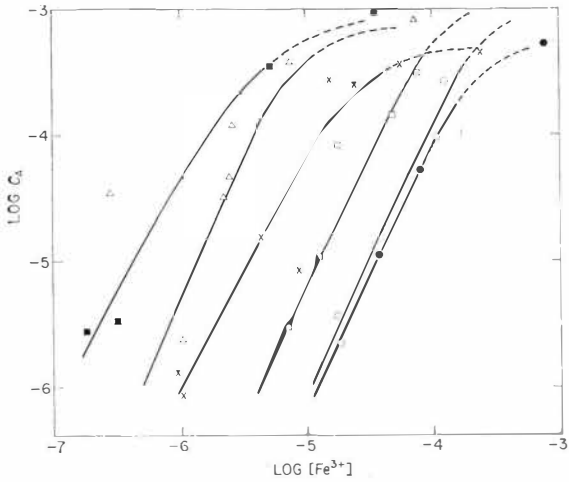

FIG. 1. *Variation of log* C_A *with log* [Fe^{3+}] *at various pH values*
● pH 2·60; ○ pH 2·75; □ pH 3·00; × pH 3·20; △ pH 3·40, ■ pH 3·70

TABLE II

Variation of D_{Fe} *with pH for various iron concentrations*

	$(C_{Fe})_0$, M									
pH	1·024 × 10^{-5}	2·048 × 10^{-5}	5·12 × 10^{-5}	1·024 × 10^{-4}	2·048 × 10^{-4}	5·12 × 10^{-4}	8·0 × 10^{-4}	1·024 × 10^{-3}	2·048 × 10^{-3}	5·12 × 10^{-3}
2·05	—	—	—	—	—	—	—	0·019	0·001	—
2·10	—	—	—	—	—	—	—	—	—	0·008
2·25	—	—	—	—	—	—	—	0·006	0·024	0·007
2·40	—	—	—	—	—	—	—	—	—	0·016
2·45	—	—	—	—	—	—	—	—	0·057	—
2·50	—	—	0·039	—	—	—	0·306	0·113	—	—
2·60	—	—	—	—	0·007	0·028	—	—	—	0·028
2·65	—	—	0·007	—	—	—	0·145	—	0·115	—
2·70	—	0·005	—	—	—	—	—	—	0·004	0·043
2·75	—	—	—	0·023	—	—	—	0·153	—	—
2·80	—	—	—	—	0·206	—	—	—	0·128	—
2·85	—	—	—	—	—	0·113	0·134	—	—	—
2·90	0·119	—	—	0·076	—	—	—	—	—	0·003
2·95	—	0·035	—	0·035	—	—	0·163	0·151	0·114	0·035
3·00	0·106	—	0·070	0·132	0·256	0·074	—	0·205	—	—
3·05	—	0·025	0·354	0·438	—	0·155	0·390	—	—	—
3·10	0·318	—	0·297	—	0·313	—	—	—	—	—
3·15	—	—	—	—	0·364	—	—	—	—	0·028
3·20	0·156	—	0·028	0·234	—	0·205	0·220	0·165	—	—
3·30	1·098	—	0·743	0·586	—	—	—	—	—	—
3·35	—	—	—	—	—	0·314	—	—	0·078	—
3·40	—	0·471	0·374	0·676	0·437	0·105	—	—	0·057	—
3·45	0·561	—	—	—	—	—	—	—	—	—
3·50	—	—	0·767	1·197	—	—	—	—	—	—
3·55	—	1·409	—	—	—	0·328	—	—	—	—
3·60	1·077	—	0·291	—	—	—	—	0·086	—	—
3·70	0·750	1·354	—	—	—	0·163	—	—	0·042	—
3·75	—	—	—	0·373	—	—	—	—	—	—
3·85	—	—	0·084	—	—	—	—	—	—	—
3·90	—	—	—	—	—	—	—	0·049	—	—

1·00M respectively. Fig. 2 shows three typical plots of log D vs. pH. From curves such as those of Fig. 2 the variation of log D_{Fe} with log $(C_{Fe})_0$ at constant pH was obtained. This is shown in Fig. 3 (in which the points shown are those obtained from the log D_{Fe} – pH plots). By drawing tangents to the curves of Fig. 3, the slopes were obtained and used to calculate values of f by Equation (37), taking $q = 2$. From 57 sets of data a value of $f = 1 \cdot 2 \pm 1 \cdot 2$ was obtained (at the 95% confidence level). Hence values of 1 or 2 for f could be equally valid. However, calculation of $(h+r)$ by Equation (36) generally gave sensible results ($(h+r) < 3$) only when f was taken as 2 and not 1. Hence the former value of f was used in all subsequent calculations. Table III shows values of $(h+r)$ obtained at different $(C_{Fe})_0$ and pH values.

TABLE III

Values of (h+r) *for various pH values and iron concentrations*

	$(C_{Fe})_0$ M									
pH	$1\cdot024 \times 10^{-5}$	$2\cdot048 \times 10^{-5}$	$5\cdot12 \times 10^{-5}$	$1\cdot024 \times 10^{-4}$	$2\cdot048 \times 10^{-4}$	$5\cdot12 \times 10^{-4}$	$8\cdot0 \times 10^{-4}$	$1\cdot024 \times 10^{-3}$	$2\cdot048 \times 10^{-3}$	$5\cdot12 \times 10^{-3}$
2·05	—	—	—	—	—	—	—	1·56	1·64	—
2·10	—	—	—	—	—	—	—	—	—	1·68
2·25	—	—	—	—	—	—	—	1·18	1·74	1·77
2·40	—	—	—	—	—	—	—	—	—	1·52
2·45	—	—	—	—	—	—	—	—	1·21	—
2·50	—	—	2·56	—	—	—	0·53	0·80	—	—
2·60	—	—	—	—	2·05	1·52	—	—	—	1·46
2·65	—	—	2·89	—	—	—	0·86	—	0·98	—
2·70	—	1·79	—	—	—	—	—	—	1·35	1·23
2·75	—	—	—	1·48	—	—	—	1·20	—	—
2·80	—	—	—	—	2·32	—	—	—	1·14	—
2·85	—	—	—	—	—	2·11	1·37	—	—	—
2·90	0·89	—	—	1·59	—	—	—	—	—	1·49
2·95	—	2·06	—	1·86	—	—	2·48	1·17	1·28	1·52
3·00	0·82	—	4·06	2·05	3·42	2·36	—	1·74	—	—
3·05	—	2·04	2·71	4·15	—	2·32	2·83	—	—	—
3·10	1·54	—	3·26	—	2·52	—	—	—	—	—
3·15	—	—	—	—	1·84	—	—	—	—	1·88
3·20	2·96	—	2·24	2·19	—	3·26	3·03	1·77	—	—
3·30	2·66	—	3·63	4·01	—	—	—	—	—	—
3·35	—	—	—	—	—	3·41	—	—	1·95	—
3·40	—	3·26	3·75	3·70	3·58	3·53	—	—	2·09	—
3·45	3·58	—	—	—	—	—	—	—	—	—
3·50	—	—	2·25	3·12	—	—	—	—	—	—
3·55	—	2·43	—	—	—	3·14	—	—	—	—
3·60	2·71	—	2·02	—	—	—	—	2·40	—	—
3·70	1·15	1·28	—	—	—	2·28	—	—	2·46	—
3·75	—	—	—	1·81	—	—	—	—	—	—
3·85	—	—	2·09	—	—	—	—	—	—	—
3·90	—	—	—	—	—	—	—	3·12	—	—

Varying C_{SCN}

Table IV shows the experimental values of D_{Fe} at various pH values for a series of values of C_{SCN} with $(C_{Fe})_0 = 1\cdot024 \times 10^{-4}$M, $\bar{C}_R = 0\cdot100$M, and $C_{NO_3} = 0\cdot25$M. Plots of log D_{Fe} vs. pH were similar to those of Fig. 2 and from them data were obtained for the plots of log D_{Fe} vs. log C_{SCN} shown in Fig. 4. Slopes of the curves in Fig. 4 were obtained by drawing tangents and used to calculate the value of s by Equation (38). Sensible values of s (positive values) were obtained only when $f = 2$ was used. When the complex, $Fe_2(SCN)_6$, was included in the complex formation sum, X_{SCN}, values of $s > 3$ were sometimes obtained. As the evidence for this species was rather inconclusive[15] it was omitted from the calculations. Values of $(h+r)$ were also calculated from log D_{Fe} vs. pH plots and corresponding values of $(h+r)$ and s are shown in Table V.

Varying $\bar{C}_R$

Table VI shows the experimental data for the variation of D_{Fe} with pH for a series of values of $\bar{C}_R$ in benzene with $(C_{Fe})_0 = 1\cdot024 \times 10^{-4}$M, $C_{SCN} = 0\cdot01$M and $C_{NO_3} = 0\cdot25$M. Plots of log D_{Fe} against pH were used to provide data for the plots of log D_{Fe} against log $\bar{C}_R$ shown in Fig. 5 whilst Fig. 6 shows a plot of log D_{Fe} vs. log $\bar{C}_R$ obtained experimentally for pH values in the range 3·0 to 3·1. Slopes obtained by drawing tangents to the plots in Figs 5 and 6 were used in Equation (40) to calculate $(m+r)$ taking $f = 2$ and corresponding values of $(h+r)$ were obtained from the plots of log D_{Fe} against pH. These are shown in Table VII. The dotted line in Fig. 6 is the regression line through the experimental points with slope = 1·8 and correlation coefficient = 0·98.

Varying C_{NO_3}

Fig. 7 shows the variation of log D_{Fe} with log C_{NO_3} at pH 3·3, $(C_{Fe})_0 = 1\cdot024 \times 10^{-4}$M, $C_{SCN} = 0\cdot01$ and 10^{-4}M, and $C_R = 0\cdot100$M. The variation of t with log C_{NO_3} as calculated from Equation (39) taking $f = 2$ is also shown.

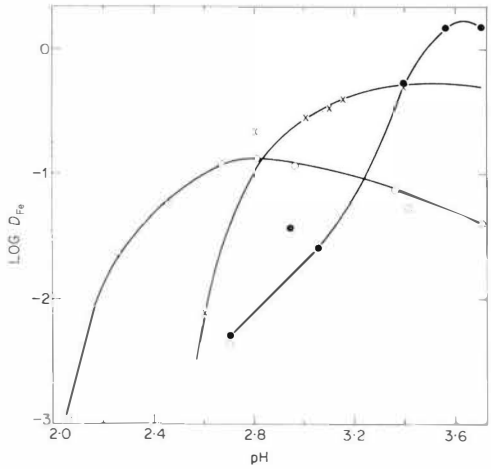

FIG. 2. *Variation of log* D_{Fe} *with pH for several initial iron concentrations*
● $(C_{Fe})_0 = 2 \cdot 048 \times 10^{-5}$M; × $(C_{Fe})_0 = 2 \cdot 048 \times 10^{-4}$M; ○$(C_{Fe})_0 = 2 \cdot 048 \times 10^{-3}$M

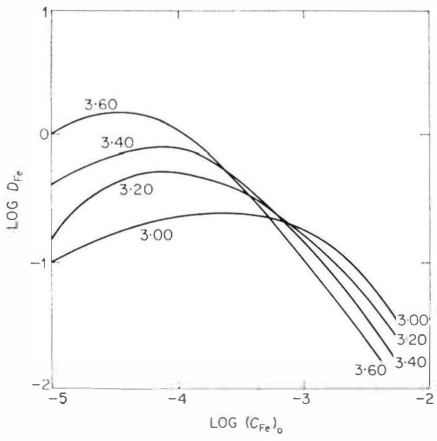

FIG. 3. *Variation of log* D_{Fe} *with log* $(C_{Fe})_0$ *for several pH values*

Varying diluent

Table VIII shows the values of D_{Fe} obtained in several different diluents with pH = 3·3, $(C_{Fe})_0 = 1 \cdot 024 \times 10^{-2}$M, $\bar{C}_R = 0 \cdot 100$M, $C_{SCN} = 0 \cdot 01$M and $C_{NO_3} = 0 \cdot 25$M.

Other carboxylic acids

Some data for D_{Fe} values at $(C_{Fe})_0 = 1 \cdot 024 \times 10^{-4}$M, $\bar{C}_R = 0 \cdot 100$M, and $C_{NO_3} = 0 \cdot 25$M was obtained for pivalic, lauric and α-bromolauric acids at one or two different pH values and C_{SCN} values and is summarised in Table IX. There is insufficient data to draw any conclusions regarding the extraction of Fe(SCN) complexes by these acids.

Discussion

Adsorption

Despite the assumptions made about the constancy of the surface area, the adsorption data is reasonably consistent and the value of $*\beta_{pq}$ is reasonably constant so that the device of treating the adsorbed iron as a non-extractable

TABLE IV
Variation of D_{Fe} *with pH at various thiocyanate concentrations*

pH	C_{SCN}, M							
	0·001	0·002	0·005	0·008	0·01	0·02	0·032	0·05
2·50	—	—	—	—	—	—	—	0·002
2·55	—	—	—	—	—	0·006	—	—
2·70	0·095	—	0·069	—	—	—	—	0·004
2·75	—	—	—	—	0·023	0·003	—	—
2·80	0·184	0·124	—	—	—	—	—	—
2·85	—	—	—	0·134	—	—	—	—
2·90	0·293	—	0·203	—	0·076	—	—	0·011
2·95	0·747	—	—	—	0·035	—	—	—
3·00	—	0·499	—	—	0·132	—	—	0·096
3·05	—	—	0·790	0·229	0·438	—	—	—
3·10	—	—	—	—	—	—	—	0·014
3·20	1·124	—	—	0·369	0·234	0·536	—	—
3·25	—	—	—	—	—	—	—	0·504
3·30	—	0·916	—	0·504	0·586	0·822	0·673	0·690
3·35	—	—	1·048	—	—	—	—	0·595
3·40	0·043	—	1·943	—	0·676	—	—	—
3·50	—	—	—	0·426	1·197	—	—	0·295
3·55	—	—	—	—	—	1·090	1·004	—
3·60	—	—	—	—	—	0·654	0·981	—
3·70	—	0·665	—	—	—	—	—	—
3·75	—	—	—	—	0·373	—	—	—

TABLE V
Variation of s *and* (h+r) *with pH and thiocyanate concentrations*

pH	C_{SCN}, M							
	0·001	0·002	0·005	0·008	0·01	0·02	0·032	0·05
				Values of $(h+r)$				
2·50	—	—	—	—	—	—	—	3·43
2·70	2·26	—	1·69	—	—	—	—	3·31
2·80	2·60	3·82	—	—	—	—	—	—
2·90	2·55	—	2·15	—	1·59	—	—	—
3·00	—	2·70	—	—	2·05	—	—	2·53
3·10	—	—	—	—	—	—	—	2·00
3·20	3·32	—	—	3·57	2·19	2·33	—	—
3·30	—	2·12	—	3·80	4·01	2·72	2·17	3·02
3·40	3·77	—	3·89	—	3·70	—	—	1·30
3·50	—	—	—	3·21	3·11	—	—	−0·48
3·60	—	—	—	—	—	2·27	3·05	—
3·70	—	3·41	—	—	—	—	—	—
				Values of s				
2·70	0·06	—	0·09	—	—	—	—	−0·43
2·80	0·05	0·02	—	—	—	—	—	—
3·00	0·01	—	0·01	—	0·26	—	—	0·67
3·10	—	−0·05	—	—	0·23	—	—	0·75
3·20	—	—	—	—	—	—	—	1·01
3·30	−0·06	—	—	−0·07	0·16	0·61	—	—
3·40	—	0·003	—	−0·08	1·62	0·45	0·82	0·68
3·50	0·37	—	0·06	—	−0·10	—	—	−0·50
3·60	—	—	—	0·52	0·04	—	—	0·68

aqueous species $Fe_2(OH)_4^{2+}$ is justifiable, although scatter in the adsorption has a marked effect on the extraction data.

Although too much should not be made of the above stoichiometry (which seems to break down at high C_A values and at pH 3·7), it is interesting to note that $Fe_2(OH)_4^{2+}$ is the dimer of the species, $Fe(OH)_2^+$, which Matar & Rudolph[19] have suggested is the principal species involved in the mechanism of activation of beryl by iron for flotation with sodium hexadecyl sulphonate, although the work of Fuerstenau *et al.*[20] suggests that $Fe(OH)^{2+}$ is the principal species involved. Regrettably, there are no data for the formation constant of $Fe_2(OH)_4^+$ in solution so that calculation of its adsorption potential is not

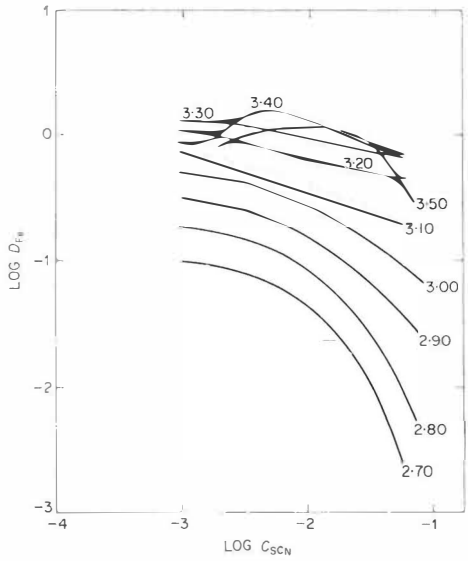

FIG. 4. *Variation of log* D_{Fe} *with log* C_{SCN} *for several pH values*

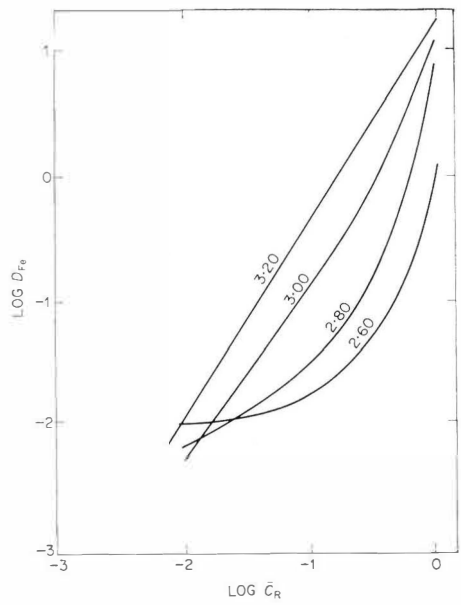

FIG. 5. *Variation of log* D_{Fe} *with log* $\bar{C}_R$ *for Versatic 911 in benzene for several pH values from* (pH – *log* D_{Fe}) *plots*

possible.[21] Adsorption of a dimeric species certainly makes more surface area available for adsorption.

Extraction

The scattered nature of the experimental data means that a great deal of much more reliable data is required before any conclusions about the nature of the complex extracted in this system can be made. The present results are very tentative and should be regarded as being of a preliminary nature. Qualitatively the variation of log D_{Fe} with pH is consistent with a system in which

TABLE VI

Variation of D_{Fe} *with pH at various concentrations of Versatic 911 in benzene*

pH	$C_{R,M}$ 0·01	0·015	0·025	0·05	0·10	0·15	0·25	0·50	0·75	1·00
2·50	0·016	—	—	—	—	—	—	—	—	—
2·60	0·010	—	—	—	—	—	0·053	—	—	0·825
2·65	—	—	—	—	—	—	—	0·088	—	—
2·75	—	—	—	—	0·023	—	—	—	—	—
2·80	—	—	—	0·019	—	—	—	—	—	5·649
2·90	—	—	—	—	0·076	—	—	1·008	—	—
2·95	—	—	—	—	0·035	—	—	—	—	—
3·00	—	—	—	0·032	0·132	0·099	0·096	—	—	—
3·05	0·005	0·006	0·013	0·229	0·438	—	—	2·039	—	—
3·10	0·004	—	—	—	—	—	0·440	3·763	5·522	9·240
3·20	0·011	—	—	0·114	0·234	—	0·845	—	—	—
3·25	—	—	—	—	—	—	0·797	0·649	—	—
3·30	—	—	—	0·240	0·586	—	—	—	—	—
3·40	—	—	—	—	0·676	—	—	—	—	—
3·50	0·012	—	—	—	1·197	—	—	—	—	—
3·75	—	—	—	—	0·373	—	—	—	—	—
3·80	0·03	—	—	—	—	—	—	—	—	—

TABLE VII

Values of (m+r) *and* (h+r) *for various pH values and Versatic 911 concentrations in benzene*

pH	$C_{R,M}$ 0·01	0·015	0·025	0·05	0·10	0·15	0·25	0·50	0·75	1·00
					Values of $(m+r)$					
2·60	0	—	—	0·27	0·52	—	0·98	1·58	—	15·4
2·80	0·46	—	—	0·69	0·94	—	1·68	2·92	—	13·3
3·00	1·01	—	—	1·44	1·59	1·93*	2·05	3·43	—	6·41
3·05	1·05*	1·20*	1·31*	1·53*	1·86*	—	2·13*	—	2·66*	—
3·10	1·14*	—	—	1·79*	2·18*	—	2·56*	3·85*	4·52*	5·52*
3·20	1·53	—	—	1·67	1·94	—	2·03	2·83	—	2·89
					Values of $(h+r)$					
2·60	—	—	—	—	—	—	2·23	—	—	1·86
2·80	—	—	—	2·48	—	—	—	—	—	2·24
3·00	—	—	—	3·05	2·05	1·67	2·43	—	—	—
3·05	1·21	2·03	2·02	3·18	—	—	—	5·35	—	—
3·10	2·21	—	—	—	—	—	3·53	4·37	3·72	3·97
3·20	2·48	—	—	3·61	2·19	—	4·14	—	—	—

* Values from Fig. 6 (others from Fig. 5).

TABLE VIII

Effect of diluent

Diluent	Dielectric constant	D_{Fe}
Chloroform	4·81	0·556
Carbon tetrachloride	2·24	0·900
Kerosene	2	0·628
Hexane	1·89	1·768
Cyclohexane	2·02	2·141
Benzene	2·28	0·586
Toluene	2·38	1·392
Xylene	2·4	1·281
Decanol	8·1	0·744
Methyl isobutyl ketone	17·0	1·246

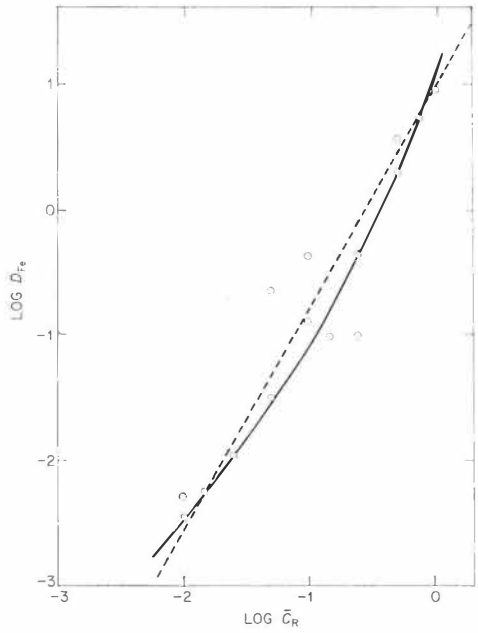

FIG. 6. *Variation of log* D_{Fe} *with log* $\bar{C}_R$ *from experimental data*

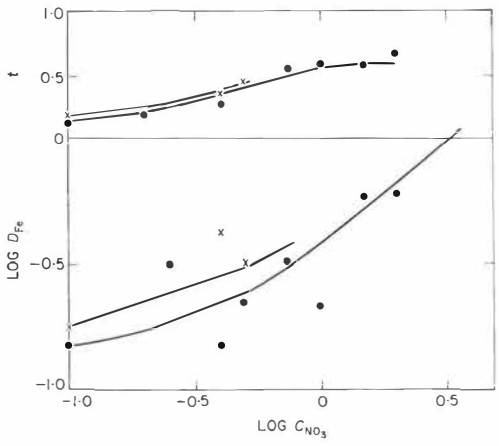

FIG. 7. *Variation of log* D_{Fe} *and* t *with log* C_{NO_3}
× $C_{SCN} = 10^{-4}$ M, ● $C_{SCN} = 0{\cdot}01$ M

hydrolysis and metal complex formation occurs in the aqueous phase.[22] The mathematical basis of the equations used appears to be valid but it appears that the values of $h+r$, s, t and $m+r$ vary with the composition of the aqueous and organic phases and it is thus necessary to include extra terms in Equations (36) (38), (39) and (40) to take this fact into account. Thus Equation (36) would become:

$$\frac{\partial \log D_{Fe}}{\partial \mathrm{pH}} = \frac{f(1+D_{Fe})}{1+f\,D_{Fe}}\left((h+r) + \mathrm{pH}\frac{\partial(h+r)}{\partial \mathrm{pH}} - X_{OH} - p\,\alpha_{pq}\right) \quad . \quad (41)$$

Solution of Equation (41) for $(h+r)$ thus becomes rather difficult and does not seem to be warranted for the present scattered data.

TABLE IX
Other carboxylic acids

Carboxylic acid	C_{SCN}	pH	D_{Fe}
Pivalic	0·001	2·55	0·054
	0·001	2·90	0·358
	0·01	3·10	0·759
	0·01	3·15	0·638
	0·01	3·40	0·753
Lauric	0·001	3·90	0·544
	0·01	3·00	2·28
	0·01	3·55	0·202
	0·01	3·90	0·715
α-Bromolauric	0·001	2·20	0·054
	0·001	2·35	3·32
	0·001	2·85	2·01
	0·01	2·60	28·94
	0·01	3·00	6·64
	0·01	3·50	1·99

Although the present data are inadequate their acquisition took rather a long time and to obtain any reasonably adequate data a system such as AKUFVE[23] is required. Such a system will have the following advantages: more points will be obtainable resulting in much more reliable experimental curves; a constant surface should be available for adsorption; it should be possible to obtain instantaneous spectra of the organic phase, eliminating the fading observed previously[8] and thus providing an alternative method of studying this phase; the kinetics of the adsorption and extraction reactions could be continuously monitored; it will be possible to start runs at pH values below those where significant adsorption occurs, thus ensuring that any adsorption only occurs during extraction and it will also be possible to tell whether any hysteresis in log D_{Fe} occurs as the pH is raised and then lowered.

The use of double labelling of both Fe and SCN^- should enable the organic phase stoichiometry to be determined independently of stability constants and thus provide a check on the precision of those used.

Acknowledgments

The author wishes to thank Miss Helen Marston and Mr. F. A. Marshall of the Department of Mining & Mineral Sciences, University of Leeds for their help in running the computer programmes used to recalculate the data on the basis of Equations (9) to (11).

References

1 Marcus, Y., & Kertes, A S., 'Ion exchange and solvent extraction of metal complexes', 1969, p. 557 (London: Wiley-Interscience)
2 Fletcher, A. W., & Flett, D. S., 'Solvent extraction chemistry of metals', (Eds McKay, H. A. C. *et al.*), 1966, p. 359 (London: MacMillan)
3 Fletcher, A. W., & Flett, D. S., *J. appl. Chem., Lond.*, 1964, **14,** 250
4 Fletcher, A. W., Flett, D. S., & Wilson, J. C., *Trans. Instn Min. Metall.*, 1964, **73,** 765
5 Flett, D. S., & West, D. W., *J. inorg. nucl. Chem.*, 1967, **29,** 1365
6 Haffenden, W. J., & Lawson, G. J., 'Advances in extractive metallurgy', 1967, p. 678 (London: Instn Min.Metall.)
7 Baes, C. F., & Baker, H. T., *J. phys. Chem., Ithaca*, 1960, **64,** 89
8 Rice, N. M., & Finkelstein, N. P., National Institute for Metallurgy Research Report No. 435, 1968 (Johannesburg: N.I.M.)
9 Rice, N. M., & Finkelstein, N. P., National Institute for Metallurgy Research Report No. 847, 1969 (Johannesburg: N.I.M.)
10 Milburn, R. M., *J. Am. chem. Soc.*, 1957, **79,** 537
11 Milburn, R. M., & Vosburgh, W. C., *J. Am. chem. Soc.*, 1955, **77,** 1352
12 Schlyter, K., *Trans. R. Inst. Technol., Stockholm*, 1962, No. 196, 37 pp.
13 Mattoo, B. N., *Z. phys. Chem. Frankf. Ausg.*, 1959, **19,** 156
14 Mironov, V. E., & Rutkovskii, Yu. I., *Russ. J. inorg. Chem.*, 1965, **10,** 580

[15] Rice, N. M., Ph.D. Thesis, University of London, 1966
[16] Burkin, A. R., Rice, N. M., & Rogers, M. J., 'Solvent extraction chemistry', (Ed. Dyrssen, D., *et al.*), 1967, p. 439 (Amsterdam: North-Holland)
[17] Irving, H. M. N. H., Rossotti, F. J. C., & Williams, R. J. P., *J. chem. Soc.*, 1955, p. 1906
[18] Rossotti, F. J. C., & Rossotti, H., 'The determination of stability constants', 1961, p. 40 (New York: McGraw-Hill)
[19] Matar, J. A. J., & Rudolph C. G., *VIII Miner. Process. Congr., Leningrad*, 1968, Paper S-10
[20] Fuerstenau, M. C., Rice, D. A., Somasundaran, P., & Fuerstenau, D. W., *Trans. Instn Min. Metall.*, 1965, **74**, 381
[21] Jowett, A., *Trans. Instn Min. Metall.*, 1966, **75**, C195
[22] Marcus, Y., & Kertes, A. S., 'Ion exchange and solvent extraction of metal complexes', 1969, p. 448 (London: Wiley-Interscience)
[23] Reinhardt, H., & Rydberg, J., *Chemy Ind.*, 1970, p. 488

Solvent extraction of yttrium and lanthanides with *N*-benzoyl-*N*-phenylhydroxylamine

by K. F. Fouché and H. J. Le Roux

Department of Chemistry, University of the Orange Free State, Bloemfontein, South Africa

A systematic investigation of the extraction of yttrium and all the lanthanides with N-*benzoyl*-N-*phenylhydroxylamine* (*HBPHA*) *has shown that a plot of the concentrations of HBPHA giving equal distribution constants versus the inverse of the ionic radius or atomic number, results in the formation of four tetrads. The antagonistic effect of tri-n-butylphosphate* (*TBP*) *on the extraction of thulium with HBPHA from benzene was quantitatively shown to be due to the formation of the association product HBPHA·TBP.*

Introduction

ALMOST ALL INVESTIGATIONS reported so far, where at least ten or more lanthanides were considered in comparative extraction studies of these elements, have been confined to phosphorus-based extractants.[1–8] These results show that, as far as extraction behaviour is concerned, the lanthanides fall into at least two subgroups—one containing the light and the other the heavy elements. Some of the more recent results can, however, best be interpreted in terms of four tetrads with gadolinium common to the two central tetrads.[4,5,7,8] Similar studies with other extractants such as thenoyltrifluoroacetone,[9,10] acetylacetone,[11] β-isopropyltropolone[12] and *N*-benzoyl-*N*-phenylhydroxylamine (HBPHA),[13,14] which have been employed for the extraction of lanthanum and europium only, are rather limited and are generally incomplete. For this reason a detailed investigation of the extraction of yttrium and the lanthanides with HBPHA was undertaken. In addition, a study was made of the effect of tri-n-butyl phosphate (TBP) on some extraction equilibria.

Experimental

Extraction of metal ions

Experimental techniques were generally the same as reported previously.[15,16] Chloroform solutions of HBPHA were equilibrated for 1 h with aqueous 0·1M sodium acetate, adjusted to pH = 5·48 with 0·1M perchloric acid and containing 50 μg/ml of the relevant lanthanide element. The metal ion content of both phases was then determined spectrophotometrically with alizarin-S[17] after the metal contained in the organic phases had first been extracted into 0·01M perchloric acid. Preliminary experiments showed that the small amount of HBPHA contained in the equilibrated aqueous phases has no effect on the spectrophotometric determination. Distribution constants (q) for all elements except lanthanum, cerium and promethium, which were determined radiometrically, were obtained in this manner. Radiometric methods, using ^{140}La and ^{144}Ce, were preferred for lanthanum and cerium as the comparatively high HBPHA concentrations used for these elements caused slight interference in the spectrophotometric determination. It was also noted that the extractability of cerium slowly increases with the extension of mixing times up to 6 h. This is most probably due to oxidation of cerium and formation of the $Ce(BPHA)_4$ complex which would be expected to have higher extractability than the Ce(III) complex.[18] (The formation of the reddish-brown Ce(IV)–HBPHA complex has recently found application in the spectrophotometric determination of cerium.[19]) The rate of oxidation is concentration dependent and when carrier-free ^{144}Ce (or ^{144}Ce in the presence of lanthanum or terbium carrier) is extracted, no increase in extraction with mixing time could be observed after the initial equilibrium had been attained. The cerium extraction curve was thus obtained from the distribution of ^{144}Ce to which terbium carrier (50 μg/ml) had been added to reduce the experimental error.

For extractions with thulium tracer into benzene solutions of HBPHA and mixtures of HBPHA with TBP, aqueous 0·01M sodium acetate solutions were adjusted to the desired pH.

Association constants

The association constants between HBPHA and TBP in organic solvents were calculated from the measured variation in the distribution constant (K_d) of HBPHA between the solvents and equal volumes of aqueous solutions as a function of TBP concentration. The distribution constants were determined spectrophotometrically by measuring the absorbance of the aqueous phases at 256 nm with a Perkin-Elmer Model 402 spectrophotometer. Aqueous phases saturated with benzene were boiled to remove the solvent and were then diluted to fixed volumes before absorbances were measured.

Metal and tracer solutions

Inactive metal oxides (Koch-Light, >99·9%) were dissolved in concentrated perchloric acid. ^{144}Ce, ^{147}Pm and ^{170}Tm tracers were obtained from The Radiochemical Centre, Amersham, U.K. ^{140}La tracer was prepared by irradiating La_2O_3 in SAFARI-1, the reactor of the South African Atomic Energy Board.

All equilibrations were carried out at 25°C.

Results and Discussion

Extractions with HBPHA

The extraction curves for yttrium and the lanthanides are shown in Fig. 1 and a plot of the HBPHA concentration for $q = 1$ against the atomic number Z and the inverse of the ionic radius is shown in Fig. 2. From the slopes shown in Fig. 1, it can be concluded that all the elements except thulium, ytterbium and lutetium are probably extracted as $M(BPHA)_3 \cdot HBPHA$ complexes; the latter three ions do not appear to be solvated significantly by undissociated HBPHA and are probably present as $M(BPHA)_3$ in the organic phases. At higher HBPHA concentrations, however, the slope of the extraction curve for thulium also approaches 4 (slope = 3·84 at pH = 4·88 and log HBPHA between −0·9 and −1·7). This indicates that the lower slopes for thulium, ytterbium and lutetium shown in Fig. 1 are due mainly to the comparatively lower HBPHA activity rather than to steric factors caused by the lower ionic

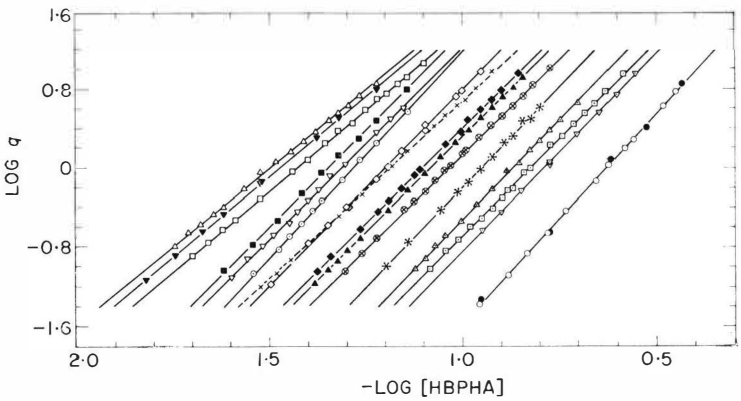

FIG. 1. *Extraction of Y and lanthanides with HBPHA from acetate solutions (pH = 5·48)*

Results marked ● and ○ on lanthanum extraction curve represent extractions in absence and presence of added carrier (50 μg/ml) respectively (slope = 4·20)
△ Lu (slope = 3·14); ▼ Yb (3·24); □ Tm (3·24); ■ Er (3·92); ▽ Ho (3·88); ○ Dy (4·14); × Y (3·70); ◇ Tb (3·94); ♦ Gd (3·92); ▲ Eu (3·92); ⊗ Sm (3·86); ✻ Pm (4·06); △ Nd (4·00); ⊡ Pr (3·96); ▽ Ce (4·00)

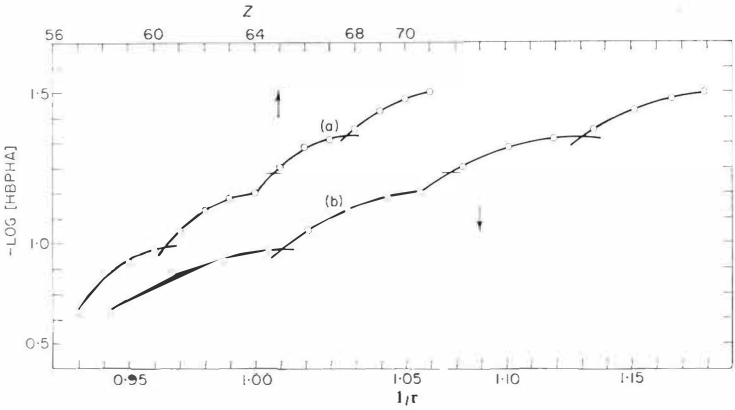

FIG. 2. (a) *Variation of* Z *and* (b) *1/r with log* [*HBPHA*] *at* q = 1

radii The good fit of cerium and promethium to the curves in Fig. 2 as well as the similar extraction behaviour of lanthanum in the presence and absence of added carrier (Fig. 1), shows that the extraction constants are not dependent on the metal concentration up to concentrations of at least 50 μg/ml.

The results shown in Fig. 2 are very similar to those obtained for phosphorous-based extractants.[4,5] The statement, 'In systems involving all 15 lanthanides(III), the points on a plot of the logarithm of a suitable numerical measure of a given property of the elements vs. Z may be grouped, through the use of four smooth curves without inflexions, into four tetrads with the gadolinium point being common to the second and third tetrads and the extended smooth curves intersecting, additionally, in the 60–61 and 67–68 Z regions',[5] is therefore also fully applicable to the present results.

It is evident from Fig. 1 that owing to the lower slopes of the extraction curves for lutetium, ytterbium and thulium, curves constructed in a similar manner as those in Fig. 2, but at different q-values, would not be identical. For $q = 0 \cdot 1$, the tetrad effect is slightly more pronounced than in Fig. 2. For $q = 10$, however, the separation between the two tetrads at high Z is not as clear and they may fuse into a single octet; the two tetrads at lower Z are again not affected significantly. Slightly different extraction behaviour by the three heaviest lanthanides would not be unexpected, as the lower solvation by HBPHA is likely to have an effect on the extractability. Apart from this deviation at high distribution ratios for lutetium, ytterbium and thulium, it is nevertheless clear that the overall extraction behaviour of the lanthanides with HBPHA is best interpreted in terms of four tetrads as in Fig. 2. Yttrium, which generally behaves as a pseudo-lanthanide,[4,20] would have a hypothetical atomic number between 64 and 65 in the present investigation.

Extraction with HBPHA–TBP

The addition of TBP (0·1M) has no effect on the extraction of europium by HBPHA in chloroform.[21] When using benzene as solvent, however, it was observed that TBP has an antagonistic effect on the extraction of lanthanides with HBPHA. Previous work on this phenomenon has shown that it could be due to interaction between the extractant and the additive as was suggested for the systems di(2-ethylhexyl)phosphoric acid–tri-n-octylphosphine oxide (TOPO),[22] mono(2-ethylhexyl)phosphoric acid–TBP,[23] dibutylphosphoric acid–TBP,[24] HBPHA–TBP[25] and alkylphosphoric acids–tri-n-octylamine[26,27] or to interaction of water in the organic phase (caused by the presence of the additive) with the extracted complex.[28,29] It could, of course, also result from a combination of both effects. To obtain more information regarding the antagonistic effect in the present investigation, an attempt was made to determine the association constant between HBPHA and TBP by a solvent extraction method.

If it is assumed that the interaction of TBP with HBPHA in the organic phase can be represented as:

$$\mathrm{HBPHA_o} + \mathrm{TBP_o} \rightleftharpoons \mathrm{HBPHA \cdot TBP_o} \qquad (1)$$

the equilibrium constant is given by (neglecting activity coefficients):

$$K = \frac{[\mathrm{HBPHA \cdot TBP}]_o}{[\mathrm{HBPHA}]_o[\mathrm{TBP}]_o}$$

This may also be written as:

$$K = \frac{[\mathrm{HBPHA}]_{to} - [\mathrm{HBPHA}]_{eo}}{[\mathrm{HBPHA}] \cdot K_d^o [\mathrm{TBP}]_{eo}}$$

$$K = \frac{K_d[\mathrm{HBPHA}] - [\mathrm{HBPHA}] \cdot K_d^o}{[\mathrm{HBPHA}] \cdot K_d^o \cdot [\mathrm{TBP}]_{eo}}$$

$$K = \frac{K_d - K_d^o}{K_d^o \cdot [\mathrm{TBP}]_{eo}} \qquad (2)$$

where $[\mathrm{HBPHA}]_{to}$ is the total HBPHA concentration in the organic phase, $[\mathrm{HBPHA}]_{eo}$ the equilibrium concentration (i.e. not complexed by TBP) in the organic phase, [HBPHA] the concentration in the aqueous phase and $[\mathrm{TBP}]_{eo}$ the equilibrium TBP concentration in the organic phase.

$$K_d = \frac{[\mathrm{HBPHA}]_{to}}{[\mathrm{HBPHA}]} \text{ and } K_d^o = \frac{[\mathrm{HBPHA}]_{eo}}{[\mathrm{HBPHA}]}$$

Equation (2) can also be written as:

$$\log K = \log (K_d - K_d^o) - \log K_d^o - \log [\mathrm{TBP}]_{eo} \qquad (3)$$

from which it can be seen that a plot of $\log (K_d - K_d^o)$ against $\log [\mathrm{TBP}]_{eo}$ should give a straight line with slope 1·0 and intercept $-\log K_d^o - \log K$ when HBPHA·TBP is the only interaction product.

From the plots shown in Fig. 3 it can be concluded that the interaction between HBPHA and TBP in benzene and carbon tetrachloride is fully represented by Equation (1) and that higher order species such as HBPHA·nTBP

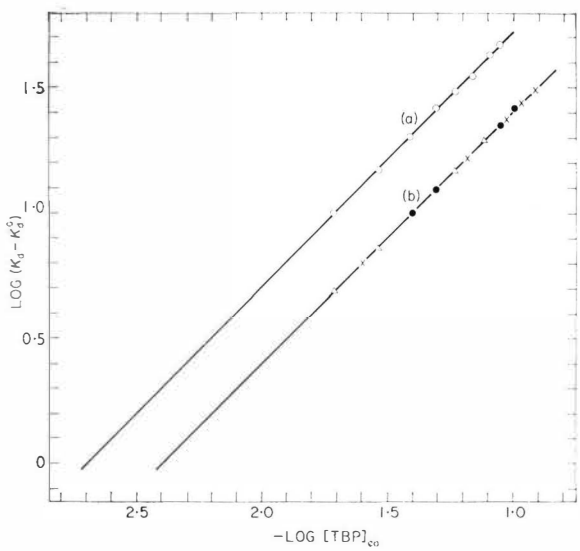

FIG. 3. *Effect of TBP on distribution constant of HBPHA*

(a) 4·18 × 10^{-3}M HBPHA–C_6H_6–water
(b) ● 4·83 × 10^{-3}M HBPHA–CCl_4–water; △ 4·83 × 10^{-3}M HBPHA–CCl_4–0·01M-$NaClO_4$; × 1·38 × 10^{-2}M HBPHA–CCl_4–water

TABLE I

Association constants (K) *for HBPHA and TBP in benzene and carbon tetrachloride*

	HBPHA	K_d^o	K
C_6H_6	$4 \cdot 18 \times 10^{-3}$	43·0	11·2
CCl_4	$4 \cdot 83 \times 10^{-3}$	14·4	16·6
	$1 \cdot 38 \times 10^{-2}$	14·8	

($n > 1$) may be ignored. The association constants obtained from these plots are given in Table I. By using these constants, equilibrium HBPHA concentrations for mixtures of TBP and HBPHA may be calculated from Equation (1). From the known variation in thulium extractability with HBPHA concentration given in Table II, a theoretical curve, relating extractability to total TBP concentration, may be constructed. These calculated values are compared with the experimental values in Table III for benzene as the organic phase. The agreement between the two sets of results is sufficiently good to conclude that the antagonistic effect of TBP is due only to interaction with HBPHA, thus causing a decrease in the equilibrium concentration of HBPHA in the organic phase.

The fact that thulium is extracted as $Tm(BPHA)_3$ into chloroform at low HBPHA concentration and that it probably adds an undissociated HBPHA

TABLE II

Extraction of thulium tracer from 0·01M acetate (pH = 5·50) with HBPHA in benzene

−log [HBPHA]	log q	−log [HBPHA]	log q
1·70	1·08	2·10	0·09
1·79	0·89	2·15	−0·06
1·82	0·87	2·22	−0·29
1·84	0·75	2·25	−0·49
1·89	0·63	2·30	−0·64
1·90	0·61	2·32	−0·69
1·95	0·49	2·40	−1·06
2·00	0·35	2·40	−1·08
2·02	0·29	2·45	−1·30
2·05	0·21		

TABLE III

Comparison of experimental and calculated results for extraction of thulium tracer from 0·01M acetate (pH = 5·50) with $8 \cdot 0 \times 10^{-3}$M HBPHA and varying TBP concentration in benzene

−log [TBP] total	log q	
	Calc.	Found
1·82	−0·17	−0·19
1·70	−0·23	−0·21
1·70	−0·23	−0·26
1·60	−0·30	−0·30
1·52	−0·37	−0·40
1·45	−0·44	−0·45
1·40	−0·49	−0·51
1·39	−0·50	−0·53
1·30	−0·61	−0·61
1·22	−0·74	−0·76
1·15	−0·86	−0·86
1·12	−0·91	−0·88
1·10	−0·96	−0·99
1·04	−1·10	−1·08
1·00	−1·20	−1·13

molecule at higher concentrations as was shown above, indicates that the complex $Tm(BPHA)_3$ is co-ordinatively unsaturated if it is assumed that the undissociated molecule is co-ordinated directly to the metal ion. It is rather surprising, therefore, that TBP and TOPO (Le Roux, H. J., unpublished results) which are likely to have stronger donor properties than HBPHA and which are probably sterically also more acceptable, apparently do not interact with $Tm(BPHA)_3$. This result appears less confusing when $Tm(BPHA)_3$ is regarded as co-ordinatively saturated with the undissociated molecule in $Tm(BPHA)_3 \cdot HBPHA$ not attached directly to the metal ion, but linked to the chelate through a hydrogen bond (possibly through the carbonyl oxygen of the co-ordinated hydroxamate ions[30]). This would also explain why a plot of the results given in Table II has limiting slope 4 (the slope decreases at high HBPHA concentration due to dimerisation of the extractant) in a concentration region where the extraction curve from chloroform would have slope 3 (Fig. 1): at low HBPHA activity, the polar chloroform molecule would compete with HBPHA for co-ordination (through hydrogen bonding) to the extracted compound, whereas the 'inert' benzene molecule would not.

Hydrogen bonding of chloroform to TBP is probably also the reason why TBP ($<0 \cdot 1$M) has no antagonistic effect on the extraction of lanthanides with HBPHA from chloroform. As TBP is added to HBPHA in chloroform, part of it reacts with chloroform, thus reducing the effect on HBPHA. Such interaction probably explains why a plot similar to Fig. 3, but with chloroform as solvent, has a slope much lower than one (Le Roux, H. J., unpublished results).

Acknowledgments

The authors wish to thank the South African Atomic Energy Board for financial support and for permission to publish this paper and Dr. D. M. Kemp for his interest in the work.

References

[1] Peppard, D. F., Driscoll, W. J., Sironen, R. J., & McCarty, S., *J. inorg. nucl. Chem.*, 1957, **4**, 326
[2] Hesford, E., Jackson, E. E., & McKay, H. A. C., *J. inorg. nucl. Chem.*, 1959, **9**, 279
[3] Duyckaerts, G., Drèze, Ph., & Simon, A., *J. inorg. nucl. Chem.*, 1960, **13**, 332
[4] Peppard, D. F., Mason, G. W., & Lewey, S., *J. inorg. nucl. Chem.*, 1969, **31**, 2271
[5] Peppard, D. F., Bloomquist, C. A. A., Horwitz, E. P., Lewey, S., & Mason, G. W., *J. inorg. nucl. Chem.*, 1970, **32**, 339
[6] Fidelis, I., & Siekierski, S., *J. inorg. nucl. Chem.*, 1966, **28**, 185
[7] Fidelis, I., *J. inorg. nucl. Chem.*, 1970, **32**, 997
[8] Siekierski, S., *J. inorg. nucl. Chem.*, 1970, **32**, 519
[9] Bronaugh, H. J., & Suttle, J. F., *Rep. Congr. atom. Energy Commn U.S.*, 1953, LA-1561
[10] Genow, L., & Kassabow, G., *Mh. Chem.*, 1967, **98**, 364
[11] Brown, W. B., Steinbach, J. F., & Wagner, W. F., *J. inorg. nucl. Chem.*, 1960, **13**, 119
[12] Dyrssen, D., *K. tek. Högsk. Handl.*, 1962, No. 188, 50 pp.
[13] Dyrssen, D., *Acta chem. scand.*, 1956, **10**, 353
[14] Sekine, T., & Dyrssen, D., *Talanta*, 1964, **11**, 867
[15] Fouché, K. F., Le Roux, H. J., & Phillips, F., *J. inorg. nucl. Chem.*, 1970, **32**, 1949
[16] Fouché, K. F., *Talanta*, 1968, **15**, 1295
[17] Rinehart, R. W., *Analyt. Chem.*, 1954, **26**, 1820
[18] Suzuki, N., & Oki, S., *Bull. chem. Soc., Japan*, 1962, **35**, 233
[19] Murugaiyan, P., & Das, M. S., *Analytica chim. Acta*, 1969, **48**, 155
[20] Moeller, T., Martin, D. F., Thompson, L. C., Ferrus, R., Feistel, R., & Randall, W. J., *Chem. Rev.*, 1965, **65**, 1
[21] Sekine, T., & Dyrssen, D., *J. inorg. nucl. Chem.*, 1967, **29**, 1475
[22] Baes, C. F., & Baker, H. T., *Rep. Congr. atom. Energy Commn U.S.*, 1957, ORNL 2433, 2451, 2486
[23] Ferraro, J. R., & Peppard, D. F., *J. phys. Chem., Ithaca*, 1961, **65**, 539
[24] Liem, D. H., *Proc. int. Conf. Solvent Extraction Chemistry, Gotenburg*, 1966, p. 264 (Amsterdam: North Holland)
[25] Hála, J., *J. inorg. nucl. Chem.*, 1967, **29**, 1777
[26] Deptula, C., & Minc, S., *J. inorg. nucl. Chem.*, 1967, **29**, 159
[27] Deptula, C., *J. inorg. nucl. Chem.*, 1967, **29**, 1097
[28] Healy, T. V., Peppard, D. F., & Mason, G. W., *J. inorg. nucl. Chem.*, 1962, **24**. 1429
[29] Wang, S. M., Walker, W. R., & Li, N. C., *J. inorg. nucl. Chem.*, 1966, **28**, 875
[30] Clarke, F. R., Steinbach, J. F., & Wagner, J. F., *J. inorg. nucl. Chem.*, 1964, **26** 1311

SESSION 3C

NUCLEAR APPLICATIONS, II

CHAIRMAN

Dr. W. Schuller

SECRETARY

Dr. A. Naylor

Plant practice in solvent extraction processing of alpha-emitting nuclides of high specific activity

by J. E. Bigelow, F. R. Chattin and V. C. A. Vaughen
Oak Ridge National Laboratory, Oak Ridge, Tennessee 37830, U.S.A.

In the Transuranium Processing Plant (TRU) at Oak Ridge National Laboratory, three solvent extraction processes are used (Pubex, Tramex and Cleanex) on the scale of up to 100 ℓ to recover transuranium elements from irradiated aluminium target assemblies. The Pubex and Cleanex processes use an acidic phosphate ester as extractive reagent in diethylbenzene or kerosene diluent. The Tramex process uses a straight-chain tertiary amine in diethylbenzene as extractant. Process solutions frequently have radiation power densities of 5–30 W/ℓ, owing to the presence of ^{244}Cm. Few problems have arisen from radiation effects at this level while processing in nitric acid solutions. However, in hydrochloric acid solutions, the radiolysis of the solution results in the loss of acid and the production of strong oxidising species, both effects requiring careful control to maintain proper operation of the processes at these radiation power densities. In addition, the presence of common chemical contaminants in process streams frequently cause difficulties as severe as those produced by radiation effects. The necessity of identifying and controlling the sources of these contaminants is a typical task encountered in the scale-up from the laboratory to the plant.

Introduction

THE TRANSURANIUM PROCESSING PLANT (TRU) was constructed at Oak Ridge National Laboratory (ORNL) to operate in conjunction with the High Flux Isotope Reactor (HFIR) for production of macroscopic amounts of the man-made transuranium elements.[1,2] The starting materials were ^{242}Pu, ^{243}Am and ^{244}Cm which were produced at the Savannah River Plant. Several hundred grams of these elements have been irradiated in the HFIR and processed at the TRU, resulting in curium which is rich in ^{246}Cm and ^{248}Cm for recycle to the HFIR, plus milligram amounts of ^{249}Bk, ^{252}Cf and ^{253}Es. As a yardstick of heavy element production, ^{252}Cf output has risen from 180 μg in 1966 to 40 mg in 1970.[3] Late in 1970 and early in 1971, > 200 mg of ^{252}Cf is expected to be recovered from targets irradiated at the Savannah River Plant under the AEC's Californium Market Evaluation Program.[4,5]

A substantial part of the technology required for operating the TRU facility had been developed previously in the Curium Recovery Facility (CRF) in Building 4507 at ORNL. These earlier efforts included the purification of ~30 g each of ^{243}Am, ^{244}Cm and ^{242}Cm during the period in which flowsheets were being developed for later use in the TRU.[6]

In virtually all the processing at the TRU, the major constituent of the process solutions is ^{244}Cm, an isotope with a half-life of 18·1 yr.[7] The high specific power generated by this isotope, 2·83 W/g, results in radiation power levels of 5–30 W/l, where many effects of radiation damage to the solution become evident. The main objectives of this paper are to discuss some of the practical problems encountered in solvent extraction technology that result from radiation damage, and to describe the solutions to these problems as developed at both the CRF and the TRU. Another objective is to cite some additional problems caused by impurities in process streams and methods for circumventing these difficulties.

In the discussion that follows, it should be kept in mind that all the processes under discussion have been operated without solvent recycle. The extensive radiation damage incurred in a single exposure to the process conditions makes recycle undesirable. The relatively small volumes of spent solvent, compared with the capacity of the ORNL radioactive waste facilities, has made it possible

to dispose of spent solvent without reuse. Had it been necessary to regenerate and recycle this material, more problems would surely have been encountered than could be covered in the scope of the present discussion.

Tramex process

The Tramex process[8] is described first, not because it is the first step, but because it is the key one. At the time that the TRU was designed, it was the only known solvent extraction process that could make a group separation between the trivalent actinide elements and the rare-earth or lanthanide series. Tramex, a contraction of 'tertiary amine extraction', requires a feed that is 11M in LiCl and <0·25M in HCl. The extractant is Adogen 364-HP (Archer-Daniels-Midland Corp.) diluted with diethylbenzene (DEB). Adogen 364-HP is a highly refined tertiary amine made from coconut oil.

In its simplest form, the process is carried out as follows. The feed is prepared by adding lithium chloride to a solution of target particles dissolved in hydrochloric acid. The excess acid is removed by evaporation. The adjusted feed is contacted with the extractant in a continuous, countercurrent contactor, and the transplutonium elements are extracted, probably as pentachloro complexes. Since the lanthanide elements are much less readily extracted (the separation factor is ~100), they remain in the raffinate. Additional purification is obtained by scrubbing the pregnant organic stream with fresh lithium chloride solution. The product americium, curium and other actinides are back-extracted with 8M-HCl. All these steps were perfected on a laboratory scale in glass and plastic equipment using analytical reagents. Scale-up, however, was more complicated.

The first difficulty arose when it was attempted to use a concentrated brine instead of crystalline lithium chloride to simplify preparation of the feed and scrub. When the new lithium chloride solutions were introduced to the mixer–settlers, the interfacial emulsion bands gradually grew wider until they filled the settling chambers. The difficulty was traced to molybdenum, present in the brine at a concentration of 150 ppm. Investigation revealed that the manufacturer had intentionally added molybdenum to some of his brines in order to reduce calcium to a very low value for another customer (calcium molybdate is extremely insoluble). When the brine was acidified for the Tramex process, the excess molybdate was converted to colloidal molybdenum blue, which collected at the interface and caused emulsification. It was a simple matter to specify molybdenum-free brine, but it had been planned to use Hastelloy C (a nickel–molybdenum alloy) as the main material of construction in the plant, then under design. As a result of this experience, the design was changed to remove Hastelloy C from all positions upstream of the Tramex process; however, it is still used for waste tanks since it is the least expensive metal that is satisfactory for hydrochloric acid service. It is interesting to note that nickel is also an undesirable corrosion product because it quantitatively follows curium through the Tramex process.

Another difficulty arose with the preparation of the extractant on a 40-l scale, rather than on the 1-l laboratory scale. During the laboratory preparation of an organic extractant, a technician will usually discard the aqueous phase along with any emulsion band that does not settle within a few minutes. If several washes are needed, he may discard a substantial amount of the organic phase. This discarded portion of the organic should contain most of the surface-active agents that might be present in the organic phase as impurities. Therefore, the clear organic phase that remains should be significantly cleaner than the starting material. In plant operation, it was difficult to prepare the solvent in this manner, at least on a reproducible basis, and operating difficulties frequently occurred owing to surfactants in the solvent. Fortunately, scientists at the Savannah River Laboratory were also working on the Tramex process at about this time. They were able to characterise several of the impurities that caused emulsification and arranged with Archer-Daniels-Midland Corp. to produce

several special high-purity batches of Adogen 364 which have been quite satisfactory. Although this material is purchased at a premium price, the cost is offset by reduced solvent preparation and operating costs.

After solving the problems of a good supply of lithium chloride and amine, we were ready to attempt operation with radioactive feed. Since highly radioactive solutions effervesce, there was concern that the gas bubbles might interfere with coalescence. However, mixer–settler systems have been operated at up to 15 W/l, pulse columns at up to 10 W/l and batch extractions at up to 30 W/l with no deleterious effects of the radiolytic gases on coalescence. On the contrary, the radioactive solutions coalesce more rapidly than their non-radioactive counterparts. It has been repeatedly observed that the operation of both mixer–settlers and pulse columns tends to smooth out after radioactive feed is admitted.

One unforseen effect of effervescence was the collection of gas in the 'hot' feed pump. Gas binding interferes with proper operation of a positive displacement pump; thus the feed pump had to be arranged with a positive suction head to obtain satisfactory control of flow rate. Hot feed systems must be designed for maximum tolerance to gas bubbles as well as solids formed by hydrolysis (*vide infra*).

Another effect, which was observed indirectly, was the difficulty of obtaining precise aliquots of solutions of power density above 5 W/l. At this level of radiation power, the quality of analytical results was typical of previous radiochemical work. But above this level, there was a noticeable drop in the reliability and consistency of analytical results. Solutions from which samples are taken for product accountability are now diluted to power densities of less than 5 W/l, and then reconcentrated before processing.

Radiation does seriously affect the chemistry of the solutions. The most apparent effect is the production of gas bubbles (hydrogen) as mentioned above. In hydrochloric acid the source of the gas is the reduction of H^+ ions. The rate has been determined both in the plant and in the laboratory[9] to be $\sim 0 \cdot 0007$ equiv./W-h (G factor $= 1 \cdot 9$). In a solution containing ~ 5 g of ^{244}Cm/l (15 W/l), the normality of the acid is decreased by $0 \cdot 01$ N per hour. If this situation is allowed to continue for ~ 24 h, all the acid in the Tramex feed would be destroyed. However, several cations present in this solution begin to hydrolyse at $0 \cdot 1$N, and acid destruction must be limited before this occurs.

Baybarz[10] suggested methanol as an agent to prevent radiolysis of the acid. This was tried with intermittent success. After some testing in the plant, it was discovered that methanol was effective in 'freezing' the acid concentration in ^{242}Cm solutions at 15 W/l if an 8-h induction period subsequent to the last boiling was permitted before the methanol was added. If the methanol was added before 8 h had elapsed, it had little or no effect. This 8-h point corresponds approximately to the point of maximum oxidant concentration. Later, in dealing with ^{244}Cm solutions with power densities of 8–10 W/l, the proper conditions could never be found, and the acid always decomposed at about the same rate regardless of whether methanol was present or not. The acidity is now simply adjusted every 12 h by adding 12M-HCl, followed by concentrated lithium chloride brine to restore the lithium chloride concentration to 11M. This method would not be practical for power densities much greater than 10 W/l. The Savannah River Laboratory uses gaseous hydrogen chloride to maintain the acidity in their version of the process.

The oxidising effect of the hydrochloric acid solutions subjected to radiolysis is the next most important consideration. Oxidising agents are also produced at $\sim 0 \cdot 0007$ equiv./W-h. Plutonium, which is normally stable in hydrogen chloride solution in the trivalent state, is oxidised mainly to the tetravalent and partly to the hexavalent states. Reducing agents are consumed. Cerium is oxidised in a dynamic equilibrium, so that $\sim 10\%$ exists in the tetravalent form, which is unstable in non-radioactive hydrochloric acid solutions. The Ce(IV) is very extractable and, once extracted, is not easily removed from the pregnant

organic phase by adding reducing agents to the scrub. It is, however, back-extracted quantitatively with the transplutonium product. Workers at the Savannah River Laboratory were the first to identify the reason for the poor ^{144}Ce decontamination that was observed in both plants. As a solution, they suggested that the cerium be kept in a reduced form by adding stannous chloride to the feed. Apparently the Ce(IV) reacts much more rapidly with stannous chloride than with Cl^-, or else the stannous chloride scavenges the radiolytically produced oxidants before the cerium becomes oxidised. At first 0·1–0·2N-$SnCl_2$ was added batchwise to the feed; however, since the methanol did not protect the stannous chloride from radiolytic oxidation, a sidestream addition to the feed line was set up just prior to the contactor. Later, it was found that 2,5-di-tert-butylhydroquinone (DBHQ), an organic-soluble reductant, could be dissolved in the Tramex extractant to the extent of 0·05M, which was enough to reduce any Ce(IV) that might have extracted and permit the 11M-LiCl scrub solution to back-extract it. This is the method that is now used. The DBHQ also prevents oxidation of berkelium and assures that it will back-extract with the product.

One other oxidising effect should be noted. Zircaloy-2, an alloy developed for water-reactor use, is resistant to non-radioactive solutions of hydrochloric acid. It belongs to a class of materials that can form a protective chloride film, as well as a protective oxide film. However, in an oxidising hydrochloric acid medium, such as in the presence of radiation, or with lithium oxychloride present, the protective film is disrupted, and corrosion can be severe. Corrosion rates of 1·5 mm/yr were found in hydrochloric acid solutions with a power density of 30 W/l.[11] Because of this high corrosion rate, some of the Zircaloy-2 equipment had to be replaced by tantalum and flowsheets had to be revised to avoid the situation as much as possible.

Zirconium causes an unusual type of difficulty when it is present in the Tramex feed. Feed adjustment requires evaporation to decrease the acid and water contents of the lithium chloride solution. After being subjected to this treatment, the zirconium apparently hydrolyses and forms a polymer. When mixed with the organic phase, the polymer forms a white 'cottony' emulsion, which is stable for many weeks. This problem was eventually handled in two ways. First, a mixture of 50% ethanol and 50% 12M-HCl will slowly disperse and dissolve the 'cotton'. This mixture was used routinely for cleanout of the solvent extraction equipment. Second, a procedure for adjusting the Tramex feed was devised which 'conditions' the zirconium polymer so that it does not form 'cotton'. The treatment[12] consists of acidifying the freshly evaporated lithium chloride solution to 1M, and then simmering at 120°C for ~0·5 h (depending on the size of the vessel) to decrease the acidity to 0·2–0·3N. Feed containing up to 1 g of zirconium/l can be successfully treated in this manner. If the feed contains more than 1 g of zirconium/l, the zirconium must be removed by some preliminary processing. Zirconium is readily extracted in all the solvent extraction processes discussed here; in most cases, it remains in the solvent when the product is back-extracted. The disposal of the solvent removes the zirconium from the system. The most convenient means of zirconium removal is by an adaptation of the Pubex process (see below).

Pubex process

Pubex is a contraction of 'plutonium batch extraction'. The Pubex process was originally adopted as an expedient when the Zircaloy-2 ion-exchange column sprang a leak due to corrosion and has proved to be very useful. The feed material is a solution of dissolved actinide oxide particles in either nitric or hydrochloric acid. The solution may contain dissolved salts. Tetravalent plutonium is readily extracted into 1M di(2-ethylhexyl)phosphoric acid (HDEHP) in DEB from any acidity and Pu(VI) will extract satisfactorily from hydrochloric acid of less than 4M. A single batch contact is sufficient to extract more than 99·5% of the plutonium. The simplest method for accom-

plishing this is to sparge the tank containing 10 l of feed and 20 l of extractant. A sparging period of 4 h provides nearly complete equilibrium, but 8 h is routinely used as a precaution. Several washes of 5M-HCl are used to wash curium and other actinides from the pregnant organic-phase and the tank, and the plutonium is then back-extracted into 5M-HCl by reducing it to the trivalent form. An aqueous-phase reductant that would have a significant effect could not be found, but Coleman[13] suggested 2,5-di-tert-butylhydroquinone (DBHQ) as an organic-soluble reducing agent. This material, dissolved in 2-ethylhexanol as a vehicle and phase modifier, is added to the organic phase. The reduction of plutonium is rapid and complete, unless the DBHQ is lost via a side reaction. One such reaction is with residual nitrate ion, so the 5M-HCl washes must free the solvent of nitrate. Another is radiolysis; however, this does not present a significant problem, since the ^{244}Cm, the main source of radiation, was not extracted and was scrubbed out of the system before the reductant was added.

The use of the Pubex process has presented very few difficulties, and has even provided several unexpected bonuses. First, the process conditions any silica that is present in the feed and makes it much more amenable to filtration prior to adjusting the Tramex feed. Second, radio-iodine is irreversibly extracted into the Pubex solvent, so that there is little concern about handling solutions in later steps of the process because of their iodine content. The best bonus is the removal of corrosion product zirconium from the Tramex feed.

Cleanex process

This process is so named because it will clean up transplutonium elements from a great variety of corrosion products, floor sweepings and other assorted contaminants. This process is regularly used here as the first step in reclaiming transplutonium elements from rework solutions. Like the Pubex process, the Cleanex process features a batch extraction that is carried out in a process tank by sparging and makes use of HDEHP as the extractive reagent. In this case, however, the use of an aliphatic diluent improves the extraction factor for curium. The acidity is reduced as far as possible, first by boiling, and then by addition of alkali. An acid concentration of 0·03–0·06N is usually satisfactory to obtain greater than 99·5% extraction, but a second extraction cycle may be required if heavily contaminated feeds are processed. The pregnant organic phase is back-extracted with acid having a concentration up to 6N. The process is applicable to either nitric or hydrochloric acid systems and can be used to convert from one medium to the other.

Radiolytic damage to the solvent is quite likely to occur in this process. 200 W-h/l (8×10^7 rad) is considered as an absolute upper limit of allowable exposure and generally it is tried to hold planned exposure below 150 W-h/l. Thus, in the case of a feed containing enough ^{244}Cm to generate 10 W/l, the extraction and scrubbing must be completed and the back-extraction begun within 15 h. No operating difficulties have been experienced with Cleanex runs made under these conditions, but several samples of curium product have been found that contained 5–8% phosphorus, presumably from radiolytic decomposition of the extractant.

There are several significant advantages in operating a process such as Cleanex batchwise. The most obvious is the extreme simplicity of the equipment. Second, the process chemistry can be adjusted during extraction; for example, additional alkali can be added to neutralise the acid that is released from the solvent when the metal ions are extracted. The most important advantage, in our opinion, is that batch operation minimises the problem of phase separation. Dirty mixtures that separate slowly may be allowed to stand for several hours. Any clear liquid that forms may be drawn off the bottom until the emulsion layer is reached. Generally speaking, successive scrubs with dilute acid cause the interface to break more and more cleanly.

Pharex process

Although tracer-scale studies of the Pharex process (Phosphonic Acid Reagent Extraction) were very promising,[8] scale-up to plant equipment proved to be nearly impossible. The process is based on the use of 2-ethylhexylphenylphosphonic acid in aliphatic diluent as an extractant. This reagent exhibits large preferential extractibilities for berkelium and californium compared with americium and curium. It is not available commercially, however, a supplier was found for a 1000-kg lot. During initial testing in the TRU facility, it was tried several times to start up the pulse columns with this reagent; each time the solvent entered the column, flooding began almost immediately. Testing of the process in glass pulse columns revealed that the extractant preferentially wetted the tantalum pulse plates. Later, Zircaloy-2 was also shown to be wetted by the solvent. We tried unsuccessfully to find a contaminant in the solvent that was the cause of the problem, but finally concluded that wetting was an inherent property of the reagent. The only alternatives were to find a non-wettable plate, such as a ceramic one, or to redesign the columns to operate with the organic phase continuous. The latter alternative was eventually chosen and it was have found that even the Tramex process operates more smoothly in this mode.

However, before the above changes could be made in the equipment, Weaver[14] began to study the likely effects of contaminant ions on the process. He found that Fe, Ni and Li ions had little effect, whereas Zr ions had a profound effect. He determined that as little as 10 ppm of zirconium in the solvent would cause a noticeable increase in the distribution coefficients but a decrease in the separation factor. If the zirconium concentration increased above 100 ppm, the separation factor became too low to give a practical process.

Since most of the equipment in the TRU is made of Zircaloy-2 (even the columns in which the Pharex process was to be carried out) and since the corrosion rates observed for Zircaloy-2 are significant, it could not be expected that the zirconium concentration in the extractant could be maintained below 100 ppm. Therefore, the Pharex process has been abandoned in favour of a lithium chloride anion-exchange process.

Conclusions

Apart from questions of shielding and containment, there is not a great deal of difference between the operation of a radiochemical processing plant and a conventional one. At the TRU, the physical effects of radiation have been minimal at power densities up to 30 W/l, and total exposures of 200 W-h/l. One exception is that pipetting aliquots of solution for analysis was unreliable above 5 W/l. Chemical effects were not serious while working in nitric acid systems, but were very important in hydrochloric acid systems. Chief among these were the production of hydrogen and loss of acid, radiolytic oxidation of cerium and berkelium, and radio-induced corrosion of Zircaloy-2.

Most of the difficulties experienced lay with lesser known properties of the non-radioactive elements of the periodic table, rather than with the transplutonium elements themselves. Working out the details of what to do and what not to do in processing these man-made elements has been a demanding but rewarding task.

Acknowledgments

This research was sponsored by the U.S. Atomic Energy Commission under contract with the Union Carbide Corporation.

The authors gratefully acknowledge the advice and encouragement of Messrs W. D. Burch and R. E. Brooksbank, under whose direction most of this work was performed.

References

[1] Ferguson, D. E., *Nucl. Sci. Engng*, 1963, **17,** 435

[2] Ferguson, D. E., & Bigelow, J. E., *Actinides Rev.*, 1969, **1,** 213

[3] Burch, W. D., Bigelow, J. E., & King, L. J., 'Transuranium processing plant semiannual report of production, status, and plans for period ending June 30, 1970', *Rep. Congr. atom. Energy Commn U.S.*, 1971, ORNL-4588

[4] Baranowski, F. J., 'Development and production of californium-252', in 'Californium-252', *Rep. Congr. atom. Energy Commn U.S.*, 1969, CONF-681032, p. 201

[5] 'Californium-252, its use and market potential', 1969 (Aiken, South Carolina: USAEC Savannah River Operations Office)

[6] Ferguson, D. E., *et al.*, 'Chemical technology division annual progress report for period ending May 31, 1966', *Rep. Congr. atom. Energy Commn U.S.*, 1966, ORNL-3945, p. 129

[7] Bentley, W. C., *J. inorg. nucl. Chem.*, 1968, **30,** 2007

[8] Leuze, R. E., Baybarz, R. D., & Weaver, B., *Nucl. Sci. Engng*, 1963, **17,** 252

[9] Costanzo, D. A., in 'Transuranium quarterly progress report for period ending October 31, 1965', *Rep. Congr. atom. Energy Commn U.S.*, 1966, ORNL-3965, p. 80

[10] Baybarz, R. D., *J. inorg. nucl. Chem.*, 1965, **27,** 725

[11] Ferguson, D. E., *et al.*, 'Chemical technology division annual progress report for period ending May 31, 1968', *Rep. Congr. atom. Energy Commn US.*, 1968, ORNL-4272, p. 98

[12] Ryon, A. D., in 'Transuranium quarterly progress report for period ending October 31, 1965', *Rep. Congr. atom. Energy Commn U.S.*, 1966, ORNL-3965, p. 48

[13] Coleman, C. F., 'Final cycle of plutonium recovery by amine extraction', *Rep. Congr. atom. Energy Commn U.S.*, 1961, ORNL-CF-61-5-74; *Nucl. Sci. Abstr.*, 1961, **15,** 19450

[14] Weaver, B., *J. inorg. nucl. Chem.*, 1968, **30,** 2233

Progress in tributyl phosphate technology at the Savannah River Plant

by D. A. Orth, J. M. McKibben, and W. C. Scotten

Savannah River Plant, E. I. du Pont de Nemours & Co., Aiken, S. Carolina, U.S.A.

Advances have been made in several aspects of irradiated fuels processing at the Savannah River Plant.

Correlation of laboratory and plant data shows that behaviour of fission-product zirconium in the solvent extraction system can be attributed to an equilibrium between two species of zirconium in the solvent phase. Residence times in the solvent extraction system determine the approach to equilibrium and affect the decontamination from zirconium.

Short-residence centrifugal contractors have given good service as the first bank in the Purex system. Maintenance requirements have been small, decontamination performance is satisfactory, degradation of solvent by radiation is low, and high-feed activities are tolerated.

Hydroxylamine nitrate reduces plutonium more rapidly and more completely than does hydroxylamine sulphate and has been substituted for the latter in the Purex second plutonium cycle and in recovery of ^{238}Pu. Loss of plutonium to various waste streams has decreased. Laboratory tests show that ferrous nitrate-hydroxylamine nitrate might be a suitable substitute for ferrous sulphamate in the partition of plutonium and uranium.

Solvent containing 15% TBP was tested as a replacement for 30% TBP in a neptunium purification cycle. Decontamination from zirconium and thorium improved, while neptunium losses to the spent solvent decreased somewhat. Conditions for the test were derived from computerised flow-sheet calculations. A graphical representation of the computer calculations was developed and has proved generally useful for flow-sheet selection.

Introduction

THE GENERAL PERFORMANCE of tributyl phosphate (TBP) solvent extraction operations at the Savannah River Plant has been discussed in two previous papers.[1,2] This paper discusses five areas of further investigation or technologic cal advancement: the solvent extraction behaviour of zirconium, short-residene, centrifugal contactors, reducing agents for plutonium, neptunium processing- and flow-sheet calculations by computer.

The laboratory studies on zirconium and analysis of its behaviour in the plant were prompted by periodic poor zirconium decontamination in several extraction steps and by the observed change in fission-product behaviour when a bank of centrifugal contactors was installed. These contactors replaced a mixer–settler unit as the Purex 1A bank and their subsequent mechanical and process performance is reviewed. The next study, reducing agents for plutonium, was undertaken to improve operation in the second plutonium cycle and other places where efficient reduction of plutonium to Pu(III) is important. The final two studies are related in that efforts to improve the performance of the second neptunium cycle led first to laboratory studies on neptunium extraction, and then to a method for evaluation and selection of flow-sheets by computer. This last item, computer flow-sheet studies, has evolved into a general, useful tool for process development.

The studies discussed are not complete, in that the solution to one problem leads directly to another; however, they have helped to develop specific improvements in operations or a better understanding of the processes.

Zirconium solvent extraction chemistry

Incomplete separation of zirconium from actinides (notably U, Pu, Np) in TBP solvent extraction processes has always been bothersome, and in some instances has been a major limitation. In the Purex process, for example,

^{95}Zr in the finished plutonium product causes radiation near, and occasionally in excess of, established limits in spite of the fact that one can calculate from published zirconium distribution coefficients that decontamination from zirconium should offer no problem.

Need for a better understanding of zirconium behaviour was emphasized by inexplicable changes in zirconium distribution in 1966 when the 'Jumbo' mixer-settler, serving as the Purex 1A bank, was replaced by the centrifugal contactors.

A laboratory programme was conducted to develop better understanding of the solvent extraction behaviour of zirconium by monitoring ^{95}Zr distribution through multiple, equal volume extractions, or scrubs, with the use of both tracer and plant process solutions. The effects of the following variables were examined: nitric acid concentration; contact time and time between contacts; and additives, such as dibutyl phosphate (DBP), SO_4^{2-}.

Experimental

In each test, the initial solvent was washed with dilute alkali to remove any traces of DBP, then pre-equilibrated with nitric acid (of the same molarity as the aqueous solution it was to contact) to avoid acidity changes during the experiment. All glassware was 'waterproofed'. The zirconium tracer was obtained from Oak Ridge National Laboratory as an oxalate salt in 0·6M oxalic acid. Shortly before use it was converted to the nitrate form by oxidising the oxalate with excess potassium permanganate, and then destroying the excess permanganate with a stoichiometric quantity of hydroxylamine nitrate. High-resolution gamma spectrometry was used for separate analyses of ^{95}Zr and ^{95}Nb.

Results and discussion

The advantage of the multiple extraction (or multiple scrub) method for determining distribution coefficients is that it clearly shows when more than one chemical form of zirconium exists. When only one form exists, a plot of activity *versus* extraction number gives a straight line on a semi-logarithmic graph. When two or more forms exist with different distribution coefficients, a curved line appears which can be resolved into two or more straight lines, each representing a separate species, provided that the rates of exchange among the species are slow relative to the time between contacts. The slope, k*, of these straight lines is related to the distribution coefficient by $e^k - 1 = D_a^o$ when performing multiple extractions from a single aqueous solution, or $(e^k - 1)^{-1} = D_a^o$ for multiple scrubs of a solvent solution.

In the tracer extractions only one aqueous species of zirconium could be seen. The distribution of this species has the acid dependence shown in Fig. 1, which is in good agreement with other investigators who made efforts to ensure that the zirconium was monomeric.[3,4] The equilibrium was achieved slowly however: 89% of equilibrium in 15 sec of vigorous mixing, 93% in 1 min, and greater than 95% in 5 min. The aqueous and solvent species are reported[4,5] to be $Zr(OH)_x^{4-x}$ and $Zr(NO_3)_4(TBP)_3$.

When solvent, freshly loaded with zirconium, is scrubbed repetitively, two solvent species are indicated if the aqueous acidity is below 4M. D_a^o for one is the same as above (Fig. 1), but the 'apparent D_a^o' of the other species, called $[Zr]_s$, is much higher, and increases with increasing time between scrubs. The fraction of the zirconium existing in this form increases with the time the solvent–Zr stands before beginning the scrubs (Fig. 2). Some of the data suggest that the fraction in the $[Zr]_s$ form (at constant time intervals) decreases with increasing solvent acidity, suggesting that free TBP (uncomplexed by nitric acid) may be involved in the formation of the second solvent species.

* k is the constant in the equations: $dA/dn = kA$ and $A_n = A_0e^{-kn}$ where A = activity and n = number of extractions or scrubs.

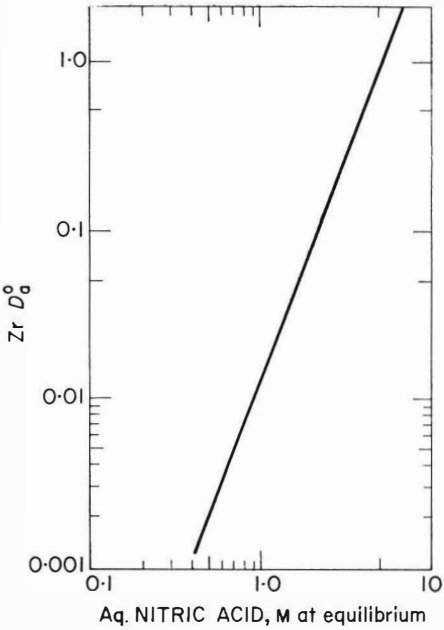

FIG. 1. *Zirconium tracer distribution coefficient in 30% TBP–'Ultrasene'*

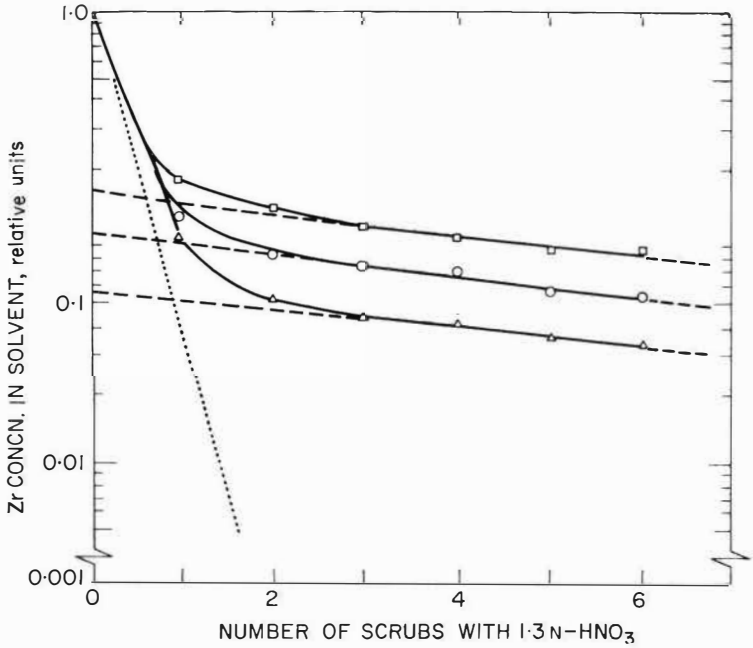

FIG. 2. *Effect of time on formation of highly solvated zirconium* $[Zr]_s$
Aqueous nitric acid 1·3N ; scrub sequence 2 min mix on–5-min intervals
Age of solvent–Zr: △—△ 15 min; ○—○ 3·5 h; □—□ 23 h
– – – – highly solvated species $[Zr]_s$

A possible explanation of the above is that the 'normal' species of solvated zirconium slowly establishes an equilibrium with a second, more highly solvated species, of unknown composition, as illustrated, below

$$\begin{array}{ll} Zr(NO_3)_4(TBP)_3 \rightleftharpoons [Zr]_s & \text{Solvent} \\ \rightleftarrows & \\ Zr(OH)_x^{(4-x)} & \text{Aqueous} \end{array}$$

By rapid, repeated scrubbing of solvent containing zirconium, all of the $Zr(NO_3)_4 \cdot (TBP)_3$-form can be removed leaving only $[Zr]_s$. On standing, the $Zr(NO_3)_4 \cdot (TBP)_3$-form grows again in the solvent, as shown in Fig. 3. The practical implication of these data is that slow scrubbing (i.e., extended residence and contact time, as in mixer-settler) should give better decontamination than rapid scrubbing.

The net effect of these two zirconium rate effects was demonstrated qualitatively by a laboratory simulation shown in Fig. 4. Two identical aliquots of solvent that contained zirconium were scrubbed as in the 1A bank (but one rapidly, one slowly) then stripped, as in the 1B bank, both as the same rate. Slower scrubbing was clearly superior.

When sulphate is present in the aqueous phase during extraction, it lowers the zirconium distribution coefficient but has no effect on subsequent scrubbing of that solvent.

When DBP is present in the solvent containing zirconium, and multiple scrubs are performed, the D_a^o for the $Zr(NO_3)_4(TBP)_3$ increases, and the fraction of $[Zr]_s$ diminishes (see Fig. 5). Both effects become greater at increasing DBP concentration. At increasing acidity the magnitude of the DBP effects are reduced.

The behaviour of ^{95}Nb in these experiments was of interest as it showed virtually no extractability, provided no silicates were added and the glassware was thoroughly 'waterproofed'. However, either addition of silicate compounds or failure to adequately coat the glassware with the silicone waterproofing agent would invariably cause detectable niobium extraction. These data support earlier indications[6] that the niobium extracted in the Purex process is a silicate complex.

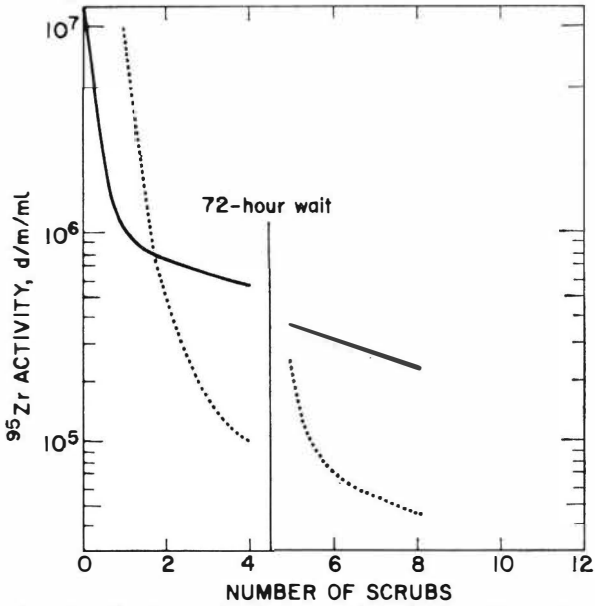

FIG. 3. *Scrub test showing conversion of solvent-Zr species*

Test conditions: 22°C; aqueous nitric acid 1·18N; 2-min scrubs on 5 min intervals
——— solvent; – – – – separate aqueous scrubs

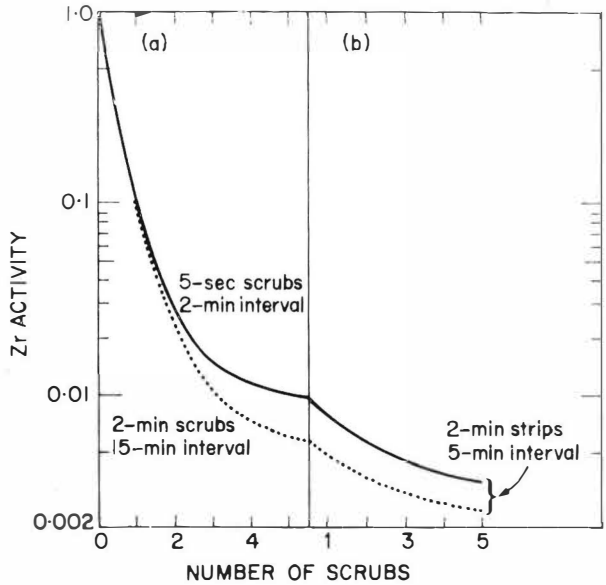

FIG. 4. *Zr rate effects on 1A scrubbing and 1B stripping*

(a) Simulating 1A bank scrub, 2·3N-HNO_3; (b) simulating 1B strip bank, 0·10N-HNO_3

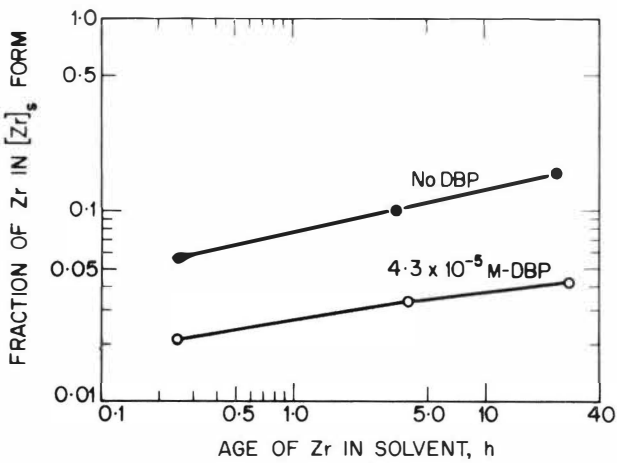

FIG. 5. *Effect of DBP on conversion of normal solvated Zr to highly solvated,* $[Zr]_s$, *form*

Fraction of $[Zr]_s$ at each ageing time determined by multiple 2-min scrubs of 30% TBP-Zr tracer with 1·18N-HNO_3 on 5-min intervals

Centrifugal contactors

To date, pulse-columns and mixer–settlers have been the contactors used in the nuclear industry for solvent extraction processes. By comparison with feed solutions processed in the past, those in the future will be more radioactive because of the economic incentives for irradiating to high burnup and for processing at minimum cooling time. There has been concern that highly active feed solutions may degrade the organic solvent sufficiently to cause poor performance in these conventional contactors.

Equipment

Centrifugal contactors were developed by the Savannah River Laboratory (SRL),; and a bank of 18 stages has been in plant service since 1966 as the 1A bank of the Purex process.[8] A schematic diagram of an individual contactor stage is shown in Fig. 6. Solvent and aqueous streams enter at the bottom, are mixed, and then discharged to the spinning bowl. Both phases leave at the top of the bowl, the aqueous at the periphery and the solvent adjacent to the centre shaft. The position of the solvent–aqueous interface is controlled by air pressure in the aqueous exit chamber.[9] Operating characteristics of the centrifugal contactor are as follows: Rotational speed, 1745 rev/min; centrifugal separation force, 300–500 g; dynamic liquid volume, 4 gal/stage; total liquid flow, 10–65 gal/min.

The Purex first cycle has three banks of contactors, as shown in Fig. 7: the first for co-extraction and decontamination of uranium and plutonium, the second for separating the plutonium from the uranium, and the third for uranium recovery. Centrifugal contactors are used only in the 1A bank, which was previously a 'Jumbo' mixer-settler. Fig. 7 gives some comparisons between the centrifugal contactor and the mixer-settler it replaced.

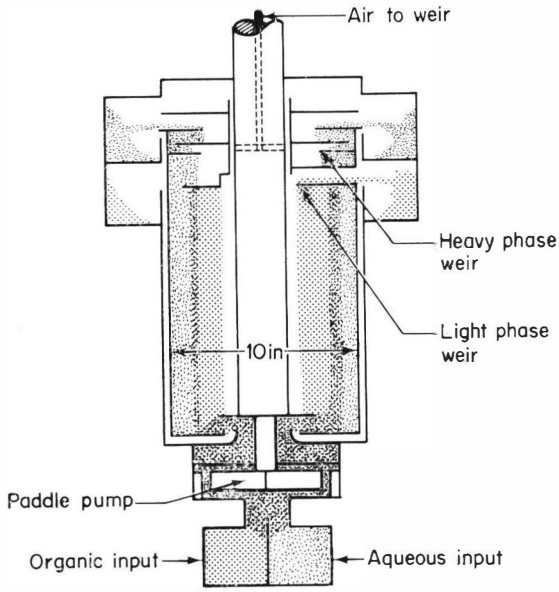

FIG. 6. *Centrifugal contactor*

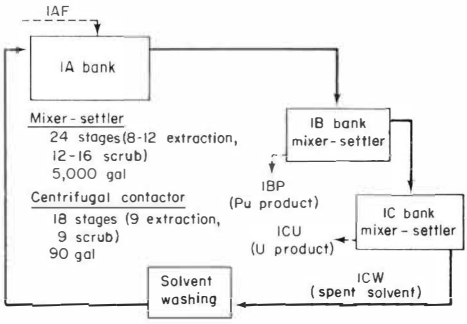

FIG. 7. *Purex first cycle*

Process performance

Equipment

Maintenance experience with the centrifugals has been satisfactory. During the first 4 years of operation, five air seals were replaced because of excessive air leakage (the first after 25 months), and one-six stage unit was rewired to replace deteriorated electrical insulation. In addition, either the shaft bearing or motor failed on six other stages; the first two after 27 and 30 months. These units had been designed for remote maintenance, and the failed parts were replaced in 3–6 h in each case except for the time required for rewiring. No routine, or preventive, maintenance is performed on these units.

By comparison with mixer–settlers, flows in centrifugal contactors must be controlled more precisely because, with the short residence times of only a few seconds per stage, small errors in flow ratios rapidly produce upsets. These control requirements have been met satisfactorily by flow ratio and specific gravity instruments connected to automatic controllers. Manual control of flow ratios also has been satisfactory, when necessary.

Discontinuous operation

Centrifugal contactors can be started up, flushed, or shut down speedily and easily. Since they were first installed, they have normally been shut down each weekend. The major penalty paid for frequent startups is in a lower average decontamination factor. At startup there is a surge of fission product activity into the product streams, probably caused by the lack of uranium saturation of the solvent during the transient period. Improved decontamination has been achieved by starting the bank on cold uranium feed and switching to hot feed after chemical equilibrium is established. In normal practice, however, there has been no cold feed or flush before startup. When shut down, the centrifugals are flushed for 45 min with 2M nitric acid.

Solvent degradation

As expected, the solvent is damaged much less by radiation in centrifugals than in mixer-settlers. Performance with the old mixer-settlers deteriorated badly when feed activities reached 150 Ci/l, and the feed for routine operation was usually held to 75–100 Ci/l. With the centrifugals, feed up to 250 Ci/l has been processed for 3 successive weeks with no evident solvent damage. No upper limit on feed activity has yet been established.

Another indicator of reduced radiation damage to the solvent with the centrifugals is the lower level of fission product activity bound in the washed solvent. This level is determined by the balance between the solvent degradation rate and the rate of removal of degradation products (fission product ligands) in the solvent washing system. When the centrifugals replaced the 'Jumbo' mixer–settler, the old solvent was retained, allowing a direct comparison between the type of contactor and the bound activity in aged solvent. The activities of ^{103}Ru, ^{106}Ru, and ^{95}Zr in the washed solvent dropped by factors of 8–20, indicating a substantially lower rate of solvent degradation on each pass through the centrifugal as compared with the mixer–settler.

Zirconium behaviour

Fission product decontamination to the end streams has also been used as a criterion for evaluating radiation damage to the solvent, but caution must be employed in such evaluations. When the centrifugals were compared with the mixer-settler (Fig. 8), a 40% improvement was observed in ^{95}Zr rejection in the 1A bank in spite of having fewer centrifugal scrub stages (tests indicate additional decontamination would be achieved with more scrub stages). Nevertheless, the actual first-cycle decontamination for plutonium and uranium is lower, because a larger fraction of the ^{95}Zr in the solvent from centrifugals can be stripped into the aqueous product streams. This effect is attributable ironically, to a lower concentration of the degradation product DBP, which, at its previous concentrations would bind the zirconium in the solvent.

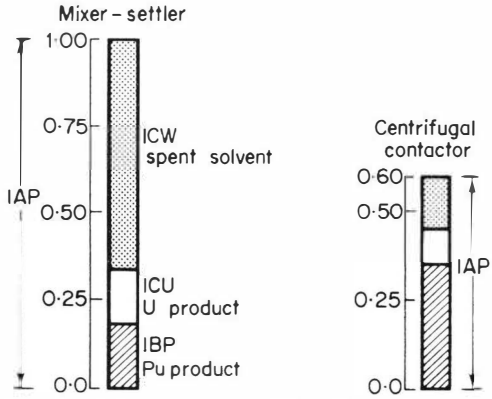

FIG. 8. *Relative quantity of Zr in first cycle streams*

At the present low level of DBP ($\sim 1 \times 10^{-4}$M) in the 1AP from the centrifugals, DBP appears to have little effect on zirconium stripping into the 1BP and 1CU. The distributions of DBP and ^{95}Zr in the first cycle differ greatly, as shown in the following figures expressed as the percentage of the total DBP and ^{95}Zr in 1AP: 1BP ^{95}Zr 60, DBP 1; 1CU ^{95}Zr15, DBP 24; 1CW ^{95}Zr25, DBP 75. The relative ease with which zirconium is stripped into the aqueous streams suggests that it is not firmly bound in the solvent in the form of the known strong DBP complex. Some other mechanism is needed to explain the quantity of ^{95}Zr present in the 1AP from the centrifugals because calculations based on published distribution coefficients[3] predict much better rejection in the 1A bank.

The laboratory tests described earlier in this report have, to some extent, clarified zirconium behaviour. For example, the slow exchange between the aqueous and 'normal' solvent form, and the slow rate of exchange between the two solvent species are both factors that tend to produce poorer DF with the centrifugals. This is illustrated, at least qualitatively, in Fig. 4, even though the speed of the centrifugal contactors could not nearly be simulated. The fraction of zirconium removed per stripping stage, with no DBP present, is consistent with present 1B bank plant performance and supports the conclusion that the current low level of DBP has little effect of zirconium stripping.

Ruthenium behaviour

When the 1A mixer–settler bank was replaced by the centrifugal contactor, the decontamination factor from ruthenium went from 7000 up to 13,000, and the bound ruthenium in washed solvent decreased by about a factor of 8. In many studies in the past decade, ruthenium behaviour in the Purex system has been shown to depend generally on the equilibria in a series of nitrato–nitrosylruthenium complexes. In addition, the long-term behaviour of ruthenium with old solvent in the mixer–settlers indicated a second mechanism for the transport of ruthenium, by radiologically produced ligands whose relative abundance in the solvent could be measured by the steady-state activity level of bound ruthenium.[1]

Early laboratory development work on miniature centrifugal contactors had shown that decontamination with short residence times was determined specifically by the characteristics of the trinitrato–nitrosylruthenium species.[10] This behaviour included a high dependency on temperature, with a large improvement in operating at 60°C instead of 40°C. However, in actual plant operation with the centrifugals, changing temperature did not significantly affect ruthenium decontamination.

A self-consistent explanation of the observations on present solvent activity, decontamination, and the effect of temperature would be that the lower degrada-

tion of the solvent in the centrifugal contactors, as compared with the mixer–settlers, gives a lower steady-state concentration of ruthenium-carrying ligands at equilibrium with a given feed activity, hence better decontamination. However, the decontamination is currently less than was attained in the mixer–settlers when they operated with solvent containing the present low level of bound ruthenium, and this effect is caused by a combination of fewer scrub stages and shorter equilibration time in the centrifugals. The relatively small effect of temperature on plant decontamination as compared with the large effect in the laboratory tests would indicate that ruthenium decontamination in the plant is not determined by straightforward trinitrato-nitrosylruthenium extraction but by the solvent degradation effect or by the presence of other ruthenium species.

Conclusions

Experience with centrifugal contactors and the related studies has led to the following conclusions relative to new plant design:

the centrifugal contactor is versatile, mechanically reliable, and relatively easy to operate;

short-residence time, low-volume contactors reduce the amount of radiation damage to solvent and increase permissible feed activity;

maximum decontamination demands an adequate number of scrub stages (12–16 is not excessive) whether the units have long or short residence times;

nine short-residence extraction stages are probably the minimum for adequate recovery of plutonium and uranium, and one or two additional stages would be a distinct help. With the nine stages, in this work plutonium losses still are quite sensitive to any change in the uranium saturation in the bank;

the best compromise between solvent degradation effects and the benefits of longer scrub residence times would be an extraction section of 10–12 short-residence stages, a scrub section of perhaps 8 short-residence stages followed by perhaps 4 long-residence scrub stages (to allow for slow equilibria);

the continuing evidence that ultimate decontamination potential is determined by a steady state between solvent degradation and cleanup means that good solvent washing facilities must be provided for stable operation if the potential of short-residence contactors in processing highly active fuels is to be realised.

Plutonium reducing agents

In large-scale processes for plutonium purification, including solvent extraction, cation exchange, and anion exchange, the plutonium generally is reduced at some step to Pu(III). The principal reductants used at the Savannah River Plant (SRP) and elsewhere, have been ferrous sulphamate (FS) and hydroxylamine sulphate (HAS). At some sites uranous–hydrazine mixtures have found application as a substitute for FS. As a result of studies on reduction rates and mechanisms (detailed below), hydroxylamine nitrate (HAN) has already been substituted for HAS in two SRP processes and there are plans to test a mixture of HAN–ferrous nitrate as a possible replacement for FS in the Purex first cycle.

Alternative reducing agents

The principal advantage of the FS and U(IV)–hydrazine is that they give very rapid reduction of Pu(IV) to (III) even in strong acid, and the principal advantage of HAS is that it contains no metallic cation to contaminate the product, or to consume sites on a cation exchange resin. These reductants are far from ideal, however. The FS is consumed in Purex first cycle greatly in excess of its stoichiometric requirements (as is uranous–hydrazine)[11] for reasons that have not been completely explained. This excess consumption of FS increases waste volume. Also the sulphate generated by the sulphamate contributes to plutonium losses (via aqueous plutonium sulphate complexes) and to stainless

steel corrosion. Reductions with HAS are slow and incomplete in addition to adding sulphate, which is detrimental for the reasons mentioned above. There are also some obvious disadvantages in using uranous ion to reduce plutonium at a step in the process where plutonium is being separated from uranium.

The second plutonium cycle

Initial interest in HAN arose from studies of Pu(IV) reduction-stripping in the Purex second cycle (see Fig. 9), where the Pu(IV) in 30% TBP–'Ultrasene' (trademark of Atlantic Richfield Co. for a refined kerosene) is stripped into an aqueous stream of HAS in dilute nitric acid. The plutonium in this aqueous stream is then concentrated by a cation exchange operation that utilises Pu(III).[12] The sulphate added with the HAS forms a series of strong complexes with Pu(IV) which retard the rate of reduction and prevent complete reduction. These sulphate–plutonium complexes are responsible both for small routine plutonium losses to the effluent from the cation exchange absorption column and for increased losses to the 2AW whenever 2BP is recycled to the 2A bank. For example, fresh cation exchange feed normally contains 5–10% Pu(IV) at an HAS concentration of ~0·03M, and the average losses from the cation exchange operation are controlled at ~0·02% of throughput. If the 2BP has been stored long enough for the HAS to decompose and the plutonium to revert to 100% (IV), the addition of HAS to give 0·03M excess gives a column feed with 10–20% Pu(IV), and column losses reach 1% if normal operating conditions are maintained.

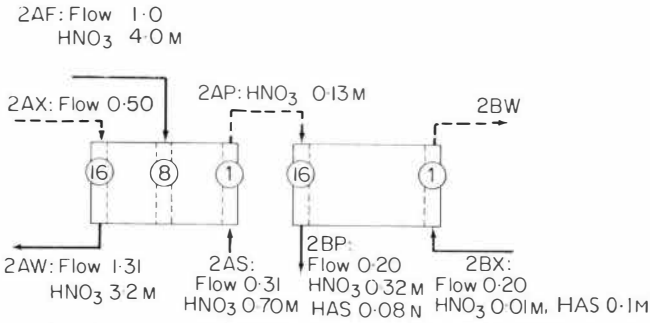

FIG. 9. *Typical flow-sheet, Purex 2nd Pu cycle*
– –→ solvent; ——→ aqueous; ○ Stage no.

Hydroxylamine nitrate (HAN) appeared a likely improvement over HAS because it would avoid the undesirable sulphate, so its properties were studied.[13] Laboratory tests showed that HAN reduces plutonium faster than either HAS or hydrazine. The data in Table I show that HAS reduces plutonium slowly and incompletely. Comparative data in Table II show that HAN reduces plutonium better than the other two agents, even at lower concentration.

TABLE I
Pu(IV) reduction with hydroxylamine sulphate
(0·3N-HNO_3, 0·1N-HAS; 22°C)

Reducing time, h	Pu(III) in solution containing 1·58 g Pu/l, %	Pu(III) in solution containing 3·04 g Pu/l, %
1·5	76·2	74·4
25·5	92·5	90·9
95	92·8	90·7
336	95·3	91·5

The plant tests and subsequent routine operation with HAN substituted for HAS in the 2BX stream (Fig. 9) have been entirely satisfactory. No change was observed in the operation of the 2B bank itself, but the plutonium in the 2BP was 100% Pu(III), whereas with HAS it was ~90–95% Pu(III).

TABLE II

Pu(IV) reductions with hydroxylamine nitrate, hydrazine nitrate, and hydrazine sulphate

(Pu, 1·5 g/l; 0·3N-HNO_3; 22°C)

Reductant	Concentration, N	Reducing time, h	Pu(III), %
$NH_2OH.HNO_3$	0·0105	1·5	99·7
		4·0	100·0
	0·0435	0·5	100·0
		150 h	99·5
		4 weeks	Still clear blue
$N_2H_4.HNO_3$	0·04	0·5	10·0
		1·0	12·7
		2·5	38·7
		18·5	86·3
		48	99·2
$(N_2H_4)_2.H_2SO_4$	0·04	2·0	<1
		1 month	~80

When fresh 2BP was processed through cation exchange, the normal small loading losses were reduced by a factor of 3·5. This improvement was anticipated, because most of the routine losses are caused by Pu-sulphate complexes which are not absorbed on the resin. Also, the absence of Pu(IV) and its sulphate complexes gives a sharper loading band, or less 'tail', on the column in repetitive loading–elution cycles. It was also demonstrated that 2BP produced with HAN could be stored until all the HAN had decomposed and the plutonium reverted to Pu(IV), then readjusted with a calculable quantity of fresh HAN to produce a feed for the cation exchange step that was nearly 100% Pu(III) and gave only ~0·01% loading losses. With HAS the plutonium was 80–90% Pu(III), and gave 1% losses unless the mode of operation was changed.

Purex partition

The success of HAN in the 2nd plutonium cycle prompted consideration of its use as a substitute for ferrous sulphamate in the Purex 1B bank. The reduction rate of plutonium with HAN decreases sharply with increasing nitric acid concentration, as shown in Fig. 10. This is of no concern in the 2nd plutonium cycle where acidity is low but presents a limitation in the 1B bank where the aqueous acidity near the middle of the bank is ~2·3M. However, ferric ion catalyses the reduction as follows:

$$2\ NH_2OH + 4\ Fe^{3+} \longrightarrow 4\ Fe^{2+} + N_2O + H_2O + 6\ H^+$$
$$4\ Fe^{2+} + 4\ Pu^{4+} \longrightarrow 4\ Pu^{3+} + 4\ Fe^{3+}$$
$$2\ NH_2OH + 4\ Pu^{4+} \xrightarrow{Fe^{2+}} 4Pu^{3+} + N_2O + H_2O + 6\ H^+$$

This catalysis by iron extends the utility of HAN reductions into higher acidities. For example, Fig. 11 shows the increased plutonium reduction rate caused by 0·1M iron, added as ferric, at 2·4N-HNO_3. In addition, tests showed that ferrous–HAN solution was as effective as ferrous sulphamate in preventing re-oxidation of Pu(III) in this nitric acid solution and that a ferrous–hydrazine mixture was ineffective for this purpose (see Table III). These data suggest that a mixture of ferrous nitrate–hydroxylamine nitrate might be used as the plutonium partitioning agent in the Purex first cycle; such tests are planned.

HAN properties

The chemical stability of HAN was examined under a variety of conditions

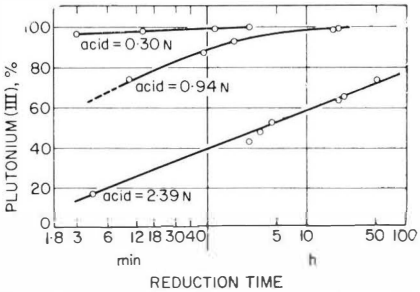

FIG. 10. *Effect of nitric acid acidity on rate of HAN reduction of Pu*
Pu, 1·6 g/l; excess HAN, 0·1N

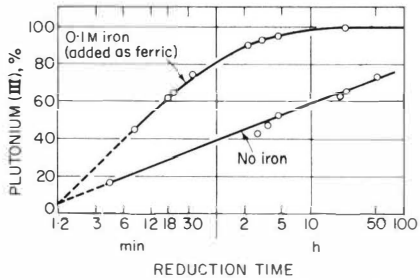

FIG. 11. *Effect of iron on rate of Pu reduction by* 0·1N-*HAN*
1·6 g Pu/l; 2·4N HNO_3

TABLE III
Comparison of Pu reductants
(Pu, 2·0 g/l; 2·5N-HNO_3)

Reductant	Analysed for	Concentrations after *n* days						
		Initial	*n* = 1	2	5	7	19	28
Ferrous sulphamate	Ferrous, N	0·102	0·092	0·086	0·079	0·076	0·052	0·041
	Sulphamate, N	0·72	0·71	—	0·66	0·67	0·65	0·527
	Pu(III),[a] %	100	→					
Hydroxylamine nitrate–ferrous nitrate	RN[b]	0·152	0·120	0·121	0·108	0·102	0·068	0·050
	Pu(III)	100	→					
Hydrazine nitrate–ferrous nitrate	Ferrous, N	0·1[c]	0 →					
	Hydrazine, N	0·1	0 →					
	Pu(III), %	100	0 →					

[a] Estimation based on observation of colour: Pu(III) is blue; Pu(IV) is brown.
[b] Total reducing normality, RN, ferrous plus hydroxylamine. The ferrous normality was 0·08 initially based on stock solution analysis.
[c] Values for ferrous and hydrazine normality are calculated from strengths of stock solutions used to prepare the mixture. Upon mixing, Pu(IV) was reduced immediately, but within 30 sec returned to brown Pu(IV). Analyses several hours later showed that no ferrous or hydrazine remained in the solution.

with the following observations:

pure aqueous solutions are stable, even while boiling;

dilute (0·1M) nitric acid solutions of HAN are stable indefinitely at room temperature, but less stable at increasing acidity, especially at elevated temperature;

decomposition of HAN in warm nitric acid, once initiated, proceeds autocatalytically, decomposing entirely to gases, as follows:

$$4NH_2OH + 2HNO_3 \rightarrow 3N_2O + 7H_2O;$$

alkali solutions are less stable than acid solutions, decomposing (again without leaving a residue) according to

$$4NH_2OH.HNO_3 + 4OH^- \rightarrow N_2O + 2NH_3 + 4NO_3^-;$$

however, cool, dilute alkali solutions are moderately stable, as indicated by a 0·2M-HAN–0·1M-NaOH solution that lost 10% of its strength in 26 days at room temperature. An attempt to distil hydroxylamine from a pH 11 sodium hydroxide solution was unsuccessful. All the hydroxylamine decomposed in less than 30 min of boiling;

HAN is extremely hygroscopic;
HAN solutions when heated under high flame produce rapid dehydration followed by decomposition but do not explode.

Low-assay ^{238}Pu

Hydroxylamine nitrate has found another use in the routine recovery of the plutonium, with moderate concentrations of ^{238}Pu, present in the waste from enriched uranium processing. This material is recovered by batch extraction with 10% TBP solvent, and is then stripped from the solvent by two batch contacts with 0·01M-HAN–0·12M-HNO. The aqueous solution is washed with 'Ultrasene' to remove dissolved TBP, evaporated, and processed through the regular solvent extraction system on a campaign basis (utilising the 3·5% TBP, enriched uranium 1st cycle and the 30% TBP neptunium 2nd cycle).

As in other operations, substituting HAN for FS or HAS eliminated sulphate in the feed to the subsequent solvent extraction processes, decreased losses, reduced waste volumes, and minimised corrosion of stainless-steel equipment especially evaporators. In addition, the product solution could be stored for indefinite time without fear that $Pu(SO_4)_2$ would precipitate from solution.

Neptunium processing

The neptunium byproduct in irradiated enriched uranium is recovered at SRP with the flow-sheet illustrated in Fig. 12.[14,15] This neptunium recovery process is under study for three reasons. First, the chemical behaviours of neptunium and zirconium in the process were not well understood, and some

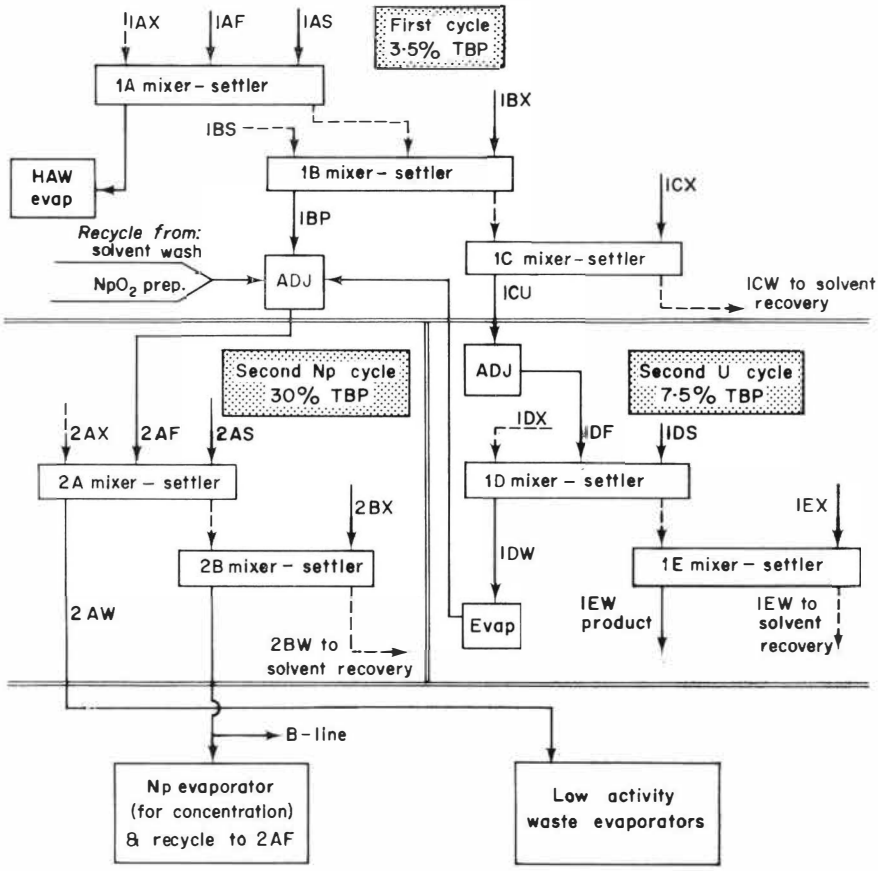

FIG. 12. *Flow-sheet for enriched U and byproduct Np recovery*
——— aqueous stream; – – – – solvent stream

improvements appeared possible. Second, any understanding of the behaviour of zirconium that was gleaned from this study could be applied as well to the Purex process. Third, the process was a convenient one to pilot the development of computational techniques for the analysis of solvent extraction flow-sheets.

Process experience

Items pertinent to this work are:

(i) Approximately 2% of the neptunium in the feed to the second neptunium cycle remains in the solvent, and accumulates in the sodium carbonate solvent washing tank. This neptunium is periodically recovered, but at some additional cost and inconvenience.

(ii) Approximately 8% of the neptunium in the feed to the first cycle remains in the solvent with the uranium in the 1B bank, and subsequently leaves in the 1DW stream. After evaporation to double its concentration the material is mixed with 1BP, at roughly equal volumes, to make the second-cycle feed. Added with the 1DW are the solvent degradation products that were produced and concentrated during the evaporation.

(iii) Decontamination from ^{95}Zr fluctuates widely, but, as in the Purex second cycle, is much below what would be expected from published distribution coefficients.

(iv) Although the routine 'reducing flow-sheet' maintains neptunium in the IV valence, occasional 'oxidising' flow-sheets' are run, in which the neptunium is extracted as Np(VI). Oxidising flow-sheets are used only to separate thorium from neptunium.

The studies presented in the following sections clarified the behaviour of neptunium and zirconium and led to work on a 15% TBP flow-sheet for neptunium. As part of this last study a convenient method was developed for calculating and analysing the effects of flow-sheet variations.

Neptunium loss to 2BW

Laboratory studies demonstrated that the chemical behaviour of the neptunium that was tightly bound in the 2BW solvent could be simulated by addition of DBP to 30% TBP-'Ultrasene' containing Np(IV). Stripping became less effective at increasing concentrations of DBP, as shown in Fig. 13, approaching

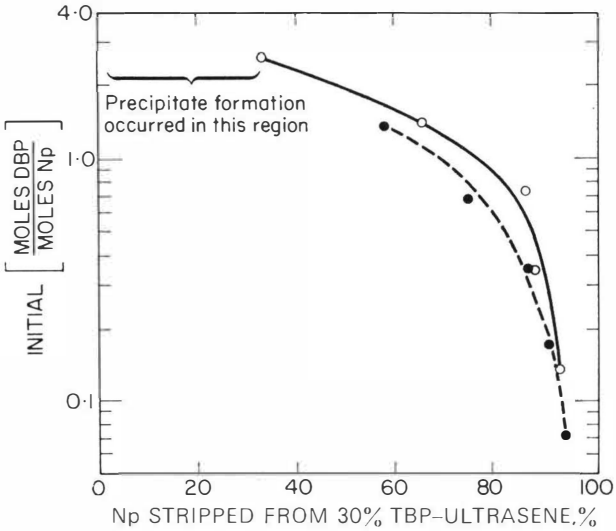

FIG. 13. *Effect of DBP on stripping of Np from 30% TBP–Ultrasene*

Conditions: 5 equal volume contacts with 0·01M-HNO_3
Initial Np concn.: ○ 0·07 g/l, ● 0·14 g/l

zero stripped at a mole ratio of 4 DBP moles per mole of neptunium. At a ratio of ~3 : 1 a precipitate began to form, which contained 4 moles of phosphate per mole of neptunium. It is therefore assumed that the bound neptunium in the process 2AW is solvated $Np(DBP)_4$. Efforts to improve stripping by addition of H_2O_2, $Ce(SO_4)_2$, or KNO_2 to the aqueous phase were unsuccessful. However, stripping was measurably better in 15% TBP than 30% TBP, as shown in Fig. 14.

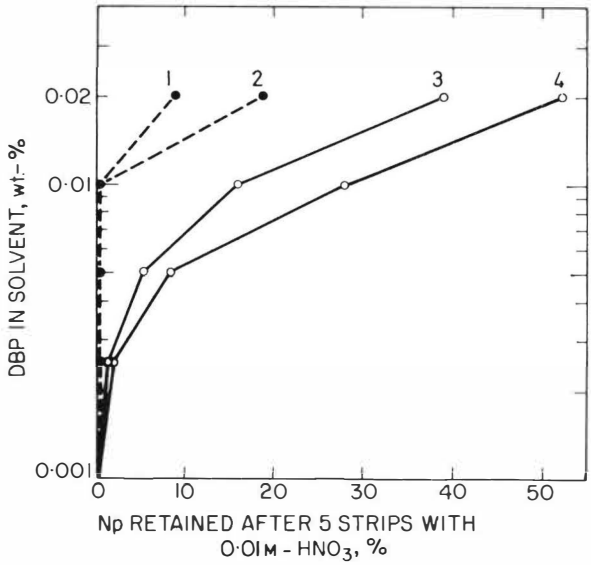

FIG. 14. *DBP stripping of Np from 15%* versus *30% TBP–Ultrasene*

Initial Np concn: (1) 0·1 g/l in 15% TBP; (2) 0·05 g/l in 15% TBP; (3) 0·14 g/l in 30% TBP (4) 0·07 g/l in 30% TBP

Zirconium decontamination

When multiple extraction and scrub tests were performed on plant 2AF no unexplainable zirconium behaviour was found. The sulphate (from sulphamate oxidation) in the sample lowered the D_a^o in extraction experiments by the approximate amount expected from the tracer experiments. Analyses of the 2AF revealed detectable quantities of DBP, and the scrub tests on solvent prepared by mixing 2AF with clean solvent were consistent with the tracer experiments when that amount of DBP was present in the tracer; i.e., increased D_a^o values, less $[Zr]_s$ at acidities of 1–2M, and no effect at ~4M.

Some tests at lower concentrations of TBP in the solvent indicated that the rate of conversion to the more highly solvated $[Zr]_s$ had a high dependence on TBP concentration. Therefore, improvement in zirconium decontamination should be possible by reducing the TBP concentration.

Neptunium distribution measurements

Additional distribution data were taken to develop a flow-sheet that utilised 15% TBP. The distribution coefficients presented in Fig. 15 are higher and have less slope than previously reported data.[16,17] The difference may lie in experimental method; the other measurements were made with tracer ^{239}Np reduced with 0·1M ferrous sulphamate, whereas in this work macro concentration (0·7 mg Np/ml) was used reduced with 0·01–0·02M-FS. The FS was always freshly prepared (<3 days old) to minimise sulphate concentration. It is possible that in the reference data, with tracer neptunium and higher sulphamate, the ratio of sulphate to Np(IV) was high enough to suppress the distribution coefficient.

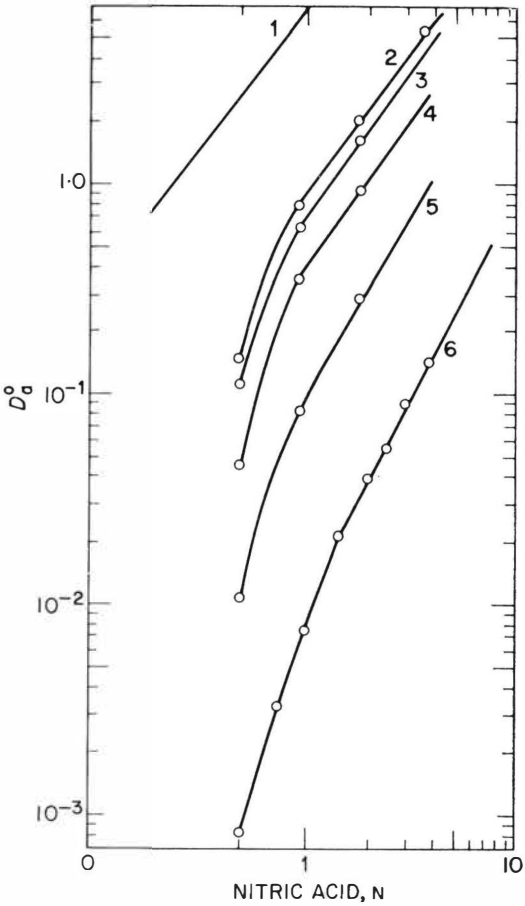

FIG. 15. *Np (IV)* D_a^o versus *nitric acid concentration*

(1) 100% TBP; (2) 30% TBP-Ultrasene; (3) 30% TBP–n-paraffin; (4) 20% TBP–n-paraffin; (5) 10% TBP–n-paraffin; (6) 3·5% TBP–Ultrasene

Plant tests

Laboratory data were utilised in a series of flow-sheet calculations (discussed in the next section), which led to a test of 15% TBP–'Ultrasene' solvent in the second neptunium cycle to explore the potential improvements in neptunium loss and zirconium decontamination. Decontamination from zirconium did improve by a factor of ten on the average. However, very low concentrations of neptunium clouded the interpretation of neptunium losses; losses to the 2BW apparently were reduced to $\frac{1}{2}$ or $\frac{1}{3}$, but were not eliminated as had been hoped. The large amount of DBP added to the system from evaporated 1DW and recycled 2BP probably overwhelms the effects of improved stripping from the more dilute solvent. Studies are now under way to improve neptunium stripping in the 1B bank in an attempt to eliminate the need to process the 1DW.

The laboratory experiments cited earlier led to plant tests on the effects of residence time and acidities. In one test, identical flow-sheets were run (flow ratios, acidities, concentrations) but at two different absolute flows (one was 70% of the other). The lower absolute flow (hence longer residence time) gave 60% improvement in Zr-DF. In another test, scrub acidities of 0·88M-HNO_3 and 2·2M-HNO_3 gave DF's of 1100 and 450, respectively. The difference between the scrubs is somewhat less than would be calculated from zirconium acid extraction data and represents the effect of the highly solvated form, $[Zr]_s$, (discussed in the laboratory studies section of this report) which is present in higher abundance at lower acidity.

Flow-sheet calculations by computer

A computer code developed by Lowe[18] was used to study the existing flow-sheet for the 2nd neptunium cycle and flow-sheets with reduced TBP in the solvent. The programme was modified slightly to permit multi-problem calculations and to permit entering distribution data in both tabular and equation form. Distribution coefficients used in these calculations, other than those of the authors, were taken from Refs 19–24.

TABLE IV

Neptunium loss versus *stage efficiency*

(2A bank; 16 stages. Reducing flow-sheet, 30% TBP)

	Stream	Flow[a]	Nitric acid, M
Conditions	2AS	31	0·88
	2AF	100	4·0
	2AX	89	0·0
	Stage efficiency, %	Np loss to 2AW, %	
Results	80	0·143	
	85	0·066	
	90	0·027	
	95	0·010	
	100	0·0031	

[a] any consistent volume flow units

Stage efficiency

Lowe's computer model,[18] like many others, combines all deviations from theoretical kinetic behaviour into one correction factor called 'stage efficiency', which is defined as the mass of component actually transferred between phases in a given stage divided by the mass that would have been transferred if equilibrium had been attained. Calculations at several stage efficiencies were made at 30% TBP under reducing conditions to establish a nominal value for this factor by comparison with plant performance. These calculations are summarised in Table IV. Since the plant generally operates at $<0{\cdot}01\%$ neptunium loss to the 2AW, the stage efficiency was conservatively set at 95% for all subsequent calculations.

Flow-sheet variation

Optimum conditions for bank operation involve a compromise between low product loss and high decontamination. In the study of the 15% TBP 'reducing flow-sheet', which utilises Np(IV), adequate fission product distribution coefficients were lacking and therefore reasonable conditions for acceptable product loss (arbitrarily set at 0·011%) were established and the independent effects of process variables on the loss were systematically explored. The calculated results are given in Fig. 16, which has been used as a guide in plant tests to seek improved decontamination at minimum product loss. All results are expressed relative to the base conditions so that the effects of all variables may be shown on one plot. As long as no exceedingly large changes are made, Fig. 16 can be used to predict the effect of simultaneous changes in two variables. For example, if better zirconium decontamination is expected at lower acidity, the 2AF acid concentration could be lowered to 3·2M (0·8 of original value) and the eight-fold increase in neptunium loss could be cancelled by raising the 2AX flow to 267 (1·3 times original value).

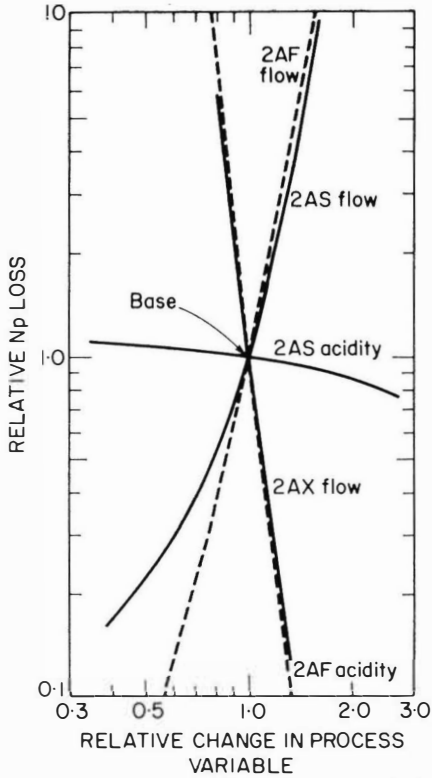

FIG. 16. *Effect of process variables on Np loss, reducing flow-sheet*
Base conditions: 2AS flow, 31; 2AF flow, 100; 2AX flow, 205; 2AS acid, 0·88M; 2AF acid, 4·0M; Np loss, 2AW, 0·011%; 15% TBP; Np(IV)

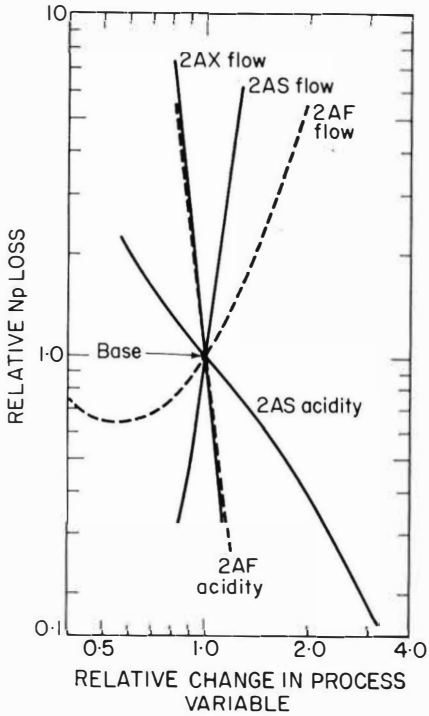

FIG. 17. *Effect of process variables on Np loss, oxidising flow-sheet*
Base conditions: 2AS flow, 80; 2AF flow, 100; 2AX flow, 270; 2AS acid, 0·5M; 2AF acid, 2·2M; Np loss, 2AW, $3{\cdot}4 \times 10^{-4}$%; 15% TBP; Np(VI)

It was also shown that very little decontamination from thorium can be obtained with a 'reducing flow-sheet', using 15% or 30% TBP.

For the 'oxidising flow-sheet', which utilises Np(IV), the effects of process variables on neptunium loss were calculated for 15% TBP and are shown in Fig. 17. The neptunium loss could be set at a lower level in this instance because thorium is the only contaminant of concern, and separation from it is quite good.

Multiparameter representation

A more interesting and useful method of presenting the data is illustrated by Fig. 18, where the effects of process variables on thorium DF and neptunium loss are given simultaneously. The solid lines correspond to the loss data from Fig. 17, i.e. variations from the same base conditions holding all variables constant except one. The labelled points along each curve show the value at that point of the variable being changed. Here again, the plot can be used to predict the effect of simultaneous small changes in two variables. For example, increasing 2AS flow from 80–89 and increasing 2AX flow from 270–300 (both increased by factor of 1·11) cause compensating changes in loss and DF equivalent to decreasing 2AF flow by a factor of 1·0/1·11 (= 0·90). In this case, the dual change can be verified by the curve given for variations in 2AF flow, the net effect falling quite close to a 2AF flow of 90.

For the dashed lines, all three of the flows were held constant, and for a given dashed line the 2AS acid was held constant and 2AF acid varied. The points are labelled by parameter numbers and the intersections of curves correspond

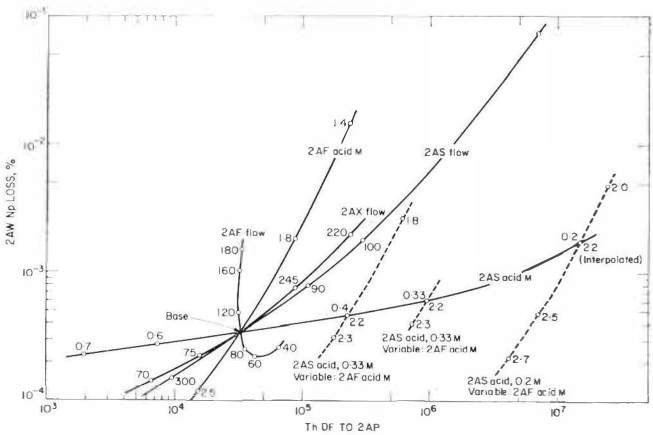

FIG. 18. *Relationship between Np loss and Th DF, oxidising flow-sheet*
Values of the variables are given on the curves

TABLE V

Effect of 2AS acidity on 2A bank neptunium inventory

(Oxidising flow-sheet, 15% TBP)

2AS flow, 80; 2AF flow, 100; 2AX flow, 270

Nitric acid, M		Peak neptunium concn. relative to 2AF 2AF concn. = 1	
2AS	2AF	Organic (stage)	Aqueous (stage)
0·7	2·2	0·5 (4)	0·4 (3)
0·5	2·2	0·6 (4)	0·8 (3)
0·33	2·2	1·0 (5)	2·0 (4)
0·2	2·7	3·2 (6)	9·4 (5)
0·2	2·0	3·4 (6)	10·3 (5)

to calculated results with the exception of the interpolated intersection on the right side of the plot.

The solid-line variations from the base conditions were calculated first. The dashed lines represent explorations in the direction of greater DF at the same neptunium loss. Greater DF's are achieved at the lower 2AS acidities because of neptunium reflux in the bank, which is indicated in Table V by changes in peak neptunium concentrations in the bank under these conditions.

Conclusion

In using this computer model of the solvent extraction process, it must be recognised that a number of effects are not considered; for example—transient start-up effects, aqueous complexants such as sulphate and phosphate, and solvent complexants such as DBP. The model is therefore not necessarily accurate in predicting absolute DF's or product losses, but should be quite useful for determining the relative effects of process variables, and as a guide, along with plant experience, for arriving at optimum conditions.

Multi-parameter plots that can be generated by the computer calculations represent a valuable visual aid in evaluating the potential effects of flow-sheet variations. The technique is being extended to aid in several studies and operations, such as nuclear safety control, partition of plutonium and uranium, and recovery and separation of trivalent actinides and lanthanides.

Acknowledgment

Information in this paper was developed during the course of work under Contract AT(07-2)-1 with the U.S. Atomic Energy Commission.

References

[1] Orth, D. A., & Olcott, T. W., *Nucl. Sci. Engng*, 1963, **17**, 593
[2] Orth, D. A., 'Solvent extraction chemistry of metals', 1965, p. 47 (New York: MacMillan & Co. Ltd.)
[3] Siddell, T. H., *Ind. Engng Chem., Ind. Edn*, 1959, **51**, 41
[4] Murbach, E. W., & McVey, W. H., *Rep. Congr. atom. Energy Commn U.S.*, 1954, LRL-115
[5] Solovkin, A. S., & Tsvetkova, S. V., *Russ. chem. Revs*, 1962, **31**, 655
[6] Wallace, R. M., & Pollock, H., *Rep. Congr. atom. Energy Commn U.S.*, 1958, DP-308
[7] Kishbaugh, A. A., *Rep. Congr. atom. Energy Commn U.S.*, 1963, DP-841
[8] Orth, D. A., & McKibben, J. M., *Trans. Am. nucl. Soc.*, 1969, **12** (1), 28
[9] Webster, D. S., & Winsche, W. E., U.S.P. 3,332,614
[10] Schlea, C. S., & Jennings, A. S., 'Solvent extraction chemistry of metals', 1965, p. 81 (New York: MacMillan & Co. Ltd.)
[11] Salomon, L., & Lopez-Menchero, E., *Ind. Engng Chem., Process Des. Dev.*, 1970, **9** (3), 345
[12] Mainland, E. W., Orth, D. A., Field, E. L., & Radke, J. H., *Ind. Engng Chem., Ind. Edn*, 1961, **53**, 685
[13] McKibben, J. M., & Bercaw, J. E., 'Hydroxylamine nitrate as a plutonium reductant in Purex solvent extraction process'. *Rep. Congr. atom. Energy Commn U.S.*, 1970, D.P. 1248
[14] Poe, W. L., Joyce, A. W., & Martens, R. I., *Ind. Engng Chem., Process Des. Dev.*, 1964, **3** (4), 314
[15] Groh, H. J., & Schlea, C. S., 'Process chemistry, progress in nuclear energy, series III', 1970, **4**, 507 (New York: Pergamon Press)
[16] Bruce, F. B., Fletcher, J. M., & Hyman, H. H., 'Process chemistry, progress in nuclear energy, series III', 1958, **2**, 501 (New York: Pergamon Press)
[17] Dawson, J. K., Elliott, R., & McKay, H. A. C., *Rep. U.K. atom. Energy Auth.*, 1953, AERE C/R 1117
[18] Lowe, J. T., *Ind. Engng Chem., Process Des. Dev.*, 1968, **7** (3), 361
[19] Codding, J. W., Haas, W. O., & Heumann, F. K., *Rep. Congr. atom. Energy Commn U.S.*, 1951, KAPL-602
[20] Siddall, T. H., Parker, S. G., & Prout, W. E., *Rep. Congr. atom. Energy Commn U.S.*, 1957, DP-53
[21] Siddall, T. H., *Rep. Congr. atom. Energy Commn U.S.*, 1956, DP-181
[22] Peppard, D. F., Mason, G. M., & Maier, J. L., *J. inorg. nucl. Chem.*, 1956, **3**, 215
[23] Ishimori, T., & Nakamura, E., *Bull. chem. Soc. Japan*, 1959, **32** (7), 713
[24] Savolainen, J. E., *Rep. Congr. atom. Energy Commn U.S.*, 1952, ORNL-CF-52-2-113

Isolation of transplutonium elements

by D. A. Orth, J. M. McKibben, W. E. Prout and W. C. Scotten

Savannah River Plant, E.I. du Pont de Nemours & Co., Aiken, S. Carolina, U.S.A.

The Savannah River Plant and Laboratory have a programme for the production of transplutonium elements. ^{239}Pu fuel was first irradiated to produce a mixture of higher plutonium isotopes which were separated, in the plant, from the fission products and refabricated into fuel. The second irradiation produced virtually pure ^{242}Pu which also was separated in the plant and refabricated for a third irradiation that is now in progress.

The first irradiation produced 1·2 kg of mixed Am and Cm isotopes as byproducts that were extracted from the raffinate from the plutonium extraction step with 50% tributyl phosphate (TBP) to test solvent extraction procedures for recovery of an actinide–lanthanide fraction. The second irradiation produced 8·6 kg of Am and Cm that were also isolated from the raffinate from the ^{242}Pu recovery operation by batch extraction with 50% TBP. The mixed actinide–lanthanide fraction was transferred to Savannah River Laboratory for purification. A large part of the material was processed through a cycle of continuous extraction with 30% TBP in the laboratory pilot mixer–settler banks in preparation for final purification. This extraction gave a substantial decontamination from the mercury, aluminium and iron present in the plant product fraction; it also gave a 36% rejection of the rare earths.

Preparations are under way for future processing of irradiated ^{242}Pu, Am–Cm, and fresh ^{239}Pu fuels. The extractions involved will utilise plant Purex extraction equipment. Studies are being made on methods of obtaining maximum separation of the actinides from the fission product lanthanides, in nitrate salt solutions compatible with plant operation. Preliminary results indicate that the separation factors (ratios of distribution coefficients) between actinides and lanthanides vary with the salt cation in solutions at the same nitrate concentration. The salting power of the cations, defined as the effect on distribution coefficients, decreases in the order Be, Li, Al, Cr, Mg, Na.

In the actinide series and the fission-product lanthanides, extractability from nitrate solutions into TBP increases as the atomic number increases. The order of extractability reverses when diethylenetriaminepentaacetic acid (DTPA), a powerful complexing agent, is added to the nitrate salt solution. Although the DTPA reduces the extractability of all the actinides and lanthanides, high concentrations of nitrate salts can raise the absolute distribution coefficients to the range necessary for extraction separations with TBP.

The laboratory data on the effects of salt strengths, acids, and DTPA concentrations were incorporated into computerised flow-sheet calculations. These calculations show that the plant should be able to provide separation from the light fission product lanthanides by extraction from aluminium-nitrate solutions, while extraction from DTPA–nitrate salt solutions should be able to discriminate against the heavier fission product lanthanides. Decontamination factors greater than 10 seem feasible and such factors would greatly ease subsequent operations. The calculations show that flow-rates and concentrations must be controlled more closely than in normal plant operations, but the required control does appear attainable.

Introduction

AT THE SAVANNAH RIVER PLANT (SRP), transplutonium elements are being produced from ^{239}Pu in successive reactor irradiations by a series of neutron captures and beta decays in the following sequence:

$$Pu \rightarrow Am \rightarrow Cm \rightarrow Bk \rightarrow Cf \rightarrow Es \rightarrow Fm$$

The Savannah River Plant programme for producing transplutonium elements in several stages is depicted graphically in Fig. 1.

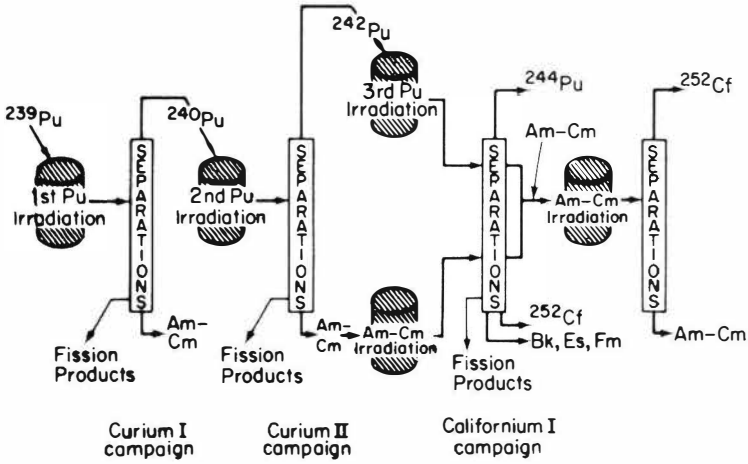

FIG. 1. *Outline of the transplutonium elements production programme at Savannah River Plant*

In the first irradiation, ^{239}Pu captured neutrons to produce heavier isotopes. The resulting mixture of plutonium isotopes was recovered (Curium I campaign) and fabricated into aluminium alloy targets for a second irradiation, in which a a portion of these plutonium isotopes was converted to ^{242}Pu, ^{243}Am and ^{244}Cm. The bulk of the ^{244}Cm from targets of this second irradiation (Curium II campaign) was separated and purified for evaluation in isotopic power sources; the ^{242}Pu and ^{243}Am were recovered and are being re-irradiated along with some of the ^{244}Cm to produce ^{252}Cf and other transplutonium elements such as Bk, Es and Fm. These elements will be separated and purified in the Californium I campaign, currently scheduled for late in 1971.

The programme to date has included initial separations in the large-scale extraction facilities at the Savannah River Plant, with subsequent processing in the high-level caves at the Savannah River Laboratory (SRL) to separate and purify the transplutonium elements. In the forthcoming Californium I campaign, all separations will be made in the plant, with final purification to be made by chromatographic ion exchange, in equipment now under construction. This paper discusses (i) plant experience with batch extractions with 50% TBP in separating a crude actinide-lanthide mixture in the Cm-I and Cm-II campaigns; (ii) Savannah River Laboratory development work on continuous extraction, in mixer-settlers with 30% TBP, to prepare a relatively pure actinide-lanthanide fraction suitable for feed to the ion exchange system; (iii) further laboratory research on methods to provide maximum separation of lanthanides and actinides during the continuous solvent extraction that will be part of plant operations when the ion exchange equipment is installed; and (iv) the use of laboratory data for evaluation and selection of flow-sheets to give maximum separation of actinides and lanthanides.

Plant processing – Cm-I and Cm-II campaigns

The principal purpose of the Cm-I irradiation and processing campaign was to produce higher plutonium isotopes for further irradiation. Recovery of the small amount of Cm and Am in this campaign was attempted primarily to pilot procedures for the Cm-II campaign.

The principal purpose of the Cm-II campaign was to produce ^{244}Cm for evaluation as a heat source material for isotopic power generators. In addition, the resulting Pu and Am and some of the Cm were made into targets for re-irradiation to produce ^{252}Cf and other transplutonium elements.

Process descriptions

In the Cm-I campaign, the irradiated Pu-Al targets were dissolved and then processed through the Purex (30% TBP) solvent extraction equipment to recover the plutonium. The Am, Cm, and fission products went into the high activity waste (HAW) stream, which was concentrated, steam-stripped to reduce nitric acid concentration, and finally adjusted to 0·4M-H^+, 6·0M-NO_3^-, in preparation for the batch extractions.[1] The Am, Cm and lanthanides were recovered from 19 separate 1200–2000 gal. batches of this waste. Each waste batch was contacted twice with 50% TBP-'Ultrasene' (trademark of Atlantic-Richfield Co. for a refined kerosene) to extract the actinides and lanthanides which were then stripped from the solvent with dilute nitric acid. Between each extraction the solvent was scrubbed with 2·5% sodium carbonate, then dilute nitric acid. The product solutions were combined and concentrated for a final batch cleanup attempt which gave considerable difficulty because of solvent radiation damage (discussed later).

In the Cm-II campaign, the Pu was extracted into 3·5% TBP in the mixer-settlers that are normally used for enriched uranium processing. Again, the actinides and lanthanides were recovered from the waste. The batch extractions were similar to those in the Cm-I campaign except that only 2 extractions were performed instead of 19, and a centrifugal separator was used to separate the phases rapidly after mixing. The reduction in the number of batches from 19 to 2 was possible because of the much lower fission product activities and the shorter time required for phase separation by centrifugal separation.

Materials accounting

The quantities of actinides processed in the Cm-I and Cm-II campaigns were respectively: Pu 65·4 and 9·7 kg; Cm 0·130 and 5·9 kg; Am 1·1 and 2·7 kg and Cf 0 and 28 mg.

The isotopic compositions of the Pu, Am and Cm are given in Table I.

TABLE I

	Atom-%			Atom-%	
	Cm-I	Cm-II		Cm-I	Cm-II
Pu-238	—	0·156	Cm-242	~30	0·40
239	22·4	0·025	244	~70	94·97
240	49·9	1·19	245	—	0·70
241	15·1	0·102	246	—	3·8
242	12·6	98·17	247	—	0·063
244	—	0·180	248	—	0·060
			Am-241	36	<1
			243	64	>99

The average yields of Cm and Am in the batch extractions were 95% for the Cm-I campaign and 99·6% for the Cm-II campaign. In the Cm-I campaign recycle batch extraction, in which severe emulsion occurred, only about 40% was recovered. The actinide–lanthanide product solution from the Cm-II campaign was transferred in small batches to SRL for further processing as described in the next section.

Radiation effects

Each of the 19 batch extractions in the Cm-I campaign irradiated the solvent to 20 W-h/l, 10% of which was from alpha radiation. The phases separated by gravity without difficulty leaving only a small amount of interface precipitate. However, the solvent washing with 2·5% sodium carbonate produced emulsions that separated quite slowly, and solvent washing became the time-limiting step in the process.

In the recycle batch extraction of the combined and concentrated Am–Cm

product batches in the Cm-I campaign, the solvent radiation exposure was nearly 500 W-h/l, which produced a stable emulsion. This emulsion persisted for about 4 months, after which the organic phase had been completely destroyed and the tank contained only an aqueous phase. Laboratory tests with the concentrated feed from the Cm-I campaign batch extractions determined that interfacial precipitates and some tendency to emulsify occur at about 15 W-h/l, which at the same time produces $\sim 8 \times 10^{-3}$M dibutyl phosphate (DBP). Stable emulsions are produced by 200 to 300 W-h/l, giving $\sim 0 \cdot 2$M-DBP. (These values apply to continuous exposure with no intermediate solvent washing.)

Based on this plant and laboratory experience, the Cm-II campaign batch extractions were designed to give a solvent exposure of less than $\sim$ 15 W-h/l (50% from alpha) per extraction cycle. Actually, in the Cm-II campaign batch extractions, an exposure of 8 W-h/l resulted, no phase separation difficulties arose, and no interfacial precipitates were observed.

SRL Work on transplutonium extraction

The crude actinide–lanthanide fraction that was produced in the SRP Cm-II campaign was transferred to the high-level caves at SRL for purification. This crude material contained large amounts of residual aluminium (carried over from batch extraction), mercury (used as a catalyst in the acid dissolution of aluminium targets), and iron (used in the valence adjustment of plutonium); it was purified in one of two processes:

1. The Tramex process[2] which consists of three cycles of extraction with a tertiary amine to separate the trivalent actinides from the lanthanides and to eliminate the other contaminants.
2. The ion-exchange chromatographic process which first utilizes one cycle of 30% TBP solvent extraction to separate the trivalent actinides and lanthanides from the aluminium, iron and mercury, then one cycle of displacement development chromatography[3] with DTPA to separate the trivalent actinides from each other and from the lanthanide fission products.

Displacement development chromatography was developed as a replacement for Tramex solvent extraction in the programme to make large quantities of ^{244}Cm and ^{252}Cf. The chromatographic process does not require the chloride solutions used in the Tramex process and suitable nitrate feeds, compatible with stainless steel equipment, can be prepared by removing aluminium, iron, and mercury (which interfere with the chromatographic process) by continuous solvent extraction with 30% TBP.

Solvent extraction as pretreatment for ion exchange

The solvent extraction flow-sheet for preparing feeds for the chromatographic separation of the trivalent actinides and lanthanides is shown in Fig. 2. In the first mixer–settler, the trivalent actinides and lanthanides (along with other actinides and the major portion of the ruthenium and zirconium) were co-extracted from a highly salted aqueous feed stream with acidified 30% TBP in n-dodecane and scrubbed with sodium nitrate or lithium nitrate solution. In the second mixer–settler, the trivalent actinides and lanthanides were selectively back-extracted into dilute nitric acid, while plutonium, uranium, zirconium and ruthenium remained in the spent solvent. The direction of transfer of the trivalent actinides and lanthanides between phases was controlled by the concentrations of aluminium nitrate in the feed, sodium nitrate in the scrub, and nitric acid in the solvent in the 1A bank and in the aqueous extractant in the 1B bank.

The solvent extraction flow-sheet, and variations, were evaluated in the miniature mixer–settlers using non-radioactive solutions containing cerium, neodymium, ytterbium, and 2M aluminium nitrate. The tests showed that:

$\geqslant 99 \cdot 5$% of the lanthanide stand-in was recovered in the product stream;

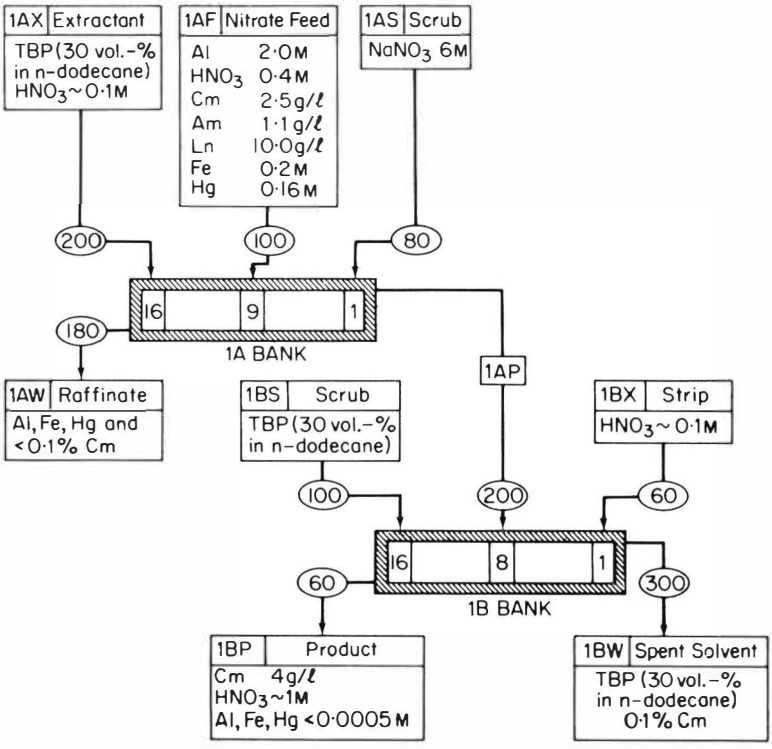

FIG. 2. *Cm Feed preparation with 30% TBP*
Ringed numbers indicate relative flow
Ln = lanthanides

decontamination factors (DFs) for aluminium and iron were greater than 10^5 and 10^4, respectively;
decrease of nitrate ion in the scrub from 8M-Li to 6M-Na improved the removal of mercury from a DF of 12 to one greater than 10^5;
since a highly salted system is used to extract the trivalent actinides, essentially all the nitric acid entering the 1A bank extracts and leaves in the product (1AP) stream. For this reason, acidified solvent must be used to prevent hydrolysis and precipitation of Fe(III) in the extraction section of the mixer-settler.

Further tests of the 30% TBP process were made with unevaporated feed containing 1·5M aluminium nitrate to define the best conditions for separating curium from the light lanthanides such as cerium. The conditions are given in Table II.

TABLE II

Stream	Composition	Relative flow
Feed (1AF)	1·5M-$Al(NO_3)_3$ 0·4M-HNO_3 0·1M-$Fe(NO_3)_3$ 0·1M-$Hg(NO_3)_2$ 0·07M lanthanides	100
Extractant (1AX)	30% TBP 0·1M-HNO_3	180–300
Aqueous scrub (1AS)	6M-$NaNO_3$	45–80
Back-extractant (1BX)	0·1M-HNO_3	75
Organic scrub (1BS)	30% TBP	75

Test results are shown in Fig. 3. The best results were obtained in test C, with 1AS/1AX = 0·28. An 11% decrease in 1AS/1AX ratio (test B) decreased the rejection of cerium from 62 to 1·6% and an 18% increase in 1AS/1AX ratio (test D) decreased the extraction of curium from 99 to 94%.

Separation of curium and cerium in the scrub section of the 1A bank is attributed to a combination of strong 'back-salting' by nitric acid in the extract and salting by 6M sodium nitrate in the scrub. At a high scrub/extractant ratio nitric acid, curium, and cerium are refluxed to near the saturation limit of the organic phase. Consequent competition for the TBP then enhances the small difference between the several equilibrium distribution coefficients, and 'back-salts' the cerium into the aqueous raffinate.

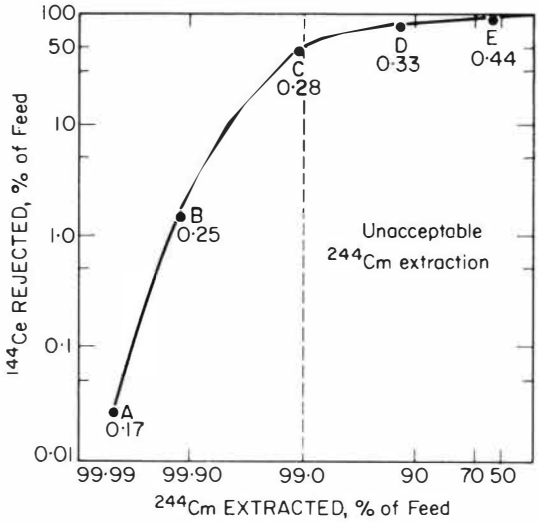

FIG. 3. *Curium–cerium separation by TBP extraction at varying 1AS/1AX flow ratios*

Curium II-campaign processing

The flow-sheet information just developed was used to process about 1·6 kg of the ^{244}Cm from the plant Cm-II campaign, as SRL converted to the ion exchange process for the separation and purification of ^{244}Cm, ^{243}Am and ^{252}Cf. Process conditions for this extraction process with 30 vol.-% TBP are those shown in Fig. 2. During normal operation, less than 0·1% of the curium remained in the waste streams (1AW and 1BW). The product stream contained less than 0·005M (Fe + Al + Hg); the curium concentration was about 4 g/l, and the nitric acid strength was about 0·8M. Analysis of process data by three analytical methods (total rare earth titration with EDTA, direct gamma counting for ^{144}Ce, and spark source mass spectrometry) indicated substantial removal of lanthanides: ~36% of total lanthanides and 30–66% of the cerium.

Studies on lanthanide–actinide separations

Batch extractions were used in plant isolation of crude actinide–lanthanide mixtures, whereas one or more cycles of multi-stage solvent extraction will be used in the Cf-I and future programme to prepare feed for the planned plant ion exchange equipment. Present plans call for a flow-sheet similar to that used at SRL, utilizing the Purex 18-stage 1A bank of centrifugal contactors for extraction and scrubbing and the 18-stage 1B mixer–settler bank for stripping. In some cases, subsequent ion-exchange processing could be eased considerably if a greater separation of actinides and lanthanides could be attained in the solvent extraction cycle. The lanthanides are undesirable because they load

the resin and limit the throughput of the ion exchange equipment. They become particularly significant for long-irradiated ^{239}Pu fuels where the mole ratio of lanthanides to actinides may be 20:1, compared with less than 2:1 for the Cf-I ^{242}Pu targets.

As a further guide to the studies, the fission product yield curve (Fig. 4) shows that a group separation of all lanthanides from all actinides is not necessary; discrimination against the light lanthanides only would give an appreciable decrease in the lanthanide–actinide ratio. The search for systems that would enhance the separation and be compatible with plant campaigns alternating with Purex operation prompted a review of nitrate-salted systems. Several investigators have reported a divergence of lanthanide coefficients when extracting into TBP from high and increasing nitric acid concentrations.[4–6] The same effect occurs with trivalent actinides. Some additional work reports that different nitrate salts have different salting effects; but little work has been published on the effect of different cations on the separation factors (ratios of distribution coefficients).

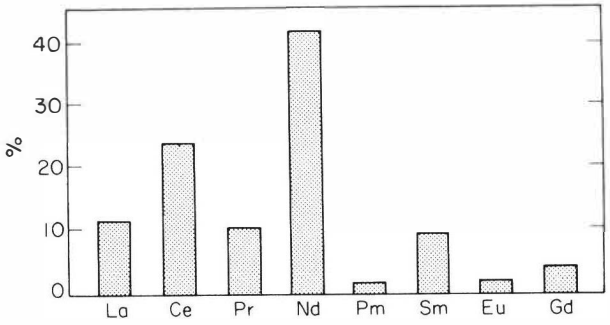

FIG. 4. *Distribution of lanthanides in 'deep burned' Pu*

Talspeak,[8] a solvent extraction system for separating lanthanides and actinides developed at ORNL, utilizes diethylenetriaminepentaacetic acid (DTPA) in the aqueous phase and di-2-ethylhexyphosphoric acid in the organic phase. DTPA, alone in the aqueous phase, is such a powerful complexant that distribution coefficients for the lanthanides and actinides are too low for workable TBP flow-sheets (this is why Talspeak utilises more powerful extractants). No work could be found that reported the addition of nitrate salts to the DTPA in efforts to raise the distribution coefficients sufficiently so that TBP would be an acceptable extractant.

This preliminary review led to complementary laboratory and numerical studies to define conditions for maximum removal of fission product lanthanides during both the extraction and stripping solvent extraction operations. The results to date are presented in the following paragraphs.

Experimental

Distribution coefficients (D_a^o) were measured for three actinides (Cf, Am, Cm) and two lanthanides (Ce, Eu) between TBP–n-paraffin and two different types of aqueous solutions. The first was a highly salted nitrate solution that would be used for preferential extraction of actinides from the light lanthanides. The second was a nitrate-salted, low-acid solution containing DTPA that gives preferential stripping of actinides from the solvent phase.

The variables investigated included type of salt, salt strength, acidity, temperature, and concentration of DPTA and TBP.

All of the aqueous solutions used in these tests were prepared by accurate mixing of separate, standardised stock solutions of tracer, salt, and acid. Tracer solutions were first fumed to dryness once with perchloric acid to destroy

any organic complexants that might have been present, then three times with concentrated nitric acid to remove chloride, sulphate, and volatile impurities. The final residue was dissolved in standardised nitric acid and the tracer concentration was determined. Immediately before each experiment, the solvent was washed three times with dilute alkali to remove TBP degradation products then equilibriated by washing three or more times with a salted acid solution of the same composition that the solvent would contact in the test. In each extraction experiment the separate tracer solutions were mixed with an equal volume of equilibriated solvent for 2 min. Each mixture was then centrifuged, although phase separation by gravity was good in all cases. The solvent activity was determined by the appropriate counting technique; alpha counting for Cf, Am, and Cm, gamma counting for Eu, and beta counting for Ce. The cerium count was made one or more hours after the extraction so that the Pr activity would have nearly reached equilibrium. Except for the Eu, the activity in the final aqueous phase was calculated by material balance (input less solvent activity) because the salt precluded direct alpha and beta counts.

Results

The laboratory extraction tests demonstrated that the distribution coefficients of all the lanthanides and actinides indeed increase with increasing nitrate concentration and that salting power (defined by effect on D_a^o) is greatly dependent on the cation. Among the cations, the order of salting power is Be > Li > Al > Cr > Mg > Na, as illustrated by Cf distribution coefficients in Fig. 5. However, the Be^{2+} ion has a finite distribution coefficient, making it impractical for plant use. Also, it gave little or no improvement in separation factor compared to lithium. If the salts are rated by their effect on separation factors (ratios of the distribution coefficients of two elements being compared), the order is the same as that just given except for Be. The very high distribution coefficients obtained with beryllium nitrate suggest that the extracted species in that case may not be the normal $M(NO_3)_3.3TBP$, but perhaps a double salt of beryllium.

The calculated separation factors from lithium nitrate and aluminium nitrate salting were averaged and are shown graphically in Fig. 6 to illustrate the divergence that occurs with increasing salt strength.

Acidity effects

The effect of varying nitric acid concentration at 1·8M aluminium nitrate is shown in Fig. 7 for extractions into 30% TBP. Additions of nitric acid sharply reduce the distribution coefficients at low acidity, and to a lesser degree at increasing acidity. Two competing effects occur when nitric acid is added: (i) Some nitric acid extracts as $TBP.HNO_3$ thus 'consuming' free TBP and depressing the actinide and lanthanide distribution coefficients and (ii) that portion of the added nitric acid that remains in the aqueous phase increases the aqueous nitrate ion activity and increases the distribution coefficients.

At low total acidity the first effect is much greater, but as the solvent approaches acid saturation the second effect becomes noticeable. Indeed, if aluminium nitrate solubility were not limiting, an extension of the distribution curves on Fig. 7 to higher acidity would show the D_a^o values turning up with increasing acidity.

As shown in Fig. 8, there is some increase in separation factors with increasing acidity, but the change is that expected from increased nitrate activity alone, which indicates that hydrogen ion activity has no separate effect on separation factors.

Temperature effects

The effect of temperature variations on distribution coefficients and separation factors was determined for both 5·4M-$LiNO_3$ and 1·8M-$Al(NO_3)_3$ from 1·0M-HNO_3. Results for the lithium nitrate are shown in Figs 9 and 10. Distri-

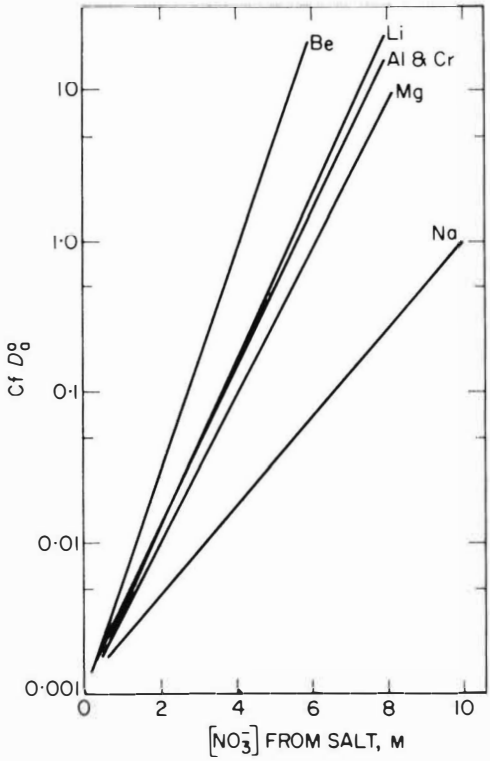

FIG. 5. *Comparison of nitrate salts on Cf distribution*
Solvent 30% TBP; acidity 1·0M-HNO_3; temperature 22°C

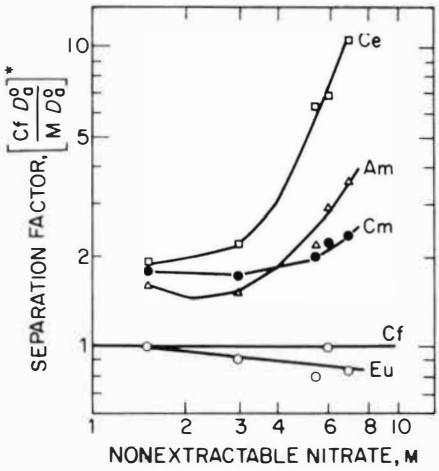

FIG. 6. *Cf Separation factors vs. salt strength*
*M is element being compared to Cf

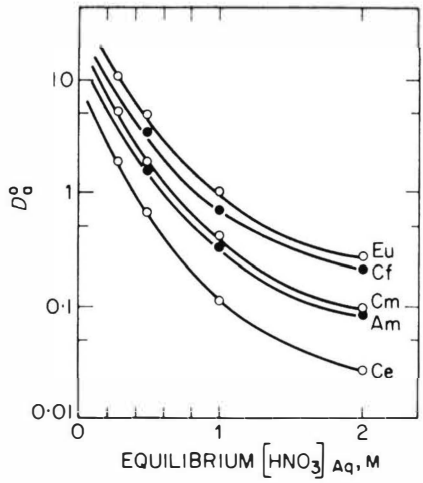

FIG. 7. *Effect of HNO_3 on* D_a^o
Salt 1·8M-$Al(NO_3)_3$; solvent 30% TBP

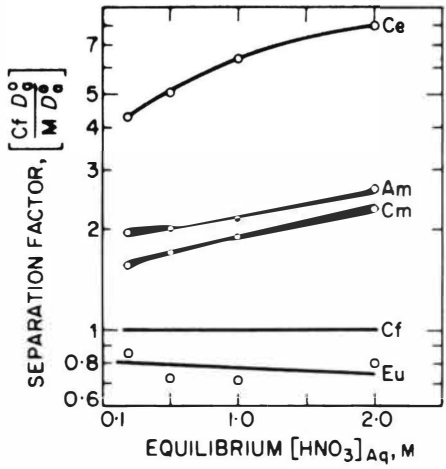

FIG. 8. *Effect of HNO_3 on separation factors*
Salt 5·4M-$LiNO_3$; solvent 30% TBP

bution coefficients declined slightly with increasing temperature, as expected. The data indicate only a slight improvement in separation factors at the higher temperatures.

TBP concentration

Previous work has established that actinide and lanthanide distribution coefficients all closely follow a third-order dependency with the TBP concentration, with little change in separation factors. Scouting tests confirmed these results, so TBP concentration was not explored in detail.

Nitric acid distribution

Measurements were made of nitric acid distribution at 22°C between 30% TBP and 1·8M-$Al(NO_3)_3$, 5·4M-$LiNO_3$, and 3·0M-$LiNO_3$. The data are presented in Fig. 11. The data for no salting, taken from Ref. 9 are also shown.

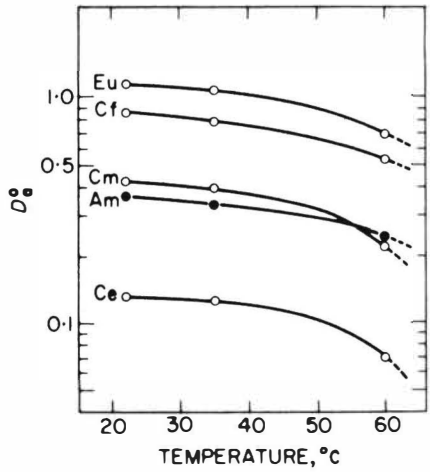

FIG. 9. *Effect of temperature on* D_a^o
Salt 5·4M-$LiNO_3$; solvent 30% TBP; acidity 1·0M-HNO_3

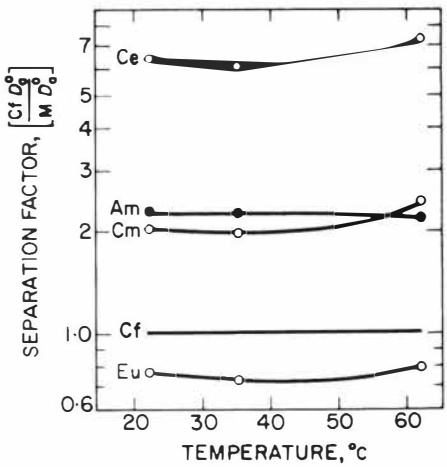

FIG. 10. *Effect of temperature on separation factors*
Salt 5·4M-$LiNO_3$; solvent 30% TBP–n–paraffin; final acidity 1·0M-HNO_3

Salt-DTPA systems

Distribution coefficients were measured in nitrate-salted DTPA solutions to see if lanthanides could be rejected in the 1B stripping bank by preferential complexation of the actinides in the aqueous phase while the lanthanides were left in the solvent.

The first work was with lithium nitrate salt which gave the results shown in Fig. 12. Without DTPA, the order of increasing D_a^o would be Ce < Am < Cm < Cf < Eu, as already shown in Fig. 9. With DTPA, the order is changed except when high acidity (low pH) diminishes the effect of DTPA and causes the D_a^o values to tend toward the order just given. Cerium, which has the highest D_a^o with DTPA and the lowest without, is the first to reach its peak with increasing acidity and to begin crossing the other curves. Presumably then, lanthanum, which has an association constant with DTPA lower than cerium,[10] will peak at a higher pH than cerium, and praseodymium, with a larger DTPA association constant, at a lower pH.

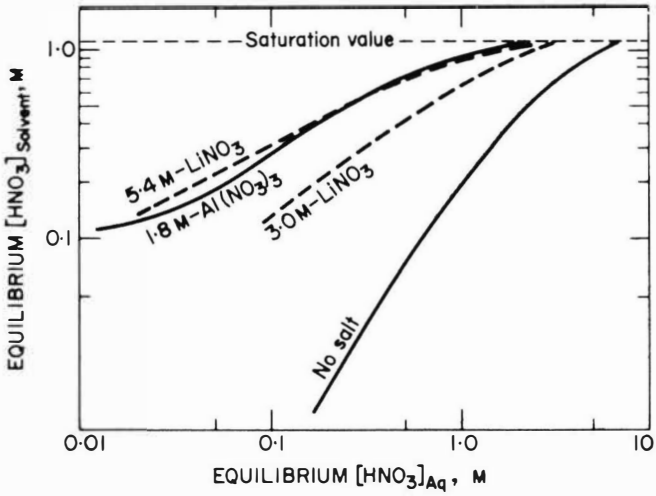

FIG. 11. *HNO_3 distribution in 30% TBP–n-paraffin*

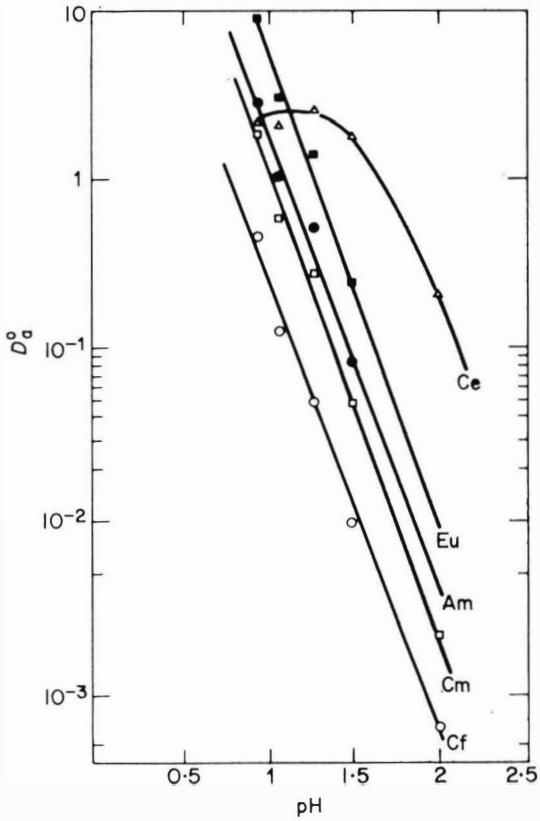

FIG. 12. *Effect of DTPA on* D_a^o

Salt 5·4M-$LiNO_3$; solvent 30% TBP; DTPA 0·05M
Separation factors: Cm/Cf 3·8; Am/Cf 7·4; Eu/Cf 17·8; Ce/Cf $\leqslant$350

At pH greater than 1·2, the separation factor between the lightest actinide, Am, and the heaviest lanthanide tested, Eu, is ~2·5. Gadolinium is the only lanthanide heavier than europium that is present to a significant extent, and, as shown in Fig. 13, its association constant with DTPA is close to that of europium. Therefore, the actinide D_a^o values will not overlap those of the lanthanides that are present.

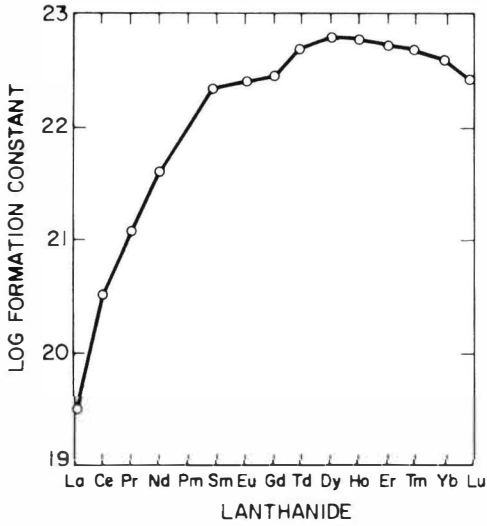

FIG. 13. *Lanthanide–DTPA formation constants*[10]

Control of pH

Separation factors in the lithium nitrate–DTPA experiments were large enough to be encouraging; however, the D_a^o values have a third-order dependence on the aqueous hydrogen ion concentration, which would require unusually close control of process feed stream acidities. The high sensitivity to pH changes is attributable to the competition between actinides (or lanthanides) and the hydrogen ion for the ionic DTPA. The salt cation, lithium, has a relatively weak association with DTPA and does not greatly affect the competition. However, competition from the hydrogen ion (and therefore sensitivity to pH change) can be substantially reduced by salting with aluminium nitrate, which buffers by hydrolysis. This buffering action is illustrated in Fig. 14. However, aluminum nitrate salting causes the crossover of cerium to occur at higher pH, thus restricting the pH range for acceptable operation. For example, the 0·8M aluminum nitrate experiments on Fig. 15 show that separation of Am from Ce is not possible below pH 2. Aluminum will begin to precipitate near pH 3, so the operable pH range lies somewhere between 2 and 3. At lower concentrations of aluminum nitrate the acceptable pH range is larger but, as also shown in Fig. 15, the absolute levels of D_a^o are becoming too low for practical use with the flow ratios available. Additions of lithium nitrate or sodium nitrate to raise the absolute D_a^o caused the cerium value to decrease relative to the others, thus defeating the objective. One experiment at 50°C indicated that the increased temperature also gave lower relative Ce distribution coefficients. However, use of 50% TBP maintained the separation factors and increased the absolute D_a^o values by a factor of 2·6 at an aqueous pH of 2·0.

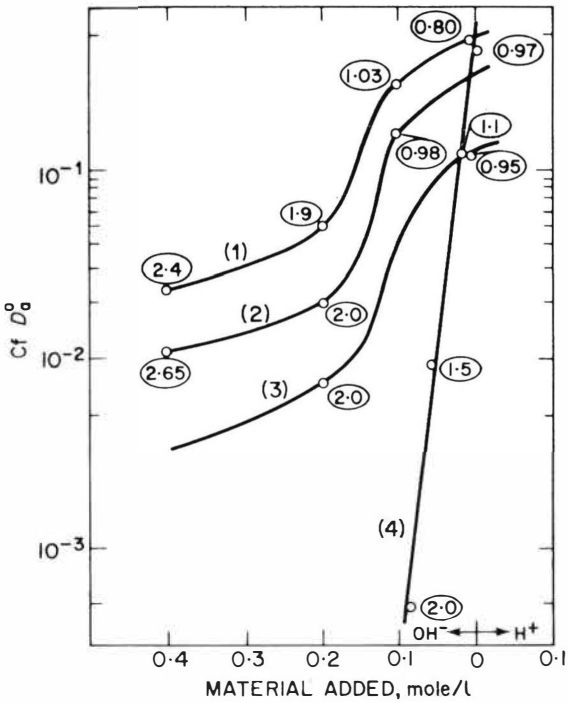

FIG. 14. *Effect of additions of acid or base on Cf* D_a^o

Ringed numbers indicate pH; DTPA 0·05M
(1) 0·8M Al^{3+}–30% TBP; (2) 0·6M Al^{3+}–50% TBP;
(3) 0·6M Al^{3+}–30% TBP; (4) 5·4M Li^{+}–30% TBP

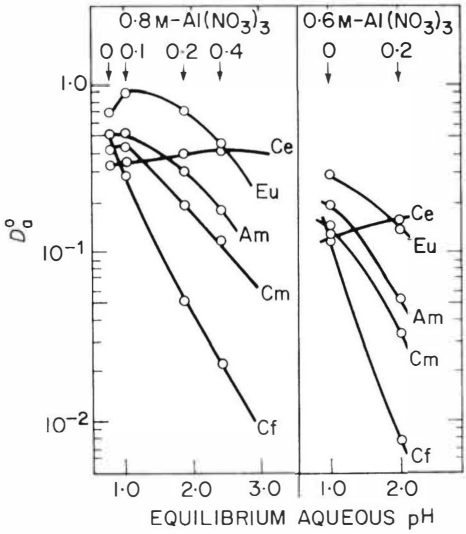

FIG. 15. *Actinide–lanthanide* D_a^o

Salt $Al(NO_3)_3$; solvent 30% TBP–Ultrasene; DTPA 0·05M
Arrowed numbers at the top represent moles of LiOH added to adjust pH

Flow-sheet: calculations

The work on salt and DTPA–salt systems showed that reasonable degrees of separation could be attained between actinides and significant fission product lanthanides. Calculations were made, parallel to the laboratory programme, to determine potential flow-sheets that might be suitable for plant extraction conditions with 18-stage centrifugal 1A bank and the 18-stage mixer–settler 1B bank. For the 1A bank, the separation of Cm and Ce was calculated under a variety of conditions in an aluminium-salted flow-sheet. Ce was picked because it is so representative of the light lanthanides that have distribution coefficients lower than those of the actinides and that should be rejected to the aqueous raffinate. For the 1B bank, the separation of Am and Eu was calculated in a DPTA–$LiNO_3$ salted flow-sheet in this case, Am is the most extractable of the actinides to be stripped and Eu is the least extractable of the intermediate lanthanides that should not be stripped from the organic.

Details

The Fortran IV computer code developed by Lowe[12] was adapted to allow systematic exploration of operating variables. Distribution coefficients were correlated as functions of aqueous acid (H_a) or pH from the experimental work of the previous section. Conditions and assumptions for computer input are given below:

Computer input bases

Acid equilibrium data were taken from Fig. 11 and presented to the computer in tabular form.

1A Bank.
- 18 centre-fed stages
- 80% stage efficiency
- 30% TBP organic phase
- 1·8M-$Al(NO_3)_3$ aqueous phase
- Distribution coefficients, D_a^o
  - Below 0·5M aqueous acid:
    - For curium, $\ln D_a^o = 3{\cdot}24 - 5{\cdot}29\ H_a$
    - For cerium, $\ln D_a^o = 2{\cdot}21 - 5{\cdot}29\ H_a$
  - Above 0·5M aqueous acid:
    - For curium, $\ln D_a^o = -2{\cdot}17 \ln H_a - 0{\cdot}913$
    - For cerium, $\ln D_a^o = -2{\cdot}40 \ln H_a - 2{\cdot}09$

1B Bank.
- 18 centre-fed stages
- 80% stage efficiency
- 30% TBP organic phase
- 5·4M-$LiNO_3$–0·05M-DTPA aqueous phase
  - Distribution coefficients:
    - For americium, $\ln D_a^o = 7{\cdot}65 - 6{\cdot}64$ pH
    - For europium, $\ln D_a^o = 8{\cdot}52 - 6{\cdot}64$ pH

For the 1B bank calculation, the base case assumed an input acid of 0·45M in the 1AP organic stream (based on a tenative 1A flow-sheet). In addition, the material balance on acid in the organic phase in the 1B bank requires that all hydrogen donors in the DTPA–$LiNO_3$ aqueous phase be considered and not just free acid. The total exchangeable hydrogen ion, here designated ΣH, in molar terms is:

$$\Sigma H = 5(DTPA) + HNO_3 \text{ added} - LiOH \text{ added}$$

The equilibrium relationship between aqueous ΣH and free hydrogen ion concentration was determined experimentally and is shown in Table III. The equilibrium relationship of organic acid to aqueous hydrogen ion concentration

was then assumed to be that shown in Fig. 11 for 5·4M-$LiNO_3$. Both relationships were presented to the computer in tabular form.

TABLE III

Free hydrogen ion and total exchangeable hydrogen ion in the 5·4M-$LiNO_3$ – 0·05M-DTPA *system*

H^+, M	ΣH, M	
0	0	
0·000355	0·126	
0·00479	0·157	
0·00794	0·163	
0·0151	0·176	
0·0251	0·188	
0·0339	0·200	
0·0525	0·219	
0·0631	0·225	
0·0794	0·238	
0·0955	0·250	
0·11	0·265	extrapolated
0·14	0·290	extrapolated

1A Bank results and process stability

The loss of curium in the aqueous waste (1AW) and the decontamination of cerium from the organic product (1AP) are shown in Fig. 16 as a function of the 1AX organic extractant flow and the 1AS aqueous scrub flow and acidity. The effects of the other two major process parameters, the 1AF feed flow and acidity, are shown in Fig. 17 to avoid confusion from overlying curves. The numbers on the curves indicate the value of the parameter and the resulting performance when that parameter alone is changed from the conditions shown for the reference point.

The sensitivity of the process to changes in these parameters is apparent from inspection; for example, a 0·05M increase (12·5%) in 1AS acid causes almost a ten-fold increase in cerium DF and a six-fold increase in curium loss. It also is apparent that the performance is much more sensitive to variations in some parameters than others. For example, on Fig. 17, a 25% increase (0·4–0·5M) in 1AF acid gives about the same effect as a 50% increase (1·0–1·5) in 1AF flow.

The sensitivity of performance to changes in the parameters is very important in evaluating and comparing flow-sheets, so a gauge that reflects the sensitivity was derived. On the figures, the total displacement along a logarithmic curve (involving changes in both DF and loss) for a given change in a parameter is a measure of the process response. This displacement, when measured with the log scale, corresponds to a ratio, which will be called the response ratio.* The stability coefficient, S, for a given process parameter will then be defined arbitrarily as the change in the parameter, expressed as relative percentage, that produces a response ratio of 2, i.e., a shift along a parameter line equivalent in length to a factor of 2 on the log scale. The locus of points for a response ratio of 2 is shown in Fig. 16 for changes from the central points.

* The response ratio, caused by a change in a given parameter is related to losses and DFs before and after the change as follows:

$$\log R_p = \sqrt{\left(\log \frac{L_2}{L_1}\right)^2 + \left(\log \frac{D_2}{D_1}\right)^2}$$

where R_p = response ratio, L_1 and L_2=initial and final curium losses, D_1 and D_2 = initial and final cerium DFs.

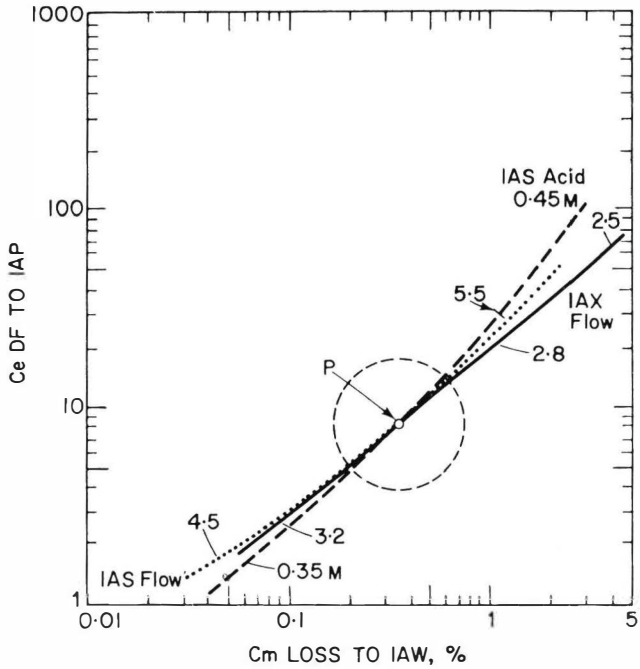

FIG. 16. *Effect of scrub and extractant on separation of curium and cerium*
30% TBP

	To Stage	Base conditions at P Flow	Acid	$Al(NO_3)_3$
IAS Aqueous	1	5·0	0·4M	1·8M
IAF Aqueous feed	10	1·0	0·4M	1·8M
IAX Organic	18	3·0	0	0

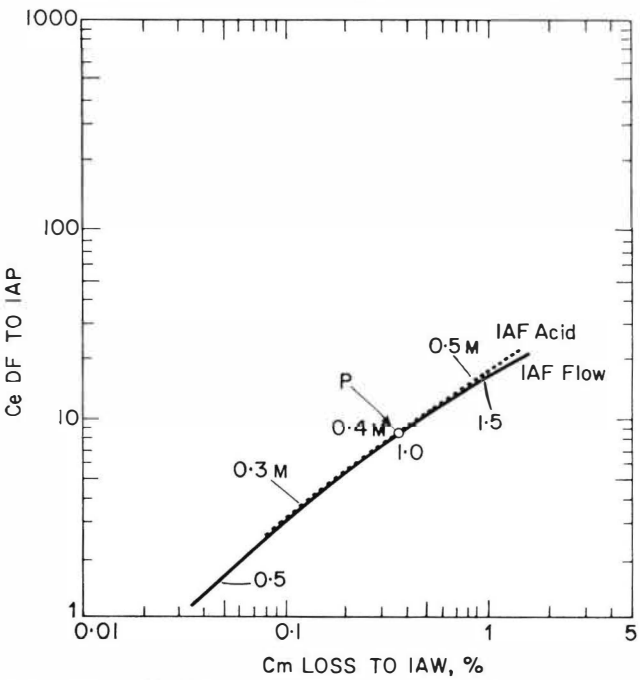

FIG. 17. *Effect of feed flow and acidity on separation of curium and cerium*
Base conditions at P as in Fig. 16

To a first approximation, the process stabilities can be calculated directly as a proportion from calculated points on the response curve. In the example cited previously, a 0·05M (12·5%) increase in 1AS acid gives a response ratio of 17, so the stability coefficient, S, equals (12·5%) (log 2/log 17) = 3·1%. To be strictly correct, however, the stabilities for a response ratio of 2 should not be deduced by proportion from a larger change. This is particularly true for those cases in which the stabilities for positive and negative changes from the central point differ significantly. The simplified calculation of stability is quite adequate, however, to illustrate the difference between parameters for this process and for comparison of this process with others currently operating.

The process stabilities derived from the 1A bank calculations are given in Table IV for each of the major process parameters and for conditions larger and smaller than those at the central point. The process stabilities can be seen to be greatest for the two parameters that are the most difficult to control, 1AF flow and acidity, and least for the three cold-stream parameters that are the easiest to control, 1AS flow and acidity and 1AX flow. From the standpoint effect of the parameters relative to one another, these are good flow-sheet conditions.

TABLE IV

Process stabilities for separation of curium and cerium in 18 stages

Parameter	Change		Response ratio, R_p	Estimated stability coefficient, %	Average stability coefficient, %
	From	To			
1AS flow	5·0	5·5	5·6	4·0	3·3
	5·0	4·5	14·2	2·6	
1AS acidity	0·40M	0·45M	17·0	3·1	3·3
	0·40M	0·35M	12·2	3·5	
1AF flow	1·0	1·5	4·0	25·0	19·2
	1·0	0·5	13·3	13·4	
1AF acidity	0·4M	0·5M	3·6	13·5	12·6
	0·4M	0·3M	4·4	11·7	
1AX flow	3·0	3·2	6·3	2·5	2·8
	3·0	2·8	4·3	3·2	

Process improvements in the 1A bank require movement on Figs 16 and 17 in the direction of lower curium loss and higher cerium DF. However, this direction is at a right angle to the bunched parameter lines and few process changes can be made to move in that direction; any that are made result in even less stability. As an example, 1AW waste volume can be decreased and cerium DF increased by decreasing the 1AS flow to 4·5 and increasing the 1AS acidity to 0·45M as shown in Fig. 18. The stability to changes in the 1AS acid and 1AS flow under these conditions decreases by ~20% to a stability coefficient of 2·5% for each. As an extreme example in the direction of lower 1AW waste volume, the following high-acid flowsheet was considered briefly:

Stream	Flow	Acid	Cm loss, %	Ce DF
1AS	0·25	1·2M	—	—
1AF	1·00	1·25M	0·6	21
1AX	1·67	0	—	—

A 4% increase in 1AF acidity to 1·30M increases the curium loss to 29·9% and the cerium DF to 500 which corresponds to a process stability coefficient of 0·55%. This flow-sheet, then, is 25 times more sensitive to changes in 1AF acidity then the Fig. 16 flow-sheet.

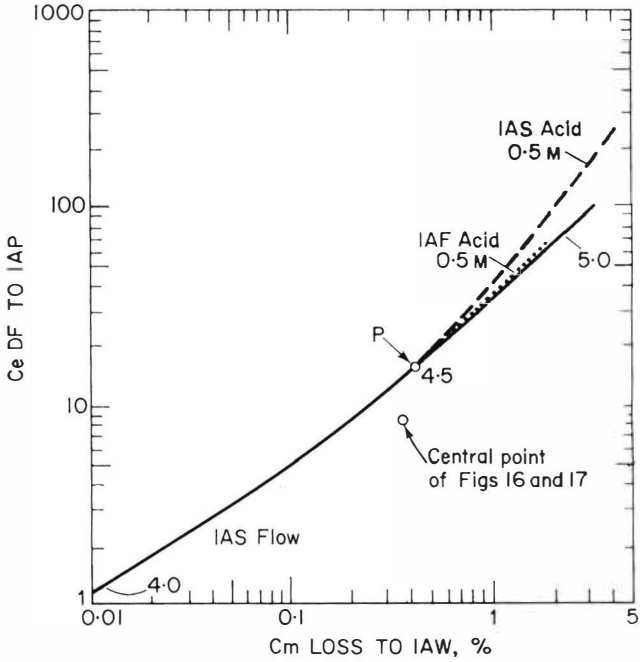

FIG. 18. *Effect of 1AS scrub stream on separation of curium and cerium*

	Base conditions at P Flow	Acid
1AS	4·5	0·45M
1AF	1·0	0·40M
1AX	3·0	0

1B Bank results

The effects of changes in the organic flows and organic feed acidity on the distribution of americium and europium between the two exit streams is shown in Fig. 19. To avoid confusion from overlying curves, the effects of changes in the other two major parameters, aqueous extractant flow and ΣH, are shown in Fig. 20. Also on Fig. 20, for illustration, is the locus of points that would correspond to a response ratio of 2 relative to the base point in the middle.

TABLE V

Stability coefficients for separation of americium and europium

Parameter	Change* (C), %	Response ratio, R_p	Estimated stability coefficient (S)**, %	Average stability coefficient, %
1BX flow	+3·6	2·8	2·5	2·4
	−3·6	3·0	2·3	
1BX ΣH	+5·6	3·6	3·0	3·3
	−5·6	2·9	3·6	
1AP flow	+10·0	5·1	4·3	4·4
	−10·0	4·6	4·5	
1AP acid	+4·4	3·0	2·8	3·0
	−4·4	2·7	3·2	
1BS flow	+8·3	2·7	5·8	5·7
	−8·3	2·9	5·5	

*Change from conditions at central points of Figs 19 and 20

$**S = C\left(\frac{\log 2}{\log R_p}\right)$.

By the previous definition, the stability coefficients of the 1BX ΣH and flow would be the changes in these parameters (expressed as percentages) that would shift performance to the intersection of the circle and the parameter line.

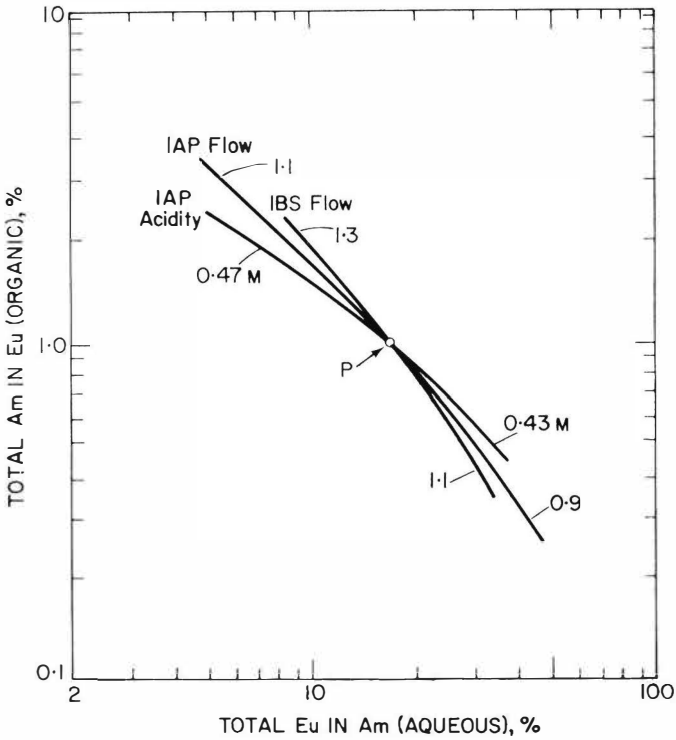

FIG. 19. *Effect of organic flows and feed acidity on separation of americium and europium*

	Base conditions at P		
	To stage	Flow*	ΣH or Acidity
1BX Aqueous extractant	1	5·5	0·18 (pH = 1·73)
1AP Organic feed	10	1·0	0·45M
1BS Organic scrub	18	1·2	—

*Volume flow relative to 1AP = 1·0

As in the 1A bank case, the direction of improvement (lower Am in Eu, lower Eu in Am) is at right angles to the parameter lines and no large improvement can be achieved.

The stability coefficients for this bank, given in Table V are only slightly less than those presented earlier for the 1A bank.

Stabilities of existing operations

The process stability coefficients for two existing operations in enriched uranium processing were calculated for comparison with the actinide–lanthanide flow-sheets. The operations selected were the 1B bank, where neptunium is separated from enriched uranium, and the second neptunium cycle 2A bank, which operates with an oxidising flow-sheet for the separation of neptunium and thorium. The stabilities for the two operations are given in Table VI. The least of the stability coefficients in Table VI is about twice as great as that for actinide separation.

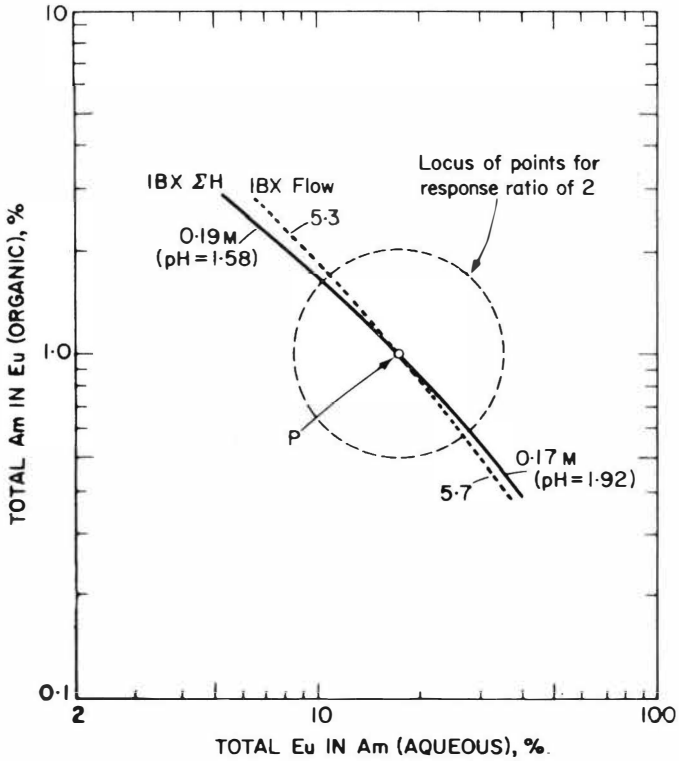

FIG. 20. *Effect of aqueous extractant flow and acidity on separation of americium and europium*

Base conditions at P as in Fig. 19

TABLE VI

Process stabilities for existing operations

1B bank, neptunium–uranium separation

Parameter	Change, M From	Change, M To	Response ratio, R_p	Estimated stability coefficient, %	Average stability coefficient, %
1BX acidity	2·75	3·25	4·4	8·5	7·2
	2·75	2·25	8·5	5·9	
1BX flow	0·84	1·00	3·0	12·0	11·5
	0·84	0·70	2·9	10·9	
1BS flow	2·45	2·90	2·3	15·7	14·3
	2·45	2·00	2·7	12·8	
2A bank, neptunium–thorium separation					
2AF acidity	2·2	2·5	3·7	7·2	6·9
	2·2	1·8	7·0	6·5	
2AS acidity	0·5	0·6	4·5	9·2	8·2
	0·5	0·4	7·0	7·1	
2AS flow	80	90	4·5	5·8	5·8
	80	70	4·4	5·9	
2AX flow	270	300	4·4	5·2	5·1
	270	245	3·6	5·0	

Conclusions

The calculations show that the 18-stage 1A bank, with the 1·8M-$Al(NO_3)_3$–30% TBP system, is limited to a cerium rejection of 90–95% at a curium loss of 1%. Reasonable rejection also would be expected for La and Pr, the lanthanides adjoining Ce, with little discrimination from higher lanthanides.

The 1B bank, with the 5·4M-$LiNO_3$–0·05M-DTPA–30% TBP system, can reject perhaps 80%–85% of the europium at an americium loss of 1%. In this case, however, there should be better separation from the lanthanides that lie between Ce and Eu, which are the ones that constitute a large fraction of the fission product lanthanides. The cerium crossover as a function of pH would work against good decontamination from Ce (and La) in the 1B bank alone. However, the combined effect of separations in both the 1A and 1B bank should be a large change in the lanthanide-actinide ratio that should ease the ion exchange load when long-irradiated ^{239}Pu fuel is processed.

These bank operations will require a high degree of control of process parameters. The actinide–lanthanide separations are a factor of 2–3 more sensitive to changes in the operating conditions than normal operations, but the control problems do not appear insurmountable.

Acknowledgment

Information in this paper was developed during the course of work under Contract AT(07-2)-1 with the U.S. Atomic Energy Commission.

References

[1] Henry, H. E., *Rep. Congr. atom. Energy Commn U.S.*, 1965, DP-972
[2] Baybarz, R. D., Weaver, B. S., & Kinser, H. B., *Nucl. Sci. Engng*, 1963, **17**, 457
[3] Hale, W. H., & Lowe, J. T., *Inorg. nucl. Chem. Lett.*, 1969, **5**, 363
[4] McKay, H. A. C., Alcock, R., & Searight, D., *Rep. U.K. atom. Energy Auth.*, 1954, AERE C6R 1524
[5] Peppard, D. F., Driscoll, W. J., Sironen, R. J., & McCarty, S., *J. inorg. nucl. Chem.*, 1957, **4**, 326
[6] Peppard, D. F., Faris, J. P., Gray, P. R., & Mason, G. W., *J. phys. Chem., Ithaca*, 1953, **57**, 294
[7] *Rep. Congr. atom. Energy Commn U.S., A. Prog. Rep. chem. tech. Div.*, May 31, 1953, ORNL-3452
[8] Weaver, B., & Kappelmann, F. A., *J. inorg. nucl. Chem.*, 1968, **30**, 263
[9] Codding, J. W., Haas, W. O., & Heumann, F. K., *Rep. Congr. atom. Energy Commn U.S.*, 1951, KAPL-602
[10] Moeller, T., & Thompson, L. C., *J. inorg. nucl. Chem.*, 1962, **24**, 499
[11] *Spec. Publs chem. Soc.*, 1964, No. 17
[12] Lowe, J. T., *Ind. Engng Chem. Process Des. Dev.*, 1968, **7** (3), 362

Optimised use of multi-purpose fuel processing facilities at the Idaho Chemical Processing Plant*

by R. D. Modrow, G. F. Offutt and B. R. Wheeler

Idaho Nuclear Corporation, P.O. Box 1845, Idaho Falls, Idaho 83401, U.S.A.

Three cycles of solvent extraction are used at the Idaho Chemical Processing Plant (I.C.P.P.) for purifying highly enriched uranium generated from reprocessing highly radioactive fuel elements in various head-end facilities. The first cycle of extraction usually uses tributyl phosphate (TBP) in this multi-purpose plant, and is followed by two extraction cycles using methyl isobutyl ketone (MIBK). Use of different solvents permits advantage to be taken of their respective characteristics for separating fission products from uranium.

Five head-end systems are currently available for dissolving spent fuel elements. Currently, these systems at the I.C.P.P. are operated sequentially, along with a waste solidification facility, to permit optimum use of manpower and facilities, to result in the lowest possible reprocessing costs. This type of alternating operation is believed ideal for a multi-purpose plant and in fact would be highly satisfactory for a single-purpose plant.

Introduction

NUMEROUS REPROCESSING PLANTS for spent nuclear fuels will be required in the 1980s to handle increasing amounts of spent fuel from commercial installations. The U.S.A. already has three commercially owned reprocessing plants that are operating or being constructed, in addition to three government-owned reprocessing plants being operated for the U.S. Atomic Energy Commission by contractor personnel. One of these plants, the Idaho Chemical Processing Plant (I.C.P.P.) is a highly versatile multi-purpose plant having a broad range of capabilities to handle many different types of fuel.

Multi-purpose fuel reprocessing plants are designed to maximise flexibility, and a common method to achieve this is to use several head-end dissolution systems with common extraction, packaging and waste storage systems. Little has been reported about how multi-purpose plants are operated to achieve optimised performance.

The I.C.P.P. is capable of processing a wide variety of reactor fuels including aluminium, zirconium, and stainless-steel alloyed fuels, clad fuels, and thorium fuels containing uranium of various enrichments and concentrations. Furthermore, this plant has facilities to handle special shapes of fuels, to convert waste solutions to solids, and to recover some isotopes and rare gases when desired. Although the plant was originally designed for high-enrichment fuels, modest quantities of low-enrichment fuels can be readily processed. Plutonium cannot currently be recovered because the I.C.P.P. lacks the packaging facilities and ventilation safeguards necessary with this material.

This paper describes the I.C.P.P. and the techniques used in its operation. In brief, sequential-type operation used at I.C.P.P. with various systems permits optimum use of manpower and facilities resulting in lowest possible reprocessing costs. This type of operation also appears ideal for other multi-purpose plants, and should be highly satisfactory for a single-purpose plant.

I.C.P.P. processes

During fuel element reprocessing at the I.C.P.P. a series of aqueous processing steps are generally used, as shown in Fig. 1. The first involves dissolution of the fuel in an acid, after which the resulting solution is processed through several cycles of counter-current solvent extraction to separate and purify the uranium. The product from the final extraction cycle is uranyl nitrate solution

*Work performed under the auspices of the United States Atomic Energy Commission, Contract AT(10–1)–1230.

with fission products removed almost to background level. This solution is generally denitrated in a fluidised bed unit to uranium trioxide for product shipment.

Usually, but not necessarily, the first extraction cycle at I.C.P.P. uses tributyl phosphate (TPB) in a kerosene diluent as the extractant because the composition requirements of a suitable dissolver product stream for TBP are less stringent than for methyl isobutyl ketone (MIBK). This is followed by two extraction cycles using MIBK. Use of different solvents permits advantage to be taken of their respective characteristics for separating fission products from uranium; MIBK is more effective for zirconium, whereas TBP is more effective for ruthenium.

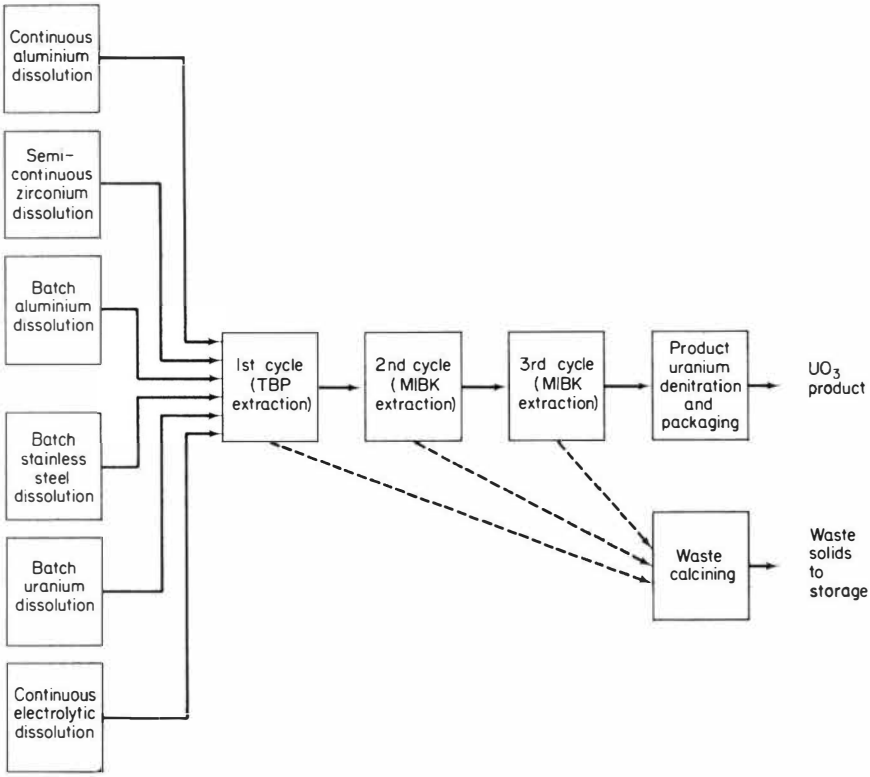

FIG. 1. *Schematic diagram of I.C.P.P. fuel and waste processes*

Dissolution

Dissolution requirements, reagent compositions, and dissolving conditions are highly dependent on the metals used in the fuel element cladding and matrix; the metals generally consist of aluminium, zirconium, or stainless steel. Five head-end systems are available at the I.C.P.P. for dissolving spent fuel elements. The most commonly used is a continuous nitric acid system having a capacity to handle that uranium associated with about 500 kg Al/day. The other dissolver systems include an hydrofluoric acid system (600 kg Zr/day), a sulphuric acid system (50 kg of stainless steel/day), a nitric acid system (for unalloyed highly enriched uranium), and a second (non-continuous) aluminium alloy–nitric acid system. A sixth head-end system currently being installed is an electrolytic dissolution process for stainless steel-clad or matrix fuels. A seventh system, which is a non-aqueous head-end process for graphite-based fuels, is in the development stage.

First cycle extraction

The uranium in the dissolver product solution, which in the case of aluminium fuels consists of uranyl nitrate, aluminium nitrate, and fission product nitrates, is isolated by contacting the liquid with TBP in counter-current extraction columns. The liquids from the hydrofluoric and sulphuric acid dissolutions are complexed with aluminium nitrate and nitric acid, respectively, so that they may be processed without excessive corrosion through the same stainless-steel extraction system. During extraction, the uranyl nitrate is preferentially dissolved in the organic material which is subsequently contacted with water to remove the uranyl nitrate. A schematic diagram of this extraction cycle is shown in Fig. 2.

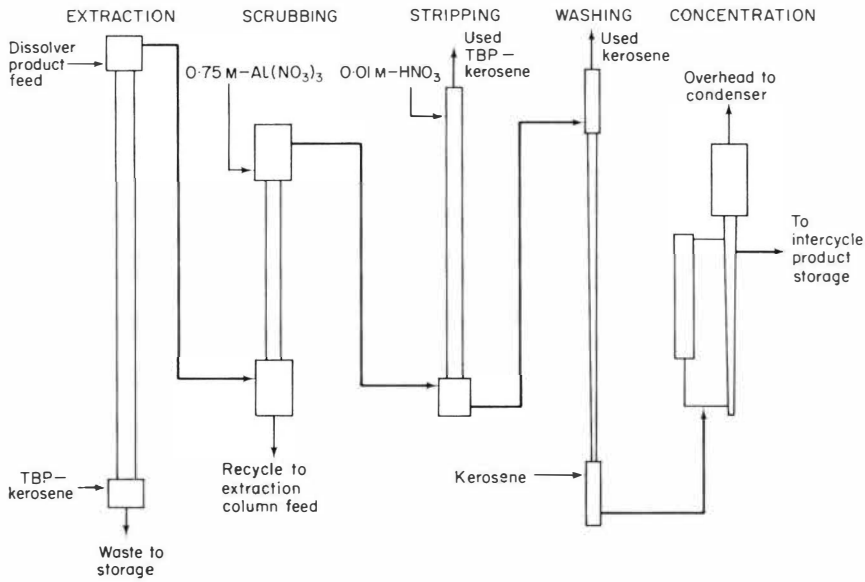

FIG. 2. *Schematic diagram of first (TBP) extraction cycle*

Dissolver solution from the various head-end systems enters the top of the first extraction column where the uranium and some acid are extracted away from the aluminium and the bulk of the fission products. 5% TBP in a kerosene diluent is commonly used as the extractant at I.C.P.P. The organic stream, containing the uranium, flows to the scrubbing column where it is contacted with aluminium nitrate solution to remove fission products and nitric acid. The spent scrubbing stream, containing a small amount of uranium, is recycled to the extraction column feed. Uranium in the organic stream leaving the scrubbing column is back-extracted into the aqueous phase in the stripping column with a dilute nitric acid stream. Prior to concentration, the stripping column product stream is washed in a fourth column with kerosene to remove dissolved TBP. The concentrated product from the evaporator may be fed directly to the second extraction cycle or placed in intercycle storage.

Nuclear safety is maintained in the first extraction cycle by making frequent rate checks of the organic stream to the extraction column, limiting the ^{235}U throughput to 1·6 kg/h (before burn-up basis), and limiting the TBP concentration. The controlling item is the head of the extraction column which has a minimum critical ^{235}U concentration limit of approximately 26 g/l. This is based on an 8-in thick layer (approximately 60 l) of solvent in the head. The solubility of ^{235}U in 5% TBP in kerosene is approximately 20 g/l so safety is assured.

Aluminium nitrate is used as a scrubbing agent in the scrubbing column rather than nitric acid, equally suitable for scrubbing fission products, because it is desirable to minimise the amount of acid that is carried over by the organic stream to the stripping column (the presence of significant quantities of acid in the column would make it more difficult to strip uranium into the aqueous phase). Separate extraction and scrubbing columns are used rather than a single combined extraction–scrubbing column because of limited cell heights at I.C.P.P. Pulsed sieve plate columns are used although mixer-settlers and other contactors would also be applicable. Calculated and actual lengths for the columns are given in Table I.

TABLE I

Typical data for I.C.P.P. solvent extraction (TBP) columns

Column	Height of a transfer unit (*HTU*), ft	Active length of column, ft	Number of transfer units (*NTU*) required	Column i.d., in
Extraction	~2·1	23	10	10
Scrubbing	~2·3	10	4	8
Stripping	~1·3	14	10	9

Plutonium and neptunium present in the dissolver product stream in the tetravalent state are extractable under the TBP first cycle conditions. These materials are reduced with ferrous sulphamate in later extraction cycles and are partitioned from the uranium at that time.

Aluminium nitrate waste solution from the TBP extraction column is stored for eventual calcination. The TBP in kerosene from the stripping column is continuously washed in three mixer-settlers for recycle to the process. The first and third washes use 0·04M nitric acid; the second wash uses 0·5M sodium carbonate. The contact time in each mixer-settler is about 30 min. Spent kerosene from the wash column and spent TBP–kerosene from extraction are steam-stripped to remove fission products and plutonium, and then they are burned in an incinerator.

Intercycle product storage

Intercycle storage for the TBP cycle product consists of geometrically safe vessels (12·7 cm i.d.) for aqueous uranium solutions. The storage capacity is approximately 4800 l and is equivalent to about 50 days of hold-up for normal I.C.P.P. operation. Solution from this storage is fed to the second and third cycle extraction systems.

Second and third cycles of extraction

The second and third extraction cycles at I.C.P.P. use MIBK as the extractant. The aqueous product stream from intercycle storage is fed to the first column of the second cycle system at about midheight, as shown in Fig. 3. The aqueous stream then flows down the column counter-current to a stream of MIBK flowing up the column. The MIBK stream entering the bottom of this compound column passes first through an extraction section and then a scrubbing section. A relatively large volume of scrubbing solution introduced at the top of the column provides a salting agent, aluminium nitrate, to force the uranium in the extraction section of the column into the organic phase. Also entering with the scrubbing solution is sufficient ammonium hydroxide to create an acid-deficient condition in the extraction part of the column for improving decontamination of uranium from fission products. The uranium in the MIBK phase leaving the first column flows to a stripping column. Here, the uranium is back-extracted into an aqueous phase with a dilute nitric acid stream. Feed is prepared for the third extraction cycle by concentrating the aqueous stream in an evaporator. The third extraction cycle is similar in most

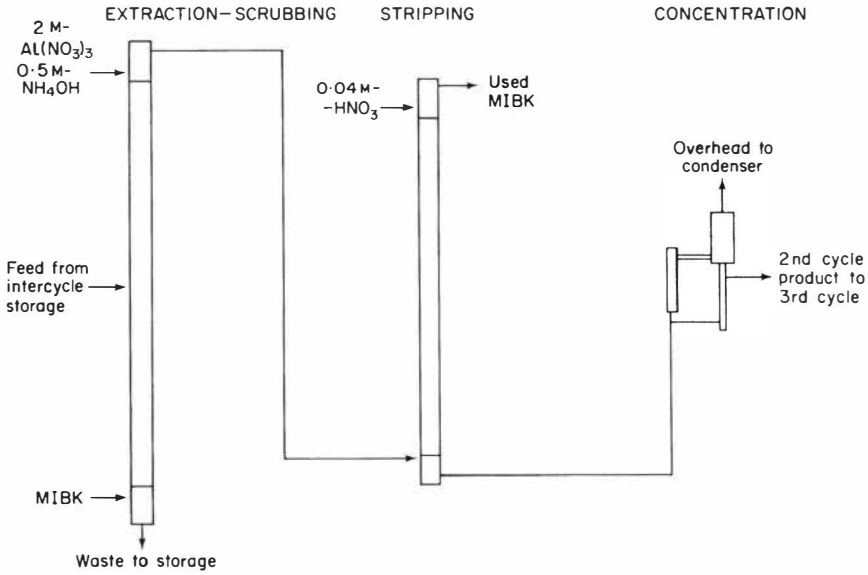

FIG. 3. *Schematic diagram of second (MIBK) extraction cycle*

respects to the second cycle and includes an evaporator in which the product solution is concentrated to about 1·5M uranyl nitrate for convenience in the subsequent denitration step using a fluidised bed denitrator.

Plutonium and neptunium follow a path similar to that of the fission products in the second and third extraction cycles. Ferrous sulphamate is added to the second cycle scrubbing stream to reduce the plutonium and neptunium to relatively inextractable valence states. Similar reducing agents may also be used in the third extraction cycle for the same purpose if additional α-decontamination is required to meet uranium product specifications; however, an available fourth extraction cycle free of ferrous ion is necessary in this case to prevent the product from being contaminated with iron.

Spent MIBK from the columns is treated with a small volume of 3·0M sodium hydroxide and then steam distilled to remove decomposition products and fission product contamination. The solvent is then recycled to the process.

The columns in the second and third cycle systems are packed with $\frac{3}{8}\times\frac{3}{8}$ in stainless-steel Raschig rings. All of the columns are 5 in o.d., small enough in diameter to be nuclearly safe under all operating conditions. Calculated and actual lengths of the columns are given in Table II. Aqueous outflow from the columns is controlled by air pressure applied to a discharge loop on each column.

TABLE II

*Typical data for I.C.P. solvent extraction (MBIK) columns**

Column	Height of a transfer unit (*HTU*), ft	Active length of column, ft	Number of transfer units (*NTU*) required
Extraction–scrubbing	~2·8	31	10
Stripping	~1·8	21	11

* Equipment in the second and third cycle processes is essentially identical

Waste storage

Aqueous waste solutions from the extraction cycles and other fuel processing operations are transferred to large volume stainless-steel tanks for interim

storage of 3–5 years before being calcined to a solid. The high-activity level waste solutions from the first extraction cycle are kept separated from the second- and third-cycle wastes. Various types of wastes are further segregated according to the acid type, i.e., nitric acid, hydrofluoric acid, and sulphuric acid.

Waste calcination

At the I.C.P.P. the Waste Calcining Facility (WCF) is used to convert radioactive waste solutions into solids which are more economical and significantly safer to store. Solution storage is now viewed as an interim means of storing wastes, and calcination is viewed as a means of converting fission products to a form desirable for long-term storage. The heart of the WCF is a well-fluidised, heated bed of granular solids. The waste solution is sprayed into the fluidised bed and coats the particles; water vapour and volatile gases flash from the spray droplets leaving the residual metal oxides uniformly deposited on bed particles. The spheroidal granular particles, ranging in diameter from 0·1 to 1·5 mm, are continuously removed from the calciner and pneumatically transported to storage facilities. With calcination, waste volumes are consistently decreased by a factor of about 10. Net processing rates are usually around 250–350 l/h.

Sequential operation

For a number of years the I.C.P.P. extraction facilities have been operated sequentially to achieve optimum use of manpower. With sequential operation, as an example, the continuous aluminium dissolution process and the first extraction cycle (TBP) are operated concurrently until the intercycle product storage tanks are filled. Then the second and third extraction cycles (MIBK) and product denitration and packaging are operated concurrently until the intercycle storage is emptied. During this time, the dissolution systems and first extraction cycle are in standby. When a fuel processing campaign is completed by alternate operation of the dissolution–TBP extraction and the MIBK–product packaging systems, the WCF is operated to convert waste solution to solids. This type of alternating operation, depicted schematically in Fig. 4, is believed ideal for a multi-purpose plant because maximum use is

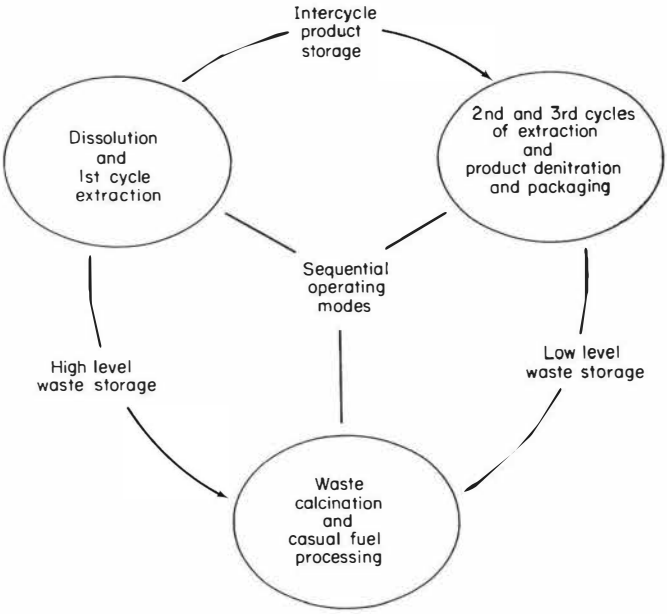

FIG. 4. *Sequential operating modes for I.C.P.P.*

made of manpower; the operating crew is sized solely for sequential-type operation of the fuel processing facilities.

During operation of the WCF, extra operations people are usually available. During this time, casual fuel processing operations can be accomplished. At I.C.P.P., casual fuel processing can involve the dissolution of significant quantities of fuel that require special handling because of hazardous or insoluble additives, special accountability requirements, or slow reaction rates. Batch dissolver systems as well as a hot cell with remote manipulators and shielding windows can be used at I.C.P.P. for fuels requiring special handling. The resulting dissolver solutions and salvage solutions from decontamination operations can be processed through the necessary extraction cycles as part of the casual operations or stored for a regular extraction campaign. In addition, the extraction systems might be operated on a casual basis to recover ^{237}Np from waste raffinate solutions.

At some point in time, the anticipated fuel load and waste inventory at I.C.P.P. will be sufficiently large to make concurrent operation of the fuel and waste processing facilities necessary to keep waste inventories within bounds. At that time, the operating crew will be enlarged sufficiently to permit operation of the WCF simultaneously with sequential operation of the fuel processing facilities. Thus, a dissolution head-end and the first cycle extraction systems could be operated simultaneously with the WCF until the intercycle storage was filled. Then, the WCF operation would continue while the second- and third-cycle extraction and product packaging systems were operated.

Sequential operation of a single-purpose plant is possible also. In this case, it is highly probable that only the fuel processing and waste solidification facilities would be operated alternately to yield the most efficient type of process. In this case, the waste solidification facility would probably be designed to process the necessary waste solution in about 2 months' time; during waste processing, necessary maintenance, repairs, and modifications to the plant facilities could be made.

Commercially owned fuel reprocessing plants for power reactor fuel must be designed and built with over-capacity to be eventually economic. Thus, for a time, these plants probably must be operated at a reduced rate until a sufficient fuel load is available for full rate. During this early period, sequential-type operation of the extraction and dissolution facilities could be economically advantageous to minimise manpower requirements.

Other strategies used to optimise economics

In addition to sequential operation and casual processing, various other strategies are used to maximise output at I.C.P.P. and thus optimise the processing economics. The techniques include: testing dissolver solutions for extraction behaviour; preparing individual dissolution and extraction flowsheets for each type of fuel; co-processing fuels; minimising non-scheduled maintenance; and preparing long-range planning and operating schedules.

Testing for extraction behaviour

At the I.C.P.P. fuel processing campaigns are characterised by frequent variation in the activity level and composition of the solvent extraction feed solution, due in part to the non-uniform nature of the fuels and the frequency with which unusual fuels are processed. Two simple and inexpensive tests have been used to study those feed solutions which cause difficulties in the pulsed solvent extraction columns and to predict operating problems prior to processing 'off-spec' solutions.

The first of these tests is designed for the detection and diagnosis of the various forms of flooding of the pulsed sieve plate columns. This test is known as a dispersion–coalescence test and involves mixing equal aliquots of the aqueous feed and organic extractant by means of a perforated plate agitator, which moves vertically across the interface. The quantitative measure-

ment consists of observing the time required to achieve a given degree of dispersion of both phases. In general, the time for coalescence is of greater sensitivity and significance than the dispersion time. Usually it is equally valuable to be able to see the nature of the emulsion that may be formed in the columns, and to observe the effect of any solids which may be present in the solutions. The most frequent application of the dispersion–coalescence test occurs when a column gives evidence of flooding. Then, dispersion–coalescence characteristics of the feed–solvent system from the plant are determined. If stable emulsion formation is experienced—indicative that flooding is actually occurring in the plant column—gelatin treatment is tried in the test. If the results are favourable, gelatin is added to the plant feed.

The second test is designed to detect a marked reduction in the distribution coefficients for either extraction or stripping of actual process solutions. In general, two stages of extraction and two stages of stripping are performed in a test using appropriate plant feed, solvent, and scrubbing and stripping reagents. The phase ratio of the second extraction or stripping stage is adjusted until the uranium loss is less than 1 % as indicated by the uranium distribution coefficient. If the distribution coefficients for both stages of extraction and stripping are as predicted by basic equilibrium data for the processes, no serious loss of uranium due to chemical interference is indicated. This test is particularly useful for the detection of a pinch in the operating diagram for the stripping operation; such a pinch is often caused by dibutyl phosphate or a similar complexing substance. Based on the results of this test, suitable process flowsheets are prepared and plant operating conditions are adjusted to achieve an optimum recovery of uranium.

These two tests have been routinely used in conjunction with normal plant control and continuing surveillance of the fuels being processed, as well as with special analyses of any 'off-spec' solutions or precipitates. In this manner, these two simple tests offer valuable diagnostic help in minimising plant operating difficulties.

Separate flowsheets

Because of the diversity of aluminium and zirconium type fuels processed at I.C.P.P., a custom flowsheet is prepared for each fuel to guarantee complete safety while minimising processing costs and uranium losses. Separate chemical flowsheets for the first cycle of extraction are necessary to increase the extraction, scrubbing, and stripping efficiencies while staying within the operating limits of the equipment. In addition, waste solution volumes and uranium losses are minimised by preparing separate flowsheets.

Co-processing

Co-processing of aluminium and zirconium alloyed fuels is now performed routinely at I.C.P.P. to optimise processing costs. During co-processing the dissolver product from aluminium fuel is used to complex and adjust the zirconium–fuel dissolver product. Prior to co-processing, aluminium nitrate solution and nitric acid were purchased and used for complexing and adjusting the zirconium dissolver product for extraction. In effect, with co-processing, less operating time and a smaller quantity of chemicals are required; the latter in turn reduces the amount of waste produced and hence the WCF operating time and the required storage volume for radioactive waste solids. An added improvement resulting from co-processing is that the fluoride in the zirconium dissolver product prevents surfactancy caused by insoluble silica (from aluminium dissolver product) in the extraction columns.

Minimising non-scheduled maintenance

Non-scheduled maintenance has been minimised at I.C.P.P., which uses a direct maintenance philosophy, by replacing or modifying mechanical or poorly

designed equipment and by installing critical equipment items (such as jets and transfer lines) in pairs. Where possible, air lifts and jets are used in place of pumps, eductors in place of blowers, and pneumatic pulsers in place of mechanically operated pulsers. Equipment with a high maintenance potential is placed in shielded cubicles outside hot cells to limit the decontamination efforts when maintenance is required. The design of all new processes or modifications to existing processes is critically examined for simplicity, reliability, and decontaminability; in addition, intensive non-radioactive testing and operating are used, and this has resulted in minimum equipment failure during initial radioactive operation. Process downtime and personnel exposure are also kept in check, and direct maintenance, when required, is accelerated by using: in-cell photographs of equipment to orient maintenance personnel with cell layout; mock-ups for training maintenance personnel; permanently installed ladders and platforms around process equipment; unattended automatic saws for cutting in-cell piping; and using leakproof, quick-disconnects in shielded cubicles.

Long-range planning

Through effective long-range planning, it is now possible to make better use of available capacity at the I.C.P.P. to permit the reprocessing of many problem-type nuclear fuels for which there are no existing commercial processing facilities in the U.S.A. The fuels involved are a wide variety of reactor fuel elements that are being used or planned for use. Most of these fuels will become available in quantities economically justifying recovery of residual fissionable material, but in quantities too small to justify individual processing facilities. When examined individually, the reprocessing economics are marginal, at best; however, on a collective basis when capital, research and development, and operating costs are apportioned realistically amongst several fuels, the economic picture at I.C.P.P. is very attractive. This is true, in part, because the versatile solvent extraction processes and other equipment, cell space, and manpower can be used to advantage for problem-type fuels to produce a more attractive cost situation than would otherwise exist. In order to produce an attractive cost situation, however, it is also imperative to use effective long-range planning techniques.

To determine a near optimum operating schedule, as well as to determine the priority for processing any particular fuel load, the economics of fuel reprocessing and waste disposal for numerous alternative cases, in which a 10–15 year period is considered, are routinely examined using a cash flow technique. With the cash flow technique, total yearly expenditures—capital, operating, research and development, and any other costs related to a programme—are subtracted from the gross annual receipts to yield a cash flow. All cash flows are discounted—put on a present value basis—so that the net effect of various programme perturbations can be interpreted in terms of present day money. The discounted cash flow concept places a greater value on current than on future money in accordance with an assumed interest rate. In this way, money to be received or spent in the future is discounted to its lower equivalent value as of today. These present worth values then can be compared directly with money to be received or spent today.

In addition to and as part of the economic analysis, the total programme is reviewed to determine the long-range needs for research and development efforts. Each fuel that might be processed is reviewed for any special requirements, such as new or modified head-end or extraction facilities.

Improvement of the procedure used to treat highly irradiated fuels

(Example of the utilisation of complexing and redox agents in a solvent extraction process)

by C. Breschet and P. Miquel

Département de Chimie, Commissariat à l'Énergie Atomique, Centre d'Études Nucléaires de Fontenay-aux-Roses, France

The procedure used at Marcoule for the treatment of irradiated uranium has been modified to obtain better fission product decontamination and also to simplify the purification cycle for plutonium nitrate.

During recent operations it has been shown that problems such as interphase precipitation and difficulties in obtaining the desired decontamination in mixer–settlers could be resolved by the addition of very small quantities of hydrofluoric acid to the aqueous feeds to the first co-decontamination cycle for uranium and plutonium.

In the second cycle, plutonium is generally concentrated and purified in pulse columns using a recycle flowsheet which uses extraction with tributyl phosphate followed by stripping in the presence of the reducing agent uranous nitrate stabilised with hydrazine. Flowsheet performance has shown that this cycle gives good decontamination (DF > 10^4) *as well as concentrating the plutonium* (CF > 100).

Introduction

THE SPENT FUEL processing method used at Marcoule since 1958[1] (Fig. 1) has been profoundly modified in order to improve efficiency and reduce reprocessing costs.

The most important changes accomplished were: in 1967, the setting up of a new plant for the 2nd cycle where plutonium is purified and concentrated by solvent extraction; in 1970, the testing of a new process involving the introduction of small quantities of hydrofluoric acid to complex fission product zirconium in the 1st cycle where uranium and plutonium are decontaminated.

This addition of hydrofluoric ions was subjected to prolonged trial in the plant with the aim of processing lightly irradiated natural uranium from graphite–gas reactors and alloys from tritium-generating reactors. Its purpose was to compensate for the inadequacy of the mixer–settler units, the geometry of which tends to promote degradation of tributyl phosphate and deleterious reactions with zirconium.

The plant for plutonium purification and concentration by tributyl phosphate in pulsed columns[2] was built with a view to simplifying and automating the plutonium production process.

These and other minor alterations have greatly contributed to the improvement of plant efficiency and their advantages and disadvantages are now in a position to be evaluated.

Decontamination by addition of HF in the 1st extraction cycle

Decontamination problems

Precipitates and their effects

Since the first spent fuel reprocessing runs at Marcoule, the presence of radioactive deposits has been observed in the settlers of the first contactor. These deposits, known as sludges or interphase precipitates, generally lead to highly irregular decontamination factors.

During fairly recent runs, βγ-irradiation fluxes of up to 10^6 r/h were observed in the loaded settlers whereas the active components in the circulating liquid phases accounted for only 10^4 rad/h.

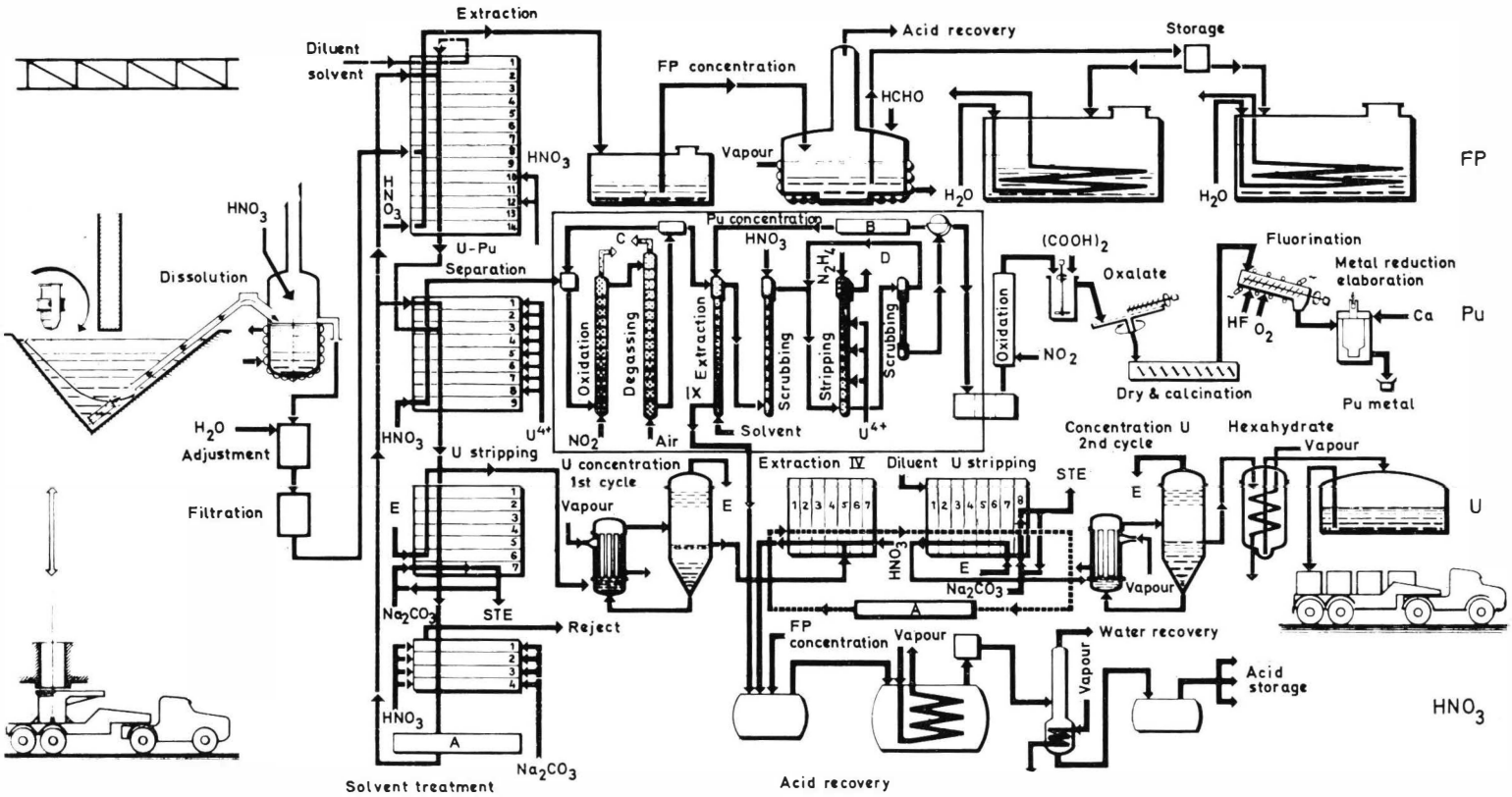

FIG. 1. *C.E.A. plutonium extraction plant at Marcoule*

A, solvent extraction; B, re-oxidation; C, ventilation; D, to solvent partition; E, H_2O recovery

During these particularly difficult periods of operation the solvent suffered considerable damage and the decontamination factors decreased. ($DF\ Zr < 1000$, $Ru < 500$).

The presence of precipitation was confirmed beyond question when the solutions from certain settlers were filtered and a black residue of high specific activity was obtained.

It was possible in addition to reproduce the phenomenon in miniature active-laboratory mixer–settlers.[3–5] All the analyses carried out on the precipitate showed that it was made up essentially of zirconium butylphosphates.

The formation of precipitates never stopped production nor blocked piping but it considerably handicapped the working of the first extraction cycle apparatus, which had to be constantly supervised from the viewpoint of hydraulic behaviour (position of the interphases, activities, densities etc.) and kept operating continuously in order to avoid prolonged stagnation of the solvent in the 'clogged' settler zone.

Well defined working conditions were also imposed, i.e. the uranium saturation of the solvent was kept high in the scrubbing section and the extraction acidity low; the 'clogging' zones are thus displaced towards the raffinate outlet stages.

Finally, plant wash-outs and complete solvent renewals were carried out in the course of several campaigns.

Formation of interphase precipitates

During the processing of spent fuels tributyl phosphate degradation seems to be considerably enhanced by the presence of fission product zirconium.

Radiolysis, which leads essentially to the formation of dibutylphosphoric acid,[6] would play a part analogous to that of temperature in the hydrolysis of tributyl phosphate in the presence of zirconium.[7] Besides the irradiation and the acidity of the medium, zirconium also greatly accelerates the process of radiolytic hydrolysis, this effect is all the more pronounced when the concentration of this element in the solvent is high.

Initially, zirconium is extracted only to a slight extent by tributyl phosphate, but it reacts with the small quantities of butyl phosphoric acids produced by radiolysis to form the highly extractable dibutyl phosphate.[8] This is the start of a process accelerated by both zirconium- and butyl-phosphoric acids. These acids raise the distribution coefficients of the elements zirconium, niobium and and uranium and spread through the plant right into the finished products.

Zirconium, partly swept back by scrubbing, concentrates more and more in the extraction section, increases the decomposition of the solvent and precipitates in the still zones of the settlers in the form of monobutyl phosphate.

This latter substance, organophilic and colloidal, adsorbs all the insoluble matter in suspension in the circulating liquid phases (silica, ruthenium, niobium) and builds up at the interphases, where solvent decomposition 'centres' are set up.

Meanwhile, portions of precipitate become detached continuously and are carried by the process solutions towards the aqueous raffinate outlet or the scrubbing section in which they are slowly resorbed, lowering the decontamination factors and leading to the 'saw-tooth' operating pattern indicated and observed in old reprocessing plants, particularly by Orth.[9]

Possible remedies

It was feared that because of this problem the process used at the plutonium extraction plant would not be suitable for the processing of highly irradiated fuels. It was, therefore, necessary to find and test a solution to the problem of interphase precipitates.

Two kinds of solution to the problem were possible: (i) technological: change of equipment for the 1st extraction cycle by the adoption of centrifugal extractors, as at the Savannah river plant,[10] or pulsed columns, which present no large

disengagement surfaces and thus allow any accumulation of insoluble products to be avoided; or alternatively to effect a compromise by replacing part of the present first extractor by a pulsed column; (ii) chemical: addition of a strong zirconium complexing agent to the feed, a process described in the following sections under the name 'HF process'.

Introduction of hydrofluoric acid

Theoretical justification

According to these assumptions, overcoming the problems of decontamination amounts in fact to preventing the interaction of fission product zirconium with the tributyl phosphate–dibutylphosphoric acid system. (This principle only applies to the processing of thermal reactor fuels where the efficiency is upset by fission product zirconium alone. In the processing of more highly irradiated fuel elements from fast neutron reactors interference from the elements Ru and Nb adds to that of zirconium, and fluoride is then only partly effective as an additive that improves decontamination additive).

It is proposed to hold the zirconium in the aqueous phase of the extraction section by addition of an appropriate quantity of fluoride ions, which can be calculated from general considerations of the distribution of fluorine between various complexes.

Degree of complexing necessary for zirconium to be non-extractable

Calculation of the amount of fluoride needed to 'fix' zirconium requires a knowledge of the degree of formation, X_M, of fluoro-complexes with each major cation, M, present in the process solution. This function is defined as the number of moles of fluoride ion complexing a given cation per mole of that cation (whether complexed or free) present in the solution. Values have been determined by Schlea & Lowe[11] for various cations in a medium of ionic strength 2; experiments at Fontenay-aux-Roses corroborated these results and also showed that the extraction of zirconium by an organic solution containing 30% tributyl phosphate and 1 g/l dibutylphosphoric acid was negligible when the degree of formation exceeded 1·5.

The degree of formation is given by the equations:

$$X_M = \frac{\sum_{i=o}^{i=n} i[MF_i]}{\sum_{i=o}^{i=n} [MF_i]} = \frac{\sum_{o}^{n} i.P_i[F^-]^i}{\sum_{o}^{n} P_i[F^-]^i} \equiv f[F^-]$$

where i is the number of fluoride ions in a complex, n is its maximum value for the cation in question, and P_i is the cumulative apparent stability constant for the formation of the complex MF_i, i.e. the product of the apparent equilibrium constants for the stepwise formation of fluoro-complexes up to and including MF_i by reactions of the type $MF_{i-1}^{r+} + F^- \rightleftharpoons MF_i^{(r-1)+}$. The degree of formation can therefore be calculated from the values of these formation constants, which are given in the literature for several ionic strengths.

The degrees of formation corresponding to the various cations simultaneously present in a solution are interdependent, since each is a function of the fluoride concentration. Thus, if the degree of formation is specified for one cation it is possible to deduce values for the others, and thence the overall fluoride concentration, F_t, since:

$$F_t = [F^-] + X_M C_M + X_{M'} C_{M'} + \ldots\ldots$$

where C_M is the overall molarity of the metal on M, and the primes distinguish different cations. The proportions of the different fluoro-complexes can also be calculated by the method of Goldstein[12] and are shown for the major cations in Fig. 2.

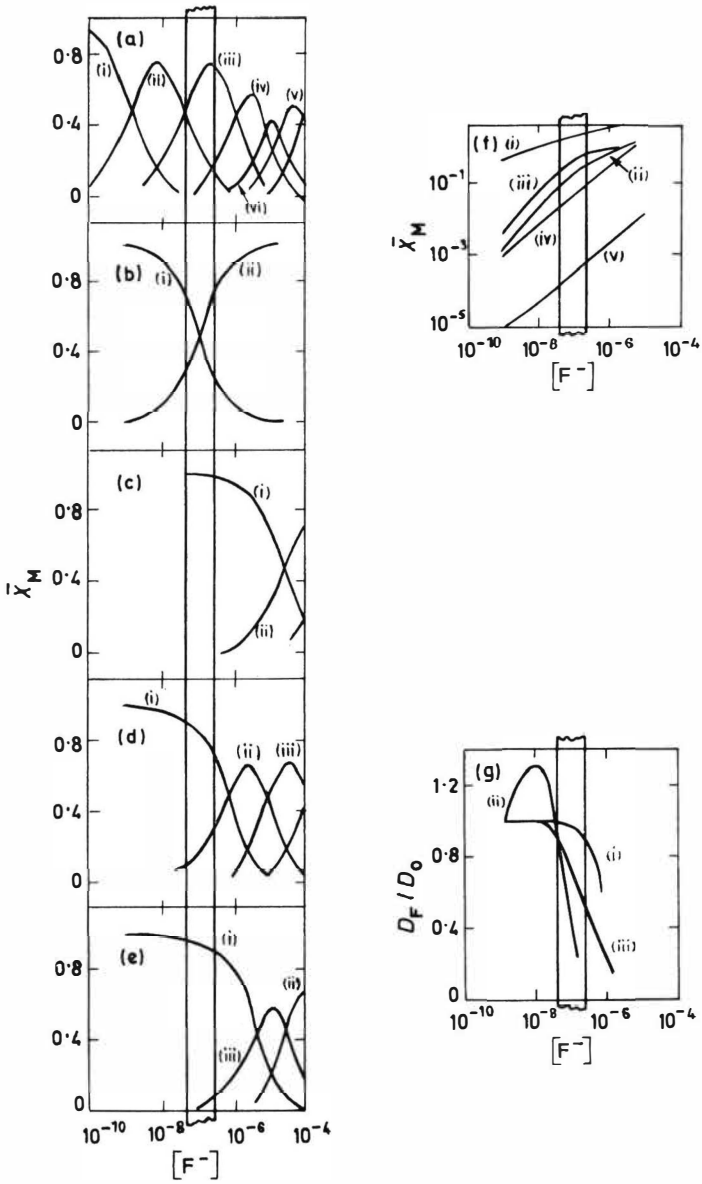

FIG. 2. *Proportions of fluoride complexes as function of free fluoride*

(a) : (i) Zr^{4+}; (ii) ZrF^{3+}; (iii) ZrF_2^{2+}; (iv) ZrF_3^{+}; (v) ZrF_3; (vi) Z_rF_5
(b) : (i) Pu^{4+}; (ii) PuF^{3+}
(c) : (i) UO_2^{3+}; (ii) UO_2F^{+}
(d) : (i) Al^{3+}; (ii) AlF^{2+}; (iii) AlF_2^{+}
(e) : (i) Fe^{3+}; (ii) FeF_2^{+}; (iii) FeF^{2+}
(f) : (i) Zr; (ii) Al; (iii) Pu; (iv) U; (v) H^{+}
(g) : (i) U; (ii) Zr; (iii) Pu

According to Schlea & Lowe, both uncomplexed zirconium ion and the first fluoro-complex ZrF^{3+} are extracted by TBP, so that a significant proportion of ZrF_2^{2+} must be formed before the addition of fluoride can be expected to improve decontamination; as mentioned earlier, a degree of complex formation greater than 1·5 is satisfactory.. On the other hand, the concentration of fluoride must not be so high as to prevent the complete extraction of plutonium.

Provided that (a) no higher fluoro-plutonium complex than PuF^{3+} is formed, (b) this complex is completely inextractable, (c) the distribution ratio for plutonium, other than that associated with fluoride, is independent of concentration, then the distribution ratios with and without fluoride are related by:

$$\frac{K_d \text{ with fluoride}}{K_d \text{ without fluoride}} = 1 - X_{Pu}$$

Goldstein's curves show that the fluoride concentration must be less than that corresponding to $X_{Zr} = 2 \cdot 2$ if the distribution ratio of plutonium is to remain satisfactory, i.e. well above unity. An attempt was therefore made to obtain values of X_{Zr} within the range $1 \cdot 5$–$2 \cdot 2$ in extractor I of the first cycle of the Marcoule reprocessing plant. For complete extraction of plutonium, if was also necessary that the adverse effect of fluoride should not be reinforced by a high concentration of uranium in the solvent.

Confinement of fluoride to the aqueous raffinate from the first cycle

Dispersion of fluoride in the apparatus must be avoided because of its corrosive action towards stainless steel.

The point of introduction of fluoride into the extraction contactor must take into account the separation coefficients of HF in tributyl phosphate ($0 \cdot 05 < K_d < 0 \cdot 1$) so that fluorine is completely eliminated from the loaded solvent leaving the scrub section.

During concentration of fission products, the fluoride is complexed by aluminium (700 ppm in fuel) in the solution, and has no corrosive properties. It may be washed back by a small flow of aluminium nitrate in the distillation column.[13]

Fluoride calculations for the Marcoule processing plant flowsheets

Taking into account all the factors mentioned below, the point at which to introduce the fluoride into the first extraction contactor, and the reflux rate in fission product concentration, were determined. The working conditions adopted are given in detail in Fig. 3.

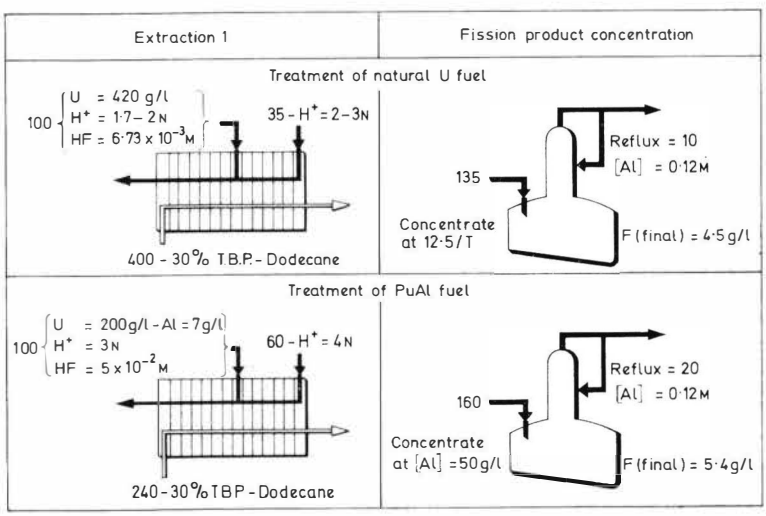

FIG. 3. *Operating conditions for the 1st extraction cycle and fission product concentration*

Results obtained with the use of hydrofluoric acid

Decontamination results

While fluoride was used, the following improvements were observed.

1. The increase in decontamination factor was considerable for zirconium ($DF > 10^4$) and less appreciable for ruthemium ($DF > 3000$). Fluoride did not seem to affect the decontamination factor for niobium, which remained low.

2. Interface activity 'peaks' were not observed by dose rate measurements in the settler zone. The main object of adding fluoride – elimination of irradiating substances at the interphases – thus appears to have been completely achieved.

3. The residual activity of the solvent remained practically steady after addition of hydrofluoric acid whereas previously it had always increased with time. This change in the residual activity, due almost exclusively to ruthenium, may be explained both by the elimination of interphase precipitates – probably the centre of reaction for highly extractable ruthenium complex formation[14] – and by the increased acidity of the scrubbing solution made possible by the introduction of hydrofluoric acid.

4. Start-up and shut-down of the first extraction cycle no longer affected efficiency; this resulted in the ability to shut-down production at week-ends. This has enabled the operational staff to be reduced.

5. The use of recycled uranium from the second cycle to load the units at the start of the run, and continuously for the dilution treatment of Pu/Al alloy (MTR type fuel), no longer led to an increased quantity of Zr in the loaded solvent. This is despite the fact that the depleted uranium contained butylphosphoric acids formed during intercycle concentration, which would enhance the extraction of Zr when it is not complexed by fluoride.

6. Uranium and plutonium left the second cycle with a higher degree of purification. The addition of hydrofluoric acid is thus a success from the viewpoint of plant efficiency.

It now remains to examine the consequences with regard to plutonium extraction and corrosion.

Plutonium extraction

The theoretical behaviour of plutonium in the first extraction cycle in the presence of fluoride, discussed above, was confirmed.

The results obtained in practice show that: the plutonium concentration can be higher in the presence of fluoride, particularly around the feed stage; and that a 'flat' plutonium concentration profile was obtained firstly by reducing the uranium saturation in the loaded output solvent product and secondly by increasing the acidity of the feed and scrub solutions.

It is also important to note that this decrease in saturation does not affect the decontamination efficiency, since it is compensated by high acidity.

Corrosion problem

Fluoride solutions can lead to general corrosion in stainless-steel apparatus depending on temperature, and nitric and hydrofluoric acid concentrations. Precautionary measures must be taken to prevent the solutions used in the 'HF process' from seriously attacking plant equipment such as extractors, connecting pipes, boilers ets., which are made of various types of stainless steel (Zr CN 18–10 and Zr CNNb 25–20 in AFNOR norm). Experiments have shown that the 3N nitric and 0·01N hydrofluoric acid solutions used do not increase corrosion at low temperatures (40°C) and that fluoride, concentrated (0·5–0·6M) but strongly complexed by cations (Al, Zr, Fe, Ce) contained in the process solutions, is practically harmless in the liquid phase even at boiling point. Also hydrofluoric acid in boiling or vaporised nitric acid does not aggravate corrosion at concentrations less than 10^{-4}M.

The fluoride distribution in the process (Fig. 4) shows that these conditions have been maintained.

Generally, no abnormal corrosion ascribable to fluoride was detected.

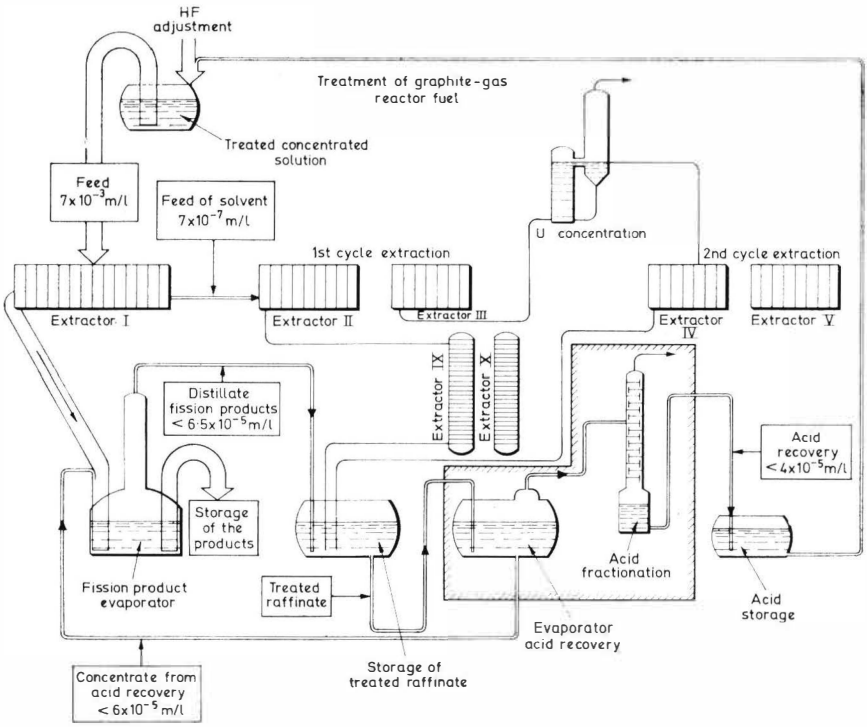

FIG. 4. *HF distribution in HA plant*

2nd cycle plutonium concentration and purification

Description of the process

The Fontenay-aux-Roses research departments[15] have also developed a tributyl phosphate extraction technique by which the plutonium solution leaving the first extraction cycle can be concentrated and purified simultaneously (Fig. 1).

This technique has replaced a cumbersome and discontinuous method using in succession a plutonium precipitation by sodium hydroxide, a tributyl phosphate purification cycle and a concentration–washing cycle by an ion-exchange process.

These difficult operations were carried out in several plant stages whereas it is now possible to process the plutonium solutions in a single, almost entirely automatic, unit equipped with pulsed columns.

The unit consists of four main sections shown on the detailed flowsheet (Fig. 5) with the following sequence of operations: oxidation of plutonium from valency three to valency four; extraction of Pu^{IV} by 30% TBP and scrubbing of the loaded solvent; re-extraction of plutonium by uranous nitrate and solvent scrubbing of the concentrate; and oxidation and recycle of part of the product stream.

Oxidation

The dilute plutonium solution from the 1st separation cycle is acidified continuously, after which the plutonium is oxidised from valency three to four by nitrous vapour bubbling in a packed column. The nitrous vapours are

formed by reaction of concentrated nitric acid on sodium nitrite and the excess eliminated by a current of air in a second packed column. (No foreign ions are introduced into the process by this method).

The oxidised and de-gassed solution is then sent to the extraction stage.

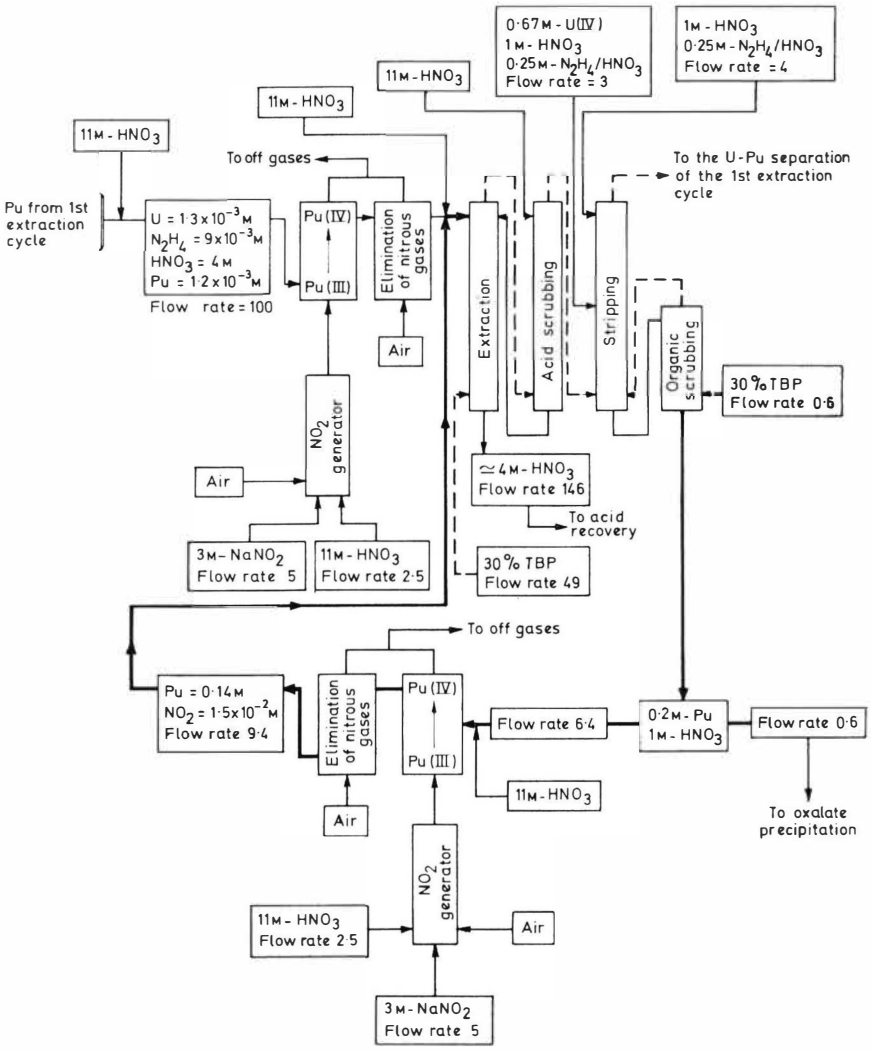

FIG. 5. *2nd cycle plutonium concentration and purification*

Extraction and scrubbing

Extraction is carried out by 30% TBP from the 1st cycle, in the first pulsed column with the organic continuous phase.

The aqueous phase, free of plutonium and containing the fission products, is sent to a nitric acid recovery process.

The loaded solvent is scrubbed with a nitric solution in a second pulsed column identical with the first and then transferred to the stripping column.

Back-extraction

The plutonium is stripped with nitric acid by reduction of Pu^{IV} to Pu^{III} with uranous nitrate containing hydrazine and concentrated in the aqueous phase.

This operation is carried out in a third pulsed column working with the aqueous phase continuous.

The concentrate obtained (Pu = 50 g/l) is purified from uranium by washing with 30% TBP in a fourth pulsed column with the organic phase continuous.

The solvent raffinate is directly recycled to the 1st extraction cycle.

Recycle

Part of the concentrated plutonium solution is recycled to the plutonium extraction column. The rest, which makes up the product of the plant, is washed with diluent to remove traces of TBP and sent to the plutonium oxalate precipitation unit.

The main innovations introduced by this new system are as follows: use of the same 30% TBP solvent as in the first extraction cycle, which means that losses to the solvent raffinate can be tolerated and that a single solvent treatment serves for both cycles; oxidation of Pu^{III} to Pu^{IV} by nitrous vapours; reductive stripping of Pu by hydrazine-stabilised uranous nitrate; and, use of pulsed columns which offer, as compared with mixer-settlers, a neat way of solving problems of nuclear safety by the adoption of a suitable geometry and a low retention volume.

Results

Oxidation of plutonium

At the outlet of the oxidation units, the oxidation yield does not exceed 85 and 95% respectively for the diluted plutonium, and for the plutonium contained in the recycled solution.

A slight improvement was obtained by increasing the nitric acid concentration, now fixed at 4N.

However, this oxidation deficiency does not affect the extraction yield, as will be seen below.

Extraction yield

Extraction. During the first months of operation some plutonium leakage was recorded in the aqueous raffinate of the extraction column, undoubtedly due to the incomplete oxidation of Pu mentioned above.

However, this was compensated by increasing the extraction acidity from 3 to 4N and by introducing nitrous vapours through the recycle solution which was deliberately incompletely degassed. The nitrous vapours thus complete the oxidation of Pu^{III} in the extraction column where Pu is now extracted with a very high yield, corresponding to a leakage of less than 0·05 mg/l of plutonium in the aqueous raffinate.

Since nitrous acid is extracted by the solvent, excess nitrous vapour must be checked and limited to about 20 mg/g of plutonium fed into the extraction column, in order to avoid the presence of nitrite ions at the plutonium stripping stage; this would lead to excessive consumption of tetravalent uranium and a risk of Pu leakage into the solvent raffinate.

Back-extraction. Generally, the results obtained during this stage corroborated the various studies made on the reductive stripping of plutonium.[15] The process takes place with a continuous aqueous phase ($7 < \frac{O}{A} < 8$) and at low acid concentration (1N) because of the instability of uranous nitrate in the organic phase. The amount of reducing agent used is equivalent to 3 times the stoichiometric quantity with respect to plutonium. The tetravalent uranium consumption

could be cut down but it is preferable to work with a slight excess, since this provides an excellent yield on stripping and thus limits plutonium leakage to a value below 5 mg/l in the solvent recycled to the first extraction cycle.

Decontamination efficiency

In the course of successive runs the decontamination efficiency was gradually improved by increasing the plutonium recycle.

Decontamination is in fact closely linked with the amount of recycle as shown by the expression:

$$DF = K\left(\frac{R}{A} + 1\right)$$

where K = constant
R = mass flow of Pu recycled
A = mass flow of Pu in the feed solution.

Another advantage of this increased recycle is that a more concentrated plutonium product solution is obtained, the limit being set by the plutonium content of the solvent raffinate.

It was thus possible to obtain a substantial degree of recycle, corresponding to a concentration of 50 g/l Pu in the product solution, without affecting the extraction yields.

Under these conditions the decontamination factors for the unit are of the order of:

$DF\ ^{95}\mathrm{Zr} = 2 \times 10^4$ to 10^5
$DF\ ^{95}\mathrm{Nb} = 10^4$ to 10^5
$DF\ ^{103+106}\mathrm{Ru} = 5 \times 10^3$ to 2×10^4

Until the 'HF process' was applied it was thus possible to compensate for the irregularity of decontamination in the first extraction cycle and to obtain plutonium with a residual γ-activity (essentially Zr–Nb) between 1 and 5 μCi/g.

Since hydrofluoric acid has been used, the overall efficiency of the 2 decontamination cycles has improved still further.

The overall plutonium decontamination factors are:

$DF\ ^{95}\mathrm{Zr} > 4 \times 10^8$
$DF\ ^{95}\mathrm{Nb} \sim 3 \times 10^8$
$DF^{103+106}\mathrm{Ru} \sim 4 \times 10^7$

The residual γ-contamination of the final plutonium is now less than 1 μCi/g.

Conclusions

The use of pulsed columns at the second decontamination cycle and the experimental introduction of a strong zirconium complexing agent (HF) at the first cycle have very favourable effects on the efficiency of the Marcoule spent fuel reprocessing plant.

Hydrofluoric acid added in very small concentrations to the dissolver solution has eliminated the formation of interphase precipitates in the mixer–settler, increased the decontamination factor and cut down degradation of the solvent during the processing of fairly lightly irradiated fuels.

It is planned to use the 'HF process', which involves no additional capital investment, *a priori*, to process the fuels of power reactors and of tritium-generating reactors in the present facilities at Marcoule.

The use of a well studied complexing agent (HF) and redox reagent (U^{4+}) improved the standard fuel reprocessing method. For the treatment of PWR and BWR fuels, the following flowsheet is suggested.

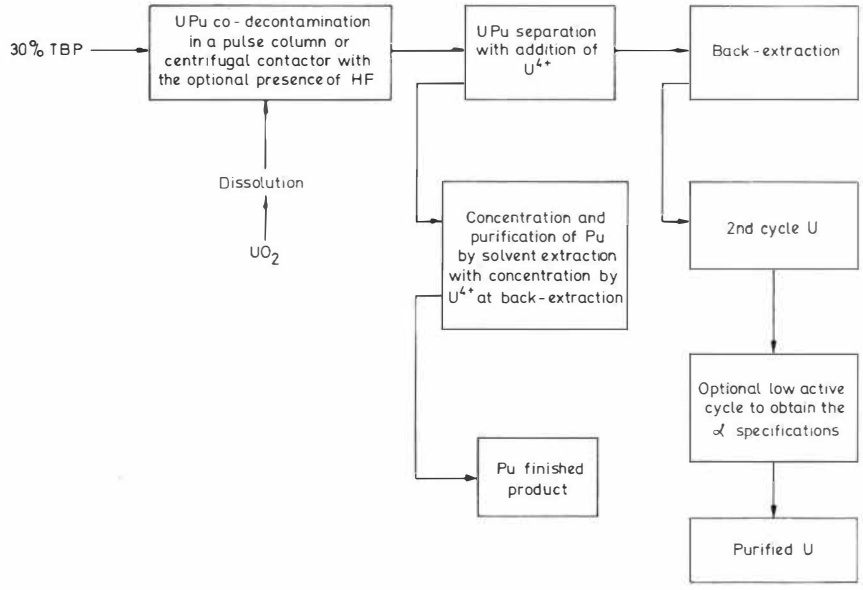

References

[1] Jouannaud, C., *Symposium sur la chimie du traitement des combustibles irradiés par voie aqueuse*, Bruxelles, 23–28 April, 1963
[2] Auchapt, P., Giraud, J. P., & Talmont, X., *Énergie nucl.*, 1968, **10** (3), 181
[3] Sauteron, J., *Inds atom.*, 1969, No. 718
[4] Lefort, C., & Miquel, P., *Notes C.E.A.*, 856, 969, 1044, 1148, 1241
[5] Faugeras, P., & Talmont, X., *11th int. Conf. Co-ord. Chem., Jerusalem*, 1968
[6] Salomon, L., & Menchero, E. L., *Rep. Congr. atom. Energy Commn U.S.*, 1967, ETR-203
[7] Moffat, A. J., & Thompson, R. D., *Rep. Congr. atom. Energy Commn U.S.*, 1961, IDO 14.543
[8] Shevchenko, V. B., & Smelov, V. S., *Ekstraktsiya teroriya primenenic Apparutura sb states*, 1962, pp. 257–263
[9] Orth, P. A., *Proc. int. Conf. Solv. Extr. Chem. of Metals*, 1965, p. 47 (London: Macmillan)
[10] Orth, P. A., & MacKiblev, J. M., Neth. Pat. Appln 69/30/1
[11] Schlea, C. S., & Lowe, J., Neth. Pat. Appln 842 (1964)
[12] Goldstein, G., *Rep. Congr. atom Energy Commn U.S.*, 1964, ORNL-3620
[13] Fr. Pat. 7003424
[14] Wallace, R. M., *Nucl. Sci. Engng*, 1964, **19**, 296
[15] Talmont, X. L. R., *Proc. int. Conf. Solv. Extr. Chem. of Metals*, 1965, p. 103 (London: Macmillan)

Chemical aspects of solvent extraction on plant scale at Eurochemic

by J. van Geel, C. Joseph, E. Detilleux, W. Heinz, J. Centeno and B. Gustafsson
Eurochemic Co., Mol, Belgium

This paper gives some chemical aspects of reprocessing fuel at Eurochemic from nuclear reactors by solvent extraction using 30% tributyl phosphate as an extractant for uranium and plutonium.

The following are discussed: application of uranous nitrate as a reductant for plutonium in air-pulsed columns, solvent stability and process performance under different radiation exposures; and formation of heavy phase and deposits under certain process conditions.

Introduction

EXPERIENCE IN REPROCESSING nuclear fuel by solvent extraction processes has shown that difficulties arise in extrapolating laboratory data to industrial scale conditions. The need for actual plant data is therefore great, in particular for those extraction processes where new techniques or extreme operating conditions are involved.

This paper discusses the Eurochemic experience gained in applying different process conditions and treating fuel elements from nuclear power reactors with different burn-up.

Application of uranium (IV) nitrate in air-pulsed columns

Since the end of 1968, uranium(IV) nitrate has been applied as a reducing agent for plutonium in the partitioning column for stripping plutonium from the tributyl phosphate (TBP) phase.

Although many laboratory studies have been reported on the behaviour of U(IV) in Purex type extraction systems, only few data, dealing with uranium (IV) nitrate in pulsed columns, are available from the literature.[1–12] Mendel[2] reported the results of some runs carried out in miniature pulsed columns in 1965 and reported high plutonium losses which he attributed to the short residence times of the TBP phase in the extraction column. The present paper describes Eurochemic experience over 2 years and shows that good separation between uranium and plutonium can be obtained on an industrial scale, provided certain process conditions are respected.

Solvent stability

Much of the data, obtained from laboratory studies on solvent stability against radiation and chemical damage, requires extensive extrapolation when used to predict the solvent performance on a plant scale.

Blake[3] recently concluded that extrapolation of most of the reported laboratory data to industrial scale operations would produce erroneous results.

The TBP solvent of the Eurochemic plant has been irradiated by radiation exposures of 0·05 Wh/l per pass in the first cycle (by treating fuel up to 26,000 MWd/t U) and 0·3 Wh/l per pass through the 2nd Pu cycle.

According to laboratory studies such exposures have a noticeable effect on the solvent performance. The solvent quality was therefore followed under the various process conditions applied at Eurochemic.

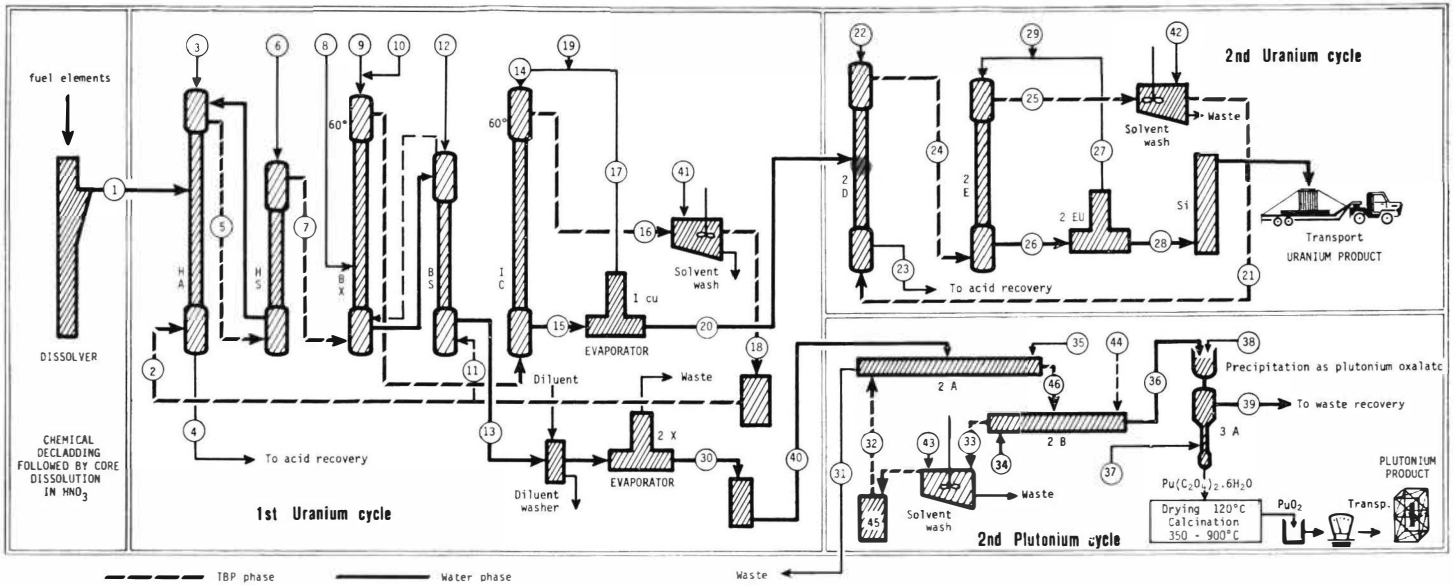

FIG. 1. *Chemical flowsheet for treatment of low-enriched uranium fuel*

Process stream numbers are referred to in the table on p. 579

Process Stream	Code	HNO_3 M	U g/l	Pu g/l	TBP vol. %	U(IV) g/l	N_2H_2 M	$H_2C_2O_4$ M	Na_2CO_3 M	Flow rate, l/h
1	HAF	3	200	~1·2						51
2	HAX				30					160
3	HAS	4								25
4	HAW	3	<0·1	$<10^{-4}$						91
5	HAP		61		30					165
6	HSS	1·5								15
7	HSP		63	~0·4						160
8	$1BXR_2$	0·5				160	0·2			~2
9	$1BXR_1$	0·5				160	0·2			~2
10	1BXH	0·1					0·2			15
11	1BSS				30					20
12	1BSA	6								1
13	1BSP	1·7	<0·4	~3						20
14	$1CX_1$	0·01								180
15	1CUF	0·04	56							180
16	1CW		<0·1		30					180
17	1CUD	0·01								145
18	1SR				30					180
19	$1CUX_2$	0·05								35
20	1CUC	0·2	300	$<10^{-3}$						35
21	2DX				30					162
22	2DS	0·5					0·1			25
23	2DW	0·35	<1							60
24	2DP		62		30					162
25	2EW		<0·1		30					162
26	2EP		61							168
27	2ED									122
28	2EUC		400							25
29	2EUW	0·05								20
30	2XC	~5	<2·5/5	25/50						2·4/1·2
31	2AW	2·5	1	<0·05						18/9
32	2AX				30					10
33	2BW		<0·1	<0·05	30					10
34	2BX	0·15								8
35	2AS	0·3								10/5
36	2BP	0·5	<1	25						8
37	3AS	2·5						0·1		6
38	3AR	2·5						0·15		5
39	3AW	2·5						0·1		19
40	2AF	5	<2·5/5	25/50						8/4
41	1SX								0·5	24
42	2SX								0·5	16
43	2BSR								0·5	1
44	2BS				30					2

Formation of heavy phase and deposits

During some process campaigns, Eurochemic suffered from intermittent process shutdowns caused by formation of heavy phases and deposits in certain parts of the equipment. The main operational difficulties concerned flooding of the mixer-settler, plugging of airlifts and sampling lines and unreproducible sample results. Evidence for heavy phase formation and deposits could be obtained from observations of samples taken from certain process streams and from visual inspection of the process equipment. The same phenomena, under similar process conditions, have been reported elsewhere,[4] although to a lesser extent. The observations in the Eurochemic plant equipment are attributed to solvent degradation in the Pu intercycle evaporator.

Extraction process at Eurochemic

The Eurochemic process has been extensively described in previous reports.[5, 6] The chemical flowsheet for treatment of low enriched fuel (<5% ^{235}U) is shown in Fig. 1 and for highly enriched fuel in Fig. 2. The low enriched uranium (LEU) process is based on chemical decanning and core dissolution.

The extraction process is a two-cycle Purex type process using 30% (by vol.) TBP in kerosene. The extraction equipment of the co-decontamination cycle, the U/Pu partitioning cycle and the second uranium cycle consists of pulsed

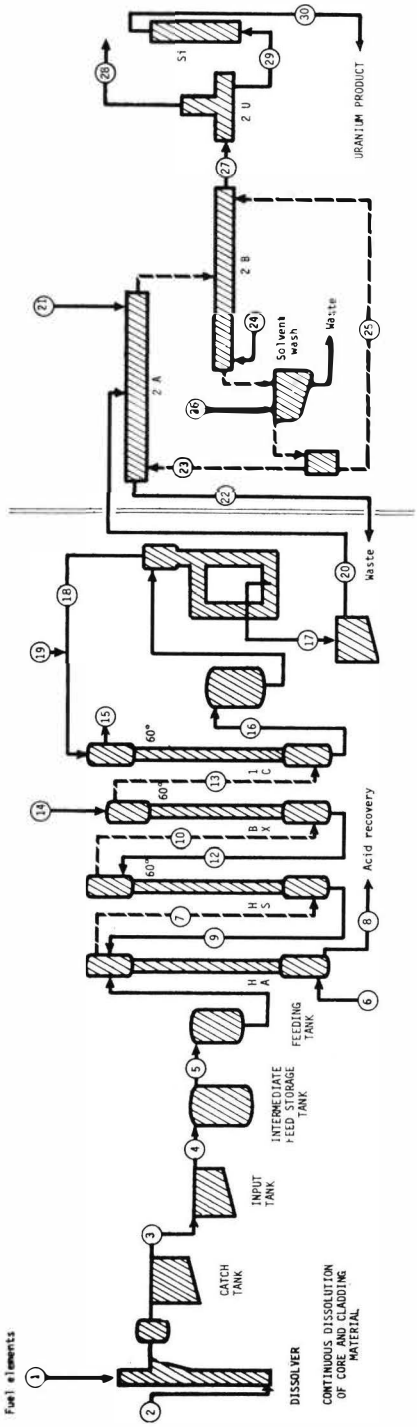

FIG. 2. *Chemical flowsheet for the treatment of highly enriched uranium fuel*

Process stream numbers are referred to in the table on p. 581

Process Stream	Code	HNO_3 M	U kg/day	Al kg/day	$Hg(NO_3)_2$ M	U g/l	Al M	TBP %	$Fe(NH_2SO_3)_2$ M	Na_2CO_3 M	α disintegrations/min/gU	Flow rate l/h
1	Fuelcharge		~6·5	~190								
2	Dissolvent	6·2			0·015							178
3	MD	0·6				1·5	1·65					
4	AFU	0·54				1·42	1·57					
5	HAF	0·5				1·35	1·5					200
6	HAX							4·5–5				80
7	HAP					3·7						80
8	HAW	~0·4				$<2\cdot5\times10^{-3}$	1·45					212
9	HSR											12
10	HSP											80
12	BXR											12
13	BXU											80
14	BXS	−0·5					1		0·02			12
15	ICW					$<2\times10^{-3}$						80
16	ICUF	0·01				3·4						80
17	MEC	0·7				~250						1·1
18	MED (dist)	0·001										79
19	MED (adj)	0·8										1
20	2AF	5				140			0·02			6
21	2AS	0·7							0·02			2
22	2AW	4				<0·1						8
23	2AX							30				10
24	2BX	0·01										12
25	2BS							30				2
26	2BSR									0·5		1
27	2BP	0·1				70						12
28	2UD											10
29	2UC	1				420					$<15\times10^{-3}$	2
30	2UP	1				420					$<15\times10^{-3}$	2

column contactors. The second plutonium cycle uses mixer–settlers as extraction equipment. The uranium tail-end consists of a treatment on silica gel for the removal of the last traces of zirconium. The plutonium tail-end involves precipitation of plutonium(IV) oxalate and calcination to PuO_2.

Until the end of 1968, ferrous sulphamate was used as a reducing agent for plutonium in the BX column for stripping plutonium from the TBP phase.

This reductant, however has certain disadvantages. Since it introduces non-volatile constituents such as iron and sulphate, the volume of radioactive waste increases and accelerates the corrosion of the evaporation equipment.

Since, 1969, hydrazine-stabilised uranous nitrate solution has therefore been applied at Eurochemic as a replacement for ferrous sulphamate.

The 2nd plutonium cycle has also been frequently modified. Elimination of sulphate addition to the 1BSP solution allowed higher Pu concentrations in the 2nd Pu extraction cycle.

The flowsheet of Fig. 1 shows Pu concentrations up to ~50 g Pu/l in the feed streams to the mixer-settler batteries.

In Table I these operating conditions are compared with those applied in other Purex-type reprocessing plants.[7] Table I shows that the Eurochemic process involves relatively high solvent loadings. It will be shown later that the radiation dose received by this solvent is accordingly high.

TABLE I

Some operating conditions in the 2nd plutonium extraction cycle in existing reprocessing plants[7]

Plant	Ref.	Pu_a g/l	Pu_o^m, g/l	[TBP] vol. %
NFS (U.S.A.)	17	1·32	3·36	30
Windscale (G.B.)	18	1·9	5·0	20
Marcoule (France)	19	8–12	<8	20
Oak Ridge (U.S.A.)	20	1·49	3·3	30
Hanford (U.S.A.)	21	1BSP not conc.	4X[1BSP]	30
Eurochemic (Belgium) until 1969		1·31	2·57	30
as from 1969		~50	12–20	30

Pu_a = Pu conc. in 2AF: Pu_o^m = max. Pu conc. in process stream 46 (see Fig. 1)

Application of uranous nitrate in the partitioning column

The application of uranium(IV) nitrate for separating plutonium from uranium by reduction of the extractable plutonium(IV) to the less extractable plutonium(III), is extensively described in the literature.[8,9].

These studies have shown that uranium(IV) and plutonium(III) are susceptible to re-oxidation by various components present in Purex-type extraction systems. Among these components nitrous acid, nitric acid and air are well known. In order to destroy the nitrous acid, uranium(IV) nitrate is stabilised with hydrazine. As hydrazine does not eliminate the other oxidising reagents, many plants use an excess of uranium(IV) nitrate with respect to the stoichiometric amount required for reduction of plutonium.

Practically no information has yet been reported on process performance in pulsed columns on an industrial scale. The choice of process conditions in the partitioning columns 1BX and 1BS of the Eurochemic plant was governed by the following considerations.

1. The process had to take place in the existing extraction equipment, originally designed to perform the partitioning process with ferrous sulphamate. The design characteristics of the 1BX and 1BS columns are discussed by Joseph *et al.*[1]

2. The α-content (mainly from plutonium) in the uranium product stream (1BXU) should be below 1×10^7 disintegration/min/g U. This corresponds to a separation factor SF_{Pu} between 10^2 and 10^3 depending on the composition of the fuel treated.
3. The uranium content in the plutonium product stream (1BSP) should be below 50,000 ppm. This corresponds to a SF_U between 10^3 and 10^4 depending on the fuel treated. A rather high uranium content of the 1BSP stream could be tolerated here as an additional DF_U of 10^4 could be expected in the subsequent final plutonium purification unit (see Fig. 1).
4. The aqueous phase in the 1BX column should be acidified to more than 1M-HNO_3 to assure good extraction of U^{4+} and U^{6+} by the TBP phase. On the other hand, a high acidity suppresses the reduction of plutonium as Equation (1) shows:
   $$2Pu^{4+} + U^{4+} + 2H_2O \rightleftharpoons 2Pu^{3+} + UO_2^{2+} + 4H^+ \quad (1)$$
   It furthermore increases the re-oxidation of Pu (III) according to:
   $$3Pu^{3+} + NO_3^- + 4H^+ \rightleftharpoons 3Pu^{4+} + NO + 2H_2O \quad (2)$$
5. The organic aqueous (O/A) flow ratio in the 1BX column should not be taken too high ($O/A \leqslant 10$) in order to avoid a high plutonium content in the uranium product stream.
6. The reductant should be distributed over the 1BX column by feeding the column with two reductant streams, one at the top of the extraction column, the other a quarter the way up from the bottom.
7. A U^{4+}/Pu mole ratio $\geqslant 5$ should be maintained. This condition was taken from French pilot trials[11] which indicated that such a ratio assures effective partitioning. The mole ratio in the Eurochemic plant was somewhat arbitrarily chosen at 8. No tests were performed at lower ratios.

Preparation of uranous nitrate

The uranous nitrate solution was prepared by electrolytic reduction of uranyl nitrate in an electrolytic cell with a graphite cathode and a platinum anode. The electrodes were separated by a ceramic diaphragm.

Reduction occurred batchwise with aqueous volumes of 115 l containing 150 gU/l, ~2M-HNO_3 and 0·3M hydrazine. The yield of U^{4+} was more than 90% applying a current of 300A maximum and 7·5 V for about 15 h.

The stability of the reductant was sufficiently high to permit storage for several days, i.e. 10 days with less than 1% re-oxidation.

Process performance

The process conditions of Fig. 1 were maintained in nearly all campaigns. A few conditions were varied occasionally, either as a result of variable feed compositions, or purposely in the hope of optimising the process and these were the flow distribution of the reductant over the two entry points into the 1BX column and the BSA/BSX flow ratio in the BS column. Table II shows these variations and their effect on the partitioning efficiency. This table shows that the process criteria for the uranium and plutonium products leaving the 1BX and 1BS columns respectively, could be met.

In Table III the partitioning efficiency for ferrous sulphamate is compared with that of uranium(IV) nitrate, treating the same type of fuel. Table III shows lower partitioning efficiency when applying uraneous nitrate instead of ferrous sulphamate.

Nevertheless, uranium(IV) nitrate has performed satisfactorily at Eurochemic i.e. yielding 1BXU and 1BSP products within the determined specifications. The plutonium fraction that left the BX column in the 1BXU stream (0·2–1%) is recovered in the 2 DW stream. This stream from the 2 D column is re-used in the plant after evaporation in an intercycle evaporator for dissolution of new fuel elements.

TABLE II

Uranium/plutonium partitioning in 1 BX and 1 BS columns during the LEU-70 Subcampaigns

Process stream	HSP		BXR_1	BXR_2	BSA	U(IV)/Pu	BSP				BXU				BSP	BXU
Sub-campaign	Pu g/l	l/h	l/h	l/h	M HNO_3	Mole ratio	l/h	Pu g/l	U g/l	U,ppm	l/h	U g/l	α disintegrations /min/l	α disintegrations /min/gU	SF_U	SF_{Pu}
LEU-70/1	0·25	180	2	2·2	1	8·2	20	2·2	0·135	$6{\cdot}1\times10^4$	160	50	4×10^8	8×10^6	5×10^3	$1{\cdot}1\times10^2$
LEU-70/2	0·45	80	1·7	1·5	1	8·2	20	2	0·060	$3{\cdot}0\times10^4$	90	35	$5{\cdot}5\times10^8$	$7{\cdot}5\times10^6$	7×10^3	3×10^2
LEU-70/3	0·5	70	1·5	1·0	2	8	20	2	0·010	5×10^3	80	40	2×10^8	5×10^6	3×10^4	5×10^2
LEU-70/4	0·1	90	0·5	0·5	2	8	20	0·70	0·030	$4{\cdot}3\times10^4$	100	30	3×10^7	1×10^6	2×10^4	$5{\cdot}6\times10^2$

TABLE III

Comparison of partitioning performance of 1BX and 1BS columns at Eurochemic applying different reductants when treating same type of fuel

Fuel characteristics: unitial U-235 content ~ 2·5%
burn-up ~ 15000 MWd/ton
cooling time ~ 150 days
Pu content ~ 5 g Pu/kgU
specific activity 300-600 Ciβ/kg U

Reductant	Separation factors	
	1 BXU SF_{pu}	1 BSP SF_U
Ferrous sulphamate mole ratio: $\frac{Fe}{Pu} \sim 2$	2×10^3	$\sim 10^5$
Uranous nitrate mole ratio: $\frac{U^{4+}}{Pu} \sim 8$	3×10^2	6×10^3

A high DF_α in the 2 D column was obtained ($\sim 10^3$). The feed solution to the 2 D column was therefore treated first with hydrazine (0·2 M) and then with uranium(IV) nitrate. The U end product could easily be kept within specifications ($\alpha < 15{,}000$ disintegrations/min/g U).

The relatively low SF_{Pu} in the BX column could be explained in terms of the kinetics of the reduction reaction in the two phases in the BX column.* According to Talmont[12] and Naylor[13] the apparent reduction rate constants are proportional to the concentration of U^{4+} in the aqueous phase and to $\frac{1}{(HNO_3)^2_{aq.}}$ SF_{Pu} may therefore be improved by lowering the acidity in the BX column.

Table II further shows that the SF_u improves by increasing the acidity in the BS column.

The following general conclusions can be drawn from experience: (i) uranous nitrate has been successfully applied as a reductant in air-pulsed column extractors on an industrial scale; (ii) an 8-fold excess of U^{4+} is sufficient to keep the plutonium breakthrough in the 1 BXU stream to less than 1·0%. By increasing this excess no major effect on the partitioning efficiency was noticed; (iii) splitting the reductant stream into two favours the efficiency as it improves the concentration profile of the reductant throughout the BX column. Variation of the $\frac{1BXR_1}{1BXR_2}$ flow ratio between 0·6 and 1·5 appeared to have no major effect on the partitioning efficiency. Experience has further shown the negative effect of feeding the reductant stream together with the HSP stream near the bottom of the BX column, as under these conditions large uranium losses were found in the 1 BSP stream; (iv) the efficiency might be improved by applying lower acidities in the BX column and higher acidities in the BS column; (v) heating the BX column to 60°C appeared to have no major effect on the partitioning efficiency, as compared to room temperature.

Solvent performance

Solvent degradation by irradiation is not only a function of absorbed radiation dose. Stieglitz *et.al* [14] recently reported the influence of certain process conditions on solvent degradation. Among these are the presence of a one-phase or mixed phase during irradiation, the acidity in the aqueous and organic phases, the concentration of U^{4+} and U^{6+} in the system and whether there is adequate

*The intensity of phase mixing in the BX column is relatively low compared with the other columns which all have more efficient cartridges (see Tables I and II of ref. 10). Bad mixing requires longer residence times in the BX column. This unfortunately favours simultaneously the re-oxidation of U^{4+} and Pu^{3+}.

washing of the solvent in between exposures. These factors make extrapolation of laboratory data to plant-scale conditions unreliable.

Among the process data which were followed during the LEU 1970 campaign were: the Zr and Ru activity of the 1st cycle solvent, before and after washing with Na_2CO_3 (see Fig. 1) and the HDBP α-and γ-activity of the 2nd plutonium solvent.

Solvent exposure

1st extraction cycle

The radiation dose received by the solvent per pass through the HA column was calculated by multiplying the radiation power density in the HA column by the residence time of the organic phase in the column during each pass. The applied equation was:

$$E = t\ (D_\beta + 0{\cdot}5\ D_\gamma) \times \frac{HAF}{HAF+HAS+HSS} \times P \qquad (3)$$

where

E=the radiation dose in Wh/l received by the solvent during each pass through the HA column.

t=the residence time of the solvent in the HA column (h).

D_β=β-power density of the HAF solutions (W/l).

D_γ=γ-power density of the HAF solution (W/l).

HAF, HAS, HSS=flow rates of respective process streams in HA column (l/h).

P=fraction of aqueous phase dispersed in the solvent of the HA column.

In calculating these various terms, the following assumptions were made: the aqueous droplet size in the mixing section of the HA column is so small that all β-energy is absorbed by the solvent phase; the γ-energy absorbed by the solvent is equal to 50% of the total γ-energy dissipated by the aqueous phase; and the power density in the bottom decanter of the HA-column is equal to that in the mixing section of the column.

The β- and γ-power densities were calculated from the fuel characteristics of the various fuels treated, such as burn-up, irradiation time and cooling time. The densities are summarised in Table IV, for all fuel treated since plant start-up. In Table IV the corresponding radiation doses per pass through HA and the accumulated dose received during each sub-campaign are also shown.

2nd plutonium cycle

The dose received by the solvent per pass through the mixer-settler equipment was calculated from the plutonium concentration in the organic phase, the isotopic composition, the average energy of the emitted α-particles and the residence time of the organic phase in the mixer–settler unit.

The assumption here is that the entire energy emitted by α-disintegration is absorbed by the solvent.

The applied equation was:

$$F = t\,[Pu]_0 \times A_\alpha \times E_\alpha \qquad (4)$$

where

F=the radiation dose received by the solvent during each pass through the mixer-settler (W.h/l).

t=residence time of the solvent in the mixer–settler equipment (h).

$[Pu]_0$=average concentration of plutonium in the organic phase (g/l).

A_α=specific activity of plutonium treated (disintegrations/h.g Pu).

E_α=energy of α particles emitted by plutonium (W.h/dis.)

Equation (4) assumes that the radiation dose from β- and γ-rays can be neglected. For calculating A_α and F_α, the variation in the isotopic composition. of the plutonium quantities treated was taken into account.

As the solvent was replaced three times during the 1970 campaigns the accumulated doses were calculated for each campaign. They are indicated in Table V.

TABLE IV

Solvent exposure and accumulated dose in HA column

Campaign	Power density fuel W/kg U		Flow rates l/h				HAF		P	Residence time per cycle, h		Exp.* Wh/l per pass	Acc. dose Wh/l	Average specific activity mCi/l			
														^{95}Zr		^{106}Ru	
	β	γ	HAF	HAS	HSS	HAX	U conc. g/l	Power dens. $D_\beta+0{\cdot}5D_\gamma$ W/l	Fraction aq. phase total vol.	Column	Decanter			HAX	ICW	HAX	ICW
LEU-68/1	1·40	0·53	60	21	15	160	200	0·33	0·15	0·8	0·2	0·030	0·32	—	—	—	—
LEU-68/2	0·23	0·08	60	21	15	160	200	0·05	0·15	0·8	0·2	0·005	0·34	—	—	—	—
LEU-68/3	1·04	0·20	60	21	15	160	150	0·28	0·15	0·8	0·2	0·027	0·38	—	—	—	—
LEU-68/4	1·01	0·19	160	20	12	125	70	0·08	0·19	1·0	0·3	0·013	0·39	0·2	0·6	0·4	0·9
LEU-68/5	0·35	0·08	60	21	18	180	250	0·10	0·15	0·7	0·2	0·008	0·41	0·3	1·5	0·5	0·9
LEU-69/1	0·28	0·08	60	21	18	180	250	0·08	0·15	0·7	0·2	0·007	0·42	0·2	1·2	0·4	0·7
LEU-69/2	0·70	0·18	70	25	15	160	190	0·15	0·15	0·8	0·2	0·015	0·50	0·03	1·0	0·2	1·5
LEU-69/3	0·16	0·04	70	25	15	160	190	0·03	0·15	0·8	0·2	0·003	0·50	0·2	0·06	0·6	2
LEU-69/4	1·04	0·22	60	25	15	160	180	0·21	0·15	0·8	0·2	0·018	0·58	0·01	0·3	1·5	2
LEU-70/1	0·37	0·10	60	25	15	150	200	0·08	0·15	0·8	0·2	0·008	0·60	1·0	1·0	3	3
LEU-70/2	1·66	0·59	40	20	11	80	175	0·37	0·11	1·7	0·5	0·051	0·66	4	4	8	5
LEU-70/3	0·51	0·16	40	20	11	80	130	0·09	0·11	1·7	0·5	0·012	0·68	10	10	10	10
LEU-70/4	2·84	1·13	80	20	11	75	60	0·23	0·13	1·8	0·5	0·051	0·70	15	30	5	6

*To obtain the exposure in Mrad, multiply by 0.438

Process performance

Solvent of 1st uranium cycle

Figs 3 and 4 show the variation of the zirconium and ruthenium content, respectively, of the 1st extraction cycle solvent before and after washing with 0·5M-Na_2CO_3.

TABLE V

Doses received by solvent of 2nd plutonium cycle during 1970 campaigns

Period indication	Dose received per pass through mixer–settler W. h/l	Dose accumulated in each period W. h/l
1	0·09–0·14	4
2	0·03–0·29	3
3	0·02–0·18	3
4	0·02–0·18	3

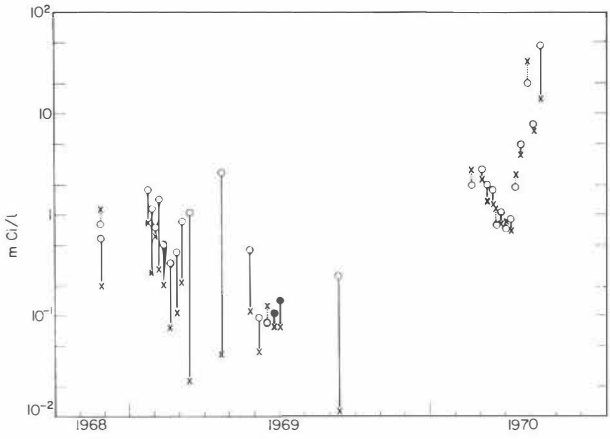

FIG. 3. ^{95}Zr *activity in solvent 1st U cycle before (ICW) and after (HAW) carbonate wash*

○ ICW; × HAW

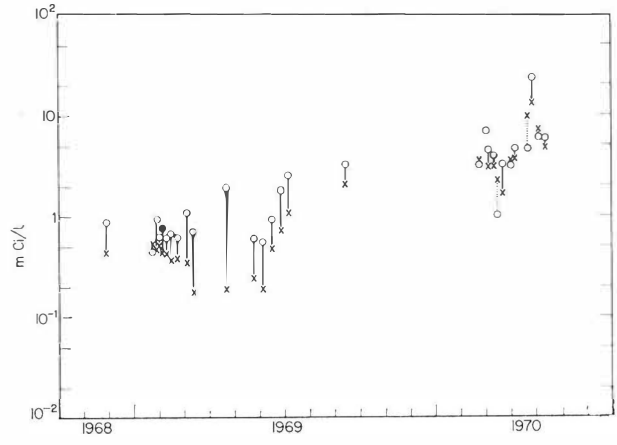

FIG. 4. ^{106}Ru *activity in solvent 1st U cycle before (ICW) and after (HAW) carbonate wash*

○ ICW; × HAW

They show that during the 1968 and 1969 campaigns the specific Zr activity could be kept below 1 mCi/l; this is in contrast with the 1970 campaigns. The relatively high specific activity of zirconium (and ruthenium) during the 1970 campaigns can be attributed to malfunctioning of the impeller in the mixer–settlers of the solvent wash unit during this period. Mixing was therefore relatively poor.

Table IV shows the specific activity of Zr and Ru as a function of the accumulated dose /l of solvent. In calculating the absorbed dose/l of solvent it is assumed that the radiation dose absorbed during each subcampaign was homogenously distributed over the entire solvent batch present in the plant.

In these calculations any volume increase of solvent and solvent refreshments during plant operations has been taken into account. It may be concluded that in spite of the low efficiency of the solvent wash unit during 1970 the solvent has performed satisfactorily even under circumstance of treating feed solutions with high power densities (up to 0·37 W/l) with solvent that has received a maximum total radiation dose of 0·7 Wh/l.

Solvent of 2nd plutonium cycle

Fig. 5 shows the variation of the HDBP content and the α- and γ-retention in the solvent during the 1970 sub-campaigns. The data refer to solvent tank 45 (see Fig. 1). During the 1970 campaigns, the solvent was refreshed three times. The reason for these refreshments was flooding of the mixer–settler resulting in a sudden increase of the specific α- and γ-activity.

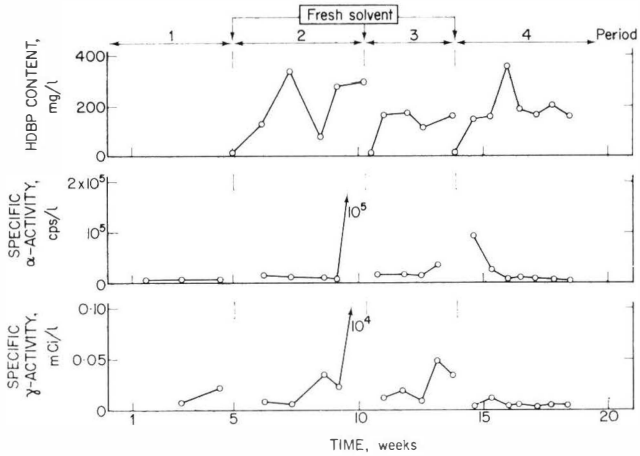

FIG. 5. *Solvent quality of 2nd Pu cycle during 1970 LEU campaign*

In both cases flooding was caused by operating difficulties. They are not believed to be directly related to radiation damage.

Fig. 5 shows variations in the HDBP content between 40 and 350 mg/l under exposures up to 0·3 W/l per pass through the mixer–settler. It further shows that the accumulated dose did not have a major effect on the HDBP content. This indicates that the removal of HDBP in the solvent wash step was adequate. Fig. 5 also shows a rather constant α- and γ-retention in the solvent. The retention seems not to be severely affected by the accumulated dose received. This could also be attributed to the solvent wash. Neither the high exposure rate in the mixer-settler equipment nor the accumulated high doses appeared to have a major effect on the solvent performance during plant operation.

The plutonium losses were of the same order of magnitude as obtained when running a 'diluted plutonium' flowsheet. The decontamination factors also

remained fairly constant. They are shown in Table VI. Although Table VI is of limited value in evaluating the effect of radiation damage on process performance of the solvent, it may be concluded that at solvent exposures of up to 0·3 Wh/l per pass, no decrease in decontamination factors for zirconium or ruthenium was observed.

TABLE VI

Decontamination factors obtained during LEU campaigns in the 2nd Pu-extraction cycle

Year	Solvent loading gPu/l	DF_{Zr}	DF_{Ru}
1967	3	4×10^2	1×10^2
1970	20	4×10^2	1×10^2

Formation of heavy phase and deposits in the 2nd Pu cycle

Operating difficulties, which were initially unrelated to solvent stability, caused intermittent process shutdowns during certain of the process campaigns. The main difficulties were: flooding of the mixer–settler equipment; plugging of airlifts and sampling lines; and unreproducible sample results. These difficulties were caused by formation of heavy phases and deposits in certain parts of the process equipment.*

Evidence for this formation has been gained from observations of samples taken from process streams and from visual inspection of the process equipment.

Operating 'disturbances'

Operating disturbances were encountered: (a) with the intercycle evaporator between the first extraction cycle and the 2nd plutonium cycle (evaporator 2X in Fig. 1). Obstructions in the bottom of the evaporator caused unstable flows through the feed leg to the evaporator, resulting in high plutonium losses in the distillate; (b) with the mixer–settler unit in the 2nd plutonium cycle. Blockage of the baffle plates between mixing- and settling-chambers resulted in flooding and distortions in the flow pattern of the process streams.

Heavy phases and deposits were observed: (a) in the heels of the vessels receiving concentrated process streams from evaporator 2X; (b) in the heels of the vessels receiving the aqueous 2BP product stream from the mixer–settler bank in the 2nd plutonium unit.

Nature of heavy phase and deposits

The heavy phase was organic in nature, containing about 0·1–1 gPu/l. The heavy phase showed a relatively high specific $^{95}Zr/^{95}Nb$ activity (~50 Ci/l) and was insoluble in kerosene, nitric acid or TBP. The solid phase was generally organic in nature containing 1–10 mg/Pu/cm^3. Sometimes the deposits dissolved in 30% by vol. TBP although the solution did not become clear. When such a solution was subsequently mixed with an aqueous phase (3M-HNO_3) the deposits reappeared. No special effort has yet been made to investigate the nature of these phases in detail. Spectrometric analysis indicated that nearly all elements which had entered into the process were present.

Test on a laboratory scale

1. Some laboratory tests were performed in concentrating solutions with a composition similar to the 1BSP stream (1·2M-HNO_3 precontacted with 30% TBP/SST). The concentration process of the intercycle evaporator

*In this paper the term heavy phase means a liquid phase, immiscible with the aqueous process solutions and a density higher than the aqueous phase. A heavy phase is not necessarily miscible with the solvent phase. The designation deposit is used for all kinds of solids observed in process solutions. They accumulate either on the surface, interphases or on the bottom of extraction mixtures.

was simulated i.e. a residence time of 50 h and a concentration factor of 10 were applied. The effect of certain process parameters, such as the presence of zirconium, DBP and stainless steel, was investigated. Thorium was used as stand-in material for plutonium. The evaporator (0·5 l volume) was made out of glass.

The study revealed that: white precipitates are formed in quantities 2–50 mg precipitate/l treated depending on the DBP content; the deposits are organic in nature containing 10·8% by wt. P; the deposits do not dissolve in 30% TBP/SST; and the main fraction of the zirconium content is contained in these deposits.

2. As heavy phase formation was feared to be caused by the relatively high plutonium loadings of the solvent in the 2nd plutonium cycle, the stability of the solvent was tested at high plutonium loadings. Fig. 6 shows the saturation curve of plutonium (IV) nitrate in the system 30% TBP/SST–plutonium (IV) nitrate–5 M-HNO_3 above which the solvent splits into two immiscible fractions, one rich in TBP and plutonium with a density higher than the aqueous phase; the other poor in TBP and plutonium and a density lower than the aqueous phase.

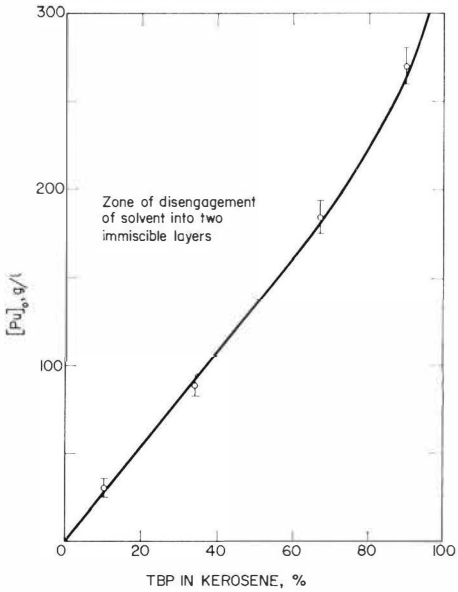

FIG. 6. *Maximum Pu concentration in solvent above which disengagement occurs*[7]
Solvent presaturated with 5M-HNO_3

Discussion

Formation of heavy phase and deposits originate from evaporators which are fed by aqueous solutions containing a significant amount of solvent. The solvent content is dictated by its solubility in the aqueous phase, the extent of solvent entrainment by this solution, and the separation efficiency in the decantation unit prior to feeding the evaporator. Under strong boiling conditions, the solvent content suffers from thermal degradation, thereby forming a heavy phase and deposits which accumulate at the bottom of the evaporator. Analysis of the heavy phase showed high Zr activities. The high complexing properties of DBP with zirconium[4, 16] support the hypothesis that thermal degradation of TBP produced DBP, MBP and other phosphates. Such degradation products may easily cause operating difficulties when fed to the mixer–settler batteries of the 2nd plutonium extraction cycle, thereby plugging the 7 mm high slots in the bottom of the settling chambers.

Spontaneous disengagement of the solvent due to over-saturation with plutonium in the mixer–settler battery is not believed to be responsible for the operating difficulties in this extraction unit. Fig. 6 shows a high plutonium loading (~90 gPu/l) solvent in 30% TBP, compared to the applied solvent loadings of 12–25 gPu/l in the 2nd Pu cycle (Fig. 1).

Conclusions

Experience of 4 years at Eurochemic has revealed that reprocessing nuclear fuel with a burn-up of up to 26,000 MWd/t can be realised in a two-cycle Purex process. Solvent loadings of up to ~20 g Pu/l have been obtained in the 2nd Pu extraction cycle.

Uranium(IV) nitrate has been successfully applied in air-pulsed columns. The required partition efficiency could be achieved. However, compared with ferrous sulphamate, uranium(IV) nitrate showed a lower partition efficiency.

Solvent exposures of up to 0·3 Wh/l solvent per pass through the mixer–settler equipment of the 2nd Pu cycle were experienced and did not have a major effect on the solvent performance. Solvent performance was satisfactory even after accumulation of radiation doses of up to 4 W/l solvent.

Under certain process conditions heavy phase formation and precipitation occurred causing many operating difficulties in subsequent process steps.

Formation of these heavy phases and deposits was found to occur mainly in evaporators, which are fed by aqueous solutions of high solvent content and in which concentration factors are relatively high.

References

1 Gaudernack, B., Lindland, K. P., & Joseph, C. J., *Proc. 3rd U.N. int. Conf. Peaceful Uses atom. Energy, Geneva*, 1964, **10,** 253

2 Mendel, J. E., *Rep. Congr. atom. Energy Commn U.S.*, 1965, HW-82103

3 Blake, C. A., *ibid.*, 1968, ORNL-4212

4 Faugeras, P., & Talmont, X., 'Radiolysis and Hydrolysis of TBP and their Effects', *C.E.A. Conf.*, 1969, 1265

5 Barendregt, T. J., Detilleux, E., & Rometsch, R., Eurochemic Technical Report ETR-210, 1967

6 Barendregt, T. J., 'Conception of the Eurochemic Reprocessing Installation', 1964 (Mol: Eurochemic Co.)

7 Salomon, L., *et al.*, Eurochemic Internal Reports IDL-21 and IDL-26, 1970

8 Chitnis, R. T., *et al. Rep. Congr. atom. Energy Commn U.S.*, 1969, BARC-430

9 Salomon, L., Lopez-Menchero, E., & Ilardi, S., Eurochemic Technical Report ETR-186, 1967

10 Joseph, C. J., van Geel, J. N. C., Detilleux, E., & Centeno J., *Proc. int. Solvent Extraction Conf., The Hague*, 1971 (London: Society of Chemical Industry)

11 Regnaut, P., *et al.*, *Proc. 2nd U.N. int. Conf. Peaceful Uses atom. Energy, Geneva*, 1958, **17,** 73

12 Talmont, X. L. R., *Proc. Symp. Solvent Extraction Chemistry of Metals*, 1965, p. 103 (London: Macmillan)

13 Naylor, A., KR-126, 1967, p. 172

14 Stieglitz, L., Ochsenfeld, W., & Schmieder, H., KFK-691, EUR-3712 d, 1968

15 Gustafsson, B., *et al.* ETR-218 1967

16 Hoffart, A. L., & Thomson, R. G., IDO-14643, 1967

17 Wischow, R. P., *et al.*, 'Safeguards Procedures Manual for the NFS Reprocessing Plant'. *TID* 23991, 1966, 2

18 Well, I., & Pepper, D., in 'Chemical Processing of Reactor Fuels, Nuclear Science and Technology', (Ed. Flagg) 1968, p. 318 (London: Academic Press)

19 Jouannaud, C., *ENEA Symp. Aqueous Reprocessing Chem., Brussels*, 1963, p. 167

20 Bruce, F. R., *et al.*, *Proc. 2nd U.N. int. Conf. Peaceful Uses atom. Energy, Geneva*, 1958, **17,** 53

21 Cooper, V. R., & Walling, M. T., jun., *Prog. Nucl. Energy (Series III, Process Chem.)*, 1961, **3,** 3229

22 Prevot, I., *et al.*, *Proc. 2nd U.N. int. Conf. Peaceful Uses atom. Energy, Geneva*, 1958, **17,** 96

Technological experience with extraction equipment at Eurochemic

by C. J. Joseph, J. van Geel, E. Detilleux and J. Centeno
Eurochemic Co., Mol, Belgium

In the reprocessing of irradiated nuclear fuel from power and materials testing reactors, the Eurochemic Company uses both air pulsed columns and geometrically safe mixer–settlers as solvent extraction equipment. A description of the applied process and equipment is given and the technological experience with the solvent extraction equipment, collected during the 4 years of operation, is presented. The influence of different parameters on the extraction performance is discussed, such as the total throughput, heating, and the presence of crud and heavy phase. The experience with direct air purge bottom interface control is dealt with, and the choice of pulsed columns for a new plutonium cycle is discussed.

Introduction

SEVERAL PAPERS describing the Eurochemic plant have already been published.[1,2] Consequently, only the outlines of the applied extraction processes and equipment are given here. Also, reference is made to another Eurochemic paper by van Geel *et al.*[3] presented at this conference.

For the processing of low enriched uranium ($<5\%^{235}U$), the following equipment is employed.

In the 1st cycle, five air-pulsed columns are used. In the first column (HA), the lower part serves for uranium and plutonium extraction and the upper part for fission product scrubbing. The heated scrub column (HS) is used for further fission product scrubbing and the IBX column for plutonium removal from the uranium stream.

In the heated IC column, uranium is stripped from the solvent and in the IBS column, uranium is removed from the plutonium stream. In the 2nd uranium cycle, two air-pulsed columns are used, of which the lower part of the 2D column is for uranium extraction, and the upper part is for fission product and plutonium scrubbing. In the heated 2E column, the uranium is stripped from the solvent.

The 2nd plutonium cycle consists of two geometrically safe mixer–settler banks. The 2A bank is used for acid washing of the solvent, plutonium extraction and fission product scrubbing; the 2B bank for diluent washing, plutonium stripping, the partial separation of the plutonium from the uranium, and for carbonate washing.

For the highly enriched uranium (HEU) process, the following equipment of the low enriched uranium (LEU) process is used.

For the 1st cycle, the HA column is used for uranium extraction and the heated HS and IBX columns for plutonium and fission product scrubbing, while the IC column is used for uranium stripping.

For the 2nd HEU cycle, the equipment of the 2nd LEU plutonium cycle is used.

In the 2A bank acid washing, uranium extraction and decontamination from plutonium and fission products are carried out, while the 2B bank is used for diluent washing, uranium stripping and carbonate washing.

The chemical flowsheets applied are given in the paper by van Geel *et al.*[3]

Equipment

The choice and characteristics of the pulsed columns, based on literature data and experiments in the Eurochemic Testing Station, have been described before.[4] The main characteristics are given in Tables I–III.

The geometrically safe mixer–settlers for 2nd cycle LEU and HEU processing have also been described before.[5] The main characteristics are as follows.

TABLE I

Design characteristics of the Eurochemic pulse columns

Column	Purpose		Continuous phase	Dia., mm	Total height, m	Cartridge type**	Cartridge height, m	Top decant.		Bottom decant.		Pulse tube dia., mm	Material
	LEU*	HEU*						Dia., mm	Height, m	Dia., mm	Height, m		
HA	Extract, scrub	Extract	Organic	150	11·20	(a)	8·980	292·0	1·0	292·0	1·2	53	Stainless steel AISI 304 L
HS	Scrub	Scrub	Organic	131·7	7·1	(b)	5·249	292	1·0	180·0	0·6	53	Stainless steel AISI 304 L
IBX	U–Pu separation	Scrub	Aqueous	100	10	(d)	8·480	292·0	1·0	121·7	0·5	36·0	Stainless steel AISI 304 L
IBS	U–Pu separation	—	Aqueous	49·8	5·1	(c)	3·980	131·7	0·7	131·7	0·4	21·6	Stainless steel AISI 304 L
IC	Strip	Strip	Aqueous	150	8·8	(c)	5·5	180	2·2	180	1·1	53	Stainless steel AISI 304 L
2D	Extract, scrub	—	Organic	131·7	11·0	(a)	9·480	292	0·9	292	0·6	53	Stainless steel AISI 304 L
2E	Strip	—	Aqueous	131·7	7·7	(c)	5·990	292	0·9	180	0·8	53	Stainless steel AISI 304 L

* LEU = low enriched process; HEU = highly enriched uranium process
** see Table II

Each bank is divided into two semi-batteries of 8–9 stages, of 1288 × 370 × 75 mm dimensions.

For reasons of criticality, the height of the organic overflow, which fixes the total depth of liquid in the batteries, is limited to 45 mm.

TABLE II

Cartridge characteristics

Cartridge type	Material	Plate type	Plate characteristics		
			Hole dia., mm	Free area, %	Plate spacing, mm
(a)	Stainless steel AISI 304 L	Nozzle* plates	3·5	22·5	50
(b)	Stainless steel AISI 304 L	Nozzle* plates	3·5	11·0	50
(c)	Stainless steel AISI 304 L	Sieve plates	3·0	22·5	50
(d)	Stainless steel AISI 304 L	Sieve plates	4·8	32·5	100

*The nozzles are directed downwards

Experience

Fuel treated

From active start-up in mid-1966 until September 1970, the Eurochemic Company has treated the following fuel: 48 tons of U metal, containing 30 kg of Pu, originating from 10 reactor batches; 48 tons of UO_2, containing 173 kg of Pu, with a maximum burn-up of 26,000 MWD/ton, originating from 11 reactor batches; and 330 kg of highly enriched U in 8 tons of Al, with a maximum burn-up of 50%, originating from 17 reactor batches.

Throughput

Low enriched uranium in pulsed columns

Before the active start-up of the plant, over a short period, tests were carried out on chemical flowsheet conditions to determine the maximum throughput of the extraction equipment, i.e. flooding capacity. It was found that the scrubbing parts of the extraction columns (HA and 2D) were the most critical ones.

Flooding capacity for the HA column scrub section was found to be 140 l/h/dm^2 at 75 cycles/min and 25 mm amplitude and 190 l/h/dm^2 for the 2D column scrub section at 60 cycles/min and 25 mm amplitude. These values correspond quite well with the design data. The known effect of flooding improvement with increased temperature was shown in a test on the 2D column. By heating the scrub part of the 2D column from 30 to 40–45°C, the flooding capacity increased by ~30 l/h/dm^2. Owing to the limitations of the extraction columns, flooding could not be achieved in the other columns. At 55°C, and 100 cycles/min with pulse amplitudes for the IC and 2E stripping columns of 20 and 25 mm, respectively, no flooding was obtained. The throughputs were 254 and 315 l/h/dm^2, respectively. During the active operation, the total capacity of the 1st cycle was increased by 20% and for the 2nd cycle by 50% without flooding, which gave the following throughputs: 2D column extraction section, 242 l/h/dm^2; 2D column scrub section, 206 l/h/dm^2; and 2E column, 340 l/h/dm^2.

It was shown that an increase in the pulse conditions improved the separation of uranium from plutonium in the IBX separation column; this separation had probably been poor as a result of the low organic hold-up caused by a cartridge of low efficiency. It was not possible to obtain more than 80 cycles/min at room temperature, but by increasing the temperature to ~50°C, 90 cycles/min were achieved.

TABLE III

Operational characteristics of the Eurochemic pulse columns for LEU processing

Column	Purpose (LEU)	Continuous phase	Pulse conditions		Flood capacity, l/h dm²	Normal operating conditions		Theoretical stages*		Operating temp., °C
			Amplitude, mm	Frequency, cycles/min		Flood capacity, %	Total flow, l/h dm²	NTS	HETS, m	
HA	Extract, scrub	Organic	25	60	320	45	145	7	0·7	30
					200	58	116	4	0·7	
HS	Scrub	Organic	25	60	240	58	138	4	0·7	60
1 BX	U–Pu separation	Aqueous	20	60	400	61	243	4	1·1	30
1 BS	U–Pu separation	Aqueous	25	60	320	56	180	4	0·7	30
1 C	Strip	Aqueous	12·5	60	400	52	208	7	0·7	60
2 D	Extract, scrub	Organic	25	60	320	43	164	5	0·7	30
					200	70	139	5	0·9	
2 E	Strip	Aqueous	12·5	60	400	58	232	9	0·7	60

* NTS = number of theoretical stages; HETS = height of equivalent theoretical stage

Highly enriched uranium in pulsed columns

The feed to the plant for reprocessing highly enriched uranium is obtained by dissolving simultaneously the uranium and the aluminium cladding and structural parts of the elements irradiated in materials testing reactors. Consequently, the extraction performance of the HA column is determined more by the aluminium than the uranium, and especially by the impurities in the aluminium alloys. Also at Eurochemic, the phenomena of emulsion stabilisation (normally attributed to the silicon in the alloy) were encountered.

Cold tests with a 97% pure aluminium alloy containing 0·3–0·7% silicon caused flooding at the low feed rate of 70 l/h. Laboratory tests with this feed showed that non-dissolved impurities caused poor phase separation. After this, column tests were made with feed solutions consisting of 1 part aluminium alloy containing 0·6–1·2% silicon and 3 parts aluminium alloy containing only 0·07–0·2% silicon (simulating the 'harder' structural and 'softer' cladding parts of the elements). With this feed, it was possible to arrive at a feed rate of 300 l/h without flooding.

During the active operation, it was not possible to obtain the same feed rates without flooding. By reducing the feed rate to 200 l/h, stable operation was possible. An analysis of the fuel data showed that for the greater part of the elements processed, the average aluminium alloy composition lay between the two cases tested during inactive runs. This indicates that at ~160–280 mg/l Si in the feed solution, the feed rate to the 1st column will have to be reduced (if no pretreatment is done).

Mixer–settlers

The geometrically safe mixer–settlers were tested inactively with the flowsheet conditions for the 2nd cycle of highly enriched uranium processing. Total aqueous plus organic flows of 57 l/h were achieved without flooding. Special problems were encountered during the plutonium processing in these mixer settlers. The 1st plutonium cycle product is concentrated 10–20 times in a geometrically safe evaporator before feeding to the mixer–settlers. As diluent washing and phase separation before feeding to the evaporator are rather poor, the feeding of solvent to the mixer–settlers cannot be excluded. On boiling, this solvent forms a heavy organic phase[3] and causes blockage when fed to the mixer–settler battery. Probably the 7-mm high slots in the aqueous outlets at the bottoms of the settling chambers are the first to clog as there is no turbulence around these low points. At least once a month, it was necessary to empty and clean the mixer–settler battery during plutonium processing.

Efficiency

Pulsed column

To determine a precise and not a minimum height of equivalent theoretical stage (HETS) in the extraction columns, the level in the raffinate stream must be above the analytical detection limit (for $U \geqslant 1$ mg/l). Because of this, precise calculations only for uranium could be made over the 2D extraction column. An average HETS of ~90 cm was found under LEU flowsheet conditions in the extraction section. For the two strip columns (IC and 2E), an average HETS of ~50 cm was found. For plutonium, the average HETS in the extraction part of the HA column under flowsheet conditions was ~1·5 m. This higher HETS can be explained by the fact that the concentration gradients for plutonium are smaller than for uranium under flowsheet conditions.

Mixer–settlers

During inactive tests of the HEU flowsheet with the mixer–settlers still open, it was possible to take samples in each settling chamber. The overall extraction efficiency of each stage for uranium in the extraction as well as in the stripping

bank was found to be ~70% of a theoretical stage with the impellers turning at ~700 rev/min. From results obtained during active operation (only sampling of feed and waste flows was possible), it was calculated that, over the extraction section of the cycle, the efficiency for plutonium extraction was 50% per stage at 700 rev/min. This lower efficiency can be explained here in the same way as with the pulsed columns.

Decontamination factors (DF)

The decontamination factors obtained at Eurochemic have already been reported[3,6–9] and will not be discussed in this paper. Data will be reported only for cases where the decontamination was directly related to the technology of solvent extraction.

Bottom interface

As is known, the advantage of the bottom interface in columns used for extraction purposes derives from the fact that the organic product flow does not have to pass the crud-containing interface, which results in improved decontamination.

This was clearly shown when comparing the results of Eurochemic (bottom interface) and Idaho (top interface)[10,11] for the processing of highly enriched uranium. The fuel and the flowsheet were similar, but the DF values for the 1st cycle at Eurochemic were ~10^2–10^3 times higher. Especially for a flowsheet for highly enriched fuel, a bottom interface is very important, as the feeds to the HEU process contain solids.

Scrub columns

The lay-out of the columns and the sampling installation for the first cycle (extraction part) made it possible to determine the DF values over the first cycle extraction and scrub columns. For the LEU flowsheet, ruthenium and zirconium DF values of 5–10 were found for the HS scrub column, and for the HEU flowsheet, DF values of ~10 and 2–3, respectively, were found for the HS and BX columns. These results support the known fact that additional scrubbing equipment does not have much effect; this is because certain proportions of the zirconium and ruthenium are present in non-scrubbable forms. This even led to additional DF values of ~10 in the stripping column, as zirconium and ruthenium stayed in the solvent and did not follow the uranium. However, sufficient stages should always be available after the feed point, because the scrubbing sections of the columns have also an important function for disentrainment of entrained feed droplets, which could greatly influence fission product decontamination.

Special instrumentation

To control the bottom interface and to detect changes which could lead to losses, the following devices have been installed and successfully operated by Eurochemic.

Bottom interface control

The special dip tube geometry needed in the bottom settler to obtain a stable signal from the interface dip tubes, in spite of the pulsation, was tested in the Eurochemic Testing Station, and has been described previously.[4] During inactive testing, the oscillation of the signal from the pneumatic-electric Foxboro transmitter was such that stable control became impossible. Pneumatic dampers in the pneumatic signal to the transmitter were not successful, but after installing two low voltage capacitors in parallel (5000 μF each) in the electrical signal from the transmitter, control became possible and there has been successful operation for 4 years. Of the three bottom interface controlled columns, two are controlled by a pressure-pot and one by an airlift in the aqueous outlet.

Column weight measurement

By following the weight of the contents of a column, useful operational information can be obtained.

The weight of the contents of a column is determined by (1) the solvent: aqueous volume ratio within the column, and (2) the densities of the two phases within the column.

Thus, a heavier column could indicate an increase in volume hold-up of the aqueous phase and/or an increase in solute (e.g. uranium) concentration in the aqueous or solvent phase, which would eventually lead to malfunctioning of the column.

A change in the solvent: aqueous volume ratio within a column can be achieved by a change in pulse conditions. Therefore, in operation, if the weight of a column is checked after each change in pulse condition, control of the column can be maintained without flooding or other malfunctioning. This system of changing the pulse product in a column can be used to obtain maximum dispersion without flooding.

To have a rather precise column weight measurement, the following set-up was installed: the highest dip tube of the bottom interface control system was connected to a 125-mm range transmitter and the pressure of the column on the membrane of the transmitter was compensated for by an adjustable mercury column.

Extraction temperature measurement

The fact that the extraction of uranium is an exothermic reaction is used at Eurochemic for the detection of the extraction zone. When the extraction zone in the column is dropping, uranium losses can be expected. Thermocouples are connected to the wall of the extraction part of the extraction column at intervals of ~1 m. Temperature increases of 5–8°C were found in the HA column and 10–15°C in the 2D column, where a more concentrated feed is used. In practice, it is not the absolute temperature that is important, but the relative temperature differences. If, for example, the measuring point that normally gives the highest temperature should decrease and the measuring point situated 1 m below should increase, uranium losses can be expected if no counter-action is taken.

Discussion

Four years of operational experience at Eurochemic have shown that the pulsed columns in the first cycle were the right choice for a multi-purpose plant. No problems were encountered in running flowsheets of different feed and extractant densities. For instance, to use the 2nd LEU pulsed column cycle for a 2nd HEU cycle (planned to operate at the beginning of 1971), the only changes that will be required will be in the piping.

Because an HA column with a continuous organic phase, was used, no breakthrough of crud particles with adsorbed fission products has occurred For the use of feed solutions containing solids the pulsed columns have been shown to be very reliable. Although the feed line (i.d. 21·6 mm) was clogged, no blockage in the column itself was encountered. In general, the design values have been shown to be correct.

The safe-geometry, slab-type mixer–settlers used for the 2nd plutonium cycle and HEU processing have been found to block very easily due to solids and heavy organic phases.

As a result of the above experience, the new 2nd plutonium cycle at Eurochemic, planned to be in operation by the end of 1971, will contain the following features: no intercycle concentration by boiling, the use of pulsed columns instead of mixer–settlers, and concentration of the product by a reducing strip and, if needed, by recycle. An additional advantage of pulsed columns in a plutonium cycle is the favourable geometry for criticality control.

Acknowledgment

Grateful acknowledgment is made of the help received from Mr. L. Geens during the non-active tests.

References

[1] Barendregt, T. J., 'Conception of the Eurochemic reprocessing installation', 1964 (Mol, Belgium: Eurochemic)

[2] Barendregt, T. J., Detilleux, E., & Rometsch, R., 'Aqueous reprocessing in a multi-purpose plant', Eurochemic Technical Report ETR-210, 1967; Paper presented at the Symposium on 'Recent Advances in Reprocessing of Irradiated Fuels', New York, Nov. 30th, 1967

[3] van Geel, J., Joseph, C. J., Detilleux, E., Heinz, W., Centeno, J., & Gustafsson, B., *Proc. int. Solvent Extraction Conf.*, 1971 (London: Society of Chemical Industry)

[4] de Witte, R., *Atompraxis*, 1966, **12**, (1), 42

[5] Ludwig, H. B., Lopez-Menchero, E., & van Geel, J., *Atompraxis*, 1966, **12** (1), 36

[6] Cao, S., Gustafsson, B., & Joseph, C. J., 'The reprocessing campaign of the fuels from the Swiss reactor Diorit', Eurochemic Technical Report ETR-215, July 1967

[7] Gustafsson, B., Joseph, C. J., Thorstensen, S., van Geel, J., & Cao, S., 'The reprocessing campaign of fuel from the German reactor FR-2 and the Belgian reactor BR-1', Eurochemic Technical Report ETC-218, Nov. 1967

[8] Detilleux, E., & Cao, S., 'Recent Eurochemic reprocessing experiences', Eurochemic Technical Report ETR-232, 1968; Paper presented at the American Nuclear Society winter meeting, 1968

[9] Joseph, C. J., van Geel, J., & Cao, S., 'The reprocessing campaigns for highly enriched uranium during 1967 and 1968 at Eurochemic', Eurochemic Technical Report ETR-238, Sept. 1969

[10] Wheeler, B. R., Offutt, G. F., & Commander, R. E., *Rep. Congr. atom. Energy Commn U.S.*, 1966, IDO 14669

[11] Palica, W. P., & Gold, M. D., *Rep. Congr. atom. Energy Commn U.S.*, 1969, IN-1153

SESSION 4A

CHEMISTRY OF METALS EXTRACTION, II

CHAIRMAN

Prof. H. Irving

SECRETARIES

Dr. N. M. Rice
Dr. G. J. Lawson

Extraction of tin and indium with tributyl phosphate from hydrochloric acid solutions

by M. Goliński
Institute of Nuclear Research, Warsaw-Żerań, Poland

The extraction of tin and indium with tributyl phosphate (TBP) from HCl solutions and the conditions of separation of these metals during extraction in static conditions, and by extraction chromatography (dynamic condition) have been studied. The mechanism of extraction of tin and indium by extraction and spectrophotometric methods has been established.

Using extraction chromatography it is possible to obtain the isotope ^{113m}In in a radiochemically pure form from ^{113}Sn. The bed of the chromatographic column contained siliconated kieselguhr and TBP as extractant.

Using the method proposed a very pure product (99·999% In) was obtained from raw material containing about 20% tin.

Introduction

NATURAL INDIUM OCCURS more frequently in association with tin than with the elements of group III of the periodic table (Al, Ga, Tl). This is connected with the isomorphism of indium and tin compounds. Various tin minerals are enriched in indium, and indium minerals often contain tin.[1]

One of the radioactive tin isotopes, ^{113}Sn, decays by K capture to ^{113m}In.

Several authors have studied the separation of indium and tin. Anion exchangers[2–4] or inorganic exchangers such as zirconium oxide,[5–8] have been used. Indium was also extracted by β-diketones or by alkylphosphoric acids tin being masked with oxalic acid. In the latter case the separation of indium from tin was achieved by a back extraction process.[9,10]

So far no use has been made of tributyl phosphate (TBP) extraction to separate indium and tin. However, literature data concerning the individual extraction of these metals indicate such a possibility.

The major part of the extraction of indium by TBP was performed at trace concentrations of the metal. The extraction experiments were carried out from halogeno-hydrogen acids,[11] hydrochloric acid,[12–15] or nitric acid containing the iodide ions.[16] The optimum extraction conditions for trace indium concentrations occur at 4–6M-HCl. From nitric acid solutions the extraction of indium is less efficient.[14] The extraction coefficients of indium (D_{In}) increase with increasing HNO_3 concentration and reach a value of about 1 in 15M-HNO_3.[14] From sulphuric acid solutions indium at trace concentrations is very poorly extracted. In the range 0·05–5M-H_2SO_4 the values of D_{In} are 10^{-4}–10^{-3}.[17]

The extraction of indium from 6–8M-HCl solutions was used for analytical purposes to separate macroquantities of this element from gallium and thallium.[18] In a patented extraction method[19] very pure indium was obtained (99·999%) using a 40% TBP solution in benzene and an initial 8–10M-HCl solution containing 40–50 g/l of indium, the extraction being performed in a counter-current apparatus. For a similar purpose a 30% TBP solution in xylene and a 10M-HCl solution were reported.[20]

Data on the extraction of tin by means of TBP are scarce and frequently at variance. It is reported that tin is extracted from a 6M-HCl solution.[21] The extraction results for tin (IV) from a solution of indefinite concentration in HCl are presented in a plot of log D_{Sn} vs. log TBP concentration.[22]

From this relationship it was found that an increase in TBP concentration from 0·025 to 0·16M brings about a rise in D_{Sn} values from 0·004 to 0·063. Extraction chromatography in the TBP (silica gel)–HCl was used to separate Sn(II) from Sn(IV). The elution of Sn(II) was carried out with 11·7M-HCl, and that of Sn(IV) with 1M-HCl.[23,24] Results reported in the literature[14] suggest that the extraction of tin is independent of its oxidation state and the concentrations of HCl and TBP, and the D_{Sn} values are close to 1 for the TBP

range 10–100% and 1–12M-HCl. In the 100% TBP–H_2SO_4–Sn (tracer) system a minimum on the extraction curve appears at 0·5–1M-H_2SO_4. Under the optimum extraction conditions, i.e. at 0·05 and 5·0M-H_2SO_4 the D_{Sn} value is about 1.[17]

It therefore follows that information on the extraction of indium and tin is not numerous and often contradictory. Since the separation of indium and tin is of interest for both the preparation of indium of high purity, and the radiochemical production of the radioisotope ^{113m}In, which finds application in medicine,[6,7] it was decided to use an extraction method with TBP and hydrochloric acid solutions. The work aimed at establishing optimum separation conditions for both metals.

Experimental

Analytical grade TBP was used and was purified before extraction by heating at boiling temperature with a 5% NaOH solution. Indium chloride solutions were obtained by dissolving the metal (99·99%) in a hydrochloric acid solution. Solutions of stannous chloride were prepared in a similar way, and Sn(II) was oxidised to Sn(IV) with gaseous chlorine.

The extraction coefficients of indium and tin were determined by means of the radioactive tracers ^{114}In and ^{113}Sn. The radioisotope ^{114}In was obtained by irradiating metallic indium in the Polish reactor 'EWA', and ^{113}Sn was obtained from the Centre of Production and Distribution of Radioisotopes of the Institute. ^{113}Sn decays to ^{113m}In with a half-life of 104 min. During the extraction process the radioactive equilibrium is disturbed and therefore the radioactivity of the phases, marked with ^{113}Sn and ^{113m}In, was measured 48 h after the phases had been separated, so that the ^{113m}In had completely decayed.

The radioactivity was measured using a well-type scintillation counter (thallium-activated sodium iodide crystal). The absorption spectra in the ultra-violet range were obtained with a Unicam SP700 spectrophotometer in a 1 cm cell. TBP solutions in toluene washed with 4, 6, 8, and 10M-HCl were used as references.

The extraction was carried out by contacting the organic and the aqueous phases for 10 min at 20 ± 3°C, the agitation being performed on an eccentric shaker. The ratio of the phases organic/water was 1. Toluene was generally used as a diluent for TBP, and the use of other diluents is noted in the text.

Results and Discussion

Effect of diluent

The results presented in Table I were obtained by extracting indium and tin (IV) with 1M solutions of TBP in various diluents from an 8M-HCl solution containing 40 g/l of In, and from a 3M-HCl solution containing 5·94 g/l Sn(IV).

TABLE I

Effect of diluent on the extraction of indium and tin (IV)

Diluent	Dielectric constant	Extraction coefficient	
		In	Sn(IV)
Chloroform	4·806	0·03	13·0
Carbon tetrachloride	2·238	0·53	4·24
Benzene	2·234	0·90	10·5
Toluene	2·379	1·03	12·4
Xylene (mixture)	—	—	13·7
Mepasine (Diesel I oil)	—	1·12	37·7
n-Heptane	1·924	1·15	30·6
n-Octane	1·948	1·17	32·4

During the extraction of indium it was found that a second organic phase was formed in the presence of aliphatic hydrocarbons owing to the decreased solubility of the TBP–In complex in these hydrocarbons as compared with aromatic hydrocarbons or halogenoderivatives. Formation of the third phase in this system was also observed by other authors.[20]

The extraction of indium and tin was better the lower the dielectric constant of the diluent (tin and chloroform are exceptional). Similar agreement (except for CCl_4) was found in the extraction of indium from sulphate solutions by alkylphosphoric acids,[25,26] uranium or thorium,[27,28] iron(III) and uranium[29,30] by mono- and di-alkylphosphoric acids. This observation may be explained by the solvation of the extractant with the diluent, which decreases the extent of extraction. The tendency towards solvation rises with increasing dielectric constant of the diluent.[27,28]

Extraction mechanism of indium and tin

The relationship between the extraction coefficient of indium and the concentration of TBP is presented in Fig. 1. The slope of the curves obtained during the extraction of trace amounts of indium (Fig. 1) was 2·3 and implies that the extracted indium is solvated in the organic phase mainly by two TBP molecules and partly by three TBP molecules. The latter value has also been confirmed[31] when indium was extracted at an excess concentration with respect to TBP. The slope of the curves then obtained was close to 3. Taking into account

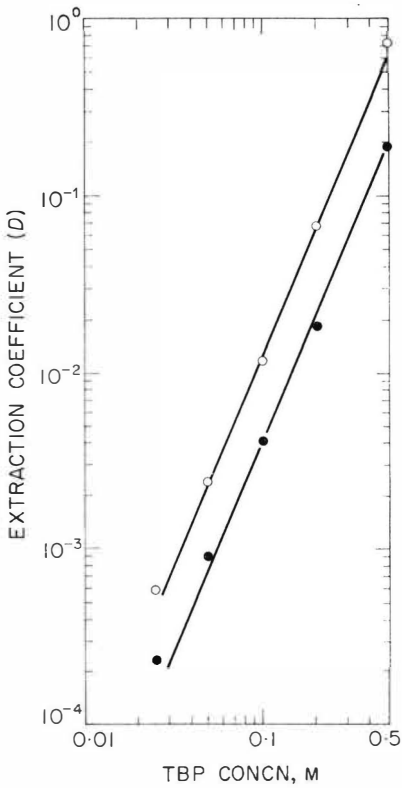

FIG. 1. *Extraction coefficient of indium as a function of the TBP concentration*

Organic phase: TBP at varying concentration in xylene; aqueous phase: trace concentration of indium
● 6M-HCl; ○ 8M-HCl

some earlier results[31] and the results discussed here it may be ascertained that the degree of solvation of indium by TBP is independent of the concentration of HCl.

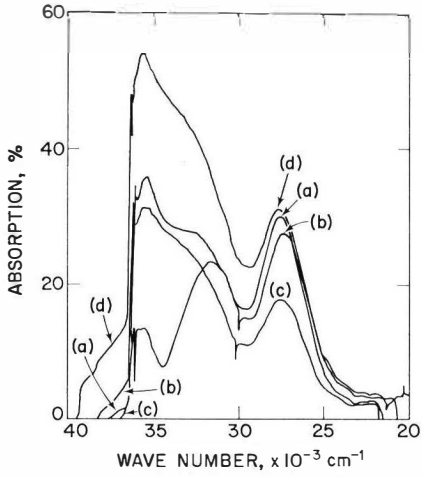

FIG. 2. *Absorption spectra of the indium extracts in the ultra-violet region*

Organic phase: 1M TBP in toluene; aqueous phase 0·1M-In
(a) 4M-HCl; (b) 6M-HCl; (c) 8M-HCl; (d) 10M-HCl
D_{In} = 0·200, 1·80, 5·50 and 5·53 respectively

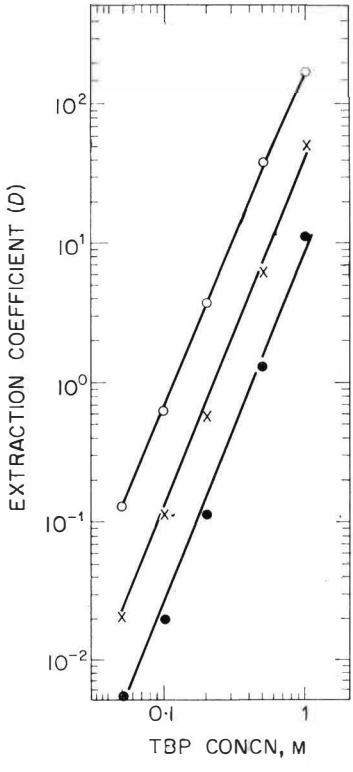

FIG. 3. *Extraction coefficient of tin(II) as a function of the TBP concentration*

Organic phase: TBP at varying concentration in toluene; aqueous phase: trace concentration of Sn(II)
● 2M-HCl; × 4M-HCl; ○ 8M-HCl

The extraction mechanism of In by TBP may be described by the following general equations:

$$In^{3+}_{(a)} + 3H^{+}_{(a)} + 3Cl^{-}_{(a)} + nTBP_{(o)} \rightleftharpoons InCl_3\text{–}nTBP_{(o)} + 3H^{+}_{(a)} \quad . \quad . \quad (1)$$

$$In^{3+}_{(a)} + 4H^{+}_{(a)} + 4Cl^{-}_{(a)} + nTBP_{(o)} \rightleftharpoons H(InCl_4)\text{–}nTBP_{(o)} + 3H^{+}_{(a)} \quad . \quad . \quad (2)$$

where $n = 2$ or 3, and *a* aqueous phase and *o* organic phase.

It seems that at lower concentrations of hydrochloric acid the extraction of indium follows the mechanism described by Equation (1), and at higher concentrations of the acid that by Equation (2).

The existence of $InCl_3$ complexes is more probable in the acid concentration range 2–6M, and at acid concentrations higher than 6M $InCl_4^-$ ions prevail.[32] This is confirmed by the changes in the absorption spectra in the ultra-violet range of the extracting TBP–In species (Fig. 2), the extraction being performed from aqueous solutions of different HCl concentrations. As the acid concentration in the aqueous phase increases, disappearance of the peaks due probably to the $InCl_3$–*n*TBP complexes, and rise in the intensity of the peaks due to the $H(InCl_4)$–*n*TBP are observed.

It should be mentioned that during the extraction of indium by TBP from iodide solutions evidence of the presence of In–2TBP complexes in the organic phase has been found.[15]

The curves in Fig. 3 imply that tin(II) is extracted by TBP in the form of

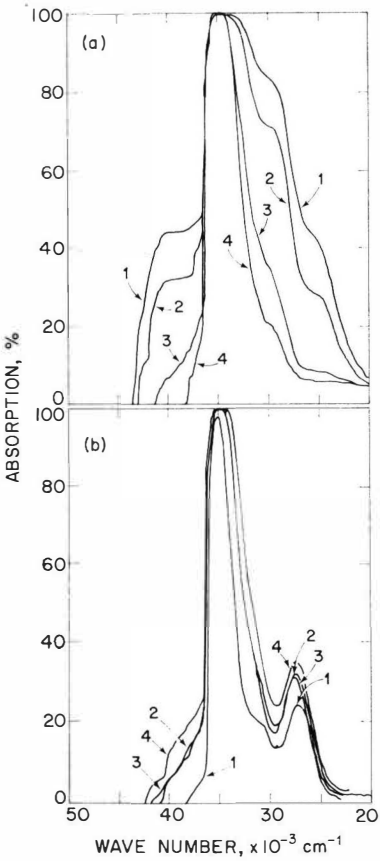

FIG. 4. *Absorption spectra of the tin extract in the ultra-violet region*

Organic Phase 1M TBP. (a) Sn(II); (b) Sn(IV) 1, 4M-HCl; 2, 6M-HCl; 3, 8M-HCl; 4, 10M-HCl
$D_{Sn(II)}$: 4·96, 9·12, 11·4 and 11·4; $D_{Sn(IV)}$: 5·05, 13·7, 20·2 and 20·5 respectively

complexes solvated by two or three molecules of TBP because the slopes of these plots are 2·5. It is of interest to mention that in the extraction of tin(IV) the slopes obtained were also equal to 2·5,[31] and in another paper[22] the extracting tin(IV) species was reported to be a Sn–2TBP complex.

Based on the above facts the extraction of tin (II) and (IV) may be presented by the following equations:

$$Sn^{2+}_{(a)} + 2H^{+}_{(a)} + 2Cl^{-}_{(a)} + nTBP_{(o)} \rightleftharpoons SnCl_2\text{–}nTBP_{(o)} + 2H^{+}_{(a)} \quad (3)$$

$$Sn^{2+}_{(a)} + 3H^{+}_{(a)} + 3Cl^{-}_{(a)} + nTBP_{(o)} \rightleftharpoons H(SnCl_3)\text{–}nTBP_{(o)} + 2H^{+}_{(a)} \quad (4)$$

$$Sn^{4+}_{(a)} + 4H^{+}_{(a)} + 4Cl^{-}_{(a)} + nTBP_{(o)} \rightleftharpoons SnCl_4\text{–}nTBP_{(o)} + 4H^{+}_{(a)} \quad (5)$$

$$Sn^{4+}_{(a)} + 6H^{+}_{(a)} + 6Cl^{-}_{(a)} + nTBP_{(o)} \rightleftharpoons H_2(SnCl_6)\text{–}nTBP_{(o)} + 4H^{+}_{(a)} \quad (6)$$

where $n = 2$ or 3.

As in the extraction of indium, it seems that at lower HCl concentrations tin extraction follows the mechanism described by Equations (3) and (5), and at higher HCl concentrations that by Equations (4) and (6). This assumption is also confirmed by the shapes of the absorption spectra of the extracting TBP–Sn species (Fig. 4), where changes are observed, depending on the composition of the initial aqueous phase.

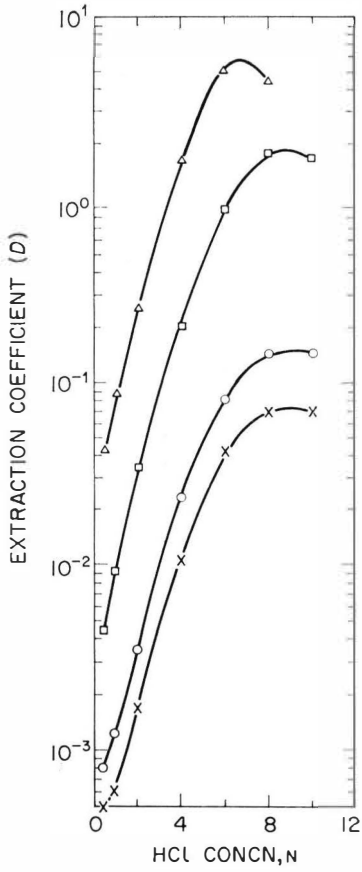

FIG. 5. *Extraction coefficient of indium as a function of the HCl concentration*

Organic phase: × 0·75M TBP; ○ 1·0 M TBP; □ 2·0M TBP; △ 3·67M TBP (100%)
Aqueous phase: 40 g/l of indium

Effect of HCl concentration

The individual extraction coefficients of indium and tin as a function of hydrochloric acid concentration are presented in Figs 5 and 6. Figs 7 and 8 present the extraction of Sn(II) and Sn(IV) ions in the presence of indium and *vice versa*.

From the results in Fig. 5 it follows that the maximum indium extraction appears in the range 6·5–9·0M-HCl, and as the extractant concentration in the organic phase increases, the maximum shifts towards lower concentrations of HCl. This may be explained by assuming an increase in the competition between the extraction of HCl by TBP with increasing concentration of the extractant in the organic phase. Fig. 5 implies that when 2M TBP is used, the percentage extraction of indium from 8–10M-HCl solution containing 40 g/l of In, reaches about 95%.

The shape of the curves in Fig. 6 indicates that, as for indium, the extraction of tin strongly increases with rising concentration of HCl. The extraction coefficients of tin under optimum conditions (7–9M-HCl) are about two orders of magnitude higher than the maximum values of D_{In}, and the curves for tin have more pronounced maxima than those for indium.

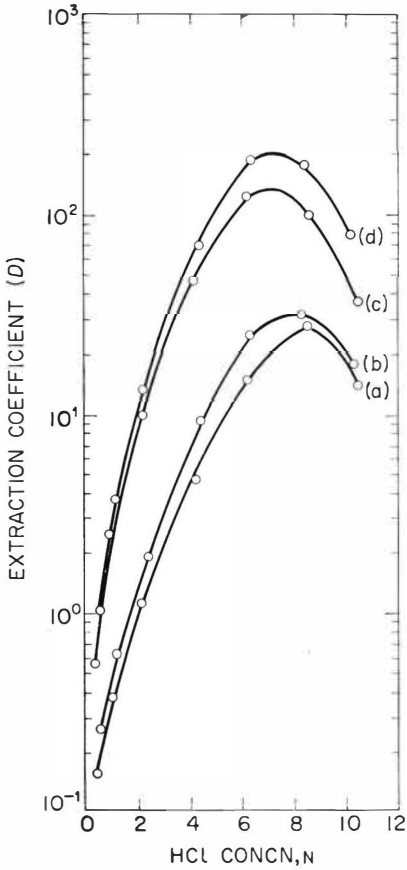

FIG. 6. *Extraction coefficient of tin as a function of the HCl concentration*
Organic phase: (a), (b) 0·5M TBP; (c), (d) 1·0 M TBP
Aqueous phase: 2·37 g/l of tin; (a), (c), 100% Sn(II); (b), (d) 85% Sn(II) and 15% Sn(IV)

In addition, from Fig. 6 (curves (b) and (d)) it follows that tin(IV) is extracted better than tin(II) particularly at higher concentrations of HCl. At equal concentrations of indium and tin (~0·1M) the extraction coefficients of tin(II) and (IV) are 2–25 higher than the values D_{In}, the differences decreasing with increasing concentration of HCl in the aqueous phase. At the same time, the relatively small (two-fold at maximum) differences between the values $D_{Sn(II)}$ and $D_{Sn(IV)}$ should be indicated. This phenomenon can be explained by two opposing factors. Firstly, because of its greater ion potential it was expected that the Sn(IV) ion would be much better extracted than the Sn(II) ion. On the other hand, the ions of tin(IV) probably have a higher tendency to polymerise and solvate in the aqueous phase than the ions of tin(II), which thus leads to relatively small differences in the extraction behaviour of tin in different oxidation states.

The effect of hydrochloric acid concentration on the extraction of tin(IV) and tin(II) in the presence of indium is presented in Fig. 7. The shape of the curves in this Fig. differs from those obtained for the individual extraction of tin (Fig. 6). The maxima of the curves are displaced towards lower concentrations of HCl (4–5M), particularly for the extraction of Sn(II) and also the extraction of Sn(IV) at higher concentrations of TBP (curve (d), Fig. 7). The observed changes in extraction of tin are, no doubt, brought about by the competitive extraction of indium, which increases at higher concentrations of HCl, as follows from the curves in Figs 5 and 8. The extraction of indium in the presence of tin is given in Fig. 8. The shape of the curves shows that the indium extraction is independent of the oxidation state of tin in the initial aqueous solution, and that the presence of tin practically does not influence the value D_{In}.

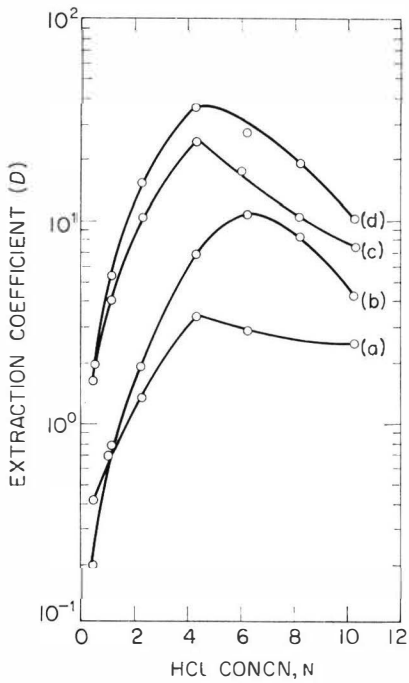

FIG. 7. *Effect of the HCl concentration on the extraction of tin in the presence of indium*

Organic phase: (a), (b) 0·5M TBP; (c), (d) 1·0M TBP
Aqueous phase: 2·37 g/l of tin; 40 g/l of indium; (a), (c) Sn(II); (b), (d) Sn(IV)

Selectivity of the extraction of tin in the presence of indium

The effect of hydrochloric acid concentration on the separation factors of Sn(II) and Sn(IV) from indium is presented in Figs 9 and 10. The relation

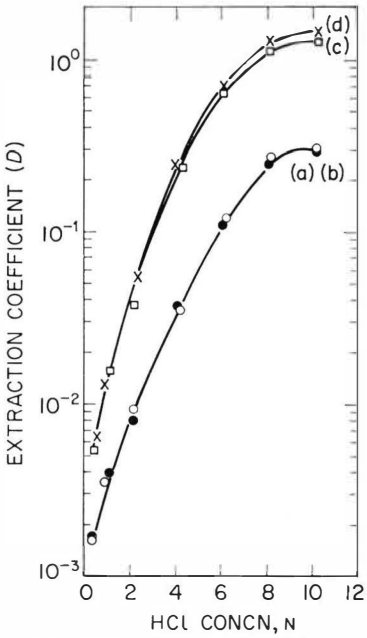

FIG. 8. *Effect of the HCl concentration on the extraction of indium in the presence of tin(II) and tin(IV)*

Organic and aqueous phases as in Fig. 7

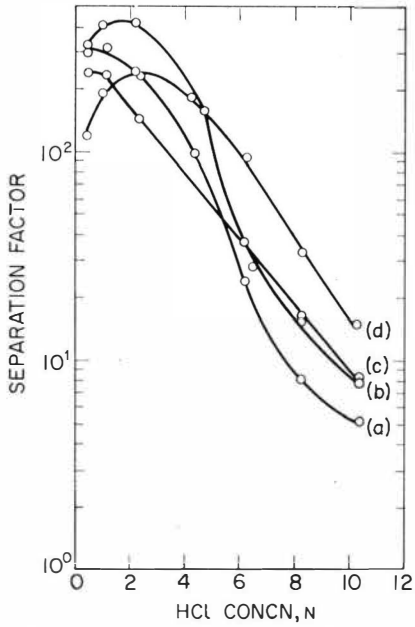

FIG. 9. *Separation factor of the pair Sn–In as a function of the HCl concentration*

Experimental conditions and (a)–(d) as in Fig. 7

between the separation factor $\beta_{Sn/In} = \frac{D_{Sn}}{D_{In}}$ and the concentration of HCl is presented in Fig. 9. In Fig. 10 analogous changes in the integral separation factor $\nu = \frac{\%E_{Sn}}{\%E_{In}}$ are shown as a function of the concentration of HCl. The value of the integral separation factor, ν, which expresses the separation effect in a more unequivocal way than the factor β does, shows that in the concentration range of the acid 0–2M a very good separation of tin and indium is achieved.

A successive three-fold extraction of tin from the same aqueous solution decreases the tin concentration to 10^{-4}% of that of indium.

The decrease in selectivity for the pair Sn–In with increasing concentration of HCl is connected with the stronger influence of the acid concentration on the extraction of indium than on tin. It should also be emphasised that the separation of tin from indium is practically independent of the tin oxidation state.

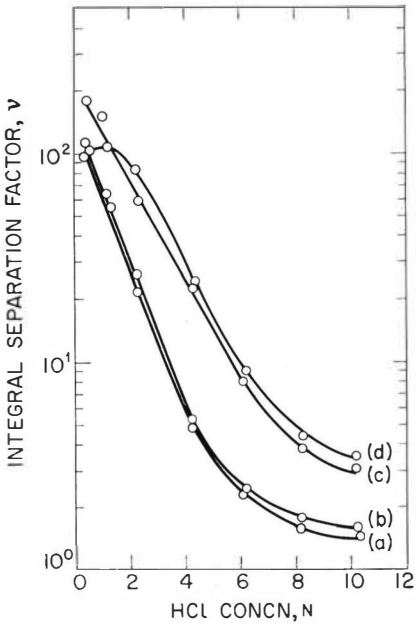

FIG. 10. *Integral separation factor of the pair Sn–In as a function of the HCl concentration*

Experimental conditions and (a)–(d) as in Fig. 6

Extraction chromatography

The results discussed above were used to separate the radioisotopes ^{113}Sn and ^{113m}In by extraction chromatography in the system TBP–siliconated silica gel–HCl. This method can be used as an isotope generator for the production of ^{113m}In.

The curves presented in Fig. 11 show that the elution of indium proceeds better when hydrochloric acid of lower concentrations is used. The measured radiochemical purity of the separated ^{113m}In indicates that in both the solutions of HCl (3 and 6M) the tin content was lower than 10^{-3}%. For practical purposes a better eluting solution is 3M-HCl, because it allows ^{113m}In solutions of higher specific activity to be obtained.

The elution curves presented in Fig. 12 show that the generator of ^{113m}In can be used several times, the recovery of indium remaining unchanged. Breakthrough experiments on the column[34] reveal that it can be used at least ten times, the radiochemical purity of ^{113m}In being undisturbed.

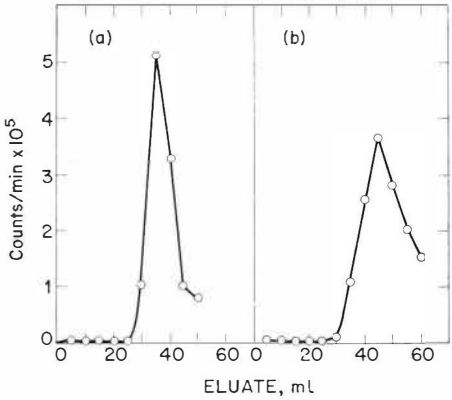

FIG. 11. *Effect of the HCl concentration on the elution of indium in the system TBP–silica gel–HCl*
(a) 3M-HCl; (b) 6M-HCl

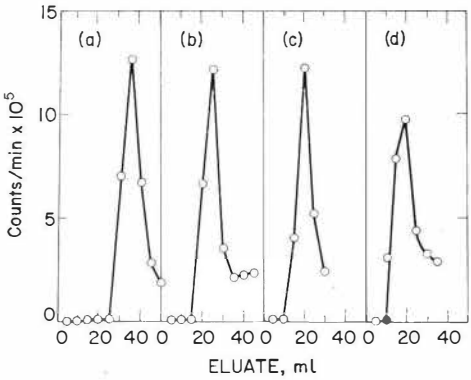

FIG. 12. *Elution efficiency of indium with 3M-HCl as a function of multiple repetition of the elution*

Obtaining high purity indium by solvent extraction

Results of the purification of indium by a two-stage extraction process are presented in Table II. Indium was first extracted by monododecylphosphoric acid (DDPA) from ~2M-H_2SO_4 then it was stripped by a dilute hydrochloric acid solution containing ammonium chloride.[35] Tin, in turn, was extracted four times by a 30% TBP solution in toluene from the strip solution of composition: 1M-HCl, 35 g/l of In and 5 g/l of Sn.

Spectrographic analysis (Table II) of the metallic indium samples deposited electrolytically show that the extraction with DDPA leads to the purification of indium by two orders of magnitude from Pb and Sb, and by a factor of 25 from iron, of 20 from Ni and Zn, and of 5 from cadmium. The tin concentration four times by a 30% TBP solution in toluene, from the strip solution of com- removes not only the tin to a concentration lower than 10^{-3}%, but at the same time lowers the concentration of Ba, Ca, Cd, Fe, Mg, Mn and Pb below 1 ppm and that of other elements up to a level of 1–10 ppm.

TABLE II

Purification of technical grade indium by solvent extraction, ppm

Element	Technical grade indium	No. of sample		
		I	II	III
Ag	<0·6	<0·2	<0·8	<0·6
Al	<0·3	3	3	3
Au	5	<2	<5	<5
Ba	4	1	<0·1	<0·1
Bi	<3	3	20	60
Ca	10	20	<0·2	<0·2
Cd	50	10	<0·1	<0·1
Cu	20	20	0·2	2
Fe	25	1	<0·1	5
Hg	<20	<600	<20	<20
Mg	1	2	<0·1	<0·1
Mn	0·1	0·1	0·03	0·03
Ni	100	5	<2	9
Pb	700	3	0·5	5
Sb	200	2	1	1
Sn	20%	13·6%	<0·1	<10
Zn	20	1	<1	<1
In	79%	86·39%	99·997%	99·991%

I—Metallic indium after the extraction with DDPA from sulphate solutions

II, III—Metallic indium after the extraction with DDPA and after the extraction of tin with TBP from the re-extract

Conclusions

The extraction of indium and tin(IV) by means of TBP increases with the diluent used in the following series: carbon tetrachloride < benzene < toluene < xylene < n-heptane < n-octane.

The extracted indium, tin(II) and tin(IV) species are solvated in the organic phase by two or three molecules of TBP, as found with the dilution method while extracting trace quantities of these metals.

The optimum extraction conditions for the separation of tin and indium appear in the hydrochloric acid range 0·1–2·0M. Under these conditions the integral separation factor reaches a value of ~100.

Extraction chromatography in the system TBP–silaca gel–HCl allows ^{113m}In to separate from ^{113}Sn efficiently and selectively.

A two-stage extraction of tin with TBP from chloride solutions enables very pure indium to be obtained.

References

[1] Levin, I. S., *Izv. Sibirsko Otd. Akad. Nauk SSSR*, 1960, **2**, 53
[2] Rybakov, W. N., & Stroński, I., *Atomn. Energ.*, 1959, **6**, 208
[3] Stroński, I., & Rybakov, W. N., *Chemia analit.*, 1959, **4**, 877
[4] Stroński, I., *Wiad. chem.*, 1961, **15**, 13
[5] Gillette, J. H., *Rep. Congr. atom. Energy Commn. U.S.*, 1965, ORNL-3802
[6] Stern, H. S., *et al.*, *Nucleonics*, 1966, **24** (10), 57
[7] *Idem.*, *ibid.*, 1967, **25** (2), 61
[8] Subramanian, J. G., & McAfee, J., *Int. J. appl. Radiat. Isotopes*, 1967, **18**, 215
[9] Levin, I. S., *Zh. prikl. Khim.*, 1962, **35**, 2368
[10] Ruman. P., 48,914
[11] Tuck, D. C., & Woodhouse, E. J., *J. chem. Soc.*, 1964, p. 6017
[12] Diamond, R. M., *J. phys. Chem.*, *Ithaca*, 1959, **63**, 659
[13] Irving, H., & Edington, D. N., *J. inorg. nucl. Chem.*, 1959, **10**, 306
[14] Ishimori, T., & Nakamura, E., *JAERI*, 1963, 1047
[15] Jackwerth, E., & Specker, H., *Z. analyt. Chem.*, 1960, **176**, 81
[16] *Idem.*, *ibid.*, 1960, **177**, 327

[17] Ishimori, T., *et al.*, *JAERI*, 1966, 1106
[18] De, A. K., & Sen, A. K., *Talanta*, 1967, **14,** 629
[19] Fr.P., 1,289,520
[20] Das, R. R., & Bhat, T. R., *Gov. India atom. Energy Commn Rep.*, 1968, BARC-324
[21] Mazońska, D., *Zesz. nauk. Politech. ślask. Chem.*, 1964, **24,** 105
[22] Specker, H., *et al.*, *Angew. Chem.*, 1959, **71,** 492
[23] Mikulski, J., & Stroński, I., *Nukleonika*, 1961, **6,** 775
[24] Stroński, I., *Polish Rep. nucl. Phys. Inst.*, *Cracow*, 1965, 427/C
[25] Goliński, M., *Przem. chem.*, 1967, **46,** 730
[26] Goliński, M., *Przem. chem.*, 1968, **47,** 631
[27] Sato, T., *J. inorg. nucl. Chem.*, 1965, **27,** 1395
[28] *Idem.*, *ibid.*, 1967, **29,** 555
[29] Urbański, T. S., *Nukleonika*, 1960, **5,** 831
[30] *Idem.*, *ibid.*, 1961, **6,** 299
[31] Goliński, M., 1970, Thesis, Nucl. Res. Inst. Warsaw
[32] Marcus, Y., *Israel atom. Energy Commn Rep.*, 1966, IA-1087
[33] Günzler, G., *et al.*, *Proc. int. Conf.*, *Gothenberg*, 1966, p. 620
[34] Goliński, M., & Zulczyk, W., *Polish Rep. nucl. Res. Inst.*, *Warsaw*, in the press
[35] Pol. P., 59,276

Comparison of selectivity of organic nitrosolvents for extraction of alkali metals

by P. Selucký, J. Rais and J. Krtil

Institute of Nuclear Research, Řež, Nr. Prague, Czechoslovakia

Heavy alkali metals are well extracted by nitrobenzene in the presence of dipicrylaminates. The extraction of alkali metal dipicrylaminates is studied with some other nitrosolvents (nitromethane, nitropropane and nitroethane) and β,β′-dichlorodiethyl ether. A comparison of extraction efficiency is made as well as of the separation properties (Cs versus *other alkali metals) and the role of dissolved water in the organic phase is shown.*

Introduction

ONLY A FEW extraction systems for caesium or other heavier alkali metals are known; one rather important group of them involves the use of nitrobenzene as organic solvent. Caesium can be extracted by this solvent in the presence of voluminous univalent anions such as dipicrylaminate,[1,2] tetraphenylborate,[3] polyiodide,[4] phosphomolybdate,[5] $[Cr(SCN)_4(aniline)_2]^-$,[6] $[As(catechol)_3]^-$,[7] etc. Whereas the mechanism of extraction has been studied thoroughly, the high distribution ratios with nitrobenzene and separation factors with caesium are not yet satisfactorily explained. Some other nitrosolvents have been tested by different workers but always with poorer results than for nitrobenzene.

The aim of this work was to discover a relevant physical property (or properties) of the water–organic nitrosolvent systems which might serve as a criterion for the estimation of the selectivity of the system. For this purpose the fact that the extraction exchange constants $K_M^{Cs}(Cs_a^+ + M_o^+ \rightleftharpoons Cs_o^+ + M_a^+)$, which were of decisive importance in this study, are independent of the kind of anion used for extraction in these systems with polar organic solvents[2,8] was used. Hence, the distribution of alkali metal dipicrylaminates has been studied for simplicity, because estimated values of K_M^{Cs} will be equally valid if another reagent is used in the given system.

Experimental

Reagents

All reagents used were of A.R. grade quality. Organic solvents were washed several times with distilled water, dried over $CaCl_2$ and distilled at atmospheric pressure. Radioisotopes ^{137}Cs, ^{86}Rb (both $< 2 \times 10^{-5}$M in final solutions) were used. The preparation of alkali metal dipicrylaminates has been described previously.[2]

Procedure

Equal volumes of an aqueous solution of the respective dipicrylaminate (with the other dissolved in the organic phase), which were 5×10^{-3}M in corresponding alkali metal hydroxide, were equilibrated in glass-stoppered test-tubes for 30 min at $25 \pm 0{\cdot}5$°C. After equilibration aliquots of the aqueuos phase were taken for colorimetric determination of the dipicrylaminate (DPA) anion content. The distribution ratios of Cs and Rb were determined radiometrically by the usual method. In estimating solubilities, an excess of solid dipicrylaminate was shaken with the given solvent for 1 week, then the aliquot of supernatant liquid was taken, evaporated to dryness, dissolved in water and the DPA anion content measured colorimetrically. Water in organic extracts was determined by Karl Fischer titration.[2]

Results and Discussion

Extraction of alkali metal dipicrylaminates into 2-nitropropane, nitroethane and β,β′-dichlorodiethyl ether as the function of their initial concentration (and in the case of 2-nitropropane also the ionic strength of the aqueous phase) was studied. The typical curves for D_{DPA} vs. $[DPA^-]_a$ were obtained and from these results two constants (i.e. the extraction constant, $K_1 = [M^+]_o[DPA^-]_a$-$([M^+]_a([DPA^-]_a)^{-1}$ and the ion-pair dissociation constant in the organic phase, $K_2 = [M^+]_o[DPA^-]_o([MDPA]_o)^{-1}$ were calculated by the method described previously.[2] The ratio of two extraction constants, i.e. K_{Cs} and K_M, gives the extraction exchange constant defined as $K_M^{Cs} = [Cs^+]_o[M^+]_a([Cs^+]_a[M^+]_o)^{-1}$.

For brevity, only the resultant values of K_1 are compared in Fig. 1 (values of K_1 for nitrobenzene and nitromethane are for higher ionic strength than for other solvents, but K_M^{Cs} values are not very sensitive to the variation of the latter[8]). From Fig. 1 it is clear that the dielectric constant of the organic solvent hardly affects the separation properties of the system, because nitrobenzene and nitromethane with comparable values of ε_S show the greatest change in the given property.

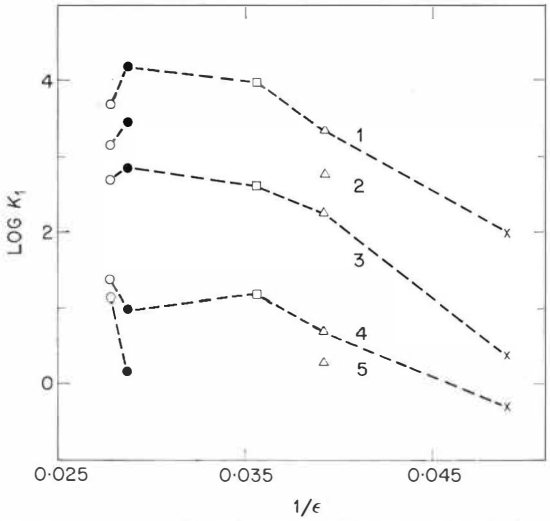

FIG. 1. *Extraction constants* $[M^+]_o[DPA^-]_o \cdot ([M^+]_a[DPA^-]_a)^{-1}$ *for alkali metal dipicrylaminates and various nitrosolvents*

1, CsDPA; 2, RbDPA; 3, KDPA; 4, NaDPA; 5, LiDPA
○ Nitromethane; ● nitrobenzene; □ nitroethane; △ 2-nitropropane; × β,β-dichlorodiethyl ether
Values for nitrobenzene ($\mu = 5 \times 10^{-2}$)[2] and for nitromethane ($\mu = 5 \times 10^{-2}$)[9,10] are from the literature; other values as estimated in this work ($\mu = 5 \times 10^{-3}$)
ε is the dielectric constant of the solvent.

The equilibrium nitromethane and nitrobenzene phases differ appreciably in their water content, a fact that may be significant. Actually, as can be seen in Fig. 2 the values of K_M^{Cs} if plotted against the equilibrium content of water in the organic nitrosolvent fall very sensitively on separate monotonic curves for each pair of cations. Moreover, the practical separation factors D_{Cs}/D_M estimated in other papers[3,11] agree well with the present values of K_M^{Cs}, thus indicating that the degree of ion-pair association in the organic phase is small. This was proved by estimates of the K_2 constants which vary in the range 2×10^{-2}–1×10^{-1} for the dipicrylaminates studied in 2-nitropropane and nitroethane. The values of K_M^{Cs} for β,β′-dichlorodiethyl ether are not compatible with the general trend in Fig. 2. This may be explained by a different solvation mechanism of alkali metal ions in this solvent.

The practically constant values of K_{Rb}^{Cs} and K_K^{Cs} for all nitrosolvents studied and the strong dependence of K_{Na}^{Cs} and K_{Li}^{Cs} on the water content may be accounted for as follows: the ions Li^+ and Na^+ pass into the organic phase in the form

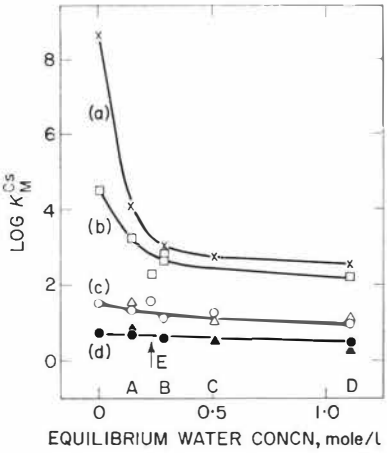

FIG. 2. *Extraction exchange constants* $[Cs^+]_o[M^+]_a([Cs^+]_a[M^+]_o)^{-1}$ *for alkali metal cations*

(a) K^{Cs}_{Li}; (b) K^{Cs}_{Na}; (c) K^{Cs}_{K}; (d) K^{Cs}_{Rb}

Values for zero water content are those for dry nitromethane and for nitromethane saturated with water.[10]
Values for nitrobenzene are from previous work[2]
△, ▲ Practical separation factors D_{Cs}/D_M;[3] □ D_{Cs}/D_{Na}.[11]
A, nitrobenzene; B, nitropropane; C, nitroethane; D, nitromethane; E, β,β′-dichlorodiethyl ether

of hydrates (with 3–4 molecules of water per ion as was found previously[2] for nitrobenzene and for nitropropane in this work; the solubility of water in nitromethane is too high to permit the same kind of experiments for this solvent), whereas K^+, Rb^+ and Cs^+ are essentially non-hydrated in the organic phase. It seems reasonable that the hydrates Li^+. nH_2O and Na^+. mH_2O will be more compatible with the solvent with higher water content and *vice versa*, owing to the hydrogen bonding of the molecules of the first hydration shell of these cations with the molecules of water dissolved in the organic phase. This effect is less pronounced for K^+ and is negligible for Rb^+ and Cs^+ (Fig. 2). From Fig. 2 moreover, it is clear that the nitrosolvents used do not differ greatly, apart from the effect of the water content, in their solvation properties towards alkali metal ions.

Considering Fig. 1, the relative enhancement of the extraction constant K_1 for LiDPA and NaDPA for nitromethane as compared with nitrobenzene becomes comprehensible in view of the foregoing discussion. The opposite effect for other dipicrylaminates may be discussed in terms of the structure-breaking concept, bearing in mind that in K_1 the sum of effects for both M^+ and DPA^- is involved. The two structure-breaker (in water) ions, Cs^+ and DPA^-, are supposed to be more strongly expelled from nitromethane saturated with water than from nitrobenzene, because the former solvent is more structured in the sense of hydrogen bonding. Additional evidence for the role of water content in the organic phase is the solubility of alkali metal dipicrylaminates in the nitrosolvents saturated with water. The solubility of all alkali metal dipicrylaminates is the highest in nitromethane saturated with water and decreases with decreasing equilibrium water content in the organic phase. On the other hand, if the water content is adjusted to the same value for the nitrosolvents studied, the solubility is again the highest in nitromethane. The solubility of LiDPA and NaDPA in water saturated with nitro-solvents is also the highest in water saturated with nitromethane. From these results it can be anticipated that the solvation of alkali metal ion by the molecules of organic solvent may probably be significant, too. It is not possible on the basis of the present results to estimate quantitatively the degree of solvation exhibited by organic nitrosolvents, but the primary effect of water dissolved in the organic phase on the separation properties for alkali metal ions has been shown unambiguously.

References

[1] Kyrš, M., & Podešva, S., *Colln Czech. chem. Commun.*, 1961, **26,** 289
[2] Rais, J., Kyrš, M., & Pivoňková, M., *J. inorg. nucl. Chem.*, 1968, **30,** 611
[3] Sekine, T., & Dyrssen, D., *Analytica chim. Acta*, 1969, **45,** 433
[4] Kyrš, M., *Zh. neorg. Khim.*, 1963, **8,** 532
[5] Rais, J., Podešva, S., & Kyrš, M., *Analytica chim. Acta*, 1966, **36,** 90
[6] Fujinaga, T., Koyama, M., & Tochiyama, O., *Analytica chim. Acta*, 1968, **42,** 219
[7] Rais, J., Selucký, P., & Dražanová, S., *Radiochem. Radioanalyt. Lett.*, 1970, **4,** 195
[8] Rais, J., *Colln Czech. chem. Commun.*, in the press
[9] Pivoňková, M., 1969, Thesis, ÚJV-Řež
[10] Haugen, G. R., & Friedman, H. L., *J. phys. Chem., Ithaca*, 1968, **72,** 4549
[11] Bray, L. A., & Roberts, F. P., *Rep. Congr. atom. Energy Commn U.S.*, 1963, HW-76222

Extraction of sodium by some di-n-alkyl phosphoric acids

by N. V. Sístková

Nuclear Research Institute of the Czechoslovak Academy of Sciences, Řež, Nr. Prague, Czechoslovakia

While studying the extraction of strontium ions by HA–NaA (where HA is some acidic organophosphorous extractant and NaA is its sodium salt), interactions in these mixtures in the organic phase were investigated. The effects of the ionic strength of the aqueous phase and of the nature of the diluent are also discussed.

MONO-ACIDIC ORGANOPHOSPHATES are effective extractants for strontium, so that extraction systems involving these extractants and strontium have been widely studied. Rather high distribution ratios for strontium are usually only reached in these systems in pH regions where the extractant is partly converted to a sodium salt. Hence evaluation of the applicability of the extractant and interpretation of the extraction mechanism is not possible without a study of the extraction equilibria of sodium under the conditions where strontium is extracted. The extraction of sodium from aqueous sodium nitrate solutions by di-n-butylphosphoric (HDBP), di-n-amylphosphoric (HDAP), di-n-hexylphosphoric (HDHP) and di-n-octylphosphoric (HDOP) acids has been examined in connexion with the previous study of strontium extraction by these extractants.[1–3] These results are reported and discussed in the present paper.

Experimental

The preparation and purification of the di-n-alkyl phosphoric acids used,[2–4] the purification of diluents[5,6] as well as the procedure for measurement of the distribution ratio of sodium (D_{Na}) and the apparatus for the measurement of the radioactivity and the hydrogen ion concentration[1,4] have been described previously. The radioactive isotope ^{22}Na was used in this work.

Results and discussion

A preliminary study showed that the simple sodium salts of di-n-alkyl phosphoric acids (NaA) are only negligibly extracted into the organic diluents. Distribution into cyclohexane from 1M-$NaNO_3$ solutions was found to be less than 10^{-5} moles for all di-n-alkyl phosphoric acids studied. However, if free di-n-alkyl phosphoric acid is also present in the system, complexes of sodium form (Fig. 1) which are more extractable than the NaA species. Thus it follows that the strontium extraction mechanism is complicated by the extraction of sodium even in those systems where the simple sodium salts of mono-acidic organophosphoric acids are negligibly soluble in the organic phase.

Fig. 1 shows that as for strontium[1] the extraction efficiency of di-n-alkyl phosphoric acids for sodium does not depend on the n-alkyl chain length in the molecule of the extractant in the pH region where log D_{Na} is a linear function of pH. The sodium complexes with the composition shown in Table I were established as the predominant species in the organic phase at very low loadings by Na(I) (the linear parts of the log D_{Na} vs. pH plots) with cyclohexane as diluent. These compositions were estimated by the analysis of the plot (log D_{Na} − log $[A^-]_{aq}$) vs. log $C_{[HA]_{mon/org.}}$ where $[A^-_{aq}]$ is the equilibrium concentration of the anion of the extractant in the aqueous phase and $C_{[HA]_{mon/org.}}$ is the equilibrium concentration of the monomeric molecules of the extractant in acid form in the organic phase. The values of the acid dissociation and polymerisation constants of the di-n-alkyl phosphoric acids and their partition coefficients used for the determination of $[A^-]_{aq}$ and $C_{[HA]_{mon/org.}}$ values were those pre-

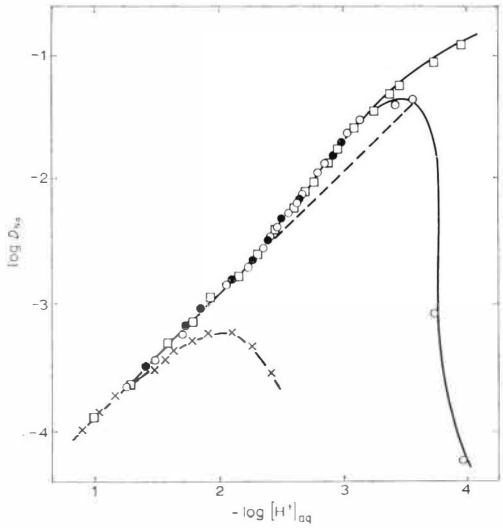

FIG. 1. *Distribution of Na(I) between 1·0M-(HNO_3 + $NaNO_3$) and 0·2F solutions of di-n-alkyl phosphoric acids in cyclohexane at °25C*
× HDBP; ○ HDAP; □ HDHP; ● HDOP

viously measured.[6–8] The correlation between x and the tendency of di-n-alkyl phosphoric acids to polymerise, which was observed in the case of lanthanides and strontium in certain diluents,[3,8] is also observed for the sodium complexes in cyclohexane (see Table I).

TABLE I

Composition of complexes NaA.xHA prevailing in the organic phase at a very low loading by Na(I) and the polymerisation constants, K_n, *of di-n-alkyl phosphoric acids*

Cyclohexane as diluent. Aqueous phase: 1·0M-(HNO_3 + $NaNO_3$); t = 23–25°C, n is the number of monomeric units in the polymer

	HDBP		HDAP		HDHP	HDOP
	$n = 2$	$n = 6$	$n = 2$	$n = 4$	($n = 2$)	($n = 2$)
Log k_n	$6{\cdot}50^7$	$21{\cdot}04^7$	$5{\cdot}32^8$	$11{\cdot}89^8$	$6{\cdot}26^8$	$3{\cdot}47^6$
x	5	5	4	4	3	3

The plot of log D_{Na} vs. pH for HDBP deviates from the straight line of slope 1 and decreases to the very low values of D_{Na} because of the considerable loss of the extractant from the organic phase.[7] In the case of di-n-alkyl phosphoric acids with larger n-alkyl groups the deviations from linearity appear at higher D_{Na} values and are positive. It has been shown[9] that these positive deviations can be most plausibly explained by polymerisation of the extracted sodium complexes. This explanation is in agreement with the equations derived for the cases of polymerisation of the extracted complexes[10] and is supported by the fact that the polymerisation of metal complexes in the organic phase has often been observed in the extraction of macro amounts of metals by mono-acidic organophosphates.[5,11–14]

The formula nNaA.mHA suggested for the polymerised sodium complexes of n-octyl hydrogen phenyl phosphate (HO[φP]), which involves molecules of the acid form of the extractant (HA) can probably be assumed for these poly-

meric species. The composition $(NaA)_n$ suggested for the sodium polymers of di-(2-ethylhexyl)phosphoric acid (HDEHP)[13] is hardly probable in view of the negligible solubility of the simple salts (NaA) of di-n-alkyl phosphoric acids in the organic phase.

The tendency of the sodium complexes NaA.xHA to polymerise in cyclohexane seems not to be dependent markedly on the n-alkyl chain length in the molecule of the extractant. Fig. 1 shows that the positive deviations connected with the polymerisation of sodium complexes appear at approximately the same values $[Na]_{tot/org.}$ for HDAP, HDHP and HDOP. The values of $C_{A,tot/org.}$ concentration of extract, at the pH value at which positive deviations from linearity occur, are also the same as the free extractant concentration and are equal to $C_{A,tot/init.}$, because the loss of the extractant from the organic phase is negligible at this pH.[3,15]

Fig. 2 shows that the polymerisation of the extracted complexes of sodium with di-n-alkyl phosphoric acids occurs in diluents other than cyclohexane.

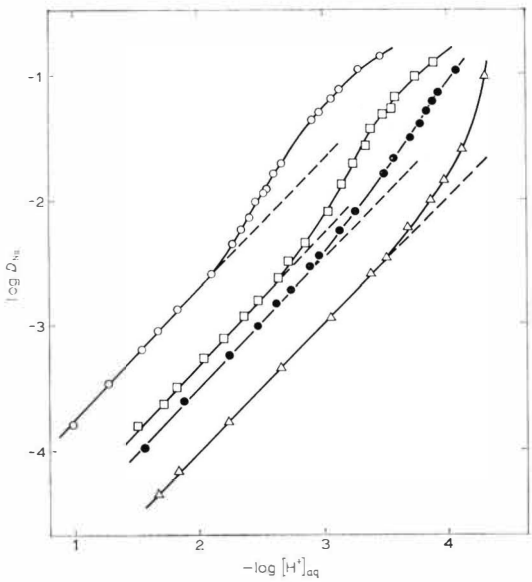

FIG. 2. *Distribution of Na(I) between 1·0M-(HNO_3 + $NaNO_3$) and 0·2F HDHP in various diluents at 25°C*

○ n-Heptane; □ dibutyl ether; ● CCl_4; △ toluene

The plots of log D_{Na} vs. pH for the extraction of sodium by solutions of HDHP in n-heptane, di-n-butyl ether, carbon tetrachloride and toluene also exhibit the positive deviations from linearity at various values of $[Na]_{tot/org.}$. These values are very similar for all the diluents studied (see Table II), indicating that the effect of the diluent on the tendency of the extracted sodium complexes to polymerise is rather insignificant.

The very low values of $[Na]_{tot/org.}$ corresponding to start of polymerisation ($[Na]_{tot/org.start}$) show that the tendency of the sodium complexes of di-n-alkyl phosphoric acids to polymerise is probably very high. The values $[Na]_{tot/org.start}$ and Y_{start} (where $Y = [Na]_{tot/org.}/C_{A,tot/org.}$) are even somewhat lower than those for the sodium complexes of HO[φP].[9] It should be noted that the polymerisation of sodium complexes in the organic phase was not observed at such low values of $[Na]_{tot/org.}$ in extraction systems with di-*p*-(1,1,3,3-tetramethylbutyl)phenylphosphoric acid.[5] The polymerisation of the sodium complexes of HDEHP in wet benzene occurs only for $Y > 0{\cdot}25$ at $C_{A,tot/org.} = 0{\cdot}1$F.[13]

This difference in the tendency of sodium complexes to polymerise is probably caused by steric effects connected with highly branched alkyl groups in the molecules of the two latter extractants. The important role of steric hindrance in the polymerisation process was shown by Wardlaw & Bradley,[16] who studied the association of the alkoxides of tri- and tetra-valent metals.

The values $[Na]_{tot/org.start}$ and Y_{start} increases with increasing $C_{A,tot/org.}$ (see Fig. 3 and Table II). This was noticed in the case of sodium complexes of HO[φP][9] and is in agreement with the equation for the polymerisation reaction:

$$n(\mathrm{NaA}.x\mathrm{HA}) \rightleftharpoons n\mathrm{NaA}.m\mathrm{HA}_{org.} + \frac{xn-m}{y}(\mathrm{HA})_{y\ org.}$$

with $(xn-m)/y > 0$.

TABLE II

Total sodium organic concentrations and the values of Y, at which polymerisation of the extracted sodium complexes of HDHP starts

$C_{A,org/tot.}$, F	$[Na^+]_{aq/init.}$, M	Start of the nNaA . mHA formation		Diluent
		$[Na]_{tot/org.}$, M	Y	
0·20	1·0	3×10^{-3}	$1{\cdot}5 \times 10^{-2}$	cyclohexane
0·10	1·0	8×10^{-4}	8×10^{-3}	cyclohexane
0·05	1·0	3×10^{-4}	6×10^{-3}	cyclohexane
0·10	0·1	8×10^{-4}	8×10^{-3}	cyclohexane
0·20	1·0	$2{\cdot}5 \times 10^{-3}$	$1{\cdot}25 \times 10^{-2}$	n-heptane
0·20	1·0	$2{\cdot}3 \times 10^{-3}$	$1{\cdot}15 \times 10^{-2}$	dibutyl ether
0·20	1·0	$2{\cdot}5 \times 10^{-3}$	$1{\cdot}25 \times 10^{-2}$	carbon tetrachloride
0·20	1·0	$3{\cdot}0 \times 10^{-3}$	$1{\cdot}5 \times 10^{-2}$	toluene

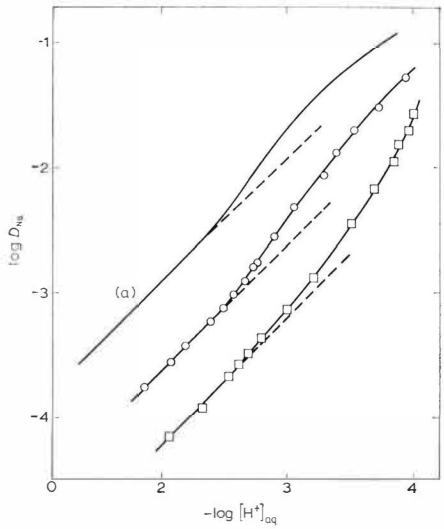

FIG. 3. *Distribution of Na(I) between 1·0M-(HNO_3 + $NaNO_3$) and solutions of HDHP in cyclohexane at 25°C*

Experimental points for 0·2F see Fig. 1
(a) 0·20; ○ 0·10; □ 0·05 F

The extent of the reaction equilibrium should be greater the lower the concentration of the free acid in the organic phase.

It was found for the sodium complexes of HO[φP][9] that their tendency to polymerise in the organic phase depends to a large extent on the ionic strength (μ) of the equilibrium aqueous phase—the value of $[Na]_{tot/org.start}$ in cyclohexane

at $C_A = 0 \cdot 1$F decreases about 10 times if the value of μ changes from $1 \cdot 0$ to $0 \cdot 1$. However, in the case of the sodium complexes of di-n-alkyl phosphoric acids the effect of the ionic strength seems to be absent. Fig. 4 shows that the positive deviation from linearity of the plot of log D_{Na} vs. pH for $C_{A,tot/org.} = 0 \cdot 1$F appears at $[Na]_{tot/org.} = 8 \times 10^{-4}$M which is identical with the value of $[Na]_{tot/org.start}$ at the same $C_{A,tot/org.}$ at $\mu = 1 \cdot 0$ (Table II). The positive

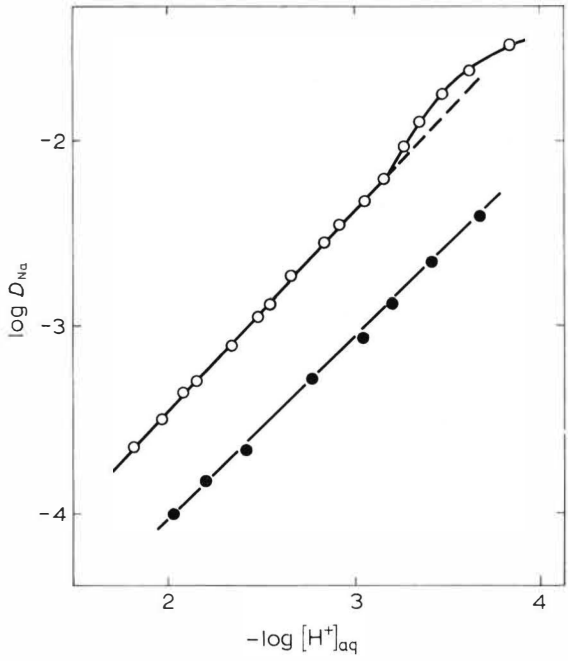

FIG. 4. *Distribution of Na(I) between 0·1M-(HNO_3 + $NaNO_3$) and the solutions of HDHP in cyclohexane at 25°C*

○ 0·10; ● 0·05 F

deviation is not observed at 0·05F for $\mu = 0 \cdot 1$ at $[Na]_{tot/org.} < 3 \times 10^{-4}$M which corresponds to $[Na]_{tot/org.start}$ at the same $C_{A,tot/org.}$ and $\mu = 1 \cdot 0$. At the moment no explanation for the difference in the effect of ionic strength on the polymerisation of the extracted sodium complexes in the organic phase has been found. The matter is being studied further.

References

[1] Kolařík, Z., Hejná, J., & Moravec, A., *J. inorg. nucl. Chem.*, 1967, **29,** 1279
[2] Šístková, N. V., Kolařík, Z., Bárta, K., & Pánková, H., *J. inorg. nucl. Chem.*, 1968, **30,** 1595
[3] Šístková, N. V., Kolařík, Z., & Chotívka, V., *J. inorg. nucl. Chem.*, 1970, **32,** 637
[4] Kolařík, Z., & Pánková, H., *J. inorg. nucl. Chem.*, 1966, **28,** 2325
[5] Šístková, N. V., Kolařík, Z., & Pánková, H., *J. inorg. nucl. Chem.*, 1969, **31,** 2911
[6] Kolařík, Z., Hejná, J., & Pánková, H., *J. inorg. nucl. Chem.*, 1968, **30,** 253
[7] Kolařík, Z., Hejná, J., & Pánková, H., *J. inorg. nucl. Chem.*, 1968, **30,** 2795
[8] Kolařík, Z., Šístková, N. V., & Hejná, J., in 'Solvent Extraction Research' (Eds Kertes, A. S., & Marcus, Y.) 1969, p. 59 (New York: John Wiley)
[9] Šístková, N. V., Kolařík, Z., Chotívka, V., & Pánková, H., in the press
[10] Gindin, L. M., & Khol'kin, A. I., *Izv. Sibirsk. Otd. Akad. Nauk SSSR*, 1969, **2** (1), 90
[11] Baes, C. F., jun., & Baker, H. T., *J. phys. Chem., Ithaca*, 1960, **64,** 89
[12] Baes, C. F., jun., Zingaro, R. A., & Coleman, C. F., *J. phys. Chem., Ithaca*, 1958, **62,** 129
[13] Myers, A. L., McDowell, W. J., & Coleman, C. F., *J. inorg. nucl. Chem.*, 1964, **26,** 2005
[14] McDowell, W. J., & Coleman, C. F., *J. inorg. nucl. Chem.*, 1965, **27,** 117
[15] Šístková, N. V., unpublished work
[16] Wardlau, W., & Bradley, D. C., *Endeavour*, 1955, **14,** 140

Mutual influence of elements during extraction (co-extraction and extraction suppression)

by Yu. A. Zolotov and V. I. Golovanov

V. I. Vernadsky Institute of Geochemistry & Analytical Chemistry, USSR Academy of Sciences, Moscow, USSR.

A suppression of the extraction of microquantities of an element (microelement) in the presence of macroquantities of another element (macroelement) during the extraction of complex metal acids and other ionic associates from halide solutions has been revealed. The causes of extraction suppression and the opposite phenomenon, co-extraction of microelements with macroelements, are discussed. The possibility of the application of extraction suppression to the purification of metals and concentration of impurities is considered.

Introduction

FOR A LONG TIME, it was thought that individual elements were extracted from mixtures independently of one another. This conclusion was sometimes extended to a wide concentration range of elements without taking into account the extraction mechanism. However, this view must be considered as out of date and essentially erroneous. Systematic investigations carried out in this and other laboratories show that instances of mutual influence of elements during extraction are very numerous and for ion associates mutual influence is normal as will be shown below. One of the principal causes of this phenomenon is dissociation and association of the compounds extracted into the organic phase. The formation of mixed-ion associates in the extract causes co-extraction of one element with another. Conversely, the dissociation of ion associates in the organic phase causes suppression of the extraction of microelements by the macroelement by the common ion effect.[1] Data on co-extraction during the separation of some ion associates by extraction were previously reported[2–5] and explained.[1,6] However, information about suppression of the extraction of one element by another is virtually non-existent, if separate observations[7,8] are not taken into consideration.

The present authors observed many cases of a decrease in the extraction of one element in the presence of another. The extraction was carried out from halide solutions by oxygenated solvents. Data for chloride solutions are considered in more detail below.

Experimental

Tri-n-butyl phosphate, β,β′-dichlorodiethyl ether, methyl isobutyl ketone, isoamyl alcohol, etc., were used as organic solvents. All solvents were purified initially. The distribution of elements was studied by means of radioactive isotopes. Equal volumes (4 ml) of an organic solvent and an aqueous solution were shaken for 20 min at 25°C in glass test-tubes. The distribution coefficient (D) was determined from the activities of equal aliquots of each phase. The mean relative error in the measurement of D did not exceed 10% at $D = 0{\cdot}01$–100 and 30% at greater or smaller values.

Results and discussion

An example of the mutual influence of elements is given in the data in Table I, where the distribution coefficients of Tl(III) and Zn are given in the absence of other elements and in the presence of macroamounts of iron(III). During extraction with ethers of low polarity, the presence of iron(III) leads to an increase in the extraction of microelements (co-extraction). Dilution of ethers by highly polar solvents, e.g. dichloroethane or nitromethane, causes an increase

in the dielectric constant of the organic phase and the value of D for microelements decreases in the presence of a macroelement (extraction suppression). The mutual influence in these systems is undoubtedly caused by interactions in the organic phase.

TABLE I

Extraction of Tl(III) and Zn (10^{-5}–10^{-4} M) from HCl solutions in the absence of other elements (D_1) *and in the presence of iron* (D_2)

Organic phase	[HCl], M	[Fe], M	D_1	D_2	D_1/D_2
			Thallium(III)		
Dibutyl ether	8	0·1	0·12	0·8	0·15
Dibutyl ether (10%) + 1,2-dichloroethane	10	0·1	10	0·08	12·5
			Zinc		
Di-isopropyl ether	10·5	0·5	0·014	0·28	0·05
Di-isopropyl ether (25%) + nitromethane	10·5	0·5	0·46	0·02	23

The character of such interactions may be deduced from the dependence of the equivalent conductivity of iron on its concentration in the extract. The conductivity in dibutyl[9] and di-isopropyl[10] ethers depends anomalously on the concentration—the corresponding curves have minima and maxima—which is obviously caused by the formation of complex ion aggregates such as ion triplets and quadruplets.[11] Thus, the cause of co-extraction may be association in the organic phase. On the other hand, in a mixture of dibutyl ether and dichloroethane, the conductivity is high and its dependence on the iron concentration has the usual form connected with the dissociation of $HFeCl_4$ (the complex acids of microelements are, of course, also dissociated). Dissociation gives rise to conditions that favour the display of the common ion effect.[1] Extraction suppression in systems with dissociation can be explained most simply as follows. The equation for the extraction of a complex acid of the microelement is:

$$H^+ + A^- = H^+_{(0)} + A^-_{(0)} ;$$

$$K_{ex} = \frac{[H^+]_0 [A^-]_0}{[H^+]\ [A^-]} .$$

Here A^- is the complex metal halide anion.
If $[A^-]_0/[A^-] = D$, then

$$D = K_{ex} \frac{[H^+]}{[H^+]_0} .$$

The value of $[H^+]$ is high and practically constant. If extraction and dissociation of HCl is negligible in comparison with extraction and dissociation of the complex acid of the macroelement, then $[H^+]_0$ depends only on the concentration of the macroelement in the organic phase. Therefore, the value of D for the microelement will be smaller in the presence of the macroelement than in its absence.

Suppression of the extraction of nine microelements has been observed during their simultaneous extraction with a large amount of iron(III). Suppression took place when solvents with a relatively high dielectric constant and/or with substantial donor capacity were used (Table II).
It can be seen that in a number of cases the D_1/D_2 ratio attains values of hundreds and even thousands. The data in Table II show that the degree of suppression depends on the nature of the organic solvent and of the micro-

TABLE II

Extraction of microelements (10^{-5}–10^{-4}M) in the presence of iron(III) (0·5M)

Organic solvent	[HCl], M	Micro-element	D_1	D_2	D_1/D_2
Nitromethane	5	Zn	0·0057	0·001	5·7
		In	0·98	0·024	42·2
		Sb(V)	5·0	1·7	2·9
		Tl(III)	250	4·6	54
		Au(III)	160	3·3	43
β,β′-Dichlorodiethyl ether	8	Ga	700	22	32
		In	0·25	0·0018	140
		Tl(III)	400	0·56	720
		Sb(V)	17	3·0	5·8
Isoamyl alcohol	6	Tl(III)	25	14	1·8
		Zn	0·92	0·60	1·5
		Co	0·145	0·145	1·0
Methyl isobutyl ketone	5	Zn	0·085	0·026	3·3
		In	36	0·06	600
		Sb(V)	7·1	5·5	1·3
Tri-n-butyl phosphate*	9	Zn	5·0	0·0033	1500
		Co	2·5	0·001	2500
		In	22	0·01	2200
		Sb(III)	3·2	0·67	4·8
		Sb(V)	1000	5·5	180
		Hg	25	0·01	2500

* Iron concentration 1·5M

element. Also the degree of suppression increases with increasing iron concentration. Similar data were obtained when gallium, thallium and certain other metals were used as the macroelement. The common ion effect (in this case the hydrogen ion) is not the sole cause of suppression of extraction. An increase in the ionic activity coefficient of the microelement in the organic phase, $f_{\pm}^{(0)}$, with an increase in the ionic strength of the extract and a decrease in the activity of the free extractant by combination with the macroelement, may also cause a decrease in microelement extraction. In this connexion, the extraction of scandium and cobalt by tributyl phosphate (TBP) is of interest. Unlike the other microelements studied, scandium and cobalt are not extracted by TBP in the form of complex acids (e.g. Fe, Tl or Zn), but as the simple halides, $ScCl_3$ and $CoCl_2$ solvated by TBP molecules.[12,13] The common ion effect must be absent in this case. Indeed, as may be seen from Fig. 1, D_{Sc} does not change in the presence of large amounts of Fe(III) and Ga. In the case of cobalt, a slight suppression of extraction is observed; obviously $CoCl_2$ is partly dissociated in TBP and $f_{\pm(Co)}^{(0)}$ increases in the presence of Fe and Ga. From corresponding equations, it follows that in this case D_{Co} must decrease. Scandium chloride is more stable and is less dissociated in the TBP phase. Therefore, the activity of the Sc complex extracted does not depend on the ionic strength of electrolytes in the organic phase. Further, the lack of suppression of scandium extraction indicates that the presence of Fe(III) and Ga in the extract does not influence the activity of the free TBP strongly. Thus, the suppression of microelement extraction is caused mainly by the dissociation of extracted compounds in the organic phase and the related effects of the common ion and ionic strength.

If the concentrations of micro- and macro-elements that are extracted by the same mechanism are reversed, a suppression of extraction will be observed in

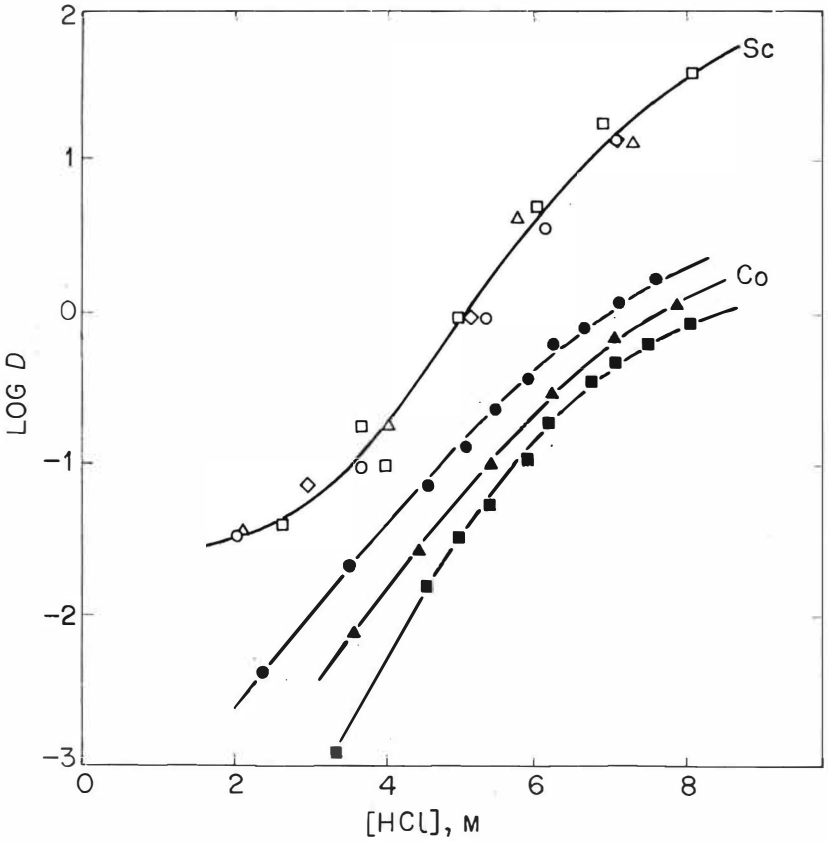

FIG. 1. *Scandium and cobalt extraction by tri-n-butyl phosphate from hydrochloric acid solutions in the absence of other elements and in the presence of Fe (0·11* and *0·5M) and Ga (0·33M)*

○ Sc; △ Sc(+Ga); □ Sc (+0·05M Fe); ◇ Sc (+0·11M Fe); ● Co; ▲ Co (+Ga); ■ Co (+0·5M Fe)

both cases. For instance, from Fig. 2 it can be seen that the decrease in the extraction of Fe(III), Sb(V) and Tl(III) by β,β′-dichlorodiethyl ether from 7·4N-HCl (the latter concentration being that at equilibrium) depends on the metal concentration itself and is analogous to the suppression of microamounts of one metal in the presence of another. This result is again a confirmation of the suppression mechanism which is connected with the dissociation of complex acids in the extract.

The suppression of the extraction of impurities can be used for purification of some metals. In the presence of 1·5M-Fe(III) (Table II), the extraction of Zn, Co, In and Hg with TBP is decreased to such an extent that no more than 1% of these metals passes into the organic phase and 99·5% of the iron is extracted. Thallium (Table III) at a concentration of 1M also substantially suppresses the extraction of certain elements with TBP. Suppression of Zn, Co, Sb(III), In and Fe(II) extraction by 0·9M gallium during TBP extraction from LiCl–HCl solutions gives a high degree of separation of these metals from gallium.

The suppression of extraction may also be used for analytical concentration of impurities. In some cases, high concentrations of metals can also be separated. During the extraction of 0·25–0·5M concentrations of In, Zn and Co with TBP, methyl isobutyl ketone and dichlorodiethyl ether in the presence of 1M-Fe(III), the suppression of extraction of these elements by iron leads to values of *D* for In, Zn, Co as low as for microconcentrations in the presence of

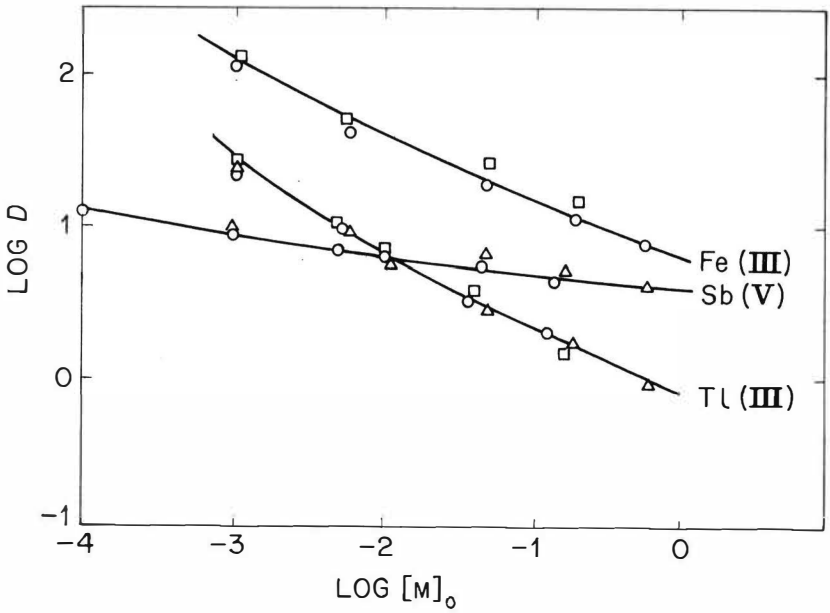

FIG. 2. *Mutual influence of elements during their extraction by β,β′-dichlorodiethyl ether from 8M-HCl*

○ Fe(III) concentration; △ Sb(V) concentration; □ Tl(III) concentration

TABLE III

Purification of thallium (1M) from microconcentrations (10^{-7}–10^{-4})M of impurities by TBP extraction from 2M-HCl

Element extracted	D_1	D_2	D_1/D_2
Tl(III)	—	94	—
Ga	10^3	0·015	6×10^4
In	68	0·0127	$5{\cdot}3 \times 10^3$
Fe(III)	330	0·07	$4{\cdot}7 \times 10^3$
Sb(V)	3·2	$8{\cdot}3 \times 10^{-4}$	$3{\cdot}8 \times 10^3$
Hg	200	$5{\cdot}9 \times 10^{-3}$	$3{\cdot}4 \times 10^4$
Zn	25	0·0165	$1{\cdot}5 \times 10^3$
Co	$4{\cdot}5 \times 10^{-3}$	1×10^{-3}	4·5

1M-Fe. Also, it has been shown that the value of D for In, Zn and Co does not depend on the concentration of these metals in the presence of 1M-Fe. It is shown that in a number of other cases, the results of experiments with micro amounts of elements will also be valid over a wide concentration range. The use of extraction suppression may be especially effective during countercurrent extraction and extraction chromatography.

In this laboratory, the present authors have accumulated extensive evidence of mutual influence in other extraction systems. For instance, macro amounts of indium and cadmium influence the extraction of Zn, Co, In, Sb(III) and other microelements when they are separated from iodide solutions by TBP and certain other solvents which cause dissociation of complex acids. During indium extraction from bromide solutions by TBP, a substantial decrease of distribution coefficients of microelements has also been observed. Numerous occurrences of extraction suppression and co-extraction have been observed during the separation of Zn, Co, In and other metals from thiocyanate solutions. Preliminary experiments with high molecular weight amines have shown that the

effect occurs with these solvents as well. Thus, indium suppresses cadmium extraction and *vice versa* during their extraction by tri-n-octylamine in benzene from chloride solutions.

Acknowledgments

The authors are grateful to A. A. Prokoshev, Z. Kh. Sultanova, A. B. Sokolov, N. Vanifatova and V. G. Revenko who investigated some of the extraction systems.

References

[1] Zolotov, Yu. A., *Dokl. Akad. Nauk SSSR*, 1968, **180**, 1367
[2] Karabash, A. G., Moseev, L. I., & Kuznetsov, V. A., *Zh. neorg. Khim.*, 1960, **5**, 1358
[3] Sokolov, A. B., Moseev, L. I., & Karabash, A. G., *Zh. neorg. khim.*, 1961, **6**, 994
[4] Moseev, L. I., & Karabash, A. G., *Zh. neorg. Khim.*, 1961, **6**, 1944
[5] Moseev, L. I., & Karabash, A. G., *Zh. neorg. Khim.*, 1964, **9**, 1720
[6] Alimarin, I. P., Zolotov, Yu. A., & Shakhova, N. V., *Trudȳ Kom. analit. Khim.*, 1963, **14**, 28
[7] Specker, H., & Shirodker, R., *Z. analyt. Chem.*, 1965, **214**, 401
[8] Günzler, G., & Mühl, P., *Z. Chemie, Lpz.*, 1965, **5**, 148
[9] Morgunov, A. F., & Fomin, V. V., *Zh. neorg. Khim.*, 1963, **8**, 508
[10] Campbell, D. E., Clark, H. M., & Bauer, W. H., *J. phys. Chem., Ithaca*, 1958, **62**, 506
[11] Izmailov, N. A., 'Electrochemistry of solutions', 2nd Edn, 1966 (Moscow: Khimia)
[12] Romanova, A. D., Favorskaya, L. V., & Ponomarev, V., *Izv. Akad. Nauk kazakh. SSR, Ser. tekh. khim. Nauk*, 1964, (4), 49
[13] Irving, H., & Edgington, D. N., *J. inorg. nucl. Chem.*, 1959, **10**, 306

Extraction of rhenium(VII) by dilute solutions of Aliquat 336 in organic solvents

by V. I. Lakshmanan and G. J. Lawson
Department of Minerals Engineering, University of Birmingham, P.O. Box 363, Birmingham B15 2TT, U.K.

The extraction of rhenium as Re(VII) with Aliquat 336 was investigated using various diluents, and the effects of electrolytes and contaminants in the aqueous phase, and of variation in pH, metal ion concentration and extractant concentration were measured. Distribution of various ions between aqueous and organic phases was measured by radio-tracer techniques.

The extraction of Re(VII) by Aliquat 336 in nitrobenzene forms the basis of an analytical method for determination of rhenium.

Introduction

THE METHODS NORMALLY used for the separation of rhenium from accompanying metal ions are based upon the fact that in its most stable valency state, Re(VII), it is present as an anion. For the separation of simple or complex anions, quaternary ammonium salts which are soluble in hydrocarbon-type solvents have been found useful;[1,2] their action is similar to that of quaternary type anion-exchange resins. Quaternary ammonium halides have been used to extract various metal ions from aqueous solution in analytical applications.[3] The object of the present work was to establish a solvent extraction procedure that could form the basis of an analytical method for rhenium, using tricaprylmethylammonium chloride (Aliquat 336) as extractant and various organic solvents as diluents.

Experimental

Reagents

Aliquat 336, a commercial grade of tricaprylmethylammonium chloride (General Mills Inc.) was supplied as a light yellow viscous liquid of average mol. wt. 442. Stock solutions of Re(VII) were made by dissolving pure potassium perrhenate (Johnson Matthey Ltd.) in water. All other reagents and solvents were of analytical reagent quality.

Extraction procedure

Portions (20 ml each) of organic and aqueous phases were transferred to open top separating funnels and equilibrated by stirring mechanically at room temperature (21 °C). The organic phases were solutions of Aliquat 336 in various solvents, and the aqueous phases were made up from aliquot portions of stock potassium perrhenate solution, radioactive tracer, acid to regulate pH, and other additions as required. Various times of stirring were tested between 5 min and 60 min; equilibrium was established in all these tests, and a standard mixing time of 5 min was adopted for all subsequent experiments. After equilibration the phases were allowed to separate; a portion of the upper phase was then removed by pipette and a portion of the lower phase through the funnel tap. These portions were centrifuged to ensure complete phase separation before aliquots were evaporated to dryness for radioactivity measurements. The equilibrium pH values of the aqueous phases were measured with a Pye Model 290 pH meter.

Rhenium tracer was obtained by irradiation of potassium perrhenate in the Herald reactor (A.W.R.E. Aldermaston). Other tracers were obtained from the Radiochemical Centre, Amersham. Measurements of radioactivity were made either with a thin-end window type Geiger–Muller counter operated with

a stabilised power supply and a dekatron scaler, or with a single channel pulse height analyser. Corrections for background, coincidence, self absorption and self scattering were applied when necessary. The sum of the activities measured in corresponding organic and aqueous phases was 100 ± 2% of the original tracer activity.

The extraction coefficient, D, was calculated from:

$$D = \frac{\text{Activity in 1 ml organic phase}}{\text{Activity in 1 ml aqueous phase}}$$

and the percentage extraction from:

$$\text{Percentage extraction} = \frac{D}{D + V_a/V_o} \times 100$$

where V_a and V_o are the volumes of the aqueous and organic phases respectively.

Results and discussion

Several series of experiments were carried out to determine the best conditions for the quantitative extraction of rhenium, free from contaminants. First, several organic solvents were examined as possible diluents, and a number proved potentially suitable (Table I). These solvents differed in dipole moment, dielectric constant, and also in their basic nature; it was decided to select for further examination three solvents, carbon tetrachloride, *o*-dichlorobenzene and nitrobenzene, which presented a wide range of dielectric constant values but were of low basicity, so that possible interaction of the solvent in the extraction process by electron donation would be minimised.

TABLE I

Extraction of rhenium from aqueous solution with Aliquat 336 in various organic diluents

Initial concentration of Re (VII): $2 \cdot 69 \times 10^{-5}$M
Initial concentration of Aliquat 336: $1 \cdot 13 \times 10^{-3}$M

Diluent	Dipole moment	Dielectric constant[4]	Rhenium extracted, %
Carbon tetrachloride	0·00	2·24	51·7
Benzene	0·00	2·28	65·0
Chloroform	1·15	4·90	99·8
o-Dichlorobenzene	2·26	9·93	99·8
Nitrobenzene	3·95	34·8	99·8
Ethyl acetate	1·81	6·40	99·9
Amyl acetate	1·82	4·60	99·9
n-Butanol	1·68	16·10	99·9
Iso-amyl alcohol	1·66	14·70	99·9
Methyl isobutyl ketone	2·79	13·11	99·9

The effect of pH on the extraction of Re(VII) with Aliquat 336 dissolved in the three chosen diluents is shown in Table II. Percentage extraction did not change progressively with pH, and the lower extraction values were obtained at pH values near the neutral point; for example the 99·4% extraction value with nitrobenzene occurred at pH 5·9, the 98·6% value at pH 5·4, and the values 51·7 and 64·7% for carbon tetrachloride occurred at pH 5·7 and pH 6·8 respectively. The results in Table II indicated that nitrobenzene was the most efficient solvent of the three; the pH values were usually adjusted with hydrochloric acid, but in two cases nitric acid was used, and this appeared to reduce the extraction efficiency. This was confirmed by experiments with larger concentrations of nitric and other acids (Table III) from the results of

TABLE II

Effect of pH on the extraction of rhenium with Aliquat 336 in various diluents

	Re(VII) concn., M	Aliquat 336 concn., M	pH range	Rhenium extracted, %
Nitrobenzene diluent:				
	$1 \cdot 35 \times 10^{-5}$	$2 \cdot 26 \times 10^{-3}$	1·33–8·40	99·8–99·9
	$2 \cdot 69 \times 10^{-5}$	$1 \cdot 13 \times 10^{-3}$	1·05–9·26	99·4–99·9
	$5 \cdot 38 \times 10^{-5}$	$6 \cdot 57 \times 10^{-4}$	1·05–9·31	98·6–99·9
	$5 \cdot 38 \times 10^{-5}$	$1 \cdot 13 \times 10^{-3}$	0·7 –8·12	99·8–99·9
	$2 \cdot 69 \times 10^{-4}$	$1 \cdot 13 \times 10^{-3}$	1·03–8·90	99·8–99·9
	$2 \cdot 69 \times 10^{-5}$	$1 \cdot 13 \times 10^{-3}$	2·12–3·57*	99·5–99·9
	$1 \cdot 35 \times 10^{-4}$	$2 \cdot 26 \times 10^{-3}$	1·49–3·04*	98·8–99·9
o-Dichlorobenzene diluent:				
	$2 \cdot 69 \times 10^{-5}$	$1 \cdot 13 \times 10^{-3}$	1·33– 9·26	98·6–99·9
	$2 \cdot 69 \times 10^{-4}$	$2 \cdot 26 \times 10^{-3}$	1·34–10·00	99·1–99·9
Carbon tetrachloride diluent:				
	$2 \cdot 69 \times 10^{-5}$	$1 \cdot 13 \times 10^{-3}$	0·66– 9·92	51·7–99·9
	$5 \cdot 38 \times 10^{-5}$	$1 \cdot 13 \times 10^{-3}$	0·78–10·08	64·7–99·5

* pH adjusted with nitric acid

TABLE III

Effect of various acids on the extraction of rhenium with Aliquat 336 in carbon tetrachloride or nitrobenzene

Initial concentration of Re(VII): $2 \cdot 69 \times 10^{-5}$M
Concentration of Aliquat 336: $1 \cdot 13 \times 10^{-3}$M

	Nature and molarity of acid	Rhenium extracted, %		Extraction coefficient (*D*)	
		Nitro-benzene	CCl_4	Nitro-benzene	CCl_4
HCl	5·5	98·6	61·8	71	1·6
	2·75	99·5	78·2	$2 \cdot 1 \times 10^2$	3·5
	1·10	99·9	83·4	$3 \cdot 8 \times 10^2$	5·0
	0·55	99·9	93·6	$7 \cdot 3 \times 10^2$	16·2
HNO_3	8·2	1·9	0·36	$1 \cdot 9 \times 10^{-2}$	$3 \cdot 6 \times 10^{-3}$
	4·1	1·3	1·74	$1 \cdot 3 \times 10^{-2}$	$1 \cdot 8 \times 10^{-2}$
	1·7	15·8	17·3	$1 \cdot 9 \times 10^{-2}$	$2 \cdot 1 \times 10^{-2}$
	0·85	51·2	41·6	1·05	0·71
CH_3COOH	8·5	—	15·3	—	0·18
	4·25	63·7	53·0	1·8	1·13
	0·83	99·8	93·8	$1 \cdot 6 \times 10^2$	15
	0·083	99·9	98·5	$1 \cdot 6 \times 10^2$	63
H_2SO_4	6·0	99·9	99·9	$> 10^3$	$> 10^3$
	4·5	99·9	99·9	$> 10^3$	$> 10^3$
	3·6	99·9	99·9	$> 10^3$	$> 10^3$
	0·9	99·9	99·9	$> 10^3$	$> 10^3$

which it appeared that both nitric and acetic acids reduced extraction efficiency; hydrochloric acid reduced extraction into nitrobenzene slightly at high concentrations, and reduced extraction into carbon tetrachloride considerably, while sulphuric acid had little effect on either diluent.

The effects on extraction efficiency of Re(VII) concentration and of Aliquat 336 concentration in the three chosen diluents were examined, with results that are shown in Tables IV and V and Fig. 1. High efficiency was obtained with nitrobenzene as diluent, even when the excess of extractant over Re(VII) was relatively small, but *o*-dichlorobenzene was less efficient. A slight reduction in percentage extraction was noted with higher extractant concentrations; this would be unlikely to affect analytical application to the small concentrations of rhenium encountered in nature. No explanation of this reduction can be offered at this stage of investigation. With carbon tetrachloride as diluent, extraction increased progressively with concentration of extractant, and the results are presented as a graph of log D vs. log [Aliquat 336] (Fig. 1). This

TABLE IV

Effect of extractant concentration on the extraction of rhenium with Aliquat 336 in nitrobenzene

Re(VII) concn., M	Aliquat 336 concn., M	Rhenium extracted, %	Extraction coefficient (D)
$5\cdot38 \times 10^{-5}$	$2\cdot26 \times 10^{-3}$	99·9	$4\cdot2 \times 10^{3}$
	$2\cdot26 \times 10^{-2}$	99·9	$1\cdot7 \times 10^{3}$
	$2\cdot26 \times 10^{-1}$	98·7	80
$2\cdot69 \times 10^{-5}$	$1\cdot13 \times 10^{-4}$	99·9	$1\cdot8 \times 10^{3}$
	$5\cdot65 \times 10^{-4}$	99·9	$1\cdot5 \times 10^{3}$
	$1\cdot13 \times 10^{-3}$	99·9	$1\cdot1 \times 10^{3}$
	$1\cdot13 \times 10^{-2}$	99·9	$2\cdot5 \times 10^{2}$
$2\cdot69 \times 10^{-4}$	$5\cdot65 \times 10^{-4}$	99·9	$3\cdot1 \times 10^{3}$
	$1\cdot13 \times 10^{-3}$	99·9	$1\cdot5 \times 10^{3}$
	$5\cdot65 \times 10^{-3}$	99·9	$7\cdot3 \times 10^{2}$
	$1\cdot13 \times 10^{-2}$	99·8	$5\cdot1 \times 10^{2}$

TABLE V

Effect of extractant concentration on the extraction of rhenium with Aliquat 336 in o*-dichlorobenzene*

Re(VII) concn., M	Aliquat 336 concn., M	Rhenium extracted, %	Extraction coefficient (D)
$2\cdot69 \times 10^{-5}$	$5\cdot67 \times 10^{-5}$	99·8	$5\cdot2 \times 10^{2}$
	$5\cdot67 \times 10^{-4}$	99·8	$6\cdot1 \times 10^{2}$
	$2\cdot26 \times 10^{-3}$	99·7	$2\cdot7 \times 10^{2}$
	$1\cdot13 \times 10^{-2}$	99·8	$6\cdot5 \times 10^{2}$
$1\cdot35 \times 10^{-4}$	$1\cdot00 \times 10^{-4}$	98·4	55
	$5\cdot67 \times 10^{-4}$	99·9	$7\cdot5 \times 10^{2}$
	$2\cdot26 \times 10^{-3}$	99·2	$1\cdot2 \times 10^{2}$
	$1\cdot13 \times 10^{-2}$	99·6	$2\cdot4 \times 10^{2}$
$2\cdot69 \times 10^{-4}$	$5\cdot67 \times 10^{-5}$	65·5	1·9
	$5\cdot67 \times 10^{-4}$	99·4	$1\cdot8 \times 10^{2}$
	$2\cdot26 \times 10^{-3}$	99·2	$1\cdot1 \times 10^{2}$
	$1\cdot13 \times 10^{-2}$	99·2	$1\cdot1 \times 10^{2}$

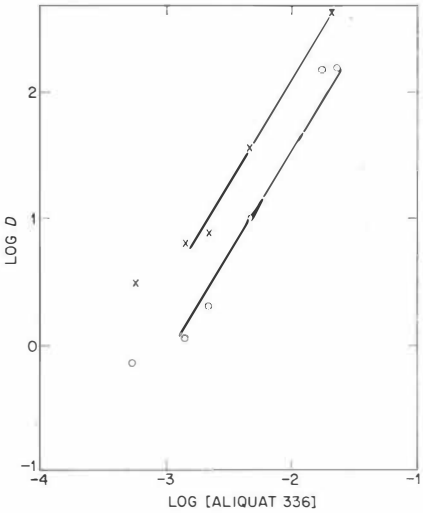

FIG. 1. *Effect of variation of extractant concentration on the extraction of rhenium by Aliquat 336 in carbon tetrachloride*

Initial concentration of Re(VII): × $1 \cdot 35 \times 10^{-4}$M; ○ $2 \cdot 69 \times 10^{-5}$M
Slope of lines = $1 \cdot 8$

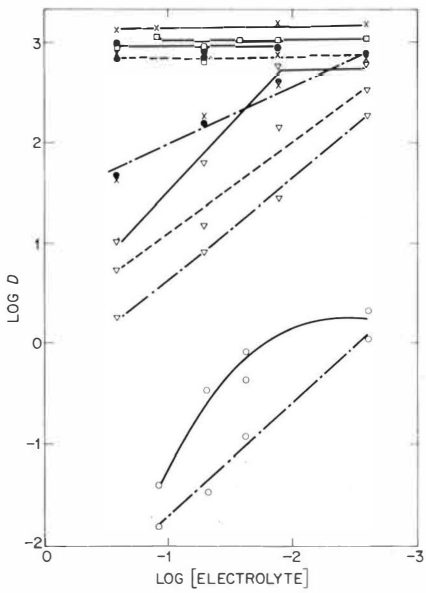

FIG. 2. *Effect of various electrolytes on the extraction of rhenium with Aliquat 336 in various diluents*

——— Nitrobenzene; — — — *o*-dichlorobenzene; —·—· carbon tetrachloride
× KCl; □ $MgCl_2$; ● NaCl; ○ $NaClO_4$; ▽ $NaNO_3$
Initial concentration of Re(VII): $2 \cdot 69 \times 10^{-5}$M
Concentration of Aliquat 336: $1 \cdot 13 \times 10^{-3}$M

behaviour may be due to dimerisation of the extractant at higher concentrations, brought about by the lower dielectric constant of carbon tetrachloride ($\varepsilon = 2 \cdot 24$; cf. nitrobenzene $\varepsilon = 34 \cdot 8$).

Various electrolytes were added to the aqueous phase in concentrations between 0·25 and 0·0025M and their effects upon extraction of rhenium were assessed (Fig. 2). The chlorides of Na^+, K^+ and Mg^{2+} did not affect the extraction of rhenium into nitrobenzene or *o*-dichlorobenzene, but $NaNO_3$ and $NaClO_4$ suppressed extraction; the effects of the three anions studied were in the order $ClO_4^- > NO_3^- > Cl^-$. In all cases nitrobenzene was the diluent least affected by the added substances.

Several other substances were tested for possible interference with extraction into nitrobenzene. These included EDTA, tartrate, citrate, oxalate, bromide, acetate, thiosulphate, phosphate and borate, none of which affected the extraction of rhenium in the concentration tested (up to 5×10^{-2}M). The extent of possible co-extraction of K^+ with ReO_4^- was also examined for the three diluents by measuring the distribution of potassium, using ^{42}K tracer, for various aqueous phase concentrations of potassium chloride. The results (Table VI) showed that co-extraction was negligible.

TABLE VI

Variation with concentration of extraction of potassium ions with Aliquat 336 in various diluents, in the presence of rhenium

Initial concentration of Re(VII): $2 \cdot 69 \times 10^{-5}$M
Concentration of Aliquat 336: $1 \cdot 13 \times 10^{-3}$M

K^+ concn., M	K^+ extraction coefficient ($\times 10^2$)		
	D_{NB}	D_{CCl_4}	D_{ODB}
0·25	1·1	1·3	2·5
5×10^{-2}	1·0	1·4	2·5
$1 \cdot 25 \times 10^{-2}$	1·2	1·5	2·3
$2 \cdot 5 \times 10^{-3}$	1·2	—	2·6

NB = nitrobenzene
ODB = *o*-dichlorobenzene

The degree to which possible contaminants might be extracted with rhenium into nitrobenzene was investigated, and in Table VII the results are presented in the form of extraction coefficients for the contaminants, separation factors with respect to rhenium (ratio of extraction coefficients), and decontamination factors:

$$\text{Decontamination factor} = \frac{\text{Total activity of contaminant}}{\text{Activity in organic phase}}$$

Most contaminants were examined in concentrations comparable with that of the rhenium present but two likely contaminants, Mo(VI) and W(VI) were tested at higher concentration. Both of these elements were extracted to a significant extent, but the extraction was suppressed on adding tartrate, which did not hinder extraction of rhenium.

Further investigations are in progress, including the examination of other potential contaminants and application to natural rhenium-bearing minerals. The present study has shown that rhenium as Re(VII) may readily be extracted selectively and quantitatively by Aliquat 336 in nitrobenzene; the useful concentration range covers that of the occurrence of rhenium. Coupled with the use of activation analysis the basis is thus formed for an analytical method for rhenium.

TABLE VII

Extraction coefficients and decontamination factors for various contaminating elements in extraction of rhenium with Aliquat 336 in nitrobenzene

Initial concentration of Re(VII): $2 \cdot 69 \times 10^{-5}$M
Concentration of Aliquat 336: $1 \cdot 13 \times 10^{-3}$M
Extraction coefficient for Re: $3 \cdot 4 \times 10^{3}$
Aqueous phase pH: 2·4–2·6

Contaminating element*	Extraction coefficient (D)	Decontamination factor	Separation factor with respect to Re
^{54}Mn(II)	$5 \cdot 6 \times 10^{-5}$	$1 \cdot 8 \times 10^{4}$	$6 \cdot 1 \times 10^{7}$
^{60}Co(II)	$4 \cdot 2 \times 10^{-5}$	$2 \cdot 4 \times 10^{4}$	$7 \cdot 9 \times 10^{7}$
^{99}Mo(VI)	$1 \cdot 6 \times 10^{-1}$	6·1	$2 \cdot 0 \times 10^{4}$
^{99}Mo(VI)†	$1 \cdot 9 \times 10^{-2}$	48	$1 \cdot 7 \times 10^{5}$
^{185}W(VI)	3·5	—	$9 \cdot 5 \times 10^{2}$
^{185}W(VI)†	$4 \cdot 0 \times 10^{-2}$	26	$8 \cdot 3 \times 10^{4}$
^{48}V(V)	$2 \cdot 1 \times 10^{-2}$	51	$1 \cdot 6 \times 10^{5}$
^{42}K(I)	$1 \cdot 2 \times 10^{-2}$	95	$2 \cdot 8 \times 10^{5}$
^{124}Sb(III)	$4 \cdot 2 \times 10^{-3}$	$2 \cdot 5 \times 10^{2}$	$7 \cdot 9 \times 10^{5}$
^{124}Sb(V)	$3 \cdot 7 \times 10^{-3}$	$2 \cdot 8 \times 10^{2}$	$9 \cdot 1 \times 10^{5}$
^{51}Cr(III)	$1 \cdot 5 \times 10^{-3}$	$7 \cdot 6 \times 10^{2}$	$2 \cdot 2 \times 10^{6}$
^{131}Cs(I)	$3 \cdot 6 \times 10^{-3}$	$2 \cdot 8 \times 10^{2}$	$9 \cdot 1 \times 10^{5}$
^{132}Te(V)	3·1	—	$1 \cdot 1 \times 10^{3}$
^{35}S(VI)	2·32	—	$1 \cdot 4 \times 10^{3}$

* Mo and W tracers used with carrier ≡ 10 mg element in 20 ml aqueous phase. Tracers only used for other elements, at concentrations 10^{-5}–10^{-6}M, i.e. comparable with concentrations of Re(VII)

† Using aqueous phases 5×10^{-2}M with respect to sodium tartrate

Acknowledgments

Grateful acknowledgment is made to Prof. S. G. Ward, Head of the Department of Minerals Engineering, for his interest and advice. Acknowledgment is also made to the Science Research Council for provision of irradiation facilities, to General Mills Inc. for a gift of Aliquat 336, and to Johnson Matthey Ltd. for providing pure potassium perrhenate.

References

1 Freiser, H., *Analyt. Chem.*, 1968, **40,** 522R
2 Wilson, A. M., Churchill, L., Kiluk, K., & Housepian, P., *Analyt. Chem.*, 1962, **34,** 203
3 Good, M. L., Srivasthava, S. L., & Holland, F. F., jun., *Analytica chim. acta*, 1964, **31,** 534
4 Marcus, Y., & Kertes, A. S., 'Ion exchange and solvent extraction of metal complexes', 1969, p. 927 (London: Wiley-Interscience)

Synergic and antagonistic effects in the extraction of chromium(VI) with a mixture of tri-n-octylamine and alkylphosphoric acids from mineral acid solutions

by C. Deptula
Institute of Nuclear Research, Centre of Production and Distribution of Isotopes, Swierk, Poland

It has been found that synergic and antagonistic effects occur in the extraction of chromium(VI) from various mineral acids solutions with a mixture of tri-n-octylamine and alkylphosphoric acids. The composition of the extracted compounds has been determined and the mechanism of the synergic and antagonistic effects is explained.

Introduction

IN PREVIOUS PAPERS,[1-4] the mechanism of the synergic and antagonistic effects in the extraction of sulphuric and chloroplatinic acids and uranyl sulphate with a mixture of amines and alkylphosphoric acids has been described. Studies of the extraction mechanism of inorganic compounds imply that the synergic effects are caused by a change in the composition of the compound extracted with a mixture of extractants as compared with those extracted with the individual components of the mixture. The antagonistic effect is caused by a decrease in the thermodynamic activity of the extractants owing to their interaction.

Hence an antagonistic effect should be expected in the extraction of inorganic compounds in systems which contain tri-n-octylamine (TOA) and alkylphosphoric acids (HX), that are stronger than orthophosphoric acid,[5] owing to the interaction:

$$R_3N + HX \rightleftharpoons R_3N...HX$$

In this case, the magnitude of the antagonistic effect should depend on the concentration of mineral acid, e.g. sulphuric acid in the aqueous phase, because an increase in sulphuric acid concentration causes replacement of the alkylphosphoric acid anion by sulphate anions in compounds of the type R_3NHX with the formation of amine sulphate and/or bisulphate and alkylphosphoric acid, i.e.:

$$2\,R_3NHX + H_2SO_4 \rightleftharpoons (R_3NH)_2SO_4 + 2\,HX$$

$$(R_3NH)_2SO_4 + H_2SO_4 \rightleftharpoons 2\,R_3NH_2SO_4$$

This causes a decrease in the concentration of the TOA salt with alkylphosphoric acids, and, consequently, a decrease in the antagonistic effects. In the extreme case, at very high concentrations of sulphuric acid, the antagonistic effect should be zero.

Studies on the extraction of sulphuric[1] and chloroplatinic acids from sulphuric acid solutions[2] have confirmed this conclusion. The synergy coefficients* for the extraction of sulphuric acid from 0·06, 0·12, 0·52 and 1·0M solutions with a mixture containing 0·10M-TOA and 0·10M di-n-butylphosphoric acid (HDBP) are −0·77, −0·51, −0·42 and −0·30, respectively. The coefficients for the extraction of chloroplatinic acid from 0·025 and 2·70M-H_2SO_4 with a mixture containing 0·05M-TOA and 0·10M-HDBP are −1·68 and −0·15, respectively.

* The synergy coefficient $S = \log E_{1,2}/E_1 + E_2$, where $E_{1,2}$, E_1 and E_2 are the extraction coefficients determined experimentally for a mixture of extractants and for the individual extractants.

In the extraction of uranium(VI) from sulphuric acid solutions with a mixture of amines and alkylphosphoric acids, a synergic effect appears as well as the antagonistic effect that occurs at low concentrations of sulphuric acid.[3,4] The synergy coefficients for the extraction of uranium(VI) from 0·025, 0·5, 1·0 and 2·0M-H_2SO_4 solutions with a mixture containing 0·05M-TOA and 0·05M-HDBP are −0·27, 0·24, 0·52 and 0·78, respectively. It was found that the extraction mechanism of uranium(VI) with the mixture of extractants examined is uniform over the whole concentration range of H_2SO_4 investigated, independently of the appearance of antagonistic or synergic effects, and can be described by the following reaction:

$$UO_2SO_4 + R_3NH^+ + (HX)_n \rightleftharpoons [UO_2SO_4X(HX)^-_{n-1}; R_3NH^+].$$

The structure of the compound extracted can be represented by:

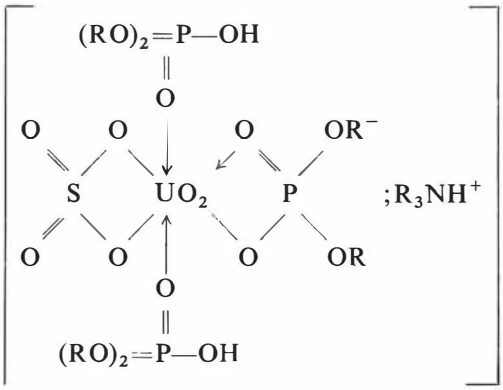

In the present work, conditions are described where synergic and antagonistic effects occur in the extraction of chromium(IV) from solutions of various mineral acids with mixtures of TOA and alkylphosphoric acids. The occurrence of a large synergic effect in these systems is caused by the formation of mixed complexes of $Cr_2O_7^{2-}$ with the amine and alkylphosphoric acids. The structure of these complexes seems to be different from that of the uranium(VI) complexes of the $Cr_2O_7^{2-}$ anion.

Experimental

The tri-n-octylamine (R_3N, TOA) and the acids di-n-butylphosphoric (HDBP), di-2-ethylhexylphosphoric (HD2EHPA) and mono-n-butylphosphoric (H_2MBP) used were obtained from Koch-Light and Co. The 2,6,8-trimethylnonylphosphoric acid (H_2DDPA) was obtained as described previously.[6] The purity of all these extractants was better than 98%.

Extraction equilibrium was achieved by mixing 20 ml of the aqueous phase with 10 ml of the organic phase in dark bottles on an electric shaker for 2 min.

Chromium(VI) was re-extracted from the organic to the aqueous phase with 0·5M sodium hydroxide solution.[7]

Measurements of the absorption spectra of chromium(VI) in an organic phase of composition 0·05M-TOA+0·05M-HDBP+carbon tetrachloride were made on a Unicam SP-500 spectrophotometer with respect to a reference solution containing the same concentrations of extractants in carbon tetrachloride. This solution was pre-equilibrated with an appropriate acid of the same concentration as that from which chromium(VI) was extracted.

Aqueous phases were prepared by dissolution of $Na_2Cr_2O_7$ in an appropriate acid.

The concentration of chromium(VI) in the aqueous phase was determined spectrophotometrically with diphenylcarbazide (for Cr concentrations up to

2 g/l) and iodometrically (for Cr concentrations > 2 g/l). The concentration of chromium(VI) in the organic phase was calculated from the difference in the chromium content in the aqueous phase before and after extraction, or else determined in the aqueous solution after back-washing from the organic phase.

The chromium(VI) balance in the aqueous and organic phases agreed to within ± 1·0%.

The concentration of chlorides in the organic phase was determined gravimetrically by precipitation of AgCl after back-washing.

Results

Reduction of chromium(VI) with solutions of tri-n-octylamine and alkylphosphoric acids

Amines and alkylphosphoric acids are relatively resistant to the action of oxidising agents.[8,9] It was found, however, that organic solutions that contained these reagents and chromium change their colour from orange to green after storing in daylight for ~ 2 days. This change was caused by the reduction of chromium(VI) to chromium(III) and was accelerated to about 1 h after irradiation of organic solutions of chromium with ultra-violet light. Photochemical reduction of chromium(VI) to chromium(III) occurs frequently.[10–12] It did not occur when the organic phase was stored in the dark (no change was found in the absorption spectrum of chromium(VI) after a 2-week storage). The extraction coefficient of chromium was determined from the difference in the chromium(VI) concentration in the aqueous phase before and after extraction, so that it was necessary to ascertain whether the chromium is reduced during the extraction process. Chromium(III) is not extracted by solutions of amines and alkylphosphoric acids,[13] thus the change in the concentration of chromium(VI) in the aqueous solution after extraction, before and after oxidation with ammonium persulphate, should indicate any reduction during extraction. The results obtained are given in Table I, from which it follows that during the extraction process no reduction of chromium(VI) occurs. However, the extractions were done in dark bottles and the duration of

TABLE I

Results for the determination of chromium(VI) in aqueous phases before and after oxidation

Mineral acid and concentration, M	Composition of organic phase	Chromium concentration, g/l Before oxidation	After oxidation
H_2SO_4, 0·025	TOA + HDBP	0·0230	0·0236
H_2SO_4, 0·90	TOA + HDBP	0·0044	0·0041
H_2SO_4, 1·80	TOA + HDBP	0·0077	0·0079
H_2SO_4, 0·025	TOA + H_2MBP	0·0076	0·0081
H_2SO_4, 0·90	TOA + H_2MBP	0·0121	0·0120
H_2SO_4, 1·80	TOA + H_2MBP	0·0268	0·0270
H_2SO_4, 0·025	TOA + H_2DDPA	0·1921	0·1920
H_2SO_4, 0·90	TOA + H_2DDPA	0·0468	0·0463
H_2SO_4, 1·80	TOA + H_2DDPA	0·0550	0·0541
H_2SO_4, 0·025	TOA + HD2EHPA	0·0202	0·0205
H_2SO_4, 0·90	TOA + HD2EHPA	0·0044	0·0040
H_2SO_4, 1·80	TOA + HD2EHPA	0·0091	0·0096
HCl, 0·25	TOA + HDBP	0·0078	0·0081
HCl, 0·90	TOA + HDBP	0·0148	0·0149
HCl, 1·80	TOA + HDBP	0·0212	0·0215
HNO_3, 0·05	TOA + HDBP	0·0206	0·0208
HNO_3, 0·90	TOA + HDBP	0·0592	0·0598
HNO_3, 2·70	TOA + HDBP	0·1440	0·1443
$HClO_4$, 0·05	TOA + HDBP	0·0987	0·0989
$HClO_4$, 0·90	TOA + HDBP	0·4442	0·4447
$HClO_4$, 2·0	TOA + HDBP	0·3700	0·3708

all operations (including analysis) was as short as possible. The stability of chromium(VI) in the systems examined is confirmed by the reproducibility of the extraction coefficients of the metal.

Composition of the organic phase: 0·05M-TOA+0·10M-HX+C_6H_6

Determination of the conditions under which the synergic and antagonistic effects appear

The influence of the composition of the aqueous and organic phases on the extraction coefficient (E_a^o) were studied to determine the conditions under which the synergic and antagonistic effect appear.

Chromium(VI) is not extracted by alkylphosphoric acids, therefore the extraction of chromium(VI) by a mixture of TOA with alkylphosphoric acids was studied, using organic phases with a constant concentration of TOA (0·05M) and alkylphosphoric acid concentrations varying from 0 to 0·30M.

Results for the extraction of chromium(VI) from sulphuric acid solutions with mixtures of TOA and the alkylphosphoric acids HDBP, HD2EHPA, H_2MBP and H_2DDPA in benzene are presented in Figs 1–4. Analogous results were obtained with nitrobenzene and carbon tetrachloride as diluents. The highest extraction coefficients were obtained with nitrobenzene, and the lowest with carbon tetrachloride.

The influence of ammonium sulphate concentration on the extraction of chromium(VI) from 0·025M-H_2SO_4 with a mixture of TOA and di-n-butylphosphoric acid is shown in Fig. 5.

Tri-n-butyl phosphate, in contrast with acidic alkylphosphoric esters, does not influence the extraction of chromium(VI) from sulphuric acid solutions with TOA (Fig. 6).

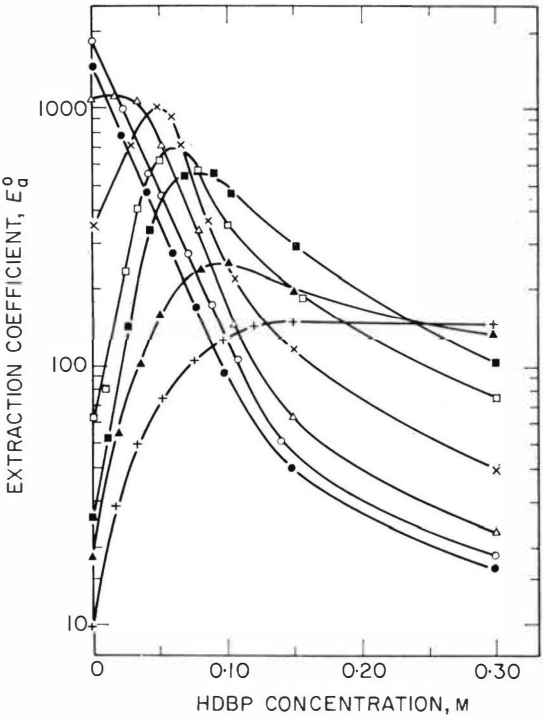

FIG. 1. *Influence of HDBP concentration on chromium(VI) extraction from sulphuric acid solutions with* 0·05 M-*TOA solution in benzene*

H_2SO_4 concentration, M: ○ 0·025; ● 0·032; △ 0·045; × 0·18; □ 0·45; ■ 0·90 ▼ 1·80; + 2·70

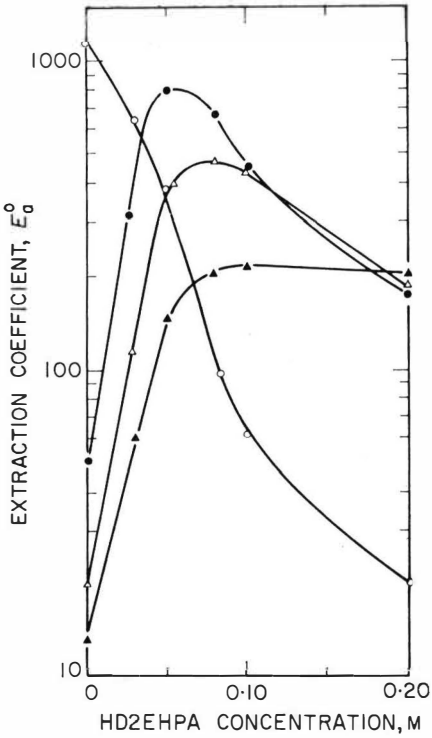

FIG. 2. *Influence of HD2EHPA concentration on chromium(VI) extraction from sulphuric acid solutions with* 0·05M-*TOA solution in benzene*

H_2SO_4 concentration, M: ○ 0·025; ● 0·50; △ 1·0; ▲ 1·80

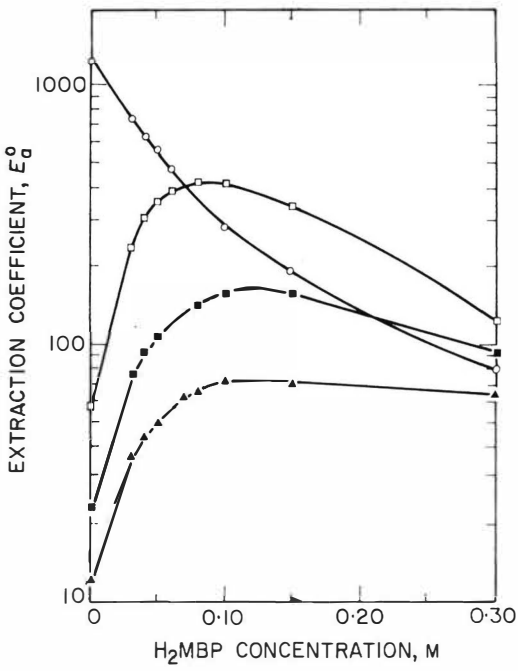

FIG. 3. *Influence of H_2MBP concentration on chromium(VI) extraction from sulphuric acid solutions with* 0·05M-*TOA solution in benzene*

H_2SO_4 concentration, M: ○ 0·025; □ 0·45; ■ 0·90; ▲ 1·80

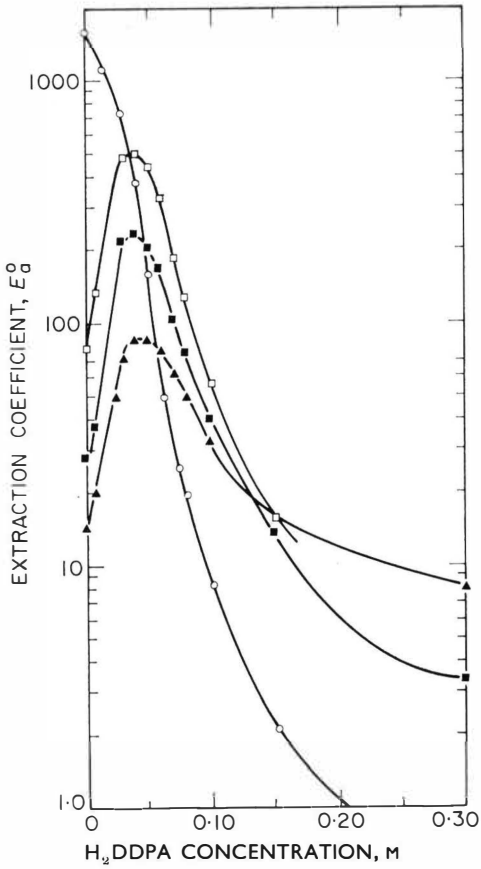

FIG. 4. *Influence of H_2DDPA concentration on chromium(VI) extraction from sulphuric acid solutions with* 0·05M-*TOA solution in benzene*

H_2SO_4 concentration, M: ○ 0·025; □ 0·45; ■ 0·90; ▲ 1·80

Results for the extraction of chromium(VI) from orthophosphoric, nitric perchloric and hydrochloric acids with a mixture of tri-n-octylamine with di-n-butylphosphoric acid are presented in Figs 7–10. The conditions under which synergic and antagonistic effects appear in the other systems were not investigated. On the basis of the results from the extraction of chromium(VI) from sulphuric acid solutions, it was assumed that the remaining alkylphosphoric acids behave similarly to di-n-butylphosphoric acid.

From the results in Figs 1–4 and 7–10, it follows that in the extraction of chromium(VI) by mixtures of tri-n-octylamine with alkylphosphoric acids, extraction coefficients differ from those expected on the basis of addition. To elucidate the mechanism of this synergic effect (the antagonistic effect is a natural sequence of the composition of the organic phase), the composition of the extracted compound was determined.

Determination of the composition of the extracted compound

The composition of the extracted chromium(VI) compound was determined by the following methods: dilution, maximum loading and spectrophotometry.

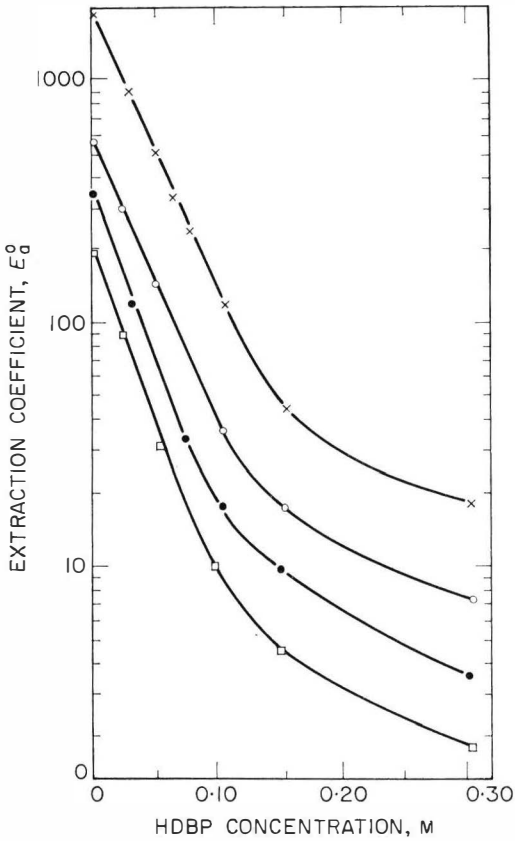

FIG. 5. *Influence of* $(NH_4)_2SO_4$ *concentration on chromium(VI) extraction from* 0·025M-H_2SO_4 *solution with tri-n-octylamine* (0·05M) *and di-n-butylphosphoric acid solutions in benzene*
$(NH_4)_2SO_4$ concentration, M: × 0; ○ 0·16; ● 0·88; □ 2·65

Dilution method

This method is commonly used to determine the composition of the extracted compounds in systems containing a mixture of extractants.[14,15] Experiments were carried out at constant concentration of tri-n-octylamine (0·05M) and varing concentrations of alkylphosphoric acids (0·01–0·30M), and at a constant concentration of alkylphosphoric acids (0·05M) and varying concentrations of tri-n-octylamine (0·01–0·20M). To eliminate extraction of the mineral acid by the tri-n-octylamine,[16,17] individual organic phases were pre-equilibrated with mineral acids at the same concentration as the chromium(VI) solutions. Under these conditions, tri-n-octylamine occurs in the organic phase as the ammonium salt. Chromium was extracted from solutions containing 0·25 g/l. The results obtained are presented in Figs 11–16, where the abscissa are the concentrations of the free extractant calculated from the equation:

$$[\text{TOA or HX}]_{\text{free}} = [\text{TOA or HX}]_{\text{total}} - [Cr_2O_7^{2-}]_0$$

where $[Cr_2O_7^{2-}]_o$ is the concentration of $Cr_2O_7^{2-}$ in the organic phase.

The deviation of the experimental points from linearity in Figs 11–16, at a large excess of one extractant with respect to the other, is probably caused by changes in their thermodynamic activity coefficients owing to their mutual action.

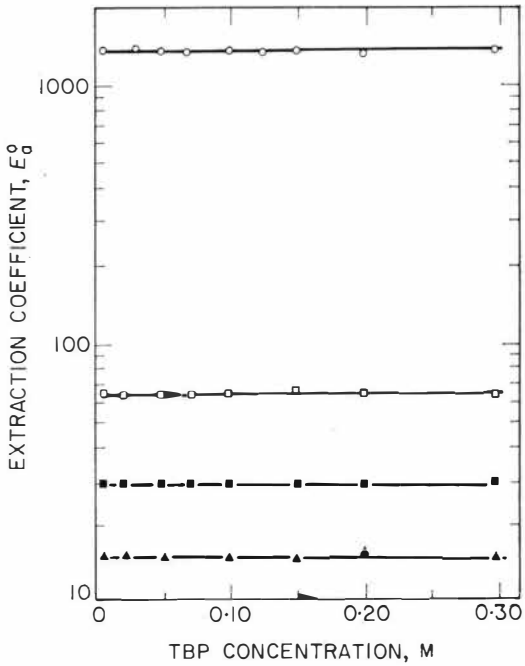

FIG. 6. *Influence of TBP concentration on chromium(VI) extraction from sulphuric acid solutions with* 0·05M-*TOA solution in benzene*

H_2SO_4 concentration, M: ○ 0·025; □ 0·45; ■ 0·90; ▲ 1·80

The dilution method is not suitable for the determination of the composition of the extracted compounds for systems with high extraction coefficients because at higher concentrations of the extractant, the errors in the determination of metal concentrations each phase are considerable. This method was therefore not used for determining the composition of the chromium(VI) compounds extracted from orthophosphoric and hydrochloric acid solutions and from sulphuric acid solutions of low concentration.

Maximum loading method

The results of chromium(VI) extraction from mineral acid solutions of varying $Na_2Cr_2O_7$ concentration with mixtures of tri-n-octylamine and di-n-butylphosphoric acid are shown in Fig. 17 (extraction equilibrium curves). Table II shows chemical analyses of the organic phases obtained under the conditions of maximum loading. In these saturated organic phases, the anions SO_4^{2-}, PO_4^{3-}, NO_3^- and ClO_4^- were not detected; Cl^- was an exception.

Spectrophotometric method

The absorption spectra of chromium(VI) in organic phases containing TOA, HDBP and CCl_4, obtained by extraction of chromium(VI) from solutions of mineral acids are shown in Fig. 18. Similar spectra were obtained for the extraction of chromium(VI) with mixtures of tri-n-octylamine and other alkylphosphoric acids.

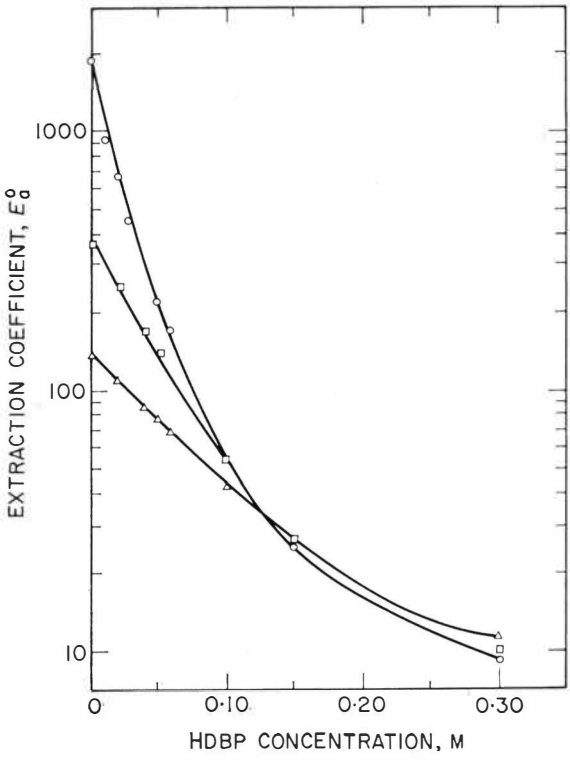

FIG. 7. *Influence of HDBP concentration on chromium(VI) extraction from phosphoric acid solutions with* 0·05M-*TOA solution in benzene*

H_2PO_4 concentration, M: ○ 0·05; □ 0·90; △ 2·70

TABLE II

Results of analysis of organic phases obtained under conditions of maximum loading with chromium(VI)

Chromium concentration in aqueous solution ~ 70 g/l

Aqueous mineral acid and concentration M,	Organic TnOA concentration M	Organic HDBP concentration M	Molar ratio Cr:TnOA	Cr:HDBP	Cr:Y
H_2SO_4, 0·10	0·05	0·05	1·04	1·04	0·00
H_2SO_4, 0·10	0·05	0·10	1·07	0·54	0·00
H_2SO_4, 1·0	0·05	0·05	1·36	1·36	0·00
H_2SO_4, 1·0	0·05	0·10	1·38	0·69	0·00
H_2SO_4, 1·0	0·05	0·20	1·32	0·33	0·00
H_2SO_4, 2·0	0·05	0·05	1·48	1·48	0·00
H_2SO_4, 2·0	0·05	0·10	1·44	0·72	0·00
H_2SO_4, 2·0	0·05	0·20	1·43	0·36	0·00
H_2SO_4, 2·0	0·10	0·10	1·50	1·50	0·00
HNO_3, 0·25	0·10	0·10	1·30	1·30	0·00
HNO_3, 0·25	0·10	0·20	1·24	0·62	0·00
HNO_3, 3·0	0·05	0·05	2·01	2·01	0·00
HNO_3, 3·0	0·05	0·10	2·05	1·03	0·00
H_3PO_4, 0·10	0·05	0·05	1·02	1·02	0·00
H_3PO_4, 2·0	0·05	0·05	1·19	1·19	0·00
H_3PO_4, 2·0	0·05	0·10	1·12	0·56	0·00
H_3PO_4, 2·0	0·05	0·20	1·11	0·28	0·00
HCl, 0·10	0·05	0·05	1·12	1·12	0·48
HCl, 1·0	0·05	0·05	1·08	1·08	1·01
HCl, 2·0	0·05	0·05	1·01	1·01	0·98
HCl, 2·0	0·05	0·10	1·03	0·52	1·02

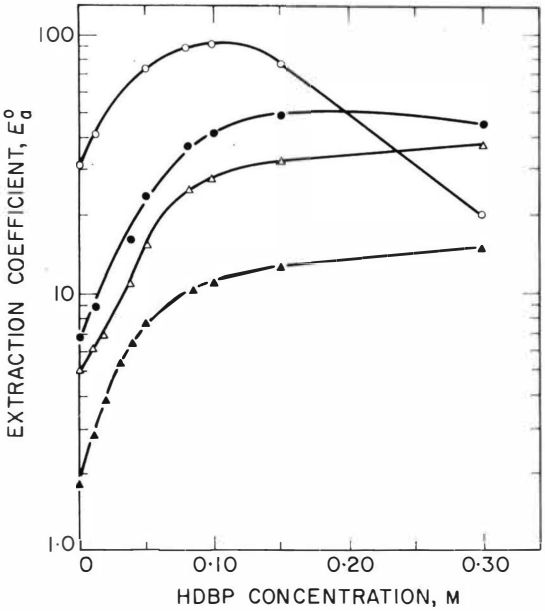

FIG. 8. *Influence of HDBP concentration on chromium(IV) extraction from nitric acid solutions with* 0·05M-*TOA solution in benzene*

HNO_3 concentration, M: ○ 0·05; ● 0·50; △ 0·90; ▼ 2·7

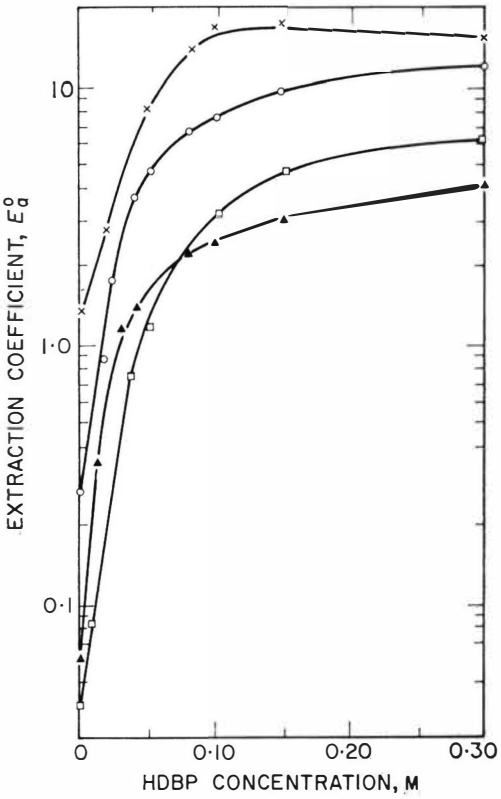

FIG. 9. *Influence of HDBP concentration on chromium(VI) extraction from perchloric acid solutions with* 0·05M-*TOA solution in benzene*

$HClO_4$ concentration, M: × 0·05; ○ 0·20; ▲ 1·0; □ 2·0

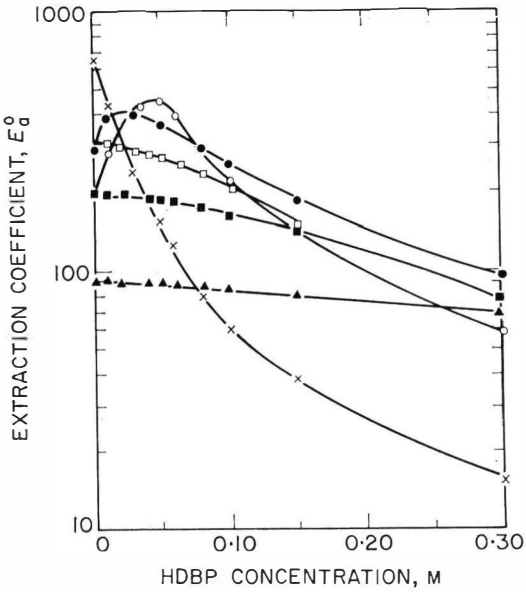

FIG. 10. *Influence of HDBP concentration on chromium(VI) extraction from hydrochloric acid solutions with* 0·05M-*TOA solution in benzene*

HCl concentration, M: × 0·05; ○ 0·10; ● 0·25; □ 0·50; ■ 0·90; ▲ 1·80

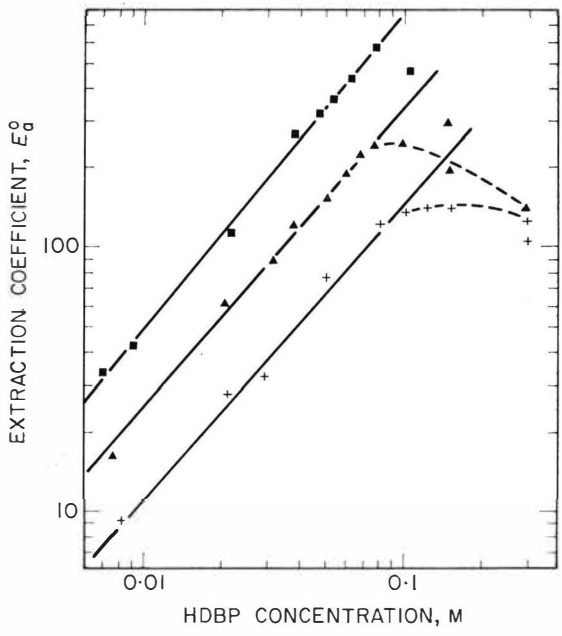

FIG. 11. *Dependence of log* E_a^o *vs. log* [*HDBP*] *at TOA concentration* 0·05M

H_2SO_4 concentration, M: ■ 0·90; ▲ 1·80; + 2·70

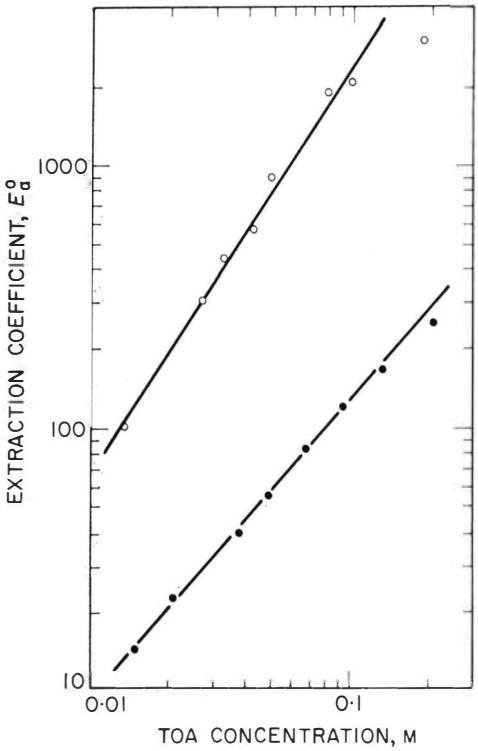

FIG. 12. *Dependence of log* E_a^o *vs. log* [*TOA*] *at HDBP concentration* 0·05M
H_2SO_4 concentration, M: ○ 1·0+4·5 M-$(NH_4)_2SO_4$; ● 3·0+3·0 M-$(NH_4)_2SO_4$

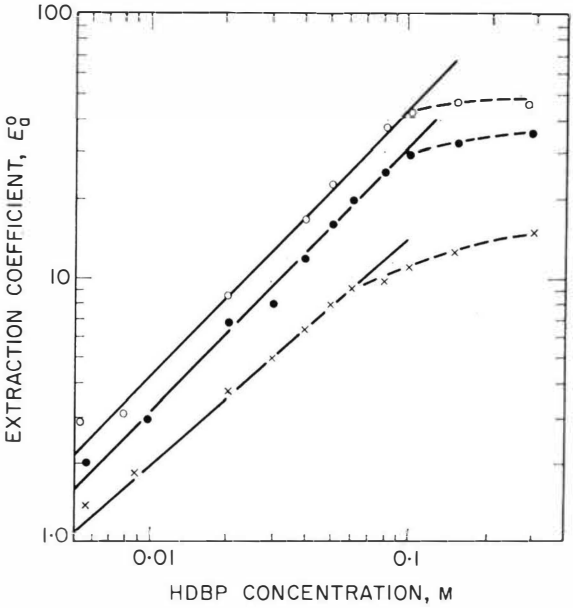

FIG. 13. *Dependence of log* E_a^o *vs. log* [*HDBP*] *at TOA concentration* 0·05M
HNO_3 concentration, M: ○ 0·50; ● 1·0; × 3·0

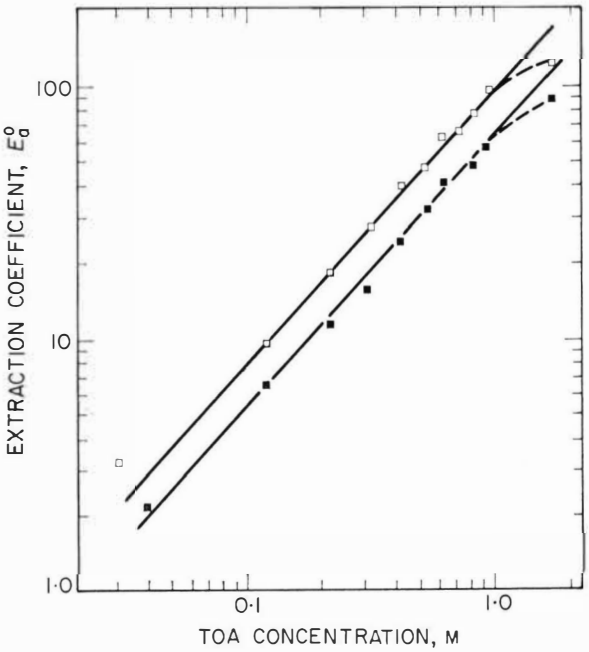

FIG. 14. *Dependence of log* E_a^o *vs. log* [*TOA*] *at HDBP concentration* 0·05M
HNO_3 concentration, M: □ 3·0; ■ 1·0+3·0 M-$NaNO_3$

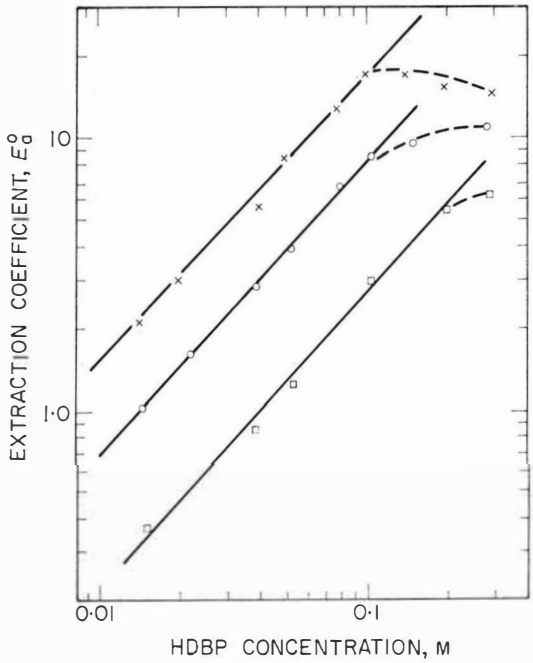

FIG. 15. *Dependence of log* E_a^o *vs. log* [*HDBP*] *at TOA concentration* 0·05M
$HClO_4$ concentration, M: × 0·05; ○ 0·20; □ 2·0

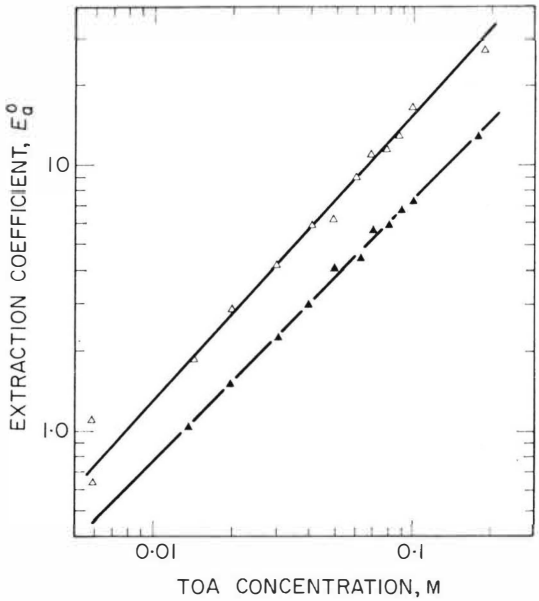

FIG. 16. *Dependence of log* E_a^o *vs. log* [*TOA*] *at HDBP concentration* 0·05M
$HClO_4$ concentration, M: △ 0·50; ▲ 1·0

Discussion

From Figs 1–5 and 7–10, both synergic and antagonistic effects appear during the extraction of chromium(VI) from sulphuric and hydrochloric acid solutions by mixtures of tri-n-octylamine and alkylphosphoric acids. During the extraction of chromium(VI) from nitric and perchloric acid solutions only the synergic effect appears. During the extraction of chromium(VI) from orthophosphoric acid solutions the antagonistic effect appears over the whole concentration range investigated.

In aqueous solutions of sulphuric, nitric, perchloric and orthophosphoric acids, chromium(VI) forms a number of complexes whose stability constants are as follows:[18–20]

$$H_2CrO_4 \rightleftharpoons H^+ + HCrO_4^- \; ; \qquad K_1 = 1{\cdot}21$$

$$HCrO_4^- \rightleftharpoons H^+ + CrO_4^{2-} \; ; \qquad K_2 = 3{\cdot}2 \times 10^{-2}$$

$$2\,HCrO_4^- \rightleftharpoons Cr_2O_7^{2-} + H_2O; \qquad K_3 = 98$$

$$H_2Cr_2O_7 \rightleftharpoons H^+ + HCr_2O_7^-; \qquad K_4 = \sim 10^6$$

$$HCr_2O_7^- \rightleftharpoons H^+ + Cr_2O_7^{-2} \; ; \qquad K_5 = 0{\cdot}85$$

In dilute solutions of hydrochloric acid, chlorochromic acid also appears.[21–22] The main factors influencing the extraction of inorganic compounds with strongly basic extractants are the strength of the acid and the size, charge and hydrophobic properties of its anion.[22] In the systems studied which contain large concentrations of chromium and hydrogen ions, the extracted anions are $Cr_2O_7^{2-}$, $HCr_2O_7^-$ and in hydrochloric acid media CrO_3Cl^-.

In the low concentration range of chromium(VI), the extraction equilibrium curves (Fig. 17) straight lines of slope ~ 1 which indicates that when excess extractant is present, the degree of polymerisation of the extracted complexes is the same as in the aqueous phase.[23]

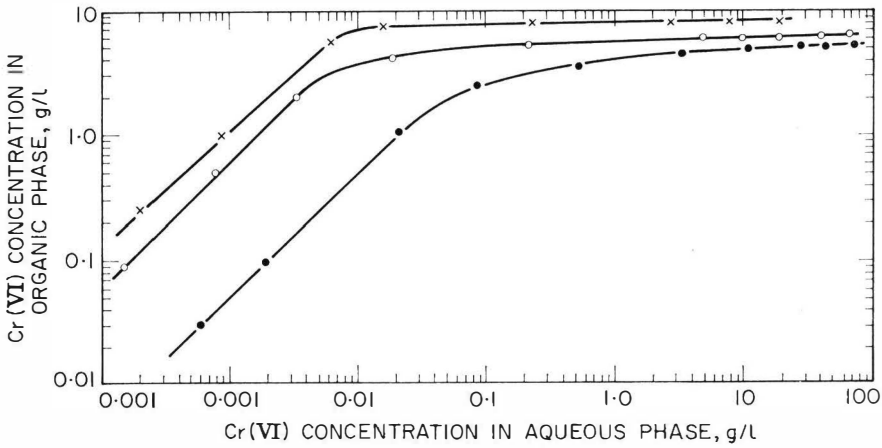

FIG. 17. *Extraction equilibrium curves in the systems* $Na_2Cr_2O_7 + HY + H_2O - TOA + HDBP + C_6H_6$

× $Na_2Cr_2O_7$ + 2·0 M-H_2SO_4–0·10 M-TOA + 0·10 M-HDBP;
○ $Na_2Cr_2O_7$ + 0·25 M-HNO_3–0·10 M-TOA + 0·20 M-HDBP;
● $Na_2Cr_2O_7$ + 3·0 M-HNO_3–0·05 M-TOA + 0·10 M-HDBP

From Figs 11–16, it follows that the composition of the extracted chromium(VI) compounds depends on the concentration of the mineral acid. The values of the slopes of the plots of log E_a^o vs. log $[R_3NH^+]$ at constant concentrations of alkylphosphoric acids, and plots of log E_a^o vs. log [HX] at a constant concentration of tri-n-octylamine are presented in Table III.

TABLE III

Values of slopes

Aqueous mineral acid and concentration, M	Slopes [HDBP] variable	[TOA] variable
H_2SO_4, 0·90	1·15	—
H_2SO_4, 1·80	1·11	—
H_2SO_4, 2·70	1·07	—
H_2SO_4, 1·0+4·5 M-$(NH_4)_2SO_4$	—	1·48
H_2SO_4, 3·0+3·0 M-$(NH_4)_2SO_4$	—	1·07
HNO_3, 0·50	1·00	—
HNO_3, 1·0	1·00	—
HNO_3, 1·0+3·0 M-$NaNO_3$	—	1·00
HNO_3, 3·0	—	1·00
$HClO_4$, 0·05	1·00	—
$HClO_4$, 0·20	1·00	—
$HClO_4$, 0·50	—	1·11
$HClO_4$, 1·0	—	1·00
$HClO_4$, 2·0	1·04	—

The values of the slopes imply that the extracted compounds contain one or two molecules of the amine and one molecule of the acid. These data are confirmed by results obtained by the maximum loading method (Table II). The molar ratio of chromium to tri-n-octylamine depends on the concentration of the mineral acid in the aqeuous phase and varies from 1·01 to 2·05. From the extraction mechanism with amines,[12,16,24] the molar ratio Cr: TOA=1·0 corresponds to the extraction of $Cr_2O_7^{2-}$ as $(R_3NH)_2Cr_2O_7$, and the molar ratio Cr; TOA=2·0 corresponds to the extraction of $HCr_2O_7^-$ as $R_3NH_2Cr_2O_7$. It follows from the data in Table II the chromium concentration in saturated organic phases is independent of the concentration of alkylphosphoric acids.

As expected the alkylphosphoric acids do not extract chromium(VI) which implies that the alkylphosphoric acids interact only with $(R_3NH)_2Cr_2O_7$ and $R_3NH_2Cr_2O_7$.

The individual compounds of chromium(VI) may be identified from their absorption spectra in the ultra-violet region.[18–20] The absorption spectra of chromium(VI) in the organic phases obtained by extraction from H_2SO_4, H_3PO_4, $HClO_4$ and HNO_3 media are analogous to the chromium(VI) spectra in the aqueous phases, respectively. In all cases absorption bands at 280 and 354 nm were observed. The ratio of the molar extinction coefficients for these wavelengths is ~2, corresponding to the $Cr_2O_7^{2-}$ complex.

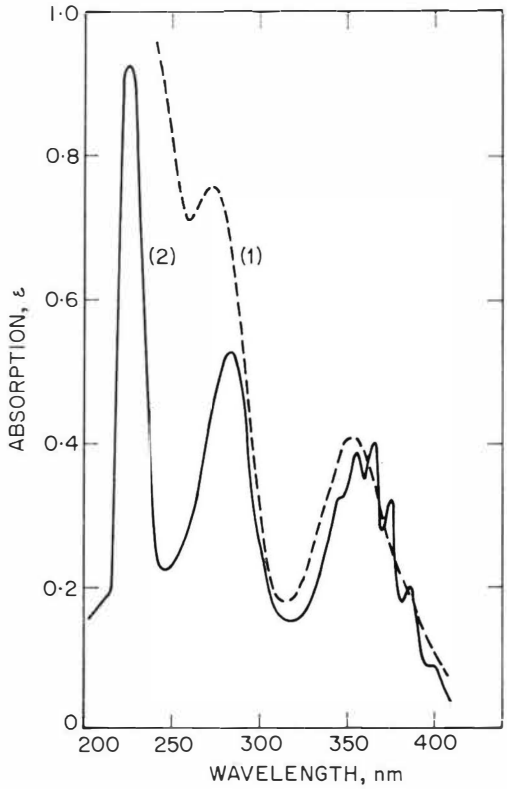

FIG. 18. *Absorption spectra of chromium(VI) in the organic phases (0·05M-TOA + 0·05M-HDBP + n-heptane) obtained by extraction of chromium*

Extraction from: (1) 0·025, 1·0 and 1·80 M-H_3PO_4, HNO_3, $HClO_4$ and H_2SO_4 solutions; (2) 2·0 B-HCl solution. Chromium concentration 0·002 M

Di- and mono-phosphoric acids are dimerised and polymerised, respectively in benzene, carbon tetrachloride and in other diluents.[25,26] It may be assumed that in the present system, dimers and polymers are also formed. Thus the extraction mechanism of chromium(VI) from solutions of sulphuric, orthophosphoric, nitric and perchloric acids with a mixture of tri-n-octylamine and alkylphosphoric acids may be represented as follows:

$$Cr_2O_{7(aq)}^{2-} + 2\,R_3NH_{(org)}^{+} + (HX)_{n(org)} \rightleftharpoons (R_3NH)_2Cr_2O_7(HX)_{n(org)}$$

$$HCr_2O_{7(aq)}^{-} + R_3NH_{(org)}^{+} + (HX)_{n(org)} \rightleftharpoons R_3NH_2Cr_2O_7.(HX)_{n(org)}$$

Tri-n-butyl phosphate, in contrast to acidic alkylphosphoric esters, does not influence the extraction of chromium(VI) with tri-n-octylamine (Fig. 6). Taking into account the differences in the structure of neutral and acidic alkylphosphoric esters, it may be assumed that the alkylphosphoric acids in the compounds $(R_3NH)_2Cr_2O_7.(HX)_n$ and $R_3NH_2Cr_2O_7.(HX)_n$ are bound by hydrogen bonds. These compounds, owing to the low dielectric constants of the organic phase, probably exist as ion pairs. Their structure may be written as:

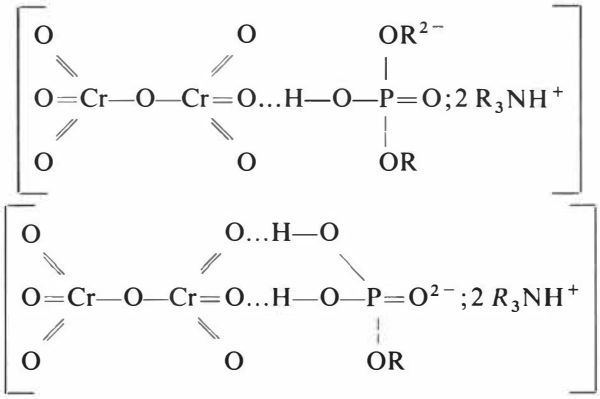

The formation of the strongly organophilic ion pairs explains the synergic effect in comparison to the extraction of chromium(VI) with tri-n-octylamine alone where the chromium is extracted as $[2\ R_3NH^+;Cr_2O_7^{2-}]$ and $[R_3NH^+;HCr_2O_7^-]$.

From previously published data,[21] it is known that chromium(VI) is extracted from hydrochloric acid solutions of concentration $>0\cdot5$M with tri-n-octylamine in benzene as $[R_3NH^+;CrO_3Cl^-]$. The absorption spectra of chromium(VI) in the organic phases obtained by extracting chromium from $1\cdot0$ and $2\cdot0$M-HCl with TOA+HX (Fig. 18) are the same as those of $[R_3NH^+;CrO_3Cl^-]$ which indicates that in this case the same compound is extracted. This conclusion is confirmed by the chemical analysis of the saturation organic phases obtained from $1\cdot0$ and $2\cdot0$M-HCl (Table II). The absence of a synergic effect in the extraction of chromium(VI) from hydrochloric acid solutions of concentration $>0\cdot5$M confirms the hypothesis that the alkylphosphoric acids are bonded by hydrogen bonds in the compounds $(R_3NH)_2Cr_2O_7.(HX)_n$ and $R_3NH_2Cr_2O_7.(HX)_n$. The presence of the strongly electronegative chlorine in chlorochromic acid decreases the basicity of the oxygen atoms, and, consequently prevents the formation of hydrogen bonds with the alkylphosphoric acids.

The synergic effect in the extraction of chromium(VI) from HCl solutions of concentration $<0\cdot5$M is caused by the presence of the compounds $(R_3NH)_2Cr_2O_7.(HX)_n$ and $R_3NH_2Cr_2O_7.(HX)_n$ in the organic phase as well as R_3NHCrO_3Cl.

It seems that a clearer elucidation of the bonding mechanism of alkylphosphoric acids in these compounds will be possible from studies of infra-red spectra.

These experiments are currently in progress and it is hoped to present the results at this Conference.

From the results obtained, the extraction mechanism of chromium(VI) with mixtures of tri-n-octylamine and alkylphosphoric acids is the same over the whole concentration range of mineral acids, independently of whether the synergic or antagonistic effects appear or not. The appearance of one of the effects depends upon the interaction of tri-n-octylamine with alkylphosphoric acids.

The reaction:

$$R_3N+HX \rightleftharpoons R_3N...HX \qquad (1)$$

causes a decrease in the thermodynamic activity of tri-n-octylamine, which is a condition for the appearance of the antagonistic effect. This factor predominates in the extraction of chromium(VI) from solutions with a low concentration of mineral acid. An increase in the concentration of the mineral acid causes displacement of the alkylphosphoric acid anion in the compound R_3NHX by the anion of the mineral acid:

$$R_3NHX + H^+ + Y^- \rightleftharpoons R_3NHY + HX \quad . \quad . \quad . \quad . \quad . \quad (2)$$

This reaction causes a decrease in the concentration of R_3NHX, and hence a decrease in the antagonistic effect. The appearance of the synergic effect in the systems studied is caused by: (i) decreasing interaction between tri-n-octylamine and alkylphosphoric acids; and (ii) differences in the composition of the extracted chromium(VI) compounds with mixtures of TOA and HX compared with those of the compounds extracted with tri-n-octylamine alone.

These considerations account for the non-occurrence of the synergic effect during extraction of chromium(VI) from solutions of low sulphuric acid concentration (0·025M) and high ammonium sulphate concentration, though the total sulphate ion concentration is within the concentration range where the effect occurs.

The curves representing the relationship between the extraction coefficient of chromium and the concentration of alkylphosphoric acids (Figs 1–5 and 7–10) display a maximum. The decrease in the extraction coefficients at high concentrations of alkylphosphoric acid is caused by the displacement of the reaction (2) equilibrium to the left.

From the papers of Coleman *et al.*,[24,27] it is known that the equilibrium constant of Reaction (2) decreases in the order $HClO_4 > NHO_3 > HCl > H_2SO_4 > > H_3PO_4$. Thus the magnitude of the antagonistic effect should be inversely proportional to the value of the equilibrium constant of this reaction. Indeed, the highest antagonistic effect was found with orthophosphoric acid, when the effect occurred over the whole concentration range studied. With sulphuric and hydrochloric acids, the synergic effect occurred in addition to the antagonistic effect. With nitric and perchloric acids, only the synergic effect was observed.

References

1 Deptuła, C., & Minc, S., *Nukleonika*, 1965, **10,** 421
2 Deptuła, C., *J. inorg. nucl. Chem.*, 1967, **29,** 1097
3 Deptuła, C., & Minc, S., *J. inorg. nucl. Chem.*, 1967, **29,** 159
4 Deptuła, C., *J. inorg. nucl. Chem.*, 1970, **32,** 227
5 Kumler, W. D., & Eiler, I. I., *J. Am. chem. Soc.*, 1943, **65,** 2365
6 Deptuła, C., & Minc, S., *Nukleonika*, 1961, **6,** 197
7 Deptuła, C., & Adamski, T., 'Possibility of application of chromate extraction with tri-n-octylamine solutions to chromium metallurgy', Inst. nucl. Res. Rep. No. 1—Ch-IV-137, Warsaw, 1961
8 Crouse, D. J., *Rep. Congr. atom. Energy Commn U.S.*, 1955, ORNL-1959
9 D. F. Peppard *et al.*, *J. inorg. nucl. Chem.*, 1957, **5,** 141
10 Udy, M. J., 'Chromium', 1956 (New York: Reinhold)
11 Dobrowolski, J., *Nukleonika*, 1960, **5,** 583
12 Deptuła, C., *J. inorg. nucl. Chem.*, 1968, **30,** 1309
13 Ishimori, T., *J. atom. Energy Soc. Japan*, 1963, **5** (2), 89
14 Irving, H., & Edgington, D. N., *J. inorg. nucl. Chem.* 1961, **21,** 158, 169
15 Healey, T. V., *J. inorg. nucl. Chem.*, 1961, **19,** 314
16 Deptuła, C., & Minc. S., *Nukleonika*, 1965, **10,** 355
17 Bertocci, U., & Rolandi, G. *J. inorg. nucl. Chem.*, 1961, **23,** 323
18 Davis, W. G., & Prue, J. E., *Trans. Faraday Soc.*, 1955, **51** (1), 45
19 Neuss, J. D., & Rieman, W., *J. Am. chem. Soc.*, 1934, **56,** 2238
20 Tong, J. Y., & King, E. L., *J. Am. chem. Soc.*, 1955, **51,** 1045
21 Deptuła, C., *Roczn. Chem.*, 1968, **42,** 725
22 Tuck, D. G., & Walters, R. N., *J. chem. Soc.*, 1963, p. 1111
23 Diamond, K. M., *J. phys. Chem., Ithaca*, 1957, **61,** 69; 75
24 Coleman, C. F. *et al.*, *Ind. Engng Chem.*, 1958, **50,** 1756
25 Kosolopoff, S. M., & Powell, J. S., *J. chem. Soc.*, 1950, p. 3535
26 Peppard, D. P. *et al.*, *J. inorg. nucl. Chem.*, 1960, **12,** 336
27 Coleman, C. F. *et al.*, *Proc. 2nd int. Conf. peaceful Uses atom. Energy, Geneva*, 1958, p. 510

Solvent extraction of gallium and zinc and their separation by aminophosphonic acids

by M. J. Herak and V. Jagodić
Rudjer Bošković Institute, Zagreb, Croatia, Yugoslavia

Solvent extraction of gallium and zinc with mono-octyl esters of α-anilinobenzylphosphonic acid and of α-(2-carboxyanilino)benzylphosphonic acid was studied. The influence of hydrochloric acid concentration and various solvents was investigated in order to establish the best conditions for separation of the metals. Over 98% of the gallium was extracted into the organic phase from diluted hydrochloric acid solutions containing up to 10^4 times more zinc, and was accompanied by only ~3% of the zinc present. The latter could easily be washed out from the organic phase with diluted acid, without affecting the extracted gallium. Radionuclides ^{72}Ga and ^{65}Zn were used in the experiments. The purity of the separated gallium was confirmed by measuring its half-life of decay.

Introduction

GALLIUM IS ONE of the elements that is highly dispersed in nature. Gallium very closely resembles aluminium in its chemical and physical properties and hence many bauxites contain traces of it. Because of the affinity of gallium with sulphur some sphalerites also contain gallium, sometimes from 0·001 to 0·1%.

Gallium has several radionuclides. Of particular interest is 68 h ^{67}Ga which is produced from zinc in a cyclotron by the nuclear reaction ^{66}Zn$(d,n)^{67}$ Ga Gallium obtained in this way contains a large amount of zinc. This paper deals with the extraction of gallium from an aqueous hydrochloric acid medium and its separation from zinc.

Among a variety of techniques that have been used for the quantitative separation of gallium from various other elements, solvent extraction has received the greatest attention. The most common systems for the extraction of gallium involve hydrochloric acid solution and oxygen-containing organic solvents.[1] Long-chain alkyl amines and quaternary ammonium salts have also been used to extract indium and gallium from an aqueous chloride medium.[2] Although a variety of different reagents[1] have been used to extract gallium, it is surprising that only a few phosphorus-based extractants have been employed for this purpose. Thus, dibutyl phosphate was used for the extraction and separation of gallium from indium[3] and tri-n-butyl phosphate for gallium.[4,5] In this study, mono-octyl ester α-anilinobenzylphosphonic acid (MOABP) and mono-octyl ester α-(2-carboxyanilino)benzylphosphonic acid (MOCABP) have been used. These reagents have the following structure:

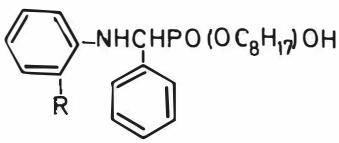

in MOABP : R = H
in MOCABP : R = COOH

Petroleum ether, carbon tetrachloride or chloroform were used as solvents for MOABP and chloroform for MOCABP. As far as is known this is the first application of aminophosphonic acids for the extraction of gallium and zinc.

Experimental

Chemicals

The synthesis of MOABP and MOCABP has been described earlier.[6,7] Radionuclides with high specific activity, ^{72}Ga (Institut 'Jozef Stefan' Ljubljana, Yugoslavia) and ^{65}Zn (Institut 'Boris Kidrič,' Vinča, Yugoslavia) in the chloride form were used. When it was necessary, they were added to inactive solutions of the metal salts. All the chemicals used were of high purity.

Determination of distribution ratios

Two equal volumes (usually 3 ml each) of the organic and aqueous solutions were shaken for 15 min, although equilibrium is attained in several minutes. The phases were separated and an aliquot (1 ml) of each phase was counted on a γ-scintillation counter. The distribution ratio, D, for a given radionuclide, was the ratio of the count rates of samples of the organic and aqueous phases. When both gallium and zinc were present together in one system then two parallel series of experiments were carried out and each of the systems was marked with the radionuclide of the other metal.

Preparation of zinc octyl anilinobenzylphosphonate complex

The zinc complex was prepared by precipitation from an aqueous solution of a metal salt with sodium octyl anilinobenzylphosphonate. Thus, the solution of 1·08 g (0·005 mole) of zinc acetate dihydrate in water was added dropwise to the warm and stirred solution of 5·95 g (0·015 mole) sodium salt of the reagent in 50 ml water. Immediately, a white precipitate formed that was filtered off, washed with warm water and ethanol, dried and analysed. Found: Zn 7·67 ($C_{42}H_{58}N_2O_6P_2Zn$ requires Zn 8·03%).

Extraction of gallium and zinc

In Fig. 1 the extraction of gallium and zinc by MOABP or MOCABP is shown as a function of hydrochloric acid concentration. It is seen that gallium is extracted from more acidic solutions than zinc. Extraction of both metals depends on the type of solvent. For a given acidity it decreases in the order petroleum ether > carbon tetrachloride > chloroform. Extraction of gallium by MOCABP in chloroform is better than with MOABP in chloroform, but not so good as with MOABP dissolved in carbon tetrachloride or petroleum ether. On the other hand, zinc is most poorly extracted by MOCABP. Although the difference in the extraction of gallium and zinc by MOCABP is the largest, this reagent is not convenient for their separation because it forms a third phase when an excess of zinc is present. Both metals can be quantitatively re-extracted into the aqueous phase by being shaken for 2 min with 1M-HCl.

Extraction of zinc as a function of its concentration

For the separation of gallium from an excess of zinc it was important to know how the extraction of the latter depends upon the increase of its own concentration in the aqueous phase. Aqueous 0·05M hydrochloric acid was chosen because at this acidity the extraction of gallium by a 5×10^{-3}M solution of MOABP in petroleum ether is the best and that of zinc the poorest. The results in Table I show that the total amount of zinc in the organic phase increases somewhat with increase in its concentration in the aqueous phase, although the percentage of zinc extracted decreases.

Extraction of gallium from the solutions containing various amounts of zinc

In Table II the extraction of gallium from the solutions containing zinc in excess is presented. Over 96% of the gallium is extracted as long as the

TABLE I

Extraction of zinc from 0·05M hydrochloric acid with 5×10^{-3}M MOABP in petroleum ether

$ZnCl_2$ concn. in aqueous phase, M	Zn extracted, %
1×10^{-6}	5·1
1×10^{-6}	5·9
1×10^{-5}	3·3
5×10^{-3}	3·9
1×10^{-2}	3·0
5×10^{-2}	1·4
1×10^{-1}	0·8

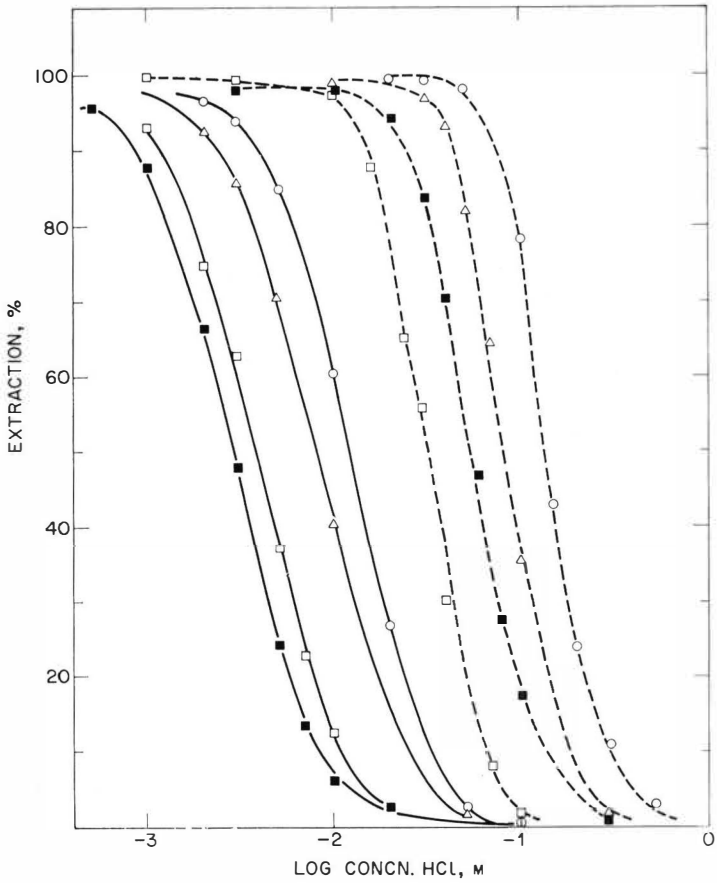

FIG. 1. *Extraction dependence of gallium(III)* (1×10^{-5}M) *and zinc(II)* (1×10^{-5}M) *on hydrochloric acid concentration*

Organic phase MOABP (5×10^{-3}M) dissolved in (○) petroleum ether, (△) carbon tetrachloride, (□) chloroform, and MOCABP (5×10^{-3}M) dissolved in (■) chloroform ——— Zn; — — — Ga

concentration of zinc does not exceed twice that of the reagent. Further increase in zinc concentration diminishes the percentage of gallium extracted, probably because the consumption of MOABP decreases the reagent available to react with gallium. It is seen in Table I that from an initial 5×10^{-2}M-$ZnCl_2$ solution 1·4% of zinc is extracted into the organic phase. Since approximately 3 moles of MOABP are bound to one zinc atom (Fig. 2), $\sim 2 \times 10^{-3}$ moles of MOABP (from the initial 5×10^{-3} moles) only are used to extract zinc. Therefore, a concentration of MOABP higher than 5×10^{-3}M should be used in order to enrich the content of gallium from samples with higher proportions of zinc to gallium than those given in Table II.

TABLE II

Extraction of gallium in the presence of zinc

Aqueous phase 0·05M hydrochloric acid.
Organic phase 5×10^{-3}M MOABP in petroleum ether.

$GaCl_3$ concn. in aqueous phase, M	$ZnCl_2$ concn. in aqueous phase, M	Ga extracted, %
1×10^{-6}	5×10^{-3}	97·2
1×10^{-6}	1×10^{-2}	96·5
1×10^{-6}	5×10^{-2}	78·5
1×10^{-6}	1×10^{-1}	61·2
1×10^{-5}	1×10^{-2}	96·0
1×10^{-5}	2×10^{-2}	84·5

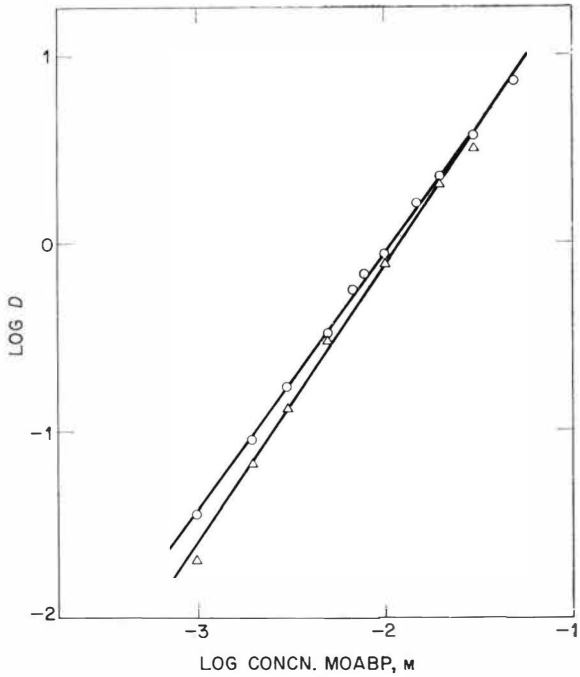

FIG. 2. *Extractant dependence of Zn(II)* (1×10^{-5}M) *into MOABP*

MOABP dissolved in (○) petroleum ether and (△) carbon tetrachloride, from (○) 0·02M and (△) 0·015M HCl
Slope: ○, 1·4; △, 1·5

Since the extraction of zinc increases with increasing MOABP concentration (Fig. 2) it would also be necessary to increase the concentration of hydrochloric acid sufficiently to suppress the extraction of zinc.

Separation of gallium from zinc

A solution of MOABP in petroleum ether was found to be the most suitable for the separation of gallium from zinc. The extraction of gallium and zinc from 0·05M hydrochloric acid solution is given in Table III.

TABLE III

Extraction of gallium and zinc from a mixture of the two

Aqueous phase 0·05M-HCl.
Organic phase 5×10^{-3}M MOABP dissolved in petroleum ether

Initial $GaCl_3$ concn., M	Initial $ZnCl_2$ concn., M	D_{Ga}	D_{Zn}	% Extracted		Separation factor, $\beta = D_{Ga}/D_{Zn}$
				Ga	Zn	
1×10^{-6}	5×10^{-3}	39·7	0·042	97·6	4·1	$0{\cdot}9 \times 10^3$
1×10^{-6}	1×10^{-2}	31·6	0·031	97·0	3·0	$1{\cdot}0 \times 10^3$

About 97% of gallium is extracted and is accompanied by 3 to 4% of zinc. In order to decrease the amount of zinc extracted the organic phase was washed with 0·05B hydrochloric acid. After a single washing, over 96% of the extracted gallium and less than 0·2% of the zinc remained in the organic phase. Two or three successive washings would further diminish the zinc content without much affecting the extracted gallium. Following this procedure ^{72}Ga was separated from ^{65}Zn and the half-life of gallium decay was found to agree with the theoretical value (Fig. 3). Since the half-life of gallium is 14·2 h and that of zinc 245 days, even a small amount of radioactive zinc, if present as an impurity, should be detected by this method.

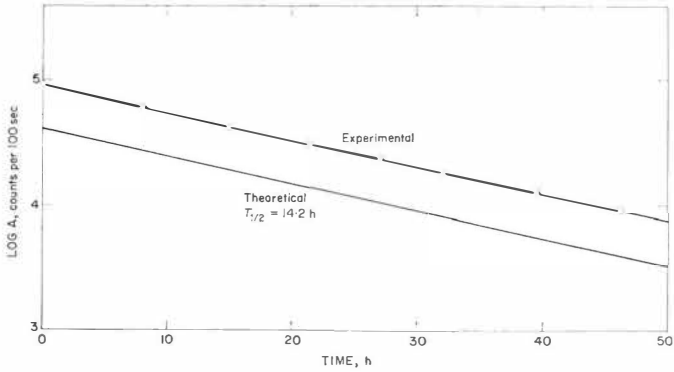

FIG. 3. *Experimental decay curve for ^{72}Ga separated from ^{65}Zn*

Extractable complexes of gallium

All the attempts to establish the dependency of distribution ratio, *D*, for gallium upon the MOABP concentration in the organic phase have failed. A linear relationship was not obtained with any of the solvents used. As yet, there is no explanation for this phenomenon. Additional experiments have only proved that gallium chloride is not extracted into the organic solvents in the absence of MOABP under the circumstances. However, by using MOCABP a 1·5 power dependence of *D* for gallium upon the reagent concentration was found (Fig. 4). With both MOABP and MOCABP it was found that the gallium distribution ratio depends inversely upon the third power of the hydrogen ion concentration in the aqueous phase (Fig. 5). These results indicate that three protons are released during the formation of an extractable

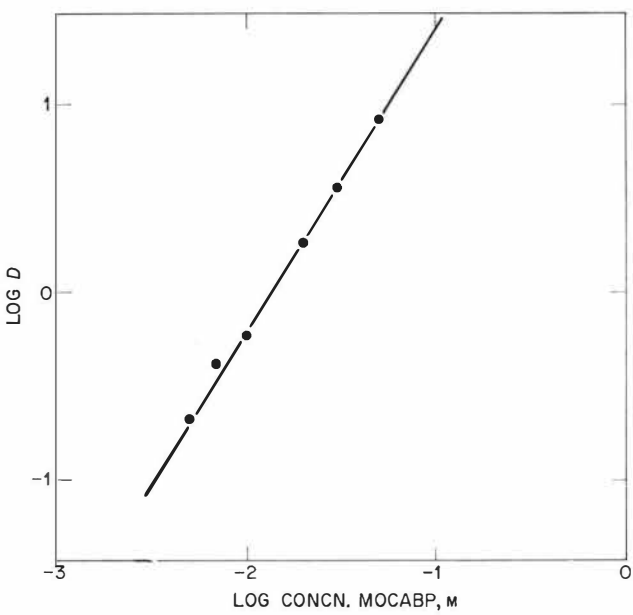

FIG. 4. *Extractant dependence of Ga(III)* (1 × 10^{-5}M) *into MOCABP dissolved in chloroform, from* 0·1M-*HCl*

Slope: 1·5

complex. The extraction mechanism with MOCABP (represented in the equations below as H_2X) is represented as:

$$Ga^{3+} + 1 \cdot 5\,(H_2X)_2 \rightleftharpoons Ga(HX)_3 + 3H^+ \quad . \quad . \quad . \quad . \quad . \quad (1)$$

Extractable complexes of zinc

In Figs 2 and 6 the slopes of plots of log D for zinc against the log MOABP concentration were found to vary with the solvent used. Values were 1·4 for petroleum ether, 1·5 for CCl_4 and 1·9 for chloroform. For MOCABP dissolved in chloroform the same 1·9 power extractant dependence has been found (Fig. 6). From Fig. 7 it is seen that D for zinc depends inversely upon the second power of the hydrogen ion concentration in the aqueous solution for both MOABP and MOCABP for all three solvents used.

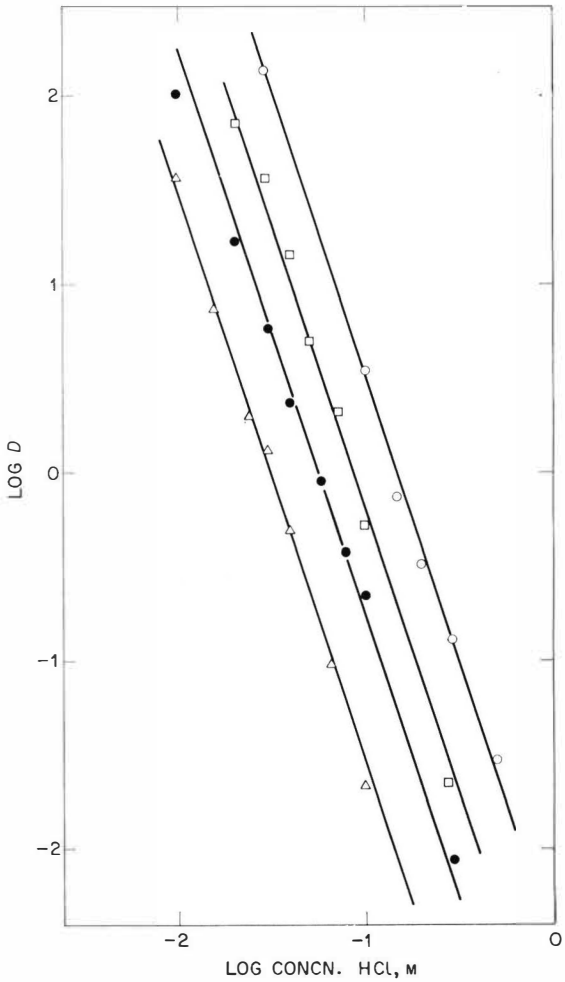

FIG. 5. *Hydrogen ion dependence of the extraction of Ga(III)* (1×10^{-5}M) *from aqueous HCl solution, into MOABP and MOCABP*

MOABP (5×10^{-3}M) dissolved in (○) petroleum ether, (□) carbon tetrachloride, (△) chloroform, and MOCABP (5×10^{-3}M) dissolved in (●) chloroform
Slope: −3·0

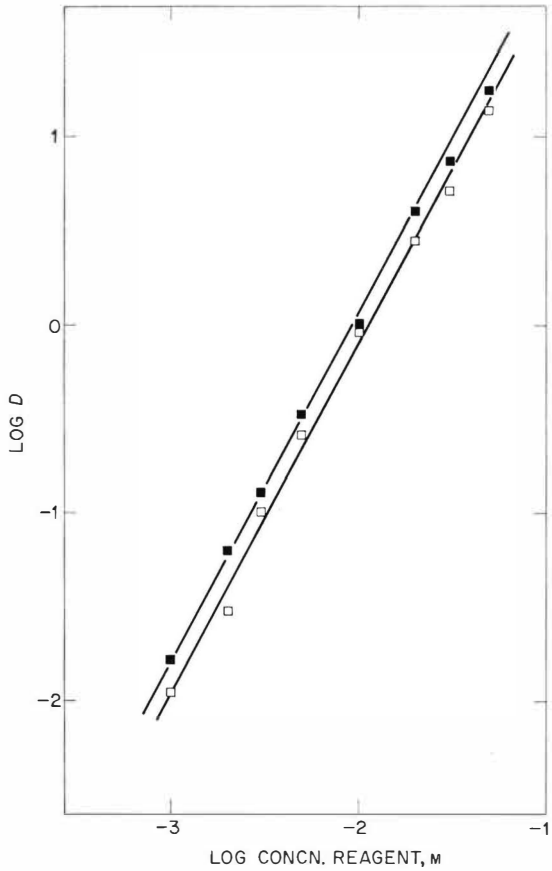

FIG. 6. *Extractant dependence of Zn(II)* (1×10^{-5}M) *into MOABP or MOCABP dissolved in chloroform, from aqueous HCl solution*
□ MOABP, 0·007M-HCl; ■ MOCABP, 0·005M-HCl
Slope: 1·9

In accordance with these results, the extraction stoichiometries for zinc with MOABP (represented as HR) in CCl_4 and petroleum ether can be represented as:

$$Zn^{2+} + 1{\cdot}5\,(HR)_2 \rightleftharpoons ZnR(HR_2) + 2H^+ \quad (2)$$

Similarly, the extraction with MOABP and MOCABP in $CHCl_3$ is represented as:

$$Zn^{2+} + 2(HR)_2 \rightleftharpoons Zn(HR_2)_2 + 2H^+ \quad (3)$$

$$Zn^{2+} + 2(H_2X)_2 \rightleftharpoons Zn(H_3X_2)_2 + 2H^+ \quad (4)$$

From aqueous solutions of zinc acetate and the sodium salt of MOABP, a white precipitate of the formula $[C_6H_5NHCH(C_6H_5)PO(C_8H_{17})O]_2Zn$ is fo med This compound is insoluble in organic solvents, but it dissolves in a chloroform solution of the reagent by giving the former complex (Equation 3). The same property was exhibited by manganese(II)[8] and europium(III)[9] octyl anilino-benzylphosphonate and uranium(IV) dioctylpyrophosphate.[10]

Acknowledgment

The authors are grateful to Mrs. E. Furić for technical assistance.

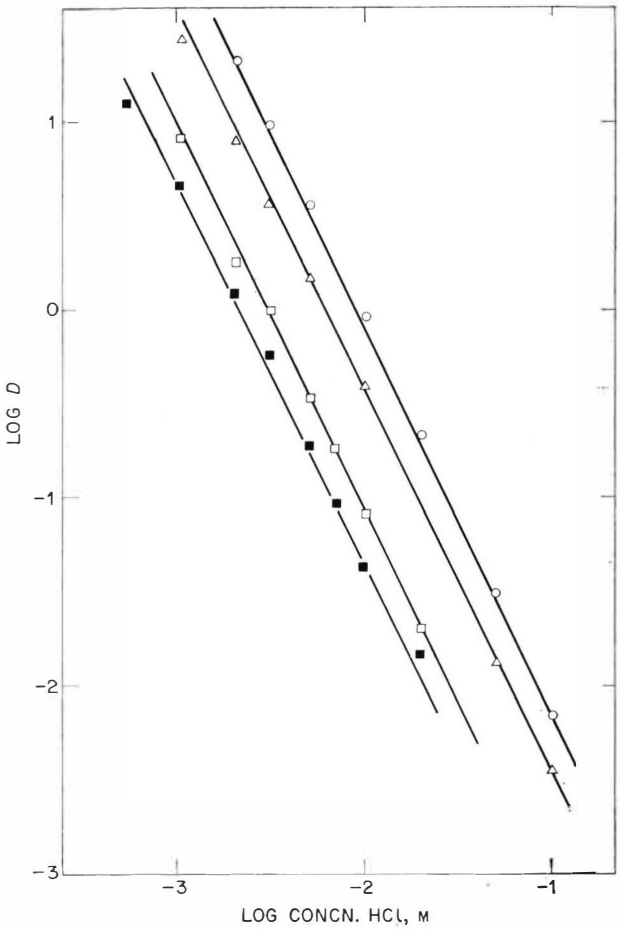

FIG. 7. *Hydrogen ion dependence of the extraction of Zn(II)* (1×10^{-5}M) *from aqueous HCl solution into MOABP and MOCABP*

MOABP (5×10^{-3}M) dissolved in (○) petroleum ether, (△) carbon tetrachloride, (□) chloroform, and MOCABP (5×10^{-3}M) dissolved in (■) chloroform
Slope: $-2 \cdot 0$

References

[1] Korkish, J., 'Modern methods for the separation of rarer metal ions', 1969, p. 311 (Oxford, London: Pergamon Press)
[2] Good, M. L., & Holland, F. F., jun., *J. inorg. nucl. Chem.*, 1964, **26,** 321
[3] Kiss, A., *Magy. kém. Foly.*, 1964, **70,** 197
[4] Morris, D. F. C., Andrews, B. D., & Short, E. L., *J. inorg. nucl. Chem.*, 1966, **28,** 2436
[5] Henning, K., & Specker, H., *Z. analyt. Chem.*, 1968, **24,** (1), 81
[6] Jagodić, V., *Chem. Ber.*, 1960, **93,** 2308
[7] Jagodić, V., & Herak, M. J., *J. inorg. Nucl. Chem.*, 1970, **32,** 1323
[8] Jagodić, V., & Grdenić, D., *J. inorg. nucl. Chem.*, 1964, **26,** 1103
[9] Herak, M. J., & Jagodić, V., *Croat. chem. Acta*, 1964, **36,** 51
[10] Grdenić, D., & Korpar, B., *J. inorg. nucl. Chem.*, 1959, **12,** 149

SESSION 4B

EXTRACTION EQUIPMENT

CHAIRMAN

Prof. J. D. Thornton

SECRETARIES

Dr. G. ten Brink

Ir. D. v.d. Meer

Droplet break-up mechanisms in a rotating disc contactor

by G. V. Jeffreys and C. J. Mumford

Department of Chemical Engineering, University of Aston in Birmingham, Gosta Green, Birmingham, U.K.

Droplet break-up mechanisms are investigated photographically in a 3-inch rotating disc contactor (RDC), (a) *with a non-wetted disc below* Re $\simeq 1 \cdot 75 \times 10^4$, *when discrete drops persist beneath the disc and* (b) *with a wetted disc, when dispersed phase coalesces into a layer beneath the disc and is redispersed from the periphery. Seven different systems are used covering a range of interfacial tension from 5 to 55·4 dynes cm*$^{-1}$. *For non-wetted discs, a criterion is discussed for droplet break-up due to dynamic pressure based on the stable drop size after Kolmogoroff, viz,*

$$r_{\text{s.d.}} \simeq \sqrt{2}\left[\frac{\sigma}{K_{\text{f}}.\rho}\right]^{3/5} \cdot \frac{L^{2/5}}{V^{6/5}}$$

V is computed from published data on velocity components in the vicinity of a rotating disc. Good agreement is found between this model and maximum observed drop sizes. The increased spread and decrease in stator impact break-up effects, associated with increasing column diameters, is discussed. For wetted discs, two regions are observed. (i) *Rim disintegration at Re* $< 1 \cdot 9 \times 10^4$, *when* d_m *is significantly greater than from a non-wetted disc and increases linearly with* $\frac{\sigma}{\Delta\rho.g}$. *Secondary drops are produced upon coalescence into the dispersed phase layer and following discrete drop detachment.* (ii) *Sheet and ligament disintegration with values of* d *predicted from published centrifugal disc atomisation equations, e.g.,*

$$d = \left[\frac{3\pi}{\sqrt{2}}\right]^{1/3} d_L \left[1 + \frac{3\mu}{(\rho_D.\sigma d_L)^{\frac{1}{2}}}\right]^{-1/6}$$

are consistently less than the measured values of d_m. *Reasons for this and the increasing disparity with increase in* $\frac{\sigma}{\Delta\rho.g}$ *are discussed.*

Practical potential is foreseen for a column with wetted discs for systems in which dispersed phase film coefficients control mass transfer.

Introduction

ROTARY AGITATED CONTACTORS, such as the Scheibel, Oldshue-Rushton and rotating disc columns, have a wide application in liquid–liquid extraction.[1] The most common design is the *RDC*, a column with equispaced stator rings which form a series of compartments each of which is agitated by a centrally located disc.[2] One phase is dispersed by the action of the rotating discs and countercurrent flow is assisted by gravity.

Numerous agitator designs have been proposed for the *RDC* including 60° arcs,[3] perforated discs,[4] a rotating cylinder[5] and alternate discs of different sizes.[6] In the conventional design, however, and in the assymetric *RDC*,[7] equisized flat rotor discs without protrusions are preferred. These discs create uniform shearing conditions and, hence, produce variation in drop sizes.

Since the droplet size is an important factor influencing both the mass transfer process and the volumetric capacity, systematic design should be made from the droplet analysis considerations. A design procedure based upon discrete drop data has been described by Misek[8] and the application to more recent models has been reviewed by Jeffreys.[9]

In general, the distribution of drop sizes produced in agitated systems results from an equilibrium between the competing effects of break-up and coalescence. Coalescence rates are related to interdroplet distances, i.e. hold-up, but vary with position in both agitated tanks and columns. Therefore, mean drop sizes can only be determined experimentally.[10,11] In addition, because mass transfer is

enhanced by coalescence and redispersion, discrete drop data cannot easily be applied. However, in work with a variety of organic liquids dispersed in water in a pilot scale *RDC* selection, it was found that, in the absence of mass transfer, interdrop coalescence was negligible until flowrates approached the floodpoint.[11] The absence of coalescence has also been considered by Davies[12] and by Misek.[13] Hence, in the absence of any special interfacial effects associated with mass transfer, the column appears to function as a discrete drop contacting device. The break-up mechanisms which determine the distribution of drop sizes therefore merit consideration.

Relationships involving experimentally determined exponents have been given[8,14] for the break-up of drops within a turbulent mixing region above $Re \simeq 6 \times 10^4$ and within a transitive mixing region down to $Re \simeq 10^4$. Operation at a lower mixing intensity, in a laminar region, is common particularly in applications involving a viscous continuous phase. In this region, according to Misek,[8] the vertical velocity of the drops is significant and drops mainly split by successive impacts on the stators and presumably rotors. By analogy with the break-up mechanismin packings, the drop diameter was assumed therefore to be determined by the ratio of buoyancy and surface forces. That is:

$$d_{12} = 0{\cdot}38 \left[\frac{\sigma}{\Delta\rho \cdot g} \right]^{0{\cdot}5} \qquad (1)$$

In this region the effect of mixing intensity is insignificant.[8]

Results of recent work indicate that the above conclusions require modification, under the following conditions:

(*a*) At rotor speeds approximating to the laminar range, when a layer of dispersed phase droplets persists beneath the rotor discs at all flowrates. Over the range of interfacial tensions studied, viz., 5–55·4 dynes cm^{-1}, with an aqueous continuous phase, this phenomenon occurs at $Re \simeq 1{\cdot}75 \times 10^4$ which is independent of hold-up as shown in Fig. 1. A similar result has been reported by Kung and Beckman.[15] The drops are discrete and the population changes continually by drops sliding to the periphery before being ejected. Their momentum is insufficient to cause impingement on the column wall and the turbulence existing in the bulk continuous phase is too small to cause shearing.

(*b*) When the dispersed phase 'wets' the disc, that is, it exhibits a contact angle of less than 90° with the disc material, droplets coalesce into a layer of dispersed phase beneath the rotor disc. The coalescence is independent of rotor speed. Redispersion occurs by streaming from the periphery as illustrated in Fig. 2.

Experimental work was performed in a 3-in diameter column section. High and normal speed cine, high speed still photography and the injection of organic soluble dye were used to study the droplet break-up. The equipment and techniques are described elsewhere.[11,16] A stationary aqueous continuous phase was employed; the dispersed phase consisted of toluene, trimethylpentane iso-amyl alcohol, ethyl acetate, isobutyl methyl ketone, amyl acetate or liquid paraffin.

Droplet break-up from a non-wetted disc in the laminar region

Break-up by impact on the stators or discs, whilst contributing to the overall spread in drop sizes produced, is not the predominant break-up mechanism. Furthermore, it has been shown, in a separate study using a flat plate suspended in a stationary aqueous phase, that over the range of drop sizes and interfacial tension encountered in this work direct impact does not cause droplet rupture. A simplified energy balance between the kinetic energy of a droplet at its terminal velocity and the cohesive and adhesive forces of the drop at an infinite non-wetted plate supports this conclusion.[17] It follows that impact rupture on a wetted plate is not possible. Smaller drops may however break-up by impact

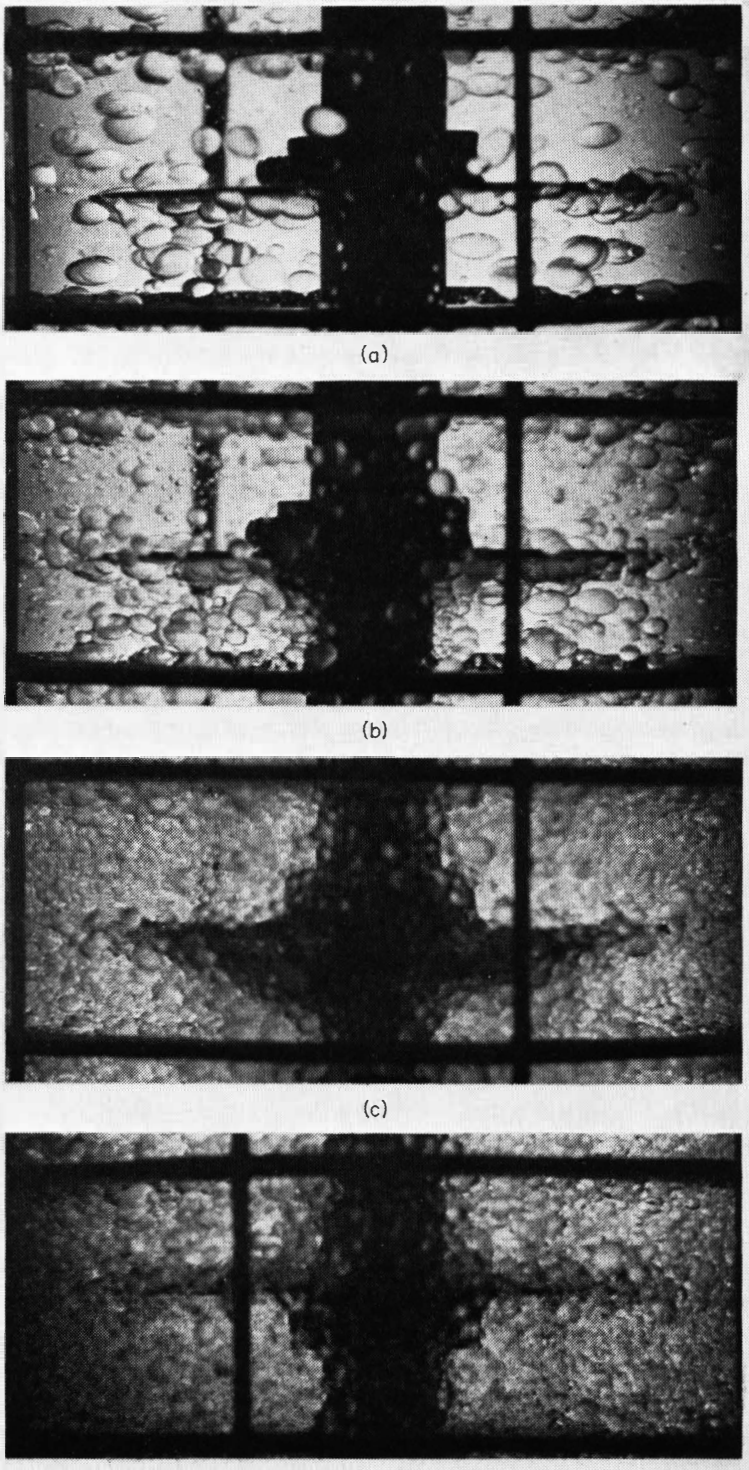

FIG. 1. *Persistence of droplets beneath a non-wetted disc at* Re $< 1 \cdot 75 \times 10^4$
MIKB–water; motor speeds (a) 400, (b) 500, (c) 600 and (d) 650 rpm.

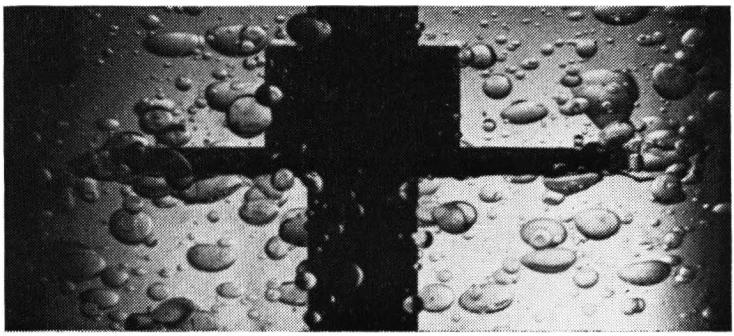

FIG. 2. *Drop formation from a wetted disc at* Re $< 1 \cdot 9 \times 10^4$
amyl acetate–water; rotor speed 500 rpm.

with the edges of the stators or discs as shown by Thornton.[18] Thus, only drops which impinge vertically within one drop diameter of the disc or stator peripheries or horizontally on the edge of a stator ring, would be expected to suffer break-up in an *RDC*. In any compartment the proportion of the former is of the order:

$$n \simeq \frac{4d\,(S+R)}{D^2} \simeq \frac{5 \cdot 4d}{D} \qquad (2)$$

in a practical column the proportion is inherently small and reduced to $3d/D$ if only stator impacts are effective.

In any liquid–liquid system, droplet rupture occurs when the difference in dynamic pressures at different points on the surface of a drop, which arises due to velocity variations within the continuous phase, exceeds the smallest value of surface force at any point. From the work of Kolmogoroff,[19] the difference in dynamic pressure exerted on opposite sides of a drop of radius r is,

$$\Delta P_1 = \frac{K_f \cdot \rho_c\,(V_1{}^2 - V_2{}^2)}{2} \qquad (3)$$

where K_f is a coefficient and V_1, V_2 are velocities of the continuous phase at distance $d = 2r$ apart. Large scale eddies that do not vary over the drops diameter will not produce deformation and break-up. Therefore only relatively small eddies need be considered. The change in eddy velocity over a length $d = 2r$ is

$$\Delta V_{2r} = (2r \cdot E)^{1/3} \qquad (4)$$

where $E = \Sigma/\rho$ is the energy dissipated per unit mass of liquid. Combining Equations (3) and (4)

$$\Delta P_1 = K_f\,\rho_c \left(\frac{2r\Sigma}{\rho}\right)^{2/3} \qquad (5)$$

This is balanced by the force due to surface tension

$$\Delta P_2 = \frac{\sigma}{d} = \frac{2\sigma}{r} \qquad (6)$$

Equating $\Delta\rho_1$ and $\Delta\rho_2$

$$K_f \cdot \rho_c \left[\frac{2r\Sigma}{\rho}\right]^{2/3} = \frac{2\sigma}{r} \qquad (7)$$

Since, however, $\Sigma = \rho(\Delta V)^3/L$ where L is a characteristic dimension of the turbulence, the radius of a stable drop is given by[19,20]

$$r_{s \cdot d \cdot} \simeq \sqrt{2} \cdot \left[\frac{\sigma}{K_f \cdot \rho}\right]^{3/5} \cdot \frac{L^{2/5}}{V^{6/5}} \qquad (8)$$

Coefficient K_f has a value of the order of 0·5 for the fragmentation of liquid drops falling in a gaseous medium;[20] this value will be used in subsequent calculations since the stable drop size is not a strong function of K_f.

If axial velocity effects are neglected, the difference in velocity across drops of diameter, (d), in the region beneath a disc results from the difference in flow velocities in horizontal planes Z and $Z + d$. Radial velocity at the disc, i.e. in plane $Z = 0$, is zero and its variation in any other horizontal plane from radius R^1 to $R^1 + d$ is small and therefore will be neglected. For the purposes of analysis, drops will be assumed to be spherical, whereas they are actually slightly elliptical with a ratio of axes of up to 1·3 to 1.

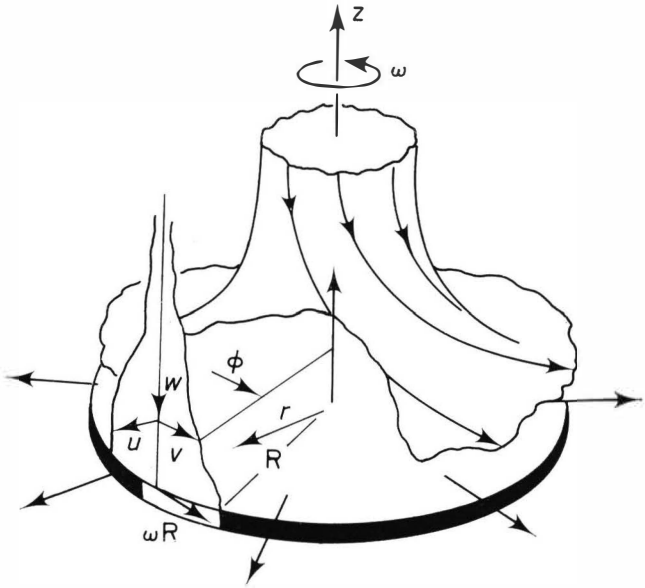

FIG. 3. *Flow in the neighbourhood of a rotating disc*

Bulk fluid at rest. Velocity components w-axial, u-radius, v-circumferential

The exact solution of the Navier–Stokes Equation for the flow around a flat disc rotating about an axis perpendicular to its plane in a fluid at rest has been given by Cochran.[21] The three dimensional flow field is shown in Fig. 3.[21,22] A velocity component (w) exists in the axial direction Z, u in the radial direction (r^1) and v in the circumferential direction (φ), when the uniform angular velocity of the disc is ω. By introducing a dimensionless distance from the disc surface, $\zeta = Z/\partial$, where ∂ is the thickness of the fluid layer carried by the disc, the velocity components are expressed as

$$u = r'\omega\, F(\zeta)$$
$$v = r'\omega\, G(\zeta)$$
$$\text{and } w = \sqrt{r'\omega}\, H(\zeta) \qquad (9)$$

The functions of F, G and H, calculated by a method of numerical integration, have been given by Cochran.[21] The axial velocity is small, of the order of $\sqrt{r'\omega}$, and as mentioned earlier, can be neglected. The axial velocity is enhanced

uniformly by the relative terminal velocity but this is not relevant to the break-up mechanism.

By means of Equation (9) and Cochran's data, the value of the resultant velocity difference across a drop can be found for any location beneath the disc. Hence by substitution in Equation (8) the stable drop size can be estimated. If the diameter of a drop (d) exceeds the stable size ($d_{s.d.}$) then provided the drop is present in the flow for sufficient time deformation and break-up will occur.

Application of this theory is complicated since the resultant velocities on either side of a drop will not be in the same direction. However, in the material range the resultants are largely tangential so that as a first approximation this will be neglected. The derivation strictly applies to a disc of infinite extent,[21] i.e. $d \ll R$. In this work drops in the range 0·2 to 0·7 cm are considered travelling vertically at a distance $r^1 = R^1$, the effective radius from the disc centre (i) at the disc underside and (ii) one drop diameter away from the disc. The resultant

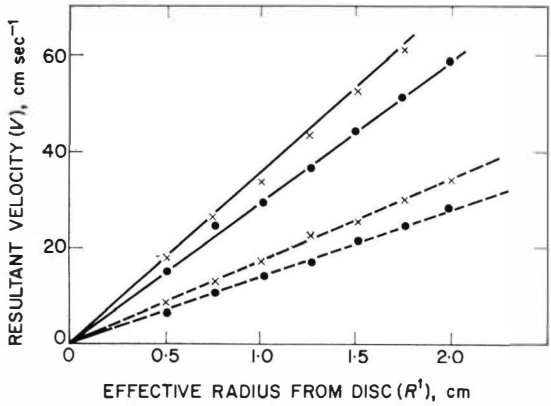

FIG. 4. *Resultant differences in velocity across droplets*

● 500 rpm; × 600 rpm
— $Z = 0$, $Z = d$; - - - - - $Z = d$, $Z = 2d$

velocities in three planes, viz., $Z = 0$, $Z = d$ and $Z = 2d$ are calculated for two rotor speeds, 500 r.p.m. and 600 r.p.m., at which the drop formation beneath the discs has well established. The calculated resultant velocities across drops are plotted in Fig. 4. Stable drop diameters from Equation (8) are plotted for drops on the disc underside in Figs 5 and 6. Curves of similar form are obtained for drops at one diameter from the discs but rupture at this distance is found to be remote.

This analysis provides a means of predicting the order of maximum drop size which can exist in an *RDC* in the laminar mixing region. Thus, for each system, minimum calculated stable drop sizes and maximum observed drop sizes, based on mean values from either determinations at two different inlet distributions, are plotted in Fig. 7. These show good agreement with the exception of trimethylpentane which has a high interfacial tension and low density. It is clearly established that drops below the minimum stable size do not break up, for example. Fig. 7 shows the effect of intact drops leaving the disc at low holdup. It follows that for any application there is a minimum speed below which the rotating disc does not affect the drop size distribution, The upper limit of can be determined by the inlet distributor[9] and the lower limit by an impact mechanism.[18]

The mean drop size cannot be predicted from fundamentals for several reasons, viz,

(a) Whilst for a given velocity (V) of a homogeneous isotropic flow, drops formed in it should be of a single size,[20] droplets are observed to produce four or more unequal sized daughter drops on rupture.

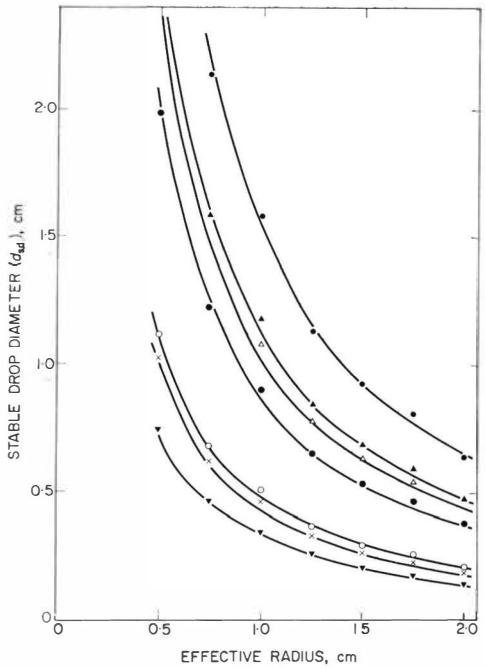

FIG. 5. *Calculated stable drop sizes at disc underside*

N 500 rpm
■ Trimethylpentane
▲ Liquid paraffin
△ Toluene
● Amyl acetate
○ MIBK
× Ethyl acetate
▼ Iso-amyl alcohol

(*b*) In small columns with large drops, the order of n in equation (2) is no longer insignificant.

(*c*) In columns with large discs, there is a wide variation of V in the unstable region and hence a spectrum of stable drop sizes.

Therefore, droplet size distribution is dependant to some extent on the disc diameter. Nevertheless, the proposed mechanism satisfactorily explains the smaller spread in drop sizes observed[11] for disc speeds below $Re \simeq 1 \cdot 75 \times 10.^4$ Mean drop sizes have been found to be largely independent of hold-up,[11] this is supported by the observation of Kung and Beckmann,[15] who showed that below a critical rotor speed the characteristic velocity (V_N) remained constant. Therefore, in practice the order of the hydraulic mean diameter can be estimated from the Equation (1) with the numerical coefficient having a value of $0 \cdot 55$.[16]

Droplet break-up from a dispersed phase wetted disc

An analogy may be drawn between drop formation from a disperse phase wetted disc and atomisation from centrifugal discs in spray driers, oil burners and humidifying equipment. In the latter, the liquid is discharged as a flat sheet and is dependant upon operating conditions; disintegration into drops follows one of the three regimes:[23]

(*a*) Rim disintegration. At very low ejection velocities the rims of the liquid sheet continually contract due to surface tension effects. Threads of liquid are pulled out during contraction to produce large droplets on break-up.

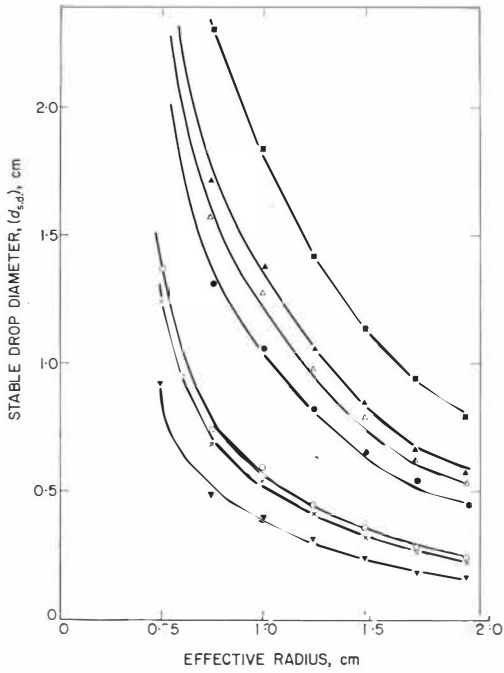

FIG. 6. *Calculated stable drop sizes at disc underside*
$N = 600$ rpm. Symbols as Fig. 5.

A theoretical equation derived for this case has the form:[24]

$$d_m = \left[\frac{0{\cdot}525 \quad 2\cdot\sigma}{N \quad R\cdot\rho}\right]^{0\cdot5} \qquad (10)$$

but small satellite drops are also formed.

(*b*) Perforated sheet disintegration. Over a narrow range of conditions the free edge disintegrates through a network of threads due to expanding perforations in an undisturbed sheet.

(*c*) Wavy sheet disintegration. Waves are produced on the sheet due to velocity differences between the two phases. At the critical wave amplitude the sheet disintegrates into unstable cylindrical ligaments which subsequently break up to form droplets.

The case (*c*) is said to be the most common regime. The ligaments are essentially jets with a predominantly longitudinal velocity. At low ejection velocities the jet is in laminar flow and varicose break-up occurs due to symmetrical swelling and contraction of increasing amplitude.

In the present case, in the vicinity of the disc, axial motion of the phases is of a lower order than that of the disperse phase in the plane of the disc. Hence break-up may be assumed to occur in a stationary continuous phase and is a special case of a liquid sheet having finite viscosity and which decreases in thickness as it moves away from the source. Dombrowski and Johns[25] have studied the growth of waves on a liquid sheet and extended this to consider the size of ligaments produced by wave disintegration of such a sheet attenuating according to $h = F.\theta^{-1}$ in a stationary gas. By a mass balance, the ligament diameter

$$d_L = \left[\frac{4h}{n''}\right]^{\frac{1}{2}} \qquad (11)$$

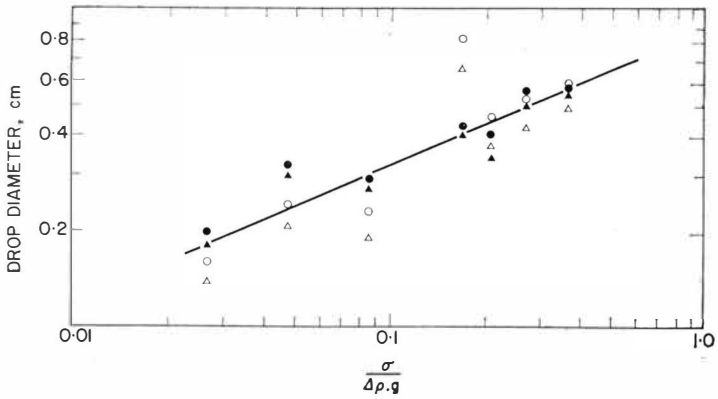

FIG. 7. *Measured* d_m *and calculated* $d_{s.d.}$

Non-wetted disc, laminar region
● measured diameter at 500 rpm.
○ calculated diameter at 500 rpm.
▲ measured diameter at 600 rpm.
△ calculated diameter at 600 rpm.

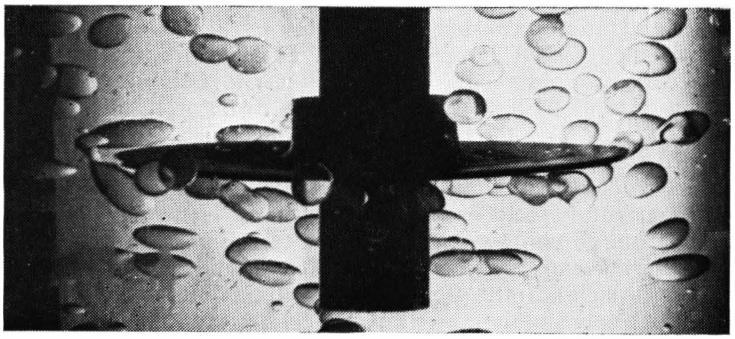

FIG. 8. *Intact droplets leaving the periphery of a non-wetted disc*

Amyl acetate–water

In order to evaluate this, the sheet thickness (h) at breakdown and the wave number (n'') were expressed in terms of the total growth of the wave (f). By means of a complex derivation and making use of the experimentally determined value, $f = 12$ at break-up independent of operating conditions, the following equation is obtained:[25]

$$d_L = 0{\cdot}9614 \cdot \left[\frac{B^2\sigma^2}{\rho_c \cdot \rho_D U^4}\right]^{\frac{1}{6}} \left[1 + 2{\cdot}6 \cdot 3\sqrt{\frac{B\rho^4 U^7}{72\rho_D^2 \sigma^5}}\right]^{\frac{1}{5}}. \quad . \quad . \quad (12)$$

Ligaments break up through symmetrical waves, whose properties, where surface tension forces predominate, have been analysed by Weber.[26] As the ligaments move transversely through the continuous phase it has no effect on the wavelength; the relevant equation is

$$n'' \cdot d_L = \left[\frac{1}{2} + \frac{3\mu}{2(\rho_D \cdot \sigma d_L)^{\frac{1}{2}}}\right]^{\frac{1}{2}} \quad . \quad . \quad . \quad . \quad . \quad . \quad . \quad (13)$$

The waves grow until they have an amplitude equal to the ligament radius and therefore one drop is produced per wavelength. Thus, by mass balance the relation between drop size and wave number is

$$d^3 = \frac{3\pi \cdot d_L{}^2}{n''} \quad . \quad . \quad . \quad . \quad . \quad . \quad . \quad . \quad . \quad (14)$$

In practice the application of Equation (14) to the prediction of drop sizes formed from cylindrical jets in immiscible liquids is not completely successful. Meister and Scheele[27] attribute this to the effects of velocity gradient in the jet which arises due to the continuous phase viscosity. However, the accuracy of the present analysis does not justify the use of their refinements. Therefore combining Equations (13) and (14)[25] gives

$$d = \left[\frac{3\pi}{\sqrt{2}}\right]^{1/3} d_L \left[1 + \frac{3\mu}{(\rho_D \cdot \sigma d_L)^{\frac{1}{2}}}\right]^{-1/6} \quad . \quad . \quad . \quad . \quad . \quad . \quad (15)$$

This equation provides an approximate means of predicting drop sizes using values of d_L calculated from Equation (12).

Experimental work was performed with a PTFE disc with which organic liquids exhibit small contact angles. The original brass stators were omitted. For all practical purposes the drop sizes emanating from the wetted disc were independent of the inlet distribution. Therefore, the results for two distributors were combined to give mean values from eight determinations at different hold-ups.

With the non-viscous systems, at rotor speeds below $Re \simeq 1 \cdot 9 \times 10^4$, discrete drop formation occurred corresponding to rim disintegration. This is illustrated in Fig. 2. The transition is dependant on dispersed phase viscosity and rim disintegration persisted beyond $Re \simeq 1 \cdot 5 \times 10^4$ but not at $Re \simeq 2 \cdot 9 \times 10^4$ in the case of liquid paraffin. Smaller drops which originated as satellites were also observed. This is a common phenomena when droplets form from a base of fluid.[16] Such secondary drops were also formed upon coalescence of drops into the dispersed phase layer beneath the disc; this has been reported elsewhere for drop-interface coalescence. The maximum drop sizes recorded under this regime are given in Fig. 9 in which no differentiation is made between rotor speeds or 400 and 500 r.p.m. Hence the points represent mean values from 16 photographs. Because of the phenomena described, no reliable correlation can be proposed for d_m, or, more particularly, for d_{vs}. However, d_m is significantly greater than values obtained with non-wetted discs in the same speed range. A similar effect has been noted for d_{12}[16].

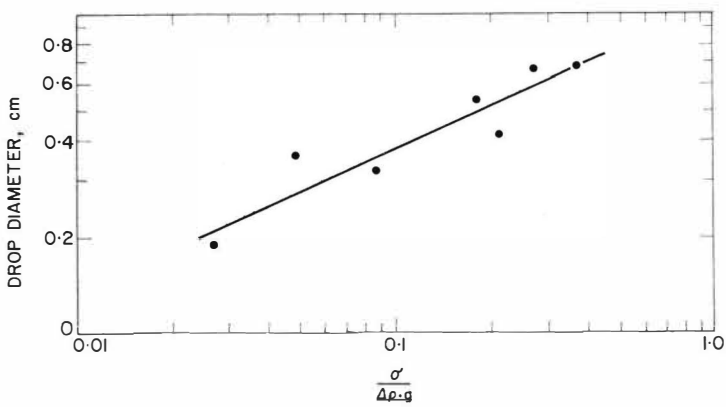

FIG. 9. *Measured* d_m
wetted disc, $Re < 1 \cdot 9 \times 10^4$

At rotor speeds such that the mechanism approximated to sheet disintegration, unlike in the two previous cases, the turbulence in the continuous phase was sufficient to produce further break-up. Hence only the upper limit of the size distribution may be determined by this mechanism. The regime is illustrated in Fig. 10. In Figs 11 and 12 maximum observed drop sizes, based on eight determinations, are compared with those predicted from Equation (15) using

radial velocities at the disc radius from Equation (9) corresponding to $Z = d/2$, to represent a mean value for the fluid carried by the disc[21] and values of x and h estimated from the photographs. Predicted values of d are consistently less than the measured values of d_m and there is increasing disparity as the ratio $(\sigma/\Delta\rho.g)$ is increased.

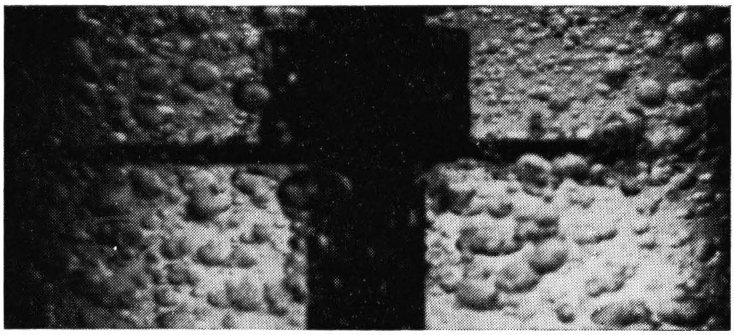

FIG. 10. *'Ligament disintegration' of dispersed phase from a wetted disc*
Amyl acetate–water, $Re > 1{\cdot}9 \times 10^{-4}$

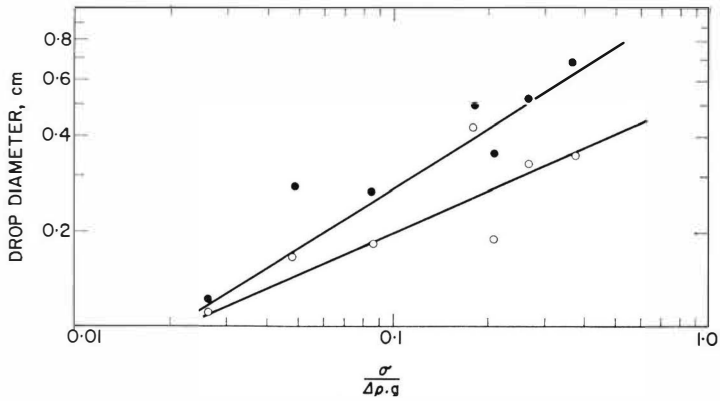

FIG. 11. *Measured* d_m *and predicted* d. *Wetted disc sheet and ligament disintegration region*
$N = 600$ rpm; ● measured diameter; ○ predicted diameter

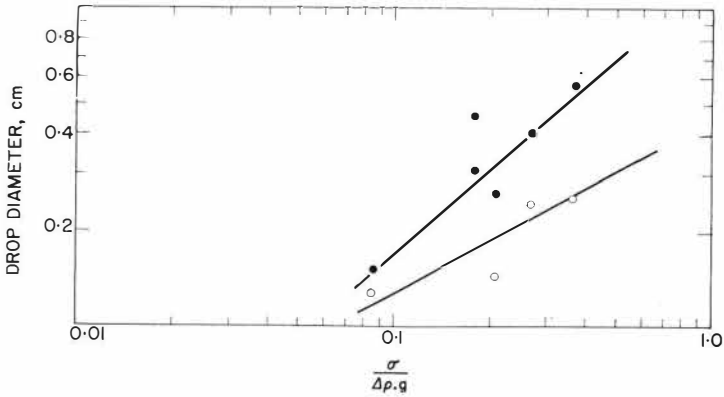

FIG. 12. *Measured* d_m *and predicted* d. *Wetted disc sheet and ligament disintegration region*
$N = 850$ rpm; ● measured diameter; ○ predicted diameter

In gaseous media, smaller drops than predicted are generally obtained since ligaments do not break down instantaneously but stretch and become thinner due to their transverse velocity component.[25] Alternatively, smaller drops can be formed when perforated break-up results from ripples created by droplet impingement on the sheet surface.[28] For liquid–liquid media other factors predominate. For example, Meister & Scheele[27] have reported that, in cylindrical jet break-up in immiscible liquids, a drop which has broken off may not have sufficient velocity to escape before the jet overtakes it causing remerging and ultimately a drop with twice the original volume. Alternatively, they found that should the jet length be between one and two wavelengths, larger drops may be formed intermittently by a force balance mechanism. For very viscous jets, such as paraffin oil in water which showed a large deviation from theory in the current work, the second node from the end of a jet sometimes ruptured causing the drop to be twice the predicted size. Probably the most significant factor however is interdroplet coalescence in the turbulence surrounding the disc periphery. A droplet break-up coalescence mechanism predominates in the *RDC* with wetted discs[16] and the tendency for coalescence is known to increase with increased interfacial tension and with decreased density difference that is large values of $(\sigma/\Delta\rho.g)$.

This study of droplet dispersion from a wetted disc was initiated since wetting of column internals may occur due to an error in materials selection, or by displacement during operation, or by a change in contact angle due to salute concentration. There is some evidence that this will reduce *RDC* efficiency[12] and capacity.[11] In the event, with operation in the wave formation region, spreading of the dispersed phase on the disc creates new interface. This may be supplemented by droplet recoalescence and break-up at the disc periphery. Hence for systems in which the dispersed phase film coefficient is controlling, mass transfer efficiency in a *RDC* type of column may be enhanced by altering the material of the discs. Some work has been carried out in establishing the potential and flexibility in operation of such a design.[29]

Nomenclature

B	hx
d	drop diameter; ligament diameter
d_{12}	hydraulic mean drop diameter
d_m	maximum drop diameter
∂	thickness of fluid layer carried by disc
D	column diameter
E	energy dissipation per unit mass
Σ	energy dissipation
F	$h\theta$
g	acceleration due to gravity
h	sheet thickness
K_f	constant
L	macroscale of turbulence
N	motor speed, revolutions per unit time
n	proportion of drops which will impinge on rotor and stator edges in any compartment.
n''	wave number $= 2\pi/\lambda$
P	force per unit area
r	drop radius
R	rotor diameter
R'	effective radius from centre of disc

Re	Reynolds number for impeller: $\frac{N^2 R \rho_c}{\mu_c}$
S	diameter of stator ring opening
u, v, w	components of velocity in directions r^1 (radial), φ (circumferential) and z (axial)
U	mean relative velocity
V	velocity
V_N	characteristic droplet velocity, i.e. the mean vertical droplet velocity at substantially zero flow rates and at rotor speed N
x	distance in radial direction from disc tip
θ	time
μ	viscosity
σ	interfacial tension
ρ	density
ω	angular velocity
ζ	dimensionless distance from disc surface
λ	wavelength

Subscripts

c	continuous phase
d	dispersed phase
L	ligament
s.d.	stable drop

References

[1] Mumford, C. J., *Br. chem. Engng*, 1968, **13,** 981
[2] Reman, G. H., 'Proc. 3rd World Petrol. Congr.', Hague, 1951, Section 111, 121 and U.S. Patents 2,601,674 (1952), 2,729,545 (1956), and 2,912,310 (1959)
[3] Nakamura, A., & Hiratsuka, S., *Kagaku Kogaku*, 1966, **30,** 1003
[4] Krishnaiah, N. M., Pai, M. U., Ramano, Rao M. V., & Sastri, S. R. S., *Br. chem. Engng*, 1967, **12,** 719
[5] Shell Internationale Research Maatschappij, N.V., Belgian Patent 632926 (1963)
[6] Sokov, Y. F., & Putilova, Z. D., 'Tr. Vses. Nauch. Tekn.', Protsessy Zhidkostnoi Elekraktsii i Khemosorbtii, 1966 (2nd Edn.) (Leningrad: Sovesch Protsessy Zhidkostnoi Elekraktsii i Khemosorbtii)
[7] Marek, J., & Misek, T., 'Conference on Solvent Extraction', London, 27th March 1969 and Czech. Patent 88415
[8] Misek, T., 'Rotating Disc Contactor', 1964 (Prague: Statni Nakadelstri Technicke Literatury)
[9] Jeffreys, G. V., *Chem. Proc. Eng.*, 1969, **49,** 11
[10] Thornton, J. D., & Bouyatiotis, B. A., *Ind. Chemist*, 1963, **39,** 298
[11] Jeffreys, G. V., & Mumford, C. J., Paper presented to the 3rd CHISA Congress, Marianske Lazne, September 1969
[12] Davies, J. T., Ritchie, J. M., & Southward, D. C., *Trans. Instn chem. Engrs*, 1960, **38,** 331
[13] Misek, T., & Rozkos, B., *Chemický Prům.*, 1965, **15,** 450
[14] Misek, T., *Colln, Czech. chem. Commun.*, 1963, **28,** 426
[15] Kung, E. V., & Beckmann, R. B., *A.I.Ch.E. Jl*, 1961, **7,** 319
[16] Mumford, C. J., Ph.D. Thesis, University of Aston in Birmingham, 1970
[17] Thomas, R., & Mumford, C. J., Unpublished work
[18] Ramshaw, C., & Thornton, J. D., *Instn chem. Engrs Symp. Ser.*, 1967, No. 26, 73 and 80
[19] Kolmogoroff, A. M., *Dokl. Akad. Nauk SSSR*, 1949, **66,** 825
[20] Levich, V. G., 'Physichochemical Hydrodynamics', 1962 (New Jersey: Prentice-Hall)
[21] Cochran, W. E., *Proc. Camb. Phil. Soc.*, 1934, **30,** 365
[22] Schlichting, H., 'Boundary Layer Theory', 1968 (6th Edn), (New York: McGraw-Hill)
[23] Fraser, R. P., & Eisenklam, P., *J. Imp. Coll. Chem. Engng Soc.*, 1953, **7,** 53
[24] Friedman, S. J., Gluckert, F. A., & Marshall, W. R., jun., *Chem. Engng Prog.*, 1952, **48,** 181
[25] Dombrowski, N., & Johns, W. R., *Chem. Engng Sci.*, 1963, **18,** 203
[26] Weber, C., *Z. Angew., Math. Mech.*, 1931, **11,** 136
[27] Meister, B. J., & Scheele, G. F., *A.I.Ch.E. Jl*, 1969, **15,** 700
[28] Fraser, R. P., Eisenklam, P., Dombrowski, N., & Hasson, D., *A.I.Ch.E. Jl*, 1962, **8,** 672
[29] Al-Hemiri, A. A. A., Unpublished work

Droplet behaviour in a Scheibel extraction column

by G. V. Jeffreys, G. A. Davies* and H. B. Piper*

Department of Chemical Engineering, University of Aston in Birmingham, Gosta Green, Birmingham, U.K.

The behaviour of droplets in a section of a 3·0-in dia. Scheibel column has been investigated and three distinct characteristics have been observed:

(i) very small drops pass through the packing without change;

(ii) medium-size drops coalesce and break up, yielding a characteristic drop size on emergence from the packing;

(iii) large drops form globules through coalescence and pass through the packing in a periodic manner.

Introduction

THE SCHEIBEL EXTRACTION COLUMN was probably the first mechanically agitated column to find widespread application in industry and in the pilot plant laboratory, and for duties requiring an extraction column of less than 12 in dia. it is still the one generally preferred.

The column consists of compartments containing alternate sections of a knitted mesh packing and mixing sections. The liquids passing through the mixing section are agitated by an impeller located centrally on a shaft that passes through the entire column. Dispersion of the desired phase is accomplished in this section and the turbulence generated there is damped out in the packed sections. For these reasons, Perry[1] describes the Scheibel extractor as a series of mixer–settlers or mixer–coalescers where the packed sections coalesce the dispersion produced by the agitator. Later workers have expressed some doubt whether coalescence always occurs in the packings and Scheibel[2] has stated that the packed sections are beneficial only for treating systems of low interfacial tension. He further stated that the packed sections could be replaced by 'stabilising baffles' when this column is employed for processing systems having high interfacial tension. In fact, the role of the packed section in the Scheibel column is rather indeterminate, although Honeykamp & Burkhart[3] found that knitted mesh packings behaved similarly to the more conventional packings in extraction columns. They found that for each system they studied, there was a 'characteristic drop size' and droplets passing through the packing tended to approach this size if sufficient packed height was available. Furthermore, the flow rate of the phases did not appear to have much influence on the size of the drops emerging from the packing. In fact the parameters controlling drop size and size distribution in Scheibel columns have not yet been elucidated. That is, the mechanism of droplet break-up and coalescence in knitted packings in Scheibel columns has not been considered hitherto and therefore it is necessary to investigate this phenomenon if the design procedures for this type of extraction column are to be placed on a more fundamental basis. This paper presents the preliminary results of studies of droplet behaviour in knitted mesh packings of the type installed in Scheibel columns.

Experimental

A schematic diagram of the apparatus employed for the investigation is shown in Fig. 1. It consisted of a 3 in dia. glass column built from two standard pipe sections, each 1·0 ft long. Elgin-type enlarged ends were installed, as shown, for phase separation of the dispersed phase leaving the top of the column, and for the dispersed phase distributor at the base of the column. The

*Department of Chemical Engineering, University of Manchester Institute of Science & Technology, Manchester, U.K.

agitator shaft was a 0·25 in stainless steel rod supported by bearings and Teflon bushes spaced 1·0ft apart. The upper bearing was a horizontal thrust ball race mounted in the upper brass end plate. The Teflon bush bearings were secured in holders and attached to a brass section fitted with gaskets in between the two pipe sections, and between the bottom pipe section and enlarged section. The brass end plates were also provided with connexion lines for entry and exit of the phases, vent lines and thermometer pockets as shown in Fig. 1.

The agitator shaft was connected by a reinforced rubber hose to a 0·25 h.p. variable-speed electric motor. The agitator speed was measured by a tachometer, and its speed was controlled at the desired value by a Variac transformer.

5-in sections of stainless steel knitmesh packing of dia. just greater than 3·0 in were placed in the column and located in position by a copper wire holder. By these means the packing could be made to fit reasonably tightly in the corrected position in the column without unduly compressing the packing or reducing its voidage.

Each mixing compartment was provided with a 1·0 in dia. four-bladed paddle and the initial dispersion was produced from nozzles in a brass perforated plate designed to give drops in the size range required for the experimental work, in accordance with the conditions proposed by Treybal & Hayworth.[4]

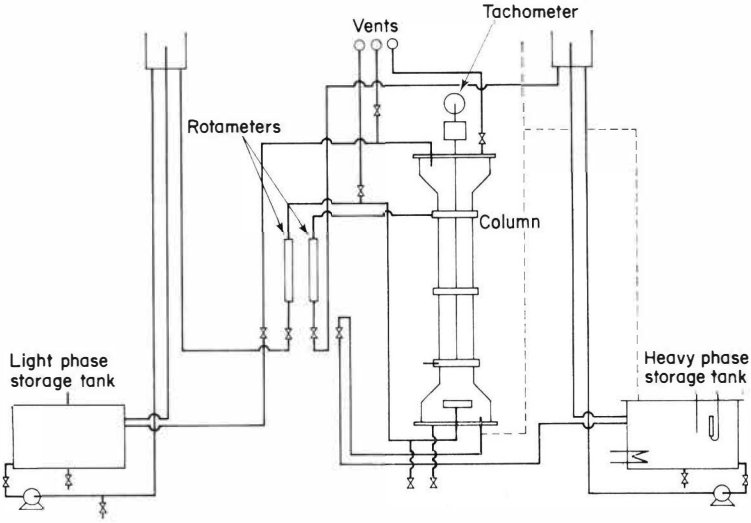

FIG. 1. *Flow diagram of experimental apparatus*

The photographic work was carried out with a 135 mm lens camera and a stroboflood in order to obtain a 0·001-sec pulse of light. The illumination was provided from the rear of the column at ~45° to the focal plane. The camera was focused on to the nearest edge of the packing holder and all photographs were taken in this plane by maintaining the camera tripod in a permanent position, and then raising or lowering the camera as required. Kodak V.P. 120 film was used throughout this investigation at a setting of *f*32. Finally, in order to measure the magnification and to be able to allow for any distortion of the drops owing to refraction, a grid, printed on a cellophane sheet, was mounted in the plane corresponding to the edge of the packing holder and photographed. In the initial experiments, the system kerosene–water was studied and before a series of experiments were carried out the entire apparatus was cleaned. The glass sections were cleaned by immersing in chromic acid, washing with water, rinsing with acetone and then thoroughly washing with distilled water. The metal sections of the column including the brass end sections and bearing supports, the copper packing holder and the Teflon bushes were cleaned by

immersing in nitric acid, washing with water, rinsing with acetone and then thoroughly washing with distilled water. The agitator shaft was cleaned with carbon tetrachloride, followed by acetone and distilled water. Finally the mesh packing was cleaned by immersion in carbon tetrachloride at 50°C for ~30 min, then washed with acetone followed by distilled water as for the other parts. The packing was stored in water before use. Finally the apparatus was assembled and water was circulated through it slowly for 24 h before the experimental work was started.

Details of the knitmesh packing are given in Table I. Type 9033 is standard Yorkmesh originally recommended by Scheibel and employed by Honeykamp & Burkhart[3] in their investigations.

TABLE I

Knitmesh packing

Type number	Density, lb/ft³	Surface area, ft²/ft³	Free volume (Voidage), %	Knitting type
9033	12·0	120·0	97·5	Standard
9036	6·0	60·0	98·75	Hi-T
4530	6·0	60·0	98·75	Standard

Comparison of the different types of knitting is seen from the illustrations of the types 9033 and 9036 in Fig. 2.

Two distributors were used in the experimental work. Both were constructed from brass plate. One contained 170 holes, each of 0·03 in dia. on a 0·1875 in square pitch and the other contained 25 holes of 0·125 in dia. on a 0·5 in square pitch.

Finally experiments were carried out at agitator speeds in the range 450–850 rev/min.

Immediately before starting an experiment, all air locks were eliminated, after which the water line valves to and from the column were closed and the kerosene phase was passed through the column. The kerosene rate was adjusted to that required for the start of the experiment and then the water flow rate was restarted and its rate adjusted to that required for the experiment. When this had been achieved, the phases were circulated until the contents of the column attained a temperature of 25°C, after which measurements were taken.

Limiting flow experiments

For this series of experiments, the continuous phase flow rate was set for the experiment and the dispersed phase flow rate was increased stepwise. On each occasion the flow rate was increased, the interface was held steady for at least 10 min before taking a reading, and as the flooding point was approached this period was extended in order to ensure that a steady state had been achieved. As the flooding point was approached drops accumulated below the packing and this warning enabled the 'flooding point' to be determined accurately.

One experiment was repeated in which the dispersed flow rate was set and the continuous phase flow rate increased stepwise, but no measurable difference in the limiting flow rate could be detected.

In the experiments involving photographic work, the phases were circulated until the temperature was steady at 25°C. Then the flow rates were set and the experimental conditions maintained steady for at least 20 min before taking any photographs. The variation in temperature could be restricted to ±0·5°C.

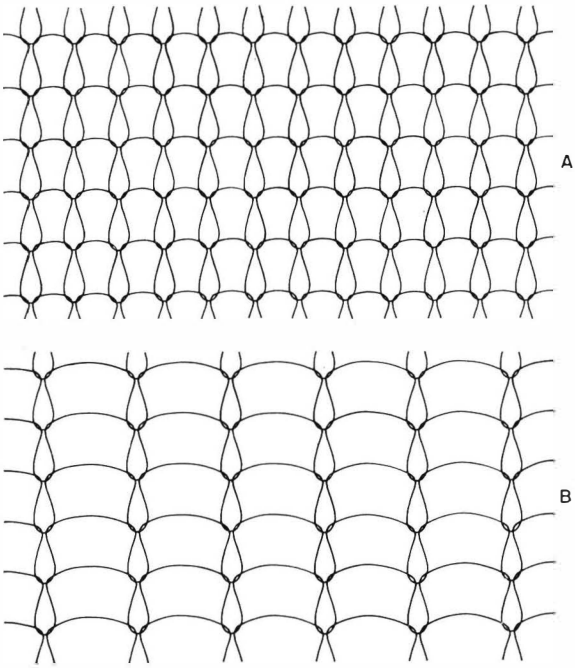

FIG. 2. *Knitmesh of packings*

A, Standard 9030 knitmesh; B, Hi-T 9036 knitmesh

Results

The results are presented in Fig. 3. It can be seen that the limiting flow rates increased from a total flow rate of 17·5 ft/h to 80·0 ft/h as the voidage increased from 97·5% to 98·75%. The maximum flow rate of 1850 ml/min corresponding to 80 ft/h compares with the maximum flow rates found by Honeykamp & Burkhart[3] using Yorkmesh packing and the system methyl isobutyl ketone –water. That is, 2000 ml/min at 600–850 rev/min. The 9036 packing, having the larger interstice size but the same voidage as the 4530 knitmesh, had a limiting flow rate of 80 ft/h compared with 55 ft/h. Also, the limiting flow rate increased when smaller drops, compared with the packing mesh size, were passed through the column. With the Yorkmesh packings, it was observed that drops from both distributors were held in the packing and that the higher throughputs were obtained when the larger drops were produced by the large nozzle distributor.

Attempts were made to correlate the flooding point results in a similar manner to that of Crawford & Wilke[5] for the flooding of packed columns. It was found that a plot of $U_c^{0\cdot5}$ vs. $U_d^{0\cdot5}$ generally did not give a straight line unless the drop size was small compared with the interstice size of the packing, conditions corresponding approximately to those found in packed columns. With drop sizes comparable with those existing in a Scheibel column, flooding occurred prematurely through the formation of a coalesced core of the dispersed phase below the packing. In some experiments, the agitator was placed close to the bottom of the packing in order to prevent the formation of the coalesced core, but with the approach of flooding and the accumulation of a drop layer it was found that the agitator tended to initiate coalescence prematurely under these conditions.

The results were analysed to estimate a 'characteristic drop size' for the three knitmesh packings, but it was found that the actual drop size distribution

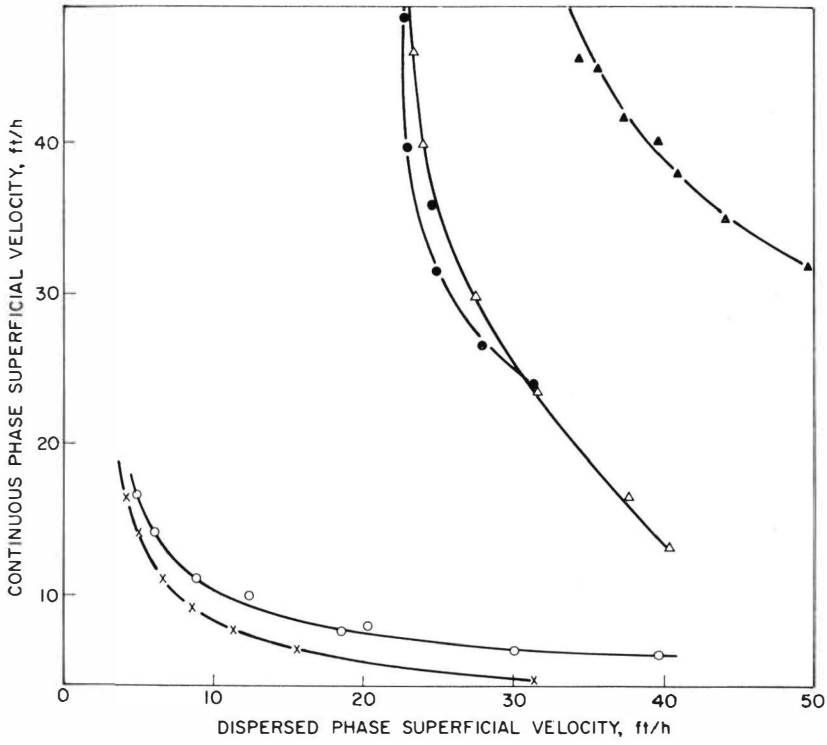

FIG. 3. *Effect of voidage on limiting flow rates*

	Packing	Hole dia., in	Voidage, %
×	9033	$\frac{1}{32}$	97·5
●	4530	$\frac{1}{32}$	98·75
▲	9036	$\frac{1}{32}$	98·75
○	9033	$\frac{1}{8}$	97·5
△	9036	$\frac{1}{8}$	98·75

observed in the column was rather more complex than that reported by Honeykamp & Burkhart.[3] Thus, it was found that the dispersion could be divided into three groups of drops as follows:

(i) Containing very small drops which passed through the packing without change.

(ii) Drops that are only relatively smaller than the interstices of the packing and which undergo no great change in passing through the packing. Honeykamp & Burkhart experimented with drops of this kind.

(iii) Drops that are large compared with the mesh size of the packing. These drops collect at the leading edge of the packing and eventually coalesce to form a large globule that passes through the packing section with a pulse-like quick movement. On reaching the upper surface of the packing this globule breaks up by a drip point mechanism. The size of the drops formed by this mechanism vary with the mesh size of the packing and with the flow rate of the globule through the packing. Globules were also noticed to form at points inside the packing where drops can be retained for sufficient time. Once a small globule formed, drops of various sizes collected below it and eventually coalesced with it. Once this occurred, the 'drip point' action set in, although there did not appear to be any globules beneath the packing. The behaviour of the drops is depicted in Fig. 4.

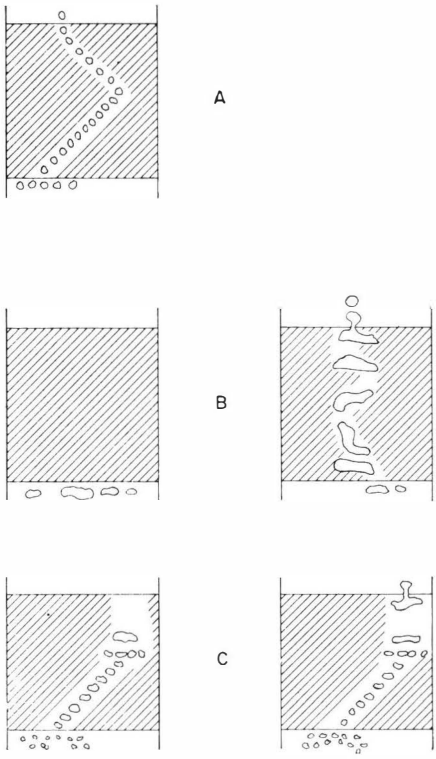

FIG. 4. *Mechanism by which drops pass through the packing*

A: Small drops pass through packing with no change in size, probably all drops following the same path.
B: Globule formation beneath packing, and pulses of globules pass rapidly through packing. Drops leaving packing formed by drip point action.
C: Globules formed by coalescence inside packing at points where drops are held up.

Photographs of drops leaving the packing were taken in the plane of the front edge of the packing holder, and photographs of drops in the mixing zone were obtained by focusing the camera onto the inside of the glass column. In each case, the magnification and distortion were measured by photographing a cellophane grid in the same plane. Three or four photographs were taken of each set of conditions and these were magnified 7× for the estimation of drop sizes. The drops analysed were either spherical or oblate spheroids. All the oblate spheroids photographed had an eccentricity of less than 1·5 and therefore, in accordance with Kintner's proposals, the major and minor axes were measured and the diameter of the sphere of equivalent volume estimated. The Sauter mean drop diameter was then calculated and histograms showing the three drop regions described above are presented in Fig. 5 which was typical of the results obtained. This figure shows that all the drops produced at the small distributor of sizes 0·3–0·4 cm coalesced in the 9033 packing to form drops of the size 0·7–0·9 cm by the drip point mechanism. These were broken up in the following agitator compartment and some of the new drops produced passed through the second packed section unchanged, while others must have coalesced to form globules and these in turn broke up to give the final distribution. These histograms indicate an approximate critical drop size for the 9033 knitmesh packing with the water–kerosene system of 2·0 mm—where the critical drop size is defined as the drop diameter above which drops behave as in group (iii), and below which size they behave as described for group (ii).

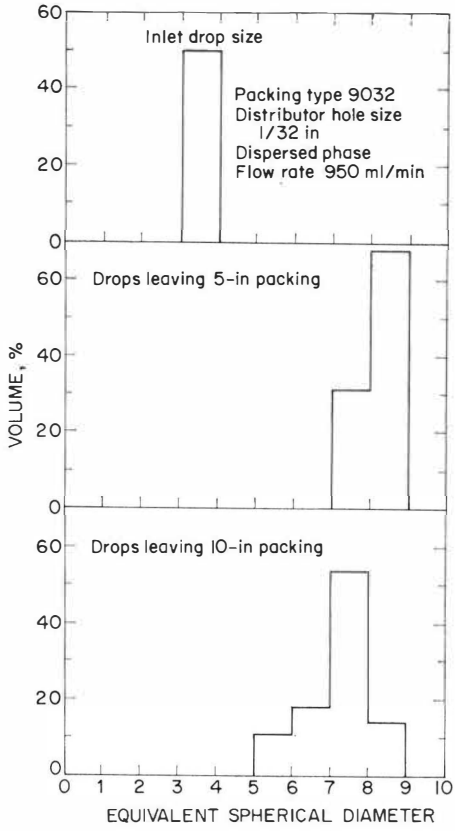

FIG. 5. *Drop size distribution analyses in packing*

Conclusions

The characteristics of droplets passing through a mesh packing of the kind installed in Scheibel columns can be divided into three regions:

Region 1. Very small drops which pass through the packing unchanged. Probably these drops follow the same passage way as already shown.

Region 2. Drops only relatively smaller than the interstice size of the packing. These drops pass through the packing by means of a series of collisions with the wire meshings until some break-up occurs through a transference of kinetic energy to surface energy. This is usually accomplished after passage through a certain minimum length of packing and results in the production of drops of a 'characteristic size'. Smaller drops entering the packing and those formed by break-up tend to coalesce in the packing, yielding an equilibrium size on emergence from the knitmesh. Honeykamp & Burkhart claim that this mechanism alone describes the drop behaviour in the packing of Scheibel columns.

Region. 3. Drops larger than the size of the interstices. Drops in this region collect at the entry to the packing and coalesce there forming large globules. These wet the packing and then rapidly spurt through the packing intermittently. A possible explanation is that the globule moves forward at a rate determined by the magnitude of the buoyancy forces over the surface forces. This is determined by the size of the globule and the wettability of the dispersed phase for the packing. In a very short time, the globules accumulate at the exit of the packing and leave through the drip point action. Probably small

jets of diameter comparable with the size of the interstice leave the packing and these are broken up through a Rayleigh type disturbance augmented through the turbulence transmitted by the agitator. Finally, globule formation can occur at the entrance or at any point within the packing where a number of drops are held up for sufficient time for coalescence to take place. Also the globule is transported through the packing so rapidly and this mechanism occurs so frequently that the column continues to operate satisfactorily. However, the contribution to the drop size distribition is uncertain at present and therefore the prediction of the drop size is not possible at the present time.

References

[1] Perry, J. H., 'Chemical engineers handbook', 4th Edn, 1966 (New York: McGraw Hill)
[2] Scheibel, E. G., *A.I.Ch.E. Jl*, 1956, **4,** 74
[3] Honeykamp, R. J., & Burkhart, L. E., *Ind. Engng Chem. Prod. Res. Dev.*, 1962, **1,**
[4] Treybal, R. E., & Hayworth, C. B., *Ind. Engng Chem.*, 1950, **42,** 1174
[5] Crawford, J. W., & Wilke, C. R., *Chem. Engng Prog.*, 1951, **47,** 423

Study of back mixing effect in a pulsed rotating disc contactor

by H. Angelino and J. Molinier
Institut du Génie Chimique, Chemin de la loge Empalot, 31-Toulouse, France

A new liquid – liquid extractor based on the combination of a pulsed column and a rotating disc contactor (RDC) *is described. Its performance is compared with that of a standard (pulsed column) apparatus, using the ternary system iodine – water – carbon tetrachloride. Concentration profiles were determined in both phases and a number of transfer units* (NTU) *and Peclet numbers were calculated using the differential back mixing model and the method of Mecklenburgh & Hartland. The influence of the various operating parameters – amplitude,* A*; frequency of pulsation,* f*; and speed of rotation,* ω *– of the agitator were studied.*

Introduction

IN 1966 A group of research workers at this Institute proposed a new apparatus for liquid–liquid extraction. They called this the 'hybrid column' since its basic design originated from the combination of two well-known devices, the pulsed column and the rotating disc contactor (*RDC*).[1–3] Initial experiments showed that the new apparatus had a higher efficiency than the standard mechanically agitated apparatus and also that it required less mechanical power to achieve an identical efficiency and that it allowed an identical flow-rate.[2] These first results were supported by a comparative systematic study of the performance of the hybrid column with that of an *RDC* and of a pulsed column using different ternary systems.[4]

Boyadzhiev & Angelino[2] attributed the increase in efficiency obtained to a decrease in the effect of back mixing. It is known that back mixing reduces the driving force along a column by depressing the concentration distribution curves. This fact led Miyauchi & Vermeulen[5] to introduce three different methods of expressing the number of transfer units (*NTU*) for mass transfer: (i) the true *NTU*, which arises from the original definition of the height of a transfer unit proposed by Chilton & Colburn:[6]

$$(NTU)_{\mathrm{v}} = \frac{KaH}{V}$$

where K is the overall mass transfer coefficient, a the interfacial area, H the height of column and V the phase velocity; (ii) the apparent *NTU* which coincides with the $(NTU)_{\mathrm{v}}$ for the combination of a piston flow model and a dilute solution:

$$(NTU)_{\mathrm{a}} = \int_{x_0}^{x'_1} \frac{\mathrm{d}x}{x^* - x'}$$

where x is the concentration in the heavy phase, x'_1, x_0, x' and x^*, are as shown in Fig. 1, and $x^* = my$, m being the slope of the distribution curve; (iii) the measured *NTU*, which is similar to the $(NTU)_{\mathrm{a}}$ but is based on the true operating curve:

$$(NTU)_{\mathrm{m}} = \int_{x_0}^{x_1} \frac{\mathrm{d}x}{x^* - x}$$

Two main models have been developed to provide a mathematical expression of the back mixing effect; the 'stagewise model' in which the apparatus is assumed to consist of several identical stages;[7–10] and the 'differential model' which introduces an eddy diffusion coefficient similar to a molecular diffusion coefficient.[8–11] In this case the apparatus is assumed to be continuous.

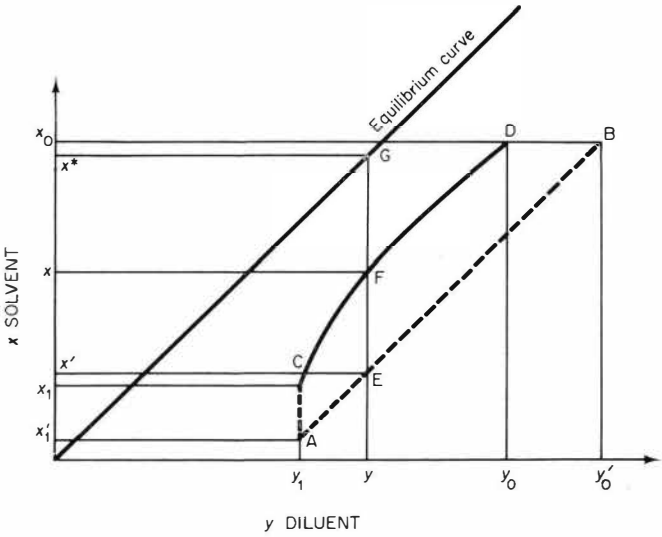

FIG. 1. *Schematic representation of concentration profiles in a differential contactor*

The relevance of either model depends on the specific case under consideration; nevertheless Mecklenburgh & Hartland[12] have established that both models are almost identical as far as numerical results are concerned.

Back-mixing may be experimentally investigated either by injection of a tracer[13] or by determining concentration profiles of the solute in both phases alongside the apparatus.[14] In the second case, the $(NTU)_v$ factor is determined in addition to the Peclet numbers P_x and P_y. When transfer occurs between the two phases in the presence of back mixing, Hartland & Mecklenburgh[15] used the three main parameters, P_x, P_y and NTU:

$$P_x = \frac{V_x H}{e_x};\ P_y = \frac{V_y H}{e_y}$$

e being the eddy diffusion coefficient and the subscripts x and y referring to the two phases.

Based on the above considerations, this paper is intended to clarify the precise reasons for the superior performance of the hybrid column and thus investigate the validity of the hypothesis of Boyadzhiev & Angelino.[2] In the work described here, concentration profiles of the solute in both phases were determined in both a hybrid column and a pulsed unit and the respective NTU and P factors were calculated using the differential back mixing model and the method of Mecklenburgh & Hartland.[12,15]

Experimental

Apparatus

A flow diagram of the pilot plant (Fig. 2) describes the system.

The hybrid column consists of three sections: a cylindrical middle 'extraction section' containing perforated plates, baffles and agitators, with two 'separating sections', one at each end of the assembly.

The extraction section was made from a 50 mm $\pm$ 1 mm dia. calibrated glass column of length 1 m. The inside of the column was fitted with 21 1-mm thick stainless-steel plates, each perforated with 126 2-mm dia. holes and offering a free cross-section area to flow of 20%. The spaces between the perforated plates constituted 20 finite compartments, every alternate of which was divided into two elementary subcompartments by a ring 30 mm i.d. and 0·2 mm thickness (Figs 2–3). Each lower elementary subcompartment was fitted with

a special agitator. This agitator was made partly of a stainless steel with a Teflon part facing upwards in which 8 3-mm holes were drilled (Fig. 3). During operation the descending heavy phase collected at the Teflon surface and was projected through the holes in the agitator towards the glass wall. The agitators which together provided a turbine effect were mounted on a central rotating drive shaft of 4 mm in dia. The minimum distance between the agitators and the adjacent ring was 3 mm.

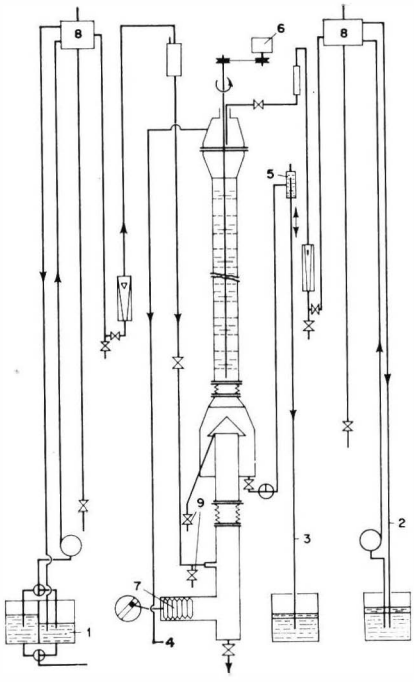

FIG. 2. *Pilot-plant flow diagram*

1, Aqueous solution of iodine; 2, discharge; 3, outlet heavy phase; 4, outlet light phase; 5, discharge and interface levelling; 6, motor; 7, Teflon bellows; 8, constant level vessel; 9, sampling device

Pulsation was produced by using a standard device involving Teflon bellows, a d.c. motor and a coupling-rod and crank. With the particular system used the amplitude of liquid could be varied up to a limit of 10 cm. The frequency was varied by changing the motor supply voltage, a maximum value of 200 mm^{-1} being attainable. The speed of rotation of the agitators could be adjusted by using a universal motor, the maximum speed being 1800 rev/min.

The heavy and light phases were supplied to the column from a constant level vessel.

When required, it was readily possible to convert the hybrid column to a pulsed column for purposes of comparison.

Since the measurement of flow, frequency, amplitude, separation and interface levelling were standard, they are not described here.

Methods

The iodine–water–carbon tetrachloride system was selected because of the following advantages: the total immiscibility of water and carbon tetrachloride, the very high value of the coefficient of distribution, which moreover remains constant and thus allows simplification of the mathematical analysis and, lastly, the fact that the mass transfer is not modified by the Marangoni effect. The aqueous phase was chosen as the continuous phase, owing to the superior wetting of the perforated plates which it provides, with the dispersed phase

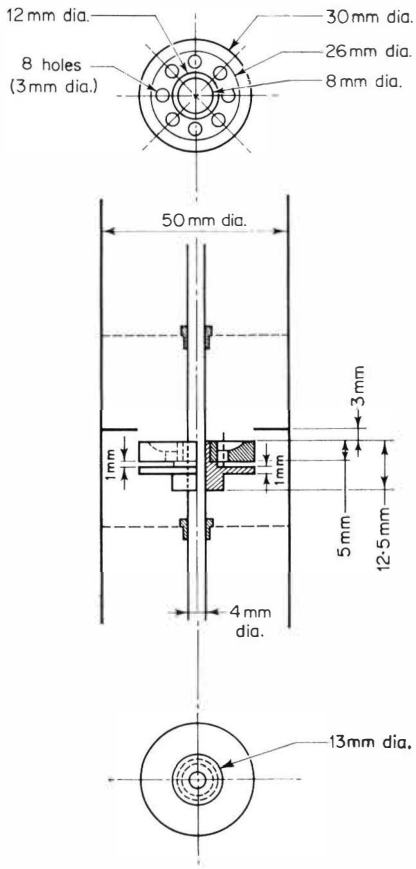

FIG. 3. *Diagram of agitator*

being the heavier carbon tetrachloride. The interface between the two phases was consequently always retained in the lower separating section during the experiments.

Only the mechanical parameters, amplitude and frequency of pulsation and in the case of the hybrid column speed of rotation of the agitators, were investigated. The flow-rates were maintained constant throughout the experiments at 40 l/h for the aqueous phase and 1 l/h for the organic phase, i.e. that the total flow-rate was equal to 20·8 $m^3/h\,m^2$ and ε the extraction factor, was 2·24, and therefore close to the economic range.

In order to establish the concentration profiles over the columns, five different samples from each phase were taken using a special hypodermic needle filled with either adsorbent or hydrophobic cotton depending on the sample for which it was being used.

Once steady-state conditions had been attained, samples were drawn as slowly as possible in order to ensure that only the desired phase was introduced into the sampling apparatus.

In order to prepare the aqueous solution of iodine a special apparatus was erected. This involved a 50 mm dia. glass column filled with alternate layers of bisublimated iodine and Raschig rings. Distilled water was passed downwards through the column thereby absorbing the iodine vapour. In order to promote the sublimation of iodine, an electrical heating wire was rolled round the column.

The technical carbon tetrachloride was regenerated using a solution of sodium

thiosulphate. The purity of the tetrachloride was determined to be 99·9% by chromatographic analysis.

The analysis of the aqueous phase was performed by using a 0·01N solution and a microburette.

Spectrophotometry was employed for the analysis of the organic phase, the defining wavelength being 580 μm for concentrations between 0·1 and 2·0 g/l and 650 μm for those between 2·0 and 12·0 g/l. Cells of 2·5, 5 and 10 mm thickness were used.

The experimental value of the coefficient of distribution, determined by using the concentrations in g/l, was 89·6. It was verified that this value remained constant over the temperature range 18 to 22°C.

About 60 experiments were performed and in each case concentration profiles were determined. Table I summarises the various experimental conditions.

TABLE I

Experimental conditions

	Pulsed column	Mixed column
A, cm	2–4	1·9–4
f, min^{-1}	81–163	61–150
ω, rev/min	—	0–800–1000 1200–1500–1800
ε	2·24	2·24
Total flow rate, m^3/h m^2	20·8	20·8

The true operating curves were deduced from the concentration profiles, a typical example of which is shown in Fig. 4. Under the operating conditions the straight-line (corresponding to the piston flow model) and the true operating curve were found to be separated to varying degrees in all cases and in some cases the operating curve was very close to the equilibrium curve.

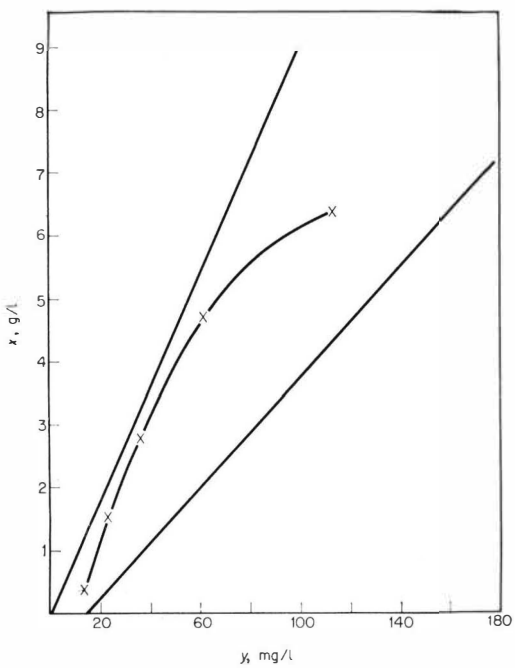

FIG. 4. *Experimental operating curve*

ω = 800 rev/min; Af = 7·42 cm/sec; A = 3·2 cm f = 139 min^{-1}

Results and discussion

In order to compare the results obtained, with those previously published,[1–5, 7–12, 14–19] the different NTU and Peclet numbers were calculated.

Fig. 5 illustrates the variation of $(NTU)_a$ as a function of the product Af. Since $\varepsilon = 2{\cdot}24$ and $m = 89{\cdot}6$, the following equations were used:

$$\text{Continuous phase: } (NTU)_a = \frac{2{\cdot}3 \log \left(\frac{y_{in}}{y_s} \times 0{\cdot}554 + 0{\cdot}446\right)}{0{\cdot}554}$$

$$\text{Dispersed phase: } (NTU)_a = \frac{2{\cdot}3 \log \left(\frac{y_{in}}{y_s} \times 0{\cdot}554 + 0{\cdot}446\right)}{2{\cdot}24 \times 0{\cdot}554}$$

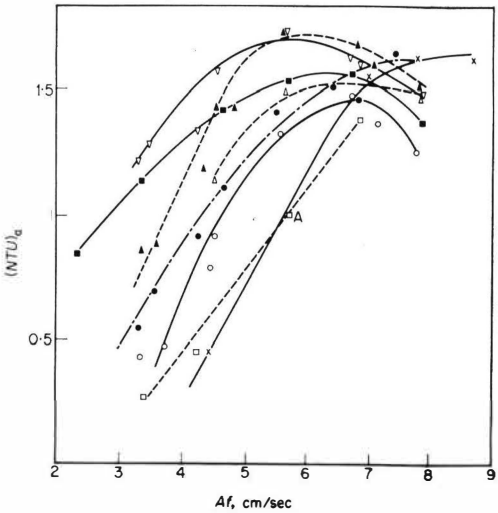

FIG. 5. *Variations of* $(NTU)_a$ *with* Af *at constant* ω

Pulsed column: ×, $A = 3{\cdot}2$ cm; □, $f = 103$ min^{-1}; Hybrid column ○, 0; ● 800; △, 1,000; ▲, 1,200; ▽, 1,500; ■ 1,800 min^{-1}

In the case of the hybrid column, the different curves correspond to a fixed value of the speed of rotation, ω. All the curves have a standard shape described by the following characteristics: $(NTU)_a$ increases with Af until a maximum value is reached, then $(NTU)_a$ decreases as Af continues to increase. The positions of the maxima change for the different curves drawn at constant values and they are also influenced by the general experimental conditions.

A comparison of the various results demonstrated that, in some cases, the maximum value of $(NTU)_a$ was greater for the hybrid column than for the pulsed column ($\omega = 1200$ rev/min and $\omega = 1500$ rev/min). The curves in both Fig. 5 and Fig. 6 indicate the existence of a maximum efficiency for values of ω between 1200 and 1500 rev/min. In addition, it is clear that the position of the maximum decreases with small values of ω although the numerical value of the efficiency increases when the product Af increases (Fig. 6). Fig. 6 also shows that the influence of agitation is much more important when the product Af is small. For example if Af is equal to 3·6 cm/sec the maximum efficiency is multiplied by a factor of 2·72 whereas it is multiplied by a factor of 1·26 when $Af = 6$ cm/sec. Furthermore, a change in the shape of the curve is evident when Af is greater than 4·5 cm/sec for values of ω of ~ 1000 rev/min. It seems that in this case, even if Af is significant, the turbulence deriving from

the presence of the agitator within the column is the major parameter. In general, the experiments made in this case confirmed that the efficiency of the hybrid column was greater than that of standard apparatus. Although in this instance the advantage amounted to only about 5%, this superior efficiency corresponded to a decrease in the power consumption, and it is known that in a different case this decrease was more than 10%.[2]

For the calculation of $(NTU)_v$ and the P_x and P_y factors the method of Mecklenburgh & Hartland[14] was used. In this method, if the variations of

$$\frac{dy/dz}{y_{in} - y} \text{ are plotted } versus \frac{\int_0^z (x^* - x)dz}{y_{in} - y} \text{ and those of } \frac{dx/dz}{x_{in} - x} \; versus \; \frac{\int_z^1 (x^* - x)dz}{x_{in} - x}$$

two straight lines are obtained. One can deduce the value of $\varepsilon/m\ T\ P_y$ and $P_x.T$ from the slopes, and P_y and P_x from the point of intersection with the ordinate axis. All the values were determined with the aid of a C.A.E. 510 computer by the method of least-mean squares. The variations of $(NTU)_v$ as a function of Af which are plotted on a log/log scale in Fig. 7, show that $(NTU)_v$ increases with Af. Furthermore, in the case of hybrid column, $(NTU)_v$ also increases with ω but the various straight lines appear to merge at one point for particular values of Af.

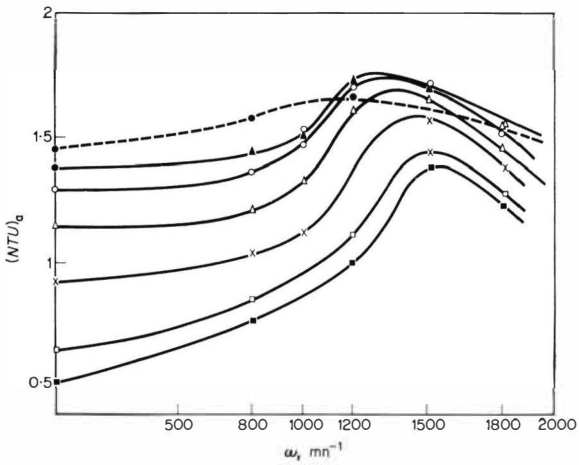

FIG. 6. *Variations of* $(NTU)_a$ *with* ω *at constant* Af

Af: ● 7; ▲ 6; ○ 5·6; △ 5; × 4·5; □ 4; ■ 3·6 cm/sec

As the $(NTU)_v$ is directly related to the product Ka, it appears that this product reaches a critical limit when the influence of agitation becomes of major significance. This may be attributed to the existence of too great a preponderance of droplets within the column resulting in a mutual hindrance, and also to the possibility that the droplet diameters are so small as thereby to attenuate the mass transfer. In the case of the pulsed column the relevance of the following equation was established for the ternary mixture involved, viz. $(NTU)_v = (Af)^{4.7} \exp(-7.82)$.

Values of $(NTU)_v$ are compared with values of $(NTU)_a$ in Fig. 8. In most cases the values differ, the degree of difference increasing with Af at constant level of ω. The flow through the column is clearly quite distinct from that defined by a piston flow model.

Variations of Peclet number, P_y, for the aqueous phase are plotted *versus* Af in Fig. 9, the straight-line corresponding to the results obtained with the standard pulsed column. P_y increases with Af which indicates a decrease in the back-mixing effect. This observation conflicts with several previous reports[16–18] but corroborates the results of Sehmel & Babb.[19] The latter authors

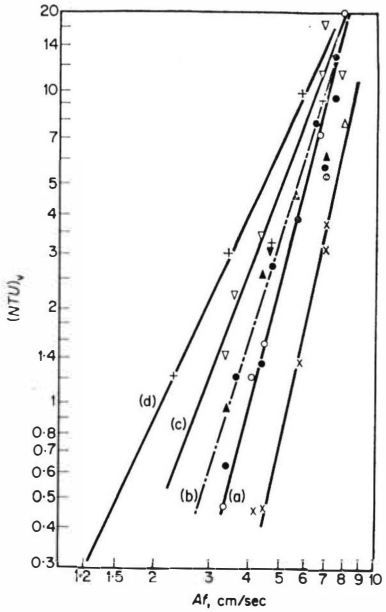

FIG. 7. *Variations of* (NTU)*v with* Af

×, Pulsed column; hybrid column: (a) $\omega = 0$; (b) $\omega = 800$; (c) $\omega = 1{,}500$; (d) $\omega = 1{,}800$ rev/min

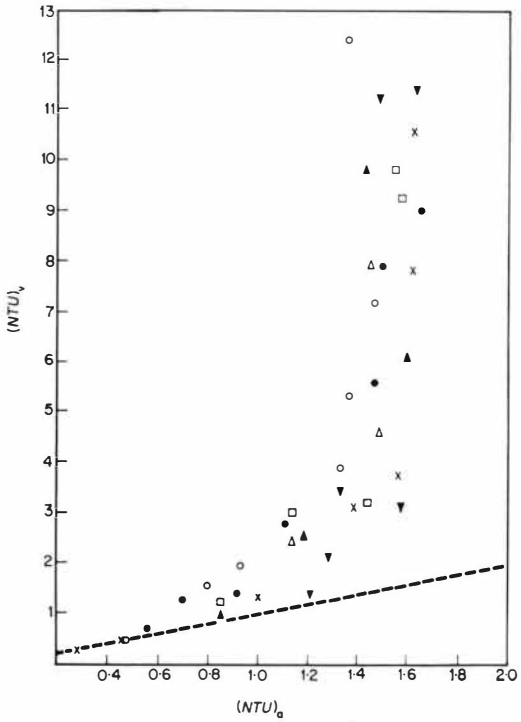

FIG. 8. *Comparison of* $(NTU)_v$ *with* $(NTU)_a$

×, Pulsed column; hybrid column, ω: ○, 0; ● 800; △ 1,000; ▲ 1,200; ▼ 1,500; □ 1,800 rev/min

established that the eddy diffusion coefficient is a decreasing function of the frequency when the apparatus is working under emulsion conditions. In fact, surveying the maximum values of the product Af involved in the various reports[16–19] it may be noticed that only Sehmel & Babb[19] had used values as high as those involved in the present study. In the other cases Af was always less than 4·5 cm/sec[17] or 2·5 cm/sec.[16,18]

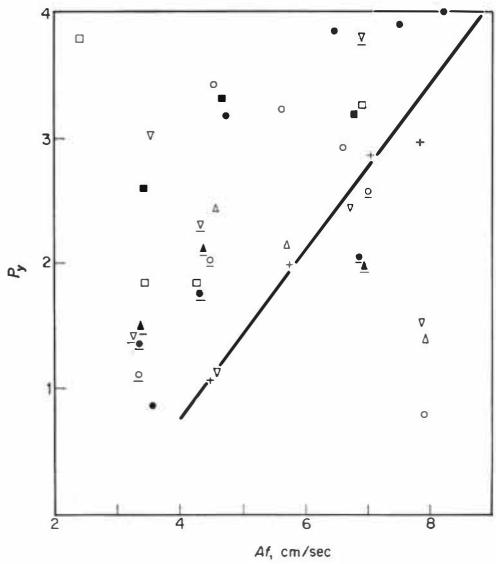

FIG. 9. *Variations of Peclet Number, for the continuous phase, with* Af

In the case of the hybrid column the experimental results are scattered and it is difficult to deduce rigid conclusions relating to the influence of the various parameters. This is not surprising in view of the probable mutual interference between the three main parameters A, f and ω which act simultaneously on both the dispersion and the retention of the organic phase. Moreover, the method of calculation is relatively satisfactory, as all the assumptions have not been reasonably well verified. This difficulty has already been encountered by other workers[20] investigating similar problems of greater simplicity. In any event, it is evident that practically all the calculated values lie above the straight line $P_y = \psi(Af)$ which corresponds with the standard pulsed column. This lends support to one of the hypotheses proposed by Boyadzhiev & Angelino[2] that the increase in efficiency derives from a decrease in the back mixing effect.

Fig. 10 illustrates the results which were calculated for the dispersed phase. As in the case of the continuous phase, some scattering exists but it can also be seen in this case that back mixing is reduced in the case of the hybrid column.

A comparison of the numerical values of P_x and P_y indicates that, for high values of the product Af, the order of magnitude of P_x and P_y is identical. This is true for the standard pulsed column and corroborates the results of Miyauchi & Oya.[17] It is also applicable to the hybrid column.

Conclusions

For the pulsed column it was established that in the range investigated, pulsation results in P_y increasing with Af while P_x decreases. In other words for one phase the back mixing is decreasing while for, the other phase, it is increasing. For very high values of Af both P_y and P_x attain the same order of magnitude.

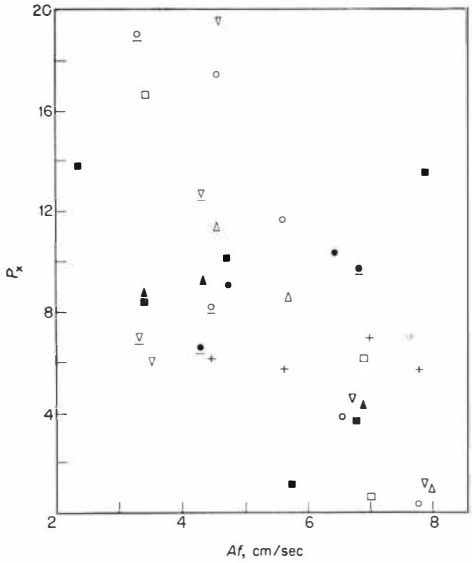

FIG. 10. *Variations of Peclet Number, for the disperse phase, with* Af

In addition, a simple relation is proposed between $(NTU)_v$ and Af and for the majority of cases:

$$(NTU)_v \geqslant (NTU)_m \geqslant (NTU)_a$$

The relevance of this inequality to the hybrid column was also shown.

It was also established that for the 'hybrid column' a maximum efficiency is attained as ω is increased at constant level of Af and also that specific combinations of Af and ω are optimal from the efficiency viewpoint. The maximum hybrid column efficiency is greater than that for the pulsed column in the case of the ternary mixture involved in this study. Scattering of the calculated values of P_y and P_x prevented the deduction of a general law; nevertheless it was established that Peclet numbers are always greater for the hybrid column than for the pulsed column. This proves that the increase in efficiency mentioned above results from a decrease in the back mixing effect in the apparatus. The scattering of the values of P_y and P_x may be attributed to the following reasons: the defects of the mathematical model; the lack of accuracy of the concentration profiles; the possible variations of e_x and e_y down the column.

In order to lessen the disadvantages it would be beneficial to increase the number of samples and/or apply an alternative technique employing pulse injection to determine the values of e_x and e_y.

Acknowledgments

The authors wish to thank G. Kuytchukov and S. Barame for their help in part of the experimental work and G. Hengl and J. Konkolewski for their technical assistance.

Nomenclature

a	= interfacial area
A	= amplitude of the pulse
Af	= pulse velocity: frequency–amplitude product
e	= eddy diffusion coefficient
f	= pulse frequency
H	= height of the column
h	= height along contactor ($h = 0$ at inlet)
K	= mass transfer coefficient

Ka = mass transfer coefficient
m = slope of the distribution curve
$(NTU)_a$ = apparent number of transfer units
$(NTU)_m$ = measured number of transfer units
$(NTU)_v$ = true number of transfer units
P = Peclet number
T = true number of transfer units in the method of Mecklenburgh & Hartland
V = superficial liquid velocity
x = concentration of solute in the dispersed phase
y = concentration of solute in the continuous phase
z $= \frac{h}{H}$
ε = extraction factor
ω = speed of rotation

Subscripts

c = continuous
d = dispersed
in = inlet
$*$ = equilibrium
s = outlet
x = x phase (disperse)
y = y phase (continuous)

References

[1] Angelino, H., Alran, C., Boyadzhiev, L., & Mukherjee, S. P., *Br. chem. Engng*, 1967, **12**, 1893
[2] Boyadzhiev, L., & Angelino, H., *CHISA Congr. Separation*, 1969, section G 3, p. 14
[3] Boyadzhiev, L., & Angelino, H., *Zh. prikl. Khim., Leningr.*, 1968, **41**, 2251
[4] Subhasavasdikul, S., 1969, Thesis, University of Toulouse
[5] Miyauchi, T., Vermeulen, T., *Ind. Engng Chem. Fundamentals*, 1963, **2**, 113
[6] Chilton, T. H., & Colburn, A. P., *Ind. Engng Chem.*, 1935, **27**, 255
[7] Sleicher, C. A., *A.I.Ch.E.Jl*, 1960, **6**, 529
[8] Hartland, S., & Wise, G. D., *Trans. Instn chem. Engrs*, 1967, **45**, 353
[9] Mecklenburgh, J. C., & Hartland, S., *Chem. Engng Sci.*, 1968, **23**, 81
[10] Hartland, S., & Mecklenburgh, J. C., *Chem. Engng Sci.*, 1966, **21**, 1209
[11] Sleicher, C. A., *A.I.Ch.E. Jl*, 1959, **5**, 145
[12] Mecklenburgh, J. C., & Hartland, S., *Can. J. chem. Engng*, 1969, **97**, 453
[13] Levenspiel, O., 'Chemical reaction engineering', 1962 (London: John Wiley)
[14] Mecklenburg, J. C., & Hartland, S., *Instn chem. Engrs Symp. Ser. No. 26*, 1967, p. 115 (London: Institution of Chemical Engineers)
[15] Hartland, S., & Mecklenburg, J. C., *Br. chem. Engng*, 1970, **15**, 216
[16] Mar, B. W., & Babb, A. L., *Ind. Engng Chem.*, 1959, **51**, 101
[17] Miyauchi, I., & Oya, H., *A.I.Ch.E. Jl*, 1965, **11**, 395
[18] Kagan, S. Z., Aerov, M. E., Lonik, V., & Volkova, T. S., *Int. chem. Engng*, 1965, **5**, 657
[19] Sehmel, G. A., & Babb, A. L., *Ind. Engng Chem. Process Des. Dev.*, 1964, p. 211
[20] Serna, P., & Lespinasse, B., 'Journée d'Études, le Calcul des Reacteurs Chimiques', 1970 (Paris: Société de Chimie Industrielle)

An improved contactor for liquid–liquid extraction

by B. J. Pope and N. R. Shah
Brigham Young University, Provo, Utah, U.S.A.

The efficiency of countercurrent contactors for physical separations is enhanced by an improvement in the phase contact in the plane orthogonal to the bulk flow. Backmixing of light or heavy fluid is always deleterious.

A highly efficient perforated rotating disc contactor (PRDC) was designed and constructed for liquid–liquid extraction to minimise axial dispersion and entrainment. The PRDC consists of a series of perforated circular discs on a common shaft mounted in a vertical cylindrical column between fixed perforated discs or stators. The device, which may be visualised as a sieve-plate column in which every other plate rotates, gives excellent phase contact with high shear rates at a given level within the vertical contactor and with minimum backmixing. Theoretical consideration of a differential model contactor as well as a survey of existing contactor design indicates the way in which efficiency and capacity of the PRDC are correlated.

An experimental perforated rotating disc liquid–liquid extraction column was operated at various disc spacings and at various rotor speeds to determine efficiency and capacity of the contactor. The tests were made with the methyl isobutyl ketone (MIBK)–acetic acid–water system, with MIBK as the discontinuous phase. Correlations are presented for capacity of the contactor at flooding and for the efficiency in terms of the height equivalent to a theoretical stage, or height of a transfer unit.

The perforated rotating disc contactor is compared with other existing devices using 'Index of Effectiveness' as suggested by Reman. On this basis, which combines both separation efficiency and capacity, the PRDC appears to be promising as one of the most efficient high capacity liquid–liquid contactors. A limited number of variables have been studied and further work is continuing.

Introduction

DESIGN OF COUNTERCURRENT contactors for separation processes strives for perfect phase mixing at each differential element orthogonal to the bulk flow axis with no axial backmixing. Treybal[1] notes that backmixing is always deleterious, that it will be a long time before the phenomenon is completely understood, and also that it would be simpler to eliminate backmixing than to study it. This paper describes the study of a new perforated rotating disc contactor of high efficiency and capacity, with reduced backmixing.

Perforated-plate or sieve-tray, spray and packed contactors have imperfect phase mixing at a given level in a column; however, backmixing or axial mixing are of small magnitude. On the other hand, mixer–settler systems or mixer–settler-type columns have complete backmixing but excellent phase contacting within a stage. Backmixing between properly designed stages is limited.

Perforated plate and packed contactors are often pulsed to increase interphase turbulence and interfacial surface renewal; always however, with the disadvantage of increasing backmixing.[2] The stages in mixer–settler contactors are often made shorter and placed within a vertical column with all of the mixing agitators on a common shaft.[3,4] A calming or settling section is placed between each mixing section to reduce backmixing.

Comprehensive reviews of extraction equipment design, scale-up, and operation have been given for U.S. equipment by Akell[5] and by Reman[6] for European equipment.

The rotating disc column (RDC) introduced and studied by Reman [7–11] is most nearly related to the new PRDC. It consists of a number of rotating discs supported on a shaft, the rotors being centered between doughnut stator rings. The central hole in the stator is usually larger than the rotor disc Reman has shown the RDC to have high volumetric efficiency, ease and economy of construction and operation. Vermijs & Kramers,[12] Kung & Backman,[13] as

well as Logsdail, Thornton and Pratt[14] have reported studies on capacity and performance of various sizes of RDC's. Probably, better data exist in the literature for scale-up of the RDC than for any other extraction equipment.

Krishnaiah *et al.*[15] and others have attempted to improve performance of the RDC by perforating the rotors.

Thomas[16] has recently described a new oscillating baffle column (OBC) device utilising vertical perforated baffles in the column in an attempt to establish truly countercurrent operation with the attendant high dispersion and high transfer rates. The performance of the column was compared with an RDC system fitted inside the same column used for the OBC studies. Under similar flow conditions with the RDC column at 1800 rev/min and the OBC at 175, oscillation gave best values of $H_{OY} = 20$ ft for both contactors on the carbon tetrachloride–acetic acid–water system. Thomas points out that the high value of 20 ft is not significant except for comparison of the particular extraction devices. The same columns with another solvent system would give entirely different but comparable values of H_{OY}.

Experimental

Description of the perforated rotating disc column (PRDC)

In the PRDC the rotors and stators are perforated discs with minimum clearance between the rotors and internal wall of the column. The fixed stator discs have a central hole with small clearance for the central shaft. The rotors are mounted on a common shaft and positioned midway between stators. The PRDC can be visualised as a sieve-plate column in which alternate plates are caused to rotate by a central power shaft.

The PRDC was constructed using a nominal 2-in i.d. Pyrex tube approximately 20 in in length. Short sections of Pyrex tubing which fit snugly inside the 20-in tube were used as spacers for holding the stators. Stators and rotating parts were of stainless steel. Details of the column construction are shown in Fig. 1. Spacers of different sizes for stators and for rotors were used to provide four stator compartment spacings, 0·5, 2·06, 3·0, 4·65 in, respectively. In each case, a rotor was located equidistant between two stators forming a compartment.

Perforations 1/4-in dia. were used on both rotors and stators. 63% of the stator and rotor area was hole area. Other possibilities for rotors design would use wire-spoked rims, thin circular wire brushes, or discs made from wire cloth.

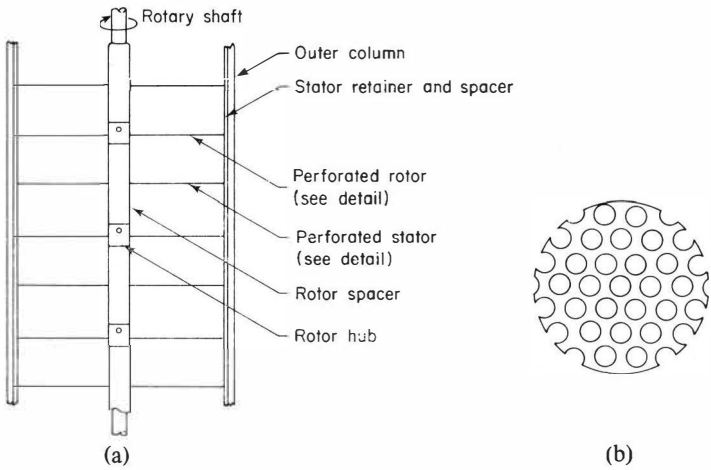

FIG. 1. *Detail of* (a) *perforated rotating disc extraction column and* (b) *disc perforation pattern*

Perforations : 1/4 in diameter; Free area : 0·63 of total; Stator diameter : 2·06 in; Rotor diameter : 1·8 in

The PRDC design, conceived by the first author, was first built and tested for capacity by Bennett[17] and was modified and tested by Su,[18] Reynolds[19] and Shah.[20] Fig. 2 is a schematic flow diagram of the PRDC system for movement of fluid, measurement and control of process variables. Auxiliaries for the extraction system as constructed by Williams[21] were of stainless steel.

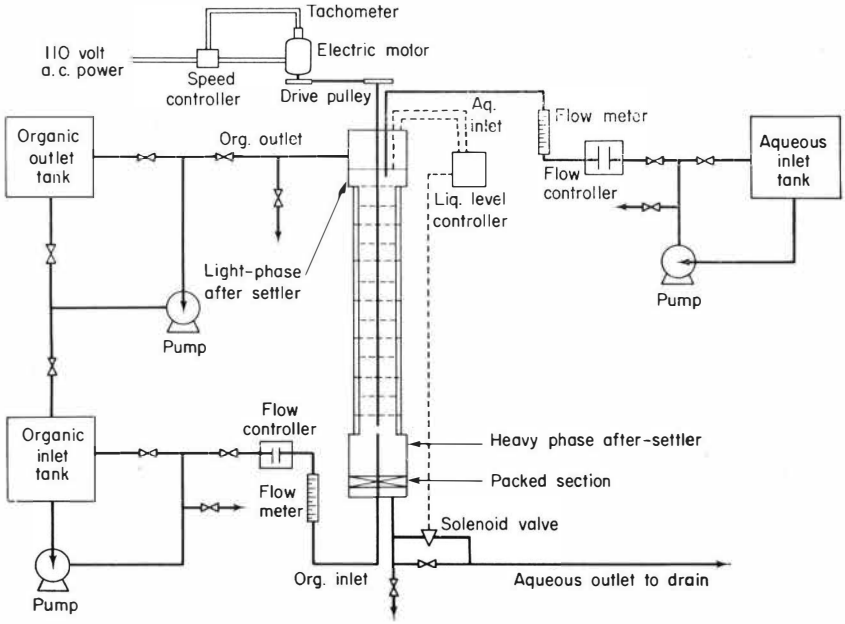

FIG. 2. *Schematic flow diagram of the extraction system for perforated rotating disc contactor*

The interface level in the light phase settler at the top of the column is maintained constant by use of a controller designed by Williams. A solenoid valve opens and closes in response to a conduction sensor which detects the aqueous interface. The organic and aqueous feed rates are controlled by M. F. Kates flow regulators and measured by Rotameters. A Clegg motor controller accurately regulates the speed of rotation.

No temperature control was required for the methyl isobutyl ketone–acetic acid–water solvent system used. Variations of temperature were found to be within 2°C.

Solvent system

Vermijs & Kramers[12] indicate the desirable characteristics of the methyl isobutyl ketone–acetic acid–water system for extraction studies. The wealth of data for other extraction equipment using MIBK–HOAc–H_2O, ease of analysis, stability against emulsion formation, and the distribution ratio between H_2O and MIBK for HOAc is near unity and the distribution coefficient is only weakly dependent on temperature or HOAc concentration.

Equilibrium distribution data for the MIBK–HOAc–H_2O system are taken from Fleming & Johnson[22] and Vermijs & Kramers.[12] The distribution coefficient varies between 0·468 for very dilute solution and 0·555 for concentrated solution, averaging 0·5 for the range in which this work was carried out.

Separation efficiency and capacity

The differential countercurrent contactor model illustrated in Fig. 3 is applied as is the usual case for all except mixer–settler types.

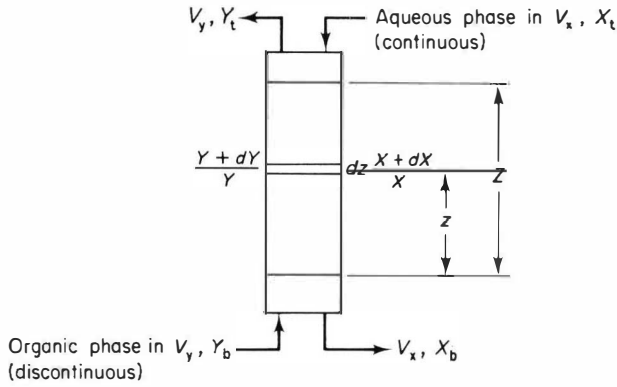

FIG. 3. *Differential contactor model*

Following the development of Treybal[23] the material balance for the element dz is:

$$V_X \mathrm{d}X = -V_Y \mathrm{d}Y \quad . \quad . \quad . \quad . \quad . \quad . \quad . \quad . \quad . \quad (1)$$

The balance assumes plug flow and for the tower height, Z, exclusive of ends, the overall material balance is:

$$V_X(X_b - X_t) = V_Y(Y_b - Y_t) \quad . \quad . \quad . \quad . \quad . \quad . \quad . \quad (2)$$

For the case where the phase ratio, V_X/V_Y, is 1 and the fresh solvent contains no solute, the material balance simplifies to:

$$X_b = Y_b - Y_t \quad . \quad . \quad . \quad . \quad . \quad . \quad . \quad . \quad . \quad (3)$$

The differential equation for rate of solute transfer is:

$$\mathrm{d}(V_Y \mathrm{d}Y) = K_Y a(Y - Y^*)\mathrm{d}z \quad . \quad . \quad . \quad . \quad . \quad . \quad . \quad (4)$$

Assuming dilute solutions leads to the expression for number of transfer units:

$$N_{OY} = K_{OY}\, a/V_Y \int_{z=0}^{z=Z} \mathrm{d}z = \int_{Y_t}^{Y_b} \frac{\mathrm{d}Y}{Y - Y^*} \quad . \quad . \quad . \quad . \quad (5)$$

The height of a transfer unit is then:

$$H_{OY} = N_{OY}/Z \quad . \quad . \quad . \quad . \quad . \quad . \quad . \quad . \quad . \quad (6)$$

N_{OY} can be calculated from measurable quantities and either H_{OY} or $K_{OY}a$ may be calculated.

Vermeulen *et al.*[24] summarise the importance of axial dispersion factors in clearly understanding column performance. For the present study, axial dispersion or backmixing was not measured specifically and overall column performance was measured using terminal X and Y values to obtain overall mass transfer coefficients and height of transfer units.

Both separation efficiency and capacity of an extractor are controlled by the size of the dispersed phase droplets. Hinze[25] has shown that in a two-phase

system being mixed, the drop size is determined by the energy input per unit mass of fluid as well as by the fluid properties and system geometry. For a given system it is a function of power input alone.

The power input of a stirrer given by Rushton & Oldshue[26] is:

$$P = f(\rho N^3 R^5) \quad (7)$$

The total mass between stators is:

$$M = \rho(\pi/4)\, D^2 H \quad (8)$$

and power unit mass is:

$$P/M = f(N^3 R^5/HD^2) \quad (9)$$

and the power number, N^3R^5/HD^2, which determines drop size, is an important function related to both separation efficiency and capacity. Reman *et al.*[10] have correlated capacity as:

$$V_X + V_Y = (Q_X + Q_Y)/S = f_1(N^3R^5/HD^2) \quad (10)$$

and separation efficiency as:

$$\frac{1}{H_{OY}} = f_2(N^3R^5/HD^2) \quad (11)$$

These same functions are used to correlate PRDC capacity and efficiency.

Mode of operation

With the light phase MIBK, as dispersed phase, droplets rise through the PRDC perforations forming new interfacial surface by the cutting and shearing action. West *et al.*[27] and Sherwood *et al.*[28] found that 20–40% of extraction occurs during the formation of drops, indicating the importance of new surface formation. The PRDC stators also cut and shear rising droplets which have radial momentum. They also act to prevent a general circular fluid motion and inhibit backmixing. In this latter respect, the stators are better than vertical, baffles.

Results

Capacity data

Flooding is defined as a condition in which the upward flow of light phase is blocked so that accumulation of light phase below a plate is increasing with time. The flooding phenomena may also occur with the heavy phase above the plate. If flooding is allowed to continue, light phase is carried from the bottom

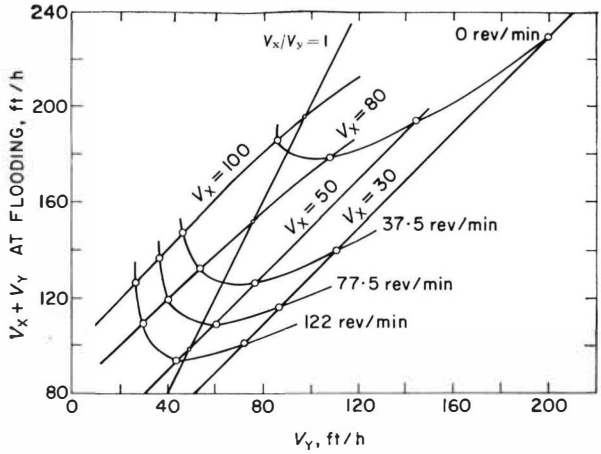

FIG. 4. *PRDC capacity at 0·5 in stator spacing*

or heavy phase from the top of the column. A stable extractor must operate below the flooding point.

Of the variables affecting flooding, or PRDC capacity, rotor speed, plate spacing, continuous and discontinuous flow rates were measured. Fig. 4 shows PRDC flooding curves for 0·5-in stator spacing at various rotor speeds in rev/min, continuous phase superficial velocity, V_X, and discontinuous phase superficial velocity, V_Y. Similar data were collected for stator spacings of 2·06, 3·0, and 4·65 in. All runs for flooding point were taken with acetic acid present in the feed; hence with mass transfer occurring. In each case, as shown in Fig. 4, the limiting total flow rate or total superficial velocity for a constant flow rate occurred at a phase ratio, V_X/V_Y, of unity.

The data for capacity are plotted in Fig. 5 as $V_X + V_Y$ at flooding vs. the power number for 4 stator spacings and several rotor speeds.

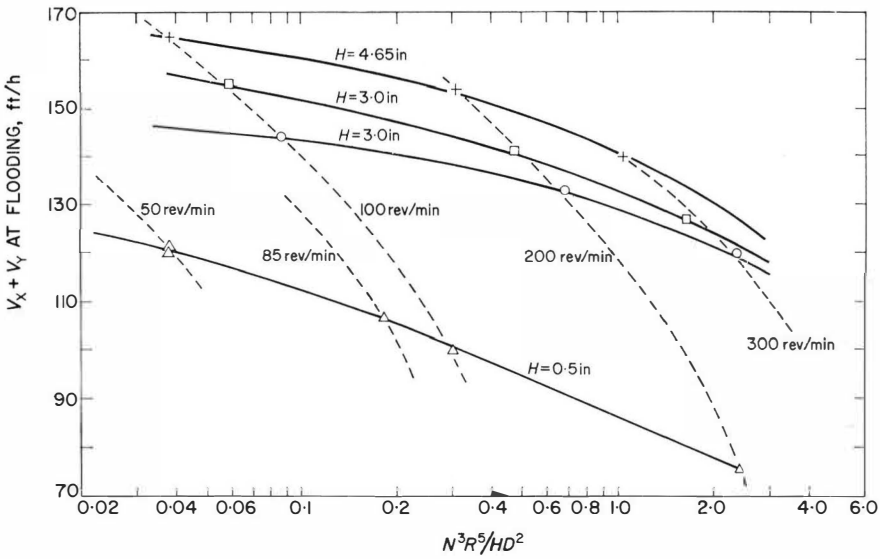

FIG. 5. *PRDC capacity vs. power number*

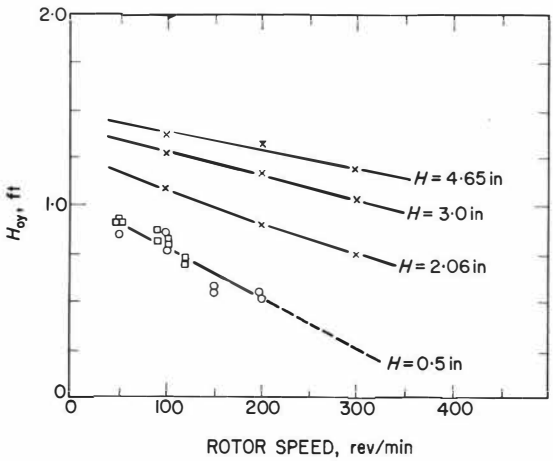

FIG. 6. *PRDC, influence of rotor speed and stator on* H_{OY}

○ Reynolds;[19] □ Su;[18] × Shah[20]

Separation efficiency

In each experiment, terminal concentrations of acid, X_b, Y_b, Y_t, were determined by titration. The inlet continuous heavy phase was water, $X_t = 0$. Inlet light phase of MIBK acetic acid concentration was as high as 5 wt.-%, but most runs were made at 1%. Runs were discarded for which the overall material balance error exceeded 2·5%. Of 42 runs, 85% checked within 1·5% error.

The separation data are shown in Fig. 6 which shows H_{OY} values for 42 individual runs at various rotor speeds and stator spacings.

The experimental data are summarised in Table I. The $V_X + V_Y$ values shown are taken at flooding for a particular rotor speed and stator spacing. The corresponding tabulated values of H_{OY} are average values for the 2 or 3 runs made at the given rotor speed and plate spacing.

Fig. 7 shows the limited effect of total throughput on H_{OY} and Fig. 8 correlates H_{OY} as a function of power number. The term $1/H_{OY}$ is sometimes termed separation efficiency.

TABLE I

Experimental results summary

Stator spacing, in	Rotor speed, rev/min	$V_X + V_Y$ at flooding, ft/h	H_{OY}, ft	$1/H_{OY}$, ft^{-1}	N^3R^5/HD^2, ft^2/sec^3	Reference
0·5	0	180				Su[18] and Reynolds[19]
0·5	50	121	0·86	1·16	0·038	,,
0·5	85	107	0·80	1·25	0·186	,,
0·5	100	100	0·76	1·32	0·304	,,
0·5	200	76	0·51	1·96	2·44	,,
2·06	100	144	1·12	0·89	0·086	Shah[21]
2·06	200	133	0·89	1·12	0·682	,,
2·06	300	120	0·77	1·30	2·37	,,
3·0	100	155	1·27	0·79	0·059	,,
3·0	200	141	1·17	0·86	0·470	,,
3·0	300	127	1·04	0·93	1·63	,,
4·65	100	165	1·37	0·73	0·038	,,
4·65	200	154	1·30	0·77	0·302	,,
4·65	300	140	1·18	0·85	1·025	,,

$V_X/V_Y = 1·0$ for all runs

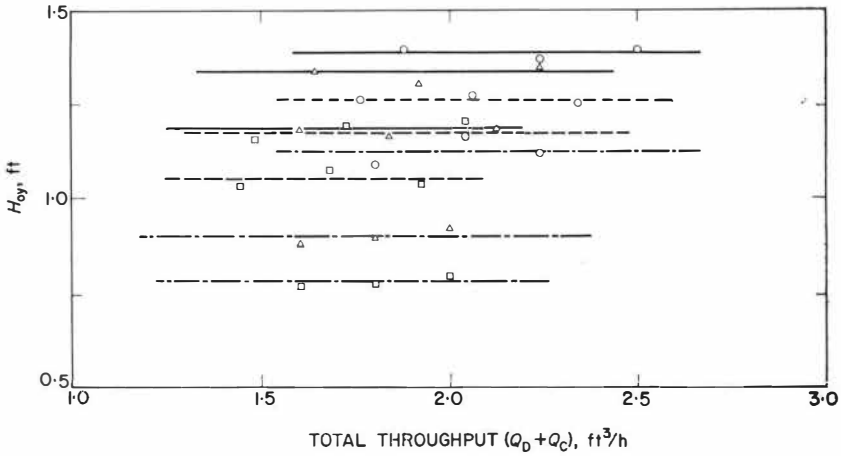

FIG. 7. *Variation of* H_{OY} *with total throughput for PRDC*

— plate spacing 4·65 in; - - - plate spacing 3·0 in;
— - — - — plate spacing 2·06 in;
○ 100 rev/min; △ 200 rev/min; □ 300 rev/min

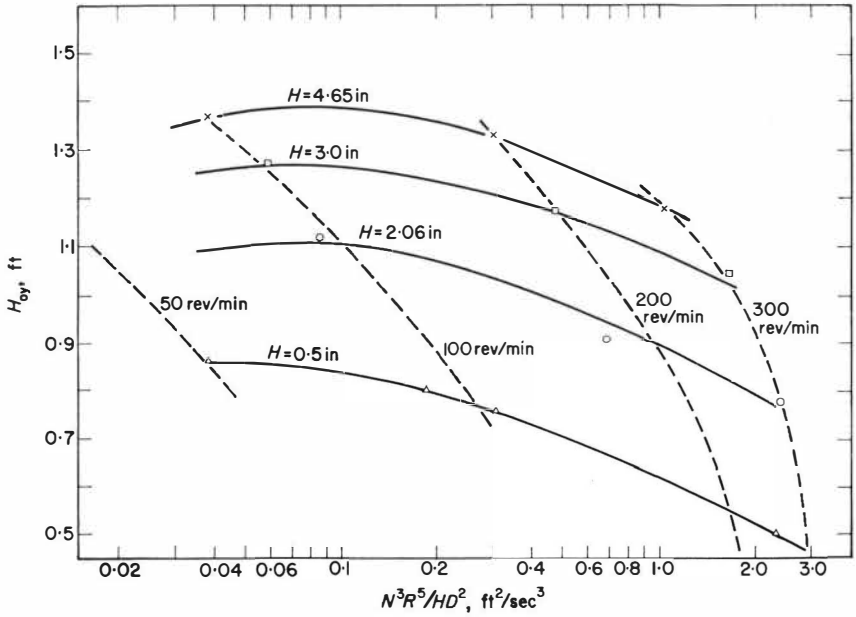

FIG. 8. H_{OY} *vs. power number for the PRDC*

Discussion

Column capacity

The data of Figs 4 and 5 show the results as predicted with capacity increasing with stator spacing and decreasing with rotor speed. In the power number region, $N^3R^5/HD^2 < 1$, an increase in power has a rather small effect on capacity. The relative effect is more pronounced at small stator spacing. In the region $N^3R^5/HD^2 > 1$, the capacity drops more rapidly with a comparable change in power number. It appears that 300 rev/min would be too high a speed for 0·5-in spacing and that much higher speeds would not be recommended for the subject column at any stator spacing.

Of the various parameters affecting capacity, only rotor speed and stator spacing have been tested. Experiments should be extended to include such variables as tower diameter, stator and rotor design, and tower height. The work of Reman[9] and others indicates the types or correlations to be expected for rotary disc extractors. For the PRDC, the experiment must as yet fill in the empirical constants because of the complicated hydrodynamics.

Separation efficiency

Values of the height of a transfer unit based on the discontinuous phase overall driving force are given in Fig. 6 for the range of rotor speeds, 50 to 300 rev/min, and stator spacings of 0·5 to 4·65 in. It is interesting to note from Fig. 7 that total throughput at a phase ratio of unity has very little effect upon H_{OY}. The merit of height of a transfer unit in design is apparent.

Fig. 8 is a plot of the data of Table I, H_{OY} versus power number with rotor speed and stator spacing as parameters. The curves of constant plate spacing are suprising in that H_{OY} for any stator spacing seems to pass through a maximum as power number increases except for 2·06-in spacing. A curve for this spacing consistent with the other three curves has been drawn on Fig. 8. The same data are shown in Fig. 9 except that H_{OY} is replaced with $1/H_{OY}$ as a measure of separation efficiency.

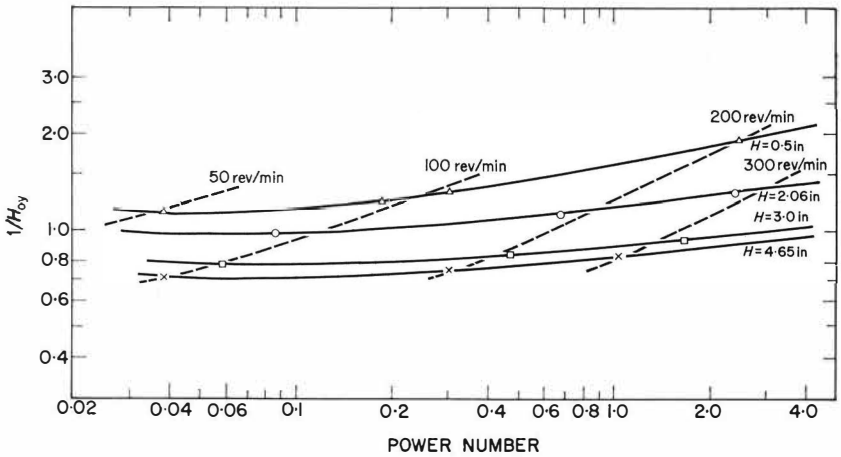

FIG. 9. *PRDC separation efficiency,* $1/H_{OX}$, *vs. power number for the PRDC*

Comparing H_{OY} values for the PRDC with Vermijs & Kramer's data,[12] values of H_{OY} for the RDC are higher until the rotor speed reaches 1800 rev/min. There is a distinct advantage in operating large rotating equipment at low speeds, not only to avoid mechanical complications, but to avoid emulsion formation. Photographic studies of the PRDC have shown that as rotor speeds increase, the droplets become smaller, but haze in the continuous phase does not form; also that the drop size is rather uniform from the bottom to top of the columns.

Effectiveness index

A combination of capacity and separation efficiency is more suitable for comparing various extraction devices than either of these factors considered separately. Reman has suggested an 'Index of Effectiveness' as the total throughput per volume of one theoretical stage.

$$I_e = \frac{\text{Total throughput}}{\text{Volume of one theoretical stage}}$$

$$= (Q_X + Q_Y)(HETS)(S)\ \text{min}^{-1}$$

$$\text{or} \quad (V_X + V_Y)/((HETS) \quad . \quad . \quad . \quad . \quad . \quad . \quad . \quad . \quad (12)$$

In the present work with dilute solutions, the H_{OY} values are used for calculation of the volume of a theoretical stage.

A comparison is made in Table II of I_e for a Scheibel column, an RDC and the PRDC for the MIBK–acetic acid–water system, for the same direction of mass transfer, with MIBK as the dispersed phase, with water as the solvent, with various acetic acid concentrations and with various speeds of rotation. The data other than the subject study are taken from Vermijs & Kramers.[12]

The PRDC appears to be a most efficient device, comparing very favourably with other high efficiency devices. Neither design nor operation have been optimised and changes in this direction may increase the capacity and efficiency even more.

TABLE II

Comparison of effectiveness of different types of equipment

Type of column	Acid content in feed, wt.-%	Rotor speed, rev/min	Column i.d., m	*HETS*, m	$V_Y + V_X = Q/S$ m³/sec (m²)	Effectiveness index, I_e, min⁻¹
Scheibel[12]	15–20	693	0·287	0·32	0·48	1·5
RDC						
Vermijs[12]	3–5	1200	0·041	0·21	0·399	1·9
Vermijs[12]	3–5	1800	0·041	0·21	0·673	3·2
Vermijs[12]	3–5	1200	0·041	0·25	0·4	1·6
Vermijs[12]	3–5	1800	0·041	0·19	0·399	2·1
Vermijs[12]	3–5	1800	0·041	0·21	0·399	1·9
PRDC						
Su[18]	0·6–0·8	50	0·0507	0·276	0·582	2·14
Su[18]	0·6–0·8	85	0·0507	0·254	0·528	2·08
Su[18]	0·6–0·8	100	0·0507	0·243	0·515	2·12
Su[18]	0·6–0·8	120	0·0507	0·217	0·495	2·28
Su[18]	0·6–0·8	37·5	0·0507	0·278	0·637	2·29
Su[18]	0·6–0·8	77·5	0·0507	0·263	0·564	2·14
Su[18]	0·6–0·8	122·5	0·0507	0·199	0·484	2·43
Reynolds[19]	1·0–1·5	50	0·0507	0·261	0·672	2·57
Reynolds[19]	1·0–1·5	77	0·0507	0·258	0·532	2·06
Reynolds[19]	1·0–1·5	100	0·0507	0·248	0·442	1·78
Reynolds[19]	1·0–1·5	122	0·0507	0·198	0·372	1·88
Reynolds[19]	1·0–1·5	150	0·0507	0·171	0·356	2·08
Reynolds[19]	1·0–1·5	170	0·0507	0·165	0·337	2·04
Reynolds[19]	1·0–1·5	200	0·0507	0·162	0·303	1·87
Shah[20]	0·9–1·5	100	0·0472	0·341	0·726	2·13
Shah[20]	0·9–1·5	200	0·0472	0·274	0·67	2·44
Shah[20]	0·9–1·5	300	0·0472	0·238	0·604	2·54
Shah[20]	0·9–1·5	100	0·0472	0·384	0·791	2·06
Shah[20]	0·9–1·5	200	0·0472	0·357	0·725	2·03
Shah[20]	0·9–1·5	300	0·0472	0·32	0·64	2·0
Shah[20]	0·9–1·5	100	0·0472	0·422	0·835	1·98
Shah[20]	0·9–1·5	200	0·0472	0·406	0·775	1·91
Shah[20]	0·9–1·5	300	0·0472	0·359	0·7	1·95

Conclusions

A new PRDC liquid–liquid extraction device has shown excellent operating characteristics and high performance in terms of 'Index of Effectiveness' as compared to other highly efficient devices.

Capacity and height transfer unit have been measured and correlated for the MIBK–acetic acid–H_2O system for limited variables. The correlations indicate other variables, which should be tested.

The low H_{OY} values plus high capacity of the PRDC are indications that the objectives of high shear with minimum backmixing are achieved. The results are so promising that further research on optimisation of design should be continued.

Nomenclature

a	interfacial area, ft^2/ft^3
D	internal column diameter, ft
H	stator spacing, ft
$HETS$	height equivalent to a theoretical stage, ft
H_{OY}	overall height of a transfer unit based on discontinuous phase, ft
I_e	index of effectiveness $= Q_X + Q_Y/(HETS)(S)$
$K_{OY}a$	overall mass transfer coefficient based on discontinuous phase, ft^3/sec
N	rotor speed, rev/min
N_{OY}	number of transfer units based on discontinuous phase, ft
P	power number $= N^3R^5/(HD^2)$ $ft^2/_{sec}{}^3$
Q	total flow rate, ft^3/h
Q_X	flow rate, continuous phase, ft^3/h
Q_Y	flow rate, discontinuous phase, ft^3/h
R	rotor diameter, ft
S	column cross-sectional area, ft^2
V	superficial velocity $=$ Q/S, ft/h
V_X	superficial velocity of continuous phase $= Q_X/S$, ft/h
V_Y	superficial velocity of discontinuous phase $= Q_Y/S$, ft/h
X	concentration of solute in continuous phase, $lb\text{-}mole/ft^3$
Y	concentration of solute in discontinuous phase, $lb\text{-}mole/ft^3$
z	distance from bottom of column, ft (exclusive of ends)
Z	column total height, ft (exclusive of ends)

Subscripts

b	bottom
t	top
o	overall
X	continuous phase
Y	discontinuous phase

References

[1] Treybal, R. E., *Chem. Engng Prog.*, 1966, **62,** 67
[2] Karr, A. E., *A.I.Ch.E. Jl*, 1959, **5,** 446
[3] Scheibel, E. G., *A.I.Ch.E. Jl*, 1956, **2,** 74
[4] Treybal, R. E., *Chem. Engng Prog.*, 1964, **60,** 77
[5] Akell, R. B., *Chem. Engng Prog.*, 1966, **62,** 50
[6] Reman, G. H., *Chem. Engng Prog.*, 1966, **62,** 56
[7] Reman, G. H., U.S. P. 2,601,674
[8] Reman, G. H., *Proc. 3rd Wld Petrol. Congr.*, 1951, Section III, 2
[9] Reman, G. H., & Olney, R. B., *Chem. Engng Prog.*, 1955, **51,** 141
[10] Reman, G. H., & Van de Vusse, *Petrol. Refiner*, 1955, **34,** 209
[11] Reman, G. H., *Petrol. Refiner*, 1957, **36,** 269
[12] Vermijs, H. J. A., & Kramers, H. A., *Chem. Engng Sci.*, 1954, **3,** 55
[13] Kung, E. V., & Backman, R. B., *A.I.Ch.E. Jl*, 1961, **7,** 319
[14] Logsdail, D. H., Thornton, J. D., & Pratt, H. R. C., *Trans. Instn chem. Engrs*, 1957, **35,** 301

[15] Krishnaiah, M. M., Pai, M. U., Ramana Rao, N. V., & Sastri, S. R. S., *Br. chem. Engng*, 1967, **12,** 719
[16] Thomas, W. J., *Trans. Instn chem. Engrs*, 1969, **47,** 304
[17] Bennett, C. D., B.S. Thesis, 1964, Provo, Utah, Brigham Young University (unpublished)
[18] Su, M. S., M.S. Thesis, 1965, Provo, Utah, Brigham Young University (unpublished)
[19] Reynolds, M. B., B.S. Thesis, 1966, Provo, Utah, Brigham Young University (unpublished)
[20] Shah, N. R., M.S. Thesis, 1970, Provo, Utah, Brigham Young University (unpublished)
[21] Williams, G. L., M.S. Thesis, 1964, Provo, Utah, Brigham Young University
[22] Fleming, J. F., & Johnson, H. F., *Chem. Engng Prog.*, 1953, **49,** 497
[23] Treybal, R. E., 'Liquid extraction', 2nd Edn, 1963 (New York: McGraw-Hill)
[24] Vermeulen, T., Moon, A., Hennico, A., & Miyauchi, T., *Chem. Engng Prog.*, 1966, **62,** 95
[25] Hinze, J. D., *A.I.Ch.E. Jl*, 1955, **1,** 219
[26] Rushton, J. H., & Oldshue, J. Y., *Chem. Engng Prog.*, 1953, **49,** 167
[27] West, F. B., Robinson, P. A., Morganthaler, A. C., Beck, T. R., & McGreggor, D. K., *Ind. Engng Chem.*, 1951, **43,** 234
[28] Sherwood, T. K., Evans, J. E., & Longcor, J. O. A., *Ind. Engng Chem.*, 1939, **31,** 1144

Axial mixing and classification phenomena in liquid–liquid fluid beds

by J.-B. Wijffels and K. Rietema
Eindhoven University of Technology, The Netherlands

Experiments were carried out with a 6 m long laboratory fluid bed of 5 cm diameter. Light organic liquids were used as the dispersed phase and doubly distilled water as the continuous phase of the droplet bed. Density differences between continuous and dispersed phase were less than 300 kgm^{-3} and droplet Reynolds numbers were greater than 100 for all cases investigated. The hydrostatic pressure profile and the droplet size distribution at different heights in the bed were measured as well as the overall residence time distribution of the continuous phase.

Fluidisation characteristics of the droplet bed were investigated. Interparticle diffusion and classification phenomena in the dispersed phase were studied. The effective axial mixing coefficient of the continuous phase was calculated from the measured residence time distribution.

Introduction

FLUIDISED BEDS BRING a continuous phase in contact with a dispersed phase, which is free to move in the bed. The motion of the continuous phase agitates the dispersed phase particles and by counteracting gravity keeps them 'weightless' in a floating state; this phenomenon is called fluidisation. Fluidised beds are used as contacting equipment or as reactors. Gas–solid fluidised beds are most frequently employed, but liquid–liquid and liquid–solid beds are also used. In gas–solid fluidised beds, often fluidisation is not homogeneous with the formation of large 'bubbles' of continuous phase which rise through the otherwise homogeneous dispersion. This phenomenon is less common in liquid–solid fluidised beds and fluidised beds of particles with a density less than that of the continuous phase are reported to be fluidised homogeneously.[1] In the present work the discussion is limited to beds in which the dispersed phase is fluidised with water and has a density similar to that of water.

Despite the fact that numerous investigators have studied fluidised beds, there is considerable disagreement with respect to the mechanics of fluidisation resulting in many empirical correlations. Two approaches are used; one group follows a hydrodynamic approach, the other a thermodynamic one. The performance of a fluidised bed is described by the relation that exists between the volume fraction of the continuous phase, the porosity and the slip velocity between the phases, i.e. the velocity of the continuous phase with respect to the dispersed phase.

In the hydrodynamic treatment, the porosity *versus* slip velocity relation is regarded as a drag equation analogous to the Ergun equations for the packed bed. Drag forces in a hydraulic model of a fluidised bed were investigated by Rowe & Henwood[3,4] and by Gunn & Malik[5]. By comparing the results from the model with the fluidised bed, Gunn & Malik concluded that for particles with Reynolds numbers of less than 1000, aggregates of particles occurred in the fluidised bed. Direct information about the structure of liquid fluidised beds was obtained by Ryan *et al.*[6] by a photographic technique. The existence of preferential paths in liquid dispersions was shown by Couderc & Angelino,[7] but they concluded that this phenomenon was not inherent to liquid fluidisation.

The mechanics of sedimentation and particulate fluidisation were studied by numerous authors. The sedimentation of particles under conditions of laminar flow was investigated by Steinour[8]. In addition, Tarján[9] studied coarse dispersion with turbulent conditions. Semi-empirical relations for fluidisation were obtained.[1, 10–12] Richardson & Zaki[10] simply equated the ratio of the slip velocity of the particles to the slip velocity at infinite dilution to some power of the porosity and obtained a convenient expression. Considerations based on the theory of turbulence were applied by Kolář[13] and Musil & Prochazka.[14]

Also, many contributions were made by Lapidus *et al.*[15–19] They established a formal relationship between fluidisation and sedimentation on the basis of the slip velocity–porosity relation, which was called 'the equation of state' of the dispersion.

The thermodynamic approach was developed by Furukawa & Ohmae[20] by analogy with liquid systems. They assumed that the particles were subjected to an oscillatory motion and they established an equation for the mean kinetic energy of the particles. According to Hetzler & Williams,[21] the fluidising medium in the bed functioned as an 'ether' which, unlike the classical ether, had both density and viscosity. These properties allowed the ether to transmit energy to the particles and led to interpretation of the fluidising velocity as a function of the temperature. These authors attempted to characterise the liquid-like properties of a fluidised system by studying expansion, viscosity, surface tension and miscibility, and the effect of temperature on these properties.

Schügerl *et al.*[22] used a similar model to interpret the effective viscosity measured in fluidised beds. Coeuret *et al.*[23] drew an analogy with a van der Waals gas. Ruckenstein[24] pointed out that the thermodynamic approach had limitations in so far that no information could be obtained concerning those physical properties of the fluidised bed which were directly dependent on the properties and flow condition of the fluidising agent.

Special aspects of fluidised bed operation were discussed by a number of authors. For instance, the scaling-up of a liquid fluidised bed was considered by Klier & Vogel[25] and Neužil[26] investigated the effect of the walls on the expansion. The flow from holes in the sides of vessels containing liquid fluidised beds was studied by Massimilla *et al.*[27] and the drop in pressure over semi-fluidised beds was measured by Fan & Wen.[28] The mechanics of three phase liquid–solid–gas systems were discussed by several workers.[29–32] The interesting paradox for liquid beds which contracted (instead of expanded as might be expected), when a gas flow was added to the liquid flow, was explained by the fact that the liquid by-passed the bed in the wake of the rapidly rising gas bubbles.

Surface dynamics were discussed by Rice & Wilhelm,[33] and the dynamic expansion was studied.[34–36] General stability was investigated by Jackson,[37] Pigford & Baron[38], Murray[39] and Molerus.[40] The occurrence of bubbles was treated by Harrison, Davidson & de Kok[41] and by Anderson & Jackson.[42] Also, work was carried out to study the propagation of kinematic density waves.[43–46]

Turbulent diffusion in fluidised beds was investigated by Hanratty *et al.*[47]; this work was based on an original treatment made by Taylor[48] who studied the diffusion by continuous movements. A statistical model analogous to that for a packed bed was used by Cairns & Prausnitz [49,50] to explain longitudinal mixing in the liquid phase. Kramers, *et al.*[51] concluded that the coefficient of longitudinal dispersion in the liquid phase was composed of two components, one of which was analogous to dispersion in a fixed bed and another was due to porosity fluctuations. A theoretical model for this phenomenon was proposed.[52] Eddy diffusivities for a large scale unit were reported by Bruinzeel, *et al.*[53] and a macroscopic model for mixing processes was described by Schügerl.[54] A comparison of various results obtained for longitudinal dispersion in the liquid was made and a generalised correlation applicable to both fixed and fluid bed was also proposed.[55]

Classification according to size of fluidised particles was much investigated,[58] which resulted in an expression for the particle size distribution being derived. Some useful methods for the determination of particle size were described by Coughlin & von Berg,[59] by Collier & Hewitt[60] and by van Heuven.[61] The forces exerted on individual spheres in liquid fluidised beds were measured by Bicknell & Whitmore.[62] Tracer particle motion was observed by Handley *et al.*[63] and individual particle velocities were measured in connection with the measurement of axial mixing coefficient.[64]

In this work a phenomenological treatment of the liquid fluidised bed is made. Classification phenomena as well as axial dispersion in continuous and dispersed phase are considered.

Experimental

General

A fluid bed is characterised by the absence of net transport of the dispersed phase, although the continuous phase flows without interruption through the apparatus. This phenomenon is due to the fact that, whenever density of the dispersed phase differs from the density of the continuous phase, the dispersed phase particles reach a certain velocity with respect to the continuous phase under influence of gravity. If the linear velocity of the continuous phase is equal in magnitude and oppositely directed to the difference in velocity averaged over the dispersed phase particles, the superficial velocity of dispersed phase equals zero and the dispersed phase is quasi-stationary in the bed. To bring this about and to distribute the continuous phase uniformly over the cross section, the bed has a sinter plate at the beginning of the continuous phase that is impermeable to the dispersed phase, but open to the continuous phase although at the cost of a considerable drop in the pressure. At the other end, where the continuous phase leaves the bed, the bed is open and a natural interface between dispersion and continuous phase is formed.

Experiments were carried out with dispersions which consisted of doubly distilled water as continuous phase and coarse droplets as dispersed phase. A number of organic liquid mixtures with densities of less than that of water were used as the dispersed phase. In the droplet bed used, distilled water flowed from the top of the bed to the bottom. For all experiments the densities of the continuous and the dispersed phase were of the same order of magnitude, the droplets being between 1 mm and 1 cm in diameter. Experiments were performed at constant ambient temperature. The droplet bed containing light organic liquids as dispersed phase exhibited homogeneous fluidisation for all values of the fluidisation velocities. Smooth homogeneous beds of 6 m length were established without difficulty.

Droplet bed

The droplet bed is shown in Fig. 1. The body of the bed (1) consists of a 'Quick Fit' glass cylinder of 2 in inner diameter and a total length of 6 m. The cylinder is built up by aligning four 1·5 m sections. At the top, the column is closed by two glass sinter plates (2) type zero, each fitted in a short glass cylinder of the same inner diameter as the bed body. A 0·5 m pressure chamber (3), with the same diameter, is situated at the top of the column. Distilled water is fed from a feed vessel (4) with a volume of about 30 l to the pressure chamber via a flowmeter (F) using a centrifugal pump. The flow rate of the continuous phase can be varied by changing the power supplied to the pump (8) and by using a by-pass (9) over the pump. The continuous phase leaves the column at the bottom (10) via a 2 in pipe and enters a separator (5) where entrained droplets, if any, are separated and then collected (6). From the separator, the continuous phase flows back into the feed vessel and thus circulates in a closed circuit. The bed itself is operated slightly above atmospheric pressure to prevent air from leaking into the system. Initially, the organic phase is let in, flowing by its weight from the supply vessel (11), which is situated approximately 2 m higher than the top of the bed, while the continuous phase is already circulating. Upon entering the bed the dispersed phase breaks up in droplets of arbitrary size. The dispersed phase inlet is closed as soon as the desired amount is present in the bed. The dispersed phase can be recovered at the completion of the experiment via the dispersed phase outlet (12), which consisted of a 5 mm diameter glass pipe with one end fused in the lowest sinter plate.

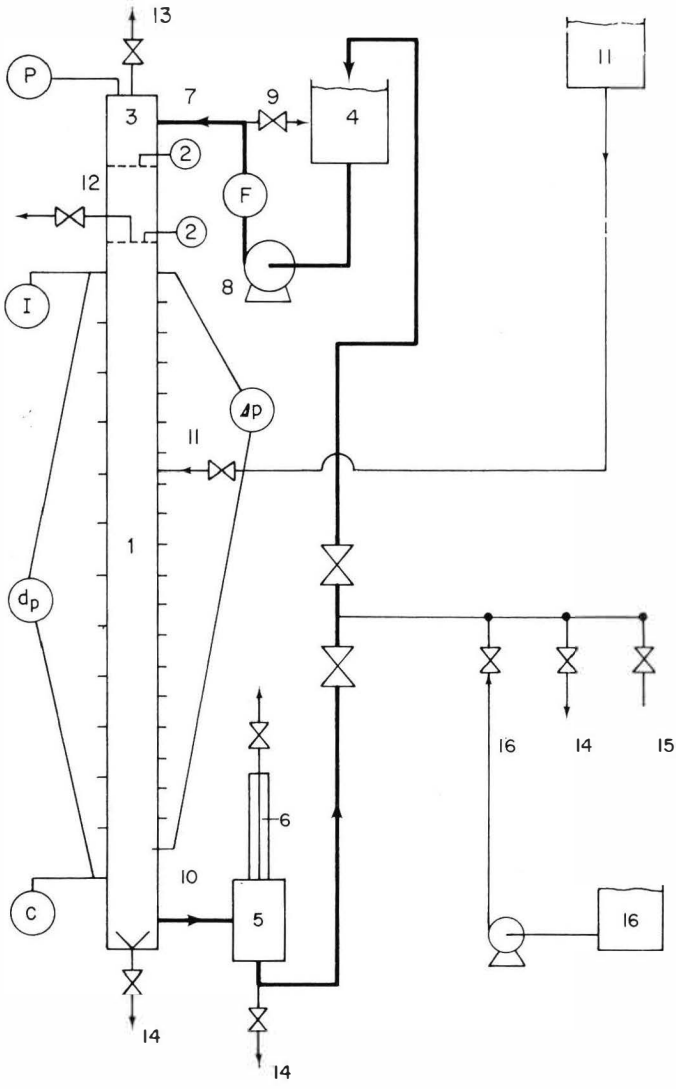

FIG. 1. *Droplet bed*

Furthermore, the bed is supplied with an air vent (13) and the necessary drains (14). The continuous phase circuit is connected with the tap water supply (15) and a supply vessel of distilled water (16). The bed is equipped with a number of instruments for measurement. The pressure chamber is supplied with a manometer (P); the bed body itself has 20 welded connections 30 cm apart with 19 difference manometers by (Δp) which the pressure in the bed could be determined. The same liquid as the dispersed phase is used as manometer liquid. Also, the bed body is equipped with 12 welded connections 50 cm apart, each of which is connected to a capillary tube for the measurement of the drop size distribution(d_p). Tracer can be added to the continuous phase at the top of the bed(I) and also coloured droplets can be introduced into the bed. The residence time distribution is measured by means of a number of electrodes installed at the bottom of the bed for the measurement of the conductivity of the continuous phase. To enable measurement of the migration of tracer droplets through the dispersion, a coordinate meter is

mounted beside the column. The droplet bed is mounted in a stainless steel rack unit.

Measurements

A number of experiments were performed with the droplet bed to determine the characteristics of liquid–liquid fluidisation and the dispersion processes occurring in both phases. For all droplet bed experiments distilled water was used as the continuous phase. For eighteen experiments, experiment nos. 1–6 and 8–19 benzene with a density of 879 kg m^{-3} were used as the droplet phase. Five experiments were performed with cyclohexane with a density of 779 kg m^{-3}, no. 20–24, and four with a cyclohexane–carbon tetrachloride mixture with a density of 940 kg m^{-3}, no. 25–28.

During each experiment the hydrostatic pressure at twenty different heights in the bed, the droplet size distribution at eleven different heights in the bed, the drunkard's random walk trajectory of a tracer droplet at approximately two meters below the top, and the overall residence time distribution of the continous phase, were measured.

The experiment was started by introducing the dispersed phase into the bed in which water was already flowing downwards at a constant rate. After the introduction of the required amount of dispersed phase, the water flow was adjusted and the bed was left for more than an hour with the continuous phase recirculating at a constant rate. A quasi-steady state was rapidly reached, due to the apparent absence of coalescence and redispersion phenomena for all but the highest flow rates of the fluidising agent, the continuous water phase. Some redispersion, however, was always taking place at the top of the bed underneath the glass sinter plate and therefore the bed was always disintegrating to some extent, however small, due to the entrainment of fines by the continuous phase. For moderate fluidisation velocities, droplet beds were operated for more than ten hours without the loss of more than a few percent of their dispersed phase holdup. After the quasi-steady state was reached, coloured droplets were injected into the bed. These droplets were clearly visible in the colourless bed and their trajectories were measured by means of a co-ordinate meter. Directly after, an extremely dilute salt solution was injected at the top of the column in order to determine the residence time distribution of the continuous phase. Next, the pressure difference manometer was read and immediately afterwards the droplet samples were taken. This last measurement destroyed the bed.

Porosity measurement

Under the experimental conditions, the wall friction of the continuous phase and the change in kinetic energy due to the gradual change in porosity over the height of the bed were negligibly small, so that the hydrostatic pressure difference over a 30 cm high section of the bed was equal to the apparent weight of that section of the bed. Because the liquid which was present in the bed as dispersed phase was also used as manometer liquid, the ratio of the difference in height of manometer liquid to the difference in height of the pressure connections was equal to the fraction of the dispersed phase in the bed. In order to eliminate errors due to misreading or malfunctioning of individual manometer legs, the manometer readings were fed into a computer and a third degree interpolation polynomial was determined using a least-square-error approach with Forsythe's method applying polynomials which are orthogonal under summation. By differentiating the interpolation polynomial the porosity can be found for any height in the bed. Some typical results are shown in Figs 2–4. The points indicated were determined by subtracting the manometer readings; the derivative of the interpolation polynomial is shown as the curve.

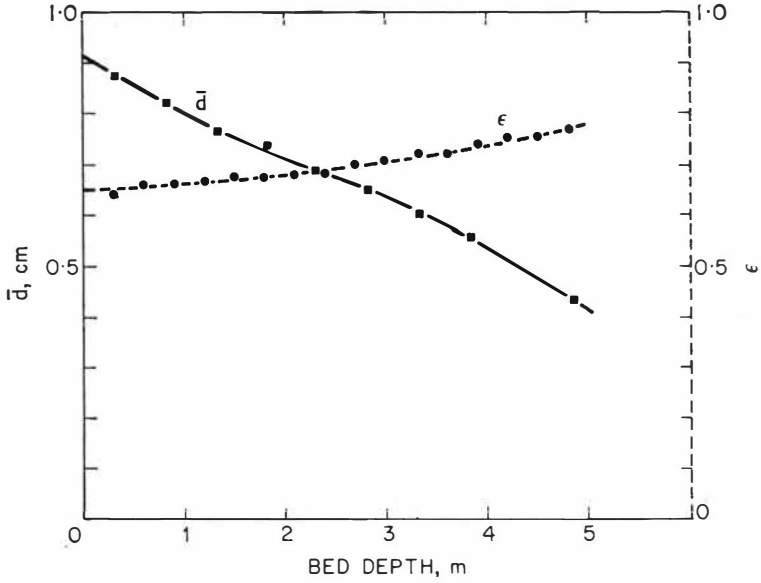

FIG. 2. *Average droplet diameter and porosity* versus *depth in the fluidised bed*
Experiment 1, benzene dispersed phase

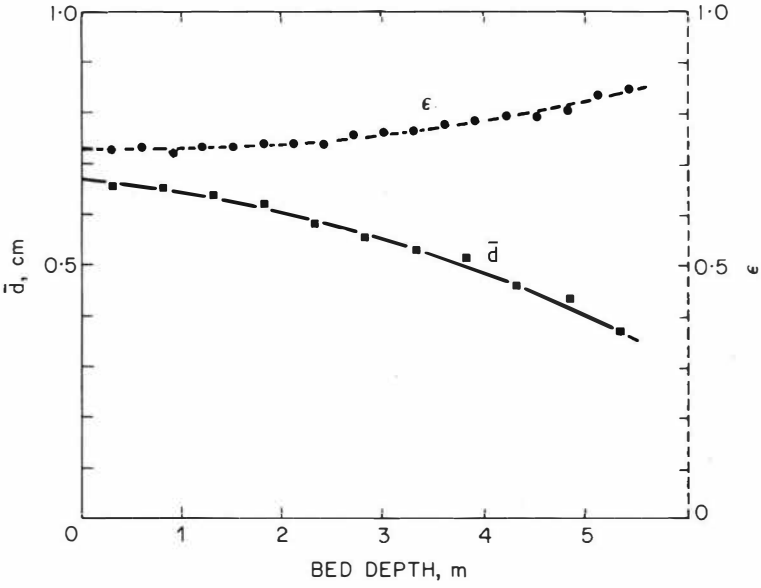

FIG. 3. *Average droplet diameter and porosity* versus *depth in the fluidised bed*
Experiment 21; cyclohexane dispersed phase

Droplet size distribution measurement

In order to determine the droplet size distribution, large samples of the dispersion were taken from the column at eleven different heights. The measurement points were provided with tubes of varying diameter. On the side where the connexion with the column was made, the tubes had an inner diameter of about 1·5 cm, while on the other side they were welded to a capillary, which was part of the measuring device. As soon as a restriction at the end of the

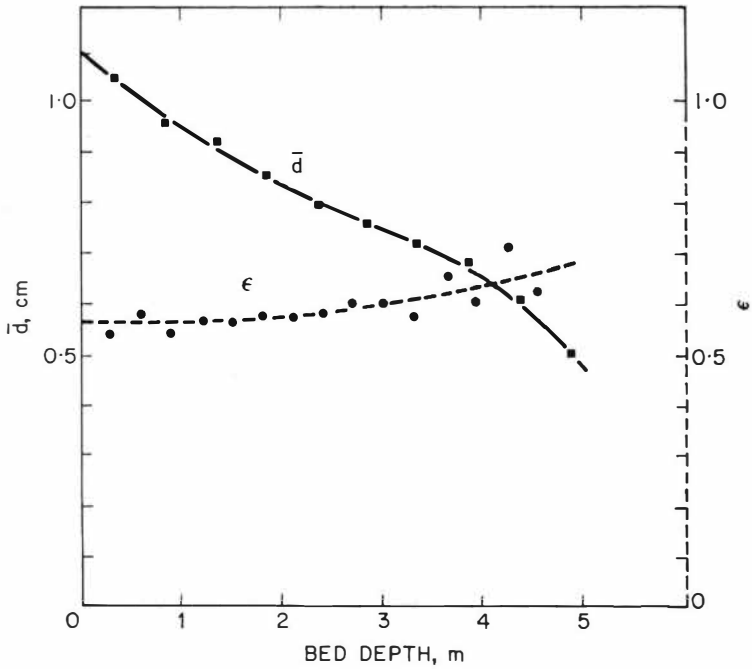

FIG. 4. *Average droplet diameter and porosity* versus *depth in the fluidised bed*
Experiment 27; cyclohexane–carbon tetrachloride dispersed phase

capillary tube was opened the dispersion started to flow through the tube due to the pressure in the column. As a result of the narrowing of the tube, the droplets were deformed and moved as plugs one after the other through the capillary. Hardly any interaction took place between neighbouring droplets in the tube, only a very small percentage were coalesced before they were measured in the capillary. The capillary itself was placed in a light beam, which, after it had passed through the capillary, excited a photosensitive diode (Fig. 5). The light beam was adjusted in such a way that it was deflected as soon as a dispersed phase plug moved in front of it and, as a consequence, the diode was darkened. The diode was connected to the measurement circuit as one arm of a four-arm direct current Wheatstone bridge so as to unbalance the bridge circuit when its resistance was changed as a result of a variation in the intensity of light that reached the diode. The bridge voltage was registered by a datalogger.

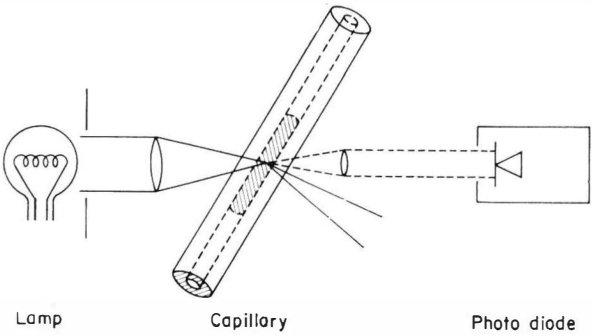

FIG. 5. *Droplet size measurement system*

Measurement was started by taking a sample from the lowest capillary, situated about 5·3 m below the glass sinter plate. The next sample was taken from the capillary directly above it and then in sequence from the other capillaries which were 50 cm apart, up to the capillary, which was situated 0·3 m below the top of the bed. Samples were taken at a flow rate of about 80 cm^3 min^{-1} for a period of one and a half minutes, so that the total measurement was performed in about a quarter of an hour. The top six capillaries connected with the lower part of the bed, had an inner diameter of 2·1 mm and the next four capillaries, connected with the upper part of the bed, had an inner diameter of 2·5 mm, so that the Reynolds number for the flow through the capillaries at experimental conditions was about 750.

A sample taken from the bed by means of a capillary contained on an average about 200 droplets. Consequently, for each experiment, the volume of 2000 droplets had to be measured and in the course of this experimental investigation a total of 50,000 droplet measurements had to be performed. It was therefore decided to take advantage of data handling routines that were available. The signals from the measurement device were recorded in full by a datalogger on a digital magnetic tape. This information was then fed into the T.H.E. EL×8 computer for data reduction and interpretation. The datalogger used was a multi-purpose registration device consisting of a multiplexer, a sample and hold amplifier, an analogue to digital converter, a core memory, a tape control and a magnetic tape unit, all assembled in one instrument.

Datalogger

Signals with a range of ±10 V could be connected directly to the datalogger input, which had an impedance of 50 MΩ. By means of the multiplexer, signals from 32 different channels could be connected sequentially at a maximum total sample rate of 10,000 samples per second with the sample and hold amplifier which offered the analogue value of a signal to the analogue to digital converter. The analogue value was converted into a ten-bit binary data word, so conversion was taking place with 20 mV resolution. The core memory contained 4096 eight-bit words. Each data word together with a two-bit channel indication was written into two memory words. As soon as the memory was about half full, new information was directed to the other half of the memory and a block of 900 data words was written on the magnetic tape without intervening with the sampling sequence. The seven track magnetic tape was written in I.B.M. compatible binary format in such a way that one data word comprised two-bit lines on the tape. Five tracks contained information bits, one track was used for channel indication and another for parity. In between logical groups of information 'end of file' marks could be written on the tape. The magnetic tape could be read by the ELx8 computer. By means of an ELAN program, provided by the T.H.E. computer centre, the tape was translated into another tape that was written in EL7bin format, which could be processed directly by means of an algol program.

The signals from the measurement points have actually been registered by means of the datalogger via one channel at a sample rate of 500 samples per second. Typical records drawn by the computer are shown in Fig. 6 with measurements taken from capillary no. 7. Because the response rate of the measurement device (about 250 V sec^{-1}) was sufficiently high and the period of time that one droplet was in front of the light beam was of the order of 0·1 to 0·2 sec, the volume of the individual droplets could be measured with a resolution of about two percent. In order to obtain a quantitative measurement of the time that the light beam was interrupted by a droplet, a criterion was required to judge whether the photo diode was dark or light. Because the signals from different measurement points did differ to some extent, however small, depending on the way the light beam was adjusted, no standard criterion could be used. Therefore, an amplitude distribution was determined for each signal and the average of the two values at which the maxima occurred was

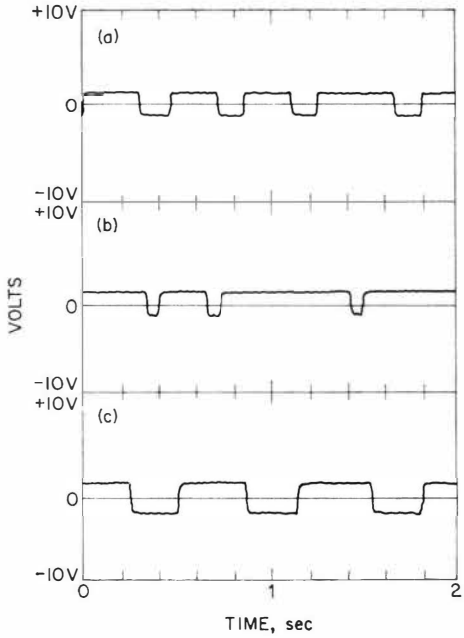

FIG. 6. *Typical measurement signals*

(*a*) experiment 1; benzene
(*b*) experiment 21; cyclohexane
(*c*) experiment 27; cyclohexane–carbon tetrachloride

used as the critical level. The amplitude distributions of the signals shown in Fig. 6 are reproduced in Fig. 7. The critical level is drawn, respectively indicated in the figures. Thus by counting the number of signal values sampled in a 'dark period' a measure for the volume of a droplet was obtained in units of 2 msec. After the volumes of all droplets had been determined in this manner, histograms were computed for the volume distribution. The histo-

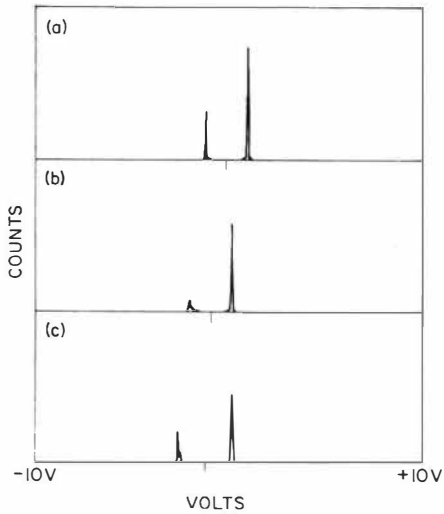

FIG. 7. *Amplitude distributions of the measurement signals*

(*a*) benzene
(*b*) cyclohexane
(*c*) cyclohexane–carbon tetrachloride

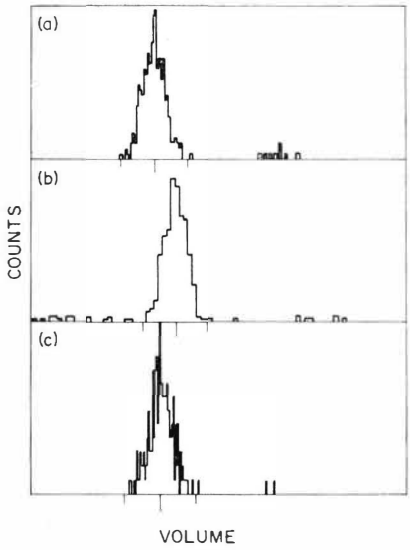

FIG. 8. *Histogram of the volume distribution of the sampled droplets*

(*a*) benzene
(*b*) cyclohexane
(*c*) cyclohexane–carbon tetrachloride

grams for the seventh capillary are shown in Fig. 8. In order to obtain a clear cut distribution, the presence of strange droplets had to be disregarded. Strange droplets were, for instance, the fines which were created underneath the glass sinter plate and which travelled down through the bed, as well as the coalesced droplets which were formed to a minor extent in the bed and in the measurement tube leading to the capillary. To achieve this, the maximum of the histogram was determined and for the set of droplets with a volume between 0·4 and 1·6 times the value at which the maximum occurred, the average volume and the standard deviation were computed. This computation was then repeated for the set of droplets with a volume larger than the average volume less three times the standard deviation and smaller than the average volume plus three times the standard deviation. This process was repeated and typically convergence was reached in about four such processes. The average volume found in this way as well as the bounds of three times the standard deviation are indicated in Fig. 8, which is drawn on an arbitrary scale; the discrete nature of the volume, or dark period, values is preserved of course. It is seen that the resolution is high enough for the determination of a distribution, in fact the resolution is higher than needed for an experiment with cyclohexane–carbon tetrachloride, where larger droplets are present than in the other experiments, due to the small difference in densities between the phases (60 kg m^{-3}).

The actual volumes of the droplets were computed by multiplication of the periods of time that the light beam was interrupted by the volume of the dispersed phase that passed through the capillary tube and divided by the total time that the photo diode was darkened. Computation from the total flow rate through the capillary gives values for the droplet volumes which are consistently about 10 per cent too high. This is because the droplet plug does not fill the capillary completely but slides over a water layer which is formed directly adjacent to the wall of the capillary tube. The accuracy of the computation of the droplet volume is estimated to be about 5 per cent. The volume frequence distribution was computed for all points where measurement was performed by transformation of the histogram. The volume frequency distributions were normalised per measurement point and are shown for

some experiments in Figs 9–11, respectively. In these figures the bed is seen from the bottom to the top. The skewness of these distributions is about +0·2 on average and the kurtosis about 2·8. The relative standard deviation equals about 0·1 depending on the experimental conditions. To a good approximation the frequency distribution may be considered to be Gaussian.

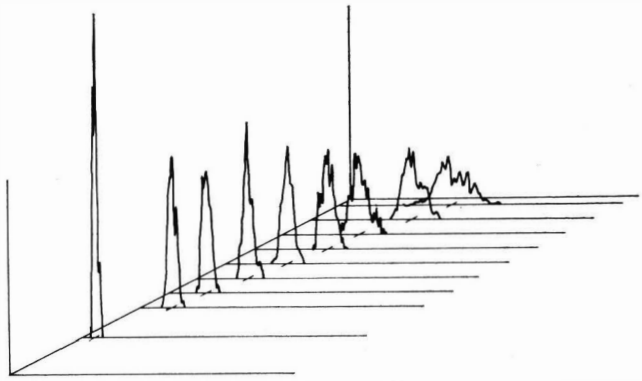

FIG. 9. *Volume frequency distribution*
Experiment 1; benzene dispersed phase

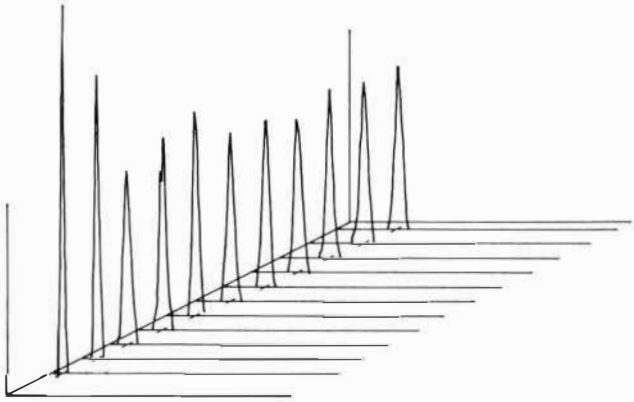

FIG. 10. *Volume frequency distribution*
Experiment 21; cyclohexane dispersed phase

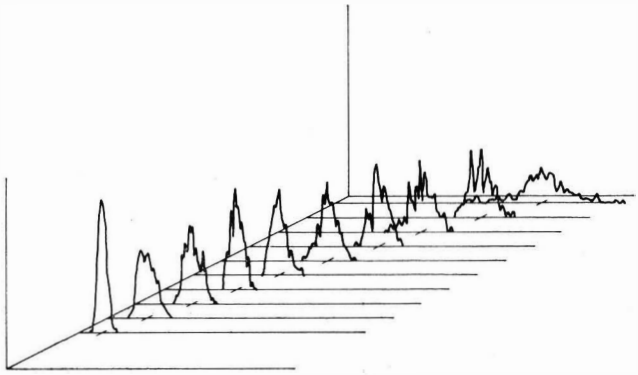

FIG. 11. *Volume frequency distribution*
Experiment 27; cyclohexane–carbon tetrachloride dispersed phase

The average diameters were computed from the histograms. They are shown in Figs 2–4 and 4 together with a third degree interpolation polynomial which was determined by Forsythe's method of application of under summation orthogonal polynomials.

As relatively large samples from the dispersion were taken from the measurement points, the part of the dispersion which was situated immediately below the measurement point was pressed through the capillary also. Consequently, during an experiment, the size of the droplets decreased. Therefore, the relationship between the droplet volume and the time elapsed since the beginning of measurement was computed and by means of a least-square-error regression line the average volume at the beginning of measurement was extrapolated. Virtually no correction for the directly computed average volume proved to be necessary for points in the middle of the bed. For the ends of the bed this correction was shown to be as large as 10 per cent. The standard deviation of the volume distribution was determined with respect to the regression line. This standard deviation was used in the description of the dispersion phenomena in the dispersed phase.

Co-ordinate measurement

The axial co-ordinate of clearly visible red tracer droplets in the colourless bed was measured with a co-ordinate meter, consisting of a pointer fitted to a chain running over a cogwheel. The cogwheel drove a precision potentiometer of high linearity. The voltage over the potentiometer was recorded. The pointer could be moved by hand over a range of about 1 m. The meter was situated at the same height as the capillaries and the uppermost point of the meter was situated 1·6 m below the glass sinter plate. The trajectory of the tracer droplets was measured by following the motion of the droplet by hand with the pointer. An example of the drunkard's walk of a droplet is shown in Fig. 12.

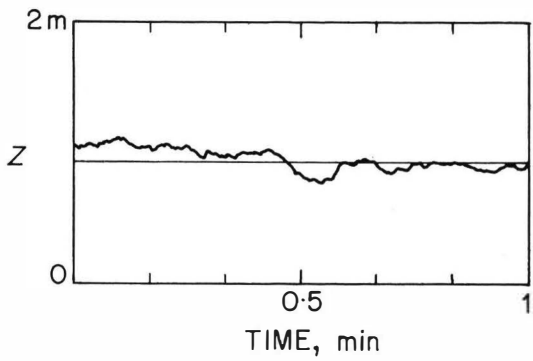

FIG. 12. *Random walk trajectory of tracer droplet*
Experiment 21

Residence time distribution measurement

The residence time distribution of the continuous phase was determined by a pulse injection of a very dilute salt solution at about 25 cm below the glass sinter plate. Conductivity was measured at a bed depth of 4·4 m and recorded, so that the overall residence time distribution was obtained. To prevent interference with the bed, the conductivity of the salt solution in the bed was chosen so that it was less than that of normal tap water.

Interpretation of results

Introduction

The stationary operation of the fluidised bed will be considered. The fluidisation characteristics will be described as well as the diffusion and classification phenomena. An interesting feature of the droplet bed is the variation of the porosity and of the average size of the droplet in the bed with the height of the column. The droplets in the bed tend to separate into layers of different sizes because of the dependence of the settling velocity on the size. Large droplets rise faster than small ones and since the droplets are free to move, the upper part of the bed consists of large droplets, the lower part of small ones. Consequently, the value of the porosity increases from the top to the bottom in the bed. Classification of droplet sizes is counteracted by axial diffusion, resulting in a spread of droplets of any given size over the height of the column. In order to evaluate these phenomena quantitatively, a general correlation for the slip velocity of the droplets has to be obtained from the experiments.

Fluidisation characteristics

For the stationary state the flow pattern in the fluidised bed is axisymmetric. If the effects of the walls are ignored, no radial gradients are present and the continuous phase can be thought to move in plug flow through the bed. The velocity of the dispersed phase equals zero and the densities of the phases are considered to be constant.

If the particle size and the porosity do not change appreciably, so that convective effects may be neglected, the pressure gradient over the bed equals

$$\frac{dp}{dz} = -\rho g \qquad (1)$$

where ρ is the average density of the bed and g the gravitational acceleration. The slip velocity v_s can be found from the force balance of the droplets by equating the buoyancy force to the drag force:

$$V_d(\rho_d - \rho)\, g = C_D A_d \tfrac{1}{2}\rho_c \,|\, v_s \,|\, v_s \qquad (2)$$

where V_d and A_d are the average volume and the average cross sectional area of the droplets, respectively. If the average diameter of the droplets ($\bar{d}$) is defined by $\bar{d} = 3V_d/2A_d$, an expression for the average dispersed phase drag coefficient C_D may be obtained directly from Equation (2).

$$C_D = \frac{4}{3}\frac{(\rho_c - \rho_d)\, g\bar{d}}{\rho_c \quad v_0^2}\varepsilon^3 \qquad (3)$$

In Equation (3) the superficial velocity of the continuous phase v_0 is introduced, which for the fluidised bed is equal to the product of the void fraction (ε) and the slip velocity

$$v_0 = \varepsilon v_s \qquad (4)$$

Equation (3) is the characteristic equation for the fluidised bed. It may be seen from this equation that if the value of the average droplet diameter varies over the column, so does the porosity. The equation was used to compute the values of the average dispersed phase drag coefficient from the experimental results. The results are tabulated in the appendix. The values for the drag coefficient near the top or the bottom of the bed were not used for further calculations. The computed values for the middle of the bed, covering a range of about 3 m height, are plotted in Fig. 13 *versus* the Reynolds number in the bed, $Re = v_0\bar{d}/\upsilon(1-\varepsilon)$, where υ is the kinematic viscosity of water. Comparison is made in the Fig. 13 with Ergun's expression for the packed bed

$$C_{DB} = 2{\cdot}33 + 200/Re \quad . \quad . \quad . \quad . \quad . \quad . \quad . \quad . \quad (5)$$

and with the limiting value for high Reynolds numbers of the drag coefficient for single droplets $C_{Dp} \sim 0{\cdot}5$.

As can be seen from Fig. 13, the values for the average dispersed phase drag coefficient of the fluidised bed are with these limits. The following simple explanation can be offered; under conditions just below minimum fluidisation

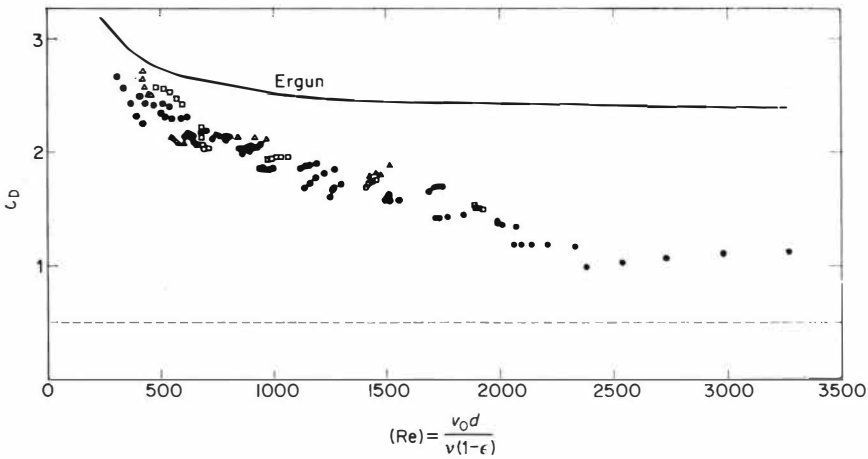

FIG. 13. *Average dispersed phase drag coefficient* versus *Reynolds number in the bed*

● benzene; □ cyclohexane;
△ cyclohexane–carbon tetrachloride

the volume of the bed is completely 'packed' and no droplet can move through the bed. The packed volume equals the sum of the volume of the droplets and the interstitial volume. Furthermore, the packed volume equals the volume of the droplets multiplied by a factor $1/(1-\varepsilon_0)$, where ε_0 denotes the porosity at minimum fluidisation. For fluidisation conditions the fraction packed volume is now supposed to be equal to $(1-\varepsilon)/(1-\varepsilon_0)$. Then the fraction of the 'free' volume through which the droplets may move freely equals $1-(1-\varepsilon)/(1-\varepsilon_0)$. An individual droplet in the bed may be in either a packed or free state. If it is assumed that neither state is preferred, the chance that an individual droplet is found in a particular state is equal to the respective volume fractions. Further, it is assumed that individual droplets rapidly change states, so that the average slip velocity is the same in both states. If the drag force acting on a droplet in a free and a packed state may be correlated by means of the drag coefficient of single particles (C_{Dp}) and the drag coefficient of packed particles (C_{DB}), respectively, then the average dispersed phase drag coefficient may be written as:

$$C_D = \left(1 - \frac{1-\varepsilon}{1-\varepsilon_0}\right) C_{Dp} + \frac{1-\varepsilon}{1-\varepsilon_0} C_{DB} \quad . \quad . \quad . \quad . \quad . \quad (6)$$

The experimentally determined values of the average dispersed phase drag coefficient are plotted in Fig. 14 *versus* the porosity. The straight line drawn can be represented by the equation

$$C_D = 0{\cdot}5 + 5(1-\varepsilon) \quad . \quad . \quad . \quad . \quad . \quad . \quad . \quad . \quad (7)$$

Actually, the relation between C_D and ε would not be expected to be linear on the basis of Equation (6). However, for the coarse dispersions considered here, where Reynolds numbers are high and the drag coefficients do not vary

appreciably with *Re*, deviations of the linear behaviour are expected to be small. If the porosity at minimum fluidisation ε_0 is estimated to be 0·4 the packed bed, the drag coefficient at minimum fluidisation is computed from Equation (7) to be about 3·5, which is in agreement with the value estimated from Ergun's Equation (5) for this condition.

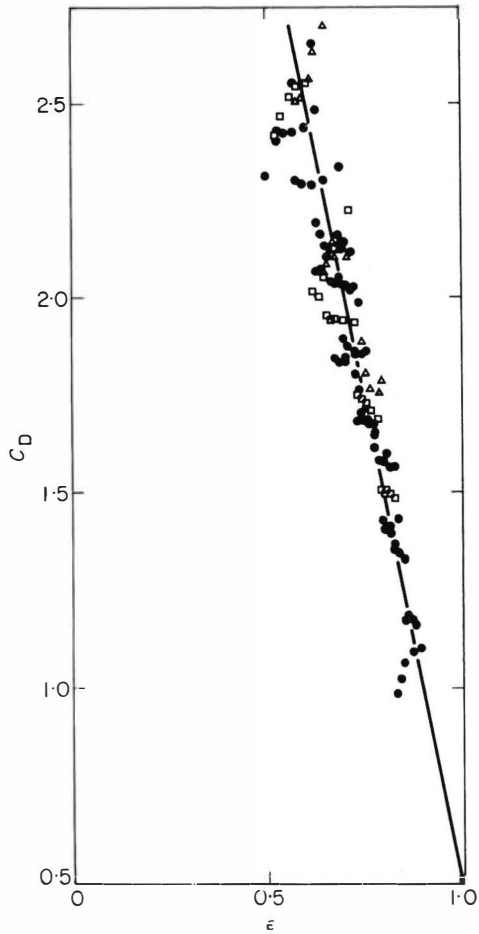

FIG. 14. *Average dispersed phase drag coefficient* versus *porosity*

Diffusion and classification phenomena

In the droplet bed, droplets are present with different diameters. Because of the dependence of the settling velocity on the size, droplets tend to separate into layers of different sizes. This tendency is counteracted by axial diffusion. Nevertheless, the average diameter of the droplets in the bed will vary with the height in the bed so that the largest droplets are nearer the top of the bed. Thus, the porosity will increase from the top to the bottom of the bed as may be seen from Equation (3). This is in agreement with the experimental findings, which are shown in Figs 2–4.

Interparticle diffusion will be considered here. Droplets with a particular diameter d may be distinguished from the rest of the dispersed phase. Their apparent relative velocity v_r with respect to the continuous phase which they would acquire by the influence of gravity solely, can be computed from

$$\frac{\pi}{6}d^3(\rho-\rho_d)\,g = C_D^*\,\frac{\pi}{4}d^2\,\tfrac{1}{2}\rho_c v_r^2 \qquad (8)$$

where C_D^* is the drag coefficient for the droplets considered. If for simplicity the drag coefficient is supposed to be dependent on the porosity only, C_D^* equals the average dispersed phase drag coefficient C_D and

$$v_r^2 = \frac{4}{3}\frac{(\rho_c-\rho_d)}{\rho_c}\frac{gd}{C_D}\varepsilon \quad . \quad . \quad . \quad . \quad . \quad . \quad . \quad . \quad (9)$$

If now at a certain height in the column a volume fraction α of the dispersed phase consists of droplets with the particular diameter d, the segregation flux φ_s of these droplets with respect to stationary co-ordinates equals

$$\varphi_s = \alpha(1-\varepsilon)(v_r+v) \quad . \quad . \quad . \quad . \quad . \quad . \quad . \quad . \quad (10)$$

where v is the linear velocity of the continuous phase which equals the slip velocity in the fluidised bed. The droplets pass through the dispersed phase in random motion. The flux φ_D of droplets with the particular diameter d due to this diffusional phenomenon may be equated to

$$\varphi_D = -(1-\varepsilon)E_i\frac{d\alpha}{dz} \quad . \quad . \quad . \quad . \quad . \quad . \quad . \quad . \quad (11)$$

where E_i denotes the interparticle diffusion coefficient in the dispersed phase. If the influence of the coalescence and redispersion phenomena may be neglected these fluxes balance each other for the steady state considered, $\varphi_s+\varphi_D=0$. The dependence of the volume fraction of the distinguished droplets on the height in the column is now described by

$$E_i\frac{d\alpha}{dz} = (v_r-\bar{v}_r)\alpha \quad . \quad . \quad . \quad . \quad . \quad . \quad . \quad . \quad . \quad (12)$$

where the average velocity of the dispersed phase with respect to the continuous phase is denoted by $\bar{v}_r=-v=-v_s$. By application of Equations (2) and (8) this may be rewritten as

$$E_i\frac{d\alpha}{dz} = \frac{v_0}{\varepsilon\bar{d}^{\frac{1}{2}}}(d^{\frac{1}{2}}-\bar{d}^{\frac{1}{2}})\alpha \quad . \quad . \quad . \quad . \quad . \quad . \quad . \quad . \quad (13)$$

The height in the column where the average diameter of the dropl ets is equa to the particular diameter d of the distinguished droplets is den oted by z_0 By means of a Taylor series for $\bar{d}^{\frac{1}{2}}$ modified in the form

$$\bar{d}^{\frac{1}{2}} = d^{\frac{1}{2}} + \frac{1}{2\bar{d}^{\frac{1}{2}}}\left\{\frac{d(\bar{d})}{dz}\right\}_{z_0}(z-z_0)+\ldots \quad . \quad . \quad . \quad . \quad . \quad (14)$$

the expression (13) can be written for the neighbourhood of z_0 by approximation as

$$E_i\frac{d\alpha}{dz} = -\frac{v_0 q}{2\varepsilon\bar{d}}\alpha(z-z_0) \quad . \quad . \quad . \quad . \quad . \quad . \quad . \quad . \quad (15)$$

where q denotes the derivative of the average diameter at z_0. By ignoring the slight variation of the group $v_0q/2\varepsilon\bar{d}E_i$ as being a second order effect, this equation may be integrated with respect to height to give

$$\alpha(z) = C_1(d)\exp\left\{-\frac{v_0 q}{4\varepsilon\bar{d}E_i}(z-z_0)^2\right\} \quad . \quad . \quad . \quad . \quad . \quad (16)$$

where the constant $C_1(d)$ is related to the total holdup of droplets with diameter d in the bed. From this equation it may be seen that droplets with any particular diameter d are distributed symmetrically around their equilibrium position.

Because the expression is derived for arbitrary d it may be rewritten if $C_1(d)$ is a slowly varying function of d and if the spread of the distribution is small, as

$$\alpha(d^{\frac{1}{2}}, \bar{d}^{\frac{1}{2}}) = C_2 \exp\left\{-\frac{v_0}{\varepsilon q E_i}(d^{\frac{1}{2}} - \bar{d}^{\frac{1}{2}})^2\right\} \quad . \quad . \quad . \quad . \quad . \quad (17)$$

Here the approximate Equation (14) has been applied. The size distribution for fixed height, in which d appears as a constant, is then given by

$$\alpha(t) = \frac{1}{\sqrt{2\pi}\sigma} \exp - \left\{\frac{t^2}{2\sigma^2}\right\} \quad . \quad . \quad . \quad . \quad . \quad . \quad . \quad (18)$$

with

$$t = \frac{d^{\frac{1}{2}}}{\bar{d}^{\frac{1}{2}}} - 1 \quad . \quad . \quad . \quad . \quad . \quad . \quad . \quad . \quad . \quad . \quad (19)$$

and

$$\sigma^2 = \frac{\varepsilon q E_i}{2 v_0 \bar{d}} \quad . \quad . \quad . \quad . \quad . \quad . \quad . \quad . \quad . \quad . \quad (20)$$

Therefore, the square-root of the droplet diameter is distributed normally. It should be noted that as long as the value of σ^2 from Equation (20) is small, the droplet diameter and even the droplet volume are distributed normally by approximation. The volume frequency distribution is then given by

$$\alpha(t_1) = \frac{1}{\sqrt{2\pi}\sigma_1} \exp\left\{-\frac{t_1^2}{2\sigma_1^2}\right\} \quad . \quad . \quad . \quad . \quad . \quad . \quad . \quad (21)$$

with

$$t_1 = \frac{\pi}{6}\frac{d^3}{V_d} - 1 \quad . \quad . \quad . \quad . \quad . \quad . \quad . \quad . \quad . \quad (22)$$

and

$$\sigma_1 = 6\sigma \quad . \quad . \quad . \quad . \quad . \quad . \quad . \quad . \quad . \quad . \quad (23)$$

The volume frequency distribution has actually been measured for the 27 experiments with the droplet bed. As was mentioned before, some typical results are shown in Figs 9–11. The interparticle diffusion coefficient can now be calculated from the experimental values of the gradient of the average diameter q and the variance of the volume frequency distribution σ_1^2. In an earlier treatment[58], the dispersed phase diffusion coefficient E_d was introduced in a slightly different manner, so that $E_d = \varepsilon E_i$. Although the present definition is preferable, the results will be stated for conformity in terms of E_d. As may be easily seen this has no influence on the results of the above analysis.

The Bodenstein number for the dispersed phase Bo_d is introduced defined as,

$$Bo_d = \frac{v_0 \bar{d}}{\varepsilon E_d} \quad . \quad . \quad . \quad . \quad . \quad . \quad . \quad . \quad . \quad . \quad (24)$$

The values of Bo_d are calculated from

$$Bo_d = 18\frac{q}{\varepsilon\sigma_1^2} \quad . \quad . \quad . \quad . \quad . \quad . \quad . \quad . \quad . \quad . \quad (25)$$

and are tabulated in the appendix. The values for this number near the top and the bottom of the bed have not been used for further calculations. The Bodenstein numbers are plotted in Fig. 15 *versus* the porosity. The straight line

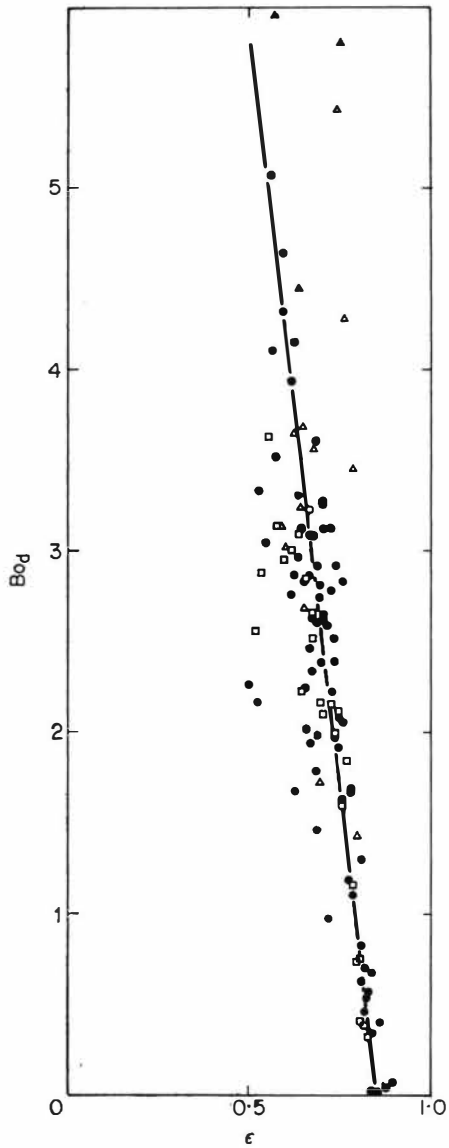

FIG. 15. *Dispersed phase Bodenstein number* versus *porosity*

drawn in the figure can be represented by the equation

$$Bo_d = \frac{50}{3}(1-\varepsilon) - 2{\cdot}5 \quad . \quad . \quad . \quad . \quad . \quad . \quad . \quad . \quad (26)$$

In order to investigate this result, the interparticle diffusion coefficient is supposed to be proportional to the mean square fluctuation velocity of the dispersed phase e_{fd} according to

$$E_i = m_d \rho_d e_{fd} \quad . \quad . \quad . \quad . \quad . \quad . \quad . \quad . \quad . \quad (27)$$

where the dispersed phase mobility is introduced defined by

$$m_d^{-1} = \frac{3}{4} C_D \rho_c |v_s| / \bar{d} \quad . \quad . \quad . \quad . \quad . \quad . \quad . \quad . \quad (28)$$

By elimination of E_i from the Bodenstein number and by substitution of C_D from Equation (7), it is found that the ratio of the fluctuation energy density in the dispersed phase to the kinetic energy density in the continuous phase equals

$$\frac{\rho_d e_{fd}}{\rho_c v_s^2} = \frac{3}{4} \cdot \frac{0{\cdot}5 + 5(1-\varepsilon)}{50(1-\varepsilon)/3 - 2{\cdot}5} \cdot \frac{1}{\varepsilon} \qquad (29)$$

For porosity values of less than 0·65, this ratio is found to be approximately equal to 3/4. For higher values, it is rapidly increased to 2 or 3 times this value. At any rate, the fluctuation energy density of the dispersed phase is not expected to be zero for conditions near minimum fluidisation. This is at variance with the results reported by Carlos & Richardson,[64] who calculated the kinetic energy of the particles from measured displacements. They found that the particle energy approaches zero near minimum fluidisation conditions. It is, however, doubtful whether their procedure would lead to a significant result when the displacements to be measured are small, as is the case near minimum fluidisation.

Diffusion in the continuous phase

The continuous phase is supposed to move in plug flow with axial diffusion through the droplet bed. The Bodenstein number for the continuous phase is introduced defined by

$$Bo_c = \frac{v\bar{d}}{E_c} \qquad (30)$$

where E_c is the axial diffusion coefficient in the continuous phase. Because the relative variance σ_r^2 of the residence time distribution is small and the contributions from different parts of the bed to the variance are additive, the Bodenstein number, if it is supposed to be constant, may be computed from the expression

$$Bo_c = \frac{\bar{d}_B}{L} \cdot \frac{2}{\sigma_r^2} \qquad (31)$$

where L is the distance between the point of injection of the salt solution and the measurement electrode and $\bar{d}_B$ denotes the droplet diameter averaged over the bed according to

$$\bar{d}_B = L\left\{ \int_0^L \varepsilon^2 \bar{d}\, dl \right\} \left\{ \int_0^L \varepsilon\, dl \right\}^{-2}$$

The values of the Bodenstein numbers computed from Equation (31) are plotted in Fig. 16 *versus* the Reynolds number in the bed $Re = v_0\bar{d}_B/\nu(1-\varepsilon)$. The average value of the Bodenstein number is calculated to be 1·02 with a standard deviation of 0·24.

Therefore, the axial diffusion in the droplet bed is approximately twice as great as that which is expected for a comparable packed bed. The Bodenstein numbers are seen to decrease slightly with the Reynolds number in the bed. This trend is indicated in the Fig. 16. No significant correlation with porosity can be obtained from these results.

Random walk of droplets

From the measured trajectories of the random walk of coloured tracer droplets in the droplet bed, a diffusion coefficient E_{rw} can be computed by application of Einstein's expression

$$E_{rw} = \frac{\overline{\Delta z^2}}{2\Delta t} \qquad (32)$$

where Δz denotes the displacement in a time interval Δt. The time interval Δt chosen should be longer than the time over which the motion of individual droplets is correlated, and the total observation should be extended over a long period of time or be repeated many times. During each experiment, a few tracer droplets were observed for about 10 minutes. Time intervals of 5 and 10 seconds were used to compute E_{rw}, which lead to comparable results. This diffusion coefficient, however, is not well defined. All ordered motions of the dispersed phase as such, i.e. all motions that do not change the relative

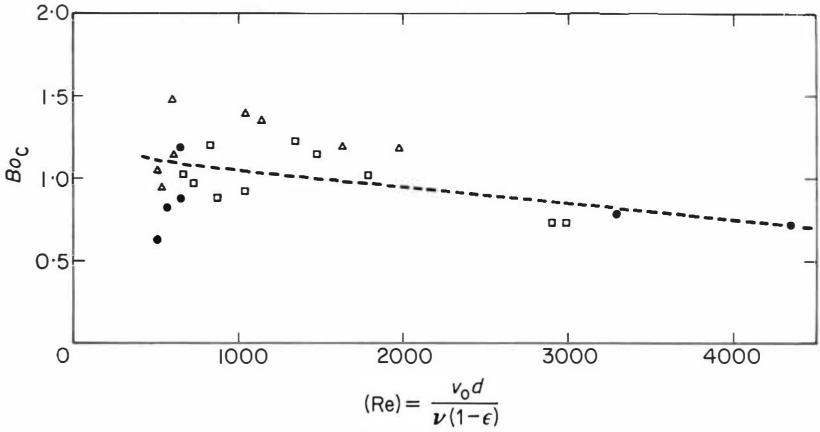

FIG. 16. *Continuous phase Bodenstein number* versus *Reynolds number in the bed*

position of the droplets, will contribute to the value of E_{rw}. Furthermore, for the special case of the droplet bed, the different positions where the tracer droplets are found during the course of observation are not equivalent and the motion of drops is influenced by classification phenomena, which also contribute to E_{rw}. In all, 46 trajectories for 8 different experiments were determined. The individual results are poorly reproducible, which would indicate that observations should be extended over a longer period of time. No significant correlation with porosity could be found for the Bodenstein number, introduced in an analogous way to definition (24). However, the average value of the Bodenstein number was found to be 2·5 with a standard deviation of 1, which is of the same order of magnitude as the values computed from the interparticle diffusion coefficient, which would indicate that the influence of ordered motions, if present, is at any rate small.

Conclusions

In this treatment the behaviour of liquid fluidised beds was studied. A droplet bed fluidised with water was used, in which water flowed from the top to the bottom to fluidise a lighter organic dispersion. The droplet bed exhibits homogeneous fluidisation for all values of the fluidisation velocity. Smooth homogeneous beds of 6 m length have been established without difficulty.

The pressure drop over the droplet bed and random walk trajectories of tracer droplets were determined for different values of the fluidisation velocity and the droplet size distribution was measured at different heights.

The fluidisation characteristics were investigated. For the homogeneously fluidized droplet bed it was found that the average dispersed phase drag coefficient C_D could be calculated as the weighted average of the drag coefficient for single droplets and the drag coefficient of the packed bed, the fractions free and packed volume in the bed being the weighting factors:

$$C_D = C_{Dp} + (C_{DB} - C_{Dp})\,(1-\varepsilon)/(1-\varepsilon_0).$$

Classification phenomena have been considered in the droplet bed. Because of the dependence of the settling velocity on the size, droplets tend to separate into layers of different sizes. This tendency is counteracted by axial diffusion. It has been shown that as a result of the balance between segregation and diffusion, droplets of any given size are normally distributed over the height around their equilibrium position in the bed. Also, the size distribution at any given height has been shown to be Gaussian.

From the experimentally determined variation of the size distribution the interparticle diffusion coefficient E_i is calculated. From the experimental results it is suggested that the decrease in E_i with holdup is due solely to the decrease of the mobility of the particles, and that the energy density of the dispersed phase is of the same order of magnitude as the kinetic energy density of the continuous phase. The interparticle diffusion coefficient is calculated from $E_i = v_s\bar{d}/C_D$, at least for porosities smaller than 0·65.

From the random walk trajectories, diffusion coefficients are calculated. Although the reproducibility of the individual experiments is poor, the average values of these diffusion coefficients are comparable in magnitude to the interparticle diffusion coefficient determined from the size distribution in the droplet bed.

References

[1] Hsiu, K., & Smirnov, N. I., *J. appl. Chem., U.S.S.R.*, 1961, **34,** 2009
[2] Ergun, S., *Chem. Engng Prog.*, 1952, **48,** 89
[3] Rowe, P. N., & Henwood, G. A., *Trans. Instn chem. Engrs*, 1961, **39,** 43
[4] Rowe, P. N., *Trans. Instn chem. Engrs*, 1961, **39,** 175
[5] Gunn, D. J., & Malik, A. A., *Trans. Instn chem. Engrs*, 1966, **44,** 371
[6] Ryan, E. J., Smith, J. W., & Hummel, R. L., *Proc. int. Symp. on Fluidisation*, 1967, p. 74
[7] Couderc, J. P., & Angelino, H., *Chim. Ind.*, 1970, **103,** 225
[8] Steinour, H. H., *Ind. Engng Chem.*, 1944, **36,** 618
[9] Tarján, G., *Acta Techn. Hung.*, 1958, **20,** 197
[10] Richardson, J. F., & Zaki, W. N., *Trans. Instn chem. Engrs*, 1954, **32,** 35
[11] Loeffler, A. L., & Ruth, B. F., *A.I.Ch.E. Jl*, 1959, **5,** 310
[12] Simpson, H. C., & Rodger, B. W., *Chem. Engng Sci.*, 1961, **16,** 153
[13] Kolář, V., *Colln. Czech. chem. Commun.*, 1962, **27,** 2816
[14] Musil, L., & Prochazka, J., *Génie Chim.*, 1966, **95,** 25
[15] Lapidus, L., & Elgin, J. C., *A.I.Ch.E. Jl*, 1957, **3,** 63
[16] Price, B. G., Lapidus, L., & Elgin, J. C., *A.I.Ch.E. Jl*, 1959, **5,** 93
[17] Weaver, E. C., Lapidus, L., & Elgin, J. C., *A.I.Ch.E. Jl*, 1959, **5,** 533
[18] Hoffman, R. F., Lapidus, L., & Elgin, J. C., *A.I.Ch.E. Jl*, 1960, **6,** 321
[19] Dunn, I., Lapidus, L., & Elgin, J. C., *A.I.Ch.E. Jl*, 1965, **11,** 158
[20] Furukawa, J., & Ohmae, T., *Ind. Engng Chem.*, 1958, **50,** 821
[21] Hetzler, R., & Williams, M. C., *Ind. Engng Chem. Fundamentals*, 1969, **8,** 668
[22] Schügerl, K., Merz, M., & Fetting, F., *Chem. Engng Sci.*, 1961, **15,** 1
[23] Coeuret, F., Le Goff, P., & Vergnes, F., *Proc. int. Symp on Fluidisation* 1967, p. 547
[24] Ruckenstein, E., Paper presented at Cluj scientific session, 1962
[25] Klier, A., & Vogel, H., *Chem. Techn.*, 1966, **18,** 195
[26] Neužil, L., & Hrdina, M., *Colln Czech. chem. Commun.*, 1965, **30,** 752
[27] Massimilla, L., Volpicelli, F., & Zenz, F., *Ind. Engng Chem. Fundamentals*, 1963, **2,** 194
[28] Fan, L. T., & Wen, C. Y., *A.I.Ch.E. Jl*, 1961, **7,** 606
[29] Stewart, P. S. B., & Davidson, J. F., *Chem. Engng Sci.*, 1964, **19,** 319
[30] Østergaard, K., & Theisen, P. I., *Chem. Engng Sci.*, 1966, **21,** 413
[31] Østergaard, K., *Chem. Engng Sci.*, 1966, **21,** 470
[32] Levsh, I. P., Krainev, N. I., & Niyazov, M. I., *Int. chem. Engng*, 1968, **8,** 311
[33] Rice, W. J., & Wilhelm, R. H., *A.I.Ch E. Jl*, 1958, **4,** 423
[34] Fan, L. T., Schmitz, J. A., & Miller, E. N., *A.I.Ch.E. Jl*, 1963, **9,** 149
[35] Massimilla, L., Volpicelli, G., & Raso, G., *A.I.Ch.E. Jl*, 1965, **11,** 549
[36] Volpicelli, G., *Proc. int. Symp. on Fluidisation*, 1967, p. 189
[37] Jackson, R., *Trans. Instn chem. Engrs*, 1963, **41,** 13
[38] Pigford, R. L., & Baron, R., *Ind. Engng Chem. Fundamentals*, 1965, **4,** 81
[39] Murray, J. D., *J. Fluid Mech.*, 1965, **21,** 465
[40] Molerus, O., *Proc. int. Symp. on Fluidisation*, 1967, p. 134
[41] Harrison, D., Davidson, J. F., & de Kock, J. W., *Trans. Instn chem. Engrs*, 1961, **39,** 230
[42] Anderson, T. B., & Jackson, R., *Chem. Engng Sci.*, 1964, **19,** 509

[43] Slis, P. L. Willemse, T., & Kramers, H., *Appl. scient. Res.*, 1959, **A8**, 209
[44] Zuber, N., *Chem. Engng Sci.*, 1964, **19**, 897
[45] Lawson, A., & Hassett, N. J., *Proc. int. Symp. on Fluidisation*, 1967, p. 113
[46] Ruckenstein, E., & Tzeculescu, M., *Chem. Engng Sci.*, 1968, **23**, 1121
[47] Hanratty, T. J., Latinen, G., & Wilhelm, R. H., *A.I.Ch.E. Jl*, 1956, **2**, 372
[48] Taylor, G. I., *Proc. London Math. Soc. A*, 1921, **20**, 196
[49] Cairns, E. J., & Prausnitz, J. M., *A.I.Ch.E. Jl*, 1960, **6**, 400
[50] Cairns, E. J., & Prausnitz, J. M., *A I.Ch.E. Jl*, 1960, **6**, 554
[51] Kramers, H., Westermann, M. D., de Groot, J. H., & Dupont, F. A. A., *Proc Symp. Interaction between Fluids and Particles* 1962, 114
[52] Ruckenstein, E., *Ind. Engng Chem. Fundamentals*, 1964, **3**, 260
[53] Bruinzeel, C., Reman, G. H., & van der Laan, E. T., *Proc. Symp. Interaction between Fluids and Particles*, 1962, p. 120
[54] Schügerl, K., *Proc. int. Symp. on Fluidisation*, 1967, p. 782
[55] Chung, S. F., & Wen, C. Y., *A.I.Ch.E. Jl*, 1959, **14**, 857
[56] Pruden, B. B., & Epstein, N., *Chem. Engng Sci.*, 1964, **19**, 696
[57] Kennedy, S. C., & Bretton, R. H., *A I.Ch.E. Jl*, 1966, **12**, 24
[58] Wijffels, J. B., & Rietema, K., 34*th Annual Chem. Engng, Symp. on Dispersed Systems* 1967, p. 15
[59] Coughlin, R. W., & von Berg, R. L., *Chem. Engng Sci.*, 1966, **21**, 6
[60] Collier, J. G., & Hewitt, G. F., *Br. chem. Engng*, 1966, **11**, 1526
[61] van Heuven, J. W., Ph.D. Thesis, Delft Univ. of Technol., 1969
[62] Bicknell, J. A., & Whitmore, R. L., *Proc. int. Symp. on Fluidisation*, 1967, p. 31
[63] Handley, D., Doraisamy, A., Butcher, K. L., & Franklin, N. L., *Trans. Instn chem. Engrs*, 1966, **44**, 260
[64] Carlos, C. R., & Richardson, J. F., *Chem. Engng Sci.*, 1968, **23**, 813

Nomenclature

A_d	average cross sectional area of droplets, m^2
Bo	Bodenstein number
C_D	average dispersed phase drag coefficient
C_D^*	droplet drag coefficient
C_{Da}	apparent drag coefficient
C_{DB}	packed bed drag coefficient
C_{Dp}	single particle drag coefficient
d	droplet diameter, m
$\bar{d}$	average droplet diameter, m
$\bar{d}_B$	average bed droplet diameter, m
E	diffusion coefficient, m^2sec^{-1}
E_i	interparticle diffusion coefficient, m^2sec^{-1}
E_{rw}	diffusion coefficient, m^2sec^{-1}
e_{fd}	mean square fluctuation velocity dispersed phase, m^2sec^{-2}
g	gravitational acceleration, $msec^{-2}$
L	length, m
m_d	dispersed phase mobility, sec m^3kg^{-1}
p	pressure, $kgm^{-1}sec^{-2}$
q	derivative of average diameter at z_0
Re	Reynolds number
t	reduced square root of droplet diameter
t_1	reduced droplet volume
V_d	average volume of droplets, m^3
v	linear velocity of the continuous phase, $msec^{-1}$
v_0	superficial velocity of the continuous phase, $msec^{-1}$
v_r	apparent relative velocity, $msec^{-1}$
$\bar{v}_r$	average dispersed phase relative velocity, $msec^{-1}$
v_s	slip velocity, $msec^{-1}$
z	distance in axial direction, m
z_0	equilibrium height, m

α volume fraction
Δt time interval, sec
Δz displacement, m
ε void fraction
ε_0 minimum fluidisation porosity
ν kinematic viscosity, m^2sec^{-1}
ρ density, kgm^{-3}
σ standard deviation of frequency distribution
σ_1 standard deviation volume frequency distribution
σ_r standard deviation residence time distribution
φ_D diffusion flux, $msec^{-1}$
φ_s segregation flux, $msec^{-1}$

Subscripts

c continuous phase
d dispersed phase

Appendix

Fluidised bed experiments

The results of the droplet bed experiments are tabulated here. A total of twenty-seven experiments were carried out using doubly distilled water as the continuous phase. The following liquids were used as the dispersed phase:

Experiments 1–6, 8–19	benzene
Experiments 20–24	cyclohexane
Experiments 25–28	cyclohexane–carbon tetrachloride

The results are reported here for those heights in the column, where the different measurement capillaries are installed. The capillaries are spaced 50 cm apart. The lowest capillary (no. 1) and the highest capillary (no. 11) are situated 5·3 m and 0·3 m below the glass sinter plate, respectively.

The porosity values ε tabulated were found by differentiation of the interpolation polynomial for the hydrostatic pressure. The average droplet diameters were computed directly from the size distribution. The values of $\bar{d}$ from the interpolation polynomial actually used for the computation of the Bodenstein number are given in the table. The Reynolds number for the droplet bed is defined by $Re = \rho_c v_0 \bar{d}/\nu(1-\varepsilon)$. The average dispersed phase drag coefficient C_D is computed from Equation (3). The Bodenstein numbers of the dispersed phase in the tables denoted by *Bo* are calculated from Equation (25). In cases where no convergence of the volume frequency distribution could be reached a dash is shown in the table.

Experiment 1
$v_0 = 4{\cdot}19$ $cmsec^{-1}$
$\rho_d = 879$ kgm^{-3}

no.	ε	$\bar{d}$	*Re*	C_D	*Bo*
1	0·79				
2	0·77	4·32	784	1·81	2·20
3	0·75				
4	0·73	5·55	864	1·99	1·97
5	0·71	6·03	885	2·02	2·58
6	0·70	6·47	902	2·03	2·62
7	0·69	6·87	918	2·04	2·74
8	0·68	7·27	939	2·06	3·60
9	0·67	7·70	966	2·09	3·59
10	0·66	8·19	1003	2·14	4·19
11	0·65	8·75	1054	2·23	3·78

Experiment 2
$v_0 = 4{\cdot}42$ $cmsec^{-1}$
$\rho_d = 879$ kgm^{-3}

no.	ε	$\bar{d}$	*Re*	C_D	*Bo*
1	0·82				
2	0·79	4·33	922	1·78	1·00
3	0·76	5·02	938	1·85	0·98
4	0·74	5·62	947	1·86	1·92
5	0·72	6·14	954	1·86	2·78
6	0·70	6·62	963	1·84	3·12
7	0·68	7·09	978	1·84	2·91
8	0·67	7·56	1002	1·85	3·08
9	0·66	8·06	1037	1·88	2·25
10	0·65	8·62	1088	1·95	3·70
11	0·65	9·27	1156	2·06	2·72

Experiment 3

$v_0 = 4{\cdot}86$ cmsec^{-1}
$\rho_d = 879$ kgm^{-3}

no.	ε	$\bar{d}$	*Re*	C_D	*Bo*
1	0·84				
2	0·82	4·33	1151	1·61	0·68
3	0·79				
4	0·77	5·35	1140	1·68	1·69
5	0·75	5·93	1163	1·72	2·82
6	0·73	6·53	1195	1·77	2·91
7	0·72	7·13	1232	1·81	3·12
8	0·70	7·72	1271	1·85	3·25
9	0·69	8·27	1309	1·88	3·76
10	0·68	8·77	1344	1·91	4·42
11	0·67	9·20	1375	1·93	1·77

Experiment 4

$v_0 = 4{\cdot}14$ cmsec^{-1}
$\rho_d = 879$ kgm^{-3}

no.	ε	$\bar{d}$	*Re*	C_D	*Bo*
1	0·80				
2	0·77	4·64	830	1·98	0·41
3	0·74				
4	0·72	5·74	853	2·03	2·22
5	0·70	6·26	868	2·03	2·61
6	0·68	6·75	885	2·04	2·60
7	0·67	7·22	905	2·04	2·33
8	0·66	7·66	926	2·05	2·86
9	0·65	8·08	948	2·06	3·41
10	0·64				
11	0·64	8·80	999	2·12	3·46

Experiment 5

$v_0 = 5{\cdot}58$ cmsec^{-1}
$\rho_d = 879$ kgm^{-3}

no.	ε	$\bar{d}$	*Re*	C_D	*Bo*
1	0·81				
2	0·80	5·82	1593	1·52	(—)
3	0·78				
4	0·77	7·04	1690	1·65	(—)
5	0·76	7·49	1712	1·68	(—)
6	0·75	7·85	1725	1·69	0·67
7	0·74	8·13	1731	1·69	1·25
8	0·73	8·35	1733	1·69	(—)
9	0·73	8·51	1734	1·69	(—)
10	0·72	8·62	1737	1·69	0·03
11	0·72	8·70	1742	1·69	0·01

Experiment 6

$v_0 = 3{\cdot}87$ cmsec^{-1}
$\rho_d = 879$ kgm^{-3}

no.	ε	$\bar{d}$	*Re*	C_D	*Bo*
1	0·79				
2	0·76				
3	0·73	4·76	694	2·03	(—)
4	0·71	5·46	734	2·12	0·97
5	0·69	6·02	757	2·15	2·38
6	0·67	6·49	772	2·14	2·65
7	0·66	6·90	785	2·13	3·09
8	0·65	7·30	802	2·14	2·01
9	0·64	7·74	827	2·16	3·26
10	0·63	8·25	865	2·23	4·80
11	0·63				

Experiment 8

$v_0 = 5{\cdot}40$ cmsec^{-1}
$\rho_d = 879$ kgm^{-3}

no.	ε	$\bar{d}$	*Re*	C_D	*Bo*
1	0·88	3·92	1831	1·50	(—)
2	0·86	4·36	1694	1·54	(—)
3	0·84	4·75	1604	1·56	(—)
4	0·82	5·10	1546	1·57	(—)
5	0·81	5·42	1510	1·57	0·70
6	0·79	5·72	1493	1·58	0·75
7	0·78	6·01	1493	1·59	1·10
8	0·77	6·31	1510	1·62	1·66
9	0·77	6·61	1546	1·66	1·78
10	0·77	6·94	1603	1·73	2·32
11	0·77	7·31	1684	1·81	3·24

Experiment 9

$v_0 = 6{\cdot}36$ cm/sec^{-1}
$\rho_d = 879$ kgm^{-3}

no.	ε	$\bar{d}$	*Re*	C_D	*Bo*
1	0·93	3·74	3314	1·19	0·14
2	0·91				
3	0·90	4·10	2512	1·18	(—)
4	0·88	4·27	2331	1·17	(—)
5	0·87	4·43	2215	1·18	(—)
6	0·86	4·58	2139	1·18	(—)
7	0·86	4·69	2090	1·18	0·09
8	0·85	4·77	2058	1·18	(—)
9	0·85	4·81	2038	1·18	(—)
10	0·85	4·80	2025	1·17	0·05
11	0·85	4·73	2015	1·16	(—)

Experiment 10

$v_0 = 5{\cdot}05$ cmsec^{-1}
$\rho_d = 879$ kgm^{-3}

no.	ε	$\bar{d}$	*Re*	C_D	*Bo*
1	0·90				
2	0·86	3·21	1153	1·29	(—)
3	0·83	4·19	1218	1·50	(—)
4	0·80	4·99	1247	1·60	1·30
5	0·77	5·65	1262	1·66	1·19
6	0·75	6·19	1271	1·68	2·05
7	0·74	6·63	1282	1·69	2·07
8	0·73	7·01	1298	1·71	2·51
9	0·72	7·34	1325	1·73	2·36
10	0·72	7·64	1365	1·78	3·12
11	0·72	7·94	1426	1·87	5·46

Experiment 11

$v_0 = 4{\cdot}68$ cmsec^{-1}
$\rho_d = 879$ kgm^{-3}

no.	ε	$\bar{d}$	*Re*	C_D	*Bo*
1	0·84				
2	0·81				
3	0·78	5·42	1145	1·88	0·69
4	0·75	5·91	1125	1·87	1·63
5	0·73	6·42	1125	1·86	2·39
6	0·72				
7	0·70	7·41	1160	1·88	3·26
8	0·69	7·85	1186	1·90	2·82
9	0·68	8·23	1214	1·93	2·64
10	0·68	8·52	1242	1·96	3·44
11	0·68	8·72	1268	2·00	1·84

Experiment 12

$v_0 = 3{\cdot}60$ cmsec^{-1}
$\rho_d = 879$ kgm^{-3}

no.	ε	$\bar{d}$	*Re*	C_D	*Bo*
1	0·77				
2	0·74	3·97	545	1·99	1·41
3	0·71	4·73	587	2·10	0·86
4	0·68	5·36	612	2·14	1·98
5	0·66	5·87	628	2·13	1·94
6	0·65	6·30	640	2·11	2·23
7	0·63	6·68	651	2·08	2·96
8	0·62	7·03	663	2·07	2·86
9	0·61	7·36	680	2·08	3·19
10	0·60	7·72	704	2·13	4·00
11	0·60	8·12	736	2·22	7·96

Experiment 13

$v_0 = 5{\cdot}87$ cmsec^{-1}
$\rho_d = 879$ kgm^{-3}

no.	ε	$\bar{d}$	*Re*	C_D	*Bo*
1	0·91	3·99	2752	1·43	0·59
2	0·89	4·51	2346	1·47	(—)
3	0·86	4·91	2105	1·48	(—)
4	0·84				
5	0·83	5·46	1842	1·44	0·34
6	0·81	5·65	1770	1·42	0·46
7	0·80	5·79	1729	1·41	0·63
8	0·80	5·93	1717	1·41	0·82
9	0·79	6·07	1737	1·43	(—)
10	0·80	6·23	1793	1·47	1·49
11	0·80	6·43	1896	1·55	2·01

Experiment 14

$v_0 = 7{\cdot}22$ cmsec^{-1}
$\rho_d = 879$ kgm^{-3}

no.	ε	$\bar{d}$	*Re*	C_D	*Bo*
1	0·97				
2	0·94	3·80	4256	0·96	0·22
3	0·91	4·62	3661	1·07	0·13
4	0·89	5·16	3274	1·11	0·07
5	0·87	5·47	2976	1·10	0·04
6	0·85	5·61	2733	1·07	0·01
7	0·84	5·61	2537	1·03	0·01
8	0·83	5·53	2381	0·99	0·02
9	0·83	5·41	2271	0·95	0·02
10	0·83	5·31	2217	0·93	0·02
11	0·83	5·25	2234	0·93	0·00

Experiment 15

$v_0 = 3{\cdot}25$ cmsec^{-1}
$\rho_d = 879$ kgm^{-3}

no.	ε	$\bar{d}$	*Re*	C_D	*Bo*
1	0·83				
2	0·77				
3	0·72	4·22	490	2·41	(—)
4	0·68	4·95	498	2·34	1·78
5	0·64	5·79	522	2·31	3·12
6	0·61	6·67	554	2·30	3·93
7	0·58	7·54	590	2·30	4·64
8	0·57	8·35	625	2·31	3·51
9	0·55	9·02	657	2·34	3·60
10	0·55	9·51	684	2·39	3·39
11	0·55	9·75	702	2·46	0·62

Experiment 16

$v_0 = 2{\cdot}89$ cmsec^{-1}
$\rho_d = 879$ kgm^{-3}

no.	ε	$\bar{d}$	*Re*	C_D	*Bo*
1	0·76				
2	0·71				
3	0·66	4·70	403	2·64	0·42
4	0·62	5·32	409	2·49	1·67
5	0·59	6·19	435	2·44	4·32
6	0·56	7·18	471	2·43	5·07
7	0·54	8·18	509	2·43	3·04
8	0·52	9·08	542	2·41	3·32
9	0·50	9·76	566	2·38	3·88
10	0·49	10·12	576	2·33	1·36
11	0·49	10·04	566	2·25	3·08

Experiment 17

$v_0 = 3{\cdot}60$ cmsec^{-1}
$\rho_d = 879$ kgm^{-3}

no.	ε	$\bar{d}$	*Re*	C_D	*Bo*
1	0·75				
2	0·72				
3	0·70				
4	0·68	5·57	624	2·17	1·47
5	0·66	5·95	630	2·13	2·45
6	0·64	6·42	650	2·14	2·82
7	0·63	6·92	676	2·17	3·30
8	0·62	7·39	702	2·20	4·14
9	0·61				
10	0·61	7·99	734	2·24	1·59
11	0·61				

Experiment 18

$v_0 = 6{\cdot}14$ cmsec^{-1}
$\rho_d = 879$ kgm^{-3}

no.	ε	$\bar{d}$	*Re*	C_D	*Bo*
1	0·90	4·30	2571	1·33	0·50
2	0·88	4·62	2321	1·34	0·19
3	0·86	4·91	2165	1·34	0·25
4	0·85	5·18	2068	1·34	0·40
5	0·83	5·42	2010	1·35	0·67
6	0·82	5·65	1982	1·36	0·54
7	0·82	5·87	1980	1·38	0·55
8	0·81				
9	0·81	6·30	2047	1·44	1·29
10	0·81	6·51	2119	1·49	1·57
11	0·81	6·72	2221	1·55	1·81

Experiment 19

$v_0 = 2{\cdot}56$ cmsec^{-1}
$\rho_d = 879$ kgm^{-3}

no.	ε	$\bar{d}$	*Re*	C_D	*Bo*
1	0·81				
2	0·74				
3	0·67				
4	0·61	4·69	310	2·66	2·75
5	0·56	5·80	341	2·56	4·01
6	0·52	6·87	370	2·43	2·16
7	0·49	7·86	397	2·32	2·26
8	0·47				
9	0·46	9·47	448	2·26	1·27
10	0·46	10·02	472	2·34	3·11
11	0·46	10·36	493	2·51	0·93

Experiment 20

$v_0 = 4{\cdot}53$ cmsec^{-1}
$\rho_d = 779$ kgm^{-3}

no.	ε	$\bar{d}$	*Re*	C_D	*Bo*
1	0·84				
2	0·79	3·34	717	2·35	1·02
3	0·74	3·97	695	2·32	0·61
4	0·70	4·49	683	2·23	2·10
5	0·67	4·95	679	2·13	2·52
6	0·64	5·35	682	2·06	2·23
7	0·63	5·71	692	2·01	3·10
8	0·61	6·05	712	2·02	3·03
9	0·61	6·38	742	2·09	3·58
10	0·61	6·71	786	2·22	3·73
11	0·62	7·06	849	2·46	5·44

Experiment 21

$v_0 = 6{\cdot}36$ cmsec^{-1}
$\rho_d = 779$ kgm^{-3}

no.	ε	$\bar{d}$	*Re*	C_D	*Bo*
1	0·83	3·68	1413	1·56	1·30
2	0·81	4·15	1412	1·62	1·50
3	0·79	4·57	1412	1·67	0·56
4	0·78	4·95	1415	1·69	1·16
5	0·76	5·28	1419	1·71	1·84
6	0·75	5·58	1427	1·72	1·60
7	0·74	5·83	1438	1·74	2·12
8	0·73	6·06	1453	1·75	1·98
9	0·73	6·25	1473	1·77	2·01
10	0·73	6·42	1499	1·80	1·68
11	0·73	6·56	1531	1·84	2·00

Experiment 22

$v_0 = 3{\cdot}60$ cmsec^{-1}
$\rho_d = 779$ kgm^{-3}

no.	ε	$\bar{d}$	*Re*	C_D	*Bo*
1	0·69				
2	0·65	3·85	400	2·44	1·81
3	0·62	4·64	441	2·53	1·22
4	0·59	5·40	477	2·56	2·96
5	0·57	6·13	510	2·55	3·14
6	0·55	6·82	540	2·52	3·63
7	0·53	7·44	566	2·47	2·88
8	0·51	7·99	588	2·42	2·56
9	0·50	8·44	606	2·38	3·47
10	0·49	8·79	619	2·34	2·97
11	0·48	9·00	627	2·31	1·42

Experiment 23

$v_0 = 5{\cdot}35$ cmsec^{-1}
$\rho_d = 779$ kgm^{-3}

no.	ε	$\bar{d}$	*Re*	C_D	*Bo*
1	0·81				
2	0·77	3·80	892	1·80	1·34
3	0·74	4·52	936	1·90	0·82
4	0·72	5·14	966	1·94	2·15
5	0·69	5·68	990	1·95	2·16
6	0·67	6·15	1011	1·95	2·65
7	0·66	6·55	1033	1·95	3·23
8	0·65	6·92	1058	1·96	2·85
9	0·64	7·24	1089	1·99	2·81
10	0·64	7·54	1127	2·05	3·40
11	0·64	7·84	1176	2·15	2·96

Experiment 24

$v_0 = 7{\cdot}25$ cmsec^{-1}
$\rho_d = 779$ kgm^{-3}

no.	ε	$\bar{d}$	*Re*	C_D	*Bo*
1	0·84	4·26	1990	1·44	0·98
2	0·83	4·50	1975	1·47	0·60
3	0·83	4·71	1955	1·48	0·32
4	0·82	4·88	1934	1·49	0·32
5	0·81	5·02	1914	1·50	0·37
6	0·80	5·15	1899	1·50	0·39
7	0·80	5·28	1890	1·50	0·75
8	0·79	5·40	1891	1·51	0·73
9	0·79	5·54	1902	1·52	0·73
10	0·79	5·70	1927	1·55	1·00
11	0·78	5·88	1968	1·58	1·12

Experiment 25

$v_0 = 3{\cdot}20$ cmsec^{-1}
$\rho_d = 940$ kgm^{-3}

no.	ε	$\bar{d}$	*Re*	C_D	*Bo*
1	0·75				
2	0·73	7·42	882	2·26	
3	0·71				
4	0·70	8·36	891	2·12	
5	0·69	8·43	865	2·13	
6	0·68	8·76	869	2·13	
7	0·67	9·22	888	2·14	
8	0·66	9·59	905	2·15	
9	0·66				
10	0·65	10·48	963	2·38	
11	0·65	12·13	1111	2·62	

Experiment 26

$v_0 = 4{\cdot}07$ cmsec^{-1}
$\rho_d = 940$ kgm^{-3}

no.	ε	$\bar{d}$	*Re*	C_D	*Bo*
1	0·86				
2	0·84	7·32	1847	2·09	0·56
3	0·82	7·24	1594	1·89	0·18
4	0·79	7·40	1468	1·79	1·43
5	0·78	7·76	1417	1·76	3·46
6	0·76	8·26	1417	1·77	4·29
7	0·75	8·88	1450	1·81	5·82
8	0·74	9·57	1509	1·89	5·44
9	0·74	10·28	1584	1·98	6·98
10	0·73	10·98	1672	2·09	6·28
11	0·73	11·63	1769	2·21	5·58

Experiment 27

$v_0 = 2{\cdot}26$ cmsec^{-1}
$\rho_d = 940$ kgm^{-3}

no.	ε	$\bar{d}$	*Re*	C_D	*Bo*
1	0·72				
2	0·69	5·15	373	2·63	2·33
3	0·66	6·04	402	2·72	1·36
4	0·64	6·71	417	2·71	3·24
5	0·62	7·23	425	2·64	3·65
6	0·60	7·67	431	2·57	3·02
7	0·58	8·06	439	2·52	3·15
8	0·57	8·48	450	2·51	6·17
9	0·57	8·97	468	2·56	6·38
10	0·56	9·60	497	2·69	10·44
11	0·56	10·41	539	2·91	4·72

Experiment 28

$v_0 = 2{\cdot}76$ cmsec^{-1}
$\rho_d = 940$ kgm^{-3}

no.	ε	$\bar{d}$	*Re*	C_D	*Bo*
1	0·78				
2	0·75				
3	0·72	5·40	531	2·11	0·33
4	0·69	6·08	546	2·12	1·73
5	0·67	6·65	558	2·11	3·56
6	0·65	7·14	568	2·09	2·69
7	0·64	7·57	578	2·07	3·69
8	0·63	7·94	590	2·07	4·45
9	0·62	8·28	606	2·10	4·60
10	0·62	8·60	627	2·17	3·59
11	0·62	8·93	655	2·27	2·06

Residence time distribution of the dispersed phase in agitated extraction columns

by V. Rod and T. Míšek*

Institute of Chemical Process Fundamentals of the Czechoslovak Academy of Sciences, Prague, Czechoslovakia.

Residence time distribution (RTD) of the dispersed phase is a very important means for the evaluation of column performance, for studying hydrodynamic behaviour and calculation of mass transfer characteristics. This paper shows the use of RTD for the study of mechanisms of longitudinal mixing.

Introduction

MEASUREMENTS of residence time distribution (RTD) carried out on the laboratory equipment, mentioned later, have shown that the method of results correlation, based on a backflow or diffusion model, widely used for the continuous phase, is not applicable to the dispersed phase.

The relation

$$\bar{\sigma}^2 = \frac{2h_m}{L}\left(A + B\,\frac{n_r D}{u}\right) \quad . \quad . \quad . \quad . \quad . \quad . \quad . \quad . \quad (1)$$

yields he best constants:

$$A = 123{\cdot}6 \text{ and } B = -16{\cdot}5 \quad . \quad . \quad . \quad . \quad . \quad . \quad . \quad (2)$$

in comparison[1] with

$$A = 0{\cdot}5 \text{ and } B = 0{\cdot}0104 \quad . \quad . \quad . \quad . \quad . \quad . \quad . \quad (3)$$

expected from measurements of RTD in the continuous phase, or:

$$A = 0{\cdot}7 \text{ and } B = 0{\cdot}006 \quad . \quad . \quad . \quad . \quad . \quad . \quad . \quad . \quad (4)$$

obtained by one of the authors[2] from measurements of solid spheres RTD in the same equipment.

The differences in orders and sign can be explained neither theoretically nor by experimental reasons as far as only the backmix or diffusion mechanism is considered. As Equation (1) with constants (3) or (4) is expected to describe the variance of RTD caused by backmixing very closely, the difference may be explained only by the effect of another additional mechanism of longitudinal mixing.

The ratio of $\bar{\sigma}^2$ calculated from Equation (1) and constant (4) to the experimental values given in Table I shows that the other dispersion mechanism prevails in the investigated column.

TABLE I

Ratio $\bar{\sigma}_c^2/\bar{\sigma}^2$

For experimental conditions see Table III

0·29	0·27	0·14	0·33
0·19	0·41	0·27	0·44
0·14	0·12	0·16	0·14
0·14	0·15	0·14	0·17
0·06	0·07	0·08	0·11
0·11	0·10	0·08	0·11
0·12	0·07	0·08	0·13
0·06	0·10	0·06	0·11

*Research Institute of Chemical Equipment, Prague, Czechoslovakia.

Theoretical

In order to describe the flow behaviour of the dispersed phase in countercurrent mixed extractors more realistically, a simple model has been suggested which takes into account three factors that affect residence time distribution, viz. backmixing, distribution of drop velocities and coalescence.

The model is represented by a series of n stages in which no coalescence of drops takes place. In each stage, drops of size a are ideally mixed, with mean residence time θ which is dependent on their size. After having passed through m stages, all drops coalesce and redisperse, so that concentration in drops is N times ($N = n/m-1$) equalised inside the cascade (Fig. 1).

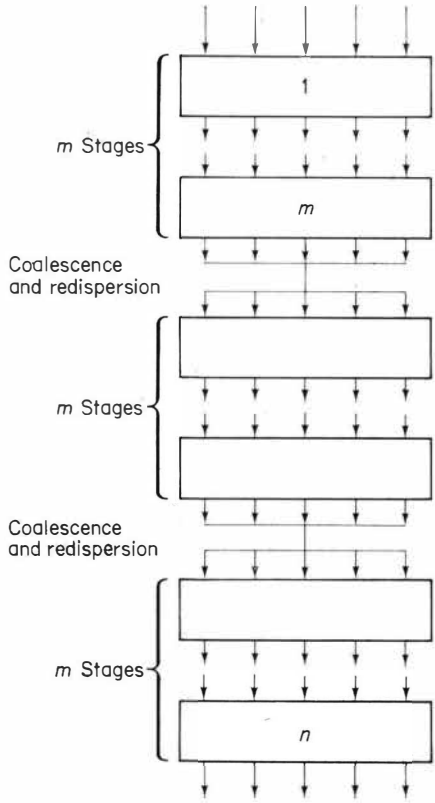

FIG. 1. *Schematic representation of dispersed phase flow*

Mean and variance of residence time distribution in the model

If the residence time distribution of drops with diameter a in m stages is denoted by the conditional probability function $\varphi(t|a)$, its mean and variance can be expressed as:

$$M(t|a) = m\theta \qquad (5)$$

and

$$\sigma^2(t|a) = m\theta^2 \qquad (6)$$

The expression derived for the m-stage cascade of ideal mixers can be applied, because there is no interaction between drops of various sizes in those m stages. If the volumetric distribution of drops entering the mixers is denoted by $g(a)$,

then the residence time distribution of drops of all sizes in m stages is given by joint distribution function:

$$f(t) = \int_0^\infty \varphi(t|a)\, g(a).\mathrm{d}a \qquad (7)$$

with mean:

$$M(t) = M\,[M(t|a)] \qquad (8)$$

and variance

$$\sigma^2(t) = \sigma^2\,[M(t|a)] + M[\sigma^2(t|a)] \qquad (9)$$

On substitution from Equations (5) and (6):

$$M(t) = M(m\theta) = mM(\theta) \qquad (10)$$

and

$$\sigma^2(t) = \sigma^2(m\theta) + M(m\theta^2) \qquad (11)$$

$$= m^2\sigma^2(\theta) + m[\sigma^2(\theta) + [M(\theta)]^2] \qquad (12)$$

As the residence time in an n-stage cascade can be regarded as the sum of $(N+1)$ independent residence times in the sections (with m stages), the additivity of variances can be applied:

$$\bar{\sigma}^2 = \frac{(N+1)\,\sigma^2(t)}{[(N+1)\,M(t)]^2}$$

$$= \left(\frac{1}{N+1}\right)\left[\frac{\sigma^2(\theta)}{[M(\theta)]^2} + \frac{1}{m}\left(\frac{\sigma^2(\theta)}{[M(\theta)]^2} + 1\right)\right] \qquad (13)$$

As

$$(N+1)m = n \qquad (14)$$

Equation (13) may be rewritten as:

$$\bar{\sigma}^2 = \left(\frac{1}{N+1}\right)\bar{\sigma}_u^2 + \frac{1}{n}(\bar{\sigma}_u^2 + 1) \qquad (15)$$

where

$$\bar{\sigma}_u^2 = \frac{\sigma^2(\theta)}{[M(\theta)]^2} \qquad (16)$$

Application of the model to continuous apparatus

By comparison of the described model with a continuous column of length L, Equation (17) is obtained:

$$L = nH_m = NH_c \qquad (17)$$

Further, the mean residence time of a drop of certain size in a stage can be related to its velocity in the column:

$$\theta = \frac{H_m}{u} \qquad (18)$$

so that Equation (16) can be written as:

$$\bar{\sigma}_u^2 = \frac{\sigma^2(1/u)}{[M(1/u)]^2} \qquad (19)$$

By combination of Equations (15) and (17), the dependence of the dimensionless variance of RTD on the column length can be written as:

$$\bar{\sigma}^2 = \left(\frac{H_c}{L+H_c}\right)\bar{\sigma}_u^2 + \frac{H_m}{L}(1+\bar{\sigma}_u^2) \quad . \quad . \quad . \quad . \quad . \quad . \quad (20)$$

This relation contains three parameters which are dependent on L, i.e. $\bar{\sigma}_u^2$, H_c and H_m. The effect of these parameters on the variance is illustrated in Fig. 2, which shows the dependence of $\bar{\sigma}^2$ on reciprocal column length.

Equation (20) can be used for analysis of the response curves obtained by a tracer injection method and the dependence of their variances on the distance between the injection and the sample points. It should be noted that on applying the injection method to a polydispersed phase, two different response curves may result, depending on whether the hold-up sampling or flow-sampling has been used. If, for example, the response is measured by radiation intensity of a tracer, which is proportional to the hold-up of the tracer in a section of column (hold-up sampling), then, in calculating $\bar{\sigma}^2$, the population of drops present in this volume and the corresponding distribution function f(a) is to be taken into account. On the other hand, if samples are taken by means of a sampling tube inserted in the column, the response is affected by a population of drops passing through the column cross-section, and, in evaluating $\bar{\sigma}^2$, the corresponding distribution function g(a) must be used.

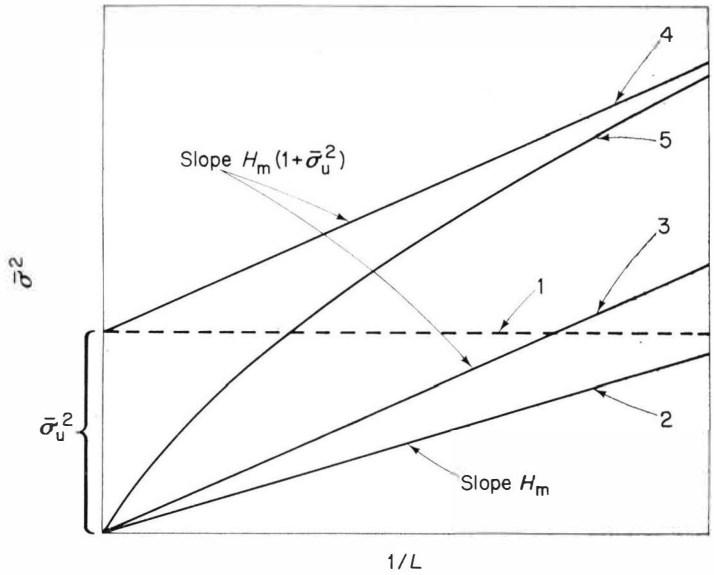

FIG. 2. *Dependence of dimensionless variance of RTD on reciprocal column length*

(1) $H_m=0$, $H_c=\infty$, no backmixing, no coalescence;
(2) $\bar{\sigma}_u^2=0$, $H_c=0$, monodispersion;
(3) $H_c=0$, infinite coalescence rate;
(4) $H_c=\infty$, no coalescence;
(5) general case

Height of a mixing stage

The value of H_m can be estimated from the knowledge of backmixing of the continuous phase. With decreasing value of $\bar{\sigma}_u^2$, it can be assumed that the flow behaviour of the dispersed phase approaches the behaviour of the continuous

phase. Hence, in the limiting case of a monodispersion ($\bar{\sigma}_u^2 = 0$), $\bar{\sigma}^2$ can be calculated from a correlation valid for backmixing of the continuous phase:

$$\lim \bar{\sigma}^2(\bar{\sigma}_u^2 \to 0) = \frac{H_m}{L} = \bar{\sigma}_c^2 \qquad (22)$$

This agrees well with results of experiments with solid particles.[2,3]

Using Equation (22), H_m can be eliminated from Equation (20):

$$\bar{\sigma}^2 = \left(\frac{H_c}{H_c+L}\right)\bar{\sigma}_u^2 + \bar{\sigma}_c^2(1+\bar{\sigma}_u^2) \qquad (23)$$

and Equation (23) can be applied to the evaluation of experimental data.

Dimensionless variance $\bar{\sigma}_u^2$

The relation between the above two distribution functions is described by the equation:

$$g(a).da = \frac{uX}{U_d} f(a).da \qquad (24)$$

where the value u is well expressed by:[4]

$$u = u_o(1-X)\exp(zX) - U_c(1-X) \qquad (25)$$

Equation (25) expresses the relation between u_o, the terminal velocity of a drop, and u, its velocity under actual conditions in the column. It has further been found[5] that:

$$f(a) = \frac{1}{6\beta^3} a^3 \exp(-a/b) \qquad (26)$$

where the only constant, β, proportional to the mean drop diameter, is a satisfactory approximation of the drop size distribution in RDC and ARD columns.

If the flow sampling is used, Equation (19) may be written as:

$$\sigma_u^2 = \frac{\int_0^\infty 1/u^2\, g(a).da}{[\int_0^\infty 1/u\, g(a).da]^2} - 1$$

and transformed by means of Equation (24) to:

$$\sigma_u^2 = \int uf(a).da \int 1/u\, f(a).da - 1 \qquad (27)$$

Assuming a linear relationship between drop velocity u_o and drop diameter:

$$u_o = (C_1 a) \qquad (28)$$

which corresponds to the intermediate law, most probably valid for drop velocities in column apparatus, Equation (27) can be solved with Equation (25) to give:

$$\bar{\sigma}_u^2 = (\bar{a}_{4,3} - C_2)\int_0^\infty \frac{f(a).da}{a-C_2} - 1 \qquad (29)$$

where

$$C_2 = \frac{U_c}{C_1(1-X)^2\exp(zX)}.$$

Equation (29) simplifies to:

$$\bar{\sigma}_u^2 = \frac{\bar{a}_{4,3}}{\bar{a}_{3,2}} - 1$$

only for the limiting condition of a stationary continuous phase.[2] Generally, the integration can be carried out on substitution of an appropriate distribution function. Even with the relatively simple distribution in Equation (26), this integration yields a complicated expression:

$$\bar{\sigma}_u^2 = \left(\frac{2}{3} - Q\right)\left\{(-Q)^3 \exp(-Q)\left[0{\cdot}5772 + \ln Q + Q + \frac{Q^2}{4} + \frac{Q^3}{18} + \ldots\right] + \right.$$
$$\left. + Q^2 + Q + 2\right\} - 1 \qquad (30)$$

where

$$Q = \frac{U_c}{C_1\, \beta(1-X)^2 \exp(zX)},$$

which is shown graphically in Fig. 3.

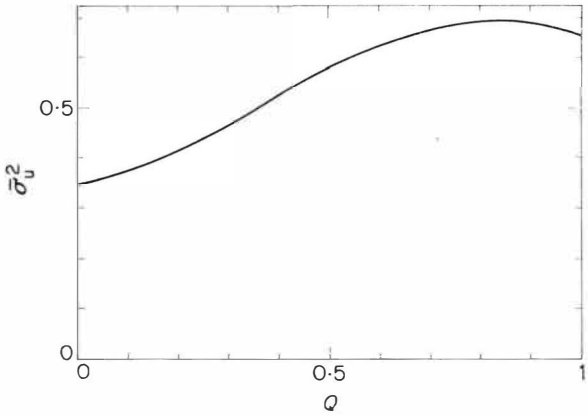

FIG. 3. *Calculated values of $\bar{\sigma}_u^2$—flow sampling*

Coalescence height

Coalescence of drops in mixed extraction columns was studied previously by one of the authors[6] who found that the Levich's theory[7] of turbulent coalescence of dispersions is in good agreement with throughput and hold-up measurements. According to this theory, the frequency of collisions in unit volume is given by:

$$\omega \sim n_o X \sqrt{\frac{\varepsilon}{\nu}} \qquad (31)$$

The average number of coagulations of a drop during its existence in the column is assumed to be proportional to the number of collisions:

$$N \sim \frac{\omega \bar{t}_L}{n_o} \qquad (32)$$

hence, with regard to Equation (17), Equation (33) can be written:

$$H_c = \frac{1}{C_3} \frac{L}{X \bar{t}_L} \sqrt{\frac{\nu}{\varepsilon}}. \qquad (33)$$

This relation is expected to be useful for the so-called 'rapid coalescence' case, where every collision between drops is efficient, i.e. a coalescence follows. In the

'slow coalescence' case, only a fraction of the collisions is efficient, and the proportionality constant C_3 is expected to be much lower.

Two approaches have been proposed for the application of Equation (23):

a. To measure the response curve at one point, while varying conditions affecting coalescence. This approach is suitable for laboratory experiments.

b. To measure response curves at several points with different distances from the injection, supposing that coalescence conditions are constant. This approach is convenient for industrial installations.

The following experimental section demonstrates the application of both methods.

Experimental

Laboratory experiments

Laboratory experiments were performed on a small RDC installation, the geometry of which is described in Table II. The operating conditions are given in Table III, and results are presented in Tables IV, V and VI in the same arrangement. The averages of at least two measurements are presented. The evaluation of (L/H_c+1) was made using Equation (23), $\bar{\sigma}_u^2$ was calculated according to Equations (1) and (3) (see Table I) and $\bar{\sigma}_c^2$ from Equation (30).

It has been found that the results fall into two groups:

TABLE II

Experimental equipment

Parameter	Laboratory	Plant
Column diameter, mm	50	2000
Effective height, mm	990	9540
Stator opening, mm	35	1500
Compartment height, mm	10–19	180
Rotor diameter, mm	26	1200
Measurement	δ Injection, 1 response	δ Injection 3 responses
Tracing	Conductivity	γ-Rays
Liquid system	Water–trichloroethylene	Water–butyl acetate (phenol)

TABLE III

Experimental conditions and run numbers

	U_c, cm/sec	0·1197		0·1709	
	U_d, cm/sec	0·0914	0·1397	0·0914	0·1397
	Rotor speed, rev/min				
h_m = 1 cm	1200	1	2	3	4
	800	5	6	7	8
h_m = 1·9 cm	1200	9	10	11	12
	800	13	14	15	16

TABLE IV

Results: Mean residence time $\bar{t}_L$, sec

181·95	146·0	193·15	147·7
177·95	107·3	185·75	123·0
131·80	96·1	115·95	92·15
117·50	88·0	99·6	84·6

TABLE V

Results: $\bar{\sigma}^2$

0·0078	0·0758	0·1530	0·0634
0·1214	0·0512	0·0870	0·0472
0·1372	0·1394	0·1214	0·1172
0·1364	0·1084	0·1404	0·0994
0·560	0·480	0·452	0·308
0·364	0·360	0·426	0·304
0·266	0·386	0·390	0·216
0·478	0·286	0·506	0·270

TABLE VI

Results: Hold-up X, %

6·55	11·65	13·2	13·15
4·35	4·39	5·42	5·9
3·03	4·31	1·69	3·8
1·82	3·26	0·96	2·86

The first (Runs 9–15) was obtained on the column with less efficient internal geometry. The calculated values of (L/H_c+1) (shown in Fig. 4) approach unity, which indicates a very low coalescence rate. As a consequence, the accuracy of determination of H_c is decreased making the evaluation of H_c uncertain.
The second group (Runs 1–8) was carried out on the column with more efficient internal geometry. Fig. 5 is a graphical representation of Equation (33), where the points denote the mean values of 2–8 measurements, performed under the same energy input conditions, and where Run 16 has been also included. The straight line is the best fit of the data with theoretical slope 0·5 and corresponds to:

$$C_3 = 4{\cdot}42 \cdot 10^{-2} \quad . \quad . \quad . \quad . \quad . \quad . \quad . \quad . \quad . \quad (34)$$

Full-scale experiments

The analysis of the dependence of the variance of the response function based on Equation (23) has been applied to the evaluation of longitudinal mixing of the dispersed phase in an industrial RDC–extractor, extracting phenol from waste water by butyl acetate. Characteristics of the extractor are given in Table II and experimental conditions in Table VII. Radioactive ^{82}Br was applied in form of bromobenzene as a tracer of the dispersed organic phase and injected into the inlet tube, immediately before the phase distributor. Response curves were recorded by a recording radiometer at distances $L = 1{\cdot}43$, $3{\cdot}45$ and $7{\cdot}55$ m from the distributor. An example of the response curves obtained is shown in Fig. 6.

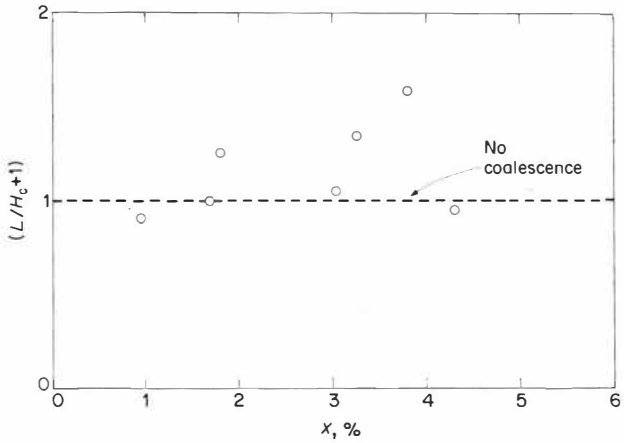

FIG. 4. *Results of laboratory experiments for slow coalescence region*

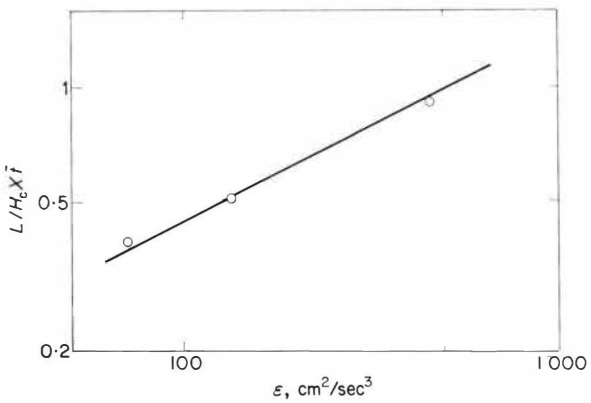

FIG. 5. *Results of laboratory experiments for rapid coalescence region*
The line represents $L/H_cXt = 0{\cdot}0442\ \sqrt{\varepsilon/\nu}$

TABLE VII

Conditions and results of full-scale experiments

Parameter	Experiment 1			Experiment 2		
Q_d, m³/h	5·2			5·8		
Q_c, m³/h	62			62		
X	0·07			0·14		
n_r rev/min	27			32		
L, m	1·43	3·41	7·55	1·43	3·41	7·55
$\bar{t}_L$, min	2·6	6·2	14·0	3·9	9·1	20·5
$\bar{\sigma}^2$	0·67	0·37	0·22	0·69	0·36	0·17
$\bar{\sigma}_c^2$	0·218	0·090	0·041	0·283	0·119	0·086
$\dfrac{1}{\bar{\sigma}^2-\bar{\sigma}_c^2(1+\bar{\sigma}_u^2)}$	2·81	4·17	6·20	3·94	5·45	11·6
σ_u^2	0·55			0·44		
H_e, m	4·2			1·5		
H_m, m	0·31			0·41		

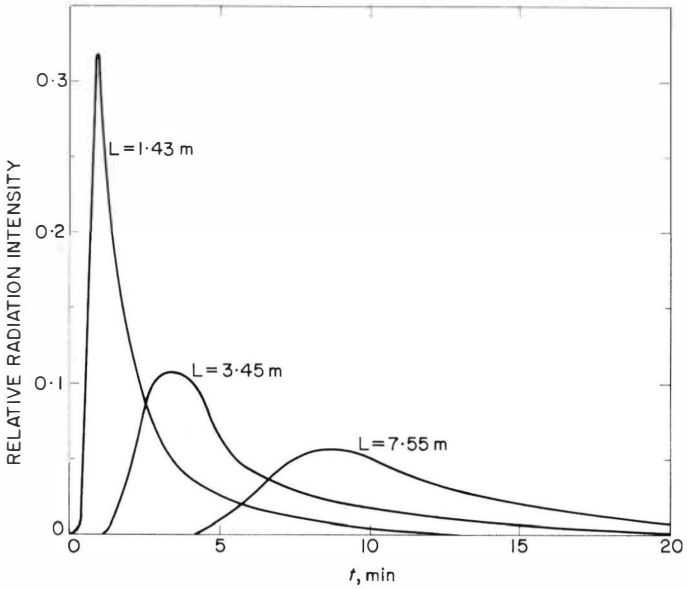

FIG. 6. *Full-scale runs response curves (example)*
Q_c 62 m³/h; Q_d 5m³/h; n_r 27 rev/min

The results of previous measurements of backmixing of the continuous phase, carried out on the same extractor by a similar injection method using an organic dyestuff as a tracer and colorimetric analyses of the response, have been correlated by Equation (1) with constants:

$$A = 0{\cdot}5 \text{ and } B = 0{\cdot}061 \quad . \quad . \quad . \quad . \quad . \quad . \quad . \quad . \quad (36)$$

which are in close agreement with results published by other authors.[3,8]

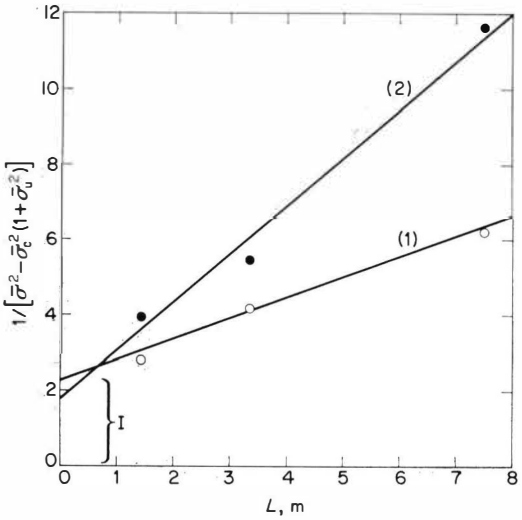

FIG. 7. *Evaluation of constants in Equation (23) from Equation (37)*
Slope $= 1/\sigma_u^2 H_c$; intercept $I = 1/\sigma_u^2$
Series (1): $\bar{\sigma}_u^2$ 0·55, H_c 4·2 m;
Series (2): $\bar{\sigma}_u^2$ 0·44, H_c 1·5 m

The average values of $\bar{t}$, $\bar{\sigma}^2$ resulting from two series of measurements as well as values of $\bar{\sigma}_c^2$ calculated from Equations (1) and (36) while using $u = L/\bar{t}$ are summarised in Table VI. Constants $\bar{\sigma}_u^2$ and H_c were obtained by an iteration procedure. In accordance with a rearranged form of Equation (23):

$$\frac{1}{\bar{\sigma}^2-\bar{\sigma}_c^2\,(1+\bar{\sigma}_u^2)} = \frac{1}{\bar{\sigma}_u^2} + \left(\frac{1}{\bar{\sigma}_u^2 H_c}\right) L \quad . \quad . \quad . \quad . \quad . \quad . \quad (37)$$

the plot of $1/[\bar{\sigma}^2-\bar{\sigma}_u^2(1+\bar{\sigma}_c^2)]$ vs. L gives a straight line with intercept $1/\bar{\sigma}_u^2$ and slope $1/\bar{\sigma}_u^2 H_c$. The best values of constants $\bar{\sigma}_u^2$ and H_c evaluated from this condition are given in Table VII and the comparison of the derived relationship with experimental data is shown in Fig. 7.

Discussion

The results indicate that Equation (23) forms a sound basis for describing the influence of individual factors on the variance of RTD in complex polydispersed systems in a column apparatus under coalescence conditions.

The coalescence height values found in both laboratory and full-scale equipment indicate two different regions of intensity, in accordance with the concept of rapid and slow coalescence. In the intensive coalescence region, the results correspond very closely to Levich's theory[7] of coalescence in turbulent flow. It may be expected that this region represents the rapid coalescence case. For the other group, the same relation may be used as a basis for correlation. The means of the laboratory results for the first group yield the constant $C_3 = 4\cdot19\times10^{-5}$ whereas the full-scale measurements may be correlated with $C_3 = 4\cdot72\times10^{-5}$ with an error of $\pm15\%$. The fact that completely different results of Runs 1 and 2 (full-scale experiments) are well correlated with a C_3 value in the 15% error range indicates the possibility of using Equation (33) even in the slow coalescence region. It is difficult to comment on the coincidence of C_3 values in both sets of results, because system dependence may be expected.

As far as $\bar{\sigma}_u^2$ is concerned, the results (Fig. 4) expressed as $\bar{\sigma}_u^2/[\bar{\sigma}^2-\bar{\sigma}_c^2(1+\bar{\sigma}_u^2)]$ being higher than unity, exclude the possibility that $\bar{\sigma}_u^2$ predicted from Equation (30) is lower than the actual value. Also, $\bar{\sigma}_u^2$ values obtained from full-scale experiments are in good agreement with the values theoretically predicted for the hold-up sampling case.

The theoretical treatment and experimental results have shown that all three factors taken into consideration, viz. backmixing, velocity distribution and coalescence, have a significant influence on RTD and that the suggested model is a convenient means for the description of dispersed phase behaviour in agitated columns.

Nomenclature

A	constant	—
B	constant	—
a	drop diameter	m
a_{pq}	$[\int_0^\infty a^{p-3}\,f(a)\,.\,da]/[\int_0^\infty a^{q-3}\,f(a)\,.\,da]$	
D	rotor diameter	m
$f(a)$	volumetric distribution of drops present in column	
$g(a)$	volumetric distribution of drops passing through a column cross-section	
h_m	compartment height	m
H_m	equivalent height of a mixing stage	m
H_c	coalescence height	m

L	column height	m
M	mean values	—
m	number of stages (see Fig. 1)	—
n	number of stages (see Fig. 1)	—
n_r	rotor speed	rev/min
n_o	number of drops in unit volume	m^{-3}
N	number of coagulations ($N = n/m-1$)	—
t	residence time of a drop in m stages	sec
t_L	mean residence time related to the distance L	sec
u	drop velocity	m sec^{-1}
u_o	terminal drop velocity	m sec^{-1}
X	hold-up	—
z	parameter of Equation (25)	—
ε	energy dissipation	m^2 sec^{-3}
υ	kinematic viscosity	m^2 sec^{-1}
$\bar{\sigma}^2$	variance of RTD	—
$\bar{\sigma}_u^2$	variance of θ	—
$\bar{\sigma}_c^2$	variance of RTD in continuous phase under equivalent flow conditions	
θ	mean residence time of a drop in one stage	sec
ω	frequency of collisions in unit volume	m^{-3} sec^{-1}

References

[1] Míšek, T., *Rep. Res. Inst. chem. Equipment, Prague*, 1966, 671/66
[2] Rod, V., *Colln Czech. chem. Commun.*, 1968, **33,** 2855
[3] Strand, C. P., Olney, R. B., & Ackermann, G. H., *A.I.Ch.E. Jl*, 1962, **8,** 252
[4] Míšek, T., *Colln Czech. chem. Commun.*, 1963, **28,** 1631
[5] Přerovská, J., & Míšek, T., Paper presented at 3rd International CHISA Congress, Mariánské Lázně, 1969
[6] Míšek, T., *Colln. Czech. chem. Commun.*, 1964, **29,** 2086
[7] Levich, V. G., *Dokl. Akad. Nauk SSSR*, 1954, **99,** 809
[8] Stemerding, I. S., *et al.*, *Chemie-Ingr-Tech.*, 1963, **35,** 844

SESSION 4C

NUCLEAR APPLICATIONS, III

CHAIRMAN
Mr. A. Chesne

SECRETARY
Dr. I. L. Jenkins

Acidic organophosphorus extractants XV.* Extraction of americium and some fission products by di-(2-ethylhexyl)phosphoric acid from perchlorate and citrate media

by Z. Kolařík

Institut für Heisse Chemie, Kernforschungszentrum Karlsruhe, West Germany

The distributions of Am(III), Eu(III), Ce(III), Sr(II), Zr(IV) and Nb(V) were measured between solutions of di-(2-ethylhexyl)phosphoric acid in n-hexane and aqueous perchlorate and perchlorate–citrate solutions. Am(III) and trivalent lanthanides can be separated from Sr(II) and Nb(V) at $-\log [H^+] = 2$–3 with an aqueous citrate concentration of $0 \cdot 25_M$; separation from Zr(IV) can be achieved by introducing nitrilotriacetic acid into the aqueous phase and/or by using short phase-contact times. If M represents Am, Eu and Ce and HA the monomeric molecule of the extractant, the composition of the complexes prevailing in the organic phase both in the presence and absence of citrates in the system can be written as $MA_3.3HA$ and $SrA_2.4HA$.

Introduction

DI-(2-ETHYLHEXYL)PHOSPHORIC acid (HDEHP) proved to be a very efficient extracting agent in the separation of trivalent lanthanides and actinides. Good separation factors between two adjacent elements can be obtained when the elements are extracted from very weakly complexing media, namely from nitrate, chloride or perchlorate solutions. On the other hand, separation of the trivalent lanthanide and actinide groups from other elements can be achieved by extracting them from aqueous solutions containing a complexing agent. Citric acid is a promising complexant for this purpose: it is not extracted by non-polar solvents and its solubility in water as well as the complexing power are sufficiently high. This paper shows the expected effects that the most important factors i.e. hydrogen ion, citric acid and extractant concentrations, have on the group separation of trivalent actinides and lanthanides from fission products, and compares the mechanism of the extraction of some elements from perchlorate–citrate and purely perchlorate media.

Experimental

Reagents and apparatus

HDEHP was purified as described previously.[1] n-Hexane (Merck Uvasol,®) citric acid, $NaClO_4$, NaOH and $HClO_4$ (all Merck reagent grade) were used without any purification. The gamma radioactivity of ^{241}Am, ^{144}Ce–^{144}Pr, $^{152,154}Eu$ and ^{85}Sr was measured by a NaI(Tl) scintillation detector and that of ^{95}Zr and ^{95}Nb by a Ge–Li detector connected with a 4096-channel gamma analyser (TMC). The measurement of the hydrogen ion concentration has been described previously.[2]

Procedure

Samples with phase volumes of 2–4 ml were shaken in polyethylene-stoppered glass bottles with total volumes of 11–13 ml. The shaking time was 20 h in the experiments with Zr(IV) and Nb(V) and 1 h in the experiments with the other elements; preliminary experiments had shown that this time was sufficient for distribution equilibrium to be attained. Improvement of the phase separation by centrifugation was found to be unnecessary even at distribution ratios > 1000. Samples of suitable volumes were taken from both phases for radioactivity measurement and the hydrogen ion concentration was measured, if necessary, in the remainder of the aqueous phase. No inactive carriers were added and the starting concentrations of the extracted elements in the aqueous phase were $\sim 10^{-5}$M. The ionic strength was adjusted to $1 \cdot 0$ with sodium perchlorate.

*Part XIV: Submitted for publication in *J. inorg. nucl. Chem.*

Symbols and abbreviations

H_nA_n, HA and A^- are the n-meric molecule, monomeric molecule and anion of HDEHP. The subscript 'org' denotes concentrations in the organic phase, while unindexed concentrations refer to the aqueous phase. The distribution ratio of a metal is denoted D_M, and C_A and C_{Cit} are the initial concentrations of HDEHP in the organic phase and of citric acid in the aqueous phase. The initial and final equilibrium concentrations were almost identical. The C_A is always given in formality (F) units defined as the number of moles of monomeric HDEHP per litre.

Results and discussion

Fig. 1 compares the dependence of the distribution ratios of Am(III), Eu(III), Ce(III), Sr(II), Zr(IV) and Nb(V) on the hydrogen ion concentration in the presence and absence of citrates in the aqueous phase. The complex formation of the extracted metal with citrate ions in the aqueous phase is evident at $-\log [H^+] > 1$ with Eu(III), Ce(III) and Am(III), at $-\log [H^+] > 3$ with Sr(II) and over the whole $-\log [H^+]$ region studied with Zr(IV) and Nb(V). Am(III), Eu(III) and Ce(III) are separated from Sr(II) and Nb(V), but not from Zr(IV) under practically equilibrium conditions (i.e. after shaking for several hours) at $-\log [H^+] = 2$–3. At shaking times of several minutes, however, good separation from Zr(IV) can be achieved, because of the slow rate of Zr(IV) extraction.

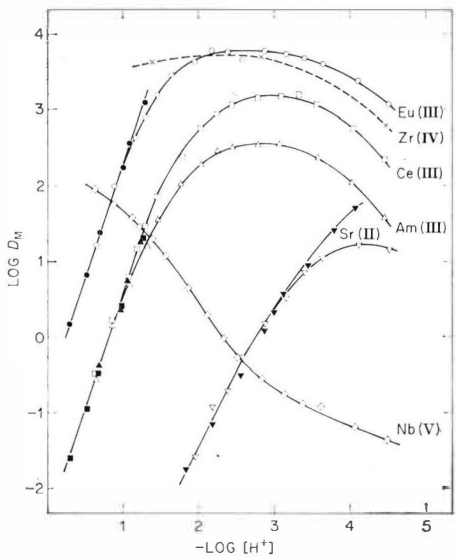

FIG. 1. *Distribution of metal species vs. hydrogen ion concentration*

Slopes of the linear ascending parts of the curves are 3·0 with Am(III), Eu(III) and Ce(III) and 2·0 with Sr(II); n-hexane diluent; ●■▼▲ without citrate; × ◇○□▽△ 0·25M citrate(aq.); 0·3F HDEHP in all cases

Nevertheless, the separation from Zr(IV) can be significantly improved even under equilibrium conditions by introducing nitrilotriacetic acid (NTA) into the aqueous phase. As seen in Fig. 2, NTA only decreases the distribution of Am(III) and Eu(III) slightly, but it markedly affects that of Zr(IV). A good separation from Zr(IV) should be attained at the short phase contact times used in practice, with both the NTA and the kinetic effects contributing to the suppression of Zr(IV) extraction. The distribution equilibrium is reached after shaking for ~3 min with trivalent elements, while the intermediate distribution of Zr(IV) is still at least 10 times less than the equilibrium one.

The effect of the aqueous citrate concentration on the distribution ratios of the trivalent elements at $-\log [H^+] = -2 \cdot 9$ is shown in Fig. 3. Curves for

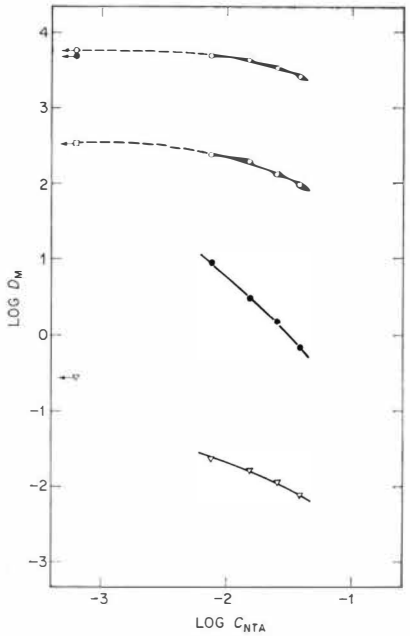

FIG. 2. *Distribution of metal species vs. concentration of nitrilotriacetic acid (NTA) in the aqueous phase*

n-Hexane diluent; ○ Eu(III), log[H⁺] = −2·87; □ Am(III), log [H⁺] = −2·83; ● Zr(IV), log [H⁺] = −2·83; ▽ Nb(V), log[H⁺] = −2·83; 0·25M citrate(aq.) and 0·3F HDEHP (org.) in all cases

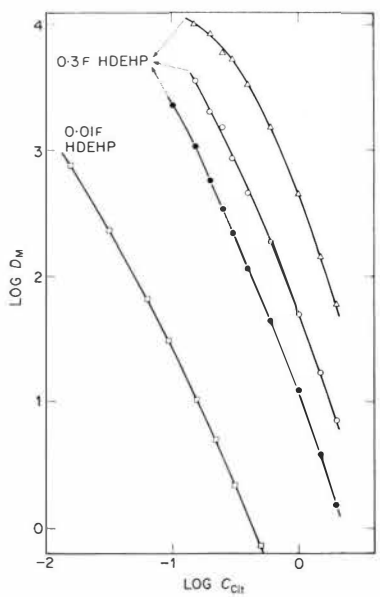

FIG. 3. *Distribution of metal species vs. total aqueous concentration of citrates*

n-Hexane diluent; △ Eu(III); ○ Ce(III); ● Am(III); △, ○, ● 0·3F HDEHP; □ Eu(III), 0·01F HDEHP; log [H⁺] = −2·85 ± 0·05 in all cases

plots of log D_M vs. log C_{Cit} were obtained in all cases; these tended to become straight lines with slopes < -2 at high citrate concentrations. This, and the, approximately zero differentiation of the log D_M vs. -log [H⁺] curve at —log

$[H^+] = 2 \cdot 9$ indicate that the most probable composition of the complexes coexisting in the aqueous phase is $M(HCit)_3^{3-}$ and $M(HCit)_2^-$ with M = Am, Eu and Ce and H_3Cit denoting the fully hydrogenated molecule of citric acid. No exact quantitative analysis of the curves shown in Fig. 3 would be justified for reasons given below.

To determine the composition of the complexes prevailing in the organic phase, the dependence of the distribution ratio on the HDEHP concentration in the organic phase was measured for each element studied, in most cases both in the absence and presence of citrate in the aqueous phase. Except for Zr(IV), the dependences shown in Figs 4–6 are in all cases curved, with D_M showing a negative deviation from the expected straight line at higher HDEHP concentrations. Thus, the curved form of the log D_M vs. log C_A plots cannot be explained by a change of the composition of the complexes in the organic phase with increasing HDEHP concentration. This would lead to a transition from a complex with a lower ligand number to a more ligand-rich complex and, consequently, an opposite curvature of the log D_M vs. log C_A plot would be observed. The partial trimerisation (or higher polymerisation) of HDEHP in the organic phase is the most plausible explanation of the curved form of the log D_M vs. log C_A plots. It was previously suggested by Dubuquoy *et al.*[3] and by Baes & Baker[4] for interpreting results obtained with HDEHP in an aliphatic diluent. However, the composition of the metal complexes predominating in the organic phase still needs clarification. In the present case the plots of log D_M vs. log C_A tend to be straight lines with slope 3 at low C_A with di- and tri-valent elements; this is especially obvious with Eu(III), where the plot covers a rather broad log C_A region (see Fig. 5). Thus the formation in the organic phase of complexes containing six monomeric units of HDEHP as ligands and Eu^{3+}, Ce^{3+}, Eu^{3+} and Sr^{2+} as central ions is a proper starting point for interpreting the log D_M–log C_A data. A very simple but illustrative analysis of the data can be carried out by plotting 3 log C_A −log D_M vs. log C_A. The points of the plot should fit the normalised curve log y = log $(1 + x)$ if, in increasing C_A, the deviation of the log D_M vs. log C_A plot from a straight line is caused only by the transition of HDEHP from the dimeric to the trimeric state. Fitting the normalised curve of the type log y = log $(x^2 + x^3)$ directly to the log D_M vs. log C_A curves is also possible, but its usefulness is much less than that of fitting of the normalised curve log y = log $(1 + x)$. The latter normalised curve is especially suitable for visual comparison with experimental data because of the zero slope of its left asymptote. The intersecting point of the asymptotes of the log y = log $(1 + x)$ curve designates a C_A value at which one half of the HDEHP in the organic phase exists in the dimeric form; this concentration will be denoted as $^\circ C_A$. Since the concentration of the monomeric HDEHP species in the organic phase is negligible in comparison with that of the dimeric and trimeric species, it is valid at $C_A = {}^\circ C_A$ that $2[H_2A_2]_{org} = 3[H_3A_3]_{org}$ and

$$C_A^{0 \cdot 5} = 1 \cdot 33\, K_2^{1 \cdot 5}\, K_3^{-1} \qquad (1)$$

where K_2 and K_3 are the dimerisation and trimerisation constants of HDEHP respectively.

The plots of data obtained here and some published data as 3 log C_A – log D_M vs. log C_A are shown in Figs 7–9. The fit between the data and the normalised curve of log y = log $(1 + x)$ is fairly good in all cases, with the exception of some points for high C_A in the presence of citrates. Thus, it can be considered as proven that the negative deviation of the log D_M vs. log C_A plots from the expected straight lines are due predominantly to the partial trimerisation of HDEHP in the organic phase. An eventual compensation of the counteracting effects owing to partial polymerisation of HDEHP beyond the trimer, and to a change in the composition of the complexes in the organic phase with increasing C_A, is not probable. The fit between the distribution data and the normalised curve shown in Figs 7–9 is observed with extracted metals ranging from Sr(II) to Fe(III) and which differ markedly in their chemical nature.

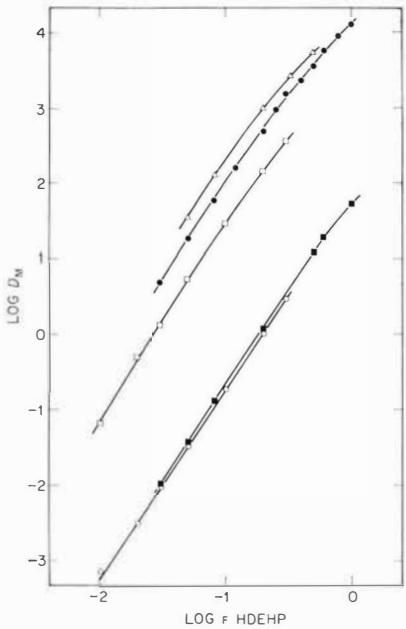

FIG. 4. *Distribution of metal species vs. organic HDEHP concentration*

n-Hexane diluent; △ Am(III), 0·1M citrate, log [H⁺] = −2·83; ● Ce(III), 0·25M citrate, log [H⁺] = −2·73; □ Am(III), 0·25M citrate, log [H⁺] = −2·83; ■ Ce(III), without citrate, log [H⁺] = −1·00; ○ Am(III), without citrate, log [H⁺] = −1·00

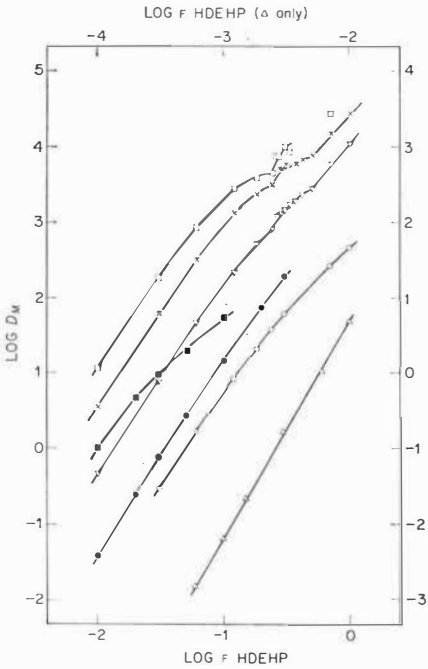

FIG. 5. *Distribution of Eu(III) vs. organic HDEHP concentration*

n-Hexane diluent; citrate, M: □ 0·15; × 0·25; ▽ 0·6; ■ 0·25: ● without citrate; ○ 2·0; △ without citrate log [H⁺]: □, × −2·87; ▽ −2·84; ■ −4·50; ● −0·70; ○ −2·79; △ −1·70

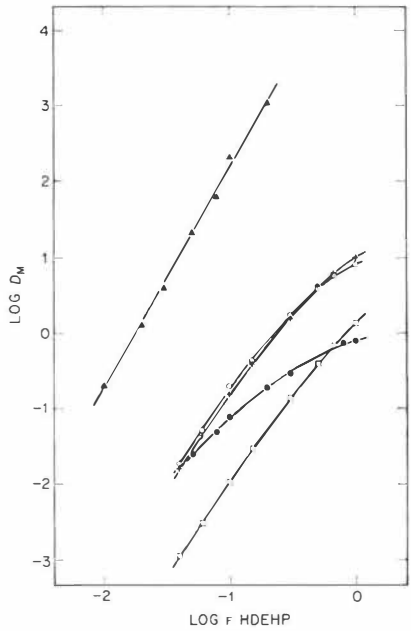

FIG. 6. *Distribution of metal species vs. organic HDEHP concentration*

Data on Sr(II) given without the correction for small $-\log[H^+]$ changes; n-hexane diluent; ▲ Zr(IV), 0·25M citrate. $\log[H^+] = -2{\cdot}83$; + Sr(II), 0·25M citrate, $\log[H^+] = -2{\cdot}80$; ○ Sr(II), 0·15M citrate, $\log[H^+] = -2{\cdot}84$; ● Nb(V), 0·25M citrate, $\log[H^+] = -2{\cdot}83$; □ Sr(II), 2·0M citrate, $\log[H^+] = -2{\cdot}70$

The following objections to this interpretation might be raised. The complexes formed by Eu(III), Am(III) and Ce(III) in the organic phase are of the type $MA_3.2HA$ (as suggested by Dubuquoy *et al.*[3]) and hence the data should be plotted as $2{\cdot}5 \log C_A - \log D_M$ vs. $\log C_A$ and fitted to the normalised curve $\log y = 0{\cdot}883 \log(1 + x)$. However, the data obtained with Eu(III) in the absence of citrates and the data of Baes & Baker[4] obtained with Fe(III) indicate clearly the formation of complexes of the type $MA_3.3HA$ and the fit of the data with the corresponding normalised curve is visibly worse with $2{\cdot}5 \log C_A$ than with $3 \log C_A$; this is shown for Fe(III) in Fig. 9. Thus, the $^{\circ}C_A$ values found in fitting the data on Eu(III) and Fe(III) with the normalised curve in the coordinate system $3 \log C_A - \log D_M$ vs. $\log C_A$ can be considered as being reliable. Consequently, of the coordination systems with $2{\cdot}5 \log C_A$ and $3 \log C_A$ that is the proper one for fitting the data on any other extracted metal in which a $^{\circ}C_A$ value is found similar to those obtained with the data on Eu(III) and Fe(III). Even though in many cases a comparably good fit of the data with a normalised curve is found in coordinate systems with both $2{\cdot}5 \log C_A$ and $3 \log C_A$, the formation of complexes with six monomeric HDEHP units in the organic phase by Sr(II) and trivalent elements is a much more probable explanation of the distribution data than the formation of complexes with five monomeric HDEHP units. This can be concluded from the fact that fitting the data to the normalised curve with $2{\cdot}5 \log C_A$ yields in all cases a $^{\circ}C_A$ value which is considerably higher than that found with Eu(III) and Fe(III) and which is taken as being reliable.

To conclude, both in the presence and absence of citrate in the aqueous phase, the composition of the complexes prevailing in n-hexane diluent at C_A up to 1F is $MA_3.3HA$ with M = Am, Eu and Ce and $SrA_2.4HA$. HDEHP exists under these conditions in n-hexane (and most probably also in other aliphatic diluents) as a mixture of comparable amounts of dimeric and trimeric species. The same interpretation applies to the data on the extraction of Sr(II) by HDEHP in

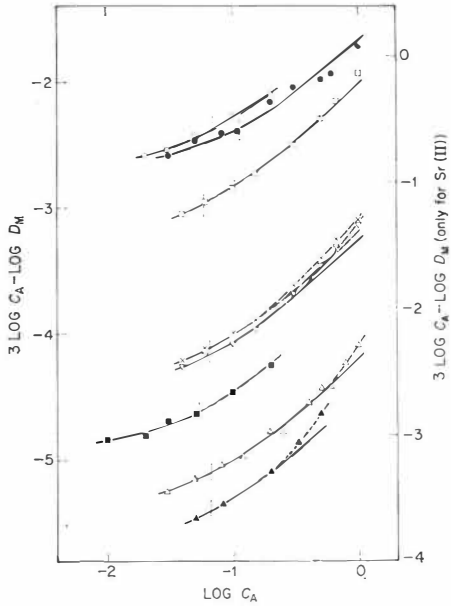

FIG. 7. *Transformation of the data given in Figs 4 and 6 and fitting of the data to the normalised curves log* y = *log* (*1*+x)

Data for Sr(II) corrected for small –log [H+] changes at high C_A; the °C_A values are marked by vertical lines ○ Am(III), without citrate; ● Ce(III), without citrate; □ Sr (II),2M citrate; × Sr(II), 0·25M citrate; ▽ Sr(II) 0·15M citrate; ■ Am(III), 0·25M citrate; △ Ce(III), 0·25M citrate; ▲ Am(III), 0·15M citrate

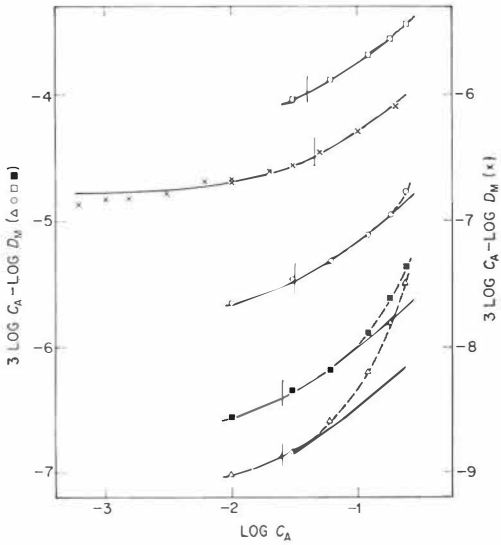

FIG. 8. *Transformation of the data on Eu(III) given in Fig. 5 and fitting of the data to the normalised curves log* y = *log* (*1*+x)

Only experimental points valid for $C_A \leqslant 0{\cdot}24$F were taken; the °C_A values a remarked by vertical lines; □ 2M citrate; × without citrate; ○ 0·6M citrate; ■ 0·25M citrate; △ 0·15M citrate

n-heptane diluent[5] and on the extraction of Sr(II) and Eu(III) by HDEHP in hexane, octane, decane and dodecane diluents.[3]

The agreement between the log °C_A values found with various extracted elements from the plots of 3 log C_A – log D_M vs. log C_A is good enough for corroborating qualitatively the above conclusions about the composition of the complexes in the organic phase. However, it is not sufficiently good for an

exact calculation of the trimerisation constant of HDEHP from Equation (1). Only a rough estimation is possible, using the value of log $K_2 = 4 \cdot 6$ taken from the papers by Ul'yanov & Sviridova[6,7] and by the present author,[8] with the result log $K_3 = 7 \cdot 7 \pm 0 \cdot 3$.

Rather significant positive deviations of some points of the plots 3 log C_A – log D_M vs. log C_A from the normalised curve are observed in the presence of citrate in the aqueous phase at high HDEHP concentrations in the organic phase. This means that the respective D_M values are lower than expected. The deviations become more significant in lowering the citrate concentration from 2·0 to 0·15M. No definite explanation has yet been found for this

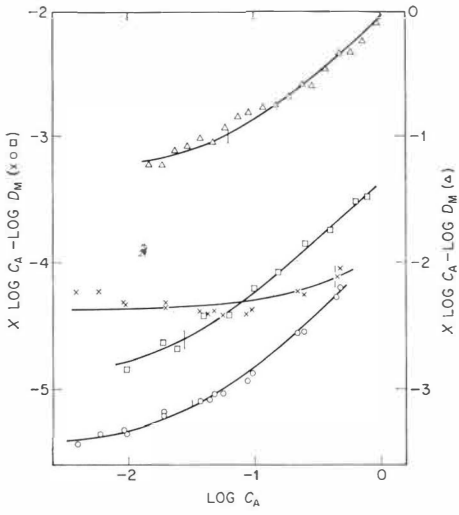

FIG. 9. *Transformation of the published data on Fe(III)*[4] *and on Eu(III) and Sr(II)*[3] *and their fitting of the data to normalised curves*

Normalised curves: log $y = 0 \cdot 883$ log $(1 + x)$ (Fe(III), $X = 2 \cdot 5$) and log $y =$ log $(1 + x)$ (other curves); the °C_A values are marked by vertical lines; △ Sr(II), $X = 3$; □ Eu(III), $X = 3$; × Fe(III), $X = 2 \cdot 5$; ○ Fe(III), $X = 3$

phenomenon; several possible explanations, however, can be definitely excluded. The deviations are not caused by a higher polymerisation than the trimer or by a change of the thermodynamic activity coefficient of HDEHP, because their extent depends markedly on the nature of the extracted metal (see Figs 7 and 8). The participation of citrate ions or citric acid molecules in the formation of metal or molecular complexes in the organic phase is very improbable; the deviations appear only at high C_A/C_{Cit} ratios and, moreover, no evidence was found for the transfer of citrates or citric acid into the organic phase either in the presence or absence of macro amounts of Eu(III) in the system. It is probable that the occurrence of the deviations is connected with the presence of HDEHP in the organic phase partially in the form of a sodium salt. The present log $[H^+]$ measurements and the data of McDowell[9] show that the fraction of HDEHP converted to a sodium salt in an aliphatic diluent is not negligible under the conditions used to obtain the log D_M – log C_A data. The unexpected shape of the log D_M vs. log C_A plot obtained with Eu(III) at very high D_M could also be connected with the partial conversion of HDEHP to a sodium salt.

The deviations described in the preceding paragraph would make it impossible to obtain an exact determination of the stability constants of metal citrate complexes by measuring the distribution of the metal species between an aqueous citrate solution and a solution of HDEHP in n-hexane.

An apparently linear log D_M vs. log C_A plot was found with Zr(IV) (Fig. 6). It must be emphasised that the accuracy of the radioactivity measurement was

lower here than in the other cases and some curvature can be hidden in the scattering of the experimental points. However, compensation of the effect of partial HDEHP trimerisation by the effect of a change of the composition of a Zr(IV) complex in the organic phase cannot be excluded. The variety of complexes formed with HDEHP in the organic phase by tetravalent elements is wider than in the case of trivalent elements (see e.g. the papers by Navrátil[10] and Peppard *et al.*[11]). No detailed interpretation can be suggested for the log D_M vs. log C_A dependence obtained with Nb(V), as the nature of Nb(V) species in solutions is extremely complex. It is obvious, nevertheless, that the Nb(V) complex (or complexes) existing in the organic phase contain less HDEHP than any other metal complexes studied in this work.

The extraction of Eu(III) from an aqueous citrate solution at $-\log [H^+] = 4 \cdot 50$ has a complicated character (see Fig. 5), which can be ascribed to nearly complete conversion of HDEHP in the organic phase to a sodium salt;[9] its tendency toward trimerisation and higher polymerisation is much more pronounced than that of the acid form of HDEHP.[12]

Acknowledgment

The author expresses his thanks to Dr. G. Koch for valuable discussions.

References

[1] Kolařík, Z., & Pánková, H., *J. inorg. nucl. Chem.*, 1966, **28,** 2325
[2] Kolařík, Z., Hejná, J., & Moravec, A., *J. inorg. nucl. Chem.*, 1967, **29,** 1279
[3] Dubuquoy, C., Guillaumont, R., & Boussières, G., *Radiochim. Acta*, 1967, **8,** 49
[4] Baes, C. F., jun., & Baker, H. T., *J. phys. Chem., Ithaca*, 1960, **64,** 89
[5] Šístková, N. V., Kolařík, Z., Bárta, K., & Pánková, H., *J. inorg. nucl. Chem.*, 1968, **30,** 1595
[6] Ul'yanov, V. S., & Sviridova, R. A., *Radiokhimiya*, 1963, **5,** 419
[7] Ul'yanov, V. S., & Sviridova, R. A., *Radiokhimiya*, 1970, **12,** 47
[8] Kolařík, Z., *Colln Czech. chem. Commun.*, 1967, **32,** 311
[9] McDowell, W. J., *J. inorg. nucl. Chem.*, 1968, **30,** 1037
[10] Navrátil, O., *J. inorg. nucl. Chem.*, 1967, **29,** 2007
[11] Peppard, D. F., Mason, G. W., & McCarty, S., *J. inorg. nucl. Chem.*, 1960, **13,** 138
[12] Myers, A. L., McDowell, W. J., & Coleman, C. F., *J. inorg. nucl. Chem.*, 1964, **26,** 2005

Solvent extraction of some diprotic nitroaromatic acids and their complexes with some actinides by tributyl phosphate

by M. M. Šečerov*, M. M. Kopečni, Z. B. Maksimović, and M. Beran

Boris Kidrič Institute of Nuclear Sciences, Belgrade, Yugoslavia, and Institute of Nuclear Research of Czechoslovak Academy of Sciences, Řež, Prague, Czechoslovakia

Solvent extraction of 3,5-dinitrosalicylic ($H_2$3,5-DNSal), 5-nitrosalicylic ($H_2$5-NSal) and 4-nitrophenol-2-sulphonic ($H_2$4-NPh-2-S) acids and of their Pu^{4+} and UO_2^{2+} complexes from 1M-(H,Na)Cl medium with tributyl phosphate in n-dodecane has been investigated. The composition of the predominant extractable species has been determined by slope analysis. The possible utilisation in separation processes is discussed in general terms.

Introduction

DURING a search into new applications of the tributyl phosphate (TBP) solvent extraction system, uses have been discovered for a group of diprotic nitroaromatic acids, the metal complexes of which are extractable by TBP. The first acid, 3-nitro-*p*-cresol-5-sulphonic acid ($H_2$3-N-*p*-Cr-5-S), has already been reported.[1] Related compounds have been investigated and the results obtained with three of them are presented in the present paper.

Experimental

Reagents

All diprotic nitroaromatic acids (or their salts) used were products of Fluka A.G. They were purified by double or triple recrystallisation. Tri-n-butyl phosphate (BDH)* was purified by vacuum distillation. All other reagents, including n-dodecane, were of analytical grade.

Radiochemically pure ^{239}Pu and ^{233}U were used in the experiments. These isotopes, and also ^{144}Ce and ^{152}Eu, supplied by U.K.A.E.A., Amersham, U.K., were used without the addition of a carrier. A solution of zirconium(IV) nitrate labelled with ^{95}(Zr + Nb) was prepared by irradiating ZrO_2 in the Boris Kidrič Institute reactor by thermal neutrons, dissolving in concentrated HNO_3 and diluting to 1 M-HNO_3.

Apparatus

The Nuclear Chicago DS5–5 gamma scintillation and Unilux II alpha liquid scintillation sets were used for the radioactivity measurements. All spectrophotometric determinations were performed in a Beckman DK-1A spectrophotometer. A Beckman research pH-meter with combined glass–calomel electrode was used for pH determinations.

Distribution experiments

The experiments were performed at $25 \pm 0 \cdot 2$°C. Equal volumes of aqueous and organic phases were shaken for 20 min in a mechanical shaker (these conditions were found to be sufficient to reach equilibrium). The organic phase was prepared by diluting TBP with n-dodecane. The aqueous phase, which contained trace amounts of the radioisotopes and the required concentrations

*Present address: Institute of Technology of Nuclear and Other Mineral Raw Materials, Belgrade, Yugoslavia.

*British Drug Houses

of the nitroaromatic acids (or salts) in 1 M–(H,Na)Cl solution with variable hydrogen ion concentration, was prepared by mixing standard solutions of HCl, NaCl and nitroaromatic acids and the stock solutions of radioisotopes. The valence state of Pu^{4+} in the aqueous phase was maintained by 10^{-2}M sodium nitrite.

Hydrogen-ion concentration (h) at $h > 0 \cdot 1$ was calculated from the amount of standard HCl solution added. Lower h values were attained by partial neutralisation with NaOH solution to the desired pH and were measured after equilibration.

Distribution coefficients of the nitroaromatic acids were determined spectrophotometrically by measurements on the initial and equilibrium aqueous phases at 310 nm ($H_2$5-NSal and $H_2$4-NPh-2-S) and 335 nm ($H_2$3,5-DNSal).

Distribution coefficients of the metals were determined by liquid scintillation alpha counting (^{239}Pu and ^{233}U) and gamma scintillation counting (^{144}Ce, ^{152}Eu and ^{95}Zr) in both equilibrated aqueous and organic phases.

Distribution experiments involving the nitrate medium were performed with $0 \cdot 4$ M-HNO_3 only.

Results

Extraction of the nitroaromatic acids themselves, at hydrogen ion concentration $> 0 \cdot 1$ M, is almost independent of their equilibrium concentrations in the aqueous phase.

Only a small reduction in the distribution coefficient can be observed at increasing total nitroaromatic acid concentration; this fall lies within the

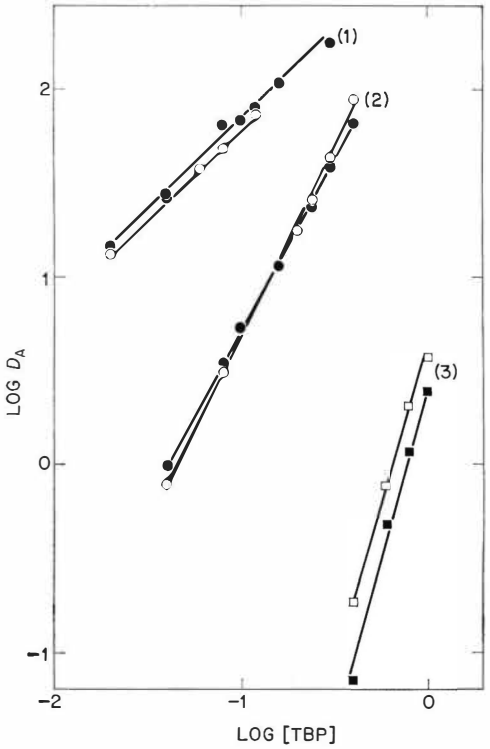

FIG. 1. *Extraction of diprotic nitroaromatic acids from* 1M-*(H,Na)Cl as a function of the TBP concentration and acidity of the aqueous phase*

h: ● 0·1 M; ○ 0·2 M; ■ 0·6M; □ 1·0M
(1) $H_2$5-NSal; (2) $H_2$3,5-DNSal; (3) $H_2$4-NPh-2-S
Slopes: (1)1; (2)2; (3)3

experimental error range and may therefore be neglected. Thus, it may be expected that the slopes of the log D_A vs. log ^eTBP plots in Fig. 1 indicate the solvation numbers of the simple molecules of nitroaromatics acids.

It was also found that the distribution coefficients of Pu^{4+} and UO_2^{2+} were independent of the total metal concentration under the given experimental conditions. It may be assumed that no polymerisation equilibria either in the organic or in the aqueous phase complicate the results of the distribution experiments with Pu^{4+} (Figs 2 and 3) and UO_2^{2+} (Figs 4 and 5).

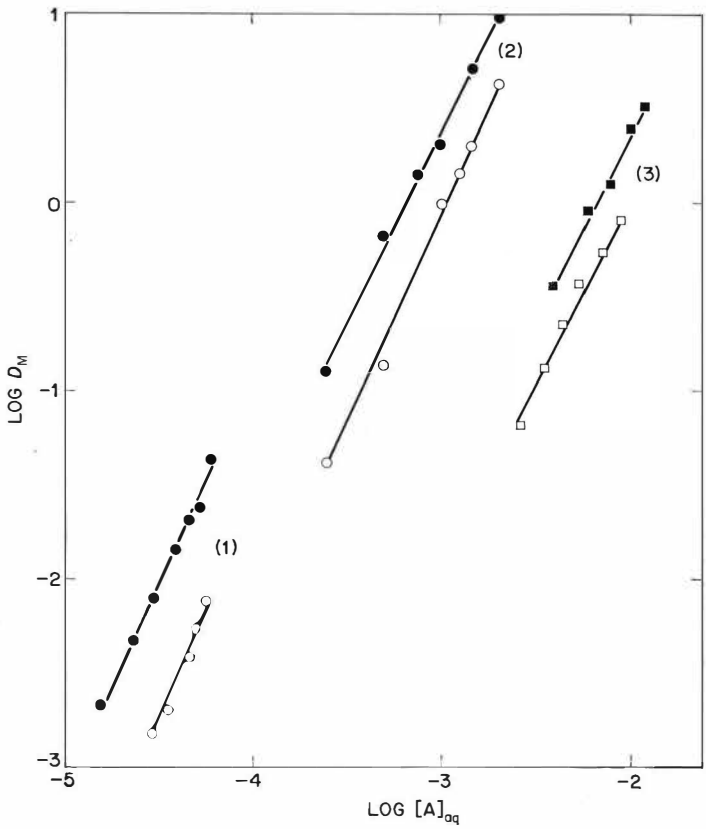

FIG. 2. *Extraction of Pu^{4+} complexes from 1M-(H,Na)Cl as a function of the equilibrium nitroaromatic acid concentration and acidity of the aqueous phase*

h : ● 0·1M, ○ 0·2M, ■ 0·25M, □ 0·85M.
[TBP] : (1) 0·05 M ($H_2$5-NSal); (2) 0·2 M ($H_2$3,5-DNSal); (3) 1·0 M ($H_2$4-NPh-2-S)
Slopes : 2 for all three cases

Extraction of trace amounts of ^{239}Pu, ^{233}U, ^{144}Ce, ^{152}Eu and $^{95}Zr + ^{95}Nb$ from 0·4 M-HNO_3 containing $H_2$3,5-DNSal or $H_2$4-NPh-2-S has been studied to verify the application of nitroaromatic acids to an actual separation system. The results are shown in Table I.

TABLE I

Extraction into TBP of ^{239}Pu, ^{233}U, ^{144}Ce, ^{152}Eu and $^{95}Zr + ^{95}Nb$ from 0·4 M-HNO_3 containing nitroaromatic acids

$[A]_{aq}$, M	D_M									
	$H_2$3,5-DNSal, [TBP] = 0·2M					$H_2$4-NPh-2-S, [TBP] = 1·0M				
	Pu	U	Ce	Eu	Zr+Nb	Pu	U	Ce	Eu	Zr+Nb
—	0·008	0·109	0·00303	0·00036	0·0365	0·03	1·77	0·00584	0·00736	0·0206
9×10^{-3}	0·767	0·112	0·00348	0·00049	0·0439	1·66	1·85	0·00624	0·00746	0·0152

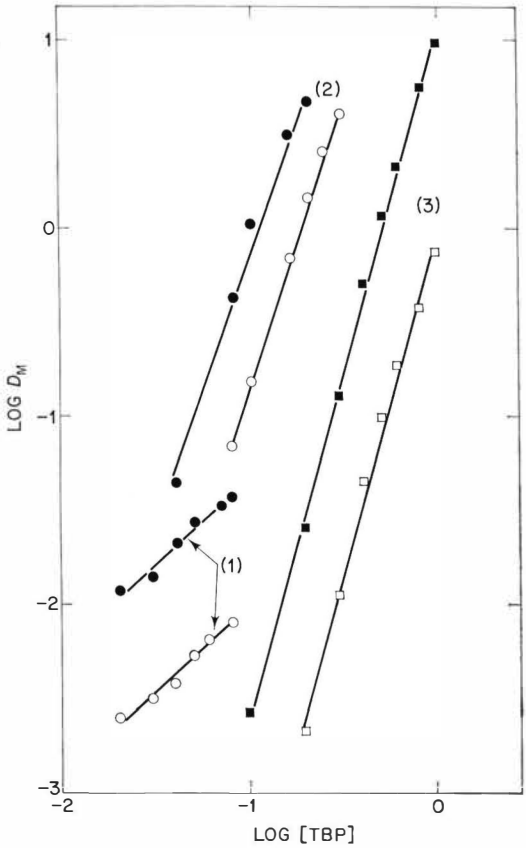

FIG. 3. *Extraction of Pu^{4+} complexes from* 1M-*(H,Na)Cl as a function of TBP concentration and acidity of the aqueous phase*

h values as in Fig. 2. $[A]_{aq}$: (1) 4×10^{-5}M ($H_2$5-NSal); (2) 1×10^{-3}M ($H_2$3,5-DNSal); (3) $1{\cdot}34 \times 10^{-2}$M ($H_2$4-NPh-2-S)
Slopes : (1) 1; (2) 3; (3) 4

Discussion

Under the experimental conditions described ($h \geqslant 0{\cdot}1$ M), the solvates $H_2$5-NSal.TBP, $H_2$3,5-DNSal.2TBP and $H_2$4-NPh-2-S.4TBP seem to be extracted. The compositions of the predominant extractable metal complexes as determined by the method of slope analysis (Figs 2–5) are Pu(5-NSal)$_2$.TBP, Pu(3,5-DNSal)$_2$.3TBP, Pu(4-NPh-2-S)$_2$.4TBP, $UO_2$5-NSal.2TBP, $UO_2$3,5-DNSal.3TBP and $UO_2$4-NPh-2-S.3TBP.

Table I shows the wide differences in distribution ratios that have been obtained for the extraction of metal ions in the presence of nitroaromatic compounds from aqueous nitric acid into TBP solutions. This could lead to high selectivity of extraction for the metal ions considered. Under certain conditions, that is, [TBP] = 0·2 M, it appears that Pu(IV) could be extracted selectively from the other metal ions present. The system with nitroaromatic acids has one other advantage compared to the classical inorganic (e.g. nitrate) system, that is, the ligand concentration can be varied through many orders of magnitude by adjustment of pH. The complicated separation of a multicomponent mixture, therefore, could possibly be realised in this way.

It should be noted that at hydrogen ion concentrations <0·1 M, there is a moderate fall in the distribution coefficients of nitroaromatic acids with increasing nitroaromatic acid concentration. This is in contrast to the negligible fall obtained at H^+ concentrations ⩾0·1 M. This effect is especially noticed in the case of nitrosalicylic acids (these results are not given in the present paper) and is very similar to that observed by Agglett & Crossley[2] for salicylic acid. It may be caused by dimerisation or a higher degree of association of nitroaromatic acids in the aqueous phase.

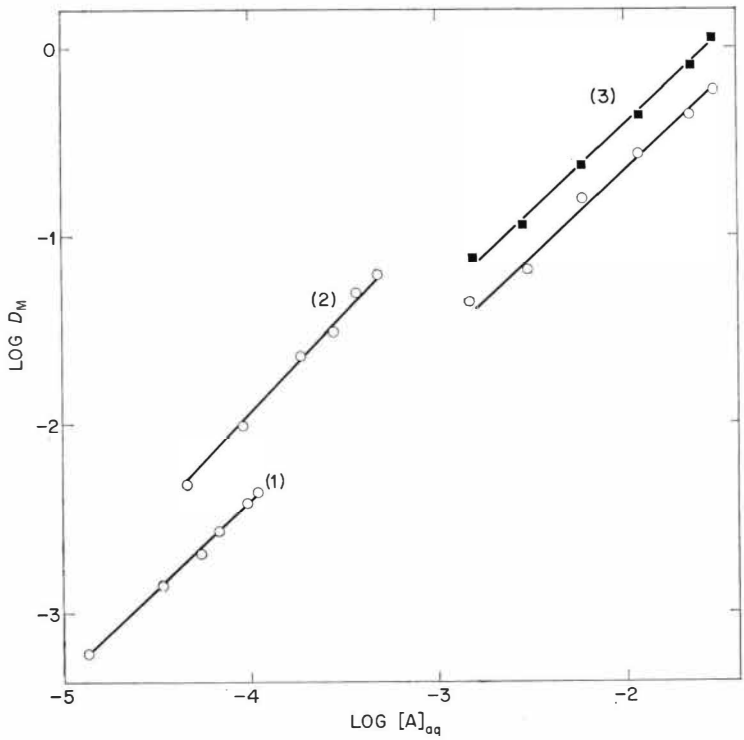

FIG. 4. *Extraction of UO_2^{2+} complexes from 1M-(H,Na)Cl as a function of the equilibrium nitroaromatic acid concentration and pH of the aqueous phase*

pH: ○ 2·0; ■ 2·5. [TBP] as in Fig. 2.
(1) $H_2$5-NSal; (2) $H_2$3,5-DNSal; (3) $H_2$4-NPh-2-S
Slopes: 1 in all three cases.

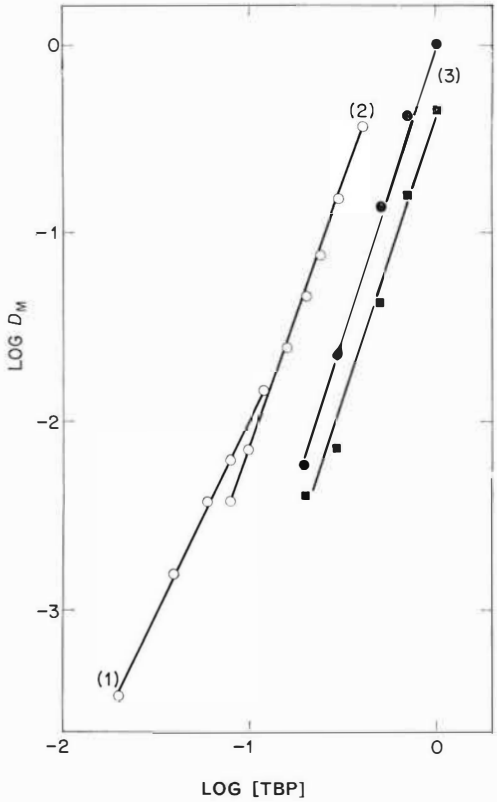

FIG. 5. *Extraction of UO_2^{2+} complexes from 1M-(H,Na)Cl as a function of TBP concentration and pH of the aqueous phase*

pH: ○ 2·0; ■ 2·5, ● 3·0
$[A]_{aq}$: (1) 4×10^{-5}M ($H_2$5-NSal); (2) 4×10^{-4}M ($H_2$3,5-DNSal); (3) $1 \cdot 8 \times 10^{-2}$M ($H_2$4-NPh-2-S)
Slopes: (1) 2: (2) and (3) 3

References

[1] Beran, M., 'Solvent Extraction Research', Eds. Kertes, A. S., & Marcus, Y., 1969, p. 75 (New York: John Wiley & Sons)
[2] Agglett, J., & Crossley, P., *J. inorg. nucl. Chem.*, 1967, **29**, 1113

Capric acid effect on actinide extraction by trilaurylammonium nitrate

by G. Koehly, C. Madic and R. Berger

Département de Chimie, Commissariat a l'Énergie Atomique,
Centre d'Études Nucléaires de Fontenay-aux-Roses, France

A decrease of the Am(III), Np(IV)–Pu(IV) and U(VI) distribution coefficients between organic solutions of trilaurylammonium nitrate and nitrate media has been observed when capric acid was added to the organic phase. A systematic study of this negative synergistic effect was then undertaken. This includes a review of the capric acid extracting properties and the effect on trilaurylamine extraction of the actinide elements at the III, IV and VI oxidation state. A tentative explanation of the extraction mechanism is proposed and the association constant of the $R_3N\ HNO_3\ (HA)_2$ *complex is calculated in the case of tetravalent species.* $\overline{K}$ *was found to be* $0{\cdot}0287 \pm 0{\cdot}0023$ *and* $p\overline{K}$ $1{\cdot}452$.

Introduction

A DECREASE OF the distribution coefficients of metallic species between trilaurylammonium nitrate solutions in inert diluents and nitric acid media has been observed when adding dinonylnaphthalene sulphonic acid in the solvent.[1] Investigations were made on organic acids, weaker extractants than dinonylnaphthalene sulphonic acid, i.e., capric, caprylic, lauric, benzoic and *o*-nitrobenzoic acids. In all the cases, the trilaurylamine extracting power was reduced and a negative synergistic effect was evidenced.[2] The utilisation of a mixture of trilaurylammonium nitrate and capric acid was therefore applied to the chemical processing of irradiated ^{237}Np.[3]

A more detailed study of this phenomenon was undertaken. The extracting properties of capric acid for the actinide elements at the III, IV and VI oxidation states were determined as well as the extraction mechanism involved. The effect of capric acid on the trilaurylamine extraction of the actinide species was also studied and a tentative explanation of the synergistic effect was proposed.

Apparatus

A Turbula mixer (Wab, Switzerland) was used to shake the centrifuge cones.

The potentiometer determinations were made with either a Metrohm Model E 336 Potentiograph or a Tacussel Autotitrigraph 3.

Reagents

Rhône-Poulenc Nuclear Grade trilaurylamine and Prolabo Reagent Grade No. 20.238 capric acid was used as received.

Progil product Solgil 54 B, consists of a mixture of mono-t-butylbenzene (> 95%) and mono-pentylbenzene (b.p. 162–172°c). All other reagents were Prolabo Analytical Grade R.P.

The radioisotopes used in this study were ^{228}Th, ^{233}U, ^{237}Np, ^{239}Pu and ^{241}Am.

Experimental

Procedure

The distribution coefficient studies were made in 15 ml glass centrifuge cones. Equal volumes of the organic and aqueous solutions (5 ml of each) were mixed for 15 min at room temperature. The actinide element concentrations in the phases were determined on aliquots evaporated down on counting planchettes and measured by α-pulse counting.

The Np(IV) and Pu(IV) distribution coefficients were measured from loaded organic solutions after scrubbing of tracer amounts of Np(VI) and Pu(VI) by the aqueous phase. For the measurement of the Am(III) and Th(IV) distribution coefficients between capric acid and aqueous solutions at pH up to 5·5, mixtures of sodium acetate–acetic acid or sodium chloroacetate–chloroacetic acid were respectively used as buffers.

The capric acid, trilaurylamine (TLA), trilaurylammonium nitrate (TLA HNO_3), and excess HNO_3 (both initial and at equilibrium) concentrations were determined by potentiometry. In the case of organic solutions a mixture of methanol and benzene was used as a solvent.

The TLA concentration associated with capric acid was graphically determined by difference between the TLA concentration in the mixture and that of TLA alone giving the same distribution coefficient.

Results

Extracting properties of capric acid

The extracting properties of capric acid for the actinide elements at the III, IV and VI oxidation states were reported in Figs. 1–4. Log–log plots of $C_{Am(III)o}$ *versus* $C_{Am(III)a}/\beta[H^+]^n$ and $C_{U(VI)o}$ *versus* $C_{U(VI)a}/\beta[H^+]^n$ were straight lines with a slope of 1. Log–log plots of $D_{Am(III)}$, $D_{Th(IV)}$ and $D_{U(VI)}$ *versus* capric acid concentrations in Fig. 2 were straight lines. Slopes of 2, 4 and 4 were respectively obtained for UO_2^{2+}, Th^{4+} and Am^{3+}. The dependence of U(VI) and Th(IV) and Am(III) distribution coefficients on $\frac{1}{[H^+]}$ are represented in Figs 3 and 4. The distribution coefficients were proportional to $1/[H^+]^2$ for U(VI) (Fig. 3) and for Th(IV) and Am(III) (Fig. 4) to $1/[H^+]^3$.

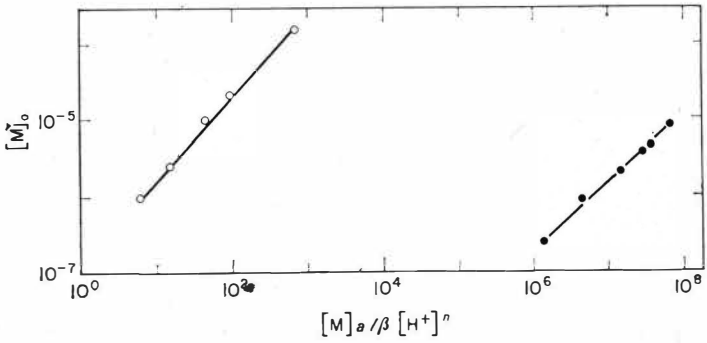

FIG. 1. *Log–log plots of* $[M]_o$ *versus* $[M]a/\beta[H]^+n$

Extractant: 1 M capric acid in benzene; aqueous phase: 1 M-$[CH_3COO^-]_{total}$ ○ UO_2^{2+}; ● Am^{3+}

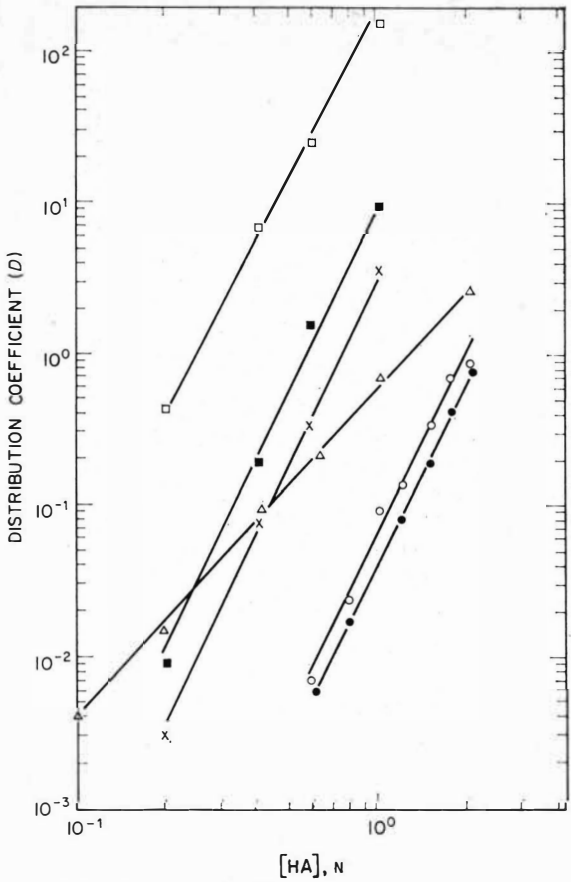

FIG. 2. *Variation of the distribution coefficients as a function of capric acid concentration*

Extractant: capric acid in benzene; aqueous phase Am^{3+}; $CH_3CO_2H/CH_3CO_2^-$ buffer □ pH 5·5; ■ pH 5; + pH 4·8; Th^{4+} $ClCH_2CO_2H/ClCH_2CO_2^-$ ○ pH 2·8; ● pH 2·6. UO_2^{2+} △ pH 3

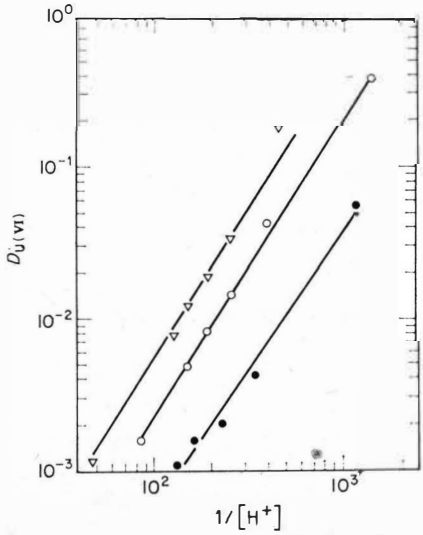

FIG. 3. *Variation of* $D_{U(VI)}$ *in capric acid as a function of* $1/[H^+]$

Extractant: ○ HA = 0·8 M in benzene; ● HA = 0·8 M in dodecane; ▽ HA = 1 M in Solgil 54 B

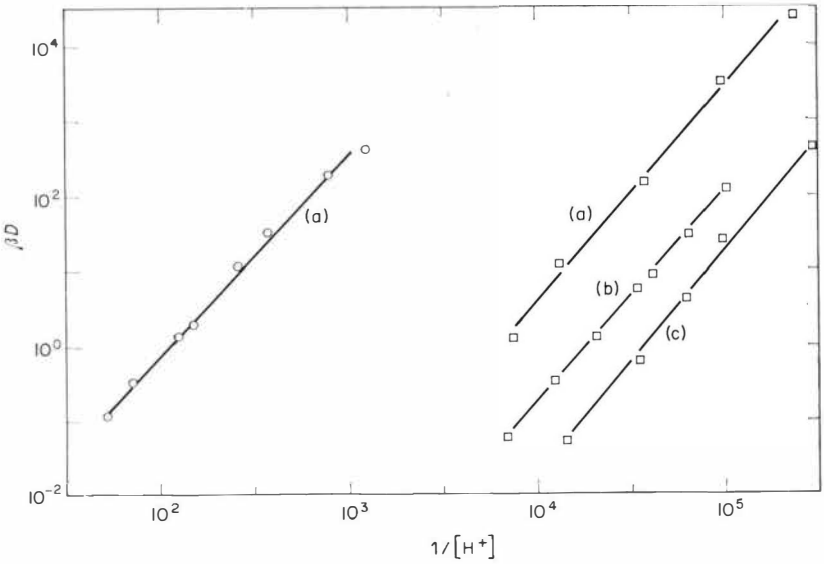

FIG. 4. *Log–log plots of* β D versus $1/[H^+]$

Extractant: capric acid in benzene: (a) = 2 M; (b) = 1 M; (c) = 0·6 M

Aqueous phase: ○ Th^{4+} $ClCH_2CO_2H/ClCH_2CO_2$ (Σ_c = 0·1 M); □ Am^{3+} $CH_3CO_2H/CH_3CO_2^-$ (Σ_c = 0·1 M)

Effect of capric acid on TLA extracting properties

The variations of the actinide elements distribution coefficients with capric acid concentration in trilaurylammonium nitrate–Solgil 54 B organic solutions are shown in Figs 5–8. In all cases the distribution coefficients decreased with the increase of capric acid concentration. The distribution coefficients of Am(III) extracted from 8 M-$LiNO_3$ solution at pH 3 were proportional to the reciprocal of capric acid concentration (Fig. 5).

The Np(IV) and Pu(IV) distribution coefficients were proportional to the reciprocal of the square of capric acid concentrations (Figs 6 and 7). Determinations of Pu(IV) distribution coefficients were made by varying the nitric acid aqueous concentration from 0·5 to 2 N and the TLA HNO_3 organic concentration from 0·08 to 0·16 M. As for Am(III), the U(VI) distribution coefficients were found to be proportional to the reciprocal of capric acid concentrations above 0·2 N (Fig. 8).

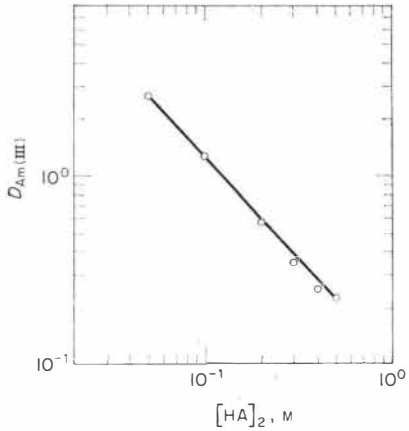

FIG. 5. *Variation of* DAm(III) *with capric acid concentration*

Extractant: 0·16 M TLA HNO_3–capric acid in Solgil 54 B; aqueous phase: 8 M-$LiNO_3$, pH 3

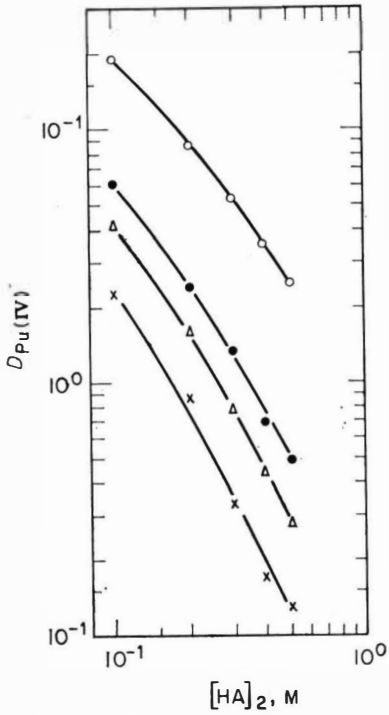

FIG. 6. *Variation of* $D_{Pu(IV)}$ *with capric acid concentration for various acidities*

Extractant: 0·16 M TLA HNO_3–capric acid in Solgil 54 B; aqueous phase: ○ 2 N-HNO_3; ● 1 N-HNO_3; △ 0·75 N-HNO_3; × 0·5 N-HNO_3

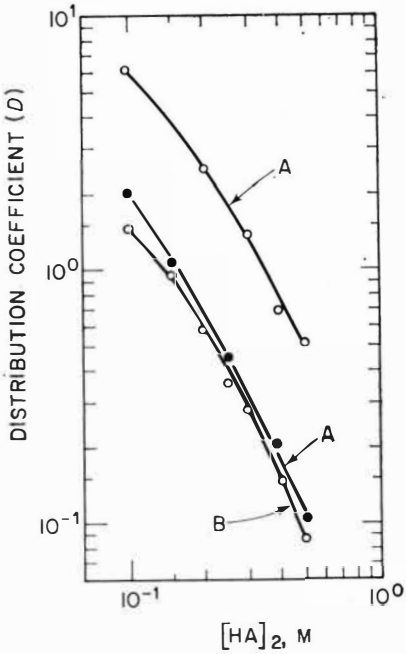

FIG. 7. *Variation of* $D_{Pu(IV)}$ *and* $D_{Np(IV)}$ *with capric acid concentration for various TLA concentrations*

Extractant A: 0·16 M TLA HNO_3–capric acid in Solgil 54 B; extractant B: 0·08 M TLA HNO_3–capric acid in Solgil 54 B

Aqueous phase: 1 N-HNO_3; ○ Pu(IV); ● Np(IV)

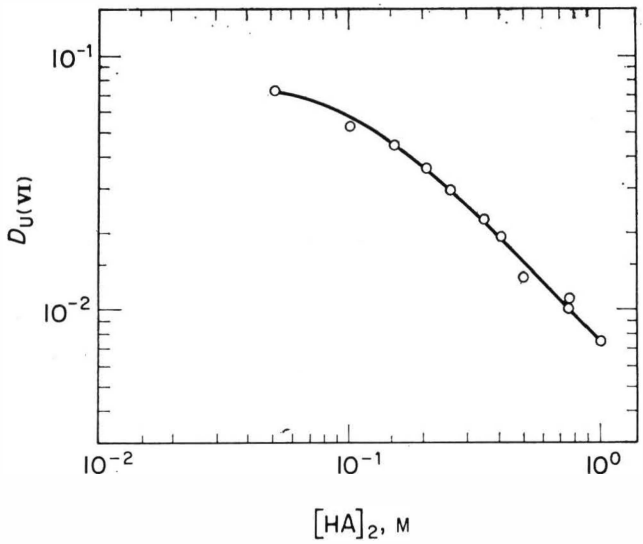

FIG. 8. *Variation of* $D_{U(VI)}$ *as a function of capric acid concentration*
Extractant: 0·16 M TLA HNO_3–capric acid in Solgil 54 B; aqueous phase: 1 N-HNO_3

The Np(IV) and Pu(IV) distribution coefficients as a function of TLA HNO_3 and TLA HNO_3–capric acid concentrations in Solgil 54 B are reported in Figs 9 and 10.

The Pu(IV) distribution coefficients between 0·16 M TLA HNO_3, 0·5 M capric acid in Solgil 54 B and 1 N-HNO_3 increased when the Pu(IV) aqueous

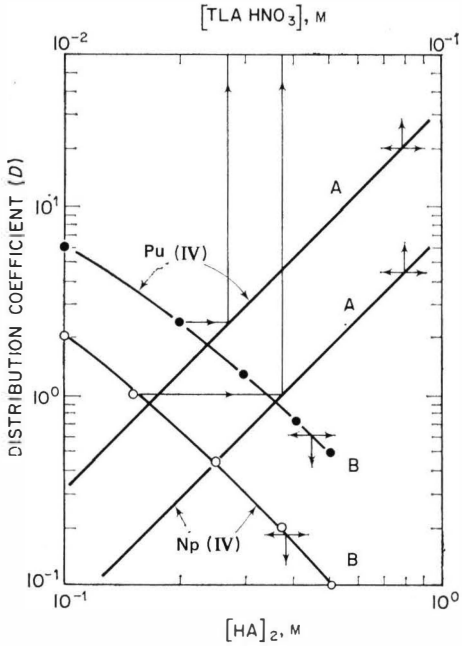

FIG. 9. *Log–log plots of* D versus *TLA or capric acid concentration for calculation of free* [*TLA* HNO_3]
Extractant A: TLA HNO_3 in Solgil 54 B; B: 0·16 M TLA HNO_3–capric acid in Solgil 54 B; aqueous phase: 1 N-HNO_3

concentrations increased up to 5×10^{-4} M and then remained constant as shown by the semi-logarithmic plot in Fig. 11. The effect of capric acid on $D_{Pu(IV)}$ as a function of the total plutonium concentration is illustrated in Fig. 12. This effect increases with the plutonium concentration.

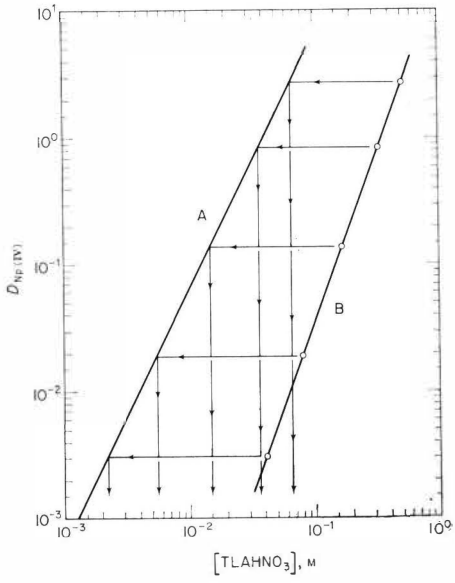

FIG. 10. *Log–log plots of* $D_{Np(IV)}$ versus *TLA or TLA capric acid mixture*

Extractant: A TLA HNO_3 in Solgil 54 B; B: TLA HNO_3–0·5 M capric acid in Solgil 54 B; aqueous phase 1 N-HNO_3

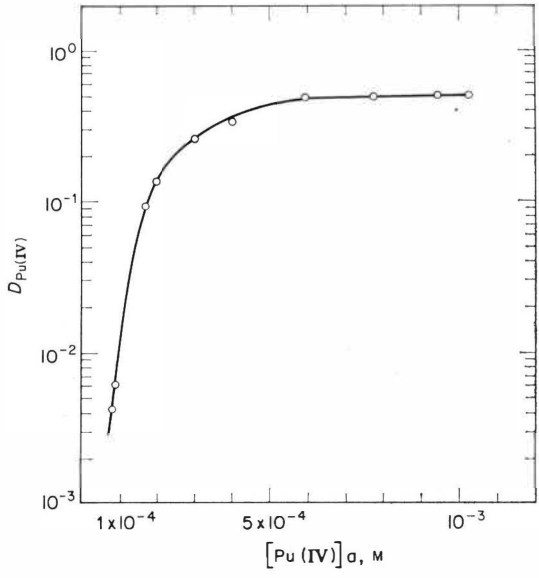

FIG. 11. *Variation of* $D_{Pu(IV)}$ *as a function of* $[Pu(IV)]_a$

Extractant: 0·16 M TLA HNO_3–0·5 M capric acid in Solgil 54 B; aqueous phase: 1 N-HNO_3

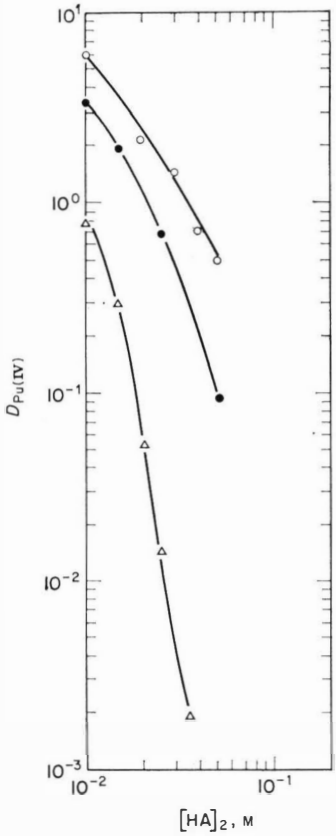

FIG. 12. *Variation of* $D_{Pu(IV)}$ *with capric acid concentration as a function of plutonium concentration*
Extractant: 0·16 M TLA HNO_3–capric acid in Solgil 54 B; aqueous phase: 1 N-HNO_3 $[Pu]_{total}$: ○ $1{\cdot}0 \times 10^{-3}$ M; ● $3{\cdot}8 \times 10^{-4}$ M; $4{\cdot}0 \times 10^{-5}$ M

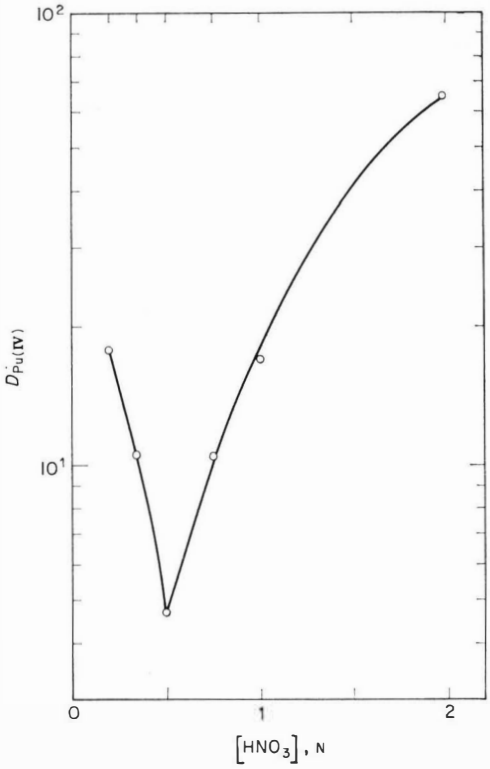

FIG. 13. *Variation of* $D_{Pu(IV)}$ *with aqueous acidity*
Extractant: 0·16 M TLA HNO_3–0·25 M capric acid in Solgil 54 B; aqueous phase: HNO_3

Enhancement of the extracting properties of capric acid at low acidity

When the aqueous acidity became very weak, an enhancement of the extracting properties of the TLA HNO_3–capric acid mixture for Pu(IV) was observed as shown by semi-logarithmic plots in Fig. 13. $D_{Pu(IV)}$ was a minimum for 0·16 M TLA HNO_3–0·25 M capric acid in Solgil 54 B and 0·5 N-HNO_3. When the capric acid concentration was raised to 0·3 M the minimum was displaced along the acidity scale to 0·2 N. The enhancement of the extracting properties of TLA HNO_3–capric acid mixtures was also demonstrated in the case of U(VI). $D_{U(VI)}$ was found to be maximum for an organic capric acid concentration of 0·32 M and 0·01 N-HNO_3 solution (Fig. 14).

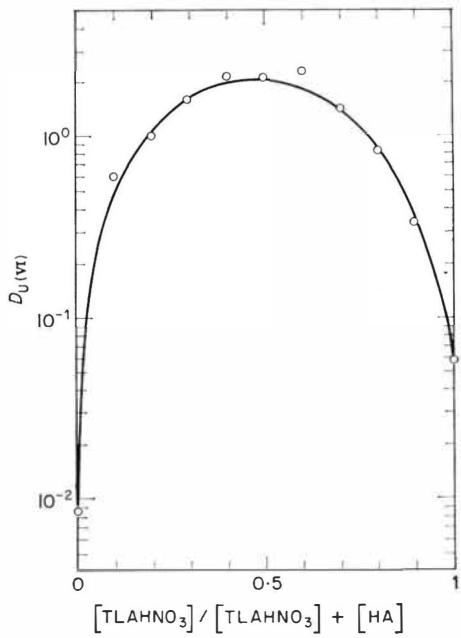

FIG. 14. *Semi-logarithmic plots of* $D_{U(VI)}$ versus $[TLA\ HNO_3]/[TLA\ HNO_3]+[HA]$

Extractant: mixtures of 0·64 M TLA HNO_3 in benzene and 0·64 M capric acid in benzene; aqueous phase: 0·01 N-HNO_3, pH 2·05

Discussion

Extraction of the actinide elements by capric acid

The extraction properties and mechanism of capric acid for metallic elements has already been studied.[4,5] The following general equation, allowing for a possible polymerisation of the metallic caprate in the organic solution, was applied to the results of this work:

$$j\,M^{n+}_{(a)} + \frac{1}{2}j\,(n+x)\,[(HA)_2]_{(o)} \rightleftharpoons (MA_n\,xHA)_{j(o)} + nj\,H^+_{(a)}$$

where j is the polymerisation number for metallic caprates,

n is the number of H^+ ions displaced from capric acid for 1 molecule of extracted metal,

x is the number of associated capric acid molecules for 1 molecule of metallic ion,

$A = CH_3(CH_2)_8COO^-$.

In the presence of complexing ions this equation can be expressed as a function of D:

$$\log D + \log C_{M(a)} = \log j\, K_{jx} + \frac{1}{2} j\,(n + x) \log C_{HA}$$

$$+ j\,(\log C_{M(a)} - \log \beta + n\,\mathrm{pH}) - \frac{1}{2} j\,(n + x) \log 2$$

$$\text{where } \beta = \left[1 + \frac{L^-}{K_1} + \frac{[L^-]^2}{K_1 K_2} + \frac{[L^-]^3}{K_1 K_2 K_3} \cdots\cdots + \frac{[L^-]^n}{K_1 K_2 K_3 \cdots K_n}\right]$$

The stability constants used in the β calculation were taken from Grenthe[6] and Day[7] respectively for Am(III) and Th(IV).

For uranyl and americium caprate the polymerisation number given by the slope of the curve in Fig. 1 was found to be 1.

In the case of Th(IV) a slope of 3 was found for the equation $\beta\, D_{Th(IV)}$ *versus* $1/[H^+]$ in Fig. 4, while $D_{Th(IV)}$ depends on the fourth power of capric acid concentration. This unexpected value is probably due to the hydrolysis of thorium.

The values of n [2 for U(VI) and 4 for Th(IV) and Am(III)] were given by the slope of the curves in Figs 3 and 4.

On the other hand, the number of capric acid molecules (x) associated with 1 molecule of metallic ion in the organic caprate can be determined from the slope (ρ) of the curves in Fig. 2:

$$\rho = \frac{1}{2}(n + x) \text{ or } x = (2\,\rho - n)$$

for americium:	$x = 5$	$Am\ A_3.5\ (HA)$
for thorium:	$x = 4$	$Th\ A_4.4\ (HA)$
for uranium:	$x = 2$	$UO_2\ A_2.2\ (HA)$

The extracting power of capric acid is weak and strictly appears at relatively high pH. For the experimental conditions taken for the study of the capric acid effect on TLA extraction, the extracting properties of capric acid could be neglected.

Effect of capric acid on the actinide extraction by TLA HNO_3

The decrease of $D_{Am(III)}$, $D_{Pu(IV)}$, $D_{Np(IV)}$ and $D_{U(VI)}$ between trilauryl-ammonium nitrate organic solution and nitric acid aqueous solutions, as a function of increasing additions of capric acid to the solvent, can be due to: (a) a complexing of metallic species in the aqueous solutions according to:

$$M^{n+} + m\,HA \rightleftharpoons MA_m^{(n-m)} + m\,H^+ \qquad (1)$$

This assumption depends on the non extractability of the $MA_m^{(n-m)}$ species; (b) a displacement of HNO_3 from trilaurylammonium nitrate in organic solution with the formation of a corresponding caprate, i.e.:

$$R_3N\,HNO_{3(o)} + (HA)_2 \rightleftharpoons_{(o)} R_3N\,(HA)_{2(o)} + H_a^+ + NO_{3(a)}^- \qquad (2)$$

or (c) an addition of capric acid to triaurylammonium nitrate:

$$R_3N\,HNO_3 + (HA)_2 \rightleftharpoons R_3N\,HNO_3\,(HA)_2 \qquad (3)$$

Because of the low solubility of capric acid in water (about 10^{-4} M)[8] its complexing effect in aqueous solutions cannot alone explain the decrease of the D values obtained in experiments carried out with plutonium aqueous concentrations ranging from 6×10^{-4} to 10^{-3} M. In fact, the capric acid effect is still very sensitive with an aqueous concentration of metallic species greater than 0·2 M.[3] Furthermore, acidity should suppress the complexing effect of capric acid in aqueous media but this was not observed in results plotted in Fig. 6. On the contrary, the complexing effect of capric acid in aqueous media becomes predominant when the Pu(IV) concentrations are lower than 4×10^{-4} M as shown in Fig. 12. Log–log plots of $D_{Pu(IV)}$ *versus* capric acid concentration likewise exhibit slopes from -2 to -6 when the plutonium concentration decreases from 10^{-3} to 4×10^{-5} M.

A tentative demonstration of the HNO_3 displacement from TLA HNO_3 by capric acid was undertaken. Increasing quantities of capric acid were added to solutions of TLA HNO_3 in Solgil 54 B and the resulting organic solutions were equilibrated with water. The HNO_3 concentrations of the corresponding aqueous phases, reported in Table I, result from both a TLA HNO_3 desalification and a HNO_3 displacement by capric acid. They are too weak to explain the capric acid effect.

TABLE I

HNO_3 displacement from TLA HNO_3 by capric acid

Initial [TLA HNO_3] N	Initial [HA], N	Aqueous [HNO_3] at equilibrium, N	[TLA caprate] at equilibrium, M
0·143	0	0·0124	0
0·138	0·0712	0·0145	$2{\cdot}1 \times 10^{-3}$
0·140	0·150	0·0165	$4{\cdot}1 \times 10^{-3}$
0·133	0·276	0·0220	$9{\cdot}6 \times 10^{-3}$

In the addition Equation (3) capric acid was represented as a dimer $(HA)_2$ because most of the carboxylic acid groups are dimerised in low polarity solvents.[9] This assumption was confirmed by a study of capric acid itself.[4] Assuming an addition reaction and no affinity between the addition species and nitrate complexes, the distribution coefficient of the actinide elements at the fourth state of oxidation is given by:

$$D_{M(IV)} = k\,[R_3N\,HNO_3]^2 \qquad (4)$$

With the help of Equation (3) D can be written as a function of $(HA)_2$:

$$D_{M(IV)} = k\left(\frac{[R_3N]_{total}}{1 + \dfrac{[(HA)_2]}{K}}\right)^2 \qquad (5)$$

with $(R_3N]_{total} = [R_3N\,HNO_3] + [R_3N\,HNO_3\,(HA)_2]$

The distribution coefficient should be proportional to the inverse square of $(HA)_2$ when 1 is small in comparison to $\frac{(HA)_2}{K}$. This result was obtained for capric acid concentrations $>0{\cdot}2$ M as shown by the slope of -2 in Figs 6 and 7.

The association constant for the addition reaction is given by:

$$K = \frac{[R_3N\,HNO_3]\,[(HA)_2]}{[R_3N\,HNO_3\,(HA)_2]} \qquad (6)$$

$[R_3N\ HNO_3]$ values were determined from Figs 9 and 10 and reported in Tables II and III respectively for Pu(IV) and Np(IV). Calculation of the mean values gives:

$$\bar{K} = 0{\cdot}0287 \text{ and } p\bar{K} = 1{\cdot}452$$

with a relative standard deviation of 8·05% for $\bar{K}$.

TABLE II

Dissociation constant of $R_3N\ HNO_3\ (HA)_2$

(Data for Pu(IV))

Total [TLA]	Total $[(HA)_2]$, M	Free $[TLA\ HNO_3]$, M	$[TLA\ HNO_3\ (HA)_2]$ M	Free $[(HA)_2]$, M	K
0·08	0·1	0·0215	0·0585	0·0415	0·0153*
0·08	0·15	0·0173	0·0627	0·0873	0·0242*
0·08	0·2	0·0132	0·0668	0·1332	0·0266
0·08	0·25	0·0107	0·0698	0·1807	0·0278
0·08	0·3	0·0093	0·0707	0·2293	0·0301
0·08	0·4	0·0067	0·0733	0·3267	0·0299
0·08	0·5	0·0052	0·0748	0·4252	0·0296
0·16	0·2	0·027	0·133	0·067	0·0137*
0·16	0·3	0·022	0·138	0·162	0·0258
0·16	0·4	0·015	0·145	0·255	0·0264
0·16	0·5	0·012	0·148	0·352	0·0293

* Erroneous K value because of uncertainty on $[(HA)_2]$

TABLE III

Dissociation constant of $R_3N\ HNO_3\ (HA)_2$

(Data for Np(IV))

Total [TLA], M	Total $[(HA)_2]$, M	Free $[TLA\ HNO_3]$, M	$[TLA\ HNO_3\ (HA)_2]$, M	Free $[(HA)_2]$, M	K
0·16	0·10	0·055	0·105		
0·16	0·15	0·039	0·121	0·029	0·0095**
0·16	0·25	0·025	0·135	0·115	0·0213**
0·16	0·375	0·018	0·143	0·233	0·0285
0·16	0·50	0·012	0·148	0·352	0·0291
0·48	0·5	0·064	0·416	0·084	0·0129*
0·32	0·5	0·036	0·284	0·215	0·0269
0·16	0·5	0·014	0·146	0·314	0·0347
0·08	0·5	0·053	0·075	0·425	0·0302
0·04	0·5	0·028	0·038	0·462	0·0267

** Erroneous K value because $[Np(IV)]_0$ (> 0·01 M) is too high
* Erroneous K value because of uncertainty on $[(HA)_2]$

Am(III) should also give a slope of −2 while a value of −1 was obtained in Fig. 5. This anomaly may be explained by the fact that the aqueous solution was weakly acidic (pH 3). In this case the formation of trilaurylammonium caprate is not negligible and it is possible that the americium caprate complexes can be extracted by capric acid or trilaurylammonium caprate according to:

$$Am\ A^{3-n}_{n(a)} + m\ R_3N\,(HA)_{2(o)} \rightleftharpoons (R_3NH)_n\ A_{m+3}\ Am_{(o)} + m\ HA_{(a)} + (n-3)\,A^-_{(a)}$$

For capric acid concentrations higher than 0·2 M the U(VI) distribution coefficient is proportional to the reciprocal of the capric acid concentration (Fig. 8) meaning that only one molecule of $R_3N\ HNO_3$ is involved in the uranium extraction:

$$UO_2^{2+} + 2\,NO_3^- + R_3N\ HNO_3 \rightleftharpoons R_3NH(NO_3)_3\ UO_2$$

In this case the distribution coefficient may be expressed by:

$$D_{U(VI)} = k\left(\frac{[R_3N]_{total}}{1 + \frac{[(HA)_2]}{K}}\right) \quad . \quad . \quad . \quad . \quad . \quad . \quad . \quad (7)$$

A review[10] of the extraction of the actinide elements at the VI oxidation state into trilaurylammonium nitrate solutions shows that for various aqueous media, e.g. $D_{\text{actinide VI}}$ is proportional to trialkylammonium nitrate concentration at a power ranging from 1 to 2, the 1 value being unusual. This uncertainty of the number of trilaurylammonium nitrate molecules associated with one uranium molecule prevents the calculation of this association constant.

Conclusions

The capric acid effect on tetravalent and hexavalent actinides extraction from nitric acid media into trilaurylammonium nitrate organic solution is explained by means of an addition reaction between one molecule of trilaurylammonium nitrate and one capric acid dimer. The association constant of the $R_3N\ HNO_3\ (HA)_2$ complex was calculated from the change of tetravalent species distribution coefficients as a function of capric acid concentration in the solvent, using a 1 N-HNO_3 medium. $\bar{K}$ was found to be $(2{\cdot}87 \pm 0{\cdot}23) \times 10^{-2}$. In weakly acid media, like those used for trivalent species extraction in trilaurylamine, there is competition between the extractants: trilaurylammonium nitrate, capric acid and trilaurylammonium caprate, which masks the phenomenon due to the trilaurylammonium nitrate–capric acid addition reaction.

Acknowledgments

The authors are indebted to A. Chesné for his advice and encouragement during this research. The experimental assistance of F. de Mora and M. Baudet is gratefully acknowledged.

References

[1] Koehly, G., Espie, J. Y., Jouan, C., *Notes CEA*, 1970,CEA-N-1241, p. 392

[2] Koely, G., Espie, J. Y., de Mora, F., & Baudet, M., *Notes CEA*, 1970 CEA-N-1341

[3] Berger, R., Koehly, G., & Espie, J. Y., *Proc. int. Solvent Extraction Conf.*, 1971, (London: Society of Chemical Industry)

[4] Tanaka, M., Nakasuka, N., & Sasane, G., *J. inorg. nucl. Chem.*, 1969, **31**, 2591

[5] Pietsch, R., & Sinic, H., *Analytica chim. Acta*, 1970, **49**, 57

[6] Grenthe, I., *Acta chem. scand.*, 1962, **16**, 1965

[7] Day, R. A., jun., & Stoughton, R. W., *J. Am. chem. Soc.*, 1950, **72**, 5662

[8] Lange, N. A., 'Handbook of Chemistry', 1956 (9th edn.), p. 448, (Sandusky, Ohio: Handbook Publishers Inc.)

[9] Marcus, Y., & Kertes, A. S., 'Ion exchange and solvent extraction of metal complexes', 1969 (London: Wiley – Interscience)

[10] Müller, W., *Actinides Rev.*, 1967, **1**, 71

Laboratory studies of nitrous acid and neptunium behaviour in TBP extraction processes

by D. Gourisse

Département de Chimie, Commissariat a l'Énergie Atomique, Centre d'Études Nucléaires de Fontenay-aux-Roses, France

The behaviour of ^{237}Np in 'Purex' extraction processes depends on the oxidation of this element to the hexavalent state according to the reaction:

$$NpO_2^+ + \frac{1}{2}NO_3^- + \frac{3}{2}H^+ \rightleftharpoons NpO_2^{2+} + \frac{1}{2}HNO_2 + \frac{1}{2}H_2O$$

nitrous acid acting as a catalyst. A systematic study of the influence of various parameters (nitric acid, uranium, nitrous acid concentrations, temperature) was made in order to determine whether it would be possible to predict and control neptunium behaviour in these extractions.

Analysis, distribution coefficients of HNO_2 in the system 30% TBP–dodecane–$UO_2(NO_3)_2$–HNO_3–H_2O, decomposition and repartition of nitrous acid in counter-current extractions experiments with laboratory mixer-settlers show that it is possible to control HNO_2 concentration in aqueous phase for every stage of the 'Purex' counter-current extractions.

Introduction

IN NITRIC ACID solutions neptunium(V) is partly oxidised to the hexavalent state according to:

$$NpO_2^+ + \tfrac{1}{2}NO_3^- + \tfrac{3}{2}H^+ \rightleftharpoons NpO_2^{2+} + \tfrac{1}{2}HNO_2 + \tfrac{1}{2}H_2O \quad . \quad . \quad (1)$$

nitrous acid acting as a catalyst.[1] This reaction allows ^{237}Np extraction with uranium and plutonium in 'Purex' processes.[2–6] To study neptunium behaviour in nuclear fuel processing plants, nitrous acid and neptunium extraction by 30 vol. % tributylphosphate (TBP) in dodecane was investigated, the equilibrium of Equation (1) was studied and counter-current mixer-settler experiments were made. This paper presents the most useful results obtained in this field.

Equilibrium experiments

Neptunium(VI) extraction

Figs 1 and 2 show the variations of tracer neptunium(VI) distribution coefficients with nitric acid and uranium concentrations respectively. The ratio of neptunium(VI) distribution coefficient to that of uranium(VI) remains constant. From 28 experimental measurements a value:

$$R(VI) = \frac{D(Np^{VI})}{D(U^{VI})} = 0{\cdot}47. \quad . \quad . \quad . \quad . \quad . \quad . \quad . \quad (2)$$

was obtained with a standard error of 11%. The simple correlations between uranium(VI), neptunium(VI) and plutonium(VI) distribution coefficients (D) are related to the formulae of the organic complexes $MO_2(NO_3)_2 \,.\, 2\,TBP$[7–10] and have been discussed in a previous paper.[11] These correlations are extremely helpful in predicting distribution coefficients of hexavalent actinide elements with TBP solutions.

Nitrous acid extraction

Nitrous acid distribution coefficients have been measured in nitric acid medium[12–14] but no reports were found in the literature of any systematic study of the influence of the organic uranium concentration on HNO_2 distribution coefficients.

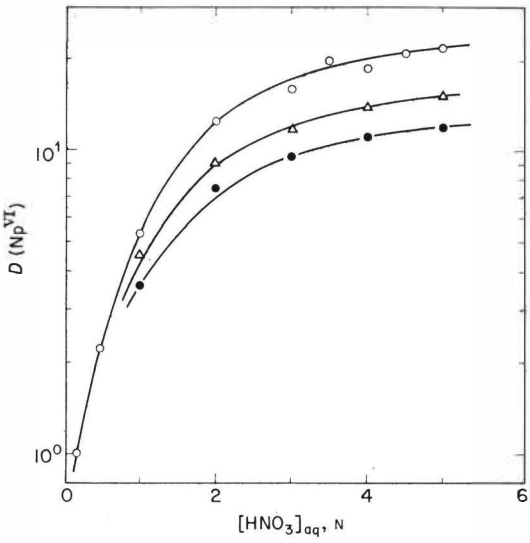

FIG. 1. *Distribution coefficients of tracer neptunium (VI) in the system 30% TBP–dodecane–HNO_3–H_2O*

○ 22°; △ 35°; ● 50°C

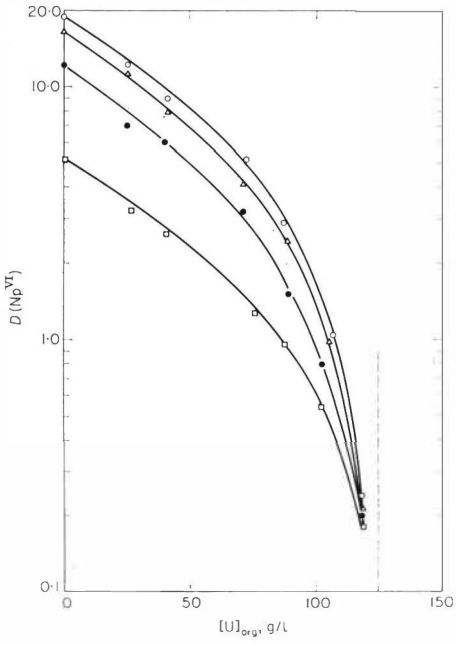

FIG. 2. *Distribution coefficients of tracer neptunium (VI) in the system 30% TBP–dodecane–HNO_3–$UO_2(NO_3)_2$–H_2O at 25°C*

○ 3·5N; △ 3N; ● 2N; □ = 1N-$(HNO_3)_{aq}$

Experimental

An original experimental method under inert atmosphere to avoid any disturbances owing to nitrous acid destruction was used. Aqueous and organic solutions were mixed and allowed to settle in closed water-jacketed vessels under an argon atmosphere saturated with nitrous vapours (mainly NO) (Fig. 3).

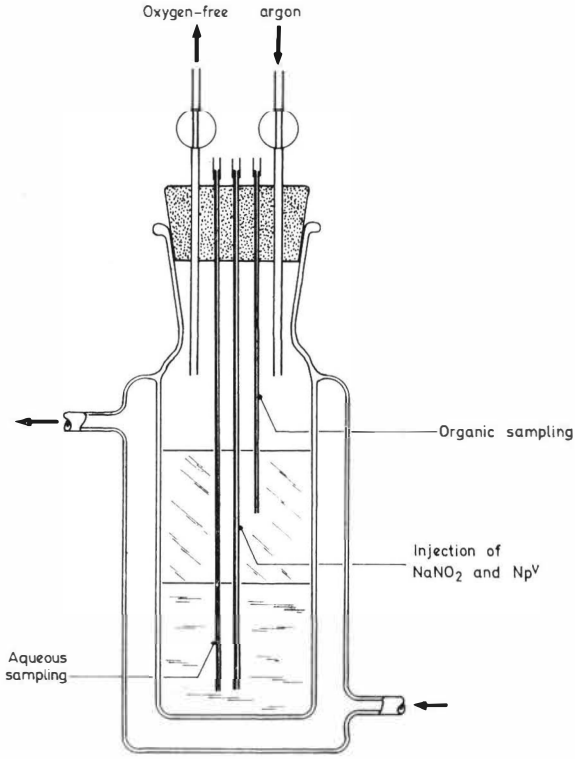

FIG. 3. *Scheme of the apparatus*

Samples were drawn up with syringes through appropriate needles to avoid any contact with the outer atmosphere. They were rapidly injected into a cooled alkaline solution and nitrous acid was determined by colorimetry of the diazonium salt which was formed with α-naphthylamine and sulphanilic acid.[15] Colorimetry was carried out at pH values between 2·0 and 2·5 in a mixture derived from monochloroacetate buffer.[16]

Results

The variations of the HNO_2 distribution coefficients with uranium concentration are plotted in Fig. 4. Nitrous acid extracts as $TBP.HNO_2$.[12–14] Consequently $D(HNO_2)$ is proportional to the free TBP activity. Neglecting variations of activity coefficients, $D(HNO_2)$ is proportional to the free TBP concentration. For a given organic uranium concentration $(U)_{org}$ and a given aqueous acidity, the free TBP concentration T is equal to:[17]

$$T = T_{x=0}(1-x)$$

$x = \dfrac{2[U]_{org}}{[TBP]_{tot}}$ uranium saturation of the organic solvent,

$T_{x=0}$ = free TBP concentration for the same aqueous acidity when no uranium is present.

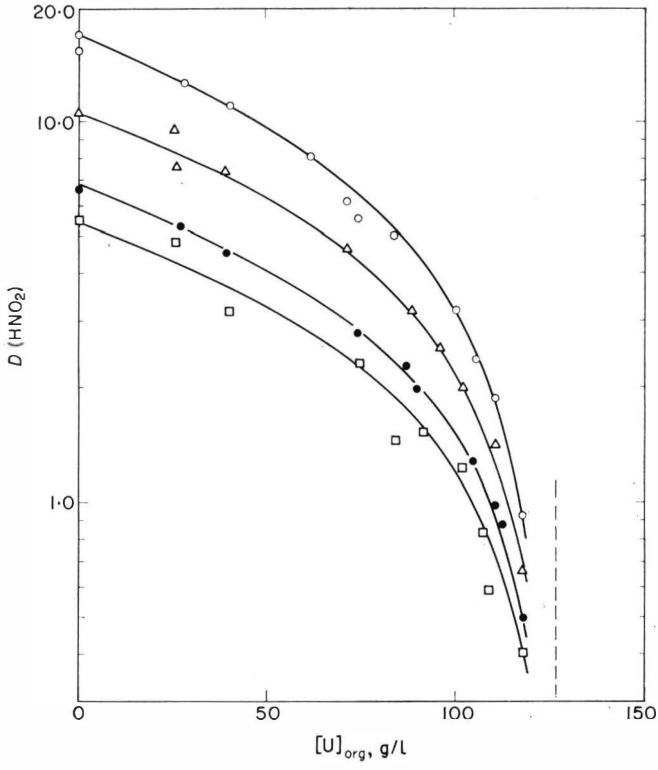

FIG. 4. *Distribution coefficients of tracer HNO_2 in the system 30% TBP–dodecane–HNO_3–$UO_2(NO_3)_2$–H_2O at 25°C*

○ 1N; △ 2N; ● 3N; □ 3·5N-$(HNO_3)_{aq}$

Neglecting activity coefficients:

$$D(HNO_2) = D(HNO_2)_{x=0}(1-x) \quad . \quad . \quad . \quad . \quad . \quad . \quad (3)$$

is obtained.

The plot in Fig. 5 shows that Equation (3) is valid within experimental accuracy. This correlation is very helpful in predicting HNO_2 distribution coefficients with uranium present.

Oxidation equilibrium

The apparent mass action law constant K of Equation (1) was measured by TBP extraction using the apparatus shown in Fig. 3. In the aqueous phase the apparent constant is:

$$K = \frac{[Np^{VI}]_{aq}}{[Np^{V}]_{aq}} \cdot \frac{[HNO_2]_{aq}^{1/2}}{[H^+]_{aq}^{3/2} \cdot [NO_3^-]_{aq}^{1/2}} \simeq \frac{[Np^{VI}]_{aq}}{[Np^{V}]_{aq}} \cdot \frac{[HNO_2]_{aq}^{1/2}}{[HNO_3]_{aq}^{2}}$$

if nitric acid is completely ionised.

If D_{app} is the apparent neptunium distribution coefficient and D_{VI} the neptunium(VI) distribution coefficient for the same conditions:

$$r = \frac{[Np^{VI}]_{aq}}{[Np^{V}]_{aq}} = \frac{D_{app} - D_V}{D_{VI} - D_{app}} \simeq \frac{D_{app}}{D_{VI} - D_{app}}$$

since $D_V \simeq$ O [neptunium(V) distribution coefficient].

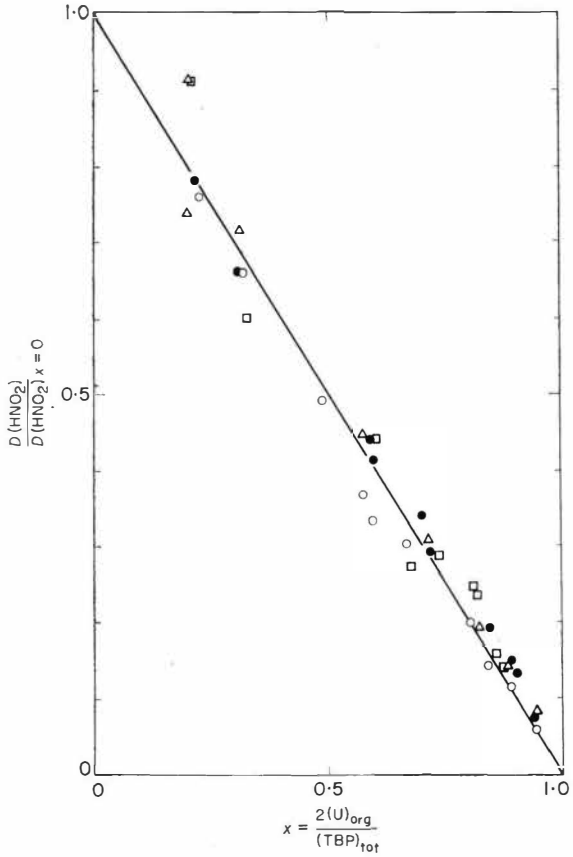

FIG. 5. *Verification of Equation (3)*
○ 1N; △ 2N; ● 3N; □ 3·5N-$(HNO_3)_{aq}$

K is calculated from D_{app} values by:

$$K = \frac{D_{app}}{D_{VI} - D_{app}} \cdot \frac{[HNO_2]_{aq}^{1/2}}{[HNO_3]_{aq}^{2}} \quad . \quad . \quad . \quad . \quad . \quad . \quad . \quad (4)$$

Fig. 6 shows the variations of K with nitric acid and temperature. Each point corresponds to a series of 10–15 measurements with a standard error $\sigma < 15\%$; for each series of measurements the HNO_2 concentration varies from 1 to 50 without any systematic variation of the K values.

These results are in agreement previously published values.[1,6] K increases with acidity and temperature. Table I shows that the oxidation is slightly

TABLE I

Thermodynamic data of Equation (1)

	$[HNO_3]_{aq}$, N			
	1	2	3	4
ΔH, kcal/mole	3·9	4·0	4·0	4·0
$\Delta S°$, cal/mole/deg	−3·0	−2·0	−1·2	−0·4
$\Delta G°$ kcal/mole	4·8	4·6	4·3	4·1

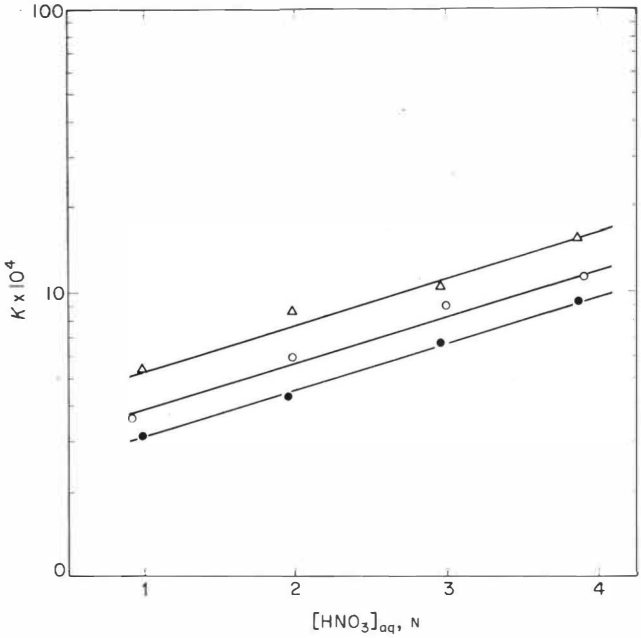

FIG. 6. *Apparent mass action law constant of Equation (1)*
● 25°; ○ 35°; △ 50°C

endothermic ($\Delta H \simeq 4 \cdot 0$ kcal/mole) and that the increase in K values results mainly due to an increase in entropy. This is in agreement with the higher complexing power of nitrate anion for NpO_2^{2+} than for NpO_2^{+}.

Equilibrium distribution of neptunium in the system 30% TBP–dodecane–HNO_3–HNO_2–H_2O

Neglecting solvent saturation by HNO_2, apparent distribution coefficients of neptunium at equilibrium were calculated from the K values (Fig. 7). Since oxidation is endothermic and neptunium(VI) extraction is exothermic, tempera-

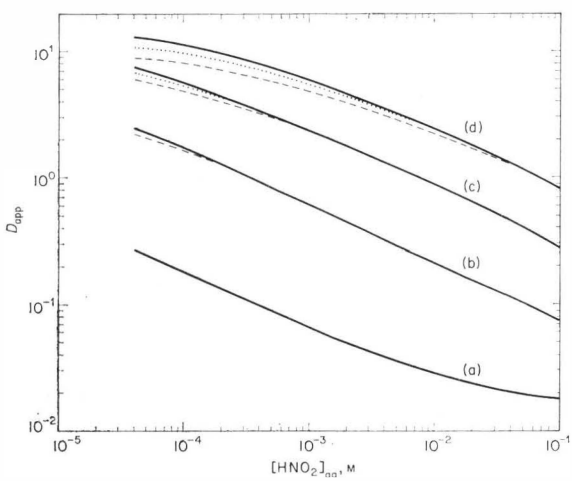

FIG. 7. *Equilibrium distribution coefficients of neptunium in the system 30% TBP–dodecane–HNO_3–HNO_2–H_2O*
—— 25°; . . . . 35°; - - - - 50°C
(a) 1N; (b) 2N; (c) 3N; (d) 4N-$(HNO_3)_{aq}$

ture variations have a minor effect on equilibrium distribution. At high acidities a small decrease of D_{app} with increasing temperature was obtained.

Counter-current experiments

The flowsheet is shown in Fig. 8. Nitrous acid is injected in stage 1 with a pre-equilibrated solvent to get an approximately constant HNO_2 concentration in the extracting section.[3,16] The nitrous acid normally present in the feed solutions (owing to radiolysis in industrial plants) is injected here in the form of an alkaline solution of $NaNO_2$ in stage 7 to avoid any destruction before injection.

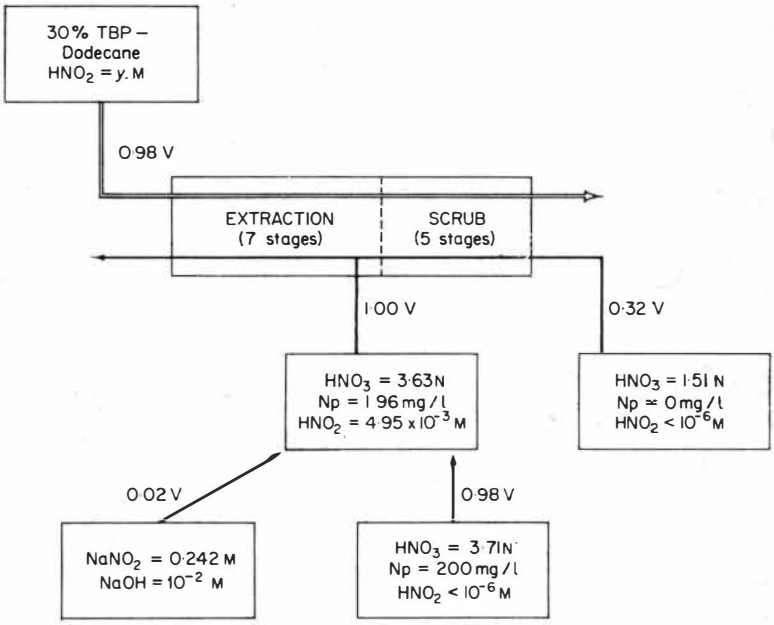

FIG. 8. *Flowsheet of counter-current experiments*

Three extraction experiments were made corresponding to: (A) $y=4\cdot70\times10^{-3}$M at $T=50°$C; (B) $y=1\cdot50\times10^{-3}$M at $T=50°$C; (C) $y=1\cdot48\times10^{-3}$M at $T=35°$C; where y=nitrous acid concentration in the TBP phase (see Fig. 8).

Comparison between extractions A and B shows the influence of HNO_2 concentration on neptunium extraction whereas comparison between extractions B and C shows the influence of temperature. Typical results corresponding to extraction B are shown in Figs 9, 10 and 11.

Nitric acid distribution

The HNO_3 distribution in the extractor was determined by the McCabe–Thiele method, using nitric acid distribution coefficients at 25°C[18] since these coefficients are relatively unaffected by temperature variations in this acidity range.[19] As shown in Fig. 9 there is good agreement between calculated and experimental values.

Nitrous acid distribution

As in previous experiments[16] nitrous acid destruction occurs only in feed stages 1 and 7 corresponding to 10–20% of the injected HNO_2 quantities (Table II).

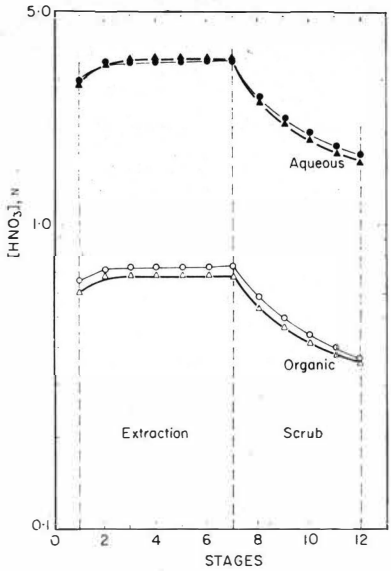

FIG. 9. *Extraction B = HNO_3 distribution*
○, ● Experimental; △, ▲ calculated

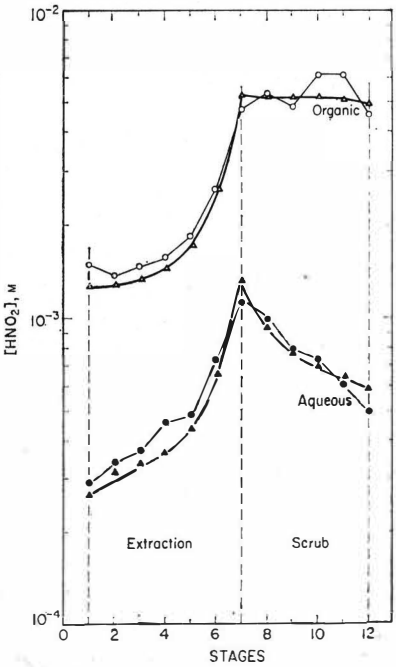

FIG. 10. *Extraction B = HNO_2 distribution*
○, ● Experimental; △, ▲ calculated

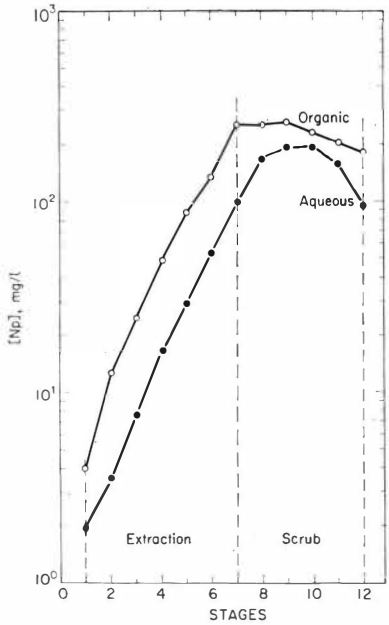

FIG. 11. *Extraction B = neptunium distribution*

TABLE II

HNO_2 destroyed in feed stages, %

	Extr. A	Extr. B	Extr. C
Stage 1	20	20	10
Stage 7	10	20	20

Subtracting the destroyed percentages from the feed and solvent concentrations, good agreement was obtained between calculated and experimental concentration (see, for example, Fig. 10).

Neptunium distribution

The neptunium extraction yields are respectively: ρNp=98·5% for extraction A; ρNp=98·9% for extraction B; ρNp=85·9% for extraction C, where ρNp= % Np extracted in the counter-current experiments.

In each stage from the apparent distribution coefficient:

$$r_{exp} = \left(\frac{[Np^{VI}]_{aq}}{[Np^{V}]_{aq}}\right)_{exp} = \frac{D_{app}}{D_{VI} - D_{app}}$$

and from the mass action law constant, K:

$$r_{eq} = \left(\frac{[Np^{VI}]_{aq}}{[Np^{V}]_{aq}}\right)_{eq} = K\,\frac{[HNO_3]^2}{[HNO_2]^{1/2}}$$

Since neptunium(V) is oxidised in the extracting section and neptunium(VI) is reduced in the scrubbing section the degree of completion of the reaction is defined as:

$$\alpha = \frac{[Np^{IV}]_{aq}}{[Np^{VI}]_{aq}+[Np^{V}]_{aq}} = \frac{r}{r+1} \quad \text{in the extracting section}$$

$$\alpha = \frac{[Np^{V}]_{aq}}{[Np^{VI}]_{aq}+[Np^{V}]_{aq}} = \frac{1}{r+1} \quad \text{in the scrubbing section}$$

Results

In Table IV values of the ratio:

$$f = \frac{\alpha_{exp}}{\alpha_{eq}}$$

are given in each stage for each experiment.

TABLE III

Degree of completion of the Equation (1) *in each stage*

Stage	Extraction A		Extraction B		Extraction C	
	$[HNO_2]_{aq}$, M × 10^4	f	$[HNO_2]_{aq}$, M × 10^4	f	$[HNO_2]_{aq}$, M × 10^4	f
1	9·0	1·04	2·6	0·69	2·0	0·13
2	10·1	0·85	3·1	0·81	2·4	0·18
3	10·5	1·00	3·3	0·69	3·5	0·22
4	10·7	0·95	3·6	0·63	2·7	0·22
5	11·4	0·96	4·4	0·66	3·1	0·32
6	13·5	0·75	6·6	0·63	4·5	0·35
7	19·4	1·09	13·1	0·81	9·4	0·62
8	12·6	0·96	9·2	0·98	6·6	0·95
9	10·5	0·95	7·5	0·91	5·7	0·87
10	9·1	0·92	6·8	0·90	5·1	0·82
11	8·5	0·91	6·3	0·85	4·8	0·69
12	7·7	0·81	5·7	0·72	4·4	0·60

Discussion

Comparison between extractions B and C shows that an increase in temperature increases the rate of Equation (1). This was expected.

Comparison between extractions A and B shows that an increase in HNO_2 concentration increases the rate of Equation (1). The rate is: [1,6]

$$\frac{d[Np^{V}]}{dt} = -k([Np^{V}]-[Np^{V}]_{eq})$$

By TBP extraction, when a large excess of nitrous acid is present as compared to neptunium, Siddall & Dukes[1] obtained values of the rate constant k which are independent of HNO_2 concentration. By spectrophotometry, with HNO_2 concentrations of the same orders of magnitude as those of neptunium, Swanson[6] obtained smaller values of the rate constant and found that the reaction is first order with respect to nitrous acid.

Preliminary kinetic experiments that were made in these laboratories by TBP extraction (Moulin, J. P., personal communication) explain these discrepancies (Fig. 12). When the ratio $\beta=[HNO_2]/[Np^{V}]$ is larger than 2, the rate constant k is independent of β and HNO_2 concentration. When the ratio β is smaller than 1, the rate constant is proportional to β but is independent of the

absolute HNO_2 concentration. Clearly the reaction mechanism is more intricate than first supposed and further kinetic studies are being made to elucidate this mechanism.

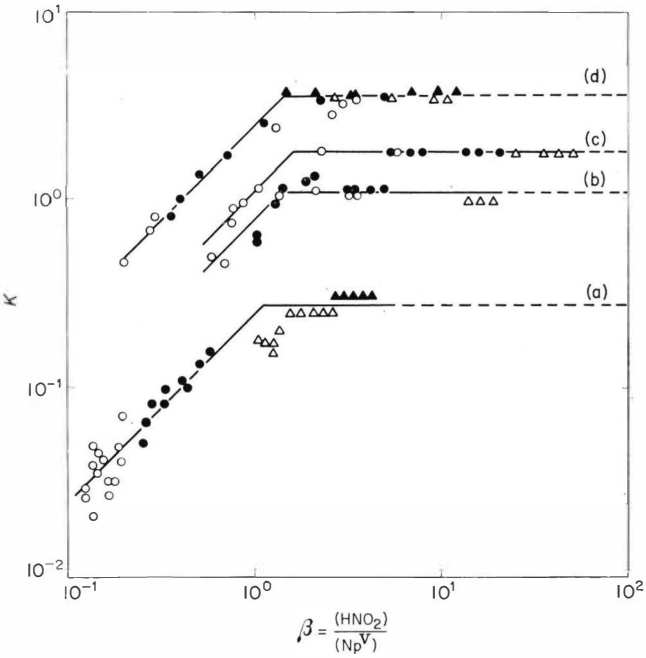

FIG. 12. *Rate constant of Equation* (1)

○ ≈ 5 × 10^{-5}M; ● ≈ 10^{-4}M; △ ≈ 4·10^{-4}M; ▲ ≈ 10^{-3}M-HNO_2
(a) 2N-HNO_3 at 25°C; (b) 3N-HNO_3 at 25°C; (c) 4N-HNO_3 at 25°C; (d) 3N-HNO_3 at 35°C

Acknowledgments

The authors are indebted to Messrs A. Chesné and A. Bathellier for the helpful advice they gave during this work and are grateful to Mlle. and Messrs D. Beucher, R. Ayache and J. C. Morisseau for skilful technical assistance.

References

1 Siddall, T. H., & Dukes, E. K., *J. Am. chem. Soc.*, 1959, **81**, 790
2 Parker, G. W., Lantz, P. M., & Martin, W. J., *Rep. Congr. atom. Energy Commn U.S.*, 1957, ORNL-2386, p. 22
3 Benedict, G. E., McKenzie, T. R., & Richardson, G. L., *Rep. Congr. atom. Energy Commn U.S.*, 1960, HW-SA-1963
4 Bähr, W., *K.F.K. Rep.*, 1968, KFK-797
5 Salomon, L., Lopez-Menchero, E., Lopez de Manterola, J., & Leynen, G., *Eurochemic Rep.*, 1968, ETR-233
6 Swanson, J. L., *Rep. Congr. atom. Energy Commn U.S.*, 1969, BNWL-1017
7 McKay, H. A. C., *Proc. 1st U. N. int. Conf. Peaceful Uses atom. Energy*, 1955, Paper P/441
8 Keder, W. E., *J. inorg. nucl. Chem.*, 1969, **16**, 138
9 Nemodruck, A. A., *Radiokhimiya*, 1967, **9**, 704
10 Siddall, T. H., & Stewart, W. E., *Inorg. nucl. chem. Lett.*, 1967, **3**, 279
11 Germain, M., Gourisse, D., & Sougnez, M., *J. inorg. nucl. Chem.*, 1970, **32**, 245
12 Burger, L. L., & Money, M. D., *Rep. Congr. atom. Energy Commn U.S.*, 1959, HW-60278
13 Woodhead, J. L., *Rep. U.K. atom. Energy Auth.*, 1960, AERE-R-3432
14 Fletcher, J. M., Scargill, D., & Woodhead, J. L., *J. chem. Soc.*, 1961, p. 1705
15 Rider, B. F., & Mellon, M. G., *Ind. Engng Chem.*, 1946, **18**, 96
16 Gourisse, D., & Gautier, A., *J. inorg. nucl. Chem.*, 1969, **31**, 839
17 Codding, J. W., Haas, W. O., & Heumann, J. F. K., *Ind. Engng Chem.*, 1958, **50**, 149
18 Leroy, P., *Rapp. CEA*, 1967, CEA-R-3207
19 Stoller, S. M., & Richards, R. S., 'Reactor Handbook', 1961, Vol. II (2nd edn), p. 158 (New York: Interscience)

Use of trilaurylamine in the processing of irradiated ^{237}Np

by R. Berger, G. Koehly and J.-Y. Espie
Département de Chimie, Commissariat à l'Énergie Atomique, Centre d'Études Nucleaires de Fontenay-aux-Roses, France

A solvent-extraction scheme for the processing of irradiated ^{237}Np using trilaurylamine and nitrate systems was developed at Fontenay-aux-Roses. The flowsheet included three extraction cycles for :

The Np(IV) and Pu(IV) separation from aluminium and fission products, the Np(IV)/Pu(III) mutual separation by selective extraction of the former and the Pu(IV) final decontamination.

Major improvements in the overall decontamination and mutual separation of neptunium and plutonium were obtained from the use of capric acid in the scrubbing steps giving decontamination factors of the order of 10^6. Furthermore, capric acid allowed a decrease in the SO_4^{2-} concentration in the back-extracting solution from 3 to 0·5N. Both advantages are due to a negative synergistic effect between trilaurylamine and capric acid resulting in a decrease of the distribution coefficients of the tetravalent species and therefore, since the reductant is in the aqueous phase, a greater reduction rate of Pu(IV).

Introduction

MOST COMMON PROCEDURES used for the recovery of ^{237}Np and ^{238}Pu from irradiated ^{237}Np are based on ion exchange techniques.[1–3] Nevertheless, solvent extraction schemes have been established using trilaurylammonium nitrate ($TLAHNO_3$) in an inert organic diluent, e.g., dodecane and, more recently, Solgil 54 B, as the extracting agent.

A review of the factors governing the choice of a $^{237}Np/^{238}Pu$ separation process has been made recently by Jenkins.[4] The oxidation–reduction reactions of neptunium and plutonium ions in aqueous media, together with the strong affinity of trilaurylammonium nitrate for the complexes of the actinide nitrates at the fourth valency state, offer two possible routes for the $^{237}Np/^{238}Pu$ separation by either extracting Pu(IV) from an oxidising medium in the presence of Np(V) or extracting of Np(IV) from a reducing medium in the presence of Pu(III). The first method has only a limited use due to the Np(V) disproportionation which is enhanced by the presence of trilaurylammonium nitrate as the organic solution. The latter method is to a lesser extent limited by the difficulty in removing small quantities of Pu(IV) in the scrubbing section. Two procedures have been proposed to overcome this difficulty, consisting of the saturation of the organic phase by Np(IV)[5] and the addition of sulphate ions in the scrubbing stream.[6] Both procedures decrease the distribution coefficients of the tetravalent species in the scrubbing section and consequently increase the reduction rate of Pu(V) by ferrous ions. However, Np(IV) distribution coefficients are decreased in the extraction.

A negative synergistic effect between trilaurylammonium nitrate and capric acid has recently been observed by Koehly. The purpose of the present work was to apply this effect to the Np(IV)/Pu(III) separation. The main advantage of this technique is its efficiency due to a strong decrease in the distribution coefficients of the tetravalent species which is strictly restricted to the scrubbing section of the countercurrent systems. Furthermore, addition of capric acid greatly facilitates the back-extraction of tetravalent species from tertiary amine solvents into sulphuric/nitric acid solutions.

The long chain capric acid (decanoic acid) was chosen because of its high solubility (>2 N) in Solgil 54 B and its very low solubility ($\sim 10^{-4}$ N) in water. Solgil 54 B was preferred to dodecane as the diluent for TLA because of the higher neptunium (or plutonium) solubility in this solvent, 18 g/l compared with 2·45 g/l in the case of dodecane. Also its chemical and radiolytic stability is satisfactory.[7]

Experimental

Procedures

Distribution coefficient measurements were carried out in 15-ml Pyrex test tubes. Equilibria between the organic and aqueous phases were obtained by mixing equal volumes of each for 20 minutes using a "Turbula" mixer (Wab. Switzerland). Phase separations were speeded up by centrifugation. Mass-transfer rates were determined by varying the mixing time. The metal ion concentrations in the aqueous solutions at equilibrium ranged from 6×10^{-4} to 10^{-3} M in order to minimise their effect on capric acid.

^{237}Np, ^{238}Pu and ^{239}Pu determinations were carried out on aliquots by α-counting and α-pulse height analysis. γ-Spectrometry measurements were performed with a Ge–Li drifted detector.

Determination of countercurrent flowsheets were carried out in mixer–settler banks both on synthetic solutions of ^{237}Np and ^{239}Pu and on active solutions formed from the dissolution of six irradiated neptunium targets in 6 N-HNO_3–0·005 M-$Hg(NO_3)_2$-0·02 M-NH_4F. The flowsheet used in the neptunium–plutonium separation shown in Fig. 1 was established from previous experiments[5] and from the results obtained in this work. The complete flowsheet for the processing of irradiated ^{237}Np is presented in Fig. 2. It includes a decontamination cycle for both neptunium and plutonium; a neptunium–plutonium separation cycle and a plutonium purification cycle. This processing was carried out on 31·8 g of initial ^{237}Np with the generation of 2·64 g of ^{238}Pu.

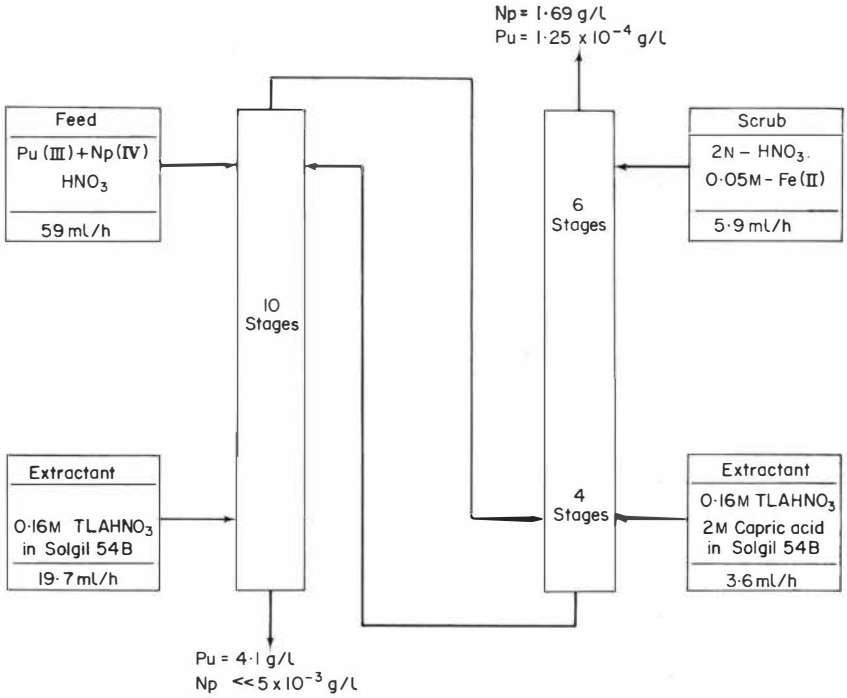

FIG. 1. *Flowsheet for the neptunium–plutonium separation in the counter-current extraction cycle*

Apparatus

The equipment used in countercurrent experiments consisted of mixer–settler banks (type Pollux) and metering pumps with mechanically actuated valves and pistons (Sonal Establishment, 95-Argenteuil).

Acidimetric determination was by a Metrohm Model E. 336 potentiograph; Tacussel Autotitrigraphe 3 was also used. Experiments were carried out either in standard glove-boxes or in hot-cells, as appropriate.

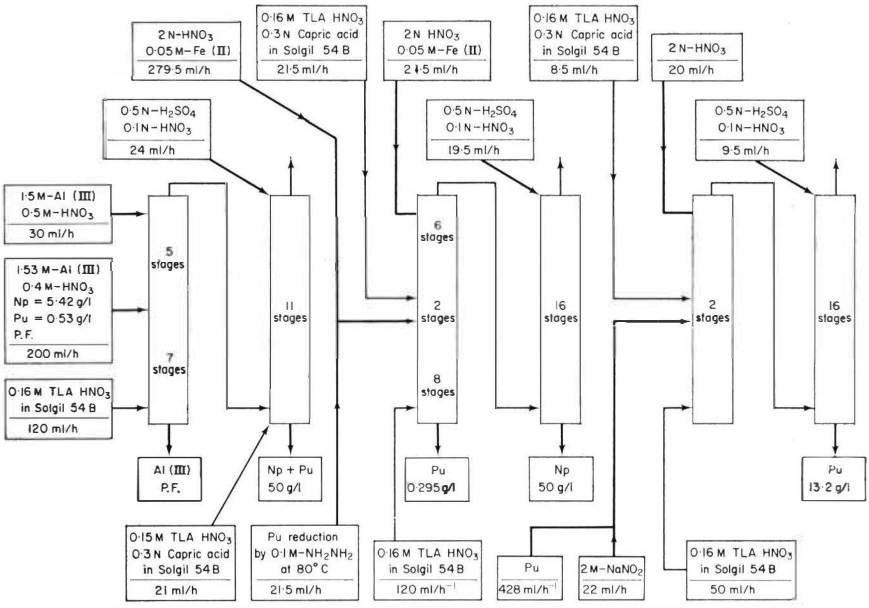

FIG. 2. *Flowsheet for the solvent extraction processing of irradiated* ^{237}Np.

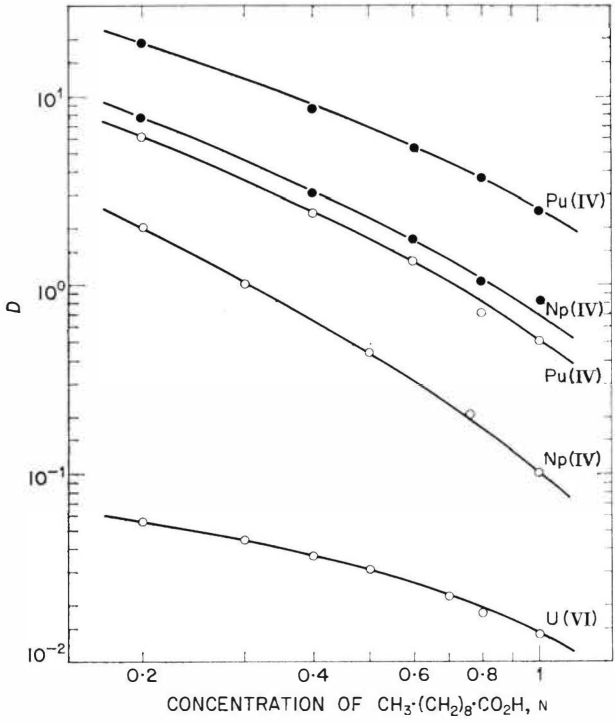

FIG. 3. *Variation of* $D_{Pu(IV)}$, $D_{Np(IV)}$ *and* $D_{U(VI)}$ *with capric acid concentration*

Extractant: 0·16 M TLAHNO3 – capric acid in Solgil 54B; Aqueous phase: ○ 1 N-HNO3, ● 2 N-HNO3.

Reagents

Standard trilaurylammonium nitrate solutions were prepared by equilibrating Rhône–Poulenc Nuclear Grade Trilaurylamine (TLA) in Solgil 54 B solutions with nitric acid in 10% excess. Progil product Solgil 54 B is a mixture of mono-tert-butylbenzene (>95%) and monopentylbenzene. Solgil 54 B consists of a distillation fraction collected between 162 and 172°C. Capric acid (Prolabo no. 20.238) was used as received. All other reagents were Prolabo Analytical Grade R.P.

Results

Influence of capric acid

The effect of capric acid on the distribution coefficients of tetravalent neptunium and plutonium between 0·16 M $TLAHNO_3$ in Solgil 54 B and nitrate solutions is shown in Fig. 3. Its effect on the back extraction rate of plutonium using a reducing solution is shown in Fig. 4.

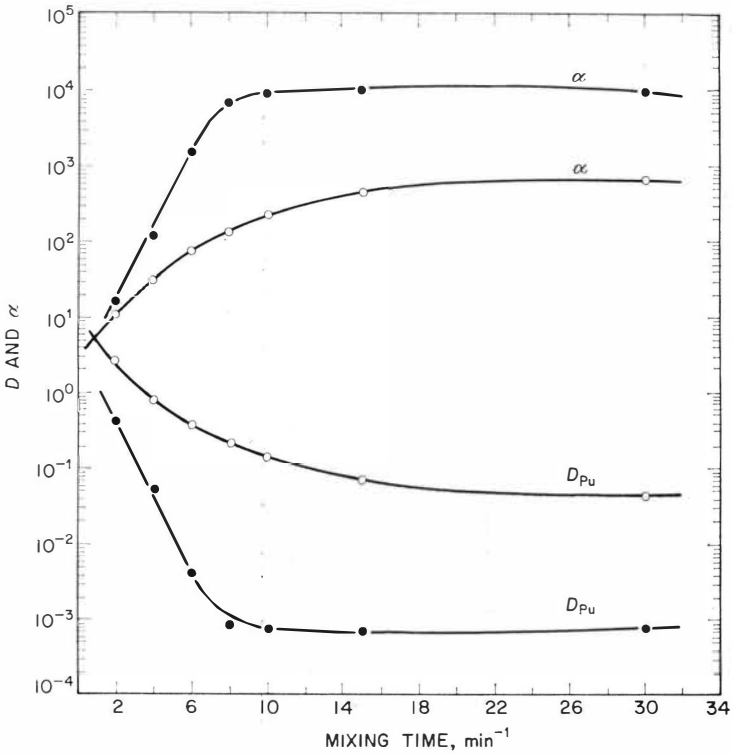

FIG. 4. *Back-extraction rate of plutonium with reducing solution.*
Extracant: ○ 0·16 M $TLAHNO_3$ in Solgil 54 B, ● 0·16 M $TLAHNO_3$ – 0·3 N capric acid in Solgil 54 B. Aqueous phase: 2 N-HNO_3 – 0·05 M-$Fe(SO_3NH_2)_2$–0·05 M-N_2-N_4

$$\alpha = \frac{D_{Np}}{D_{Pu}}$$

The distribution coefficients of plutonium between an organic solution, 0·16 M $TLAHNO_3$–0·3 N capric acid in Solgil 54 B, and aqueous sulphuric/nitric acid solutions were measured. They are reported in Fig. 5. The distribution line at room temperature of Np(IV) between 0·16 M TLA HNO_3–0·3N capric acid in Solgil 54 B and 0·5 N-H_2SO_4–0·1 N-HNO_3 is reported in Fig. 6.

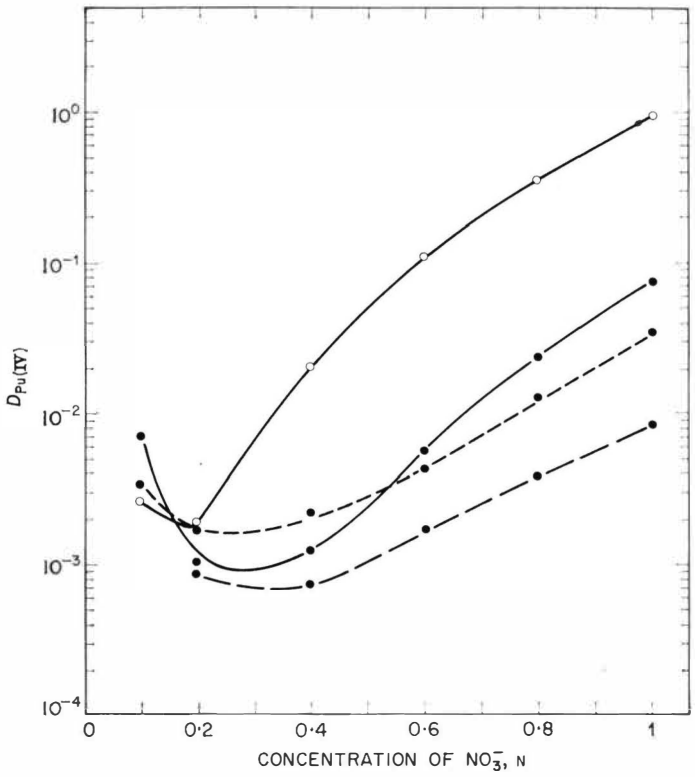

FIG. 5. *Variation of* $D_{Pu(IV)}$ *with nitrate concentration*

Extractant: ○ 0·16 M TLA HNO_3 in Solgil 54 B, ● 0·16 M TLA HNO_3–0·3 N capric acid in Solgil 54 B. Aqueous phase: ——— 0·5 N-H_2SO_4–HNO_3, — — — — 0·5 N-H_2SO_4–0·2 N-HNO_3–NH_4NO_3 - - - - 1N-H_2SO_4–HNO_3

Neptunium–plutonium separation

The mutual decontamination factors for neptunium and plutonium and the recovery of these elements given by the countercurrent demonstration are reported in Table I. The corresponding neptunium and plutonium extraction and scrubbing profiles are shown in Fig. 7.

TABLE I

Yield of recovery and decontamination factors obtained in the countercurrent extraction cycle

Decontamination factors of Np in Pu	
extraction	53
scrubbing	7
back-extraction	270
Total	10^5
Decontamination factor of Pu in Np	$\gg 10^2$
Yield of recovery in	
neptunium	> 0·99
plutonium	> 0·999

^{237}Np and ^{238}Pu recovery

The results obtained in the processing of irradiated ^{237}Np are also compared with those obtained from a previous run in absence of capric acid. The

α-losses, the neptunium and plutonium decontamination factors and the cross-contamination of the finished products are reported in Tables II to IV, respectively.

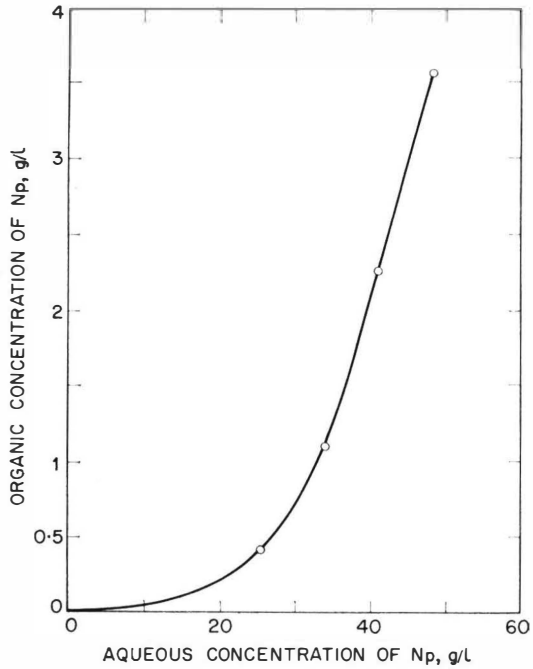

FIG. 6. *Distribution line of Np(IV) at room temperature*

Extractant: 0·16 M $TLAHNO_3$–0·3 N capric acid in Solgil 54 B; Aqueous phase: 0·5 N-H_2SO_4–0·1 N-HNO_3.

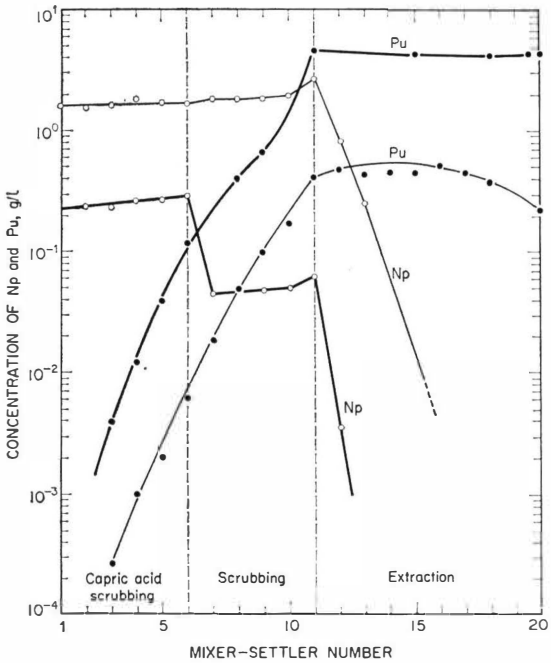

FIG. 7. *Np and Pu extraction and scrubbing profiles in the counter-current extraction cycle*

——— organic concentration, ——— aqueous concentration

TABLE II

Alpha losses in the processing of irradiated ^{237}Np

Flowsheet	Solvent extraction losses (% of α activity in feed) run 1	run 2 (capric acid)
1st cycle		
extraction	0·3	0·3
back-extraction	<0·1	<0·1
2nd cycle		
back-extraction	<0·1	<0·1
3rd cycle		
extraction	<1	<0·5
back-extraction	<0·1	<0·1
Overall	<1·6	<1·1

TABLE III

Neptunium decontamination in the processing of irradiated ^{237}Np

Flowsheet run	Decontamination factors ($\times 10^{-3}$) *1st cycle* 1	*1st cycle* 2*	*2nd cycle* 1	*2nd cycle* 2*	*overall* 1	*overall* 2*
Pu			1·0	1000	1·0	1000
Ru	12	1·3	0·017	1·25	200	1600
Zr	4·5	1·0	0·3	>10	1350	> 10
Nb		> 1·0		> 0·7		>700
Ce		>10		>10		> 10^5
Cs		>10		>10		> 10^5
gross γ		–		0·73		–

* capric acid present

TABLE IV

Plutonium decontamination in the processing of irradiated ^{237}Np

Flow sheet run	Decontamination factors ($\times 10^{-3}$) *1st cycle* 1	*1st cycle* 2*	*2nd cycle* 1	*2nd cycle* 2*	*3rd cycle* 1	*3rd cycle* 2*	*overall* 1	*overall* 2*
Np			>1·0	>1·0		>0·1		> 100
Ru	12	1·3			0·008	0·53	96	690
Zr	4·5	1·0			0·13	>10	590	> 10^4
Nb		> 1·0				1·1		>1100
Ce		>10				>10		> 10^5
Cs		>10				>10		> 10^5
gross γ		–				–		–

* capric acid present

TABLE V

Cross-contamination of finished ^{237}Np and ^{238}Pu products

	Concentration (10^{-6}) run 1	run 2 (capric acid)
Pu content in finished Np products	100	0·1
Np content in finished Pu products	4200	<100

Discussion

Influence of capric acid on the neptunium–plutonium separation

The effect of capric acid on $D_{Pu(IV)}$, $D_{Np(IV)}$ and $D_{U(IV)}$ (Fig. 3) was recently studied.[8] It is explained by the following addition reaction with trilauryl-ammonium nitrate involving one capric acid dimer:

$$R_3N\ HNO_3 + [CH_3\ (CH_2)_8CO_2H]_2 \rightleftarrows R_3N\ HNO_3\ [CH_3(CH_2)_8CO_2H]_2$$

where $R = CH_3(CH_2)_{10}\ CH_2-$

The choice of the capric acid concentration is a compromise between decreasing the distribution coefficient of plutonium in the reducing scrub and leaving the extracted neptunium in the solvent. For a capric acid concentration of 0·3 N and a solvent to aqueous volume ratio of 4, the extraction coefficient for neptunium is still greater than 10 while those for plutonium decrease to 4×10^{-2} and 4×10^{-3}, respectively, for 5 minutes of mixing time and at equilibrium.

Decontamination factors for neptunium in plutonium of 10^3 and 4×10^3 respectively, were obtained in saturating the solvent with Np(IV) and adding SO_4^{2-} in the scrub. Values of 10^5 were achieved when using capric acid.

Influence of capric acid on the back-extraction of neptunium and plutonium

When used in the neptunium–plutonium separation, capric acid follows the organic stream in the neptunium back-extraction. Therefore its effect on the back-extraction of tetravalent species was studied. For instance, Fig. 5 shows that the back-extraction of tetravalent plutonium into 0·5 N-H_2SO_4 and up to 1N-HNO_3 aqueous solutions can be performed with a concentration factor of 10 when using 0·3 N capric acid in the solvent. In fact much lower SO_4^{2-} ion concentrations are required when using capric acid in the back-extraction; 0·5 N-H_2SO_4 is required instead of 2 N-$(NH_4)_2SO_4$–1 N-H_2SO_4 whereas higher nitric acid concentrations are allowed (1 N instead of 0·55 N).

The back-extraction reaction can be represented as follows:

$$(R_3NH)_2\ M\ (NO_3)_6 + nHSO_4^- \rightleftarrows 2\ R_3N\ HNO_3 + M(SO_4)_n^{-(2n-4)} + nH^+ + 4NO_3^-$$

showing that 4 moles of nitrate ions are liberated from the organic complex into the aqueous phase with one mole of metal ion. On the other hand, the lowest HNO_3 concentration of the back-extracting solution required for a proper exchange of the M(IV) ions in the metal-depleted end of the counter-current system is 0·1N. An additional 0·9 M-NO_3^- ions coming from the organic phase can therefore be tolerated in the aqueous phase without exceeding the limit of 1M NO_3^- ions mentioned earlier. This addition corresponds to an aqueous concentration of neptunium, plutonium or a mixture of both of about 50 g/l which is, in practice, the chosen maximum concentration. Fig. 6 shows that the Np(IV) distribution coefficient at this aqueous concentration is still sufficiently low ($7 \cdot 5 \times 10^{-2}$). In this process, the loading of the solvent (10% by vol. TLA) is in practice maintained at about 10g/l, thus a concentration factor of about 5 is needed in the back-extraction.

Influence of capric acid on the decontamination of neptunium and plutonium

The processing of irradiated ^{237}Np was carried out using the same solvent in all the extraction steps and adding capric acid in the scrubbing of cycles 2 and 3 and in all the back-extractions. Furthermore, all back-extractions were carried out with a 0·5N-H_2SO_4–0·1 N-HNO_3 solution and an organic to aqueous volume ration of 5·85.

These results are compared with those obtained in a previous processing run in which capric acid was not used.[5] The losses of α- activity were similar in both runs (Table II).

The decontamination factors from ruthenium and zirconium obtained in run 1 were slightly higher in the first cycle and lower in the other two cycles than those given in run 2 (Tables III and IV).

The higher decontamination obtained in the absence of capric acid may be explained by the use of a greater concentration factor in the first extraction step (3 instead of 1·66). On the other hand, the introduction of capric acid in the back-extraction displaces the extracted ruthenium and zirconium species along with neptunium and plutonium, while, when introduced in the scrubbing section, as, in the second and third cycles of run 2, capric acid improves the neptunuim and plutonium decontamination.

Finally it must be noticed that a good uranium-plutonium separation occurs in the third cycle due to the absence of a salting agent and to the high decontamination factors obtained when using capric acid. The reason for the latter effect is that, although the distribution coefficient of Pu(IV) decreases more rapidly than that of U(VI) with increasing capric acid concentration (Fig. 3), the operating conditions are such that addition of capric acid significantly improves the back extraction of uranium with only a slight increase in plutonium recycle.

Conclusions

A comparison between trilaurylamine solvent-extraction processes for irradiated ^{237}Np using in the presence or absence of capric acid clearly shows the advantages of the former process. Introduction of capric acid in the scrubbing section results in a better neptunium–plutonium mutual separation, an increase of the overall decontamination factors for zirconium and ruthenium by a factor of about 10 and decontamination factors for the other fission-products of $>10^4$ for each cycle. Furthermore, addition of capric acid in the back-extractions allows a decrease in the SO_4^{2-} ions to neptunium and/or plutonium molar ratio in the aqueous stream by a factor of 6, thus facilitating the further extraction or oxalate-precipitation steps.

Acknowledgments

The authors wish to thank R. Sontag who kindly supplied the hot cell and processing equipment for this work and R. Pottier for performing the γ-spectrometry measurements. The experimental assistance of F. de Mora, M. Baudet and C. Jouan is also gratefully acknowledged.

References

[1] Poe, W. L., Joyce, A. W. & Martens, R. I., *Ind. Engng Chem. Process Des. Dev.* 1964, **3**, 314
[2] Burney, G. A., *Ind. Engng. Chem. Process Des. Dev.* 1964, **3**, 328
[3] Jenkins, I. L., Shorthill, C. G. C., Streeton, R. J. W., & Wain, A. G., *Rep. U.K. atom. Energy Auth.*, 1966 AERE R-5074
[4] Jenkins, I. L., *Actinides Rev.*, 1969, **1**, 187
[5] Berger, R., Koehly, G., & Sontag, R. *Notes CEA*, 1968, N-1044, 283
[6] Gourisse, D., & Bathellier, A. *Radiochim. Acta*, 1970, **13**, 191
[7] Bathellier, A. *et al.*, *Notes CEA*, 1969, N-1241, 215
[8] Koehly, G., & Madic, C., & Berger, R., *Proc. int Solvent Extraction Conf.*, 1971, Paper 105 (London: Society of Chemical Industry)

A process for the extraction of plutonium-238 from a neptunium solution circulating through a reactor

by Miss C. J. Hynes, I. L. Jenkins and A. G. Wain
Atomic Energy Research Establishment, Harwell, U.K.

The advantages of making ^{238}Pu by irradiating an aqueous solution of neptunium(V) nitrate in a reactor loop are discussed, and a process for the rapid separation of ^{238}Pu is described. The plutonium can be extracted efficiently into a dilute solution of a tertiary amine in a diluent, leaving the neptunium and the fission products in the aqueous phase which can be recycled through the reactor.

Introduction

PLUTONIUM-238 is produced by the irradiation of compacts of $^{237}NpO_2$ and aluminium in a nuclear reactor.[1] Factors affecting the choice of a $^{237}Np/^{238}Pu$ separation process have been reviewed,[2] but little work has been published on the possibility of producing ^{238}Pu by circulating solutions of ^{237}Np through a reactor and processing the circulating solution. Such a system has been examined by Burton (Burton, W. R., personal communication) who concluded that production of kilogram amounts of ^{238}Pu per year was feasible by circulating solutions of neptunium nitrate in nitric acid in a loop installed in a nuclear reactor. The main reactions are:

$$\begin{array}{ccccccc}
^{237}Np & \xrightarrow{n,\gamma} & ^{238}Np & \xrightarrow{\beta\ \text{decay}} & ^{238}Pu & \xrightarrow{n,\gamma} & ^{239}Pu \\
 & & \downarrow \theta_f = 1600\ \text{barns} & & \downarrow \theta_f = 16\cdot 8\ \text{barns} & & \downarrow \theta_f = 750\ \text{barns} \\
 & & \text{fission products} & & \text{fission products} & & \text{fission products}
\end{array}$$

Processing the neptunium at intervals limits losses as ^{239}Pu, which is produced by neutron capture of the more valuable ^{238}Pu, and also ensures that the product has a high specific activity, which is desirable when the ^{238}Pu is to be used as a concentrated heat source. The material to be processed consists predominantly of neptunium containing fairly small amounts of plutonium and fission products.

The frequency of processing also depends on the build-up of neutron-absorbing poisons, e.g. the rare earths which will lower the reactivity of the reactor and decrease the yield of ^{238}Pu by absorbing neutrons that would otherwise be utilised to produce ^{238}Np. The worst neutron-absorbing poison is ^{135}Xe ($\sigma_c = 3\cdot 4 \times 10^6$ barns), but during reactor operation the ^{135}Xe equilibrium concentration is low and the poisoning effect is small. In addition the xenon can be removed by scrubbing the radiolytic off-gas so that its effect on neutron absorption of ^{237}Np will also be small. ^{149}Sm and ^{157}Gd also have high neutron capture cross-sections ($6\cdot 6 \times 10^6$ barns and $1\cdot 6 \times 10^5$ barns, respectively) and the cumulative fission yields (in ^{235}U fission) are $1\cdot 3$ and $0\cdot 15\%$ respectively. The fission yields will be slightly greater for ^{238}Np fission, but the total quantities of the poisons will be small relative to the ^{237}Np present since the equilibrium concentration of the fissile ^{238}Np is only about $0\cdot 3\%$ of the total neptunium (for a flux of 6×10^{13} n/cm^2 sec). It is likely, therefore, that the main consideration governing the frequency of processing the recycled solution is the permissable quantity of ^{239}Pu. Calculations by Milsted (Milsted, J., personal communication) show that in 30 days irradiation of ^{237}Np at a flux of 7×10^{13} n/cm^2 sec the ^{239}Pu concentration is $\sim 3\cdot 6\%$ based on ^{238}Pu

and after 100 days it is ~11%. Processing is needed approximately once a month to keep the ^{239}Pu content below 5%; more frequent processing is needed if a lower ^{239}Pu content is required.

A circulating aqueous system has one great advantage over the conventional method of ^{238}Pu production in that the fabrication and canning of NpO_2–Al compacts is avoided. This paper describes a possible processing scheme in which neptunium nitrate solutions circulated through a reactor are processed to remove the ^{238}Pu preferentially, and where the neptunium can be recycled with little delay. Solvent extraction was selected in preference to anion exchange as it is easier to operate on a continuous basis should this be desired but, in principle, an ion-exchange scheme based on the preferential removal of Pu(IV) from the circulating solution could be used. Moreover, a solvent extraction process can be operated at 1M-HNO_3 as against >4·5M-HNO_3 for an anion-exchange separation process. The use of a higher nitric acid concentration could lead to difficulties.

In choosing an extractant, tertiary amines were preferred to organophosphorus reagents as, in general, their degradation products are less troublesome than those of extractants such as tri-n-butyl phosphate. This is particularly important in the processing scheme described because, as discussed above, the concentration of plutonium in the solution to be processed is low and the amounts of degradation products from the extractant may be comparable to the plutonium content.

Published data for the distribution of plutonium and neptunium between tertiary amines and nitric acid (see for example ref. 3) suggest that several possible processing schemes can be used. Three possible methods may be considered: the co-extraction of Np(IV) and Pu(IV) followed by selective backwashing to separate them; selective extraction of neptunium as Np(IV) leaving the plutonium as Pu(III); and selective extraction of Pu(IV), leaving neptunium in the pentavalent state in the aqueous phase which is recycled.

The selective extraction of Pu(IV) is favoured since it avoids extraction of the major component. The volatile fission products are absorbed from the radiolytic gases evolved and the non-volatile ones are recycled with the neptunium. A schematic flow sheet based on experimental work is given later.

The degradation of one of the amine–diluent combinations examined, viz. Alamine 336/dibutyl Cellosolve, has been studied by Lane *et al.*,[4] and countercurrent solvent extraction trials using the same extractant and diluent have been carried out by Streeton & Holdoway[5] for the separation of plutonium from uranium in a nitrate system. The latter authors obtained solvent loadings of up to 10·5 g Pu/l for 15% Alamine 336/DBC. This is rather a low value for a solvent extraction process where a large amount of plutonium is to be extracted, but it is ample for the type of process envisaged here where small amounts of plutonium are preferentially extracted from much larger amounts of neptunium.

For some applications, e.g. for use in heart pacers, it is desirable to produce ^{238}Pu containing less than 1 ppm of ^{236}Pu.[6] This isotope is formed by the $^{237}Np(n,2n)^{236}Np \xrightarrow{\beta} {}^{236}Pu$ process and has a decay chain containing some very penetrating gamma rays, especially those from ^{208}Tl. The irradiation conditions, therefore, need to be chosen to minimise the production of ^{236}Pu. Topp[7] has calculated the amounts of ^{236}Pu that are likely to be found as contaminants in ^{238}Pu when using different types of reactors (with different neutron spectra). Although of interest in the choice of irradiation conditions, the ^{236}Pu content does not affect the processing of the irradiated neptunium.

Experimental

Neptunium

Solutions of neptunium nitrate were prepared by dissolving the dioxide, NpO_2, in 12M nitric acid containing about 0·05M-HF, precipitating the neptunium as the hydroxide, redissolving in nitric acid and fuming down several times to near dryness with concentrated HNO_3 to remove the fluoride. Finally,

the solution was evaporated nearly to dryness and the product taken up in nitric acid of the desired strength.

Plutonium

Aged solutions stock of plutonium nitrate (^{239}Pu) in 6M-HNO_3 were purified from ^{241}Am, the daughter of ^{241}Pu, by anion exchange in 8M-HNO_3. ^{238}Pu produced by the neutron irradiation of ^{237}Np, had been prepared previously[8] and was available as a highly pure product in 2M-HCl. The chloride was removed by repeated heating to near dryness with concentrated nitric acid.

Alamine 336, a mixture of tertiary amines but mainly tricaprylamine, from General Mills, Inc., U.S.A., and trilaurylamine (TLA), nuclear grade, from the Société des Usines Chimiques, Rhône Poulenc, Paris, were used without further purification. Their basicity was checked by non-aqueous titration with 0·1M perchloric acid in glacial acetic acid using oracet blue B indicator, and solutions in various diluents were made up by volume.

Odourless kerosene, 'Analar' xylene and Solvesso 100, an aromatic diluent consisting of a mixture of alkyl benzenes, were used without further purification but dibutyl Cellosolve (DBC, 1,2-di-n-butoxyethane), was purified as described by Lane *et al.*[4]

Plutonium and neptunium were determined by alpha scintillation counting. Where both were present in the same sample, alpha pulse height analysis was used to differentiate between them.

The different valency states of neptunium and plutonium were determined with a Cary 14 automatic recording spectrophotometer or with a Cambridge SP 500 spectrophotometer. Distribution measurements were made by stirring together equal volumes of the organic and aqueous phases in a centrifuge tube at 25°C ± 0·1°. The mixed phases were then centrifuged and the phases separated. All the organic phases were pre-equilibrated with aqueous acid of the required concentration before use. In many cases the equilibrated organic phase was re-equilibrated with fresh aqueous phase of the correct acidity to obtain a 'backwash' value for the distribution coefficient; this eliminated any errors due to inextractable α-emitters, e.g. ^{241}Am, in the initial aqueous phase.

Stirring times of 2 min, 10 min and 2 h were used to check the rate of attainment of extraction equilibrium in the Pu(IV)/1M-HNO_3–10% TLA/kerosene system and equilibrium was attained within 2 min. Stirring times of 10 min were normally used, unless it is noted otherwise in the text. The rate of attainment of extraction equilibrium was much slower when stripping plutonium from the organic phase; this is discussed later.

Results and discussion

Distribution data for Np(VI)

Hexavalent neptunium was prepared by oxidising the lower valency states with sodium bromate, argentic oxide or ozone. Distribution data are plotted in Fig. 1 and the salting-out effect of aluminium nitrate in the aqueous phase is shown in Table I.

TABLE I

Effect of a salting-out agent on $D_{Np(n)}$, *10% Alamine 336/DBC, 25°C*

Aqueous phase	$D_{Np(VI)}$
0·5M-HNO_3	0·75
0·5M-HNO_3 + 1·5M-$Al(NO_3)_3$	3·2
1·0M-HNO_3 + 1·5M-$Al(NO_3)_3$	17·5, 17·5
2·0M-HNO_3 + 1·5M-$Al(NO_3)_3$	55

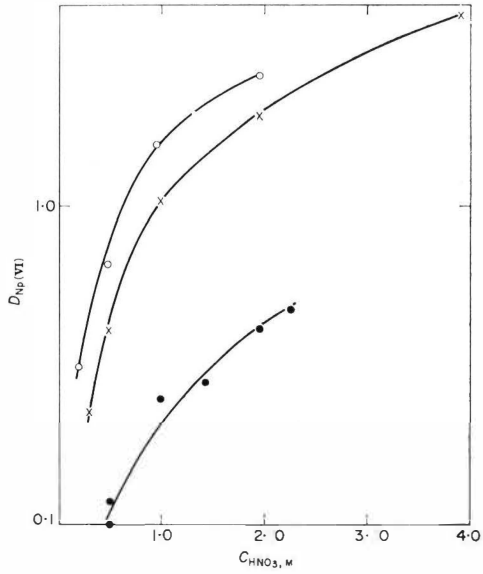

FIG. 1. *Variation of* $D_{Np(VI)}$ *with acidity at 25°C*
○ 10% Alamine 336/DBC; × 10% TLA/kerosene; ● 2·5% Alamine 336/DBC

In the absence of a salting-out agent the slope of the log $D_{Np(VI)}$ vs. log C_{amine} line is ~1·3 at 1M and 2M-HNO_3. This is in qualitative agreement with the work of Keder *et al.*,[3] who found a slope of 'less than two but greater than unity'.

Distribution data for Np(V)

Tertiary amines do not extract Np(V) very efficiently as shown in Table II. Neptunium was conditioned to the pentavalent state by first oxidising it all to the (VI) state and then reducing it to Np(V) with oxides of nitrogen.

With kerosene as diluent, consistent results could not be obtained for the dependence of $\log D_{Np(V)}$ on log C_{amine}. A linear dependence with a slope of 0·85 was found at amine concentrations less than 2% but very erratic results were found with higher amine concentrations. The inconsistencies may be connected with the kerosene since with TLA in xylene a linear dependence (with a slope of 2·1) was found at concentrations of TLA up to at least 20%. The inconsistencies are unlikely to be due to disproportionation of Np(V) as the equilibrium constant for the reaction ($2\ Np(V) \rightleftharpoons Np(IV) + Np(VI)$) is 4×10^{-7} in 1M-HCl or 1M-$HClO_4$.[9] At 1M-HNO_3 with little or no nitrate complexing,[10] Np(V) should be stable with respect to disproportionation.

TABLE II

Values of $D_{Np(V)}$ *at 25°C*

Extractant	Aqueous phase	$D_{Np(V)}$
10% Alamine 336/DBC	1M-HNO_3	$7 \cdot 5 \times 10^{-3}$
10% Alamine 336/DBC	1M-HNO_3 + 1·5M-$Al(NO_3)_3$	3×10^{-2}
10% TLA/kerosene	1M-HNO_3	$2 \cdot 3 \times 10^{-2}$ } See text
5% TLA/kerosene	1M-HNO_3	$3 \cdot 3 \times 10^{-2}$ } See text
2·5% TLA/kerosene	1M-HNO_3	$2 \cdot 0 \times 10^{-2}$ } See text
10% TLA/xylene	1M-HNO_3	8×10^{-3}

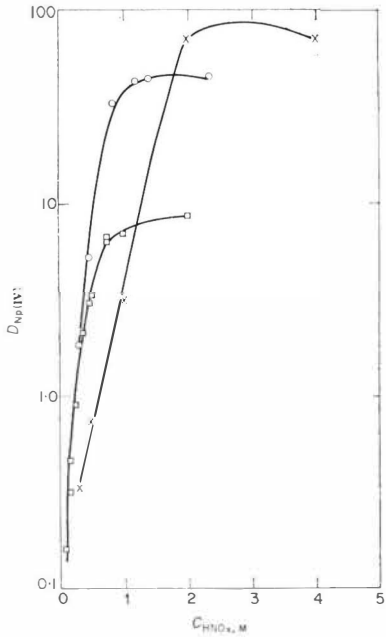

FIG. 2. *Variation of* $D_{Np\ (IV)}$ *with acidity at 25°C*
○ 10% Alamine 336/DBC; × 10% TLA/kerosene; □ 5% Alamine 336/DBC

Distribution data for Np(IV)

The variation of $D_{Np(IV)}$ with the concentration of nitric acid in the aqueous phase for both amine–diluent combinations is given in Fig. 2. Np(IV) is not likely to be found in process solutions of the type under consideration and none was observed when solutions of Np(V) in 1M-HNO_3 were irradiated (see later). Any Np(IV) in the amine phase is difficult to strip with dilute nitric acid alone as polymerisation and hydrolysis of the neptunium are probable at the acid concentrations needed for efficient stripping. Stripping can be carried out either by oxidising the neptunium to the relatively inextractable pentavalent state or by complexing the neptunium, e.g. with acetic or sulphuric acids. Coleman *et al.*[11] have used hydrogen peroxide to oxidise Np(IV) to Np(V) in stripping neptunium from 0·3M (~15%) Alamine 336 in a diluent and have shown that stripping by this method can be carried out satisfactorily in a mixer–settler. Sulphuric acid has been found to be more effective than acetic acid in stripping neptunium from Alamine 336 but the removal of Np(IV) from the amine phase has not been studied in detail, as the problem should not arise in the process under consideration.

Distribution data for Pu(VI)

The variation of $D_{Pu(VI)}$ with acidity for both amine–diluent combinations is given in Fig. 3. The results show that with 10% Alamine 336/DBC, plutonium can be extracted easily from 1M-HNO_3 even if it is all present as Pu(VI). With 10% TLA/kerosene a high solvent : aqueous ratio would be needed to extract Pu(VI) and it would be necessary to use a higher amine concentration, say 15% TLA, to obtain better extraction. The slope of the log $D_{Pu(VI)}$ vs. log C_{amine} plot is between 1 and 2 for tri-n-octylamine in xylene;[3] a slope of ~unity (1·1) has been found for the TLA/kerosene system.

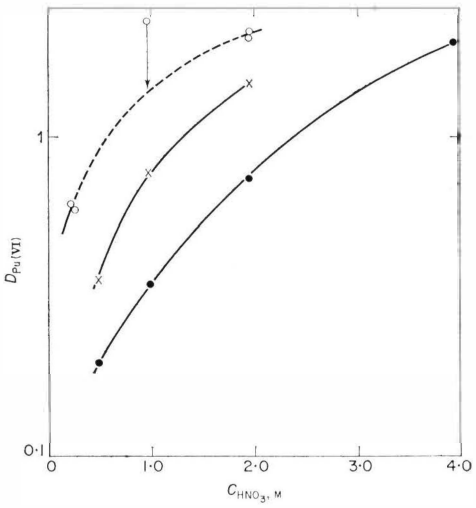

FIG. 3. *Variation of* $D_{Pu(VI)}$ *with acidity at 25°C*
O 10% Alamine 336/DBC; × 10% TLA/kerosene; ● 5% TLA/kerosene

Distribution data for Pu(IV)

A plot of log $D_{Pu(IV)}$ against log C_{amine} for Alamine 336/DBC yields a slope of nearly 2,[12] and $D_{Pu(IV)}$ is very high where the loadings are low, e.g. for 1M-HNO_3 and 10% Alamine 336/DBC, $D_{Pu(IV)}$ is about 192 for trace plutonium, 81 for 1 mg Pu/ml and 23 for 10 mg Pu/ml in the aqueous phase. Plutonium loadings of up to 10·5 g Pu/l in 15% Alamine 336/DBC have been observed by Streeton & Holdoway[5] without third phase formation, and loadings of 1·5 g Pu/l and 3 g Pu/l have been determined in this work for 5% and 10% TLA/kerosene respectively. Higher plutonium loadings, e.g. ~20 g Pu/l, are possible with 20% TLA/Solvesso 100.[13] The variation of $D_{Pu(IV)}$ with acidity for 5% TLA/kerosene and for 5% Alamine 336/DBC is shown in Fig. 4; the slope of the log $D_{Pu(IV)}$ vs. log C_{amine} plot was 1·4 for the TLA/kerosene system (1M-HNO_3, 25°C).

The values of $D_{Pu(IV)}$ are so high with both amine–diluent combinations that it is impractical to strip plutonium (IV) from the amine phase with dilute nitric acid. Alternative methods of removal are: (i) a reducing strip, (ii) an oxidising strip and (iii) a complexing strip; these are considered below.

(i) Champion & Chesne[14] have shown that the rate of removal of plutonium from a tertiary amine by reduction of the Pu(IV) in the organic phase to Pu(III) with ferrous ion is time dependent, and studies on the stripping of plutonium from 15% Alamine 336/DBC (initially containing 2 mg Pu/ml) with 0·5M-HNO_3 + 0·1M-Fe^{2+} show that 20–30 min contact time is required to reach equilibrium. This must be considered when stripping plutonium in, say, a mixer–settler or a pulsed column. Bathellier[15] has stripped plutonium from 5% TLA/dodecane as Pu(III) in a mixer–settler using nitrite as reducing agent. He concludes that a pulsed column is preferable to a mixer–settler for stripping with nitrous acid and that any actinide can easily be displaced from TBP (tri-n-butyl phosphate) or TLA by nitrous acid. This method gives an aqueous phase free of foreign ions, e.g. Fe(II) and Fe(III), and re-extraction into an amine phase for a second purification cycle is easy. It should, however, be borne in mind that any secondary or primary amines present either in the original amine or as a result of radiolytic degradation of the tertiary amine may react with nitrous acid. Primary amines can yield alcohols, or in some cases

olefins, while secondary amines form nitroso compounds. More work, therefore, needs to be carried out before the use of nitrous acid to strip plutonium from TLA or Alamine 336 can be considered as a firmly established practical method in a system where severe radiolytic attack on the solvent is possible.

(ii) $D_{Pu(VI)}$ is much lower than $D_{Pu(IV)}$ in both the amine–diluent combinations examined. In the 10% Alamine 336/DBC–nitric acid system, $D_{Pu(VI)}$ is equal to 0·62 at 0·25M-HNO_3 and it should therefore be possible to strip plutonium from 10% Alamine 336/DBC if the plutonium is oxidised to the hexavalent state. A high aqueous : solvent volumetric flow ratio would be needed for the 10% amine system but if a 5% amine system were used, stripping would be easier. Stripping plutonium by oxidation to Pu(VI) is easier in the TLA/kerosene system as the values of $D_{Pu(VI)}$ are lower, but with both amine–diluent combinations information is needed on the rates of reduction under the desired experimental conditions.

(iii) The removal of plutonium from the organic phase by complexing with acetic acid is also time dependent but plutonium has been successfully stripped from a solution of 10·5 g Pu/l in 15% Alamine 336/DBC using 1M acetic acid + 0·05 M-HNO_3.[5] The plutonium concentration in the organic phase was reduced from 10·5 g/l to 10^{-3} g/l in eleven stages with a solvent : aqueous volumetric flow ratio of unity. This result was achieved with an average hold-up time of about 2 min per stage in the mixer–settler. The apparently dangerously low nitric acid concentration did not lead to hydrolysis and polymerisation of the plutonium as, in addition to the hydrogen ions supplied by the acetic acid, more nitric acid was stripped from the organic phase.

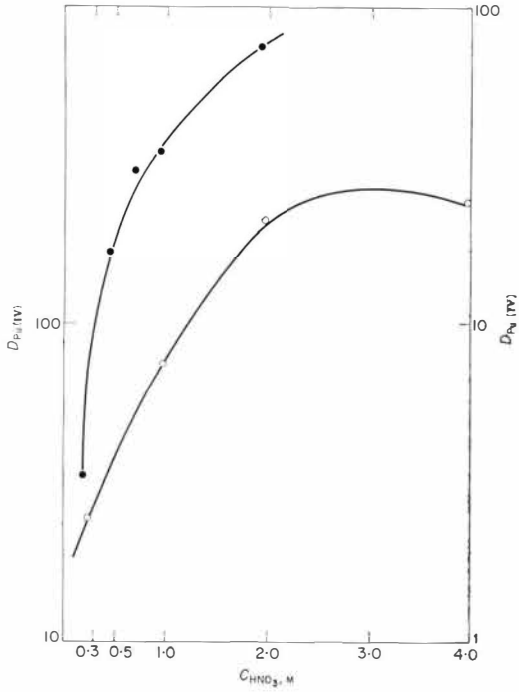

FIG. 4. *Variation of* $D_{Pu(IV)}$ *with acidity at 25°C*

● (right-hand ordinate), 5% Alamine 336/DBC; ○ (left-hand ordinate), 5% TLA/kerosene

Distribution data for Pu(III)

It is well known that plutonium can be extracted by tertiary amines from aqueous nitric acid in which the plutonium is kept predominantly in the trivalent state by an excess of reductant, the plutonium in the amine being in the tetravalent state. The results in Fig. 5 are taken from ref. 2 and show that, nevertheless, in the presence of the Fe(III)/Fe(II) couple, provided the mole ratio of Fe(III) to Fe(II) is kept low, the extraction of plutonium is also low. It should therefore be possible to extract only Np(IV) from a mixed Np(IV)/Pu(III) system provided the Fe(III)/Fe(II) ratio can be kept low.

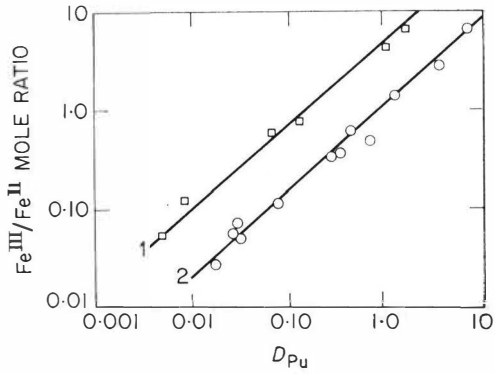

FIG. 5. *Plot of log* D_{Pu} *as a function of the Fe(III)/Fe(II) mole ratio*

Effects of irradiation of neptunium and plutonium solutions

The irradiations were carried out with gamma rays from irradiated fuel elements stored in the Technical Irradiation Group (TIG) pond at A.E.R.E. Two dose rates were used: 0·1 and 1 Mrad/h and the highest integrated dose given to any sample was 60 Mrad. The initial solutions to be irradiated were treated with nitrous fumes (nitric oxide from a cylinder) to ensure that, at the start, the neptunium and plutonium were in the (V) and (IV) states respectively. Neptunium spectra were examined with a Cary automatic recording spectrophotometer; Np(IV) could not be determined by its absorption at 960 nm because of interference by that of Np(V) at 980 nm. Plutonium spectra were examined with a Cambridge Unicam SP 500 spectrophotometer. The conditions used are given in Table III and the results are discussed below.

TABLE III

Conditions used for irradiation tests

Run	Np, mg/ml	Pu, mg/ml	HNO_3, M	Dose rate, Mrad/h	Comments
1	2·9	—	2·2	0·1	Np spectra examined
	16·4	—	2·2	0·1	Np spectra examined
2	2·4	trace	1·01	0·1	D_{Np} and D_{Pu} determined
	10·5	trace	1·01	0·1	D_{Np} and D_{Pu} determined
3	—	1·4	1·0	0·1	D_{Pu} determined Pu spectra examined
4	—	0·74	1·03	0·1	Pu spectrum examined Total dose = 59·9 Mrad
5	—	0·58	0·99	1·0	Pu spectra examined

Two series of neptunium concentrations were studied in Runs 1 and 2. Small amounts of Np(VI) were found in the irradiated samples in Run 1 but as equal amounts were also found in unirradiated samples, kept the same length of time, the Np(VI) was probably formed by the disproportionation of Np(V) in 2·2M-HNO_3. At 1M-HNO_3 (Run 2) where the Np(V) is more stable, no Np(VI) was detected in either irradiated or unirradiated solutions.

All the values of D_{Np} (for both series of neptunium concentrations) in Run 2 were found to lie between $1 \cdot 47 \times 10^{-2}$ and $2 \cdot 15 \times 10^{-2}$ using 10% TLA/kerosene, and the neptunium was still present as 100% Np(V) as shown by the absorption spectrum. The values of D_{Pu} were dependent on the initial neptunium concentration and also on the irradiation dose as shown in Fig. 6. The fall of D_{Pu} with irradiation dose indicates the presence of a plutonium species less extractable than Pu(IV). This was assumed to be Pu(IV) produced by the disproportionation of Pu(IV).

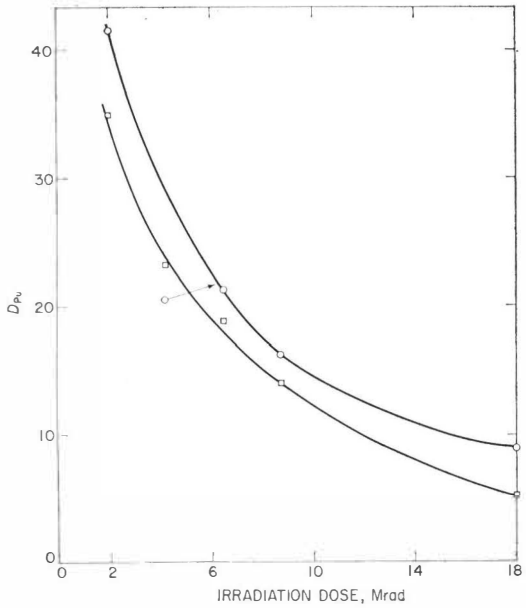

FIG. 6. *Plot of* D_{Pu} *vs. irradiation dose, 25°C*
○ ^{238}Pu(trace), ^{237}Np(10·5 mg/ml); □ ^{238}Pu(trace), ^{237}Np(2·4 mg/ml)

Pu(III) would not be expected to exist under the irradiation conditions since nitrite formed by the radiolysis of nitric acid would oxidise it to Pu(IV) and therefore the irradiated solution should be a mixture of Pu(IV) and Pu(VI). Runs 3 and 4 were carried out with plutonium concentrations high enough to enable the valency states to be examined spectrophotometrically. Pu(III) was not detected but, as expected, the Pu(IV) concentration was found to decrease and that of Pu(VI) increased. The absorption spectrum of Pu(VI) in nitric acid has been studied by many workers and values for the molar extinction coefficient at 831 nm range from 300 to 500 in 2M-HNO_3,[16] making quantitative measurements very difficult, and it was not possible to confirm the stoichiometry of the valency changes. The results of Runs 3 and 4 (Fig. 7), however, show that the decrease in Pu(IV) content depends linearly on the irradiation dose and the increase in Pu(VI) also seems to be linear. Similar results were found for Run 5 where a dose rate of 1 Mrad/h was used, but at the increased

dose rate more Pu(IV) was destroyed and more Pu(VI) formed for a given total integrated dose than was formed at the lower dose rate. The build-up of Pu(VI) therefore appears to depend on the dose rate as well as on the total integrated dose.

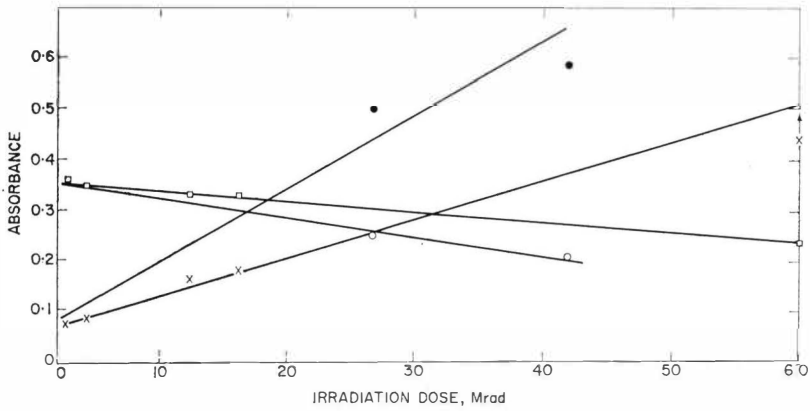

FIG. 7. *Changes in the absorbance due to Pu(IV) and Pu(VI) in irradiated solutions*

● Pu(VI) Run 5; × Pu(VI) Runs 3 and 4; □Pu(IV) Runs 3 and 4; ○Pu(IV) Run 5
Pu(VI) absorbance measured at 837 nm
Pu(IV) absorbance measured at 475 nm

Possible flowsheet

General comments

A schematic diagram of a possible flowsheet is given in Fig. 8. The feed to the first solvent extraction cycle consists of neptunium(V) at a concentration of, say, 0·05M (~12 g Np/l) together with plutonium at about 0·0025M (~0·6 g Pu/l) and the associated fission products. The plutonium is extracted with 10% Alamine 336/DBC and the neptunium and fission products are recycled through the reactor. Various aspects of the flow sheet are discussed below. The conditioning of the feed to the first solvent extraction cycle, to the plutonium purification cycle and to the neptunium recycle are discussed first. The passage of plutonium through the process is then dealt with and finally the recycling of neptunium is discussed. The behaviour of fission products has not been studied as it is well known that, in general, tertiary amines do not extract fission products efficiently (see for example ref. 12 and 17).

Conditioning

Feed to first cycle

The feed to the first cycle is not expected to need any pretreatment as the neptunium should be in the pentavalent state and the plutonium in the tetra- or hexavalent states. There will however be an equilibrium between the Pu(VI)/Pu(V) and the Np(VI)/Np(V) couples,

$$Np(VI) + Pu(V) \rightleftharpoons Pu(VI) + Np(V).$$

The electrode potentials of the Pu(VI)/Pu(V) and Np(VI)/Np(V) couples in 1M-$HClO_4$ are −0·912 and −1·138V respectively. Similar values may be assumed for 1M-HNO_3 because Np(VI) complexing is small and there is no Np(V) complexing by nitrate.[10] Plutonium would be expected to behave similarly so that the differences in the potentials in 1M-HNO_3 will be ~ −0·226V.

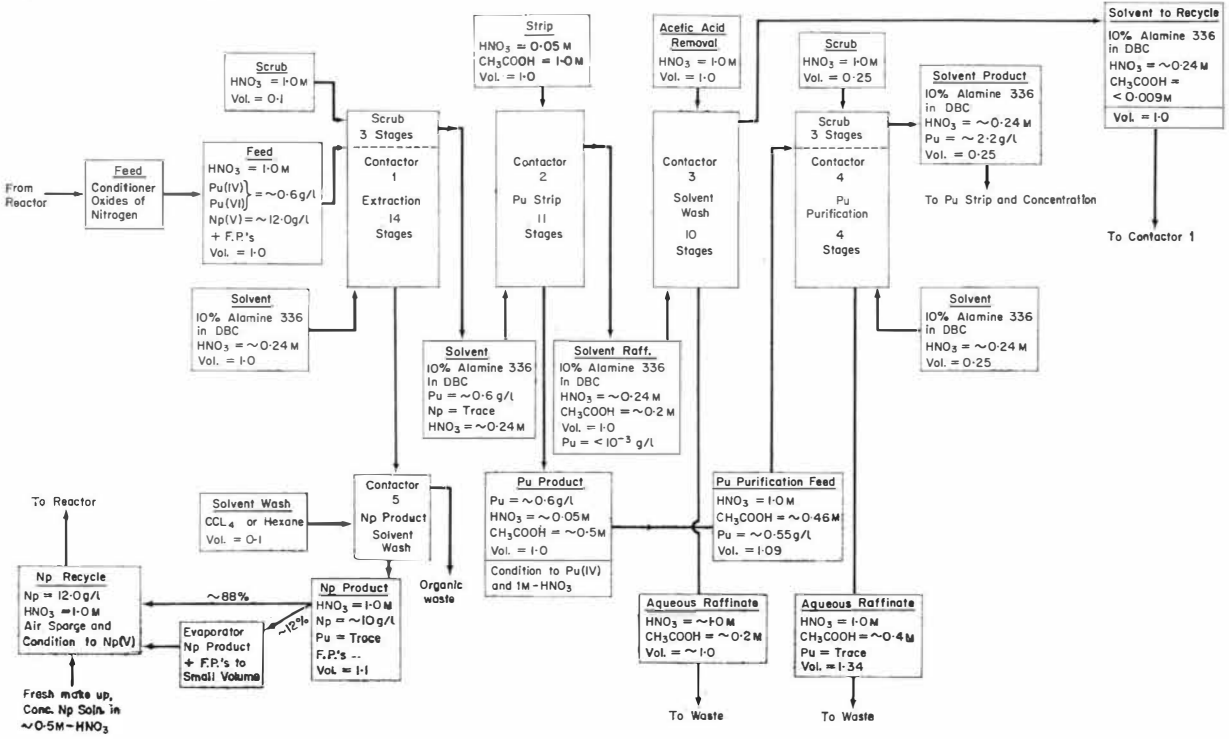

FIG. 8. *Outline flowsheet*

The equilibrium constant for the above reaction is:

$$K = \frac{[\mathrm{Pu(VI)}]\,[\mathrm{Np(V)}]}{[\mathrm{Np(VI)}]\,[\mathrm{Pu(V)}]}$$

and log K is related to the potentials by

$$\log K = \frac{n}{0{\cdot}0591}(E_1 - E_2)$$

$$= \frac{0{\cdot}226}{0{\cdot}0591} = 3{\cdot}8$$

$$\therefore\ K = 6{\cdot}6 \times 10^3$$

The equilibrium for the reaction will favour the right-hand side of the equation making Pu(VI) and Np(V) the predominant species; any Np(VI) could be converted to Np(V) by bubbling oxides of nitrogen through the solution. This conditioning must be kept to a minimum because it increases the acidity of the solution which would then need to be adjusted to 1M-HNO_3.

Pu(VI) formed during the irradiation (Fig. 7) would be extracted quantitatively into the amine using the extraction conditions given in the outline flowsheet (Fig. 8).

Feed to plutonium purification cycle

Any Pu(III) formed by disproportionation of Pu(IV) during processing can be converted to Pu(IV) by passing in oxides of nitrogen. The nitric acid concentration also has to be increased to enable the plutonium to be extracted in the presence of acetic acid (see later).

Conditioning of recycled neptunium

All the neptunium can be converted to Np(V) by passing in oxides of nitrogen.

Contactor I – plutonium extraction and scrub

The outline flowsheet (Fig. 8) shows that at 1M-HNO_3 and with volumetric flow ratios of aqueous feed : 10% Alamine 336/DBC : aqueous scrub = 1 : 1 : 0·1, plutonium can be efficiently extracted in 14 stages even if the plutonium is present entirely as Pu(VI); with TLA/kerosene an amine concentration of about 15% would be needed. Np(V) extraction by these solvents is very small ($D_{\mathrm{Np(V)}} \sim 1 \times 10^{-2}$) so that a plutonium–neptunium separation is possible.

Introducing a scrub section in contactor I increases the volume of neptunium solution by 9%. This together with the conversion of neptunium to plutonium decreases the neptunium concentration of the aqueous product from contactor I to 10 ~g/l. A portion (~12%) of this product is bled off, evaporated and mixed with fresh neptunium at a high concentration to blend with the irradiated neptunium solution before conditioning and recycling.

An alternative is to have a separate contactor for scrubbing but this leads to extra operations before the neptunium solution is fed back into the reactor.

Plutonium loadings of 10·5 g/l have been achieved in the 15% Alamine 336/DBC case,[5] and up to 3 g Pu/l in 10% TLA/kerosene have been obtained without the formation of three phase systems. These loadings are ample in a system where the initial concentration of plutonium in the aqueous phase is low. Higher loadings can be obtained with 20% TLA/Solvesso 100.[13]

Contactor II – plutonium strip

Either a reducing or a complexing strip can be used and the feasibility of both methods has been demonstrated, e.g. by Bathellier[15] in the case of reduction of

Pu(IV) and by Streeton & Holdoway[5] for stripping with an acetic acid–nitric acid mixture. The latter method is preferred as there is no danger of unwanted reactions with primary and secondary amines, and there is no need to exclude air from the contacting equipment.

Contactor III – solvent clean-up cycle

The amine phase from contactor II (plutonium strip) will contain acetic acid, and if the amine is to be recycled and used for the plutonium extraction cycle the adverse effect of this acetic acid on the extraction of plutonium must be minimised. This can be carried out by displacing the acetic acid from the amine phase with nitric acid. Complete removal of the acetic acid is not necessary as it has been shown that for 5% Alamine 336/DBC in contact with 2M-HNO_3, the presence of 0·05M acetic acid in the organic phase does not have any significant effect on $D_{Pu(IV)}$. In practice, Streeton & Holdoway[5] have demonstrated inactively that the acetic acid content of 15% Alamine 336/DBC can be reduced from 0·281M to below 0·009M in nine stages of a counter-current mixer–settler by stripping with 1·06M-HNO_3 and using a solvent : aqueous volumetric flow ratio of unity.

Contactor IV – plutonium purification

The purity of the plutonium product from contactor II can be improved by further solvent extraction cycles. In order to extract plutonium from the mixed acetic acid–nitric acid solution from contactor II the nitric : acetic acid mole ratio has to be increased to 2 : 1. The effect on $D_{Pu(IV)}$ of increasing the nitric acid concentration at a fixed acetic acid concentration is illustrated in Fig. 9 (Jenkins, I. L., & Lidington, D., unpublished information) for 5% Alamine 336 in Solvesso 100. Efficient extraction of the plutonium can be achieved from a 1M-HNO_3 + 0·5M-CH_3COOH solution at volumetric flow ratios of aqueous feed: 10% Alamine 336/DBC : aqueous scrub = 1 : 0·25 : 0·25 using 4 extraction and 3 scrub stages.

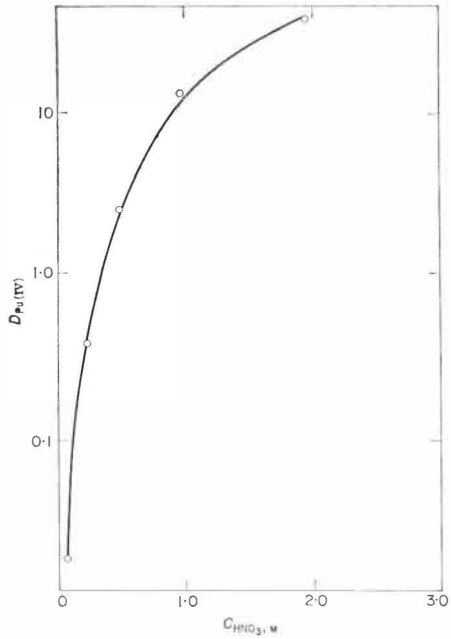

FIG. 9. *Variation of* $D_{Pu(IV)}$ *with nitric acid concentration at a fixed acetic acid concentration of 0·5M*, 25°C
5% Alamine 336/Solvesso 100

Contactor V – removal of dissolved solvent

The aqueous stream from contactor I will contain dissolved extractant as well as some entrained organic phase and it will be neccesary to remove this before returning the neptunium solution to the reactor. This part of the process has not been studied but it would be possible to remove organic matter by scrubbing the aqueous phase with, for example, hexane. Any hexane left in the aqueous phase can be removed by air sparging.

Acknowledgments

The authors wish to thank Mrs. D. Lidington and Mr. C. G. C. Shorthill for experimental assistance and Dr. H. A. C. McKay for advice and encouragement.

References

[1] *Ind. Engng Chem. Process Des. Dev.*, 1964, **3**, 293
[2] Jenkins, I. L., *Actinides Rev.*, 1969, **1**, 187
[3] Keder, W. E., Sheppard, J. C., & Wilson, A. S., *J. inorg. nucl. Chem.*, 1960, **12**, 327
[4] Lane, E. S., Pilbeam, A., & Fletcher, J. M., *Rep. U.K. atom. Energy Auth.*, 1965, AERE-R 4440, Part 1
[5] Streeton, R. J. W., & Holdoway, M. J., *Rep. U.K. atom. Energy Auth.*, 1965, AERE-R 4440, Part 3
[6] Matlack, G. M., & Metz, C. F., *Rep. Congr. atom. Energy Commn. U.S.*, 1967, LA-3696
[7] Topp, S. V., *Nucl. Appl. Tech.*, 1969, **7**, 139
[8] Jenkins, I. L., Shorthill, C. G. C., Streeton, R. J. W., & Wain, A. G., *Rep. U.K. atom. Energy Auth.*, 1966, AERE-R 5074
[9] Katz, J. J., & Seaborg, G. T., 'The chemistry of the actinide elements', 1957 (London: Methuen & Co. Ltd.)
[10] Al-Niaimi, N. S., Wain, A. G., & McKay, H. A. C., *J. inorg. nucl. Chem.*, 1970, **32**, 977
[11] Coleman, C. F., Kappelmann, F. A., & Weaver, B., *Nucl. Sci. Engng*, 1960, **8**, 507
[12] Jenkins, I. L., McKay, H. A. C., Shorthill, C. G. C., & Wain, A. G., *Rep. U.K. atom. Energy Auth.*, 1965, AERE-R 4440, Part 2
[13] Detilleux, E., Rolandi, G., Lopez-Menchero, J., & Geoffroy, A., Eurochemic Technical Report, ETR-90, 1962
[14] Champion, C., & Chesne, A., *Rapp. cea*, 1964, no. 2607
[15] Bathellier, A., 'Solvent extraction of metals', (Eds Healy, T. V., McKay, H. A. C., Jenkins, I. L., & Naylor, A.), 1965, p. 295 (London: MacMillan)
[16] Buijs, K., De Dalmassy, B. C., & Maurice, M. J., *Analytica chim. Acta*, 1969, **43**, 409
[17] Zifferero, M., 'Symposium on aqueous reprocessing chemistry for irradiated fuels,' Brussels, 1963, p. 107

Synergistic extraction and its use in analytical chemistry of transplutonium elements

by B. F. Myasoedov, M. K. Chmutova and I. A. Lebedev
V. I. Vernadsky Institute of Geochemistry & Analytical Chemistry, Moscow, USSR.

Introduction

THE NUMBER OF extraction systems which allow quantitative extraction of trivalent transplutonium elements from relatively acid media, without resorting to high concentration of salting out agents, is very limited.

In some cases, the use of a mixture of reagents for extraction leads to an increase in the distribution coefficient of the metal compared with the sum of the distribution coefficients which is obtained on the basis of the additivity of reagent action. This phenomenon, called the 'synergistic effect', has been investigated in the extraction of transplutonium elements in systems consisting of chelate-forming reagents with donor-active additives, and has been used for the separation and extraction of these elements from relatively acid media.

Experimental and Results

1-Phenyl-3-methyl-4-benzoylpyrazolone-5 (PMBP) was used as a chelate-forming reagent and alcohols and neutral phosphoro-organic reagents—tributyl phosphate (TBP), trioctylphosphine oxide (TOPO), and tributylphosphine oxide (TBPO)—were used as donor-active additives.

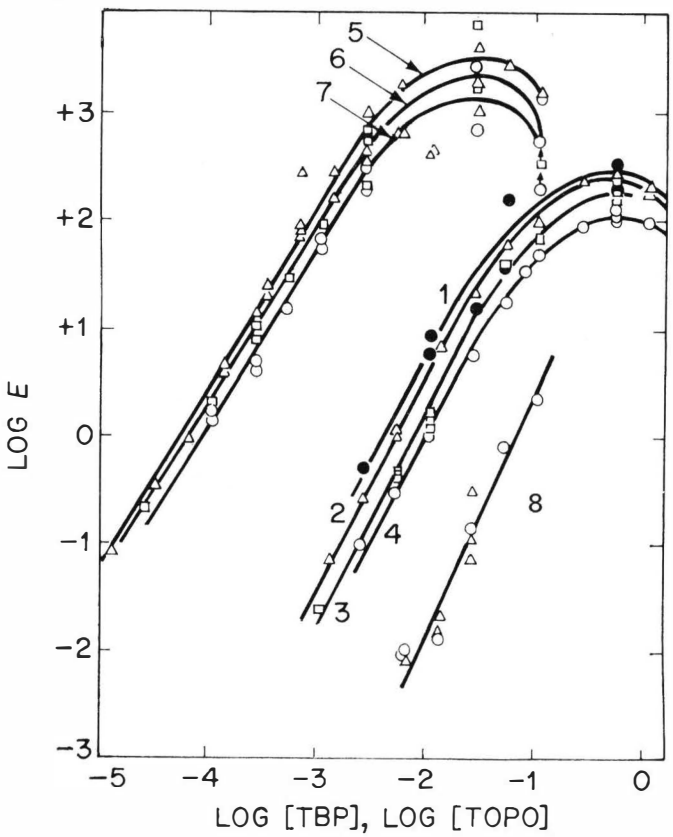

FIG. 1. *Dependence of Am, Cm, Bk, Eu extraction on the TBP and TOPO concentration in cyclohexane*

0·05M PMBP, 0·1M-HNO_3
Curves 1, 2, 3, 4 PMBP+TBP; Curves 5, 6, 7 PMBP+TOPO; Curve 8 TOPO without PMBP
△ Eu; ● Bk; □ Am; ○ Cm

The substitution of benzene for alcohols (isoamyl, n-butyl, benzyl) as solvent in systems with PMBP, increases the distribution coefficient of curium by 4–5 orders of magnitude and, therefore, curium (and other transplutonium elements) may be extracted from 0·1N-HNO_3 solutions. The slopes of curves, showing the logarithmic dependence of the curium distribution coefficient on the water phase acidity and on the concentrations of reagents, indicate the extraction of a $CmA_3 \cdot XS$ compound, where A is the anion of PMBP and S the molecule of alcohol.

The use of TBP and TOPO (cyclohexane solvent) as additives gives a still greater effect and the dependence of Am, Cm, Bk and Eu extraction by a mixture of 0·05M-PMBP and TBP (or TOPO) on the concentration of the latter is shown in Fig. 1. After the maximum, the fall in extraction is due to the lowering of the effective concentration of the reagents as a result of their interaction.

Investigation of the dependence of the Cm and Eu extraction on the water phase acidity and on the concentrations of reagents led to the assumption that the extraction of these elements proceeds in the form of a compound $MeA_3 \cdot 2TBP$ (or of the compounds $MeA_2(NO_3) \cdot 2TOPO$ and $MeA_3 \cdot 2TOPO$ in the case of TOPO).

Thus the addition of 0·25M TBP or 0·0025M TOPO to 0·05M-PMBP in cyclohexane allows the quantitative extraction of trivalent transplutonium elements from 0·1N-HNO_3 and the addition of 0·025M-TOPO allows extraction from 0·3N-HNO_3. Quantitative re-extraction is achieved with 3–5N-HNO_3.

The nature of the diluent greatly influences the magnitude of the synergistic effect. Table I shows that the americium extraction constants decrease as the diluent dielectric constant increases.

TABLE I

Influence of the solvent nature upon the Am(III) extraction in the system PMBP–TBP–solvent–0·1M-HNO_3

Solvent	Dielectric constant	log K_{ex}
η-Hexane	1·890	5·18
η-Heptane	1·924	4·99
η-Octane	1·948	4·84
Cyclohexane	2·023	4·77
CCl_4	2·238	2·23
Toluene	2·379	1·63
Benzene	2·284	1·35

K = americium extraction constant

Investigation of the influence of high concentrations of salts (Al, Mg, Li, Na, NH_4 nitrates; Na perchlorate) on the degree of extraction of the transplutonium elements and on the magnitude of the synergistic effect has shown that Am extraction by a TBP–PMBP mixture first decreases as the concentration of salts increases (Fig. 2).

One of the causes of the decrease in extraction (in the case of nitrates) is the complexing of the transplutonium elements with the nitrate ion. The second possible cause (in the case of nitrates and perchlorates) is the decrease of the free TBP and PMBP concentrations due to the complexing of the reagents with cations of the salting out agents and due to the formation of TBP compounds with HNO_3.

If the concentration of Al, Mg, Li nitrates or Na perchlorate further increases, an increase in extraction is observed; this is caused by the dehydrating action of the salts. Such a rise was not observed in the case of sodium or ammonium nitrates which are weak salting-out agents.

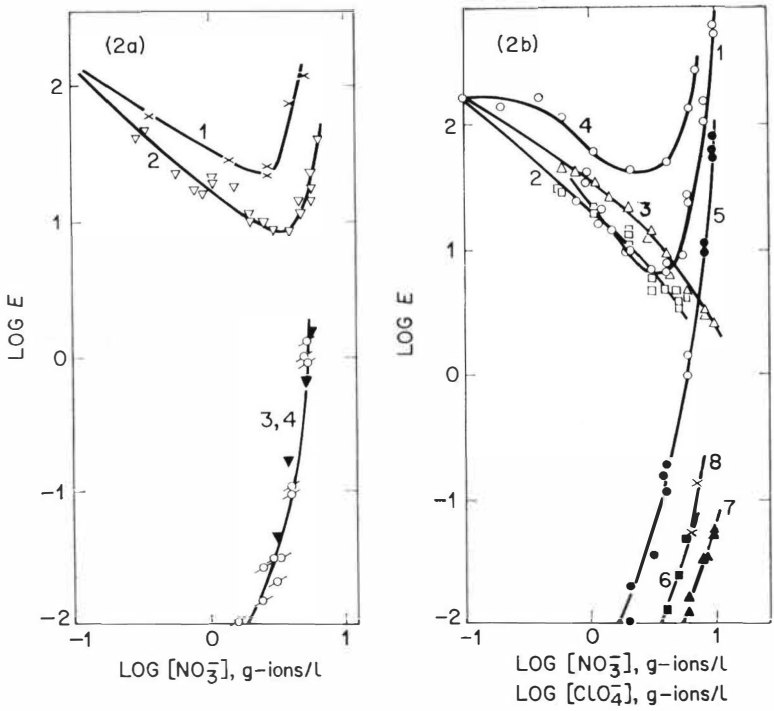

FIG. 2. *Dependence of americium extraction by a mixture of 0·05M-PMBP, 0·25M-TBP and 0·25M-TBP in cyclohexane on the concentration of salts in the water phase*

Initial concentration of HNO_3 is 0·1M

2a. Curves 1 and 2 represent extraction by a mixture of reagents from $Al(NO_3)_3$ and $Mg(NO_3)_2$, respectively Curves 3 and 4 represent extraction by TBP from $Al(NO_3)_3$ and $Mg(NO_3)_2$, respectively.

2b. Curves 1, 2 and 3 represent extraction by a mixture of reagents from $LiNO_3$, $NaNO_3$ and NH_4NO_3, respectively; Curve 4 represents extraction by a mixture of reagents from $NaClO_4$; Curves 5, 6 and 7 represent extraction by TBP from $LiNO_3$, $NaNO_3$ and NH_4NO_3, respectively; Curve 8 represents extraction by TBP from $NaClO_4$.

The data of Fig. 2 show that in all cases when salts are introduced, the synergistic effect in the given system is lowered. For practical purposes, regions of salt concentrations may be singled out, in which quantitative extraction of transplutonium elements by a mixture of reagents is possible from 0·1N-HNO_3.

PMBP and TOPO mixtures in cyclohexane were used in an effective method of americium and curium separation based on the extraction of trivalent curium from weakly acid solutions, under conditions when americium, being oxidised to the hexavalent state, remains in the water phase. The use of this mixture has a number of advantages, it permits curium extraction with a high distribution coefficient under conditions which are optimal for americium oxidation. In addition, contact with the mixture of PMBP and TOPO causes the aqueous Am(VI) to be reduced to the inextractable Am(V) thus improving the Cm/Am separation. This method of obtaining Am in the pentavalent state is particularly useful as there are no direct ways of oxidising Am to Am(V) in an acid medium. The separation coefficient for the Cm/Am separation is greater with the PMBP and TOPO mixture than with PMBP and TOPO alone.

Americium oxidation was carried out by heating with ammonium persulphate in 0·1M-HNO_3 in the absence of silver ions. Experiments carried out with macroquantities of americium ($\sim 10^{-3}$M) have shown that, under these conditions, americium is quantitatively oxidised to the hexavalent state (Fig. 3). On contacting an aqueous solution, containing Am(VI), with the PMBP and TOPO mixture in cyclohexane, reduction of americium to the pentavalent state begins immediately. According to spectrophotometric data, the completeness of Am(VI) reduction to Am(V) is $\nless 99\%$ (Fig. 3, curve 3). In the solution thus obtained, pentavalent americium was fairly stable (no change of the spectrum was ob-

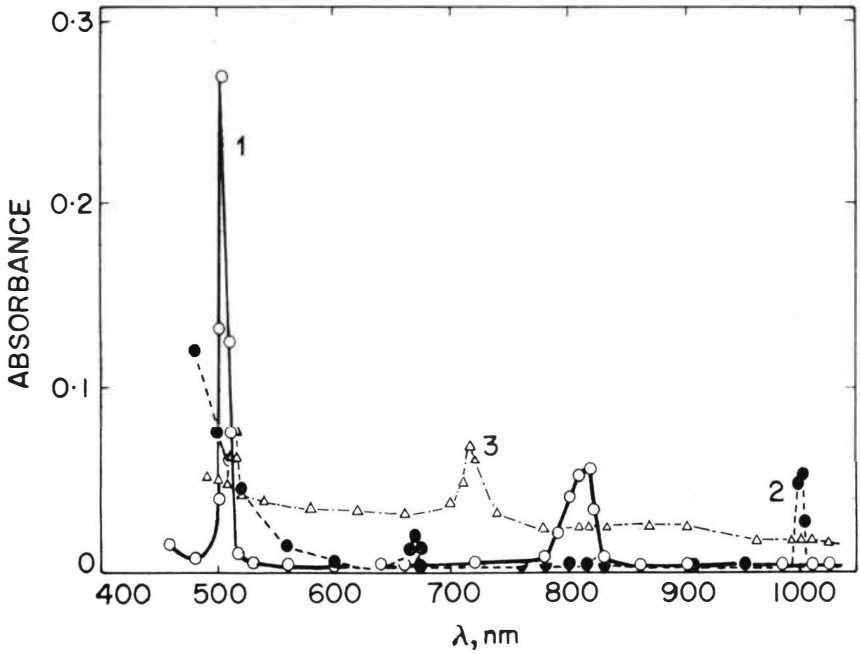

FIG. 3. *Absorption spectra of Am in 0·1M-HNO_3*
Am = 0·35 g/l; —— before oxidation, Am(III); - - - after oxidation, Am(VI); - · - · - after contact with the organic phase, Am(V)

served during 15 hours). In the presence of other α-emitters (Cm^{242}, Cm^{244}), the rate of Am(V) reduction increases and is 0·6% and 6% per hour in the presence of 0·1 g/l and 1 g/l of Cm^{244}, respectively.

Am and Cm extraction by 0·05M-PMBP in cyclohexane from 0·1M-HNO_3, containing 50 g/l of $(NH_4)_2S_2O_8$ (after 15 min. heating to oxidise americium), was examined as a function of TOPO concentration. It was found that, in the presence of persulphate ions, the introduction of donor additives (TOPO, TBPO) also substantially increased the distribution coefficient of trivalent curium (Fig. 4, curve 2), whereas the extraction of pentavalent americium hardly increased (Fig. 4, curve 3). Optimum americium and curium separation was attained during extraction by a mixture of 0·05M-PMBP+0·025M-TOPO ($E_{Cm}/E_{Am} = 4 \times 10^3$).

After curium separation, americium may be isolated from the salt-laden aqueous phase by hydroxide precipitation or by extraction after reduction to Am(III). The quantitative reduction of americium occurs when the aqueous phase is heated for 20 min in the presence of hydroxylamine (0·05–0·2M).

The method was successfully used for the separation of an americium and curium mixture and for the quantitative isolation of americium, from highly radioactive solutions, in a radiochemically pure state for its subsequent radiometric determination. Data for americium and curium separations by this method are given in Table II.

TABLE II

Am^{241} and Cm^{244} separation by extraction of 0·05M-PMBP+0·025M-TOPO in cyclohexane

Initial solution, count/min	Am/Cm	Org. phase (two extractions), count/min	Cm/Am	Org. phase (after Am red.), count/min	Cm/Am	Separation factor	
						Am/Cm	Cm/Am
$9·6 \times 10^3$	1	$4·8 \times 10^3$	50	$4·8 \times 10^3$	3×10^3	3×10^3	5×10
$5·4 \times 10^6$	10^{-2}	$5·4 \times 10^6$	—	$5·41 \times 10^4$	24	$2·4 \times 10^3$	—
$5·84 \times 10^7$	2×10^{-3}	$5·81 \times 10^7$	—	$1·17 \times 10^5$	13	$6·5 \times 10^3$	—

The americium yield by this method is 95+0·45% (6 determinations). Table III shows the extent of americium separation from some interesting radioactive elements.

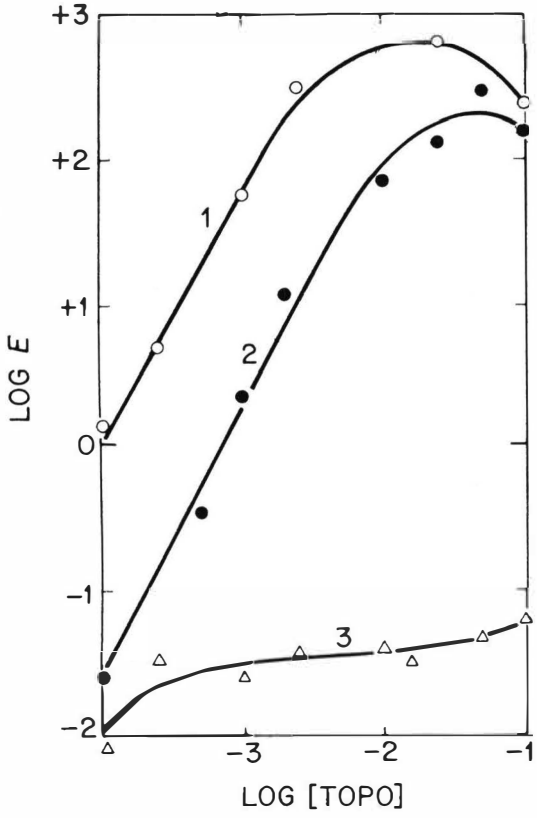

FIG. 4. *Cm*(III) *and Am*(V) *extraction by a mixture of 0·05M-PMBP + 0·025M-TOPO in cyclohexane*

Curve 1, Cm from 0·1M-HNO_3; curve 2, Cm from 0·1M-HNO_3+$(NH_4)_2S_2O_8$(50g/l); curve 3, Am(V) from 0·1M-HNO_3+$(NH_4)_2S_2O_8$(50g/l)

TABLE III

^{241}Am separation from other elements by extraction with 0·05M-PMBP+ 0·025M-TOPO in cyclohexane

Isotope	Found in Am, %	Isotope	Found in Am, %
^{90}Sr	0·38	^{233}U	0·46
^{134}Cs	0·13	^{237}Np	0·73
^{95}Zr+ ^{95}Nb	0·78	^{239}Pu	0·47
^{103}Ru	1·2	^{244}Cm	0·033
^{152}Eu	0·006	^{249}Bk	0·6
^{144}Ce	0·09	^{249}Cf	2·0

A method developed for the determination of ^{243}Am by the selective synergistic extraction of ^{239}Np, uses a mixture of PMBP and TBP as extractant, and 1×10^{-7} mg of Am can be detected. Decontamination factors of $\sim 10^5$ can be obtained for Zr, Nb and Ru; 10^8 for Cm and Ce and 10^{12} for Cs.